2017

# Photoredox Generated Radicals In Csp2-Csp3 Bond Construction

David Neal Primer
*University of Pennsylvania*, dave.primer@gmail.com

# Photoredox Generated Radicals In Csp2-Csp3 Bond Construction

**Abstract**
The routine application of Csp3-hybridized nucleophiles in cross-coupling has been an ongoing pursuit in the agrochemical, pharmaceutical, and materials science industries for over 40 years. Unfortunately, despite numerous attempts to circumvent the problems associated with alkyl nucleophiles, application of these reagents in transition metal-catalyzed C-C bond-forming reactions has remained largely restricted. In recent years, many chemists have noted the lack of reliable, turnkey reactions that exist for the installation of Csp3-hybridized centers - reactions that would be useful for delivering molecules with enhanced three-dimensional topology and altered chemical properties. As such, a general method for alkyl nucleophile activation in cross-coupling would offer access to a host of compounds inaccessible by other means.

From a mechanistic standpoint, the continued failure of alkylmetallics is inherent to the high energy intermediates associated with a traditional transmetalation. To overcome this problem, we have pioneered an alternate, single-electron pathway involving 1) initial oxidation of an alkylmetallic reagent, 2) oxidative alkyl radical capture at a metal center, and 3) subsequent reduction of the metal center to return its initial oxidation state. This series of steps constitutes a formal transmetalation that avoids the energy-demanding steps that plague a traditional anionic approach. Under this enabling paradigm, a host of alkyl precursors (alkyl-trifluoroborates and -silicates) have been generally used in cross-coupling for the first time.

In summary, the synergistic use of an Ir photoredox catalyst and a Ni cross-coupling catalyst to mediate the cross-coupling of (hetero)aryl bromides with diverse alkyl radical precursors will be discussed. Methods for coupling various trifluoroborate classes (α-alkoxy, α-trifluoromethyl, secondary and tertiary alkyl) will be covered, focusing on their complementarity to traditional protocols. Finally, a discussion of novel silicate radical precursors and their advantages in a single-electron transmetalation regime will be included.

**Degree Type**
Dissertation

# PHOTOREDOX GENERATED RADICALS IN $C_{sp^2}$-$C_{sp^3}$ BOND CONSTRUCTION

David Neal Primer

A DISSERTATION

in

Chemistry

Presented to the Faculties of the University of Pennsylvania

in

Partial Fulfillment of the Requirements for the
Degree of Doctor of Philosophy

2017

Supervisor of Dissertation

_____

Gary A. Molander
Hirschmann-Makineni Professor of Chemistry

Graduate Group Chairperson

_____

Gary A. Molander
Hirschmann-Makineni Professor of Chemistry

Dissertation Committee:

David M Chenoweth, Assistant Professor of Chemistry
Madeleine Joullié, Professor of Chemistry
Jeffrey D. Winkler, Merriam Professor of Chemistry

PHOTOREDOX GENERATED RADICALS IN $C_{sp^2}$-$C_{sp^3}$ BOND CONSTRUCTION

*Dedicated to Benjamin M. Primer III,*

*the man who forgot while I learned to remember.*

# ABSTRACT


PHOTOREDOX GENERATED RADICALS IN $C_{sp2}$-$C_{sp3}$ BOND CONSTRUCTION

David N Primer

Gary A. Molander

The routine application of $C_{sp3}$-hybridized nucleophiles in cross-coupling has been an ongoing pursuit in the agrochemical, pharmaceutical, and materials science industries for over 40 years. Unfortunately, despite numerous attempts to circumvent the problems associated with alkyl nucleophiles, application of these reagents in transition metal-catalyzed C-C bond-forming reactions has remained largely restricted. In recent years, many chemists have noted the lack of reliable, turnkey reactions that exist for the installation of $C_{sp3}$-hybridized centers - reactions that would be useful for delivering molecules with enhanced three-dimensional topology and altered chemical properties. As such, a general method for alkyl nucleophile activation in cross-coupling would offer access to a host of compounds inaccessible by other means.

From a mechanistic standpoint, the continued failure of alkylmetallics is inherent to the high-energy intermediates associated with a traditional transmetalation. To overcome this problem, we have pioneered an alternate, single-electron pathway involving 1) initial oxidation of an alkylmetallic reagent, 2) oxidative alkyl radical capture at a metal center, and 3) subsequent reduction of the metal center to return its initial oxidation state. This series of steps constitutes a formal transmetalation that avoids the energy-demanding steps that plague a traditional anionic approach. Under this enabling paradigm, a host of alkyl precursors (alkyl-trifluoroborates and -silicates) have been generally used in cross-coupling for the first time.

In summary, the synergistic use of an Ir photoredox catalyst and a Ni cross-coupling catalyst to mediate the cross-coupling of (hetero)aryl bromides with diverse alkyl radical precursors will be discussed. Methods for coupling various trifluoroborate classes (α-alkoxy, α-trifluoromethyl, secondary and tertiary alkyl) will be covered, focusing on their complementarity to traditional protocols. Finally, a discussion of novel silicate radical precursors and their advantages in a single-electron transmetalation regime will be included.

TABLE OF CONTENTS

**ABSTRACT** ..... **iv**

**Chapter 1. Background on Cross-Coupling of $C_{sp}3$ Nucleophiles: Design of a New Radical-Based Approach to Alkyl Transfer** ..... **1**

1.1 Introduction to Alkyl Cross-Coupling and Its Limitations ..... 1

1.2 Photoredox Catalysis for the Generation of Organic Radicals ..... 8

1.3 Fusion of Transition Metal Catalysis and Photoredox Catalysis ..... 12

1.4 References ..... 14

**Chapter 2. Proof of Concept: Photoredox/Ni Dual Catalysis for the Cross-Coupling of Benzylic Trifluoroborates with Aryl Halides** ..... **19**

2.1 Introduction ..... 19

2.2 Results and Discussion ..... 22

2.3 Conclusions ..... 28

2.4 Experimental ..... 28

2.5 References ..... 54

Appendix A1. $^{1}H$, $^{13}C$, $^{11}B$, and $^{19}F$ NMR Spectra Relevant to Chapter 2 ..... 58

**Chapter 3. Extension to Activated Primary Systems** ..... **109**

3.1 Introduction ..... 109

3.2 Results and Discussion ..... 110

3.3 Conclusion ..... 116

3.4 Experimental ..... 117

3.5 References ..... 143

Appendix A2. $^{1}H$, $^{13}C$, $^{11}B$, and $^{19}F$ NMR Spectra Relevant to Chapter 3 ..... 146

**Chapter 4. Unactivated Secondary Alkyltrifluoroborates as Radical Precursors** ..... **201**

4.1 Introduction ..... 201

4.2 Results and Discussion ..... 203

4.3 Conclusion ..... 207

4.4 Experimental ..... 208

4.5 References ..... 226

Appendix A3. $^{1}H$, $^{13}C$, $^{11}B$, and $^{19}F$ NMR Spectra Relevant to Chapter 4 ..... 230

**Chapter 5. Synthesis of 1,1'-Diaryl-2,2,2-trifluoroethanes via Photoredox/Nickel Dual Catalytic Cross-Coupling ..... 261**

5.1 Introduction ..... 261

5.2 Results and Discussion ..... 264

5.3 Conclusion ..... 271

5.4 Experimental ..... 271

5.5 References ..... 283

Appendix A4. Cyclic Voltammetry (CV) Data Relevant to Chapter 5 ..... 285

Appendix A5. Chiral SFC Chromatograms Relevant to Chapter 5 ..... 286

Appendix A6. $^{1}H$, $^{13}C$, and $^{19}F$ NMR Spectra Relevant to Chapter 5 ..... 296

**Chapter 6. Construction of Quaternary Centers via Radical Mediated Alkyl Transfer 324**

6.1 Introduction ..... 324

6.2 Results and Discussion ..... 325

6.3 Conclusion ..... 333

6.4 Experimental ..... 334

6.5 References ..... 361

Appendix A7. $^{1}H$, $^{13}C$, $^{11}B$, and $^{19}F$ NMR Spectra Relevant to Chapter 6 ..... 365

**Chapter 7. Hypervalent Silicates as Alternative Radical Precursors ..... 411**

7.1 Introduction ..... 411

7.2 Results and Discussion ..... 413

7.3 Conclusion ..... 420

7.4 Experimental ..... 421

7.5 References ..... 458

Appendix A8. $^{1}H$, $^{13}C$, and $^{19}F$ NMR Spectra Relevant to Chapter 7 ..... 461

Appendix A9. Cyclic Voltammetry Data Relevant to Chapter 7 ..... 525

**Chapter 8. Computational and Experimental Investigations into Reaction Mechanism 528**

8.1 Introduction ..... 528

8.2 Results and Discussion ..... 530

8.3 Conclusion ..... 536

8.4 Experimental ..... 537
8.5 References ..... 542
Appendix A10. $^{1}H$, $^{13}C$ Spectra and Chiral SFC Chromatograms Relevant to Chapter 8 ..... 545

**Chapter 9. Photoredox Generated Radicals in Minisci Chemistry ..... 552**
9.1 Introduction ..... 552
9.2 Results and Discussion ..... 556
9.3 Conclusion ..... 575
9.4 Experimental ..... 576
9.5 References ..... 606
Appendix A11. $^{1}H$, $^{13}C$, $^{11}B$, $^{19}F$ Spectra Relevant to Chapter 9 ..... 611

# PART I

## Chapter 1. Background on Cross-Coupling of $C_{sp3}$ Nucleophiles: Design of a New Radical-Based Approach to Alkyl Transfer

### 1.1 Introduction to Alkyl Cross-Coupling and Its Limitations

Palladium and nickel have transformed the landscape of catalytic chemistry over the past century.[1] Although hardly the first metals to be used in carbon-carbon bond-forming reactions, they have quickly become the catalysts of choice over early copper- and cobalt-based methods. In particular, nickel has recently grown in popularity relative to palladium because of its low cost, greater abundance, and lower toxicity.[2] Especially for achieving alkyl-aryl couplings, nickel possesses a number of notable advantages, including its higher barriers for β-hydride elimination,[3] stable odd-electron oxidation states,[4] and enhanced inner sphere reduction potential toward alkyl halides.[5]

As indicated by the 2010 Nobel Prize in Chemistry, the importance of transition metal catalyzed cross-coupling to organic synthesis cannot be overstated.[6] To date, these methods continue to be among the most broad, reliable, and powerful tools for constructing C–C bonds in the chemical literature. A typical cross-coupling proceeds through the following catalytic cycle: (1) oxidative addition of an aryl electrophile to a low-valent metal center, (2) transmetalation of an organometallic nucleophile to displace a weakly coordinating ligand, and (3) reductive elimination to forge a desired C-C bond and regenerate the catalyst (**Figure 1.1**).[7,8]

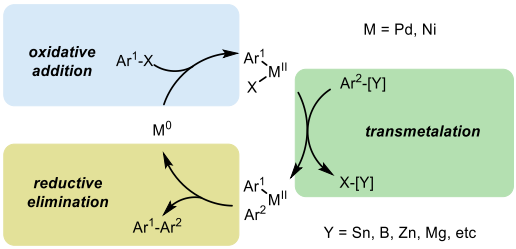


**Figure 1.1:** Standard cross-coupling catalytic cycle

These reactions work exceptionally well for $C_{sp2}$-$C_{sp2}$ and $C_{sp2}$-$C_{sp}$ bond formation. Unfortunately, because of the nature of the transmetalation step (vide infra), these reactions are much less amenable to $C_{sp2}$-$C_{sp3}$ cross-coupling. To illustrate this point, as of 2014, over 32,000 articles had been published on cross-coupling methods, but a mere 600 (less than 2%) have been related to the use of alkylmetallic reagents in these reactions.[9]

Driven by this clear methodological gap, the use of $C_{sp3}$-hybridized nucleophiles in cross-coupling has been a continued goal of the synthetic organometallic community since the development of Pd-catalyzed cross-coupling over 40 years ago.[10] However, unlike the development of the related $C_{sp2}$ couplings, the unique challenges associated with alkylmetallics has limited their development and widespread adoption. Among the issues associated with these reagents include the following: (1) the greater propensity to undergo protodemetalation,[11,12] (2) the often pyrophoric nature of these reagents, requiring fresh preparation and superstoichiometric loadings, (3) the high barrier for efficient transmetalation[13] in the catalytic cycle, typically requiring additives,[14] and finally (4) in the case of successful alkyl transfer, the ready possibility for β-hydride elimination/reinsertion sequences,[8,15] which afford a mixture of both olefinic byproducts and regioisomeric coupling products (**Figure 1.2**).

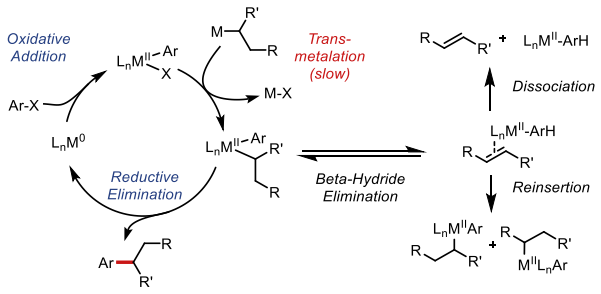


**Figure 1.2:** Possible side reactivity with secondary organometallics

Despite these challenges, successful use of alkyllithium,[16] -zinc,[17–19] -magnesium,[20–23] -indium,[24] -boron,[25–27] -silicon,[28,29] and -tin[15] reagents in the cross-coupling with aryl electrophiles has been realized with a variety of catalysts systems (Pd, Ni, and Fe). Typically, these cross-coupling methods work best for primary alkyl systems where potential isomerization favors the less sterically hindered position. Moving to secondary alkyl nucleophiles, only Kumada[23] and Negishi[17,19] reagents have been widely employed, but these methods suffer from limited functional group tolerance as both protic and electrophilic handles are sensitive to these highly reactive reagents.[18,30] Isolated examples of success exist for secondary alkyl -boron[26,27] and -stannane[15] reagents. For the former, these methods are completely intolerant of steric bulk and give complex product mixtures when bulky organoboron reagents are engaged (**Figure 1.3**). For the latter, these reagents remain untested for isomerization, but the perceived toxicity of alkylstannanes limits their broader use in academic and industrial settings. A qualitative comparison of these reagents and their properties can be found in **Figure 1.4**.

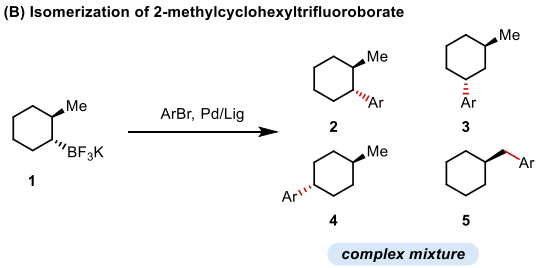


**Figure 1.3:** Isomerization of bulky organoboron reagents

A closer look at Figure 1.4 highlights the overall advantages of organoboron reagents when stacked up against their competitors in alkyl cross-coupling. Organoboron reagents, in particular alkyltrifluoroborates, exist as indefinitely bench-stable, fluffy powders that do not require fresh preparation before use and release innocuous waste after the reaction is complete (borate and potassium halide salts). These properties are particularly advantageous in medicinal chemistry where libraries of compounds are made in a parallel manner. Unfortunately, the low nucleophilicity of these organoborons has always limited their general use in cross-coupling. Therefore, to improve

| Reagent | Stability | FG Tolerance | Synthetic Accessibility | Toxicity | 2° alkyl XC? |
|---|---|---|---|---|---|
| RLi | 🔴 | 🔴 | 🔴 | 🟢 | 🟢 |
| RMgX | 🔴 | 🔴 | 🔴 | 🟢 | 🟢 |
| RZnX | 🟡 | 🟡 | 🟡 | 🟢 | 🟢 |
| $RSnR'_3$ | 🟢 | 🟢 | 🟢 | 🔴 | 🟢 |
| $RB(X)_n$ | 🟢 | 🟢 | 🟢 | 🟢 | 🔴 |

**Figure 1.4:** Qualitative comparison of alkylmetallic reagents

these organoboron reagents as potential partners in cross-coupling, it seemed prudent to consider the key steps in the classical cross-coupling which were responsible for their failure. Here, it was recognized that for nearly all organoboron cross-couplings, the transmetalation step is rate-determining (**Figure 1.5**)

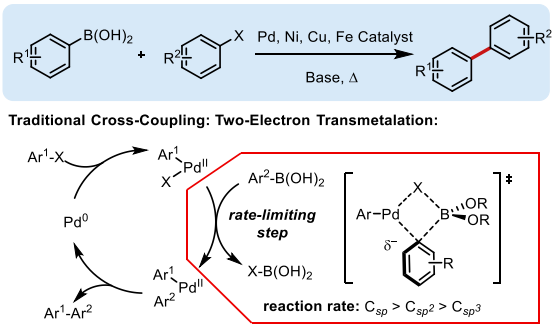


**Figure 1.5:** Rate-determining step in organoboron cross-couplings

Examination of this step shows that significant anionic charge builds up on the transferring carbon in the transition state. Therefore, reagents best able to stabilize this negative charge such as the $C_{sp}$ and $C_{sp2}$ hybridized organometallics typically perform best in cross-coupling. Furthermore, the most successful *alkyl* cross-couplings have generally defaulted to the more anionic reagents (zinc-, magnesium-, lithium-based organometallics) to overcome this high barrier for transmetalation.

Instead of attempting to override the inherent mechanistic hierarchy of classical cross-coupling, it was hypothesized that an odd-electron manifold for achieving a formal transmetalation might be possible through the intermediacy of an alkyl radical precursor. Notably, this single-electron approach to transmetalation should exhibit complementary reactivity to traditional cross-coupling as the trends in radical stability are inverted relative to their anionic counterparts (**Figure 1.6**).

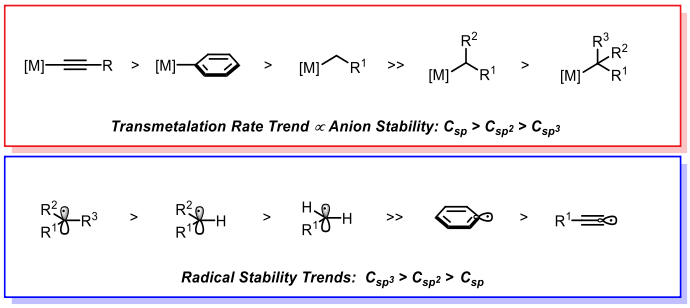


**Figure 1.6**: Relative stability trends for alkyl-centered anions and radicals

This concept of using radicals as transmetalating agents in cross-coupling was not unprecedented. Key mechanistic investigation of Ni-catalyzed reductive coupling chemistry from the Weix group[31,32] (**Figure 1.7**) as well as radical rebound oxidative addition of alkyl halides pioneered by the Fu group[33,34] suggested that this strategy would indeed be possible. These experiments delineated the clear presence of radical intermediates in Ni-catalyzed cross-coupling, observing cyclization products when using alkyl halides containing pendant olefins. Furthermore, nickel loading in these experiments drastically affected the amount of cyclization observed indicating that the radicals generated by inner sphere reduction at the nickel center escape the solvent cage and participate in radical chain events. Beyond these reports, radical addition processes at metal centers were believed to be virtually barrierless based on computational and experimental evaluation.[35] However, unlike all hitherto reported methods, the proposed radical intermediates from organometallics needed to be generated via oxidation instead of reduction.

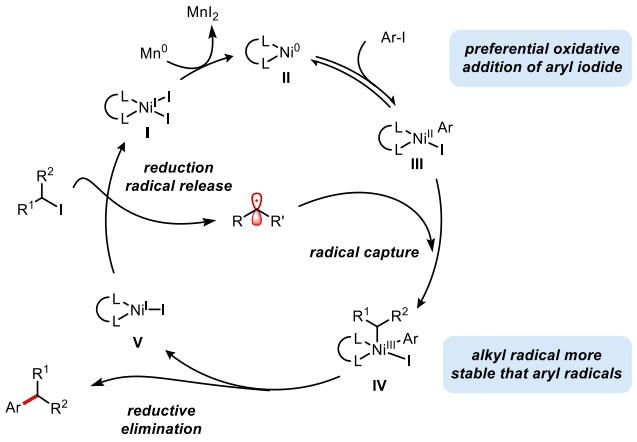


**Figure 1.7.** Weix's mechanism for selectivity in nickel catalyzed reductive coupling

Here, examination of the alkyltrifluoroborate literature gave numerous examples of stoichiometric radical generation under oxidizing conditions employing [Dess-Martin periodinane/$Cu^{II}$,[36] $Mn(OAc)_2$,[37] Ag salts,[38] etc]. Furthermore, there were even reports of radical generation of alkyltrifluoroborates under photoredox catalysis.[39] Based on these reports, we were confident that facile radical generation from alkyltrifluoroborates would indeed be possible. However, generation of an alkyl radical and its addition to a metal center is an incomplete transmetalation; instead, addition of a radical to a metal center results in a metal center that is formally oxidized by one electron.[40] Therefore, in order to achieve the overall redox-neutral profile of a traditional transmetalation, a subsequent single-electron reduction event would be required. (**Figure 1.8**)

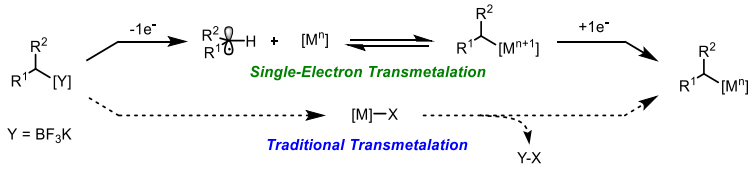


**Figure 1.8.** Comparison between radical capture at metal and traditional transmetalation

The solution to this challenge is certainly non-obvious, given that the proposed oxidation and reduction events need to occur simultaneously within the confines of the same flask. A proposal based on stoichiometric reagents in this context was likely to be ineffectual as the reagents would self-quench unproductively instead of performing the desired oxidation and reduction events at the appropriate times within the catalytic cycle.[41,42] Here, an ideal solution would be the ability to transiently generate both a single electron oxidant and reductant in a reaction mixture without significant side reactivity or reagent quenching. Fortunately, it was anticipated that photoredox catalysis would serve as an enabling technology for this exact purpose.[43]

## 1.2 Photoredox Catalysis for the Generation of Organic Radicals

Photoredox catalysis has been a rapidly growing field in organic synthesis over the last 20 years, accelerated by publications from a number of high-profile groups.[44–46] However, the origins of this field extend back over 80 years. For example, the most well-recognized photoredox catalyst $Ru(bpy)_3^{2+}$ was first synthesized in 1936 by Burstall and co-workers, and is noted for its phosphorescent properties and remarkable configurational stability.[47] Since its discovery, this complex has found uses in understanding electron transfer chemistry, observing photophysical phenomenon, assisting molecular labeling, etc.[48] However, it was not until the late 1970s that $Ru(bpy)_3^{2+}$ saw its first use as a catalytic photosensitizer in organic synthesis.[49]

The photochemistry of these complexes has been studied extensively since these initial forays into catalytic electron transfer; therefore, a full picture of their excitation and relaxation pathways is now well-understood (**Figure 1.9**).[50,51] First, visible light excitation of $Ru(bpy)_3^{2+}$ complex **I** ($\lambda_{max}$ = 452 nm) leads to efficient excitation to the lowest singlet excited state **II**. This initially generated

singlet state ($^1$MLCT state, MLCT = metal-to-ligand charge transfer) then undergoes an intersystem crossing to afford the long-lived, luminescent triplet excited state $^3Ru(bpy)_3^{2+}$* (**III**). This triplet state has a number of possible relaxation pathways to afford the ground state complex **I**.[41] In the absence of quencher, phosphorescent decay pathways can occur from the triplet state, emitting in the orange spectrum (dashed green line). In the presence of an organic acceptor, outer sphere electron transfer from the ligand affords the oxidized $Ru(bpy)_3^{3+}$ complex **IV** and the reduced acceptor. This oxidized catalyst can then accept an electron from a donor to return the catalyst to its ground state, $Ru(bpy)_3^{2+}$ (**I**). Alternatively, in the presence of an organic donor, a reductive quenching manifold can occur where the photocatalyst accepts an electron at the metal center to afford complex (**V**). Followed by subsequent single-electron transfer from the ligand to an appropriate acceptor, the catalyst can then return to the ground state. In addition to these single-electron transfer relaxation events, energy transfer events can occur to give triplet excitation in the presence of appropriate acceptor molecules (e.g., diarylketones).[52] Each of these quenching events must be carefully considered when designing any photocatalytic transformation to avoid undesired off-cycle intermediates.

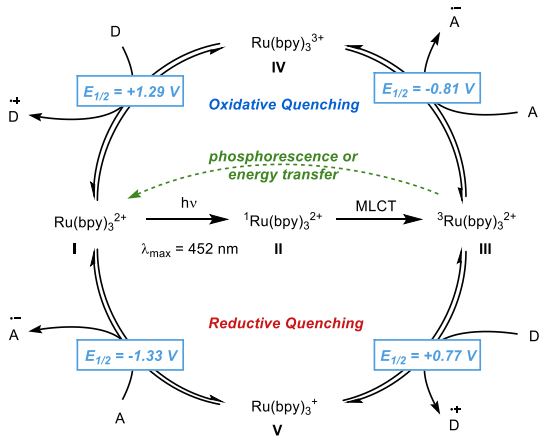


**Figure 1.9:** Possible quenching pathways for $Ru(bpy)_3^{2+}$

As referenced above, the earliest reports of photosensitizers in organic synthesis began in the late 1970s, but these transformations largely explored the use of photoredox catalysts in purely overall reductive or overall oxidative transformations. In these methods, a readily reducible or oxidizable functional group is converted into a higher or lower oxidation state via successive single-electron transfer events (**Schemes 1.1 and 1.2**). Typically, a stoichiometric terminal reductant (e.g., 1,4-dihydropyridine)[49] or terminal oxidant (e.g., aryldiazonium salt)[53] is used to turn over the photocatalytic cycle with the sensitizer serving only as an electron shuttle between the two reagents. Most notably, under this paradigm an entire equivalent of material is sacrificed to achieve a desired transformation.

**Scheme 1.1.** Net reduction of acylsulfonium salts

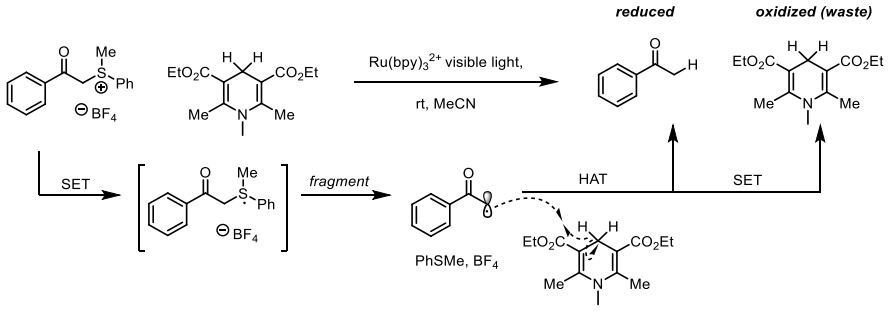


**Scheme 1.2.** Net oxidation of benzylic alcohols

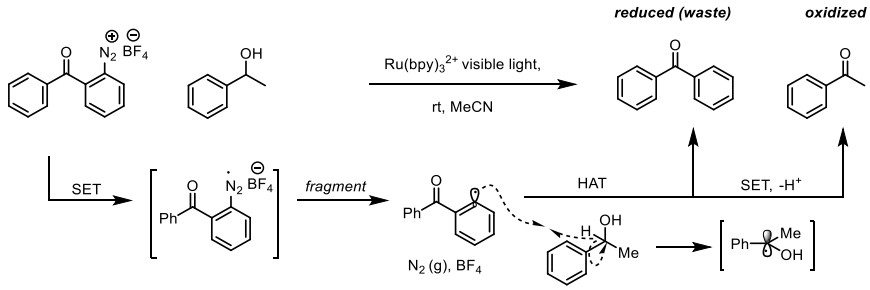


Although these transformations were the first to establish the feasibility of performing photoredox catalysis in batch format on organic molecules, the resultant products often could be accessed in identical yields using stoichiometric quantities of an appropriate reductant or oxidant.

Therefore, the use of these photosensitizers languished in the materials and photophysics arenas for another fifteen years before being rediscovered by modern synthetic laboratories.

The modern renaissance for photoredox chemistry was likely triggered by Barton and co-workers in 1994.[54] In a modified atom transfer radical addition reaction (ATRA), Barton was able to use both individual single-electron steps in a productive manner for the first time. In his work, initial oxidation of a *Se*-phenyl *p*-tolueneselenosulfonate generates a sulfonyl radical which is captured by a vinyl ether. The generated α-alkoxy radical is then oxidized to afford an oxocarbenium ion which readily intercepts the phenylselenoate byproduct of the first step. The Stephenson group[55] was able to extend this chemistry further to alkyl halides as shown in **Figure 1.10.**

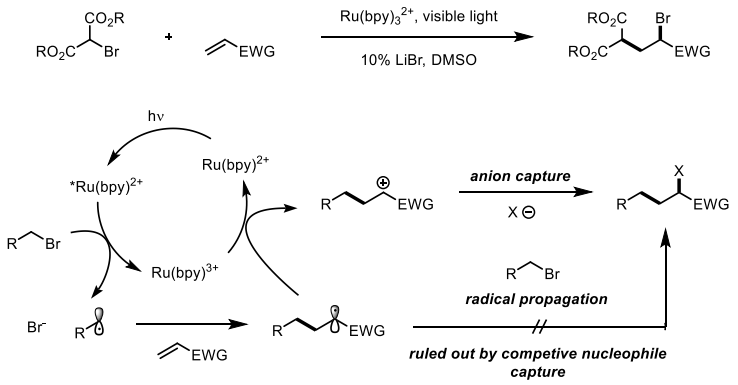


**Figure 1.10.** Redox neutral 1,2-halofunctionalization of alkenes

Following these two pioneering contributions, the most powerful photoredox transformations to date have sought to use each of the catalytic single-electron steps in a productive manner. Successful integration of this concept has led to some remarkable bond disconnections, particularly in cases where long-lived radicals are selectively coupled with concomitantly generated transient radicals. Selected recent highlights of redox-neutral photoredox transformations include the following: (1) enantioselective α-alkylation of in situ generated iminium ions,[44] (2) decarboxylative

alkylation of electron-poor arenes,[56,57] (3) trifluoromethylation of arenes,[58] (4) enamine coupling with silyl enols,[59] and (5) anti-Markovnikov hydrofunctionalization of olefins.[60] In addition to these fully organic redox-neutral transformations, the use of photoredox catalysts to modulate transition-metal catalyzed reactions has rapidly evolved into its own unique field as discussed in Chapter 1.3.

## 1.3 Fusion of Transition Metal Catalysis and Photoredox Catalysis

Beginning in the early 2000s, many chemists began to question the possible effect that single-electron photosensitizers might have on transition metal-catalyzed reactions. Given that oxidation state has been shown to perturb the overall reaction pathway significantly by improving catalyst stability,[61] accelerating reductive elimination,[62,63] altering oxidative addition rates,[64] and enabling C–H activation,[65] the use of photoredox catalysts to modulate transition-metal oxidation states was an inevitable outcome. An interesting review by the Toste group discussing this realization has recently been published outlining the use of single-electron transfer for all elementary steps in transition metal catalysis.[66]

The first report on this concept focused purely on rate acceleration observed in previously reported Pd-catalyzed Sonogashiri couplings. Here, addition of $Ru(bpy)_3^{2+}$ led to improved reaction times and electrophile scope relative to methods using more traditional stoichiometric additives (Cu, Ag).[67] Unfortunately, in this report, no attempt was made to understand the underlying mechanism. Instead, the authors suggest broadly that an energy transfer or single-electron oxidation event may be responsible for the Pd catalyst's greater propensity for both oxidative addition and alkyne coordination.

A second application of dual photoredox/palladium catalysis in cross-coupling chemistry was introduced in a seminal contribution by Sanford and co-workers.[68] This transformation involves the

direct arylation of arenes by C–H bond activation. Previous studies on this transformation had identified diaryliodonium salts as a suitable aryl coupling partner, but high reaction temperatures (>95 ºC) were always required to overcome oxidative addition to a crowded palladium center.[69] Anticipating that aryl radicals might offer an alternative, highly oxidizing aryl group source, a dual catalytic system was proposed based on the well-established photoredox-mediated reduction of aryldiazonium salts.[70] In contrast to other synthetic routes to aryl radicals, this process occurs at room temperature, showcasing how photoredox catalysis can generate reactive species under remarkably mild conditions. A summary of the reaction manifold can be found in **Figure 1.11**.

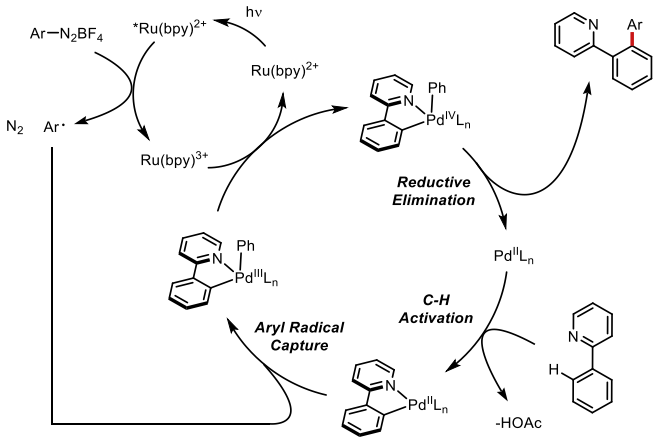


**Figure 1.11.** Merger of Pd C-H activation with photoredox generated radicals

After the introduction of this concept to the literature, numerous reports have highlighted the fusion of photoredox catalysis with a variety of transition metal catalysts to achieve useful and unprecedented reactivity. For example, trifluoromethylation of boronic acids using copper has been achieved using a photoredox catalysts for the reduction of trifluoromethyl iodide.[71] Here, the photocatalyst is integral in the oxidation of the Cu to its high valent $Cu^{III}$ state to facilitate reductive elimination. Gold catalysis has also been combined with photoredox catalysis to access highly reactive $Au^{III}$ to facilitate the alkoxyarylations of alkenes.[72,73] Given the infancy of this field, further

reports on the merger of photocatalysis with various transition metal catalysts will likely continue to occur with greater and greater frequency.[74,75]

## 1.4 References


(1) Kronberg, B. I.; Coatsworth, L. L.; Usselman, M. C. *Ambix* **1981**, *28*, 20.

(2) Tasker, S. Z.; Standley, E. A.; Jamison, T. F. *Nature* **2014**, *509*, 299.

(3) Bo-Lin, L.; Lei, L.; Yao, F.; Shi-Wei, L.; Qian, C.; Guo, Q.-X. *Organometallics* **2004**, *23*, 2114.

(4) Cornella, J.; Gómez-Bengoa, E.; Martin, R. *J. Am. Chem. Soc.* **2013**, *135*, 1997.

(5) Choi, J.; Fu, G. C. *Science* **2017**, *356*.

(6) Halford, B. *Chem. Eng. News* **2010**, *88*.

(7) Carrow, B. P.; Hartwig, J. F. *J. Am. Chem. Soc.* **2011**, *133*, 2116.

(8) Hartwig, J. F. *Organotransition Metal Chemistry: From Bonding to Catalysis*; University Science Books: Sausalito, CA, 2009.

(9) Johansson Seechurn, C. C. C.; DeAngelis, A.; Colacot, T. J. In *New Trends in Cross-Coupling: Theory and Applications*; Royal Society of Chemistry: Cambridge, **2014**, 1–19.

(10) Jana, R.; Pathak, T. P.; Sigman, M. S. *Chem. Rev.* **2011**, *111*, 1417.

(11) Rilatt, I.; Jackson, R. F. W. *J. Org. Chem.* **2008**, *73*, 8694.

(12) Lozada, J.; Liu, Z.; Perrin, D. M. *J. Org. Chem.* **2014**, *79*, 5365.

(13) Miyaura, N.; Ishiyama, T.; Sasaki, H.; Ishikawa, M.; Satoh, M.; Suzuki, A. *J. Am. Chem. Soc.* **1989**, *111*, 314.

(14) Zou, G.; Reddy, Y. K.; Falck, J. R. *Tetrahedron Lett.* **2001**, *42*, 7213.

(15) Li, L.; Wang, C.-Y.; Huang, R.; Biscoe, M. R. *Nat. Chem.* **2013**, *5*, 607.

(16) Vila, C.; Giannerini, M.; Hornillos, V.; Fañanás-Mastral, M.; Feringa, B. L. *Chem. Sci.* **2014**, *5*, 1361.

(17) Han, C.; Buchwald, S. L. *J. Am. Chem. Soc.* **2009**, 7532.

(18) Manolikakes, G.; Schade, M. A.; Hernandez, C. M.; Mayr, H.; Knochel, P. *Org. Lett.* **2008**, *10*, 2765.

(19) Pompeo, M.; Froese, R. D. J.; Hadei, N.; Organ, M. G. *Angew. Chem. Int. Ed.* **2012**, *51*, 11354.

(20) Michael E. Limmert; Amy H. Roy, A.; Hartwig, J. F. *J. Org. Chem.* **2005**, *70*, 9364.

(21) Katayama, T.; Umeno, M. *Chem. Lett.* **1991**, *20*, 2073.

(22) Kanemura, S.; Kondoh, A.; Yorimitsu, H.; Oshima, K. *Synthesis* **2008**, *2008*, 2659.

(23) Joshi-Pangu, A.; Wang, C.-Y.; Biscoe, M. R. *J. Am. Chem. Soc.* **2011**, *133*, 8478.

(24) Ignacio Pérez; José Pérez Sestelo, A.; Sarandeses, L. A. *J. Am. Chem. Soc.* **2001**, *123*, 4155.

(25) Littke, A. F.; Dai, C.; Fu, G. C. *J. Am. Chem. Soc.* **2000**, *122*, 4020.

(26) Dreher, S. D.; Dormer, P. G.; Sandrock, D. L.; Molander, G. A. *J. Am. Chem. Soc.* **2008**, *130*, 9257.

(27) Li, L.; Zhao, S.; Joshi-Pangu, A.; Diane, M.; Biscoe, M. R. *J. Am. Chem. Soc.* **2014**, *136*, 14027.

(28) Nakao, Y.; Takeda, M.; Matsumoto, T.; Hiyama, T. *Angew. Chem. Int. Ed.* **2010**, *49*, 4447.

(29) Hatanaka, Y.; Hiyama, T. *Tetrahedron Lett.* **1990**, *31*, 2719.

(30) Melzig, L.; Metzger, A.; Knochel, P. *Chemistry* **2011**, *17*, 2948.

(31) Everson, D. A.; Shrestha, R.; Weix, D. J. *J. Am. Chem. Soc.* **2010**, *132*, 920.

(32) Biswas, S.; Weix, D. J. *J. Am. Chem. Soc.* **2013**, *135*, 16192.

(33) Zultanski, S. L.; Fu, G. C. *J. Am. Chem. Soc.* **2013**, *135*, 624.

(34) Wilsily, A.; Tramutola, F.; Owston, N. A.; Fu, G. C. *J. Am. Chem. Soc.* **2012**, *134*, 5794.

(35) Breitenfeld, J.; Ruiz, J.; Wodrich, M. D.; Hu, X. *J. Am. Chem. Soc.* **2013**, *135*, 12004.

(36) Sorin, G.; Martinez Mallorquin, R.; Contie, Y.; Baralle, A.; Malacria, M.; Goddard, J.-P.; Fensterbank, L. *Angew. Chem. Int. Ed.* **2010**, *49*, 8721.

(37) Presset, M.; Fleury-Brégeot, N.; Oehlrich, D.; Rombouts, F.; Molander, G. A. *J. Org. Chem.* **2013**, *78*, 4615.

(38) Lockner, J. W.; Dixon, D. D.; Risgaard, R.; Baran, P. S. *Org. Lett.* **2011**, *13*, 5628.

(39) Yasu, Y.; Koike, T.; Akita, M. *Adv. Synth. Catal.* **2012**, *354*, 3414.

(40) Tellis, J. C.; Kelly, C. B.; Primer, D. N.; Jouffroy, M.; Patel, N. R.; Molander, G. A. *Acc. Chem. Res.* **2016**, *49*, 1429.

(41) Tucker, J. W.; Stephenson, C. R. J. *J. Org. Chem.* **2012**, *77*, 1617.

(42) Narayanam, J. M. R.; Stephenson, C. R. J. *Chem. Soc. Rev.* **2011**, *40*, 102.

(43) Prier, C. K.; Rankic, D. A.; MacMillan, D. W. C. *Chem. Rev.* **2013**, *113*, 5322.

(44) Nicewicz, D. A.; MacMillan, D. W. C. *Science* **2008**, *322*, 77.

(45) Ischay, M. A.; Lu, Z.; Yoon, T. P. *J. Am. Chem. Soc.* **2010**, *132*, 8572.

(46) Narayanam, J. M. R.; Tucker, J. W.; Stephenson, C. R. J. *J. Am. Chem. Soc.* **2009**, *131*, 8756.

(47) Morgan, G. T.; Burstall, F. H. *J. Chem. Soc.* **1936**, *0*, 41.

(48) Balzani, V.; Bergamini, G.; Campagna, S.; Puntoriero, F. In *Photochemistry and Photophysics of Coordination Compounds I*; Springer Berlin Heidelberg: Berlin, Heidelberg; pp. 1–36.

(49) Hedstrand, D. M.; Kruizinga, W. H.; Kellogg, R. M. *Tetrahedron Lett.* **1978**, *19*, 1255.

(50) Demas, J. N.; Harris, E. W.; McBride, R. P. *J. Am. Chem. Soc.* **1977**, *99*, 3547.

(51) Wrighton, M.; Morse, D. L. *J. Am. Chem. Soc.* **1974**, *96*, 998.

(52) Wrighton, M.; Markham, J. *J. Phys. Chem.* **1973**, *77*, 3042.

(53) Cano-Yelo, H.; Deronzier, A. *Tetrahedron Lett.* **1984**, *25*, 5517.

(54) Barton, D. H. R.; Csiba, M. A.; Jaszberenyi, J. C. *Tetrahedron Lett.* **1994**, *35*, 2869.

(55) Nguyen, J. D.; Tucker, J. W.; Konieczynska, M. D.; Stephenson, C. R. J. *J. Am. Chem. Soc.* **2011**, *133*, 4160.

(56) Zuo, Z.; MacMillan, D. W. C. *J. Am. Chem. Soc.* **2014**, *136*, 5257.

(57) Prier, C. K.; MacMillan, D. W. C. *Chem. Sci.* **2014**, *5*, 4173.

(58) Nagib, D. A.; MacMillan, D. W. C. *Nature* **2011**, *480*, 224.

(59) Yasu, Y.; Koike, T.; Akita, M. *Chem. Commun.* **2012**, *48*, 5355.

(60) Margrey, K. A.; Nicewicz, D. A. *Acc. Chem. Res.* **2016**, *49*, 1997.

(61) Proutiere, F.; Aufiero, M.; Schoenebeck, F. *J. Am. Chem. Soc.* **2012**, *134*, 606.

(62) Camasso, N. M.; Sanford, M. S. *Science* **2015**, *347*.

(63) Ball, N. D.; Gary, J. B.; Ye, Y.; Sanford, M. S. *J. Am. Chem. Soc.* **2011**, *133*, 7577.

(64) Gutierrez, O.; Tellis, J. C.; Primer, D. N.; Molander, G. A.; Kozlowski, M. C. *J. Am. Chem. Soc.* **2015**, *137*, 4896.

(65) Hickman, A. J.; Sanford, M. S. *Nature* **2012**, *484*, 177.

(66) Levin, M. D.; Kim, S.; Toste, F. D. *ACS Cent. Sci.* **2016**, *2*, 293.

(67) Osawa, M.; Nagai, H.; Akita, M.; Whitten, D. G.; Astruc, D.; Nishihara, Y. *Dalt. Trans.* **2007**, *101*, 827.

(68) Kalyani, D.; McMurtrey, K. B.; Neufeldt, S. R.; Sanford, M. S. *J. Am. Chem. Soc.* **2011**, *133*, 18566.

(69) Deprez, N. R.; Sanford, M. S. *J. Am. Chem. Soc.* **2009**, *131*, 11234.

(70) Hari, D. P.; König, B. *Angew. Chem. Int. Ed.* **2013**, *52*, 4734.

(71) Ye, Y.; Sanford, M. S. *J. Am. Chem. Soc.* **2012**, *134*, 9034.

(72) Sahoo, B.; Hopkinson, M. N.; Glorius, F. *J. Am. Chem. Soc.* **2013**, *135*, 5505.

(73) Shu, X.; Zhang, M.; He, Y.; Frei, H.; Toste, F. D. *J. Am. Chem. Soc.* **2014**, *136*, 5844.

(74) Ravelli, D.; Protti, S.; Fagnoni, M. *Chem. Rev.* **2016**, *116*, 9850.

(75) Skubi, K. L.; Blum, T. R.; Yoon, T. P. *Chem. Rev.* **2016**, *116*, 10035.

(76) Lowry, M. S.; Goldsmith, J. I.; Slinker, J. D.; Rohl, R.; Pascal, R. A.; Malliaras, G. G.; Bernhard, S. *Chem. Mater.* **2005**, *17*, 5712.

# PART II

# Chapter 2. Proof of Concept: Photoredox/Ni Dual Catalysis for the Cross-Coupling of Benzylic Trifluoroborates with Aryl Halides

## 2.1 Introduction

As highlighted in Chapter 1, the use of alkyl nucleophiles has been an ongoing challenge for cross-coupling chemistry.[i] However, it was speculated that radical intermediates could potentially be funneled into a base metal cross-coupling cycle to overcome a number of the key issues associated with traditional catalysis. To test this hypothesis experimentally, benzylic trifluoroborates were selected as an optimal radical nucleophile for three main reasons. First, the generation of these radicals under photoredox conditions was well-established.[1] Second, their superb stability under the reaction conditions would avoid potential H-atom abstraction[2] byproducts and other radical chain processes.[3] And, finally, their use as coupling partners removed β-hydride elimination as a possible challenge in reaction development.

With the radical nucleophile selected, screening of a broad array of potential photocatalysts, electrophiles, and transition metal complexes to achieve the desired coupling was initiated (**Figure 2.1**). This broad examination quickly narrowed focus to nickel-based systems given the formation of dehalogenation products (an indicator of oxidative addition) in the presence

[i] Reproduced in part from *Science*, **2014**, *354*, 433

of a variety of photocatalysts and electrophiles. By contrast, the use of a variety of alternative cross-coupling metals (Pd, Cu, and Fe) typically returned starting materials under the reaction conditions.

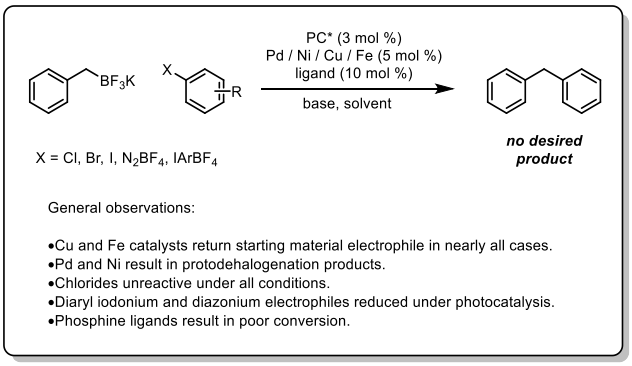


**Figure 2.1.** Screening of electrophile, metal, and photocatalyst scope

Based on these initial screens and a careful examination of the literature, we were able to key in on the combination of heteroleptic iridium catalyst **1** and Ni(bpy)$X_2$ complexes as having ideally matched properties for productive coupling (**Figure 2.2**). For the nickel catalyst, bipyridyl ligated nickel systems had been shown to be productive scaffolds for radical-mediated reductive couplings.[4] Additionally, the redox potentials of these nickel catalysts had been previously reported in the literature, giving us confidence that single electron reduction of the most likely Ni states ($Ni^{I}$ or $Ni^{II}$) would indeed be possible with our selected photocatalyst. For the photocatalyst, **1** had been successfully used in alkyltrifluoroborate oxidation to carbon-centered radicals, engaging those radicals in trapping with α,β-unsaturated carbonyl compounds and long-lived radicals such as TEMPO.[1] Furthermore, the Ir catalysts return reduction potential was cathodic enough to achieve reduction of any of the possible nickel intermediates of interest. For reference, the photochemical half-cell potential that results from reduction of Ni(bpy)X to $Ni^{0}$ in the presence of $Ir^{II}$ to the ground state $Ir^{III}$ is exothermic by greater than 0.27 V.

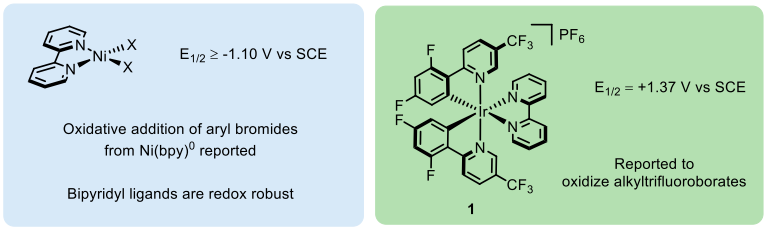


**Figure 2.2.** Catalyst combination for photoredox cross-coupling

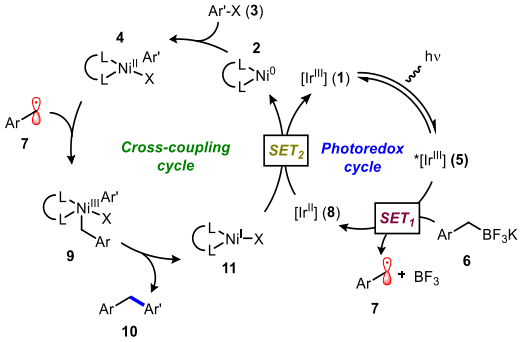


**Figure 2.3.** Proposed catalytic cycle for photoredox coupling of benzylic trifluoroborates

Based on the high reactivity of nickel, it was anticipated that the combination of a monomeric Ni(0) catalyst **2** and an aryl halide **3** would result in rapid oxidative addition, generating Ni(II) species **4**. Concomitantly, visible light irradiation of Ir[dFCF$_3$ppy]$_2$(bpy)PF$_6$ **1** would generate excited state complex **5**, the reduction potential of which is sufficiently high ($E_{red}$ = +1.21 V vs SCE)[5] to induce single-electron oxidation of an activated alkyltrifluoroborate **6** ($E_{ox}$ = -1.10 V vs SCE),[1] affording the desired alkyl radical **7** upon fragmentation. Subsequent capture of the alkyl radical at Ni(II) would then yield high-valent Ni(III) intermediate **9**, which was expected to undergo reductive elimination to generate the desired cross-coupled product **10** and Ni(I) complex **11**. From here, reduction of **11** ($E_{1/2}$ > -1.10 V vs SCE)[6] by the reduced form of the photocatalyst **8** ($E_{1/2}$ = +1.37 V vs SCE)[5] would regenerate both the Ni(0) catalyst **2** and the Ir catalyst **1**, closing the dual catalytic cycle (**Figure 2.3**).

Applying this dual catalytic, single-electron transmetalation approach to the cross-coupling of benzylic trifluoroborates and aryl bromides (Figure 2.4), efforts were quickly gratified, as a catalytic system consisting of photocatalyst **4**, $Ni(COD)_2$ (COD = 1,5-cyclooctadiene), and 2,2'-bipyridine (bpy) as a ligand in acetone effected the cross-coupling of potassium benzyltrifluoroborate and bromobenzonitrile in 54% yield upon exposure to visible light from a 26W compact fluorescent light bulb (CFL) at room temperature for 24 hours. Further optimization of these reaction conditions significantly improved both yield and conversion. Use of more electron-rich ligand systems such as 4,4'-di-*tert*-butyl-2,2'bipyridine (dtbbpy) improved overall conversions, presumably by accelerating oxidative addition. The use of MeOH as a cosolvent and lutidine as additive also significantly accelerated the reactions. In this cases, it is surmised that the alcohol serves to esterify the boron trifluoride generated under the reaction conditions, and lutidine then sequesters the generated hydrogen fluoride. Most importantly, control reactions performed in the absence of photocatalyst, Ni catalyst, or light resulted in no detectable product formation, confirming the essential role of each of these components in the dual catalytic process.

## 2.2 Results and Discussion

With reaction concept and optimized conditions established, a full analysis of reaction scope was initiated on both the benzylic trifluoroborate and aryl halide **(Figure 2.4)**. Expectedly, electronic modification of the trifluoroborate component had a moderate effect on reaction yield, with more electron rich, and thus more highly stabilized, radical precursors (**12** and **18**) performing better than those substituted with electron withdrawing groups (**15** and **17**). Substrates possessing an ortho-substituent were well tolerated, evidenced by isolation of product **13** in 82% yield. The

reaction also exhibited increased efficiency on scale, as diarylmethane **12** was isolated in 97% yield on gram scale with reduced catalyst loading [1 mol % **4** and 1.5 mol % of $Ni(COD)_2$ and ligand].

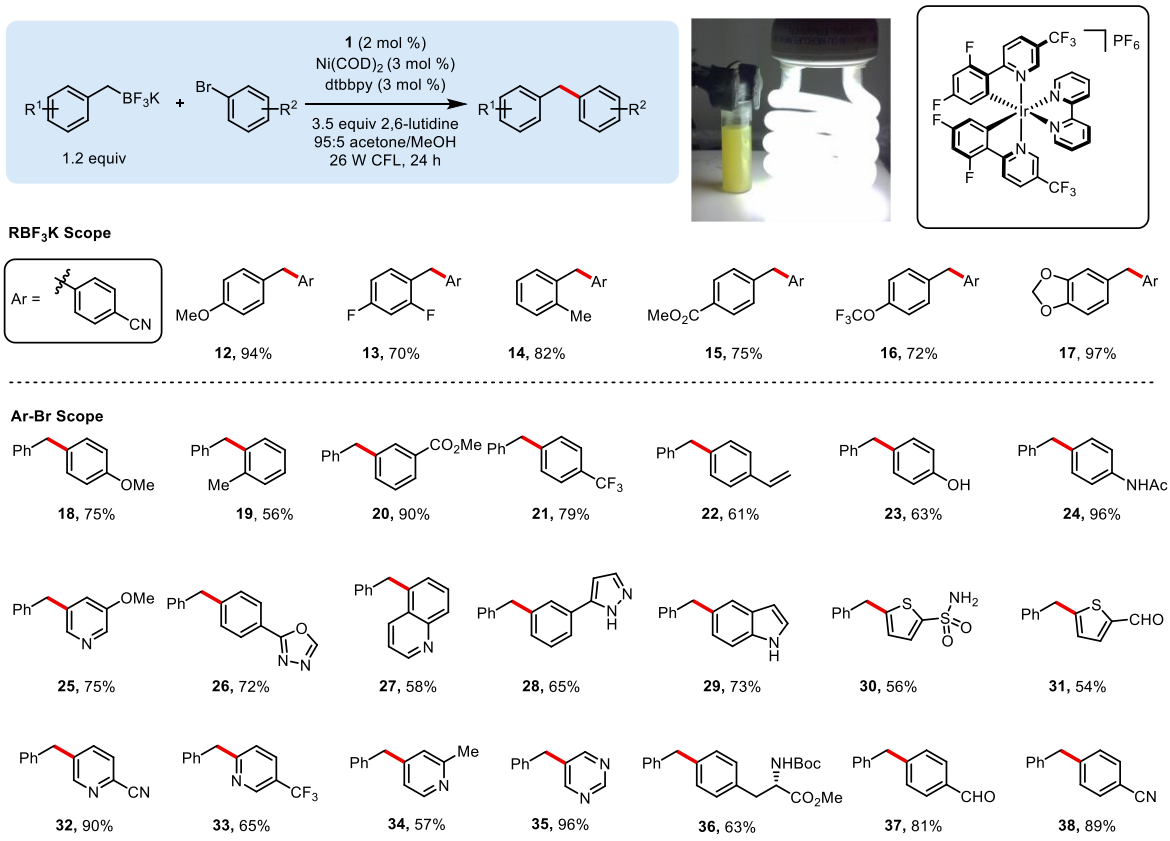


All yields are percent isolated yield of pure material after chromatography. Reactions were performed on 0.5 mmol aryl halide. Boc = *tert*-butoxycarbonyl, Me = methyl, Ph = phenyl, Ac = acetyl.

**Figure 2.4**. Photoredox cross-coupling of benzylic trifluoroborates and aryl bromides.

High levels of versatility and functional group tolerance were observed with regard to the aryl halide partner. Substrates bearing electrophilic functional groups that would be incompatible with more highly reactive organometallic nucleophiles were well tolerated. Protic functional groups, including amide **24**, sulfonamide **30**, phenol **23**, pyrazole **28**, and NHBoc **36**, could also be

employed. Substrates possessing substituents ortho to the halide (**19**, **27**) were tolerated, albeit in diminished yield.

A variety of nitrogen-containing heteroaryl bromides, classically challenging yet highly valued substrates as a result of their prevalence in biologically active compounds,[7] performed well under the optimized reaction conditions. Pyridine substrates were coupled in all possible regioisomeric configurations (**25**, **32**, **33**, **34**). Other important *N*-heterocycles, including pyrimidine **35**, indole **29**, and quinoline **27** proved to be competent partners. Although five-membered heterocyclic bromides generally exhibited poor reactivity, electron deficient thienyl bromides were coupled in moderate yields, leading to **30** and **31**.

Several practical and more sustainable features derive from this approach to cross-coupling. Previous approaches to the cross-coupling of benzylboron compounds with aryl halides have required excess (3 equiv) aqueous base and temperatures no lower than 60 °C.[8–10] Furthermore, the present reaction makes use of air stable and inexpensive bipyridine ligands with low loading of the Ni catalyst. A derivative of photocatalyst **1** has recently been made commercially available and is similarly effective in promoting the desired reactivity.

The reported cross-coupling reactions generally exhibited levels of efficiency and functional group tolerance equal to or surpassing those of traditional cross-coupling reactions on similar substrates. Most reactions cleanly afforded the desired product, with the remaining mass balance consisting of only unreacted aryl halide. Competing homocoupling of the trifluoroborate to afford bibenzyl derivatives was undetectable by crude HPLC analysis, allowing use of only a slight excess (1.2 equiv) of this reaction partner, which is typical in traditional Suzuki-Miyaura cross-couplings. Also of note is the compatibility of this reaction manifold with functional groups susceptible to single-electron oxidation or potentially reactive toward the radical intermediates, including phenol, anilide, and thienyl substructures, as well as 5-membered nitrogen heterocycles.

Remarkably, even 4-bromostyrene could be employed as an electrophile without competitive radical capture or polymerization, affording diarylmethane **22** in 61% yield.

As a demonstration of the broader potential of the application of single-electron transmetalation in this dual catalytic cross-coupling, the conditions optimized for use with primary benzylic trifluoroborates were directly applied to the cross-coupling of a secondary (α-alkoxy)alkyltrifluoroborate (**Eq. 2.2**). Comparable single-electron oxidation potentials serve as the singular commonality between these structurally dissimilar reagents. Thus, C-C bond formation via single-electron transmetalation proceeded smoothly under these extremely mild and unoptimized conditions. The differential reactivity between the two-electron and single-electron transmetalation processes is underscored by the stark differences in conditions previously reported for (α-alkoxy)alkyltrifluoroborate cross-coupling (5 equiv CsOH, 105 °C, 24 h) compared to those described herein.[11] The observed reactivity also serves to demonstrate tolerance of substrates possessing β-hydrogens, a characteristic that is requisite of any general method for the cross-coupling of alkyl substructures.

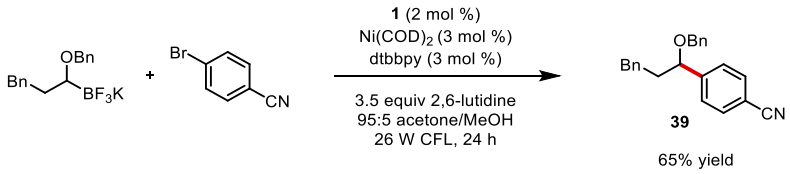


**Eq. 2.2.** Photoredox cross-coupling of a secondary (α-alkoxy)alkyltrifluoroborate

To highlight further the differences between this activation mode and that of traditional cross-coupling, a competition experiment was performed between potassium benzyltrifluoroborate and potassium phenyltrifluoroborate. Exposure of these two nucleophiles to the photoredox cross-coupling conditions resulted in isolation of diarylmethane product **38** in 91% isolated yield, with no observable biaryl formation (**Eq. 2.3**). The ability to engage a $C_{sp3}$-hybridized organometallic

reagent selectively in a transition metal-catalyzed C-C bond-forming reaction in the presence of an equivalent $C_{sp2}$-hybridized organometallic represents a dramatic reversal of the reactivity hierarchy of all previously reported cross-coupling reactions. This effectively demonstrates the complementary reactivity patterns observed between the single-electron and two-electron transmetalation modes.

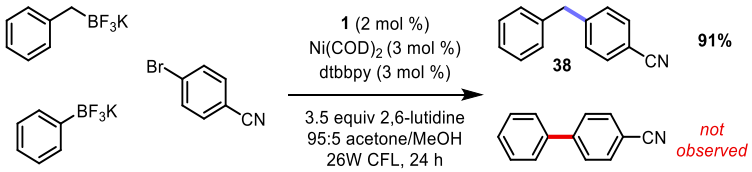


**Eq. 2.3:** Competition experiment between potassium benzyltrifluoroborate and potassium phenyltrifluoroborate under photoredox cross-coupling conditions.

Another important implication of the single-electron transmetalation manifold is related to the stereochemical outcome of the alkyl transfer. Nearly all cross-coupling reactions of stereo-defined nucleophiles reported heretofore have demonstrated the transmetalation event to be stereospecific.[12] Thus, enantioenriched products may only be accessed from nonracemic and configurationally stable organometallic reagents, which are often difficult to access. Isolated examples of stereoconvergence in transmetalation exist, specifically in the context of secondary benzylmagnesium reagents, a pyrrolidine-based organozinc, and a diastereoconvergent cross-coupling of substituted cyclohexylzinc reagents.[13–15] Stereoconvergence in the former is thought to be enabled by dynamic kinetic resolution of the configurationally unstable Grignard reagent, while the origin of selectivity in the latter is not fully understood. None of these approaches constitute a general strategy for stereoconvergent transmetalation beyond the scope of the directly explored reagents.

In contrast, the stereochemical outcome of the single-electron transmetalation is dictated by facial selectivity of the addition of a prochiral alkyl radical to a ligated Ni center. Thus,

application of a chiral ligand framework renders this process asymmetric and provides a general reaction manifold in which stereoconvergent transmetalation can be achieved. Well-known stereoconvergent cross-couplings of alkyl halides, which putatively employ a similar mechanistic step, provide guidance for selection of appropriate ligand scaffolds to maximize the stereoselectivity of the radical capture.[16]

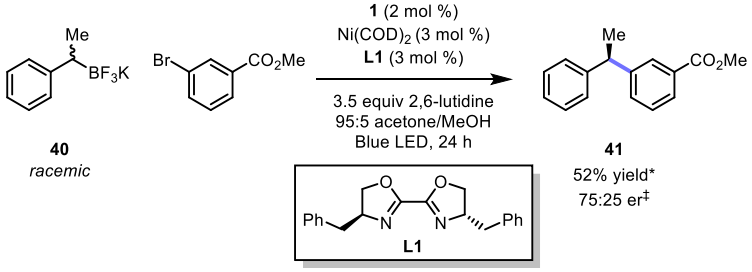


Reactions performed on 0.5 mmol aryl bromide. * Determined by chiral supercritical fluid chromatography (SFC). ‡ Absolute configuration was assigned as (S) based on data reported in the literature. er = enantiomeric ratio.

**Eq. 2.4.** Stereoconvergent cross-coupling of a racemic trifluoroborate **39** and aryl bromide to afford an enantioenriched product

Indeed, employing commercially available ligand **L1** under slightly modified conditions, racemic trifluoroborate **40** was engaged in stereoconvergent cross-coupling with methyl 3-bromobenzoate, affording 1,1-diarylethane product **41** in 52% yield and a promising 75:25 er (**Eq. 2.4**). The observed stereoconvergence serves as an effective mechanistic probe, supporting the role of the organotrifluoroborate as a carbon radical precursor, providing evidence that the radical is intercepted by the ligated Ni complex, and suggesting that C-C bond formation occurs via reductive elimination from Ni. This preliminary result strongly implies that high levels of stereoselectivity are possible in the photoredox cross-coupling of secondary alkyl nucleophiles with appropriate modification of reaction conditions and ligand structure. Refinement of this approach to asymmetric cross-coupling will provide a powerful advancement to the field by alleviating the need for synthesis of enantioenriched organometallic reagents. Taken together, these findings effectively

validate the single-electron transmetalation manifold and dual photoredox/cross-coupling cycle as a viable alternative to conventional cross-coupling of $C_{sp3}$-hybridized nucleophiles.

## 2.3 Conclusions

In summary, the first successful integration of photoredox catalysis with Ni cross-coupling catalysis has been realized. The developed protocol allows the facile synthesis of diarylmethanes from commercially available aryl halides and benzylic trifluoroborates. The functional group tolerance of this coupling is unmatched by any previously reported protocol - allowing the coupling of sensitive electrophilic sites, protic functional handles, and a wide array of heterocyclic halides.

Beyond the advancements in reaction scope, the use of benzylic and secondary alkoxy radicals in this single-electron transmetalation manifold indicate that this concept is a general strategy for overcoming the classical challenges of secondary alkyl cross-coupling with alkyl nucleophiles. Continued development of this concept should yield protocols extending to unactivated secondary and hopefully tertiary alkyl systems

## 2.4 Experimental

All reactions were carried out under an inert atmosphere of nitrogen or argon unless otherwise noted. Acetone (99.9%, extra dry), MeOH (99.8% extra dry), and DMF (99.8%, anhydrous) were used as received. 2,6-Lutidine (>99%, purified by redistillation) was used without further purification (high purity lutidine was found to be important for reproducibly obtaining high yields. Commercially redistilled lutidine or lutidine distilled from $AlCl_3$ and stored under $N_2$ gave similar results). CuI, $IrCl_3 \cdot xH_2O$, and $Ni(COD)_2$ were from commercial sources. Potassium

benzyltrifluoroborate was purchased or prepared using a published procedure.[10] Potassium (1-(benzyloxy)-3-phenylpropyl)trifluoroborate and potassium trifluoro(1-phenylethyl)borate were prepared according to published procedures.[11,17] All other reagents were purchased commercially and used as received. Photoredox reactions were irradiated with a standard 26W compact fluorescent light bulb. Stereoconvergent cross-couplings were irradiated with blue LED light strips (~425 nm). Melting points (°C) are uncorrected. NMR spectra were recorded on a 500 or 400 MHz spectrometer. $^{19}$F NMR chemical shifts were referenced to external $CFCl_3$ (0.0 ppm). $^{11}$B NMR spectra were obtained on a spectrometer equipped with the appropriate decoupling accessories. All $^{11}$B NMR chemical shifts were referenced to an external $BF_3{\cdot}OEt_2$ (0.0 ppm) with a negative sign indicating an upfield shift. Data are presented as follows: chemical shift (ppm), multiplicity (s = singlet, d = doublet, t = triplet, dd = doublet of doublets, m = multiplet, br = broad), coupling constant *J* (Hz) and integration. The $^{13}$C signal of the carbon bonded to boron was not observed in some cases due to quadrupolar relaxation.

**General procedure A for synthesis of benzylic trifluoroborates**

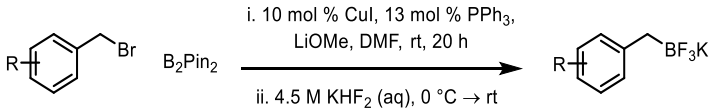


According to an unoptimized procedure derived from that reported by Liu and coworkers,[18] to a flame-dried 20 mL vial was added benzylic bromide (5 mmol) and $PPh_3$ (173 mg, 0.66 mmol). The vial was taken into a glovebox, and CuI (95 mg, 0.5 mmol), LiOMe (380 mg, 10 mmol, 2 equiv), and bis(pinacolato)diboron (1.93 g, 7.6 mmol, 1.52 equiv) were added. The vial was sealed with a Teflon-lined silicone septum, DMF was added, and the mixture was stirred vigorously under an inert atmosphere at rt for 20 h. The resultant brown, viscous mixture was filtered through a pad of silica gel, washing with EtOAc (60–100 mL). The filtrate was diluted with MeOH (HPLC grade,

~50 mL) and cooled to 0 °C. Then sat. aq. $KHF_2$ (9 mL, 40.5 mmol, 8.1 equiv) was added dropwise over 15 to 30 min, and the soln was allowed to warm to rt. The resultant suspension was concentrated under reduced pressure. Pinacol and $H_2O$ were azeotropically removed by suspension in toluene (100–150 mL) followed by rotary evaporation. The remaining solid was dried under high vacuum and then suspended in hot acetone (3 x 100 mL) and filtered. The filtrate was concentrated to a minimal volume (5–20 mL) and hexane (~200 mL) was added to yield a white precipitate. The precipitate was isolated by filtration, washing with hexane (~30 mL), and $CH_2Cl_2$ (~30 mL) to afford the desired benzylic trifluoroborate.

**General procedure B for synthesis of benzylic trifluoroborates**

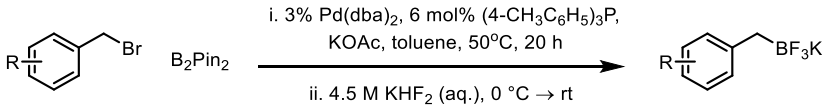


According to an unoptimized procedure derived from that reported by Miyaura and coworkers,[19] to a flame dried 100 mL round bottom flask equipped with a stir bar was added benzylic bromide (5 mmol), KOAc (736 mg, 7.5 mmol), and $(4\text{-}MeC_6H_4)_3P$ (91 mg, 0.30 mmol). The flask was taken into the glovebox, and $Pd(dba)_2$ (86 mg, 0.15 mmol) and bis(pinacolato)diboron (1.40 g, 5.5 mmol) were added. The flask was sealed with a rubber septum, toluene was added (30 mL), and the mixture was stirred vigorously under inert atmosphere for 20 h. The resultant yellow-brown mixture was concentrated to near dryness and then diluted with MeOH (HPLC grade, 20 mL), cooled to 0 °C, and sat. $KHF_2$ (9 mL, 40.5 mmol, 8.1 equiv) was added dropwise by an addition funnel under inert atmosphere for 30 min. The resulting suspension was concentrated under reduced pressure. Pinacol and $H_2O$ were azeotropically removed by suspension in toluene (100-150 mL) followed by rotary evaporation. The remaining solid was dried under high vacuum and then suspended in hot acetone (3 x 100 mL) and filtered. The filtrate was concentrated to a minimal volume (5 – 20 mL) and hexane (~200 mL) was added to yield a white precipitate. The precipitate was isolated by filtration,

washing with hexanes (~30 mL) and $CH_2Cl_2$ (~30 mL), to afford the desired benzylic trifluoroborate.

**Synthesis of photocatalyst 1**

The synthesis of photocatalyst **1** has been documented in literature reports, though never compiled in one location. In an effort to aid the practicing chemist, the procedures found to be most effective in our hands are compiled below. Alternatively, the 4,4'-di-*tert*-butyl bipyridine derivative of **1** is commercially available.

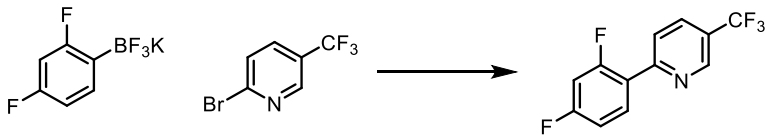


**S1** **S2** **S3**

To a large vial equipped with a magnetic stir bar was added **S1** (3.3 g, 15 mmol), **S2** (2.26 g, 10 mmol), anhyd $K_2CO_3$ (6.9 g, 50 mmol), and $Pd(PPh_3)_4$ (1.16 g, 1 mmol). The vial was sealed tightly with a Teflon-coated septum cap and evacuated and purged with $N_2$ three times. The contents were dissolved in THF (32 mL) and degassed $H_2O$ (16 mL), then stirred at 80 °C for 24 h. After cooling to rt, the reaction mixture was diluted with $H_2O$ and extracted with $CH_2Cl_2$ (3 x 60 mL). The combined organic layers were dried ($MgSO_4$), filtered, concentrated under reduced pressure, and purified by silica gel column chromatography, eluting with 5% EtOAc in hexanes to afford ligand **S3** as white solid (2.54 g, 98%). mp = 55-58 °C. A small amount of $PPh_3$ was usually observed after column chromatography (<5 mol %) which did not interfere with subsequent reactions. $^1$H NMR (500 MHz, $CDCl_3$): δ = 8.96 (s, 1H), 8.12-8.07 (m, 1H), 7.98 (dd, *J* = 8.5, 2.0 Hz, 1H), 7.90 (d, *J* = 8.5 Hz, 1H), 7.06-7.02 (m, 1H), 6.97-6.92 (m, 1H). $^{13}$C NMR (125.8 MHz, $CDCl_3$): δ = 163.8 (dd, *J* = 253.1, 12.5 Hz), 161.1 (dd, *J* = 253.5, 12.0 Hz), 155.8, 133.8 (d, *J* = 3.1 Hz), 132.6 (dd, *J* = 9.7, 4.0 Hz), 128.6 (d, *J* = 6.9 Hz), 125.2 (q, *J* = 33.1 Hz), 123.70 (q, *J* = 272.2 Hz), 123.68 (d, *J* = 10.9 Hz), 122.5 (dd, *J* = 11.2, 3.8 Hz), 112.3 (dd, *J* = 21.1, 3.5 Hz), 104.7 (dd, *J* = 26.0, 26.0

Hz). $^{19}$F NMR ($CDCl_3$, 470.8 MHz): δ = -62.3, -107.1 (d, *J* = 8.5 Hz), 112.0 (d, *J* = 8.5 Hz). IR: ν = 2925, 2337, 1601, 1321, 1119, 1058 $cm^{-1}$. HRMS: (ESI) m/z calc. for $C_{12}H_7NF_5$ (M+H) 259.0499, found 259.0421

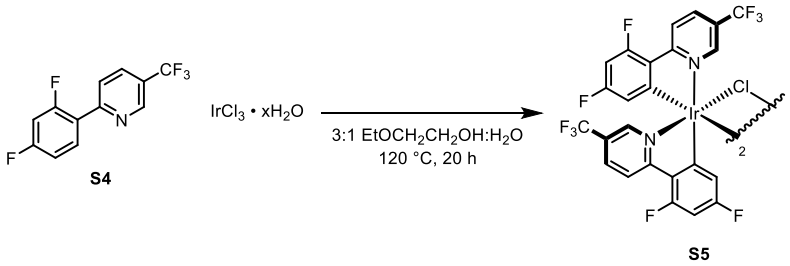


To a 20 mL round-bottom flask equipped with a magnetic stir bar was added ligand **S4** (428 mg, 1.65 mmol) and $IrCl_3$ hydrate (224 mg, 0.75 mmol). The flask was equipped with a cold water condenser and evacuated and purged with $N_2$ five times. The contents were suspended in rigorously degassed ethoxyethanol (9 mL) and $H_2O$ (3 mL) and then heated with stirring to 120 °C for 20 h, during which time a yellow precipitate was observed to form. After cooling to rt, the precipitate was collected by vacuum filtration. The filter cake was washed copiously with $H_2O$ (~75 mL) and hexanes (~30 mL) to afford iridium μ-Cl-dimer **S5** as a fine yellow powder (84%). mp = >250 °C. Characterization data for this compound matched that reported in the literature.[5]

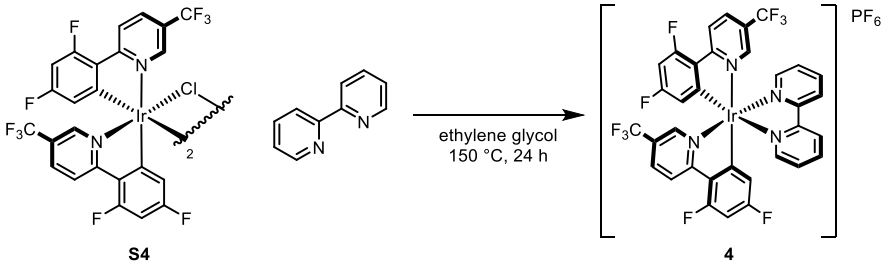


To a 15 mL round-bottom flask equipped with a magnetic stir bar was added iridium dimer **S4** (130 mg, 0.087 mmol) and 2,2'-bipyridine (32 mg, 0.21 mmol). The flask was attached to a reflux condenser and the contents were placed under an inert atmosphere by three evacuation/purge cycles. The reaction components were dissolved in degassed ethylene glycol (6 mL) and heated with stirring at 150 °C for 24 h. Upon cooling to rt, the reaction mixture was diluted with an equal

volume of deionized $H_2O$ and transferred to a separatory funnel. The aqueous phase was washed three times with hexanes (10 mL), then drained into an Erlenmeyer flask and heated to ~85 °C for 5-15 min. to remove residual hexanes. Upon cooling to rt, an aq soln of $NH_4PF_6$ (10 mL, 0.1 g/mL) was added, resulting in the formation of a fine yellow precipitate that was isolated by vacuum filtration, washing with $H_2O$ (20 mL) and hexanes (15 mL). The solid was dried under high vacuum to remove residual $H_2O$ and then dissolved in acetone and recrystallized by vapor diffusion with pentane to yield **1** as large yellow crystals (172 mg, 88%). mp = 199-202 °C. Characterization data for this compound matched that reported in the literature.[20]

**Selected reaction optimization studies**

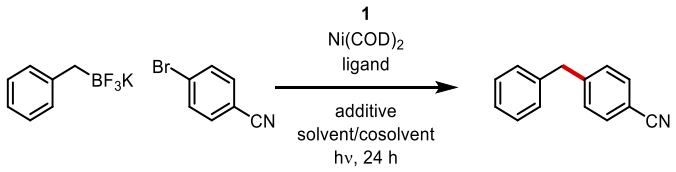


*Procedure for reaction screening at 0.01 or 0.05 mmol scale:* To a reaction vial equipped with a Teflon coated magnetic stir bar in a glovebox was added a soln of $Ni(COD)_2$ and ligand [1:1 $Ni(COD)_2$:ligand] dissolved in THF (0.1 M). The solvent was removed *in vacuo* under an inert atmosphere, then a soln of potassium benzyltrifluoroborate (1 equiv), 4-bromobenzonitrile (1 equiv), and 4,4'-di-*tert*-butylbiphenyl (0.1 equiv) in 1 mL of solvent (0.1 M) was added, followed by a soln of photocatalyst **1**. If desired, an alcoholic cosolvent or amine base was added before the vial was sealed and stirred over blue LED lights. After 24 h the reactions were opened to air, diluted with acetonitrile, and analyzed by reversed phase analytical HPLC using product:internal standard (4,4'-di-*tert*-butylbiphenyl) ratios as a qualitative assessment of reaction yield.

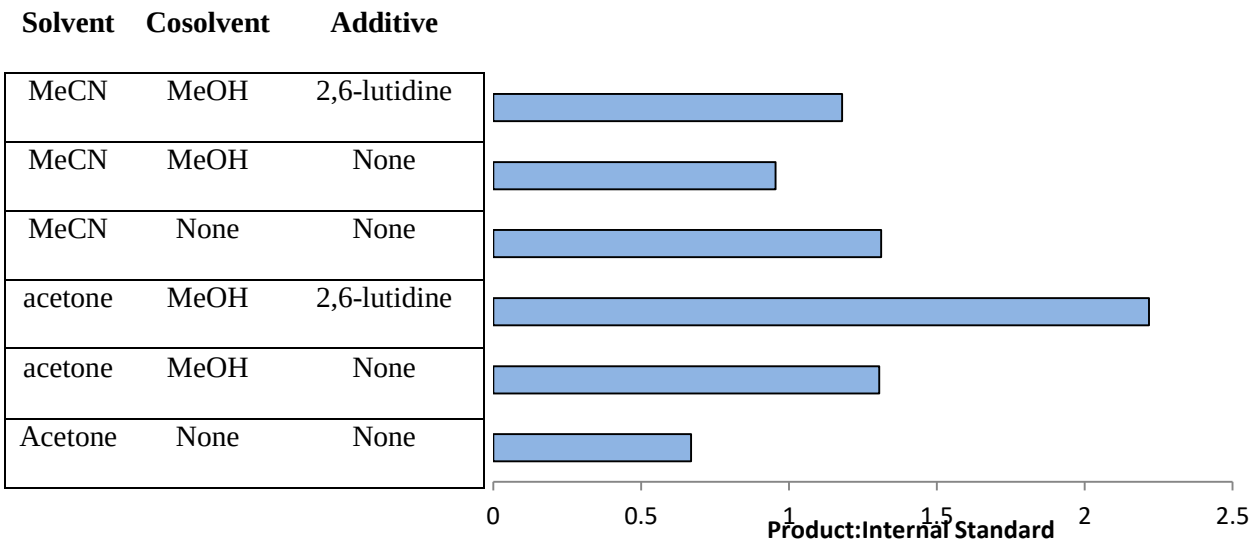


**Figure 2.5.** Conditions: 2 mol % **1**, 10 mol % $Ni(COD)_2$, 10 mol % 2,2'-bipyridine, 0.1 M, 24 h, 0.01 mmol

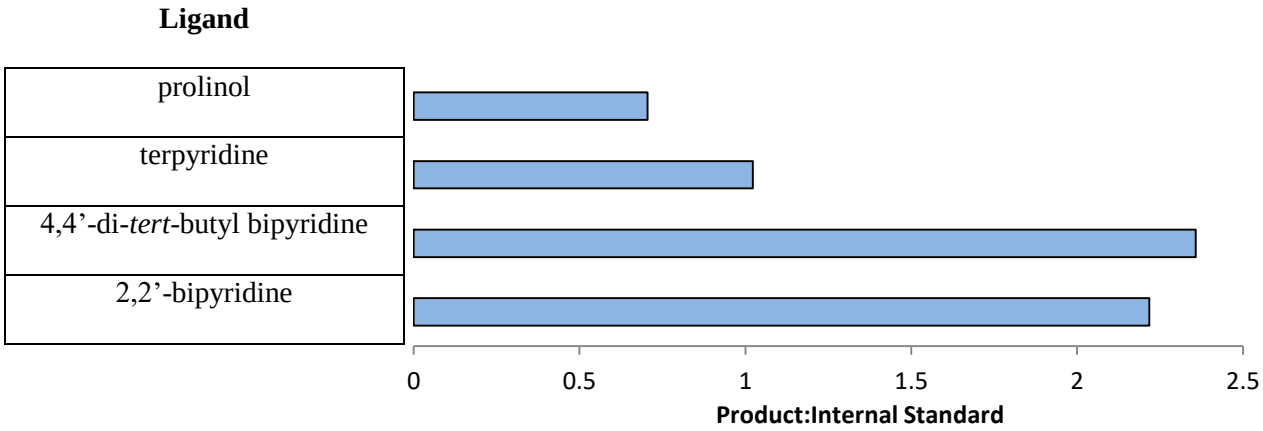


**Figure 2.6.** Conditions: 2 mol % **1**, 10 mol % $Ni(COD)_2$, 10 mol % ligand, 10:1 acetone/MeOH, 2 equiv 2,6-lutidine, 0.1 M, 24 h, 0.01 mmol

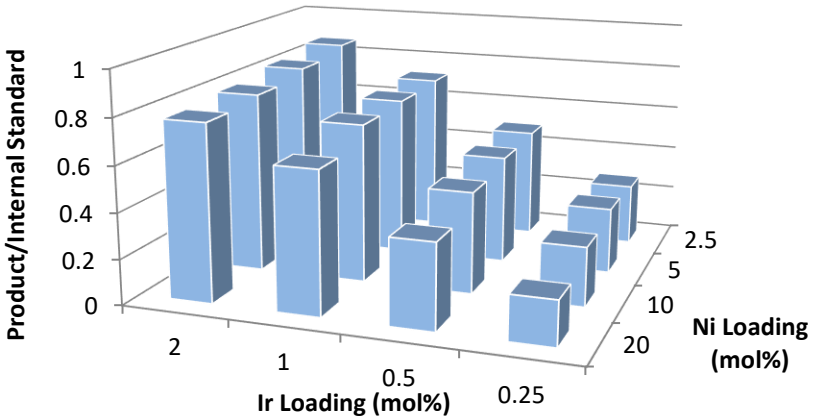


**Figure 2.7.** Conditions: 1:1 $Ni(COD)_2$/dtbbpy, 10:1 acetone/MeOH, 2 equiv 2,6-lutidine, 0.1 M, 24 h, 0.05 mmol

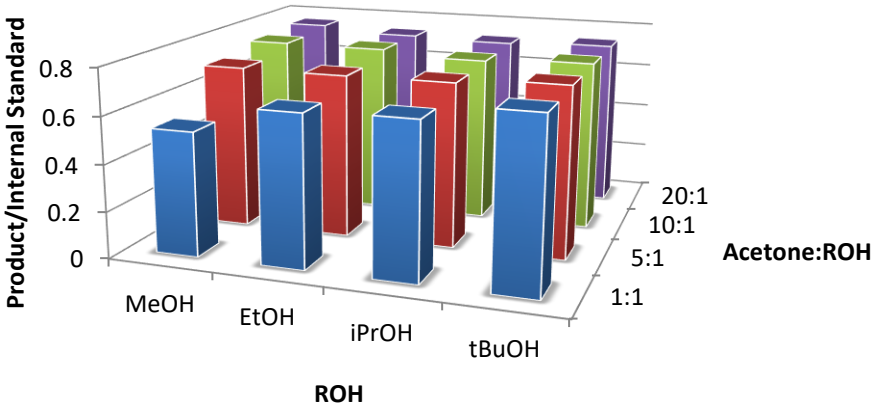


**Figure 2.8.** Conditions: 1 mol % **1**, 5 mol % $Ni(COD)_2$, 5 mol % dtbbpy, 10:1 acetone/alcohol, 2 equiv 2,6-lutidine, 0.1 M, 24 h, 0.05 mmol

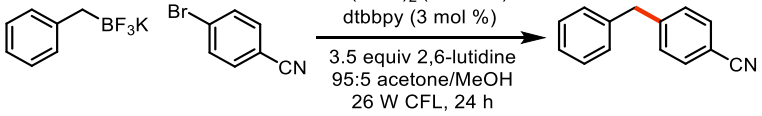


| *Variation from Standard Condition* | *Yield* [a] |
|---|---|
| None | 80 |
| Photocatalyst omitted | 0 |
| $Ni(COD)_2$/dtbbpy omitted | 0 |
| No light | 0 |
| Ligand omitted | 45 |
| Lutidine omitted | 43 |
| MeOH omitted | 75 |

Reactions performed on 0.05 mmol scale; [a] Yield determined by calibrated HPLC analysis

**Figure 2.9**. Conditions: 2 mol % **1**, 3 mol % $Ni(COD)_2$, 3 mol % dtbbpy, 95:5 acetone/methanol, 3.5 equiv 2,6-lutidine, 0.1 M, 24 h, 0.05 mmol

**General procedure for photoredox cross-coupling reactions**

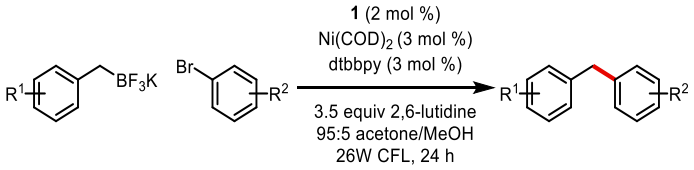


To a two dram (8 mL) borosilicate glass vial equipped with a Teflon-coated magnetic stir bar was added aryl bromide (0.5 mmol, 1 equiv) (liquid aryl bromides were added with solvent), benzylic trifluoroborate (0.6 mmol, 1.2 equiv), $Ir[dFCF_3ppy]_2(bpy)PF_6$ **1** (10 mg, 0.01 mmol), and 4,4'-di-*tert*-butyl-2,2'-bipyridine (4.0 mg, 0.015 mmol). The vial was taken into a glovebox and $Ni(COD)_2$ (4.1 mg, 0.015 mmol) was added. The vial was sealed with a plastic screw cap containing a Teflon-lined silicone septum, removed from the glovebox, and evacuated and purged with inert gas three times. Under inert atmosphere was introduced successively acetone (4.75 mL), methanol (0.25 mL), and 2,6-lutidine (202 μL, 1.75 mmol, 3.5 equiv). The vial was sealed with Teflon ribbon, electrical tape, and parafilm and stirred for 24 hours approximately 3 cm from a 26 W fluorescent light bulb. The crude reaction mixture was filtered through an approximately 2 cm x 2 cm cylindrical plug of Celite, washing with EtOAc (30–50 mL). The residue was purified by column chromatography on silica gel, eluting with EtOAc and hexanes, to obtain products in pure form.

**Figure 2.10:** Photoredox cross-coupling reaction set-up (0.5 mmol scale)

**Gram scale reaction:** To a ~75 mL Schlenk flask equipped with a Teflon-coated magnetic stir bar was added 4-bromobenzonitrile (1.000 g, 5.49 mmol, 1 equiv), benzyl trifluoroborate (1.306 g, 6.59 mmol, 1.2 equiv), $Ir[dFCF_3ppy]_2(bpy)PF_6$ **1** (55.0 mg, 0.055 mmol, 0.01 equiv), and 4,4'-di-*tert*-butyl-2,2'-bipyridine (22.0 mg, 0.082 mmol, 0.015 equiv). The flask was taken into the glovebox, and $Ni(COD)_2$ (22.5 mg, 0.082 mmol, 0.015 equiv) was added. The flask was sealed, and under an inert atmosphere, acetone (47.5 mL), MeOH (2.5 mL), and 2,6-lutidine (2.24 mL, 19.2 mmol, 3.5 equiv) were added successively. The reaction was stirred ~5 cm from two 26 watt compact fluorescent light bulbs for 24 h. After filtration though Celite, the residue was purified by column chromatography on silica gel, eluting with EtOAc and hexanes, to obtain the product in pure form.

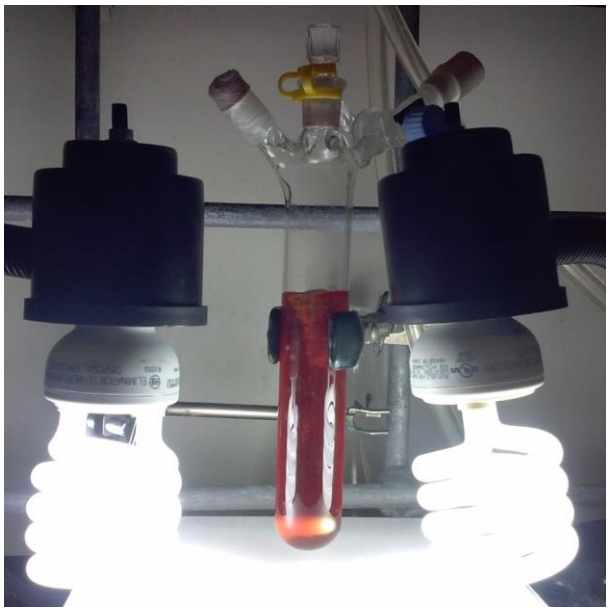

**Figure 2.11:** Gram scale photoredox cross-coupling reaction set-up (5.5 mmol)

**Benzyl-aryl competition experimental details**

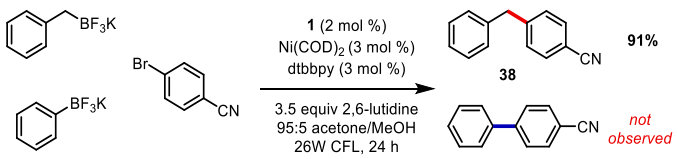

The reaction was performed according to the general procedure for photoredox cross-coupling at 0.5 mmol scale using 1.2 equiv $BnBF_3K$ and 1.2 equiv $PhBF_3K$. The crude reaction was analyzed by reversed phase analytical HPLC. A product standard for biaryl was synthesized according to a literature procedure.[21] After workup and purification according to the general procedure, diarylmethane product **38** was isolated in 91% yield (88 mg).

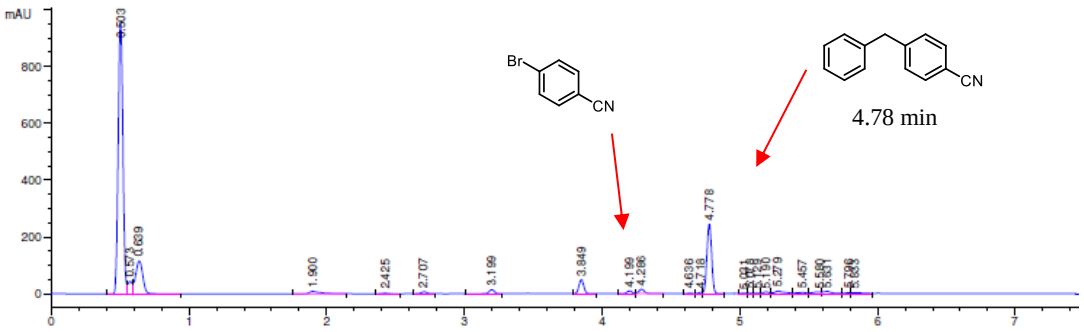


**Figure 2.12:** Crude HPLC chromatogram for benzyl-aryl competition experiment under photoredox cross-coupling conditions.

A traditional Suzuki-Miyaura cross-coupling was performed for comparison of the product distribution in the photoredox cross-coupling to that of a cross-coupling employing a traditional transmetalation. The reaction was performed on 0.2 mmol scale using 1.2 equiv $BnBF_3K$, 1.2 equiv $PhBF_3K$, and 1 mol % $Pd(OAc)_2$. The crude reaction mixture was analyzed by reversed phase analytical HPLC.

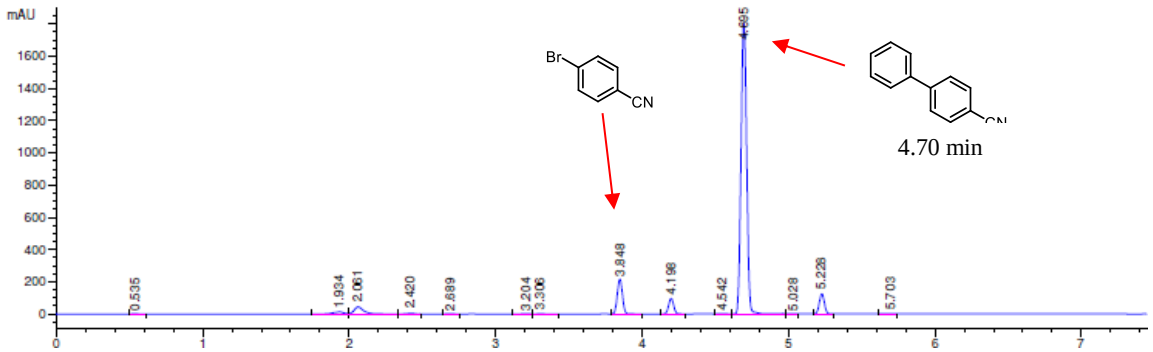


**Figure 2.13:** Crude HPLC chromatogram for benzyl-aryl competition experiment under conventional Suzuki-Miyaura cross-coupling conditions

**Procedure for stereoconvergent cross-coupling**

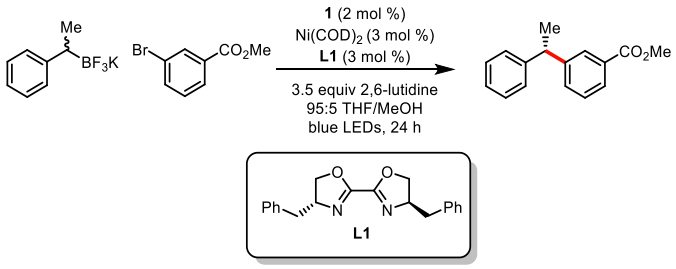


To a two dram (8 mL) borosilicate glass vial equipped with a Teflon-coated magnetic stir bar was added methyl 3-bromobenzoate (108 mg, 0.5 mmol, 1 equiv), potassium trifluoro(1-phenylethyl)borate (127 mg, 0.6 mmol, 1.2 equiv), $Ir[dFCF_3ppy]_2(bpy)PF_6$ **1** (10 mg, 0.01 mmol), and **L1** (4.8 mg, 0.015 mmol). The vial was taken into a glovebox, and $Ni(COD)_2$ (4.1 mg, 0.015 mmol) was added. The vial was sealed with a plastic screw cap containing a Teflon-lined silicone septum, removed from the glovebox, and evacuated and purged with inert gas three times. Under inert an atmosphere, THF (4.75 mL), MeOH (0.25 mL), and 2,6-lutidine (202 μL, 1.75 mmol, 3.5 equiv) were introduced successively. The vial was sealed with Teflon ribbon, electrical tape, and Parafilm and stirred for 24 h in a crystallization dish surrounded by blue LED lights. The crude reaction mixture was filtered through an approximately 2 cm x 2 cm cylindrical plug of Celite, washing with EtOAc (30–50 mL). The residue was purified by column chromatography on silica gel, eluting with EtOAc and hexanes, to obtain product in pure form.

**Compound Characterization Data**

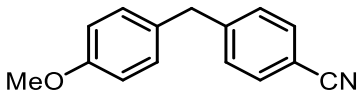


**12**

**4-(4-Methoxybenzyl)benzonitrile (12)**: obtained as a white solid (105 mg, 94%), mp = 48-50 °C. $^1$H NMR ($CDCl_3$, 500 MHz): δ = 7.56 (d, *J* = 8.0 Hz, 2H), 7.27 (d, *J* = 7.5 Hz, 2H), 7.07 (d, *J* = 8.5 Hz, 2H), 6.85 (d, *J* = 9.0 Hz, 2H), 3.97 (s, 2H), 3.79 (s, 3H). $^{13}$C NMR ($CDCl_3$, 125.8 MHz): δ =

158.5, 147.4, 132.4, 131.6, 130.1, 129.7, 119.2, 114.3, 110.0, 55.4, 41.2. Characterization data matched that reported in the literature.[22]

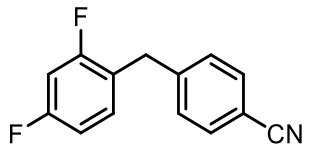


**13**

**4-(2,4-Difluorobenzyl)benzonitrile (13)**: obtained as a white crystalline solid (80 mg, 70%), Mp = 63-65 °C. $^{1}$H NMR ($CDCl_3$, 500 MHz): δ = 7.59 (d, *J* = 8.0 Hz, 2H), 7.30 (d, *J* = 8.0 Hz, 2H), 7.13-7.11 (m, 1H), 6.86-6.82 (m, 2H), 4.02 (s, 2H) $^{13}$C NMR ($CDCl_3$, 125.8 MHz): δ = 162.3 (dd, *J* = 148.6, 11.8 Hz), 160.3 (dd, *J* = 148.9, 11.8 Hz), 145.1, 132.3, 131.5 (dd, *J* = 9.7, 6.2 Hz), 129.3, 122.2 (dd, *J* = 12.5, 3.6 Hz), 118.7, 111.4 (dd, *J* = 21.1, 3.8 Hz), 110.3, 104.0 (dd, *J* = 25.5, 25.5 Hz). $^{19}$F NMR ($CDCl_3$, 470.8 MHz): δ = -111.7, -113.0. IR: ν = 2225, 1604, 1500, 1269, 1136, 968, 852 $cm^{-1.}$ HRMS: (ESI) m/z calc. for $C_{14}H_{10}NF_2$ (M+H) 230.0781, found 230.0772.

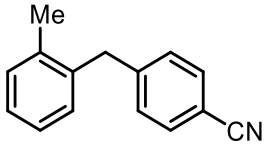


**14**

**4-(2-Methylbenzyl)benzonitrile (14)**: obtained as a white solid (85 mg, 82%), mp = 50-52 °C. $^{1}$H NMR ($CDCl_3$, 500 MHz): δ = 7.57 (d, *J* = 8.5 Hz, 2H), 7.26-7.21 (m, 5H), 7.13-7.12 (m, 1H), 4.07 (s, 2H), 2.24 (s, 3H). $^{13}$C NMR ($CDCl_3$, 125.8 MHz): δ = 146.2, 137.2, 136.5, 132.2, 130.5, 130.0 129.3, 127.0, 126.2, 118.9, 109.9, 39.5, 19.6. Characterization data matched that reported in the literature.[23]

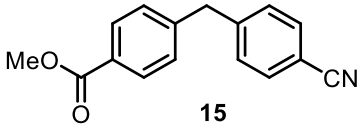


**15**

**Methyl 4-(4-Cyanobenzyl)benzoate (15)**: obtained as a colorless oil (94 mg, 75%). $^{1}$H NMR ($CDCl_3$, 500 MHz): δ = 7.97 (d, *J* = 8.0 Hz, 2H), 7.57 (d, *J* = 8.0 Hz, 2H), 7.27 (d, *J* = 8.0 Hz, 2H), 7.22 (d, *J* = 8.0 Hz, 2H), 4.08 (s, 2H), 3.89 (s, 3H). $^{13}$C NMR ($CDCl_3$, 125.8 MHz): δ = 167.0, 145.8, 144.7, 132.6, 130.2, 129.8, 129.1, 128.8, 119.0, 110.5, 52.3, 42.0. Characterization data matched that reported in the literature.[23]

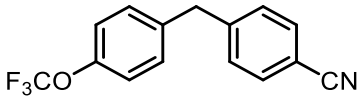


**16**

**4-(4-(Trifluoromethoxy)benzyl)benzonitrile** (**16)**: obtained as a colorless oil (106 mg, 76%). $^{1}$H NMR ($CDCl_3$, 500 MHz): δ = 7.58 (d, *J* = 8.0 Hz, 2H), 7.28 (d, *J* = 8.0 Hz, 2H), 7.19-7.15 (m, 4H), 4.04 (s, 2H). $^{13}$C NMR ($CDCl_3$, 125.8 MHz): δ = 147.9, 145.9, 138.0, 132.3, 130.1, 129.5, 121.2, 120.4 (q, *J* = 257.3 Hz), 118.7, 110.3, 41.1. $^{19}$F NMR ($CDCl_3$, 470.8 MHz): δ = -57.9. IR: ν = 2920, 2228, 1608, 1508, 1257, 1222, 1161, 1020, 921, 811 $cm^{-1.}$ HRMS (ESI) m/z calc. for $C_{15}H_{11}NOF_3$ (M+H) 178.0793, found 178.0795.

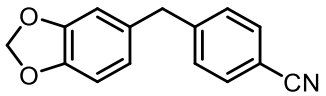


**17**

**4-(Benzo[d][1,3]dioxol-5-ylmethyl)benzonitrile** (**17)**: obtained as a white crystalline solid (115 mg, 97%) , mp = 106-108 °C. $^{1}$H NMR ($CDCl_3$, 500 MHz): δ = 7.56 (d, *J* = 8.0 Hz, 2H), 7.27 (d, *J* = 8.0 Hz, 2H), 6.75 (d, *J* = 8.0 Hz, 1H), 6.64-6.61 (m, 2H), 5.92 (s, 2H), 3.93 (s, 2H). $^{13}$C NMR ($CDCl_3$, 125.8 MHz): δ = 148.1, 147.0, 146.5, 133.2, 132.4, 129.6, 122.1, 119.1, 110.2, 109.5, 108.6, 101.2, 41.8. IR: ν = 2920, 2362, 2226, 1604, 1491, 1254, 1038, 927, 816 $cm^{-1.}$ HRMS: (ESI) m/z calc. for $C_{15}H_{12}NO_2$ (M+H) 238.0868, found 238.0860.

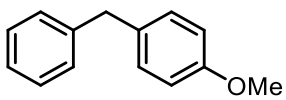


**18**

**1-Benzyl-4-methoxybenzene (18)**: obtained as a colorless oil (74 mg, 75%). $^{1}$H NMR ($CDCl_3$, 500 MHz): δ = 7.31-7.28 (m, 2H), 7.22-7.19 (m, 3H), 7.12 (d, *J* = 8.5 Hz, 2H), 6.85 (d, *J* = 8.5 Hz, 2H), 3.95 (s, 2H), 3.80 (s, 3H). $^{13}$C NMR ($CDCl_3$, 125.8 MHz): δ = 158.1, 141.7, 133.4, 130.0, 129.0. 128.5, 126.1, 114.0, 55.4, 41.2. Characterization data matched that reported in the literature.[24]

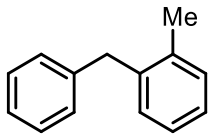


**19**

**1-Benzyl-2-methylbenzene** (**19)**: obtained as a colorless oil (51 mg, 56%). $^{1}$H NMR ($CDCl_3$, 500 MHz): δ = 7.30-7.27 (m, 2H), 7.21-7.11 (m, 7H), 4.01 (s, 2H) 2.26 (s, 3H). $^{13}$C NMR ($CDCl_3$, 125.8 MHz): δ = 140.6, 139.1, 136.8, 130.5, 130.2, 129.0, 128.6, 126.7, 126.2, 126.1, 39.7, 19.9. Characterization data matched that reported in the literature.[25]

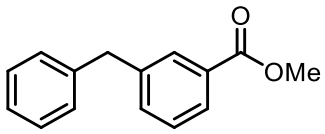


**20**

**Methyl 3-Benzylbenzoate** (**20)**: obtained as a pale yellow oil (102 mg, 90%). $^{1}$H NMR ($CDCl_3$, 500 MHz): δ = 7.93-7.89 (m, 2H), 7.40-7.35 (m, 2H), 7.32-7.30 (m, 2H), 7.24-7.20 (m, 3H), 4.04 (s, 2H), 3.91 (s, 3H). $^{13}$C NMR ($CDCl_3$, 125.8 MHz): δ = 167.3, 141.6, 140.7, 133.7, 130.5, 130.2, 129.0, 128.8, 128.7, 127.6, 126.5, 52.3, 41.9. Characterization data matched that reported in the literature.[26]

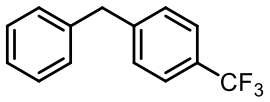


**21**

**1-Benzyl-4-(trifluoromethyl)benzene** (**21)**: obtained as a colorless oil (93 mg, 79%). $^{1}$H NMR ($CDCl_3$, 500 MHz): δ = 7.52 (d, *J* = 8.0 Hz, 2H), 7.30-7.26 (m, 4H), 7.22-7.19 (m, 1H), 7.16 (d, *J* = 7.5 Hz, 2H), 4.01 (s, 2H). $^{13}$C NMR ($CDCl_3$, 125.8 MHz): δ = 145.4, 140.2, 129.4, 129.1, 128.9, 128.7 (q, *J* = 32.2 Hz), 126.7, 125.6 (q, *J* = 3.9 Hz), 123.4, 41.9. $^{19}$F NMR ($CDCl_3$, 470.8 MHz): δ = -62.3. Characterization data matched that reported in the literature.[27]

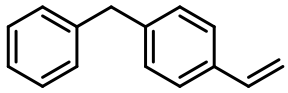

**22**

**1-Benzyl-4-vinylbenzene (22)**: obtained as a colorless oil (59 mg, 61%). $^{1}$H NMR ($CDCl_3$, 500 MHz): δ = 7.38-7.27 (m, 4H), 7.23–7.18 (m, 5H), 6.73 (dd, *J* = 17.5, 11.0 Hz, 1H), 5.74 (d, *J* = 17.5, 1H), 5.23 (d, *J* = 11.0, 1H), 4.01 (s, 2H). $^{13}$C NMR ($CDCl_3$, 125.8 MHz): δ = 140.9, 140.7, 136.5, 135.5, 129.0, 128.8, 128.4, 126.3, 126.0, 113.1, 41.6. Characterization data matched that reported in the literature.[25]

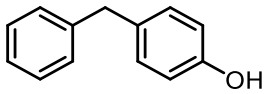


**23**

**4-Benzylphenol** (**23)**: obtained as a white solid (58 mg, 63%), mp = 80-82 °C. $^{1}$H NMR ($CDCl_3$, 500 MHz): δ = 7.32-7.29 (m, 2H), 7.23-7.18 (m, 3H), 7.07 (d, *J* = 8.0 Hz, 2H), 6.76 (d, *J* = 8.0 Hz, 2H) 4.84 (s, 1H), 3.93 (s, 2H). $^{13}$C NMR ($CDCl_3$, 125.8 MHz): δ = 153.9, 141.7, 133.6, 130.3, 129.0, 128.6, 126.2, 115.5, 41.2. Characterization data matched that reported in the literature.[28]

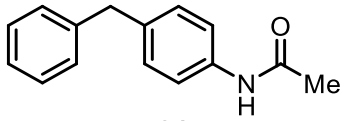


**24**

***N*-(4-Benzylphenyl)acetamide (24):** obtained as a white solid (107 mg, 96%), mp = 117-119 °C. $^{1}$H NMR ($CDCl_3$, 500 MHz): δ = 7.40 (d, *J* = 8.5 Hz, 2H), 7.28 (t, *J* = 7.5 Hz, 1H), 7.21-7.13 (m, 5H), 3.94 (s, 2H), 2.16 (s, 3H).$^{13}$C NMR ($CDCl_3$, 125.8 MHz): (* denotes minor rotamer) δ = 168.8,

141.0, 137.1, 136.0, 131.7*, 129.3, 129.0, 128.4, 126.0, 121.5*, 120.3, 41.3, 24.3. IR: ν = 3249, 3186, 3120, 2898, 2362, 1659, 1604, 1552, 1511, 1410, 1322, 1271, 850, 731 $cm^{-1.}$ HRMS (ESI) m/z calc. for $C_{15}H_{16}NO$ (M+H) 226.1232, found 226.1235.

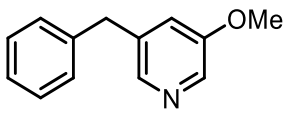


**25**

**3-Benzyl-5-methoxypyridine** (**25)**: obtained as a dark yellow oil (74 mg, 75%). $^{1}H$ NMR ($CDCl_3$, 500 MHz): δ = 8.17 (s, 1H), 8.13 (s, 1H), 7.31-7.28 (m, 2H), 7.23-7.17 (m, 3H), 6.97 (s, 1H), 3.96 (s, 2H), 3.80 (s, 3H). $^{13}C$ NMR ($CDCl_3$, 125.8 MHz): δ = 147.9, 145.9, 138.0, 132.3, 130.1, 129.5, 121.2, 120.4 (q, *J* = 257.3 Hz), 118.7, 110.3, 41.1. IR: ν = 3027, 2940, 2838, 1586, 1426, 1281, 1184, 1156, 1051, 843, 718, 669 $cm^{-1.}$ HRMS (ESI) m/z calc. for $C_{13}H_{14}NO$ (M+H) 200.1075, found 200.1066.

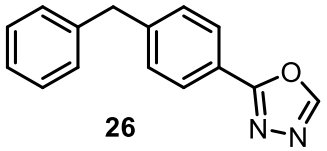


**26**

**2-(4-Benzylphenyl)-1,3,4-oxadiazole (26)**: obtained as a yellow solid (85 mg, 72%), mp = 71-73 °C. $^{1}H$ NMR ($CDCl_3$, 500 MHz): δ = 8.43 (s, 1H), 8.00 (d, *J* = 8.0 Hz, 2H), 7.34 (d, *J* = 8.0 Hz, 2H), 7.32 (d, *J* = 7.5 Hz, 2H), 7.25-7.19 (m, 3H), 4.06 (s, 2H). $^{13}C$ NMR ($CDCl_3$, 125.8 MHz): δ = 164.9, 152.6, 145.8, 140.1, 129.8, 129.1, 128.8, 127.4, 126.6, 121.5, 42.0. IR: ν = 2924, 2854, 1614, 1493, 1094, 1065, 865, 712 $cm^{-1.}$ HRMS (ESI) m/z calc. for $C_{15}H_{13}N_2O$ (M+H) 237.1028, found 237.1034.

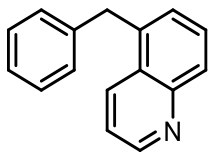


**27**

**5-Benzylquinoline (27):** obtained as a white solid (64 mg, 58%), mp = 80-81 °C. $^{1}$H NMR ($CDCl_3$, 500 MHz): δ = 8.90 (dd, *J* = 4, 1.5 Hz, 1H), 8.30 (d, *J* = 8.5 Hz, 1H), 8.04 (d, *J* = 8.5 Hz, 1H), 7.67 (dd, *J* = 8.4, 7.2 Hz, 1H), 7.61-7.24 (m, 4H), 7.13 (m, 3H), 4.45 (s, 2H). $^{13}$C NMR ($CDCl_3$, 125.8 MHz): δ = 149.9, 148.8, 140.0, 137.0, 132.5, 129.1, 128.5, 127.7, 127.1, 126.2, 120.8, 38.4. Characterization data matched that reported in the literature.[29]

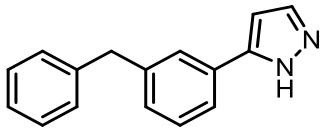


**28**

**5-(3-Benzylphenyl)-1H-pyrazole (28):** obtained as a white solid (76 mg, 65%), mp = 78-79 °C. $^{1}$H NMR ($CDCl_3$, 500 MHz): δ = 11.46 (br s, 1H), 7.63 (s, 1H), 7.60 (d, *J* = 8.0 Hz, 1H), 7.54 (d, *J* = 2 Hz, 1H), 7.33 (d, *J* = 8.0 Hz, 1H), 7.31-7.27 (m, 2H), 7.22-7.19 (m, 3H), 7.16 (d, *J* = 7.5 Hz, 2H), 6.58 (d, *J* = 1.5 Hz, 1H), 4.01 (s, 2H). $^{13}$C NMR ($CDCl_3$, 125.8 MHz): δ = 141.8, 141.0, 133.3, 132.4, 129.10, 129.09, 128.9, 128.7, 126.5, 126.3, 125.9, 123.8, 102.9, 42.1. IR: ν = 3166, 3068, 2919, 2850, 1559, 1494, 1472, 1452, 1357, 1052, 822, 771, 706 $cm^{-1.}$ HRMS (ESI) m/z calc. for $C_{16}H_{15}N_2$ (M+H) 235.1235, found 235.1235.

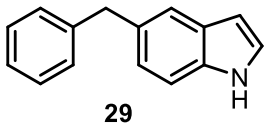


**29**

**5-Benzyl-1H-indole (29):** obtained in pure form as a white solid (57 mg, 55%), mp = 40-42 °C, and as a mixture with aryl bromide starting material [30 mg (mass of mixture), 18% (based on $^{1}$H NMR purity analysis)]. $^{1}$H NMR ($CDCl_3$, 500 MHz): δ = 7.99 (br s, 1H), 7.50 (s, 1H), 7.33-7.21 (m, 6H), 7.16 (d, *J* = 2.5 Hz, 1H), 7.08 (d, *J* = 8.0 Hz, 1H), 6.52 (s, 1H), 4.13 (s, 2H). $^{13}$C NMR ($CDCl_3$, 125.8 MHz): δ = 142.3, 134.4, 132.5, 128.9, 128.3, 128.1, 125.8, 124.3, 123.5, 120.6, 110.9, 102.4, 42.0. IR: ν = 3401, 2923, 2853, 2358, 1453, 1338, 1090, 1028, 762, 730, 699 $cm^{-1}$ HRMS (ESI) m/z calc. for $C_{15}H_{14}N$ (M+H) 208.1126, found 208.1135.

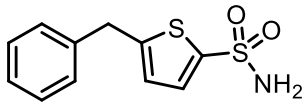


**30**

**5-Benzylthiophene-2-sulfonamide (30):** obtained as a white solid (71 mg, 56%), mp =89-90 °C $^{1}$H NMR ($CDCl_3$, 500 MHz): δ = 7.78 (d, *J* = 3.5 Hz, 1H), 7.34 (m, 2H), 7.29-7.23 (m, 3 H), 6.76 (d, *J* = 3.5 Hz, 1H), 4.93 (s, 2H), 4.15 (s, 2H). $^{13}$C NMR ($CDCl_3$, 125.8 MHz): δ = 152.1, 140.8, 138.9, 132.1, 129.0, 128.8, 127.3, 125.5, 36.5. IR: ν = 3382, 3276, 3109, 2918, 1566, 1443, 1330, 1163, 1142, 1020, 908, 704 $cm^{-1.}$ HRMS (ESI) m/z calc. for $C_{11}H_{10}NO_2S_2$ (M-H) 252.0153, found 252.0164.

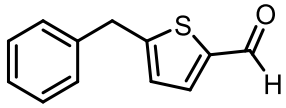


**31**

**5-Benzylthiophene-2-carbaldehyde (31):** obtained as a colorless oil (55 mg, 54%). $^{1}$H NMR ($CDCl_3$, 500 MHz): δ = 9.81 (s, 1H), 7.60 (d, *J* = 3.5 Hz, 1H), 7.35-7.32 (m, 2H), 7.28-7.24 (m, 3H), 6.90 (d, *J* = 3.5 Hz, 1H), 4.19 (s, 2H). $^{13}$C NMR ($CDCl_3$, 125.8 MHz): δ = 182.8, 155.9, 142.6, 138.9, 137.0, 129.0, 128.8, 127.2, 126.8, 37.0. Characterization data matched that reported in the literature.[28]

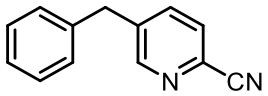


**32**

**5-Benzylpicolinonitrile (32)**: obtained as a colorless oil (87 mg, 90%). $^{1}$H NMR: ($CDCl_3$, 500 MHz): δ = 8.60 (s, 1H), 7.60 (m, 2H), 7.33 (dd, *J* = 7.0, 7.0 Hz, 2H), 7.27 (m, 1H), 7.16 (d, *J* = 7.0 Hz, 2H), 4.06 (s, 2H). $^{13}$C NMR ($CDCl_3$, 125.8 MHz): δ = 151.7, 141.1, 138.3, 137.2, 131.8, 129.2, 129.1, 128.4, 127.2, 117.5, 39.2. IR: ν = 3027, 2920, 2851, 2362, 2234, 1586, 1566, 1496, 1470,

1454, 1392, 1027, 741, 706 $cm^{-1.}$ HRMS (ESI) m/z calc. for $C_{13}H_{11}N_2$ (M+H) 195.0922, found 195.0924.

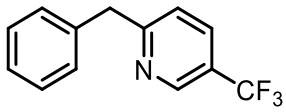


**33**

**2-Benzyl-5-(trifluoromethyl)pyridine** (**33)**: obtained as a colorless oil (77 mg, 65%). $^{1}H$ NMR ($CDCl_3$, 500 MHz): δ = 8.84 (s, 1H), 7.82 (d, *J* = 7.0 Hz, 1H), 7.34-7.32 (m, 2H), 7.28-7.24 (m, 4H), 4.25 (s, 2H). $^{13}C$ NMR ($CDCl_3$, 125.8 MHz): δ = 165.2, 146.5 (d, *J* = 3.5 Hz), 138.6, 133.8, 129.3, 129.0, 127.0, 124.6 (q, *J* = 33.2), 123.9 (q, *J* = 271.9), 122.9, 44.8. $^{19}F$ NMR ($CDCl_3$, 470.8 MHz): δ = -62.3. IR: ν = 3030, 2360, 1605, 1495, 1322, 1327, 1124, 1017, 735 $cm^{-1.}$ HRMS (ESI) m/z calc. for $C_{13}H_{11}F_3N$ (M+H) 208.0844, found 208.0842.

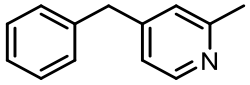


**34**

**4-Benzyl-2-methylpyridine (34):** obtained as a light yellow oil (52 mg, 57%). $^{1}H$ NMR ($CDCl_3$, 500 MHz): δ = 8.38 (d, *J* = 5.0 Hz, 1H), 7.32 (m, 2H), 7.25 (m, 1 H), 7.17 (d, *J* = 7.0 Hz, 2H), 6.97 (s, 1H), 6.91 (d, *J* = 5.0 Hz, 1H), 3.92 (s, 2H), 2.51 (s, 3H). $^{13}C$ NMR ($CDCl_3$, 125.8 MHz): δ = 158.6, 150.4, 149.3, 139.3, 129.2, 128.8, 126.7, 123.8, 121.5, 41.4, 24.5. IR: ν = 3027, 2923, 2358, 1600, 1558, 1495, 1453, 734, 699 $cm^{-1.}$ HRMS (ESI) m/z calc. for $C_{13}H_{14}N$ (M+H) 184.1126, found 184.1117.

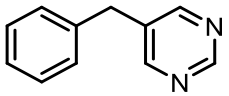


**35**

**5-Benzylpyrimidine** (**35)**: obtained as yellow crystals (82 mg, 96%), mp = 45-47 °C. $^{1}H$ NMR ($CDCl_3$, 500 MHz): δ = 9.07 (s, 1H), 8.57 (s, 2H), 7.33-7.30 (m, 2H) 7.25-7.22 (m, 2H) 7.17-7.15

(m, 2H), 3.95 (s, 2H). $^{13}$C NMR ($CDCl_3$, 125.8 MHz): δ = 157.15, 157.08, 138.4, 134.4, 129.1, 128.9, 127.1, 36.7. IR: ν = 3032, 2916, 2850, 1560, 1408, 1230, 1100, 987, 924, 749, 729 $cm^{-1.}$ HRMS (ESI) m/z calc. for $C_{11}H_{11}N_2$ (M+H) 171.0922, found 171.0919.

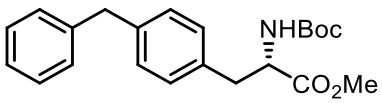


**36**

**Methyl (*S*)-3-(4-Benzylphenyl)-2-((*tert*-butoxycarbonyl)amino)propanoate (36)** obtained as a yellow oil after purification by preparatory reverse phase high pressure liquid chromatography (19 x 100 mm Waters XBridge Prep BHE130 C18 column, 10% → 90% MeCN/$H_2O$, 20 mL/min flow rate) (116 mg, 63%). $^1$H NMR ($CDCl_3$, 500 MHz): δ = 7.30-7.27 (m, 2H), 7.22-7.17 (m, 3H), 7.11 (d, *J* = 8.0 Hz, 2H), 7.04 (d, *J* = 8.0 Hz, 2H), 4.96 (d, *J* = 7.5 Hz, 1H), 4.57 (dd, *J* = 14.0, 6.0 Hz, 1H), 3.95 (s, 2H), 3.71 (s, 3H), 3.10-2.99 (m, 2H), 1.41 (s, 9H). $^{13}$C NMR ($CDCl_3$, 125.8 MHz): δ = 172.4, 155.2, 141.0, 139.0, 133.8, 129.5, 129.2, 129.0, 128.5, 126.2, 100.0, 79.9, 54.5, 52.2, 41.6, 38.0, 28.4. IR: ν = 3363, 2978, 2362, 1745, 1715, 1494, 1366, 1166 $cm^{-1.}$ HRMS (ESI) m/z calc. for $C_{22}H_{27}NO_4Na$ (M+Na) 392.1838, found 392.1822. Chiral SFC (ChiralPak AD-H column: 10% MeOH in $CO_2$, 5.0 mL/min) $t_r$ = 2.017 (major peak).

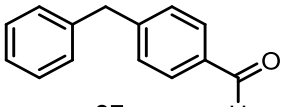


**37**

**4-Benzylbenzaldehyde (37):** obtained as a colorless oil (79 mg, 81%). $^1$H NMR ($CDCl_3$, 500 MHz): δ = 9.98 (s, 1H), 7.81 (d, *J* = 8.0 Hz, 2H), 7.36 (d, *J* = 8.0 Hz, 2H), 7.31 (dd, *J* = 7.5, 7.0 Hz, 2H), 7.24 (t, *J* = 7.0 Hz, 1H), 7.19 (d, *J* = 7.5 Hz, 2H), 4.06 (s, 2H). $^{13}$C NMR ($CDCl_3$, 125.8

MHz): δ = 192.1, 148.6, 139.9, 134.8, 130.2, 129.7, 129.1, 128.8, 126.7, 42.2. Characterization data matched that reported in the literature.[9]

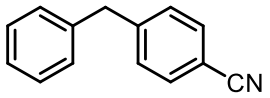


**38**

**4-Benzylbenzonitrile (38)**: obtained as a white crystalline solid (86 mg, 89%); gram scale (1029 mg, 97%), mp = 47-50 °C. $^{1}$H NMR ($CDCl_3$, 500 MHz): δ = 7.57 (d, *J* = 8.5 Hz, 2H), 7.25-7.32 (m, 5H), 7.17 (d, *J* = 7.5 Hz, 2H), 4.04 (s, 2H). $^{13}$C NMR ($CDCl_3$, 125.8 MHz): δ = 146.9, 139.5. 132.4, 129.8, 129.1, 128.9, 126.8, 119.1, 110.2, 42.1. Characterization data matched that reported in the literature.[30]

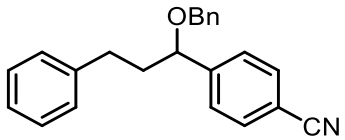


**39**

**4-(1-(benzyloxy)-3-phenylpropyl)benzonitrile (40)**: prepared using the general procedure for primary benzyl cross-couplings, obtained as a colorless oil (106 mg, 65%). $^{1}$H NMR ($CDCl_3$, 500 MHz): δ = 7.67 (d, *J* = 8.0 Hz, 2H), 7.46 (d, *J* = 8.0 Hz, 2H), 7.40-7.37 (m, 2H), 7.34-7.32 (m, 3H), 7.30-7.26 (m, 2H), 7.22-7.18 (m, 1H), 7.14 (d, *J* = 7.5 Hz, 2H), 4.46 (d, *J* = 11.5 Hz, 1H), 4.38 (dd, *J* = 8.5, 4.5 Hz, 1H), 4.29 (d, *J* = 11.5 Hz, 1H), 2.83-2.77 (m, 1H), 2.72-2.67 (m, 1H), 2.19-2.14 (m, 1H), 1.97-1.92 (m, 1H). $^{13}$C NMR ($CDCl_3$, 125.8 MHz): δ = 148.2, 141.3, 137.9, 132.4, 128.5, 128.40, 128.38, 127.78, 127.76, 127.3, 125.9, 118.8, 111.4, 79.8, 71.0, 39.8, 31.8. IR: ν = 3028, 2924, 2228, 1607, 1496, 1094, 853, 698, 737 $cm^{-1}$ HRMS (ESI) m/z calc. 328.1701 for (M+H), found 328.1709.

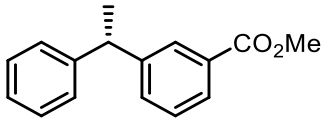


**41**

**Methyl 3-(1-Phenylethyl)benzoate (41):** obtained as a colorless oil (62 mg, 52%). $^{1}$H NMR ($CDCl_3$, 500 MHz): δ = 7.96 (m, 1H), 7.87 (m, 1H), 7.41-7.28 (m, 4H), 7.22-7.18 (m, 3H), 4.21 (q, *J* = 7.5 Hz, 1H), 3.90 (s, 3H), 1.67 (d, *J* = 7.5 Hz, 3H). $^{13}$C NMR ($CDCl_3$, 125.8 MHz): δ = 167.4, 146.9, 145.9, 132.5, 130.4, 128.8, 128.64, 128.61, 127.7, 127.6, 126.4, 52.2, 44.8, 21.9. $[\alpha_D]^{25}$ = -4.4 ($CDCl_3$, c = 1.0 mg/mL). Chiral SFC (ChiralPak OJ-H column: 5% iPrOH in $CO_2$, 2.0 mL/min) $t_r$ = 8.37 (minor peak) $t_r$ = 9.17 (major peak) Absolute configuration of the major enantiomer was assigned as (*S*) based on literature data. Characterization data matched that reported in the literature.[31]

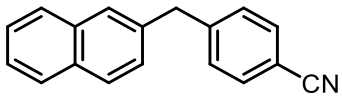


**42**

**4-(Naphthalen-2-ylmethyl)benzonitrile (42)**: obtained as a white solid (121 mg, 99%), Mp = 105-110 °C. $^{1}$H NMR ($CDCl_3$, 500 MHz): δ = 7.83-7.77 (m, 3H), 7.62 (s, 1H), 7.58 (m, 2H), 7.48 (m, 2H), 7.33 (d, *J* = 8.0 Hz, 2H), 7.27-7.25 (m, 1H), 4.20 (s, 2H). $^{13}$C NMR ($CDCl_3$, 125.8 MHz): δ = 146.5, 136.8, 133.6, 132.3, 129.7, 128.5, 127.7, 127.5, 127.4, 126.3, 125.8, 119.0, 110.1, 42.1. Characterization data matched that reported in the literature.[32]

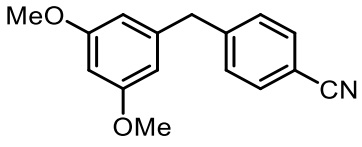


**43**

**4-(3,5-Dimethoxybenzyl)benzonitrile** (**43)**: obtained as a colorless oil (108 mg, 86%). $^{1}$H NMR ($CDCl_3$, 500 MHz): δ = 7.57 (d, *J* = 8.5 Hz, 2H), 7.29 (d, *J* = 8.0 Hz, 2H), 6.34 (s, 1H), 6.30 (s, 2H), 3.95 (s, 2H,), 3.76 (s, 6H). $^{13}$C NMR ($CDCl_3$, 125.8 MHz): δ = 161.2, 146.5, 141.7, 132.4, 129.7, 119.1, 110.2, 107.4, 98.4, 55.4, 42.3. IR: ν = 2937, 2838, 2358, 2227, 1594, 1461, 1430, 1205, 1156, 1065, 822 $cm^{-1.}$ HRMS (ESI) m/z calc. for $C_{16}H_{16}NO_2$ (M+H) 254.1181, found 254.1182.

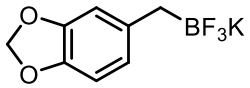


**S5**

**Potassium (Benzo[d][1,3]dioxol-5-ylmethyl)trifluoroborate (S5)**: prepared following general procedure A, obtained as a white solid (498 mg, 41%), mp = 258 °C (dec.). $^{1}$H NMR (acetone-$d_6$, 500 MHz): δ = 6.65 (s, 1H), 6.54-6.50 (m, 2H), 5.79 (s, 2H), 1.55 (br s, 2H). $^{13}$C NMR (DMSO-$d_6$, 125.8 MHz): δ = 146.8, 143.1, 141.2, 121.2, 109.8, 107.7, 100.3. $^{19}$F NMR (acetone-$d_6$, 282.4 MHz): δ = -136.3 (q, *J* = 70.6 Hz). $^{11}$B NMR (acetone-$d_6$, 128.4 MHz): δ = 4.12 (q, *J* = 50.2 Hz) IR: ν = 3067, 1482, 1436, 1230, 1040, 960, 775, 630 $cm^{-1.}$ HRMS (ESI) m/z calc. for $C_8H_7O_2BF_3$ (M-) 203.0491, found 203.0486.

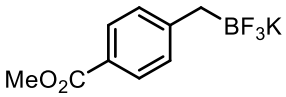


**S6**

**Potassium Trifluoro(4-(methoxycarbonyl)benzyl)borate (S6)**: prepared following general procedure B, obtained as a white solid (706 mg, 55%), mp = 205°C (dec.). $^{1}$H NMR (acetone-$d_6$, 500 MHz): δ = 7.73 (d, *J* = 8.0 Hz, 2H), 7.18 (d, *J* = 8.0 Hz, 2H), 3.81 (s, 3H), 1.75 (br s, 2H). $^{13}$C NMR (acetone-$d_6$, 125.8 MHz): δ = 166.9, 153.7, 128.5, 128.3, 124.3, 50.7. $^{19}$F NMR (acetone-$d_6$, 470.8 MHz): δ = -140.7 (q, *J* = 55.6 Hz). $^{11}$B NMR (acetone-$d_6$, 128.4 MHz): δ = 4.70 (q, *J* = 57.9

Hz). IR: ν = 3038, 1690, 1607, 1444, 1293, 1233, 1056, 993, 959, 782, 720, 642. HRMS: (ESI) m/z calc. for $C_9H_9O_2BF_3$ (M-) 217.0648, found 217.0647.

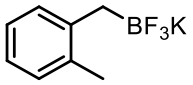


**S7**

**Potassium Trifluoro(2-methylbenzyl)borate (S7)**: prepared following general procedure A, obtained as a white solid (850 mg, 80%), mp = 230 °C (dec.). $^1$H NMR (acetone-$d_6$, 500 MHz): δ = 7.05 (d, *J* = 8.0 Hz, 1H), 6.93 (d, *J* = 7.5 Hz, 1H), 6.90-6.87 (m, 1H), 6.81-6.78 (m, 1H), 2.24 (s, 3H), 1.66 (br s, 2H). $^{13}$C NMR (acetone-$d_6$, 125.8 MHz): δ = 145.0, 135.3, 129.4, 129.0, 124.8, 122.5, 19.9. $^{19}$F NMR (acetone-$d_6$, 470.8 MHz): δ = -138.3. $^{11}$B NMR (acetone-$d_6$, 128.4 MHz): δ = 5.27 (q, *J* = 51.0 Hz). IR: ν = 2941, 1488, 1228, 1049, 975, 781, 734, 636 cm$^{-1.}$ HRMS (ESI) m/z calc. for $C_8H_9BF_3$ (M-) 173.0749, found 173.0753.

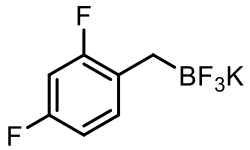


**S8**

**Potassium (2,4-Difluorobenzyl)trifluoroborate (S8):** prepared following general procedure A, obtained as a white solid (422 mg, 36%), mp = 225-227 °C. $^1$H NMR (acetone-$d_6$, 500 MHz): δ = 7.23 (q, *J* = 7.5 Hz, 1H), 6.70-6.66 (m, 2H), 1.59 (br s, 2H). $^{13}$C NMR (acetone-$d_6$, 125.8 MHz): δ = 160.7 (dd, *J* = 131, 11 Hz), 158.8 (dd, *J* = 129, 11 Hz), 131.7 (t, *J* = 8 Hz), 128.0 (d, *J* = 17 Hz), 109.7 (dd, *J* = 20, 3 Hz), 102.0 (dd, *J* = 28, 25 Hz), 18.5. $^{19}$F NMR (acetone-$d_6$, 470.8 MHz): δ = -114.9, -119.4, -139.9. $^{11}$B NMR (acetone-$d_6$, 128.4 MHz): δ = 4.98. IR: ν = 2928, 1622, 1601, 1504, 1253, 1087, 1071, 986, 949, 846 cm$^{-1.}$ HRMS (ESI) m/z calc. for $C_7H_5BF_5$ (M-) 195.0404, found 195.0402.

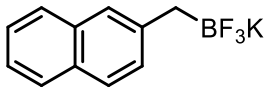


**S9**

**Potassium Trifluoro(naphthalen-2-ylmethyl)borate (S9):** prepared following general procedure A, obtained as a white solid (323 mg, 26%), mp: 199-202 °C. $^{1}$H NMR (acetone-$d_6$, 500 MHz): δ = 7.70 (d, *J* = 8.1 Hz, 1H), 7.65 (d, *J* = 8.2 Hz, 1H), 7.57 (d, *J* = 8.4 Hz, 1H), 7.49 (s, 1H), 7.38 (d, *J* = 8.5 Hz, 1H), 7.35-7.28 (m, 1H), 7.27-7.21 (m, 1H), 1.81 (br s, 2H). $^{13}$C NMR (acetone-$d_6$, 125.8 MHz): δ = 144.0, 134.0, 130.9, 129.4, 127.3, 126.8, 126.3, 125.4, 124.9, 123.3. $^{19}$F NMR (acetone-$d_6$, 470.8 MHz): δ = -139.1. $^{11}$B NMR (acetone-$d_6$, 128.4 MHz): δ = 5.34. IR: ν = 3054, 2891, 1631, 1597, 1505, 1239, 1074, 953, 746. HRMS (ESI) m/z calc. for $C_{11}H_9BF_3$ (M-) 209.0749, found 209.0749.

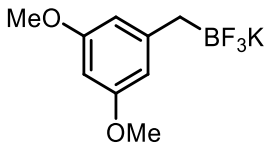


**S10**

**Potassium (3,5-Dimethoxybenzyl)trifluoroborate (S10):** prepared following general procedure A, obtained as a white solid (809 mg, 63%), mp: 220-222 °C. $^{1}$H NMR (DMSO-$d_6$, 500 MHz): δ = 6.16 (s, 2H), 6.02 (s, 1H), 3.64 (s, 6H), 1.40 (br s, 2H). $^{13}$C NMR (DMSO-$d_6$, 125.8 MHz): δ = 159.4, 149.3, 106.7, 94.5, 54.6. $^{19}$F NMR (DMSO-$d_6$, 470.8 MHz): δ = -136.3. $^{11}$B NMR (DMSO-$d_6$, 128.4 MHz): δ = 4.20. IR: ν = 2837, 1614, 1588, 1315, 1240, 1156, 1147, 1068, 978, 934 cm$^{-1.}$ HRMS (ESI) m/z calc. for $C_9H_{11}BF_3O_2$ (M-) 219.0804, found 219.0812.

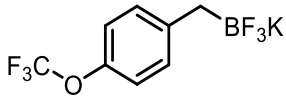


**S11**

**Potassium (3,5-Dimethoxybenzyl)trifluoroborate (S11):** reaction performed on 3 mmol scale according to general procedure A, obtained as a white solid (466 mg, 55%), mp = 165-168 °C. $^{1}$H NMR (acetone-$d_6$, 500 MHz): δ = 7.16 (d, *J* = 8.5 Hz, 2H), 6.97 (d, *J* = 8.0 Hz, 2H), 1.66 (br s, 2H). $^{13}$C NMR (acetone-$d_6$, 125.8 MHz): δ = 146.7, 145.0, 130.0, 120.9 (q, *J* = 253 Hz), 119.8. $^{19}$F NMR (acetone-$d_6$, 470.8 MHz): δ = -59.0, -141.0 (q, *J* = 62 Hz). $^{11}$B NMR (acetone-$d_6$, 128.4 MHz): δ = 4.88. Characterization data matched that reported in the literature.[17]

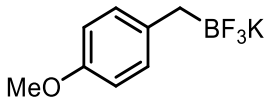


**S12**

**Potassium Trifluoro(4-methoxybenzyl)borate (S12):** prepared following general procedure A, obtained as a white solid (403 mg, 35%), mp = 162-165 °C. $^{1}$H NMR (acetone-$d_6$, 500 MHz): δ = 7.01 (d, *J* = 8.0 Hz, 2H), 6.64 (d, *J* = 8.0 Hz, 2H), 3.68 (s, 3H), 1.56 (br s, 2H). $^{13}$C NMR (acetone-$d_6$, 125.8 MHz): δ = 156.4, 138.0, 129.8, 113.3, 54.9. $^{19}$F NMR (acetone-$d_6$, 470.8 MHz): δ = -140.7 (q, *J* = 58.9 Hz). $^{11}$B NMR (acetone-$d_6$, 128.4 MHz): δ = 5.14. Characterization data matched that reported in the literature.[8]

## 2.5 References

(1) Yasu, Y.; Koike, T.; Akita, M. *Adv. Synth. Catal.* **2012**, *354*, 3414.

(2) Blanksby, S. J.; Ellison, G. B. *Acc. Chem. Res.* **2003**, *36*, 255.

(3) Motherwell, W. B.; Crich, D. Free Radical Chain Reactions in Organic Synthesis; Academic Press: London, 1992.

(4) Everson, D. A.; Shrestha, R.; Weix, D. J. *J. Am. Chem. Soc.* **2010**, *132*, 920.

(5) Lowry, M. S.; Goldsmith, J. I.; Slinker, J. D.; Rohl, R.; Pascal, R. A.; Malliaras, G. G.; Bernhard, S. *Chem. Mater.* **2005**, *17*, 5712.

(6) Cannes, C.; Labbe, E.; Durandetti, M.; Devaud, M.; Nedelec, J. Y. *J. Electroanal. Chem.* **1996**, *412*, 85.

(7) Welsch, M. E.; Snyder, S. A.; Stockwell, B. R. *Curr. Opin. Chem. Biol.* **2010**, *14*, 347.

(8) Jain, P.; Yi, S.; Flaherty, P. T. *J. Heterocycl. Chem.* **2013**, *50*, 166.

(9) Flaherty, A.; Trunkfield, A.; Barton, W. *Org. Lett.* **2005**, *7*, 4975.

(10) Molander, G. A.; Ito, T. *Org. Lett.* **2001**, *3*, 393.

(11) Molander, G. A.; Wisniewski, S. R. *J. Am. Chem. Soc.* **2012**, *134*, 16856.

(12) Li, L.; Wang, C.-Y.; Huang, R.; Biscoe, M. R. *Nat. Chem.* **2013**, *5*, 607.

(13) Hayashi, T.; Tajika, M.; Tamao, K.; Kumada, M. *J. Am. Chem. Soc.* **1976**, *98*, 3718.

(14) Hayashi, T.; Konishi, M.; Fukushima, M.; Mise, T.; Kagotani, M.; Tajika, M.; Kumada, M. *J. Am. Chem. Soc.* **1982**, *104*, 180.

(15) Cordier, C. J.; Lundgren, R. J.; Fu, G. C. *J. Am. Chem. Soc.* **2013**, *135*, 10946.

(16) Do, H.-Q.; Chandrashekar, E. R. R.; Fu, G. C. *J. Am. Chem. Soc.* **2013**, *135*, 16288.

(17) Cazorla, C.; Métay, E.; Lemaire, M. *Tetrahedron* **2011**, *67*, 8615.

(18) Yang, C.-T.; Zhang, Z.-Q.; Tajuddin, H.; Wu, C.-C.; Liang, J.; Liu, J.-H.; Fu, Y.; Czyzewska, M.; Steel, P. G.; Marder, T. B.; Liu, L. *Angew. Chem. Int. Ed.* **2012**, *51*, 528.

(19) Ishiyama, T.; Oohashi, Ã. Z.; Ahiko, T.; Miyaura, N. *Chem. Lett.* **2002**, *31*, 780.

(20) Hanss, D.; Freys, J. C.; Bernardinelli, G.; Wenger, O. S. *Eur. J. Inorg. Chem.* **2009**, *2009*, 4850.

(21) Molander, G. A.; Biolatto, B. *J. Org. Chem.* **2003**, *68*, 4302.

(22) Kofink, C. C.; Knochel, P. *Org. Lett.* **2006**, *8*, 4121.

(23) Schäfer, G.; Bode, J. W. *Angew. Chem. Int. Ed.* **2011**, *50*, 10913.

(24) Schmink, J. R.; Leadbeater, N. E. *Org. Lett.* **2009**, *11*, 2575.

(25) Chen, C.-R.; Zhou, S.; Biradar, D. B.; Gau, H.-M. *Adv. Synth. Catal.* **2010**, *352*, 1718.

(26) Chupak, L. S.; Wolkowski, J. P.; Chantigny, Y. A. *J. Org. Chem.* **2009**, *74*, 1388.

(27) Bedford, R. B.; Huwe, M.; Wilkinson, M. C. *Chem. Commun.* **2009**, *5*, 600.

(28) Burns, M. J.; Fairlamb, I. J. S.; Kapdi, A. R.; Sehnal, P.; Taylor, R. J. K. *Org. Lett.* **2007**, *9*, 5397.

(29) Maity, P.; Shacklady-Mcatee, D. M.; Yap, G. P. A.; Sirianni, E. R.; Watson, M. P. *J. Am. Chem. Soc.* **2013**, *135*, 280.

(30) Liu, Z.; Dong, N.; Xu, M.; Sun, Z.; Tu, T. *J. Org. Chem.* **2013**, *78*, 7436.

(31) Fessard, T. C.; Andrews, S. P.; Motoyoshi, H.; Carreira, E. M. *Angew. Chem. Int. Ed.* **2007**, *46*, 9331.

(32) Giannangeli, M.; Baiocchi, L. *Tetrahedron* **1980**, *36*, 1381.

**Author Contributions:**

D.N.P. contributed to the design and conception of the project. D.N.P. optimized the enantioselctive cross-coupling conditions, prepared some of the compounds, and assisted in writing and editing the manuscript. John C. Tellis contributed to the design and conception of the project, wrote and edited the manuscript, and planned the competition experiments and α-alkoxyalkyl cross-coupling examples. John C. Tellis also prepared some of the compounds in this study.

## Appendix A1. $^{1}H$, $^{13}C$, $^{11}B$, and $^{19}F$ NMR Spectra Relevant to Chapter 2

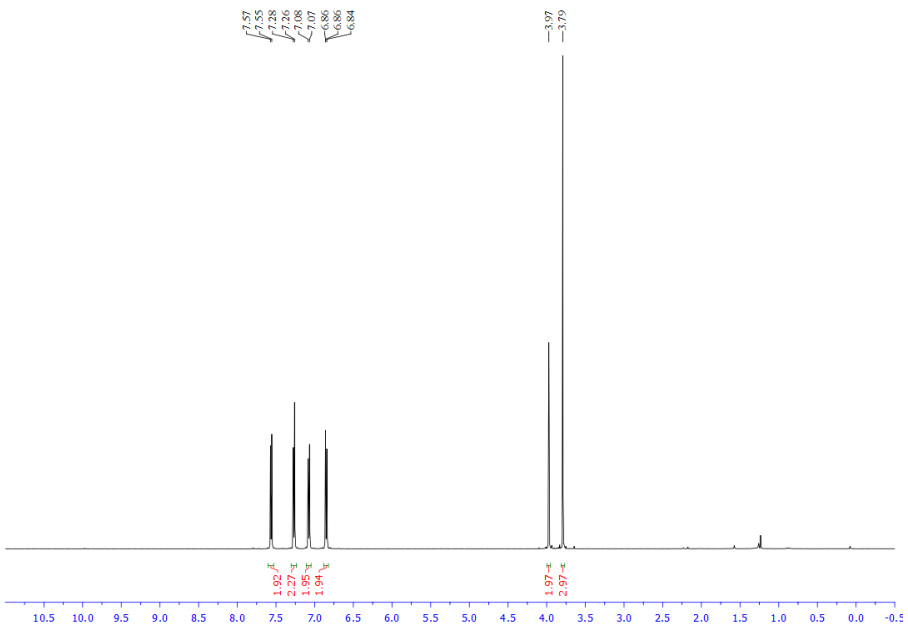


**Figure A1.1.** $^{1}$H NMR ($CDCl_3$, 500 MHz) spectrum of 4-(4-methoxybenzyl)benzonitrile (**12**)

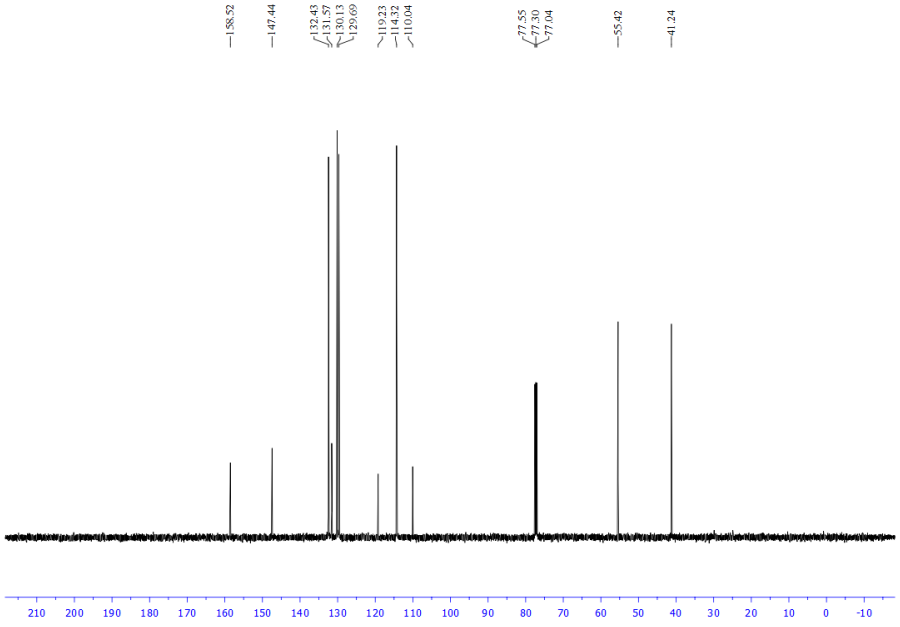


**Figure A1.1.** $^{13}$C NMR ($CDCl_3$, 125.8 MHz) spectrum of 4-(4-methoxybenzyl)benzonitrile (**12**)

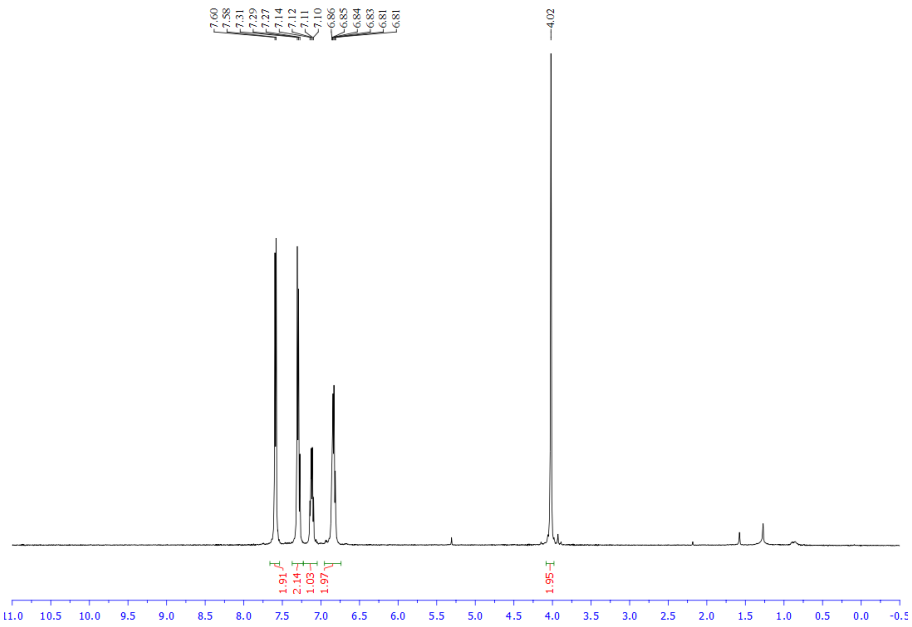

**Figure A1.3.** $^{1}$H NMR ($CDCl_3$, 500 MHz) spectrum of 4-(2,4-difluorobenzyl)benzonitrile (**13**)

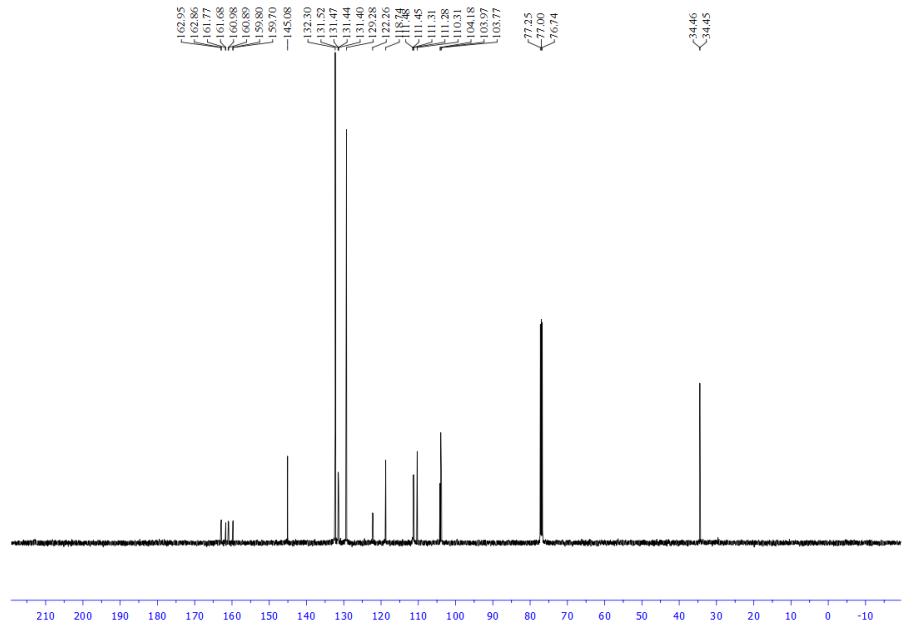

**Figure A1.4.** $^{13}$C NMR ($CDCl_3$, 125.8 MHz) spectrum of 4-(2,4-difluorobenzyl)benzonitrile (**13**)

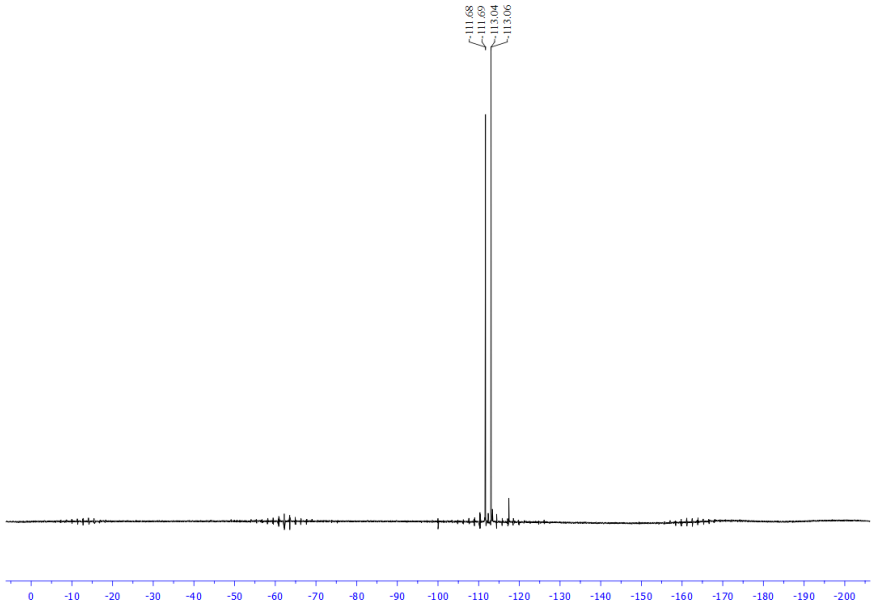


**Figure A1.5.** $^{13}C$ NMR ($CDCl_3$, 470.8 MHz) spectrum of 4-(2,4-difluorobenzyl)benzonitrile (**13**)

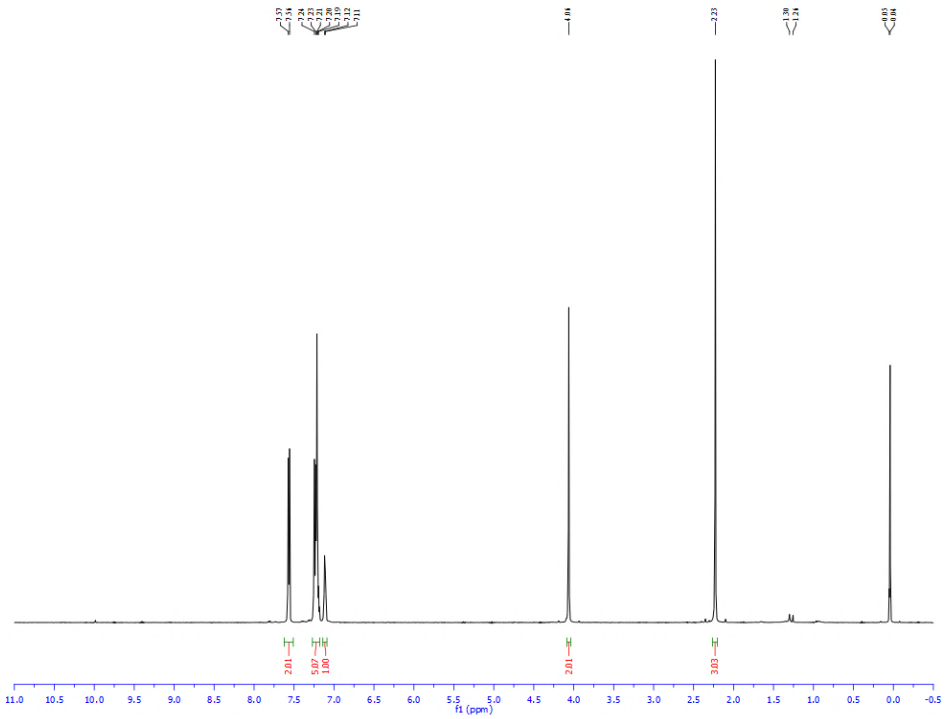


**Figure A1.6.** $^{1}H$ NMR ($CDCl_3$, 500 MHz) spectrum of 4-(2-methylbenzyl)benzonitrile (**14**)

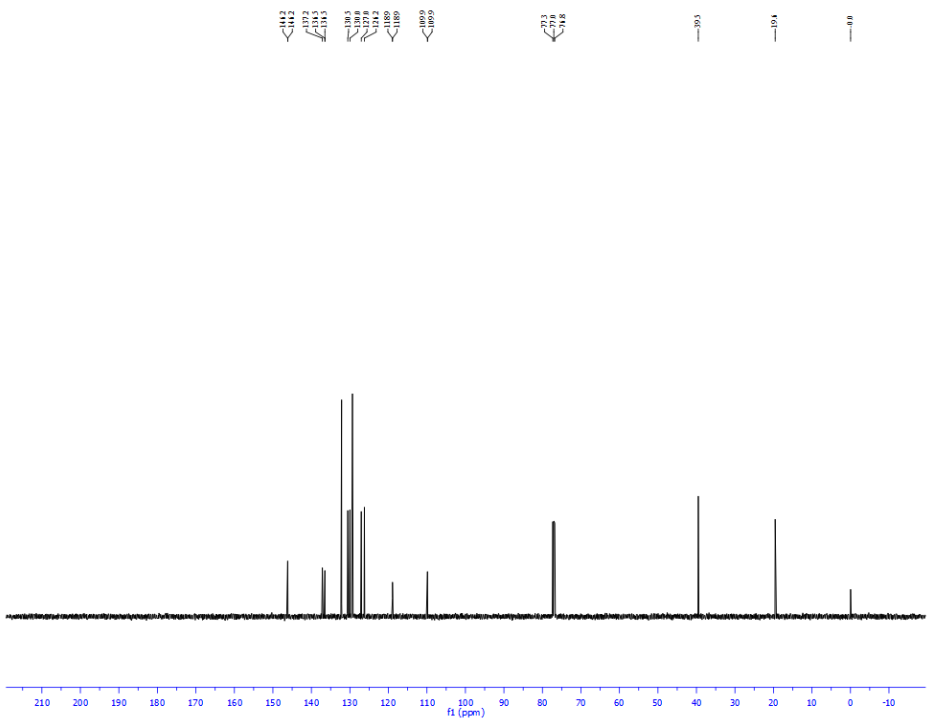

**Figure A1.7.** $^{13}C$ NMR ($CDCl_3$, 125.8 MHz) spectrum of 4-(2-methylbenzyl)benzonitrile (**14**)

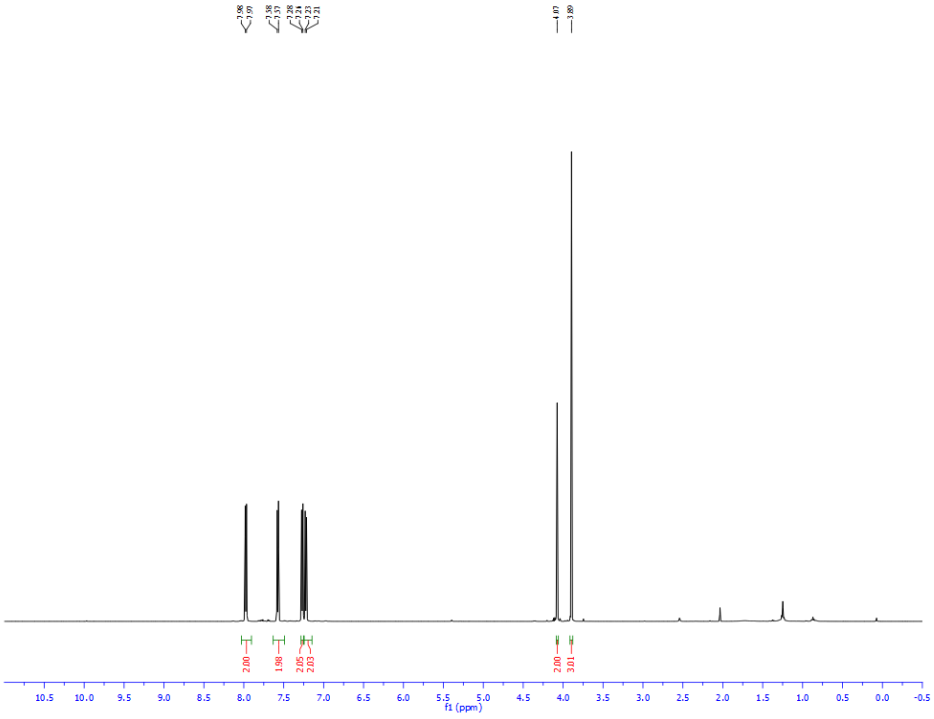

**Figure A1.8.** $^{1}H$ NMR ($CDCl_3$, 500 MHz) spectrum of methyl 4-(4-cyanobenzyl)benzoate (**15**)

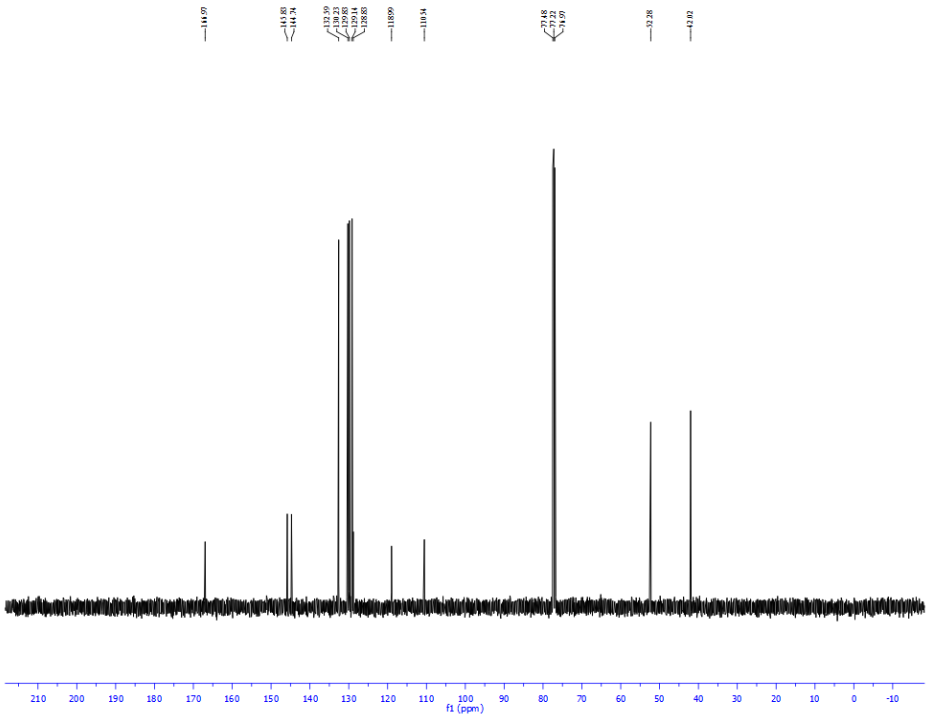

**Figure A1.9.** $^{13}C$ NMR ($CDCl_3$, 125.8 MHz) spectrum of methyl 4-(4-cyanobenzyl)benzoate (**15**)

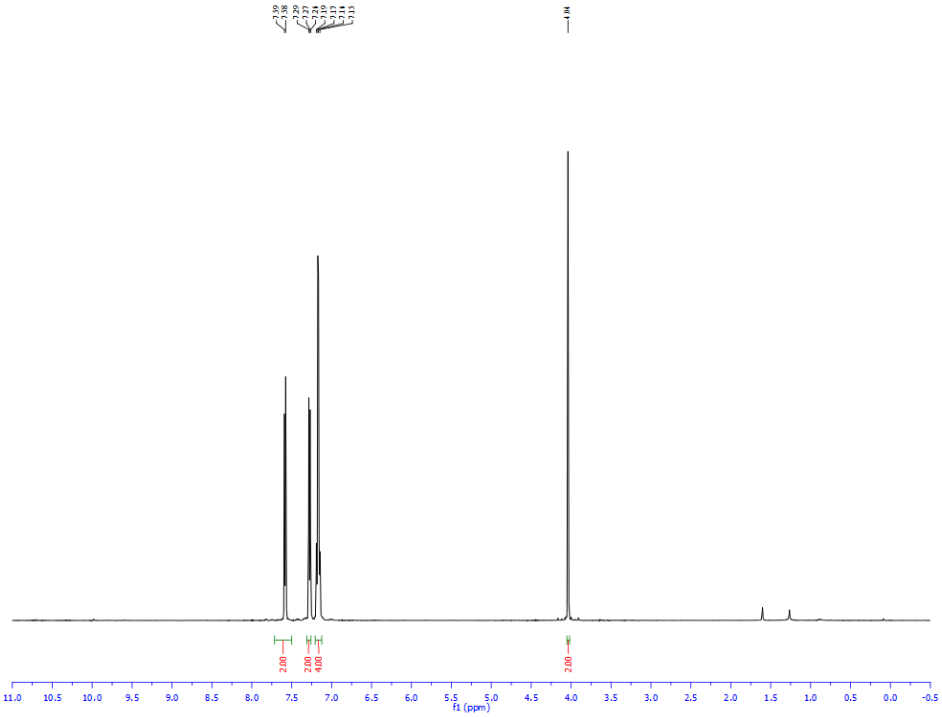

**Figure A1.10.** $^{1}H$ NMR ($CDCl_3$, 500 MHz) spectrum of 4-(4-(trifluoromethoxy)benzyl)benzonitrile (**16**)

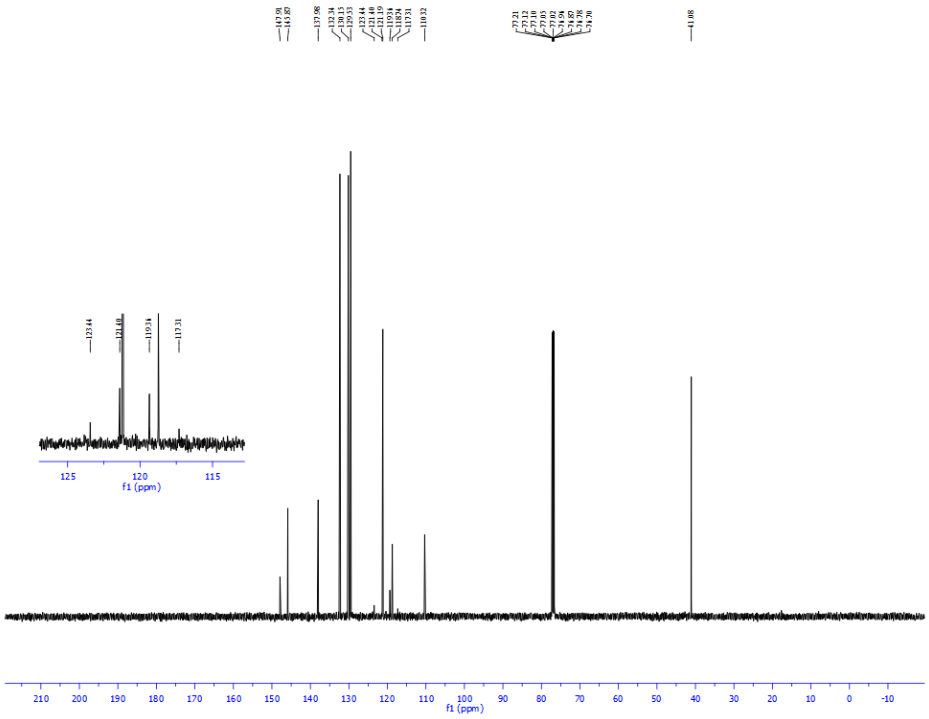

**Figure A1.11.** $^{13}C$ NMR ($CDCl_3$, 125.8 MHz) spectrum of 4-(4-(trifluoromethoxy)benzyl)benzonitrile (**16**)

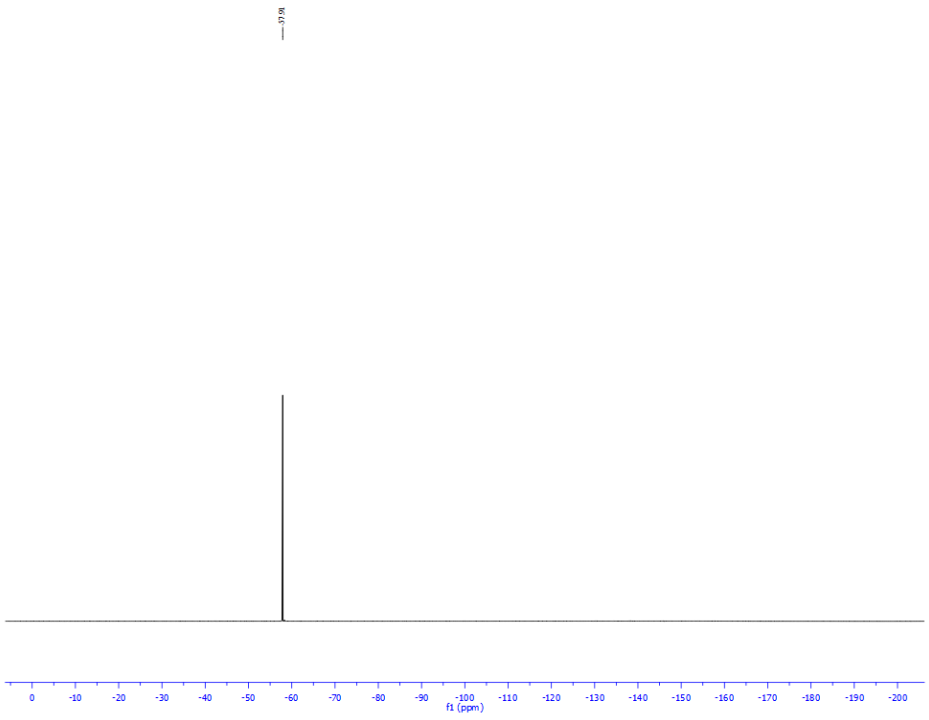

**Figure A1.12.** $^{19}F$ NMR ($CDCl_3$, 470.8 MHz) spectrum of 4-(4-(trifluoromethoxy)benzyl)benzonitrile (**16**)

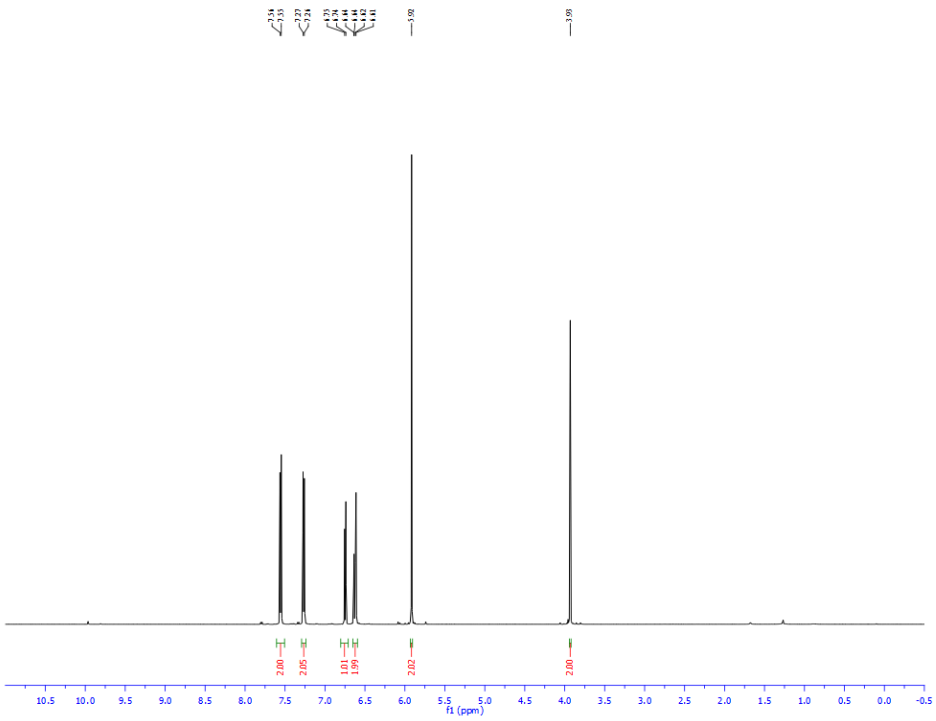

**Figure A1.13.** $^{1}$H NMR ($CDCl_3$, 500 MHz) spectrum of 4-(benzo[d][1,3]dioxol-5-ylmethyl)benzonitrile (**17**)

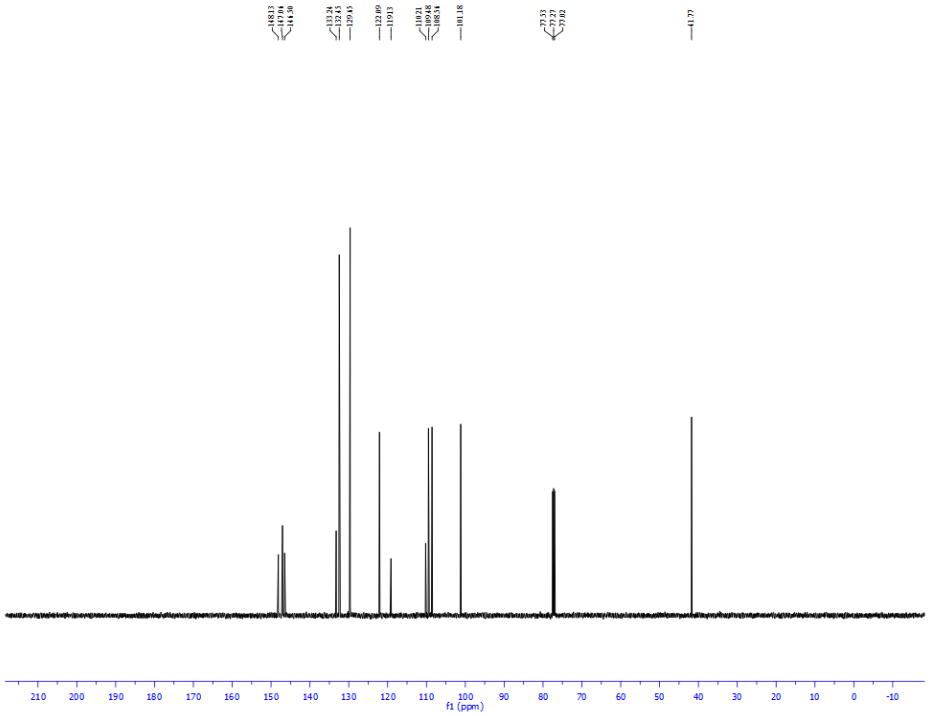

**Figure A1.14.** $^{13}$C NMR ($CDCl_3$, 125.8 MHz) spectrum of 4-(benzo[d][1,3]dioxol-5-ylmethyl)benzonitrile (**17**)

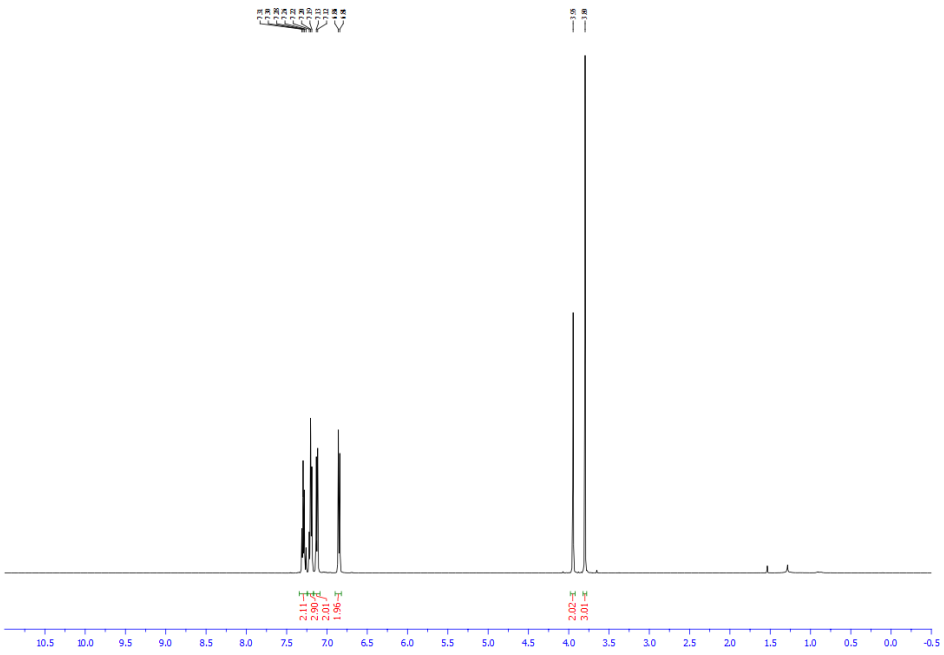

**Figure A1.15.** $^{1}H$ NMR ($CDCl_3$, 500 MHz) spectrum of 1-benzyl-4-methoxybenzene (**18**)

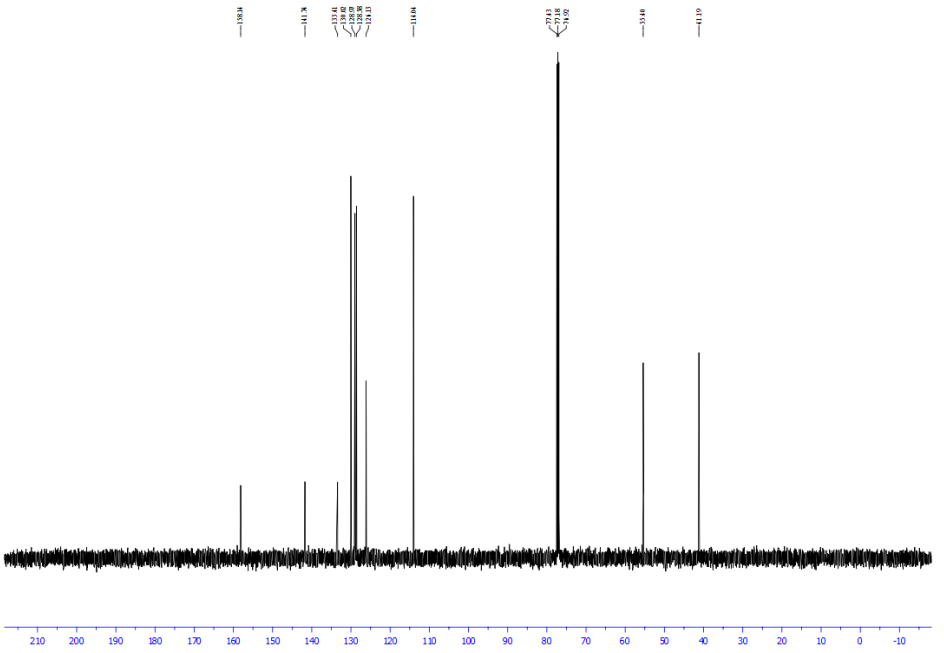

**Figure A1.16.** $^{13}C$ NMR ($CDCl_3$, 125.8 MHz) spectrum of 1-benzyl-4-methoxybenzene (**18**)

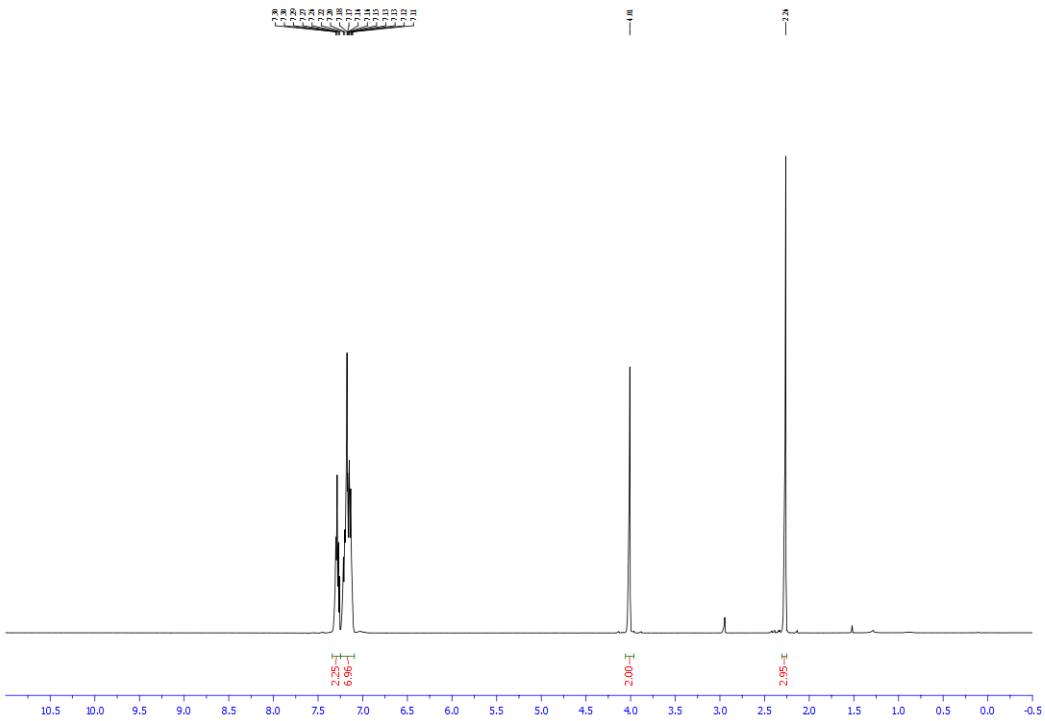

**Figure A1.17.** $^{1}$H NMR ($CDCl_3$, 500 MHz) spectrum of 1-benzyl-2-methylbenzene (**19**)

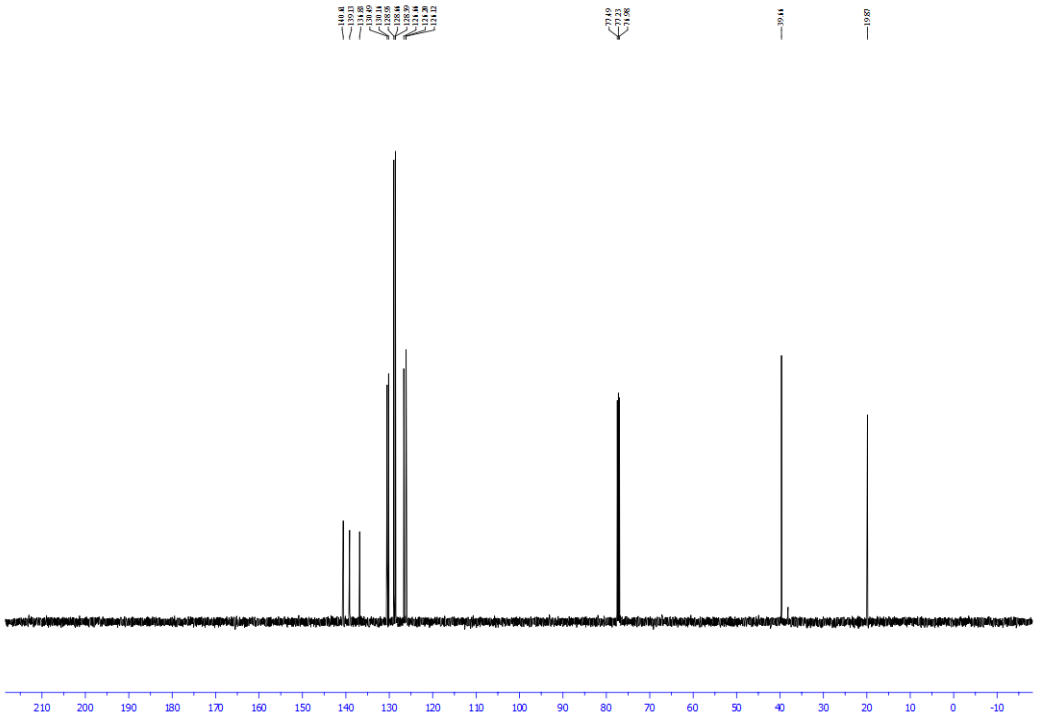

**Figure A1.18.** $^{13}$C NMR ($CDCl_3$, 125.8 MHz) spectrum of 1-benzyl-2-methylbenzene (**19**)

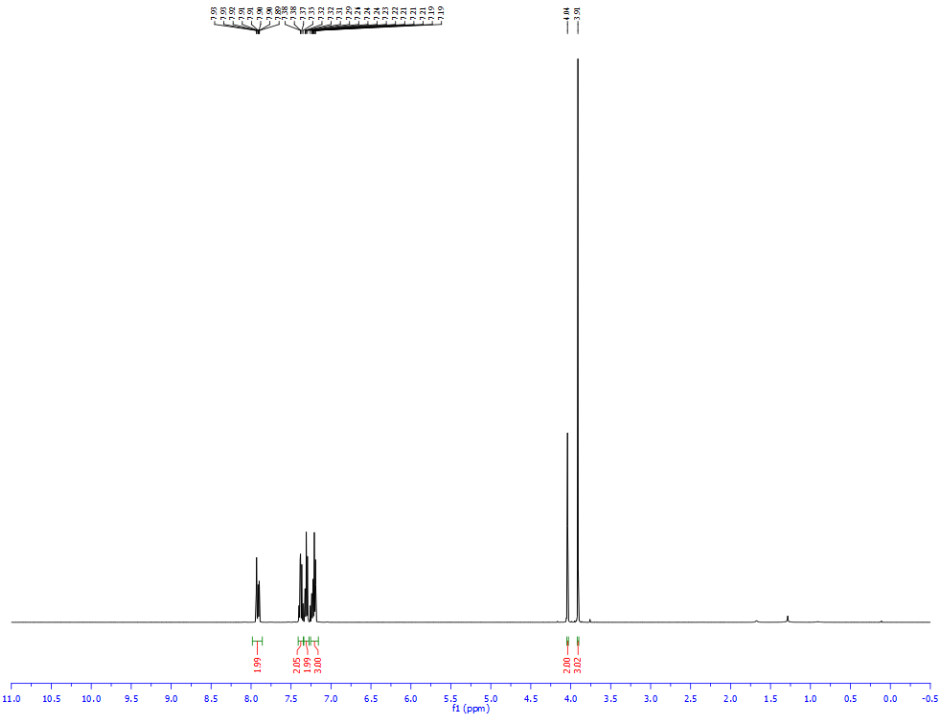

**Figure A1.19.** $^{1}$H NMR ($CDCl_3$, 500 MHz) spectrum of methyl 3-benzylbenzoate (**20**)

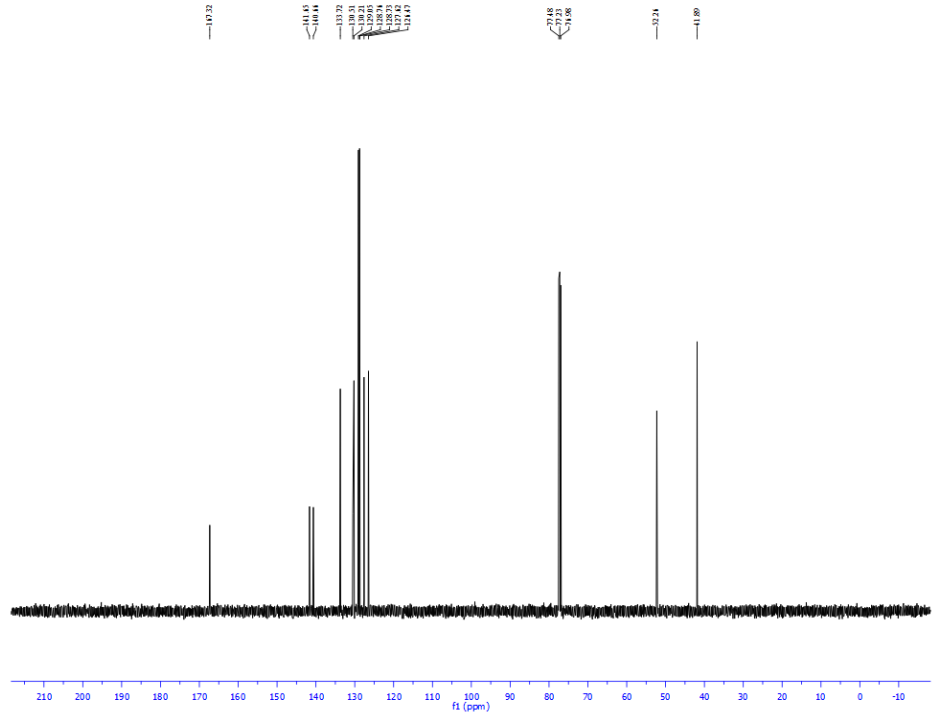

**Figure A1.20.** $^{13}$C NMR ($CDCl_3$, 125.8 MHz) spectrum of methyl 3-benzylbenzoate (**20**)

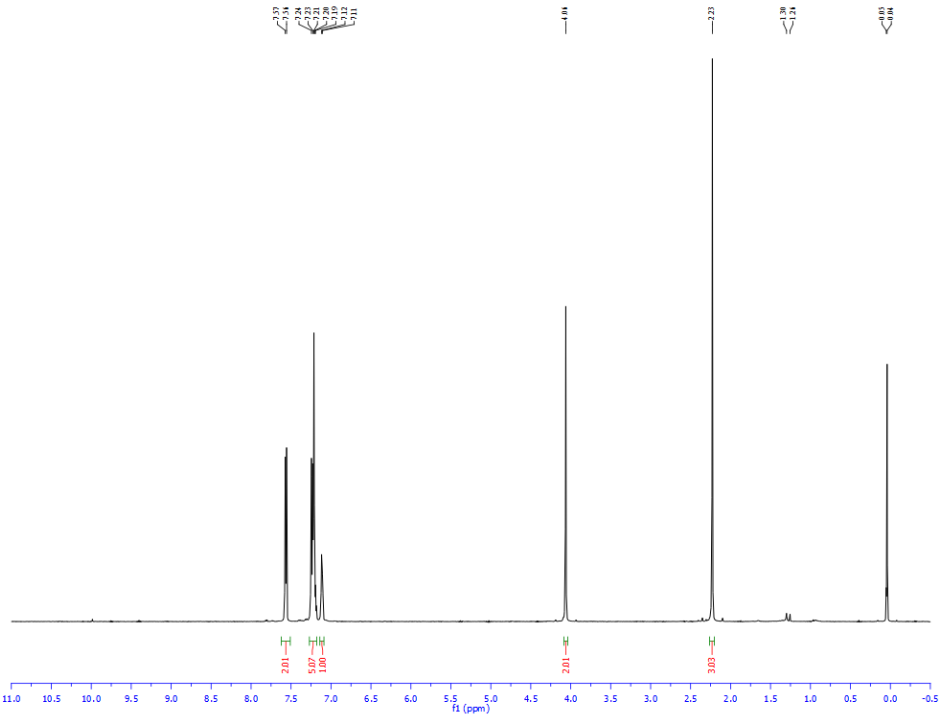

**Figure A1.21.** $^{1}$H NMR ($CDCl_3$, 500 MHz) spectrum of 1-benzyl-4-(trifluoromethyl)benzene (**21**)

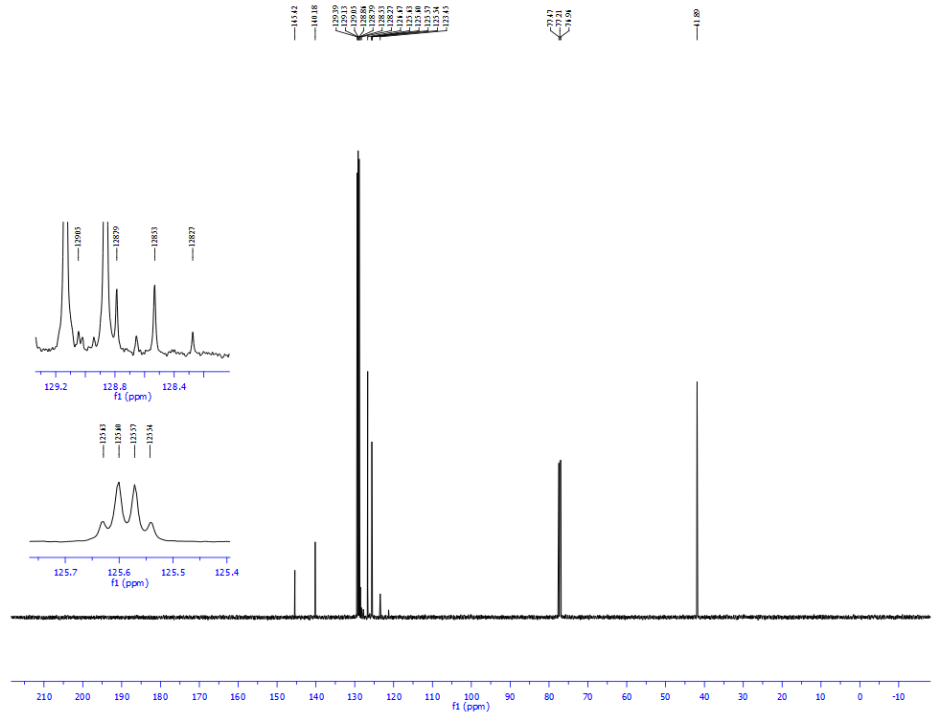

**Figure A1.22.** $^{13}$C NMR ($CDCl_3$, 125.8 MHz) spectrum of 1-benzyl-4-(trifluoromethyl)benzene (**21**)

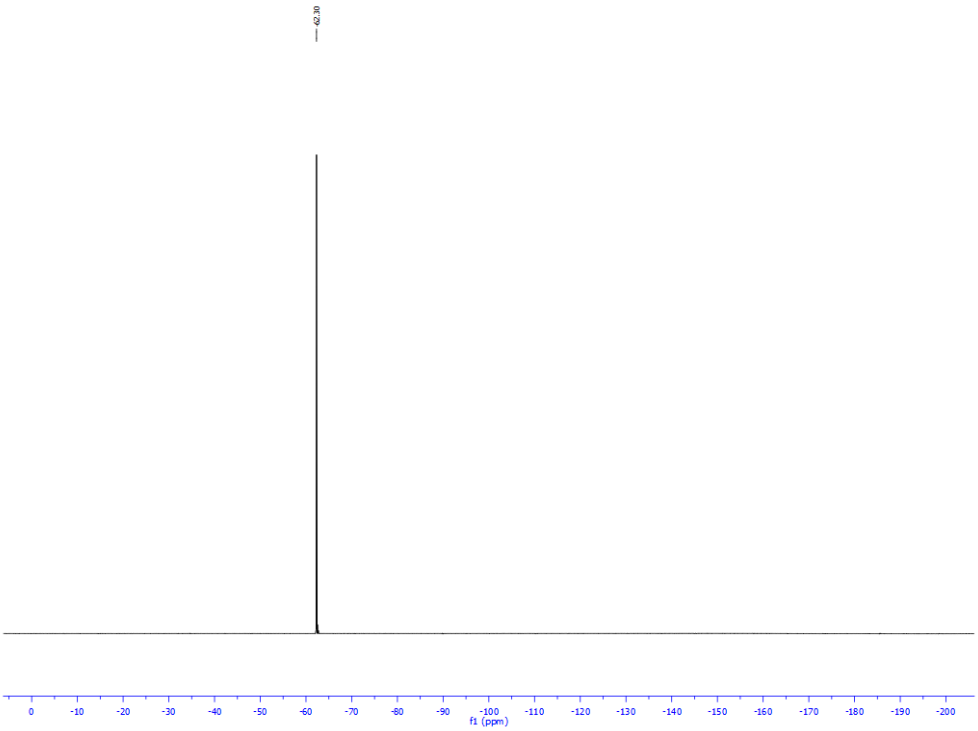


**Figure A1.23.** $^{19}F$ NMR ($CDCl_3$, 470.8 MHz) spectrum of 1-benzyl-4-(trifluoromethyl)benzene (**21**)

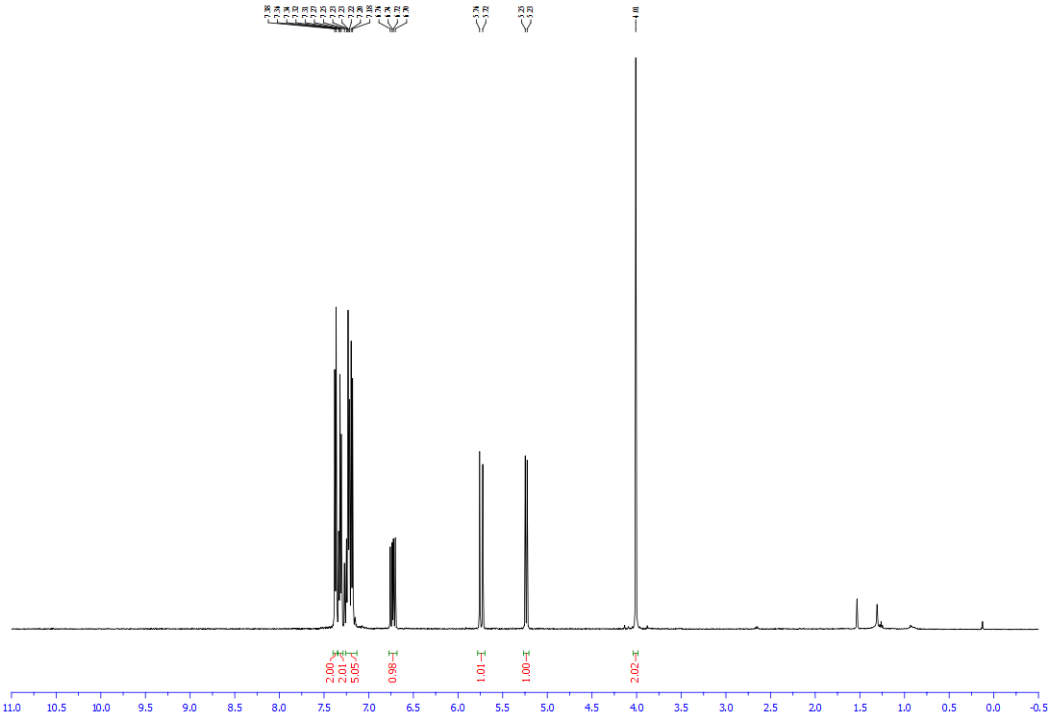


**Figure A1.24.** $^{1}H$ NMR ($CDCl_3$, 500 MHz) spectrum of 1-benzyl-4-vinylbenzene (**22**)

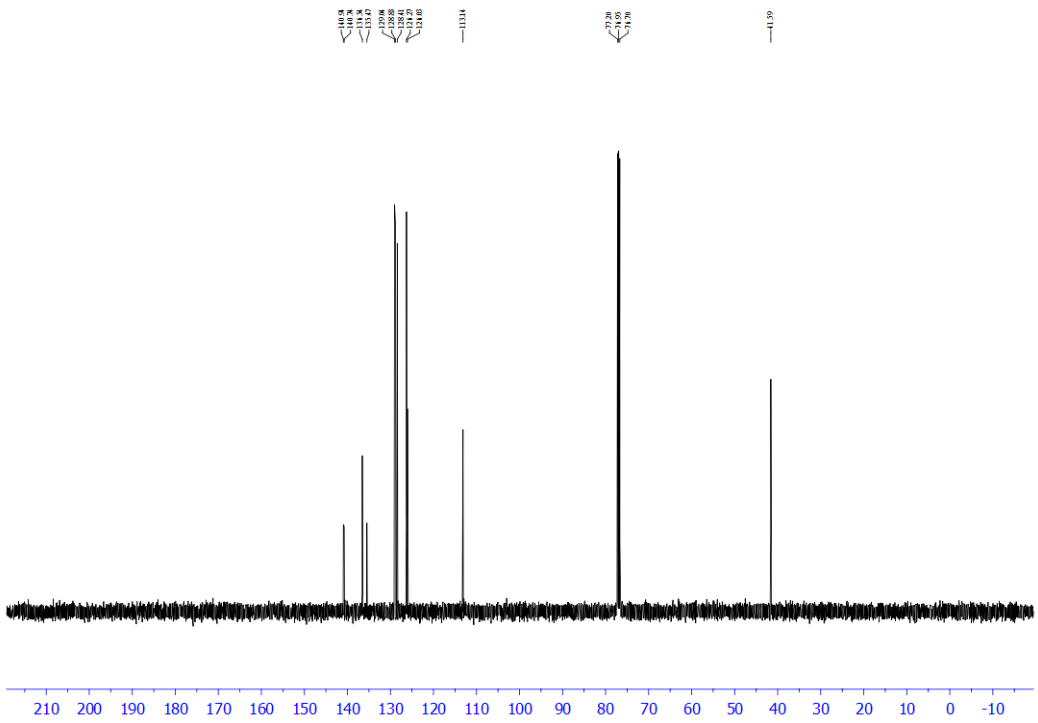

**Figure A1.25.** $^{13}C$ NMR ($CDCl_3$, 125.8 MHz) spectrum of 1-benzyl-4-vinylbenzene (**22**)

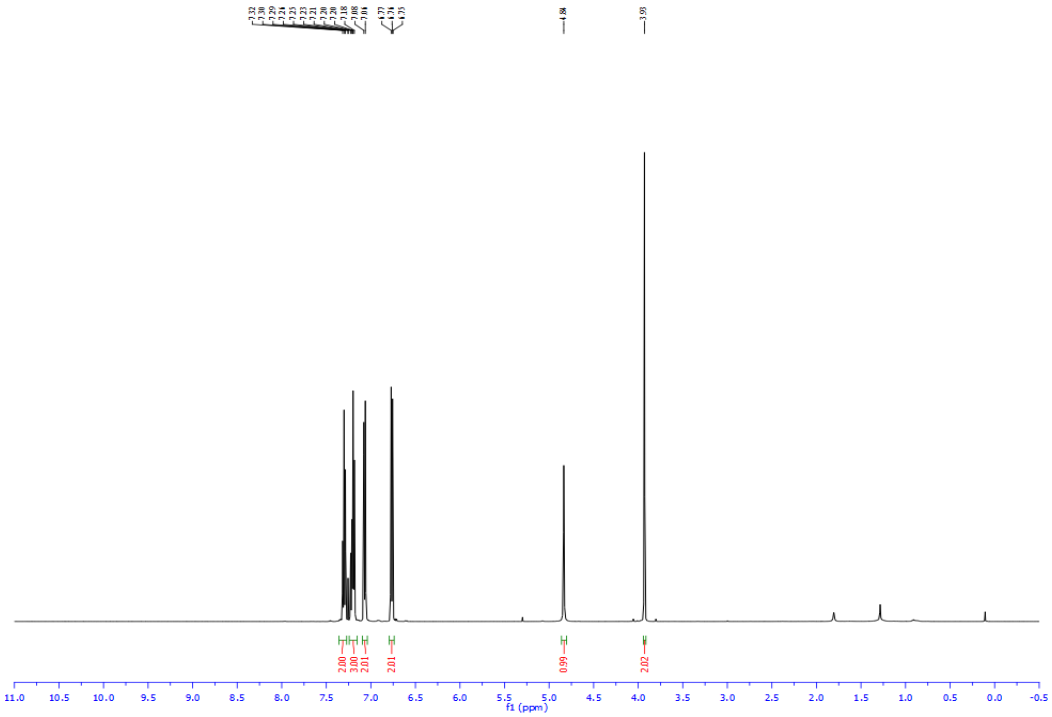

**Figure A1.26.** $^{1}H$ NMR ($CDCl_3$, 500 MHz) spectrum of 4-benzylphenol (**23**)

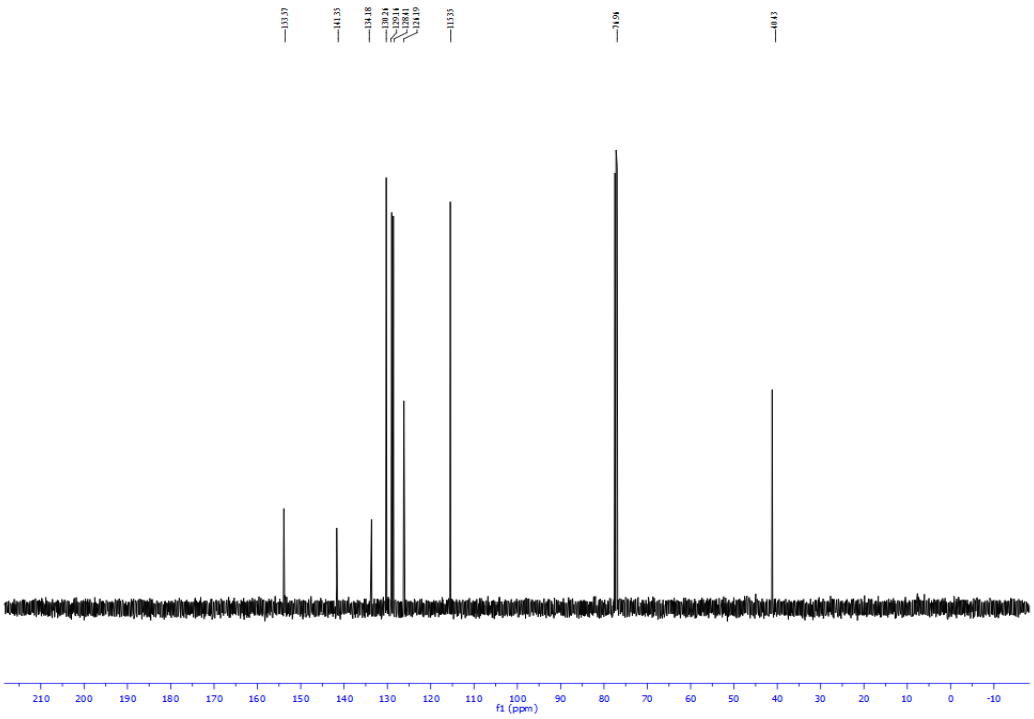

**Figure A1.27.** $^{13}C$ NMR ($CDCl_3$, 125.8 MHz) spectrum of 4-benzylphenol (**23**)

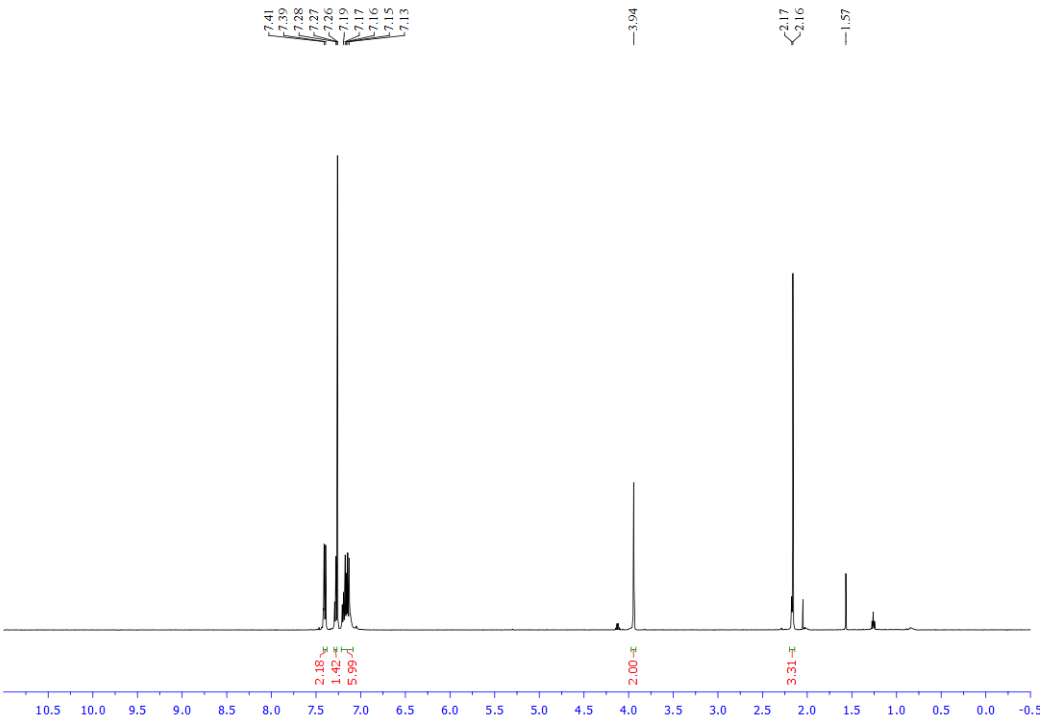

**Figure A1.28.** $^{1}H$ NMR ($CDCl_3$, 500 MHz) spectrum of N-(4-benzylphenyl)acetamide (**24**)

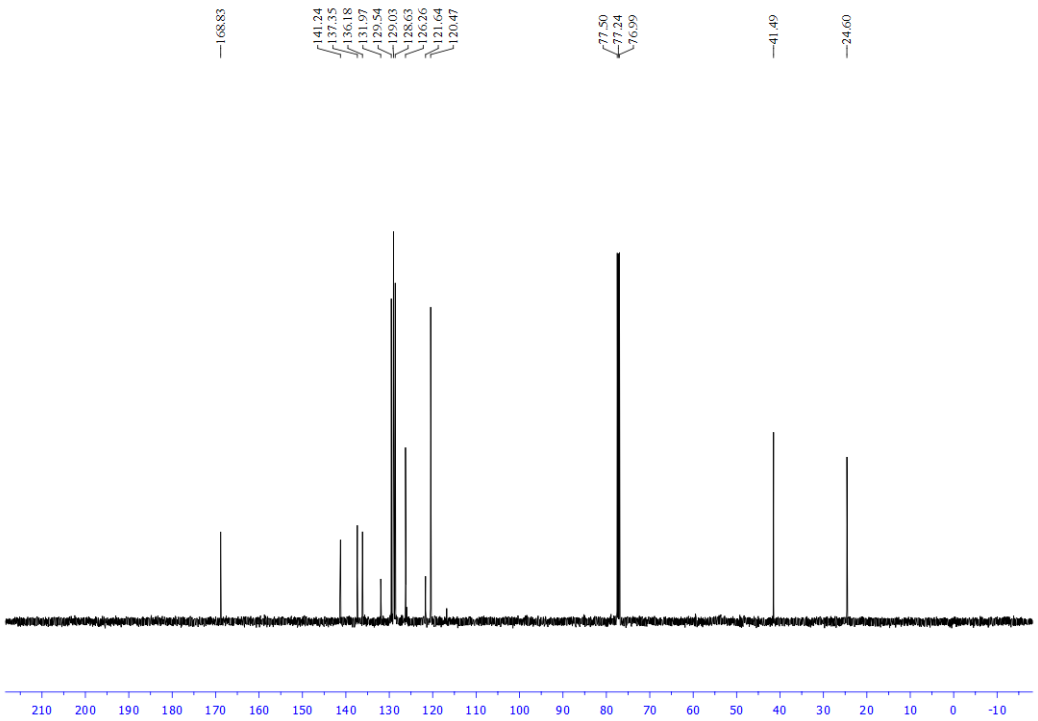


**Figure A1.29.** $^{13}C$ NMR ($CDCl_3$, 125.8 MHz) spectrum of N-(4-benzylphenyl)acetamide (**24**)

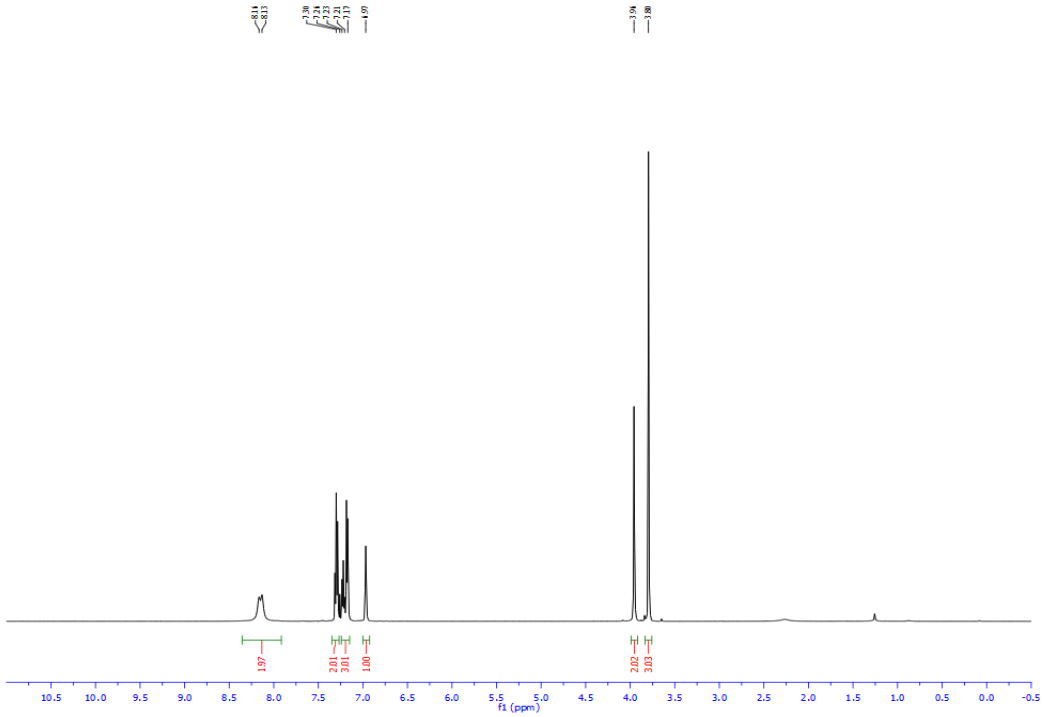


**Figure A1.30.** $^{1}H$ NMR ($CDCl_3$, 500 MHz) spectrum of 3-benzyl-5-methoxypyridine (**25**)

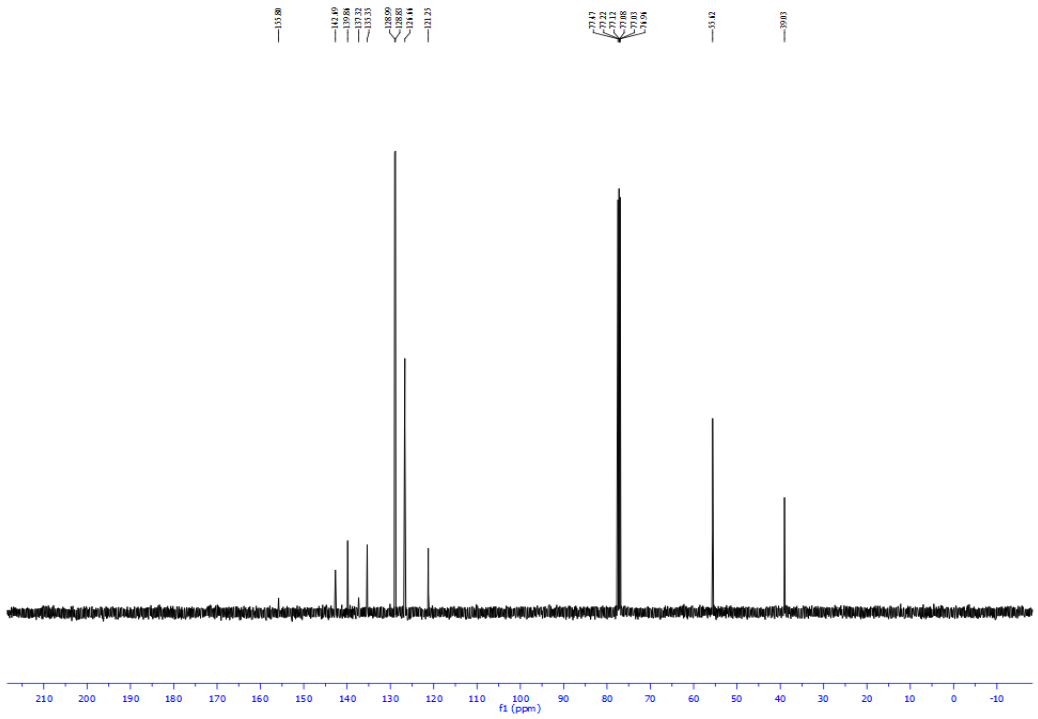

**Figure A1.31.** $^{13}C$ NMR ($CDCl_3$, 125.8 MHz) spectrum of 3-benzyl-5-methoxypyridine (**25**)

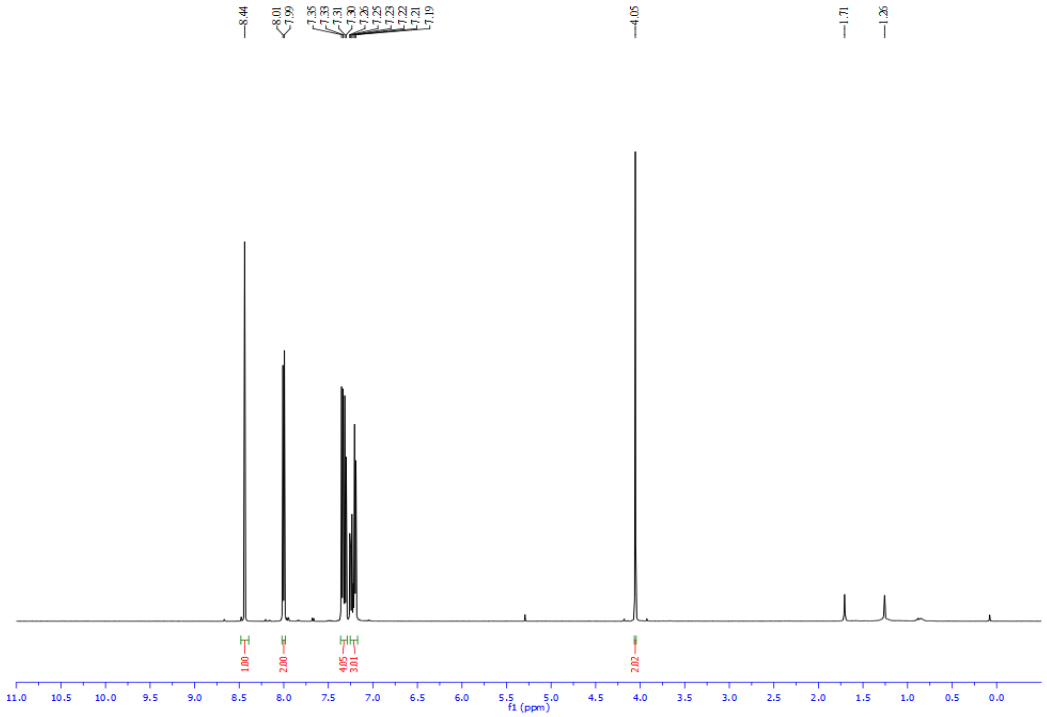

**Figure A1.32.** $^{1}H$ NMR ($CDCl_3$, 500 MHz) spectrum of 2-(4-benzylphenyl)-1,3,4-oxadiazole (**26**)

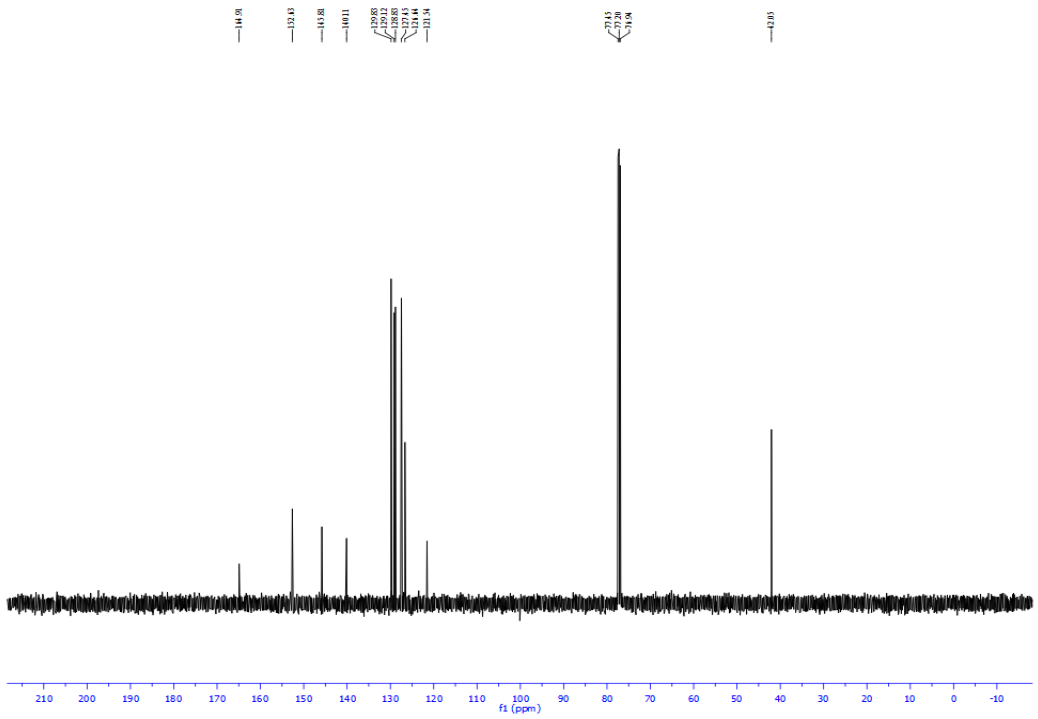

**Figure A1.33.** $^{13}C$ NMR ($CDCl_3$, 125.8 MHz) spectrum of 2-(4-benzylphenyl)-1,3,4-oxadiazole (**26**)

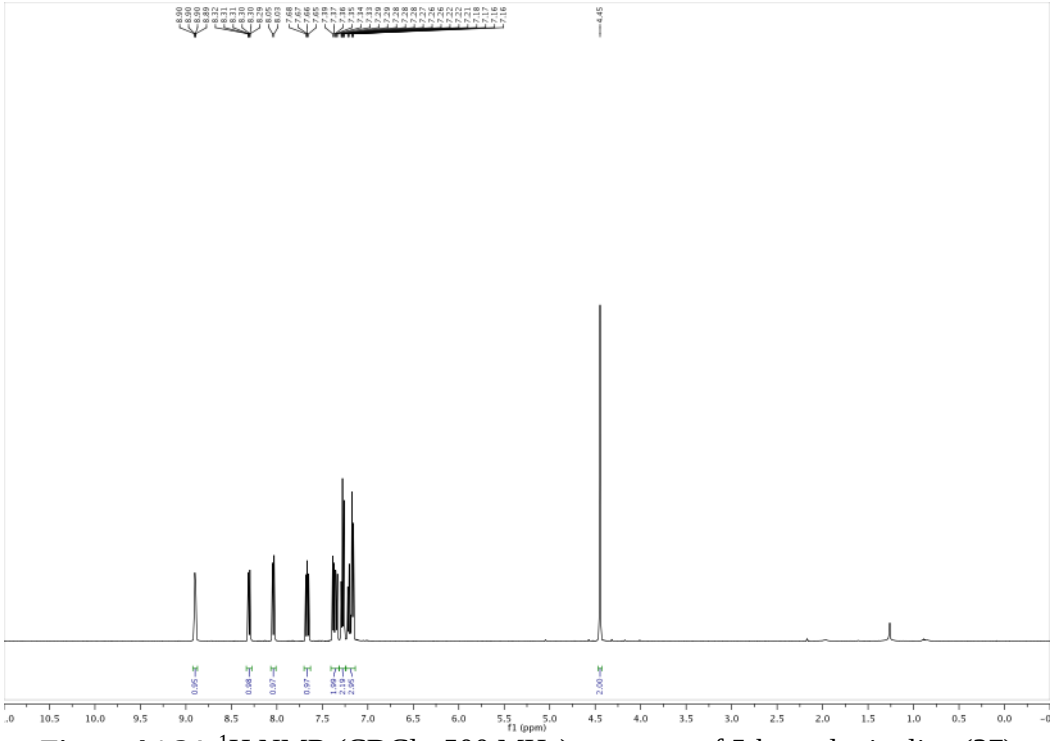

**Figure A1.34.** $^{1}H$ NMR ($CDCl_3$, 500 MHz) spectrum of 5-benzylquinoline (**27**)

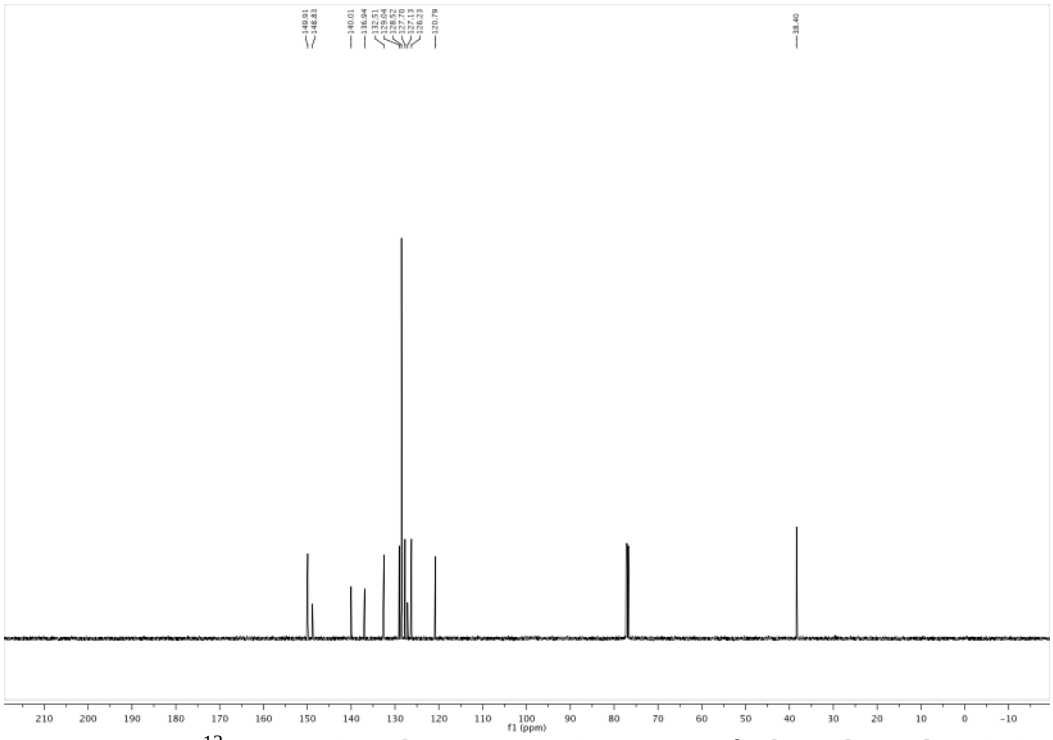

**Figure A1.35.** $^{13}C$ NMR ($CDCl_3$, 125.8 MHz) spectrum of 5-benzylquinoline (**27)**

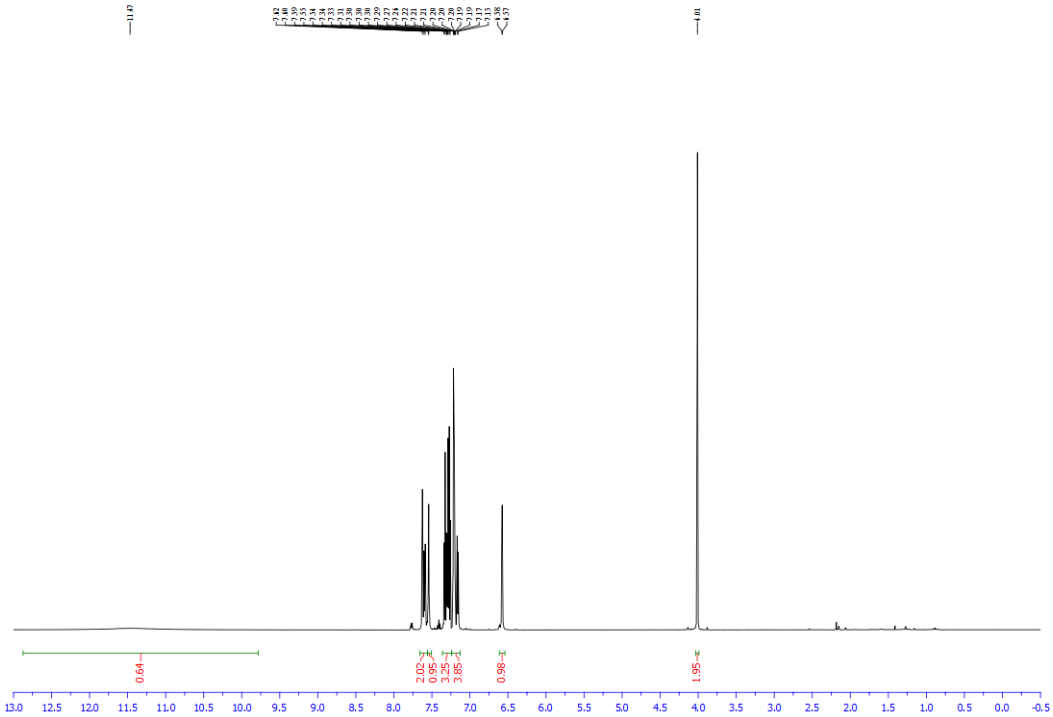

**Figure A1.36.** $^{1}H$ NMR ($CDCl_3$, 500 MHz) spectrum of 5-(3-benzylphenyl)-1H-pyrazole (**28)**

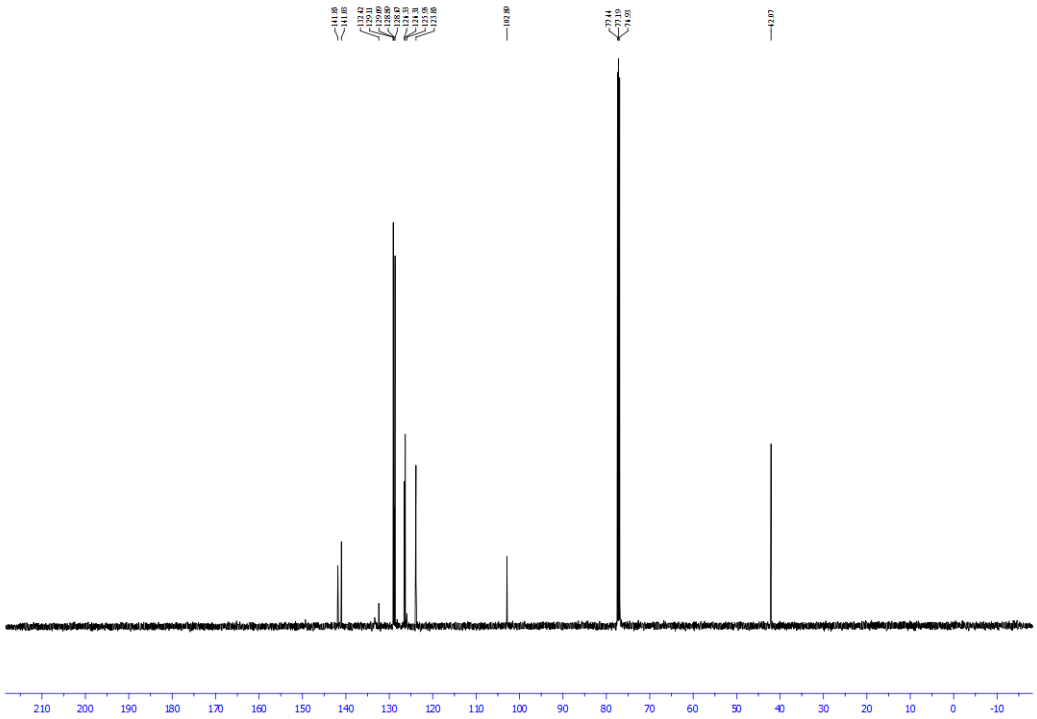

**Figure A1.37.** $^{13}C$ NMR ($CDCl_3$, 125.8 MHz) spectrum of 5-(3-benzylphenyl)-1H-pyrazole (**28)**

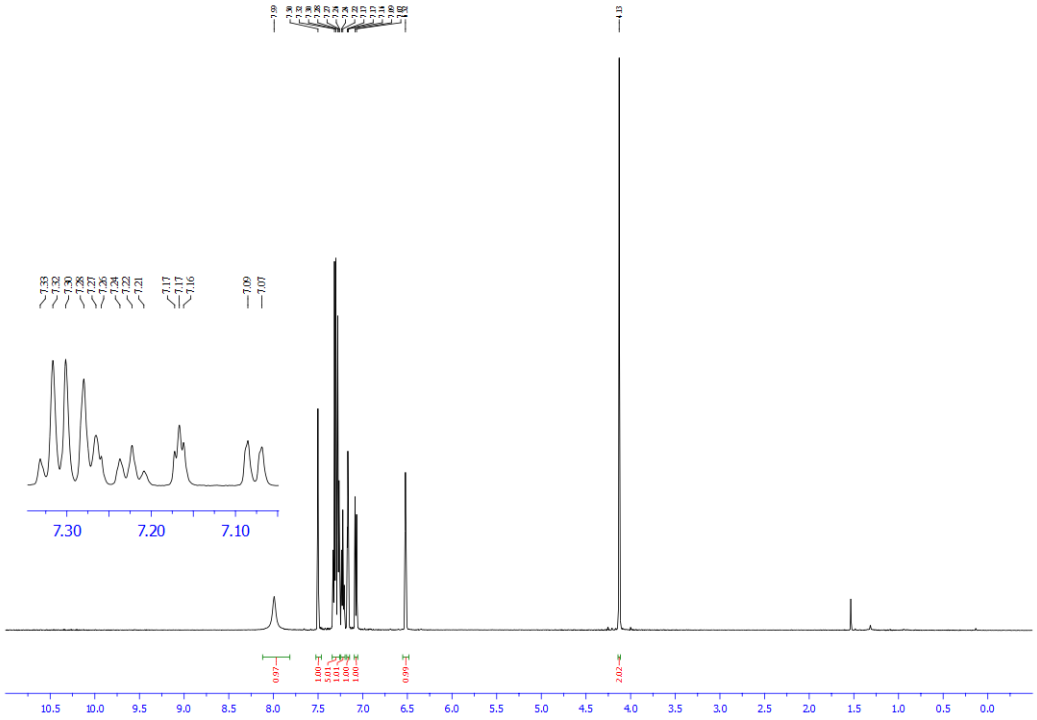

**Figure A1.38.** $^{1}H$ NMR ($CDCl_3$, 500 MHz) spectrum of 5-benzyl-1H-indole (**29)**

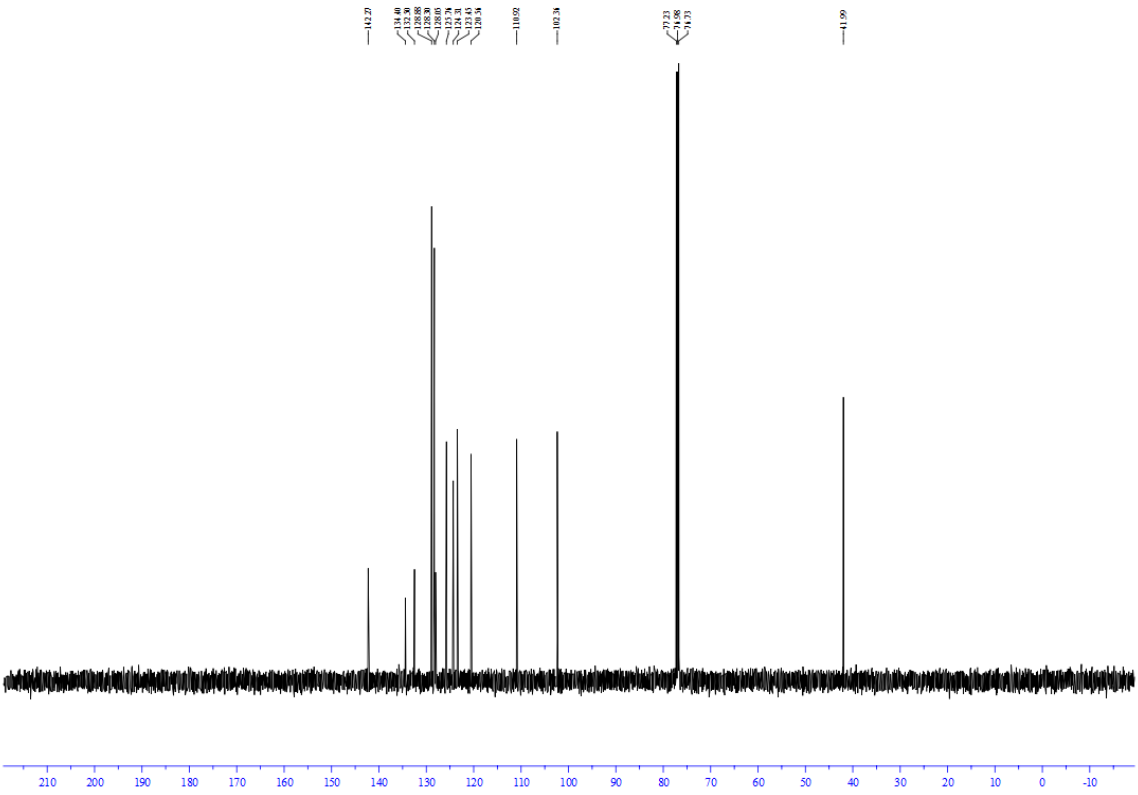

**Figure A1.39.** $^{13}C$ NMR ($CDCl_3$, 125.8 MHz) spectrum of 5-benzyl-1H-indole (**29)**

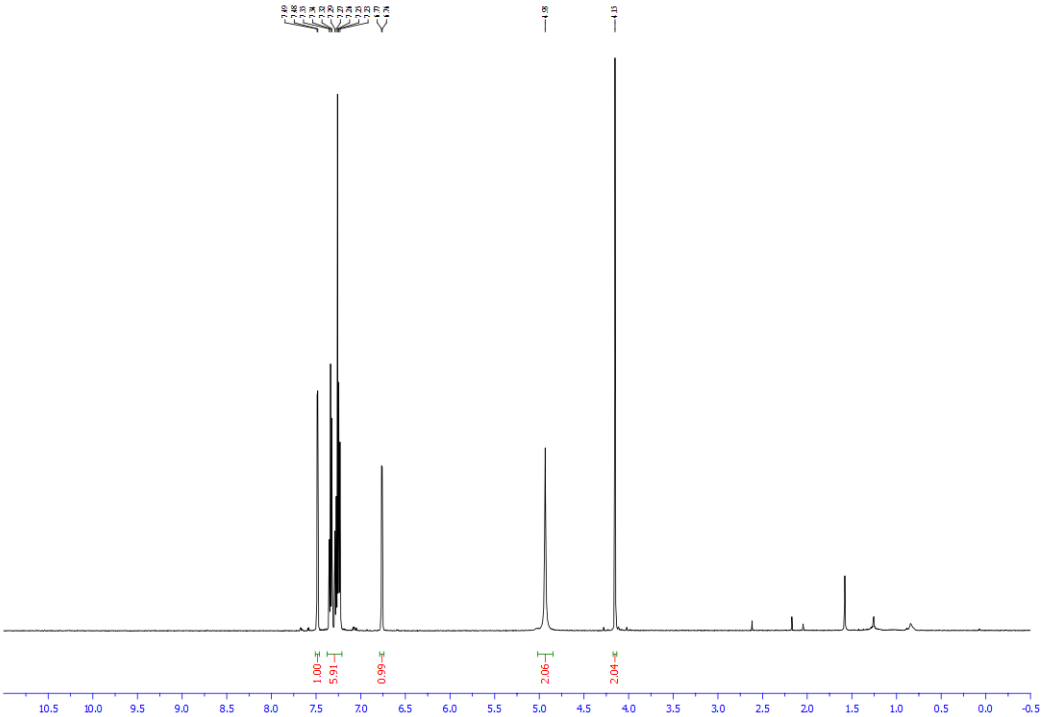

**Figure A1.40.** $^{1}H$ NMR ($CDCl_3$, 500 MHz) spectrum of 5-benzylthiophene-2-sulfonamide (**30)**

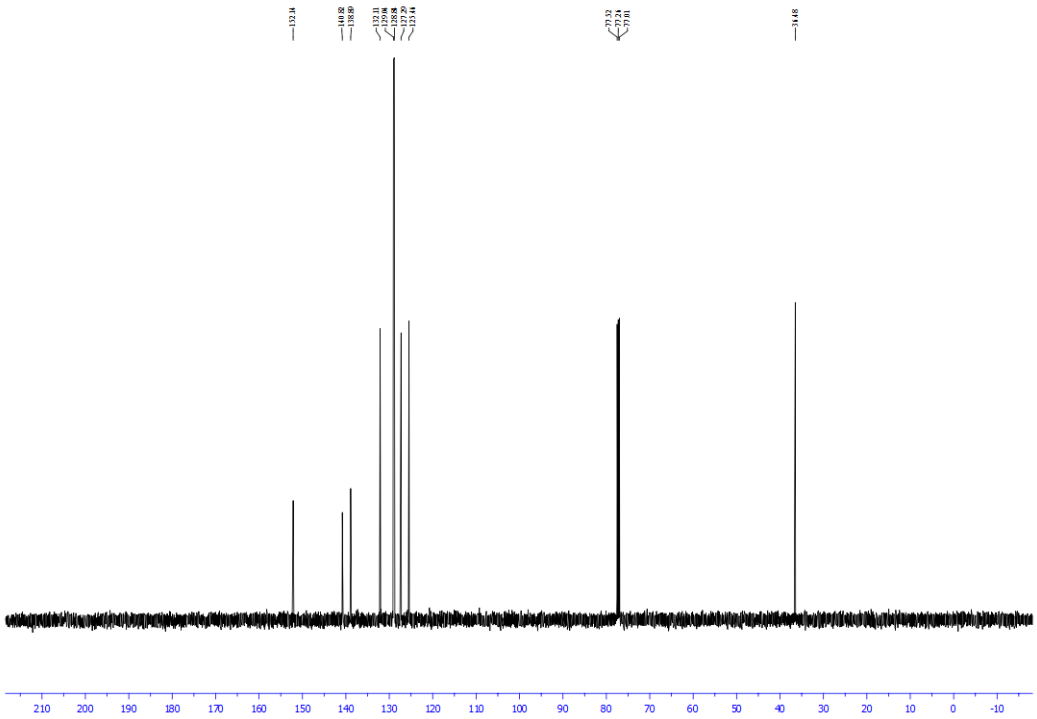

**Figure A1.41.** $^{13}C$ NMR ($CDCl_3$,125.8 MHz) spectrum of 5-benzylthiophene-2-sulfonamide (**30)**

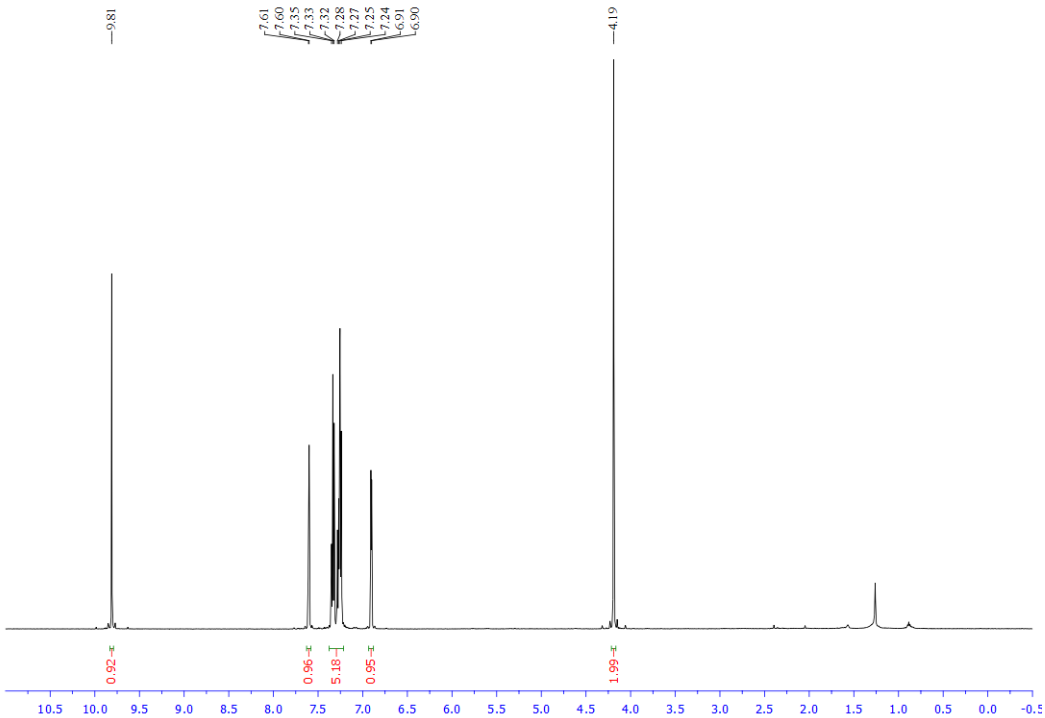

**Figure A1.42.** $^{1}H$ NMR ($CDCl_3$, 500 MHz) spectrum of 5-benzylthiophene-2-carbaldehyde (**31)**

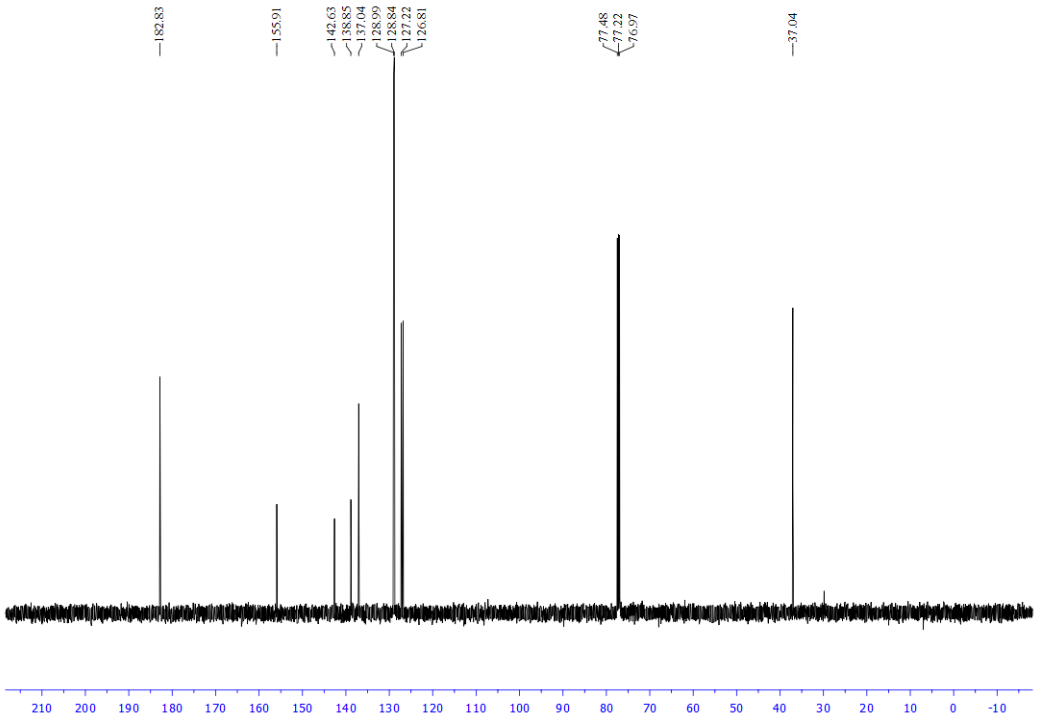


**Figure A1.43.** $^{13}C$ NMR ($CDCl_3$,125.8 MHz) spectrum of 5-benzylthiophene-2-carbaldehyde (**31)**

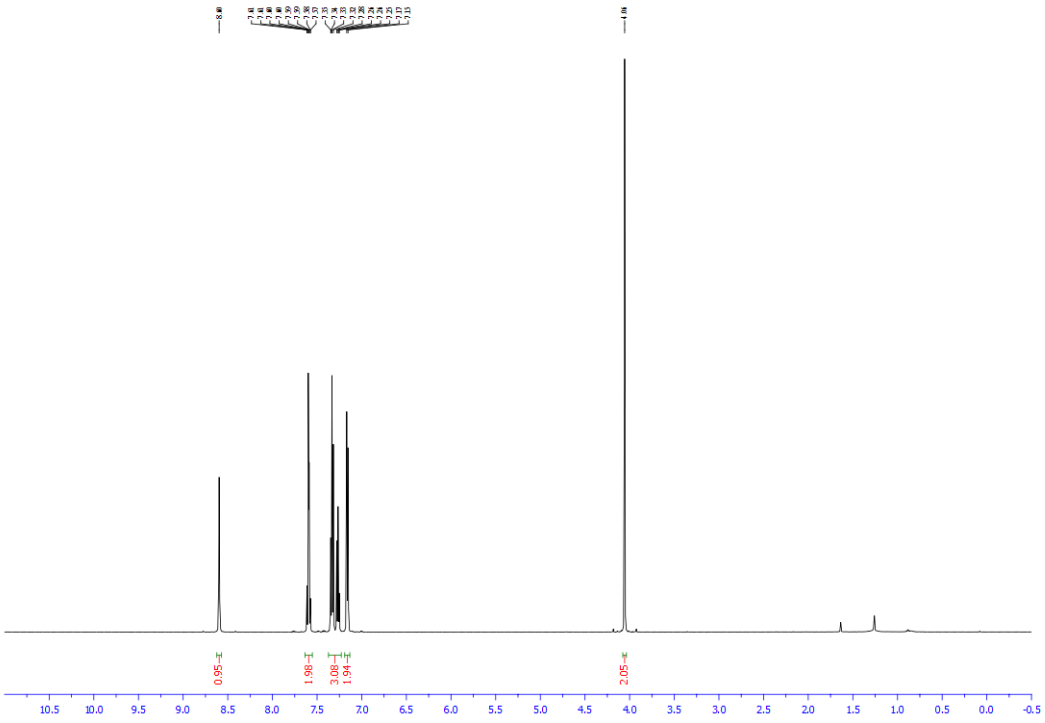


**Figure A1.44.** $^{1}H$ NMR ($CDCl_3$, 500 MHz) spectrum of 5-benzylpicolinonitrile (**32)**

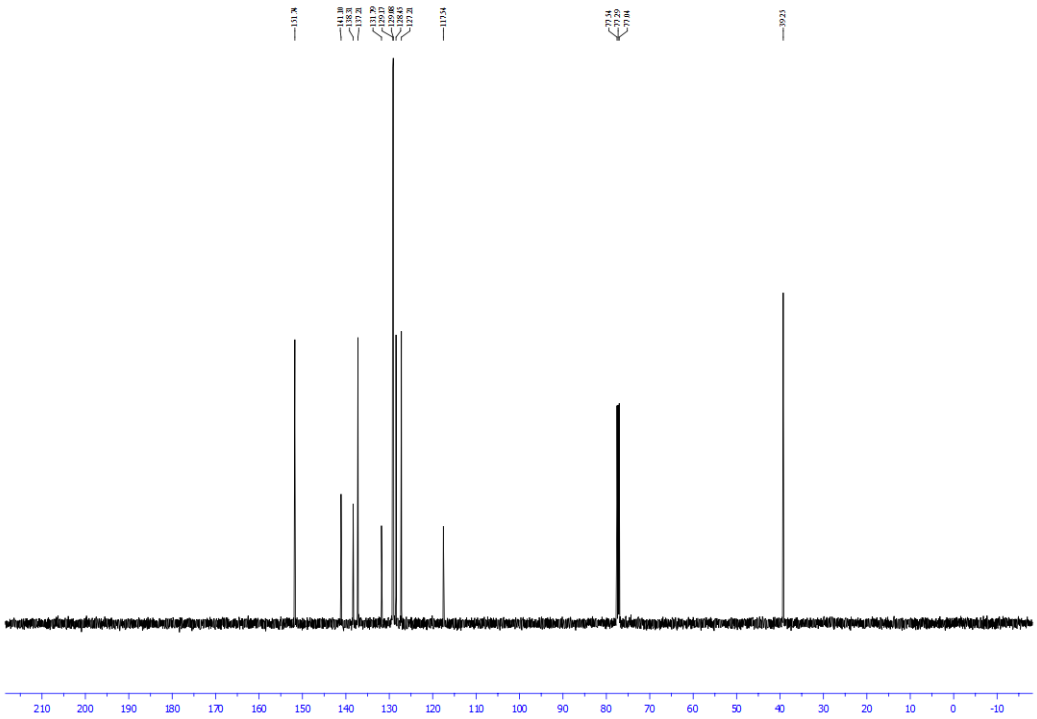

**Figure A1.45.** $^{13}C$ NMR ($CDCl_3$, 125.8 MHz) spectrum of 5-benzylpicolinonitrile (**32)**

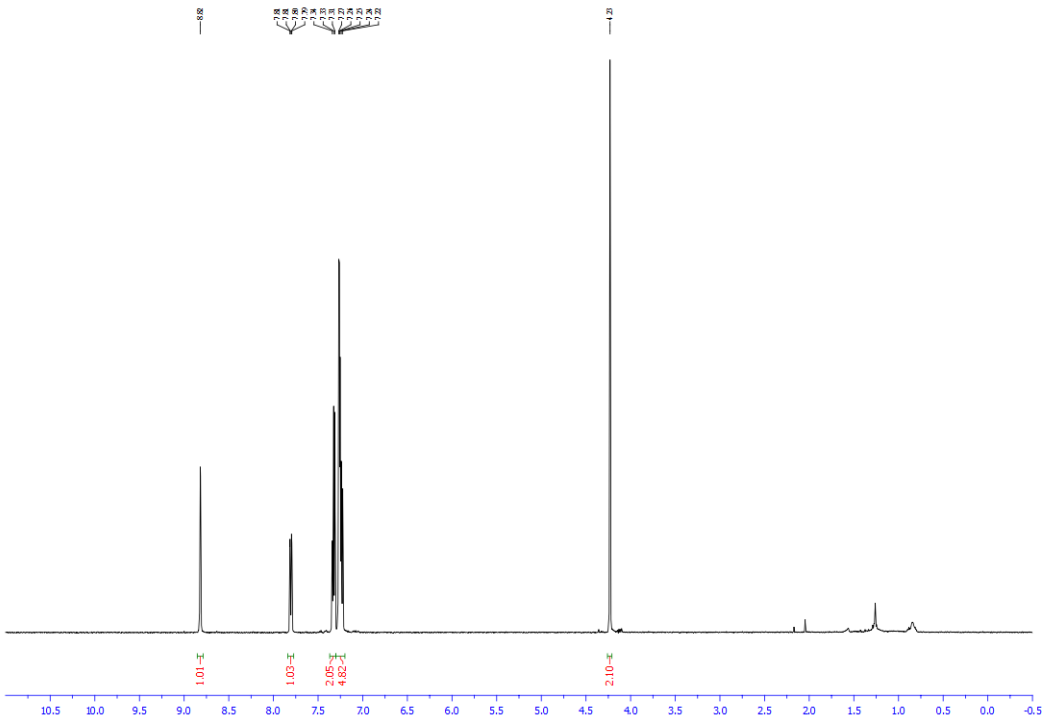

**Figure A1.46.** $^{1}H$ NMR ($CDCl_3$, 500 MHz) spectrum of 2-benzyl-5-(trifluoromethyl)pyridine (**33)**

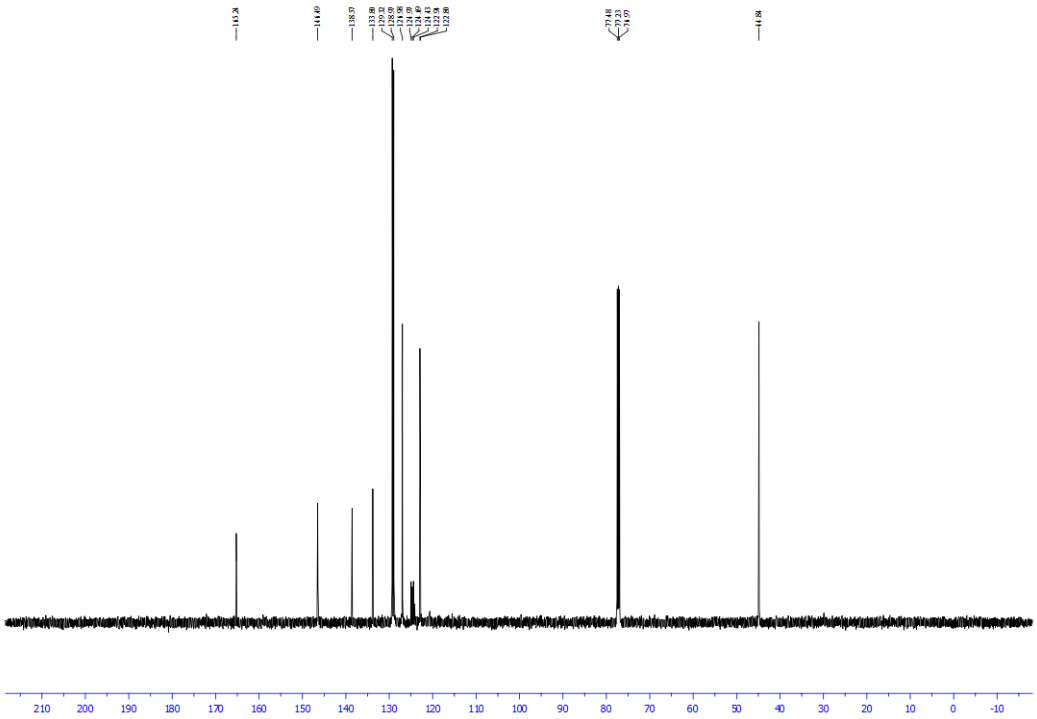

**Figure A1.47.** $^{13}C$ NMR ($CDCl_3$, 125.8 MHz) spectrum of 2-benzyl-5-(trifluoromethyl)pyridine (**33)**

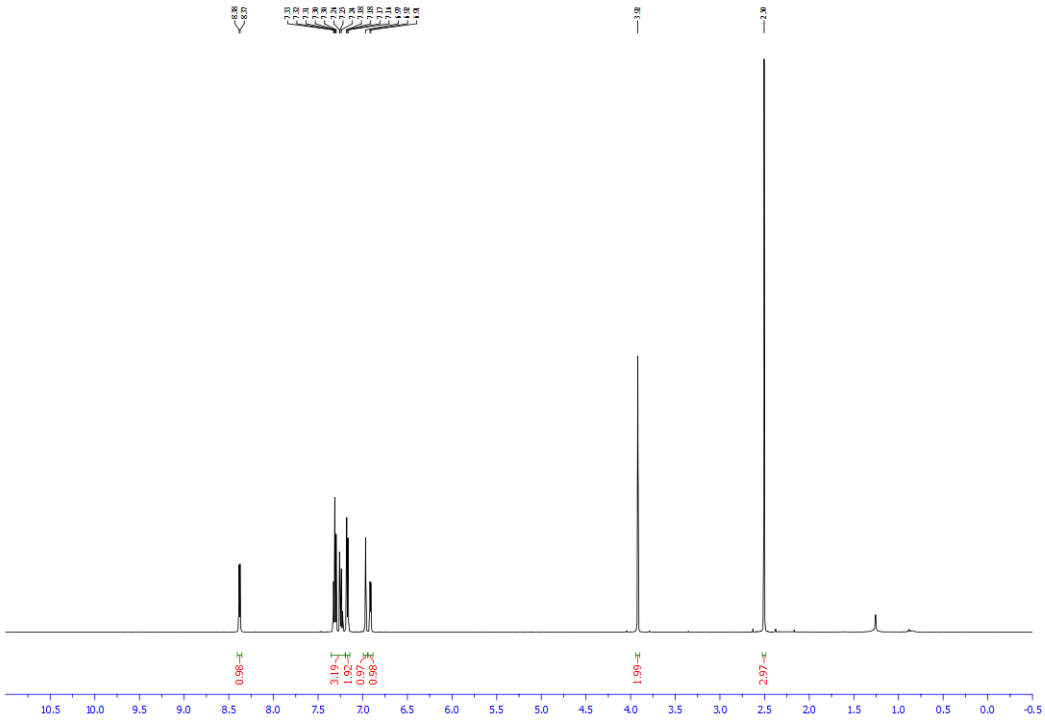

**Figure A1.48.** $^{1}H$ NMR ($CDCl_3$, 500 MHz) spectrum of 4-benzyl-2-methylpyridine (**34)**

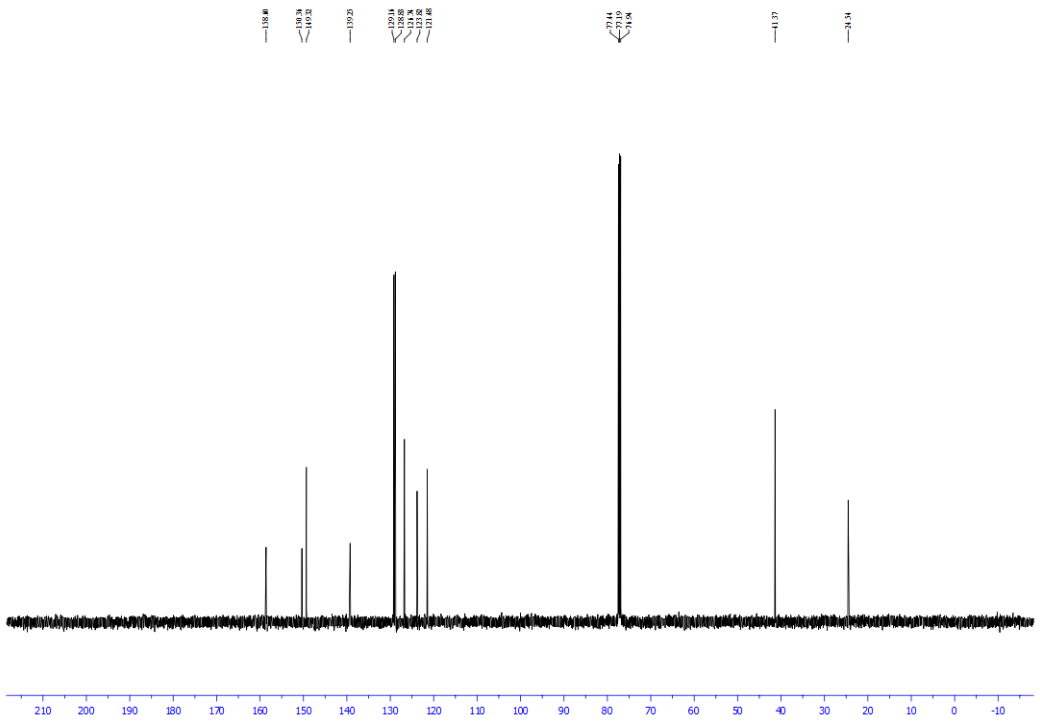

**Figure A1.49.** $^{13}C$ NMR ($CDCl_3$, 125.8 MHz) spectrum of 4-benzyl-2-methylpyridine (**34)**

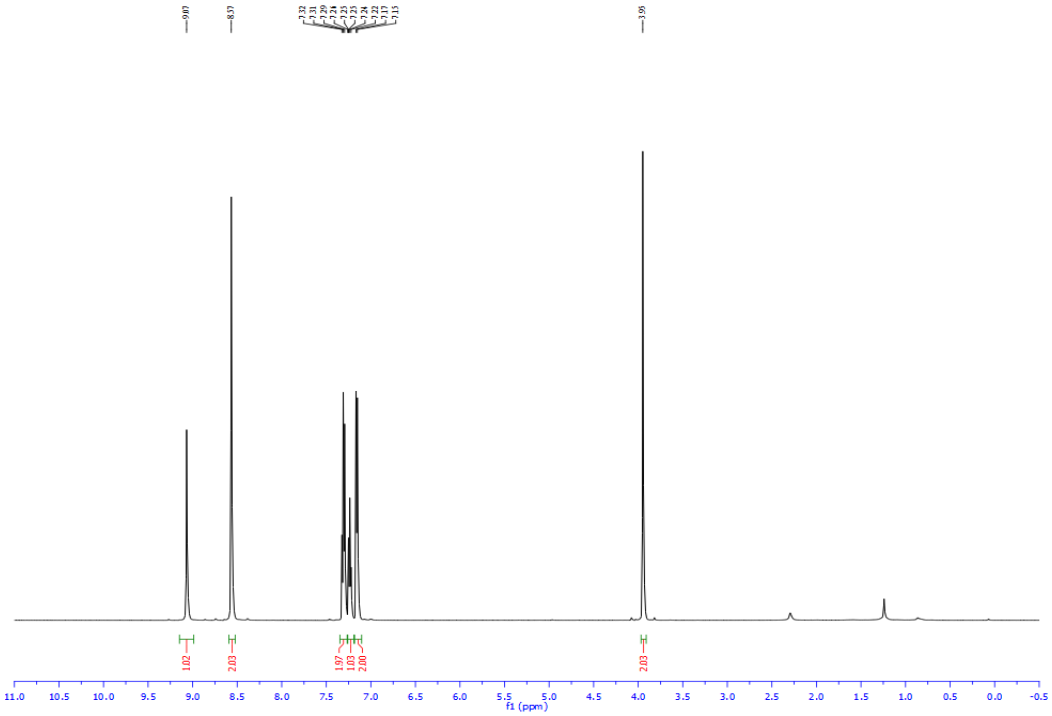

**Figure A1.50.** $^{1}H$ NMR ($CDCl_3$, 500 MHz) spectrum of 5-benzylpyrimidine (**35)**

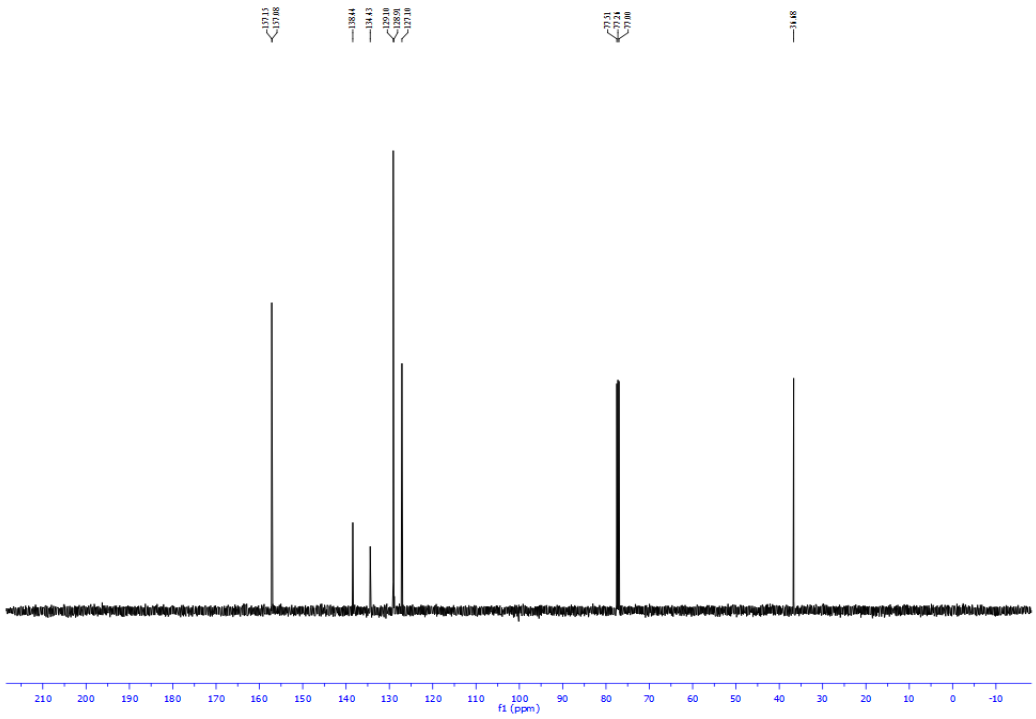

**Figure A1.51.** $^{13}C$ NMR ($CDCl_3$,125.8 MHz) spectrum of 5-benzylpyrimidine (**35)**

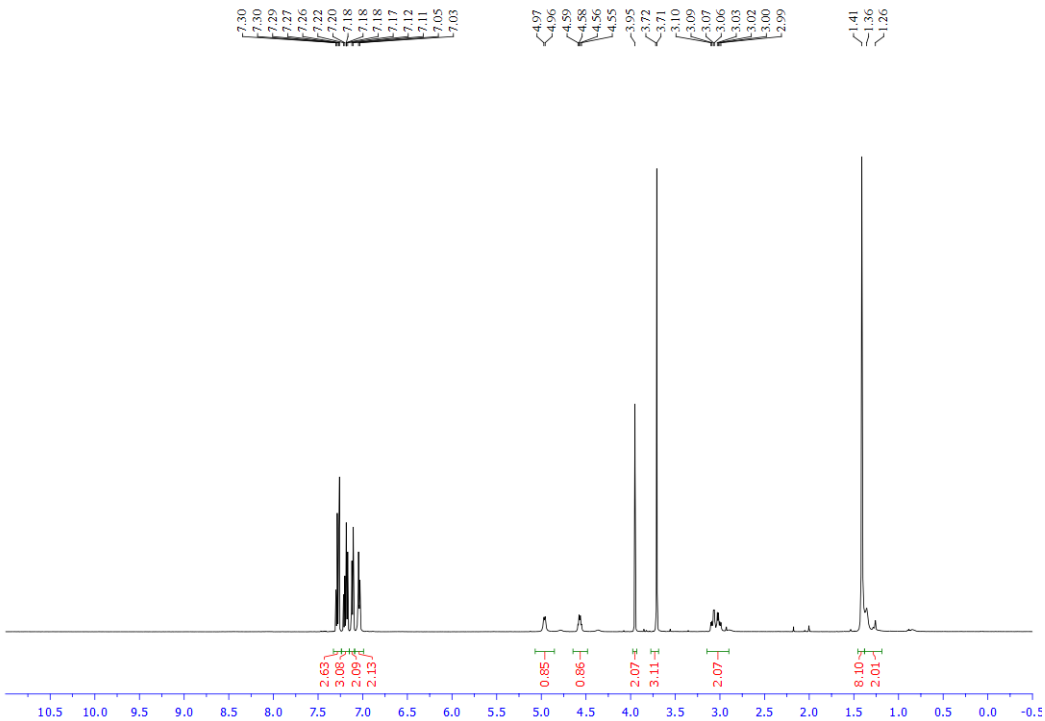

**Figure A1.52.** $^{1}H$ NMR ($CDCl_3$, 500 MHz) spectrum of methyl (S)-3-(4-benzylphenyl)-2-((tert-butoxycarbonyl)amino)propanoate (**36)**

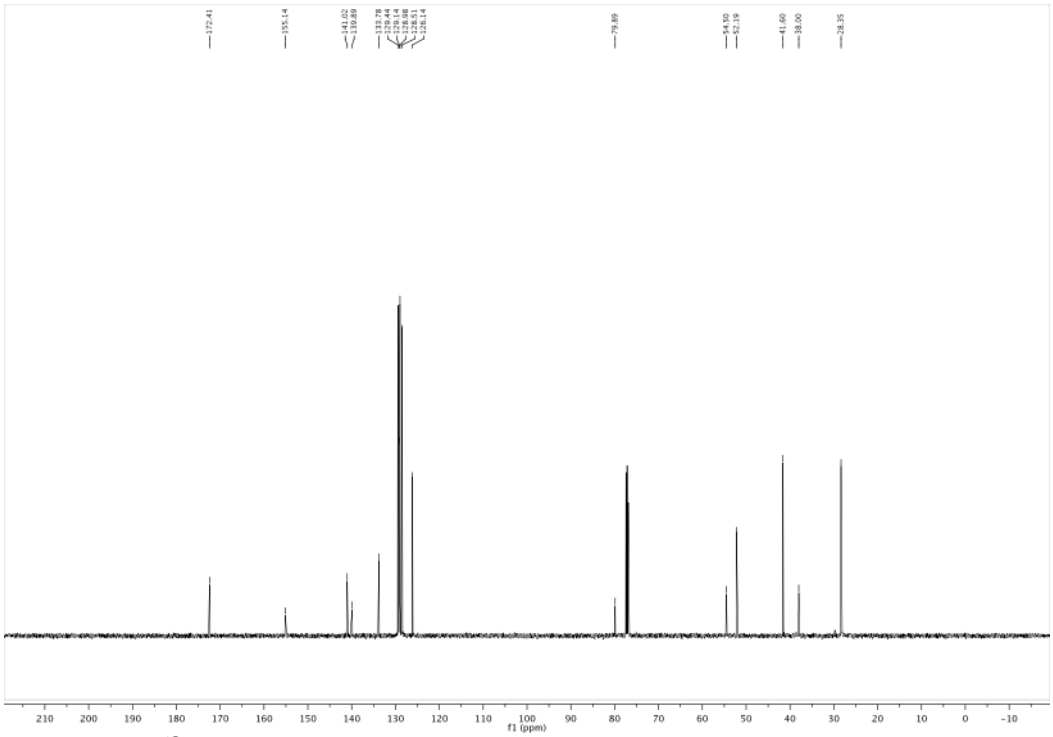

**Figure A1.53.** $^{13}C$ NMR ($CDCl_3$,125.8 MHz) spectrum of methyl (S)-3-(4-benzylphenyl)-2-((tert-butoxycarbonyl)amino)propanoate (**36)**

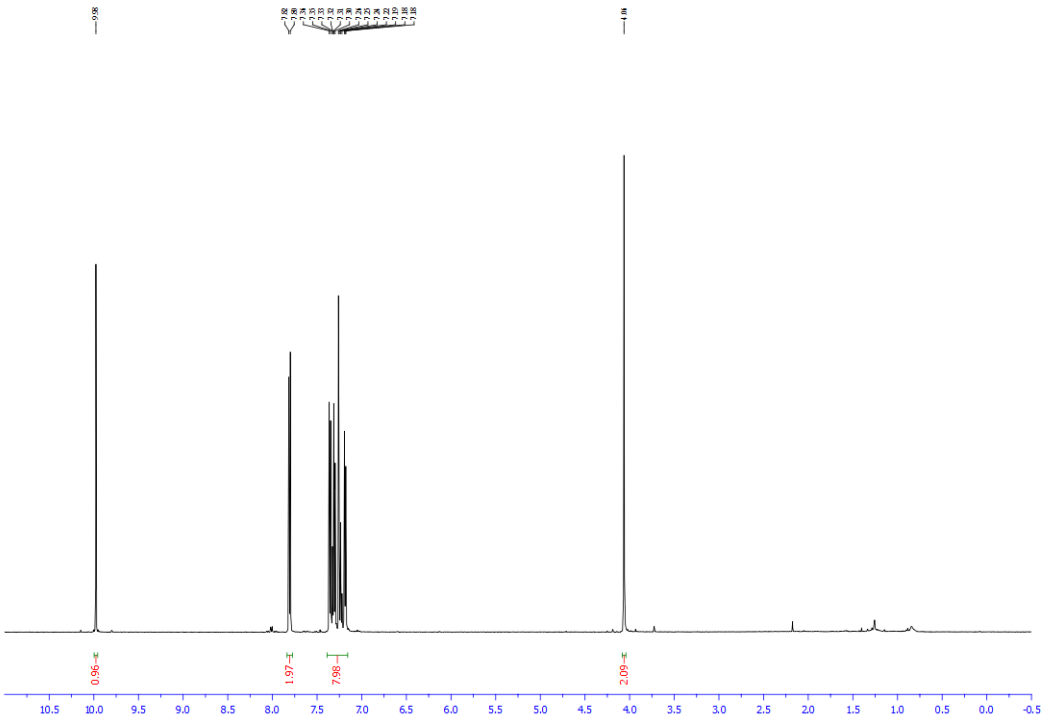

**Figure A1.54.** $^{1}H$ NMR ($CDCl_3$, 500 MHz) spectrum of 4-benzylbenzaldehyde (**37)**

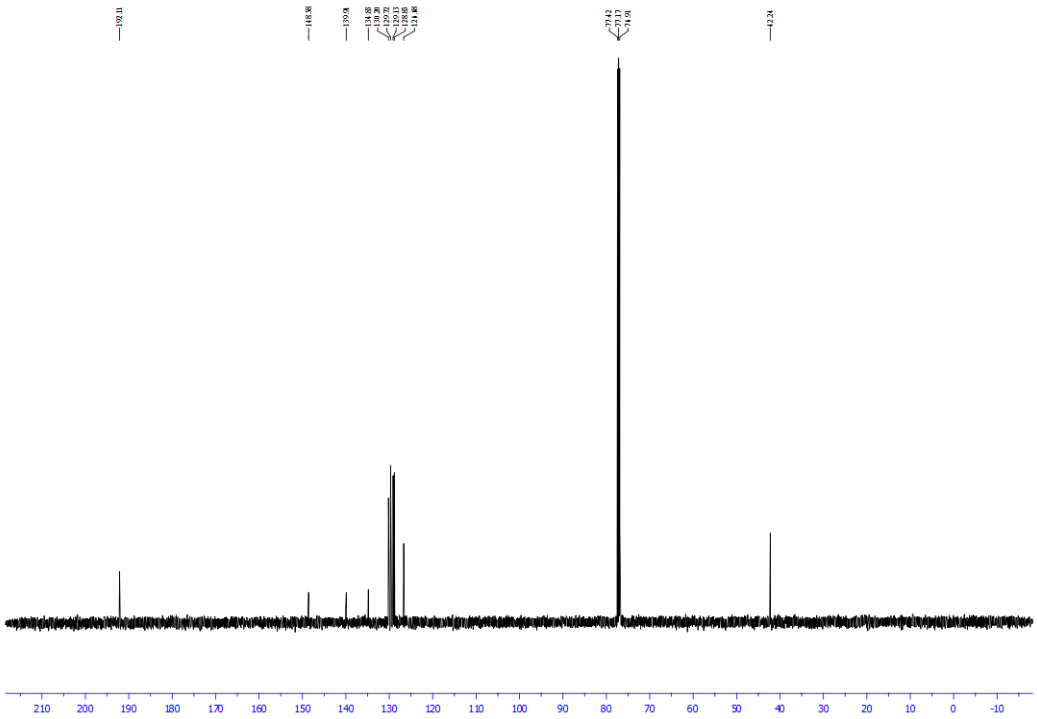

**Figure A1.55.** $^{13}C$ NMR ($CDCl_3$, 125.8 MHz) spectrum of 4-benzylbenzaldehyde (**37)**

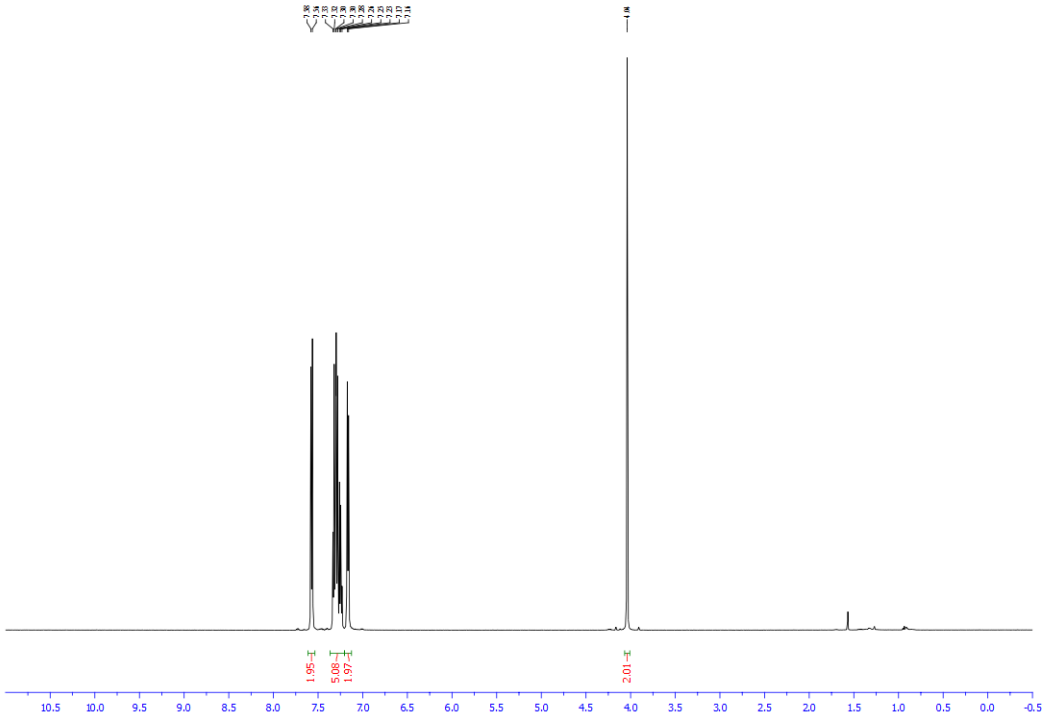

**Figure A1.56:** $^{1}H$ NMR ($CDCl_3$, 500 MHz) spectrum of 4-benzylbenzonitrile (**38**)

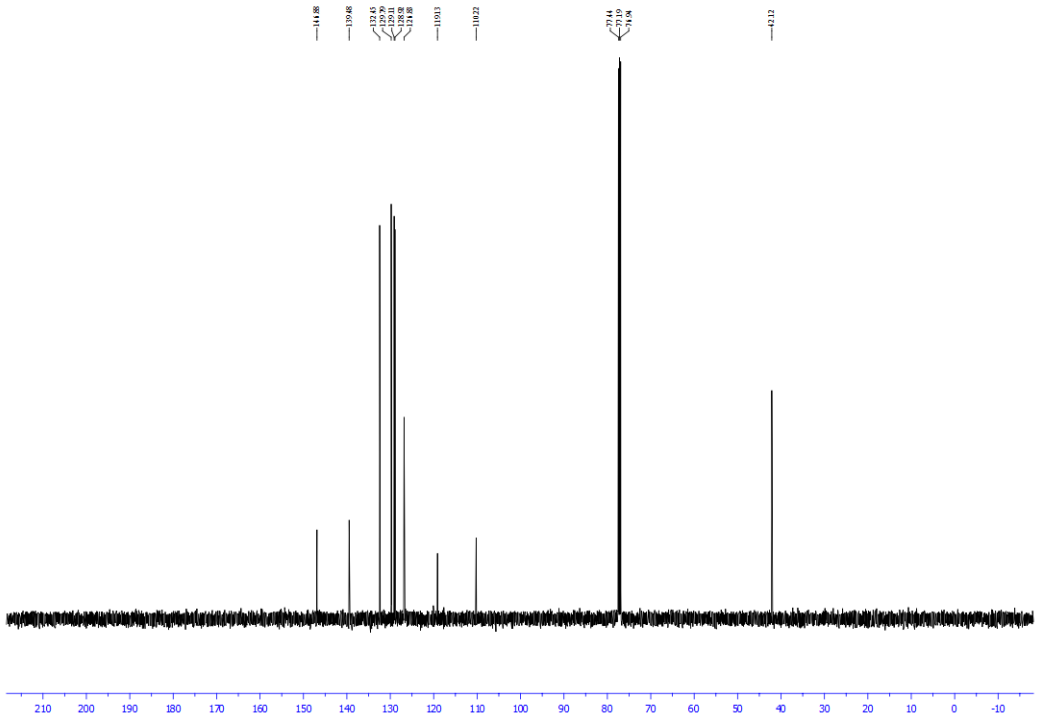

**Figure A1.57:** $^{13}C$ NMR ($CDCl_3$, 125.8 MHz) spectrum of 4-benzylbenzonitrile (**38**)

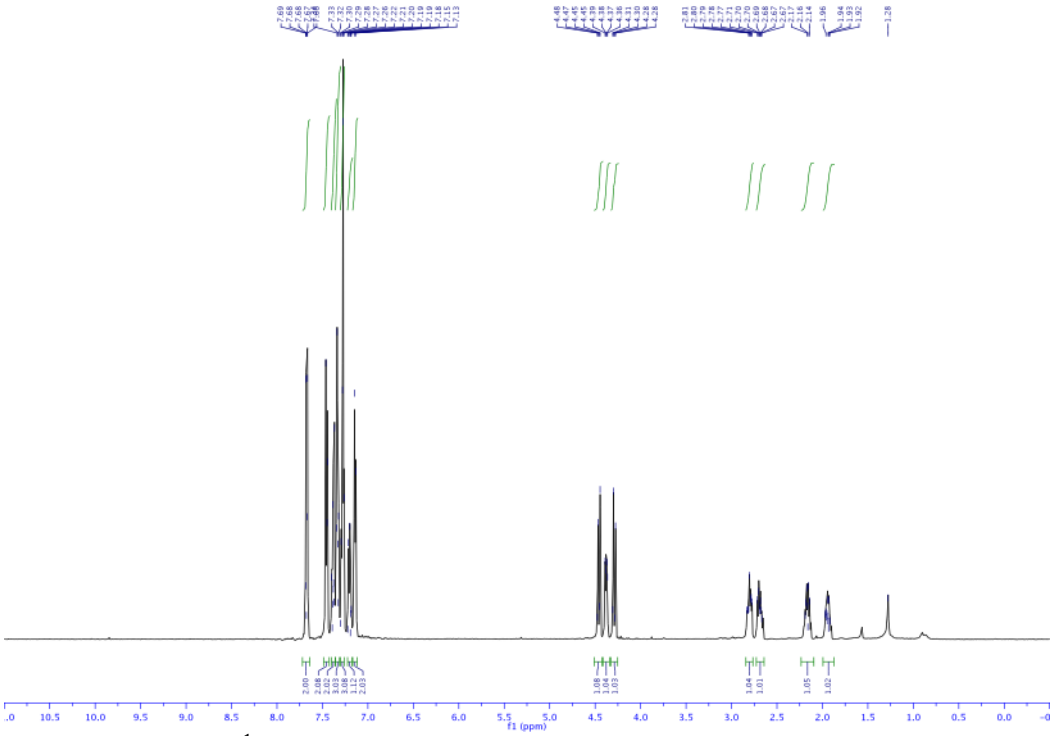

**Figure A1.58:** $^{1}H$ NMR ($CDCl_3$, 500 MHz) spectrum of 4-(1-(benzyloxy)-3-phenylpropyl)benzonitrile (**39**)

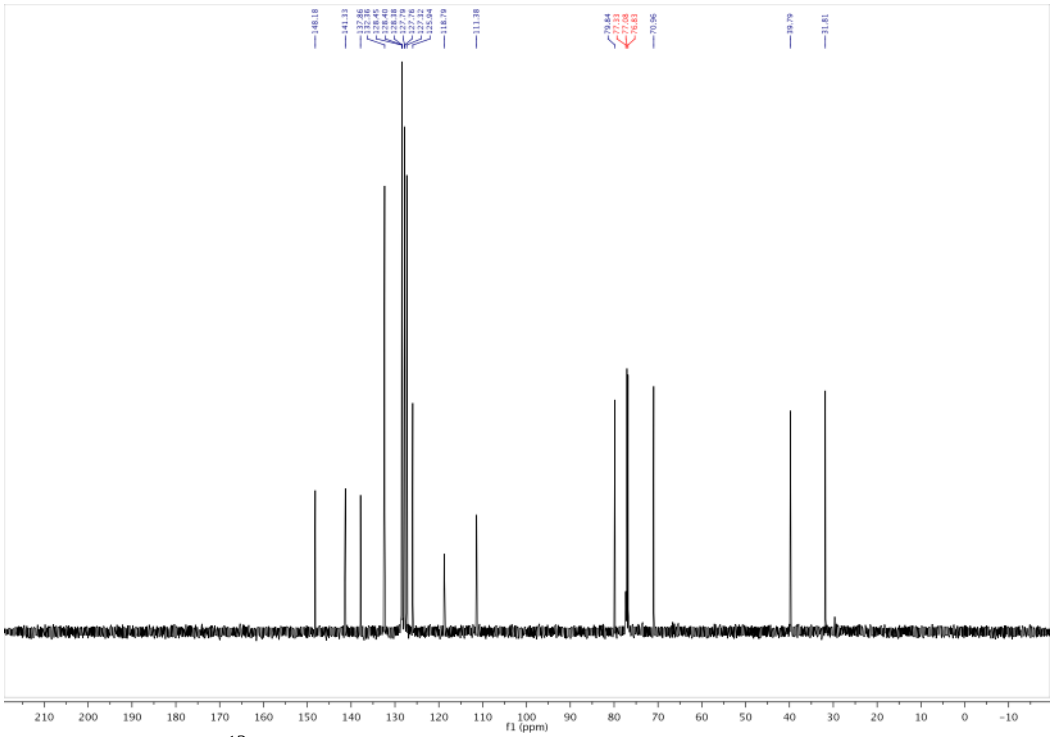

**Figure A1.59:** $^{13}C$ NMR ($CDCl_3$, 125.8 MHz) spectrum of 4-(1-(benzyloxy)-3-phenylpropyl)benzonitrile (**39**)

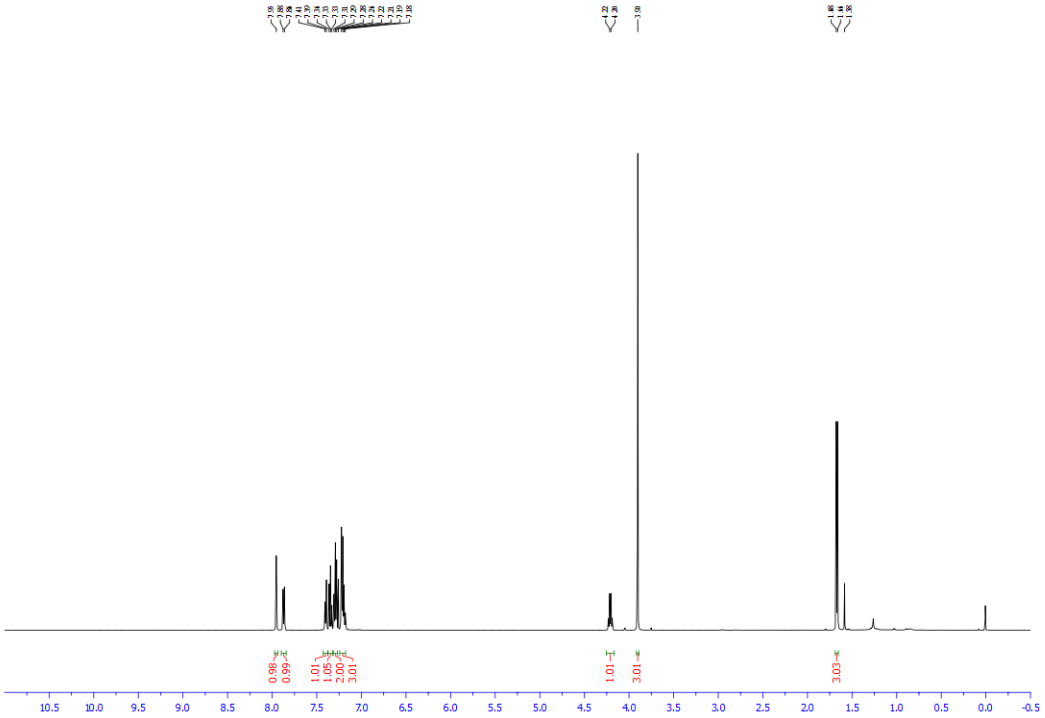

**Figure A1.60:** $^{1}H$ NMR ($CDCl_3$, 500 MHz) spectrum of methyl 3-(1-phenylethyl)benzoate (**41**)

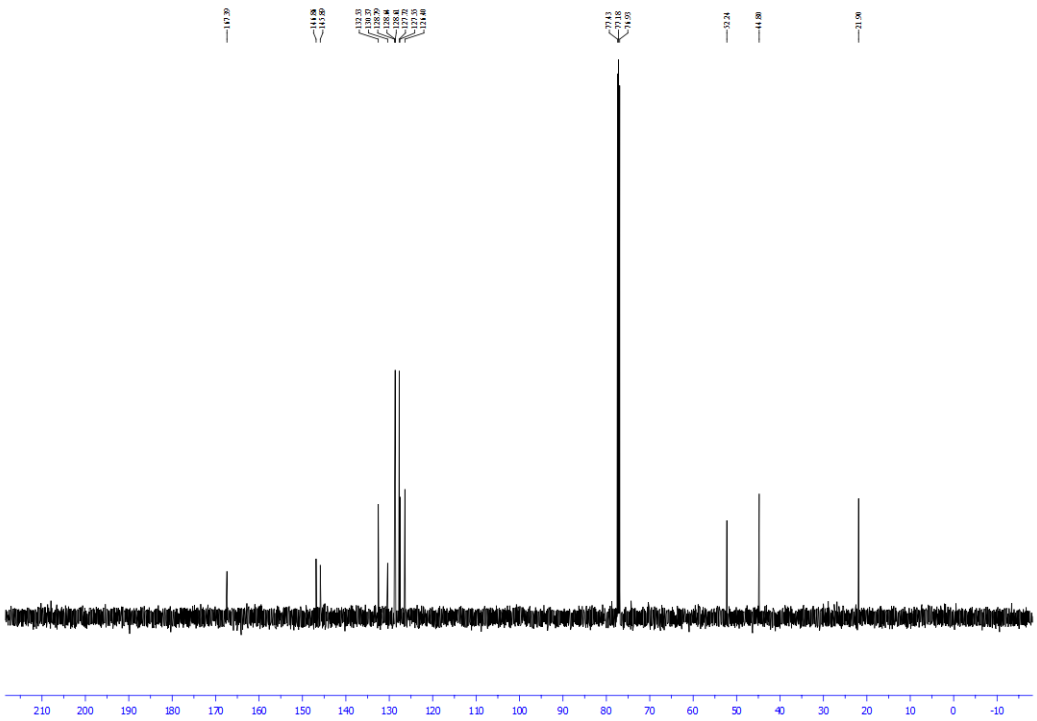

**Figure A1.61:** $^{13}C$ NMR ($CDCl_3$, 125.8 MHz) spectrum of methyl 3-(1-phenylethyl)benzoate (**41**)

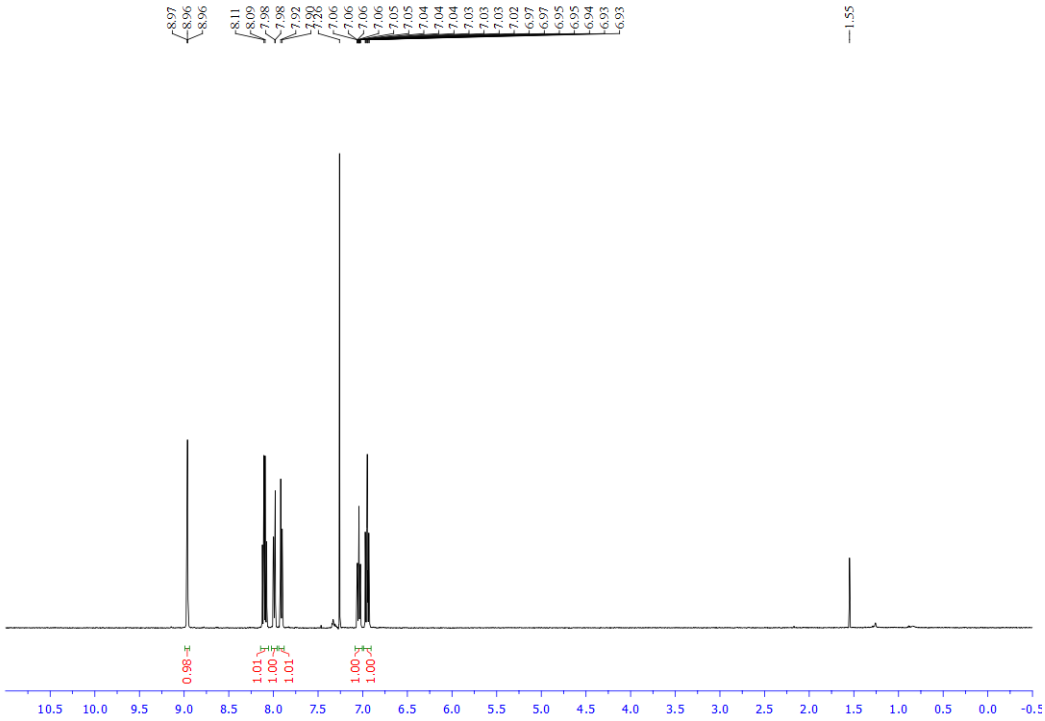

**Figure A1.62:** $^{1}H$ NMR ($CDCl_3$, 500 MHz) spectrum of 2-(2,4-difluorophenyl)-5-(trifluoromethyl)pyridine (**S3**)

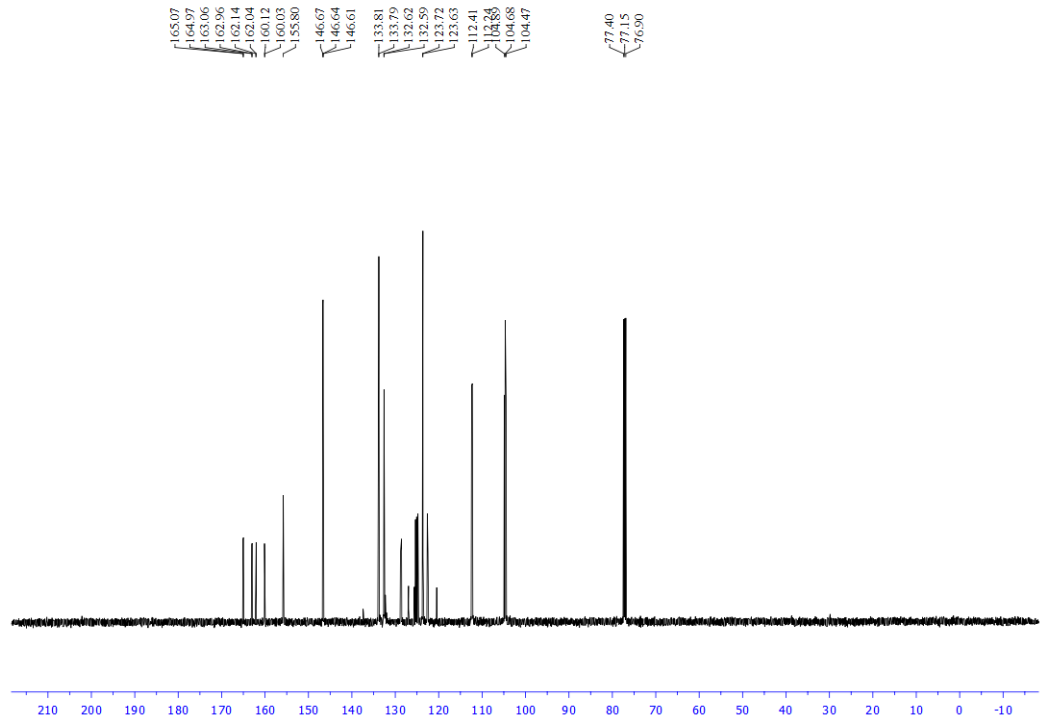


**Figure A1.63:** $^{13}C$ NMR ($CDCl_3$, 125.8 MHz) spectrum of 2-(2,4-difluorophenyl)-5-(trifluoromethyl)pyridine (**S3**)

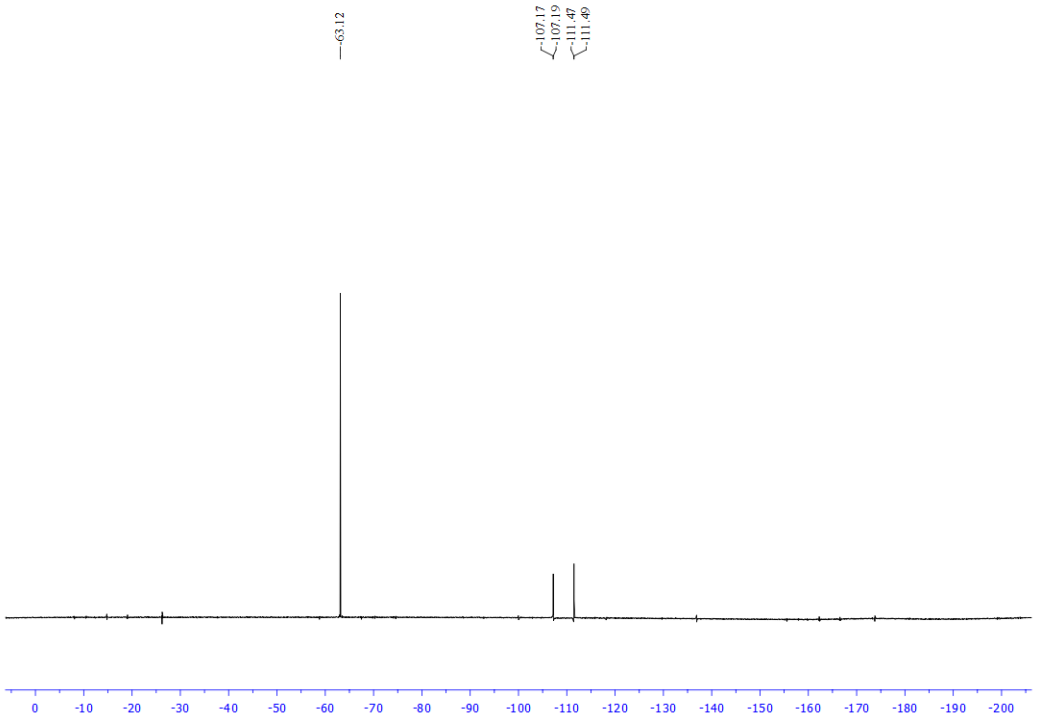


**Figure A1.64:** $^{19}F$ NMR ($CDCl_3$, 470.8 MHz) spectrum of 2-(2,4-difluorophenyl)-5-(trifluoromethyl)pyridine (**S3**)

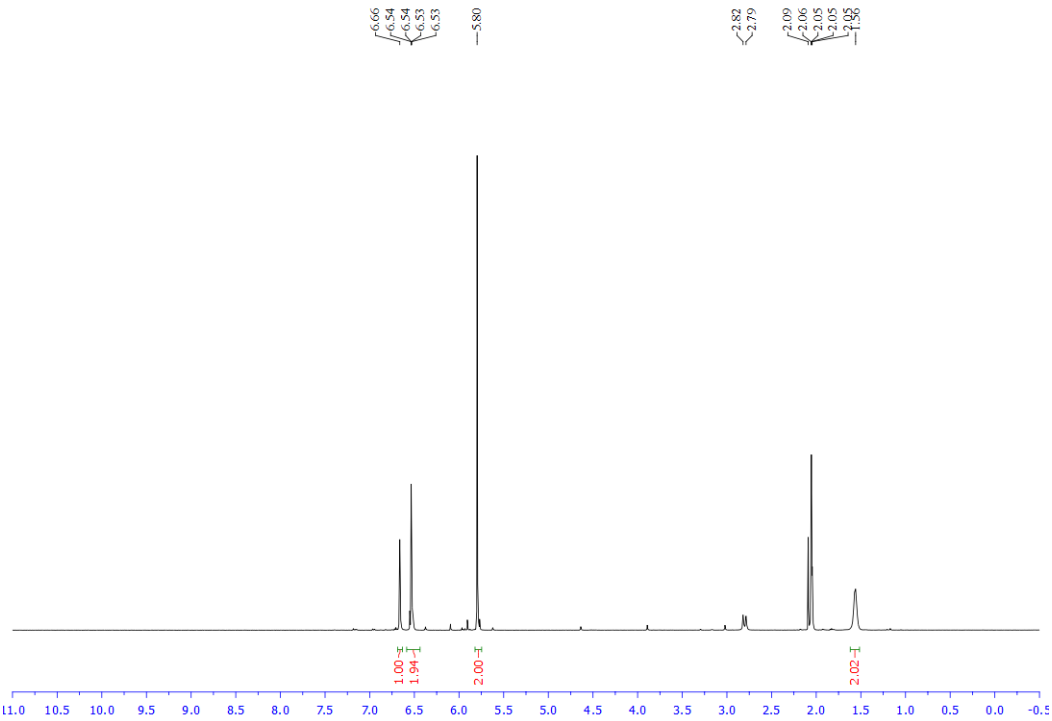


**Figure A1.65:** $^{1}$H NMR (acetone-d$^{6}$, 500 MHz) spectrum of potassium (benzo[d][1,3]dioxol-5-ylmethyl)trifluoroborate (**S5**)

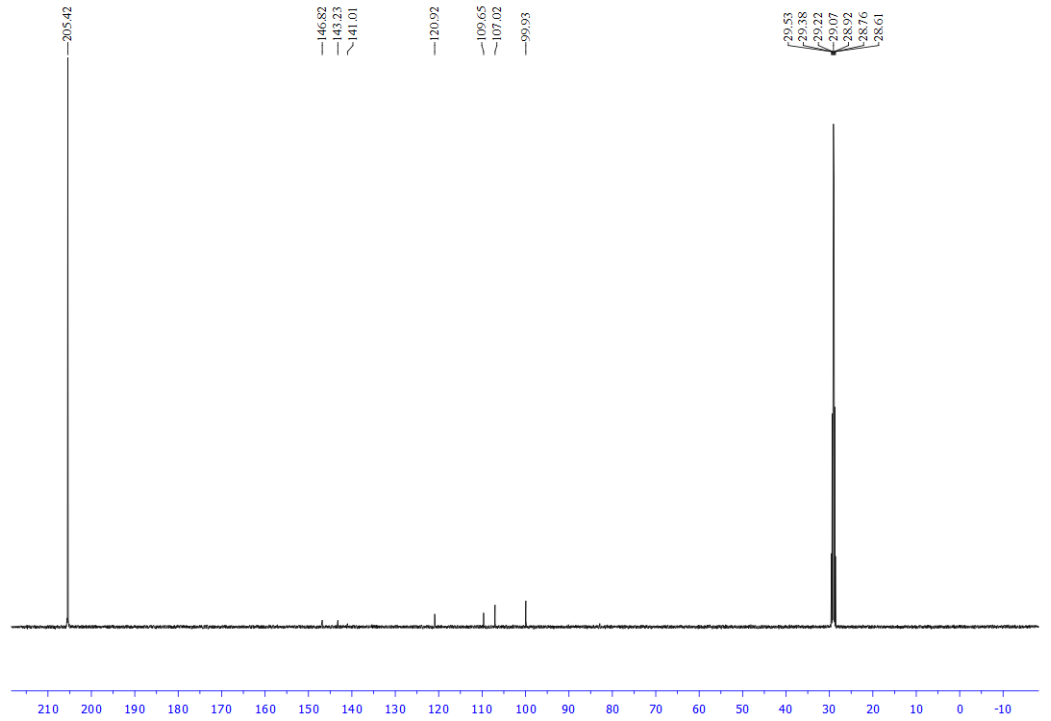


**Figure A1.66:** $^{13}$C NMR (acetone-d$^{6}$, 125.8 MHz) spectrum of potassium (benzo[d][1,3]dioxol-5-ylmethyl)trifluoroborate (**S5**)

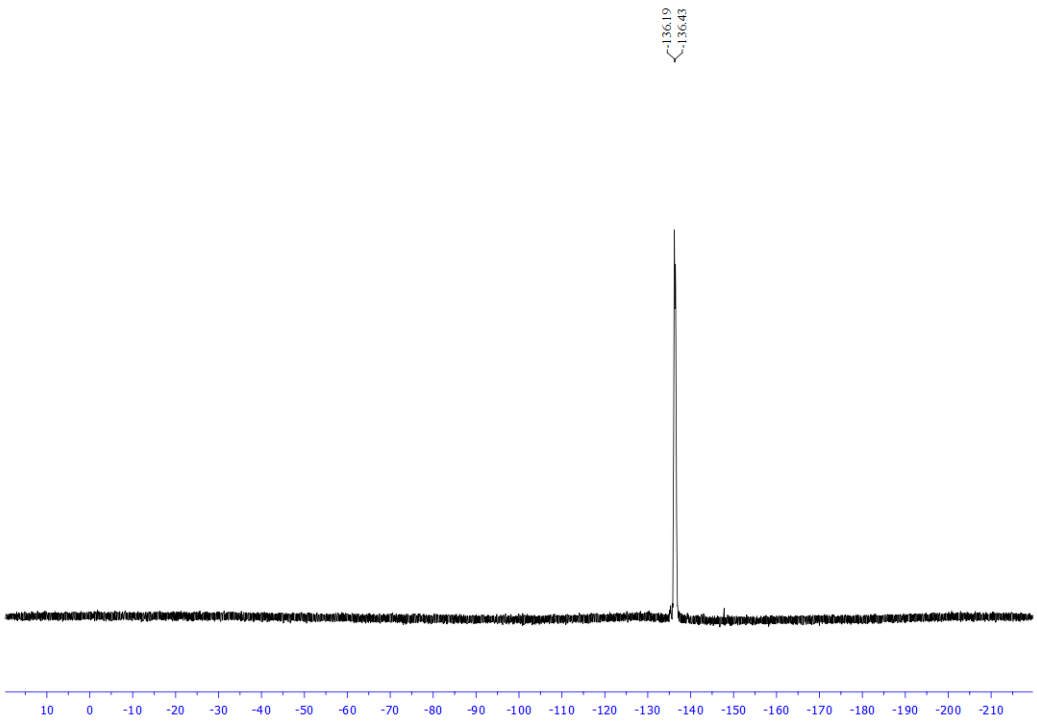


**Figure A1.67:** $^{19}$F NMR (acetone-d$^{6}$, 282.4 MHz) spectrum of potassium (benzo[d][1,3]dioxol-5-ylmethyl)trifluoroborate (**S5**)

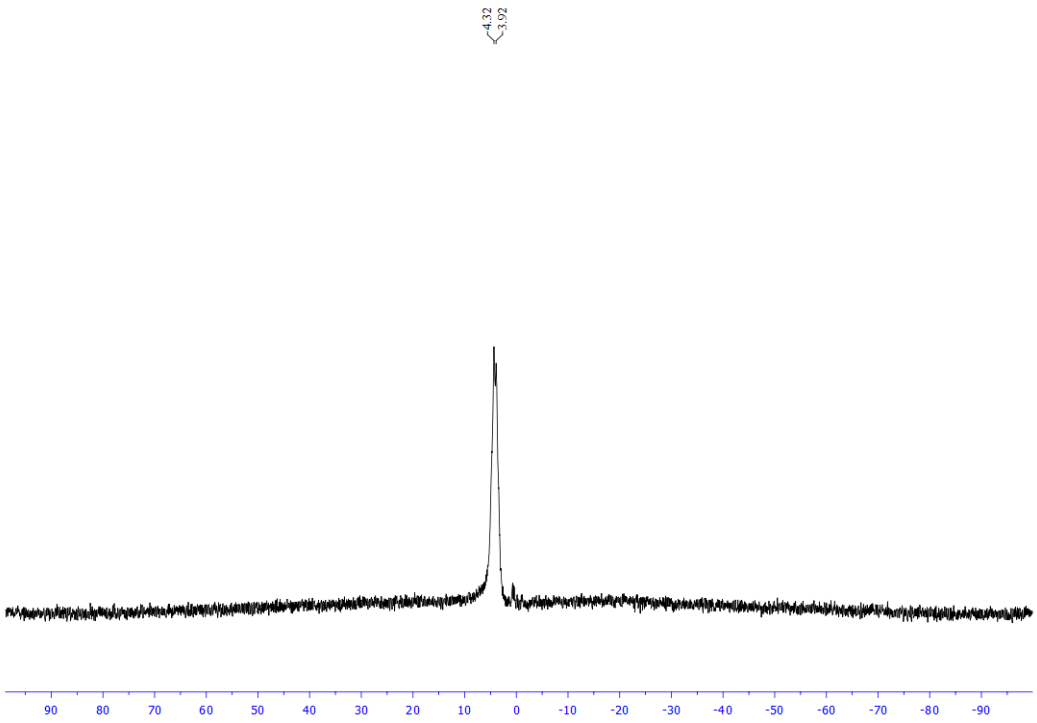


**Figure A1.68:** $^{11}$B NMR (acetone-d$^{6}$, 128.4 MHz) spectrum of potassium (benzo[d][1,3]dioxol-5-ylmethyl)trifluoroborate (**S5**)

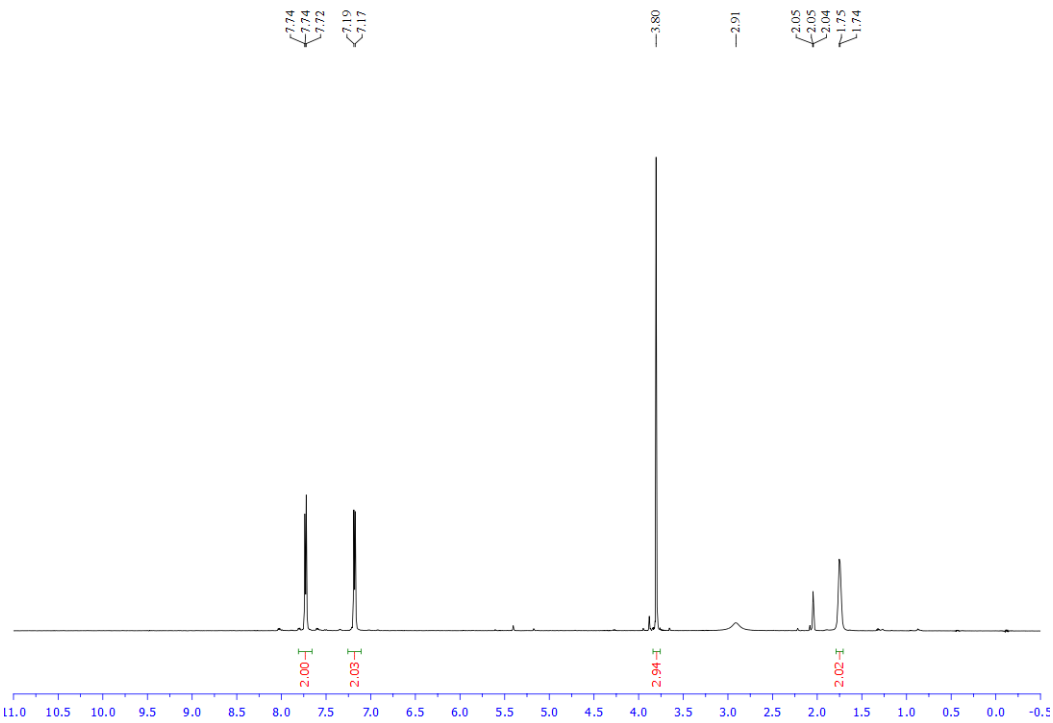


**Figure A1.69.** $^{1}$H NMR (acetone-d$^{6}$, 500 MHz) spectrum potassium trifluoro(4-(methoxycarbonyl)benzyl)borate (**S6**)

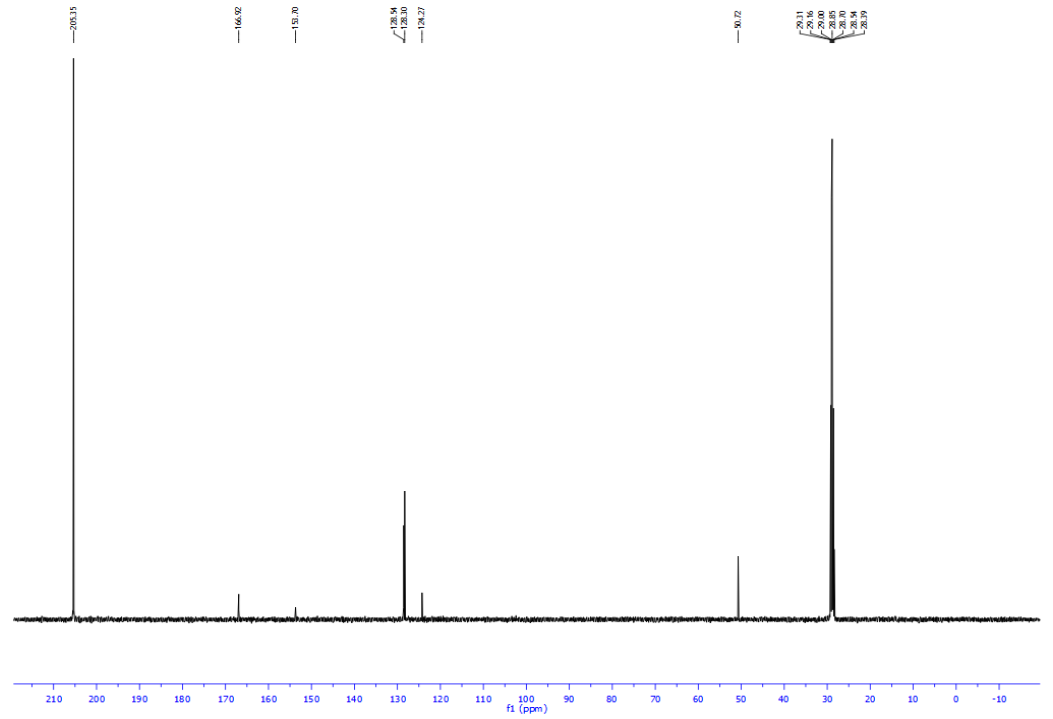


**Figure A1.70.** $^{13}$C NMR (acetone-d$^{6}$, 125.8 MHz) spectrum potassium trifluoro(4-(methoxycarbonyl)benzyl)borate (**S6**)

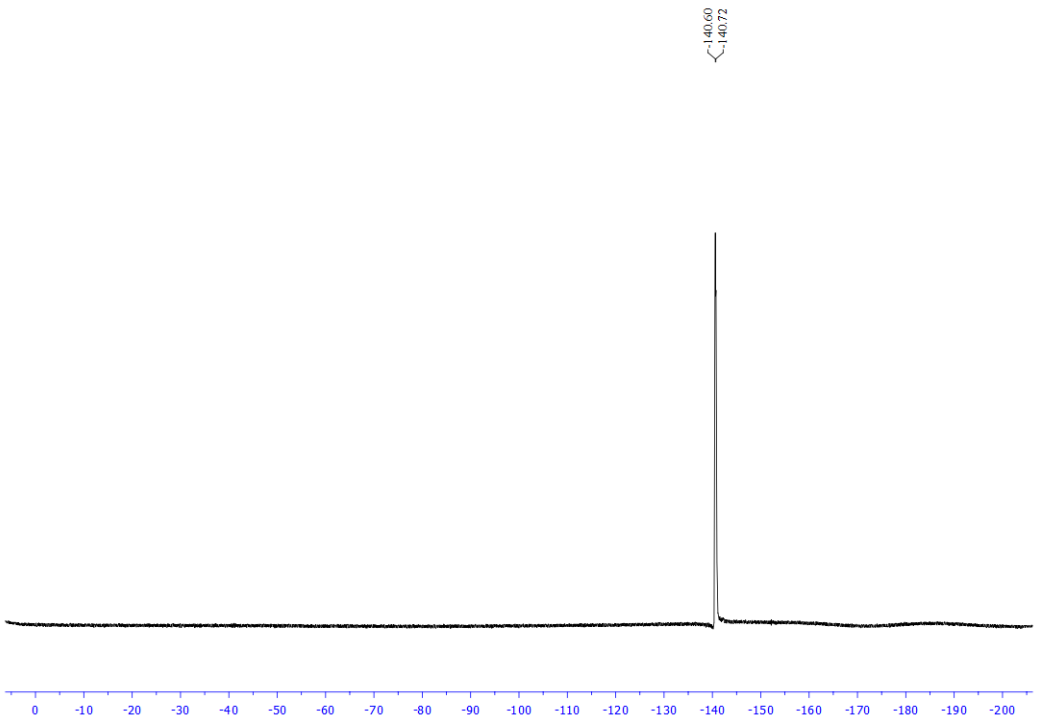


**Figure A1.71.** $^{19}$F NMR (acetone-d$^6$, 470.8 MHz) spectrum potassium trifluoro(4-(methoxycarbonyl)benzyl)borate (**S6**)

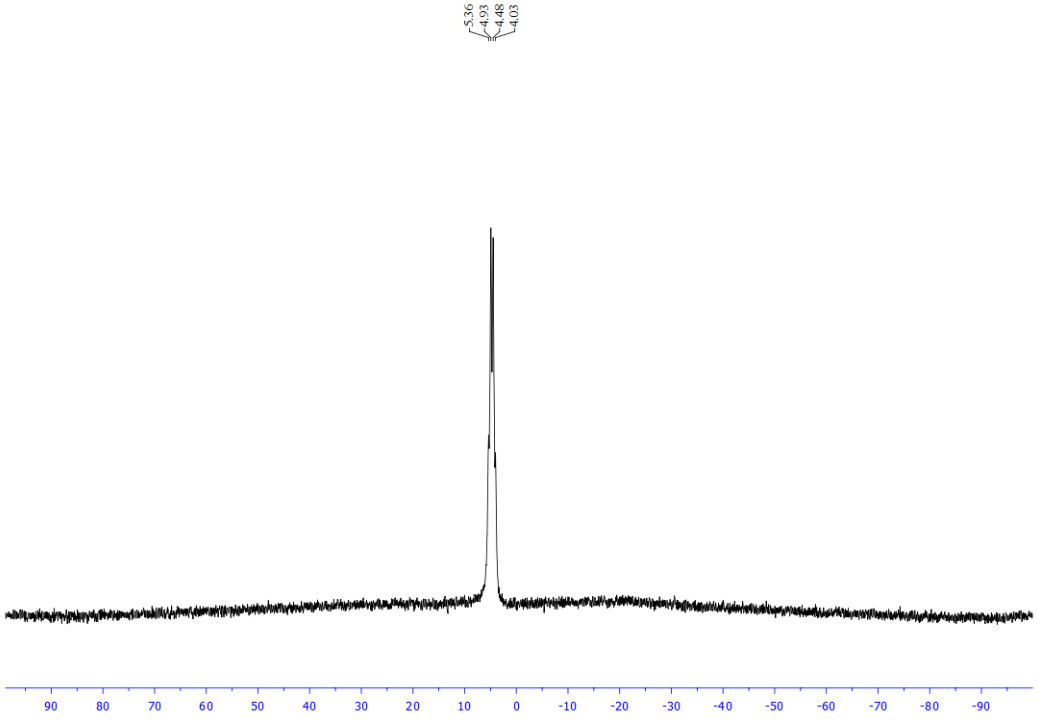


**Figure A1.72.** $^{11}$B NMR (acetone-d$^6$, 128.4 MHz) spectrum potassium trifluoro(4-(methoxycarbonyl)benzyl)borate (**S6**)

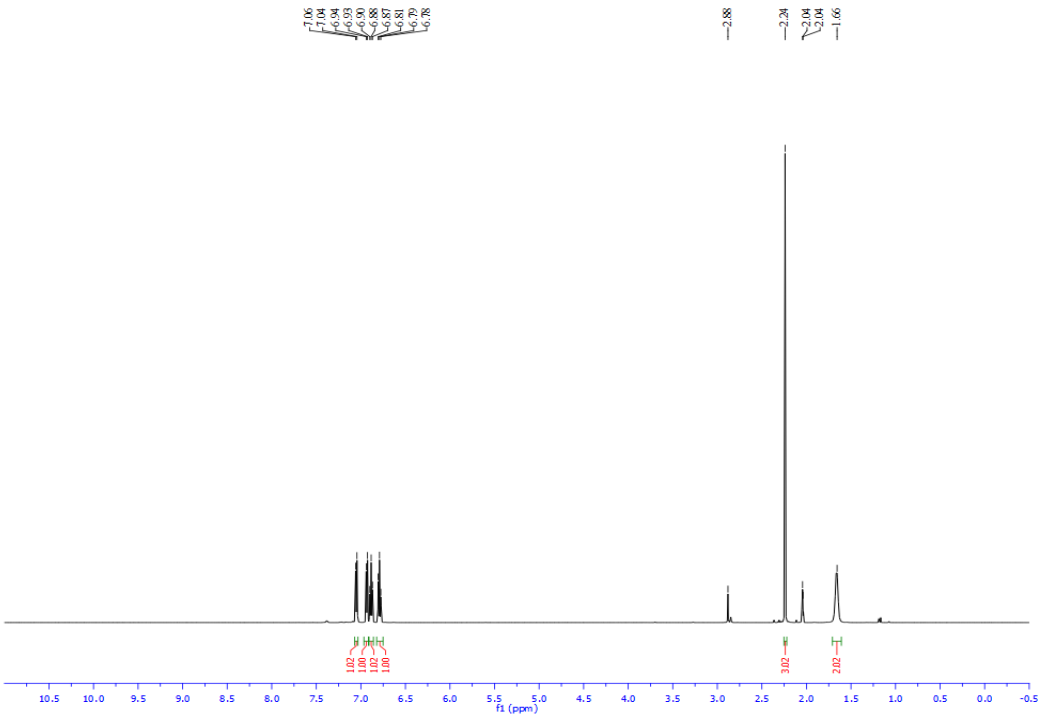


**Figure A1.73.** $^{1}$H NMR (acetone-d$^{6}$, 500 MHz) spectrum of potassium trifluoro(2-methylbenzyl)borate (**S7**)

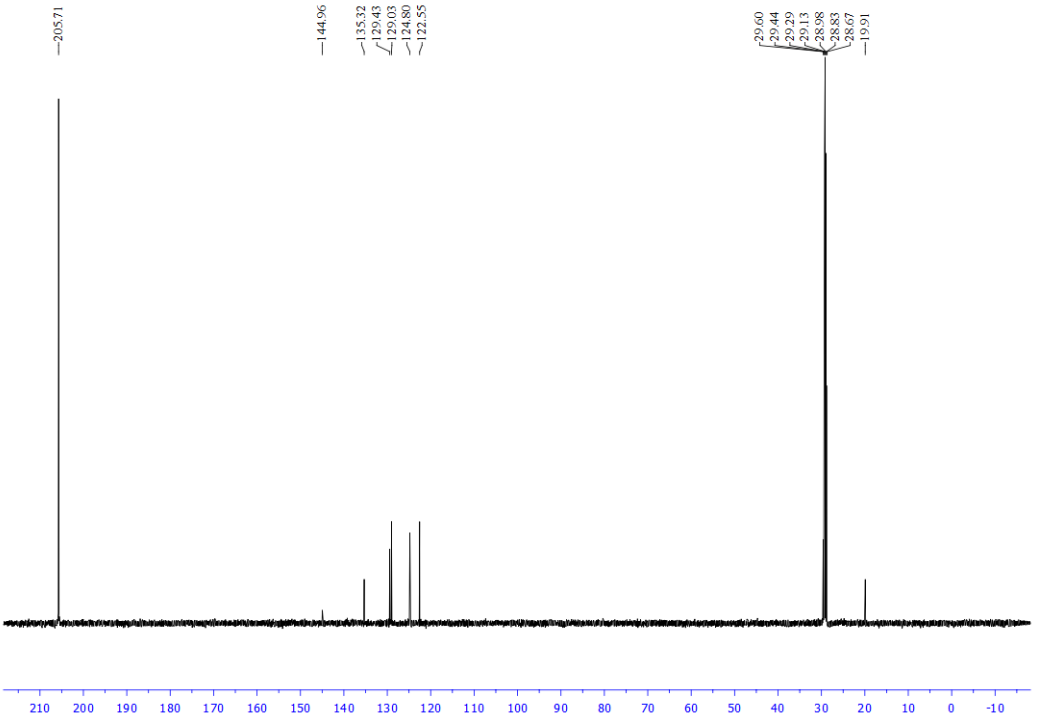


**Figure A1.74.** $^{13}$C NMR (acetone-d$^{6}$, 125.8 MHz) spectrum of potassium trifluoro(2-methylbenzyl)borate (**S7**)

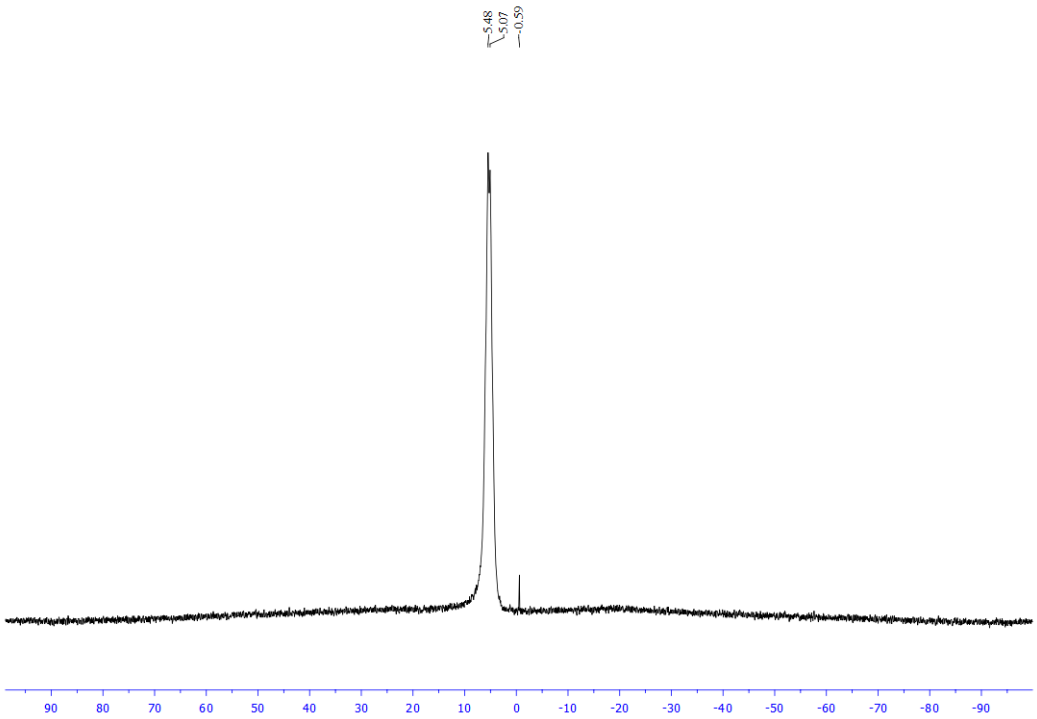


**Figure A1.75.** $^{11}$B NMR (acetone-d$^6$, 128.4 MHz) spectrum of potassium trifluoro(2-methylbenzyl)borate (**S7**)

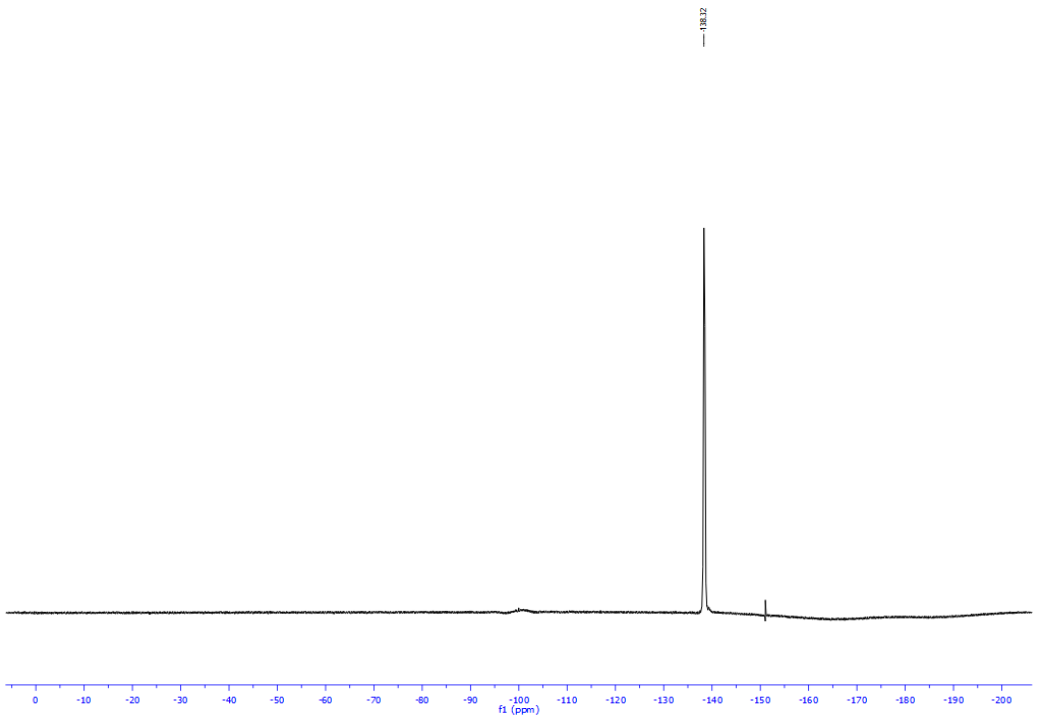


**Figure A1.76.** $^{19}$F NMR (acetone-d$^6$, 470.8 MHz) spectrum of potassium trifluoro(2-methylbenzyl)borate (**S7**)

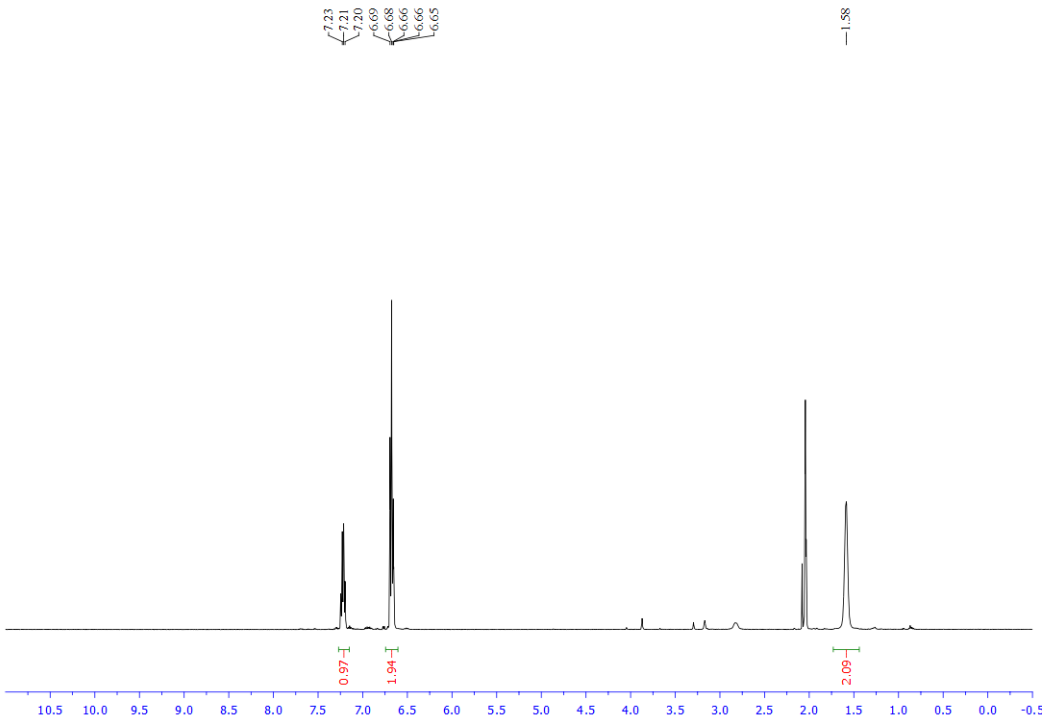


**Figure A1.77.** $^{1}$H NMR (acetone-d$^{6}$, 500 MHz) spectrum of potassium (2,4-difluorobenzyl)trifluoroborate (**S8**)

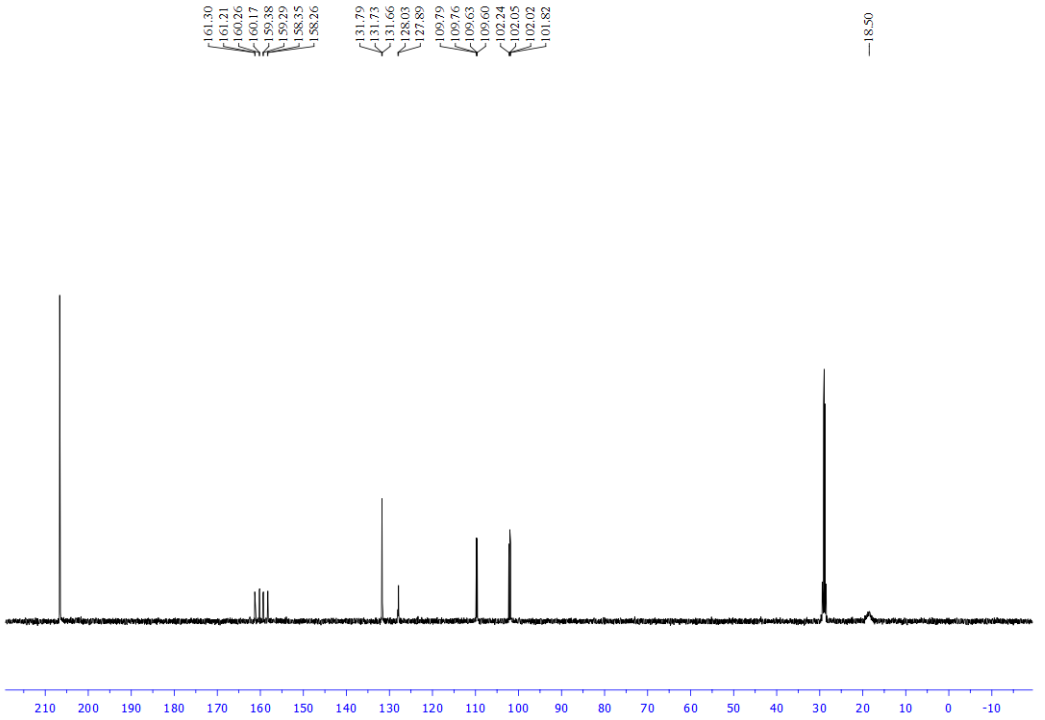


**Figure A1.78.** $^{13}$C NMR (acetone-d$^{6}$, 125.8 MHz) spectrum of potassium (2,4-difluorobenzyl)trifluoroborate (**S8**)

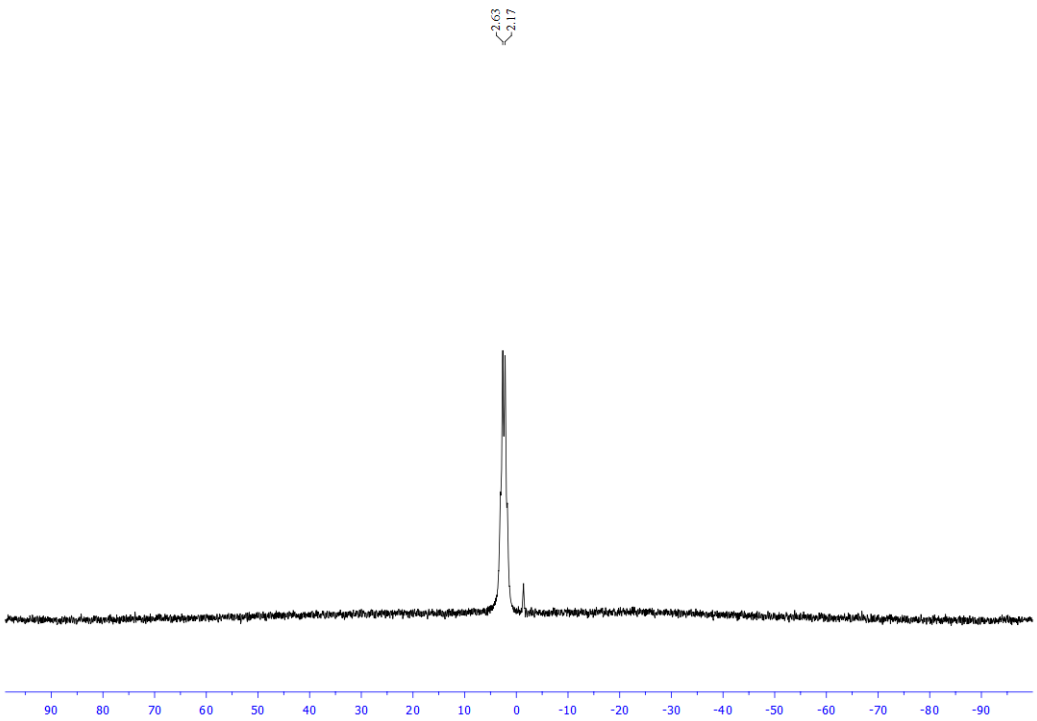


**Figure A1.79.** $^{11}$B NMR (acetone-d$^6$, 128.4 MHz) spectrum of potassium (2,4-difluorobenzyl)trifluoroborate (**S8**)

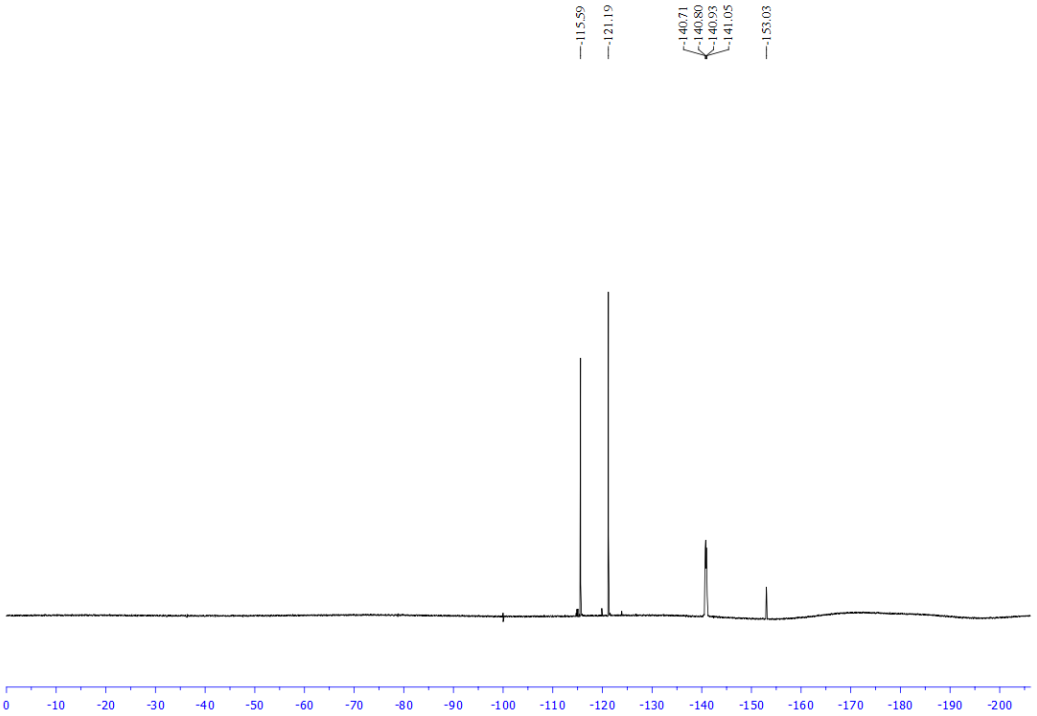


**Figure A1.80.** $^{19}$F NMR (acetone-d$^6$, 470.8 MHz) spectrum of potassium (2,4-difluorobenzyl)trifluoroborate (**S8**)

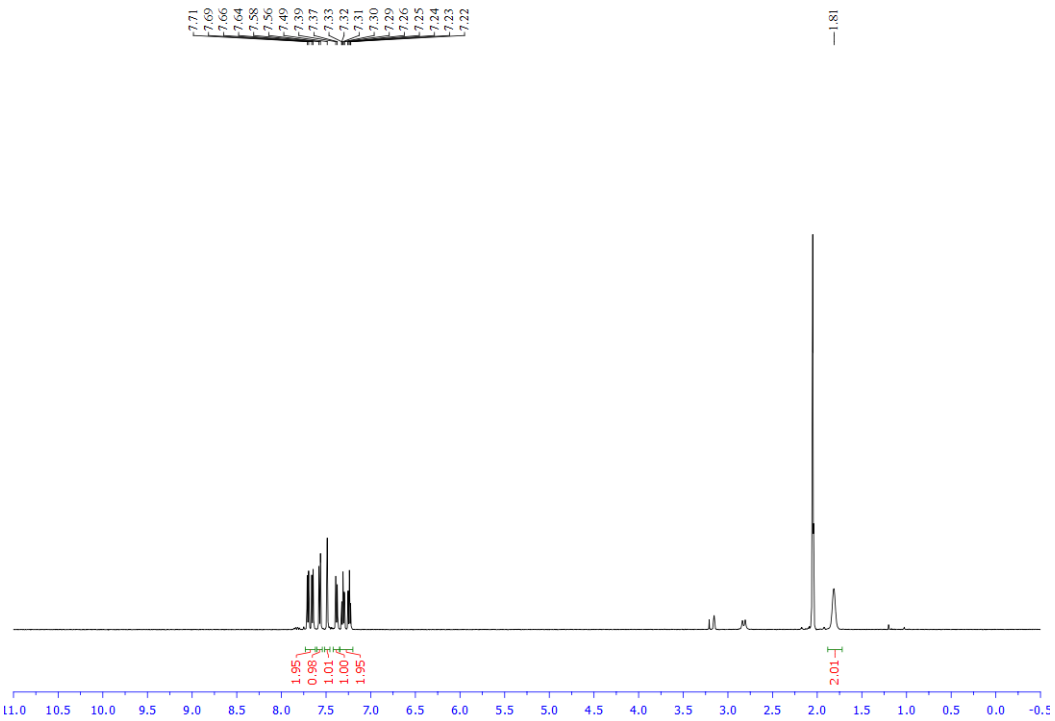

**Figure A1.81.** $^{1}$H NMR (acetone-$d_6$, 500 MHz) spectrum of potassium trifluoro(naphthalen-2-ylmethyl)borate (**S9**)

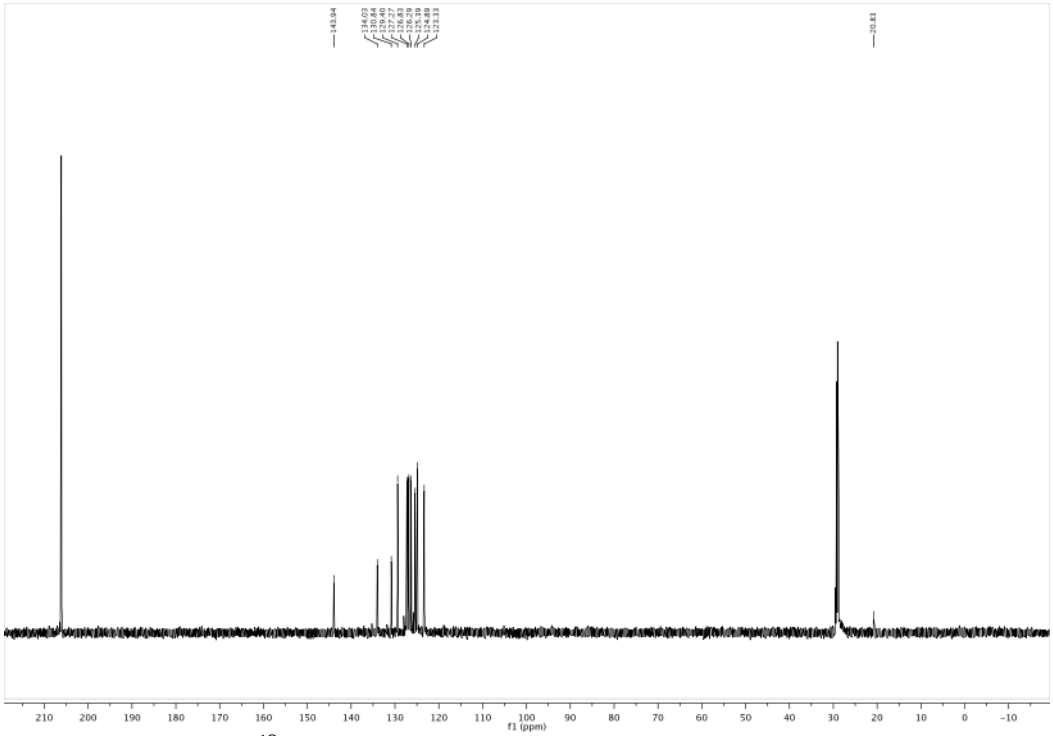

**Figure A1.82.** $^{13}$C NMR (acetone-$d_6$, 125.8 MHz) spectrum of potassium trifluoro(naphthalen-2-ylmethyl)borate (**S9**)

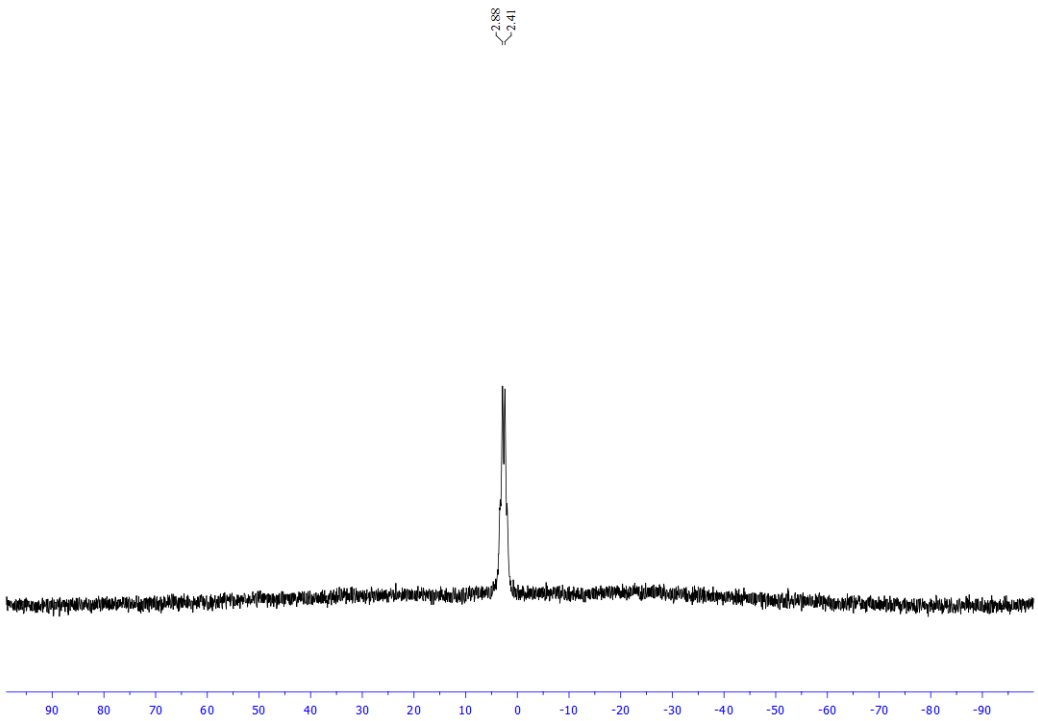


**Figure A1.83.** $^{11}$B NMR (acetone-$d_6$, 128.4 MHz) spectrum of potassium trifluoro(naphthalen-2-ylmethyl)borate (**S9**)

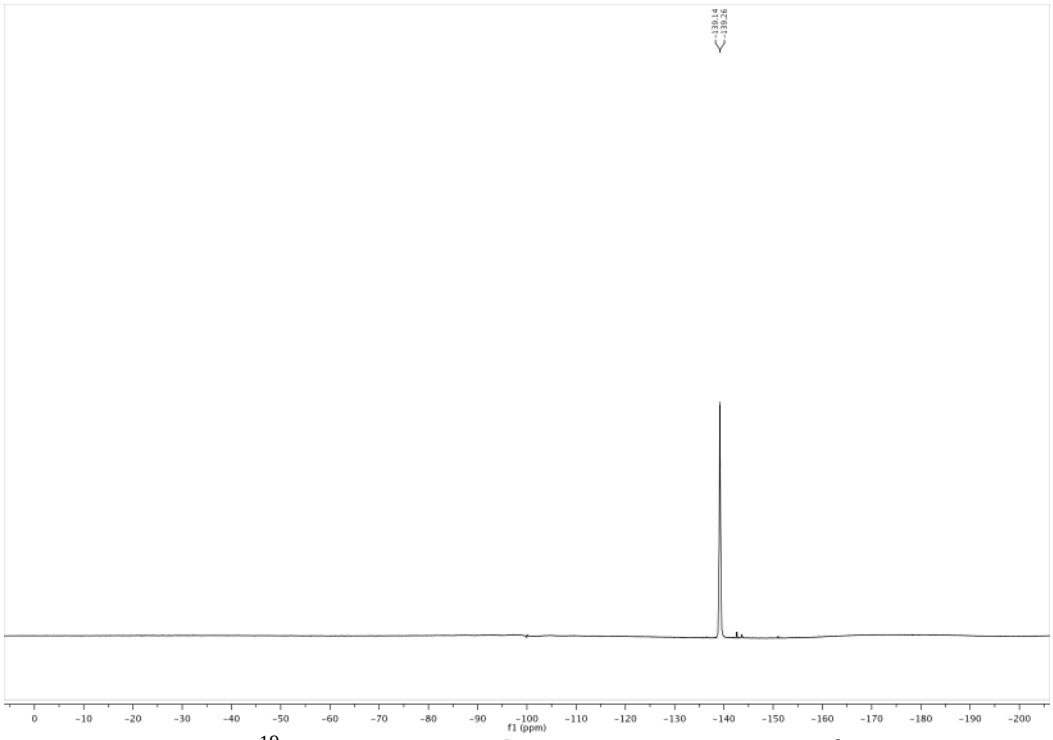


**Figure A1.84.** $^{19}$F NMR (acetone-$d_6$, 400.7 MHz) spectrum of potassium trifluoro(naphthalen-2-ylmethyl)borate (**S9**)

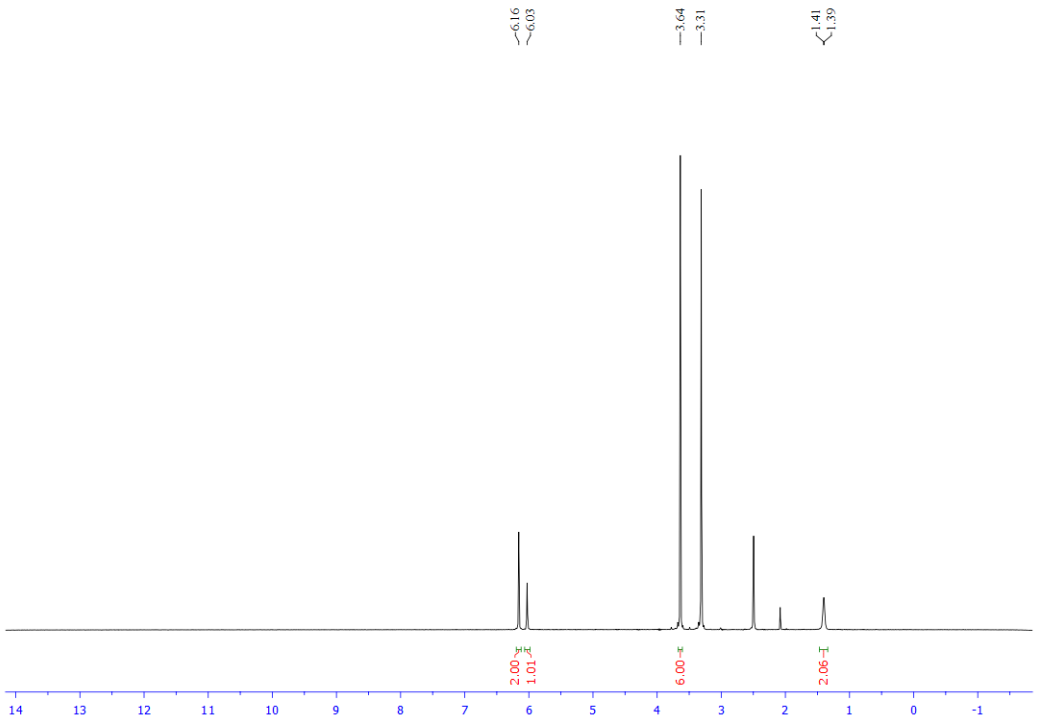


**Figure A1.85.** $^{1}$H NMR (DMSO-d$^{6}$, 500 MHz) spectrum of potassium (3,5-dimethoxybenzyl)trifluoroborate (**S10**)

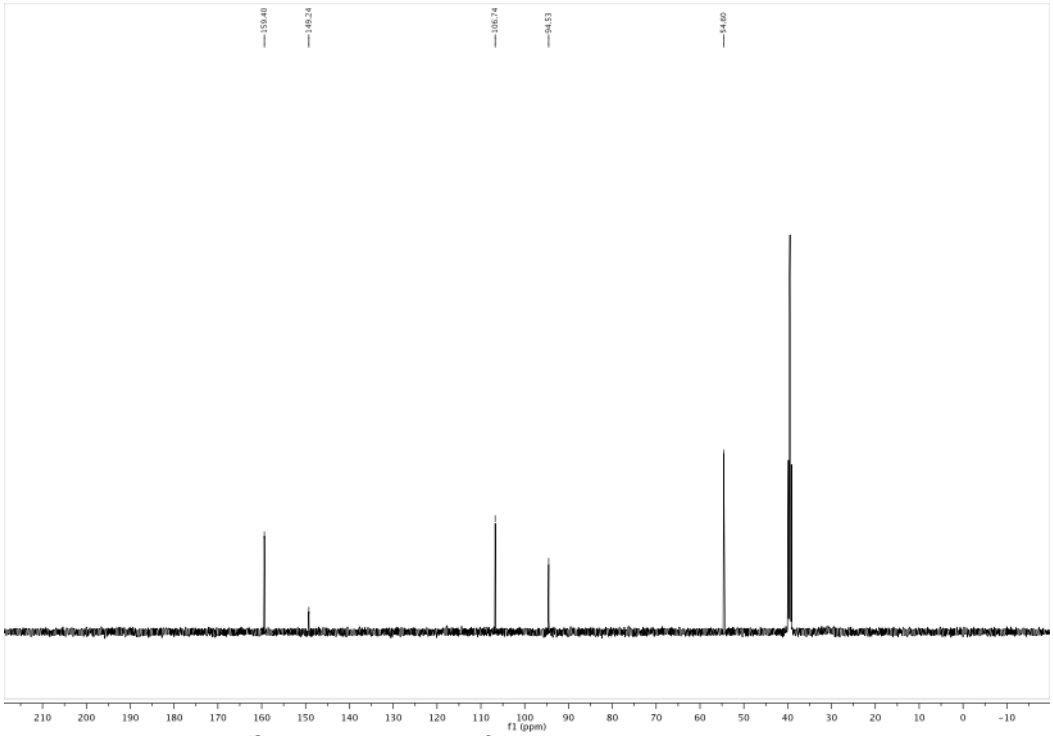


**Figure A1.86.** $^{13}$C NMR (DMSO-d$^{6}$, 125.8 MHz) spectrum of potassium (3,5-dimethoxybenzyl)trifluoroborate (**S10**)

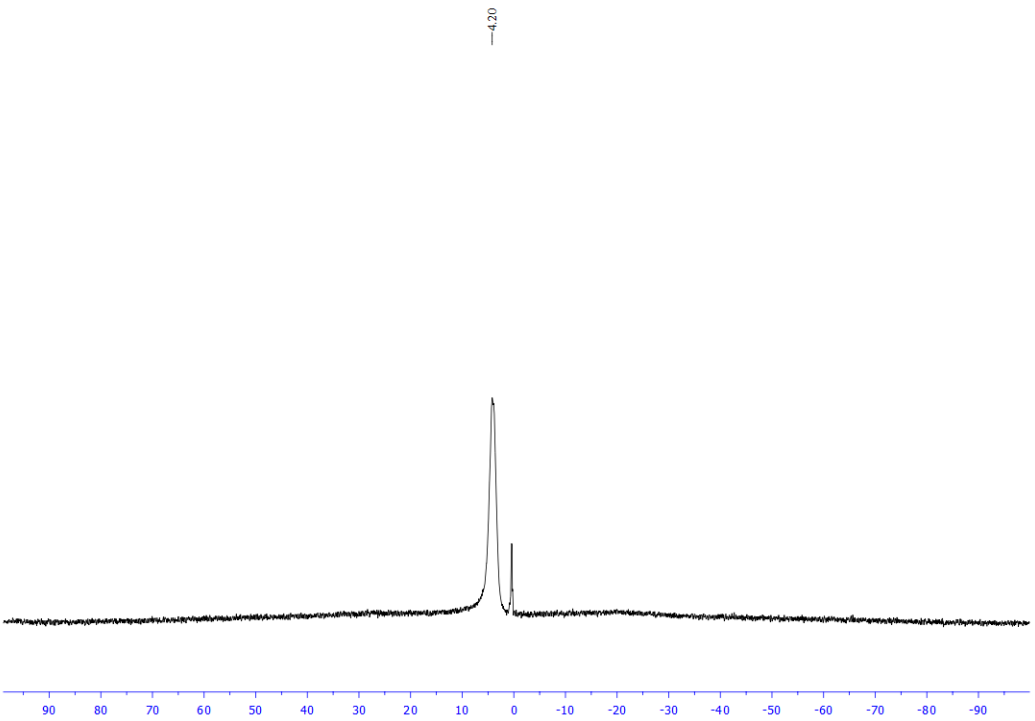


**Figure A1.87.** $^{11}$B NMR (DMSO-d$^6$, 128.4 MHz) spectrum of potassium (3,5-dimethoxybenzyl)trifluoroborate (**S10**)

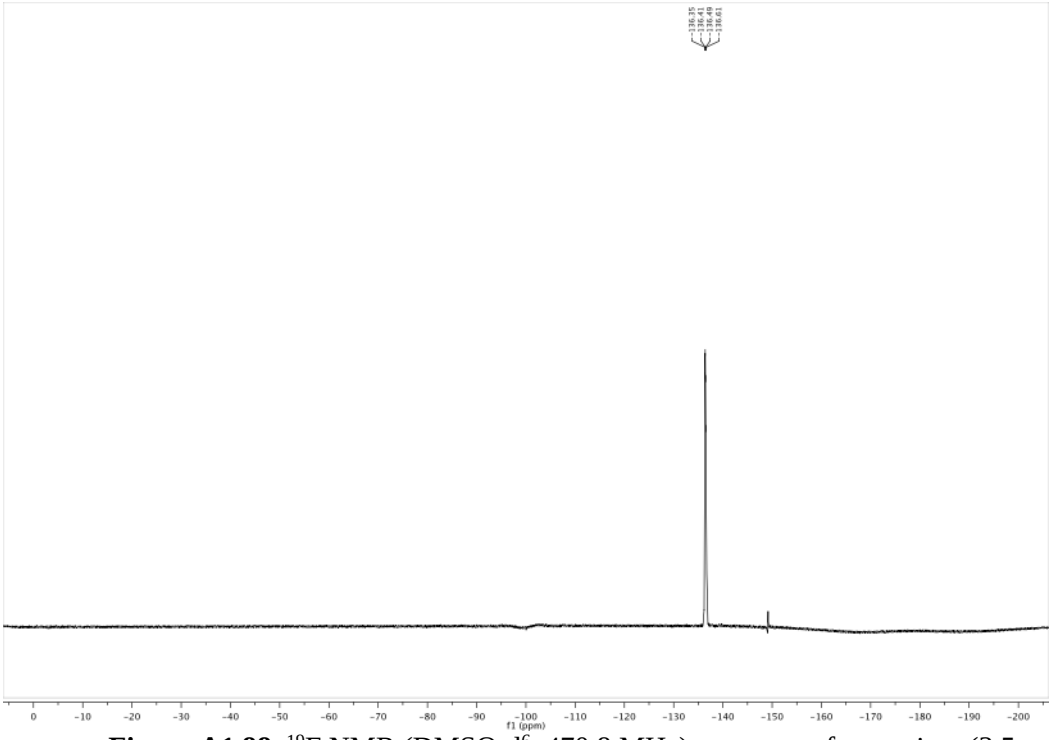


**Figure A1.88.** $^{19}$F NMR (DMSO-d$^6$, 470.8 MHz) spectrum of potassium (3,5-dimethoxybenzyl)trifluoroborate (**S10**)

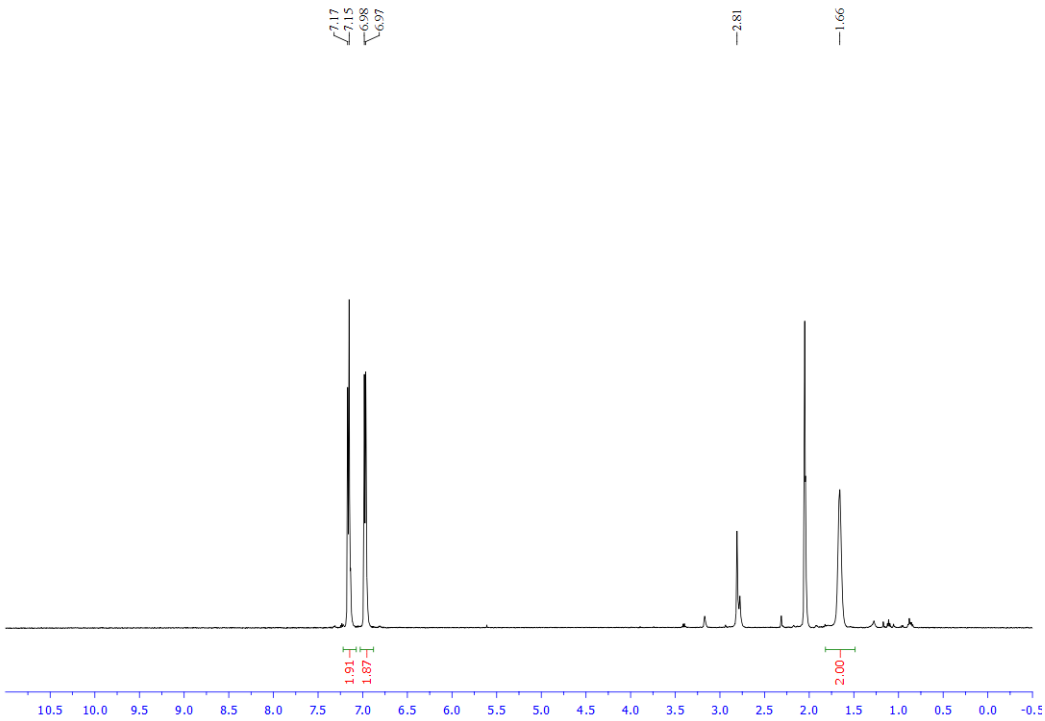


**Figure A1.89.** $^{1}$H NMR (acetone-d$^{6}$, 500 MHz) spectrum of potassium trifluoro(4-(trifluoromethoxy)benzyl)borate (**S11**)

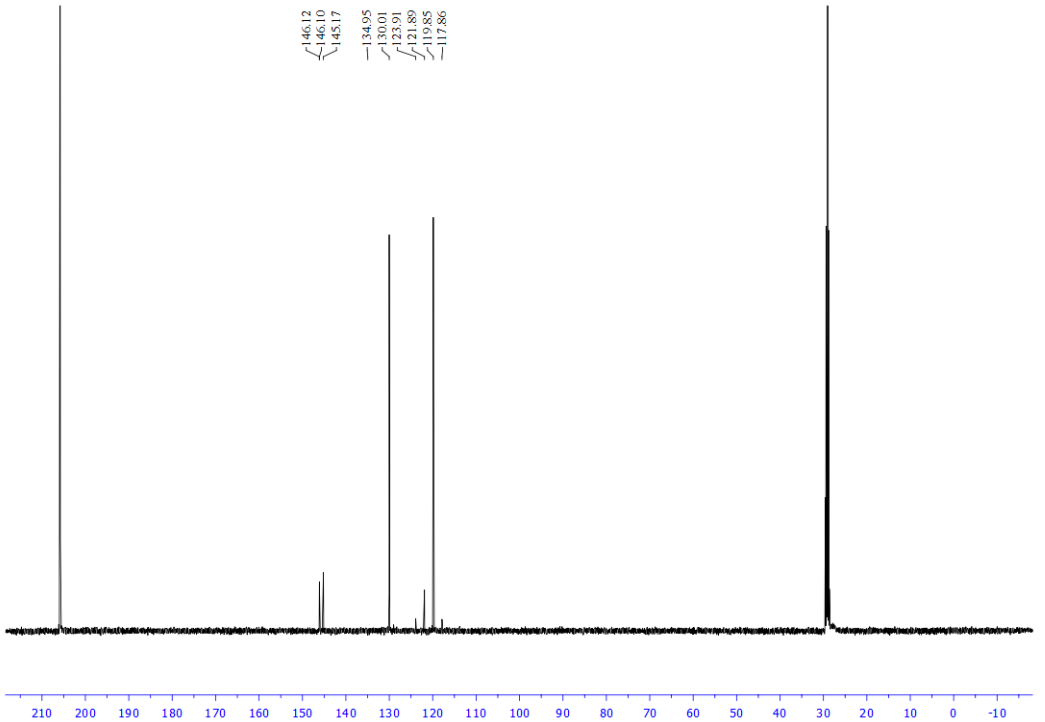


**Figure A1.90.** $^{13}$C NMR (acetone-d$^{6}$, 125.8 MHz) spectrum of potassium trifluoro(4-(trifluoromethoxy)benzyl)borate (**S11**)

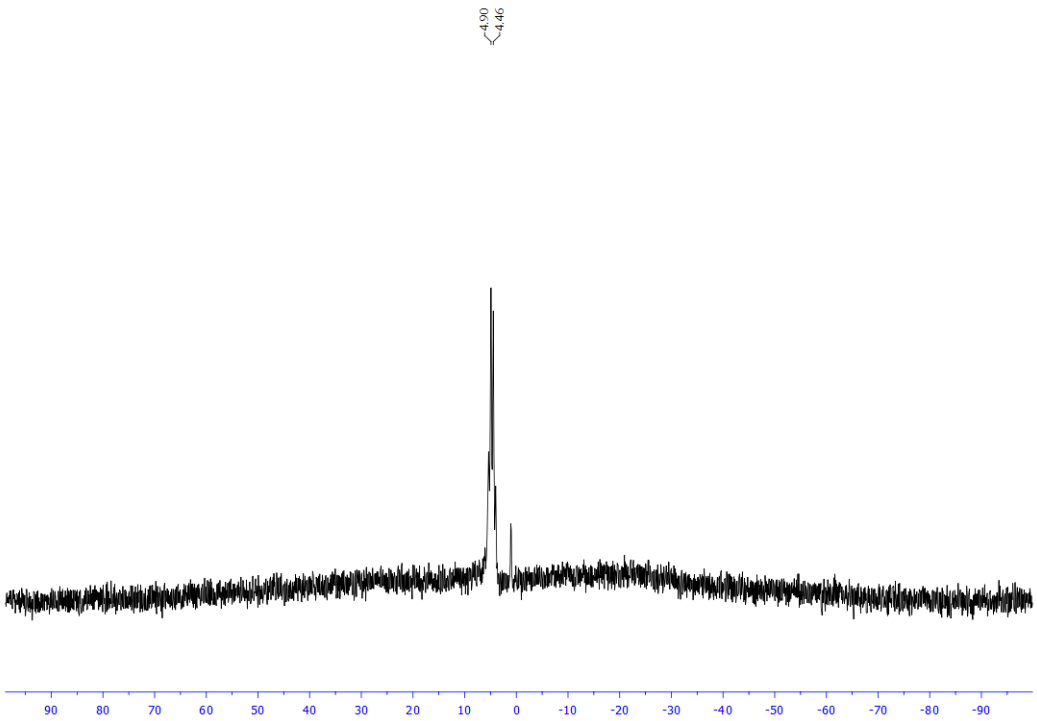


**Figure A1.91.** $^{11}$B NMR (acetone-d$^6$, 128.4 MHz) spectrum of potassium trifluoro(4-(trifluoromethoxy)benzyl)borate (**S11**)

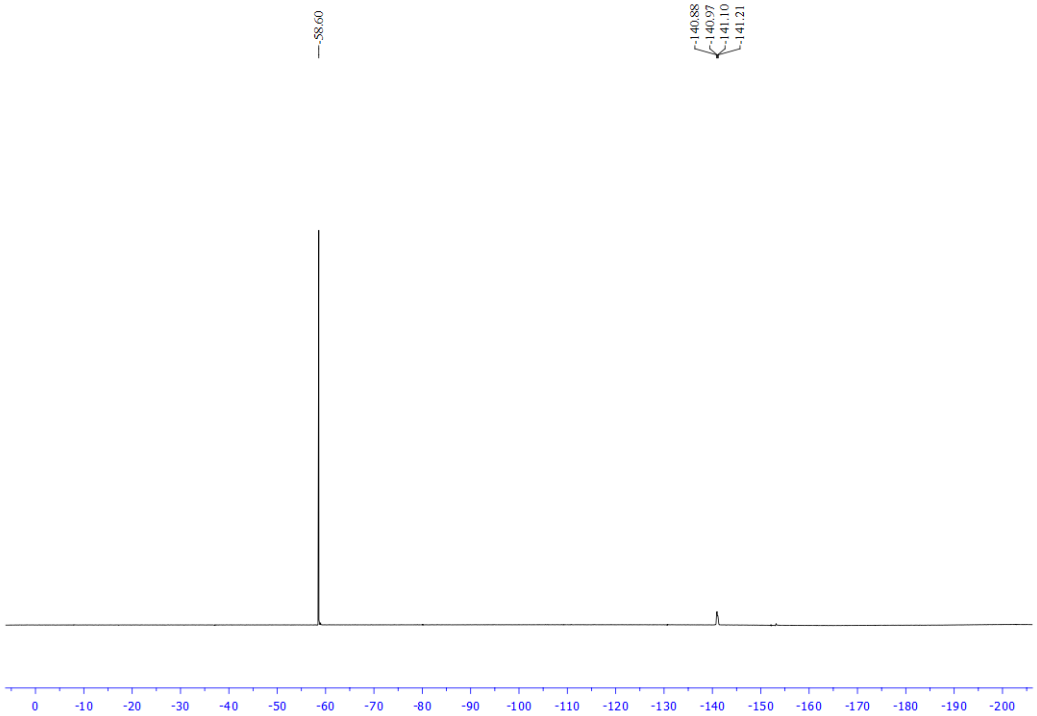


**Figure A1.92.** $^{19}$F NMR (acetone-d$^6$, 470.8 MHz) spectrum of potassium trifluoro(4-(trifluoromethoxy)benzyl)borate (**S11**)

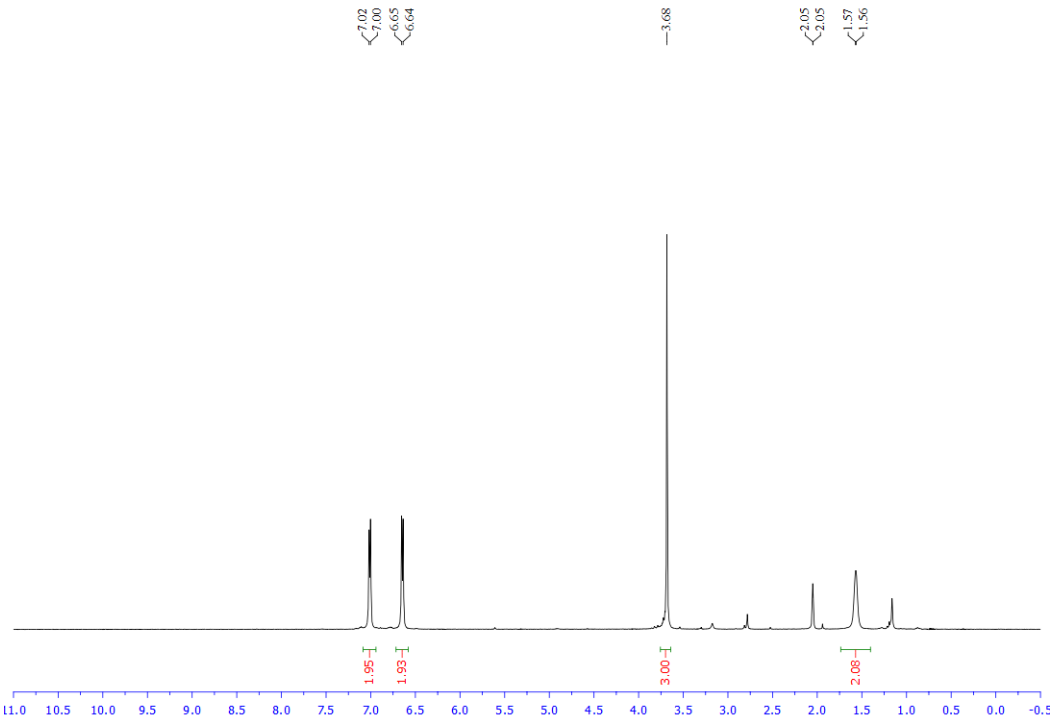


**Figure A1.93.** $^{1}$H NMR (acetone-d$^{6}$, 500 MHz) spectrum of potassium trifluoro(4-methoxybenzyl)borate (**S12**)

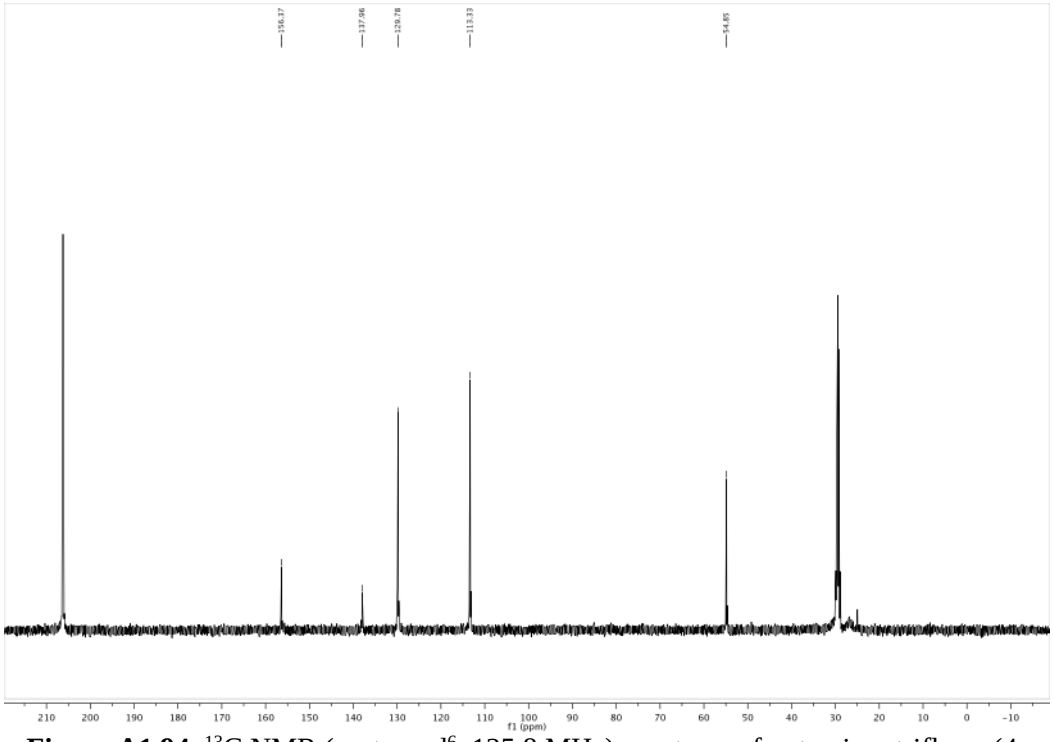


**Figure A1.94.** $^{13}$C NMR (acetone-d$^{6}$, 125.8 MHz) spectrum of potassium trifluoro(4-methoxybenzyl)borate (**S12**)

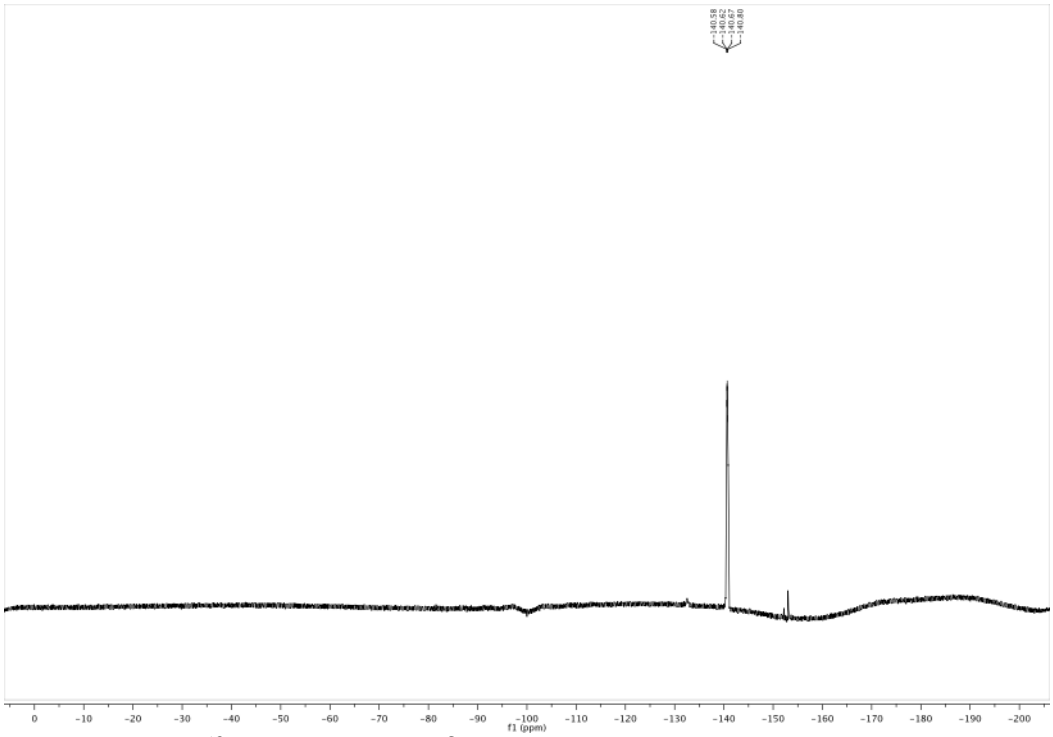


**Figure A1.95.** $^{19}F$ NMR (acetone-$d^6$, 470.8 MHz) spectrum of potassium trifluoro(4-methoxybenzyl)borate (**S12**)

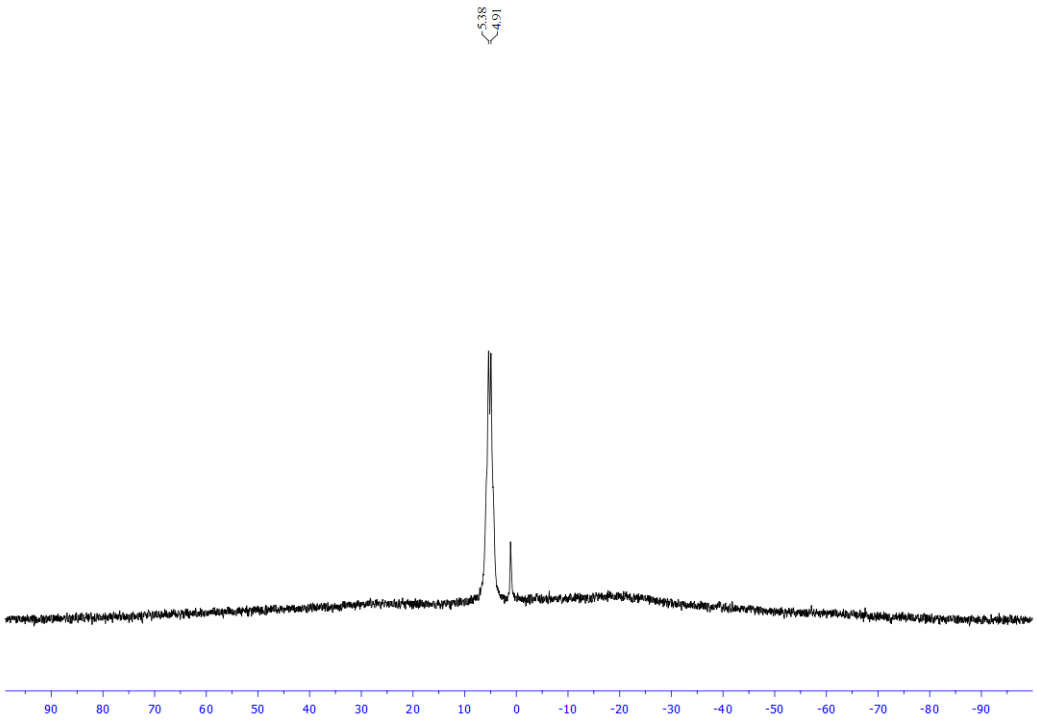


**Figure A1.96.** $^{11}B$ NMR (acetone-$d^6$, 128.4 MHz) spectrum of potassium trifluoro(4-methoxybenzyl)borate (**S12**)

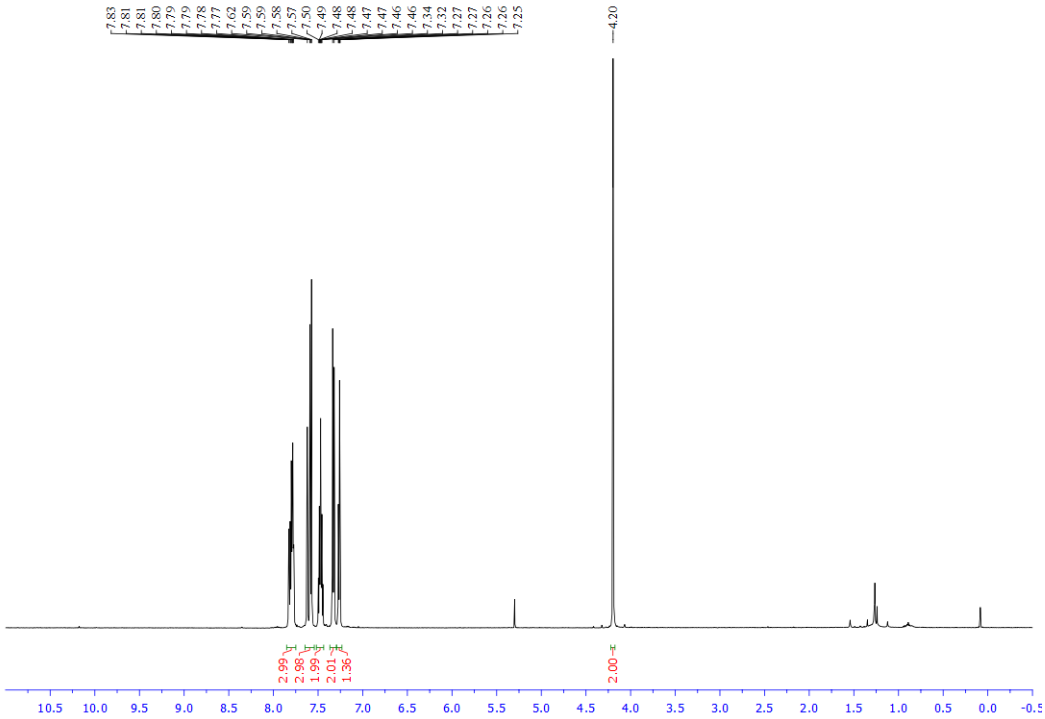


**Figure A1.97.** $^{1}$H NMR ($CDCl_3$, 500 MHz) spectrum of 4-(naphthalen-2-ylmethyl)benzonitrile (**42**)

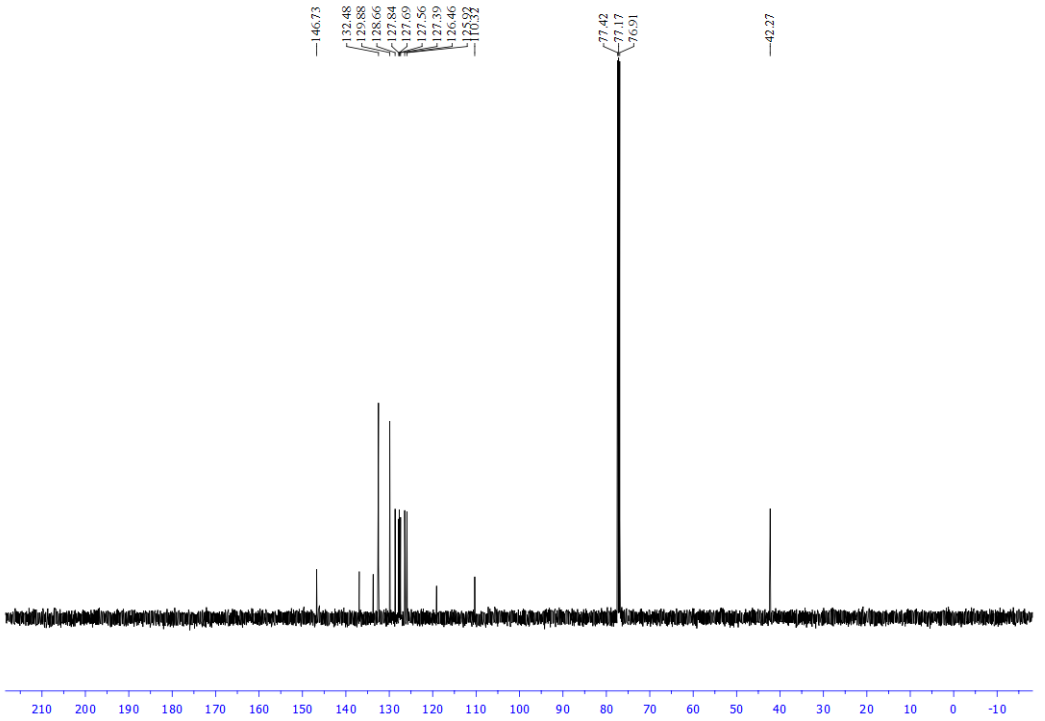


**Figure A1.98.** $^{13}$C NMR ($CDCl_3$, 125.8 MHz) spectrum of 4-(naphthalen-2-ylmethyl)benzonitrile (**42**)

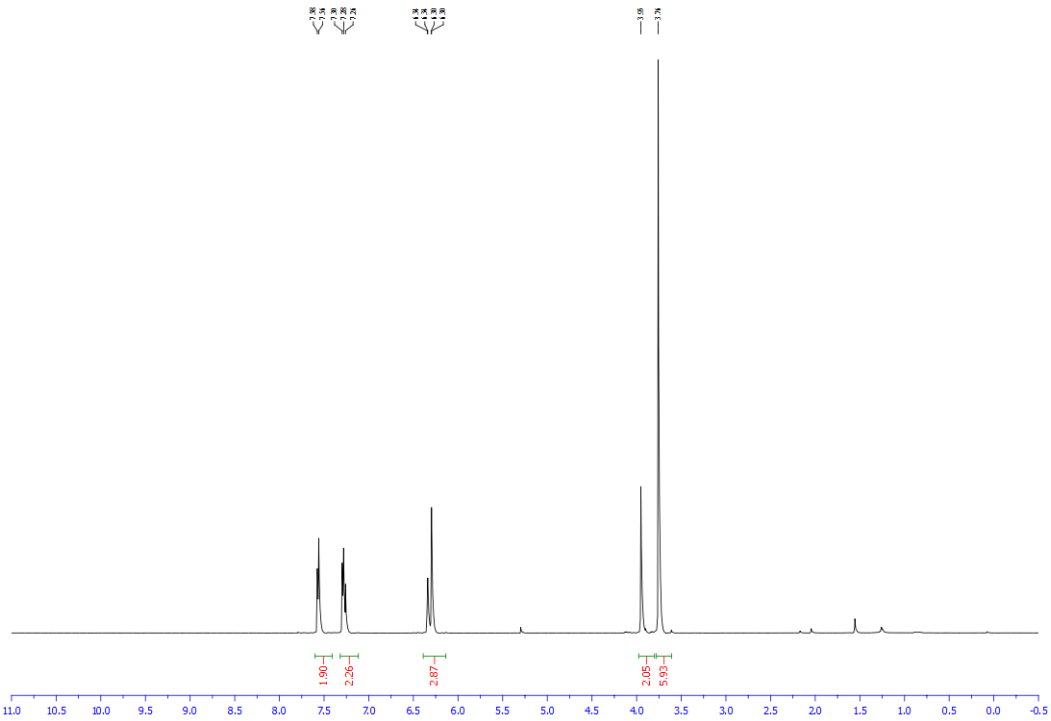

**Figure A1.99.** $^{1}H$ NMR ($CDCl_3$, 500 MHz) spectrum of 4-(3,5-dimethoxybenzyl)benzonitrile (**43**)

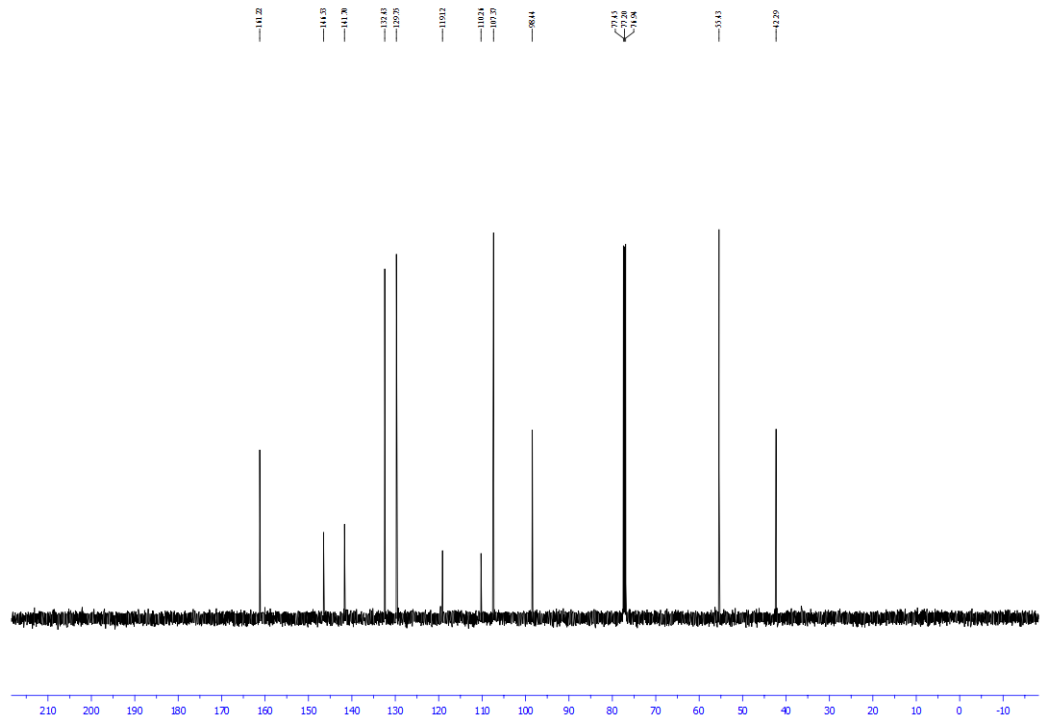

**Figure A1.99.** $^{13}C$ NMR ($CDCl_3$, 125.8 MHz) spectrum of 4-(3,5-dimethoxybenzyl)benzonitrile (**43**)

# Chapter 3. Extension to Activated Primary Systems

## 3.1 Introduction

Moving forward from the initial success in benzylic couplings, it was anticipated that success might be realized more broadly with an array of primary and secondary alkyl trifluoroborates. However, access to these radicals from alkyl precursors is not as trivial a process as one might expect. First off, primary, unactivated systems, such as *n*-hexyl trifluoroborate, exhibit prohibitively high oxidation potentials (1.9 V vs SCE)[1] for direct incorporation into the developed photoredox/Ni catalytic cycle. Although incorporation of unactivated, primary alkyl systems appeared inaccessible with the current technology, the use of stabilizing groups had enabled the generation of benzylic systems previously,[2] so the use of alternative stabilized moieties was considered to allow efficient radical generation.

Radical stability, similar to carbocation stability, can be influenced by a number of factors. As a singularly occupied orbital, these species tend to be electron-poor and benefit from any interaction that can donate electron density into the radical center. Three of the most well recognized phenomena for achieving this donation are hyperconjugative stabilization,[3] resonance stabilization,[4] and adjacent lone pair donation (**Figure 3.1**).[5]

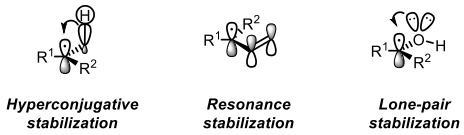


**Figure 3.1: Stabilization of radicals**

Given the stabilization afforded by α-heteroatom substitution, it was anticipated that the use of α-alkoxymethyltrifluoroborates would significantly lower the oxidation potential required to

access these radical species. Access to these radical synthons would serve to complement existing anionic approaches in cross-coupling.[i] Prior work on α-alkoxy anions[6,7] has included methods employing alkoxymethylzincs,[8,9] alkoxymethylstannanes,[10–13] and alkoxymethylboron derivatives.[14,15] However, the current methods are severely limited by the use of toxic and/or air- and moisture-sensitive reagents under often harsh conditions that inhibit the incorporation of reactive functional groups. As such, improved methods in this arena would allow access to benzylic ethers, which are an important motif in pharmaceutical[16–18] and supramolecular chemical architectures.[19,20]

## 3.2 Results and Discussion

At the start of this optimization, direct application of previously developed conditions afforded trace amounts of the desired α-alkoxymethyl cross-coupling product (**Eq. 3.1**). However, the alkyltrifluoroborate used in this initial investigation was deemed only sparingly soluble in room temperature acetone.

**Eq 3.1.** Previously optimized conditions with α-alkoxymethyltrifluoroborates

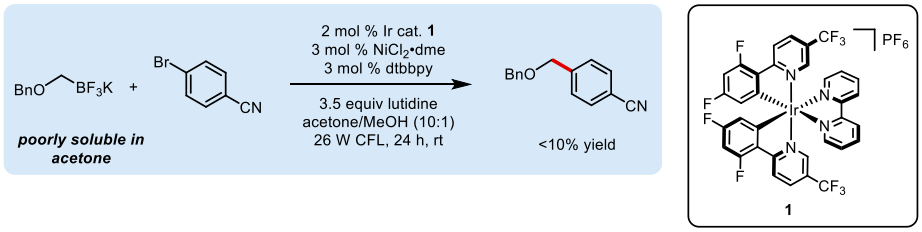


To overcome this issue, an extensive solvent screen was commenced to enhance contact between the photocatalyst and the alkyltrifluoroborate in solution (see Experimental). Solubility is

[i] Reproduced in part from *Org. Lett.*, **2015**, *17*, 3294

particularly important for these reactions as insoluble material disrupts light penetration and can serve to decouple the integrated catalytic cycles. In our experience, maintaining the homogeneity of the reaction mixture has always led to significant improvements. Using methyl 4-bromobenzoate, potassium [(benzyloxy)methyl]trifluoroborate (1.2 equiv), $NiCl_2$•dme (5.0 mol %), dtbbpy (5.0 mol %), Ir cat **1** (2.0 mol %), and a cosolvent system consisting of dioxane with added DMA was determined to provide the right balance of solubility and reactivity for the dual catalytic cross-coupling.

An investigation of additives, proposed to be key for sequestering generated $BF_3$ during trifluoroborate oxidation, also improved the yields significantly. Without added base, the reactions tend to stall out around 40-60% conversion (~10 h), leading us to suspect that byproduct inhibition is principally responsible. Among those bases examined, $K_2HPO_4$ led to full consumption of the starting material after 16 h.

With reasonably effective conditions in hand, alternate ligands and Ni sources were examined to identify scaffolds that might be useful in extending this chemistry. Although a number of these Ni sources and ligands served as competent catalysts (see Experimental), our model ligand remained a clear front-runner in both conversion and yield. Considering the commercial availability and low cost of this established catalytic system ($NiCl_2$•dme, dtbbpy), we moved forward with this combination to evaluate the full scope of this reaction.

Beginning with the aryl bromide partner, it was important to emphasize the ability of this catalyst system to engage a range of electronically differentiated aryl bromides. Reaction with electron-withdrawing 4-bromoacetophenone and electron-neutral 4-bromotoluene led to isolation of **4** and **13** in 86% and 62% yields, respectively. Even electron-rich bromides were competent electrophiles, as reaction with 4-bromoanisole gave rise to product **12**, albeit in a modest 52% yield.

*ortho*-Substitution was tolerated in trifluoromethyl-, cyano-, methyl-, and methoxy-substituted aryl bromides, leading to ethers **6-9**. Selective cross-coupling was observed exclusively at the bromide for both a bifunctional aryl triflate and a heteroaryl chloride, affording products **10** and **17**, respectively. Aldehydes contained in products **3** and **16** survived the reaction untouched.

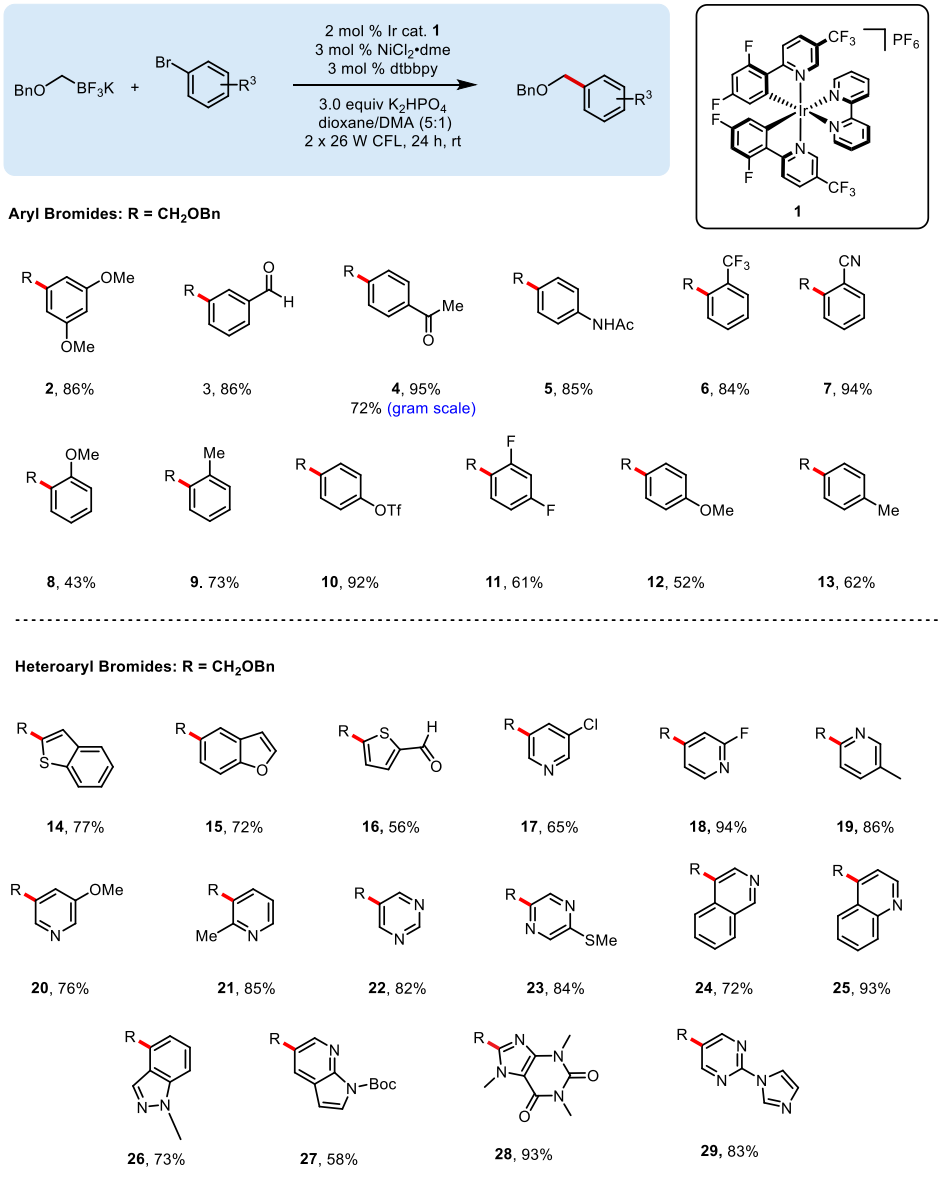


**Figure 3.2.** α-Alkoxymethyltrifluoroborate photoredox cross-coupling: halide scope

Considering the sensitivity of aldehydes to reduction under Pd-catalysis[21] as well as their electrophilicity toward harsher organometallic nucleophiles in cross-coupling, this method provides the opportunity to circumvent protection and/or oxidation-reduction sequences that may be required to access the same structural architecture. To ensure the scalability of this transformation, a gram-scale reaction was performed with 4-bromoacetophenone using reduced catalyst loadings (1.0 mol % Ir cat. **1** and 1.5 mol % $NiCl_2$•dme). Although extended reaction times were required for full conversion (48 h), the desired ether **4** was obtained in good yield (72%). The generality for the cross-coupling with heteroaryl substructures makes this method particularly attractive for late-stage diversification. In addition to the products derived from well-behaved benzofuran- and benzothiophene-containing bromides (**14, 15**), more challenging pyrazine-, pyrimidine-, quinoline-, and isoquinoline-containing bromides gave the desired products in excellent yield (**22-25**). Bromopyridines substituted at all regioisomeric positions were used to access products **17-21** in good yields. Even 8-bromocaffeine allowed access to product **28** in excellent yield. Unfortunately, protection was required for indazole- and azaindole-containing bromides, affording products **26** and **27**, respectively. Although satisfactory methods for cross-coupling of these protic heteroaryl bromides remain elusive, it should be noted that previous Pd-catalyzed conditions [3 mol % $Pd(OAc)_2$, 6 mol % RuPhos, 3 equiv $Cs_2CO_3$, dioxane/$H_2O$, 100° C] have proved wholly ineffective or low yielding for a number of the heteroaryl bromides shown.[14] Therefore, this method represents a marked improvement over the current state of the art.

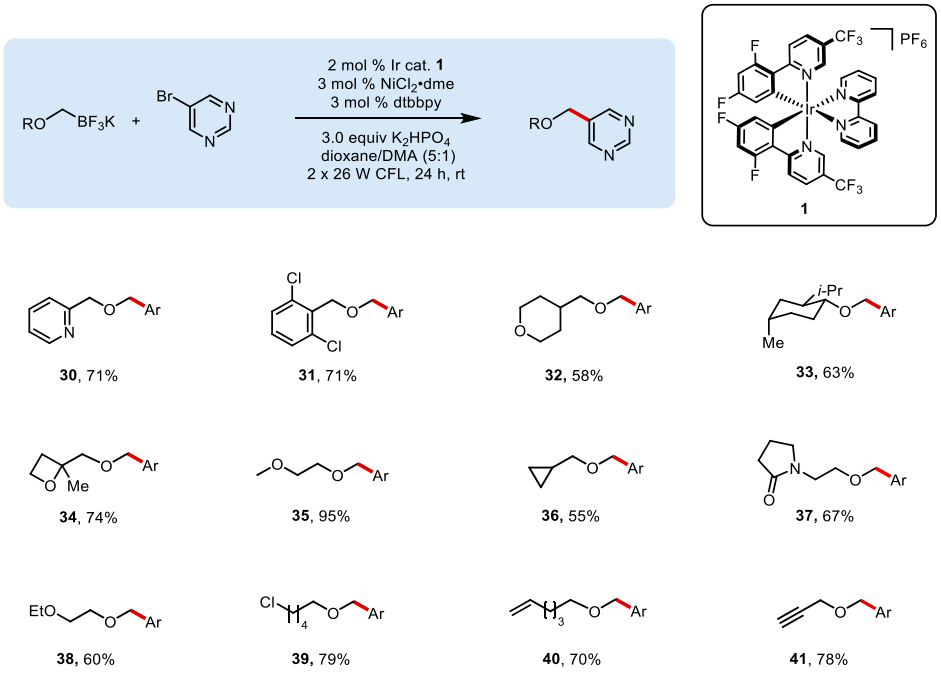


**Figure 3.3.** α-Alkoxymethyltrifluoroborate photoredox cross-coupling: Organotrifluoroborate scope

To highlight further the heteroaryl tolerance of this coupling, 5-bromopyrimidine was used as an electrophile to evaluate the alkoxymethyltrifluoroborate scope (**Figure 3.3**). To this end, a pyridyl-containing organotrifluoroborate was successfully employed to yield compound **30** in reasonable yield – showing tolerance of a heteroaryl functional unit in both reaction partners. Aryl chlorides were also tolerated on the trifluoroborate partner to give the dichlorinated arene **31** with no competitive reaction at the chlorides.

As expected, ethers were tolerated throughout the functionalized organotrifluoroborate core to give products such as **32**, **34**, and **35**. For **35**, the ability to incorporate PEG linkers on target molecules at a late stage could serve as a means to modulate in vivo drug solubility.[22] Steric bulk, although distal from the reacting radical, led to isolation of menthol derivative **33** and *tert*-butyl ether product **44** (**Figure 3.4**) in acceptable yields.

Beyond the largely aliphatic functional groups shown, amides and alkyl chlorides were untouched under the reaction conditions, leaving a site for further manipulation in products **37** and **39**. Also to be noted is that products containing alkenes and alkynes were isolated in excellent yields (**40-42**). Considering the intermediacy of radical intermediates during this process, the tolerance of these functional handles for later derivatization is particularly intriguing.

As a final testament to the utility of this transformation, a variety of α-alkoxymethyltrifluoroborates substituted with simple protecting groups were prepared (**Figure 3.4**). Currently, the facile preparation of many benzylic alcohols is predicated on commercial access to the corresponding esters and aldehydes. Even in cases where these precursors are readily available, the generated alcohols can be sensitive to ambient oxidation to afford a mixture of alcohol, aldehyde, and other oxidation byproducts.[23,24] Consequently, a method for the preparation of protected benzylic alcohol variants from the far more widely available aryl- and heteroaryl halides serves as an attractive method for reliable synthesis and long-term storage. To that end, allyl-, *para*-methoxybenzyl-, *tert*-butyl-, and trimethylsilylethyl-protected α-alkoxymethyltrifluoroborates were synthesized and employed as cross-coupling partners to give products **42-45**. Subsequent deprotection of these protected alcohols allows the formation of benzylic alcohols in two steps from readily accessible bromoarenes.

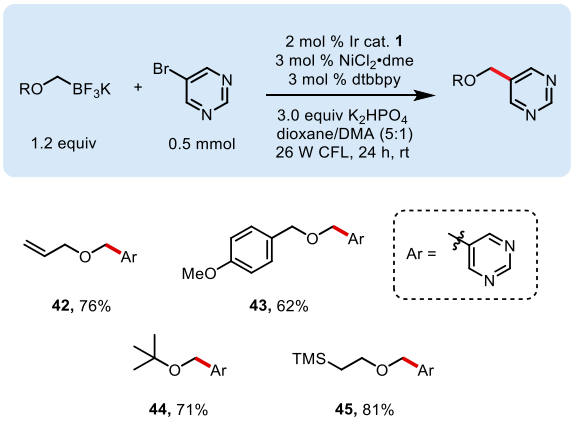


**Figure 3.4.** α-Alkoxy photoredox cross-coupling: formation of protected alcohols

## 3.3 Conclusion

In summary, room temperature conditions for the cross-coupling of α-alkoxymethyltrifluoroborates with an array of aryl bromides has been communicated. Previous reports for the cross-coupling of these substrates with aryl chlorides have taken place at 100 ºC in the presence of strong aqueous base and have suffered from significant limitations in scope when applied to both heteroaryl chlorides and -bromides. Consequently, the developed couplings address key substrate limitations of the former methods. Furthermore, the delineated procedures provide a method for the synthesis of benzylic ethers that can be readily deprotected to afford the corresponding alcohols – many of which are challenging to access in high purity.

Finally, although the products derived from these reactions can often be made by other means, the use of these reagents serves to validate further the photoredox cross-coupling manifold as a means of engaging $C_{sp3}$ nucleophiles in alkyl transfer under mild conditions. Most importantly, the ability to cross-couple late stage bromides with an ever-expanding library of $C_{sp3}$ hybridized nucleophiles using a single robust catalyst system is anticipated to enable practitioners to diversify synthetic molecular architecture quickly and expand three-dimensional chemical space.

## 3.4 Experimental

### General considerations

All reactions were carried out under an inert atmosphere of nitrogen or argon unless otherwise noted. Dioxane (99.9%, extra dry) and dimethyl acetamide (purity, extra dry) were used as received. $K_2HPO_4$ was used as received. $IrCl_3 \cdot xH_2O$, and $NiCl_2$•dme were purchased from commercial sources. All other reagents were purchased commercially and used as received. Photoredox reactions were irradiated with two to three standard 26 W compact fluorescent light bulbs. Melting points (°C) are uncorrected. NMR spectra were recorded on a 500 or 400 MHz spectrometer. $^{19}F$ NMR chemical shifts were referenced to external $CFCl_3$ (0.0 ppm). $^{11}B$ NMR spectra were obtained on a spectrometer equipped with the appropriate decoupling accessories. All $^{11}B$ NMR chemical shifts were referenced to an external $BF_3 \cdot OEt_2$ (0.0 ppm) with a negative sign indicating an upfield shift. Data are presented as follows: chemical shift (ppm), multiplicity (s = singlet, d = doublet, t = triplet, q = quartet, m = multiplet), coupling constant *J* (Hz) and integration. The $^{13}C$ signal of the carbon bonded to boron was not observed in some cases due to quadrupolar relaxation.

### Synthesis of α-alkoxymethyltrifluoroborates:

Most potassium α-alkoxymethyltrifluoroborates were purchased commercially. In cases where the desired potassium organotrifluoroborate was unavailable, the corresponding alcohol derivative was converted to the trifluoroborate by the following procedure.

**General procedure for α-alkoxymethyltrifluoroborate synthesis:**

NaH (96 mg, 4 mmol) was added to a 50 mL 2-neck round-bottom-flask and purged with $N_2$ three times. The content was diluted with dry THF (10 mL) and precursor alcohol (4.0 mmol) was then added dropwise to the reaction mixture at 0 °C under $N_2$. After stirring for 15 min at 0 °C, the temperature was increased to rt and further stirred for 30 min. Bromomethyltrifluoroborate (267 mg, 1.33 mmol) was added in one portion to the suspension at 0 °C, and the reaction was stirred at rt for 3 h. The reaction was quenched by adding 4.5 M $KHF_2$ (pH 6, ~ 4.5 mL). The final mixture was stirred for 30 min and then concentrated and dried overnight under high vacuum to remove trace solvent. The crude residue was suspended in hot acetone (3 x 50 mL) and filtered. The filtrate was concentrated to a minimal volume (5 – 10 mL) and $Et_2O$ (~150 mL) was added to precipitate. The white precipitate was isolated by filtration, washing with hexanes (~30 mL) and $CH_2Cl_2$ (~30 mL), to give the desired trifluoroborate in good yield.

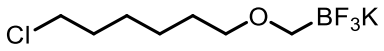


**S1**

**Potassium (((6-Chlorohexyl)oxy)methyl)trifluoroborate (S1)**: Obtained as a white solid (296 mg, 87%). mp = 177-181 °C, $^1$H NMR (DMSO, 500 MHz): 3.60-3.58 (m, 2H), 3.15-3.14 (m, 2H), 2.46-2.45 (m, 2H), 1.69-1.66 (m, 2H), 1.41-1.40 (m, 2H), 1.34-1.33 (m, 2H), 1.25-1.24 (m, 2H), $^{13}$C NMR (DMSO, 126 MHz) δ 73.9, 46.0, 32.6, 29.9, 26.9, 25.7, $^{19}$F NMR (DMSO, 471 MHz) δ -141.5, $^{11}$B NMR (DMSO, 128 MHz) δ 3.1, IR: ν = 2936, 2856, 1444, 1402, 1353, 1230, 1221, 1068, 1008, 961, 920, 804, 732 cm$^{-1}$, HRMS (ESI) m/z calc. for $C_7H_{14}BClF_3O$ ($M^-$) 217.0767, found 217.0773.

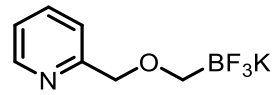

**S2**

**Potassium ((Pyridin-2-ylmethoxy)methyl)trifluoroborate (S2):** Obtained as a white solid (213 mg, 70%), mp = 162-164 ºC, $^{1}$H NMR (DMSO, 500 MHz) δ 8.45-8.44 (m, 1H), 7.74 (t, *J* = 7.5 Hz, 1H), 7.39 (d, *J* = 7.8 Hz, 1H), 7.25 – 7.14 (m, 1H), 4.35 (s, 2H), 2.62 (s, 2H), $^{13}$C NMR (DMSO, 126 MHz) δ 160.7, 149.2, 136.9, 122.5, 121.5, 76.4, $^{19}$F NMR (DMSO, 471 MHz) δ -141.4, $^{11}$B NMR (DMSO, 128 MHz) δ 3.2, IR: ν = 3773, 2834, 1593, 1435, 1352, 1304, 1234, 1121, 1060, 1022, 985, 918, 801 cm$^{-1}$, HRMS (ESI) m/z calc. for $C_7H_8BF_3NO$ ($M^-$) 190.0657, found 190.0653.

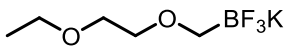

**S3**

**Potassium ((2-Ethoxyethoxy)methyl)trifluoroborate (S3):** Obtained as a colorless oil, 5 mmol scale (610 mg, 58%), $^{1}$H NMR (500 MHz, $(CD_3)_2CO$) δ $^{1}$H NMR (acetone-$d_6$, 500 MHz,) δ 3.58 – 3.50 (m, 4H), 3.49-3.46 (m, 2H), 2.80 (s, 2H), 1.16 (t, *J* = 7.0 Hz, 3H), $^{13}$C NMR (acetone-$d_6$, 126 MHz) δ 72.9, 69.2, 66.0, 14.4, $^{19}$F NMR (acetone-$d_6$, 471 MHz) δ -145.0, $^{11}$B NMR (acetone-$d_6$, 128 MHz) δ -4.8, IR: ν = 3606, 3054, 2977, 2870, 2305, 1712, 1608, 1447, 1265, 1072, 735 cm$^{-1}$, HRMS (ESI) m/z calc. for $C_5H_{11}BF_3O_2$ ($M^-$) 171.0804, found 171.0806.

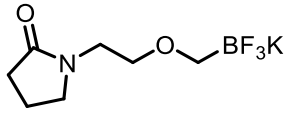

**S4**

**Potassium ((Methoxy)methyl)pyrrolidin-2-onetrifluoroborate (S4):** Obtained as a white solid (256 mg, 82%), mp = 120-123 ºC $^{1}$H NMR (DMSO, 500 MHz) δ 3.36-3.35 (m, 4H), 3.25 (s, 4H), 2.18-2.16 (m, 2H), 1.88-1.87 (m, 2H), $^{13}$C NMR (DMSO, 126 MHz) δ 174.5, 71.0, 47.5, 42.3, 30.8, 17.8, $^{19}$F NMR (DMSO, 471 MHz) δ 141.8, $^{11}$B NMR (DMSO, 128 MHz) δ 3.3, IR: ν = 3053,

2987, 2305, 1669, 1422, 1265, 1071, 895, 739, 705 $cm^{-1}$, HRMS (ESI) m/z calc. for $C_7H_{12}BF_3NO_2$ ($M^-$) 210.0913, found 210.0914.

**Selected reaction optimization studies**

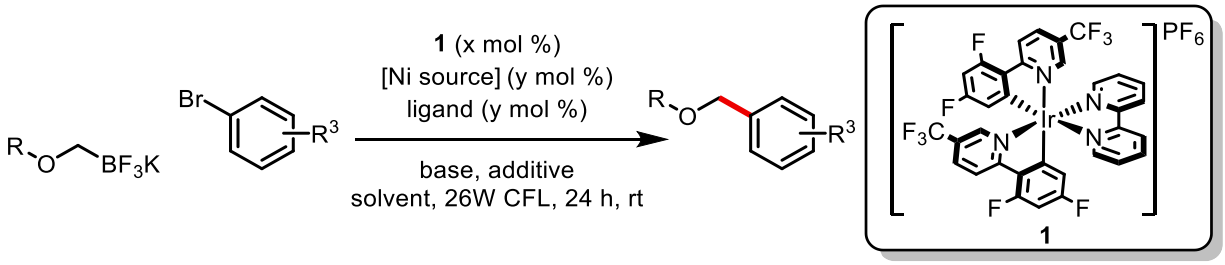


A 1:1 ratio of Ni source and ligand were dissolved in THF in a 1 gram reaction vial equipped with a Teflon coated magnetic stir bar. After stirring about 10 min, the solvent was removed *in vacuo*. Other solid additives were weighed into the vials. The vials were then brought into the glovebox where a stock solution of aryl bromide (0.1 mmol), alkoxymethyltrifluoroborate, Ir catalyst **1**, and internal standard were then added by syringe and stirred for 24 h in front of a single 26 W CFL at an ambient temperature of ~$35^0$ C. Reactions were analyzed using GC and compared within sets by crude product to internal standard (P/IS) ratios. Note: P/IS can only be compared within each table; fresh stock solutions were prepared for each screen.

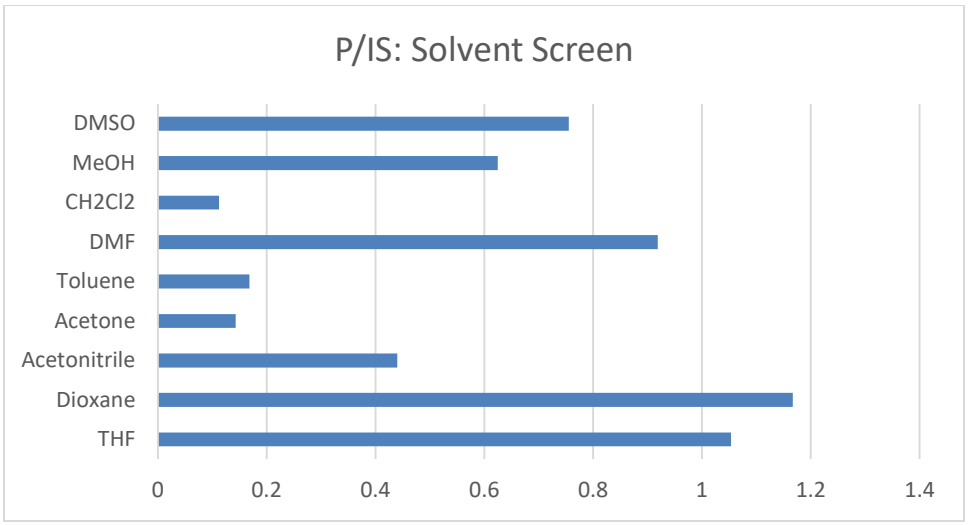


**Figure 3.5.** Comparison of Solvents
Conditions: 0.1 mmol Ph-Br, 1.2 equiv R-$BF_3K$, 2.0 % $Ir(dFCF_3ppy)_2bpy•PF_6$, 5.0 % $NiCl_2$•dme/dtbbpy, 0.05 M in solvent

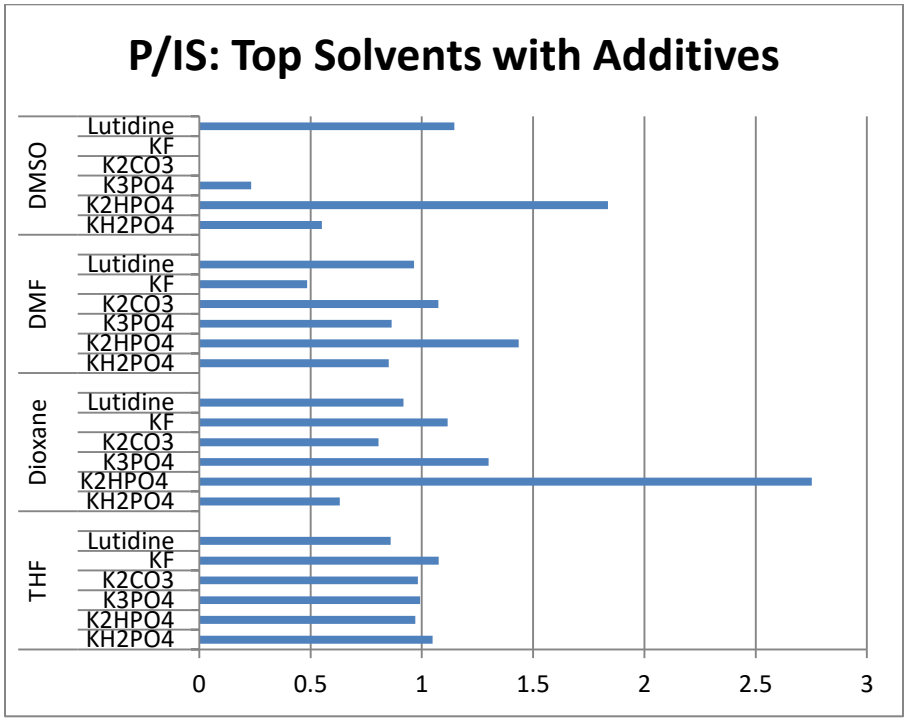


**Figure 3.6.** Comparison of Solvents and Bases
Conditions: 0.1 mmol Ph-Br, 1.2 equiv R-$BF_3K$, 2.0 % $Ir(dFCF_3ppy)_2bpy•PF_6$, 5.0 % $NiCl_2$•dme/dtbbpy, 1.0 equiv base, 0.05 M in solvent

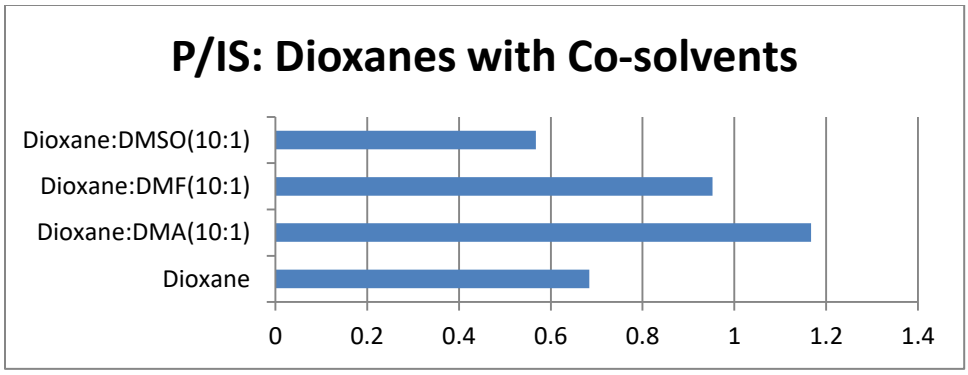


**Figure 3.7.** Comparison of Solvent Mixtures
Conditions: 0.1 mmol Ph-Br, 1.2 equiv R-$BF_3K$, 2.0 % $Ir(dFCF_3ppy)_2bpy•PF_6$, 5.0 % $NiCl_2$•dme/dtbbpy, 1.0 equiv $K_2HPO_4$, 0.05 M in solvent

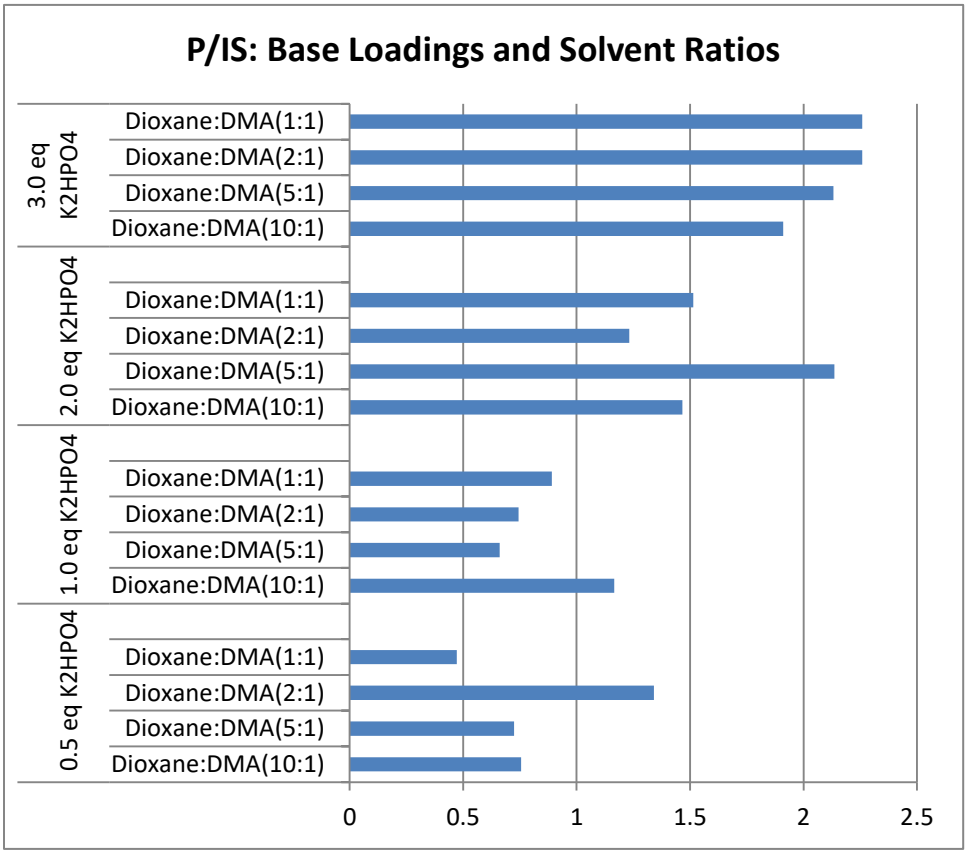


**Figure 3.8.** Comparison of Solvent Mixture and Base Ratios
Conditions: 0.1 mmol Ph-Br, 1.2 equiv R-$BF_3K$, 2.0 % $Ir(dFCF_3ppy)_2bpy•PF_6$, 5.0 % $NiCl_2$•dme/dtbbpy, 0.05 M in solvent

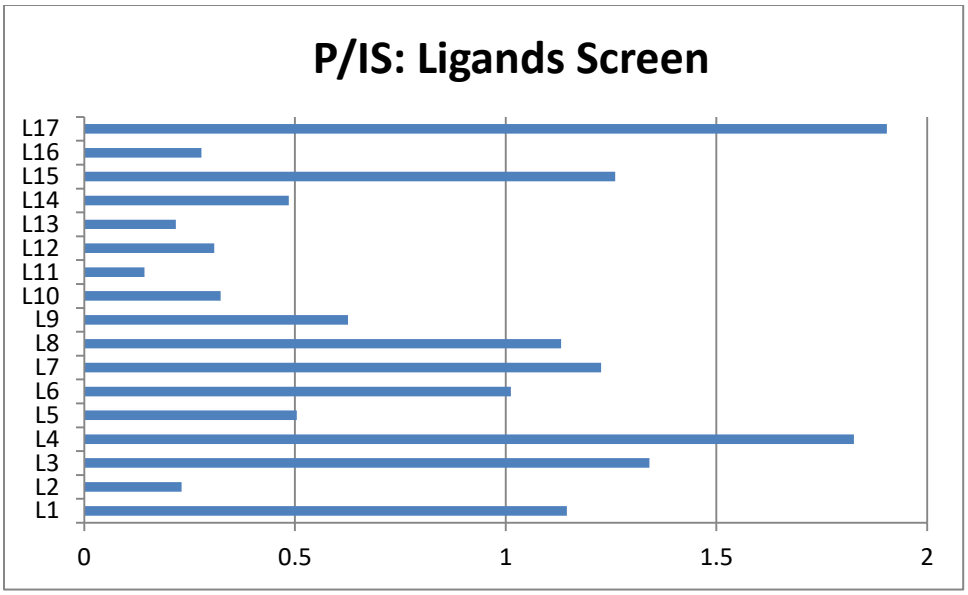


**Figure 3.9.** Comparison of Ligands
Conditions: 0.1 mmol Ph-Br, 1.2 equiv R-$BF_3K$, 2.0 % $Ir(dFCF_3ppy)_2bpy•PF_6$, 5.0 % $NiCl_2$•dme/ligand, 3.0 equiv $K_2HPO_4$, 0.05 M in solvent

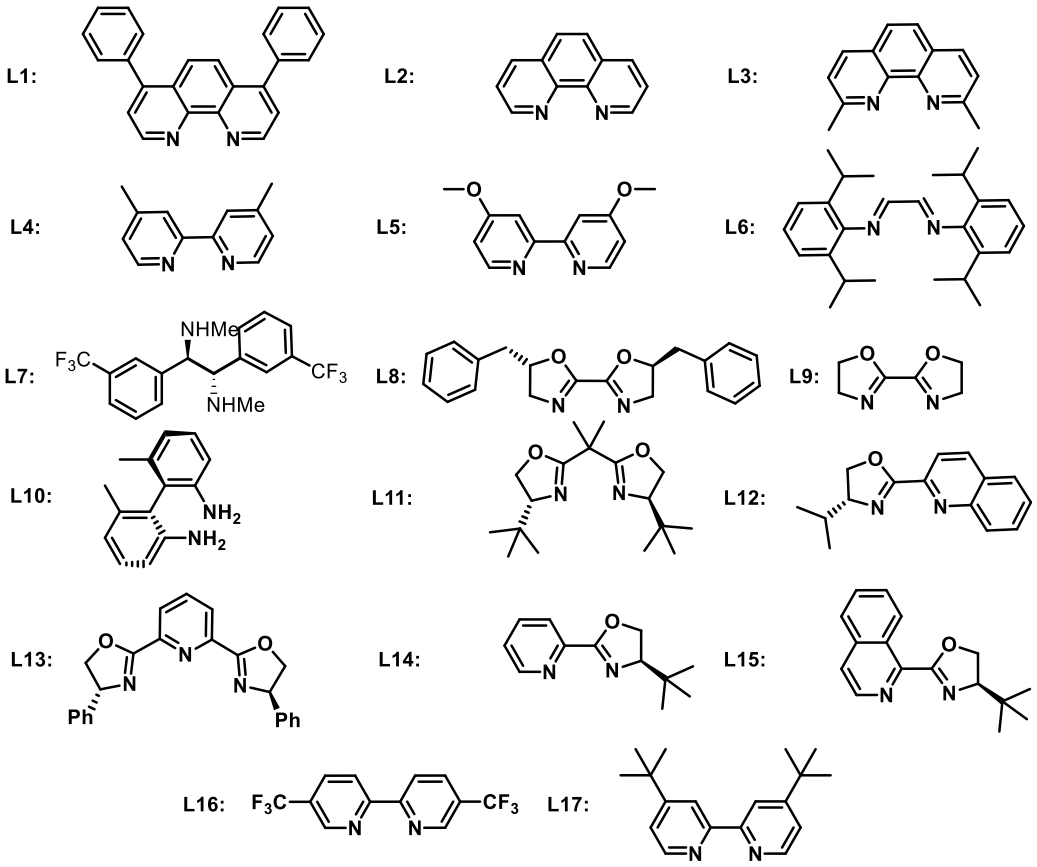

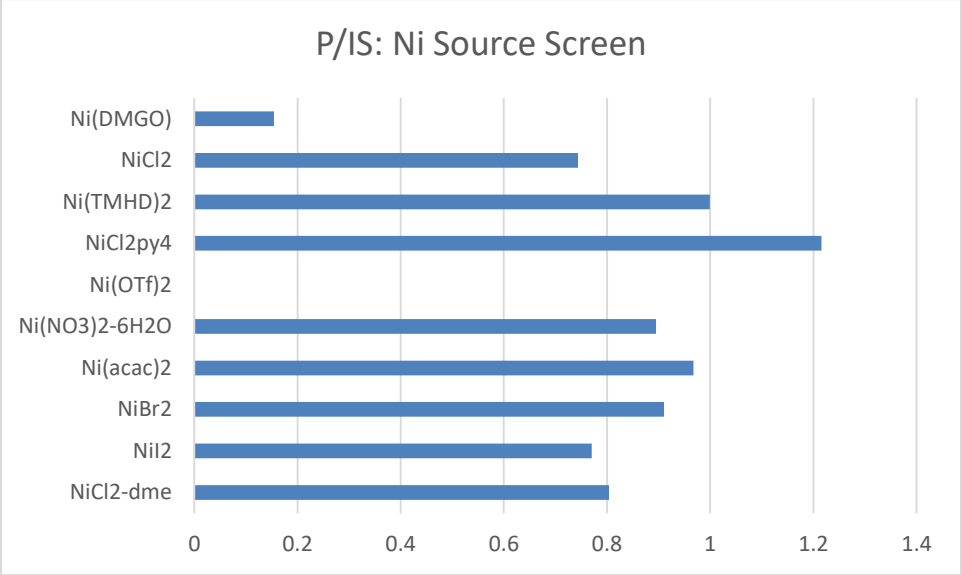


**Figure 3.10.** Comparison of Ni Sources
Conditions: 0.1 mmol Ph-Br, 1.2 equiv R-$BF_3K$, 2.0 % $Ir(dFCF_3ppy)_2bpy•PF_6$, 5.0 % Ni source / dtbbpy, 3.0 equiv $K_2HPO_4$, 0.05 M in solvent

Ni(DMGO) = Nickel(II) dimethylglyoxime; $Ni(TMHD)_2$ = Nickel(II) bis(2,2,6,6-tetramethyl-3,5-heptanedionate); $NiCl_2py_4$ = Nickel(II) chloride tetrapyridine

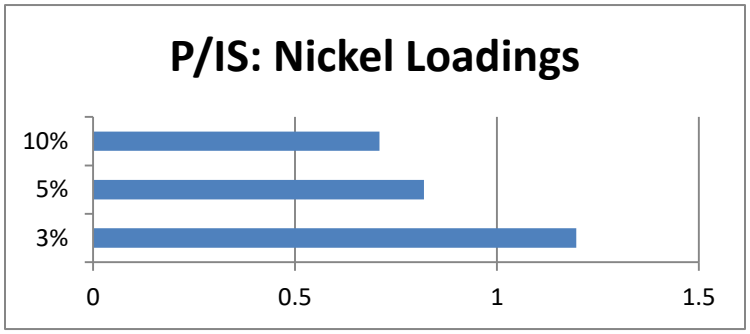


**Figure 3.11.** Comparison of $NiCl_2$•dme/dtbbpy loadings
Conditions: 0.1 mmol Ph-Br, 1.2 equiv R-$BF_3K$, 2.0 % $Ir(dFCF_3ppy)_2bpy•PF_6$, 3.0 equiv $K_2HPO_4$, 0.05 M in solvent

**General Procedure for Photoredox Cross-Coupling Reactions**

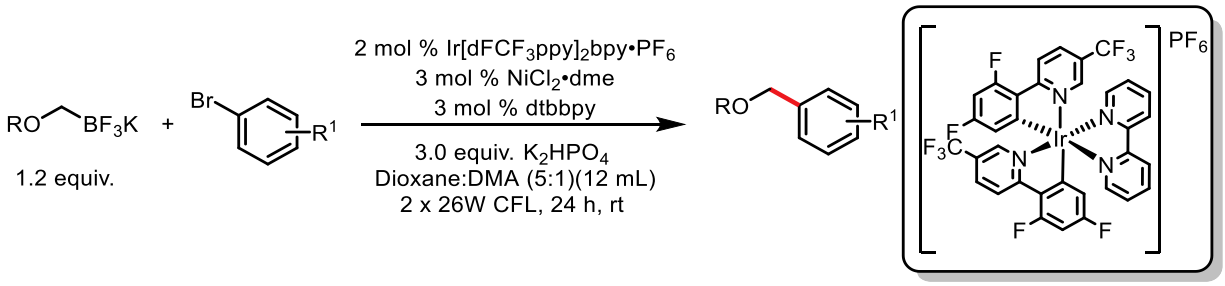


4,4'-di-*tert*-Butyl-2,2'-bipyridine (4.0 mg, 0.015 mmol) and $NiCl_2$•dme (3.3 mg, 0.015 mmol) were weighed into a 20 mL oven-dried, long, thin (~20 mL) glass vial. Approximately 1 mL of dry, degassed THF was added and the mixture was heated briefly until obtaining a pale green solution. The solvent was then removed under vacuum to yield a ligated nickel complex that was pale evergreen color. Next, aryl bromide (0.5 mmol, 1 equiv) (liquid aryl bromides were added with solvent), alkoxymethyltrifluoroborate (0.6 mmol, 1.2 equiv), $Ir[dFCF_3ppy]_2(bpy)•PF_6$ **1** (10.1 mg, 0.02 mmol) and $K_2HPO_4$ (261 mg, 1.5 mmol) were added sequentially. Afterwards, the tube was sealed and subsequently purged and evacuated four times. Dioxane/DMA (5:1) (12 mL) was next added under inert atmosphere. The resulting mixture was stirred for 24 h approximately 4 cm away from two 26 W fluorescent light bulbs while a fan was blown across the reaction setup to maintain an ambient temperature of 24 $^oC$. The crude reaction mixture was filtered through a cylindrical plug of Celite and rinsed with $CH_2Cl_2$ and EtOAc (10-20 mL). The resulting solution was concentrated, and the residue was purified by column chromatography on silica gel, eluting with EtOAc and hexanes, to obtain products in pure form.

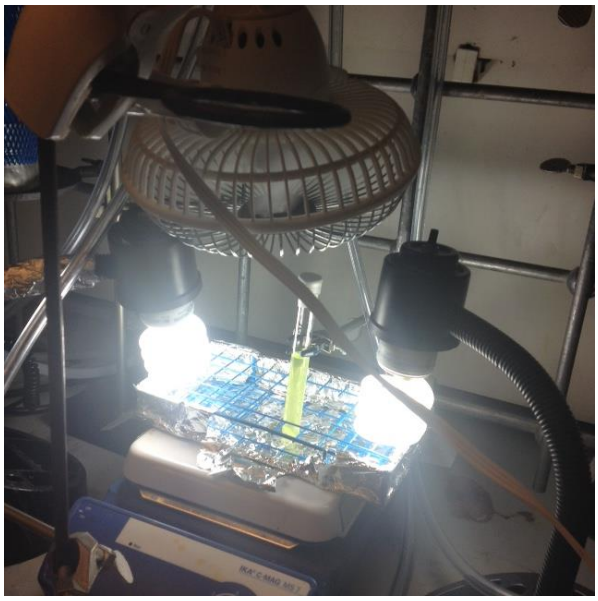

**Figure 3.12.** Photoredox cross-coupling reaction set-up (0.5 mmol scale)

**Gram scale reaction:** To a ~125 mL long, thin-walled vacuum flask equipped with a Teflon-coated magnetic stir bar was added $NiCl_2$•dme (16.5 mg, 0.075 mmol, 0.015 equiv) and 4,4'-di-*tert*-butyl-2,2'-bipyridine (20 mg, 0.075, 0.015 equiv), and 5.0 mL of THF. The vial was capped, and the resulting suspension was heated briefly with a heat gun until the nickel and ligand were fully solubilized, yielding a pale green solution. The solvent was then removed under vacuum to give a fine coating of the ligated nickel complex (pale evergreen in color). Once fully evacuated, 1-(4-bromophenyl)ethan-1-one (1.000 g, 5.025 mmol, 1.00 equiv), potassium (benzyloxy)methyltrifluoroborate (1.37 g, 6.03 mmol, 1.20 equiv), $Ir[dFCF_3ppy]_2(bpy)$•$PF_6$ **1** (53 mg, 0.0525 mmol, 0.01 equiv), and $K_2HPO_4$ (2.6 g, 15.07 mmol, 3.0 equiv) was added. The vial was then capped with a rubber septum and purged and evacuated four times. Under inert atmosphere, dioxane (92 mL) and DMA (18 mL) was introduced. The vial containing all the reagents was further sealed with parafilm and stirred vigorously (a small vortex should be observed toward the top of the reaction mixture) for 48 h approximately 4 cm away from three 26 W

fluorescent light bulbs. A fan was blown across the reaction setup to maintain an ambient temperature around 24 °C. After completion, the crude reaction mixture was filtered through an approximately 4 cm x 2 cm cylindrical plug of Celite, washing with EtOAc (40 mL). The resulting solution was concentrated, and the residue was purified by column chromatography on silica gel, eluting with EtOAc and hexanes, to obtain product in pure form.

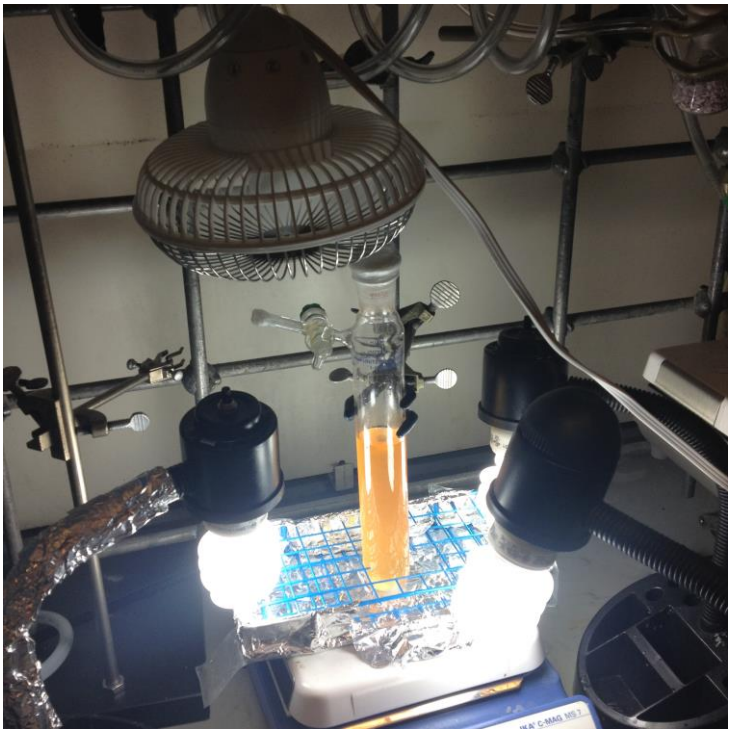

**Figure 3.13.** Gram scale photoredox cross-coupling reaction set-up (4.65 mmol)

## Compound Characterization Data

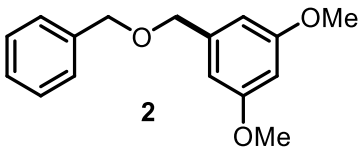


2

**1-((Benzyloxy)methyl)-3,5-dimethoxybenzene (2):** Obtained as a colorless oil (111 mg, 86%), $^{1}$H NMR ($CDCl_3$, 500 MHz): δ 7.42-7.37 (m, 4H), 7.34-7.33 (m, 1H), 6.59 (s, 2H), 6.45 (s, 1H), 4.59 (s, 2H), 4.55 (s, 2H), 3.82 (s, 6H), $^{13}$C NMR ($CDCl_3$, 126 MHz): δ 161.1, 141.0, 138.4, 128.6, 128.0, 127.8, 105.6, 99.9, 72.3, 72.2, 55.5, IR: ν = 2838, 1597, 1455, 1430, 1358, 1320, 1204, 1153, 1098, 1065, 1055, 833, 737, 698 $cm^{-1}$; HRMS (ESI) m/z calc. for $C_{16}H_{18}O_3Na$ (M+Na) 281.1154, found 281.1162.

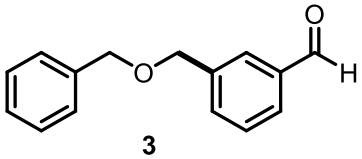


3

**3-((Benzyloxy)methyl)benzaldehyde (3):** Obtained as a semi solid (97 mg, 86%), $^{1}$H NMR ($CDCl_3$, 500 MHz): δ 10.03 (s, 1H), 7.89 (s, 1H), 7.82 (d, *J* = 7.6 Hz, 1H), 7.65 (d, *J* = 7.6 Hz, 1H), 7.53 (t, *J* = 7.6 Hz, 1H), 7.41 – 7.35 (m, 4H), 7.33-7.31 (m, 1H), 4.63 (s, 2H), 4.61 (s, 2H), $^{13}$C NMR ($CDCl_3$, 126 MHz): δ 192.4, 139.7, 138.0, 136.7, 133.7, 129.3, 129.1, 128.9, 128.7, 128.0, 128.0, 72.7, 71.5, IR: ν = 2856, 1694, 1606, 1590, 1453, 1285, 1203, 1099, 1072, 1028, 750, 697 $cm^{-1}$; HRMS (ESI) m/z calc. for $C_{15}H_{14}O_2Na$ (M+Na) 249.0891, found 249.0896.

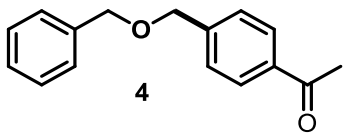


4

**1-(4-(Benzyloxy)methyl)phenyl)ethan-1-one (4):** Obtained as a colorless oil (114 mg, 95%) On gram scale with 1% Ir cat. **1** and 1.5% $NiCl_2$.dme/dtbbpy (868 mg, 72% yield), $^{1}$H NMR ($CDCl_3$, 500 MHz): δ 7.96 (d, *J* = 8.4 Hz, 2H), 7.47 (d, *J* = 8.4 Hz, 2H), 7.40 – 7.35 (m, 4H), 7.33-7.30 (m,

1H), 4.62 (s, 2H), 4.60 (s, 2H), 2.60 (s, 3H), $^{13}$C NMR ($CDCl_3$, 126 MHz): δ 197.9, 144.0, 138.1, 136.6, 128.7, 128.6, 128.0, 127.9, 127.6, 72.7, 71.6, 26.8, IR: ν = 2919, 2851, 1682, 1609, 1413, 1358, 1267, 1092, 1073, 1016, 957, 820, 699 $cm^{-1}$; HRMS (ESI) m/z calc. for $C_{16}H_{16}O_2Na$ (M+Na) 263.1048, found 263.1035.

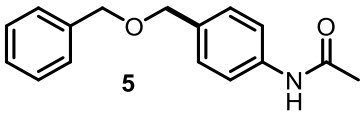


**5**

***N*-((4-(Benzyloxy)methyl)phenyl)acetamide (5):** Obtained as a white solid (108 mg, 85%), mp = 84-85 °C, $^1$H NMR ($CDCl_3$, 500 MHz): 8.06 (s, 1H), 7.50 (d, *J* = 8.2 Hz, 2H), 7.45 – 7.26 (m, 7H), 4.54 (s, 2H), 4.51 (s, 2H), 2.12 (s, 3H), $^{13}$C NMR ($CDCl_3$, 126 MHz): δ 169.0, 138.3, 137.7, 134.2, 128.7, 128.5, 127.9, 127.8, 120.1, 72.2, 71.8, 24.5, IR: ν = 3309, 2866, 2342, 1614, 1611, 1555, 1544, 1517, 1358, 1326, 1270, 1091, 1073, 824, 730 $cm^{-1}$; HRMS (ESI) m/z calc. for $C_{16}H_{17}NO_2Na$ (M+Na) 278.1157, found 278.1147.

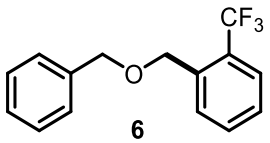


**6**

**1-(Benzyloxy)methyl)-2-(trifluoromethyl)benzene (6):** Obtained as a colorless oil (112 mg, 84%), $^1$H NMR ($CDCl_3$, 500 MHz): δ 7.80 (d, *J* = 7.8 Hz, 1H), 7.68 (d, *J* = 7.8 Hz, 1H), 7.59 (m, 1H), 7.42-7.39 (m, 5H), 7.35-7.32 (m, 1H), 4.81 (s, 2H), 4.66 (s, 2H), $^{13}$C NMR ($CDCl_3$, 126 MHz): δ 138.1, 137.3, 132.1, 129.1, 128.6, 127.9, 127.9, 127.5, 125.8 (q, *J* = 5.7 Hz), 124.6 (q, *J* = 273.6 Hz), 73.0, 68.4 (q, *J* = 2.7 Hz), $^{19}$F NMR (471 MHz, $CDCl_3$) δ -59.97, IR: ν = 2854, 1451, 1365, 1314, 1163, 1117, 1059, 1038, 769, 697 $cm^{-1}$; HRMS (ESI) m/z calc. for $C_{15}H_{14}F_3O$ (M+H) 267.0997, found 267.0992.

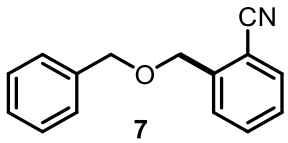


7

**2-((Benzyloxy)methyl)benzonitrile (7):** Obtained as a colorless oil (105 mg, 94%), $^{1}$H NMR ($CDCl_3$, 500 MHz): δ 7.66-7.58 (m, 3H), 7.43-7.37 (m, 5H), 7.34-7.31 (m, 1H), 4.76 (s, 2H), 4.67 (s, 2H), $^{13}$C NMR ($CDCl_3$, 126 MHz): δ 142.2, 137.8, 133.0, 132.9, 128.8, 128.7, 128.2, 128.1, 128.1, 117.5, 111.7, 73.37, 70.0, IR: ν = 2919, 2850, 2225, 1600, 1453, 13612, 1214, 1111, 1075, 763, 738, 698 cm$^{-1}$; HRMS (ESI) m/z calc. for $C_{15}H_{14}NO$ (M+H) 224.1075, found 224.1077.

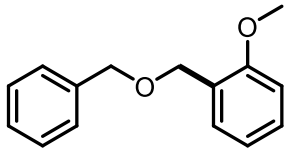


8

**1-((Benzyloxy)methyl)-2-methoxybenzene (8):** Obtained as a colorless oil (49 mg, 43%), $^{1}$H NMR ($CDCl_3$, 500 MHz): δ 7.48 – 7.36 (m, 5H), 7.33-7.27 (m, 2H), 7.01-6.98 (m, 1H), 6.91-6.89 (m, 1H), 4.64 (s, 4H), 3.85 (s, 3H), $^{13}$C NMR ($CDCl_3$, 126 MHz): δ 157.1, 138.5, 128.9, 128.6, 128.3, 127.7, 127.4, 126.6, 120.4, 110.1, 72.3, 66.9, 55.2, IR: ν = 3865, 2838, 1603, 1494, 1464, 1361, 1244, 1092, 1029, 753 cm$^{-1}$; HRMS (ESI) m/z calc. for $C_{15}H_{16}O_2$ (M+) 228.1150, found 228.1143.

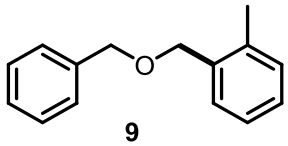


9

**1-((Benzyloxy)methyl)-2-methylbenzene (9):** Obtained as a colorless oil (77 mg, 73%), $^{1}$H NMR ($CDCl_3$, 500 MHz): δ 7.41-7.37 (m, 5H), 7.34-7.32 (m, 1H), 7.26 – 7.18 (m, 3H), 4.61 (s, 2H), 4.59 (s, 2H), 2.37 (s, 3H), $^{13}$C NMR ($CDCl_3$, 126 MHz): δ 138.3, 136.7, 136.0, 130.2, 128.6, 128.3, 127.8, 127.7, 127.6, 125.7, 72.2, 70.5, 18.8, IR: ν = 3029, 2855, 1605, 1495, 1454, 1358, 1213, 1090, 1072, 742, 697 cm$^{-1}$; HRMS (ESI) m/z calc. for $C_{15}H_{15}O$ (M-H) 211.1123, found 211.1129.

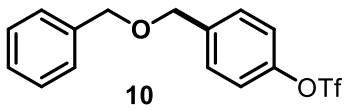


10

**4-((Benzyloxy)methyl)phenyl trifluoromethanesulfonate (10):** Obtained as a colorless oil (160 mg, 92%), $^{1}$H NMR ($CDCl_3$, 500 MHz): δ 7.48-7.26 (m, 2H), 7.41-7.38 (m, 4H), 7.36-7.33 (m, 1H), 7.31-7.27 (m, 2H), 4.62 (s, 2H), 4.59 (s, 2H), $^{13}$C NMR ($CDCl_3$, 126 MHz): δ 149.0, 139.2, 138.0, 129.4, 128.7, 128.0, 128.0, 121.4, 119.0 (q, *J* = 320.8 Hz), 72.8, 71.1, $^{19}$F NMR (471 MHz, $CDCl_3$) δ -72.76, IR: ν = 2853, 1501, 1422, 1249, 1210, 1139, 1094, 1017, 887, 697 cm$^{-1}$; HRMS (ESI) m/z calc. for $C_{15}H_{13}F_3O_4SNa$ (M+Na) 369.0384, found 369.0383.

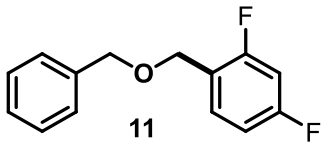


11

**1-((Benzyloxy)methyl)-2,4-difluorobenzene (11):** Obtained as a colorless oil (71 mg, 61%), $^{1}$H NMR ($CDCl_3$, 500 MHz): δ 7.45-7.41 (m, 1H), 7.39 – 7.35 (m, 4H), 7.31-7.30 (m, 1H), 6.91 – 6.85 (m, 1H), 6.84 – 6.78 (m, 1H), 4.59 (s, 2H), 4.58 (s, 2H), $^{13}$C NMR ($CDCl_3$, 126 MHz): δ 162.8 (dd, *J* = 220.7, 12.1 Hz), 160.9 (dd, *J* = 221.8, 12.2 Hz) 138.1, 131.2 (dd, *J* = 9.7, 5.6 Hz), 128.6, 127.9, 121.5 (dd, *J* = 15.3, 3.5 Hz), 111.3 (dd, *J* = 21.0, 3.6 Hz), 103.8 (dd, *J* = 25.4, 25.4 Hz), 72.7, 65.3 (d, *J* = 3.4 Hz), $^{19}$F NMR ($CDCl_3$, 471 MHz): δ -110.9 (d, *J* = 7.4 Hz), -114.6 (d, *J* = 7.4 Hz), IR: ν = 2864, 1620, 1606, 1505, 1454, 1430, 1277, 1139, 1101, 1072, 1029, 962, 849, 735, 697 cm$^{-1}$; HRMS (ESI) m/z calc. for $C_{14}H_{12}F_2O$ (M+) 234.0856, found 234.0857.

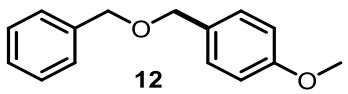


12

**1-((Benzyloxy)methyl)-4-methoxybenzene (12):** Obtained as a colorless oil (60 mg, 52%), $^{1}$H NMR ($CDCl_3$, 500 MHz): δ 7.41 – 7.35 (m, 4H), 7.32 (m, 3H), 6.92 (d, *J* = 8.6 Hz, 2H), 4.56 (s, 2H), 4.52 (s, 2H), 3.83 (s, 3H), $^{13}$C NMR ($CDCl_3$, 126 MHz): δ 159.1, 138.3, 130.3, 129.4, 128.3, 127.7, 127.5, 113.7, 71.7, 71.6, 55.2, IR: ν = 3893, 2853, 1652, 1513, 1454, 1360, 1302, 1247,

1172, 1088, 1071, 1034, 822, 737, 697 $cm^{-1}$; HRMS (ESI) m/z calc. for $C_{15}H_{16}O_2$ (M+) 228.1150, found 228.1155.

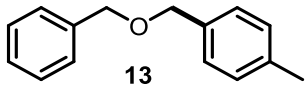


13

**1-((Benzyloxy)methyl)-4-methylbenzene (13):** Obtained as a colorless oil (66 mg, 62%), $^1$H NMR ($CDCl_3$, 500 MHz): δ 7.46 – 7.38 (m, 4H), 7.36-7.33 (m, 3H), 7.23-7.22 (m, 2H), 4.60 (s, 2H), 4.58 (s, 2H), 2.41 (s, 3H), $^{13}$C NMR ($CDCl_3$, 126 MHz): δ 138.3, 137.3, 135.2, 129.1, 128.3, 127.9, 127.7, 127.5, 71.9, 71.8, 21.2, IR: ν = 3028, 2854, 1615, 1516, 1496, 1453, 1359, 1204, 1092, 1073, 1028, 803, 735, 697 $cm^{-1}$; HRMS (ESI) m/z calc. for $C_{15}H_{15}O$ (M-H) 211.1123, found 211.1124.

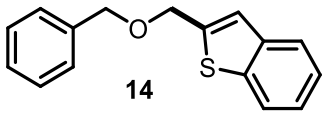


14

**2-((Benzyloxy)methyl)benzo[b]thiophene (14):** Obtained as a white solid, mp = 51-53 °C (98 mg, 77%), $^1$H NMR ($CDCl_3$, 500 MHz): δ 7.87 (d, *J* = 7.3 Hz, 1H), 7.78 (d, *J* = 7.2 Hz, 1H), 7.45 – 7.31 (m, 7H), 7.26 (s, 1H), 4.85 (s, 2H), 4.65 (s, 2H), $^{13}$C NMR ($CDCl_3$, 126 MHz): δ 142.2, 140.2, 139.4, 137.7, 128.4, 127.9, 127.8, 126.3, 124.2, 123.4, 122.6, 122.4, 71.8, 67.2, IR: ν = 3031, 2923, 2851, 1496, 1455, 1355, 1140, 1129, 1086, 1070, 1061, 841, 746, 727, 696 $cm^{-1}$; HRMS (ESI) m/z calc. for $C_{16}H_{14}OSNa$ (M+Na) 277.0663, found 277.0673.

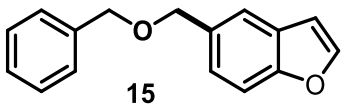


15

**5-((Benzyloxy)methyl)benzofuran (15):** Obtained as a colorless oil (86 mg, 72%), $^1$H NMR ($CDCl_3$, 500 MHz): δ 7.65-7.64 (m, 2H), 7.53-7.51 (m, 1H), 7.46 – 7.37 (m, 4H), 7.36 – 7.29 (m, 2H), 6.79-6.78 (m, 1H), 4.68 (s, 2H), 4.61 (s, 2H), $^{13}$C NMR ($CDCl_3$, 126 MHz): δ 154.8, 145.5, 138.5, 133.0, 128.6, 128.0, 127.8, 127.7, 124.7, 120.9, 111.4, 106.8, 72.5, 72.1, IR: ν = 2854, 1538,

1496, 1469, 1453, 1444, 1362, 1264, 1126, 1108, 1089, 1070, 1031, 884, 760, 734 $cm^{-1}$; HRMS (ESI) m/z calc. for $C_{16}H_{14}O_2Na$ (M+Na) 261.0891, found 261.0899.

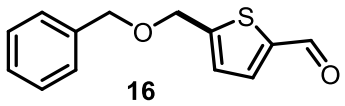


**16**

**5-((Benzyloxy)methyl)thiophene-2-carbaldehyde (16)**: Obtained as a colorless oil (65 mg, 56%), $^1H$ NMR ($CDCl_3$, 500 MHz): 9.87 (s, 1H), 7.66 (d, *J* = 3.8 Hz, 1H), 7.37 (d, *J* = 4.4 Hz, 4H), 7.34 – 7.26 (m, 1H), 7.09 (d, *J* = 3.7 Hz, 1H), 4.73 (s, 2H), 4.61 (s, 2H), $^{13}C$ NMR ($CDCl_3$, 126 MHz): δ 183.1, 152.6, 143.5, 137.5, 136.6, 128.7, 128.2, 128.0, 126.6, 72.7, 66.9, IR: ν = 2854, 1713, 1668, 1464, 1454, 1359, 1227, 1206, 1086, 816, 738, 698 $cm^{-1}$; HRMS (ESI) m/z calc. for $C_{13}H_{12}O_2SNa$ (M+Na) 255.0456, found 255.0462.

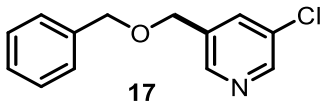


**17**

**1-((Benzyloxy)methyl)-3-chlorobenzene (17):** Obtained as a colorless oil (75 mg, 64%), $^1H$ NMR ($CDCl_3$, 500 MHz): δ 8.52 (m, 1H), 8.46 (s, 1H), 7.73 (s, 1H), 7.38 (m, 4H), 7.34 (m, 1H), 4.61 (s, 2H), 4.56 (s, 2H), $^{13}C$ NMR ($CDCl_3$, 126 MHz): δ 147.9, 146.6, 137.3, 135.1, 134.9, 132.0, 128.5, 127.9, 127.7, 72.7, 68.6, IR: ν = 2921, 1566, 1336, 1265, 1165, 1059, 1035, 911, 732, $cm^{-1}$; HRMS (ESI) m/z calc. for $C_{13}H_{13}ClNO$ (M+H) 234.0686, found 234.0685.

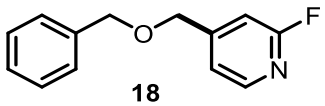


**18**

**4-((Benzyloxy)methyl)-2-fluoropyridine** (**18)**: Obtained as a colorless oil (102 mg, 94%), $^1H$ NMR ($CDCl_3$, 500 MHz): δ 8.17 (d, *J* = 5.1 Hz, 1H), 7.39-7.38 (m, 4H), 7.35-7.32 (m, 1H), 7.15-7.14 (m, 1H), 6.97 (s, 1H), 4.63 (s, 2H), 4.59 (s, 2H), $^{13}C$ NMR ($CDCl_3$, 126 MHz): δ 165.0, 163.1, 153.7 (d, *J* = 7.6 Hz), 147.5 (d, *J* = 15.1 Hz), 137.3, 128.5, 127.8 (d, *J* = 32.9 Hz), 119.2 (d, *J* = 4.1 Hz), 107.2 (d, *J* = 38.2 Hz), 72.9, 69.7 (d, *J* = 2.9 Hz), $^{19}F$ NMR (471 MHz, $CDCl_3$) δ -68.1, IR: ν

= 2858,1615, 1570, 1453, 1411, 1359, 1277, 1148, 1097, 958, 830, 737, 698 $cm^{-1}$; HRMS (ESI) m/z calc. for $C_{13}H_{13}FNO$ (M+H) 218.0981, found 218.0977.

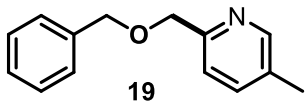

**19**

**2-((Benzyloxy)methyl)-5-methylpyridine (19)**: Obtained as a colorless oil (91 mg, 86%), $^{1}H$ NMR ($CDCl_3$, 500 MHz): δ 8.40 (s, 1H), 7.51-7.49 (m, 1H), 7.40-7.34 (m, 5H), 7.31-7.29 (m, 1H), 4.67 (s, 2H), 4.64 (s, 2H), 2.33 (s, 3H), $^{13}C$ NMR ($CDCl_3$, 126 MHz): δ 155.4, 149.4, 138.0, 137.1, 131.7, 128.3, 127.7, 127.6, 121.0, 73.0, 72.7, 18.1, IR: ν = 2922, 2855, 1603, 1573, 1490, 1454, 1356, 1099, 1030, 824, 734, 698 $cm^{-1}$; HRMS (ESI) m/z calc. for $C_{14}H_{15}NONa$ (M+Na) 236.1051, found 236.1062.

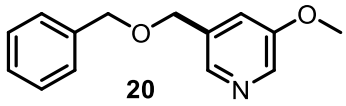

**20**

**3-((Benzyloxy)methyl)-5-methoxypyridine (20)**: Obtained as a colorless oil (87 mg, 76%), $^{1}H$ NMR ($CDCl_3$, 500 MHz): δ 8.25-8.24 (m, 1H), 8.18 (s, 1H), 7.37-7.36 (m, 4H), 7.34 – 7.28 (m, 1H), 7.24 (s, 1H), 4.58 (s, 2H), 4.55 (s, 2H), 3.85 (s, 3H), $^{13}C$ NMR ($CDCl_3$, 126 MHz): δ 155.9, 141.4, 137.9, 137.3, 134.5, 128.7, 128.0, 128.0, 119.7, 72.7, 69.4, 55.7, IR: ν = 2840, 1591, 1468, 1429, 1287, 1192, 1178, 1097, 1051, 865, 740, 701 $cm^{-1}$; HRMS (ESI) m/z calc. for $C_{14}H_{16}NO_2$ (M+H) 230.1181, found 230.1185.

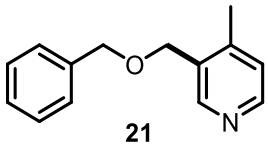

**21**

**3-((Benzyloxy)methyl)-4-methylpyridine (21):** Obtained as a colorless oil (90 mg, 85%), $^{1}H$ NMR ($CDCl_3$, 500 MHz): δ 8.48 (s, 1H), 8.41 (d, *J* = 4.9 Hz, 1H), 7.35-7.32 (m, 4H), 7.29 (dd, *J* = 8.6, 4.2 Hz, 1H), 7.07 (d, *J* = 4.9 Hz, 1H), 4.55 (s, 2H), 4.53 (s, 2H), 2.33 (s, 3H), $^{13}C$ NMR

($CDCl_3$, 126 MHz): δ 150.0, 149.6, 146.7, 138.0, 132.0, 128.6, 128.0, 127.9, 125.4, 72.7, 68.3, 18.5, IR: ν = 3052, 2861, 1597, 1559, 1506, 1496, 1456, 1362, 1265, 1076, 738 $cm^{-1}$, HRMS (ESI) m/z calc. for $C_{14}H_{16}NO$ (M+H) 214.1232, found 214.1230.

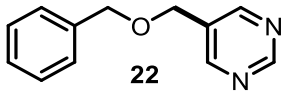


**22**

**5-((Benzyloxy)methyl)pyrimidine (22)**: Obtained as a colorless oil (82 mg, 82%), $^1H$ NMR ($CDCl_3$, 500 MHz): δ 9.14 (s, 1H), 8.71 (s, 2H), 7.38 – 7.33 (m, 4H), 7.31-7.39 (m, 1H), 4.60 (s, 2H), 4.53 (s, 2H), $^{13}C$ NMR ($CDCl_3$, 126 MHz): δ 158.3, 156.4, 137.4, 131.7, 128.7, 128.2, 128.0, 73.1, 67.3, IR: ν = 2917, 2851, 1722, 1564, 1410, 1271, 1164, 1109, 1092, 1074, 728 $cm^{-1}$; HRMS (ESI) m/z calc. for $C_{12}H_{13}N_2O$ (M+H) 201.1028, found 201.1027.

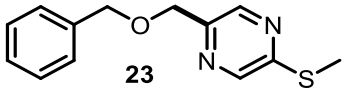


**23**

**2-((Benzyloxy)methyl)-5-(methylthio)pyrazine (23):** Obtained as a colorless oil (103 mg, 84%), $^1H$ NMR ($CDCl_3$, 500 MHz): δ 8.52-8.51 (m, 1H), 8.41-8.40 (m, 1H), 7.40 – 7.33 (m, 4H), 7.31-7.29 (m, 1H), 4.65 (s, 2H), 4.64 (s, 2H), 2.56 (s, 3H), $^{13}C$ NMR ($CDCl_3$, 126 MHz): δ 156.3, 148.0, 142.9, 142.4, 137.8, 128.6, 128.0, 128.0, 73.1, 71.0, 12.8, IR: ν = 3030, 2856, 1497, 1463, 1357, 1317, 1116, 1023, 736, 698 $cm^{-1}$; HRMS (ESI) m/z calc. for $C_{13}H_{15}N_2OS$ (M+H) 247.0905, found 247.0903.

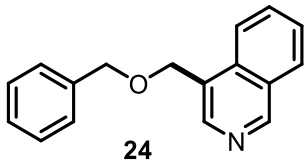


**24**

**4-((Benzyloxy)methyl)isoquinoline (24):** Obtained as a colorless oil (89 mg, 72%), $^1H$ NMR ($CDCl_3$, 500 MHz): δ 9.24 (s, 1H), 8.52 (s, 1H), 8.13 (d, *J* = 8.3 Hz, 1H), 7.99 (d, *J* = 8.3 Hz, 1H), 7.75-7.72 (m, 1H), 7.63-7.61 (m, 1H), 7.39 – 7.34 (m, 4H), 7.33 – 7.28 (m, 1H), 4.95 (s, 2H), 4.62 (s, 2H), $^{13}C$ NMR ($CDCl_3$, 126 MHz): δ 153.6, 143.3, 138.0, 134.9, 130.8, 128.7, 128.3, 128.1,

128.0, 127.4, 127.0, 123.6, 72.5, 68.4, IR: ν = 3053, 2985, 2861, 2305, 1624, 1420, 1362, 1265, 1075, 896, 738, 703 $cm^{-1}$, HRMS (ESI) m/z calc. for $C_{17}H_{16}NO$ (M+H) 250.1232, found 250.1235.

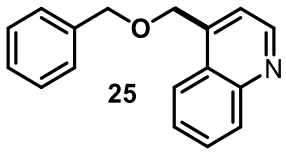


25

**4-((Benzyloxy)methyl)quinoline (25):** Obtained as a semisolid (116 mg, 93%), $^1$H NMR ($CDCl_3$, 500 MHz): δ 8.91 (d, *J* = 4.2 Hz, 1H), 8.15 (d, *J* = 8.4 Hz, 1H), 7.95 (d, *J* = 8.4 Hz, 1H), 7.73-7.71 (m, 1H), 7.60-7.51 (m, 2H), 7.39 (m, 4H), 7.33 (m, 1H), 5.01 (s, 2H), 4.68 (s, 2H), $^{13}$C NMR ($CDCl_3$, 126 MHz): δ 150.3, 148.0, 143.5, 137.6, 130.1, 129.1, 128.5, 127.8, 127.7, 126.5, 126.1, 123.1, 119.4, 72.8, 68.5, IR: ν = 2863, 1712, 1596, 1510, 1453, 1352, 1242, 1109, 852, 758, 737 $cm^{-1}$; HRMS (ESI) m/z calc. for $C_{17}H_{16}NO$ (M+H) 250.1232, found 250.1238.

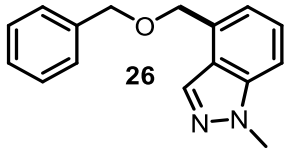


26

**4-((Benzyloxy)methyl)-1-methyl-1H-indazole (26)**: Obtained as a colorless oil (92 mg, 73%), $^1$H NMR ($CDCl_3$, 500 MHz): δ 8.12 (s, 1H), 7.42 – 7.34 (m, 6H), 7.33-7.30 (m, 1H), 7.14 (d, *J* = 5.8 Hz, 1H), 4.90 (s, 2H), 4.61 (s, 2H), 4.10 (s, 3H), $^{13}$C NMR ($CDCl_3$, 126 MHz): δ 140.1, 138.0, 131.8, 131.6, 128.4, 127.8, 127.6, 126.0, 122.8, 119.4, 108.5, 72.2, 70.3, 35.5 , IR: ν = 2854, 2358, 2340, 1611, 1453, 1354, 1275, 1162, 1093, 1074, 980, 781, 735, 698 $cm^{-1}$; HRMS (ESI) m/z calc. for $C_{16}H_{16}N_2ONa$ (M+Na) 275.1160, found 275.1161.

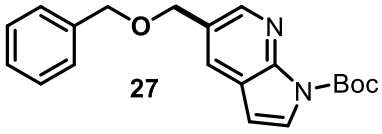


27

**(*tert*-Butyl 5-(Benzyloxy)methyl)-1H-pyrrolo[2,3-b]pyridine-1-carboxylate (27):** Obtained as a colorless oil (98 mg, 58%), $^1$H NMR ($CDCl_3$, 500 MHz): δ 8.47 (d, *J* = 1.9 Hz, 1H), 7.90 (d, *J* =

1.9 Hz, 1H), 7.64 (d, *J* = 4.0 Hz, 1H), 7.35 (d, *J* = 4.3 Hz, 4H), 7.30-7.28 (m, 1H), 6.48 (d, *J* = 4.1 Hz, 1H), 4.65 (s, 2H), 4.55 (s, 2H), 1.66 (s, 9H), $^{13}$C NMR ($CDCl_3$, 126 MHz): δ 148.3, 148.0, 145.3, 138.1, 129.0, 128.6, 128.0, 127.9, 127.2, 123.1, 104.6, 84.2, 72.2, 70.0, 28.2, IR: ν = 2860, 1753, 1729, 1532, 1477, 1392, 1370, 1318, 1254, 1159, 1092, 1028, 734 cm$^{-1}$; HRMS (ESI) m/z calc. for $C_{20}H_{23}N_2O_3$ (M+H) 339.1725, found 339.1719.

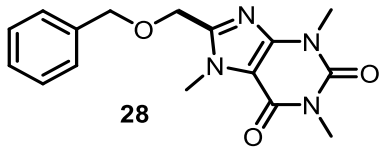

**28**

**8-((Benzyloxy)methyl)-1,3,7-trimethyl-3,7-dihydro-1H-purine-2,6-dione (28):** Obtained as a white solid, mp = 124-125 °C (146 mg, 93%), $^1$H NMR ($CDCl_3$, 500 MHz): δ 7.37 – 7.23 (m, 5H), 4.62 (s, 2H), 4.55 (s, 2H), 3.94 (s, 3H), 3.53 (s, 3H), 3.36 (s, 3H), $^{13}$C NMR ($CDCl_3$, 126 MHz): δ 155.5, 151.7, 149.3, 147.5, 137.0, 128.7, 128.3, 128.2, 108.6, 73.2, 63.7, 32.4, 29.8, 28.1, IR: ν = 3055, 2359, 2343, 1705, 1660, 1544, 1457, 1265, 1073, 849, 738, 703 cm$^{-1}$, HRMS (ESI) m/z calc. for $C_{16}H_{19}N_4O_3$ (M+H) 315.1457, found 315.1457.

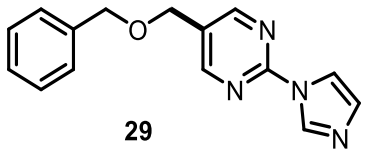

**29**

**5-((benzyloxy)methyl)-2-(1H-imidazol-1-yl)pyrimidine (29):** Obtained as a white solid, mp = 59-61 °C (111 mg, 83%), $^1$H NMR ($CDCl_3$, 500 MHz): δ 8.68 – 8.59 (m, 3H), 7.89 (s, 1H), 7.42 – 7.30 (m, 5H), 7.17 (s, 1H), 4.60 (s, 2H), 4.52 (s, 2H), $^{13}$C NMR ($CDCl_3$, 126 MHz): δ 158.9, 158.3, 154.5, 137.3, 130.9, 129.3, 128.8, 128.3, 128.0, 119.1, 73.1, 66.8, IR: ν = 3051, 2925, 2859, 2305, 1700, 1573, 1476, 1454, 1266, 1097, 1052, 981, 737 cm$^{-1}$, HRMS (ESI) m/z calc. for $C_{15}H_{15}N_4O$ (M+H) 267.1246, found 267.1247.

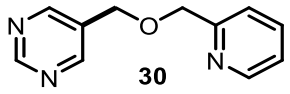

30

**5-((Pyridin-2-ylmethoxy)methyl)pyrimidine (30):** Obtained as a white solid, mp = 38-39 °C (71 mg, 71%), $^{1}$H NMR ($CDCl_3$, 500 MHz): δ 9.13 (s, 1H), 8.73 (s, 2H), 8.54-8.53 (m, 1H), 7.70-7.68 (m, 1H), 7.42-7.40 (m, 1H), 7.23 – 7.15 (m, 1H), 4.71 (s, 2H), 4.64 (s, 2H), $^{13}$C NMR ($CDCl_3$, 126 MHz): δ 158.4, 157.5, 156.4, 149.4, 137.0, 131.4, 122.9, 121.7, 74.0, 68.1, IR: ν = 2858, 1718, 1590, 1564, 1439, 1412, 1111, 1046, 1029, 764, 729 $cm^{-1}$; HRMS (ESI) m/z calc. for $C_{11}H_{11}N_3ONa$ (M+Na) 224.0800, found 224.0807.

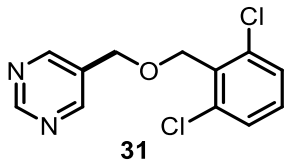

31

**5-(((2,6-Dichlorobenzyl)oxy)methyl)pyrimidine (31):** Obtained as a white solid, mp = 77-78 °C (95 mg, 71%), $^{1}$H NMR ($CDCl_3$, 500 MHz): δ 9.13 (s, 1H), 8.74 (s, 2H), 7.32-7.30 (m, 2H), 7.20-7.17 (m, 1H), 4.86 (s, 2H), 4.62 (s, 2H), $^{13}$C NMR ($CDCl_3$, 126 MHz): δ 158.4, 156.4, 137.0, 132.8, 131.5, 130.5, 128.6, 67.9, 67.5, IR: ν = 2923, 2853, 1184, 1565, 1436, 1407, 1104, 1090, 1080, 941, 792, 760, 729 $cm^{-1}$; HRMS (ESI) m/z calc. for $C_{12}H_{11}Cl_2N_2O$ (M+H) 269.0248, found 269.0248.

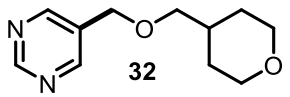

32

**5-((Tetrahydro-2H-pyran-4-yl)methoxy)methyl)pyrimidine (32):** Obtained as a colorless oil (61 mg, 58%), $^{1}$H NMR ($CDCl_3$, 500 MHz): δ $^{1}$H NMR (500 MHz, $CDCl_3$) δ 9.14 (s, 1H), 8.69 (s, 2H), 4.50 (s, 2H), 3.98 – 3.92 (m, 2H), 3.44 – 3.30 (m, 4H), 1.93 – 1.83 (m, 1H), 1.68 – 1.60 (m, 2H), 1.41 – 1.28 (m, 2H), $^{13}$C NMR ($CDCl_3$, 126 MHz): δ 158.3, 156.2, 131.8, 76.2, 68.4, 67.7,

35.6, 30.0, IR: ν = 2918, 2847, 1728, 1564, 1442, 1407, 1288, 1237, 1148, 1111, 1091, 728 $cm^{-1}$; HRMS (ESI) m/z calc. for $C_{11}H_{17}N_2O_2$ (M+H) 209.1290, found 209.1287.

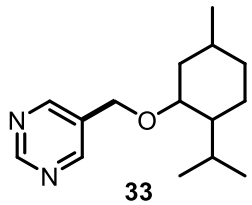

33

**5-(((1*S*)-2-Isopropylcyclohexyl)oxy)methyl)pyrimidine (33):** Obtained as a colorless oil (78 mg, 63%), $^1$H NMR ($CDCl_3$, 500 MHz): δ 9.11 (s, 1H), 8.69 (s, 2H), 4.66 (d, *J* = 12.1 Hz, 1H), 4.37 (d, *J* = 12.1 Hz, 1H), 3.20-3.15 (m, 1H), 2.24 – 2.09 (m, 2H), 1.66-1.60 (m, 2H), 1.37-1.33 (m, 1H), 1.29-1.24 (m, 1H), 0.93-0.80 (m, 9H), 0.71 (d, *J* = 7.0 Hz, 3H), $^{13}$C NMR ($CDCl_3$, 126 MHz): δ 158.1, 156.3, 132.5, 79.9, 65.7, 48.3, 40.3, 34.5, 31.6, 25.8, 23.4, 22.4, 21.0, 16.2, IR: ν = 3354, 2959, 2871, 1565, 1453, 1410, 1370, 1161, 1110, 953, 727 $cm^{-1}$; HRMS (ESI) m/z calc. for $C_{15}H_{25}N_2O$ (M+H) 249.1967, found 249.1978.

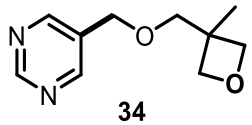

34

**5-(((2-Methyloxetan-2-yl)methoxy)methyl)pyrimidine (34):** Obtained as a colorless oil (72 mg, 74%), $^1$H NMR ($CDCl_3$, 500 MHz): δ 9.13 (s, 1H), 8.69 (s, 2H), 4.56 (s, 2H), 4.47 (d, *J* = 5.6 Hz, 2H), 4.34-4.33 (m, 2H), 3.56 (s, 2H), 1.29 (s, 3H), $^{13}$C NMR ($CDCl_3$, 126 MHz): δ 158.2, 156.1, 131.4, 79.9, 76.2, 68.6, 39.9, 21.3, IR: ν = 2868, 1729, 1584, 1564, 1407, 1290, 1111, 1093, 1045, 977, 833, 727 $cm^{-1}$; HRMS (ESI) m/z calc. for $C_{10}H_{15}N_2O_2$ (M+H) 195.1134, found 195.1133.

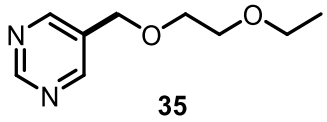

35

**5-((2-Ethoxyethoxy)methyl)pyrimidine (35):** Obtained as a colorless oil (55 mg, 60%), $^1$H NMR ($CDCl_3$, 500 MHz): δ 9.11 (s, 1H), 8.70 (s, 2H), 4.57 (s, 2H), 3.66-3.64 (m, 2H), 3.60-3.58 (m, 2H),

3.49 (q, *J* = 7.0 Hz, 2H), 1.18 (t, *J* = 7.0 Hz, 3H), $^{13}$C NMR ($CDCl_3$, 126 MHz): δ 158.0, 156.1, 131.4, 70.3, 69.7, 68.4, 66.7, 15.0, IR: ν = 3053, 2980, 2873, 2306, 1734, 1565, 1410, 1265, 1110, 896, 739 $cm^{-1}$, HRMS (ESI) m/z calc. for $C_9H_{14}N_2O_2Na$ (M+Na) 205.0953, found 205.0958.

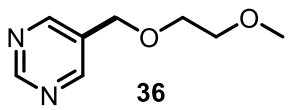

**36**

**5-((2-Methoxyethoxy)methyl)pyrimidine (36):** Obtained as a colorless oil (80 mg, 95%), $^1$H NMR ($CDCl_3$, 500 MHz): δ 9.09 (s, 1H), 8.68 (s, 2H), 4.54 (s, 2H), 3.69-3.67 (m, 2H), 3.58-3.57 (m, 2H), 3.33 (s, 3H), $^{13}$C NMR ($CDCl_3$, 126 MHz): δ 158.2, 156.4, 131.6, 72.0, 70.4, 68.6, 59.2, IR: ν = 3420, 2894, 1628, 1568, 1410, 1111, 1092, 847, 727, 630 $cm^{-1}$; HRMS (ESI) m/z calc. for $C_8H_{12}N_2O_2Na$ (M+Na) 191.0796, found 191.0799.

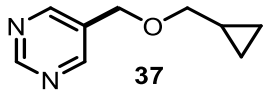

**37**

**5-((Cyclopropylmethoxy)methyl)pyrimidine (37):** Obtained as a colorless oil (45 mg, 55%), $^1$H NMR ($CDCl_3$, 500 MHz): δ 9.14 (s, 1H), 8.72 (s, 2H), 4.54 (s, 2H), 3.37 (d, *J* = 6.9 Hz, 2H), 1.14 – 1.04 (m, 1H), 0.59 – 0.52 (m, 2H), 0.23-0.20 (m, 2H), $^{13}$C NMR ($CDCl_3$, 126 MHz): δ 158.0, 156.1, 131.7, 75.7, 67.6, 10.3, 3.0, IR: ν = 2858, 1586, 1564, 1440, 1409, 1376, 1110, 1089, 1045, 728 $cm^{-1}$; HRMS (ESI) m/z calc. for $C_9H_{13}N_2O$ (M+H) 165.1028, found 165.1026.

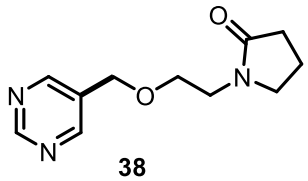

**38**

**1-(2-(Pyrimidin-5-ylmethoxy)ethyl)pyrrolidin-2-one (38):** Obtained as a colorless oil (74 mg, 67%), $^1$H NMR ($CDCl_3$, 500 MHz): δ 9.12 (s, 1H), 8.66 (s, 2H), 4.50 (s, 2H), 3.65-3.63 (m, 2H), 3.50-3.48 (m, 2H), 3.45-4.42 (m, 2H), 2.35-2.42 (m, 2H), 2.02-1.94 (m, 2H),$^{13}$C NMR ($CDCl_3$, 126 MHz): δ 175.4, 158.3, 156.2, 131.4, 69.2, 68.2, 48.7, 42.4, 30.9, 18.2, IR: ν = 2923, 2870, 2239,

1677, 1566, 1408, 1289, 1115, 912, 728 $cm^{-1}$, HRMS (ESI) m/z calc. for $C_{11}H_{15}N_3O_2Na$ (M+Na) 244.1062, found 244.1059.

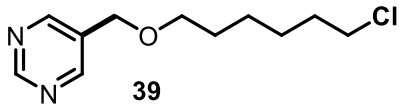


**39**

**5-((5-Chloropentyl)oxy)methyl)pyrimidine (39):** Obtained as a colorless oil (90 mg, 79%), $^1H$ NMR ($CDCl_3$, 500 MHz): δ 9.10 (s, 1H), 8.67 (s, 2H), 4.47 (s, 2H), 3.50-3.46 (m, 4H), 1.76-1.70 (m, 2H), 1.63-1.57 (m, 2H), 1.45-1.35 (m, 4H), $^{13}C$ NMR ($CDCl_3$, 126 MHz): δ 158.2, 156.2, 131.9, 71.1, 68.2, 45.1, 32.6, 29.6, 26.7, 25.5, IR: ν = 2934, 2860, 1727, 1564, 1440, 1406, 1112, 1095, 727 $cm^{-1}$; HRMS (ESI) m/z calc. for $C_{11}H_{18}ClN_2O$ (M+H) 229.1108, found 229.1112.

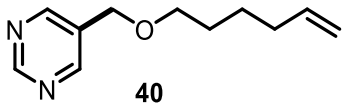


**40**

**5-((Hex-5-en-1-yloxy)methyl)pyrimidine (40):** Obtained as a colorless oil (67 mg, 70%), $^1H$ NMR ($CDCl_3$, 500 MHz): δ 9.13 (s, 1H), 8.69 (s, 2H), 5.82 – 5.72 (m, 1H), 5.00-4.91 (m, 2H), 4.49 (s, 2H), 3.52-3.49 (m, 2H), 2.12 – 2.02 (m, 2H), 1.69 – 1.57 (m, 2H), 1.52 – 1.41 (m, 2H), $^{13}C$ NMR ($CDCl_3$, 126 MHz): δ 158.2, 156.2, 138.6, 131.9, 114.8, 71.2, 68.2, 33.6, 29.1, 25.5, IR: ν = 3391, 2968, 2934, 2861, 1731, 1643, 1565, 1408, 1112, 1099, 952, 910, 728 $cm^{-1}$; HRMS (ESI) m/z calc. for $C_{11}H_{17}N_2O$ (M+H) 193.1341, found 193.1345.

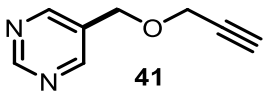


**41**

**5-((Prop-2-yn-1-yloxy)methyl)pyrimidine (41):** Obtained as a white semi-solid (58 mg, 78%), $^1H$ NMR ($CDCl_3$, 500 MHz): δ 9.15 (s, 1H), 8.72 (s, 2H), 4.61 (s, 2H), 4.23 (s, 2H), 2.51 (s, 1H), $^{13}C$ NMR ($CDCl_3$, 126 MHz): δ 158.5, 156.5, 131.0, 78.8, 75.8, 66.8, 58.1, IR: ν = 3276, 1566, 1444, 1409, 1388, 1276, 1233, 1164, 1107, 1091, 1046, 724 $cm^{-1}$; HRMS (ESI) m/z calc. for $C_8H_9N_2O$ (M+H) 149.0715, found 149.0712.

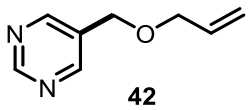

42

**5-((Allyloxy)methyl)pyrimidine (42):** Obtained as a colorless oil (57 mg, 76%), $^{1}$H NMR ($CDCl_3$, 500 MHz): δ 9.11 (s, 1H), 8.69 (s, 2H), 5.96 – 5.83 (m, 1H), 5.30-5.20 (m, 2H), 4.49 (s, 2H), 4.04 (d, *J* = 5.6 Hz, 2H), $^{13}$C NMR ($CDCl_3$, 126 MHz): δ 158.3, 156.3, 134.0, 131.7, 118.1, 72.0, 67.3, IR: ν = 3050, 2982, 2858, 1588, 1564, 1410, 1267, 1086, 931, 737 $cm^{-1}$, HRMS (ESI) m/z calc. for $C_8H_{11}N_2O$ (M+H) 151.0871, found 151.0867.

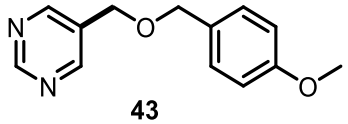

43

**5-(((4-Methoxybenzyl)oxy)methyl)pyrimidine (43):** Obtained as a colorless oil (71 mg, 62%), $^{1}$H NMR ($CDCl_3$, 500 MHz): δ 9.19 (s, 1H), 8.76 (s, 2H), 7.30 (d, *J* = 8.5 Hz, 2H), 6.92 (d, *J* = 8.5 Hz, 2H), 4.57 (s, 2H), 4.54 (s, 2H), 3.83 (s, 3H),$^{13}$C NMR ($CDCl_3$, 126 MHz): δ 159.7, 158.3, 156.4, 132.0, 129.7, 129.4, 114.1, 72.8, 67.0, 55.4, IR: ν = 3047, 2859, 1613, 1586, 1564, 1514, 1441, 1410, 1302, 1249, 1174, 1082, 1034, 820, 728 $cm^{-1}$, HRMS (ESI) m/z calc. for $C_{13}H_{15}N_2O_2$ (M+H) 231.1134, found 231.1126.

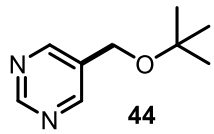

44

**5-(*Tert*-butoxymethyl)pyrimidine (44):** Obtained as a colorless oil (59 mg, 71%), $^{1}$H NMR ($CDCl_3$, 500 MHz): δ 9.09 (s, 1H), 8.67 (s, 2H), 4.43 (s, 2H), 1.27 (s, 9H), $^{13}$C NMR ($CDCl_3$, 126 MHz): δ 157.9, 156.1, 133.0, 74.3, 59.7, 27.6, IR: ν = 2974, 2359, 2341, 1723, 1564, 1490, 1392, 1365, 1197, 1082, 877, 727 $cm^{-1}$; HRMS (ESI) m/z calc. for $C_9H_{15}N_2O$ (M+H) 167.1184, found 167.1183.

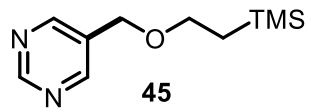


45

**5-(2-(Trimethylsilyl)ethoxy)methyl)pyrimidine (45):** Obtained as a colorless oil (85 mg, 81%), $^{1}$H NMR ($CDCl_3$, 500 MHz): δ 9.09 (s, 1H), 8.67 (s, 2H), 4.45 (s, 2H), 3.57 (dd, *J* = 11.1, 5.2 Hz, 2H), 0.95 (dd, *J* = 11.1, 5.42 Hz, 2H), -0.03 (s, 9H), $^{13}$C NMR ($CDCl_3$, 126 MHz): δ 158.1, 156.2, 132.0, 68.7, 67.6, 18.3, -1.3, IR: ν = 2953, 1563, 1409, 1360, 1249, 1182, 1110, 1087, 859, 836, 727 $cm^{-1}$; HRMS (ESI) m/z calc. for $C_{10}H_{18}N_2OSiNa$ (M+Na) 233.1079, found 233.1076.

## 3.5 References

(1) Yasu, Y.; Koike, T.; Akita, M. *Adv. Synth. Catal.* **2012**, *354*, 3414.

(2) Tellis, J. C.; Primer, D. N.; Molander, G. A. *Science.* **2014**, *345*, 433.

(3) Ingold, K. U.; DiLabio, G. A. *Org. Lett.* **2006**, *8*, 5923.

(4) Van Hoomissen, D. J.; Vyas, S. *J. Org. Chem.* **2017**, *82*, 5731.

(5) Henry, D. J.; Parkinson; C. J.; Mayer, P. M.; Radom, L. *J. Phys. Chem. A*, **2001**, *105*, 6750

(6) Hutchinson, D. K.; Fuchs, P. L. *J. Am. Chem. Soc.* **1987**, *109*, 4930.

(7) Tamao, K.; Ishida, N.; Ito, Y.; Makoto, K. *Org. Synth.* **1990**, *69*, 96.

(8) Blanc, R.; Groll, K.; Bernhardt, S.; Stockmann, P.; Knochel, P. *Synthesis* **2014**, *46*, 1052.

(9) Sakata, K.; Urabe, D.; Inoue, M. *Tetrahedron Lett.* **2013**, *54*, 4189.

(10) Masanori, K.; Takashi, S.; Toshimi, O.; Hiroshi, S.; Toshihiko, M. *Chem. Lett.* **1984**, 1225.

(11) Majeed, A. J.; Antonsen, O.; Benneche, T.; Undheim, K. *Tetrahedron* **1989**, *45*, 993.

(12) Falck, J. R.; Patel, P. K.; Bandyopadhyay, A. *J. Am. Chem. Soc.* **2007**, *129*, 790.

(13) Goli, M.; He, A.; Falck, J. R. *Org. Lett.* **2011**, *13*, 344.

(14) Molander, G. A.; Canturk, B. *Org. Lett.* **2008**, *10*, 2135.

(15) Murai, N.; Yonaga, M.; Tanaka, K. *Org. Lett.* **2012**, *14*, 1278.

(16) Lawrence, N. J.; Rennison, D.; Woo, M.; McGown, A. T.; Hadfield, J. A. *Bioorg. Med. Chem. Lett.* **2001**, *11*, 51.

(17) Thompson, A. M.; Blaser, A.; Anderson, R. F.; Shinde, S. S.; Franzblau, S. G.; Ma, Z.; Denny, W. A.; Palmer, B. D. *J. Med. Chem.* **2009**, *52*, 637.

(18) Güven, O. O.; Erdoğan, T.; Göker, H.; Yildiz, S. *Bioorg. Med. Chem. Lett.* **2007**, *17*, 2233.

(19) Helms, B.; Mynar, J. L.; Hawker, C. J.; Fréchet, J. M. J. *J. Am. Chem. Soc.* **2004**, *126*, 15020.

(20) Percec, V.; Heck, J.; Lee, M.; Ungar, G.; Alvarez-Castillo, A. *J. Mater. Chem.* **1992**, *2*, 1033.

(21) Wang, A.; Yang, Z.; Liu, J.; Gui, Q.; Chen, X.; Tan, Z.; Shi, J.-C. *Synth. Commun.* **2014**, *44*, 280.

(22) Harris, J. M.; Chess, R. B. *Nat. Rev. Drug Discov.* **2003**, *2*, 214.

(23) Urakami, K.; Kobayashi, C.; Miyazaki, Y.; Nishijima, K.; Yoshimura, Y.; Hashimoto, K. *Chem. Pharm. Bull.* **2000**, *48*, 1299.

(24) Abend, A. M.; Chung, L.; Bibart, R. T.; Brooks, M.; McCollum, D. G. *J. Pharm. Biomed. Anal.* **2004**, *34*, 957.

**Author Contributions:**

D.N.P. wrote and edited the manuscript, performed the reaction optimization, and prepared some compounds and alkyltrifluoroborates used in this study. Idris Karakaya synthesized all the remaining compounds prepared in this study and edited the manuscript.

# Appendix A2. $^{1}H$, $^{13}C$, $^{11}B$, and $^{19}F$ NMR Spectra Relevant to Chapter 3

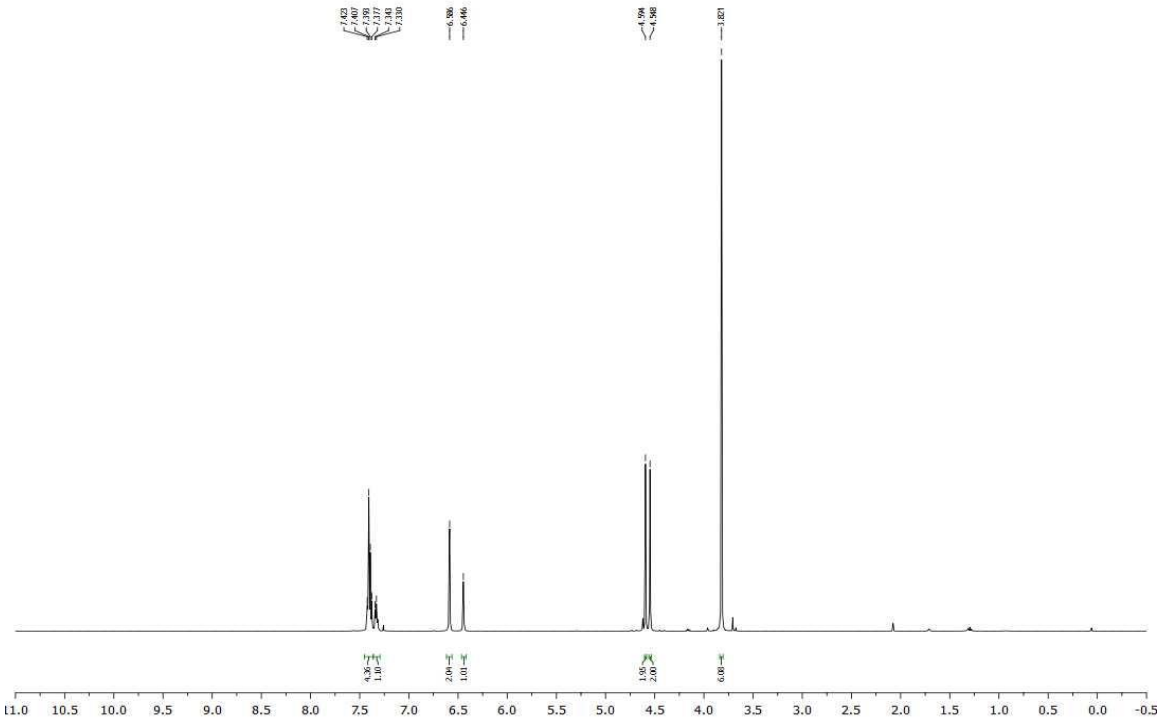

**Figure A2.1.** $^{1}$H NMR ($CDCl_3$, 500 MHz) spectrum of 1-((benzyloxy)methyl)-3,5-dimethoxybenzene (**2**)

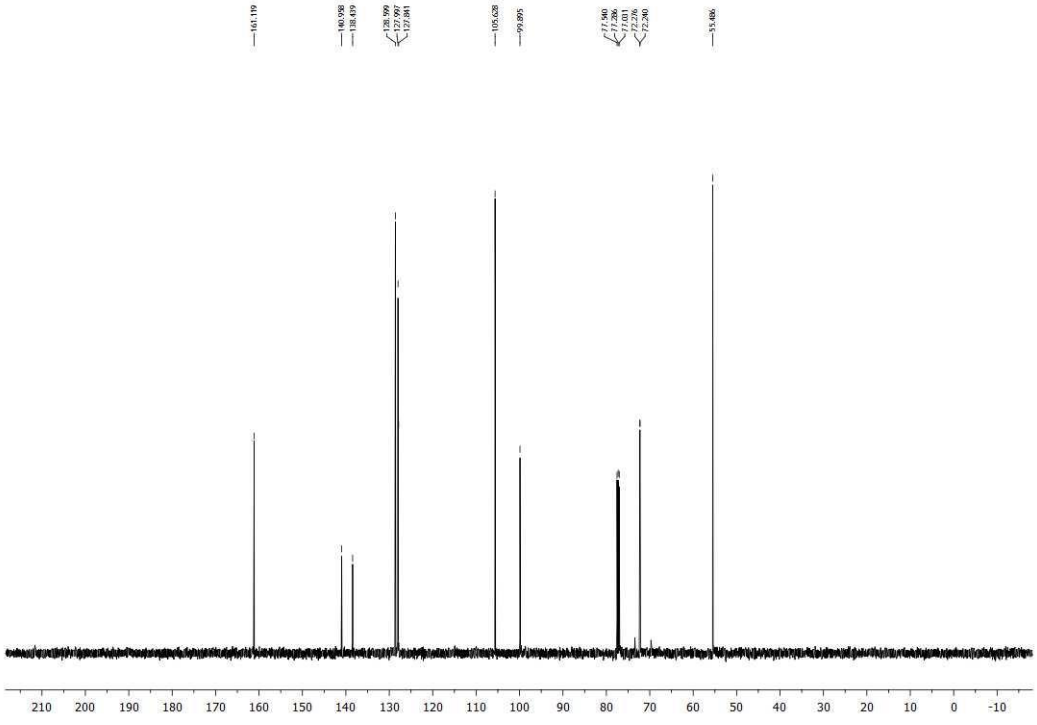

**Figure A2.2.** $^{13}$C NMR ($CDCl_3$, 125.8 MHz) spectrum of 1-((benzyloxy)methyl)-3,5-dimethoxybenzene (**2**)

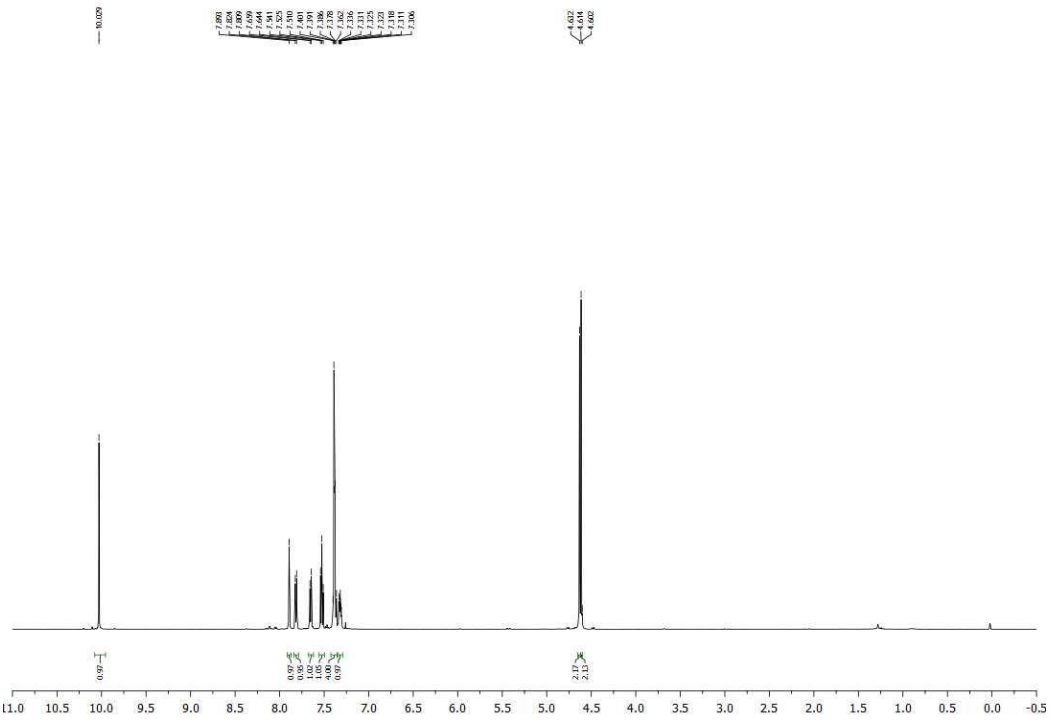

**Figure A2.3.** $^{1}H$ NMR ($CDCl_3$, 500 MHz) spectrum of 3-((benzyloxy)methyl)benzaldehyde (**3**)

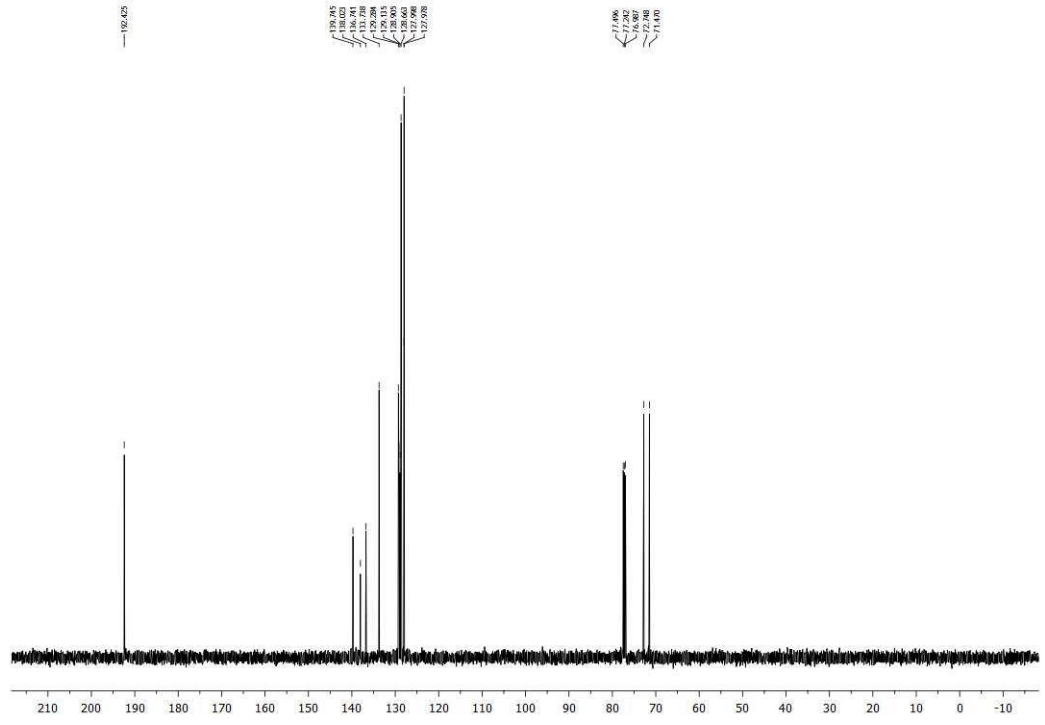

**Figure A2.4.** $^{13}C$ NMR ($CDCl_3$, 125.8 MHz) spectrum of 3-((benzyloxy)methyl)benzaldehyde (**3**)

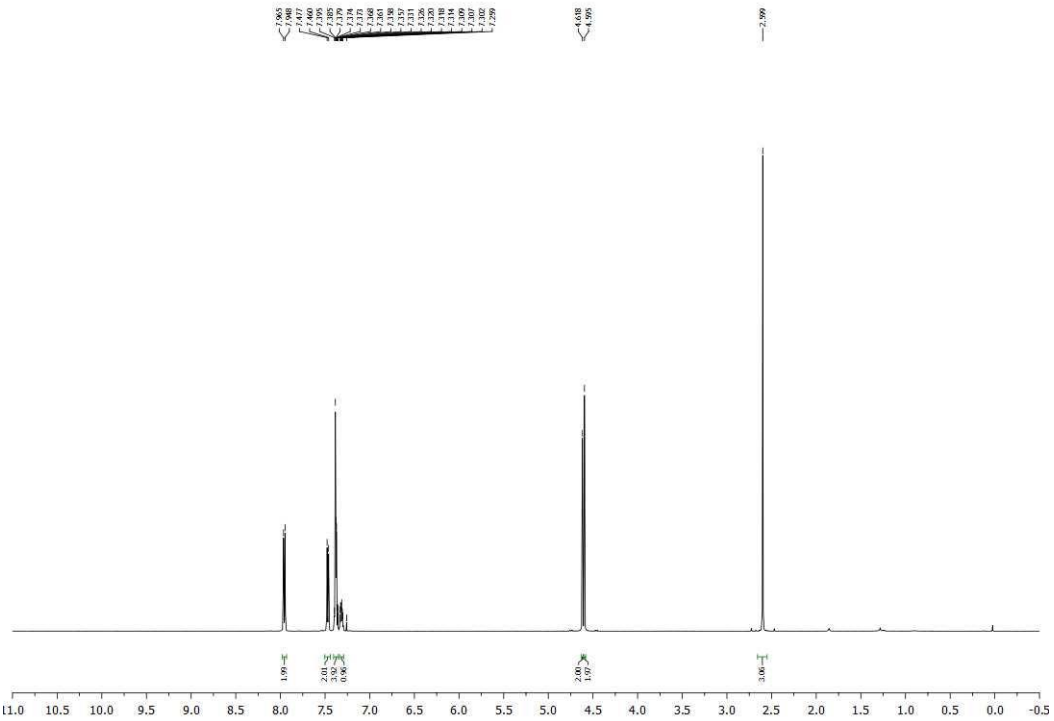

**Figure A2.5.** $^{1}$H NMR ($CDCl_3$, 500 MHz) spectrum of 1-(4-(benzyloxy)methyl)phenyl)ethan-1-one (**4**)

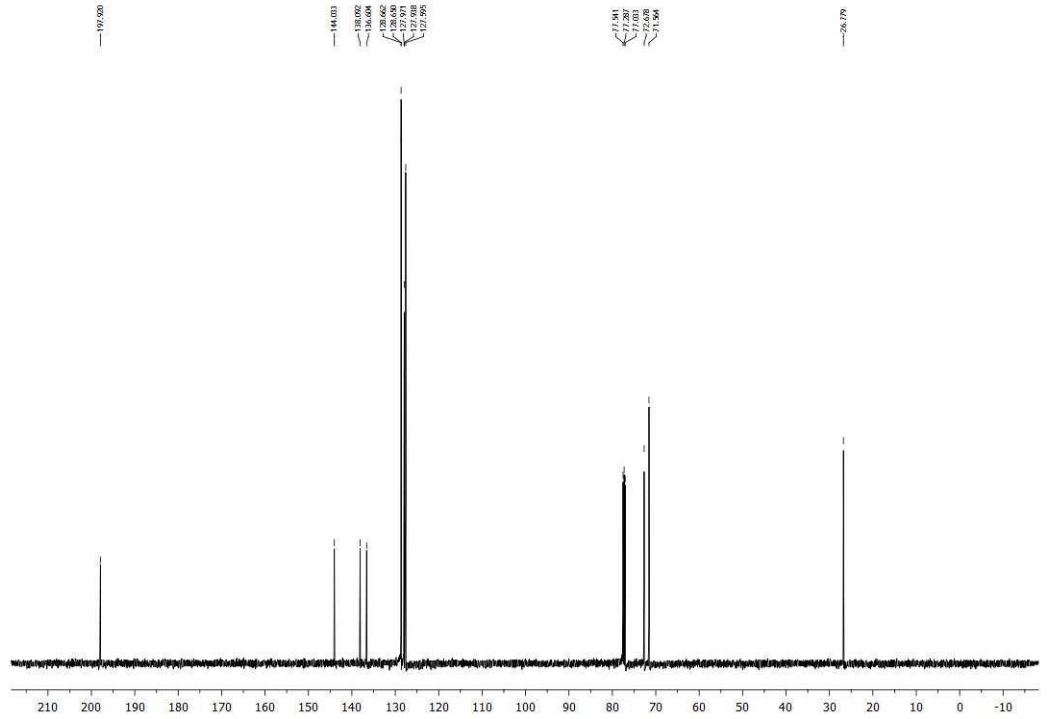

**Figure A2.6.** $^{1}$H NMR ($CDCl_3$, 500 MHz) spectrum of 1-(4-(benzyloxy)methyl)phenyl)ethan-1-one (**4**)

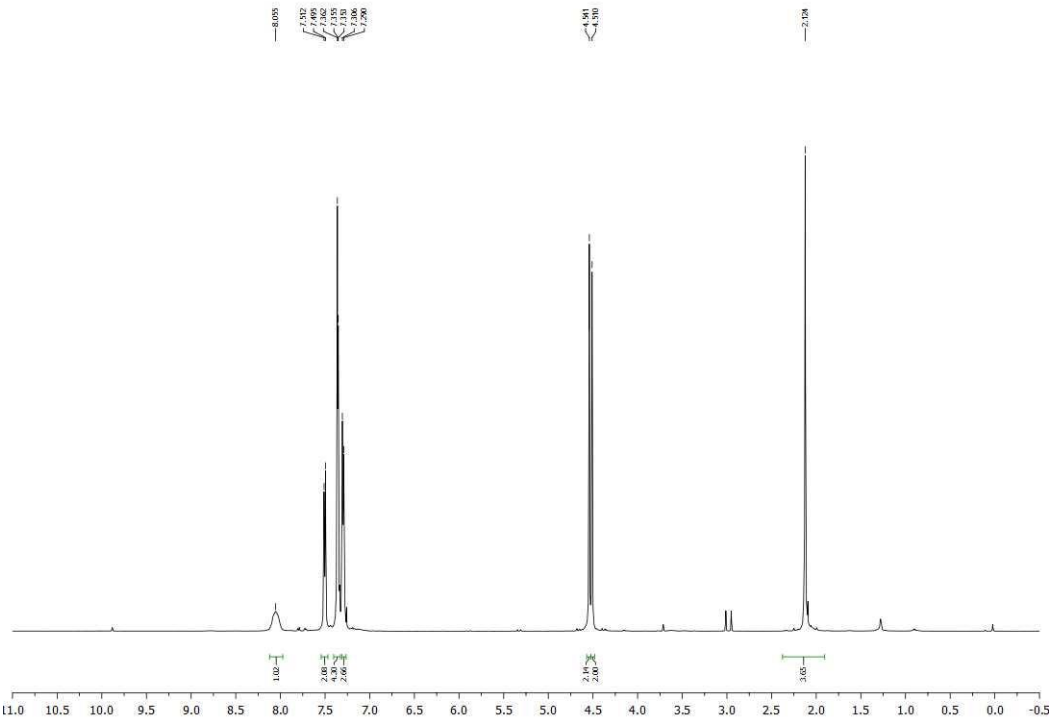

**Figure A2.7.** $^{1}$H NMR ($CDCl_3$, 500 MHz) spectrum of *N*-((4-(benzyloxy)methyl)phenyl)acetamide (**5**)

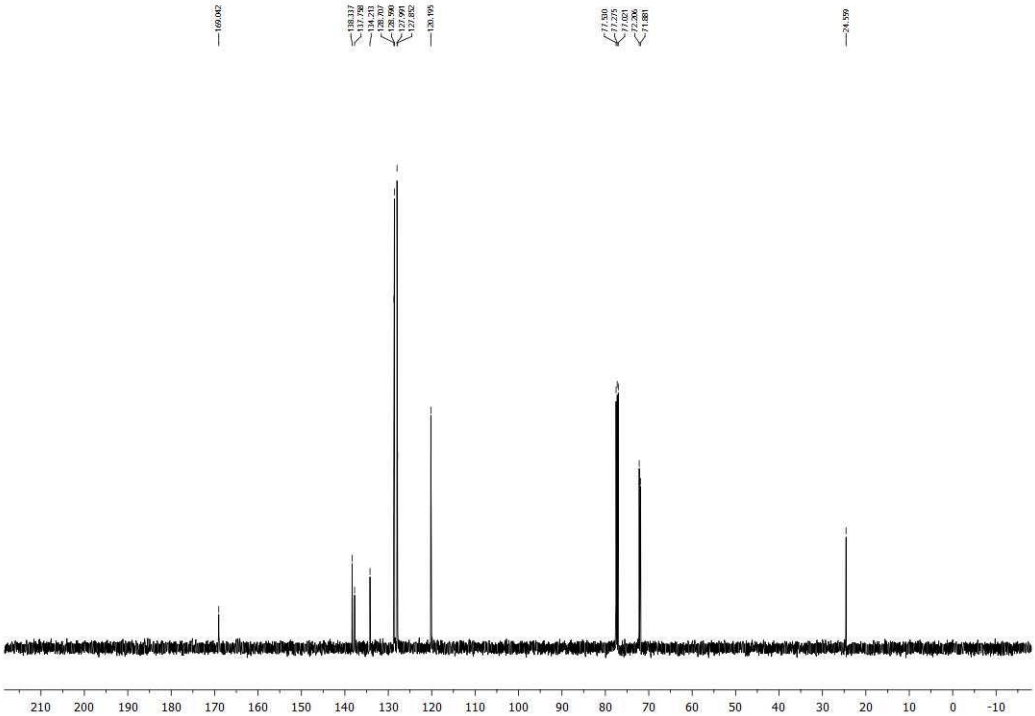

**Figure A2.8.** $^{13}$C NMR ($CDCl_3$, 125.8 MHz) spectrum of *N*-((4-(benzyloxy)methyl)phenyl)acetamide (**5**)

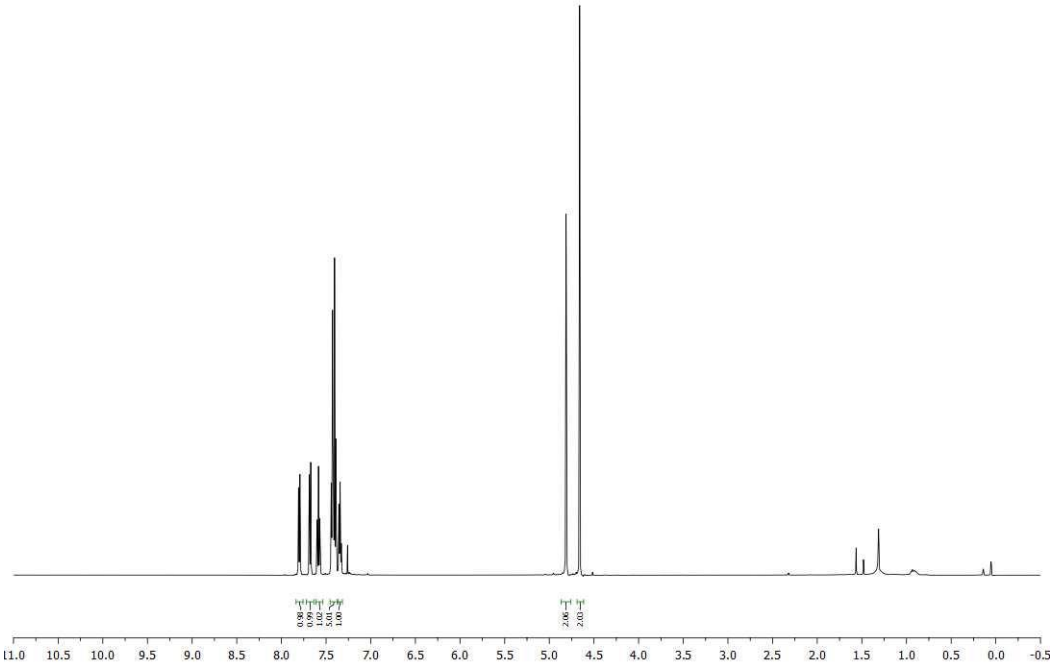

**Figure A2.9.** $^{1}$H NMR ($CDCl_3$, 500 MHz) spectrum of 1-(benzyloxy)methyl)-2-(trifluoromethyl)benzene (**6**)

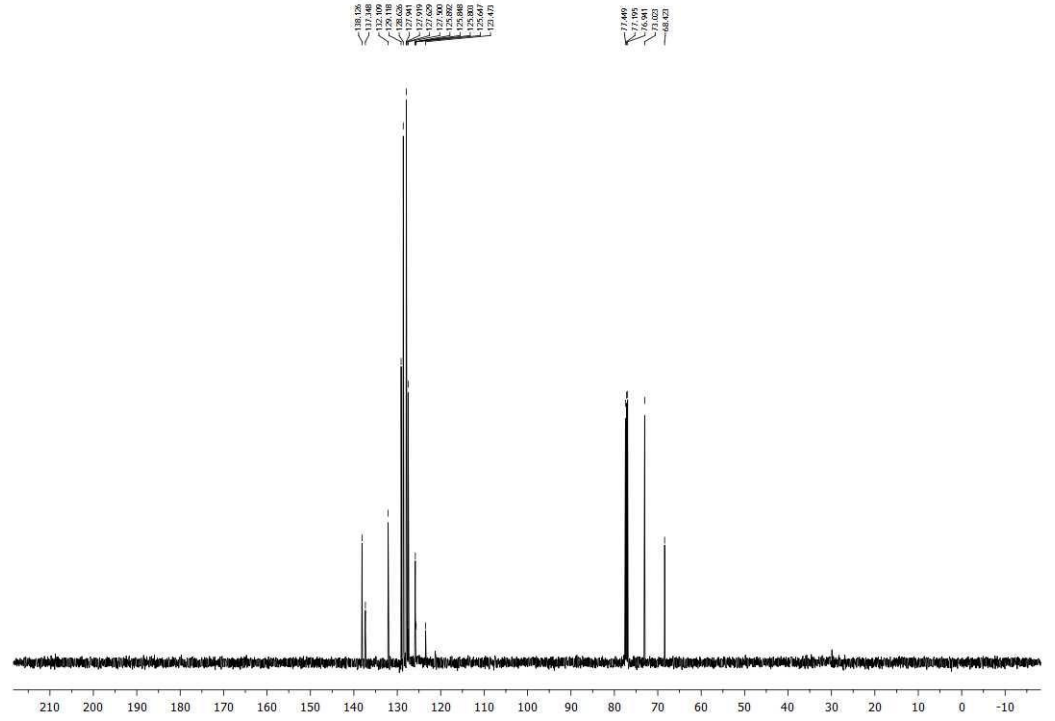

**Figure A2.10.** $^{13}$C NMR ($CDCl_3$, 125.8 MHz) spectrum of 1-(benzyloxy)methyl)-2-(trifluoromethyl)benzene (**6**)

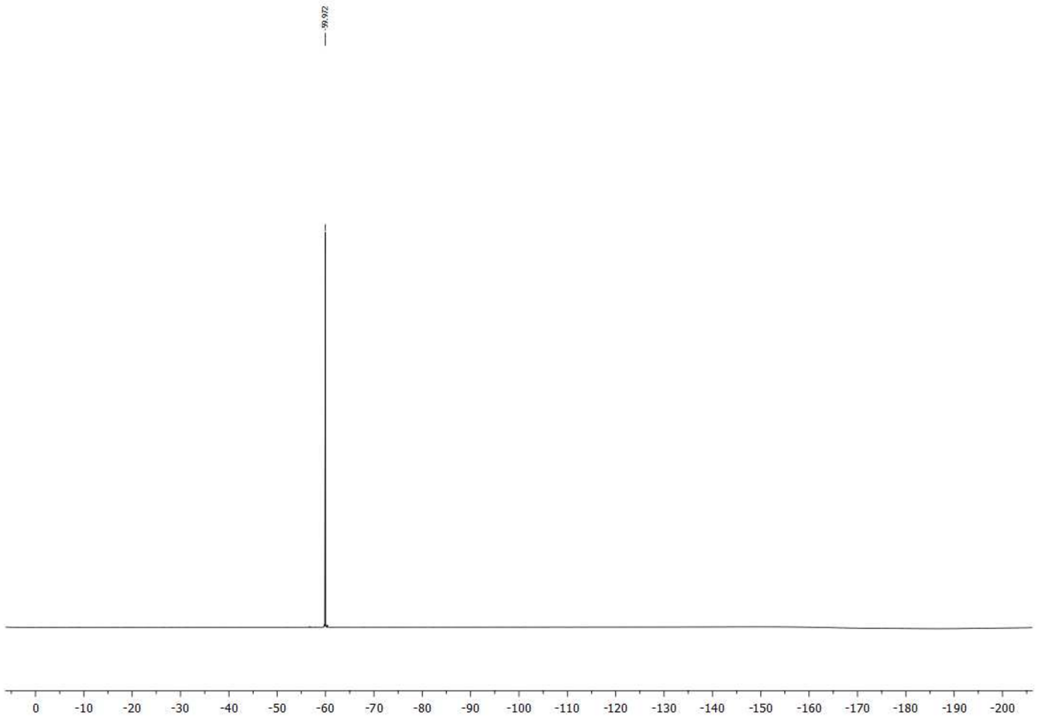


**Figure A2.11.** $^{19}F$ NMR ($CDCl_3$, 470.8 MHz) spectrum of 1-(benzyloxy)methyl)-2-(trifluoromethyl)benzene (**6**)

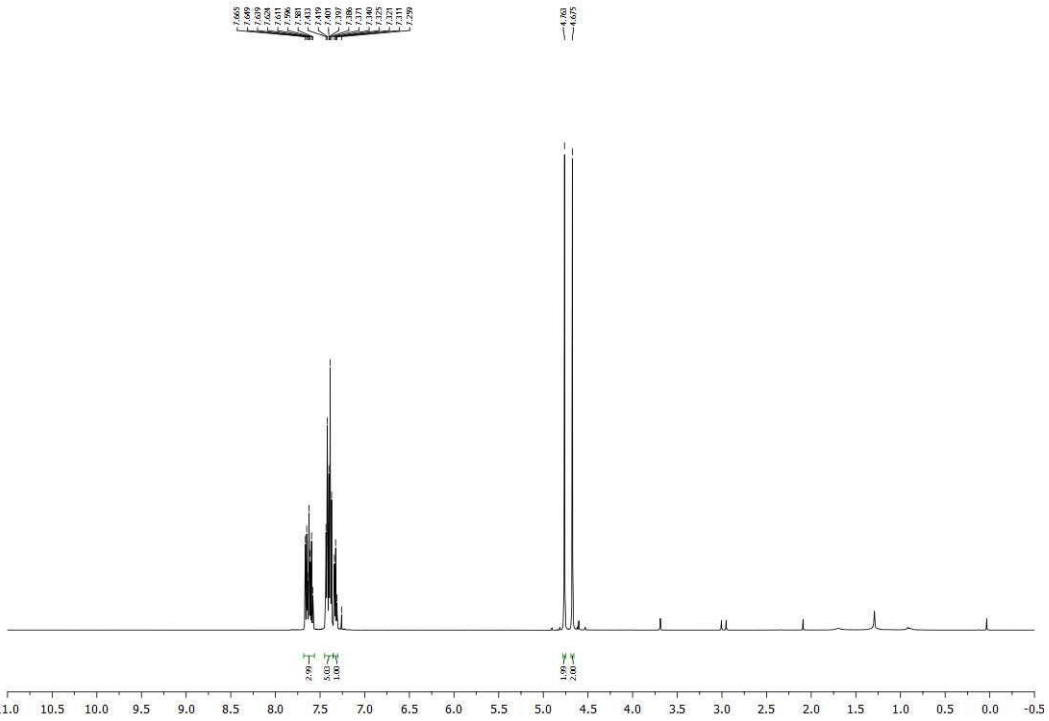


**Figure A2.12.** $^{1}H$ NMR ($CDCl_3$, 500 MHz) spectrum of 2-((benzyloxy)methyl)benzonitrile (**7**)

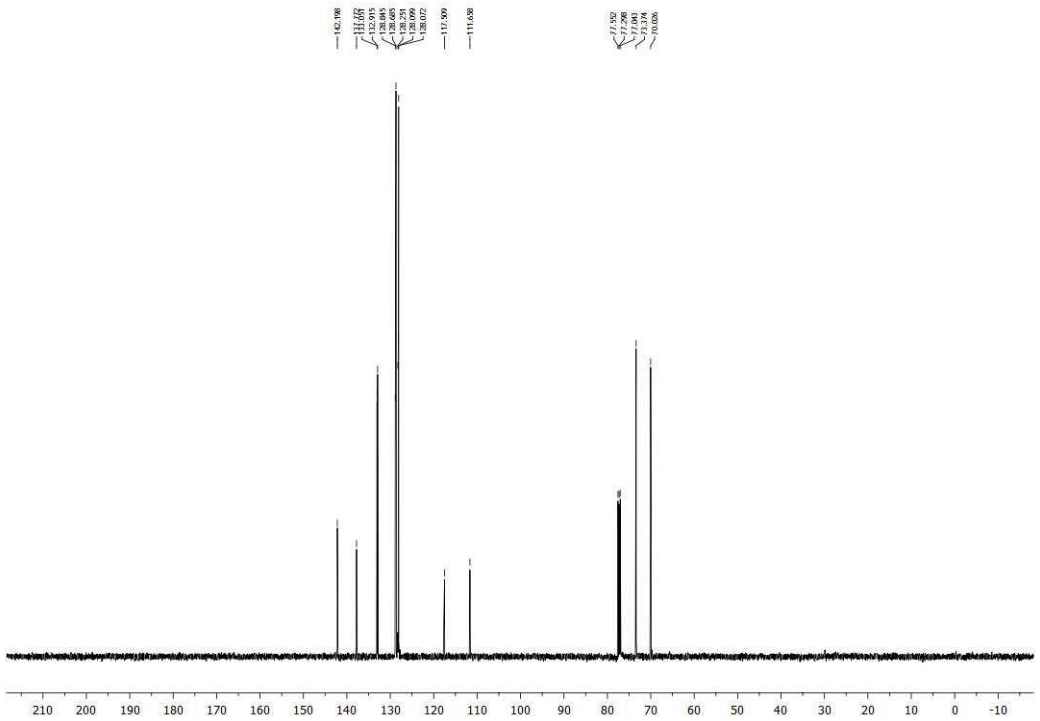

**Figure A2.13.** $^{13}C$ NMR ($CDCl_3$, 125.8 MHz) spectrum of 2-((benzyloxy)methyl)benzonitrile (**7**)

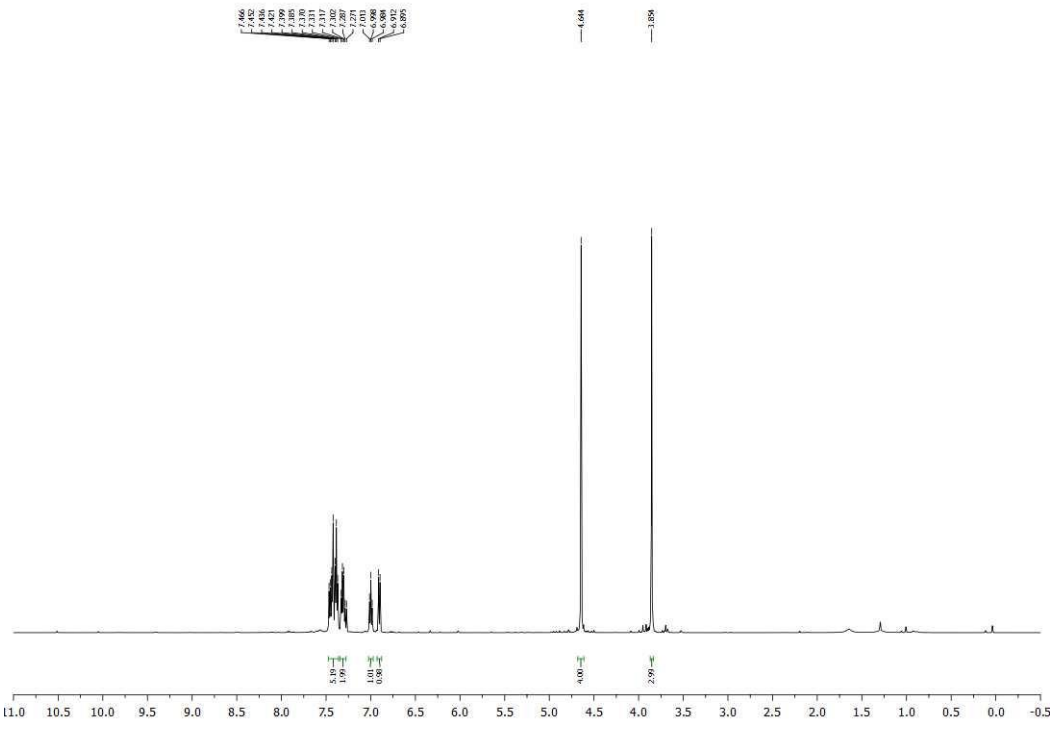

**Figure A2.14.** $^{1}H$ NMR ($CDCl_3$, 500 MHz) spectrum of 1-((benzyloxy)methyl)-2-methoxybenzene (**8**)

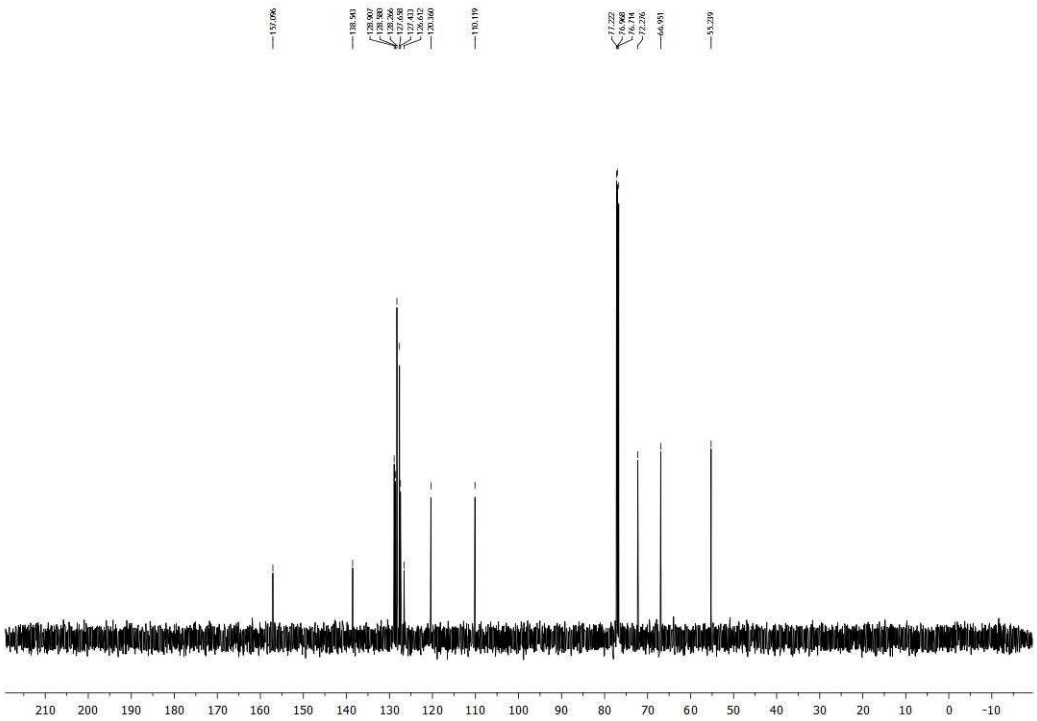

**Figure A2.15.** $^{13}C$ NMR ($CDCl_3$, 125.8 MHz) spectrum of 1-((benzyloxy)methyl)-2-methoxybenzene (**8**)

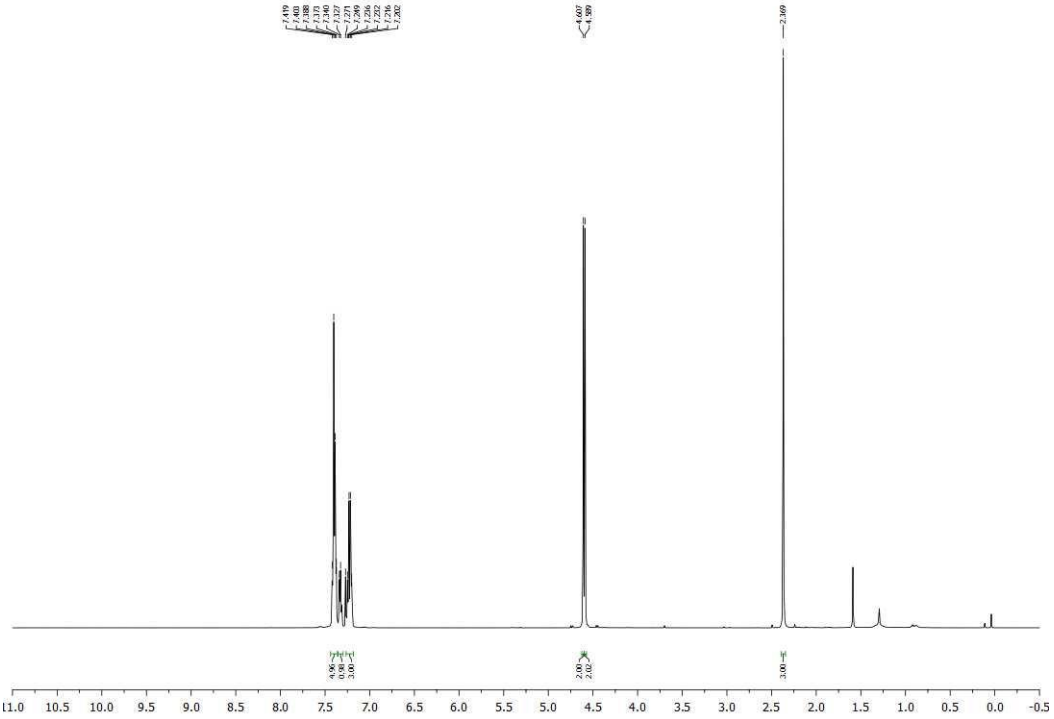

**Figure A2.16.** $^{1}H$ NMR ($CDCl_3$, 500 MHz) spectrum of 1-((benzyloxy)methyl)-2-methylbenzene (**9**)

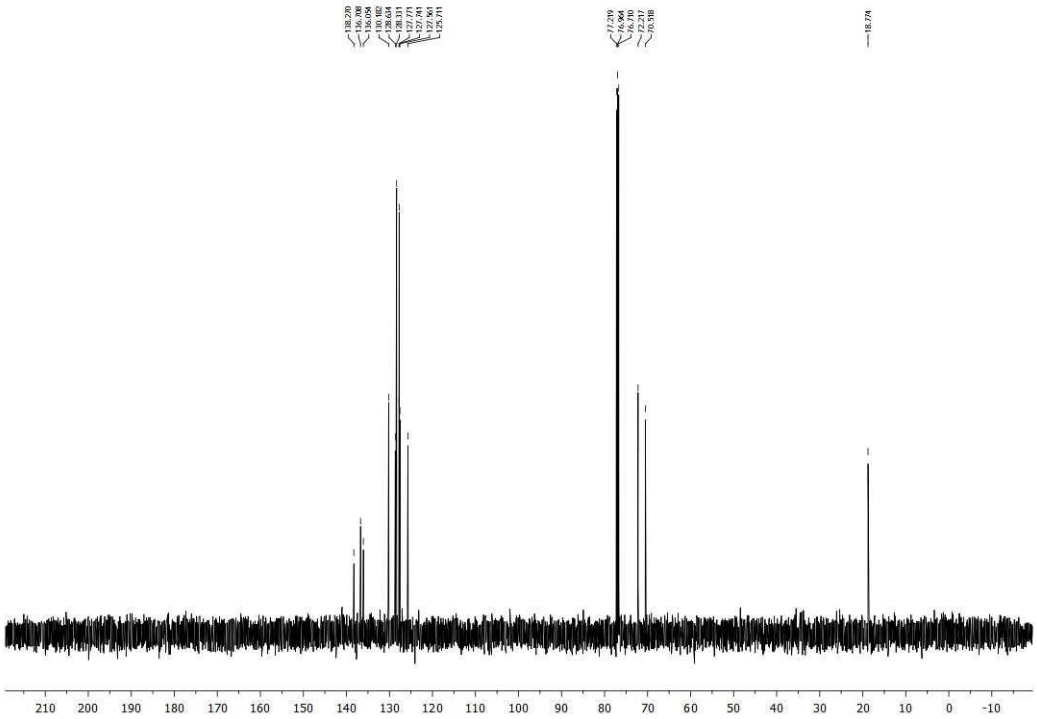

**Figure A2.17.** $^{13}C$ NMR ($CDCl_3$, 125.8 MHz) spectrum of 1-((benzyloxy)methyl)-2-methylbenzene (**9**)

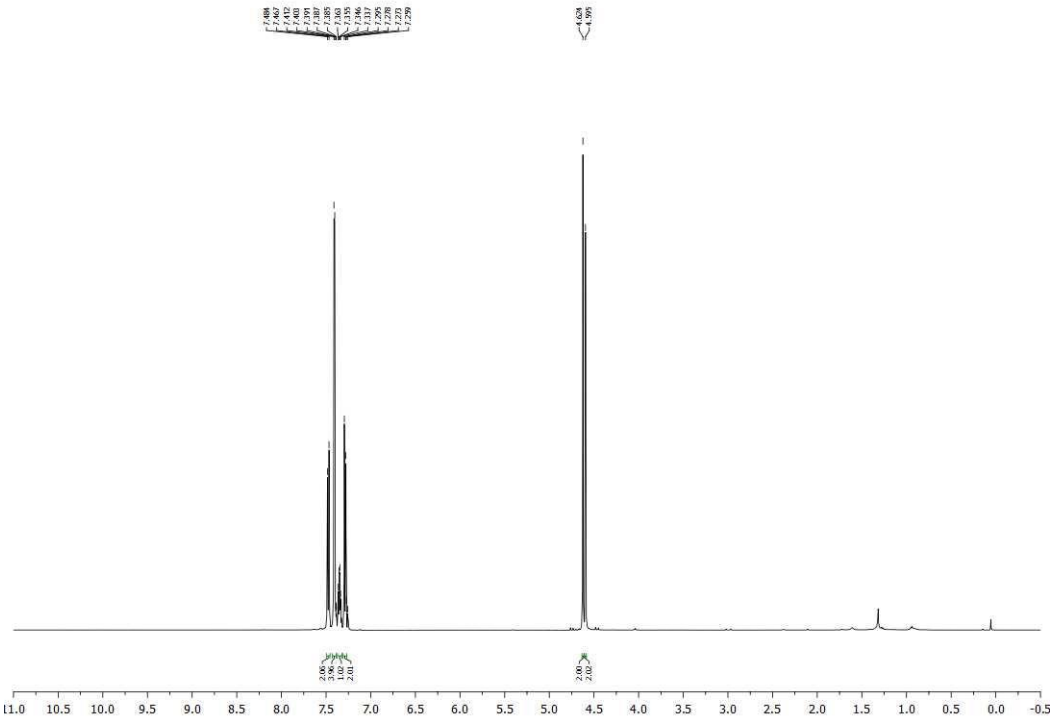

**Figure A2.18.** $^{1}H$ NMR ($CDCl_3$, 500 MHz) spectrum of 4-((benzyloxy)methyl)phenyl trifluoromethanesulfonate (**10**)

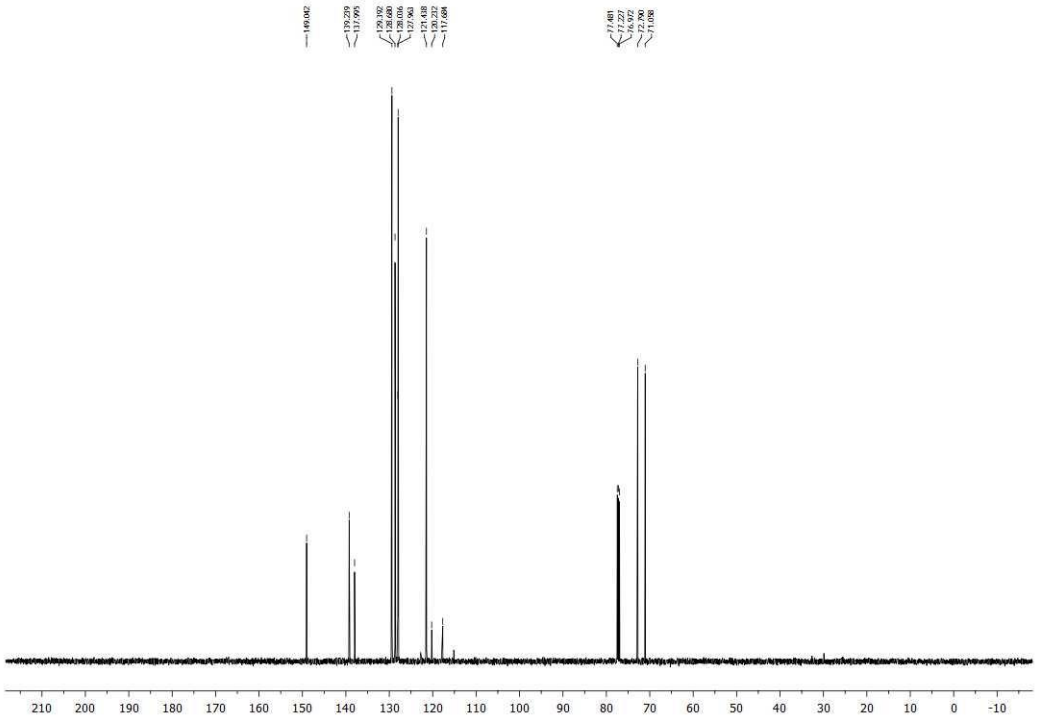

**Figure A2.19.** $^{13}C$ NMR ($CDCl_3$, 125.8 MHz) spectrum of 4-((benzyloxy)methyl)phenyl trifluoromethanesulfonate (**10**)

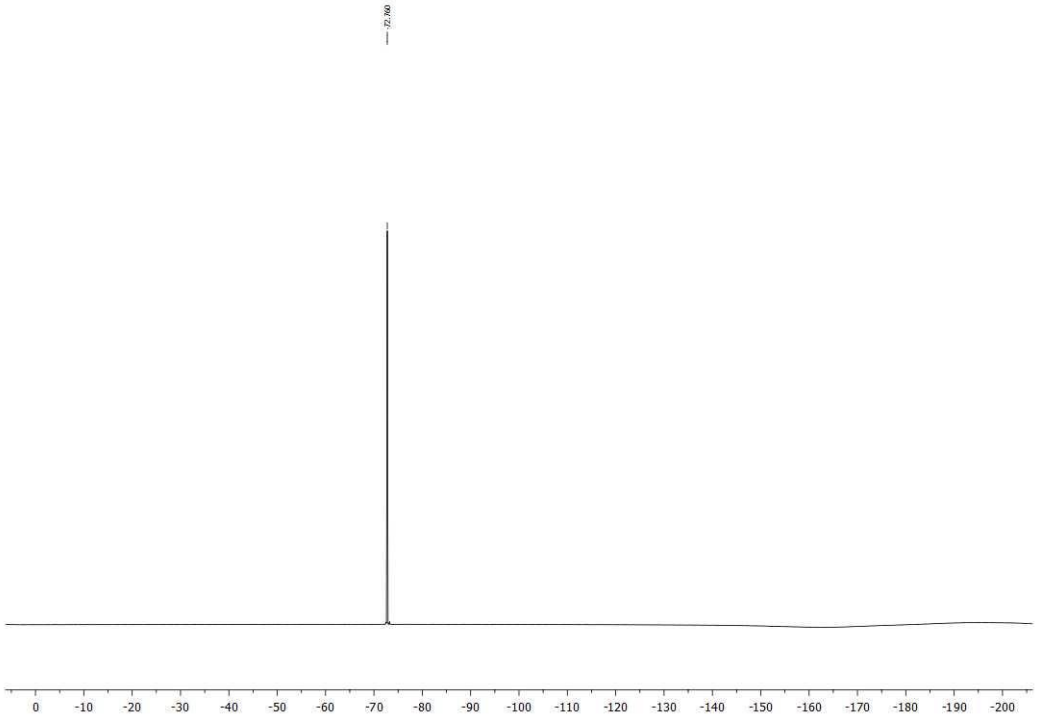

**Figure A2.20.** $^{19}F$ NMR ($CDCl_3$, 470.8 MHz) spectrum of 4-((benzyloxy)methyl)phenyl trifluoromethanesulfonate (**10**)

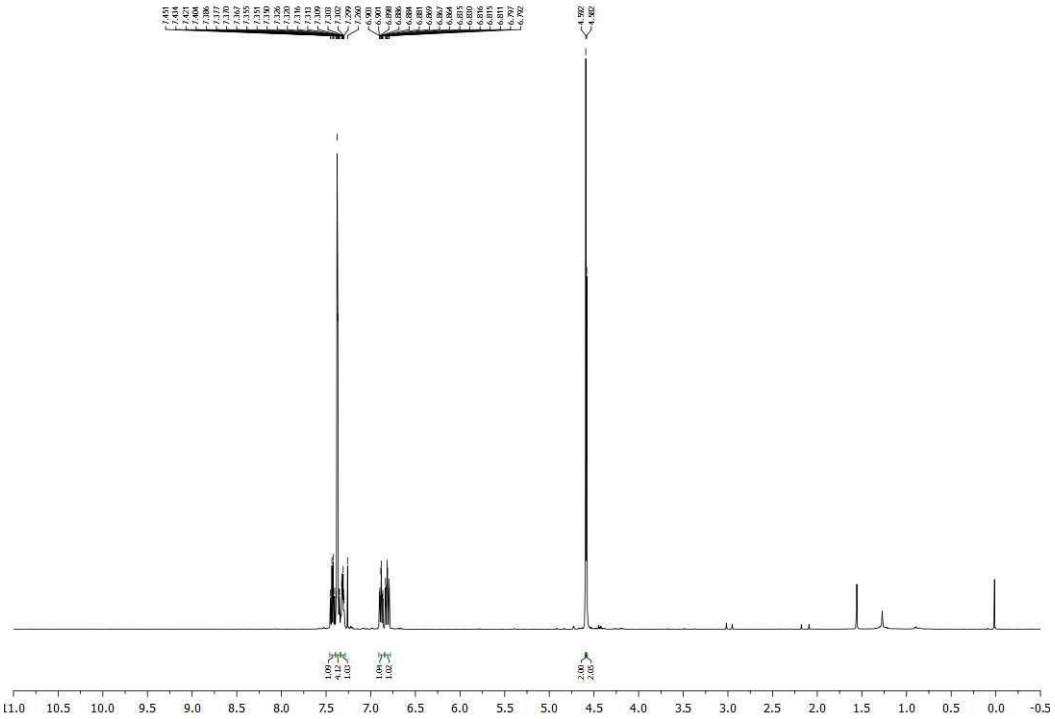

**Figure A2.21.** $^{1}$H NMR ($CDCl_3$, 500 MHz) spectrum of 1-((benzyloxy)methyl)-2,4-difluorobenzene (**11**)

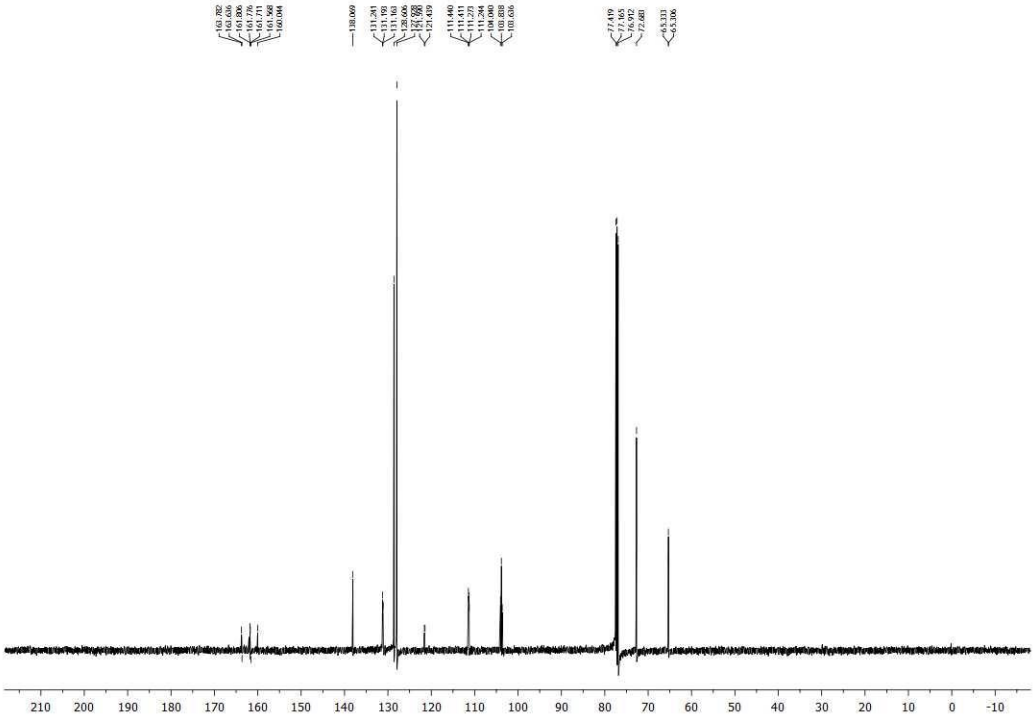

**Figure A2.22.** $^{13}$C NMR ($CDCl_3$, 125.8 MHz) spectrum of 1-((benzyloxy)methyl)-2,4-difluorobenzene (**11**)

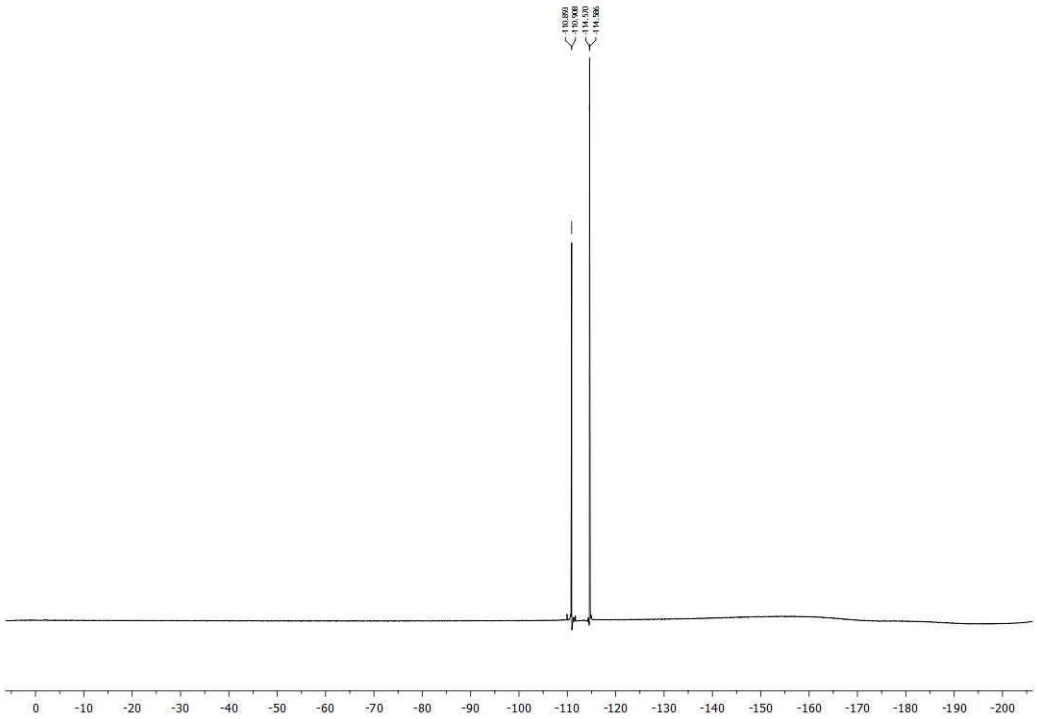

**Figure A2.23.** $^{19}F$ NMR ($CDCl_3$, 470.8 MHz) spectrum of 1-((benzyloxy)methyl)-2,4-difluorobenzene (**11**)

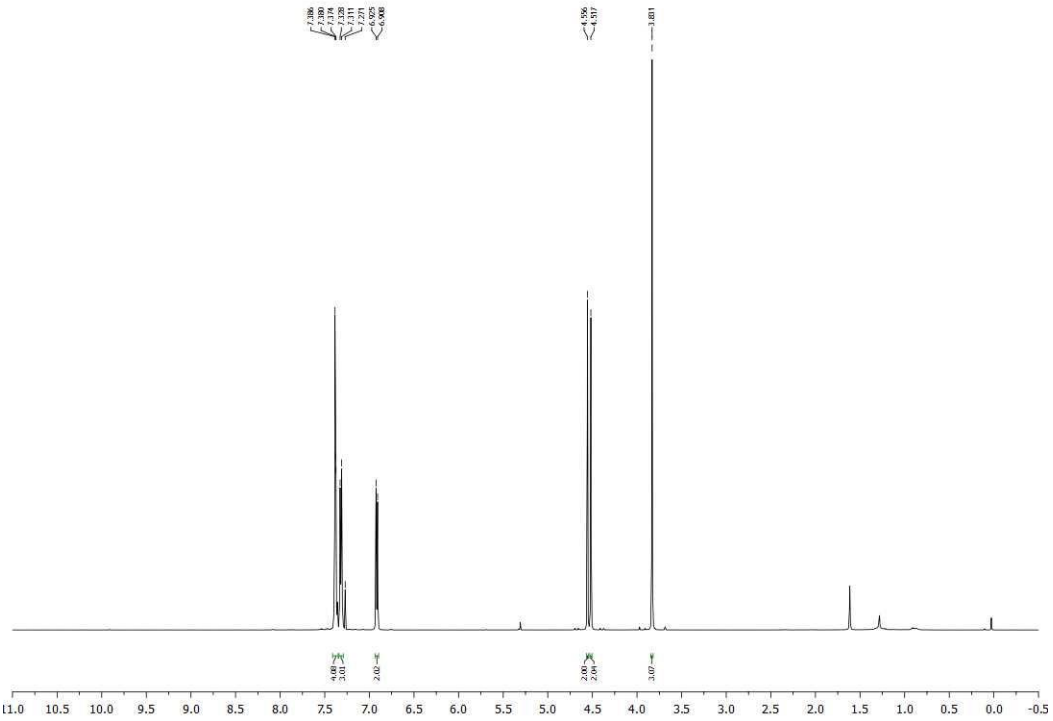

**Figure A2.24.** $^{1}H$ NMR ($CDCl_3$, 500 MHz) spectrum of 1-((benzyloxy)methyl)-4-methoxybenzene (**12**)

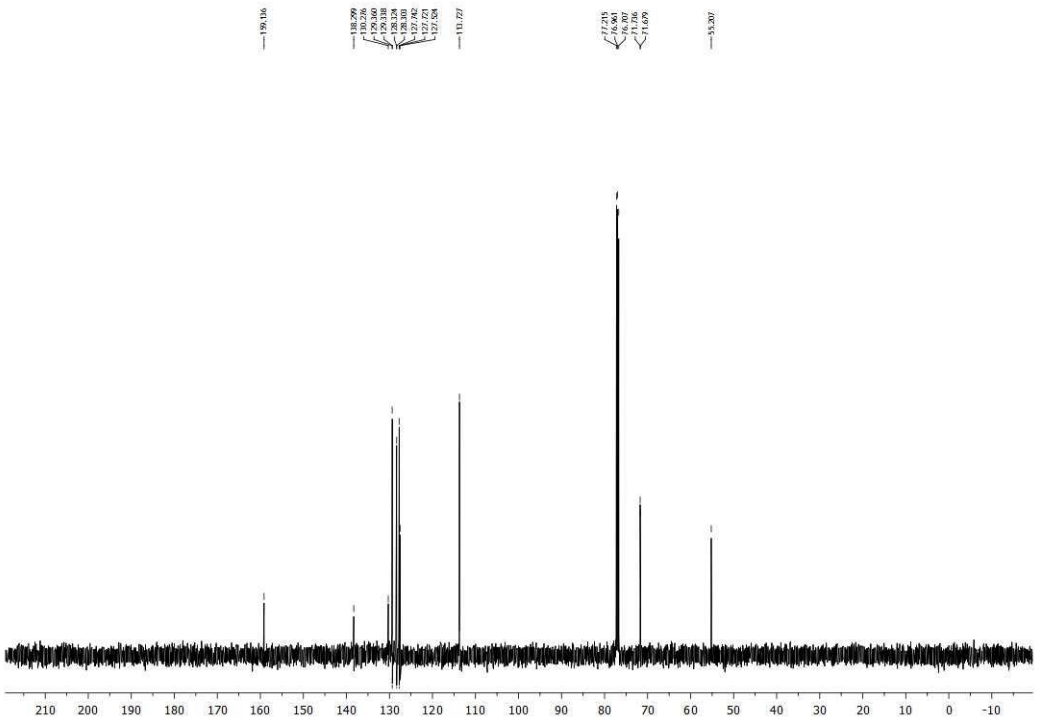

**Figure A2.25.** $^{13}C$ NMR ($CDCl_3$, 125.8 MHz) spectrum of 1-((benzyloxy)methyl)-4-methoxybenzene (**12**)

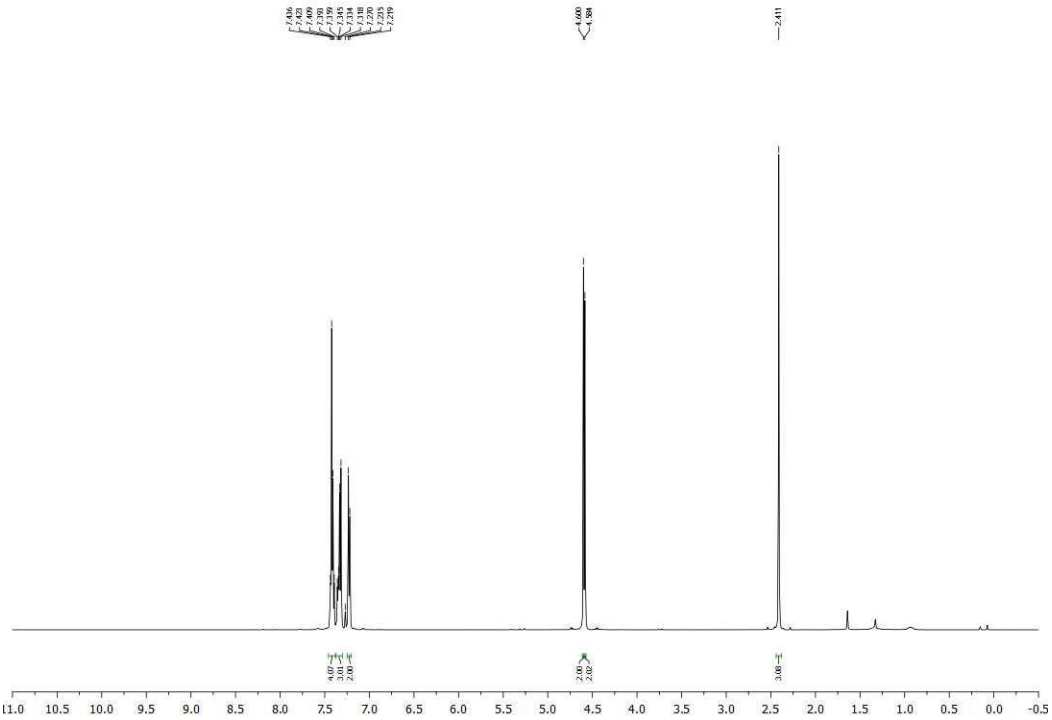

**Figure A2.26.** $^{1}H$ NMR ($CDCl_3$, 500 MHz) spectrum of 1-((benzyloxy)methyl)-4-methylbenzene (**13**)

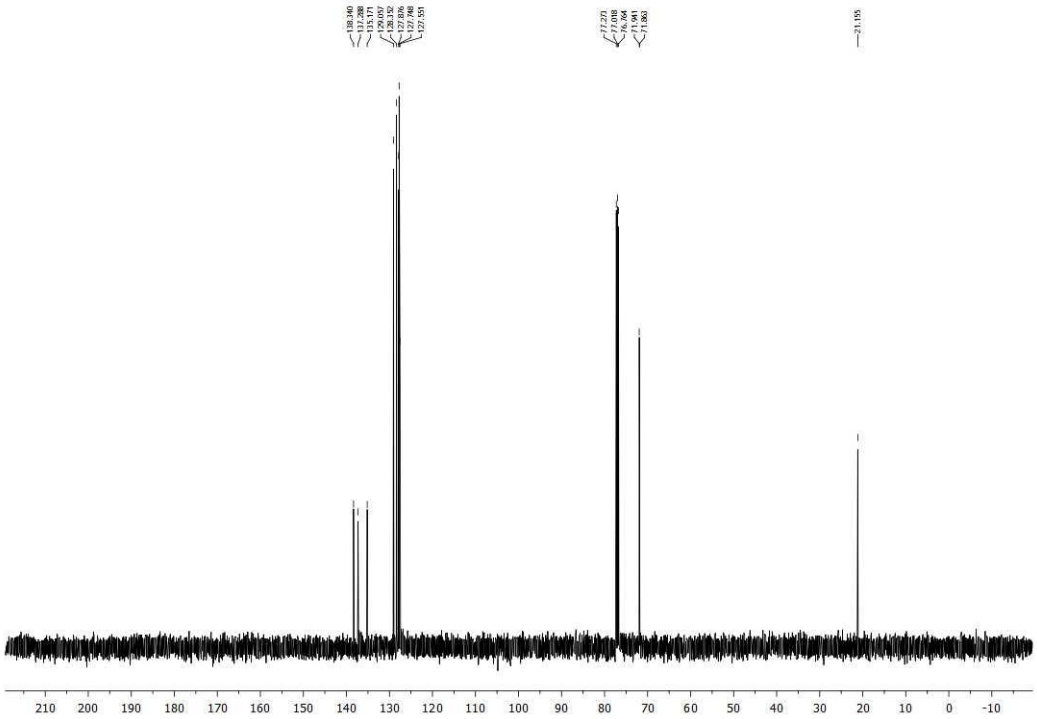

**Figure A2.27.** $^{13}C$ NMR ($CDCl_3$, 125.8 MHz) spectrum of 1-((benzyloxy)methyl)-4-methylbenzene (**13**)

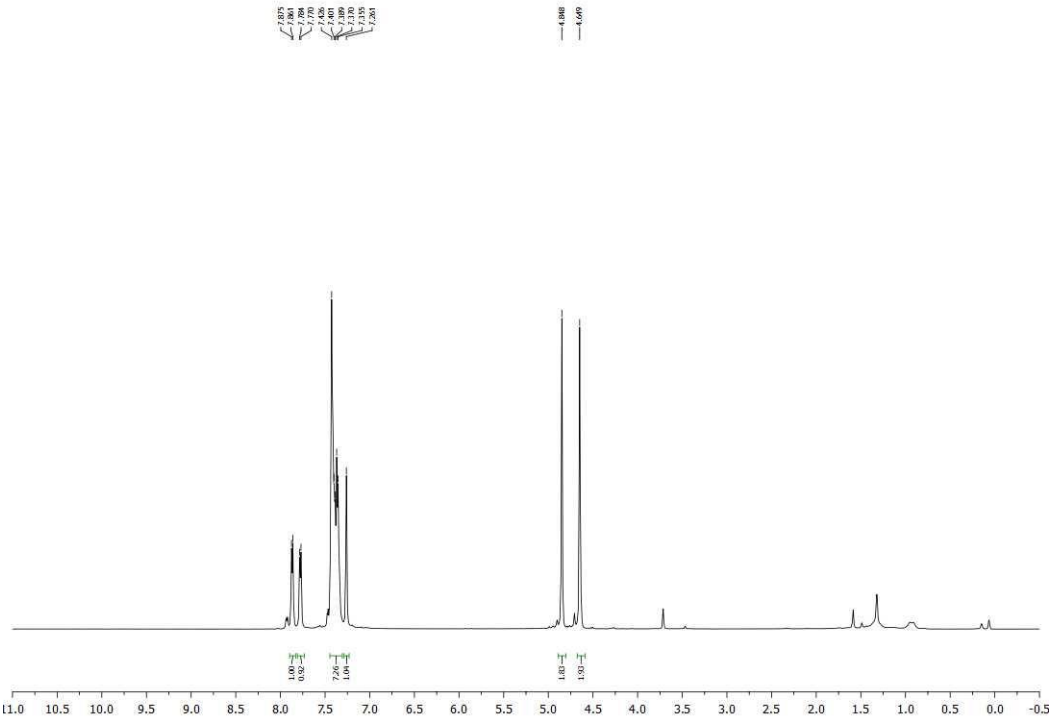

**Figure A2.28.** $^{1}H$ NMR ($CDCl_3$, 500 MHz) spectrum of 2-((benzyloxy)methyl)benzo[b]thiophene (**14**)

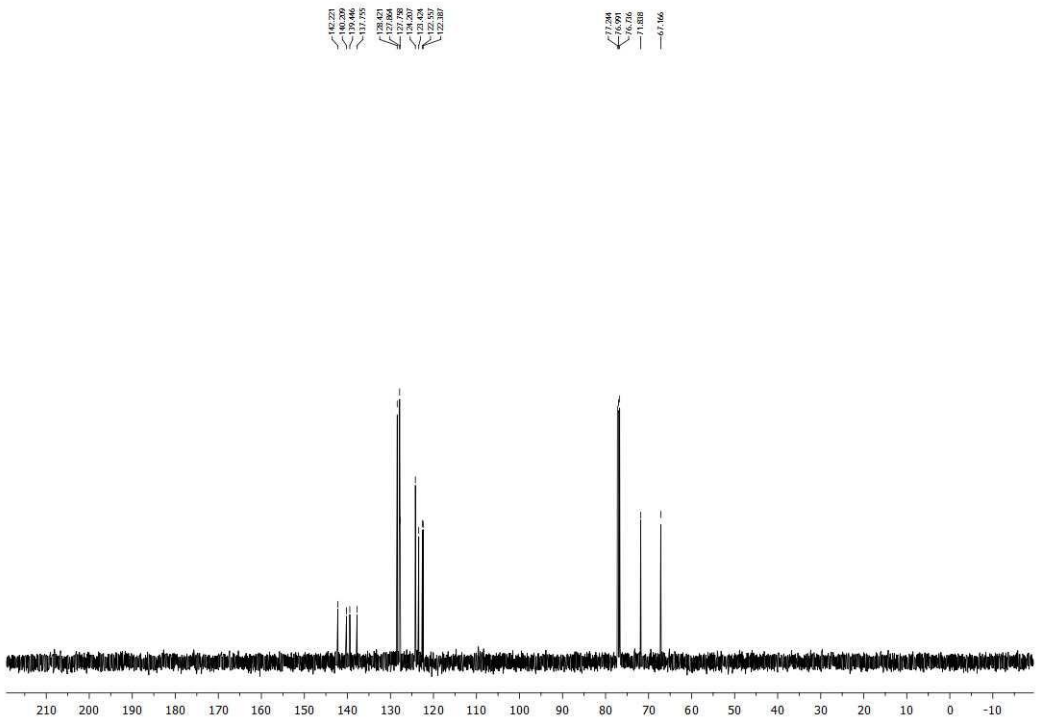

**Figure A2.29.** $^{13}C$ NMR ($CDCl_3$, 125.8 MHz) spectrum of 2-((benzyloxy)methyl)benzo[b]thiophene (**14**)

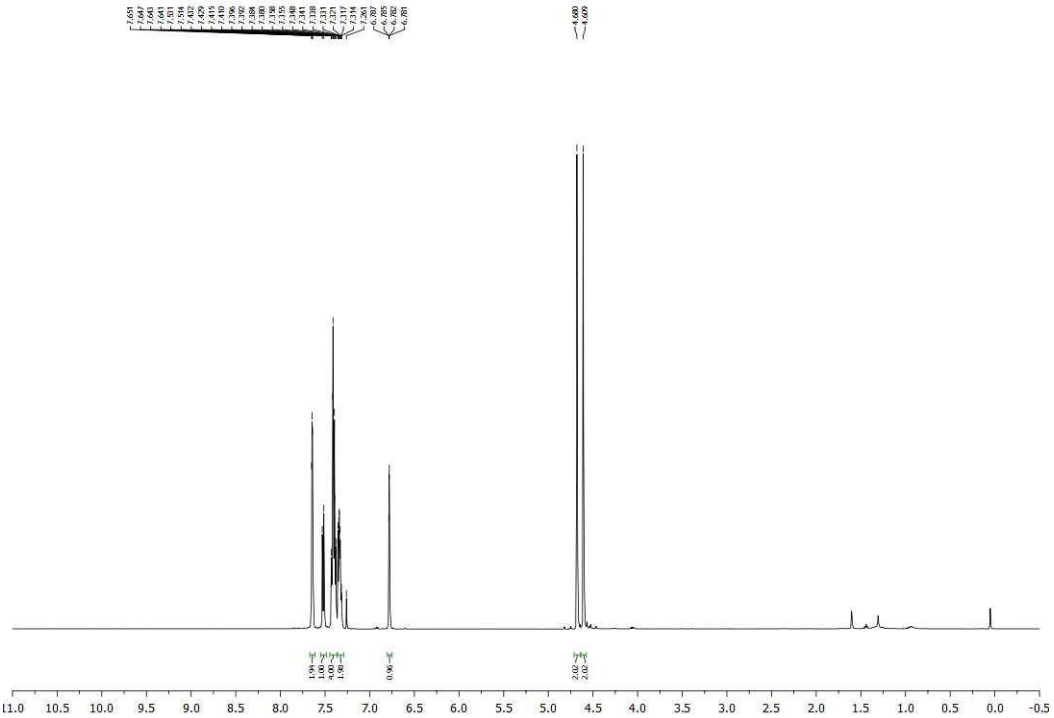

**Figure A2.30.** $^{1}H$ NMR ($CDCl_3$, 500 MHz) spectrum of 5-((benzyloxy)methyl)benzofuran (**15**)

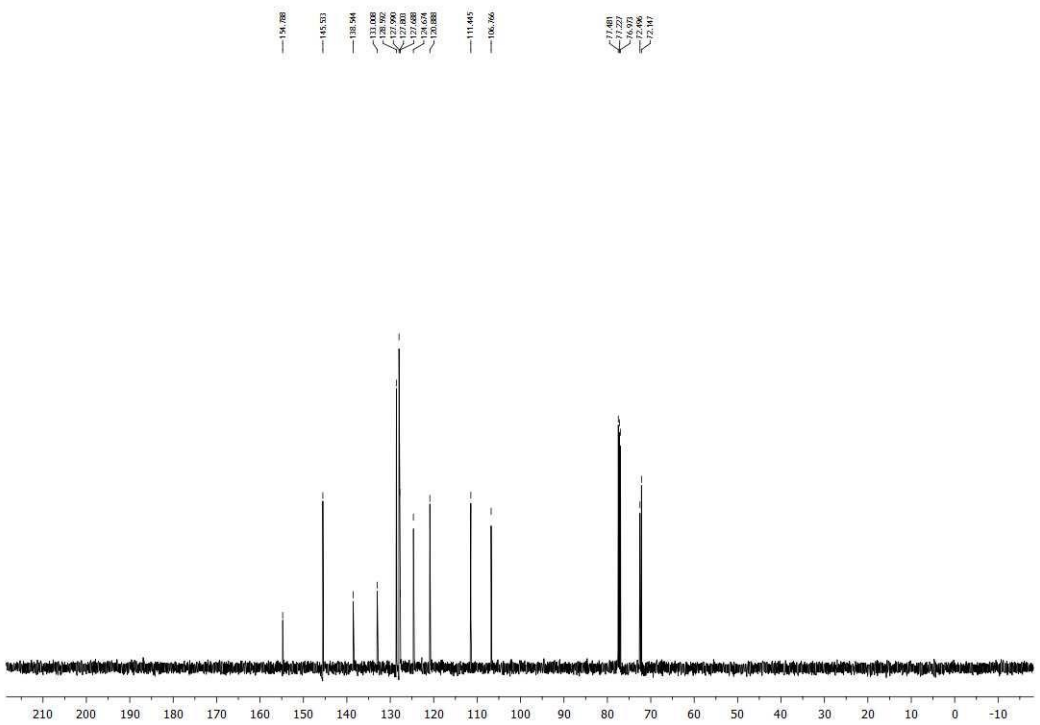

**Figure A2.31.** $^{13}C$ NMR ($CDCl_3$, 125.8 MHz) spectrum of 5-((benzyloxy)methyl)benzofuran (**15**)

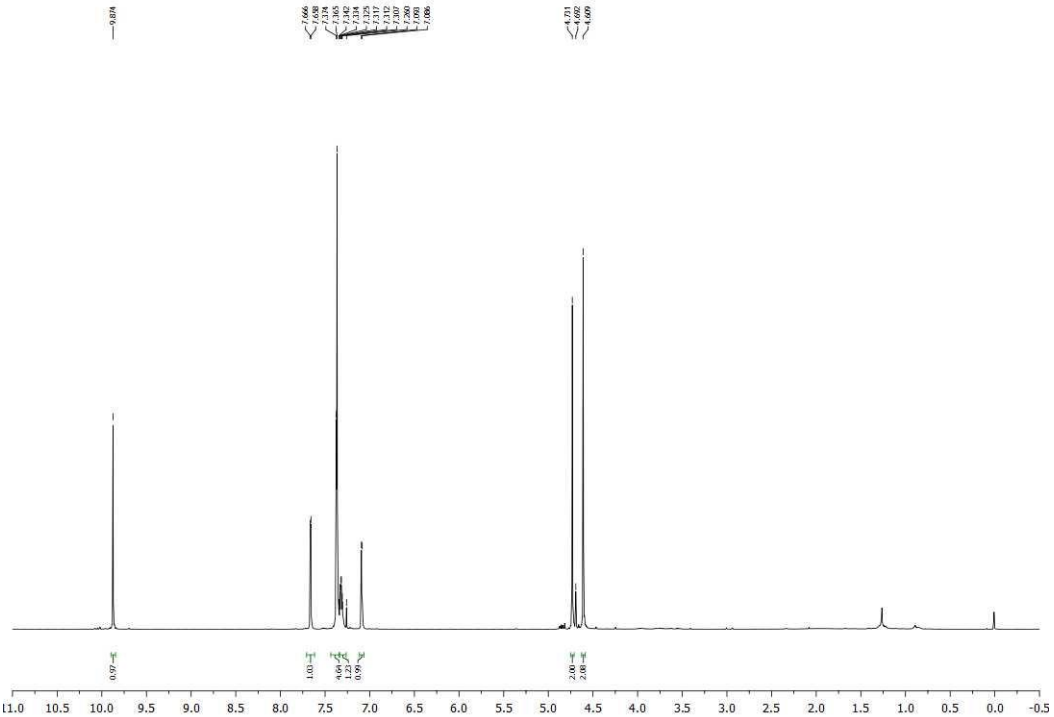

**Figure A2.32.** $^{1}H$ NMR ($CDCl_3$, 500 MHz) spectrum of 5-((benzyloxy)methyl)thiophene-2-carbaldehyde (**16**)

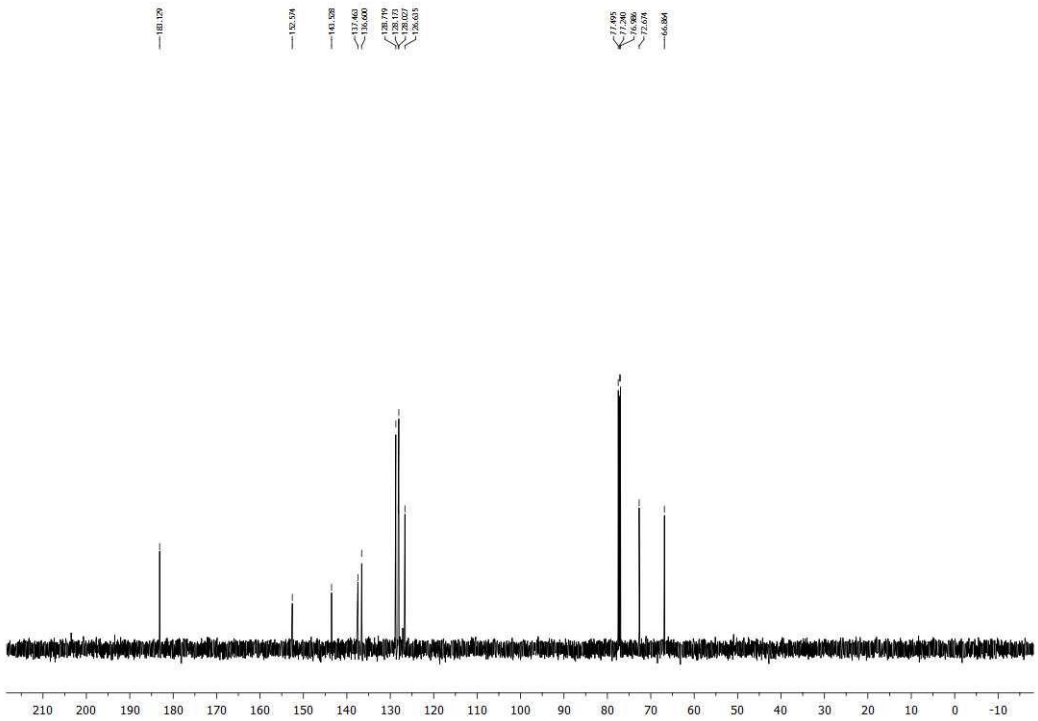

**Figure A2.33.** $^{13}C$ NMR ($CDCl_3$, 125.8 MHz) spectrum of 5-((benzyloxy)methyl)thiophene-2-carbaldehyde (**16**)

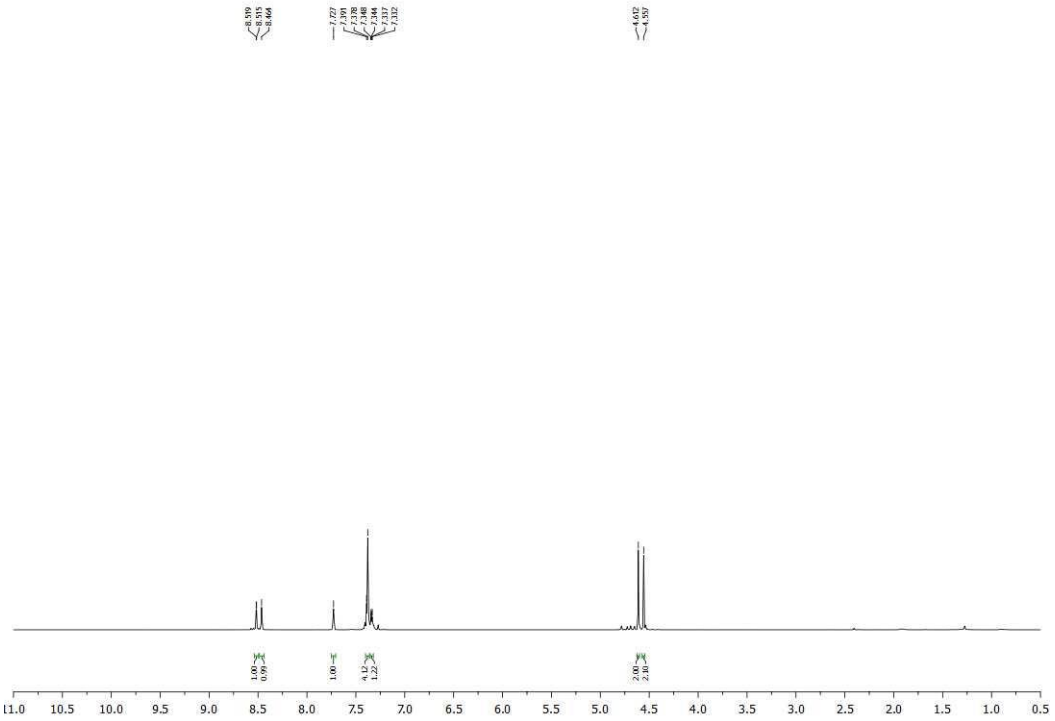

**Figure A2.34.** $^{1}H$ NMR ($CDCl_3$, 500 MHz) spectrum of 1-((benzyloxy)methyl)-3-chlorobenzene (**17**)

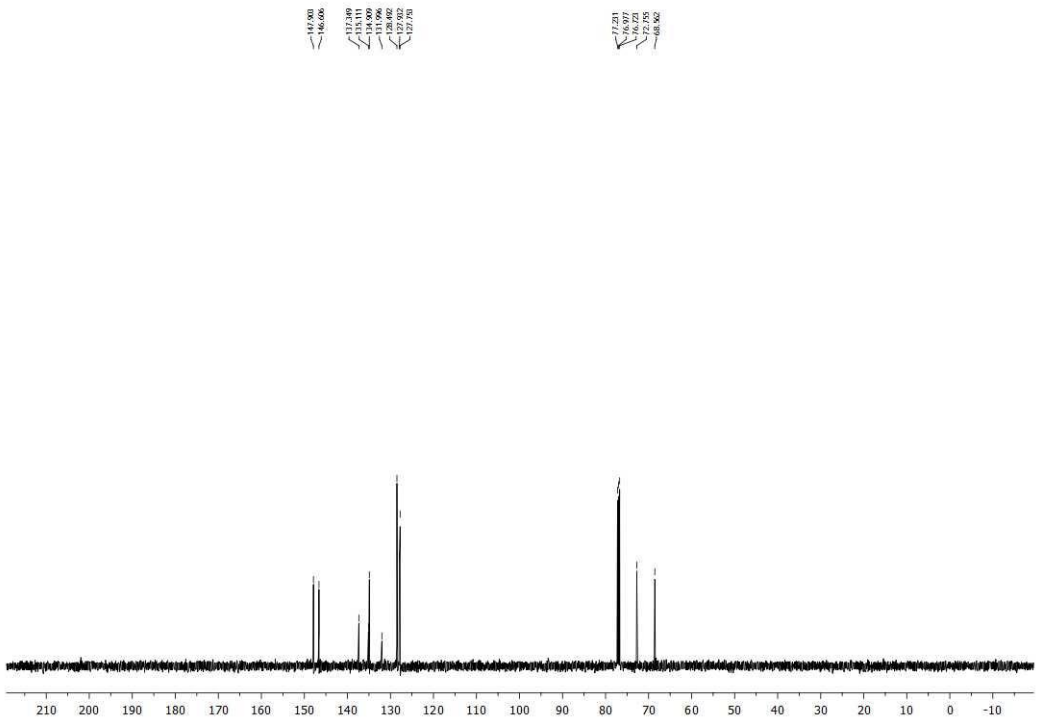

**Figure A2.35.** $^{13}C$ NMR ($CDCl_3$, 125.8 MHz) spectrum of 1-((benzyloxy)methyl)-3-chlorobenzene (**17**)

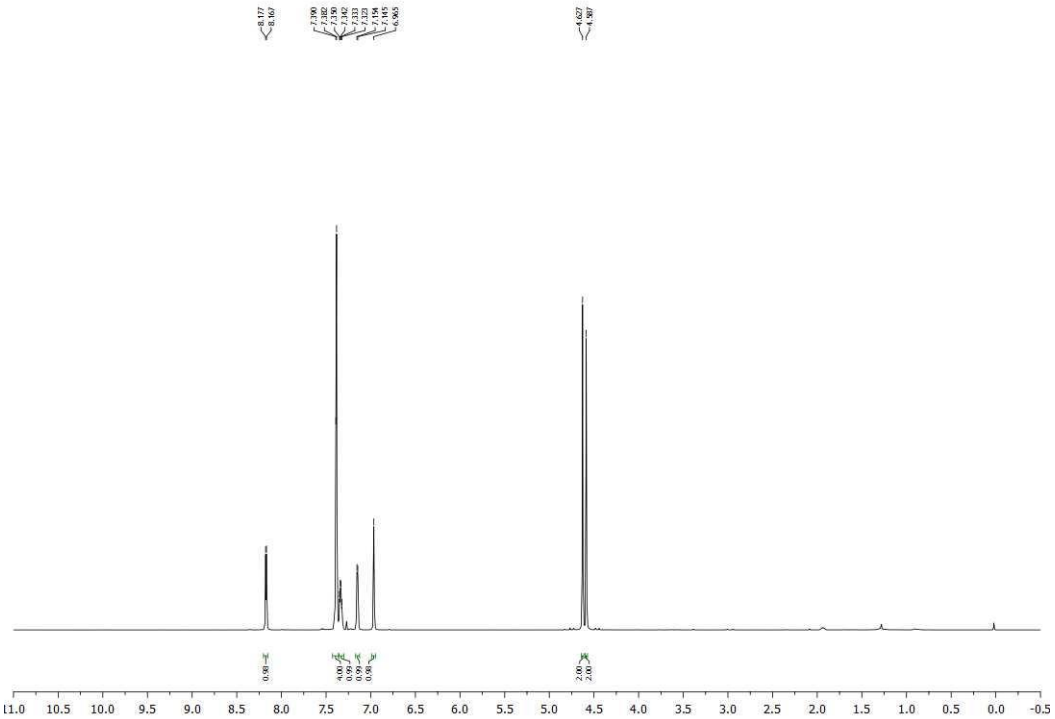

**Figure A2.36.** $^{1}H$ NMR ($CDCl_3$, 500 MHz) spectrum of 4-((benzyloxy)methyl)-2-fluoropyridine (**18**)

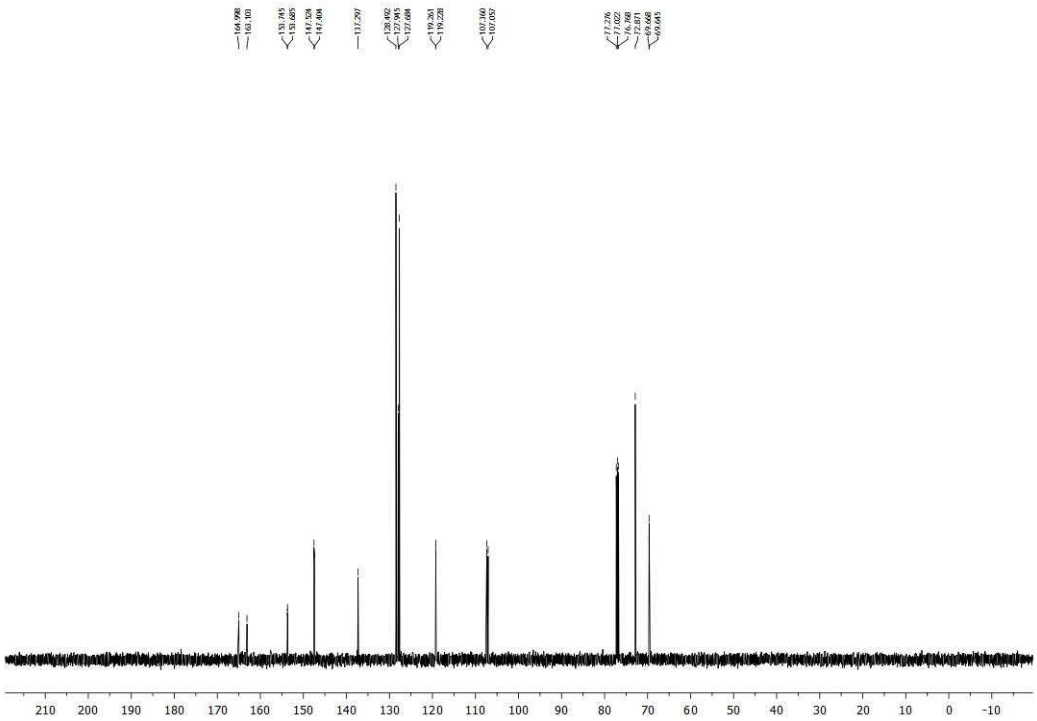

**Figure A2.37.** $^{13}C$ NMR ($CDCl_3$, 125.8 MHz) spectrum of 4-((benzyloxy)methyl)-2-fluoropyridine (**18**)

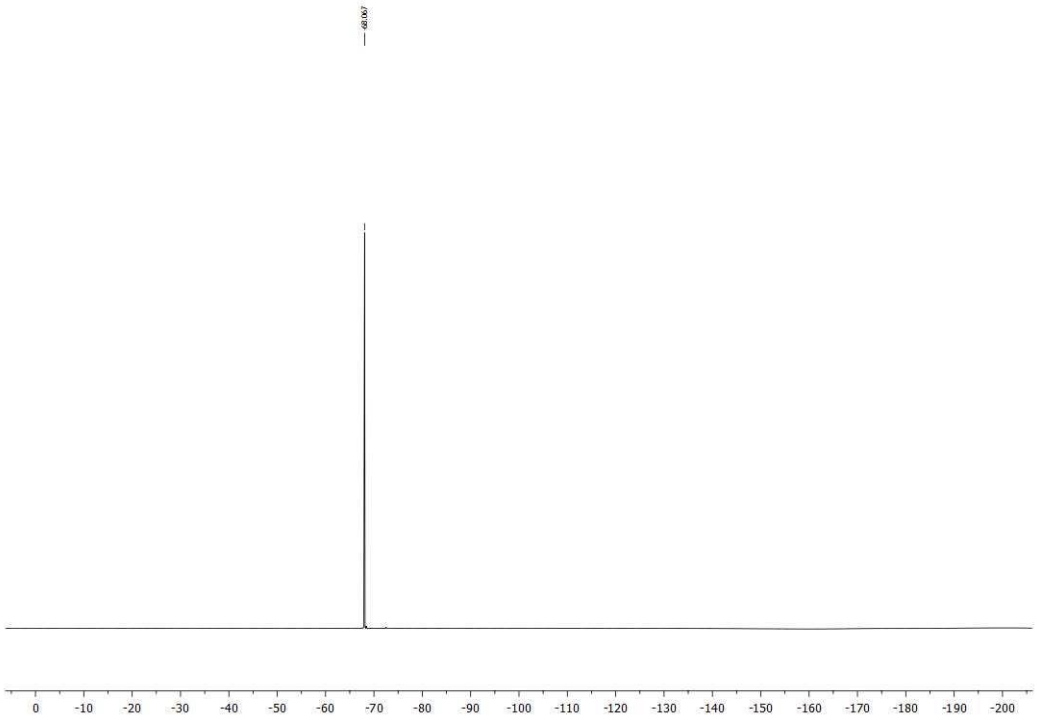

**Figure A2.38.** $^{1}H$ NMR ($CDCl_3$, 470.8 MHz) spectrum of 4-((benzyloxy)methyl)-2-fluoropyridine (**18**)

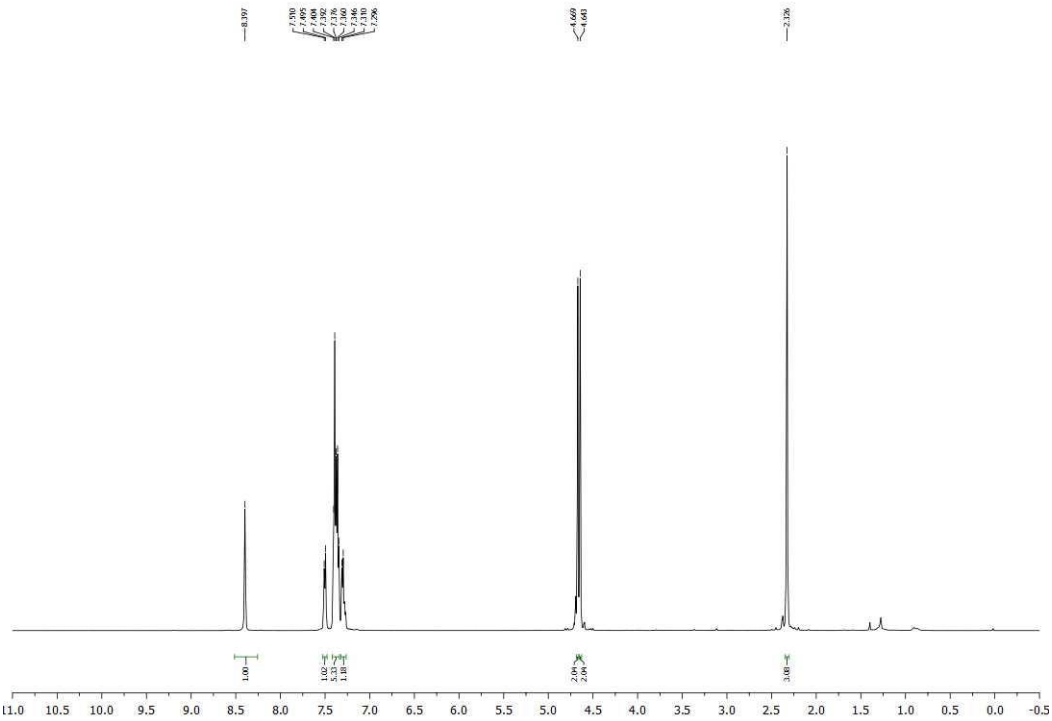

**Figure A2.39.** $^{1}$H NMR ($CDCl_3$, 500 MHz) spectrum of 2-((benzyloxy)methyl)-5-methylpyridine (**19**)

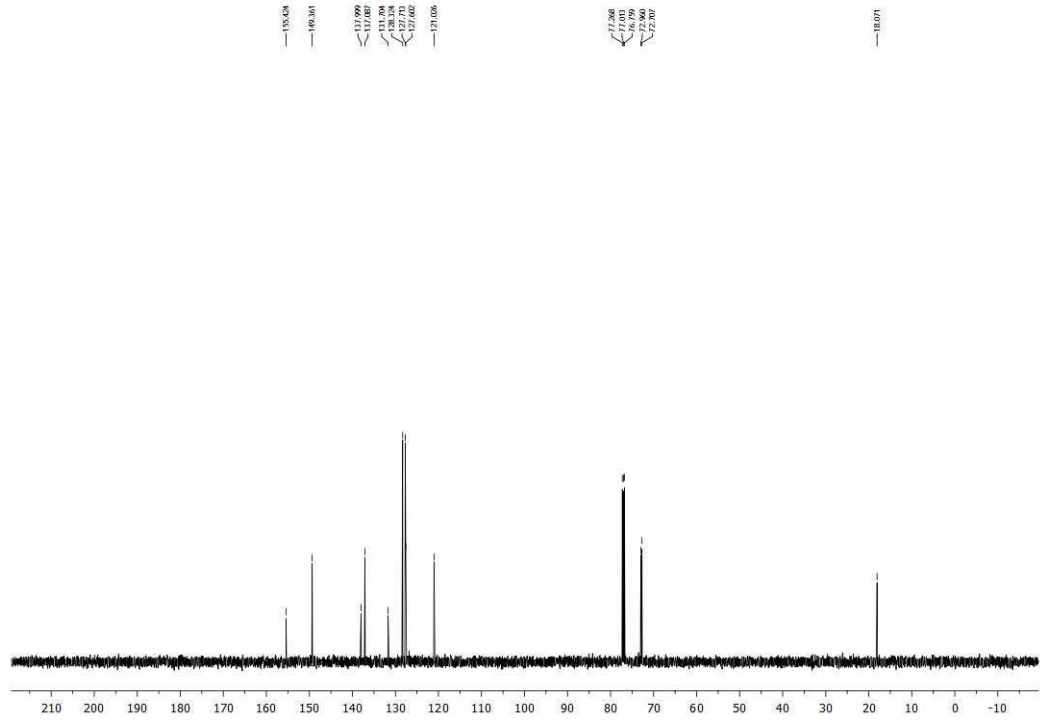

**Figure A2.40.** $^{13}$C NMR ($CDCl_3$, 125.8 MHz) spectrum of 2-((benzyloxy)methyl)-5-methylpyridine (**19**)

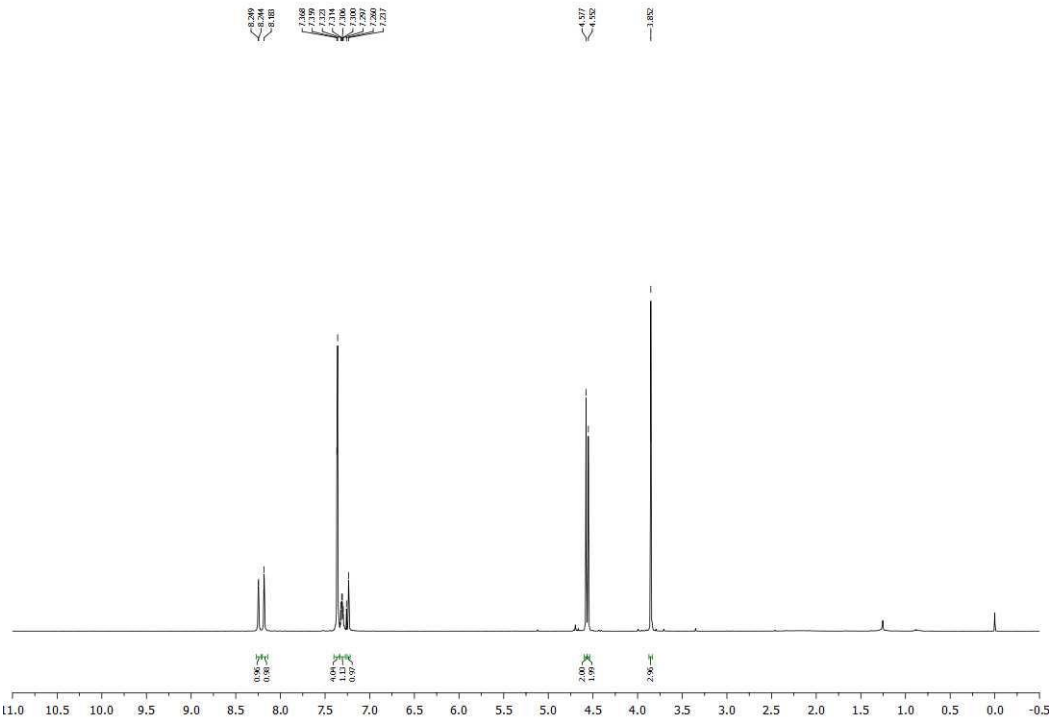

**Figure A2.41.** $^{1}H$ NMR ($CDCl_3$, 500 MHz) spectrum of 3-((benzyloxy)methyl)-5-methoxypyridine (**20**)

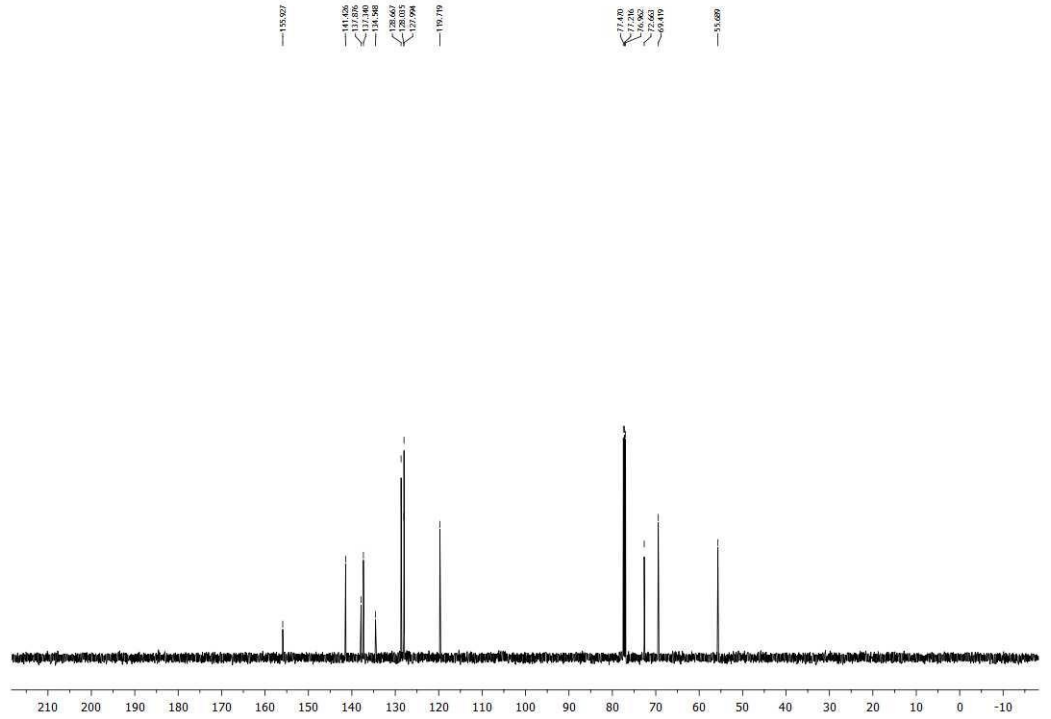

**Figure A2.42.** $^{13}C$ NMR ($CDCl_3$, 125.8 MHz) spectrum of 3-((benzyloxy)methyl)-5-methoxypyridine (**20**)

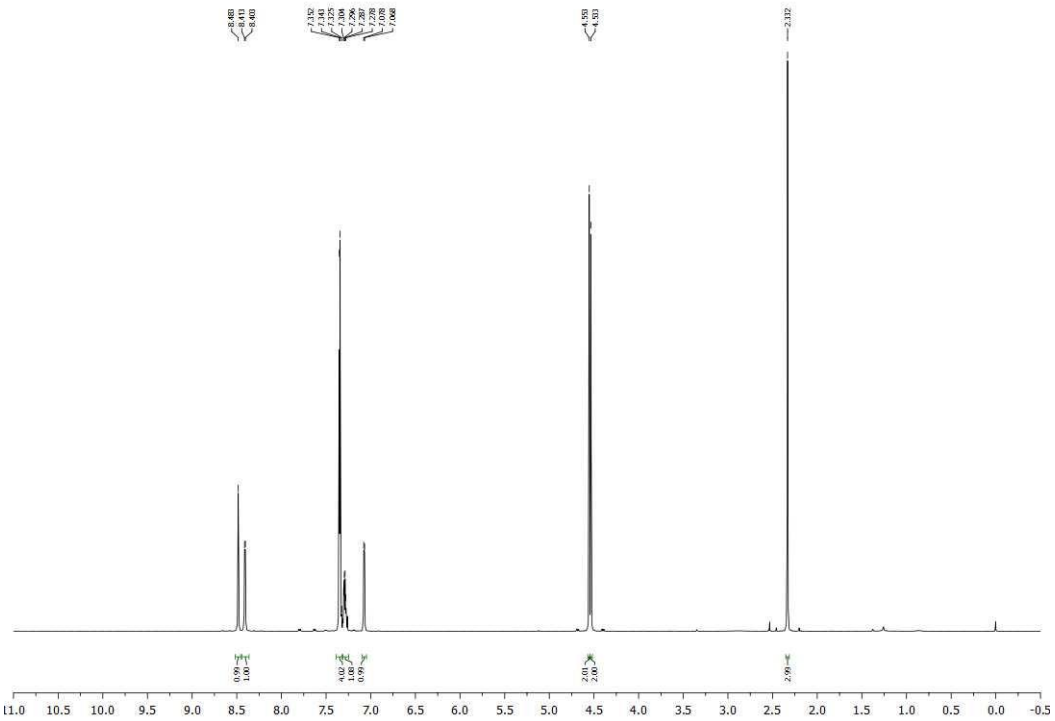

**Figure A2.43.** $^{1}$H NMR ($CDCl_3$, 500 MHz) spectrum of 3-((benzyloxy)methyl)-4-methylpyridine (**21**)

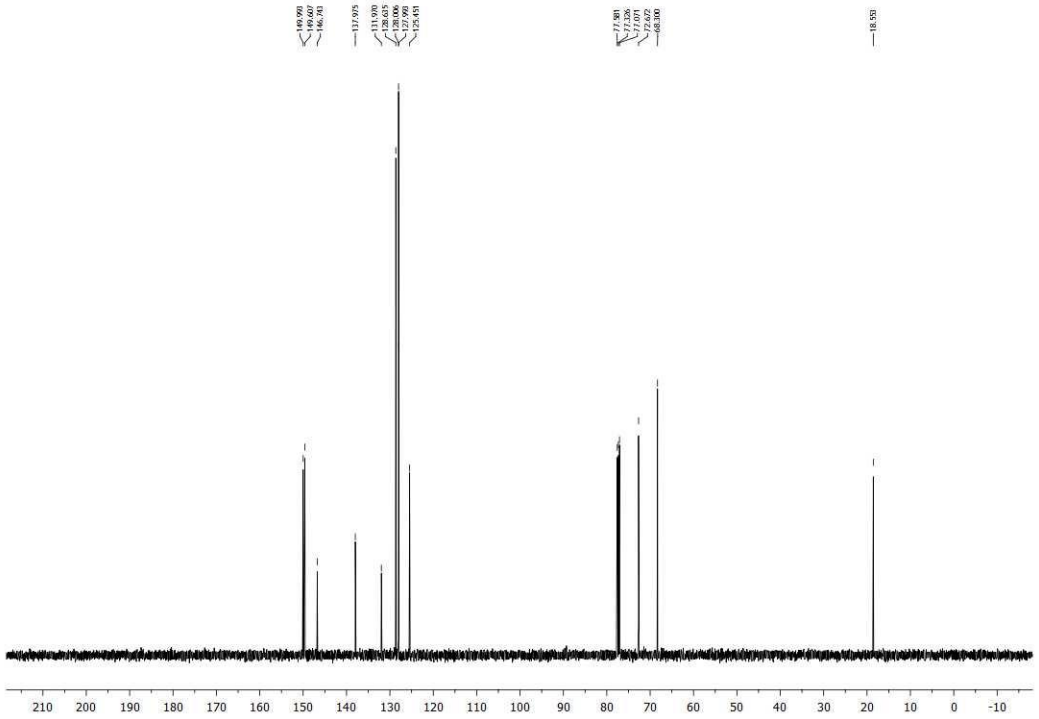

**Figure A2.44.** $^{13}$C NMR ($CDCl_3$, 125.8 MHz) spectrum of 3-((benzyloxy)methyl)-4-methylpyridine (**21**)

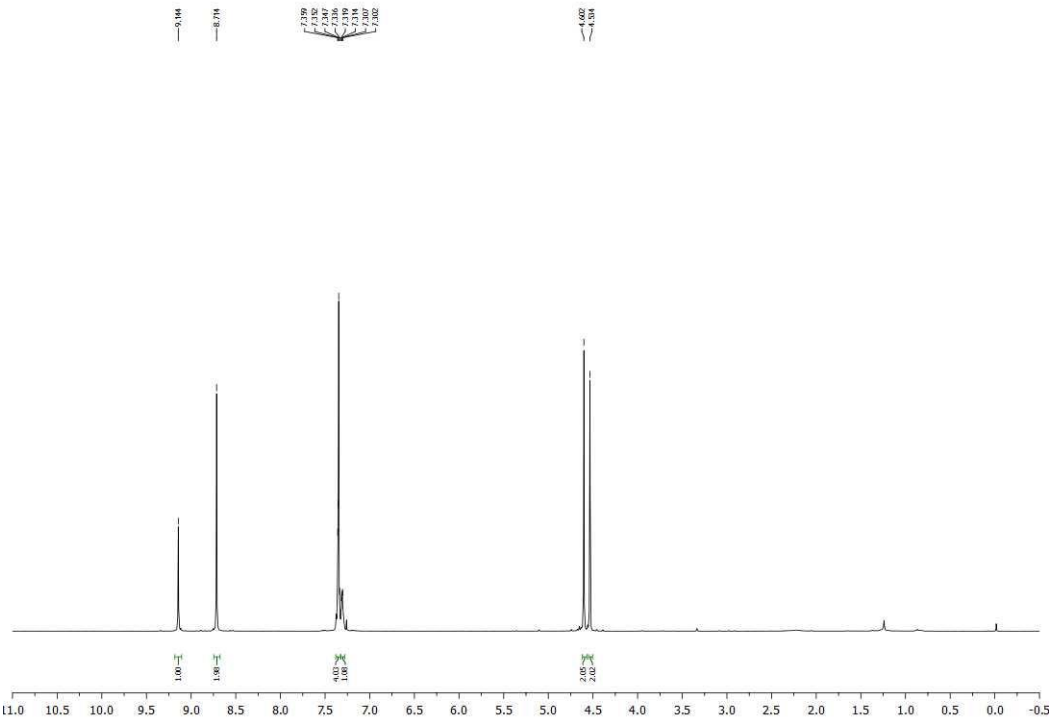

**Figure A2.45.** $^{1}$H NMR ($CDCl_3$, 500 MHz) spectrum of 5-((benzyloxy)methyl)pyrimidine (**22**)

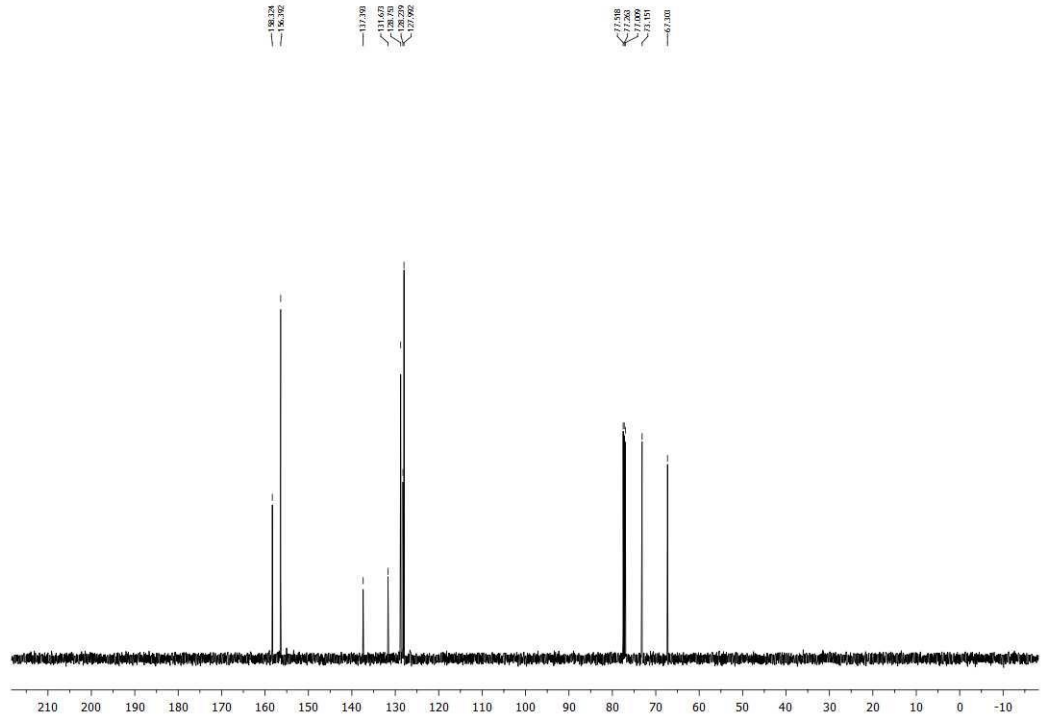

**Figure A2.46.** $^{13}$C NMR ($CDCl_3$, 125.8 MHz) spectrum of 5-((benzyloxy)methyl)pyrimidine (**22**)

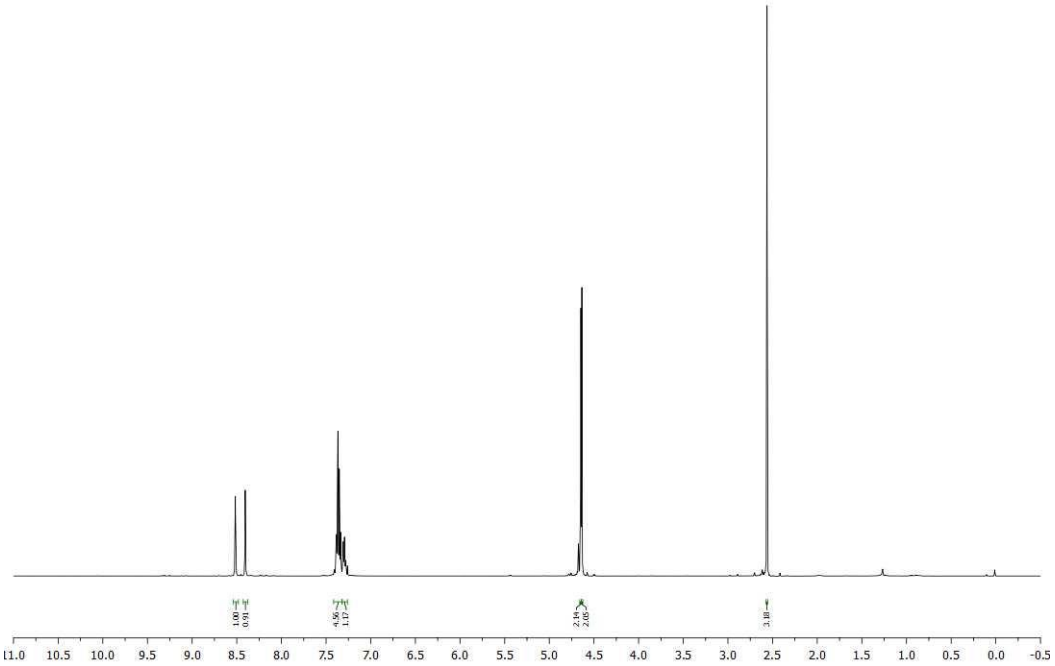

**Figure A2.47.** $^{1}$H NMR ($CDCl_3$, 500 MHz) spectrum of 2-((benzyloxy)methyl)-5-(methylthio)pyrazine (**23**)

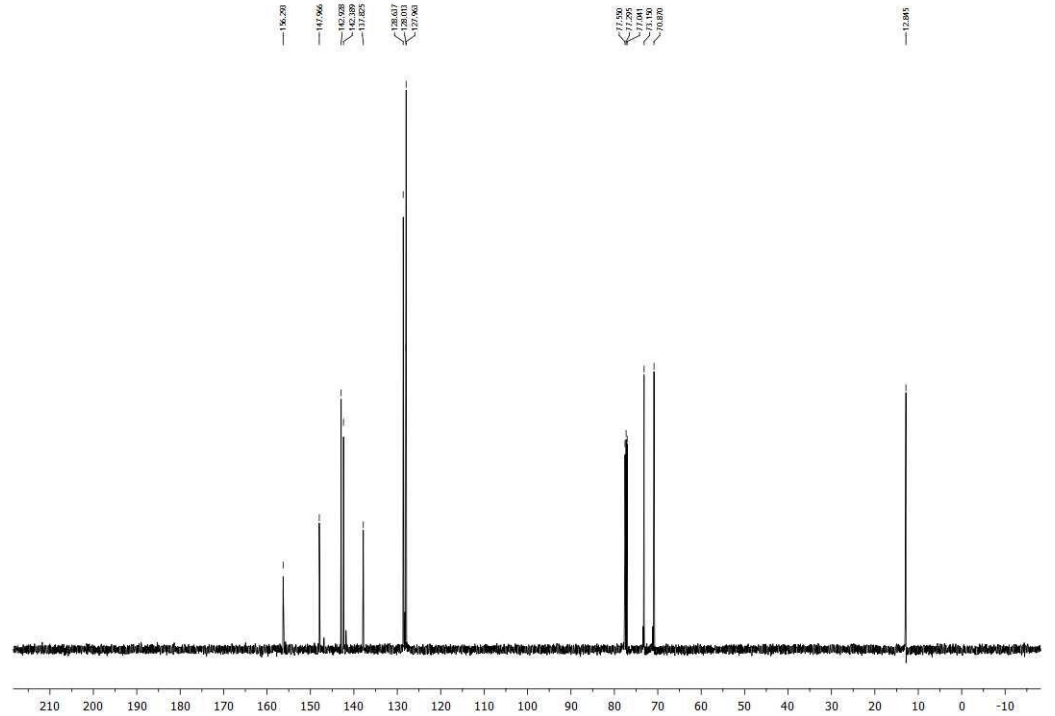

**Figure A2.48.** $^{13}$C NMR ($CDCl_3$, 125.8 MHz) spectrum of 2-((benzyloxy)methyl)-5-(methylthio)pyrazine (**23**)

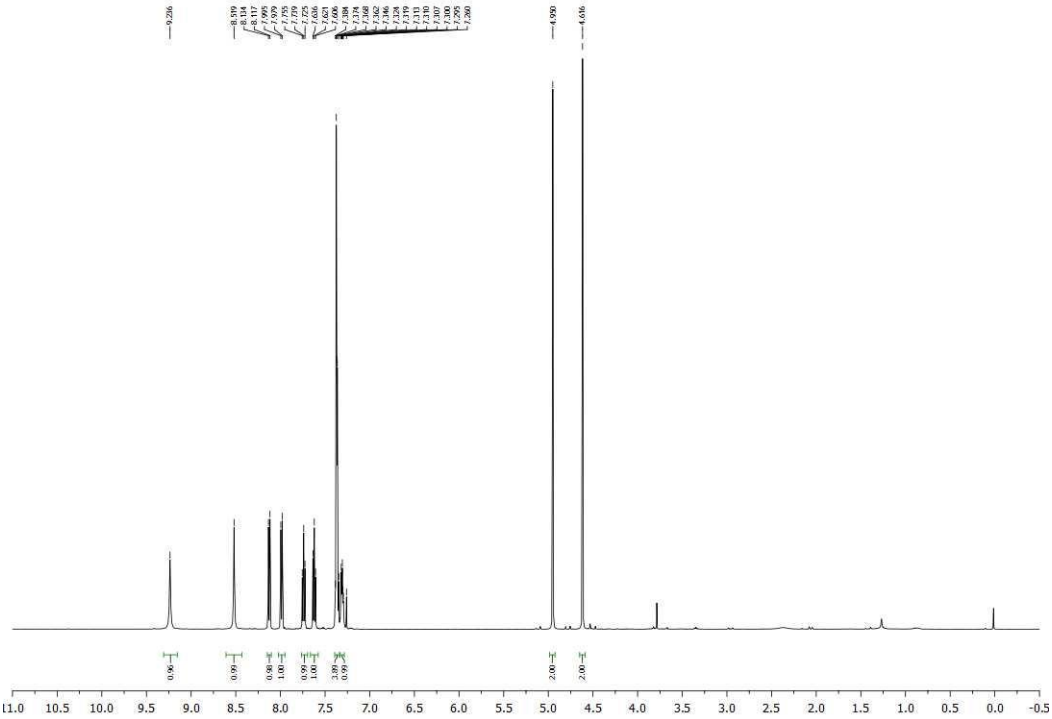

**Figure A2.49.** $^{1}$H NMR ($CDCl_3$, 500 MHz) spectrum of 4-((benzyloxy)methyl)isoquinoline (**24**)

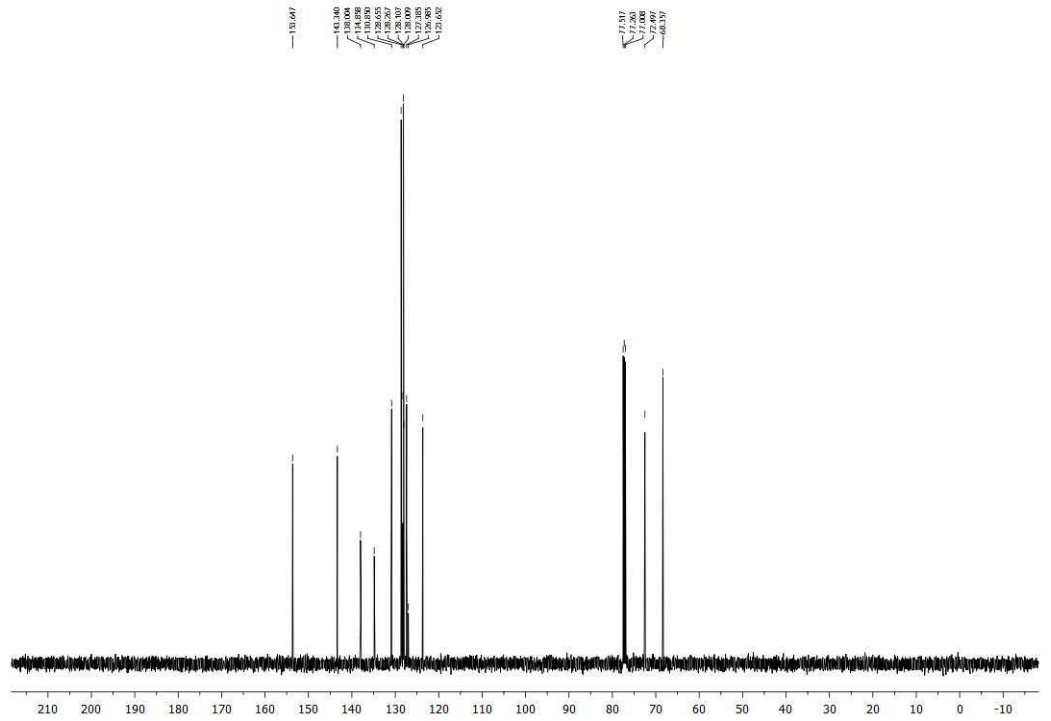

**Figure A2.50.** $^{13}$C NMR ($CDCl_3$, 125.8 MHz) spectrum of 4-((benzyloxy)methyl)isoquinoline (**24**)

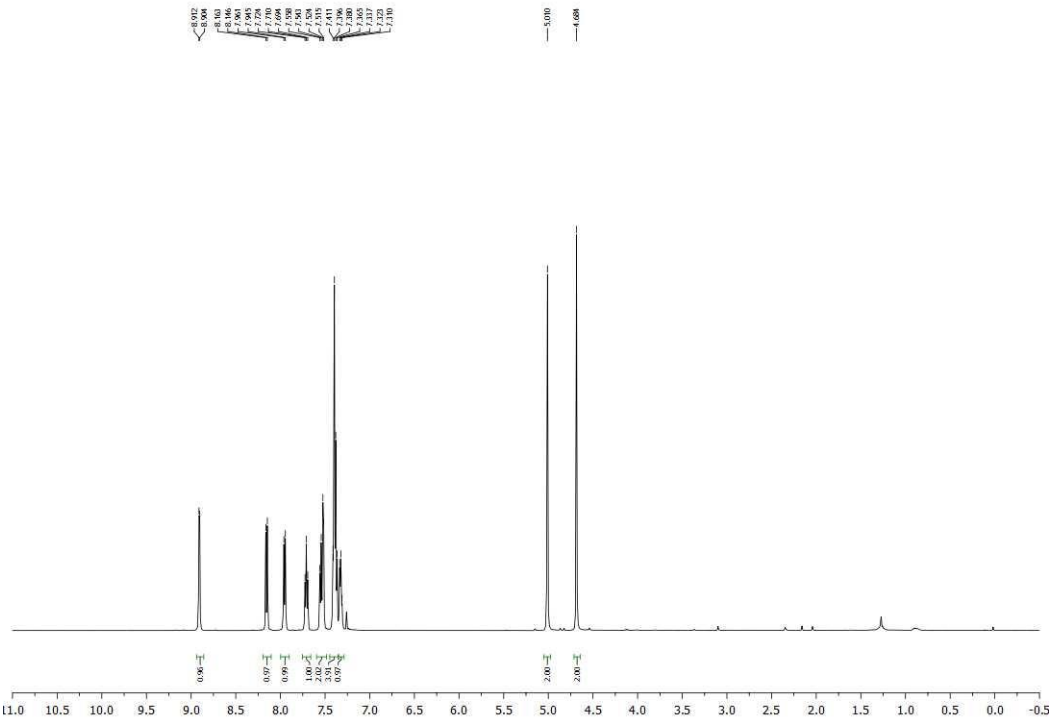

**Figure A2.51.** $^{1}$H NMR ($CDCl_3$, 500 MHz) spectrum of 4-((benzyloxy)methyl)quinoline (**25**)

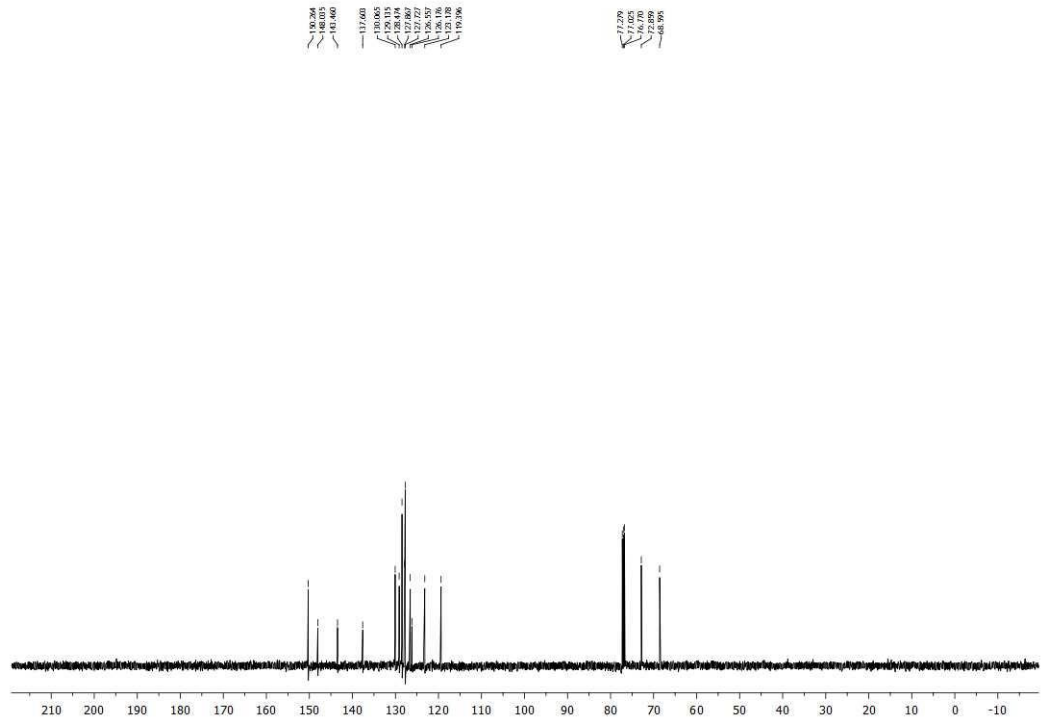

**Figure A2.52.** $^{13}$C NMR ($CDCl_3$, 125.8 MHz) spectrum of 4-((benzyloxy)methyl)quinoline (**25**)

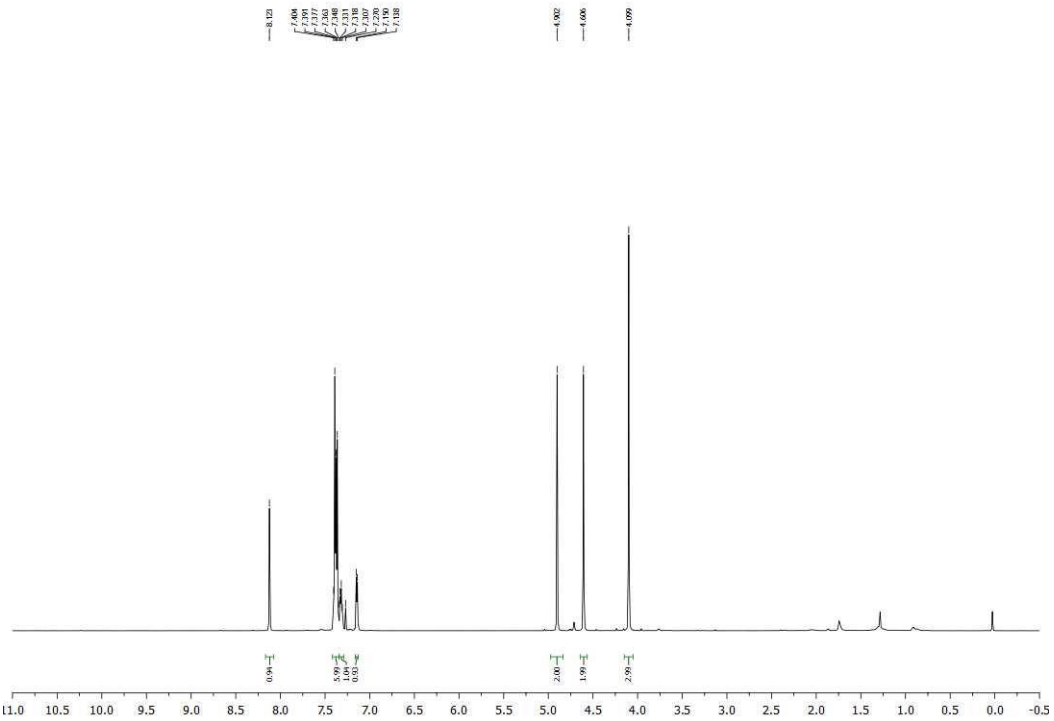

**Figure A2.53.** $^{1}$H NMR ($CDCl_3$, 500 MHz) spectrum of 4-((benzyloxy)methyl)-1-methyl-1H-indazole (**26**)

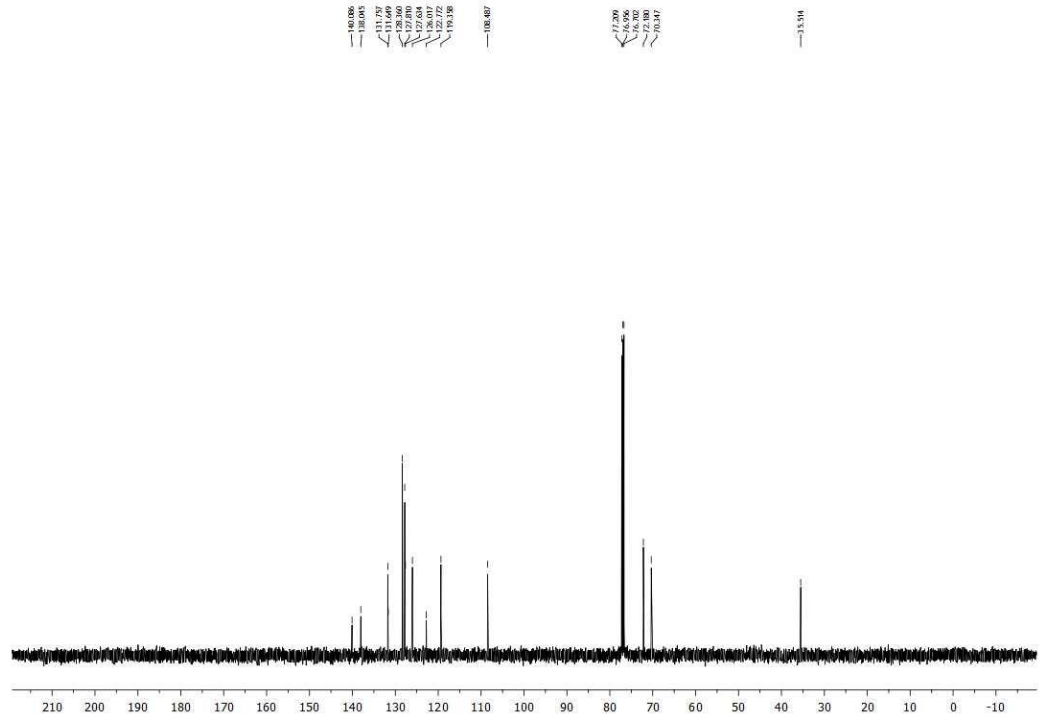

**Figure A2.54.** $^{13}$C NMR ($CDCl_3$, 125.8 MHz) spectrum of 4-((benzyloxy)methyl)-1-methyl-1H-indazole (**26**)

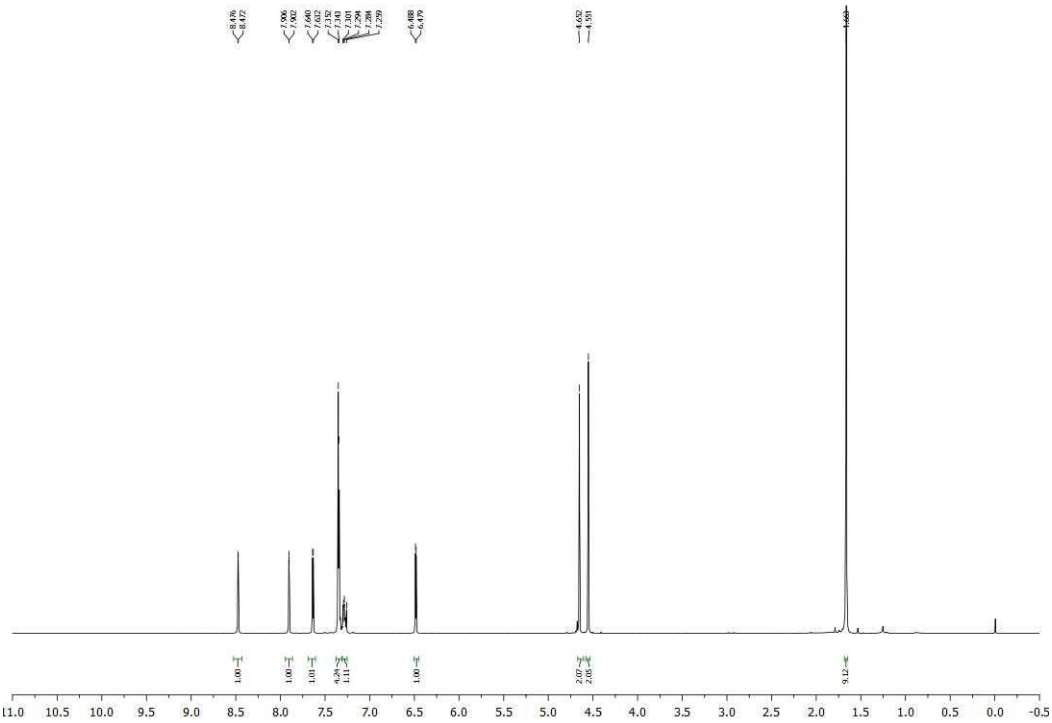

**Figure A2.55.** $^{1}$H NMR ($CDCl_3$, 500 MHz) spectrum of (*tert*-butyl 5-(benzyloxy)methyl)-1H-pyrrolo[2,3-b]pyridine-1-carboxylate (**27**)

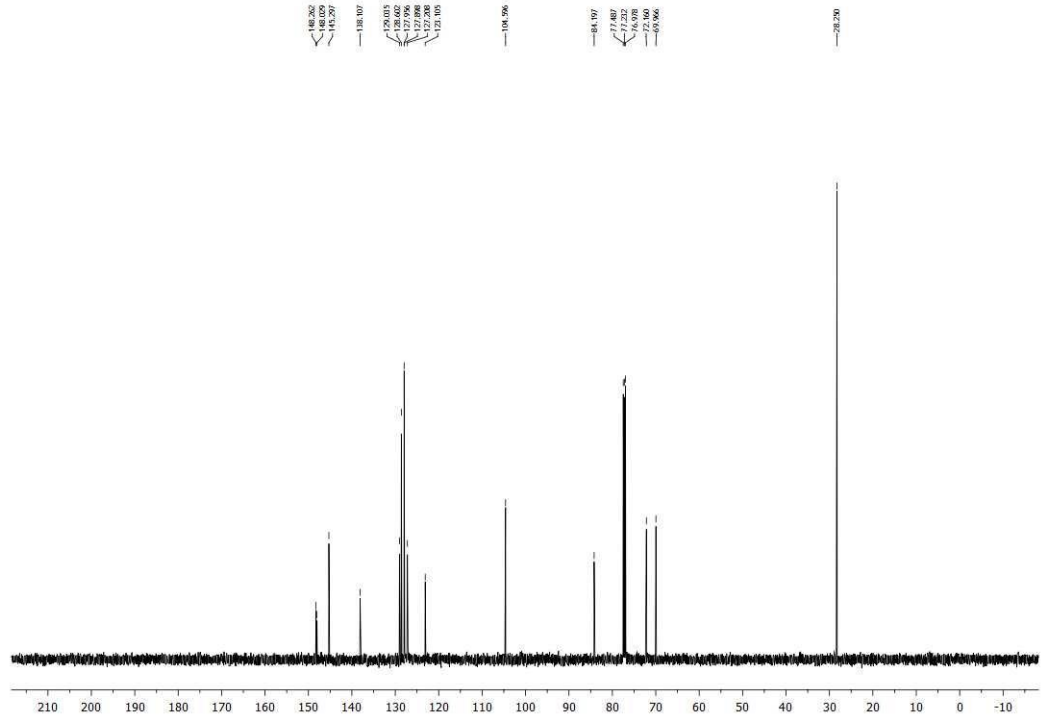

**Figure A2.56.** $^{13}$C NMR ($CDCl_3$, 125.8 MHz) spectrum of (*tert*-butyl 5-(benzyloxy)methyl)-1H-pyrrolo[2,3-b]pyridine-1-carboxylate (**27**)

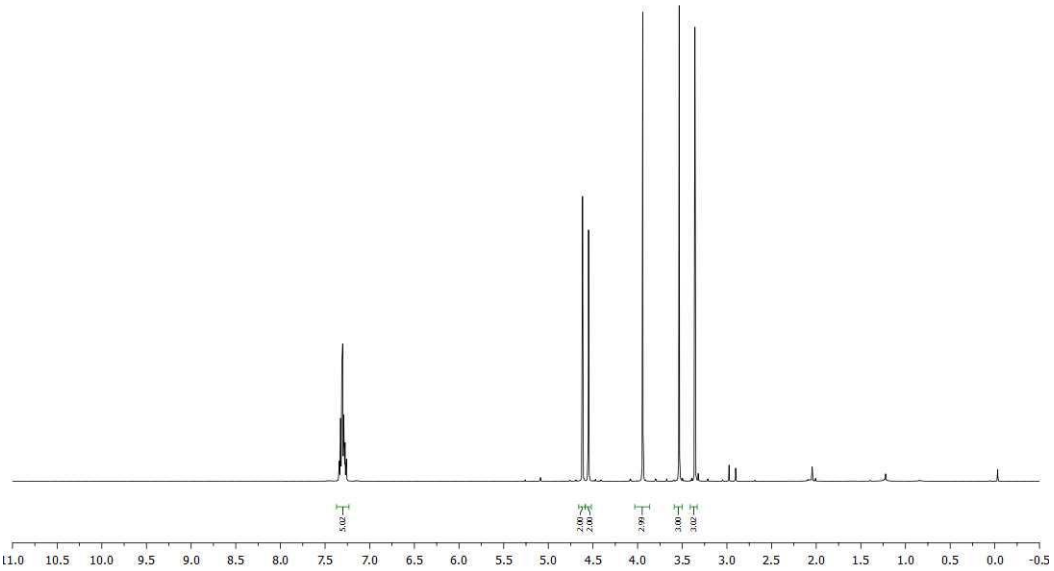

**Figure A2.57.** $^{1}$H NMR ($CDCl_3$, 500 MHz) spectrum of 8-((benzyloxy)methyl)-1,3,7-trimethyl-3,7-dihydro-1H-purine-2,6-dione (**28**)

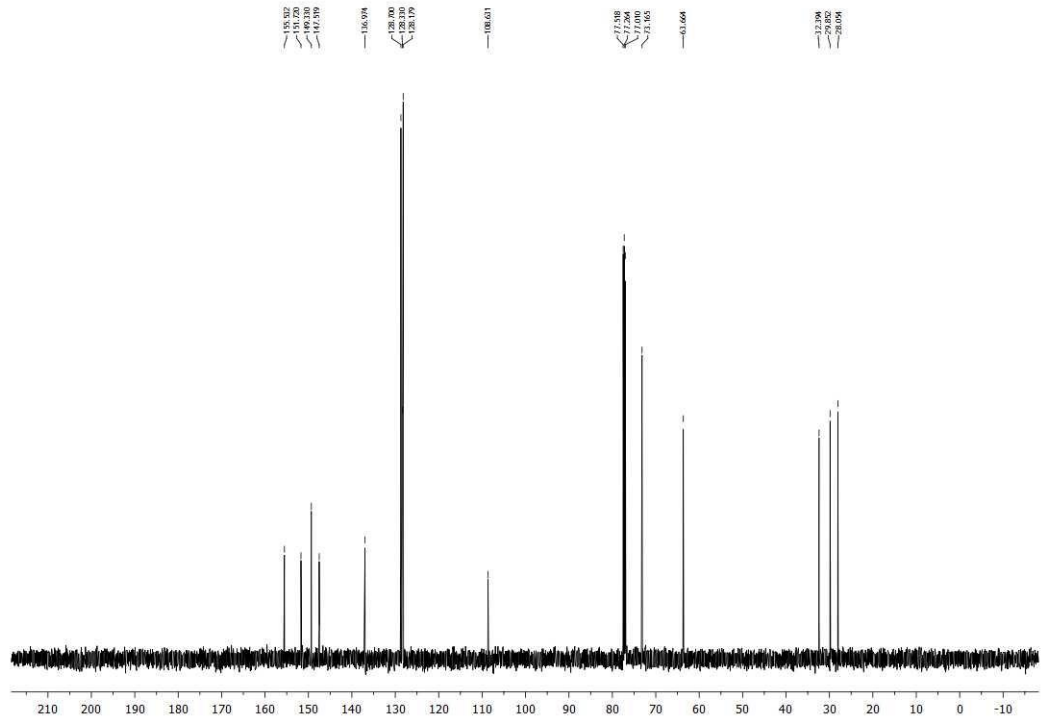

**Figure A2.58** $^{13}$C NMR ($CDCl_3$, 125.8 MHz) spectrum of 8-((benzyloxy)methyl)-1,3,7-trimethyl-3,7-dihydro-1H-purine-2,6-dione (**28**)

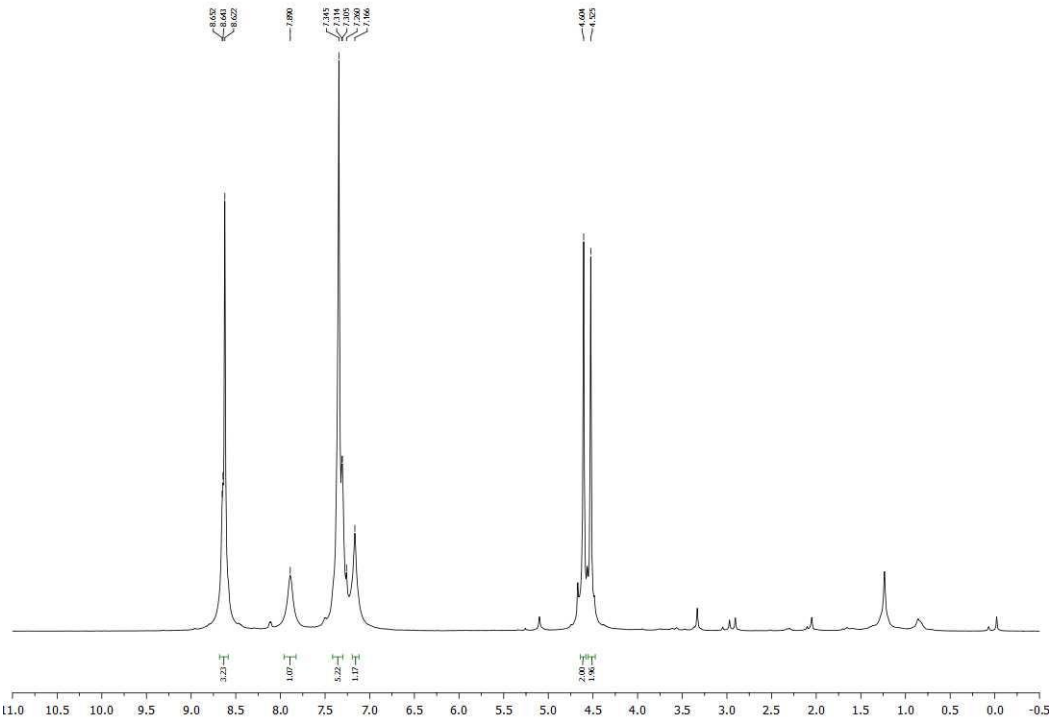

**Figure A2.59.** $^{1}$H NMR ($CDCl_3$, 500 MHz) spectrum of 5-((benzyloxy)methyl)-2-(1H-imidazol-1-yl)pyrimidine (**29**)

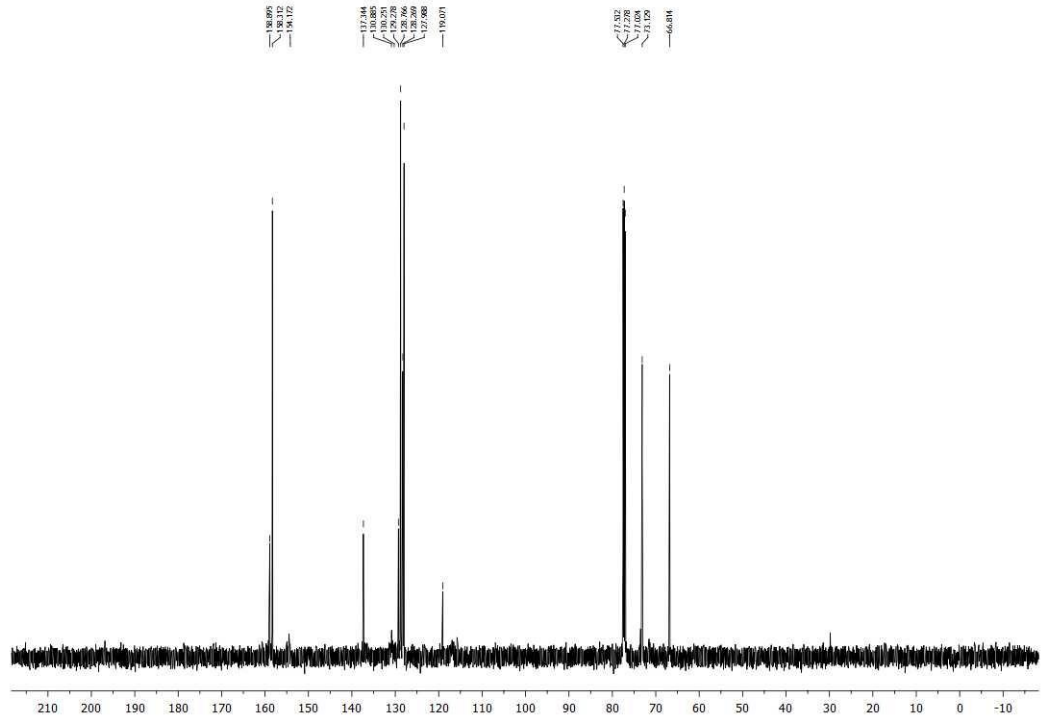

**Figure A2.60.** $^{13}$C NMR ($CDCl_3$, 125.8 MHz) spectrum of 5-((benzyloxy)methyl)-2-(1H-imidazol-1-yl)pyrimidine (**29**)

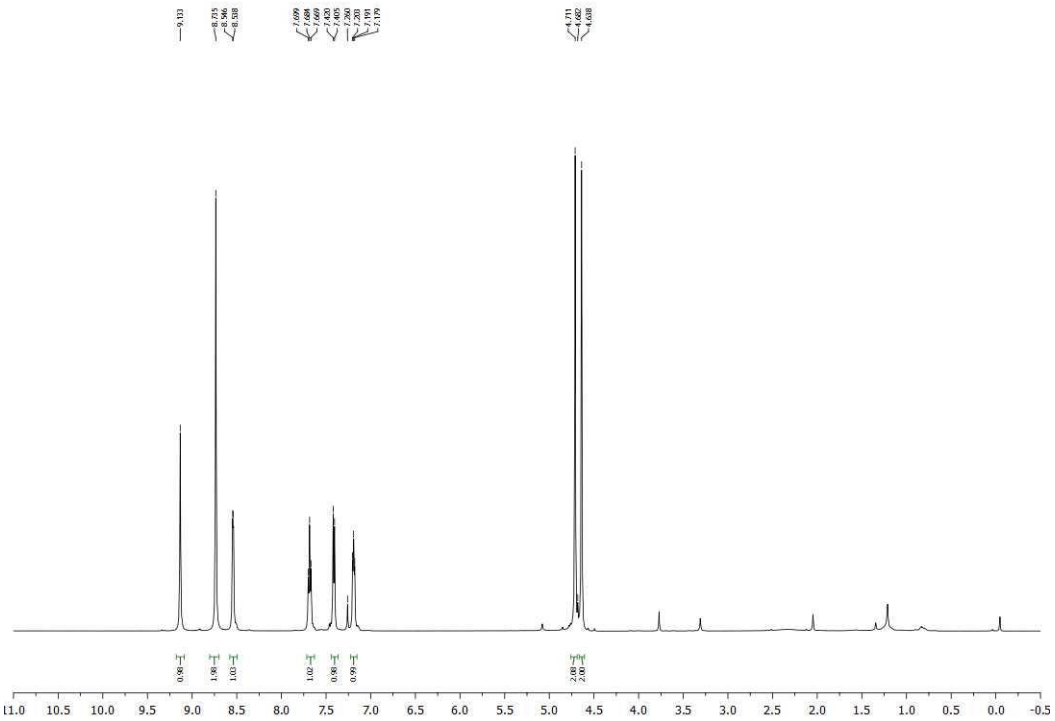

**Figure A2.61.** $^{1}$H NMR ($CDCl_3$, 500 MHz) spectrum of 5-((pyridin-2-ylmethoxy)methyl)pyrimidine (**30**)

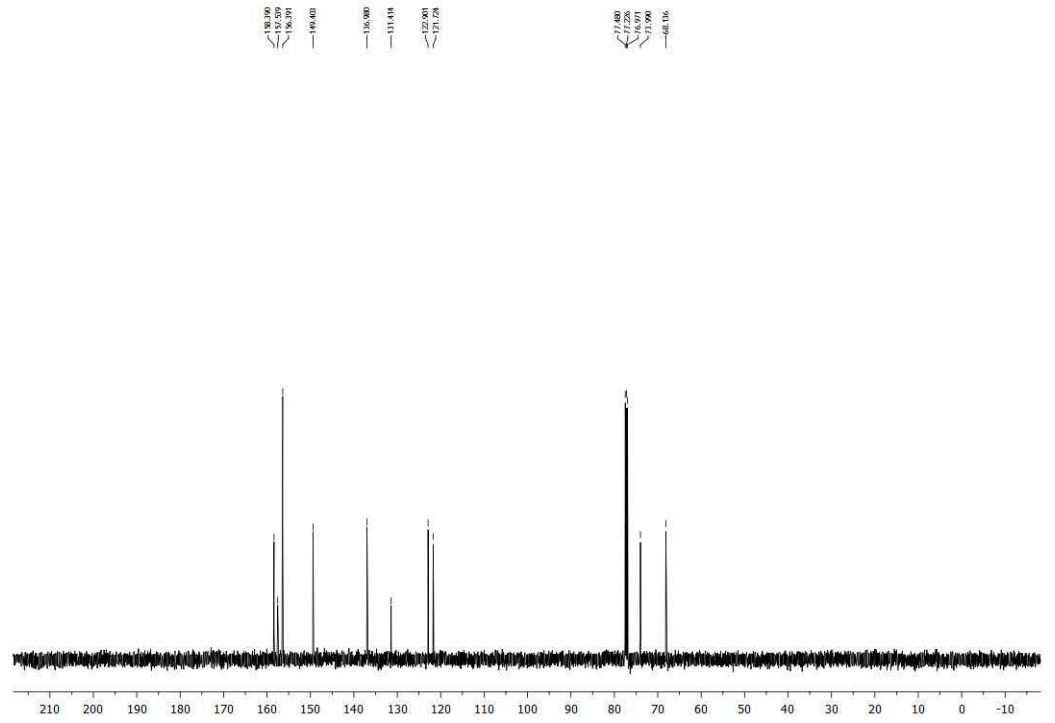

**Figure A2.62.** $^{13}$C NMR ($CDCl_3$, 125.8 MHz) spectrum of 5-((pyridin-2-ylmethoxy)methyl)pyrimidine (**30**)

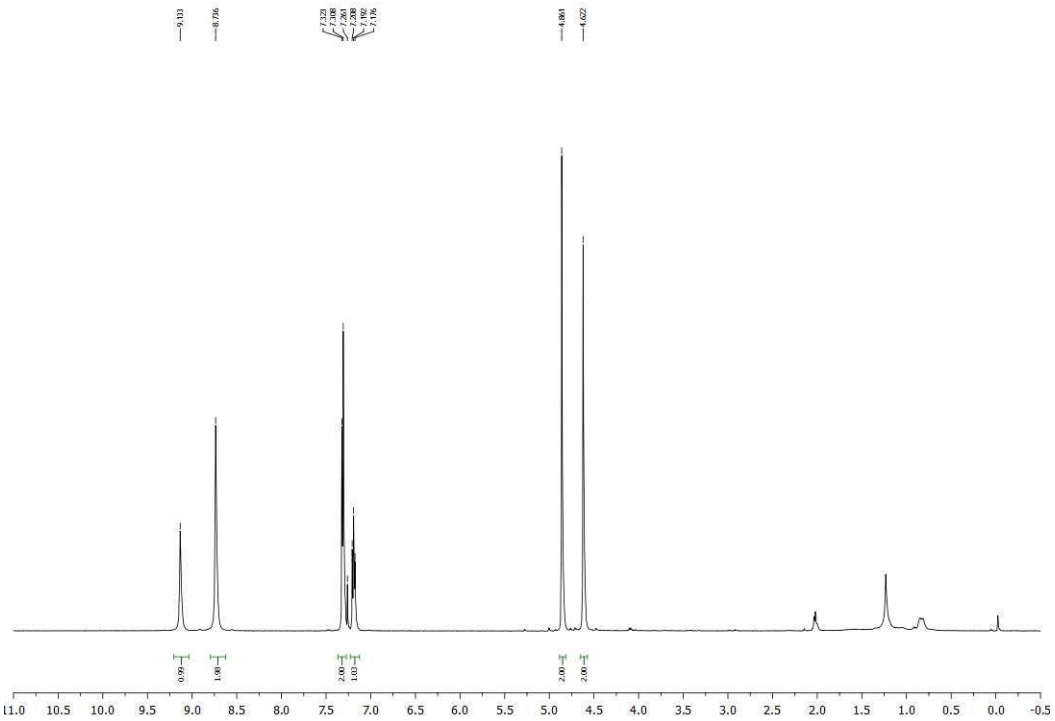

**Figure A2.63.** $^{1}$H NMR ($CDCl_3$, 500 MHz) spectrum of 5-(((2,6-dichlorobenzyl)oxy)methyl)pyrimidine (**31**)

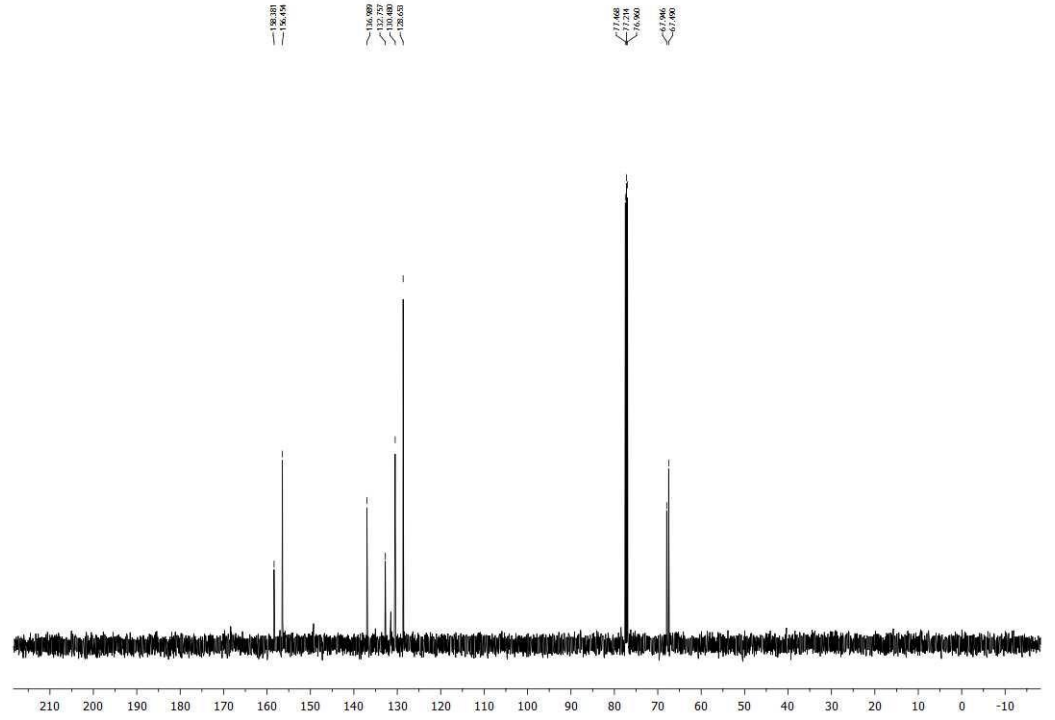

**Figure A2.64.** $^{13}$C NMR ($CDCl_3$, 125.8 MHz) spectrum of 5-(((2,6-dichlorobenzyl)oxy)methyl)pyrimidine (**31**)

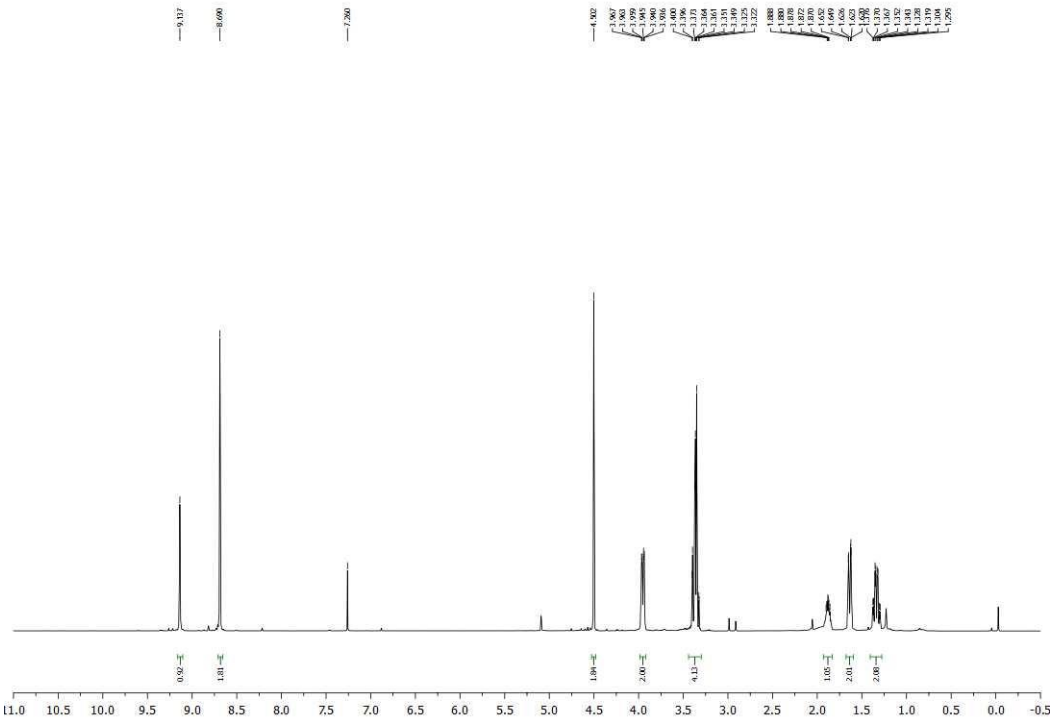

**Figure A2.65.** $^{1}$H NMR ($CDCl_3$, 500 MHz) spectrum of 5-((tetrahydro-2H-pyran-4-yl)methoxy)methyl)pyrimidine (**32**)

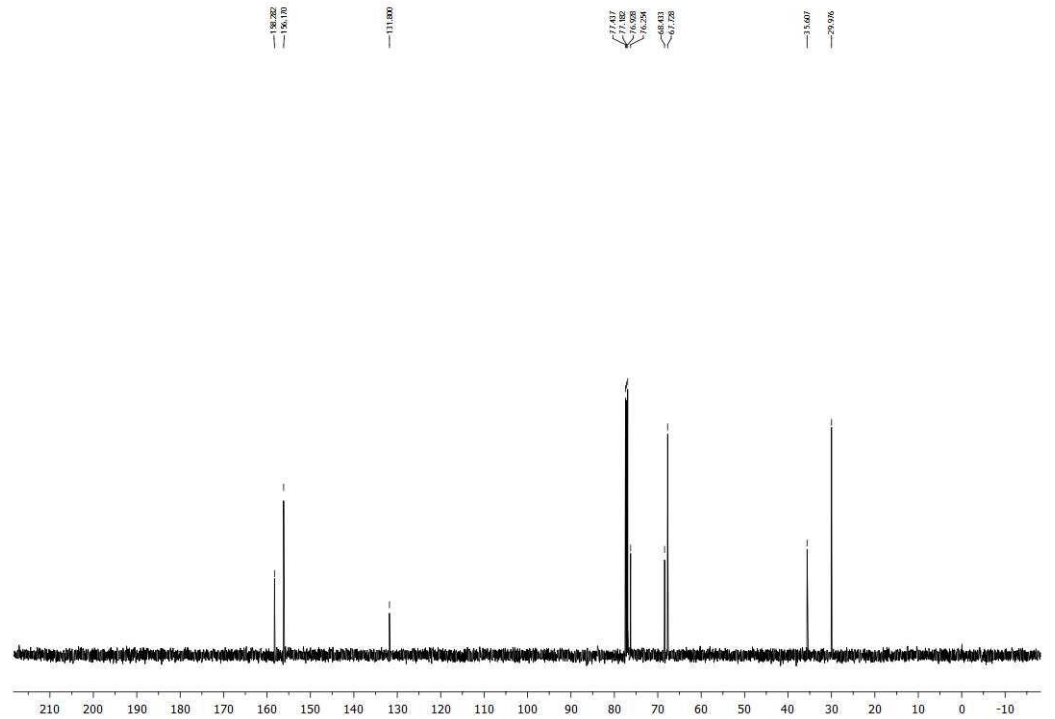

**Figure A2.66.** $^{13}$C NMR ($CDCl_3$, 125.8 MHz) spectrum of 5-((tetrahydro-2H-pyran-4-yl)methoxy)methyl)pyrimidine (**32**)

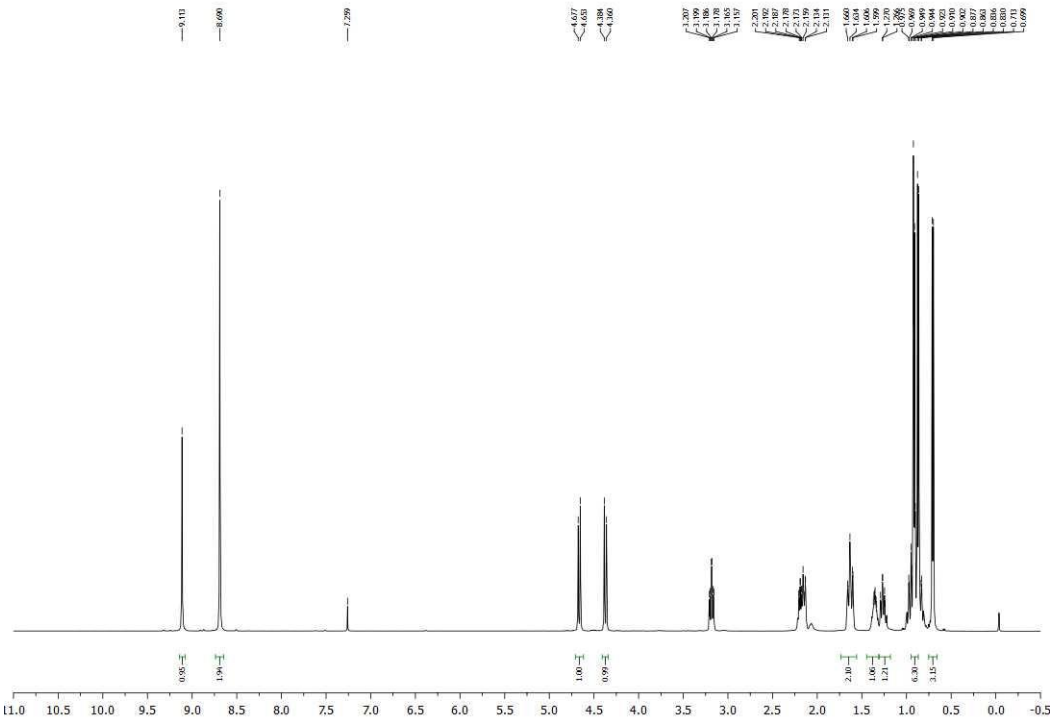

**Figure A2.67.** $^{1}$H NMR ($CDCl_3$, 500 MHz) spectrum of 5-(((1*S*)-2-isopropylcyclohexyl)oxy)methyl)pyrimidine (**33**)

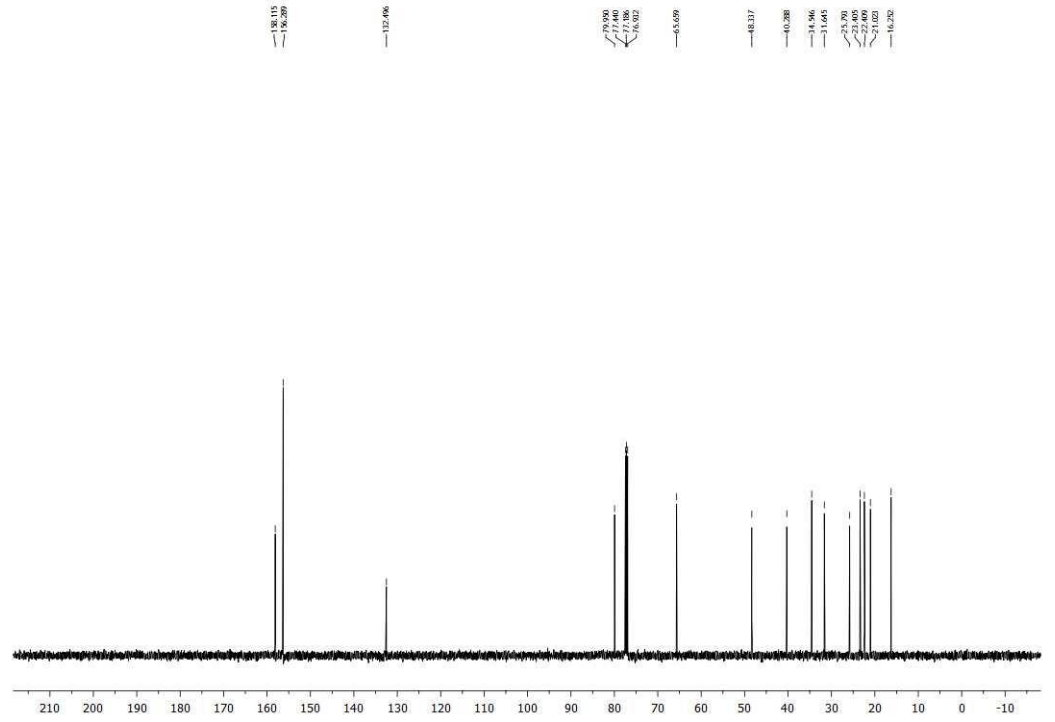

**Figure A2.68.** $^{13}$C NMR ($CDCl_3$, 125.8 MHz) spectrum of 5-(((1*S*)-2-isopropylcyclohexyl)oxy)methyl)pyrimidine (**33**)

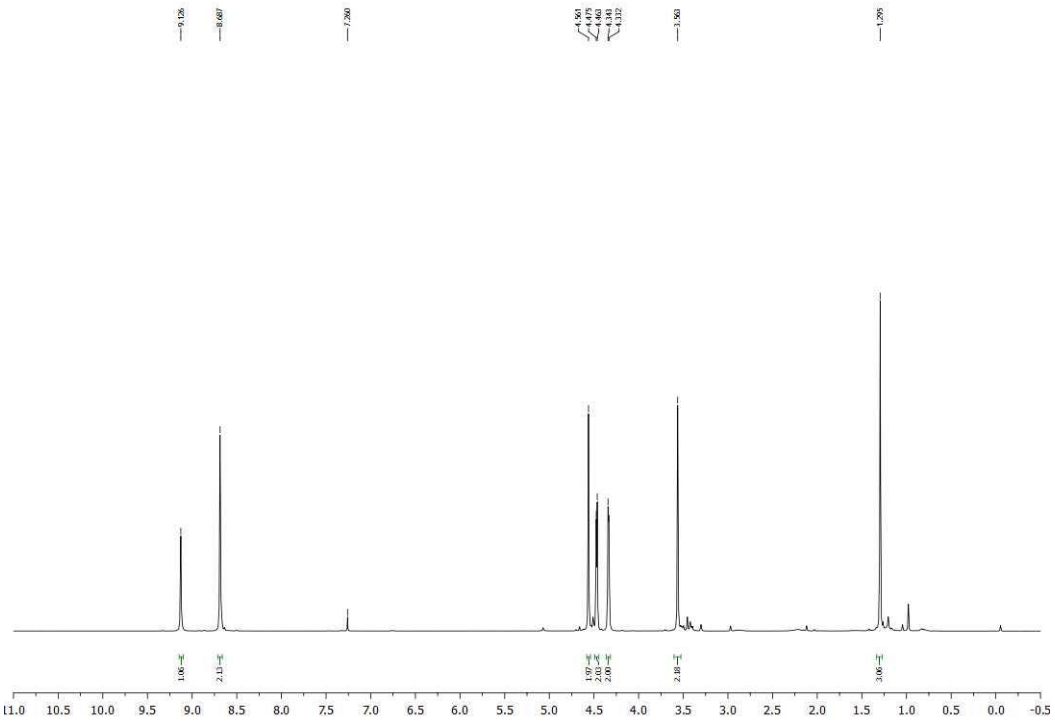

**Figure A2.69.** $^{1}$H NMR ($CDCl_3$, 500 MHz) spectrum of 5-(((2-methyloxetan-2-yl)methoxy)methyl) (**34**)

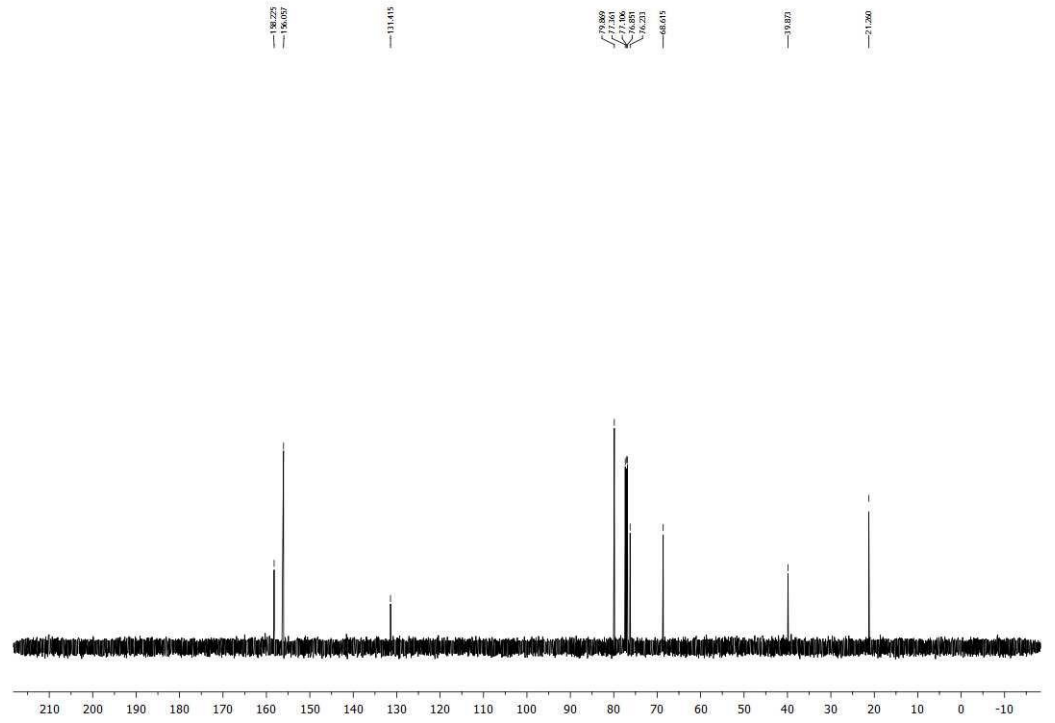

**Figure A2.70.** $^{13}$C NMR ($CDCl_3$, 125.8 MHz) spectrum of 5-(((2-methyloxetan-2-yl)methoxy)methyl) (**34**)

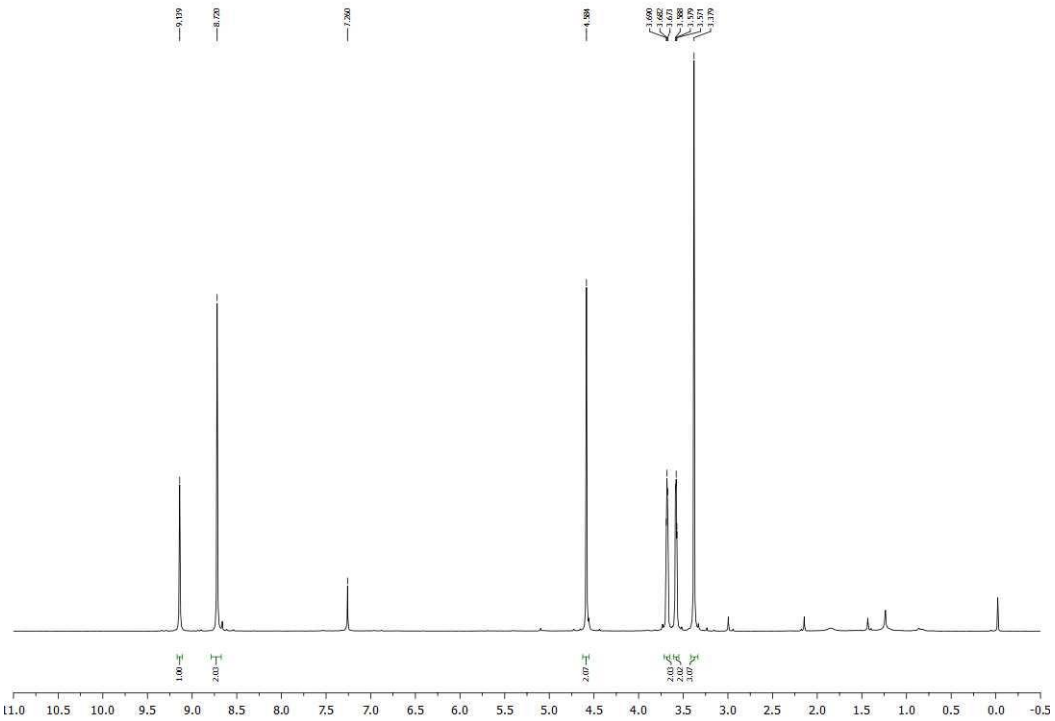

**Figure A2.71.** $^{1}$H NMR ($CDCl_3$, 500 MHz) spectrum of 5-((2-methoxyethoxy)methyl)pyrimidine (**35**)

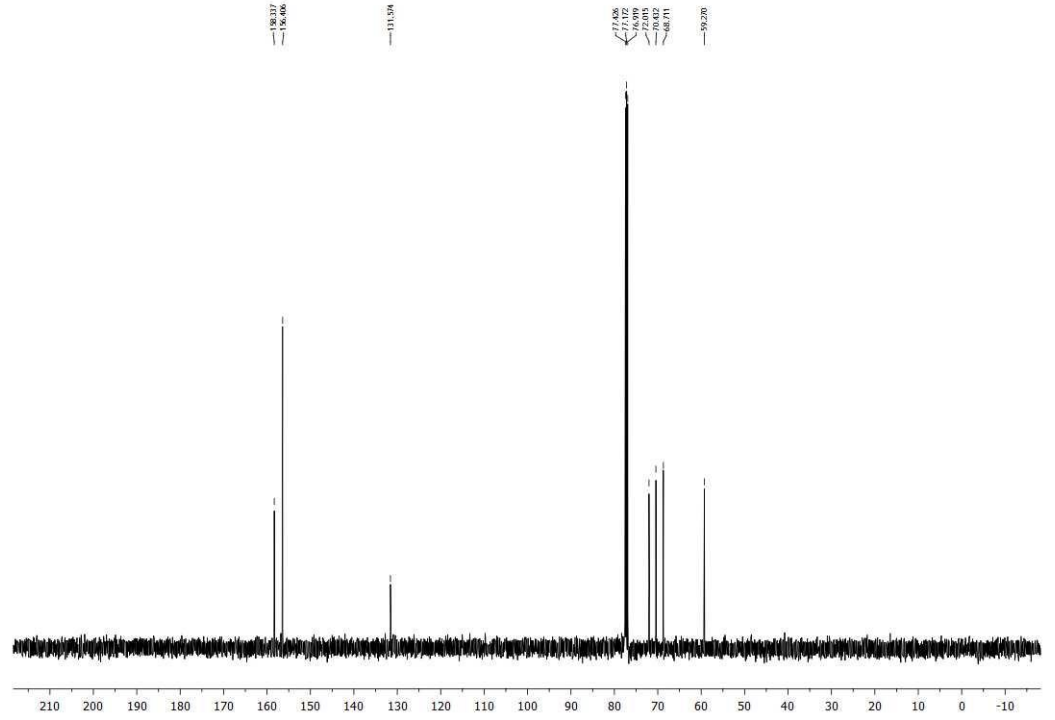

**Figure A2.72.** $^{13}$C NMR ($CDCl_3$, 125.8 MHz) spectrum of 5-((2-methoxyethoxy)methyl)pyrimidine (**35**)

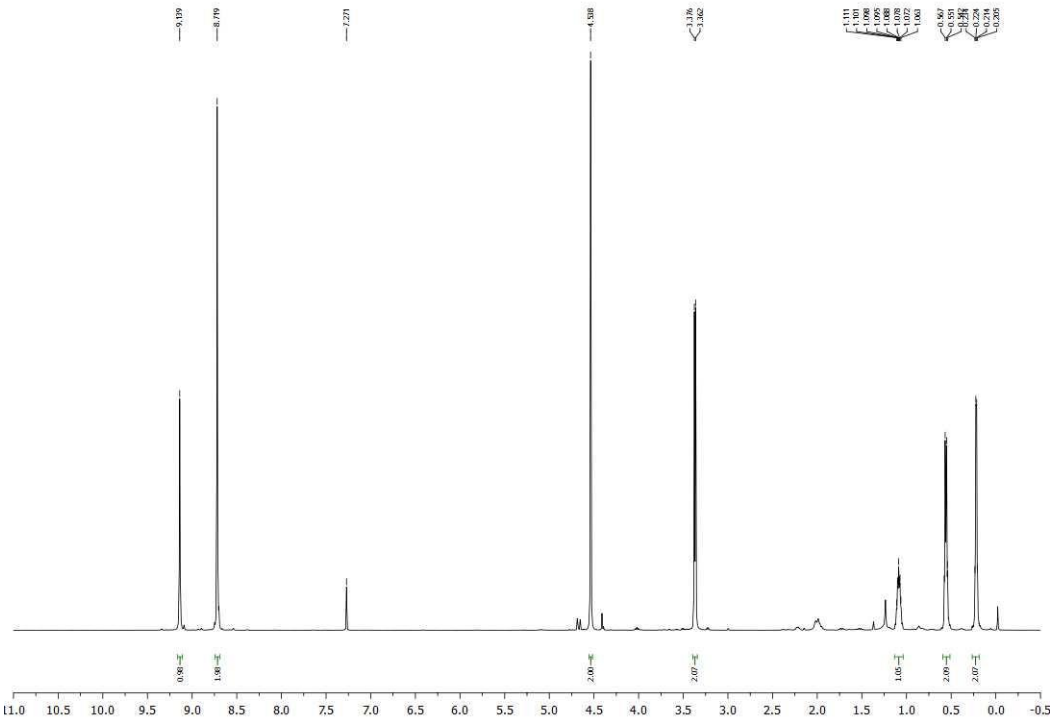

**Figure A2.73.** $^{1}$H NMR ($CDCl_3$, 500 MHz) spectrum of 5-((cyclopropylmethoxy)methyl)pyrimidine (**36**)

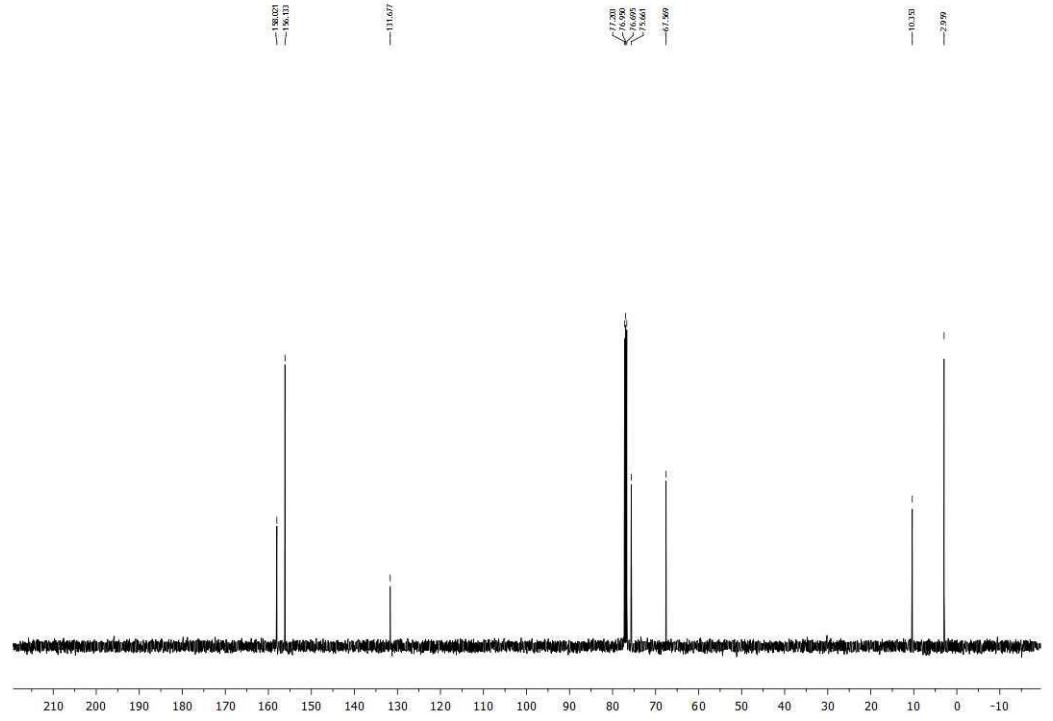

**Figure A2.74.** $^{13}$C NMR ($CDCl_3$, 125.8 MHz) spectrum of 5-((cyclopropylmethoxy)methyl)pyrimidine (**36**)

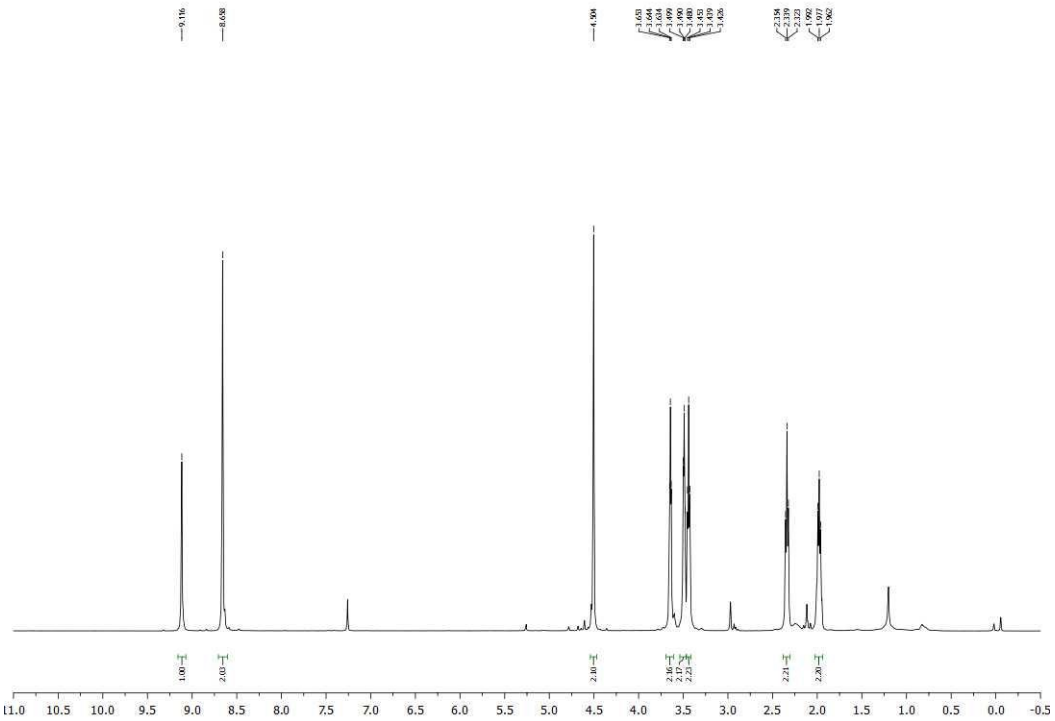

**Figure A2.75.** $^{1}$H NMR ($CDCl_3$, 500 MHz) spectrum of 1-(2-(pyrimidin-5-ylmethoxy)ethyl)pyrrolidin-2-one (**37**)

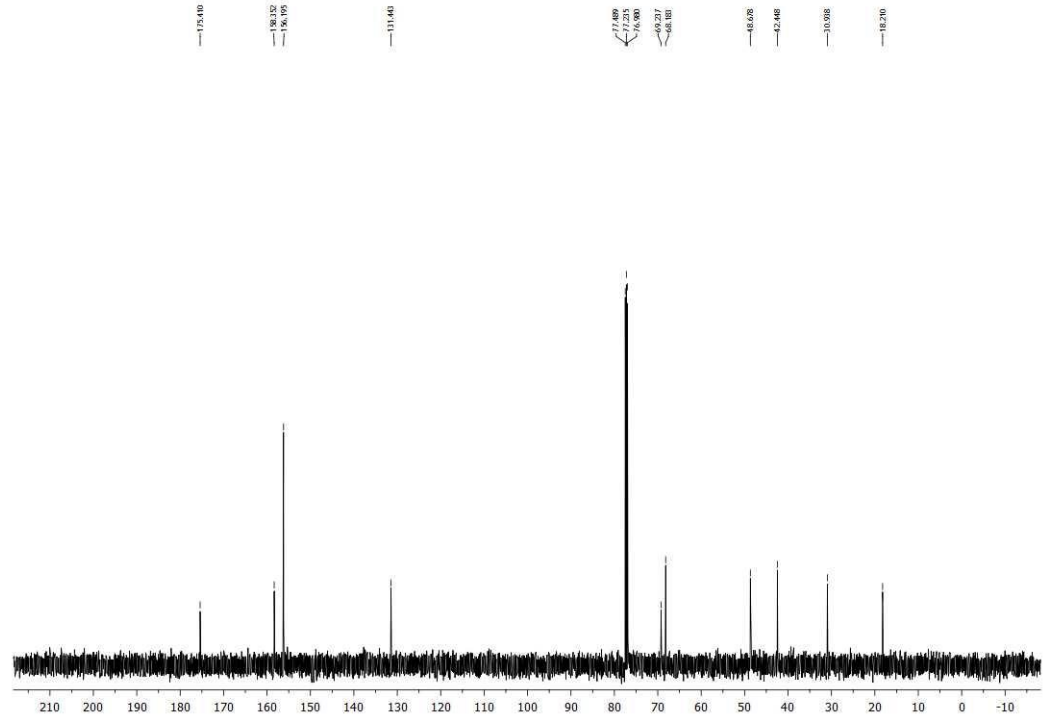

**Figure A2.76.** $^{13}$C NMR ($CDCl_3$, 125.8 MHz) spectrum of 1-(2-(pyrimidin-5-ylmethoxy)ethyl)pyrrolidin-2-one (**37**)

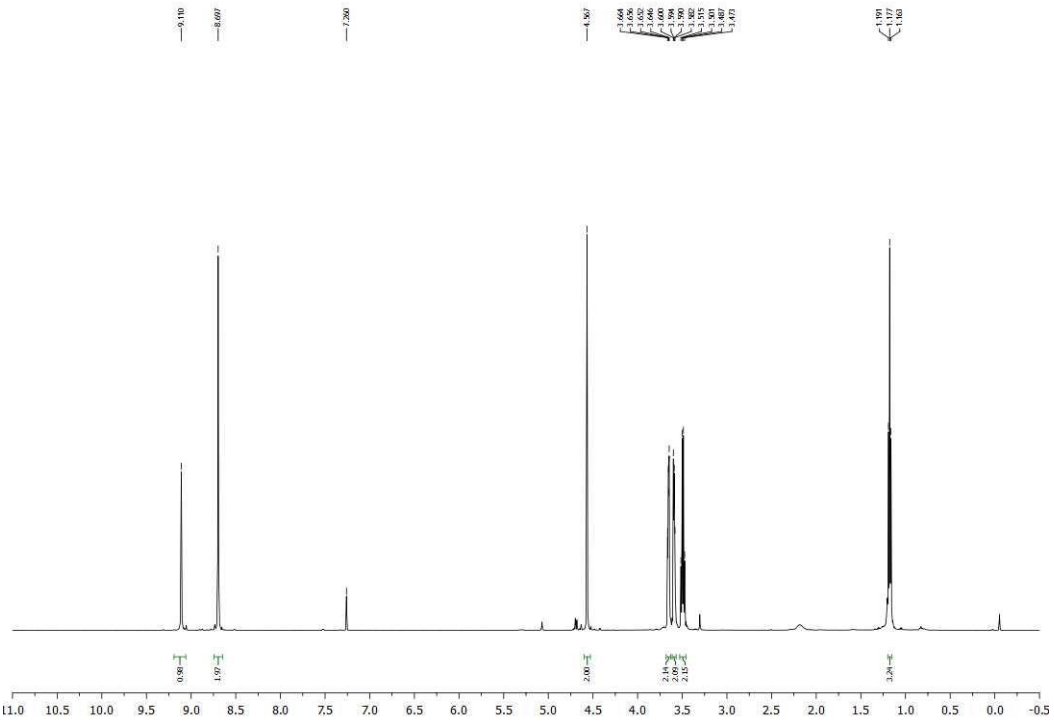

**Figure A2.77.** $^{1}$H NMR ($CDCl_3$, 500 MHz) spectrum of 5-((2-ethoxyethoxy)methyl)pyrimidine (**38**)

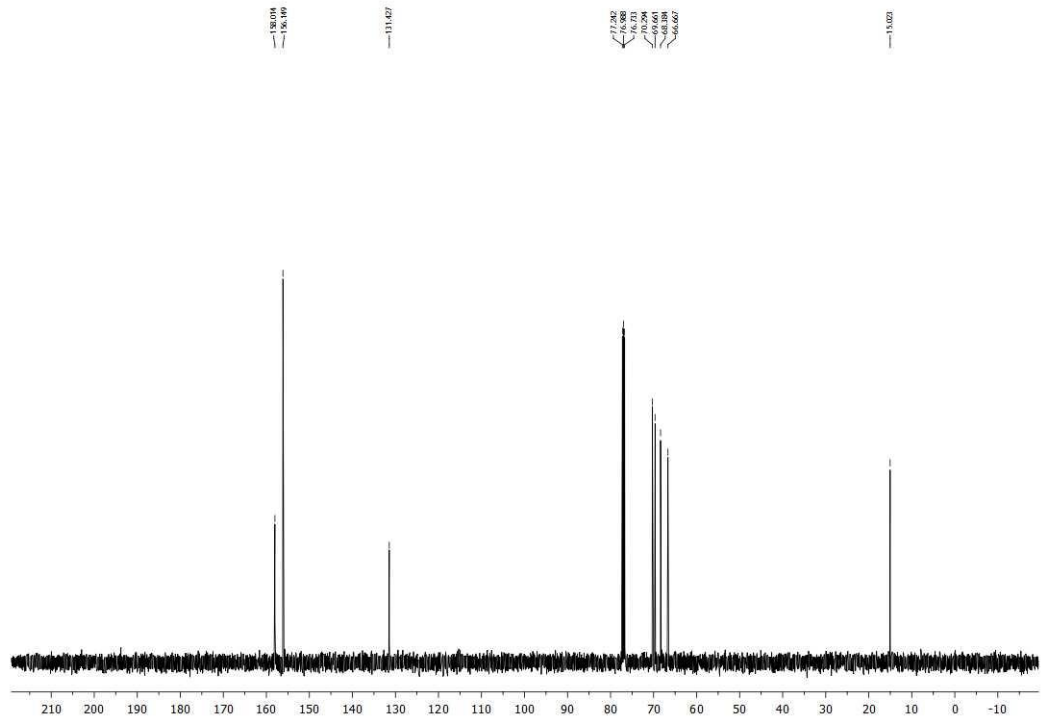

**Figure A2.78.** $^{13}$C NMR ($CDCl_3$, 125.8 MHz) spectrum of 5-((2-ethoxyethoxy)methyl)pyrimidine (**38**)

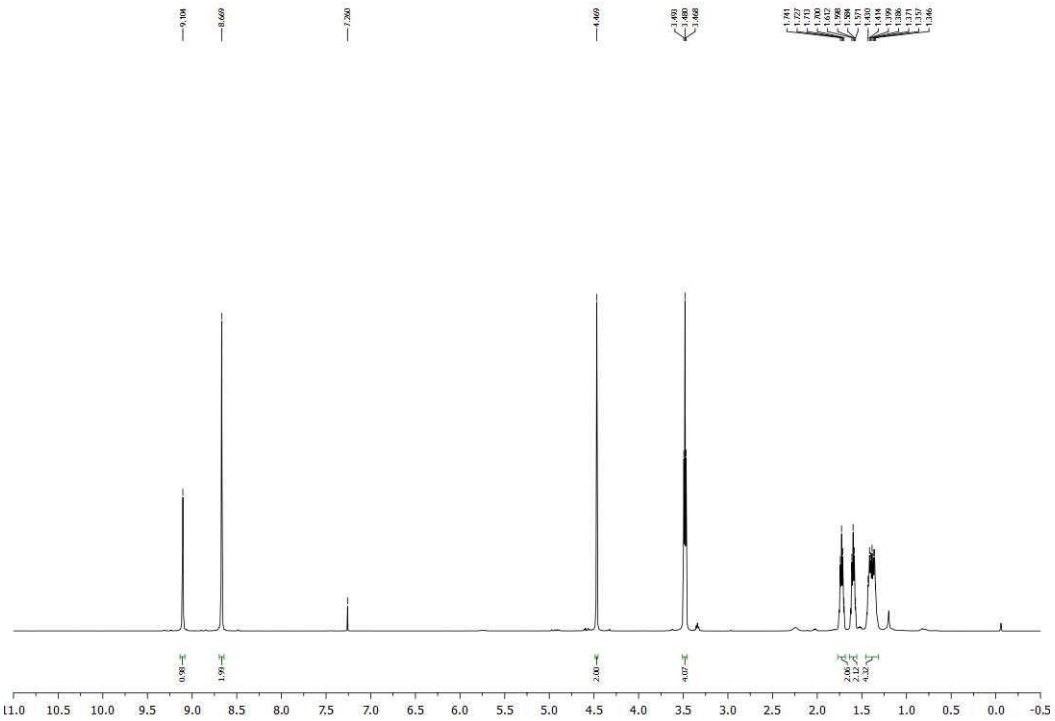

**Figure A2.79.** $^{1}$H NMR ($CDCl_3$, 500 MHz) spectrum of 5-((5-chloropentyl)oxy)methyl)pyrimidine (**39**)

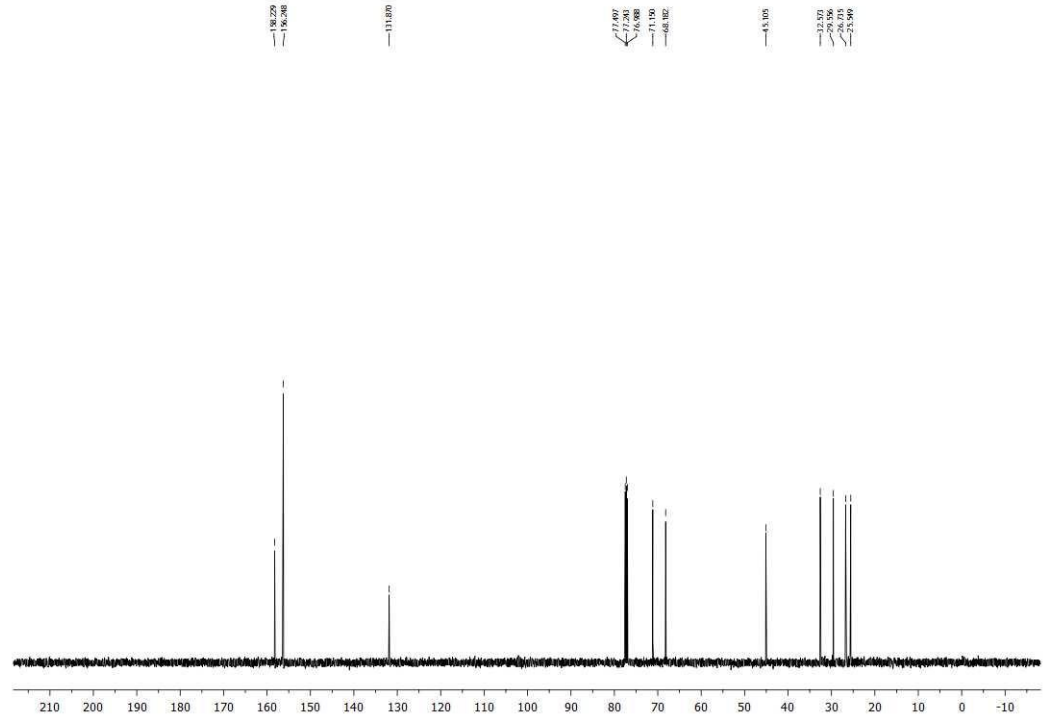

**Figure A2.80.** $^{13}$C NMR ($CDCl_3$, 125.8 MHz) spectrum of 5-((5-chloropentyl)oxy)methyl)pyrimidine (**39**)

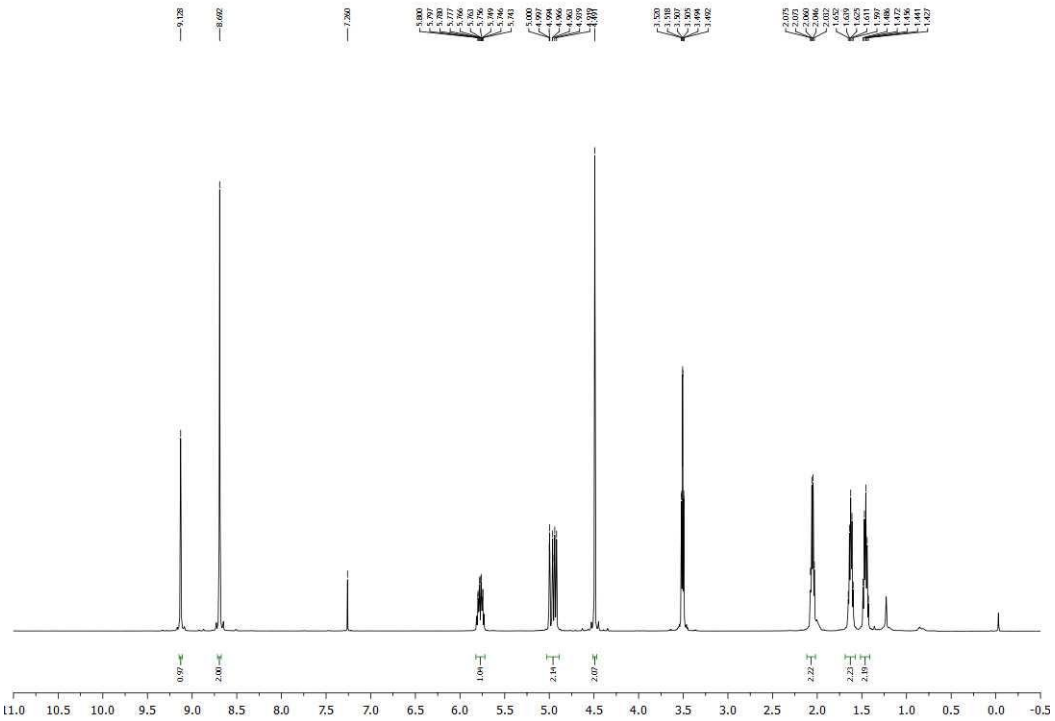

**Figure A2.81.** $^{1}$H NMR ($CDCl_3$, 500 MHz) spectrum of 5-((hex-5-en-1-yloxy)methyl)pyrimidine (**40**)

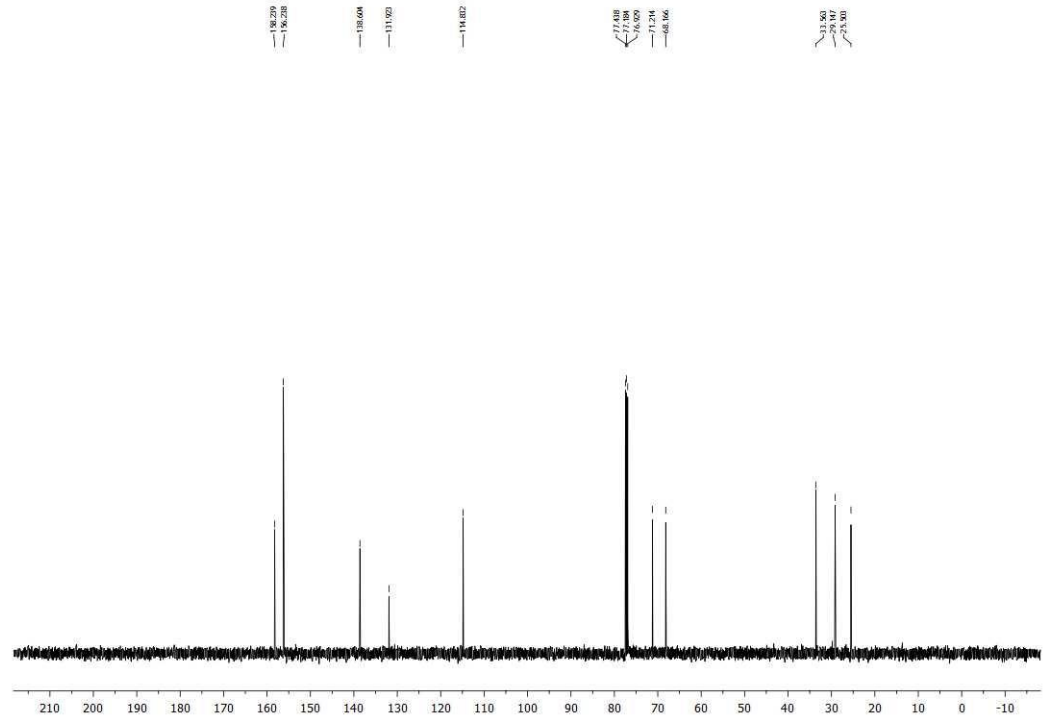

**Figure A2.82.** $^{13}$C NMR ($CDCl_3$, 125.8 MHz) spectrum of 5-((hex-5-en-1-yloxy)methyl)pyrimidine (**40**)

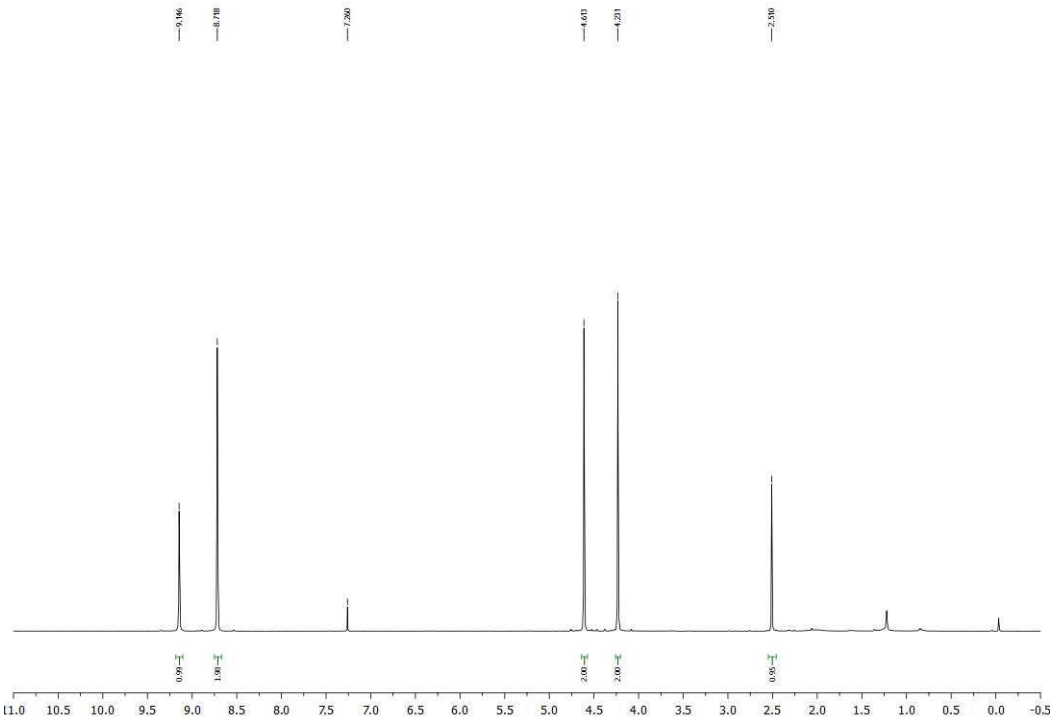

**Figure A2.83.** $^{1}$H NMR ($CDCl_3$, 500 MHz) spectrum of 5-((prop-2-yn-1-yloxy)methyl)pyrimidine (**41**)

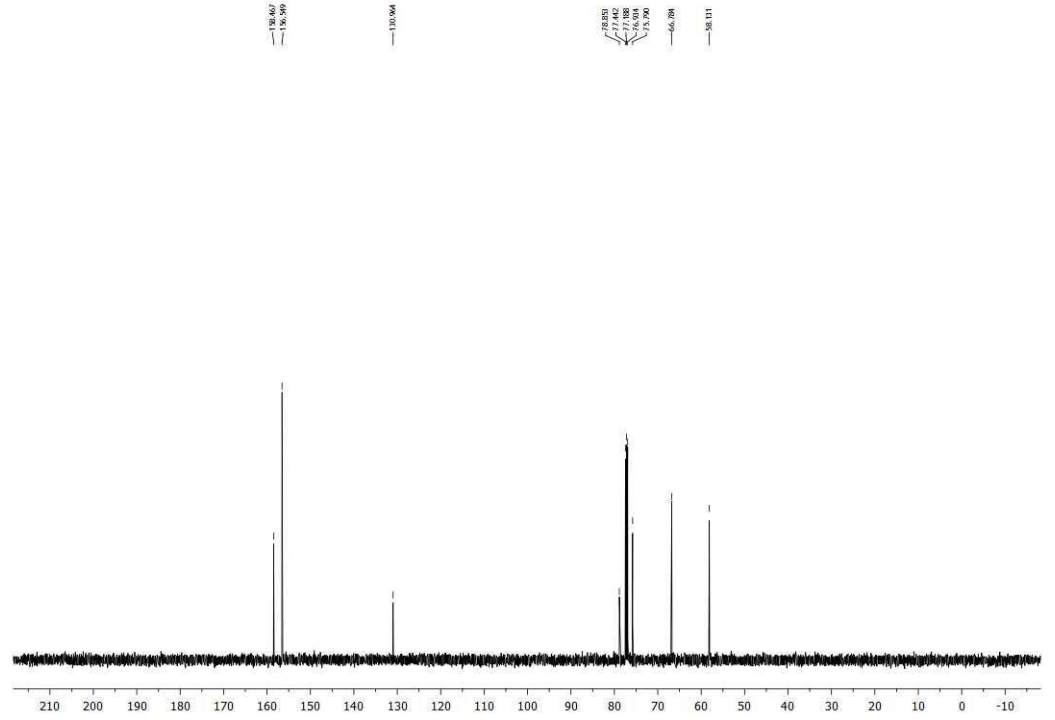

**Figure A2.84.** $^{13}$C NMR ($CDCl_3$, 125.8 MHz) spectrum of 5-((prop-2-yn-1-yloxy)methyl)pyrimidine (**41**)

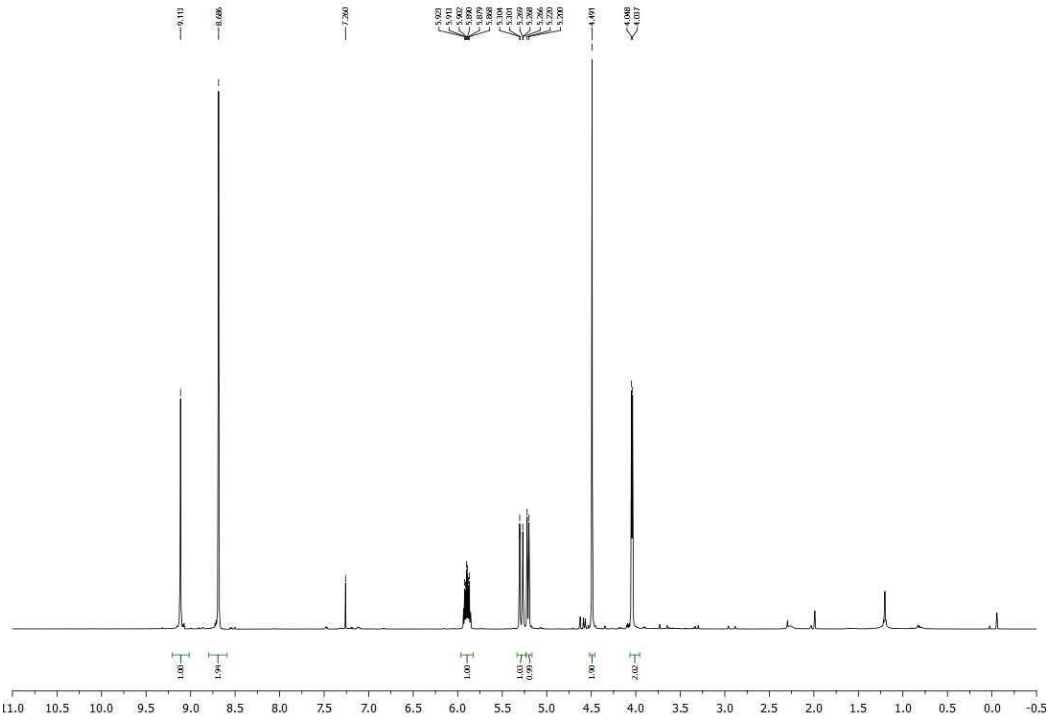

**Figure A2.85.** $^{1}$H NMR ($CDCl_3$, 500 MHz) spectrum of 5-((allyloxy)methyl)pyrimidine (**42**)

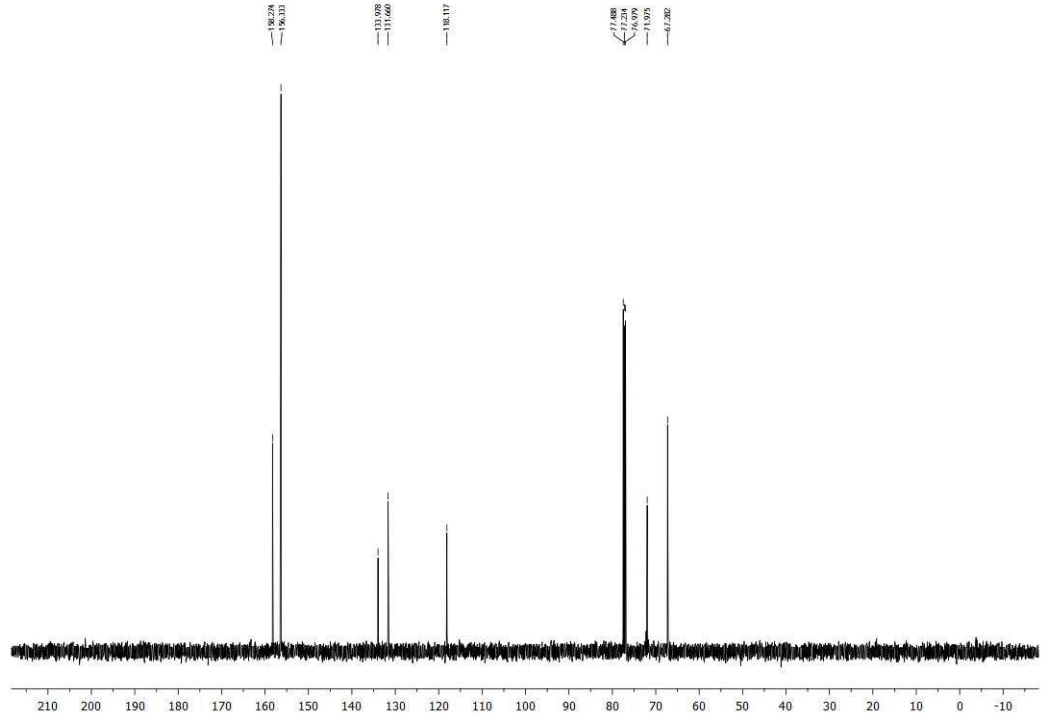

**Figure A2.86.** $^{13}$C NMR ($CDCl_3$, 125.8 MHz) spectrum of 5-((allyloxy)methyl)pyrimidine (**42**)

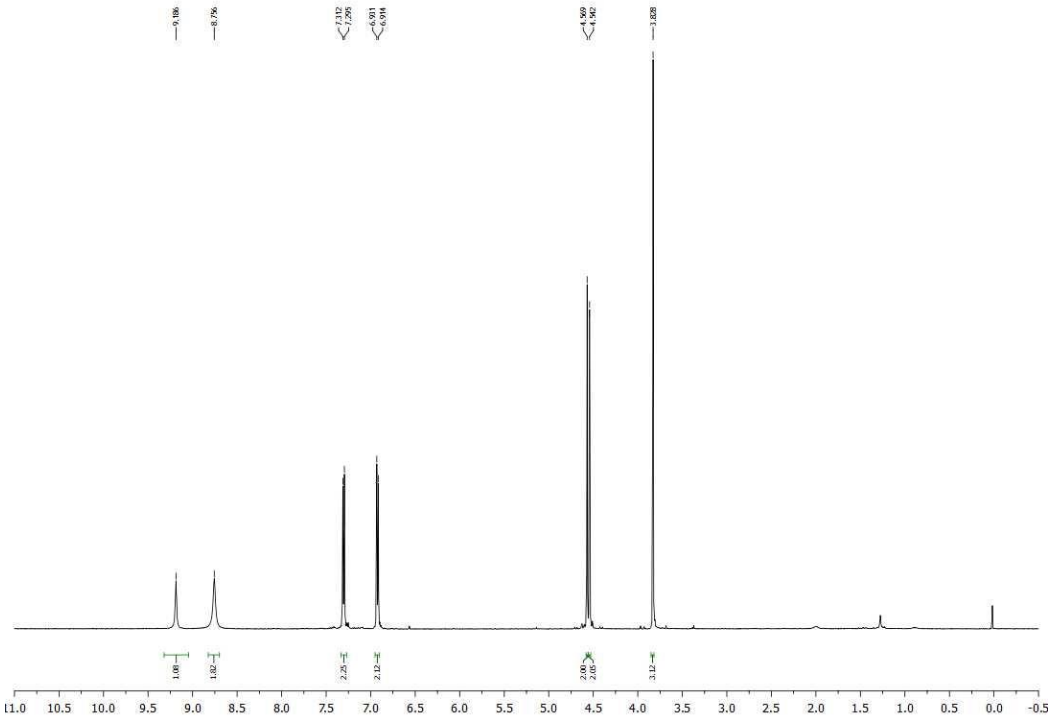

**Figure A2.87.** $^{1}$H NMR ($CDCl_3$, 500 MHz) spectrum of 5-(((4-methoxybenzyl)oxy)methyl)pyrimidine (**43**)

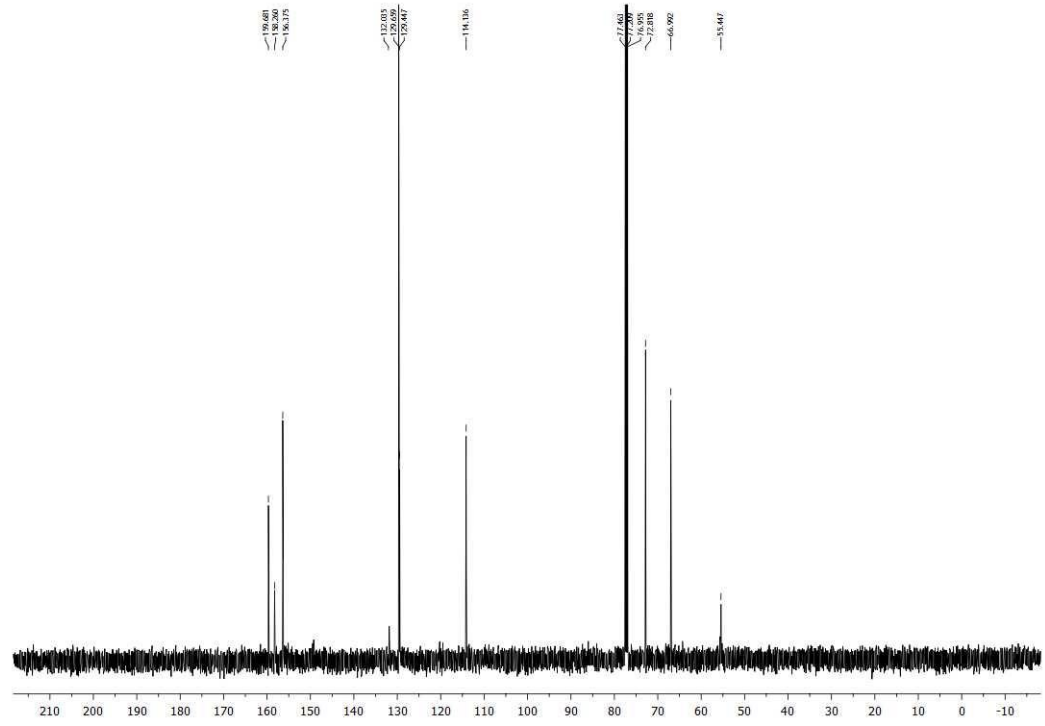

**Figure A2.88.** $^{13}$C NMR ($CDCl_3$, 125.8 MHz) spectrum of 5-(((4-methoxybenzyl)oxy)methyl)pyrimidine (**43**)

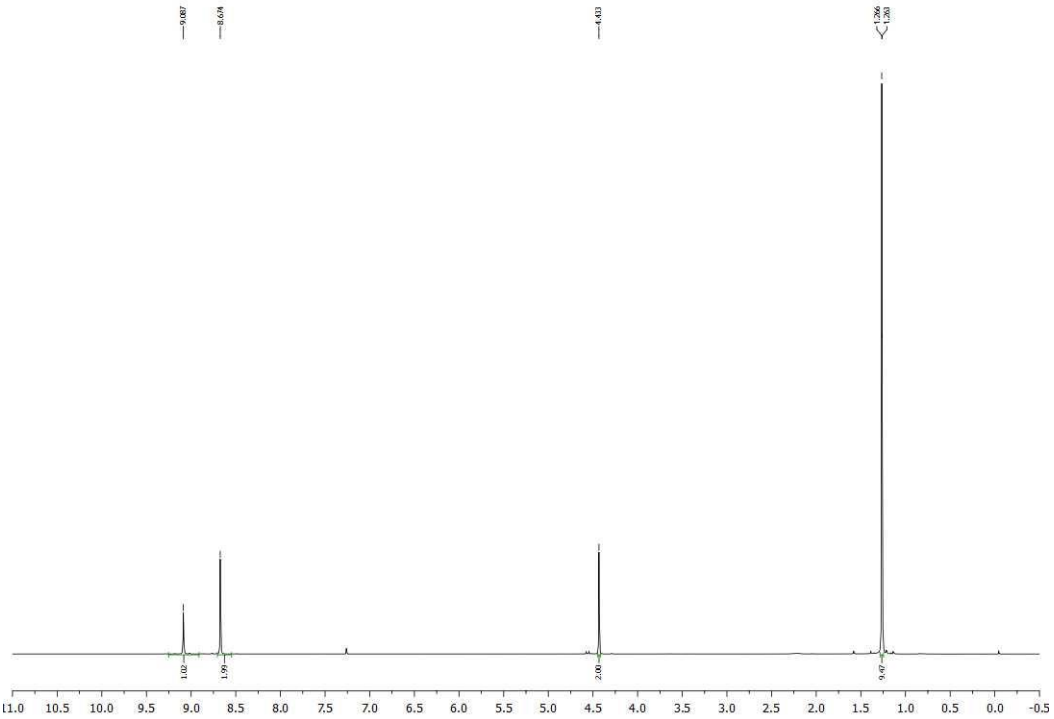

**Figure A2.89.** $^{1}$H NMR ($CDCl_3$, 500 MHz) spectrum of 5-(*tert*-butoxymethyl)pyrimidine (**44**)

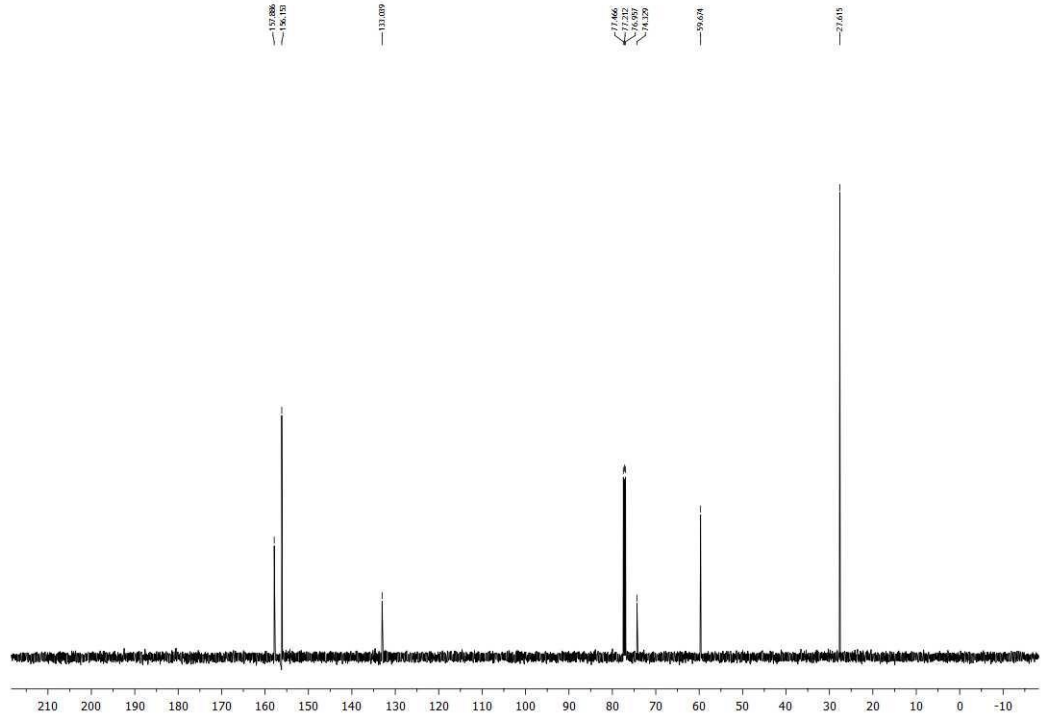

**Figure A2.90.** $^{13}$C NMR ($CDCl_3$, 125.8 MHz) spectrum of 5-(*tert*-butoxymethyl)pyrimidine (**44**)

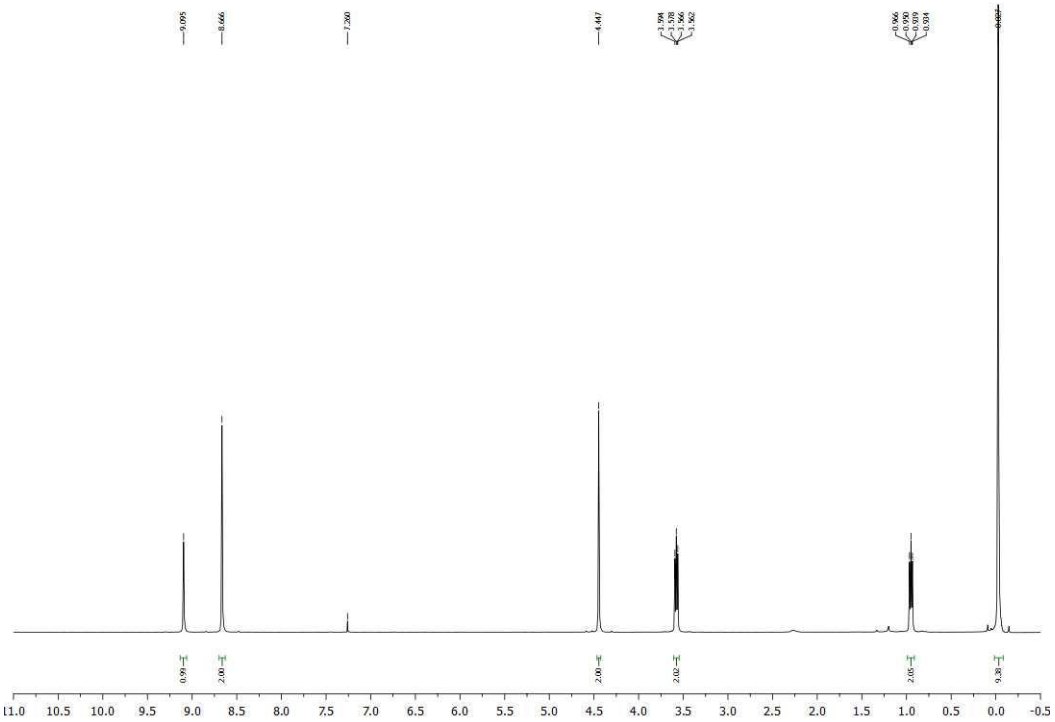

**Figure A2.91.** $^{1}$H NMR ($CDCl_3$, 500 MHz) spectrum of 5-((tetrahydro-2H-pyran-4-yl)methoxy)methyl)pyrimidine (**45**)

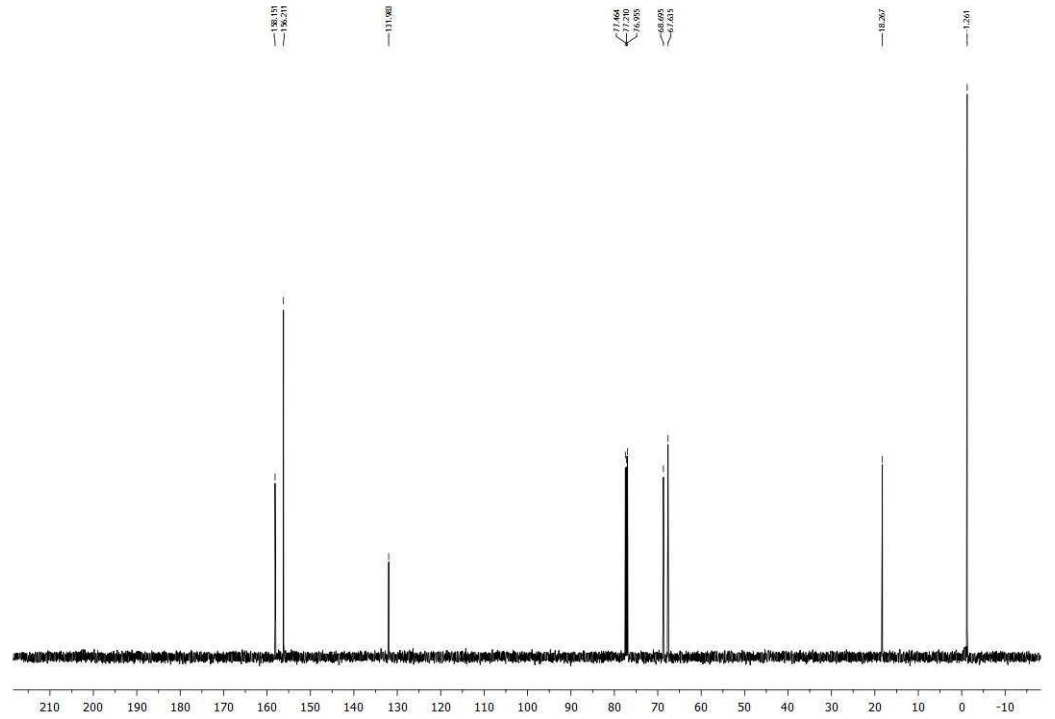

**Figure A2.92.** $^{13}$C NMR ($CDCl_3$, 125.8 MHz) spectrum of 5-((tetrahydro-2H-pyran-4-yl)methoxy)methyl)pyrimidine (**45**)

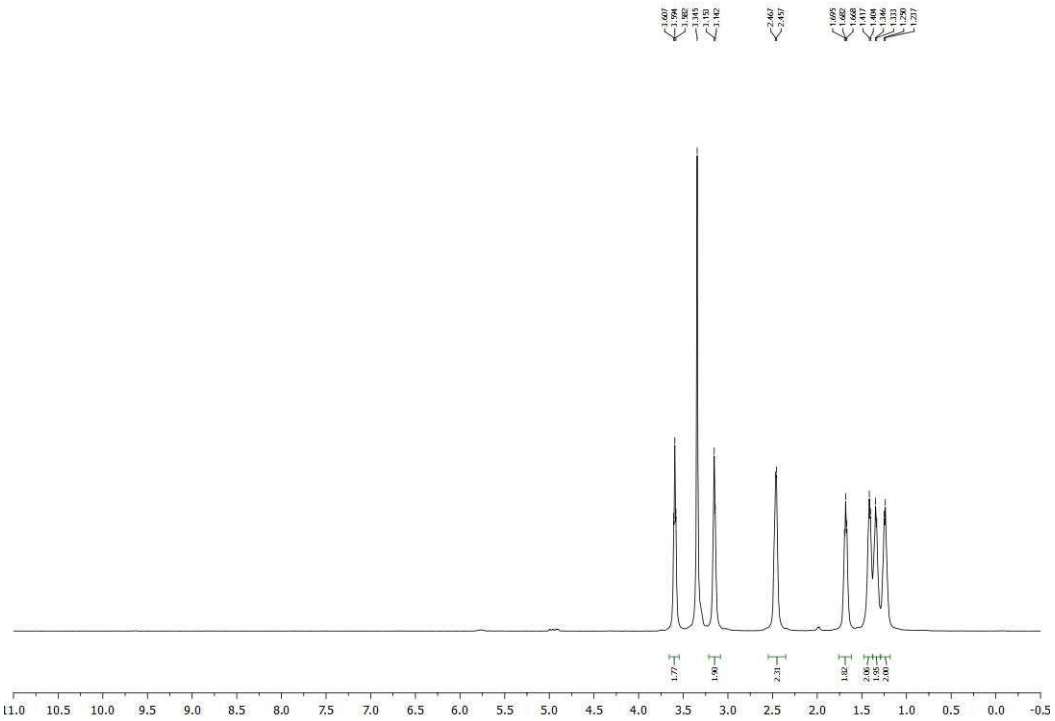

**Figure A2.93.** $^{1}H$ NMR ($CDCl_3$, 500 MHz) spectrum of Potassium (((6-chlorohexyl)oxy)methyl)trifluoroborate (**S1**)

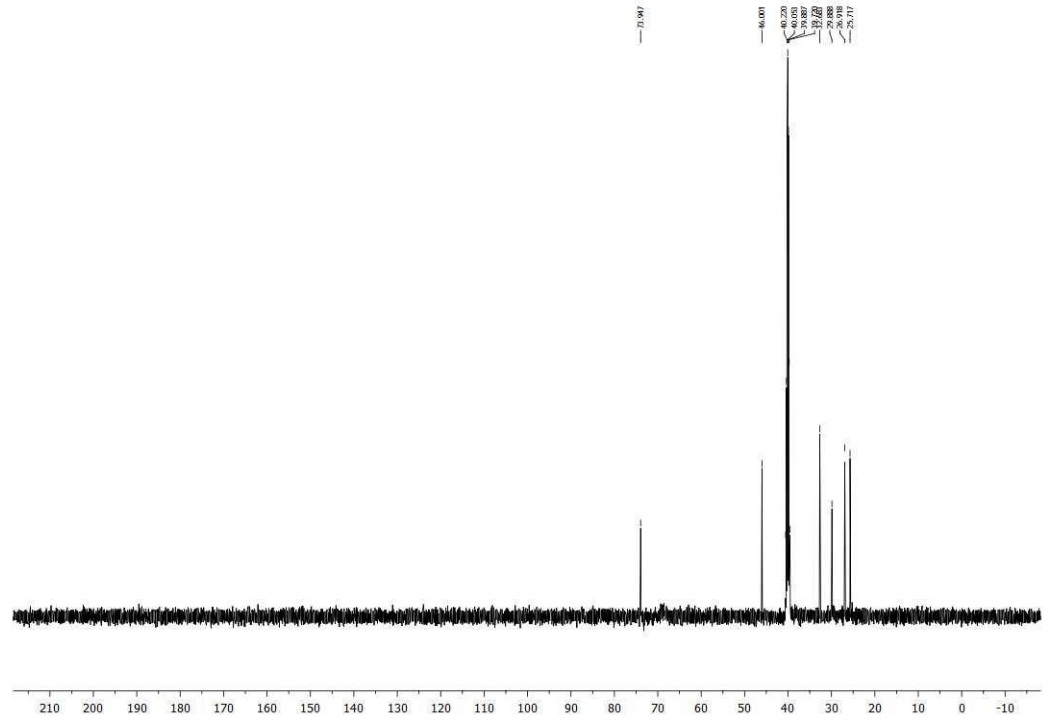

**Figure A2.94.** $^{13}C$ NMR ($CDCl_3$, 125.8 MHz) spectrum of Potassium (((6-chlorohexyl)oxy)methyl)trifluoroborate (**S1**)

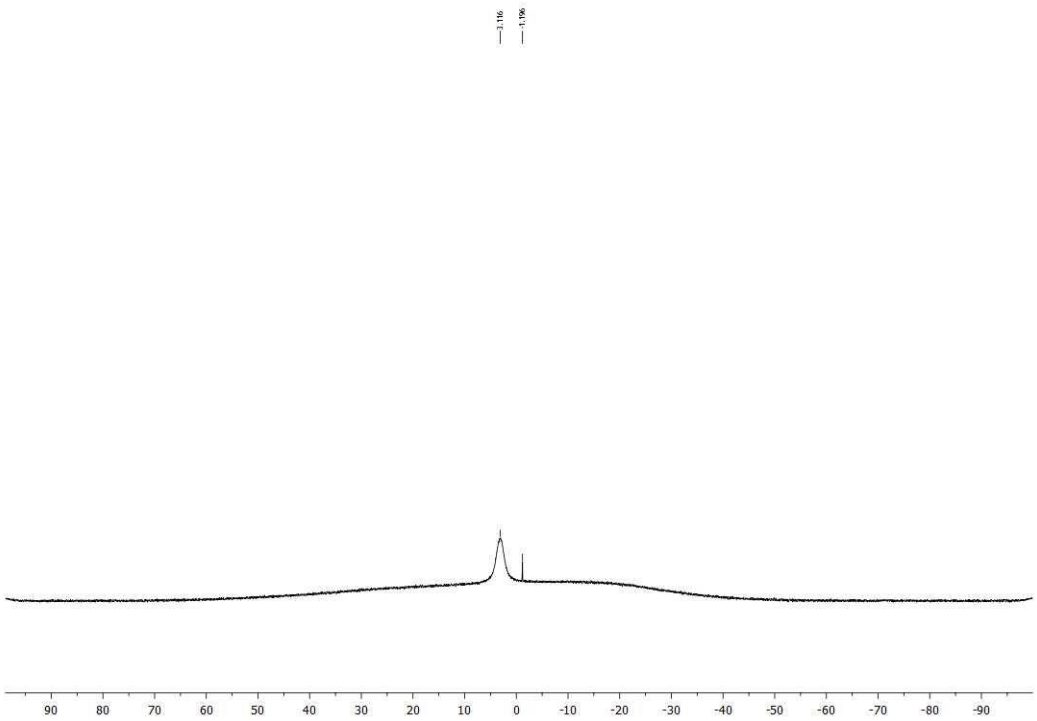


**Figure A2.95.** $^{11}B$ NMR ($CDCl_3$, 128.4 MHz) spectrum of Potassium (((6-chlorohexyl)oxy)methyl)trifluoroborate (**S1**)

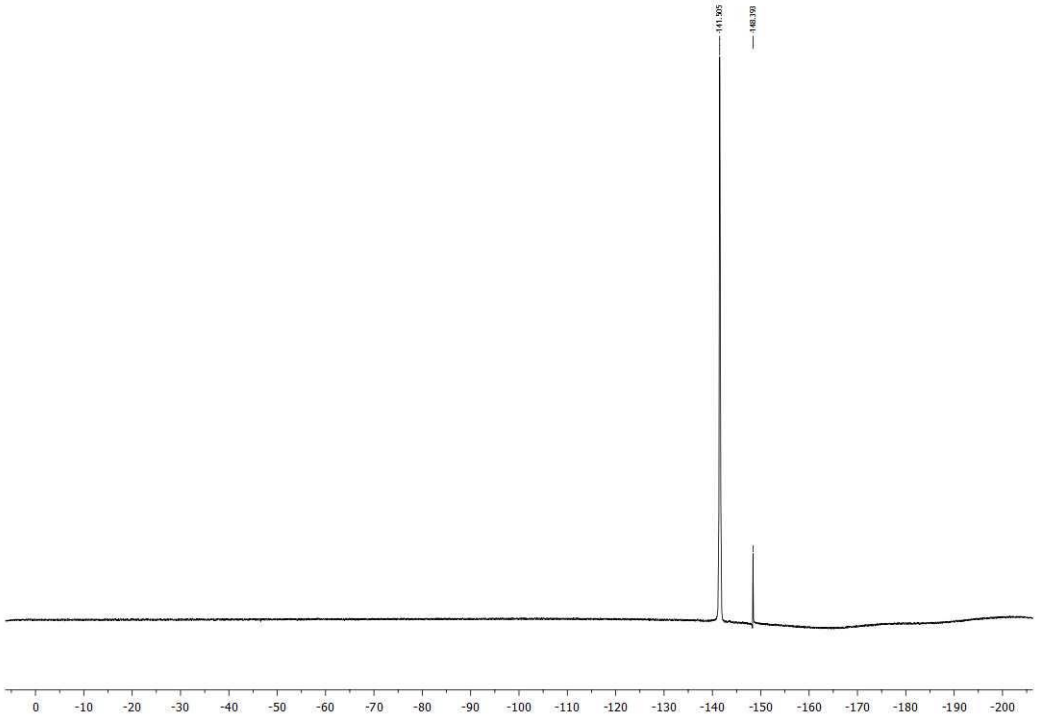


**Figure A2.96.** $^{19}F$ NMR ($CDCl_3$, 470.8 MHz) spectrum of Potassium (((6-chlorohexyl)oxy)methyl)trifluoroborate (**S1**)

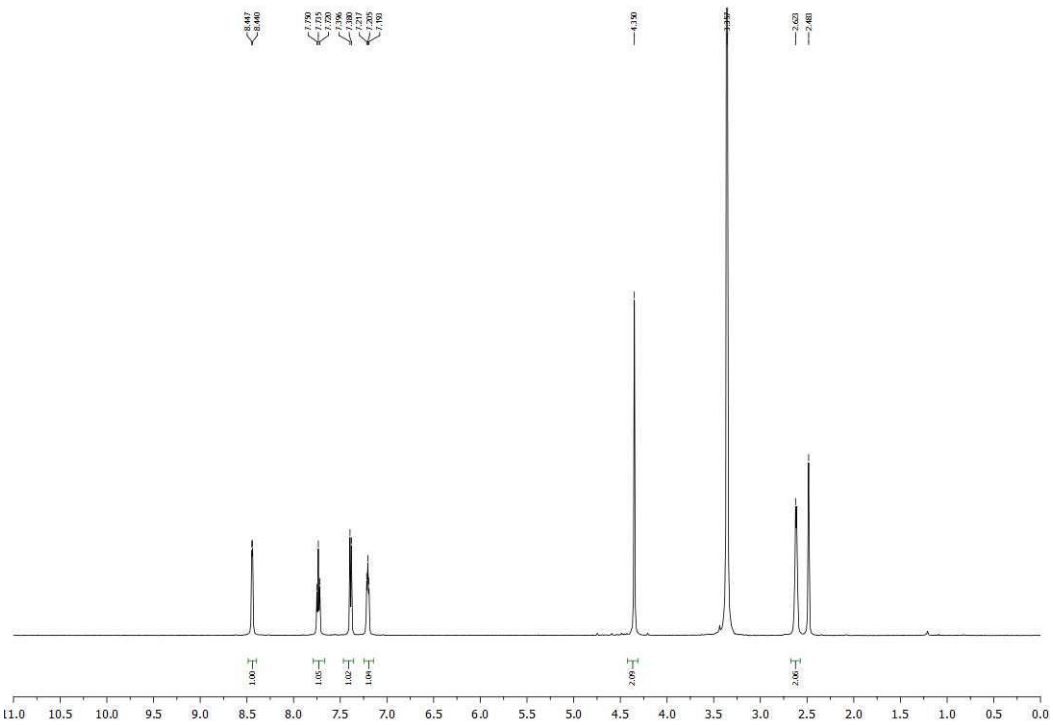

**Figure A2.97.** $^{1}$H NMR ($CDCl_3$, 500 MHz) spectrum of Potassium ((pyridin-2-ylmethoxy)methyl)trifluoroborate (**S2**)

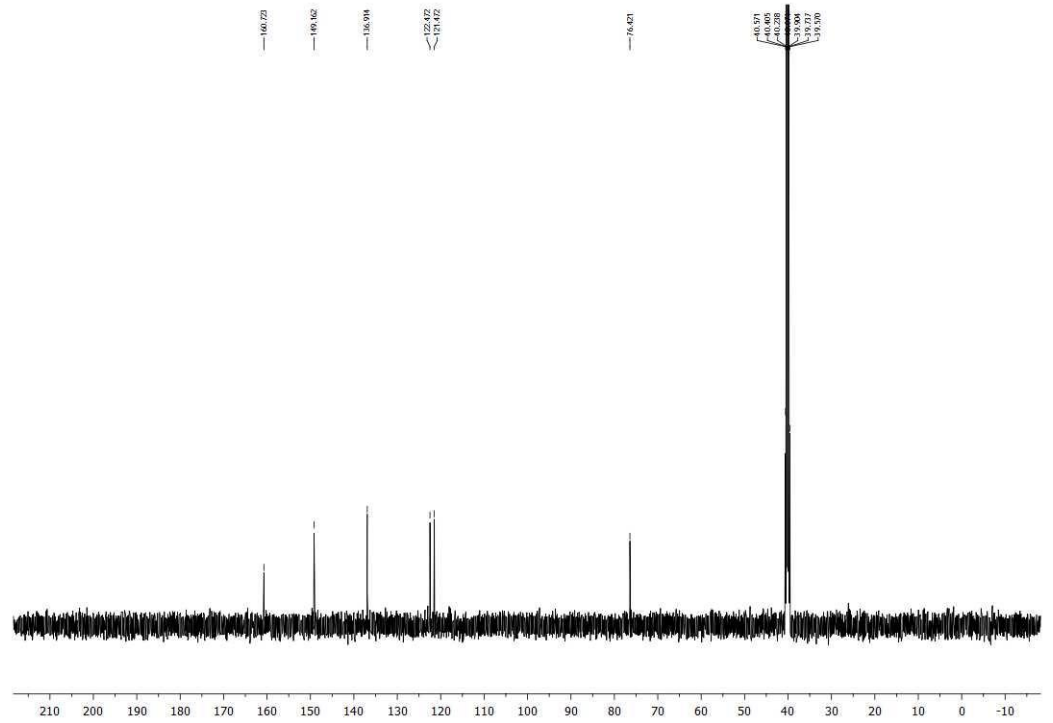

**Figure A2.98.** $^{13}$C NMR ($CDCl_3$, 125.8 MHz) spectrum of Potassium ((pyridin-2-ylmethoxy)methyl)trifluoroborate (**S2**)

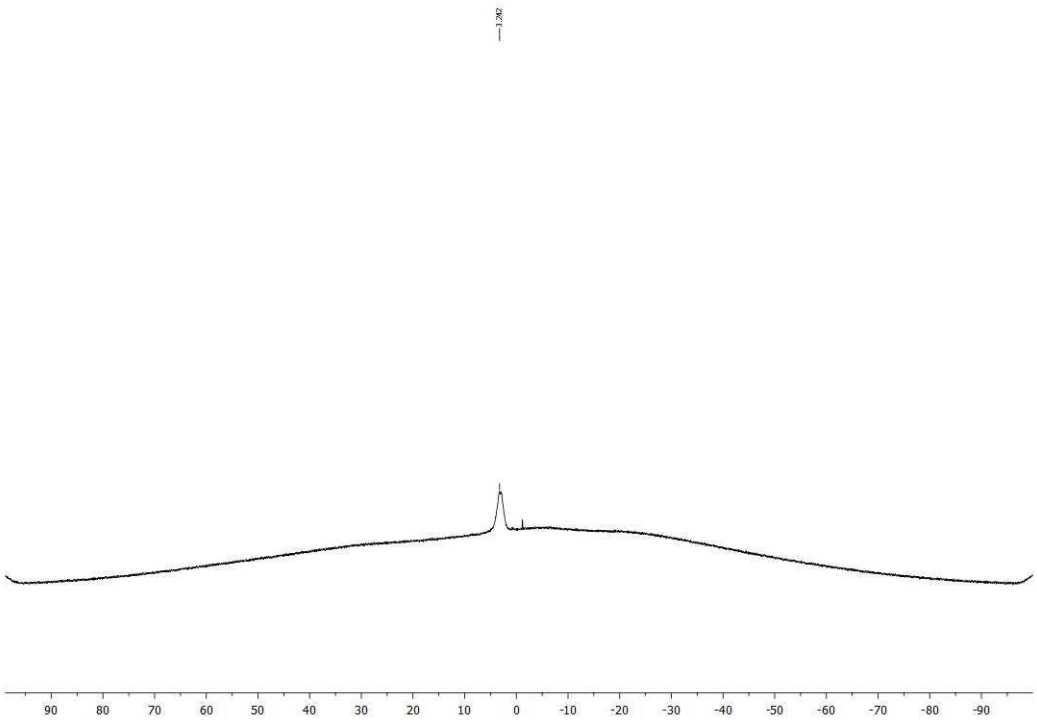


**Figure A2.99.** $^{11}B$ NMR ($CDCl_3$, 128.4 MHz) spectrum of Potassium ((pyridin-2-ylmethoxy)methyl)trifluoroborate (**S2**)

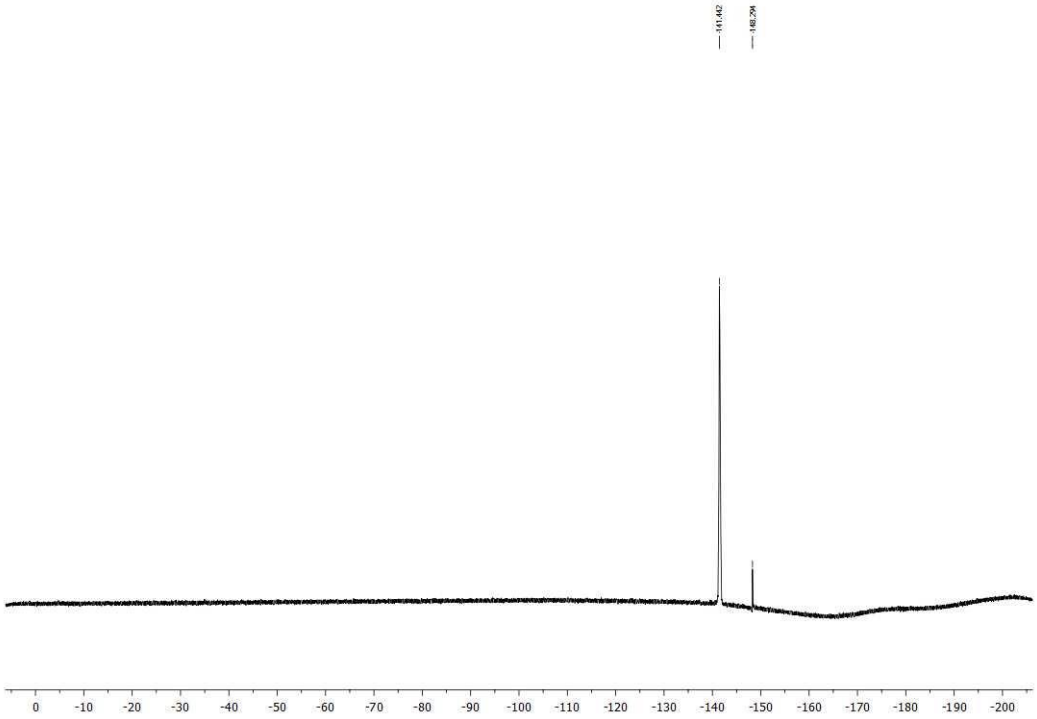


**Figure A2.100.** $^{19}F$ NMR ($CDCl_3$, 470.8 MHz) spectrum of Potassium ((pyridin-2-ylmethoxy)methyl)trifluoroborate (**S2**)

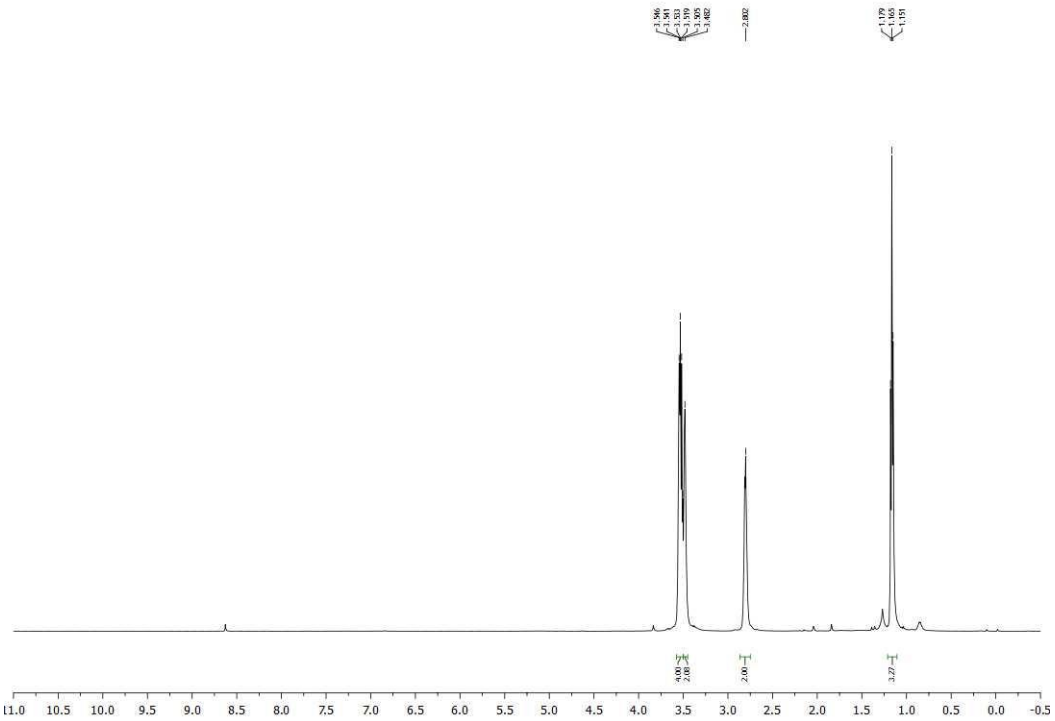

**Figure A2.101.** $^{1}$H NMR ($CDCl_3$, 500 MHz) spectrum of Potassium ((2-ethoxyethoxy)methyl)trifluoroborate (**S3**)

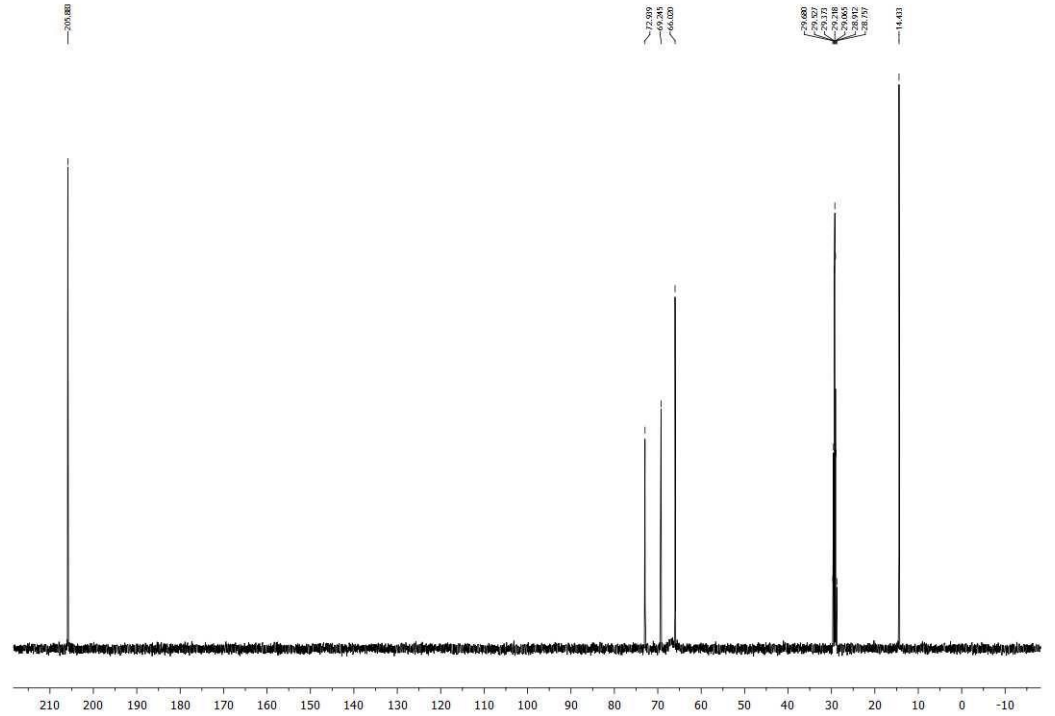

**Figure A2.102.** $^{13}$C NMR ($CDCl_3$, 125.8 MHz) spectrum of Potassium ((2-ethoxyethoxy)methyl)trifluoroborate (**S3**)

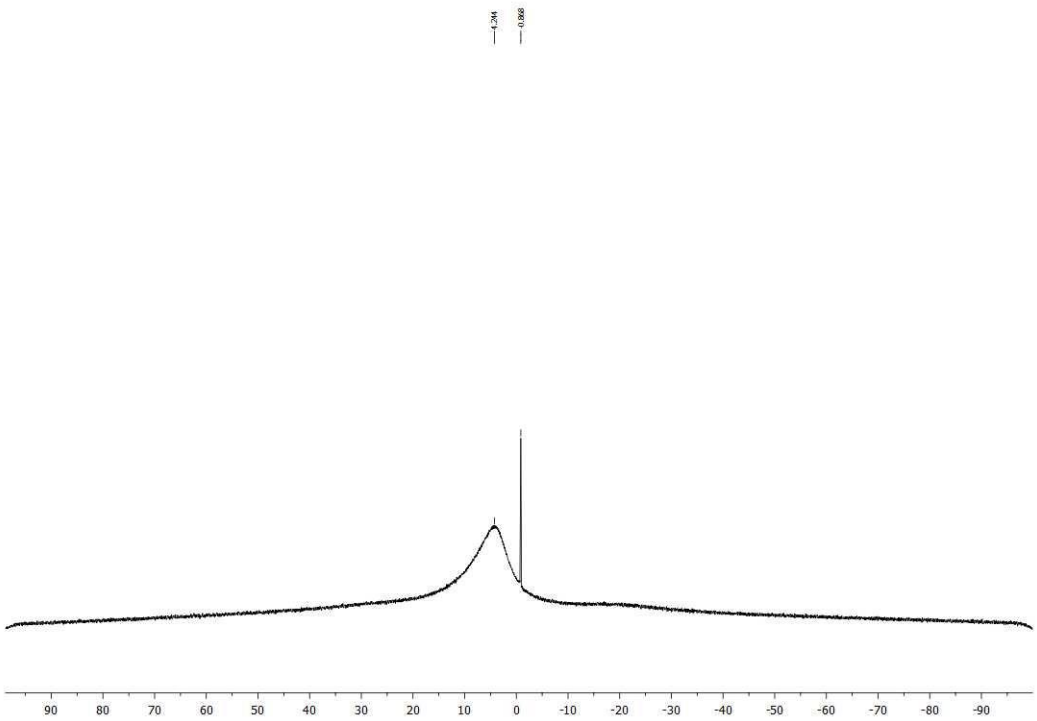


**Figure A2.103.** $^{11}B$ NMR ($CDCl_3$, 128.4 MHz) spectrum of Potassium ((2-ethoxyethoxy)methyl)trifluoroborate (**S3**)

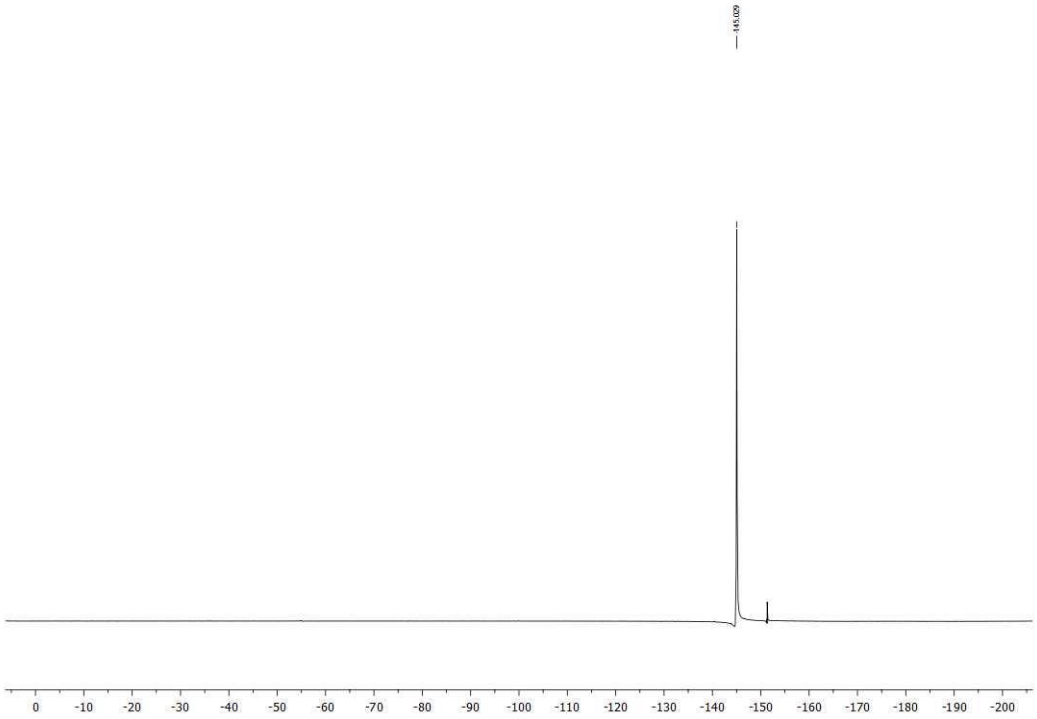


**Figure A2.104.** $^{19}F$ NMR ($CDCl_3$, 470.8 MHz) spectrum of Potassium ((2-ethoxyethoxy)methyl)trifluoroborate (**S3**)

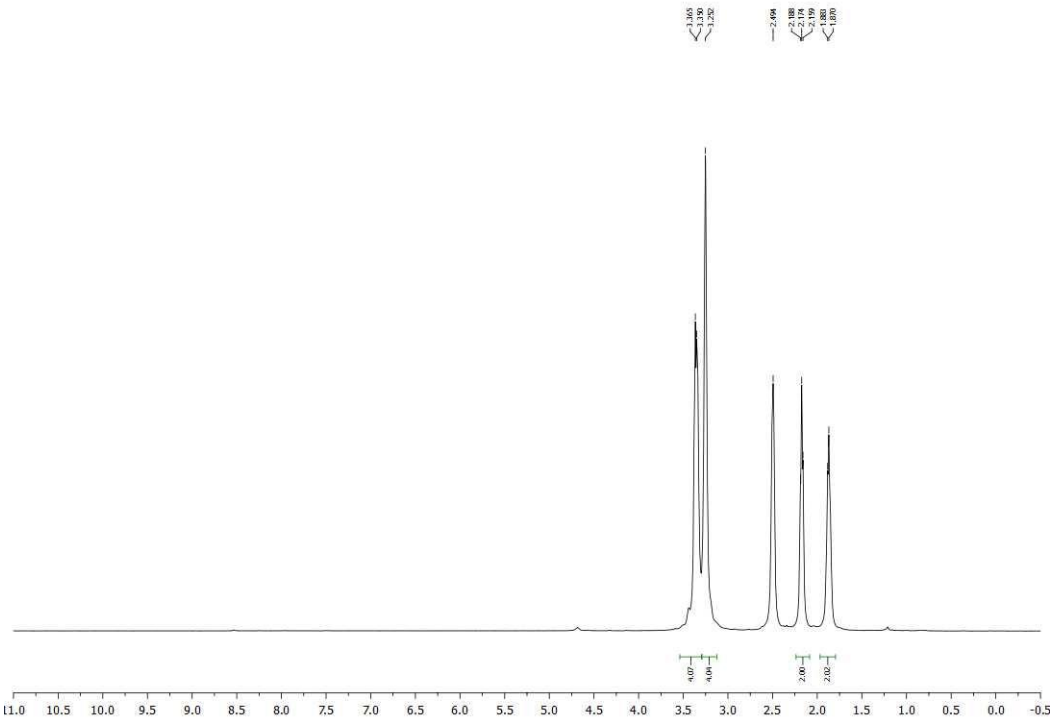

**Figure A2.105.** $^{1}$H NMR ($CDCl_3$, 500 MHz) spectrum of Potassium ((methoxy)methyl)pyrrolidin-2-onetrifluoroborate (**S4**)

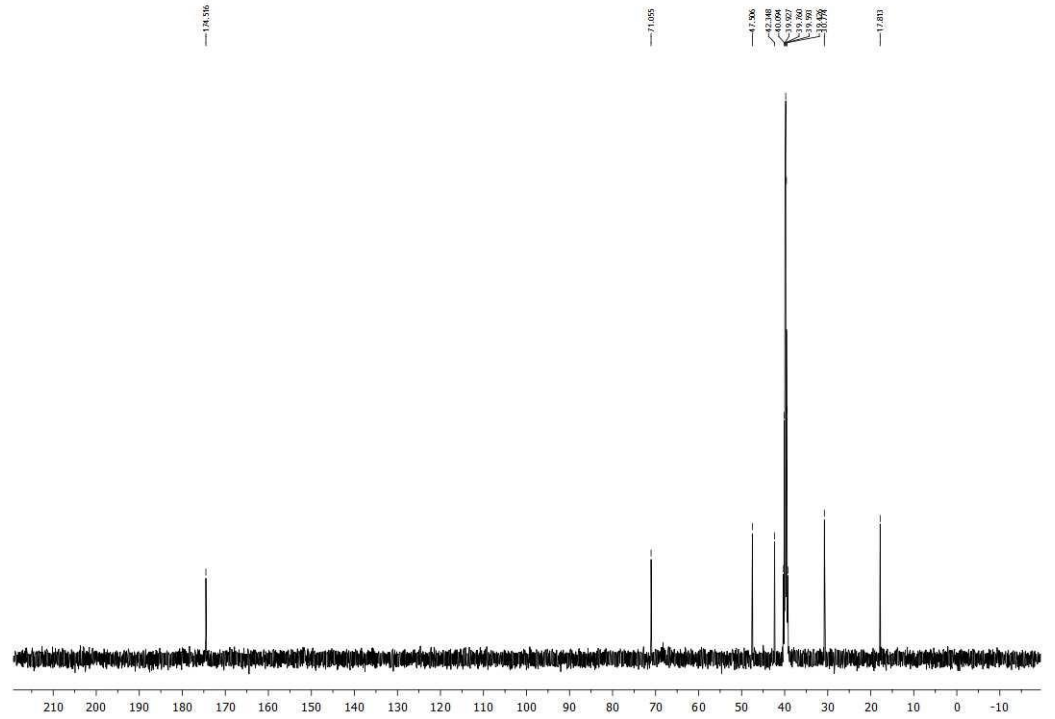

**Figure A2.106.** $^{13}$C NMR ($CDCl_3$, 125.8 MHz) spectrum of Potassium ((methoxy)methyl)pyrrolidin-2-onetrifluoroborate (**S4**)

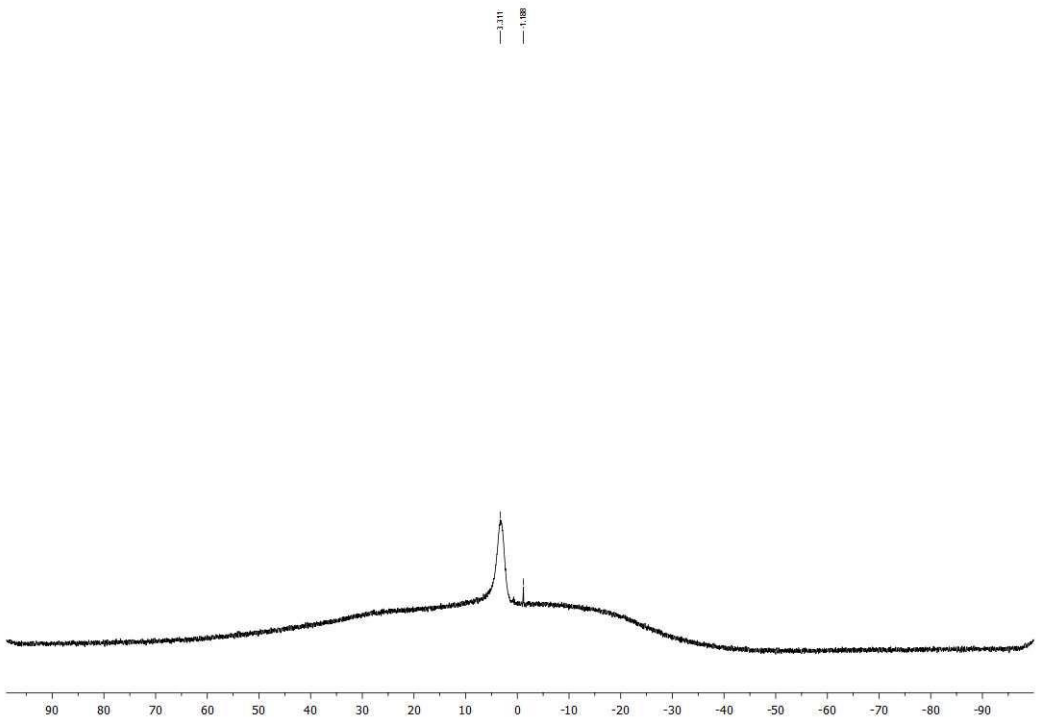


**Figure A2.107.** $^{11}B$ NMR ($CDCl_3$, 128.4 MHz) spectrum of Potassium ((methoxy)methyl)pyrrolidin-2-onetrifluoroborate (**S4**)

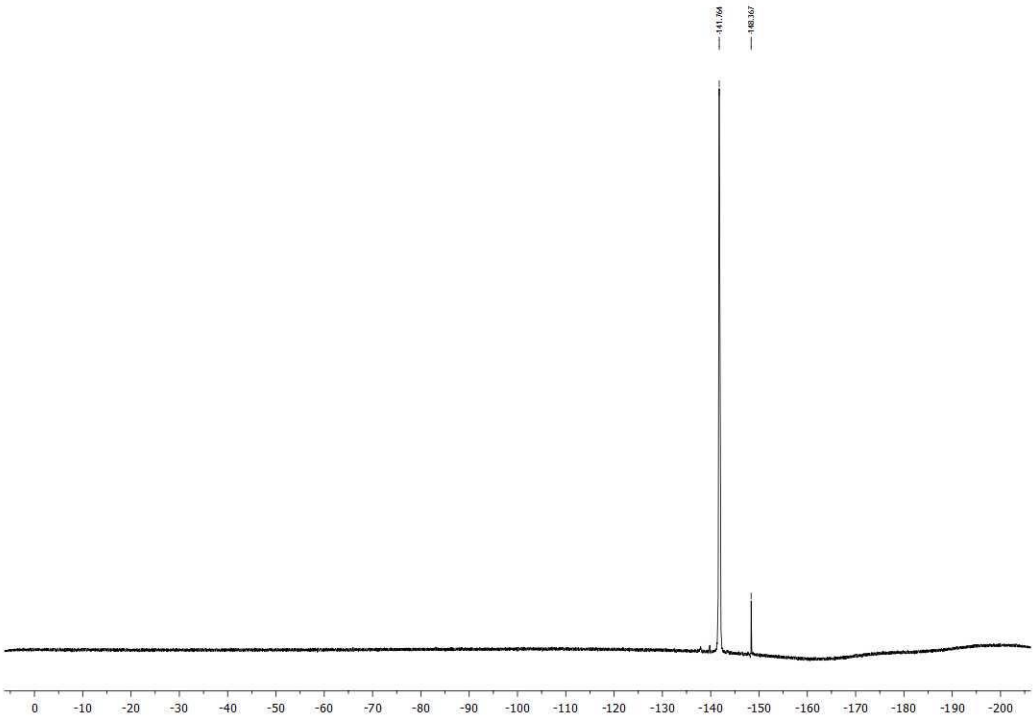


**Figure A2.108.** $^{19}F$ NMR ($CDCl_3$, 470.8 MHz) spectrum of Potassium ((methoxy)methyl)pyrrolidin-2-onetrifluoroborate (**S4**)

# Chapter 4. Unactivated Secondary Alkyltrifluoroborates as Radical Precursors

## 4.1 Introduction

At this point in the development of this new cross-coupling paradigm, all successful radical partners (benzylic, α-alkoxymethyl) had been previously employed in Pd cross-coupling via their analogous carbon-centered anion intermediates. Although the scope of the photoredox Ni catalyzed variants often far exceeded and surpassed that of previously recorded methods, many of the products obtained in these coupling could be accessed by alternative strategies – cross-coupling or otherwise. The true test of a new method should be whether it can overcome or complement weaknesses in the current state of the art and, in the case of organoboron cross-coupling, the truest limitation has always been sterically hindered secondary and tertiary alkyl nucleophiles.

Given these classical restraints, the expectation from the outset of this research was to surmount the far greater challenge of secondary alkyl coupling.[i] As alluded to in Chapter 1, the most challenging aspect of traditional alkylboron cross-coupling is the slow rate of transmetalation,[1–3] a problem innate to the two-electron nature of the process. Because of the inherently low nucleophilicity of organoboron reagents and the associated high energy of activation in the transmetalation, general approaches to secondary alkyl cross-coupling have defaulted to the more reactive alkylboranes,[1] alkylzincs,[4,5] alkyl Grignard reagents,[6] and alkyllithiums.[7] Although

[i] Reproduced in part from *J. Am. Chem. Soc.*, **2015**, *137*, 2195

these reagents can normally be cross-coupled in high yields, their poor shelf life and lack of functional group tolerability limits their widespread application - particularly in the context of parallel synthesis for medicinal chemistry.

Among the more preferable organoboron reagents, a number of substrate-specific secondary alkyl cross-coupling reactions have been reported, but these have always required electronic or functional group stabilization (β-carbonyl,[8] α-boryl,[9] α-alkoxy,[10] benzylic,[11,12] or allylic[13]) to allow effective reaction.[14] A few isolated examples of cross-coupling with unactivated boronic acid derivatives exist, but these do not comprise a general strategy for alkyl cross-coupling.[15,16] The most universal transformations to date have involved cross-coupling with alkyltrifluoroborates or boronic acids under rigorous reaction conditions (3 equiv $K_2CO_3$, 60 – 100 $^0$C, 24 – 48 h).[17–19] *Most importantly, these methods are uniformly ineffective for more highly substituted systems such as 2-methylcycloalkylboron reagents.*

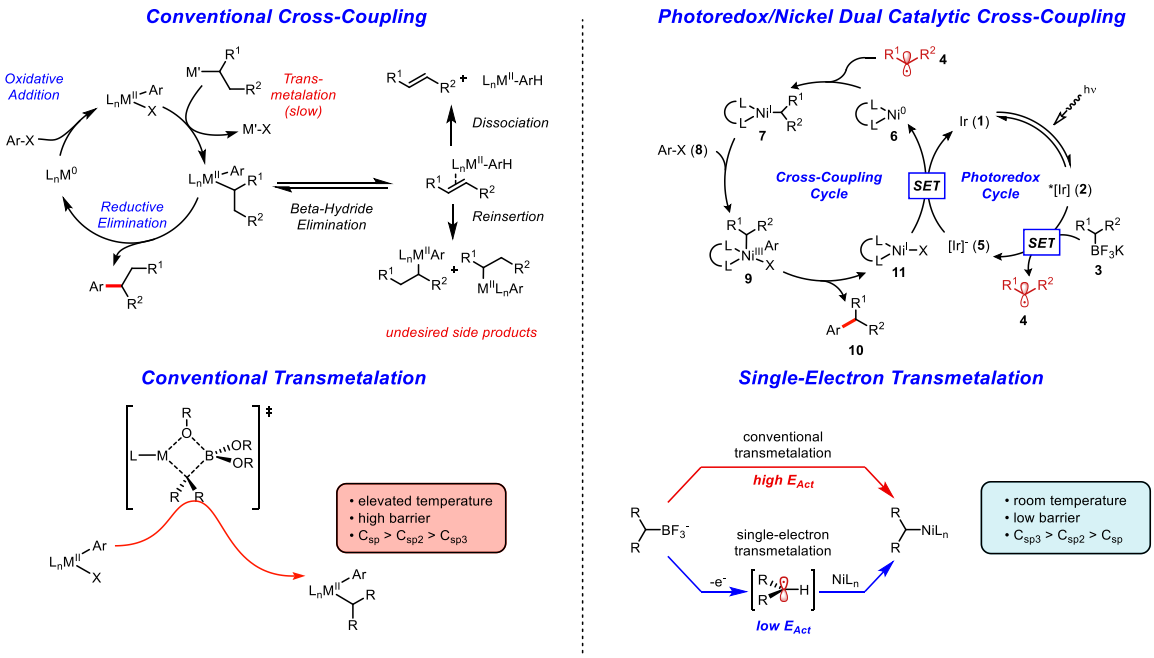


**Figure 4.1.** Comparison between traditional and radical cross-coupling

Here, our approach to transmetalation was anticipated to circumvent the traditional four-coordinate transition structure[20] and replace alkyl transfer with a series of SET processes,[21,22] enabling cross-coupling at room temperature. It was recognized that this method had profound implications for $C_{sp3}$-$C_{sp2}$ cross-coupling because of the mild nature of the reaction conditions. Instead of a high activation energy transmetalation, alkyl transfer could be effected through radical combination with a transition metal-based catalyst complex – a nearly barrierless energetic process.[23] In such a transformation, excitation of the photocatalyst serves as a targeted energy shuttle to enable the transmetalation event, alleviating the necessity to heat the reactions. These conditions were anticipated to increase yields by limiting the side reactions that have doomed previous alkyl Suzuki couplings. A comparison between the two strategies is summarized in **Figure 4.1**

## 4.2 Results and Discussion

Direct application of the previously reported SET strategy to secondary alkyltrifluoroborates was recognized as challenging because of their relatively high oxidation potentials (+1.50 V vs SCE)[24] as compared to that of their benzylic counterparts (+1.10 V vs SCE).[24] Exceeding the electrochemical potentials of highly oxidizing photocatalyst $Ir(dFCF_3ppy)_2bpy\ PF_6$ (+1.32 V vs SCE),[25] these substrates appeared to be destined for failure because of their high electrochemical demands. Nevertheless, encouragement was found in cases where thermodynamically unfavorable single electron transfers occur – particularly within the context of an irreversible oxidation or reduction.[24,26] Thus, only a small portion of the oxidation wave need overlap with the potential of the photocatalyst for the reaction to proceed, driven forward by irreversible C-B bond fragmentation.

Initially, attempts to apply previous conditions for the cross-coupling of benzylic and secondary α-alkoxyalkyltrifluoroborates [2.0 mol % $Ir[dFCF_3ppy]_2(bpy)PF_6$ **1**, 3.0 mol % $Ni(COD)_2$/dtbbpy, acetone/MeOH (10:1), 3.5 equiv of lutidine] proved ineffective (<10% yield). The low yields achieved using that protocol appeared to be a consequence of the differing nature of the unstabilized, secondary alkyl radicals, where radical alkylation of arenes[27] and H-atom abstraction from the solvent[28] could outcompete combination with the nickel catalyst, which was present in low concentration. Using knowledge of established H-atom abstraction rates,[29] suppression of these side reactions could be achieved by the use of dioxane as solvent with careful monitoring of the reaction temperature. Next, various additives were determined to have a profound effect on the rate of the reaction and the amount of protodehalogenation side product observed. Of those additives screened, $Cs_2CO_3$ was the best for maximizing productive cross-coupling while limiting side reactions. Although the precise role of the base has not been defined, rate studies have revealed that $BF_3$ appears to inhibit the reaction. Its removal by added base allows reactions to proceed to completion in a more timely manner. Application of these conditions to the cross-coupling of methyl 4-bromobenzoate with potassium cyclopentyltrifluoroborate furnished product **14** in a satisfactory 92% yield (see experimental). Control experiments in the absence of nickel, iridium, and light all confirmed the dual catalytic nature of this cross-coupling.

With suitable conditions [2.5 mol % Ir cat **1**, 5 mol % $NiCl_2$•dme, 5 mol % dtbbpy, 1.5 equiv $Cs_2CO_3$, dioxane, 26-Watt compact fluorescent lightbulb (CFL), 24 ºC, 24 h] in hand, an exploration of the scope of the alkyltrifluoroborate component was initiated (Table 1). Organoboron reagents possessing various ring sizes were coupled in good to excellent yields. To ensure the scalability and efficiency of this secondary alkyl coupling, a gram scale reaction generating **2** was performed with reduced loadings of iridium and nickel catalyst. Importantly, only 1.0 mol % of the photoredox catalyst and 2.0 mol % of the nickel catalyst was required, and under

these conditions the cross-coupling of methyl 4-bromobenzoate with potassium cyclohexyltrifluoroborate was accomplished to afford **2** in 73% yield after 36 h.

When moving to smaller ring sizes, particularly cyclobutyl- and cyclopropyl systems, where occupying an orbital with greater s-character destabilizes the resultant radical, yields suffered. In fact, for the cyclopropyl substrate, no reaction was observed. This poor reactivity serves to highlight the complementary nature of this method when compared to established methods for $C_{sp2}$- and $C_{sp2}$-like cross-coupling; an area where the two-electron transmetalation regime has proven quite effective.[30] Isopropyl- and *sec*-butyltrifluoroborates were also coupled in good yields. For these substrates, where isomerization would lead to different products, only the desired regioisomer was observed.

To probe further the limits of the isomeric fidelity observed in this transformation, several more bulky secondary alkyltrifluoroborates were explored. Gratifyingly, products derived from 2-methylcyclopentyl and 2-methylcyclohexyl substrates were also isolated without rearrangement. In addition, the products were exclusively the trans diastereomer. Remarkably, an even more sterically demanding pinene derivative could be coupled to afford **12.**

Aliphatic heterocyclic ring systems containing oxygen (**11**) and protected nitrogen (**10**), which have proven to be recalcitrant in previous cross-coupling methods,[18] did not significantly reduce yields under the photoredox cross-coupling protocol. In particular, aryl piperidines structurally analogous to **10**, which are highly desired for incorporation into pharmaceutical libraries,[31] could be accessed in excellent yield. To explore the scope of functional group tolerance, attention was turned to the screening of substituted aryl bromides (Table 4.2). During this process, a variety of trifluoroborates were used, particularly those that were *both unsymmetrical and sterically encumbered* in an effort to showcase the mild nature of these cross-couplings. In previous work under palladium catalysis, 2-methylcycloalkylborons were observed to isomerize during the reaction, leading to a complex mixture where cross-coupling at the less sterically crowded positions

was preferred.[18,19] In contrast, the ability to couple even more crowded trifluoroborates with a range of aryl bromides under the current paradigm serves to highlight the mechanistic differences between a traditional transmetalation and the radical-mediated alkyl transfer described herein.

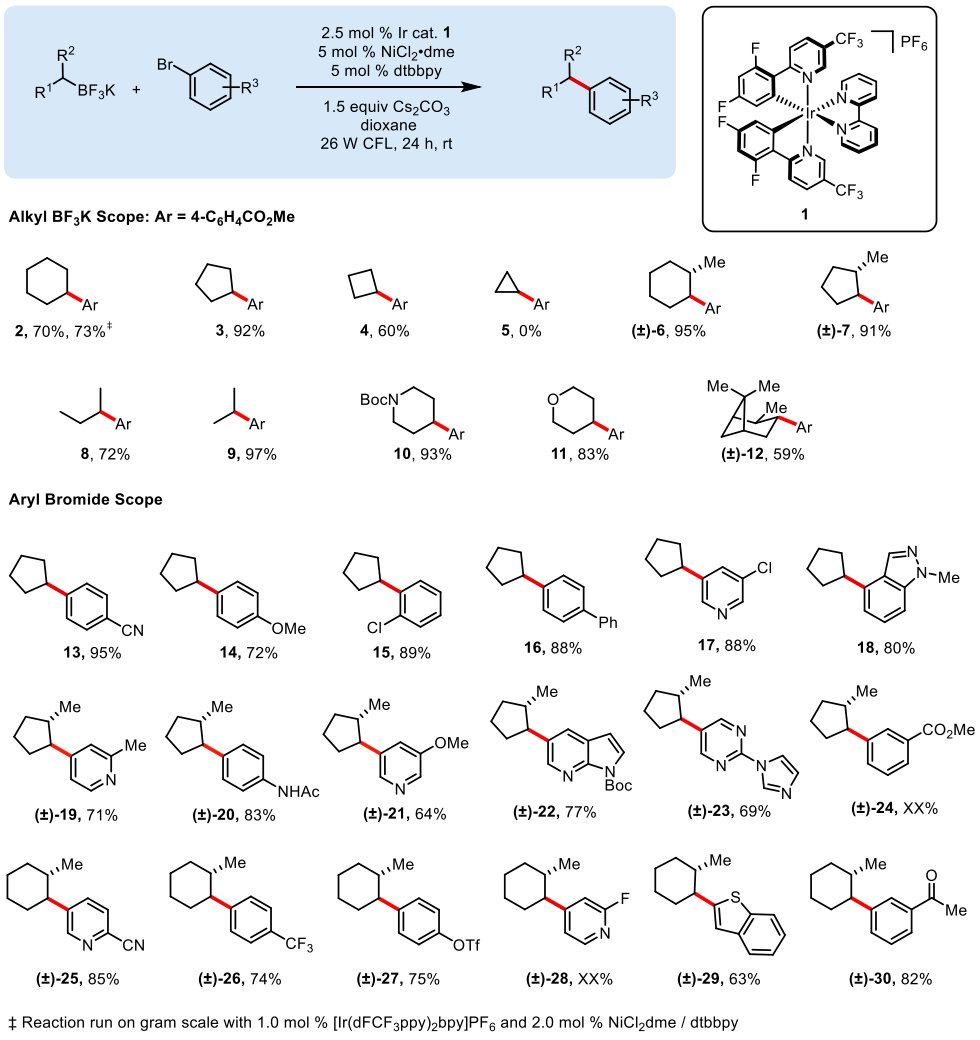


**Figure 4.2**. Scope of secondary alkyltrifluoroborates and aryl halides in Ni/photoredox cross-coupling

For the aryl bromide component, both electron-poor (**13**) and electron-rich systems (**14**) were coupled in good to excellent yields. Substitution ortho to the halide in **15** and **18** was tolerated without significant reduction in yield. Selective cross-coupling was observed in compounds with multiple electrophilic handles; both bifunctional aryl chlorides (leading to **15** and **17)** and an aryl

triflate, providing **27**, coupled exclusively at the bromide. Ketones and esters (**24** and **30**), which can be intolerant of Kumada-type conditions, could be embedded within substrates to afford products in excellent yields. Further, nitrile-substituted bromides **13** and **25,** which were unreactive under the previously developed Pd chemistry for alkyltrifluoroborates,[18] served as competent reaction partners.

Protic groups did not diminish reactivity for the acetanilide substrate leading to **20**. A number of N-heterocyclic bromides, providing privileged substructures of use in medicinal chemistry,[31] readily participated in the cross-coupling. Pyridines (**17**, **19**, **21**, **25, 28**), pyrimidine (**23**), and protected heterocycles (indazole **18**, azaindole **22**) were all accessed in acceptable yields. In addition to the more desirable N-heterocycles, a bromobenzothiophene was also reactive under the conditions, returning coupled product **29** in reasonable yield. Overall, the functional group tolerance for bromides shown here rivals or exceeds that of any previously developed method for secondary alkyl Suzuki cross-coupling – particularly within the context of heteroaryl substrates.

## 4.3 Conclusion

In summary, extremely mild conditions (rt, 1.5 equiv base, 26 W CFL irradiation) for the cross coupling of secondary alkyltrifluoroborates with aryl bromides have been developed. The best previously reported, palladium-catalyzed conditions for secondary alkylboron coupling[18,19] have required significant excess of base and elevated temperatures to achieve less general overall results. Moreover, extensive Pd source, ligand, and reaction condition screening have so far failed to identify satisfactory results for systems such as 2-methyl-substituted cycloalkylboron reagents. In contrast, only slight modification of the initially reported conditions for benzylic coupling were required to extend both the nucleophilic and electrophilic scope of secondary alkyl cross-couplings

with the photoredox/cross-coupling dual catalytic system. The ease of this transformation across a broad array of radical precursors (α-amino,[32] α-alkoxy,[32,33] benzylic,[33] and now secondary alkyl) speaks to the power of the SET-mediated approach. Further investigations into Ni precatalysts and ligands (entities that have yielded vast improvements in analogous Pd chemistry[34,35]) can arguably afford similar gains when applied to this system. With proper screening and catalyst design, extensions to extremely hindered electrophiles and aryl chlorides appear feasible.

Finally, it should be noted that several Pd-catalyzed processes allow the conversion of enantiomerically enriched organoboron reagents to cross-coupled products with high stereochemical fidelity.[7,17,19-22] Although such a process is clearly not feasible under the current paradigm, where radical intermediates are generated from the organoboron precursors, the prochiral radicals generated can be engaged in stereoconvergent transformations by employing enantioenriched ligands around the Ni catalyst.[33,36,37] The fine tuning of stereoconvergent protocols by ligand development and screening has the potential to provide a unique and significant advancement to the field by eliminating the need to synthesize optically active organometallic reagents, approaches to which are often long, tedious, and intolerant of sensitive functional groups.[38–40]

Possibly the most attractive feature of the reported photoredox cross-coupling is its operational simplicity. By eliminating the need to prepare sensitive organometallics, titrate reagents, or use glovebox techniques, these methods greatly enhance the approachability of secondary alkyl cross-couplings. Consequently, the methods described herein provide a significant advancement to $C_{sp3}$-$C_{sp2}$ cross-coupling.

## 4.4 Experimental

**General considerations**

All reactions were carried out under an inert atmosphere of nitrogen or argon unless otherwise noted. Dioxane (99.9%, extra dry) was used as received. $Cs_2CO_3$ was used as received. $IrCl_3 \cdot xH_2O$, and $NiCl_2$•dme were purchased from commercial sources. All other reagents were purchased commercially and used as received. Photoredox reactions were irradiated with two or three standard 26 W compact fluorescent light bulbs. Melting points (°C) are uncorrected. NMR spectra were recorded on a 500- or 400 MHz spectrometer. $^{19}F$ NMR chemical shifts were referenced to external $CFCl_3$ (0.0 ppm). $^{11}B$ NMR spectra were obtained on a spectrometer equipped with the appropriate decoupling accessories. Data are presented as follows: chemical shift (ppm), multiplicity (s = singlet, d = doublet, t = triplet, sept = septet, m = multiplet, br = broad), coupling constant *J* (Hz) and integration.

**Synthesis of Secondary Alkyltrifluoroborates:**

Most potassium organotrifluoroborates were purchased commercially. In cases where the desired potassium organotrifluoroborate was unavailable, the corresponding boronic acid derivative was converted to the trifluoroborate by the following procedure.

**General Procedure for conversion of boronic acid to trifluoroborate:**

To a solution of boronic acid derivative in acetone or MeOH (0.1 M) at 0 °C was added saturated aq $KHF_2$ (4.5 M) dropwise over 30 min. The resulting suspension was concentrated under reduced pressure. $H_2O$ was azeotropically removed by suspension in toluene (100-150 mL) followed by rotary evaporation. The remaining solid was dried under high vacuum and then suspended in hot

acetone (3 x 100 mL) and filtered. The filtrate was concentrated to a minimal volume (5 – 20 mL) and hexane or $Et_2O$ (~200 mL) were added to yield a white precipitate. The precipitate was isolated by filtration, washing with hexanes (~30 mL) and $CH_2Cl_2$ (~30 mL), to afford the desired secondary alkyltrifluoroborate.

**Selected reaction optimization studies**

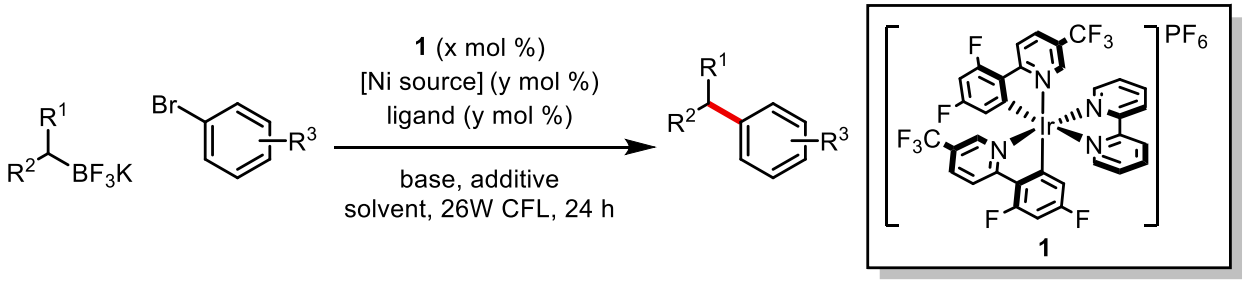


*Procedure for reaction screening at 0.10 or 0.05 mmol scale:* To a reaction vial equipped with a Teflon-coated magnetic stir bar in a glovebox was added a soln of nickel source and ligand (1:1) dissolved in THF. The solvent was removed *in vacuo* under an inert atmosphere. Additives were weighed into the vials (liquid additives were added after the stock solution). A stock solution of aryl bromide, secondary alkyltrifluoroborate, Ir catalyst **1**, and internal standard were then added by syringe and stirred for 16-24 h in front of a single 26 W CFL. Aliquots were then taken, diluted, and analyzed by HPLC or GC/MS. Reactions were compared within sets by crude product to internal standard (P/IS) ratios.

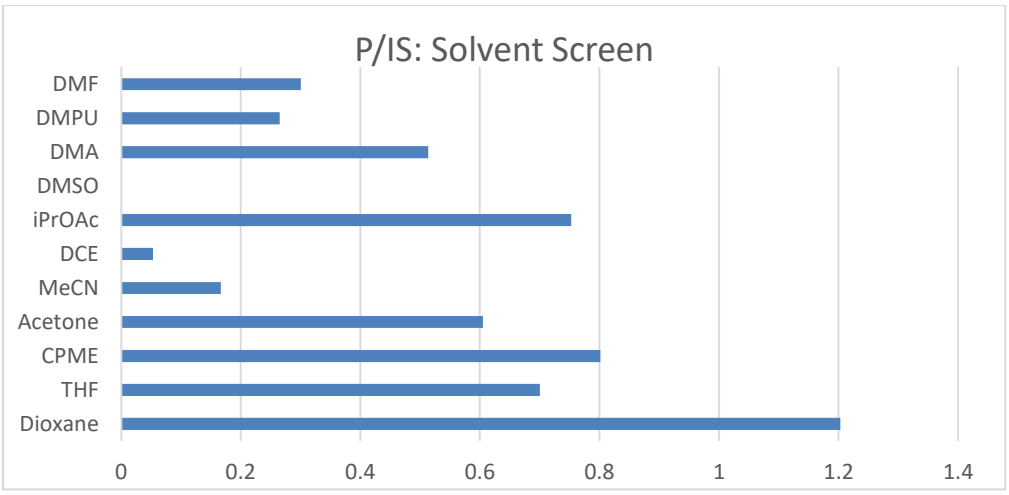


**Figure 4.3. Comparison of Solvents**
Conditions: 0.1 mmol Ar-Br, 1.5 equiv $RBF_3K$, 2.0 %
$Ir(dFCF_3ppy)_2bpy\ PF_6$, 10.0 % Ni/dtbbpy, $K_2CO_3$ (1.0 equiv), 0.05 M

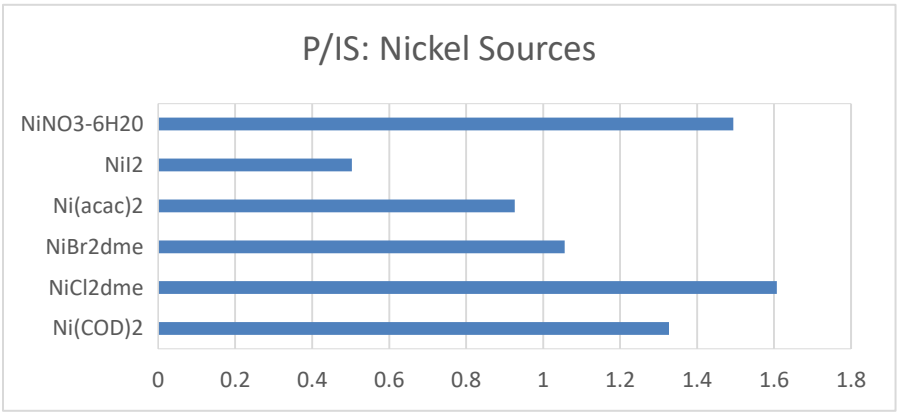


**Figure 4.4. Nickel Sources**
Conditions: 0.1 mmol Ar-Br, 1.5 equiv $RBF_3K$, 2.0%
$Ir(dFCF_3ppy)_2bpy\ PF_6$, 10.0 % Ni source/dtbbpy, $K_2CO_3$ (1.0 equiv), 0.05 M in dioxane

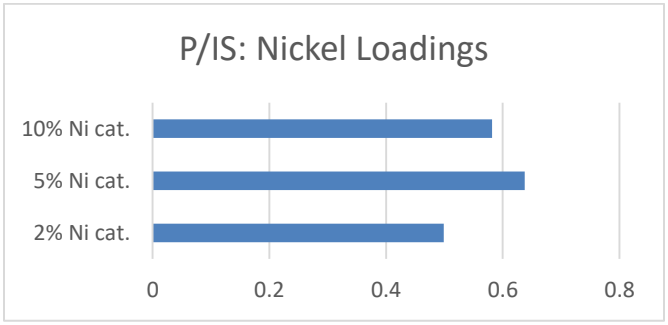


**Figure 4.5. Nickel Loadings**
Conditions: 0.1 mmol Ar-Br, 1.5 equiv $RBF_3K$, 2.0%
$Ir(dFCF_3ppy)_2bpy\ PF_6$, 1.5 equiv $K_2CO_3$ 0.05 M in dioxane

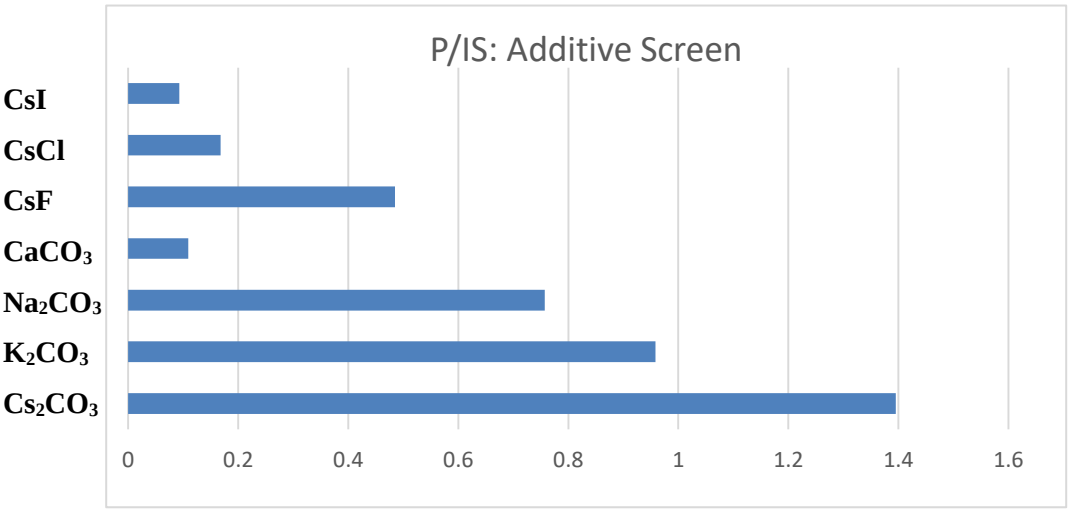


**Figure 4.6. Comparison of Carbonate Bases and Cesium Salts**
**Conditions: 0.1 mmol Ar-Br, 1.5 equiv $RBF_3K$, 2.5% $Ir(dFCF_3ppy)_2bpy\ PF_6$, 5.0% Ni/dtbbpy, 1.5 equiv additive, 0.05 M in dioxane**

**General procedure for photoredox cross-coupling reactions**

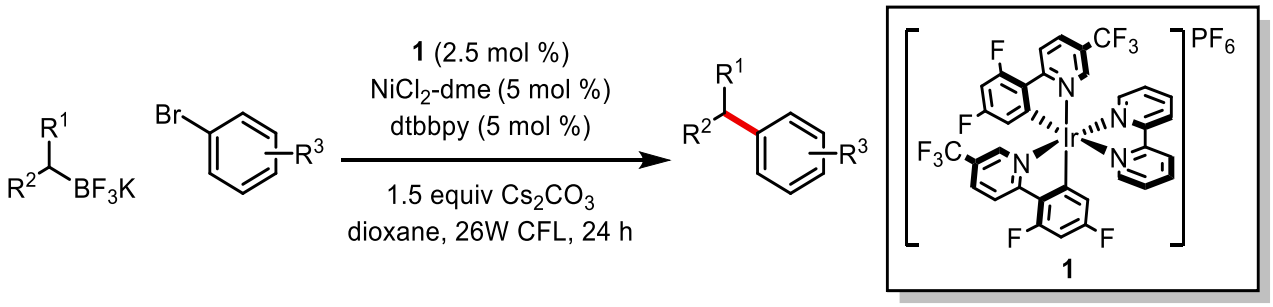


To a long, thin (~20 mL) borosilicate glass vial equipped with a Teflon-coated magnetic stir bar was added 4,4'-di-*tert*-butyl-2,2'-bipyridine (6.7 mg, 0.025 mmol) and $NiCl_2$•dme (5.5 mg, 0.025 mmol) and 1.0 mL THF. The vial was capped and the resulting suspension was heated briefly with a heat gun until the nickel and ligand were fully solubilized, yielding a pale green solution. The solvent was then removed under vacuum to give a fine coating of the ligated nickel complex (pale evergreen in color). Once dry, aryl bromide (0.5 mmol, 1 equiv) (liquid aryl bromides were added with solvent), secondary alkyltrifluoroborate (0.75 mmol, 1.5 equiv), $Ir[dFCF_3ppy]_2(bpy)PF_6$ **1** (12.8 mg, 0.025 mmol) and $Cs_2CO_3$ (243 mg, 0.75 mmol) were added in succession. The vial was

then capped and purged and evacuated four times. Under inert atmosphere, dioxane (10 mL) was introduced. The vial containing all the reagents was further sealed with parafilm and stirred for 24 hours approximately 4 cm away from two 26 W fluorescent light bulbs. A fan was blown across the reaction setup to maintain an ambient temperature around 24 $^{o}$C. After 16-24 h, an aliquot was taken and analyzed on a GC/MS to monitor reaction completion and confirm formation of a single regioisomer (when applicable). Then, the crude reaction mixture was filtered through an approximately 2 cm x 2 cm cylindrical plug of Celite, washing with EtOAc (10–20 mL). The resulting solution was concentrated and the residue was purified by column chromatography on silica gel, eluting with EtOAc and hexanes, to obtain products in pure form.

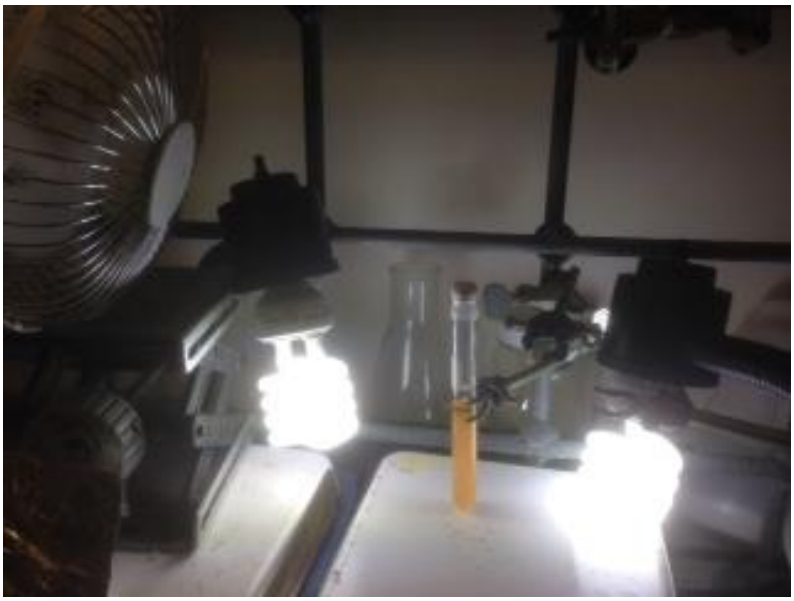

**Figure 4.7.** Photoredox cross-coupling reaction set-up (0.5 mmol scale)

**Gram scale reaction:** To a ~125 mL long thin-walled vacuum flask equipped with a Teflon-coated magnetic stir bar was added $NiCl_2$•dme (20 mg, 0.093 mmol, 0.02 equiv) and 4,4'-di-*tert*-butyl-2,2'-bipyridine (25 mg, 0.093, 0.02 equiv) and 5.0 mL of THF. The vial was capped and the resulting suspension was heated briefly with a heat gun until the nickel and ligand were fully solubilized, yielding a pale green solution. The solvent was then removed under vacuum to give a

fine coating of the ligated nickel complex (pale evergreen in color). Once dry, methyl 4-bromobenzoate (1.000 g, 4.65 mmol, 1.00 equiv), potassium cyclohexyltrifluoroborate (1.325 g, 6.98 mmol, 1.50 equiv), $Ir[dFCF_3ppy]_2(bpy)PF_6$ **1** (47.0 mg, 0.047 mmol, 0.01 equiv), and $Cs_2CO_3$ (2.267 g, 6.98 mmol, 1.50 equiv) was added. The vial was then capped with a rubber septum and purged and evacuated four times. Under inert atmosphere, dioxane (95 mL, 0.05 M) was introduced. The vial containing all the reagents was further sealed with parafilm and stirred vigorously (a small vortex should be observed toward the top of the reaction mixture) for 36 h approximately 4 cm away from three 26 W fluorescent light bulbs. A fan was blown across the reaction setup to maintain an ambient temperature around 24 $^oC$. After completion, the crude reaction mixture was filtered through an approximately 4 cm x 2 cm cylindrical plug of Celite, washing with EtOAc (60 mL). The resulting solution was concentrated and the residue was purified by column chromatography on silica gel, eluting with EtOAc and hexanes, to obtain product in pure form.

**Figure 4.8.** Gram scale photoredox cross-coupling reaction set-up (4.65 mmol)

**Compound Characterization Data**

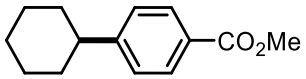


**2**

**Methyl 4-cyclohexylbenzoate** (**2)**: obtained as a white crystalline solid (76 mg, 70%), on gram (4.65 mmol) scale (740 mg, 73%), mp = 38-40 ºC. $^{1}$H NMR ($CDCl_3$, 500 MHz): δ 7.97 (d, *J* = 8.0 Hz, 2H), 7.28 (d, *J* = 8.0 Hz, 2H), 3.90 (s, 3H), 2.58-2.54 (m, 1H), 1.87 (m, 4H), 1.77 (d, *J* = 12.5 Hz, 1 H), 1.48-1.31 (m, 4H), 1.29-1.25 (m, 1H). $^{13}$C NMR ($CDCl_3$, 125.8 MHz): δ 167.1, 153.4, 129.6, 127.7, 126.8, 51.8, 44.6, 34.0, 26.7, 26.0. IR: ν = 2926, 2852, 1720, 1436, 1276, 1180, 1112, 1101, 1019, 762, 706 $cm^{-1}$. HRMS (ESI) m/z calc. for $C_{14}H_{18}O_2Na$ (M+Na) 241.1204, found 241.1214.

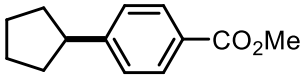


**3**

**Methyl 4-cyclopentylbenzoate (3)**: obtained as a white amorphous solid (94 mg, 92%), mp = 32-33 °C. $^{1}$H NMR ($CDCl_3$, 500 MHz): δ 7.95 (d, *J* = 8.5 Hz, 2H), 7.29 (d, *J* = 8.5 Hz, 2H), 3.89 (s, 3H), 3.04 (q, *J* = 8.5 H, 1H), 2.08 (m, 2H), 1.82-1.59 (m, 6H) – a small amount of methyl 4-bromobenzoate (<5%) was inseparable from the starting material after column chromatography. $^{13}$C NMR ($CDCl_3$, 125.8 MHz): δ 167.1, 152.1, 129.5, 127.6, 127.0, 51.8, 45.9, 34.4, 25.5 Characterization data matched that reported in the literature.[41]

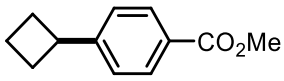


**4**

**Methyl 4-cyclobutylbenzoate** (**4)**: obtained as a pale yellow oil (57 mg, 60%). $^{1}$H NMR ($CDCl_3$, 500 MHz): δ 7.96 (d, *J* = 8.5, 2H), 7.26 (d, *J* = 8.5, 2H) 3.90 (s, 3H), 3.59 (m, 1H), 2.39-2.34 (m, 2H), 2.20-2.00 (m, 3H), 1.90-1.84 (m, 1H). $^{13}$C NMR ($CDCl_3$, 125.8 MHz): δ 167.3, 151.8, 129.7,

127.8, 126.4, 52.1, 40.4, 29.7, 18.4. IR: ν = 2951, 1721, 1609, 1435, 1276, 1108, 1020, 768, 646 $cm^{-1}$. HRMS (ESI) m/z calc. for $C_{12}H_{15}O_2$ (M+H) 191.1072, found 191.1065.

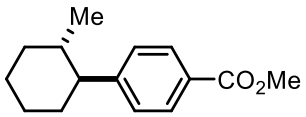


**6**

**Methyl *trans*-4-(2-methylcyclohexyl)benzoate** (**6)**: obtained as a colorless oil (110 mg, 95%) $^1$H NMR ($CDCl_3$, 500 MHz): δ 7.95 (d, *J* = 8.0, 2H), 7.22 (d, *J* = 8.0, 2H), 3.89 (s, 3H), 2.16-2.11 (m, 1H), 1.84-1.76 (m, 4H), 1.64-1.58 (m, 1H), 1.46-1.32 (m, 3H), 1.12-1.10 (m, 1H), 0.64 (d, *J* = 6.5 Hz, 3H). $^{13}$C NMR ($CDCl_3$, 125.8 MHz): δ 167.1, 152.4, 129.6, 127.7, 127.5, 52.5, 51.8, 37.4, 35.5, 35.2, 26.7, 26.5, 20.6. IR: ν = 2924, 2853, 1722, 1609, 1435, 1276, 1180, 1112, 1102, 772, 708 $cm^{-1}$. HRMS (ESI) m/z calc. for $C_{15}H_{21}O_2$ (M+H) 233.1542, found 233.1539. GCMS analysis of the reaction mixture after 16 hours confirms formation of a single regioisomer.

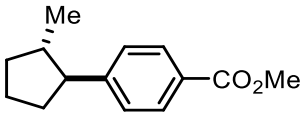


**7**

**Methyl *trans*-4-(2-methylcyclopentyl)benzoate** (**7)**: obtained as a pale yellow oil (99 mg, 91%) $^1$H NMR ($CDCl_3$, 500 MHz): δ 7.96 (d, *J* = 8.0, 2H), 7.27 (d, *J* = 8.0, 2H), 3.90 (s, 3H), 2.50-2.44 (m, 1H) 2.10-2.08 (m, 1H), 2.00-1.92 (m, 2H), 1.78-1.71 (m, 3H), 1.34-1.30 (m, 1H), 0.91 (d, *J* = 6.5 Hz, 3H) $^{13}$C NMR ($CDCl_3$, 125.8 MHz): δ 167.3, 151.4, 129.8, 128.0, 127.7, 54.7, 52.1, 43.4, 35.4, 34.9, 24.1, 18.6. IR: ν = 2951, 2868, 1723, 1610, 1435, 1278, 1179, 1112, 770 $cm^{-1}$

HRMS (ESI) m/z calc. for $C_{14}H_{19}O_2$ (M+H) 219.1385, found 219.1394. GCMS analysis of the reaction mixture after 16 hours confirms presence of a single regioisomer.

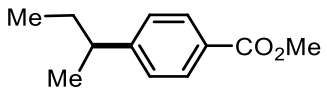


**8**

**Methyl 4-(sec-butyl)benzoate (8):** obtained as a colorless oil (73 mg, 76%). $^{1}$H NMR ($CDCl_3$, 500 MHz): δ 7.96 (m, 2H), 7.25 (m, 2H), 3.89 (s, 3H), 2.65 (m, 1H), 1.61 (m, 2H), 1.24 (m, 3H), 0.81 (m, 3H). $^{13}$C NMR ($CDCl_3$, 125.8 MHz): δ 167.3, 153.3, 129.8, 127.9, 127.2, 52.1, 41.9, 31.1, 21.7, 12.3. GCMS analysis of the reaction mixture after 24 hours confirms presence of a single regioisomer. Characterization data matched that reported in the literature. [42]

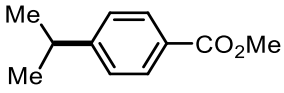


**9**

**Methyl 4-isopropylbenzoate (9):** obtained as a colorless oil (68 mg, 76%). $^{1}$H NMR ($CDCl_3$, 500 MHz): δ 7.96 (d, *J* = 8.5 Hz, 2H), 7.28 (d, *J* = 8.5 Hz, 2H), 3.90 (s, 3H), 2.96 (sept, *J* = 7.0 Hz, 1H), 1.26 (d, *J* = 7.0 Hz, 6H). $^{13}$C NMR ($CDCl_3$, 125.8 MHz): δ 167.3, 153.3, 129.8, 127.9, 127.2, 52.1, 41.9, 31.1, 21.7, 12.3. Characterization data matched that reported in the literature.[43]

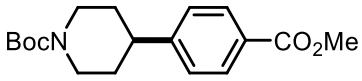


**10**

***tert*-Butyl 4-(4-(methoxycarbonyl)phenyl)piperidine-1-carboxylate** (**10)**: obtained as a white amorphous solid (147 mg, 92%), mp = 118-120 ºC. $^{1}$H NMR ($CDCl_3$, 500 MHz): δ 7.95 (d, *J* = 8.5 Hz, 2H), 7.24 (d, *J* = 8.5 Hz, 2H), 4.23 (bs, 2H), 3.87 (s, 3H), 2.80-2.65 (m, 3H), 1.81-1.78 (m, 2H), 1.62-1.58 (m, 2H), 1.46 (s, 9H). $^{13}$C NMR ($CDCl_3$, 125.8 MHz): δ 167.1, 154.9, 151.2, 130.0, 128.4, 127.0, 79.7, 52.1, 44.3 (br), 42.9, 33.0, 28.6, 24.9. IR: ν = 2845, 1701, 1421, 1365, 1268, 1229, 1155, 1126, 1012, 770 $cm^{-1}$. HRMS (ESI) m/z calc. for $C_{18}H_{25}NO_4Na$ (M+Na) 342.1681,

found 342.1685. GC analysis of the crude mixture after 24h confirms the formation of a single regioisomer.

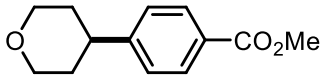


**11**

**Methyl 4-(tetrahydro-2H-pyran-4-yl)benzoate** (**11)**: obtained as a white crystalline solid (91 mg, 83%), mp = 74-75 °C. $^{1}$H NMR ($CDCl_3$, 500 MHz): δ 7.97 (d, *J* = 8.0 Hz, 2H), 7.28 (d, *J* = 8.0 Hz, 2H), 4.08 (d, *J* = 10.5 Hz, 2H), 3.89 (s, 3H), 3.52 (t, *J* = 11.5 Hz, 2H), 2.82-2.78 (m, 1H), 1.83-1.74 (m, 4H). $^{13}$C NMR ($CDCl_3$, 125.8 MHz): δ 167.2, 151.2, 130.0, 128.4, 126.9, 68.3, 52.2, 41.8, 33.7. IR: ν = 2964, 2932, 2862, 1718, 1609, 1440, 1275, 1109, 1098, 1017, 764 cm$^{-1}$. HRMS (ESI) m/z calc. for $C_{13}H_{17}O_3$ (M+H) 221.1178, found 221.1179.

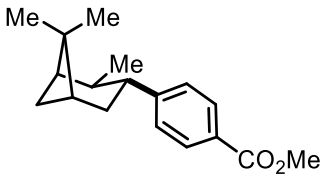


**(±)-12**

**Methyl 4-((1R*,2R*,3R*,5R*)-3,6,6-trimethylbicyclo[3.1.1]heptan-2-yl)benzoate (12):** obtained as a yellow oil (80 mg, 59%). $^{1}$H NMR ($CDCl_3$, 500 MHz): δ 7.99 (d, *J* = 8.5 Hz, 2H), 7.37 (d, *J* = 8.5 Hz, 2H), 3.91 (s, 3H), 3.10-3.06 (m, 1H), 2.53-2.51 (m, 1H), 2.45-2.42 (m, 1H), 2.09-2.04 (m, 2H), 1.92-1.87 (m, 2H), 1.29 (s, 3H), 1.17-1.15 (m, 4H), 1.00 (d, *J* = 7.0 Hz, 3H). $^{13}$C NMR ($CDCl_3$, 125.8 MHz): δ 167.1, 154.8, 129.6, 128.3, 127.5, 51.8, 47.9, 45.6, 44.9, 41.7, 39.1, 37.2, 34.8, 28.4, 22.9, 20.8. IR: ν = 2950, 2904, 1723, 1610, 1434, 1278, 1112, 1019, 770, 707 cm$^{-1}$. HRMS (ESI) m/z calc. for $C_{18}H_{25}O_2$ (M+H) 273.1855, found 273.1850.

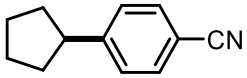


**13**

**4-Cyclopentylbenzonitrile (13)**: obtained as a colorless oil (81 mg, 95%). $^{1}$H NMR ($CDCl_3$, 500 MHz): δ 7.56 (d, *J* = 8.0 Hz, 2H), 7.32 (d, *J* = 8.0 Hz, 2H), 3.04 (q, *J* = 8.0 Hz, 1H), 2.10-2.08 (m, 2H), 1.84-1.81 (m, 2H), 1.73-1.70 (m, 2H), 1.60-1.57 (m, 2H). $^{13}$C NMR ($CDCl_3$, 125.8 MHz): δ 152.5, 132.2, 128.1, 119.4, 109.6, 46.1, 34.6, 25.7. IR: ν = 2955, 2869, 2227, 1607, 1504, 1451, 1416, 1178, 830, 657 $cm^{-1}$. HRMS: (ESI) m/z calc. for $C_{12}H_{13}N$ (M+) 171.1048, found 171.1044.

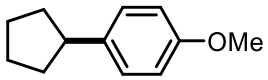


**14**

**1-Cyclopentyl-4-methoxybenzene (14)**: obtained as a colorless oil (63 mg, 72%). $^{1}$H NMR ($CDCl_3$, 500 MHz): δ 7.19 (d, *J* = 9.0 Hz, 2H), 6.86 (d, *J* = 9.0 Hz, 2H), 3.81 (s, 3H), 3.00-2.93 (m, 1H), 2.10-2.04 (m, 2H), 1.83-1.55 (m, 6H). $^{13}$C NMR ($CDCl_3$, 125.8 MHz): δ 157.8, 138.7, 128.1, 113.8, 55.4, 45.3, 34.9, 25.6. IR: ν = 2950, 2866, 1612, 1513, 1463, 1245, 1178, 1033, 826 $cm^{-1}$. HRMS: (ESI) m/z calc. for $C_{12}H_{16}O$ (M+) 176.1201, found 176.1199.

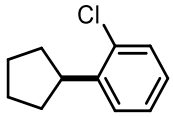


**15**

**1-Chloro-2-cyclopentylbenzene (15)**: obtained as a yellow oil (80 mg, 89%). $^{1}$H NMR ($CDCl_3$, 500 MHz): δ 7.36-7.22 (m, 2H), 7.13-7.10 (m, 2H), 3.46 (q, *J* = 9 Hz, 1H), 2.16-2.07 (m, 2H), 1.83-1.72 (m, 4H), 1.59-1.57 (m, 2H). $^{13}$C NMR ($CDCl_3$, 125.8 MHz): δ 143.8, 134.3, 129.5, 127.2, 127.0, 126.9, 42.3, 33.3, 25.6. IR: ν = 2951, 2868, 1475, 1442, 1355, 1035, 744 $cm^{-1}$. HRMS: (ESI) m/z calc. for $C_{11}H_{13}Cl$ (M+) 180.0706, found 180.0711.

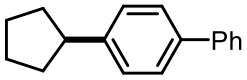


**16**

**4-Cyclopentyl-1,1'-biphenyl (16)**: obtained as a pale yellow semi-solid (98 mg, 88%). $^{1}$H NMR ($CDCl_3$, 500 MHz): δ 7.67-7.65 (m, 2H), 7.60 (d, *J* = 8.5 Hz, 2H), 7.51-7.48 (m, 2H), 7.41-7.38 (m, 3H) 3.11 (q, *J* = 7.5 Hz, 1H), 2.19-2.17 (m, 2H), 2.00-1.90 (m, 2H) 1.80-1.70 (m, 4H). $^{13}$C NMR ($CDCl_3$, 125.8 MHz): δ 145.9, 141.4, 138.9, 129.0, 127.8, 127.23, 127.22, 127.17 45.9, 34.9, 25.8. IR: ν = 2952, 2869, 1598, 1486, 831, 764, 735, 698 $cm^{-1}$. HRMS: (ESI) m/z calc. for $C_{17}H_{18}$ (M+) 222.1409, found 222.1406.

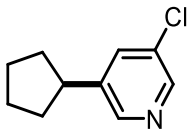


**17**

**3-Chloro-5-cyclopentylpyridine (17)**: obtained as a pale yellow oil (80 mg, 88%). $^{1}$H NMR ($CDCl_3$, 500 MHz): δ 8.39 (d, *J* = 2.5 Hz, 1H), 8.37 (d, *J* = 1.5 Hz, 1H), 7.53-7.52 (dd, *J* = 2.5, 1.5 Hz, 1H), 3.00 (m, 1H), 2.13-2.10 (m, 2H), 1.85-1.83 (m, 2H), 1.75-1.69 (m, 2H), 1.59-1.52 (m, 2H). $^{13}$C NMR ($CDCl_3$, 125.8 MHz): δ 146.9, 146.0, 143.0, 134.0, 131.7, 42.8, 34.2, 25.3. IR: ν = 2954, 2868, 2361, 1580, 1440, 1420, 1295, 1233, 1107, 1022, 935, 879, 709 $cm^{-1}$. HRMS: (ESI) m/z calc. for $C_{10}H_{13}NCl$ (M+H) 182.0737, found 182.0740.

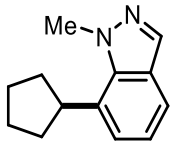


**18**

**7-Cyclopentyl-1-methyl-1H-indazole (18)**: obtained as a dark yellow oil (80 mg, 80%). $^{1}$H NMR ($CDCl_3$, 500 MHz): δ 8.08 (s, 1H), 7.35-7.32 (m, 1H), 7.23 (d, *J* = 8.0 Hz, 1H), 7.03 (d, *J* = 7.0 Hz, 1H), 4.07 (s, 3H), 3.46 (m, 1H), 2.22-2.18 (m, 2H), 1.90-1.78 (m, 6H). $^{13}$C NMR ($CDCl_3$, 125.8 MHz): δ 140.2, 140.0, 131.7, 126.3, 123.5, 116.8, 106.4, 43.6, 35.5, 33.6, 25.6. IR: ν = 2950, 2868, 1606, 1508, 1447, 1272, 1237, 982, 783, 740 $cm^{-1}$. HRMS: (ESI) m/z calc. for $C_{13}H_{17}N_2$ (M+H) 201.1392, found 201.1390.

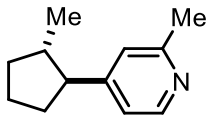


**19**

***trans*-2-Methyl-4-(2-methylcyclopentyl)pyridine (19)**: obtained as a yellow oil (62 mg, 71%). $^{1}$H NMR ($CDCl_3$, 500 MHz): δ 8.36 (d, *J* = 5.0 Hz, 1H), 6.97 (s, 1H), 6.91 (d, *J* = 5.0 Hz, 1H), 2.51 (s, 3H), 2.35 (m, 1H), 2.07-1.90 (m, 3H), 1.77-1.67 (m, 3H), 1.33-1.28 (m, 1H), 0.91 (d, *J* = 6.5 Hz, 3H). $^{13}$C NMR ($CDCl_3$, 125.8 MHz): δ 158.3, 155.1, 149.1, 122.6, 120.2, 53.9, 42.9, 34.9, 24.6, 24.1, 18.6. IR: ν = 2934, 2837, 1698, 1611, 1512, 1247, 1173, 1096, 1034, 818 $cm^{-1}$. HRMS (ESI) m/z calc. for $C_{12}H_{18}N$ (M+H) 176.1439, found 176.1439.

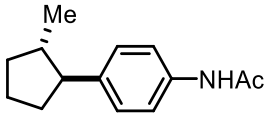


**20**

***trans*-*N*-(4-(2-Methylcyclopentyl)phenyl)acetamide (20)**: obtained as a white crystalline solid (90 mg, 83%), mp = 118-124 °C. $^{1}$H NMR ($CDCl_3$, 500 MHz): δ 7.60 (br s, 1H), 7.41 (d, *J* = 8.0 Hz, 2H), 7.14 (d, *J* = 8.0 Hz, 2H), 2.37 (q, *J* = 9.0 Hz, 1H), 2.15 (s, 3H), 2.05-1.72 (m, 6H), 1.31-1.27 (m, 1H), 0.90 (d, *J* = 6.5 Hz, 3H). $^{13}$C NMR ($CDCl_3$, 125.8 MHz): δ 168.6, 141.7, 135.8, 128.0, 120.3, 54.2, 43.2, 35.5, 34.8, 24.6, 23.9, 18.7. IR: ν = 3246, 3123, 2946, 2865, 1661, 1610, 1557, 1512, 1413, 1369, 1327, 826 $cm^{-1}$. HRMS (ESI) m/z calc. for $C_{14}H_{20}NO$ (M+H) 218.1545, found 218.1545.

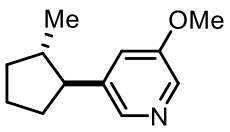


**21**

***trans*-3-Methoxy-5-(2-methylcyclopentyl)pyridine** (**21**): obtained as a yellow oil (61 mg, 64%). $^{1}$H NMR ($CDCl_3$, 500 MHz): δ 8.12 (d, *J* = 2.5 Hz, 1H), 8.07 (m, 1H), 7.02-7.01 (m, 1H), 3.84 (s, 3H), 2.43-2.38 (m, 1H), 2.09-2.07 (m, 1H), 2.00-1.98 (m, 1H), 1.94-1.89 (m, 1H), 1.76-1.69 (m, 3H), 1.31-1.29 (m, 1H), 0.91 (d, *J* = 6.5 Hz, 3H). $^{13}$C NMR ($CDCl_3$, 125.8 MHz): δ 155.8, 142.2, 141.6, 134.8, 119.6, 55.6, 51.7, 43.2, 35.3, 34.8, 24.0, 18.5. IR: ν = 2953, 2868, 1587, 1454, 1427, 1318, 1296, 1176, 1164, 1049, 867, 714 $cm^{-1}$. HRMS: (ESI) m/z calc. for $C_{12}H_{18}NO$ (M+H) 192.1388, found 192.1386.

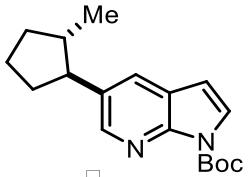


**22**

***tert*-Butyl *trans*-5-(2-methylcyclopentyl)-1H-pyrrolo[2,3-b]pyridine-1-carboxylate (22)**: obtained as a yellow oil (115 mg, 77%). $^{1}$H NMR ($CDCl_3$, 500 MHz): δ 8.34 (d, *J* = 2.0 Hz, 1H), 7.68 (d, *J* = 2.0 Hz, 1H), 7.58 (d, *J* = 4.0 Hz, 1H), 6.43 (d, *J* = 4.0Hz, 1H), 2.53-2.47 (m, 1H), 2.12-2.10 (m, 1H), 2.02-1.90 (m, 2H), 1.81-1.72 (m, 3H), 1.65 (s, 9H), 0.90 (d, *J* = 6.5 Hz, 3H). $^{13}$C NMR ($CDCl_3$, 125.8 MHz): δ 148.2, 147.4, 145.5, 135.4, 127.4, 126.7, 123.1, 104.5, 83.9, 52.0, 43.6, 35.7, 34.8, 28.3, 23.9, 18.4. IR: ν = 2951, 2868, 1757, 1728, 1532, 1472, 1398, 1356, 1318, 1253, 1145, 1092, 730 $cm^{-1}$. HRMS (ESI) m/z calc. for $C_{19}H_{25}N_2O_2$ (M+H) 301.1916, found 301.1905.

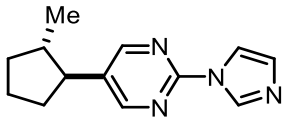


**23**

***trans*-2-(1H-Imidazol-1-yl)-5-(2-methylcyclopentyl)pyrimidine** (**23)**: obtained as a dark yellow oil (79 mg, 69%). $^{1}$H NMR ($CDCl_3$, 500 MHz): δ 8.63 (s, 1H), 8.52 (s, 2H), 7.88 (s, 1H), 7.17 (s, 1H), 2.48-2.42 (m, 1H), 2.20-2.13 (s, 1H), 2.10-2.03 (m, 1H), 1.98-1.92 (m, 1H), 1.87-1.71 (m, 3H), 1.42-1.34 (m, 1H), 0.98 (d, *J* = 6.5 Hz, 3H).$^{13}$C NMR ($CDCl_3$, 125.8 MHz): δ 159.4, 157.6, 136.0, 135.6, 130.3, 116.4, 48.9, 43.0, 34.7, 34.4, 23.6, 18.2. IR: ν = 3127, 2947, 2866, 1568, 1477, 1450, 1314, 1097, 931, 795, 754, 651 $cm^{-1}$. HRMS (ESI) m/z calc. for $C_{13}H_{17}N_4$ (M+H) 229.1453, found 229.1453.

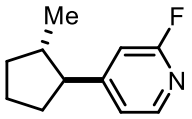


**24**

***trans*-2-Fluoro-4-(2-methylcyclopentyl)pyridine** (**24)**: obtained as a pale yellow oil (70 mg, 78%). $^{1}$H NMR ($CDCl_3$, 500 MHz): δ 8.09 (d, *J* = 5.0 Hz, 1H), 7.01-6.99 (m, 1H), 6.75 (s, 1H), 2.49-2.43 (m, 1H), 2.15-2.08 (m, 1H), 2.04-1.89 (m, 2H), 1.83-1.65 (m, 3H), 1.37-1.29 (m, 1H), 0.94 (d, *J* = 6.5 Hz, 3H). $^{13}$C NMR ($CDCl_3$, 125.8 MHz): δ 164.1 (d, *J* = 237.7 Hz), 160.9 (d, *J* = 7.4 Hz), 147.2 (d, *J* = 15.4 Hz), 120.6 (d, *J* = 3.6 Hz), 108.0 (d, *J* =36.6 Hz), 53.6 (d, *J* = 2.6 Hz), 42.9, 34.7, 34.6, 23.9, 18.3.IR: ν = 2953, 2869, 1610, 1563, 1482, 1414, 1273, 996, 974, 832 $cm^{-1}$ HRMS (ESI) m/z calc. for $C_{11}H_{15}NF$ (M+H) 180.1189, found 180.1189.

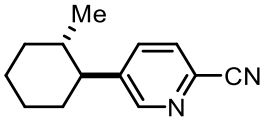


**25**

***trans*-5-(2-Methylcyclohexyl)picolinonitrile (25)**: Reaction was run on 0.40 mmol scale; obtained as a pale yellow oil (68 mg, 85%). $^{1}$H NMR ($CDCl_3$, 500 MHz): δ 8.52 (s, 1H), 7.63-7.59 (m, 2H), 2.22-2.17 (m, 1H), 1.87-1.77 (m, 4H), 1.62-1.58 (m, 1H), 1.44-1.33 (m, 3H), 1.15-1.10 (m, 1H), 0.65 (d, *J* = 6.5 Hz, 3H). $^{13}$C NMR ($CDCl_3$, 125.8 MHz): δ 151.3, 146.5, 135.6, 131.6, 128.5, 117.6, 50.1, 37.5, 35.5, 35.2, 26.6, 26.4, 20.7. IR: ν = 2925, 2854, 2234, 1566, 1470, 1024, 845, 652, 632 $cm^{-1}$. HRMS (ESI) m/z calc. for $C_{13}H_{17}N_2$ (M+H) 201.1392, found 201.1385.

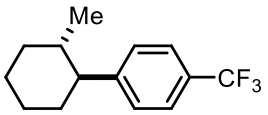


**26**

***trans*-1-(2-Methylcyclohexyl)-4-(trifluoromethyl)benzene (26)**: obtained as a colorless oil (90 mg, 74%). $^{1}$H NMR ($CDCl_3$, 500 MHz): δ 7.53 (d, *J* = 8.0 Hz, 2H), 7.26 (d, *J* = 8.0 Hz, 2H), 2.17-2.12 (m, 1H), 1.82-177 (m, 4H), 1.61-1.57 (m, 1H), 1.45-1.35 (m, 3H), 1.13-1.10 (m, 1H), 0.65 (d, *J* = 6.5 Hz, 3H). $^{13}$C NMR ($CDCl_3$, 125.8 MHz): δ 151.1, 128.2 (q, *J* = 32.1 Hz), 128.0, 125.3 (q, *J* = 3.9 Hz), 124.6 (q, *J* = 271.6 Hz), 52.6, 37.7, 35.7, 35.6, 26.9, 26.7, 20.8. $^{19}$F NMR ($CDCl_3$, 470 MHz): δ -62.2. IR: ν = 2928, 2858, 1618, 1325, 1163, 1124, 1069, 1020, 830 $cm^{-1}$. HRMS (ESI) m/z calc. for $C_{14}H_{17}F_3$ (M+) 242.1282, found 242.1283.

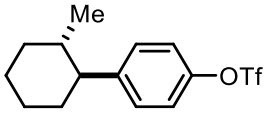


**27**

***trans*-4-(2-Methylcyclohexyl)phenyl trifluoromethanesulfonate (27)**: obtained as a colorless oil (120 mg, 75%). $^{1}$H NMR ($CDCl_3$, 500 MHz): δ 7.22 (d, *J* = 8.5 Hz, 2H), 7.17 (d, *J* = 8.5 Hz, 2H), 2.14-2.09 (m, 1H), 1.85-1.78 (m, 4H), 1.60-1.53 (m, 1H), 1.44-1.35 (m, 3H), 1.13-1.06 (m, 1H), 0.65 (d, *J* = 6.5 Hz, 3H). $^{13}$C NMR ($CDCl_3$, 125.8 MHz): δ 147.5, 147.3, 129.0, 120.9, 118.7 (q, *J* = 320.7 Hz), 51.8, 37.6, 35.5, 35.4, 26.7, 26.4, 20.5. $^{19}$F NMR ($CDCl_3$, 470 MHz): δ -72.9. IR: ν =

3339, 2970, 2929, 1426, 1379, 1213, 1142, 1131, 952, 883, 817 $cm^{-1}$. HRMS (ESI) m/z calc. for $C_{14}H_{16}O_3F_3S$ (M-H) 321.0772, found 321.0787.

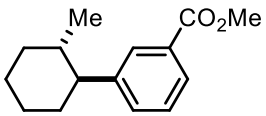


**28**

***trans*-Methyl 3-(2-methylcyclohexyl)benzoate (28)**: obtained as a colorless oil (100 mg, 86%). $^1H$ NMR ($CDCl_3$, 500 MHz): δ 7.87-7.86 (m, 2H), 7.36-7.34 (m, 2H), 3.92 (s, 3H), 2.17-2.15 (m, 1H), 2.13-1.80 (m, 4H), 1.64-1.62 (m, 1H), 1.51-1.28 (m, 3H), 1.14-1.06 (m, 1H), 0.66 (d, *J* = 6.5 Hz, 3H). $^{13}C$ NMR ($CDCl_3$, 125.8 MHz): δ 167.3, 147.1, 132.2, 130.0, 128.5, 128.2, 127.0, 52.3, 51.9, 37.5, 35.6, 35.5, 26.8, 26.5, 20.6. IR: ν = 2923, 2852, 1723, 1445, 1432, 1285, 1196, 1107, 1086, 752, 698 $cm^{-1}$. HRMS (ESI) m/z calc. for $C_{15}H_{21}O_2$ (M+H) 233.1542, found 233.1553.

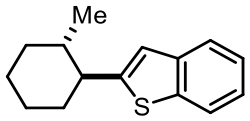


**29**

***trans*-2-(2-Methylcyclohexyl)benzo[b]thiophene (29)**: obtained as a colorless crystal (73 mg, 63%). $^1H$ NMR ($CDCl_3$, 500 MHz): δ 7.78 (d, *J* = 8.0 Hz, 1H), 7.67 (d, *J* = 8.0 Hz, 1H), 7.33-7.24 (m, 2H), 7.01 (s, 1H), 2.52-2.47 (m, 1H), 2.02 (dd, *J* = 3.0, 1.0 Hz, 1H), 1.85-1.78 (m, 3H), 1.60-1.36 (m, 4H), 1.15-1.13 (m, 1H), 0.83 (d, *J* = 6.5 Hz, 3H). $^{13}C$ NMR ($CDCl_3$, 125.8 MHz): δ 152.1, 140.1, 139.0, 124.1, 123.4, 122.8, 122.4, 119.8, 48.4, 39.3, 36.8, 35.7, 26.9, 26.5, 21.0

IR: ν = 2923, 2851, 1445, 1443, 1309, 1128, 819, 744, 655, 636 $cm^{-1}$. HRMS (ESI) m/z calc. for $C_{15}H_{19}S$ (M+H) 231.1207, found 231.1208.

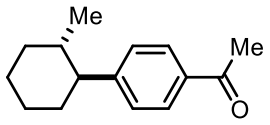


30

***trans*-1-(4-(2-Methylcyclohexyl)phenyl)ethan-1-one (30)**: obtained as a colorless oil (89 mg, 82%).$^{1}$H NMR ($CDCl_3$, 500 MHz): δ 7.78-7.77 (m, 2H), 7.38-7.37 (m, 2H), 2.61 (s, 3H), 2.19-2.14 (m, 1H), 1.86-1.78 (m, 4H), 1.65-1.62 (m, 1H), 1.49-1.27 (m, 3H), 1.14-1.08 (m, 1H), 0.66 (d, *J* = 6.5 Hz, 3H). $^{13}$C NMR ($CDCl_3$, 125.8 MHz): δ 198.4, 147.4, 137.1, 132.4, 128.4, 127.1, 126.0, 52.3, 37.5, 35.6, 35.5, 26.8, 26.6, 26.5, 20.6.IR: ν = 2922, 2853, 1685, 1600, 1444, 1359, 1266, 1229, 1186, 799, 698 $cm^{-1}$. HRMS (ESI) m/z calc. for $C_{15}H_{21}O$ (M+H) 217.1592, found 217.1586.

## 4.5 References

(1) Miyaura, N.; Ishiyama, T.; Sasaki, H.; Ishikawa, M.; Satoh, M.; Suzuki, A. *J. Am. Chem. Soc*. **1989**, *111*, 314.

(2) Trends in organoboron transmetalation rate mirror that observed for the corresponding alkylstannanes as shown in reference 3

(3) Labadie, J. W.; Stille, J. K. *J. Am. Chem. Soc.* **1983**, *105*, 6129.

(4) Han, C.; Buchwald, S. L. *J. Am. Chem. Soc.* **2009**, *131*, 7532.

(5) Pompeo, M.; Froese, R. D. J.; Hadei, N.; Organ, M. G. *Angew. Chem. Int. Ed.* **2012**, *51*, 11354.

(6) Hayashi, T.; Konishi, M.; Kobori, Y.; Makoto, K.; Taiichi, H.; Hirotsu, K. *J. Am. Chem. Soc*. **1984**, *106*, 158.

(7) Vila, C.; Giannerini, M.; Hornillos, V.; Fañanás-Mastral, M.; Feringa, B. L. *Chem. Sci.* **2014**, *5*, 1361.

(8) Sandrock, D. L.; Jean-Gerard, L.; Chen, C.; Dreher, S. D.; Molander, G. A. *J. Am. Chem. Soc*. **2010**, *132*, 17108.

(9) Endo, K.; Ohkubo, T.; Hirokami, M.; Shibata, T. *J. Am. Chem. Soc.* **2010**, *132*, 11033.

(10) Molander, G. A.; Wisniewski, S. R. *J. Am. Chem. Soc.* **2012**, *134*, 16856.

(11) Imao, D.; Glasspoole, B. W.; Laberge, S.; Crudden, C. M. *J. Am. Chem. Soc.* **2009**, 5024.

(12) Ohmura, T.; Awano, T.; Suginome, M. *J. Am. Chem. Soc.* **2010**, *132*, 13191.

(13) Glasspoole, B. W.; Ghozati, K.; Moir, J. W.; Crudden, C. M. *Chem. Commun.* **2012**, *48*, 1230.

(14) Leonori, D.; Aggarwal, V. K. *Angew. Chem. Int. Ed.* **2014**, *53*, 2.

(15) Littke, A. F.; Dai, C.; Fu, G. C. *J. Am. Chem. Soc.* **2000**, *122*, 4020.

(16) Kataoka, N.; Shelby, Q.; Stambuli, J. P.; Hartwig, J. F. *J. Org. Chem.* **2002**, *67*, 5553.

(17) van den Hoogenband, A.; Lange, J. H. M.; Terpstra, J. W.; Koch, M.; Visser, G. M.; Visser, M.; Korstanje, T. J.; Jastrzebski, J. T. B. H. *Tetrahedron Lett.* **2008**, *49*, 4122.

(18) Dreher, S. D.; Dormer, P. G.; Sandrock, D. L.; Molander, G. A. *J. Am. Chem. Soc.* **2008**, *130*, 9257.

(19) Li, L.; Zhao, S.; Joshi-Pangu, A.; Diane, M.; Biscoe, M. R. *J. Am. Chem. Soc.* **2014**, *136*, 14027.

(20) Lennox, A. J. J.; Lloyd-Jones, G. C. *Angew. Chem. Int. Ed.* **2013**, *52*, 7362.

(21) Schultz, D. M.; Yoon, T. P. *Science.* **2014**, *343*, 985.

(22) Hopkinson, M. N.; Sahoo, B.; Li, J.-L.; Glorius, F. *Chem. Eur. J.* **2014**, *20*, 3874.

(23) Breitenfeld, J.; Ruiz, J.; Wodrich, M. D.; Hu, X. *J. Am. Chem. Soc.* **2013**, *135*, 12004.

(24) Yasu, Y.; Koike, T.; Akita, M. *Adv. Synth. Catal.* **2012**, *354*, 3414.

(25) Koike, T.; Akita, M. *Inorg. Chem. Front.* **2014**, *1*, 562.

(26) Shih, H.-W.; Vander Wal, M. N.; Grange, R. L.; MacMillan, D. W. C. *J. Am. Chem. Soc.* **2010**, *132*, 13600.

(27) Giese, B. *Radicals in Organic Synthesis: Formation of Carbon-Carbon Bonds*: Pergamon Press Ltd., 1986.

(28) For example, in tetrahydrofuran as solvent, coupling at the carbon alpha to oxygen was observed alongside the desired alkyl cross-coupling product.

(29) Hallen, R. T.; Gleicher, G. J.; Mahiou, B.; Clapp, G. E. *J. Phys. Org. Chem.* **1989**, *2*, 367.

(30) Molander, G. A.; Gormisky, P. E. *J. Org. Chem.* **2008**, *73*, 7481.

(31) Welsch, M. E.; Snyder, S. A.; Stockwell, B. R. *Curr. Opin. Chem. Biol.* **2010**, *14*, 347.

(32) Zuo, Z.; Ahneman, D.; Chu, L.; Terrett, J.; Doyle, A. G.; MacMillan, D. W. C. *Science* **2014**, *345*, 437.

(33) Tellis, J. C.; Primer, D. N.; Molander, G. A. *Science* **2014**, *345*, 433.

(34) Bruno, N. C.; Niljianskul, N.; Buchwald, S. L. *J. Org. Chem.* **2014**, 79, 4161.

(35) Martin, R.; Buchwald, S. L. *Acc. Chem. Res.* **2008**, *41*, 1461.

(36) Tasker, S. Z.; Standley, E. A.; Jamison, T. F. *Nature* **2014**, *509*, 299.

(37) Binder, J. T.; Cordier, C. J.; Fu, G. C. *J. Am. Chem. Soc.* **2012**, *134*, 17003.

(38) Matteson, D. S. *Tetrahedron* **1998**, *54*, 10555.

(39) Brown, H. C.; Bakthan, S. *Acc. Chem. Res.* **1988**, *21*, 287.

(40) Larouche-Gauthier, R.; Fletcher, C. J.; Couto, I.; Aggarwal, V. K. *Chem. Commun.* **2011**, *47*, 12592.

(41) Liu, Z.; Dong, N.; Xu, M.; Sun, Z.; Tu, T. *J. Org. Chem.* **2013**, *78*, 7436.

(42) Phapale, V. B.; Guisán-Ceinos, M.; Buñuel, E.; Cárdenas, D. J. *Chem. A Eur. J.* **2009**, *15*, 12681.

(43) Zhu, Y.; Yan, H.; Lu, L.; Liu, D.; Rong, G.; Mao, J. *J. Org. Chem.* **2013**, *78*, 9898.

**Author Contributions:**

D.N.P. participated in the conception and design of the project, wrote and edited the manuscript, optimized the reaction, and prepared most of the compounds in this study. Idris Karakaya prepared some of the compounds. John C. Tellis assisted in the conception and design of the project. John C. Tellis also edited the manuscript.

# Appendix A3. $^{1}H$, $^{13}C$, $^{11}B$, and $^{19}F$ NMR Spectra Relevant to Chapter 4

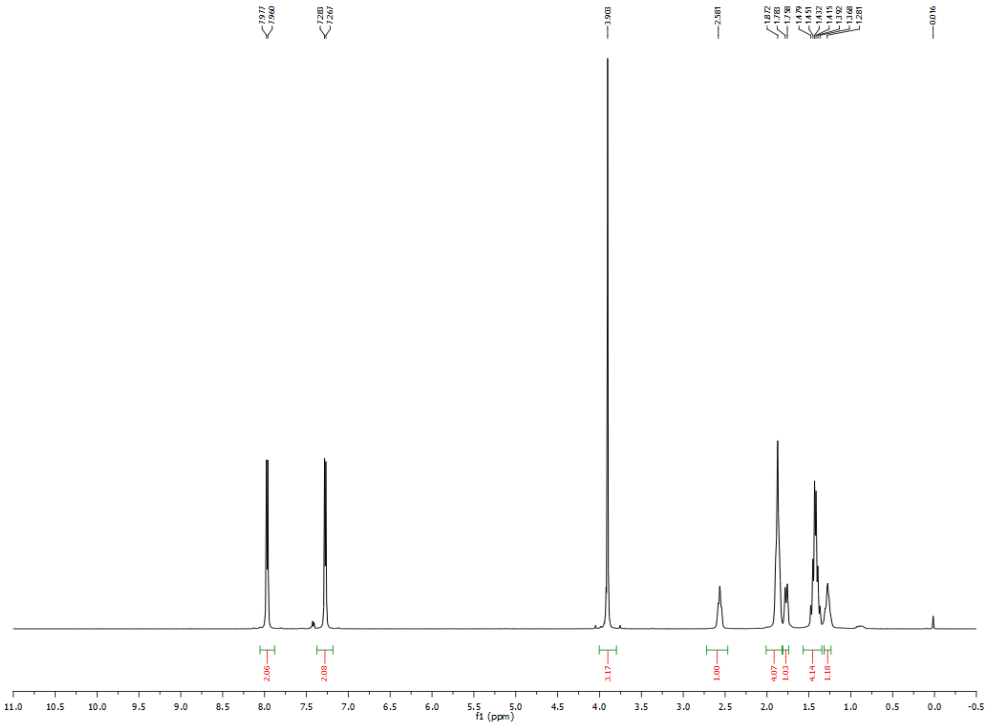

**Figure A3.1.** $^{1}$H NMR ($CDCl_3$, 500 MHz) spectrum of methyl 4-cyclohexylbenzoate (**2**)

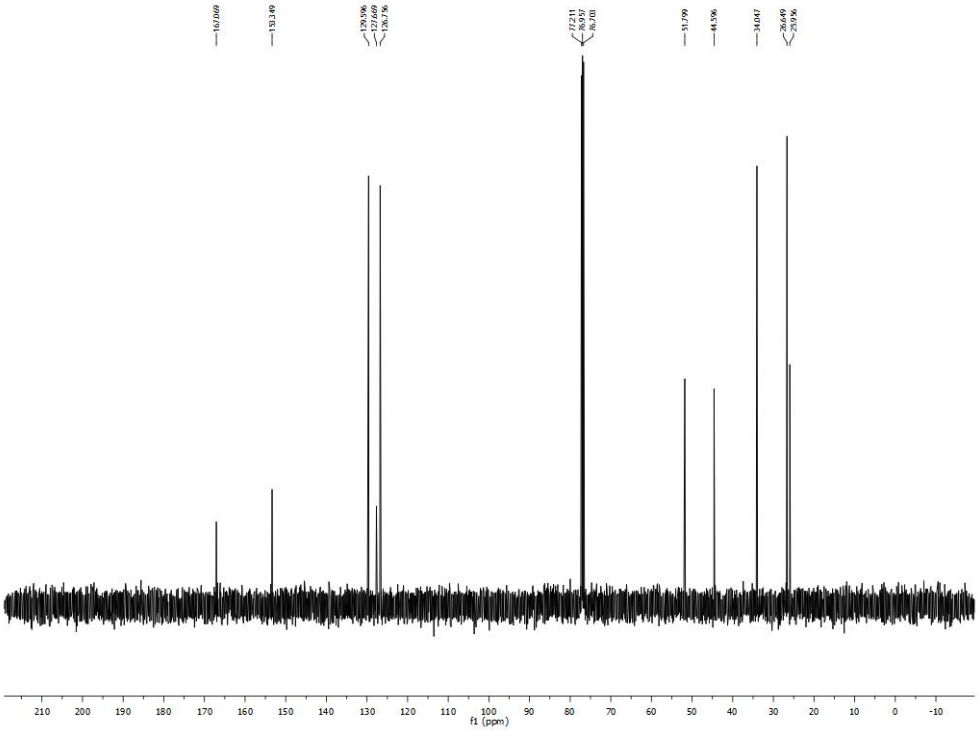

**Figure A3.2.** $^{13}$C NMR ($CDCl_3$, 125.8 MHz) spectrum of methyl 4-cyclohexylbenzoate (**2**)

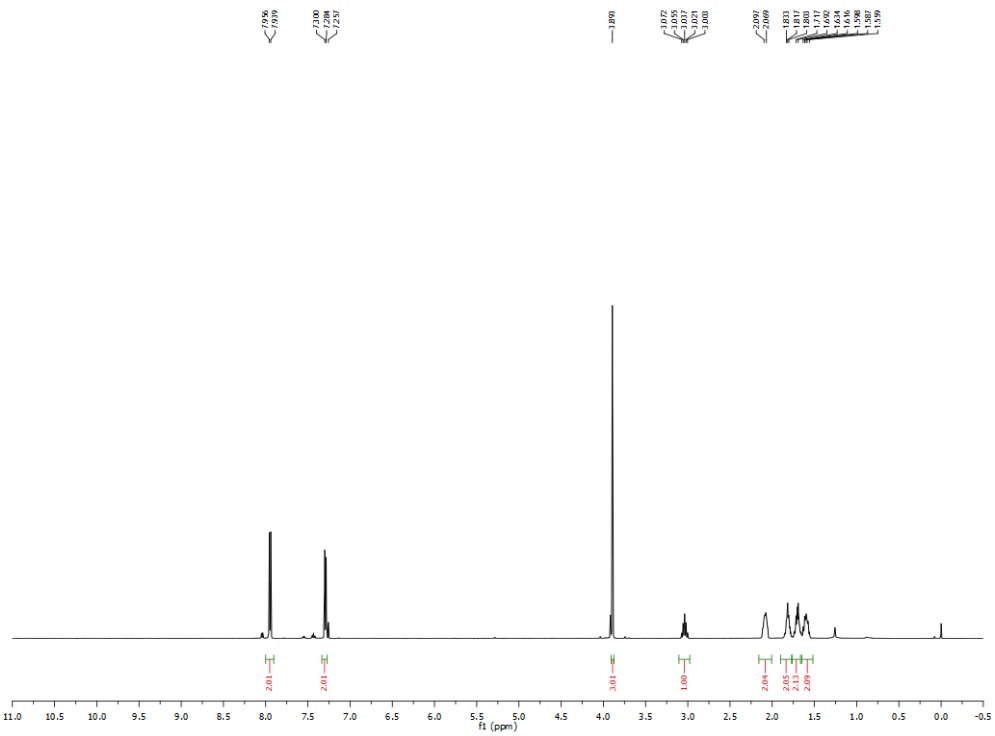

**Figure A3.3.** $^{1}H$ NMR ($CDCl_3$, 500 MHz) spectrum of methyl 4-cyclopentylbenzoate (**3**)

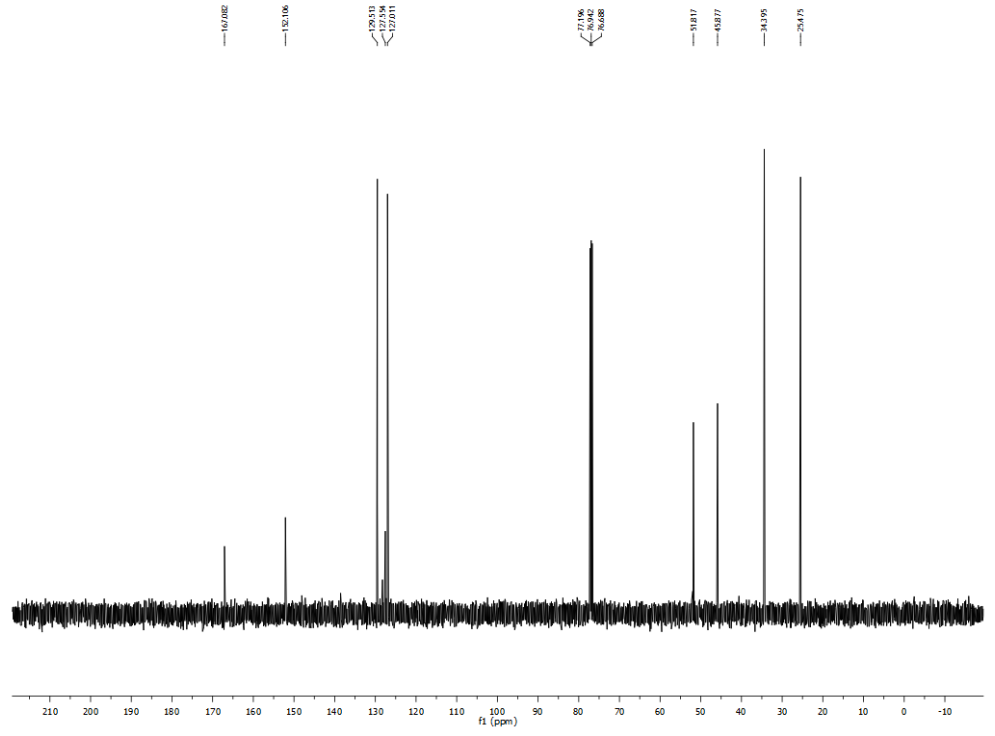

**Figure A3.4.** $^{13}C$ NMR ($CDCl_3$, 125.8 MHz) spectrum of methyl 4-cyclopentylbenzoate (**3**)

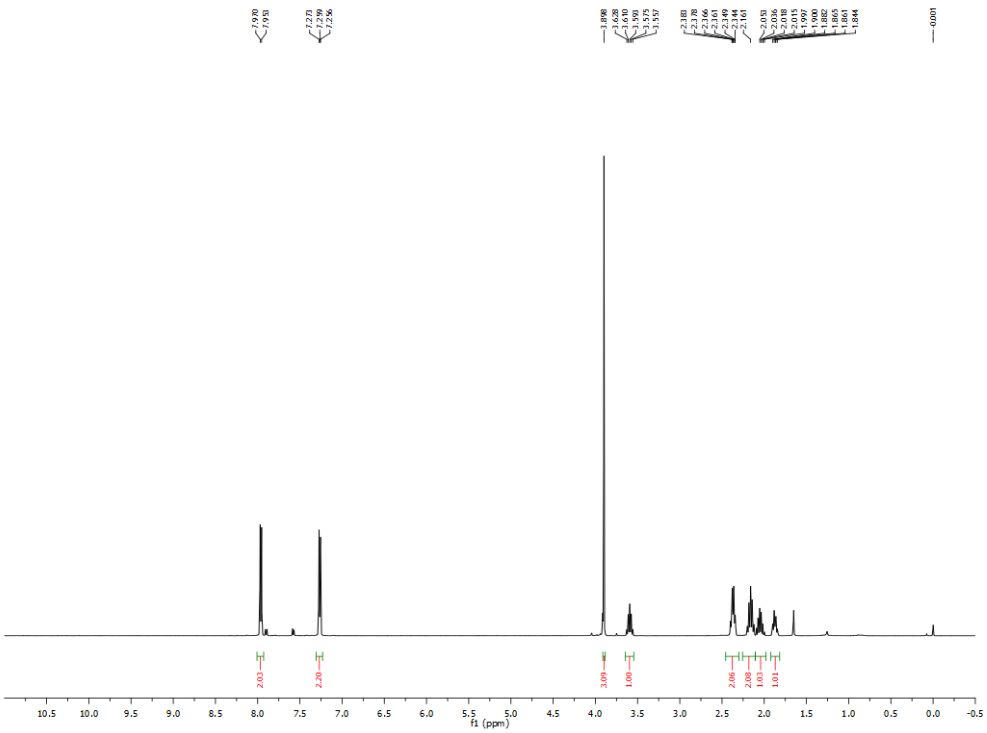

**Figure A3.5.** $^{1}$H NMR ($CDCl_3$, 500 MHz) spectrum of methyl 4-cyclobutybenzoate (**4**)

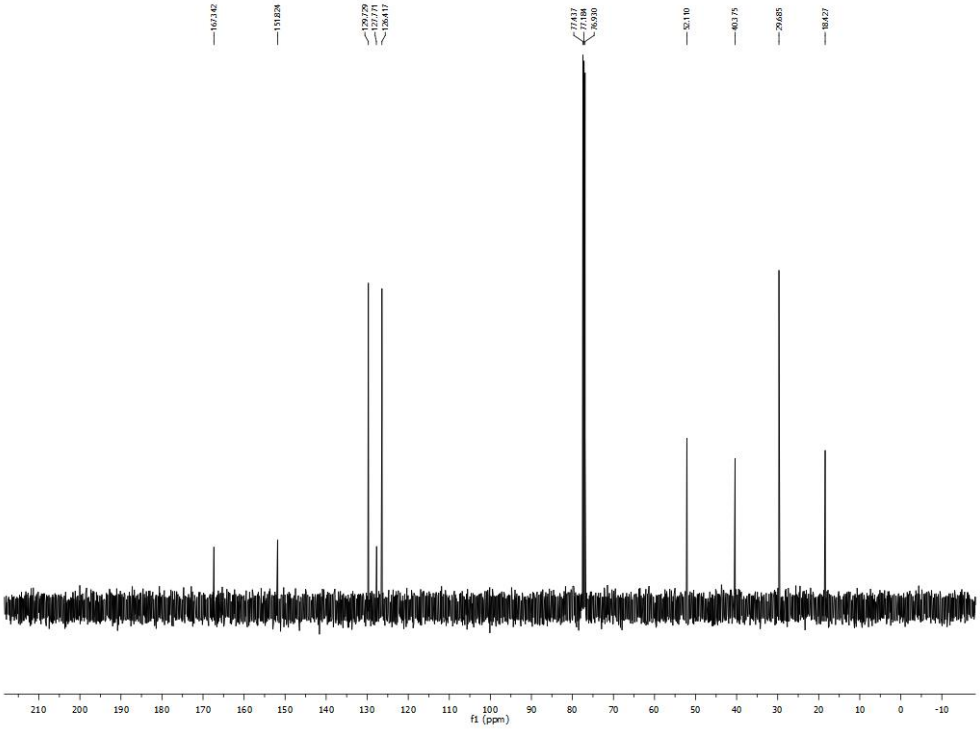

**Figure A3.6.** $^{13}$C NMR ($CDCl_3$, 125.8 MHz) spectrum of methyl 4-cyclobutybenzoate (**4**)

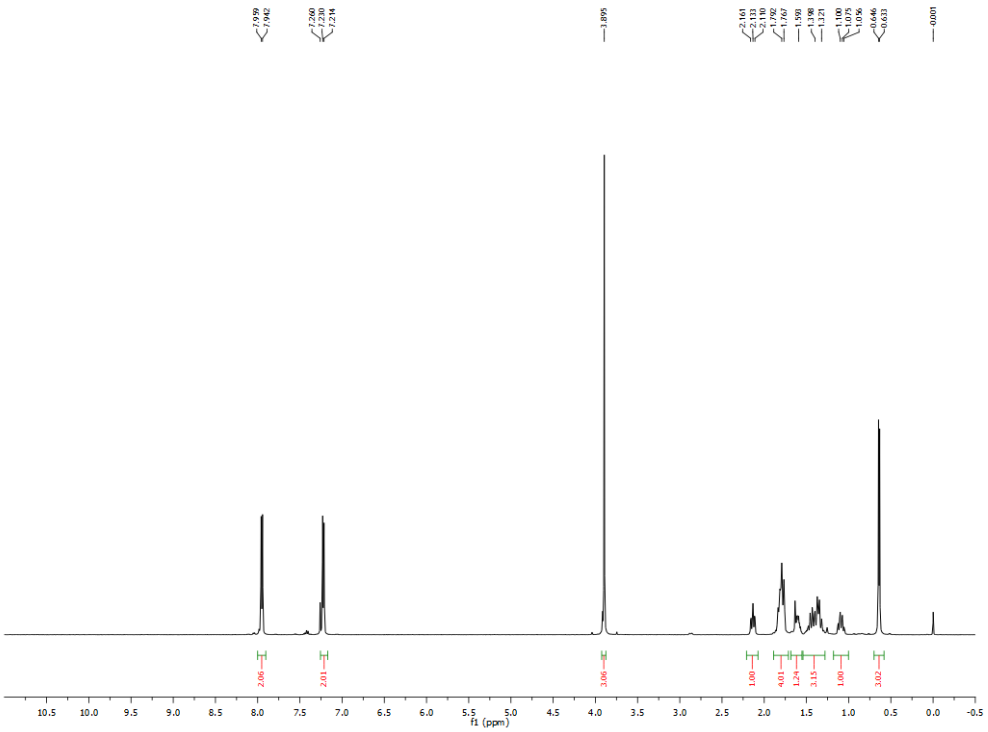

**Figure A3.7.** $^{1}$H NMR ($CDCl_3$, 500 MHz) spectrum of methyl 4-(2-methylcyclohexyl)benzoate (**6**)

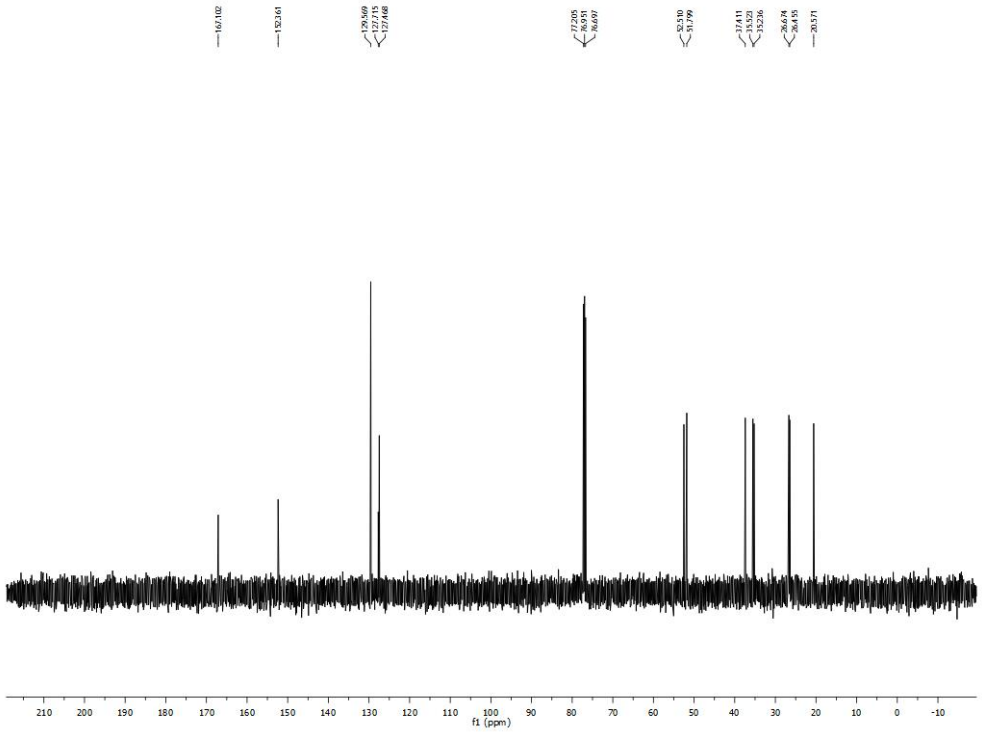

**Figure A3.8.** $^{13}$C NMR ($CDCl_3$, 125.8 MHz) spectrum of methyl 4-(2-methylcyclohexyl)benzoate (**6**)

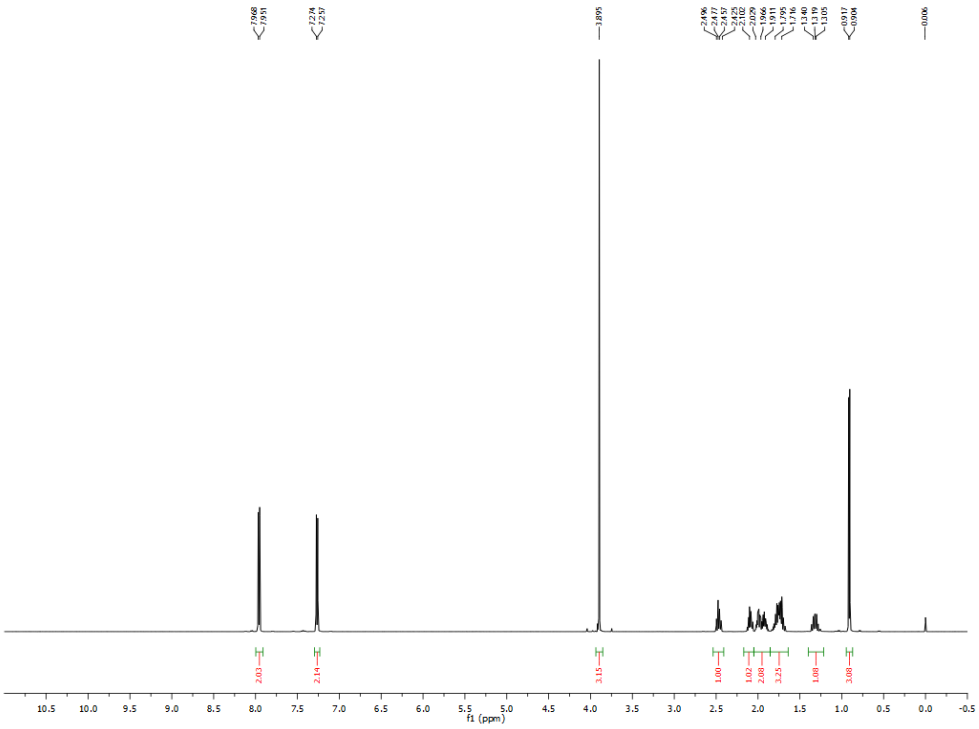

**Figure A3.9.** $^{1}$H NMR ($CDCl_3$, 500 MHz) spectrum of methyl 4-(2-methylcyclopentyl)benzoate (**7**)

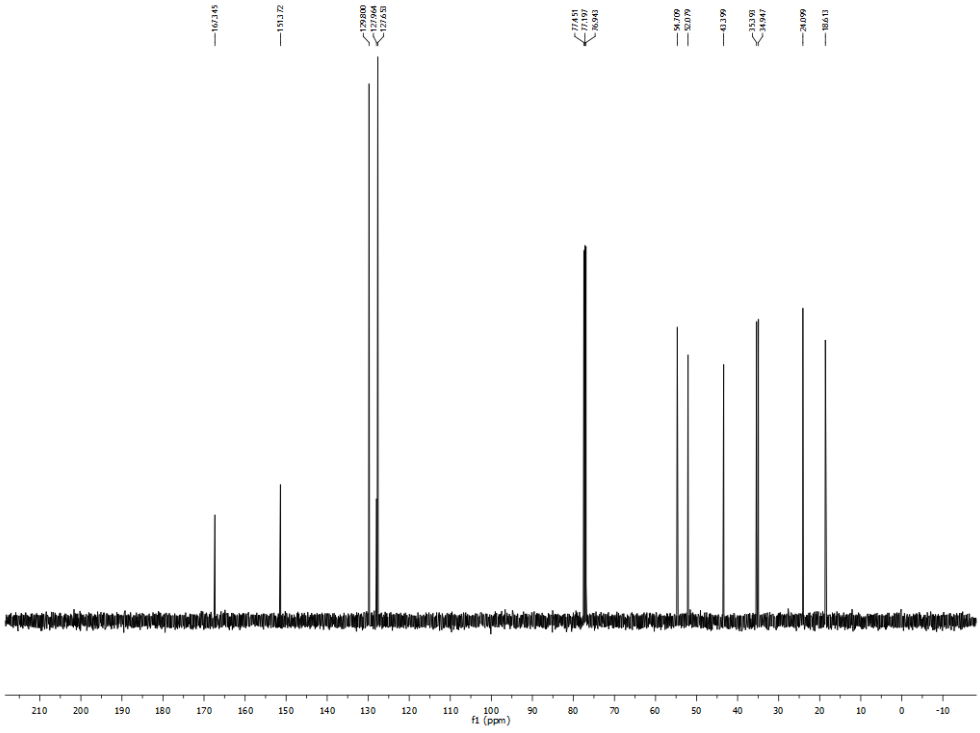

**Figure A3.10.** $^{13}$C NMR ($CDCl_3$, 125.8 MHz) spectrum of methyl 4-(2-methylcyclopentyl)benzoate (**7**)

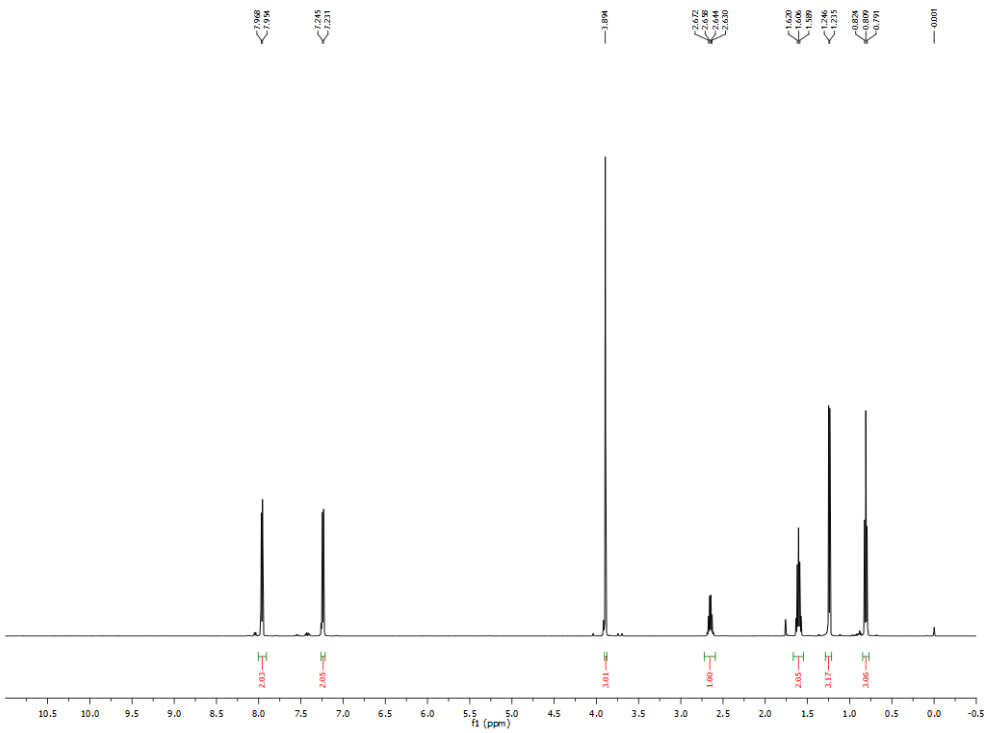

**Figure A3.11.** $^{1}$H NMR ($CDCl_3$, 500 MHz) spectrum of methyl 4-(sec-butyl)benzoate (**8**)

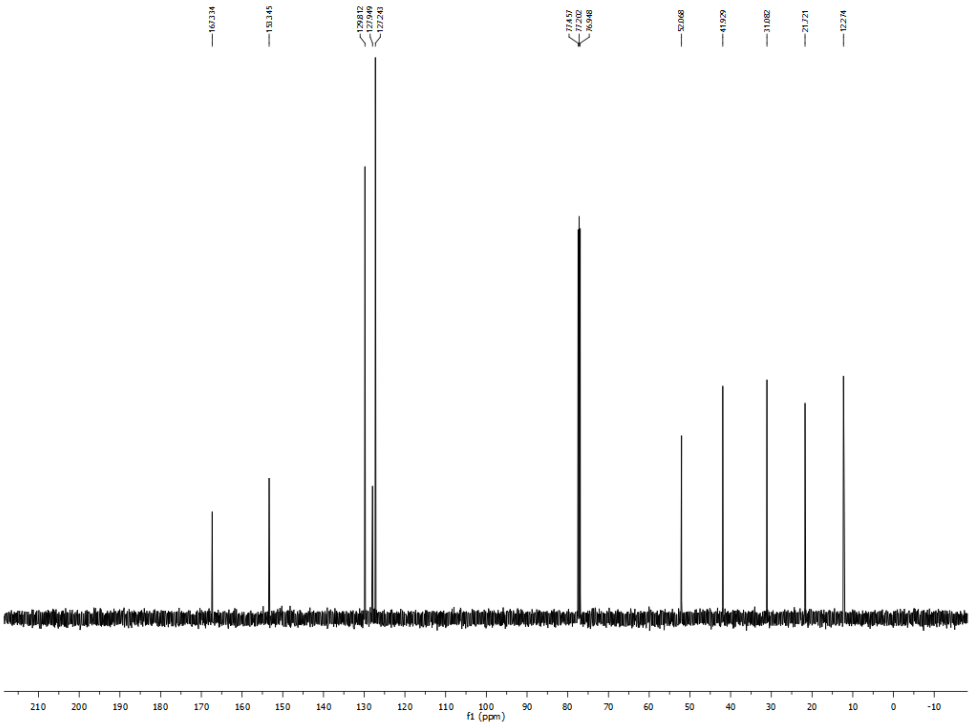

**Figure A3.12.** $^{13}$C NMR ($CDCl_3$, 125.8 MHz) spectrum of methyl 4-(sec-butyl)benzoate (**8**)

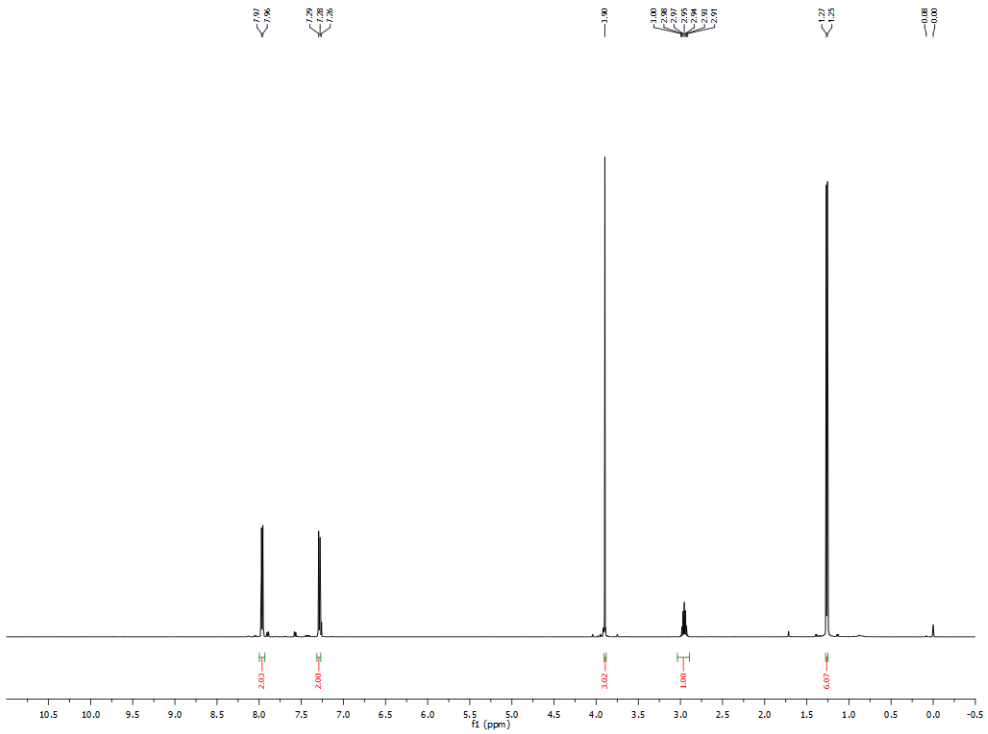

**Figure A3.13.** $^{1}$H NMR ($CDCl_3$, 500 MHz) spectrum of methyl 4-isopropylbenzoate (**9**)

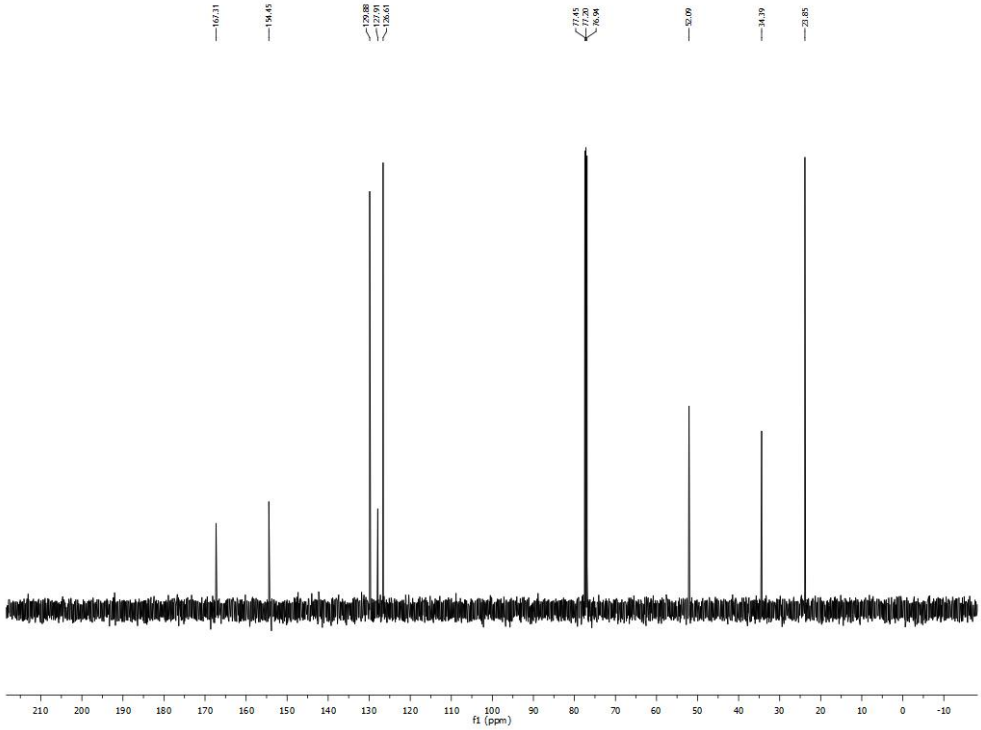

**Figure A3.14.** $^{13}$C NMR ($CDCl_3$, 125.8 MHz) spectrum of methyl 4-isopropylbenzoate (**9**)

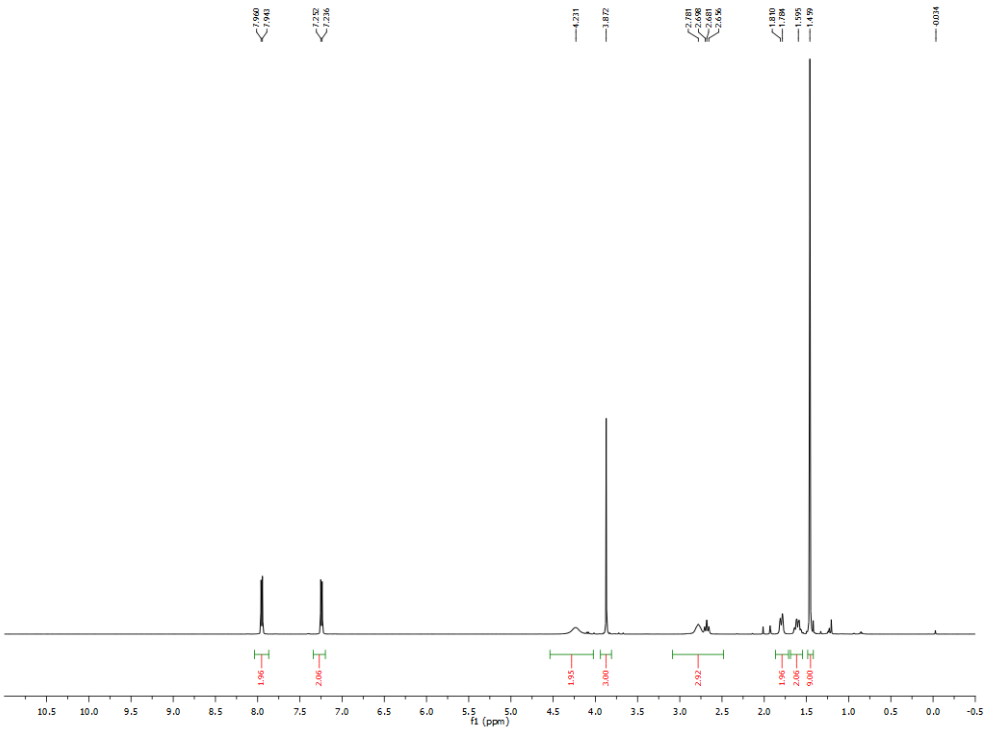

**Figure A3.15.** $^{1}$H NMR ($CDCl_3$, 500 MHz) spectrum of *tert*-butyl 4-(4-(methoxycarbonyl)phenyl)piperidine-1-carboxylate (**10**)

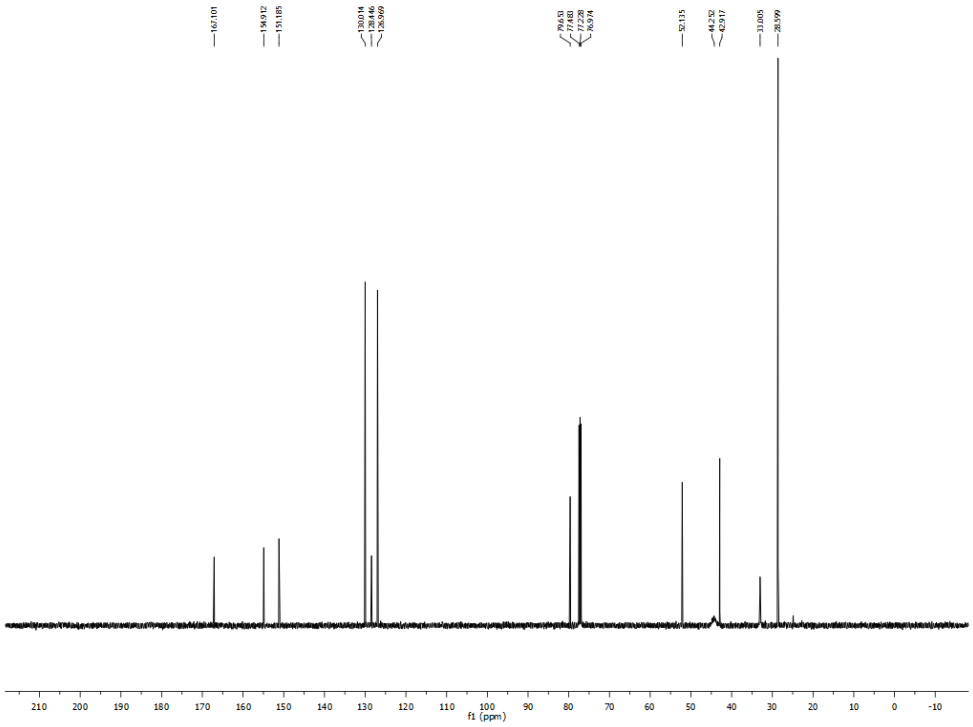

**Figure A3.16.** $^{13}$C NMR ($CDCl_3$, 125.8 MHz) spectrum of *tert*-butyl 4-(4-(methoxycarbonyl)phenyl)piperidine-1-carboxylate (**10**)

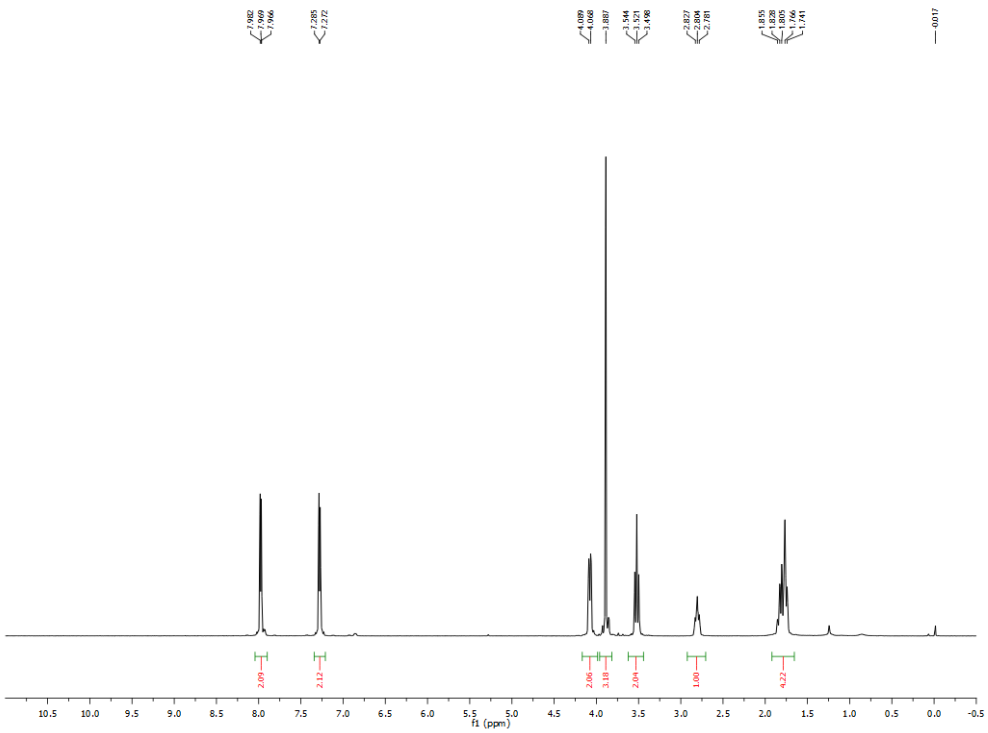

**Figure A3.17.** $^{1}$H NMR ($CDCl_3$, 500 MHz) spectrum of methyl 4-(tetrahydro-2H-pyran-4-yl)benzoate (**11**)

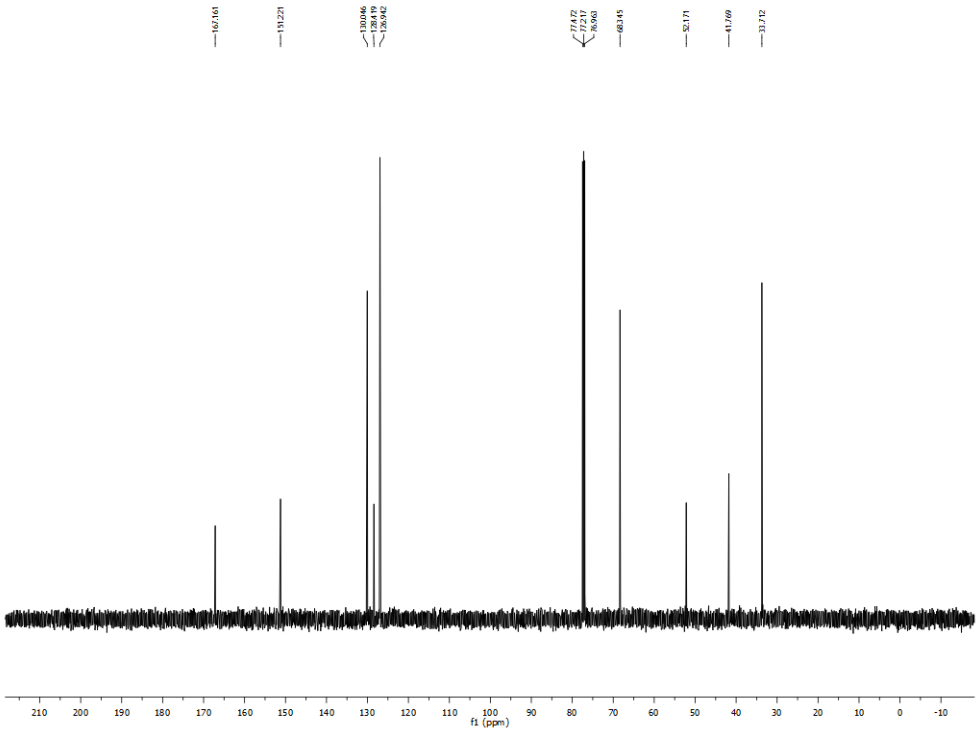

**Figure A3.18.** $^{13}$C NMR ($CDCl_3$, 125.8 MHz) spectrum of methyl 4-(tetrahydro-2H-pyran-4-yl)benzoate (**11**)

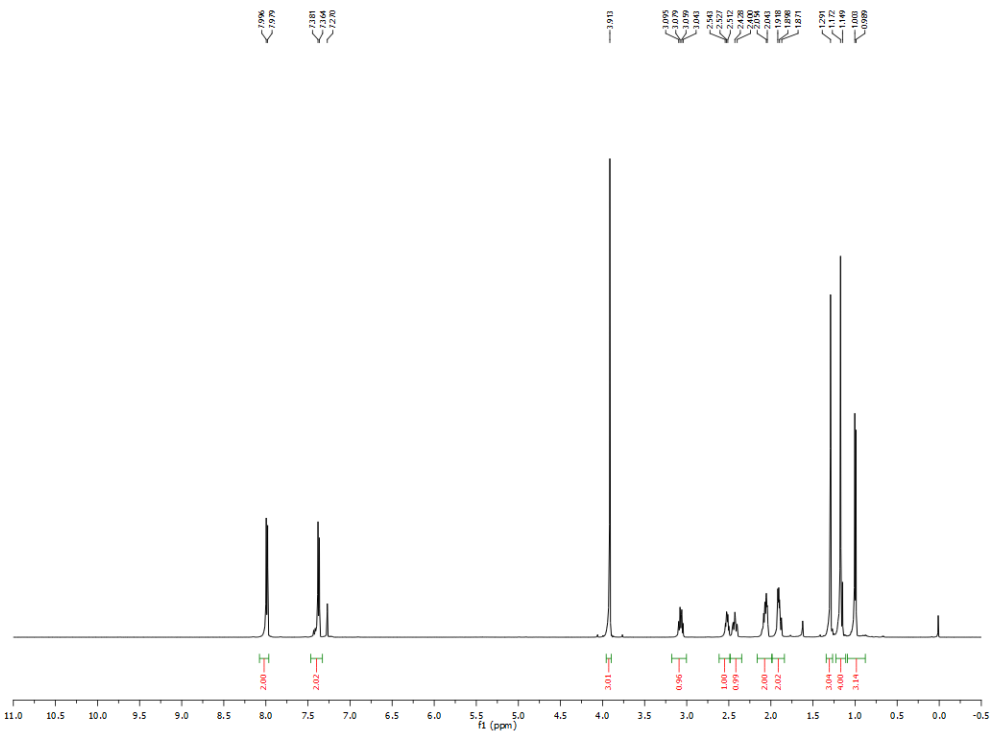

**Figure A3.19.** $^{1}$H NMR ($CDCl_3$, 500 MHz) spectrum of methyl 4-((3,6,6-trimethylbicyclo[3.1.1]heptan-2-yl)benzoate (**12**)

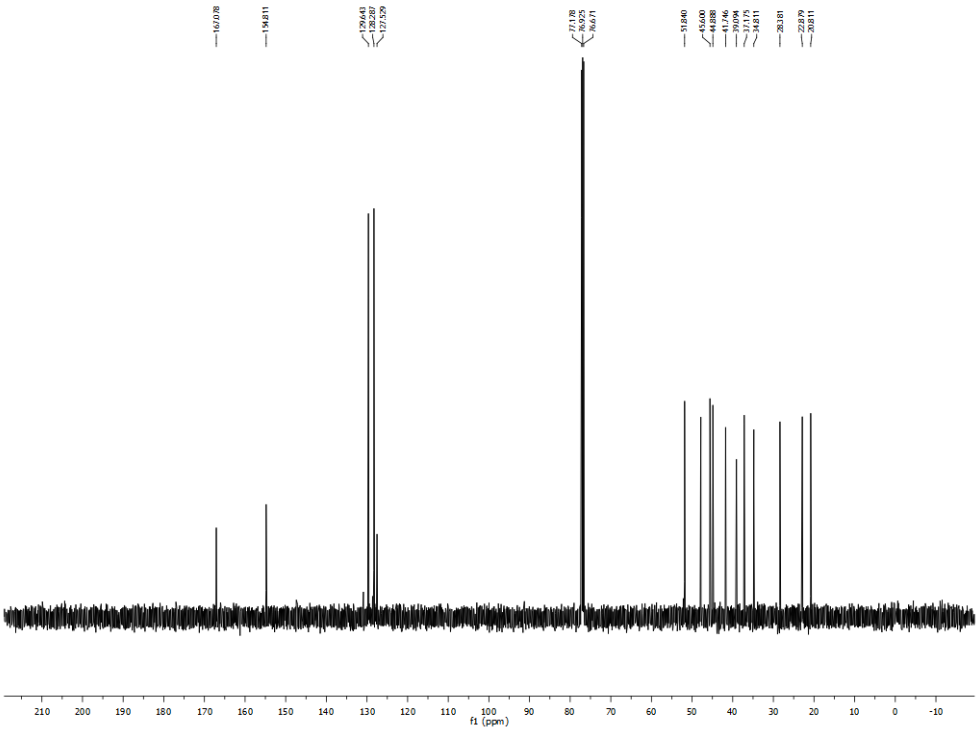

**Figure A3.20.** $^{13}$C NMR ($CDCl_3$, 125.8 MHz) spectrum of methyl 4-((3,6,6-trimethylbicyclo[3.1.1]heptan-2-yl)benzoate (**12**)

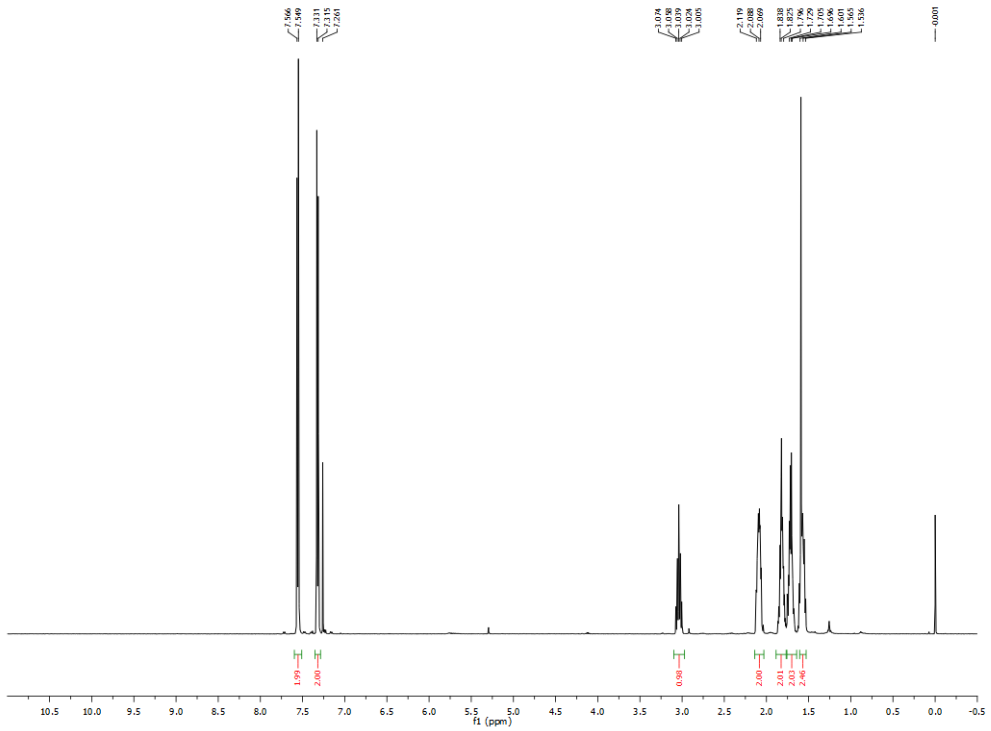

**Figure A3.21.** $^{1}$H NMR ($CDCl_3$, 500 MHz) spectrum of 4-cyclopentylbenzonitrile (**13**)

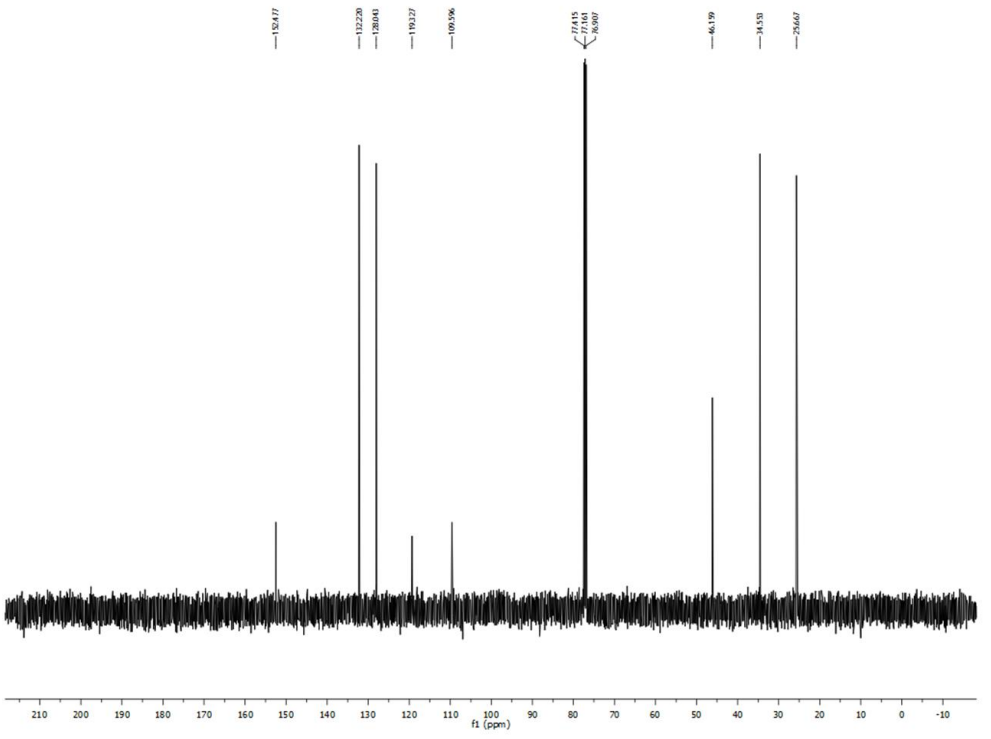

**Figure A3.22.** $^{13}$C NMR ($CDCl_3$, 125.8 MHz) spectrum of 4-cyclopentylbenzonitrile (**13**)

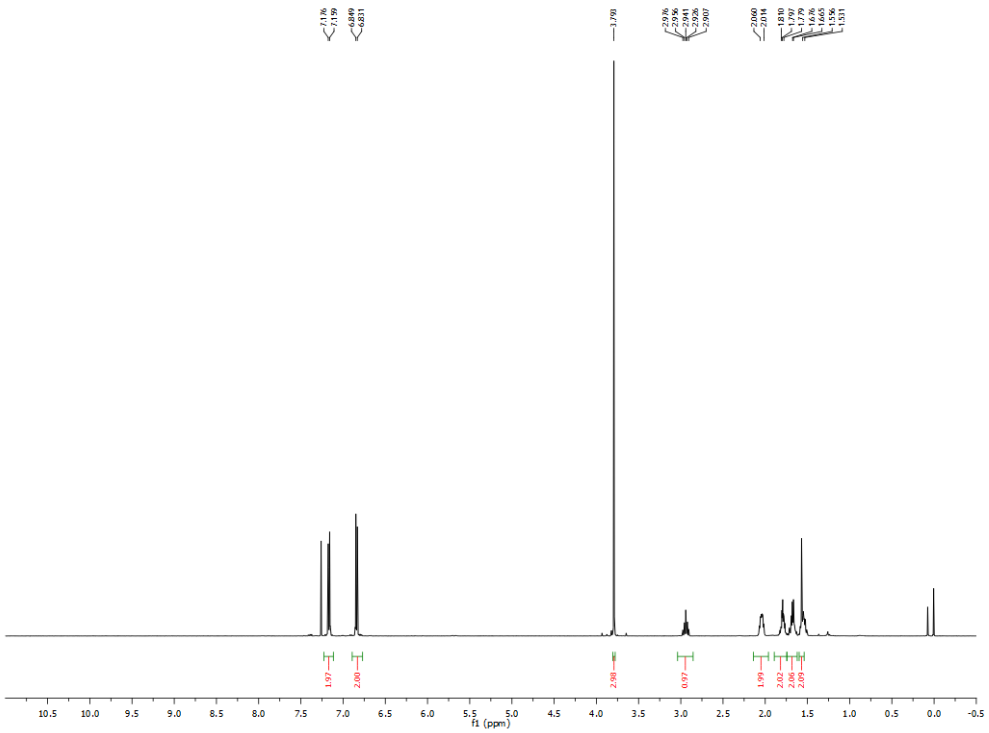


**Figure A3.23.** $^{1}$H NMR ($CDCl_3$, 500 MHz) spectrum of 1-cyclopentyl-4-methoxybenzene (**14**)

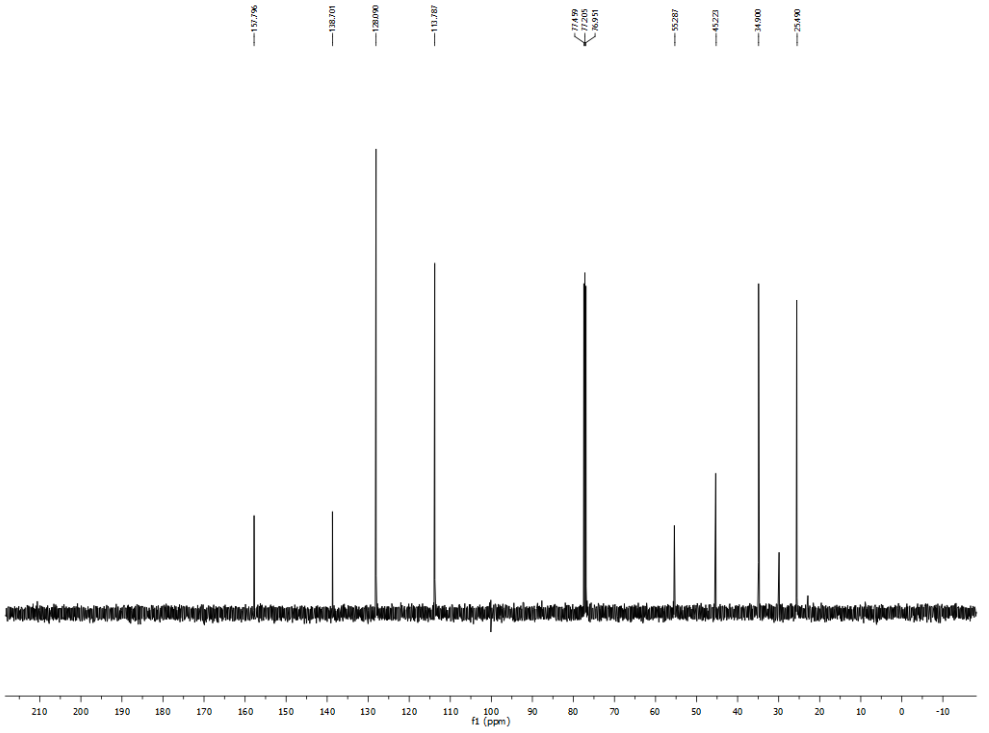


**Figure A3.24.** $^{13}$C NMR ($CDCl_3$, 125.8 MHz) spectrum of 1-cyclopentyl-4-methoxybenzene (**14**)

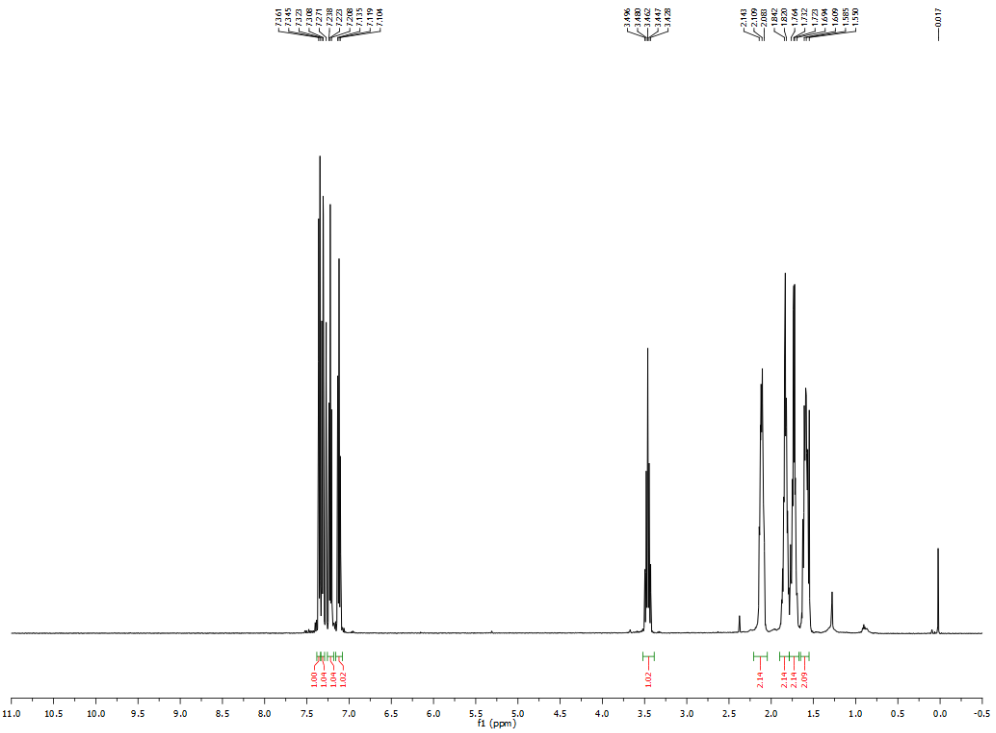

**Figure A3.25.** $^{1}$H NMR ($CDCl_3$, 500 MHz) spectrum of 1-chloro-2-cyclopentylbenzene (**15**)

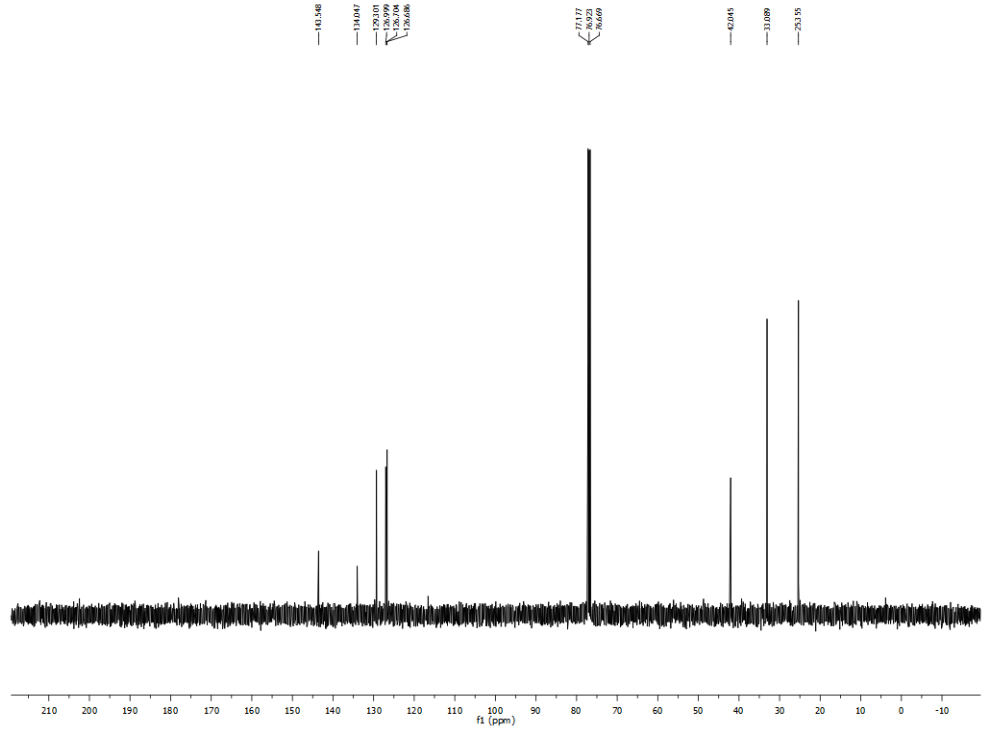

**Figure A3.26.** $^{13}$C NMR ($CDCl_3$, 125.8 MHz) spectrum of 1-chloro-2-cyclopentylbenzene (**15**)

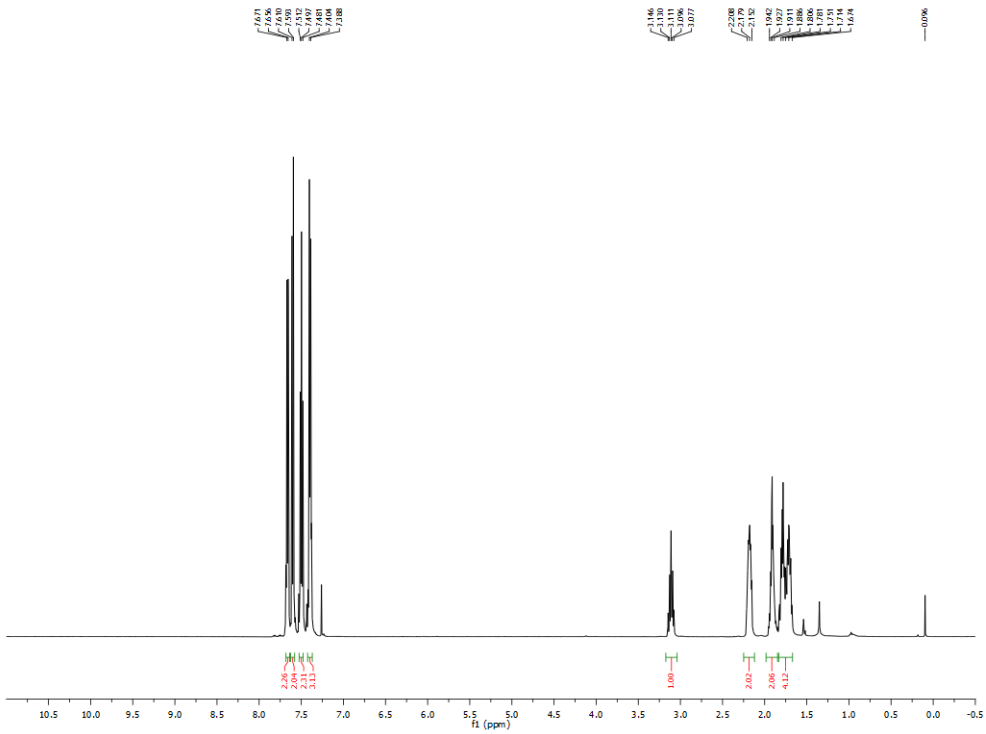

**Figure A3.27.** $^{1}$H NMR ($CDCl_3$, 500 MHz) spectrum of 4-cyclopentyl-1,1'-biphenyl (**16**)

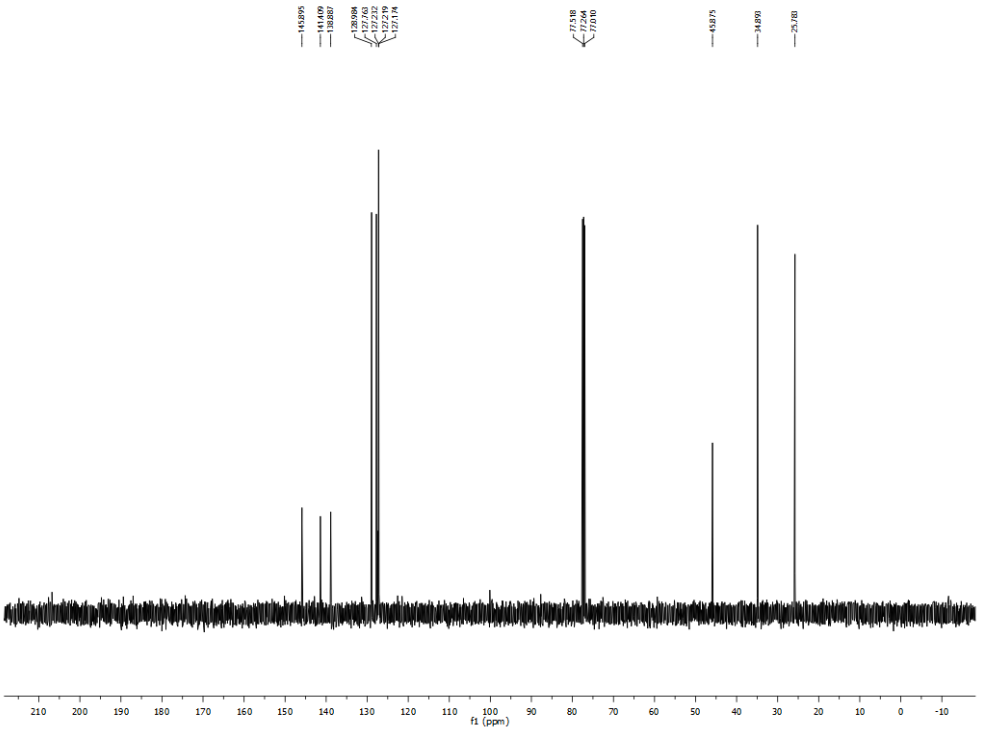

**Figure A3.28.** $^{13}$C NMR ($CDCl_3$, 125.8 MHz) spectrum of 4-cyclopentyl-1,1'-biphenyl (**16**)

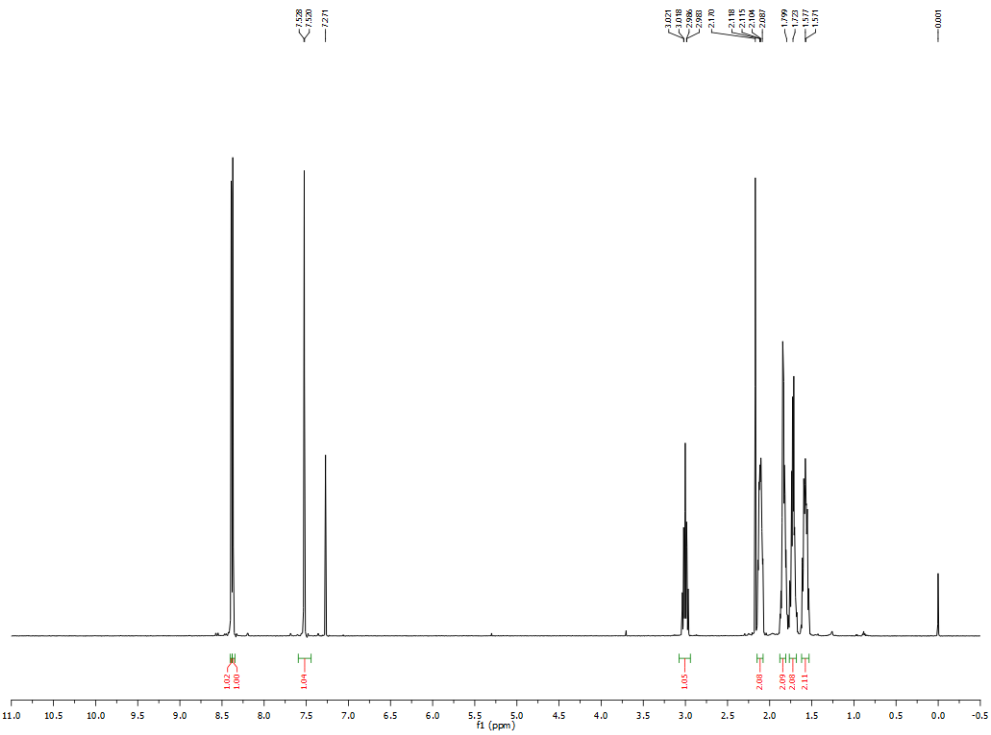

**Figure A3.29.** $^{1}$H NMR ($CDCl_3$, 500 MHz) spectrum of 3-chloro-5-cyclopentylpyridine (**17**)

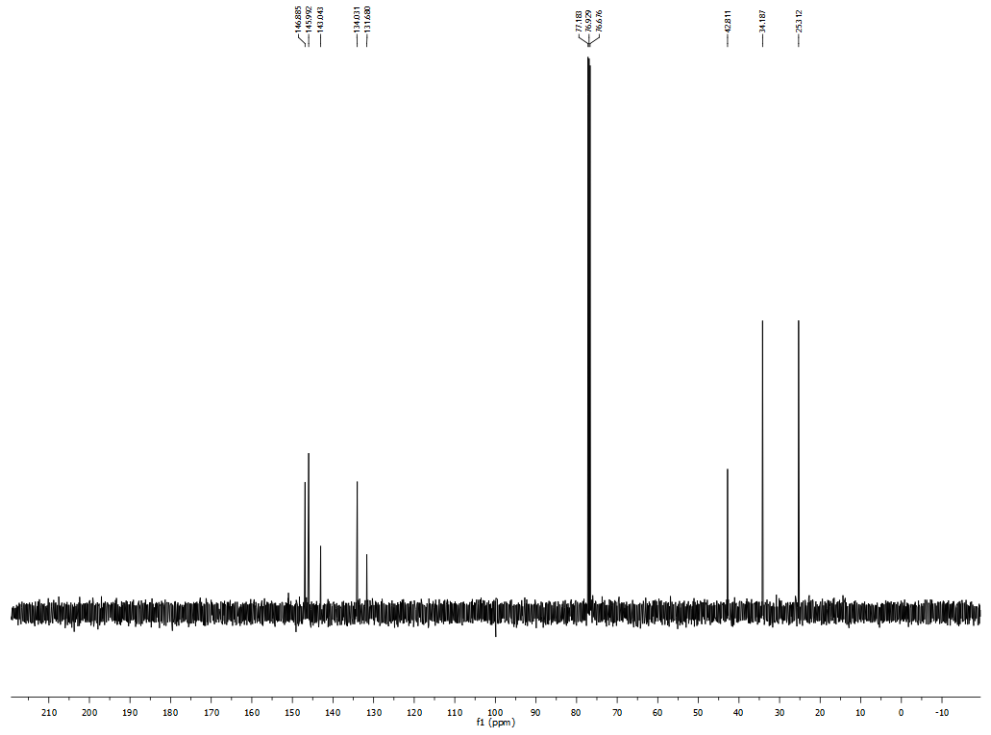

**Figure A3.30.** $^{13}$C NMR ($CDCl_3$, 125.8 MHz) spectrum of 3-chloro-5-cyclopentylpyridine (**17**)

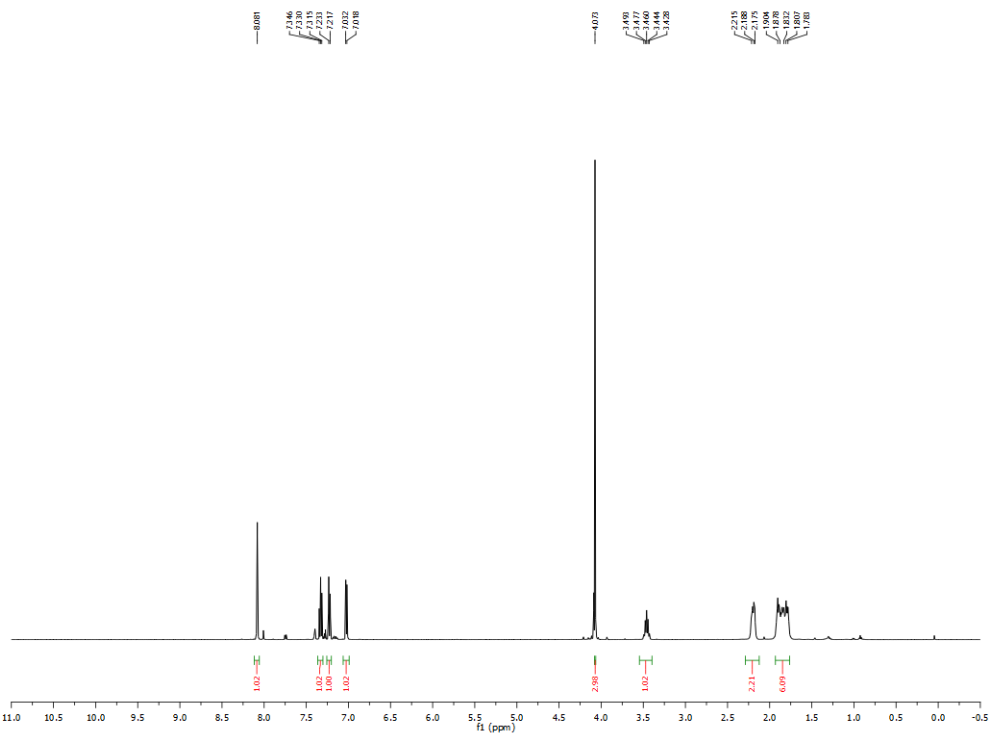

**Figure A3.31.** $^{1}$H NMR ($CDCl_3$, 500 MHz) spectrum of 7-cyclopentyl-1-methyl-1H-indazole (**18**)

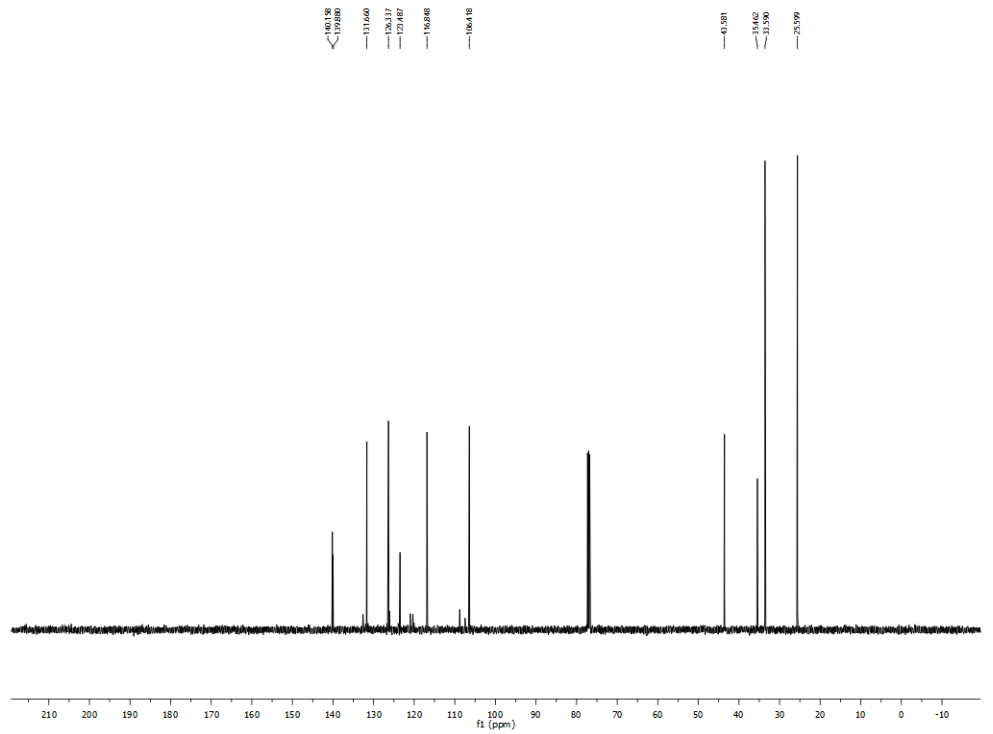

**Figure A3.32.** $^{13}$C NMR ($CDCl_3$, 125.8 MHz) spectrum of 7-cyclopentyl-1-methyl-1H-indazole (**18**)

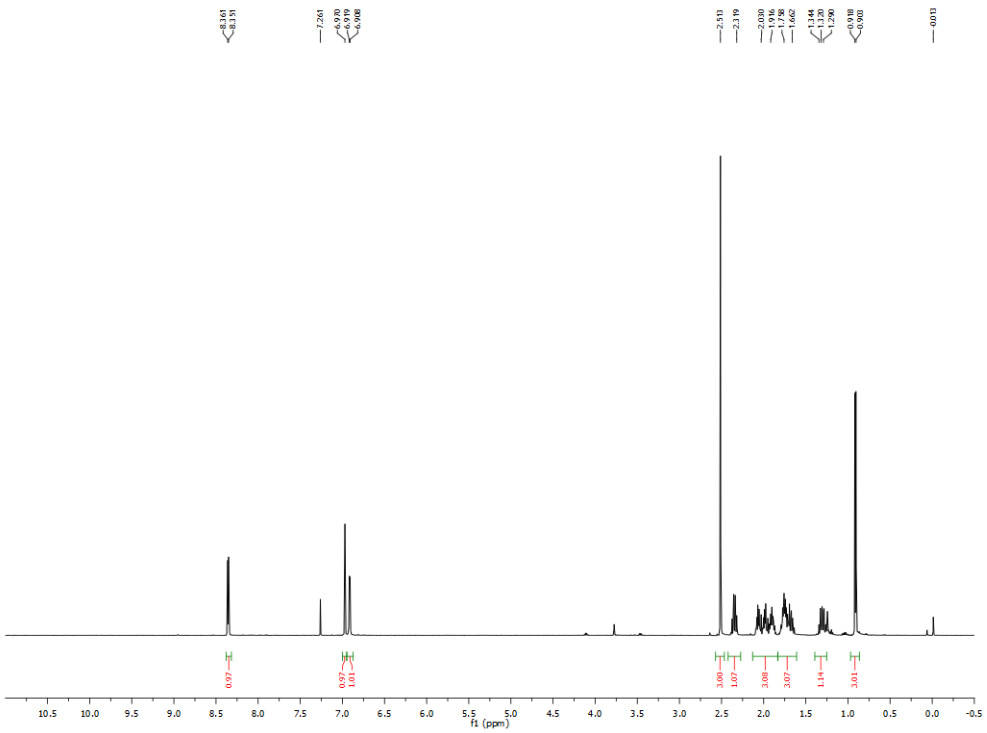

**Figure A3.33.** $^{1}$H NMR ($CDCl_3$, 500 MHz) spectrum of (±)-*trans*-2-methyl-4-(2-methylcyclopentyl)pyridine (**19**)

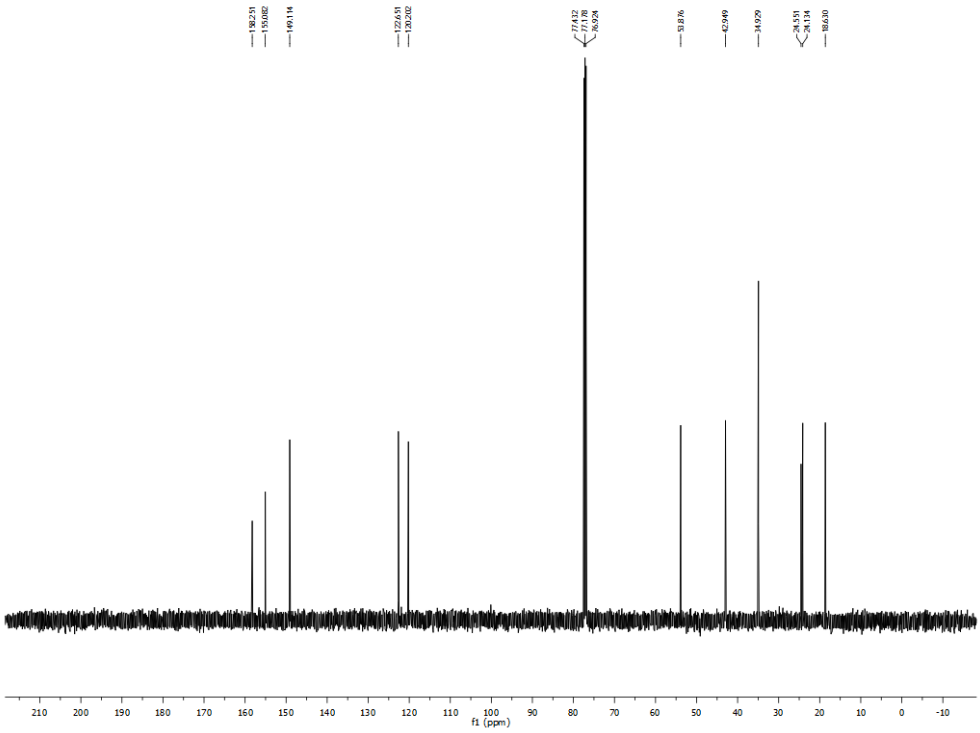

**Figure A3.34.** $^{13}$C NMR ($CDCl_3$, 125.8 MHz) spectrum of (±)-*trans*-2-methyl-4-(2-methylcyclopentyl)pyridine (**19**)

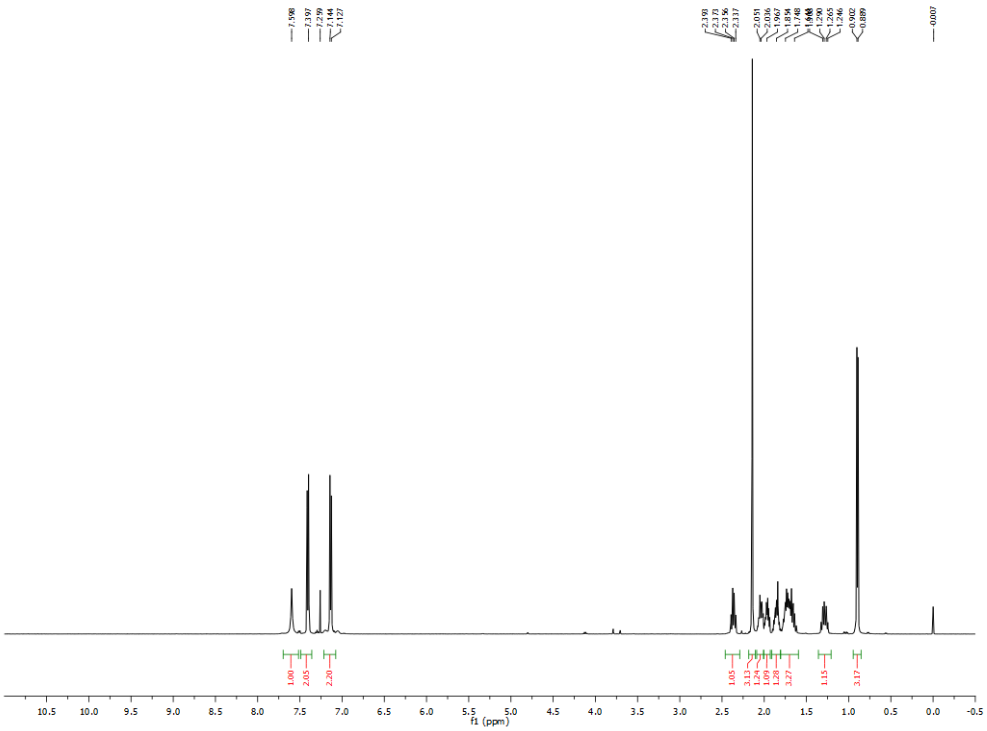

**Figure A3.35.** $^{1}$H NMR ($CDCl_3$, 500 MHz) spectrum of (±)-*trans* -N-(4-(2-methylcyclopentyl)phenyl)acetamide (**20**)

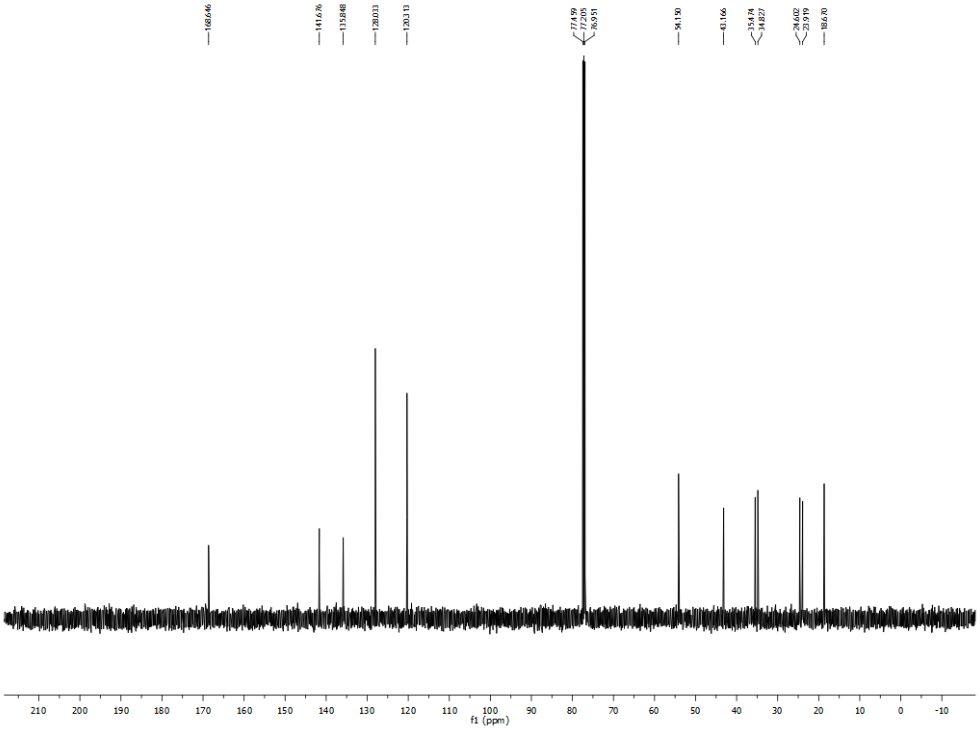

**Figure A3.36.** $^{13}$C NMR ($CDCl_3$, 125.8 MHz) spectrum of (±)-*trans* -N-(4-(2-methylcyclopentyl)phenyl)acetamide (**20**)

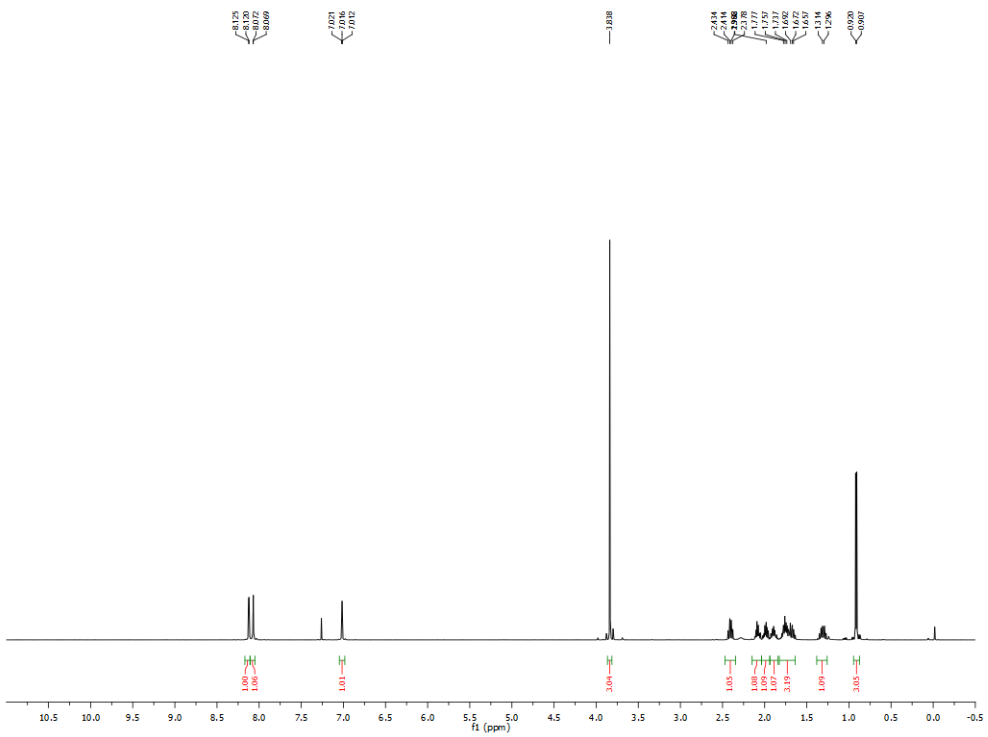

**Figure A3.37.** $^{1}$H NMR ($CDCl_3$, 500 MHz) spectrum of (±)-*trans*-3-methoxy-5-(2-methylcyclopentyl)pyridine (**21**)

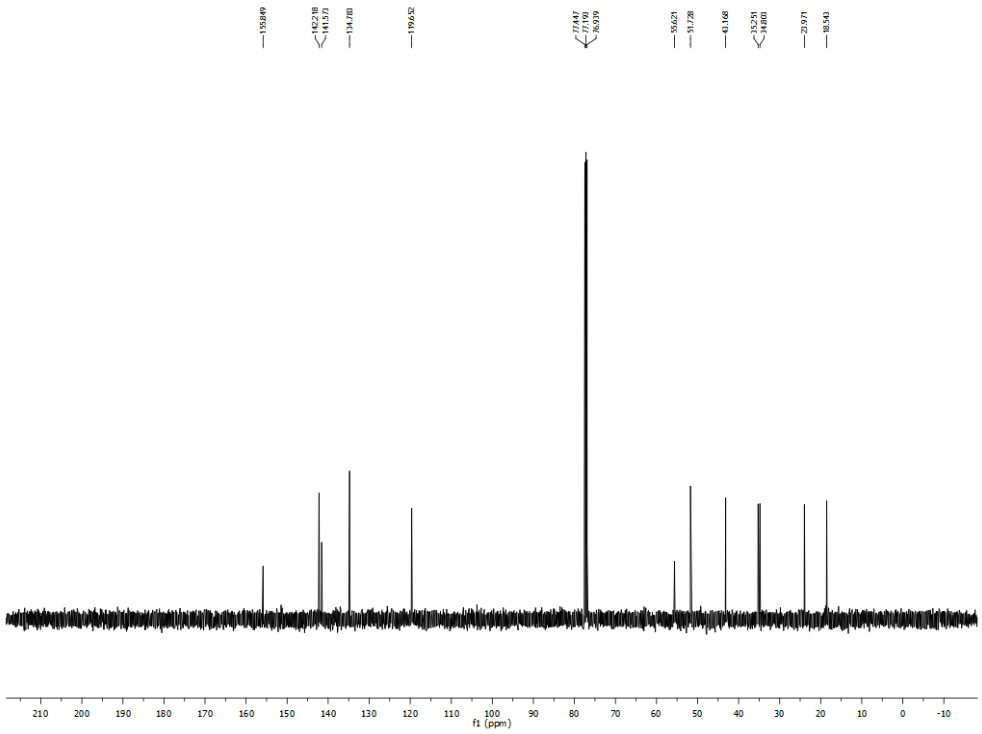

**Figure A3.38.** $^{13}$C NMR ($CDCl_3$, 125.8 MHz) spectrum of (±)-*trans*-3-methoxy-5-(2-methylcyclopentyl)pyridine (**21**)

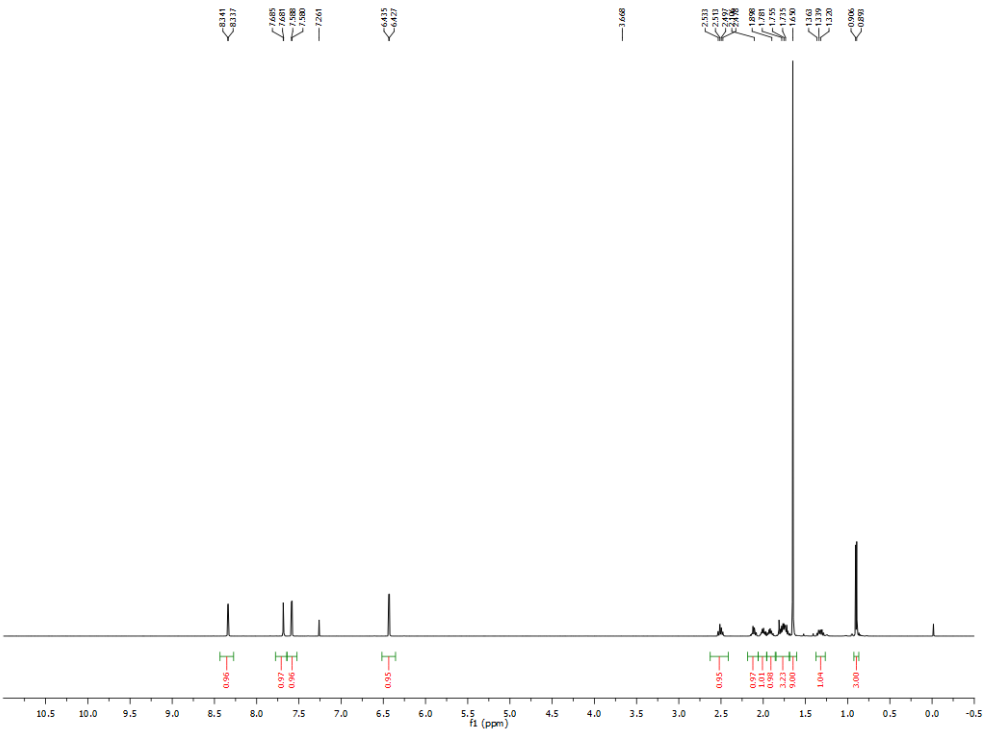

**Figure A3.39.** $^{1}$H NMR ($CDCl_3$, 500 MHz) spectrum of (±)-*tert*-butyl *trans*-5-(2-methylcyclopentyl)-1H-pyrrolo[2,3-b]pyridine-1-carboxylate (**22**)

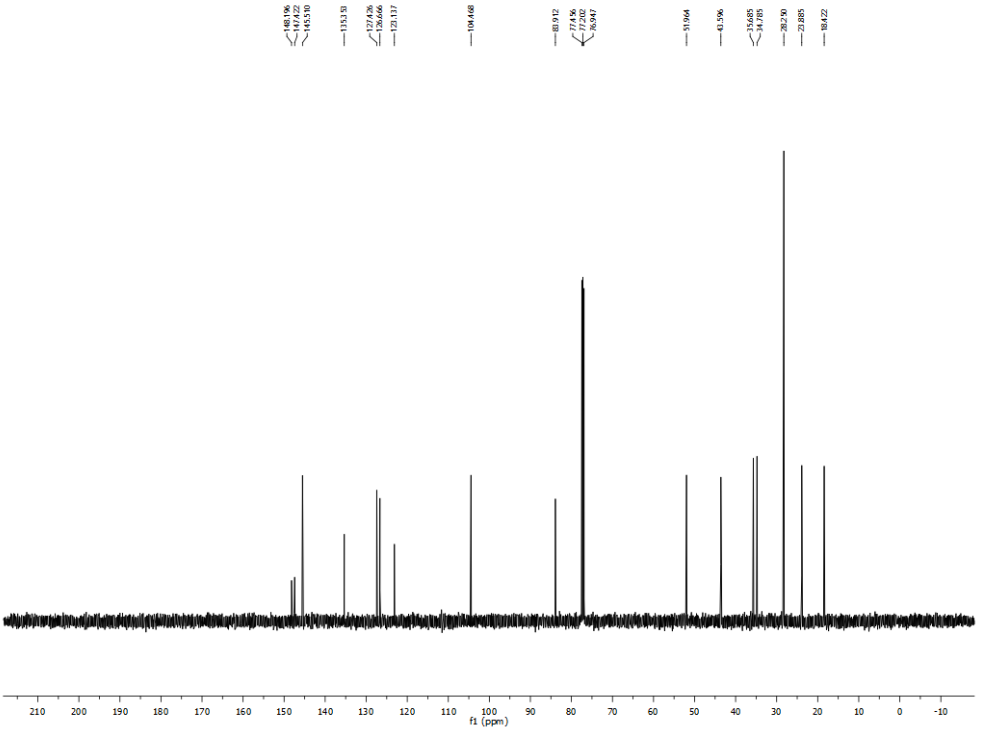

**Figure A3.40.** $^{13}$C NMR ($CDCl_3$, 125.8 MHz) spectrum of (±)-*tert*-butyl *trans*-5-(2-methylcyclopentyl)-1H-pyrrolo[2,3-b]pyridine-1-carboxylate (**22**)

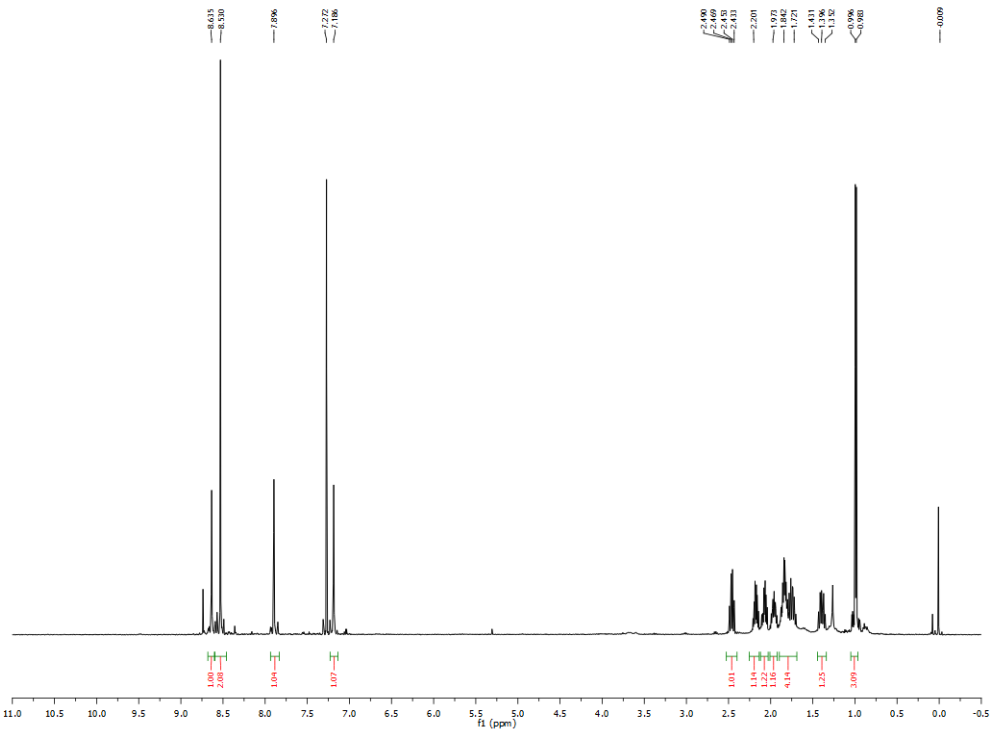

**Figure A3.41.** $^{1}$H NMR ($CDCl_3$, 500 MHz) spectrum of (±)-*trans*-2-(1H-Imidazol-1-yl)-5-(2-methylcyclopentyl)pyrimidine (**23**)

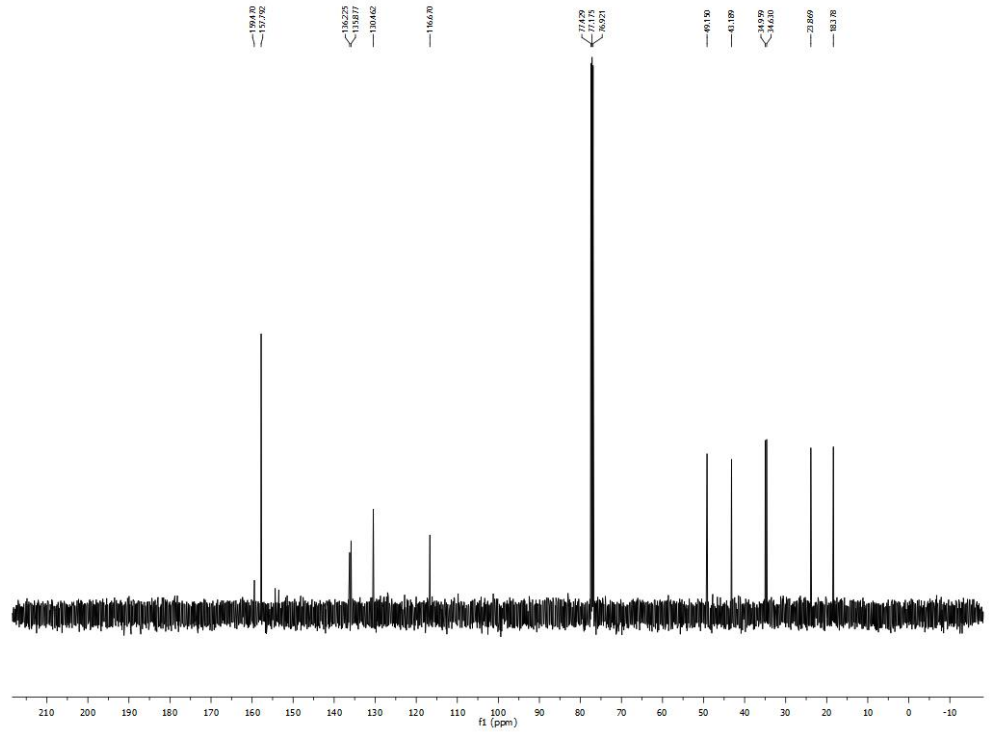

**Figure A3.42.** $^{13}$C NMR ($CDCl_3$, 125.8 MHz) spectrum of (±)-*trans*-2-(1H-Imidazol-1-yl)-5-(2-methylcyclopentyl)pyrimidine (**23**)

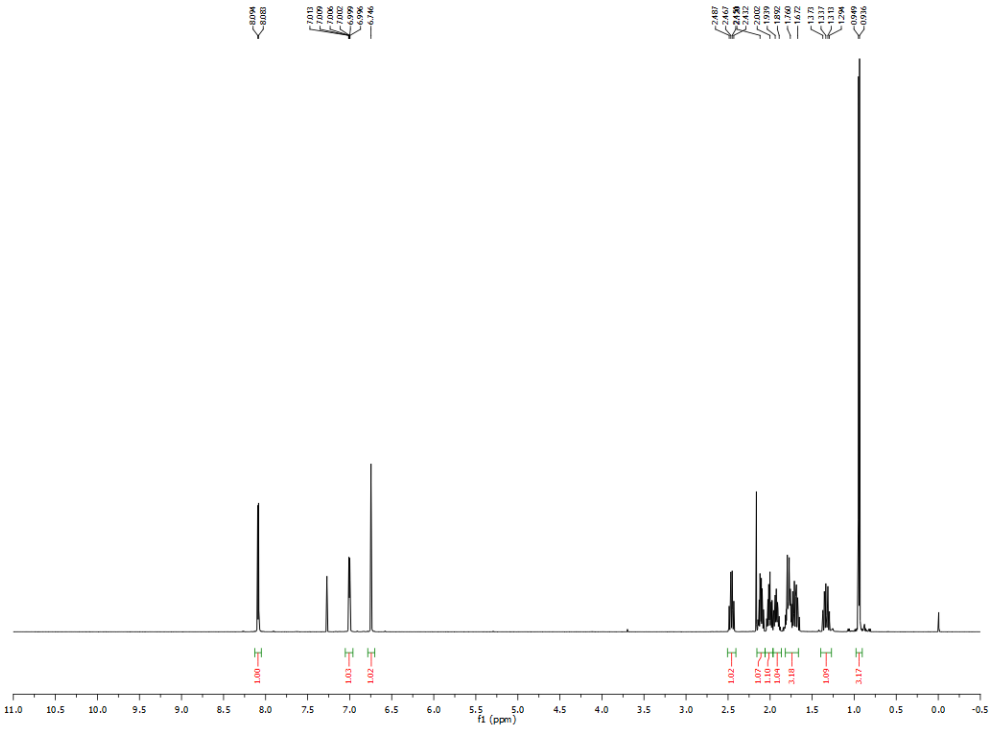

**Figure A3.43.** $^{1}$H NMR ($CDCl_3$, 500 MHz) spectrum of (±)-*trans*-2-fluoro-4-(2-methylcyclopentyl)pyridine (**24**)

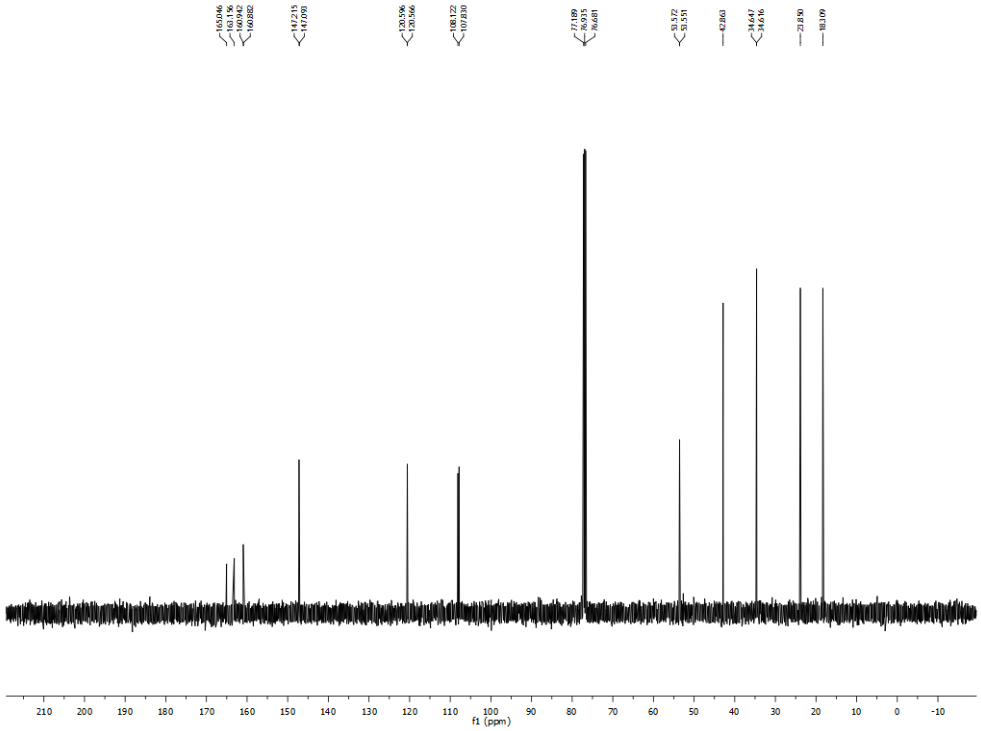

**Figure A3.44.** $^{13}$C NMR ($CDCl_3$, 125.8 MHz) spectrum of (±)-*trans*-2-fluoro-4-(2-methylcyclopentyl)pyridine (**24**)

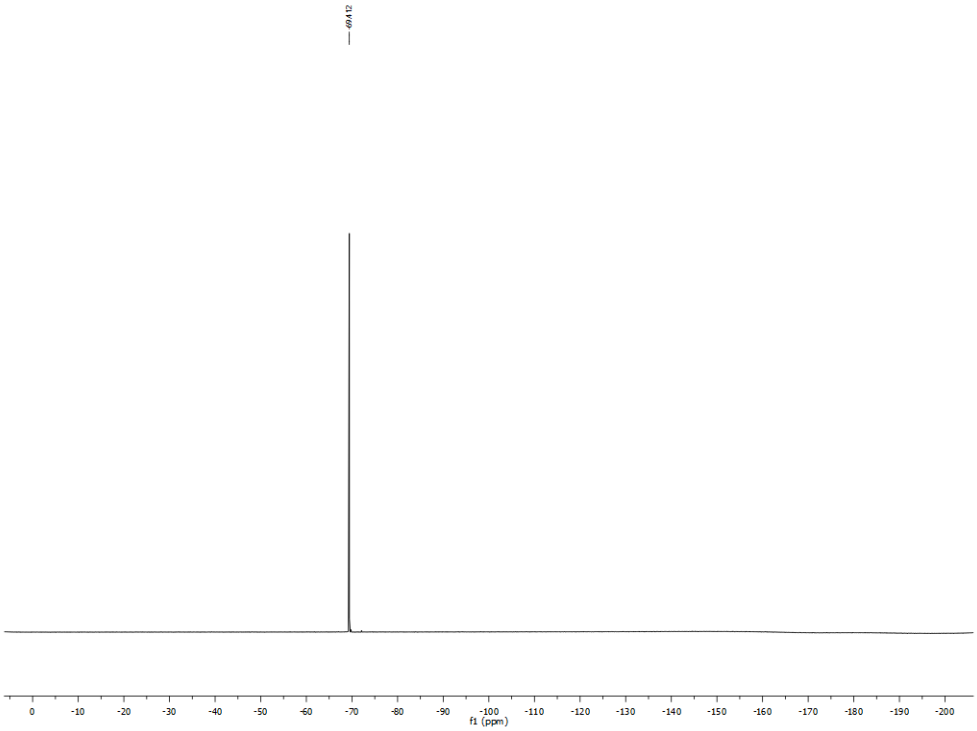


**Figure A3.45.** $^{19}F$ NMR ($CDCl_3$, 470.8 MHz) spectrum of (±)-*trans*-2-fluoro-4-(2-methylcyclopentyl)pyridine (**24**)

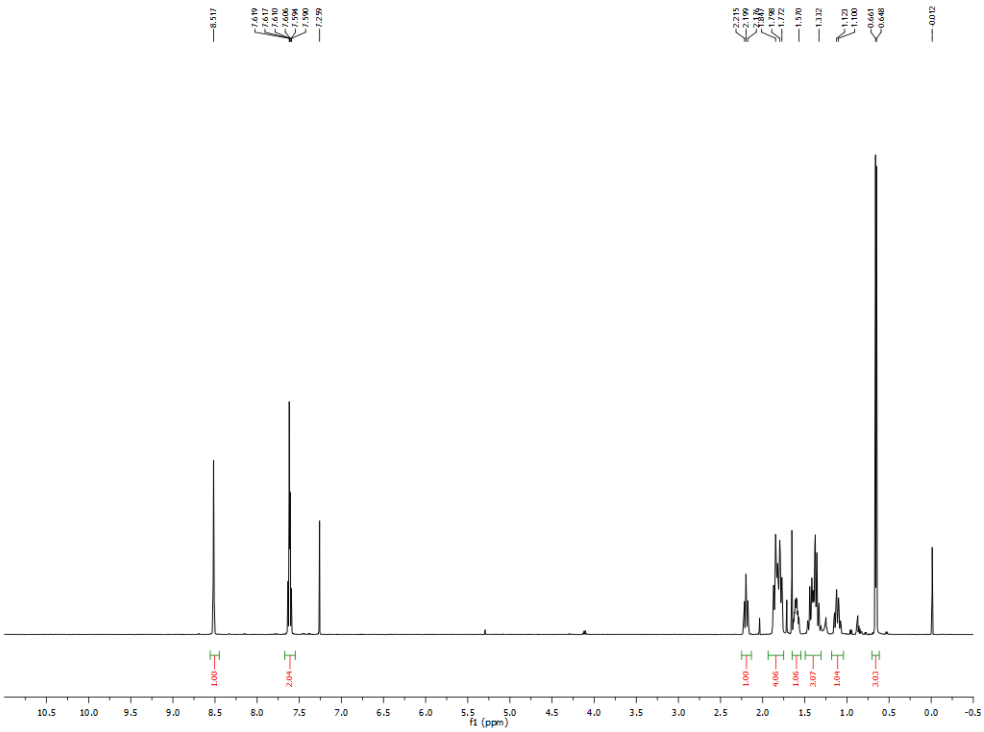


**Figure A3.46.** $^{1}H$ NMR ($CDCl_3$, 500 MHz) spectrum of (±)-*trans*-5-(2-methylcyclopentyl)picolinonitrile (**25**)

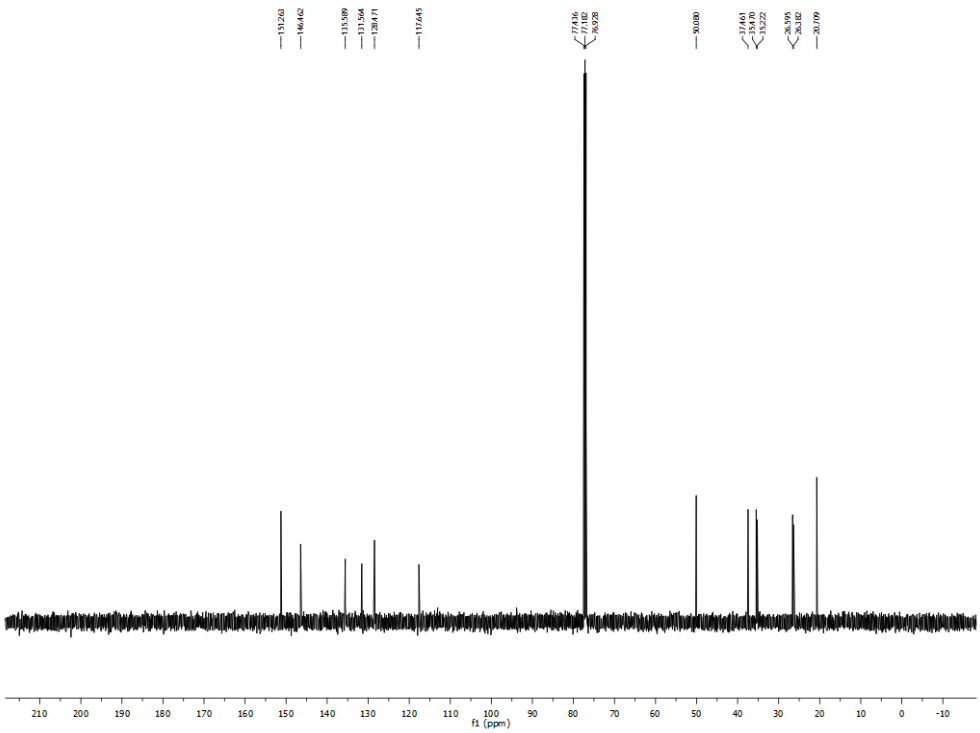

**Figure A3.47.** $^{13}C$ NMR ($CDCl_3$, 125.8 MHz) spectrum of (±)-*trans*-5-(2-methylcyclopentyl)picolinonitrile (**25**)

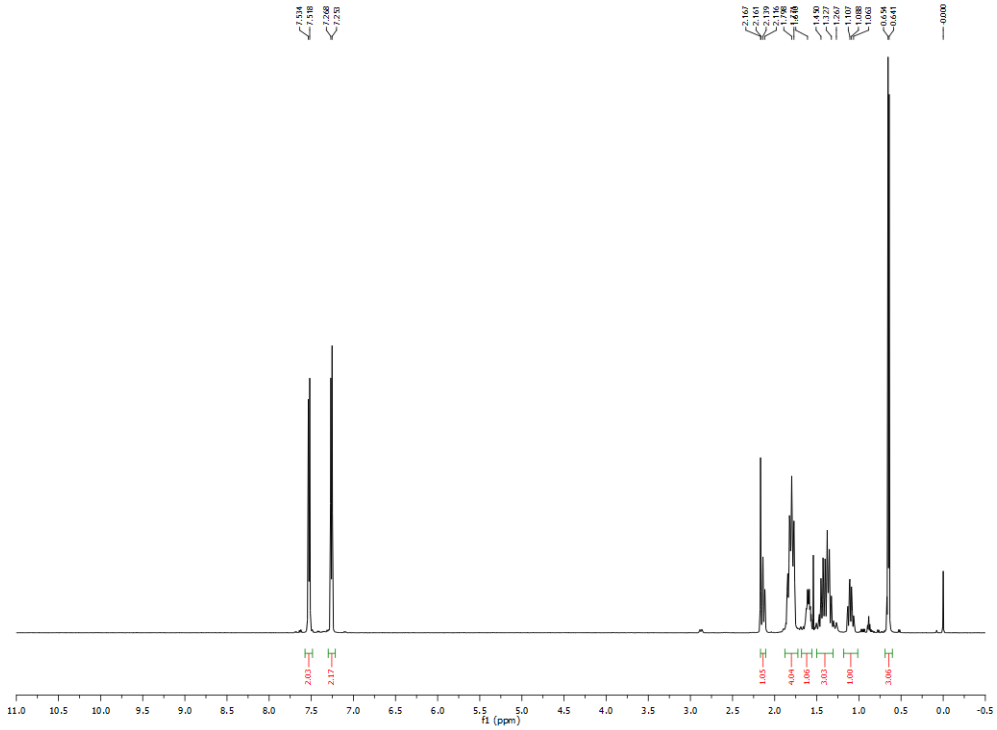

**Figure A3.48.** $^{1}H$ NMR ($CDCl_3$, 500 MHz) spectrum of (±)-*trans*-1-(2-methylcyclohexyl)-4-(trifluoromethyl)benzene (**26**)

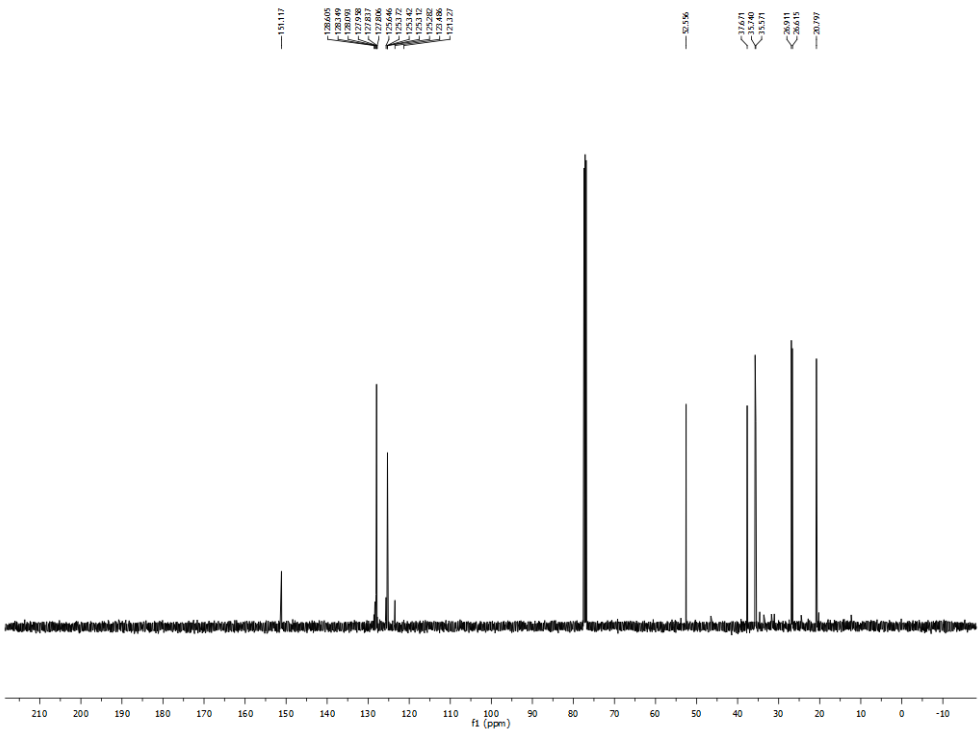

**Figure A3.49.** $^{13}C$ NMR ($CDCl_3$, 125.8 MHz) spectrum of (±)-*trans*-1-(2-methylcyclohexyl)-4-(trifluoromethyl)benzene (**26**)

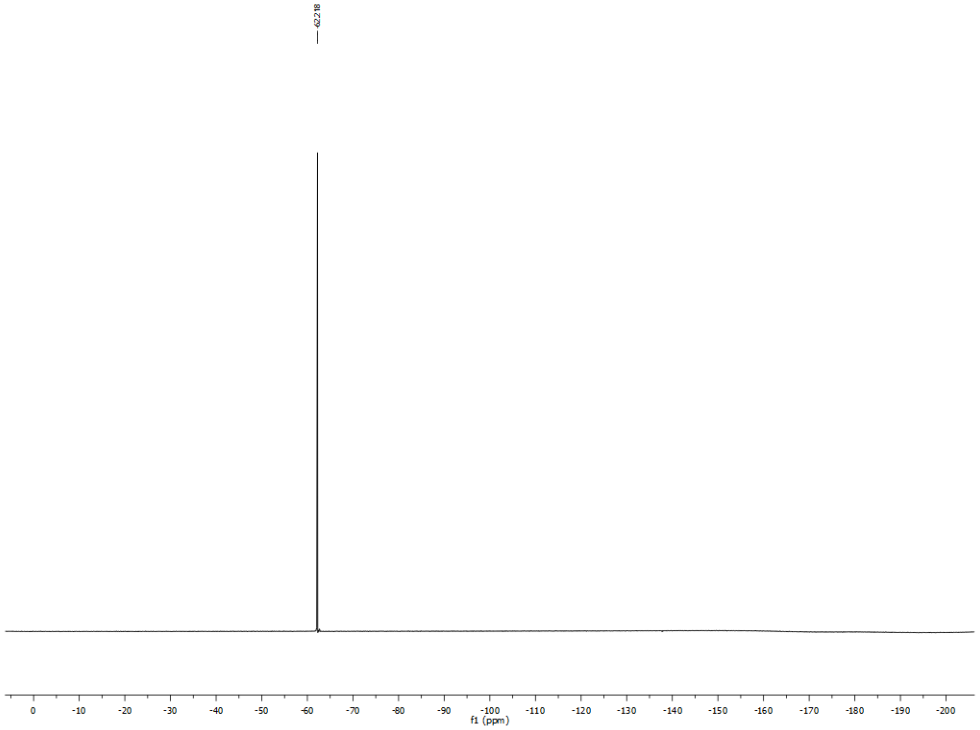

**Figure A3.50.** $^{19}F$ NMR ($CDCl_3$, 470.8 MHz) spectrum of (±)-*trans*-1-(2-methylcyclohexyl)-4-(trifluoromethyl)benzene (**26**)

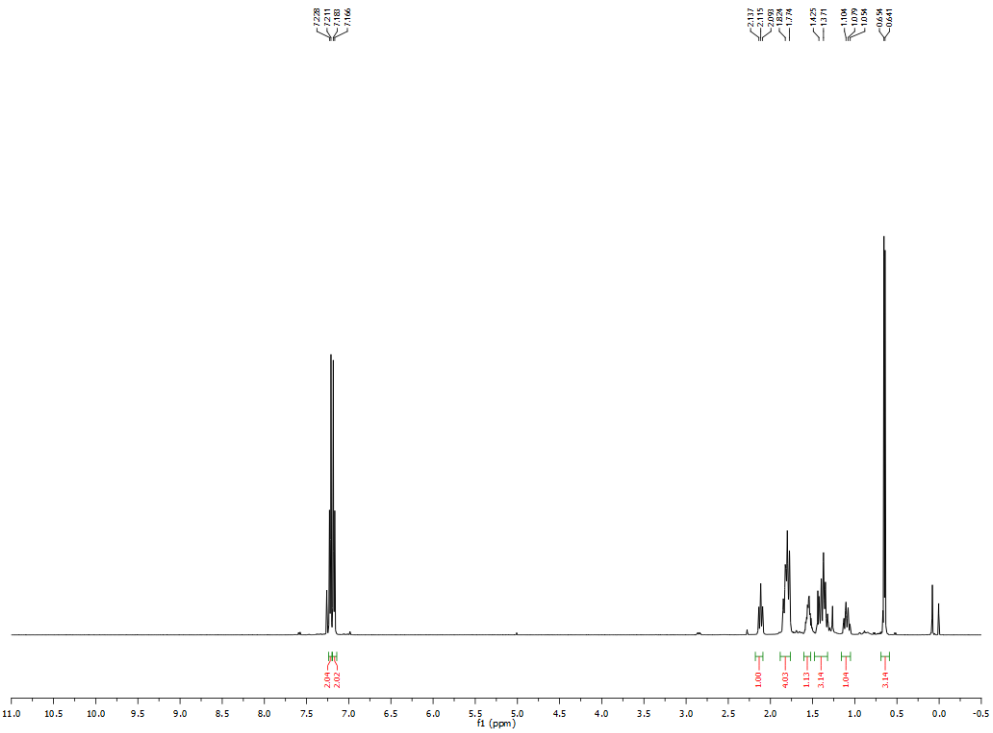

**Figure A3.51.** $^{1}$H NMR ($CDCl_3$, 500 MHz) spectrum of (±)-*trans*-4-(2-methylcyclohexyl)phenyl trifluoromethanesulfonate (**27**)

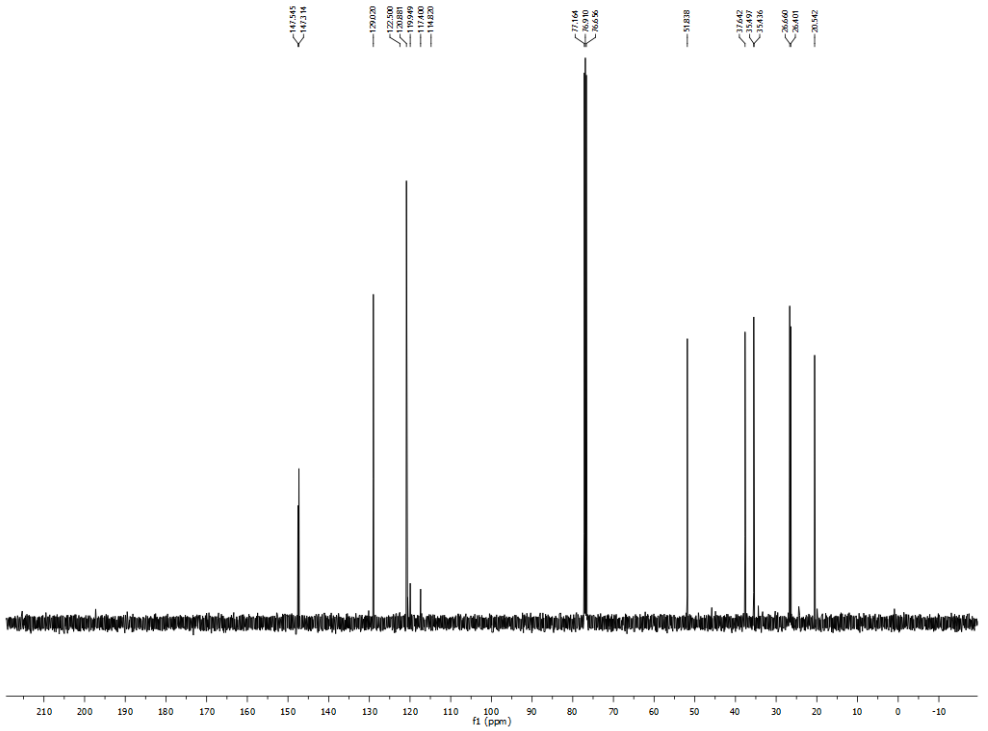

**Figure A3.52.** $^{13}$C NMR ($CDCl_3$, 125.8 MHz) spectrum of (±)-*trans*-4-(2-methylcyclohexyl)phenyl trifluoromethanesulfonate (**27**)

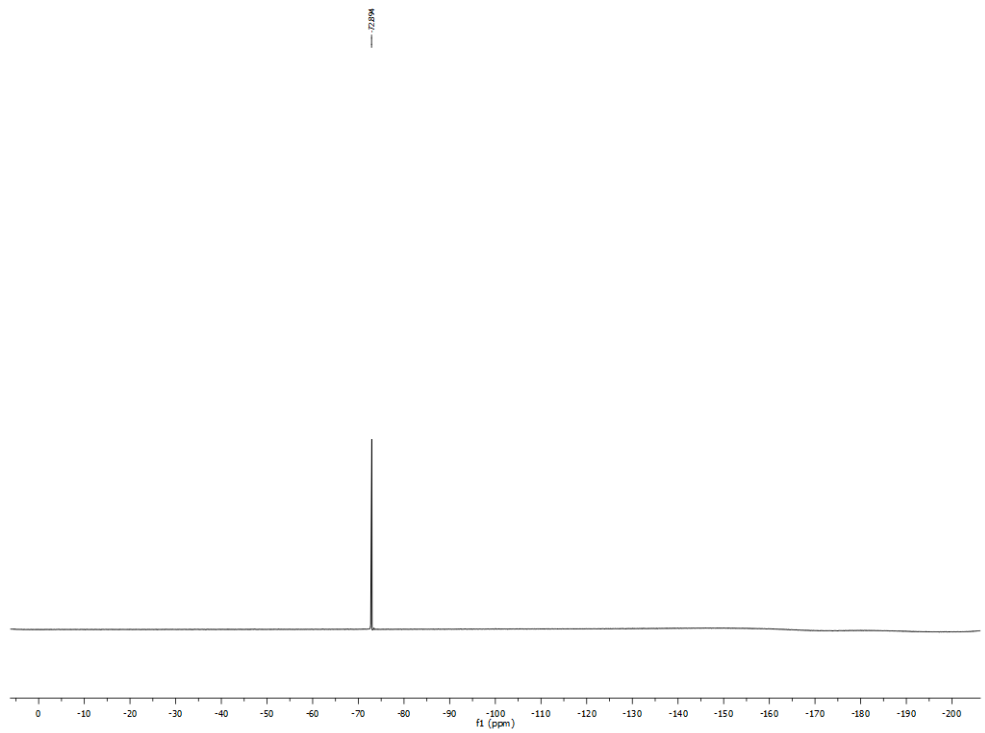


**Figure A3.53.** $^{19}F$ NMR ($CDCl_3$, 470.8 MHz) spectrum of (±)-*trans*-4-(2-methylcyclohexyl)phenyl trifluoromethanesulfonate (**27**)

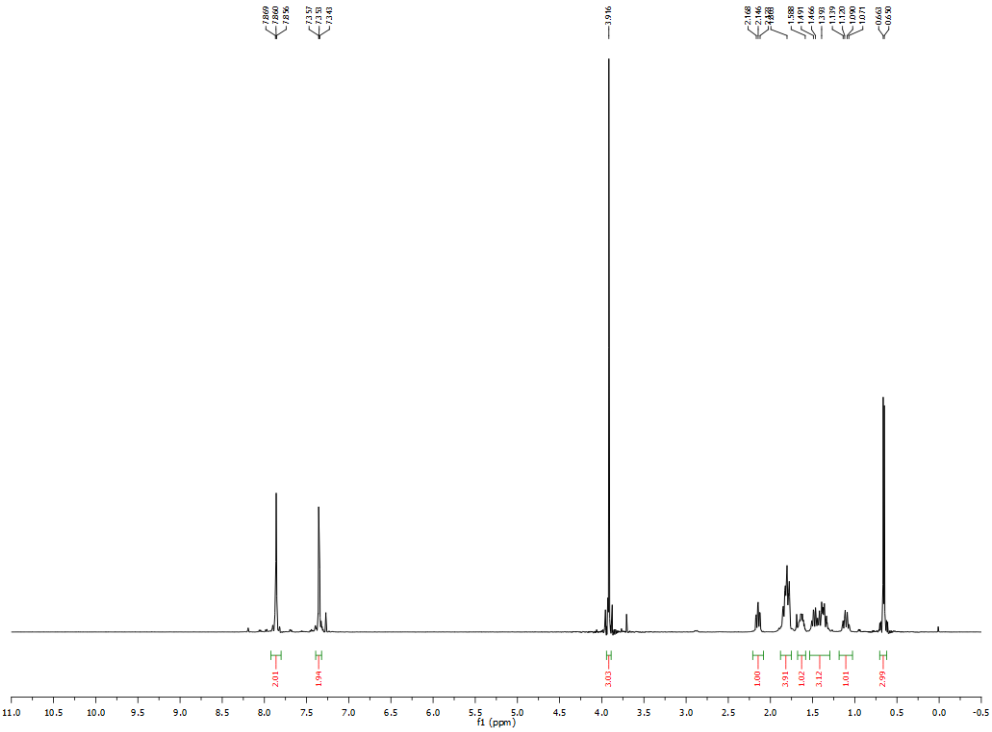


**Figure A3.54.** $^{1}H$ NMR ($CDCl_3$, 500 MHz) spectrum of (±)-*trans*-methyl 3-(2-methylcyclohexyl)benzoate (**28**)

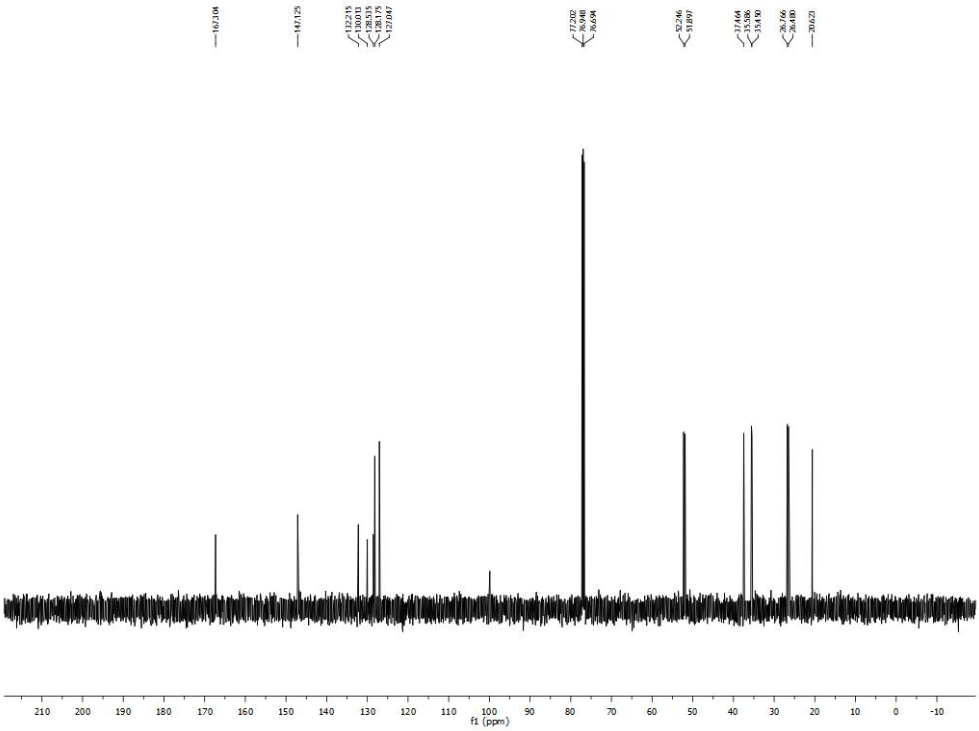

**Figure A3.55.** $^{13}C$ NMR ($CDCl_3$, 125.8 MHz) spectrum of (±)-*trans*-methyl 3-(2-methylcyclohexyl)benzoate (**28**)

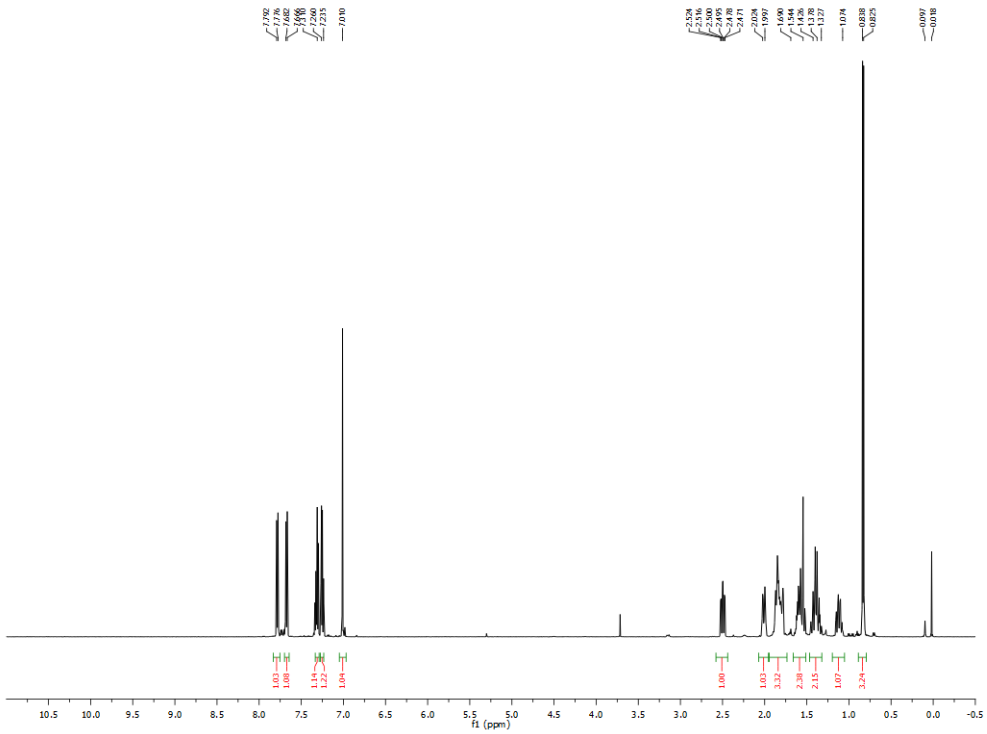

**Figure A3.56.** $^{1}H$ NMR ($CDCl_3$, 500 MHz) spectrum of (±)-*trans*-2-(2-Methylcyclohexyl)benzo[b]thiophene (**29**)

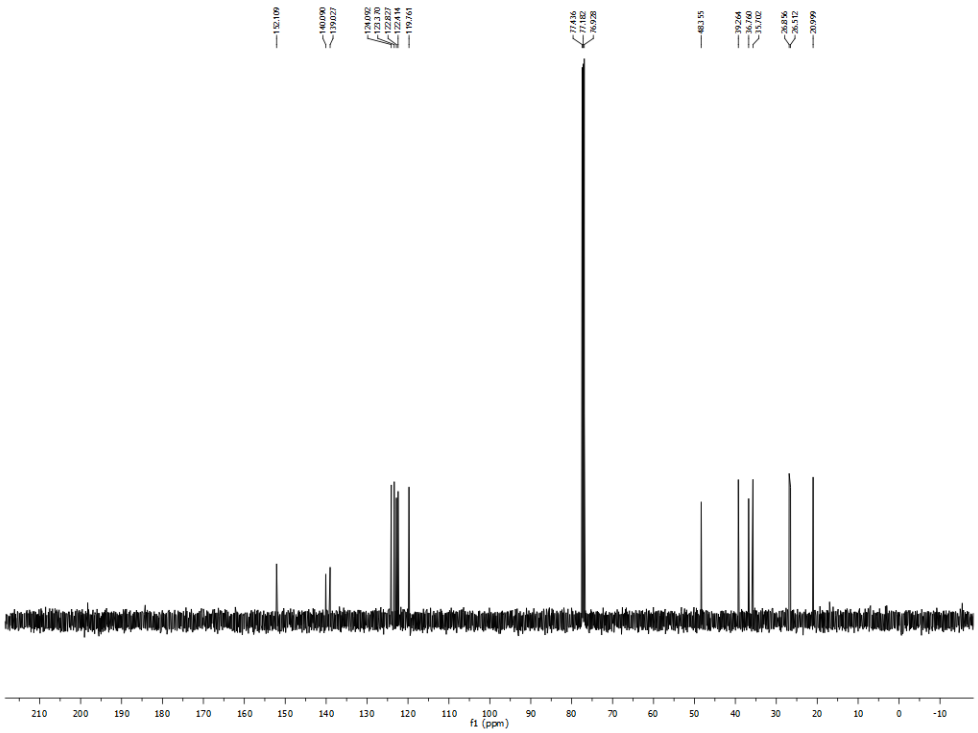

**Figure A3.57.** $^{13}C$ NMR ($CDCl_3$, 125.8 MHz) spectrum of (±)-*trans*-2-(2-Methylcyclohexyl)benzo[b]thiophene (**29**)

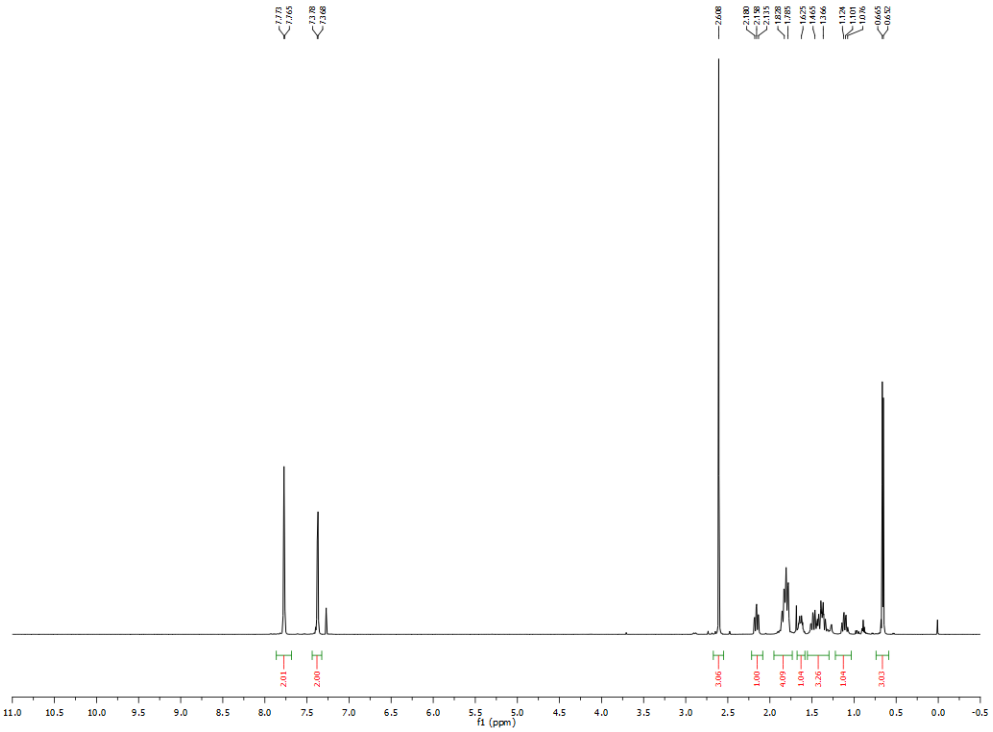

**Figure A3.58.** $^{1}H$ NMR ($CDCl_3$, 500 MHz) spectrum of (±)-*trans*-1-(4-(2-Methylcyclohexyl)phenyl)ethan-1-one (**30**)

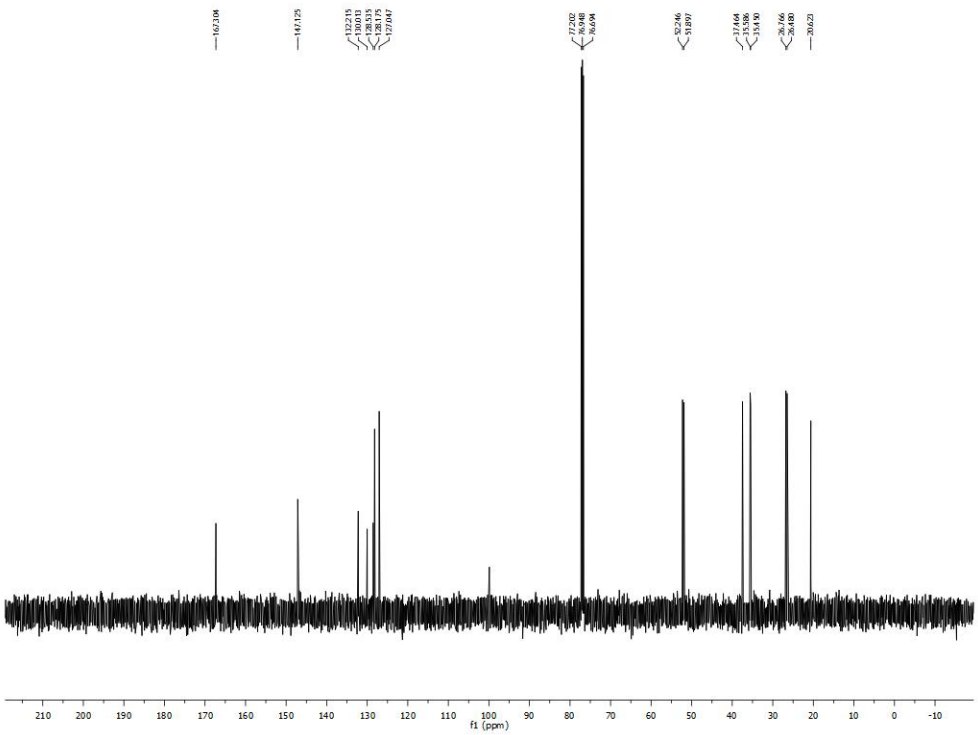


**Figure A3.59.** $^{13}C$ NMR ($CDCl_3$, 125.8 MHz) spectrum of (±)-*trans*-1-(4-(2-Methylcyclohexyl)phenyl)ethan-1-one (**30**)

# Chapter 5. Synthesis of 1,1'-Diaryl-2,2,2-trifluoroethanes via Photoredox/Nickel Dual Catalytic Cross-Coupling

## 5.1 Introduction

The importance of fluorinated molecules in diverse applications has driven interest in the development of methods for accessing unexplored chemical space in hopes of providing new molecular architectures with desirable physical and biological properties. Toward this end, it was anticipated that α-trifluoromethylated alkylboron reagents would be broadly reactive in established protocols for organoboron elaboration. Indeed, these compounds were found to participate in a variety of C-B bond functionalization reactions, including oxidation, halogenation, ethyl diazoacetate (EDA) insertion, and protodemetalation (**Figure 5.1**).[1]

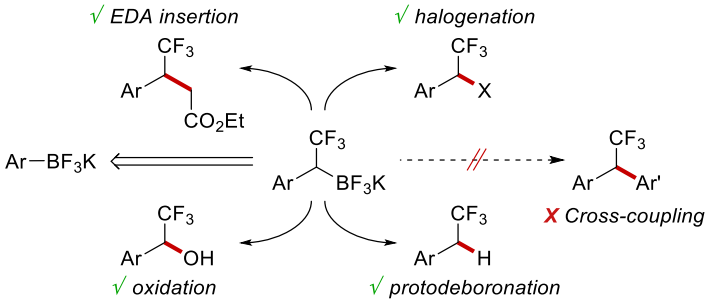


**Figure 5.1.** C-B bond functionalization reactions of α-trifluoromethylated alkylborons

These reagents were next examined in Suzuki cross-coupling with aryl halides. This process was particularly attractive as currently, 1,1-diaryl-2,2,2-trifluoroethane substructures can only be accessed through methods that require multiple steps and/or are severely limited in scope. In fact, at the outset of this project, less than 20 compounds had been reported in the literature with only one compound reported with full characterization. Among known methods, two main

strategies predominate: (1) deoxygenation of diaryltrifluoromethylcarbinols (Eq 5.1, Eq 5.2)[2] and (2) Friedel-Crafts alkylation of arenes with aryltrifluoroethyl cations derived from ionization of the corresponding benzylic alcohols (Eq 5.3, Eq 5.4).[3] The harsh conditions employed in these transformations significantly limit functional group tolerance, and reactions are often low yielding. Furthermore, approaches based on Friedel-Crafts alkylation are typically limited to electron rich arenes, suffer from regiochemical restrictions, and usually afford mixtures of *ortho*- and *para*-alkylated products.

**Eq 5.1.** Published in 1960

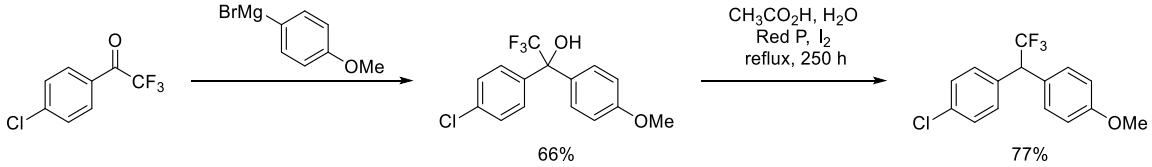


**Eq 5.2.** Published in 1982

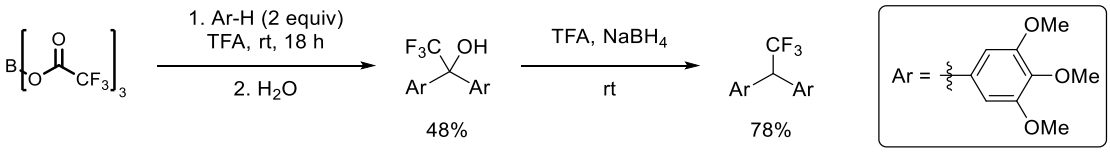


**Eq 5.3.** Published in 1985

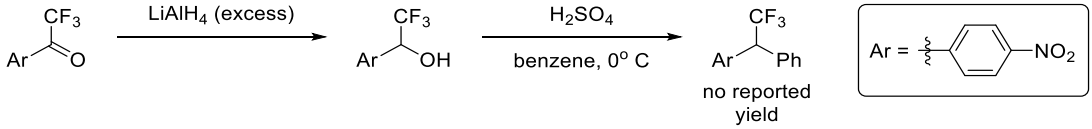


**Eq 5.4.** Published in 2011

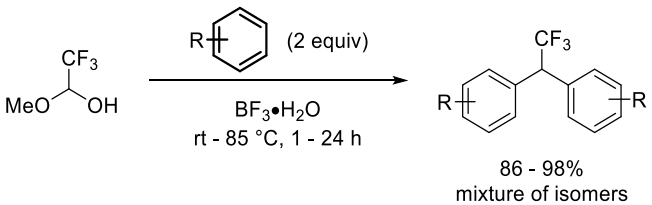

Notwithstanding these challenges, diaryltrifluoroethanes remain attractive targets in medicinal and agricultural chemistry. The addition of a trifluoromethyl functional group onto a biologically active diarylmethane skeleton could prove a viable strategy for reduction of metabolic susceptibility in this class of drug candidates.[4] Moreover, as fluoro-analogs of 1,1,1-trichloro-2,2-bis(*p*-chlorophenyl)ethane (DDT), these compounds serve as potential alternatives to the environmentally harmful DDT, in which case the ability to manipulate their structures would be crucial in altering their physical properties.

In pursuit of conditions for achievement of the desired Suzuki cross-coupling,[i] microscale high throughput experimentation techniques[5] were employed to screen a variety of Pd sources, ligands, bases, solvents, and temperatures. Despite significant efforts to identify optimal conditions, only trace amounts (less than 5%) of the cross-coupled product were detected by HPLC analysis of the crude reaction mixtures. Furthermore, this insignificant conversion was invariably accompanied by side products arising from protodeboronation, C-B bond oxidation, and β-fluoride elimination to afford the corresponding difluoroalkene.

These outcomes suggested that application of these reagents in conventional Pd-catalyzed cross-coupling is hindered by two principal challenges rooted in the two-electron nature of alkylboron transmetalation. First and foremost, the low nucleophilicity of these electron-poor, secondary alkylboron reagents necessitates both high temperature and strong base for efficient transmetalation. Second, the strong affinity of transition metal complexes for fluoride leads to $\beta$-fluoride elimination from the intermediate organopalladium in preference to the desired reductive elimination.[6] Notably, in analogy to the related β-hydride elimination, this side reaction is likely to

[i] Reproduced in part from *Chem. Eur. J.* **2016**, *22*, 120.

be exacerbated at the elevated temperatures required for efficient transmetalation. This unfortunate dichotomy of reactivity was feared to preclude this useful class of reagents from participating in all types of transition metal-catalyzed C-C bond forming reactions.

Although these novel organoboron reagents proved unreactive in conventional cross-coupling protocols, productive reactivity was anticipated to result through application of the mechanistically distinct single-electron transmetalation manifold developed recently in our laboratory.[7] Here, the problematic high energy transition state associated with transmetalation of the secondary alkylboron is, in effect, replaced by a lower energy pathway involving oxidative fragmentation of the trifluoroborate followed by capture at a transition metal center. This low barrier, odd-electron pathway was anticipated to permit cross-coupling to occur at room temperature, thereby reducing the problematic side reactions that had doomed previous efforts (**Figure 5.2**).

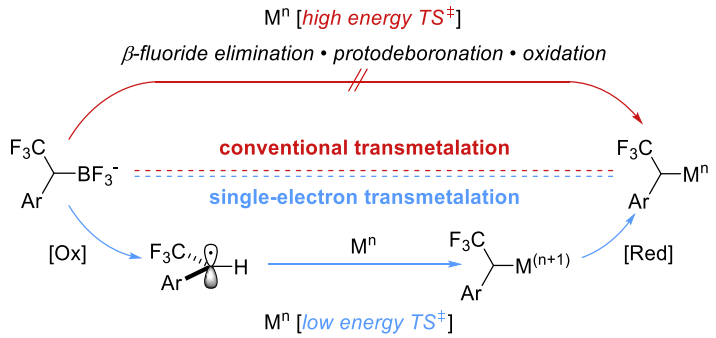


**Figure 5.2.** Comparison between traditional and single-electron transmetalations

## 5.2 Results and Discussion

Iridium complex **1** was expected to be sufficiently oxidizing to fragment the C-B bond of **2** to generate the corresponding α-trifluoromethyl radical **3**, which would rapidly add to a ligated

$Ni^0$ complex **5**. The resultant alkylnickel(I) complex was then expected to engage an aryl bromide in oxidative addition to afford high-valent diorganonickel(III) complex **8** which was predicted to exist in equilibrium with Ni(II) complex **9** and free radical **3**.[8] Reductive elimination from **8** was then expected to afford the desired diaryltrifluoroethane **10** and Ni-Br species **11**. Subsequent reduction of the complex **11** by the reduced form of the photocatalyst then completes both catalytic cycles simultaneously (**Figure 5.3**).

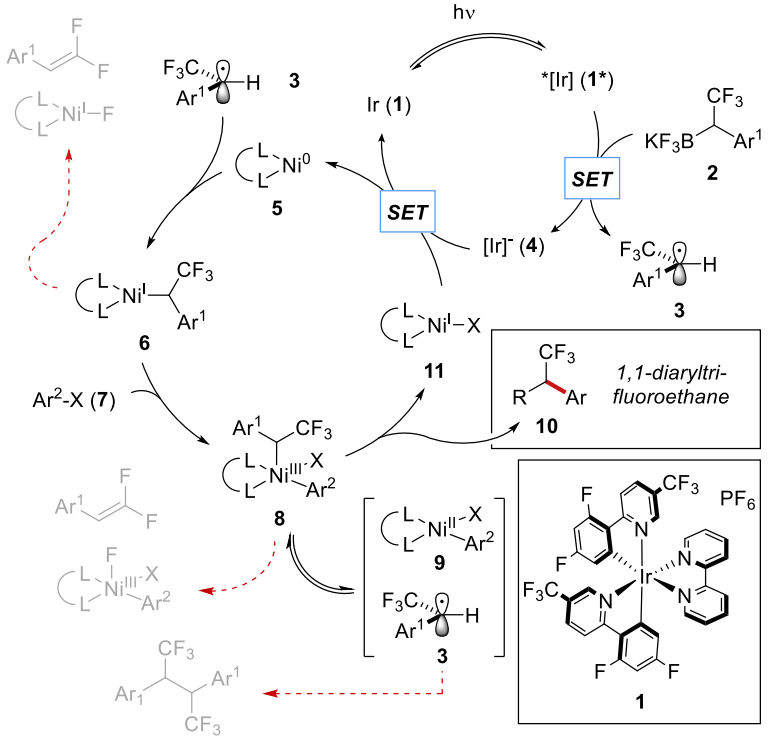


**Figure 5.3.** Proposed catalytic cycle with depiction of possible side reactions

It is worth noting that this proposed catalytic cycle is rife with challenges and potential deleterious side reactions. Both the feasibility of generating the putative benzylic α-trifluoromethyl radicals and their affinity for transition metal complexes were uncertain at the outset of this study. Furthermore, it was not clear if reductive elimination from Ni(III) complex **8** would be favored

over the β-fluoride elimination observed under palladium catalysis. Even if the rate of β-fluoride elimination were slowed sufficiently by the milder reaction temperatures, slow reductive elimination could result in excessive homocoupling of the trifluoroborate fragment through reversible homolysis of the Ni(III) intermediate followed by radical-radical coupling (Figure 5.3).

Undaunted, investigations were initiated with measurement of the single-electron oxidation potential of organotrifluoroborate **2** ($Ar^1$ = *p*-methoxyphenyl) via cyclic voltammetry. Expectedly, the electronic influence of the trifluoromethyl group affords an organoboron intermediate much less susceptible to oxidation ($E_{Red}$ = + 1.17 V vs SCE, see Appendix A8) than related non-fluorinated reagents ($E_{Red}$ = + 1.10 V and + 0.91 V vs SCE for benzyltrifluoroborate and 1-phenylethyltrifluoroborate, respectively). Nonetheless, this data suggested that the oxidation is thermodynamically feasible based on the reported reduction potential of the excited state of photocatalyst **1** ($E_{Red}$ = + 1.32 V vs SCE),[9] providing support for the viability of the proposed cross-coupling.

Reaction optimization began with investigation of the cross-coupling of organotrifluoroborate **2** with methyl 4-bromobenzoate (**Table 5.1**). Dioxane was quickly recognized as the solvent of choice with 2,2'-bisoxazoline ligand **L1** inducing promising levels of the desired reactivity (entry 1). Screening of various additives revealed the beneficial effect of fluoride bases and $Cs_2CO_3$, with a mixture of KF and $Cs_2CO_3$ ultimately proving optimal (entry 9). In this case, the additives appear to be primarily responsible for reducing the prevalence of products arising from β-fluoride elimination and homocoupling of radical **3**. The nature of this effect has yet to be identified, although it is reasonable to suggest that these anionic additives may act as transient ligands, occupying coordination sites on the Ni center to retard the β-fluoride elimination process.

**Table 5.1.** Optimization table

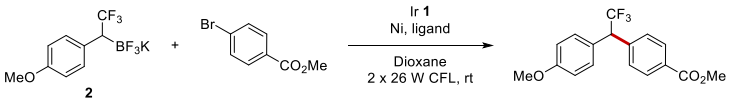


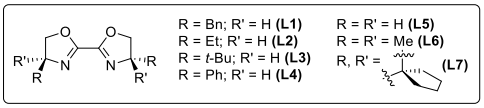


| Entry | $BF_3K$ **2** (equiv) | Ir **1** (mol %) | Ni source (mol %) | **L1** (mol %) | Additive (equiv) | Conc. (M) | Yield[a] (%) |
|---|---|---|---|---|---|---|---|
| 1 | 1.3 | 1 | $Ni(COD)_2$ (10) | 10 | - | 0.05 | 12 |
| 2 | 1.3 | 1 | $Ni(COD)_2$ (10) | 10 | CsF (3) | 0.05 | 32 |
| 3 | 1.5 | 2 | $NiCl_2$•dme (5) | 5 | CsF (3) | 0.05 | 37 |
| 4 | 1.5 | 2 | $NiBr_2$•dme (5) | 7.5 | CsF (3) | 0.05 | 43 |
| 5 | 1.5 | 3 | $NiBr_2$•dme (5) | 7.5 | CsF (3) | 0.02 | 62 |
| 6 | 2.0 | 3 | $NiBr_2$•dme (5) | 7.5 | CsF (3) | 0.02 | 71 |
| 7 | 2.0 | 3 | $NiBr_2$•dme (5) | 7.5 | $Cs_2CO_3$ (4) | 0.02 | 78 |
| 8 | 2.0 | 3 | $NiBr_2$•dme (5) | 7.5 | $Cs_2CO_3$ (4)[b] | 0.02 | 0 |
| 9 | 2.0 | 3 | $NiBr_2$•dme (5) | 7.5 | $Cs_2CO_3$ (4), KF (1) | 0.02 | 82 |
| 10[c] | 2.0 | 3 | $NiBr_2$•dme (5) | 7.5 | $Cs_2CO_3$ (4), KF (1) | 0.02 | 60 |

[a] based on $^{19}F$ NMR yield with trifluorotoluene as the internal standard;
[b] $Cs_2CO_3$ stored on benchtop; [c] reaction performed at 40 °C

A variety of novel 2,2'-bisoxazoline ligands (**L2-L7**) were synthesized[10] and tested in the cross-coupling, but benzyl derivative **L1** exhibited the best performance among the ligands analyzed. This observation underscores the challenges associated with this particular cross-coupling, as the ligand must satisfy a highly delicate balance of electronic and steric effects to promote the desired reactivity while simultaneously suppressing numerous detrimental side reactions.

Exchange of $Ni(COD)_2$ for Ni(II) sources such as $NiBr_2$•dme in combination with reduced Ni loading and higher ligand/Ni ratio (1.5:1) was effective in decreasing homocoupling of the aryl bromide and providing increased conversion to product (entries 3-4). Adventitious water from hygroscopic $Cs_2CO_3$ (entry 8) and increased reaction temperature (entry 10) proved detrimental to the desired reactivity.

Concentration proved an important variable in achieving high yields (entry 5), as reactions performed at higher dilution exhibited significantly faster rates and fewer side products. We attribute this concentration dependence primarily to increased penetration of light into the reaction mixture, because reactions at higher concentration suffer from decreased light input per unit area because of inner filter effects.[11] A brief exploration of alternative photocatalysts revealed other related derivatives to be inferior to **1** for this cross-coupling.

With optimized conditions in hand, a variety of aryl bromides were engaged in cross-coupling with trifluoroborate **2 (Figure 5.4**).

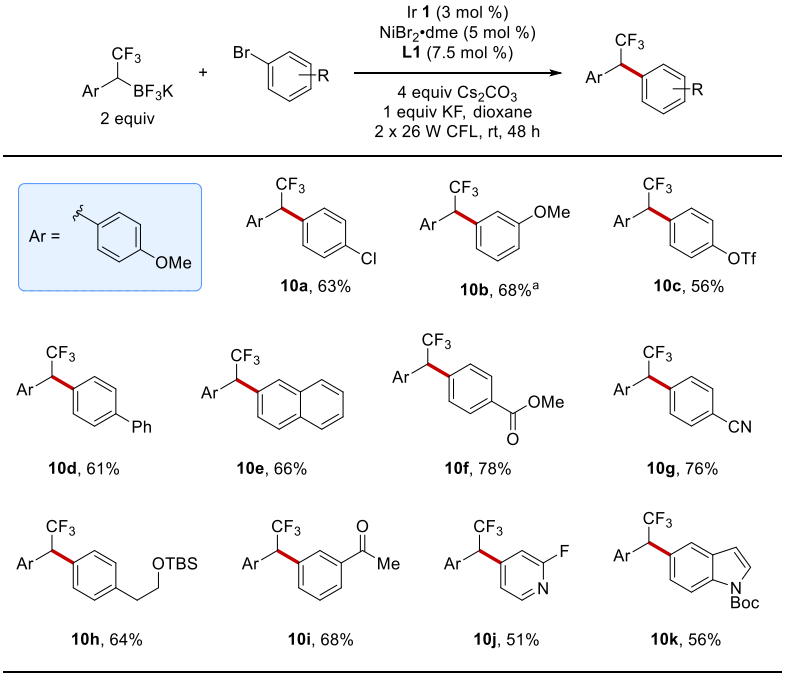


[a] Based on $^{19}F$ NMR analysis of crude reaction mixture, product isolated by preparative UPLC.

**Figure 5.4.** Substrate scope of aryl bromides

Both electronically activated and electron neutral bromides smoothly participated in cross-coupling to afford the corresponding unsymmetrical 1,1-diaryl-2,2,2-trifluoroethanes. Selective

cross-coupling of the C-Br bond was observed in preference to both triflates and aryl chlorides (products **10a** and **10c**). In addition, numerous functional groups, including esters **10f**, nitriles **10g**, and ketones **10i**, were well tolerated. Protected alcohol derivatives also afforded products in good yield (**10h**). Tolerance of medicinally and agrochemically relevant heterocyclic bromides was demonstrated in the cross-coupling of 4-pyridyl (**10j**) and protected indolyl (**10k**) substrates. Unfortunately, some nitrogen-containing aryl bromides (e.g., 4-acetamido, 4-dimethylamino, etc.) proved unreactive under the reported conditions, affording only trace amounts of product even with prolonged reaction times.

Attention was next turned to the compatibility of this reaction manifold with electronically and structurally diverse trifluoroborates (**Figure 5.5**). Expectedly, substrates adorned with electron donating groups (**11c**, **11d**) afforded products in the highest yields, presumably because of the greater stability of the intermediate radical. Electron neutral substrates (**11a**, **11e**) were also engaged in cross-coupling in moderate yields. Although electron poor substrates were generally sluggish – requiring extended reaction times, diarylethane **11b** was generated in 43% yield despite the presence of the electron-withdrawing 4-fluoro substituent. Heteroaromatic fragments were also coupled, affording products **11f** and **11g**.

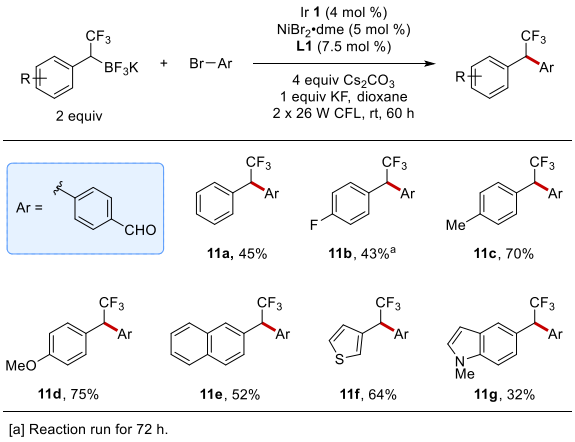


**Figure 5.5.** Substrate scope of trifluoroborates

Some degree of enantioselectivity was observed in several of the products generated via reaction in the presence of **L1** (0-60% ee, see 5.4 Experimental and Appendix A7). According to the mechanistic studies, enantioselectivity arises from Ni(III) complex **8** where one of the two equilibrating diastereomeric Ni(III) complexes undergoes reductive elimination at a faster rate.[8] In this study, reaction conditions were optimized purely on yields, and no attempt was made to identify conditions under which higher levels of enantioinduction could be afforded.

Although the yields afforded by the methods reported herein are often moderate, it is noteworthy that all of the reported compounds are entirely new chemical entities (only **10a** has been synthesized previously with only elemental analysis provided for characterization [2a]). This fact effectively highlights both the difficulties associated with synthesis of these materials using conventional methods and the vast, untapped chemical space that these products occupy. Furthermore, the variety of useful functional groups demonstrated to be compatible in this novel cross-coupling permit rapid diversification and complexity building operations, thereby multiplying the quantity of readily accessible molecular architectures.

## 5.3 Conclusion

The first general synthesis of differentially substituted 1,1-diaryl-2,2,2-trifluoroethanes through photoredox/nickel dual catalytic cross-coupling of α-trifluoromethylated trifluoroborates with (hetero)aryl bromides has been developed. Key to the success of this method is the exploitation of a mechanistically distinct activation mode for transmetalation of these alkylboron reagents that avoids the high temperatures and strong bases that have thwarted attempts to effect their cross-coupling using conventional protocols. These dual catalytic cross-couplings occur under mild conditions, in satisfactory yields, and demonstrate tolerance of a variety of useful functional groups. In addition to the significant synthetic value offered by the reported method, the success of the single-electron transmetalation manifold in a case where conventional approaches have failed entirely stands as a testament to the power of this complementary reactivity mode in realizing the cross-coupling of conventionally challenging substructures.

## 5.4 Experimental

*General considerations*

New bottles of $Cs_2CO_3$ and KF were opened in the glove box and stored within. Dioxane was stored over 3Å molecular sieves overnight and purged with argon for 1 h prior to being brought into the glove box. $NiBr_2$•dme was stored in the desiccator under vacuum.

The cross-coupling reactions were performed on a 0.1 mmol scale. Reactions performed on larger scales gave a lower conversion to the desired products. Three separate 0.1 mmol reactions were run for each substrate and then combined prior to purification in order to get accurate isolated yields (yields were calculated accordingly).

Photocatalyst **1**[7] and potassium trifluoro(2,2,2-trifluoro-1-arylethyl)borates **2**[1] were synthesized according to previous reports.

The compounds were purified using an ISCO CombiFlash system equipped with 254 nm, 280 nm, and ELS detectors. All pure compounds were characterized by $^{1}H$, $^{13}C$, and $^{19}F$ NMR spectroscopy, IR spectroscopy, high-resolution mass spectrometry (HRMS), chiral SFC, and melting point (for solids). $^{1}H$, $^{13}C$, and $^{19}F$ NMR spectra were recorded at 500.4, 125.8, and 470.8 MHz, respectively.

**Procedure for photoredox cross-coupling reactions – varying (het)aryl bromides:**

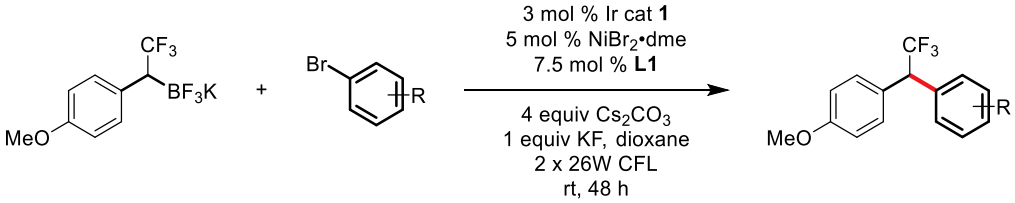


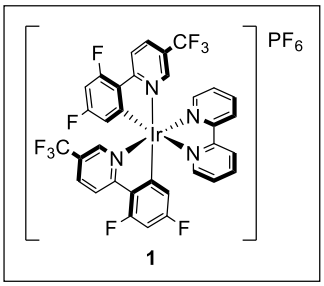


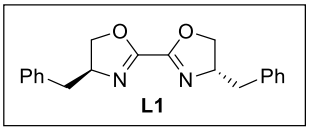


To a 2-dram vial (8 mL) equipped with a Teflon-coated magnetic stir bar was added **L1** (0.0024 g, 0.0075 mmol) and $NiBr_2$•dme (0.0015 g, 0.005 mmol) and 1.0 mL THF (from a JC Meyer solvent system). The resulting suspension was heated briefly with a heat gun until the nickel and ligand

were fully solubilized, yielding an orange solution. The solvent was then removed under vacuum to give a fine coating of the ligated nickel complex, and the vial was placed under high vacuum. Once dry, (het)aryl bromide (0.1 mmol, 1 equiv) (liquid aryl bromides were added in the glove box after adding the solvent), potassium trifluoro[2,2,2-trifluoro-1-(4-methoxyphenyl)ethyl]borate (0.0592 g, 0.2 mmol), and $Ir(dFCF_3ppy)_2(bpy)PF_6$ **1** (0.0030 g, 0.0030 mmol) were added. The vial was then transported into the glove box where $Cs_2CO_3$ (0.0130 g, 0.4 mmol) and KF (0.0058 g, 0.1 mmol) and dioxane (5 mL) were added, and the vial was then sealed tightly with a PTFE-lined PP storage cap. Once brought out of the glove box, the vial was further sealed with Parafilm and placed in front of two 26 W fluorescent light bulbs with a fan blowing across to maintain an ambient temperature around 24 °C. After stirring for 48 h, the crude reaction mixture was filtered through a plug of Celite, washed with $CH_2Cl_2$, and then concentrated under vacuum. Purification of the mixture by column chromatography, eluting with EtOAc and hexanes, was performed to obtain products in pure form.

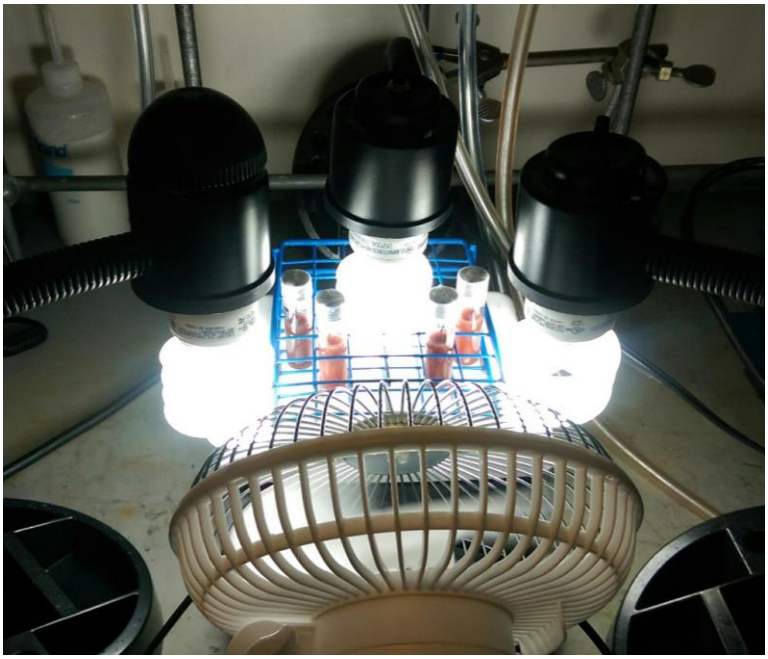

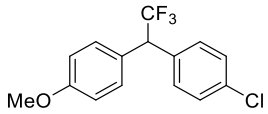


**1-Chloro-4-(2,2,2-trifluoro-1-phenylethyl)benzene (10a):** Pale yellow oil (63%); IR (KBr) 3052, 2987, 2306, 1424, 1269, 1260, 897, 757, 708 $cm^{-1}$; $^{1}H$ NMR (500 MHz, $CDCl_3$) δ 7.33-7.24 (m, 8H), 4.60 (q, *J* = 9.8 Hz, 1H), 3.80 (s, 3H); $^{13}C$ NMR (126 MHz, $CDCl_3$) δ 159.5, 134.4, 134.0, 130.5, 130.3, 129.0, 127.1, 126.8 (q, *J* = 280.6 Hz), 114.3, 55.4, 54.3 (q, *J* = 27.7 Hz); $^{19}F$ NMR (471 MHz, $CDCl_3$) δ -66.3; HRMS (ESI-TOF) *m/z* calcd. for $C_{15}H_{12}OF_3Cl$ $[M]^+$ 300.0529, found 300.0529; Chiral SFC (ChiralPak OJ-H column: 5% *i*-PrOH in $CO_2$, 1.5 mL/min) $t_r$ = 8.16 min (61%), 9.00 min (39%).

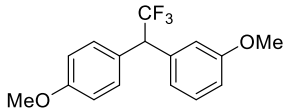


**1-Methoxy-3-(2,2,2-trifluoro-1-(4-methoxyphenyl)ethyl)benzene (10b):** Pale yellow oil (68%); IR (KBr) 3438, 3055, 2987, 2306, 1611, 1515, 1263, 1158, 896, 752, 706 $cm^{-1}$; $^{1}H$ NMR (500 MHz, $CDCl_3$) δ 7.32–7.27 (m, 3H), 6.97 (d, *J* = 7.8 Hz, 1H), 6.95–6.82 (m, 4H), 4.61 (q, *J* = 9.9 Hz, 1H), 3.80 (s, 3H), 3.80 (s, 3H); $^{13}C$ NMR (126 MHz, $CDCl_3$) δ 159.6, 159.1, 137.0, 130.1, 129.6, 127.3, 126.4 (q, *J* = 280.6 Hz), 121.2, 115.1, 114.0, 112.7, 55.2, 55.1, 54.6 (q, *J* = 27.7 Hz); $^{19}F$ NMR (471 MHz, $CDCl_3$) δ -66.0; HRMS (ESI-TOF) *m/z* calcd. for $C_{16}H_{15}O_2F_3$ $[M]^+$ 296.1024, found 296.1021; Chiral SFC (ChiralPak OJ-H column: 5% *i*-PrOH in $CO_2$, 1.5 mL/min) $t_r$ = 10.78 min (47%), 14.00 min (53%).

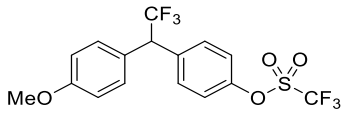


**4-(2,2,2-Trifluoro-1-(4-methoxyphenyl)ethyl)phenyl trifluoromethanesulfonate (10c):** Colorless oil (56%); IR (KBr) 3052, 2983, 2302, 1422, 1263, 1181, 1140, 895, 738, 704 $cm^{-1}$; $^{1}H$

NMR (500 MHz, $CDCl_3$) δ 7.46 (d, *J* = 8.9 Hz, 2H), 7.28-7.25 (m, 4H), 6.91 (d, *J* = 8.8 Hz, 2H), 4.68 (q, *J* = 9.7 Hz, 1H), 3.81 (s, 3H); $^{13}C$ NMR (126 MHz, $CDCl_3$) δ 159.4, 148.9, 136.2, 130.8, 130.1, 126.3, 125.8 (q, *J* = 280.2 Hz), 121.5, 118.6 (q, *J* = 320.5 Hz), 114.2, 55.2, 54.0 (q, *J* = 27.7 Hz); $^{19}F$ NMR (471 MHz, $CDCl_3$) δ -66.2, -72.8; HRMS (ES*i*-TOF) *m/z* calcd. for $C_{16}H_{12}O_4F_6S$ $[M]^+$ 414.0361, found 414.0361; Chiral SFC (ChiralPak OJ-H column: 5% *i*-PrOH in $CO_2$, 1.5 mL/min) $t_r$ = 4.08 min (75%), 5.23 min (25%).

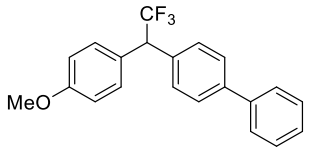


**4-(2,2,2-Trifluoro-1-(4-methoxyphenyl)ethyl)-1,1'-biphenyl (10d):** White solid (61%): mp 69-71 °C; IR (KBr) 3052, 2983, 2366, 1422, 1267, 895, 749, 706 $cm^{-1}$; $^1H$ NMR (500 MHz, $CDCl_3$) δ 7.60 (d, *J* = 7.7 Hz, 4H), 7.47-7.44 (m, 4H), 7.39 - 7.34 (m, 3H), 6.92 (d, *J* = 8.0 Hz, 2H), 4.71 (q, *J* = 9.9 Hz, 1H), 3.82 (s, 3H); $^{13}C$ NMR (126 MHz, $CDCl_3$) δ 159.3, 140.7, 140.5, 134.7, 130.3, 129.4, 128.8, 127.5, 127.5, 127.4, 127.1, 126.3 (q, *J* = 280.6 Hz), 114.2, 55.3 (q, *J* = 3.8 Hz), 54.5 (q, *J* = 27.7 Hz); $^{19}F$ NMR (471 MHz, $CDCl_3$) δ -66.0; HRMS (ESI-TOF) *m/z* calcd. for $C_{21}H_{17}OF_3$ $[M]^+$ 342.1232, found 342.1231; Chiral SFC (ChiralPak OJ-H column: 5% *i*-PrOH in $CO_2$, 1.5 mL/min) $t_r$ = 4.25 min (58%), 8.75 min (42%).

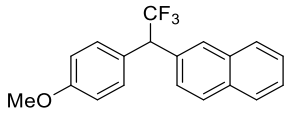


**2-(2,2,2-Trifluoro-1-(4-methoxyphenyl)ethyl)naphthalene (10e):** Pale yellow solid (66%): mp 57-59; IR (KBr) 3052, 2983, 2301, 1512, 1422, 1267, 1153, 897, 740, 704 $cm^{-1}$; $^1H$ NMR (500 MHz, $CDCl_3$) δ 7.90 (s, 1H), 7.87-7.82 (m, 3H), 7.53-7.49 (m, 2H), 7.45 (d, *J* = 8.5 Hz, 1H), 7.35 (d, *J* = 8.3 Hz, 2H), 6.91 (d, *J* = 7.8 Hz, 2H), 4.84 (q, *J* = 9.9 Hz, 1H), 3.81 (s, 3H); $^{13}C$ NMR (126 MHz, $CDCl_3$) δ 159.4, 133.4, 133.3, 132.8, 130.5, 128.6, 128.2, 128.1, 127.8, 127.6, 126.9, 126.6,

126.5 (q, $J$ = 280.6 Hz), 126.5, 114.3, 55.4, 55.0 (q, $J$ = 27.7 Hz); $^{19}$F NMR (471 MHz, $CDCl_3$) δ -65.8; HRMS (ESI-TOF) *m/z* calcd. for $C_{19}H_{15}OF_3$ $[M]^+$ 316.1075, found 316.1075; Chiral SFC (ChiralPak OJ-H column: 5% *i*-PrOH in $CO_2$, 1.5 mL/min) $t_r$ = 28.85 min (57%), 33.15 min (43%).

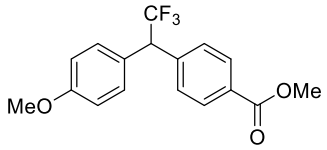


**4-(2,2,2-Trifluoro-1-(4-methoxyphenyl)ethyl)benzoate (10f):** Pale yellow oil (78%); IR (KBr) 3052, 2983, 2306, 1723, 1516, 1439, 1265, 1159, 1108, 899, 740, 706 cm$^{-1}$; $^1$H NMR (500 MHz, $CDCl_3$) δ 8.02 (d, $J$ = 8.4 Hz, 2H), 7.44 (d, $J$ = 8.1 Hz, 2H), 7.26 (d, $J$ = 8.6 Hz, 2H), 6.88 (d, $J$ = 8.7 Hz, 2H), 4.69 (q, $J$ = 9.8 Hz, 1H), 3.91 (s, 3H), 3.79 (s, 3H); $^{13}$C NMR (126 MHz, $CDCl_3$) δ 166.7, 159.6, 140.8, 130.4, 130.1, 129.8, 129.1, 126.8, 126.1 (q, $J$ = 280.6 Hz), 114.4, 55.4, 54.8 (q, $J$ = 27.7 Hz), 52.3; $^{19}$F NMR (471 MHz, $CDCl_3$) δ -66.0;HRMS (ESI-TOF) *m/z* calcd. for $C_{17}H_{15}O_3F_2$ $[M]^+$ 324.0973, found 324.0973; Chiral SFC (ChiralPak OJ-H column: 5% *i*-PrOH in $CO_2$, 1.5 mL/min) $t_r$ = 9.48 min (50%), 11.23 min (50%).

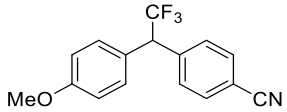


**4-(2,2,2-Trifluoro-1-(4-methoxyphenyl)ethyl)benzonitrile (10g):** Pale yellow oil (76%); IR (KBr) 3056, 2987, 2306, 2233, 1613, 1512, 1422, 1263, 1162, 895, 738, 706 cm$^{-1}$; $^1$H NMR (500 MHz, $CDCl_3$) δ 7.64 (d, $J$ = 8.3 Hz, 2H), 7.48 (d, $J$ = 8.0 Hz, 2H), 7.23 (d, $J$ = 8.4 Hz, 2H), 6.89 (d, $J$ = 8.8 Hz, 2H), 4.69 (q, $J$ = 9.6 Hz, 1H), 3.80 (s, 3H); $^{13}$C NMR (126 MHz, $CDCl_3$) δ 159.5, 140.8, 132.4, 130.1, 129.7, 125.9, 125.6 (q, $J$ = 280.2 Hz), 118.3, 114.3, 111.9, 55.2, 54.6 (q, $J$ = 28.1 Hz); $^{19}$F NMR (471 MHz, $CDCl_3$) δ -66.0; HRMS (ESI-TOF) *m/z* calcd. for $C_{16}H_{12}NOF_3$ $[M]^+$ 291.0871, found 291.0871; Chiral SFC (ChiralPak OD-H column: 5% *i*-PrOH in $CO_2$, 1.5 mL/min) $t_r$ = 9.16 min (60%), 10.08 min (40%).

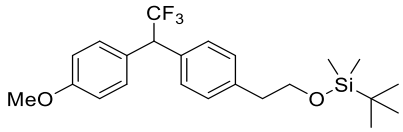


***tert*-Butyldimethyl(4-(2,2,2-trifluoro-1-(4-methoxyphenyl)ethyl)phenethoxy)silane (10h):** Pale yellow oil (64%); IR (KBr) 3056, 2953, 2310, 1514, 1422, 1265, 895, 738, 704 $cm^{-1}$; $^{1}H$ NMR (500 MHz, $CDCl_3$) δ 7.31–7.26 (m, 4H), 7.20 (d, *J* = 7.3 Hz, 2H), 6.88 (d, *J* = 8.8 Hz, 2H), 4.62 (q, *J* = 9.7 Hz, 1H), 3.82-3.79 (m, 5H), 2.82 (t, *J* = 7.0 Hz, 2H), 0.87 (s, 9H), -0.02 (s, 6H); $^{13}C$ NMR (126 MHz, $CDCl_3$) δ 159.0, 138.8, 133.4, 130.1, 129.4, 128.7, 127.6, 126.2 (q, *J* = 280.6 Hz), 113.9, 64.2, 55.1, 54.3 (q, *J* = 27.3 Hz), 39.0, 25.8, 18.2, -5.5; $^{19}F$ NMR (471 MHz, $CDCl_3$) δ -66.2; HRMS (ESI-TOF) *m/z* calcd. for $C_{23}H_{32}O_2F_3Si$ $[M+H]^+$ 425.2124, found 425.2140; Chiral SFC (ChiralPak OJ-H column: 3% *i*-PrOH in $CO_2$, 1.5 mL/min) $t_r$ = 9.42 min (55%), 11.97 min (45%).

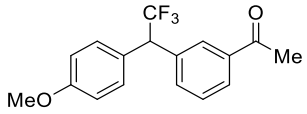


**1-(3-(2,2,2-Trifluoro-1-(4-methoxyphenyl)ethyl)phenyl)ethan-1-one (10i):** Pale yellow oil (68%); IR (KBr) 3056, 2841, 1686, 1516, 1267, 1159, 1103, 740, 706 $cm^{-1}$; $^{1}H$ NMR (500 MHz, $CDCl_3$) δ 7.97 (s, 1H), 7.89 (d, *J* = 7.5 Hz, 1H), 7.59 (d, *J* = 7.8 Hz, 1H), 7.46 (t, *J* = 7.8 Hz, 1H), 7.28 (d, *J* = 8.3 Hz, 2H), 6.89 (d, *J* = 6.7 Hz, 2H), 4.71 (q, *J* = 9.8 Hz, 1H), 3.79 (s, 3H), 2.59 (s, 3H); $^{13}C$ NMR (126 MHz, $CDCl_3$) δ 197.8, 159.5, 137.7, 136.6, 133.5, 130.3, 129.2, 128.9, 128.1, 126.9, 126.2 (q, *J* = 280.6 Hz), 114.4, 55.4 (q, *J* = 6.3 Hz), 54.7 (q, *J* = 27.7 Hz), 26.8; $^{19}F$ NMR (471 MHz, $CDCl_3$) δ -66.1; HRMS (ESI-TOF) *m/z* calcd. for $C_{17}H_{16}O_2F_3$ $[M+H]^+$ 309.1102, found 309.1100; Chiral SFC (ChiralPak OJ-H column: 5% *i*-PrOH in $CO_2$, 1.5 mL/min) $t_r$ = 12.40 min (38%), 14.65 min (62%).

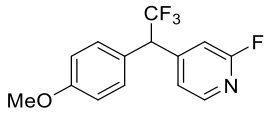


**2-Fluoro-4-(2,2,2-trifluoro-1-(4-methoxyphenyl)ethyl)pyridine (10j):** Pale yellow oil (51%); IR (KBr) 3052, 2987, 2302, 1613, 1514, 1422, 1267, 1166, 895, 734, 706 $cm^{-1}$; $^{1}H$ NMR (500 MHz, $CDCl_3$) δ 8.20 (d, *J* = 6.6 Hz, 1H), 7.22 (d, *J* = 7.9 Hz, 2H), 7.17 (d, *J* = 5.2 Hz, 1H), 6.94 (s, 1H), 6.90 (d, *J* = 10.3 Hz, 2H), 4.65 (q, *J* = 9.5 Hz, 1H), 3.80 (s, 3H); $^{13}C$ NMR (126 MHz, $CDCl_3$) δ 164.2 (d, *J* = 239.1 Hz), 159.9, 150.2 (d, *J* = 7.6 Hz), 148.2 (d, *J* = 15.1 Hz), 130.5, 125.2, 124.0 (q, *J* = 280.2 Hz), 121.8 (d, *J* = 3.8 Hz), 114.6, 110.1 (d, *J* = 39.0 Hz), 55.4, 54.1 (q, *J* = 27.7 Hz); $^{19}F$ NMR (471 MHz, $CDCl_3$) δ -66.0, -66.9; HRMS (ESI-TOF) *m/z* calcd. for $C_{14}H_{12}NOF_4$ $[M+H]^+$ 286.0855, found 286.0854; Chiral SFC (ChiralPak OD-H column: 3% *i*-PrOH in $CO_2$, 1.5 mL/min) $t_r$ = 11.68 min (80%), 19.58 min (20%).

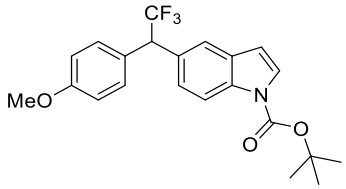


***tert*-Butyl 5-(2,2,2-trifluoro-1-(4-methoxyphenyl)ethyl)-1*H*-indole-1-carboxylate (10k):** Pale yellow oil (56%); IR (KBr) 3056, 2987, 2301, 1733, 1512, 1265, 1155, 895, 736, 706 $cm^{-1}$; $^{1}H$ NMR (500 MHz, $CDCl_3$) δ 8.09 (s, 1H), 7.59 (d, *J* = 15.4 Hz, 2H), 7.32-7.28 (m, 3H), 6.87 (d, *J* = 7.5 Hz, 2H), 6.55 (d, *J* = 3.8 Hz, 1H), 4.74 (q, *J* = 10.0 Hz, 1H), 3.79 (s, 3H), 1.66 (s, 9H); $^{13}C$ NMR (126 MHz, $CDCl_3$) δ 159.2, 149.8, 134.6, 130.9, 130.3, 130.2, 128.1, 126.7, 126.6 (q, *J* = 280.2 Hz), 125.4, 121.5, 115.5, 114.2, 107.4, 84.0, 55.4 (q, *J* = 3.8 Hz), 54.7 (q, *J* = 27.7 Hz), 28.3; $^{19}F$ NMR (471 MHz, $CDCl_3$) δ -66.1; HRMS (ESI-TOF) *m/z* calcd. for $C_{22}H_{23}NO_3F_3$ $[M+H]^+$ 406.1630, found 406.1637; Chiral SFC (ChiralPak OJ-H column: 5% *i*-PrOH in $CO_2$, 1.5 mL/min) $t_r$ = 14.19 min (35%), 16.06 min (65%).

**Procedure for photoredox cross-coupling reactions – varying $RBF_3K$'s:**

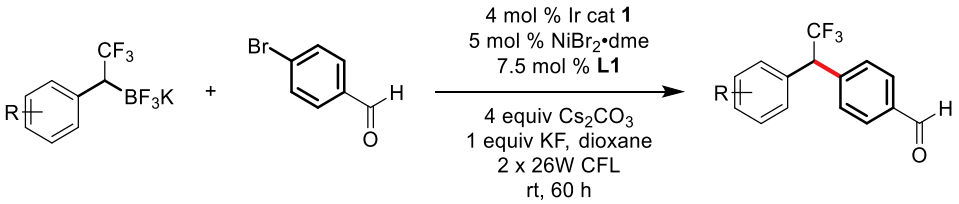


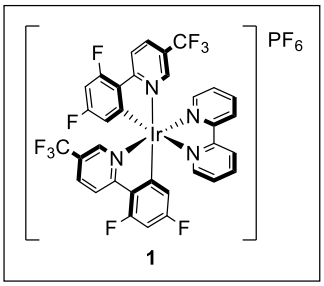


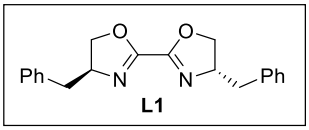


To a 2-dram vial vial (8 mL) equipped with a Teflon-coated magnetic stir bar was added **L1** (0.0024 g, 0.0075 mmol) and $NiBr_2$•dme (0.0015 g, 0.005 mmol) and 1.0 mL THF (from a JC Meyer solvent system). The resulting suspension was heated briefly with a heat gun until the nickel and ligand were fully solubilized, yielding an orange solution. The solvent was then removed under vacuum to give a fine coating of the ligated nickel complex, and the vial was placed under high vacuum. Once dry, 4-bromobenzaldehyde (0.0185 g, 0.1 mmol, 1 equiv), potassium trifluoro(2,2,2-trifluoro-1-arylethyl)borates (0.2 mmol, 2 equiv), and $Ir(dFCF_3ppy)_2(bpy)PF_6$ **1** (0.0040 g, 0.0040 mmol) were added. The vial was then transported into the glove box where $Cs_2CO_3$ (0.0130 g, 0.4 mmol) and KF (0.0058 g, 0.1 mmol) and dioxane (5 mL) were added, and the vial was then sealed tightly with a PTFE-lined PP storage cap. Once brought out of the glove box, the vial was further sealed with parafilm and placed in front of two 26 W fluorescent light bulbs with a fan blowing across to maintain an ambient temperature around 24 °C. After stirring for 60 h, the crude reaction mixture was filtered through a plug of Celite, washed with $CH_2Cl_2$, and then concentrated under vacuum.

Purification of the mixture by column chromatography, eluting with EtOAc and hexanes, was performed to obtain products in pure form.

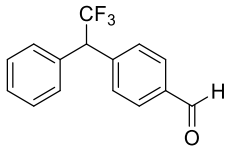

**4-(2,2,2-Trifluoro-1-phenylethyl)benzaldehyde (11a):** Pale yellow oil (45%); IR (KBr) 3943, 3688, 3054, 2987, 2305, 1704, 1422, 1266, 1161, 910, 738, 705 $cm^{-1}$; $^{1}H$ NMR (500 MHz, $CDCl_3$) δ 10.02 (s, 1H), 7.87 (d, *J* = 6.2 Hz, 2H), 7.55 (d, *J* = 7.8 Hz, 2H), 7.39-7.33 (m, 5H), 4.77 (q, *J* = 9.5 Hz, 1H); $^{13}C$ NMR (126 MHz, $CDCl_3$) δ 191.7, 142.1, 136.0, 134.6, 130.2, 130.0, 129.3, 129.1, 128.5, 125.9 (q, *J* = 280.6 Hz), 55.72 (q, *J* = 27.7 Hz); $^{19}F$ NMR (471 MHz, $CDCl_3$) δ -65.6; HRMS (ESI-TOF) *m/z* calcd. for $C_{15}H_{10}OF_3$ $[M-H]^-$ 263.0684, found 263.0673; Chiral SFC (ChiralPak OJ-H column: 5% *i*-PrOH in $CO_2$, 1.5 mL/min) $t_r$ = 12.24 min (46%), 15.68 min (54%).

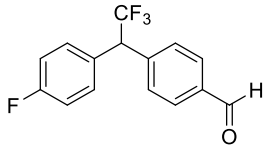

**4-(2,2,2-Trifluoro-1-(4-fluorophenyl)ethyl)benzaldehyde (11b):** Yellow oil (43%); IR (KBr) 3607, 3054, 2987, 2306, 1702, 1421, 1266, 1162, 896, 739, 705 $cm^{-1}$; $^{1}H$ NMR (500 MHz, $CDCl_3$) δ 10.02 (s, 1H), 7.88 (dd, *J* = 8.3, 1.8 Hz, 2H), 7.54 (d, *J* = 8.0 Hz, 2H), 7.34–7.31 (m, 2H), 7.08-7.04 (m, 2H), 4.77 (q, *J* = 9.6 Hz, 1H); $^{13}C$ NMR (126 MHz, $CDCl_3$) δ 191.7, 162.5 (d, *J* = 124.1 Hz), 141.7, 136.1, 131.0 (d, *J* = 8.8 Hz), 130.4 (d, *J* = 2.5 Hz), 130.2, 129.8, 125.8 (q, *J* = 280.6 Hz), 116.1 (d, *J* = 21.4 Hz), 54.9 (q, *J* = 28.1 Hz); $^{19}F$ NMR (471 MHz, $CDCl_3$) δ -65.9, -113.3; HRMS (ESI-TOF) *m/z* calcd. for $C_{15}H_{10}OF_4$ $[M]^+$ 282.0668, found 282.0673; Chiral SFC (ChiralPak OJ-H column: 5% *i*-PrOH in $CO_2$, 1.5 mL/min) $t_r$ = 7.00 min (39%), 7.93 min (61%).

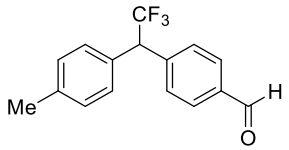


**4-(2,2,2-Trifluoro-1-(*p*-tolyl)ethyl)benzaldehyde (11c):** Yellow oil (70%); IR (KBr) 3435, 3047, 2983, 2310, 1703, 1421, 1264, 895, 740, 704 $cm^{-1}$; $^{1}H$ NMR (500 MHz, $CDCl_3$) δ 10.01 (s, 1H), 7.87 (d, *J* = 8.0 Hz, 2H), 7.56 (d, *J* = 7.9 Hz, 2H), 7.25 (d, *J* = 7.9 Hz, 2H), 7.18 (d, *J* = 7.9 Hz, 2H), 4.74 (q, *J* = 9.7 Hz, 1H), 2.35 (s, 3H); $^{13}C$ NMR (126 MHz, $CDCl_3$) δ 191.8, 142.3, 138.4, 135.9, 131.6, 130.1, 129.9, 129.8, 129.1, 126.0 (q, *J* = 280.6 Hz), 55.4 (q, *J* = 27.7 Hz), 21.2; $^{19}F$ NMR (471 MHz, $CDCl_3$) δ -65.7; HRMS (ESI-TOF) *m/z* calcd. for $C_{16}H_{13}OF_3$ $[M]^+$ 278.0918, found 278.0920; Chiral SFC (ChiralPak OJ-H column: 5% *i*-PrOH in $CO_2$, 1.5 mL/min) $t_r$ = 12.81 min (46%), 17.34 min (54%).

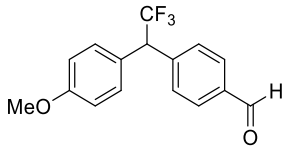


**4-(2,2,2-Trifluoro-1-(4-methoxyphenyl)ethyl)benzaldehyde (11d):** Pale yellow oil (75%); IR (KBr) 3436, 3054, 2987, 2306, 1703, 1422, 1266, 1160, 896, 740, 706 $cm^{-1}$; $^{1}H$ NMR (500 MHz, $CDCl_3$) δ 10.02 (s, 1H), 7.88 (d, *J* = 8.3 Hz, 2H), 7.56 (d, *J* = 8.0 Hz, 2H), 7.27 (d, *J* = 6.7 Hz, 2H), 6.90 (d, *J* = 8.8 Hz, 2H), 4.73 (q, *J* = 9.7 Hz, 1H), 3.81 (s, 3H); $^{13}C$ NMR (126 MHz, $CDCl_3$) δ 191.8, 159.6, 142.4, 135.9, 130.4, 130.1, 129.8, 126.6, 126.0 (q, *J* = 280.6 Hz), 114.4, 55.4, 54.9 (q, *J* = 27.7 Hz); $^{19}F$ NMR (471 MHz, $CDCl_3$) δ -65.9; HRMS (ESI-TOF) *m/z* calcd. for $C_{16}H_{13}O_2F_3$ $[M]^+$ 294.0868, found 294.0864; Chiral SFC (ChiralPak OJ-H column: 3% *i*-PrOH in $CO_2$, 1.5 mL/min) $t_r$ = 37.48 min (49%), 40.63 min (51%).

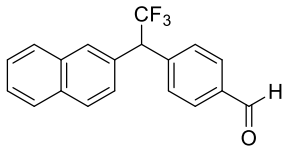


**4-(2,2,2-Trifluoro-1-(naphthalen-2-yl)ethyl)benzaldehyde (11e):** Pale yellow oil (53%); IR (KBr) 3686, 3054, 2986, 2305, 1708, 1421, 1266, 1159, 896, 741, 706 $cm^{-1}$; $^{1}H$ NMR (500 MHz, $CDCl_3$) δ 10.02 (s, 1H), 7.89–7.83 (m, 6H), 7.60 (d, *J* = 8.0 Hz, 2H), 7.54-7.50 (m, 2H), 7.40 (d, *J* = 8.6 Hz, 1H), 4.95 (q, *J* = 9.6 Hz, 1H); $^{13}C$ NMR (126 MHz, $CDCl_3$) δ 191.7, 142.0, 136.0, 133.3, 133.0, 131.9, 130.2, 130.1, 128.9, 128.5, 128.2, 127.8, 126.9, 126.8, 126.6, 126.0 (q, *J* = 280.6 Hz), 55.8 (q, *J* = 27.7 Hz); $^{19}F$ NMR (471 MHz, $CDCl_3$) δ -65.3; HRMS (ESI-TOF) *m/z* calcd. for $C_{19}H_{13}OF_3$ $[M]^+$ 314.0918, found 314.0915; Chiral SFC (ChiralPak OJ-H column: 10% *i*-PrOH in $CO_2$, 1.5 mL/min) $t_r$ = 15.95 min (59%), 17.67 min (41%).

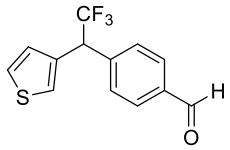


**4-(2,2,2-Trifluoro-1-(thiophen-3-yl)ethyl)benzaldehyde (11f):** Pale yellow oil (64%); IR (KBr) 2836, 1705, 1610, 1265, 1160, 1108, 826, 781, 738, 703 $cm^{-1}$; $^{1}H$ NMR (500 MHz, $CDCl_3$) δ 10.02 (s, 1H), 7.88 (d, *J* = 8.2 Hz, 2H), 7.54 (d, *J* = 7.7 Hz, 2H), 7.35-7.33 (m, 1H), 7.27 (s, 1H), 7.01 (d, *J* = 5.0 Hz, 1H), 4.86 (q, *J* = 9.4 Hz, 1H); $^{13}C$ NMR (126 MHz, $CDCl_3$) δ 191.7, 141.6, 136.2, 134.2, 130.2, 130.1, 127.9, 126.7, 125.7 (q, *J* = 280.6 Hz), 124.3, 51.6 (q, *J* = 28.5 Hz); $^{19}F$ NMR (471 MHz, $CDCl_3$) δ -66.8; HRMS (ESI-TOF) *m/z* calcd. for $C_{13}H_9OF_3S$ $[M]^+$ 270.0326, found 270.0326; Chiral SFC (ChiralPak OJ-H column: 5% *i*-PrOH in $CO_2$, 1.5 mL/min) $t_r$ = 10.95 min (51%), 13.41 min (49%).

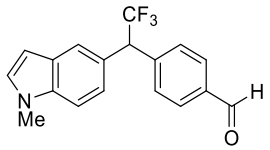


**4-(2,2,2-Trifluoro-1-(1-methyl-1*H*-indol-5-yl)ethyl)benzaldehyde (11g):** Red oil (32%); IR (KBr) 3054, 2987, 2325, 1708, 1265, 1166, 896, 741, 706 $cm^{-1}$; $^{1}H$ NMR (500 MHz, $CDCl_3$) δ 10.00 (s, 1H), 7.86 (d, *J* = 6.5 Hz, 2H), 7.67–7.57 (m, 3H), 7.30 (d, *J* = 8.5 Hz, 1H), 7.16 (d, *J* = 8.5 Hz, 1H), 7.08 (d, *J* = 3.2 Hz, 1H), 6.48 (d, *J* = 3.1 Hz, 1H), 4.87 (q, *J* = 9.8 Hz, 1H), 3.78 (s, 3H); $^{13}C$ NMR (126 MHz, $CDCl_3$) δ 191.9, 143.2, 136.4, 135.7, 130.1, 130.0, 129.9, 128.8, 126.3 (q, *J* = 280.6 Hz), 125.4, 122.7, 121.8, 109.8, 101.4, 55.8 (q, *J* = 27.7 Hz), 33.1; $^{19}F$ NMR (471 MHz, $CDCl_3$) δ -65.6; HRMS (ESI-TOF) *m/z* calcd. for $C_{18}H_{15}NOF_3$ $[M+H]^+$ 318.1106, found 318.1105; Chiral SFC (ChiralPak AS-H column: 10% *i*-PrOH in $CO_2$, 1.5 mL/min) $t_r$ = 8.22 min (53%), 9.42 min (47%).

## 5.5 References

(1) Argintaru, O. A.; Ryu, D.; Aron, I.; Molander, G. A. *Angew. Chem. Int. Ed.* **2013**, *52*, 13656-13660.

(2) a) Kaluszyner, A. *J. Org. Chem.* **1960**, *25*, 473-474; b) Briody, J. M.; Marshall, G. L. *Synthesis* **1982**, 939-940.

(3) a) Jarczewski, A.; Schroeder, G.; Galezowski, W.; Leffek, K. T.; Maciejewska, U. *Can. J. Chem.* **1985**, *63*, 576-580; b) Guy, A.; Lobgeois, A.; Lemaire, M. *J. Fluorine Chem.* **1986**, *32*, 361-366; c) Prakash, G. K. S.; Paknia, F.; Mathew, T.; Mlostoń, G.; Joschek, J. P.; Olah, G. A. *Org. Lett.* **2011**, *13*, 4128-4131.

(4) Wang, Z.; Ai, F.; Wang, Z.; Zhao, W.; Zhu, G.; Lin, Z.; Sun, J. *J. Am. Chem. Soc.* **2015**, *137*, 383-389.

(5) Schmink, J. R.; Bellomo, A.; Berritt, S. *Aldrichim. Acta* **2013**, *46*, 71-80.

(6) Furuya, T.; Kamlet, A. S.; Ritter, T. *Nature* **2011**, *473*, 470-477.

(7) a) Tellis, J. C.; Primer, D. N.; Molander, G. A. *Science* **2014**, *345*, 433-436; b) Primer, D. N.; Karakaya, I.; Tellis, J. C.; Molander, G. A. *J. Am. Chem. Soc.* **2015**, *137*, 2195–2198.

(8) Gutierrez, O.; Tellis, J. C.; Primer, D. N.; Molander, G. A.; Kozlowski, M. C. *J. Am. Chem. Soc.* **2015**, *137*, 4896-4899.

(9) Koike, T.; Akita, M. *Inorg. Chem. Front.* **2014**, *1*, 562-562.

(10) Denmark, S. E.; Stavenger, R. A.; Faucher, A.-M.; Edwards, J. P. *J. Org. Chem.* **1997**, *62*, 3375-3389.

(11) Lakowicz, J. R. *Principles of Fluorescence Spectroscopy*; 3 ed.; Springer: New York, 2007.

**Author Contributions:**

D.N.P. assisted in the design of the project, wrote and edited the manuscript, and prepared some of the compounds made in this study. DaWeon Ryu optimized the reaction, prepared the compounds, and edited the manuscript. John C. Tellis assisted in the conception of the project and helped write and edit the manuscript.

## Appendix A4. Cyclic Voltammetry (CV) Data Relevant to Chapter 5

Electrochemical measurements were recorded on a CH Instruments: Model 600E Series Electrochemical Analyzer (observed in 0.002 M MeCN; $[N(Bu)_4](PF_6)$ = 0.1 M; Ag/AgCl = electrode; reported in SCE based on a ferrocene internal standard).

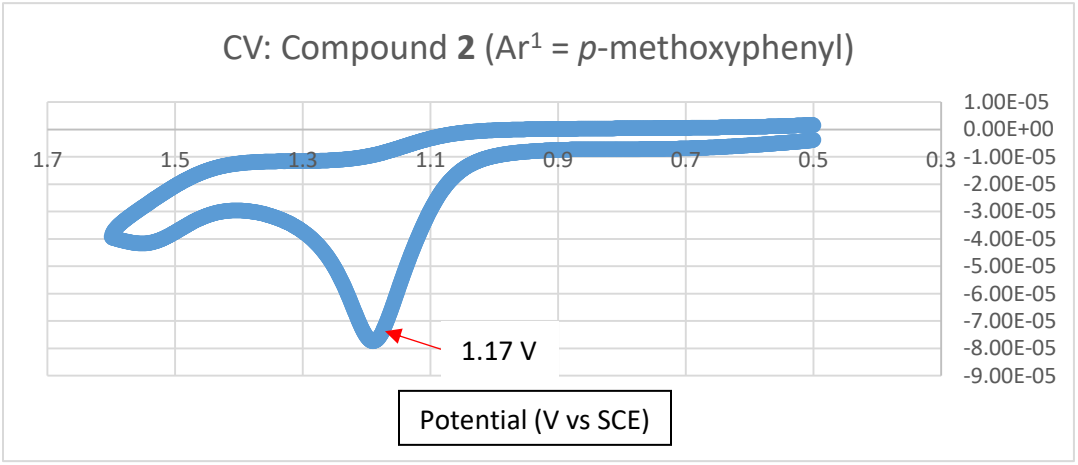


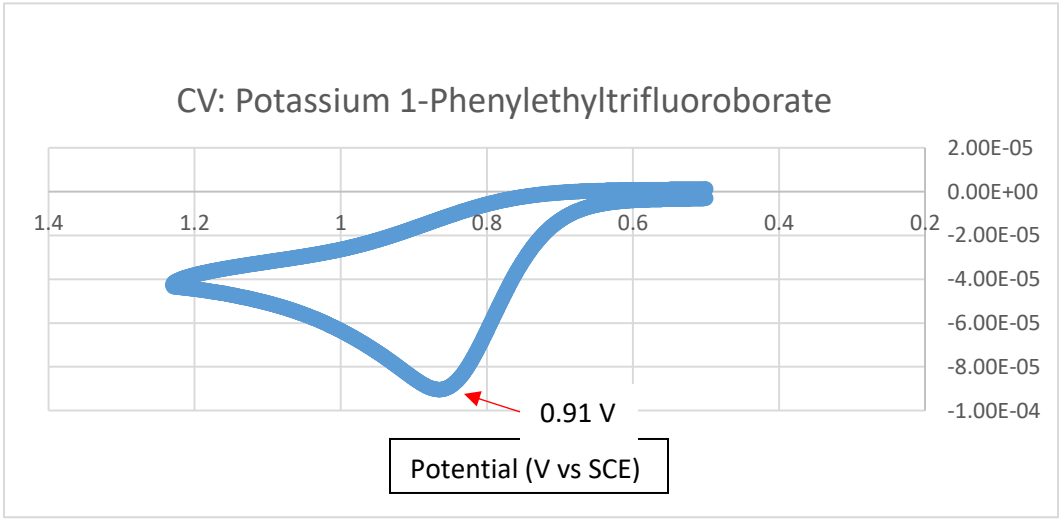

# Appendix A5. Chiral SFC Chromatograms Relevant to Chapter 5

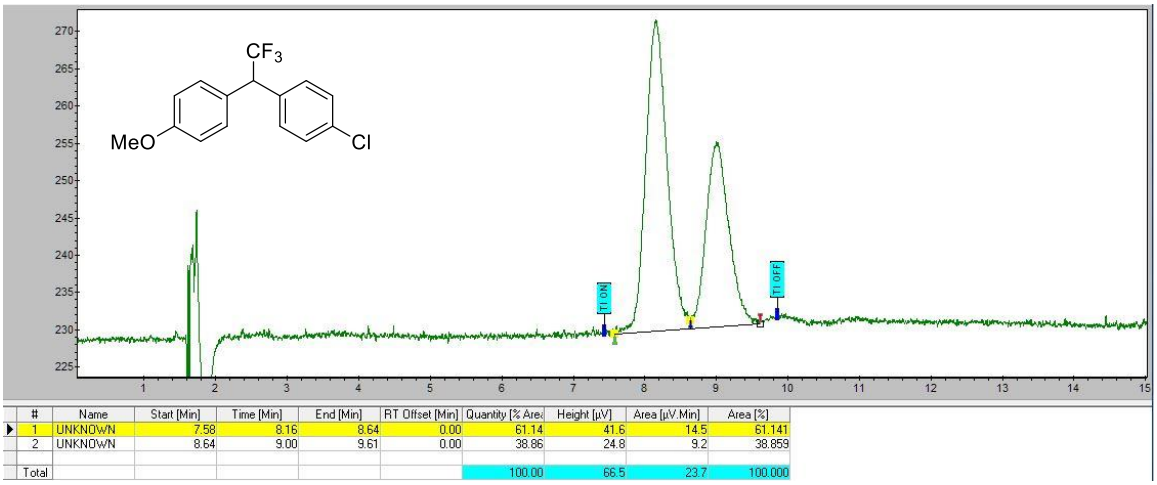


| # | Name | Start [Min] | Time [Min] | End [Min] | RT Offset [Min] | Quantity [% Area] | Height [µV] | Area [µV.Min] | Area [%] |
|---|---|---|---|---|---|---|---|---|---|
| 1 | UNKNOWN | 7.58 | 8.16 | 8.64 | 0.00 | 61.14 | 41.6 | 14.5 | 61.141 |
| 2 | UNKNOWN | 8.64 | 9.00 | 9.61 | 0.00 | 38.86 | 24.8 | 9.2 | 38.859 |
| Total | | | | | | 100.00 | 66.5 | 23.7 | 100.000 |

**Figure A5.1.** Chiral SFC (OJ-H column: 5% *i*-PrOH in $CO_2$, 1.5 mL/min) chromatogram of 1-chloro-4-(2,2,2-trifluoro-1-phenylethyl)benzene (**10a**)

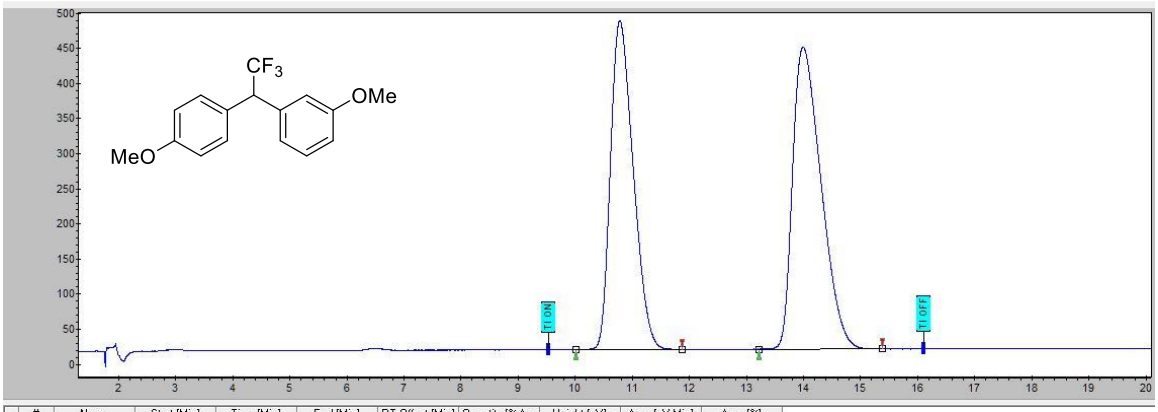


| # | Name | Start [Min] | Time [Min] | End [Min] | RT Offset [Min] | Quantity [% Area] | Height [µV] | Area [µV.Min] | Area [%] |
|---|---|---|---|---|---|---|---|---|---|
| 1 | UNKNOWN | 10.02 | 10.78 | 11.88 | 0.00 | 46.52 | 468.8 | 216.8 | 46.517 |
| 2 | UNKNOWN | 13.22 | 14.00 | 15.39 | 0.00 | 53.48 | 430.6 | 249.2 | 53.483 |
| Total | | | | | | 100.00 | 899.4 | 466.0 | 100.000 |

**Figure A5.2.** Chiral SFC (OJ-H column: 5% *i*-PrOH in $CO_2$, 1.5 mL/min) chromatogram of 1-methoxy-3-(2,2,2-trifluoro-1-(4-methoxyphenyl)ethyl)benzene (**10b**)

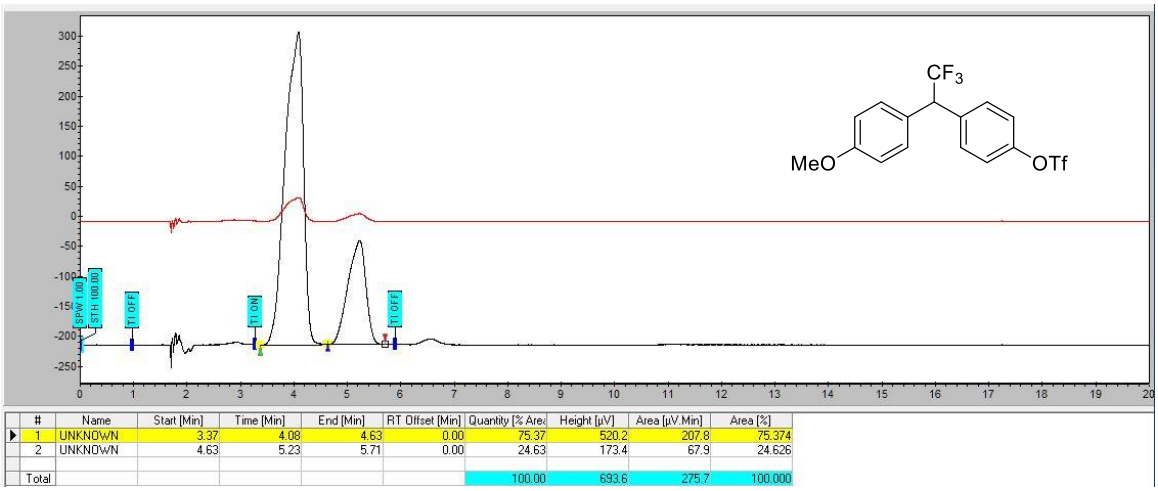


| # | Name | Start [Min] | Time [Min] | End [Min] | RT Offset [Min] | Quantity [% Area] | Height [µV] | Area [µV.Min] | Area [%] |
|---|---|---|---|---|---|---|---|---|---|
| 1 | UNKNOWN | 3.37 | 4.08 | 4.63 | 0.00 | 75.37 | 520.2 | 207.8 | 75.374 |
| 2 | UNKNOWN | 4.63 | 5.23 | 5.71 | 0.00 | 24.63 | 173.4 | 67.9 | 24.626 |
| Total | | | | | | 100.00 | 693.6 | 275.7 | 100.000 |

**Figure A5.3.** Chiral SFC (OJ-H column: 5% *i*-PrOH in $CO_2$, 1.5 mL/min) chromatogram of 4-(2,2,2-trifluoro-1-(4-methoxyphenyl)ethyl)phenyl trifluoromethanesulfonate (**10c**)

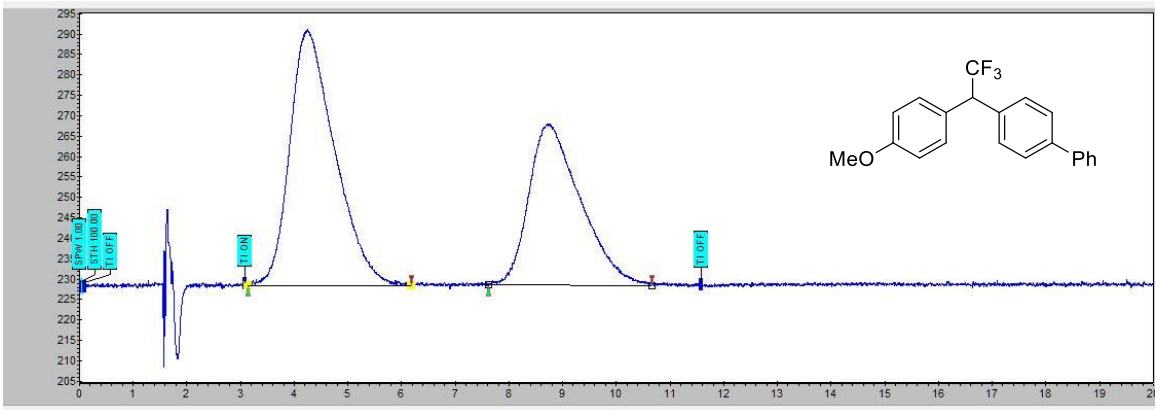


| # | Name | Start [Min] | Time [Min] | End [Min] | RT Offset [Min] | Quantity [% Area] | Height [µV] | Area [µV.Min] | Area [%] |
|---|---|---|---|---|---|---|---|---|---|
| 1 | UNKNOWN | 3.13 | 4.25 | 6.19 | 0.00 | 58.05 | 62.7 | 61.1 | 58.051 |
| 2 | UNKNOWN | 7.62 | 8.75 | 10.66 | 0.00 | 41.95 | 39.5 | 44.1 | 41.949 |
| Total | | | | | | 100.00 | 102.2 | 105.2 | 100.000 |

**Figure A5.4.** Chiral SFC (OJ-H column: 5% *i*-PrOH in $CO_2$, 1.5 mL/min) chromatogram of 4-(2,2,2-trifluoro-1-(4-methoxyphenyl)ethyl)-1,1'-biphenyl (**10d**)

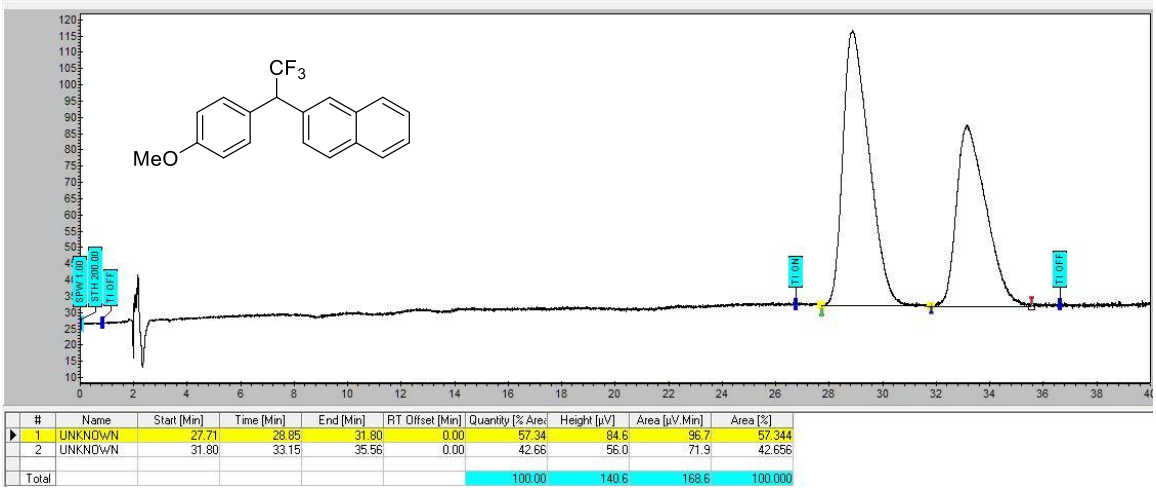


| # | Name | Start [Min] | Time [Min] | End [Min] | RT Offset [Min] | Quantity [% Area] | Height [µV] | Area [µV.Min] | Area [%] |
|---|---|---|---|---|---|---|---|---|---|
| 1 | UNKNOWN | 27.71 | 28.85 | 31.80 | 0.00 | 57.34 | 84.6 | 96.7 | 57.344 |
| 2 | UNKNOWN | 31.80 | 33.15 | 35.56 | 0.00 | 42.66 | 56.0 | 71.9 | 42.656 |
| Total | | | | | | 100.00 | 140.6 | 168.6 | 100.000 |

**Figure A5.5.** Chiral SFC (OJ-H column: 5% *i*-PrOH in $CO_2$, 1.5 mL/min) chromatogram of 2-(2,2,2-trifluoro-1-(4-methoxyphenyl)ethyl)naphthalene (**10e**)

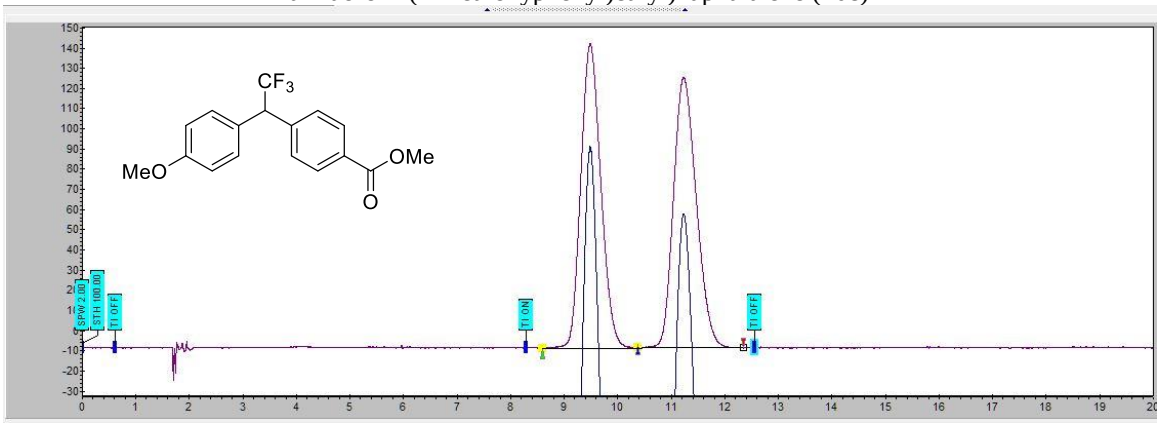


| # | Name | Start [Min] | Time [Min] | End [Min] | RT Offset [Min] | Quantity [% Area] | Height [µV] | Area [µV.Min] | Area [%] |
|---|---|---|---|---|---|---|---|---|---|
| 1 | UNKNOWN | 8.59 | 9.48 | 10.38 | 0.00 | 49.60 | 150.9 | 65.3 | 49.598 |
| 2 | UNKNOWN | 10.38 | 11.23 | 12.35 | 0.00 | 50.40 | 134.0 | 66.3 | 50.402 |
| Total | | | | | | 100.00 | 284.9 | 131.6 | 100.000 |

**Figure A5.6.** Chiral SFC (OJ-H column: 5% *i*-PrOH in $CO_2$, 1.5 mL/min) chromatogram of methyl 4-(2,2,2-trifluoro-1-(4-methoxyphenyl)ethyl)benzoate (**10f**)

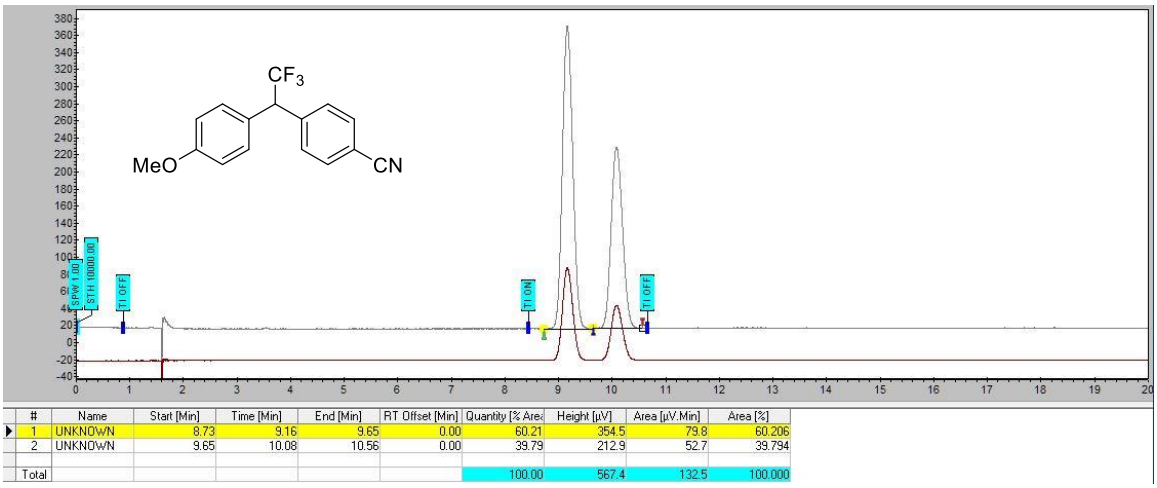


| # | Name | Start [Min] | Time [Min] | End [Min] | RT Offset [Min] | Quantity [% Area] | Height [µV] | Area [µV.Min] | Area [%] |
|---|---|---|---|---|---|---|---|---|---|
| 1 | UNKNOWN | 8.73 | 9.16 | 9.65 | 0.00 | 60.21 | 354.5 | 79.8 | 60.206 |
| 2 | UNKNOWN | 9.65 | 10.08 | 10.56 | 0.00 | 39.79 | 212.9 | 52.7 | 39.794 |
| Total | | | | | | 100.00 | 567.4 | 132.5 | 100.000 |

**Figure A5.7.** Chiral SFC (OD-H column: 5% *i*-PrOH in $CO_2$, 1.5 mL/min) chromatogram of 4-(2,2,2-trifluoro-1-(4-methoxyphenyl)ethyl)benzonitrile (**10g**)

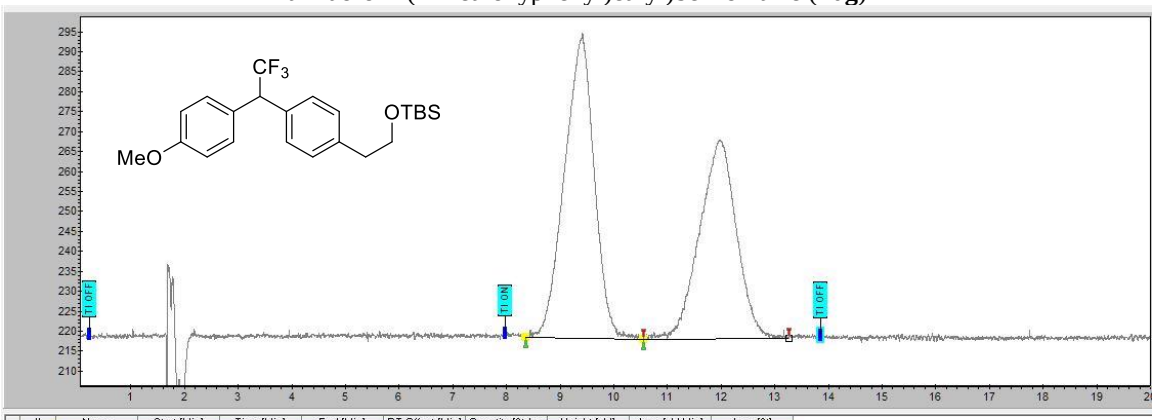


| # | Name | Start [Min] | Time [Min] | End [Min] | RT Offset [Min] | Quantity [% Area] | Height [µV] | Area [µV.Min] | Area [%] |
|---|---|---|---|---|---|---|---|---|---|
| 1 | UNKNOWN | 8.36 | 9.42 | 10.56 | 0.00 | 55.10 | 76.4 | 49.1 | 55.103 |
| 2 | UNKNOWN | 10.56 | 11.97 | 13.26 | 0.00 | 44.90 | 49.9 | 40.0 | 44.897 |
| Total | | | | | | 100.00 | 126.2 | 89.0 | 100.000 |

**Figure A5.8.** Chiral SFC (OJ-H column: 3% *i*-PrOH in $CO_2$, 1.5 mL/min) chromatogram of *tert*-butyldimethyl(4-(2,2,2-trifluoro-1-(4-methoxyphenyl)ethyl)phenethoxy)silane (**10h**)

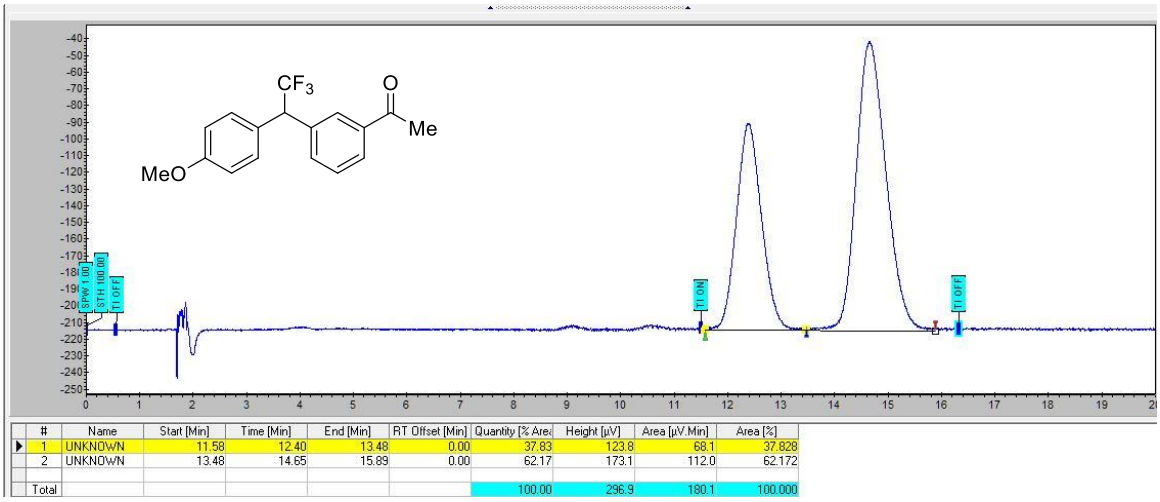


| # | Name | Start [Min] | Time [Min] | End [Min] | RT Offset [Min] | Quantity [% Area] | Height [µV] | Area [µV.Min] | Area [%] |
|---|---|---|---|---|---|---|---|---|---|
| 1 | UNKNOWN | 11.58 | 12.40 | 13.48 | 0.00 | 37.83 | 123.8 | 68.1 | 37.828 |
| 2 | UNKNOWN | 13.48 | 14.65 | 15.89 | 0.00 | 62.17 | 173.1 | 112.0 | 62.172 |
| Total | | | | | | 100.00 | 296.9 | 180.1 | 100.000 |

**Figure A5.9.** Chiral SFC (OJ-H column: 5% *i*-PrOH in $CO_2$, 1.5 mL/min) chromatogram of 1-(3-(2,2,2-trifluoro-1-(4-methoxyphenyl)ethyl)phenyl)ethan-1-one (**10i**)

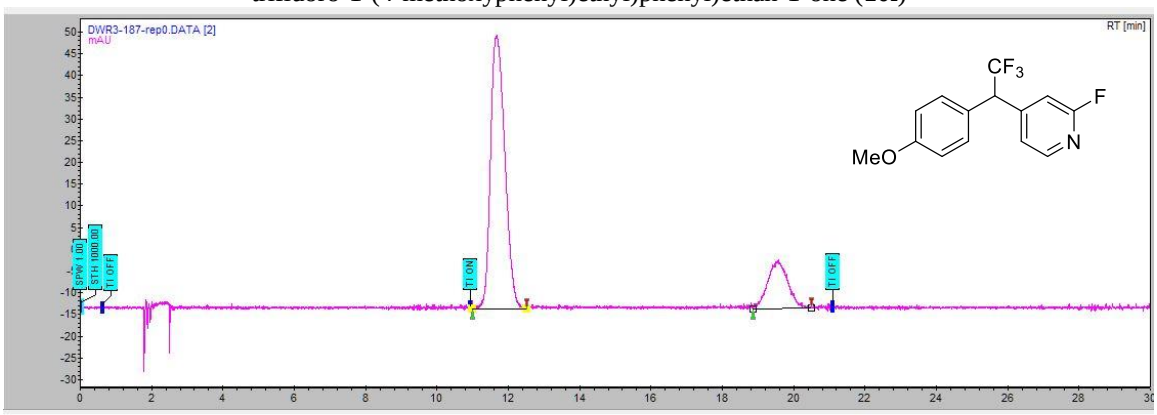


| # | Name | Start [Min] | Time [Min] | End [Min] | RT Offset [Min] | Quantity [% Area] | Height [µV] | Area [µV.Min] | Area [%] |
|---|---|---|---|---|---|---|---|---|---|
| 1 | UNKNOWN | 11.00 | 11.68 | 12.50 | 0.00 | 80.15 | 62.9 | 29.3 | 80.145 |
| 2 | UNKNOWN | 18.86 | 19.58 | 20.49 | 0.00 | 19.85 | 11.3 | 7.3 | 19.855 |
| Total | | | | | | 100.00 | 74.2 | 36.6 | 100.000 |

**Figure A5.10-1.** Chiral SFC (OD-H column: 3% *i*-PrOH in $CO_2$, 1.5 mL/min) chromatogram of 2-fluoro-4-(2,2,2-trifluoro-1-(4-methoxyphenyl)ethyl)pyridine (**10j**)

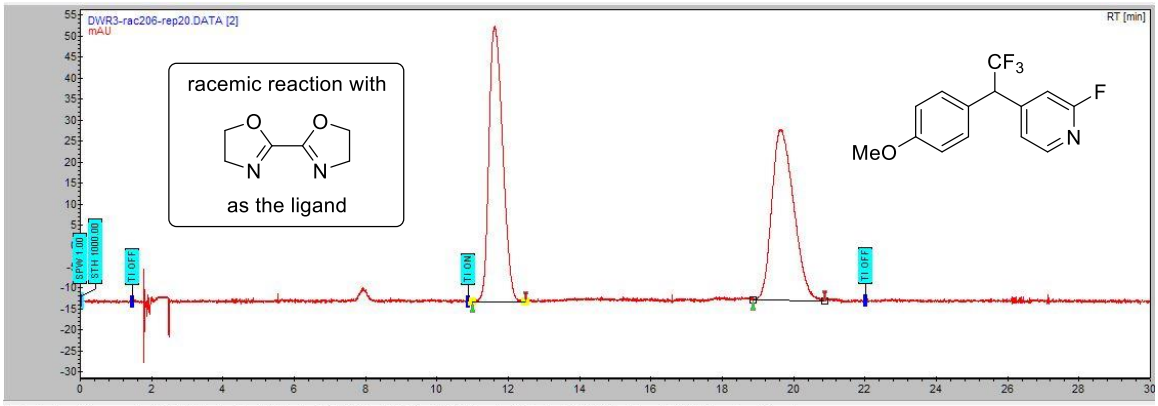


| # | Name | Start [Min] | Time [Min] | End [Min] | RT Offset [Min] | Quantity [% Area] | Height [µV] | Area [µV.Min] | Area [%] |
|---|---|---|---|---|---|---|---|---|---|
| 1 | UNKNOWN | 11.01 | 11.62 | 12.49 | 0.00 | 50.37 | 65.7 | 29.4 | 50.369 |
| 2 | UNKNOWN | 18.87 | 19.65 | 20.87 | 0.00 | 49.63 | 40.8 | 29.0 | 49.631 |
| Total | | | | | | 100.00 | 106.5 | 58.4 | 100.000 |

**Figure A5.10-2.** Chiral SFC (OD-H column: 3% *i*-PrOH in $CO_2$, 1.5 mL/min) chromatogram of 2-fluoro-4-(2,2,2-trifluoro-1-(4-methoxyphenyl)ethyl)pyridine (**1j**) from a racemic reaction

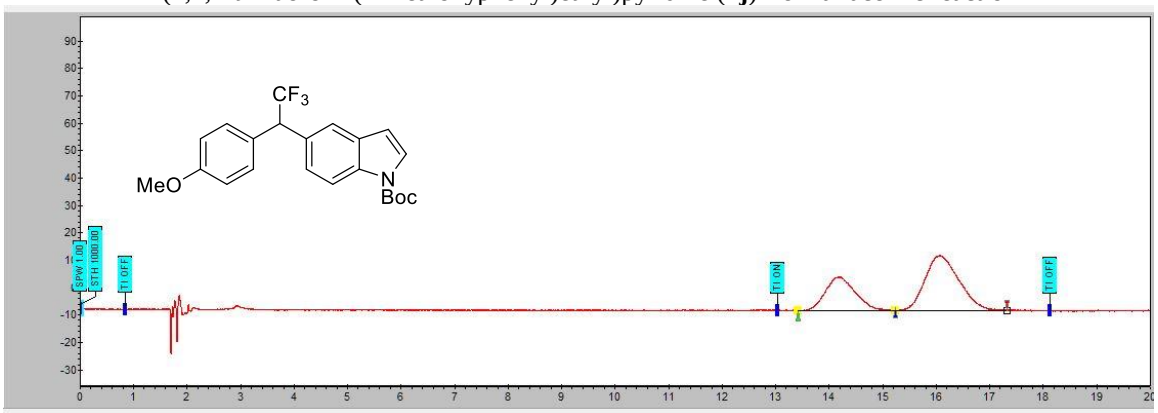


| # | Name | Start [Min] | Time [Min] | End [Min] | RT Offset [Min] | Quantity [% Area] | Height [µV] | Area [µV.Min] | Area [%] |
|---|---|---|---|---|---|---|---|---|---|
| 1 | UNKNOWN | 13.42 | 14.19 | 15.24 | 0.00 | 35.27 | 12.4 | 8.1 | 35.270 |
| 2 | UNKNOWN | 15.24 | 16.06 | 17.33 | 0.00 | 64.73 | 20.1 | 14.8 | 64.730 |
| Total | | | | | | 100.00 | 32.5 | 22.9 | 100.000 |

**Figure A5.11.** Chiral SFC (OJ-H column: 5% *i*-PrOH in $CO_2$, 1.5 mL/min) chromatogram of *tert*-butyl 5-(2,2,2-trifluoro-1-(4-methoxyphenyl)ethyl)-1*H*-indole-1-carboxylate (**10k**)

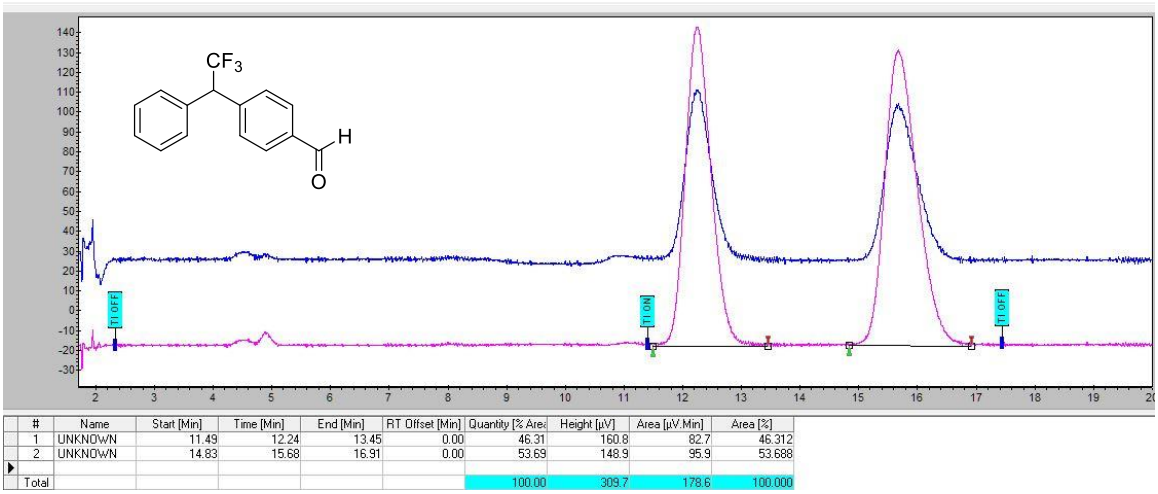


| # | Name | Start [Min] | Time [Min] | End [Min] | RT Offset [Min] | Quantity [% Area] | Height [µV] | Area [µV.Min] | Area [%] |
|---|---|---|---|---|---|---|---|---|---|
| 1 | UNKNOWN | 11.49 | 12.24 | 13.45 | 0.00 | 46.31 | 160.8 | 82.7 | 46.312 |
| 2 | UNKNOWN | 14.83 | 15.68 | 16.91 | 0.00 | 53.69 | 148.9 | 95.9 | 53.688 |
| Total | | | | | | 100.00 | 309.7 | 178.6 | 100.000 |

**Figure A5.12.** Chiral SFC (OJ-H column: 5% *i*-PrOH in $CO_2$, 1.5 mL/min) chromatogram of 4-(2,2,2-trifluoro-1-phenylethyl)benzaldehyde (**11a**)

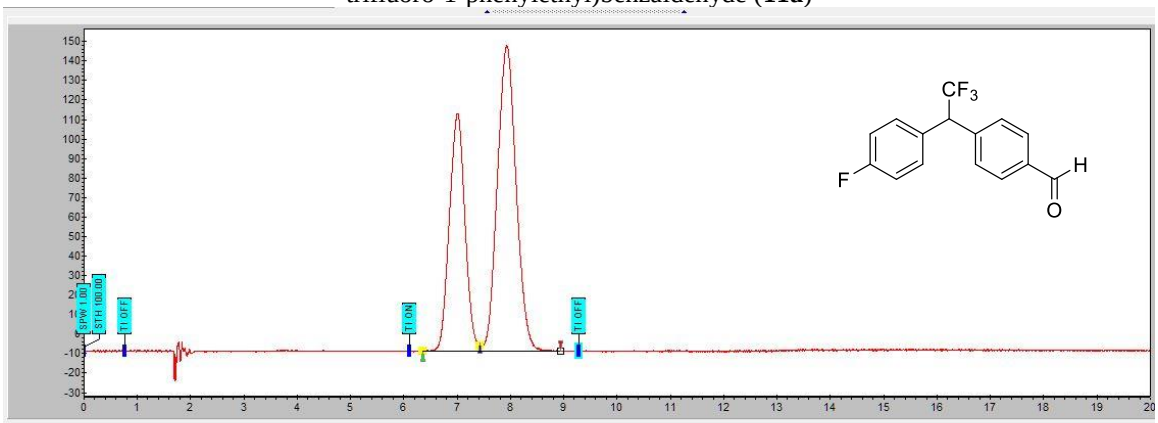


| # | Name | Start [Min] | Time [Min] | End [Min] | RT Offset [Min] | Quantity [% Area] | Height [µV] | Area [µV.Min] | Area [%] |
|---|---|---|---|---|---|---|---|---|---|
| 1 | UNKNOWN | 6.35 | 7.00 | 7.44 | 0.00 | 39.19 | 121.9 | 41.5 | 39.189 |
| 2 | UNKNOWN | 7.44 | 7.93 | 8.95 | 0.00 | 60.81 | 156.8 | 64.4 | 60.811 |
| Total | | | | | | 100.00 | 278.7 | 105.9 | 100.000 |

**Figure A5.13.** Chiral SFC (OJ-H column: 5% *i*-PrOH in $CO_2$, 1.5 mL/min) chromatogram of 4-(2,2,2-trifluoro-1-(4-fluorophenyl)ethyl)benzaldehyde (**11b**)

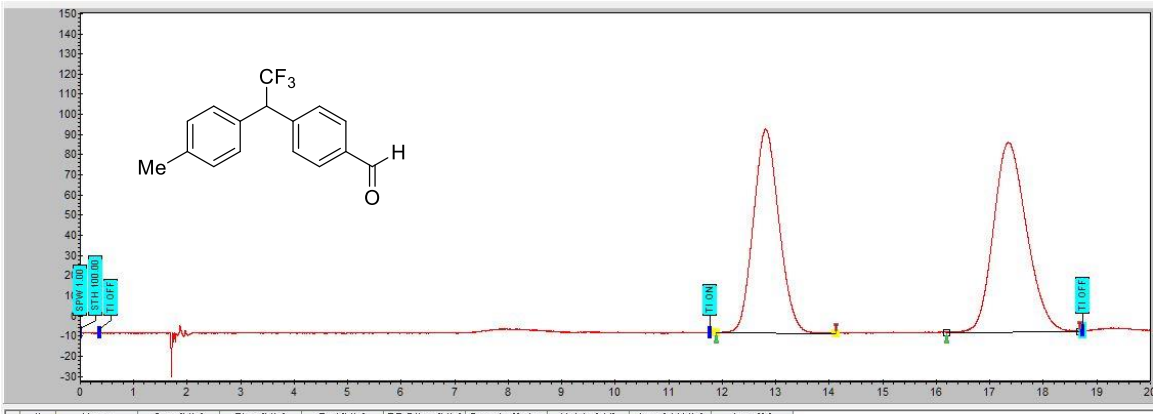


| # | Name | Start [Min] | Time [Min] | End [Min] | RT Offset [Min] | Quantity [% Area] | Height [µV] | Area [µV.Min] | Area [%] |
|---|---|---|---|---|---|---|---|---|---|
| 1 | UNKNOWN | 11.88 | 12.81 | 14.13 | 0.00 | 45.59 | 101.3 | 56.5 | 45.594 |
| 2 | UNKNOWN | 16.19 | 17.34 | 18.68 | 0.00 | 54.41 | 94.0 | 67.5 | 54.406 |
| Total | | | | | | 100.00 | 195.3 | 124.0 | 100.000 |

**Figure A5.14.** Chiral SFC (OJ-H column: 5% *i*-PrOH in $CO_2$, 1.5 mL/min) chromatogram of 4-(2,2,2-trifluoro-1-(*p*-tolyl)ethyl)benzaldehyde (**11c**)

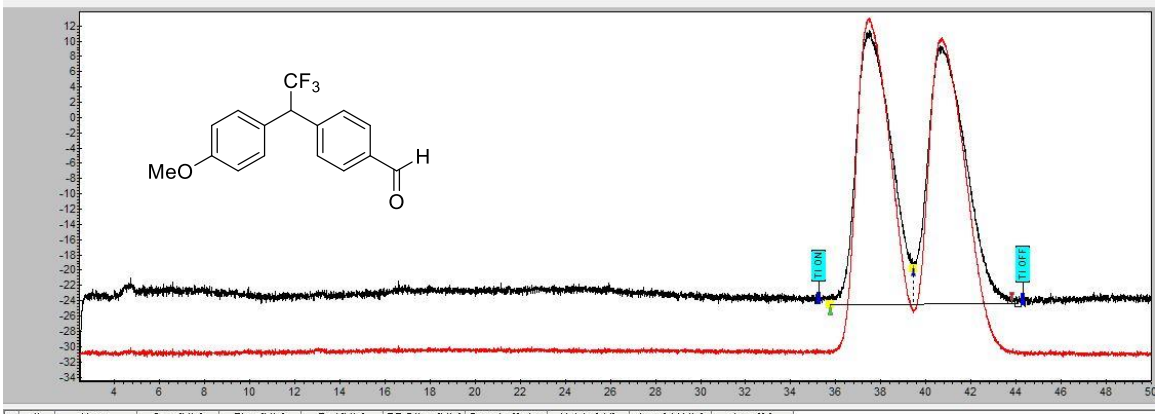


| # | Name | Start [Min] | Time [Min] | End [Min] | RT Offset [Min] | Quantity [% Area] | Height [µV] | Area [µV.Min] | Area [%] |
|---|---|---|---|---|---|---|---|---|---|
| 1 | UNKNOWN | 35.74 | 37.48 | 39.45 | 0.00 | 49.37 | 35.9 | 64.4 | 49.368 |
| 2 | UNKNOWN | 39.45 | 40.63 | 43.80 | 0.00 | 50.63 | 33.8 | 66.0 | 50.632 |
| Total | | | | | | 100.00 | 69.7 | 130.4 | 100.000 |

**Figure A5.15.** Chiral SFC (OJ-H column: 3% *i*-PrOH in $CO_2$, 1.5 mL/min) chromatogram of 4-(2,2,2-trifluoro-1-(4-methoxyphenyl)ethyl)benzaldehyde (**11d**)

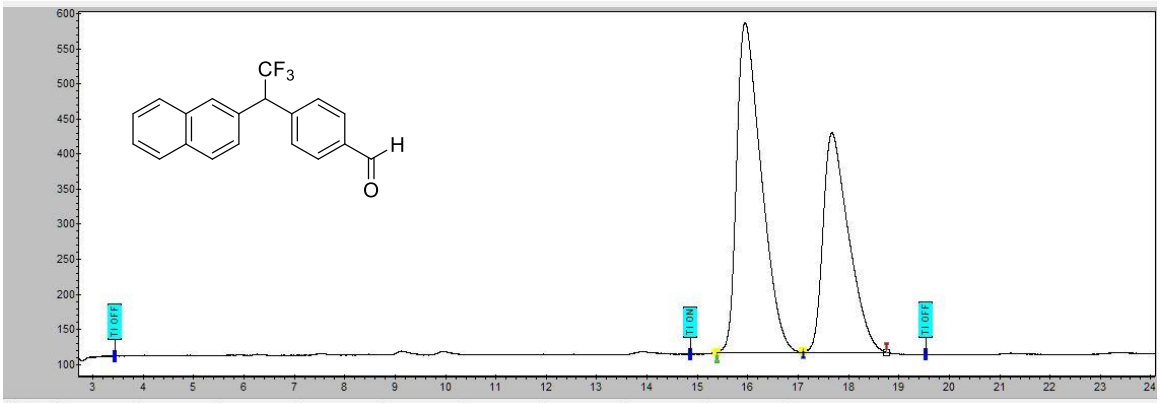


| # | Name | Start [Min] | Time [Min] | End [Min] | RT Offset [Min] | Quantity [% Area] | Height [µV] | Area [µV.Min] | Area [%] |
|---|---|---|---|---|---|---|---|---|---|
| 1 | UNKNOWN | 15.39 | 15.95 | 17.11 | 0.00 | 58.95 | 470.2 | 265.8 | 58.948 |
| 2 | UNKNOWN | 17.11 | 17.67 | 18.75 | 0.00 | 41.05 | 313.1 | 185.1 | 41.052 |
| Total | | | | | | 100.00 | 783.3 | 450.8 | 100.000 |

**Figure A5.16.** Chiral SFC (OJ-H column: 10% *i*-PrOH in $CO_2$, 1.5 mL/min) chromatogram of 4-(2,2,2-trifluoro-1-(naphthalen-2-yl)ethyl)benzaldehyde (**11e**)

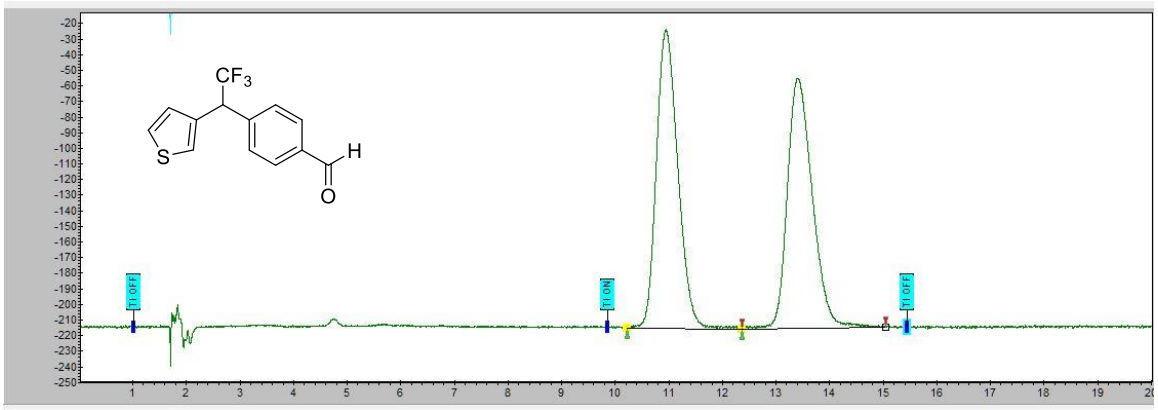


| # | Name | Start [Min] | Time [Min] | End [Min] | RT Offset [Min] | Quantity [% Area] | Height [µV] | Area [µV.Min] | Area [%] |
|---|---|---|---|---|---|---|---|---|---|
| 1 | UNKNOWN | 10.21 | 10.95 | 12.36 | 0.00 | 50.53 | 191.2 | 88.8 | 50.531 |
| 2 | UNKNOWN | 12.36 | 13.41 | 15.04 | 0.00 | 49.47 | 160.2 | 86.9 | 49.469 |
| Total | | | | | | 100.00 | 351.5 | 175.7 | 100.000 |

**Figure A5.17.** Chiral SFC (OJ-H column: 5% *i*-PrOH in $CO_2$, 1.5 mL/min) chromatogram of 4-(2,2,2-trifluoro-1-(thiophen-3-yl)ethyl)benzaldehyde (**11f**)

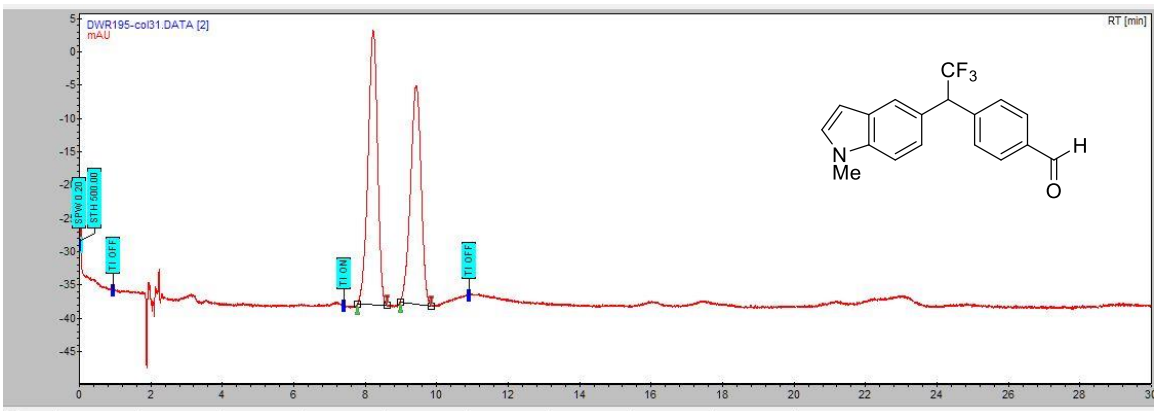


| # | Name | Start [Min] | Time [Min] | End [Min] | RT Offset [Min] | Quantity [% Area] | Height [µV] | Area [µV.Min] | Area [%] |
|---|---|---|---|---|---|---|---|---|---|
| 1 | UNKNOWN | 7.79 | 8.22 | 8.61 | 0.00 | 52.93 | 41.2 | 12.7 | 52.928 |
| 2 | UNKNOWN | 8.97 | 9.42 | 9.86 | 0.00 | 47.07 | 32.9 | 11.3 | 47.072 |
| Total | | | | | | 100.00 | 74.1 | 24.0 | 100.000 |

**Figure A5.18.** Chiral SFC (AS-H column: 10% *i*-PrOH in $CO_2$, 1.5 mL/min) chromatogram of 4-(2,2,2-trifluoro-1-(1-methyl-1*H*-indol-5-yl)ethyl)benzaldehyde (**11g**)

# Appendix A6. $^{1}H$, $^{13}C$, and $^{19}F$ NMR Spectra Relevant to Chapter 5

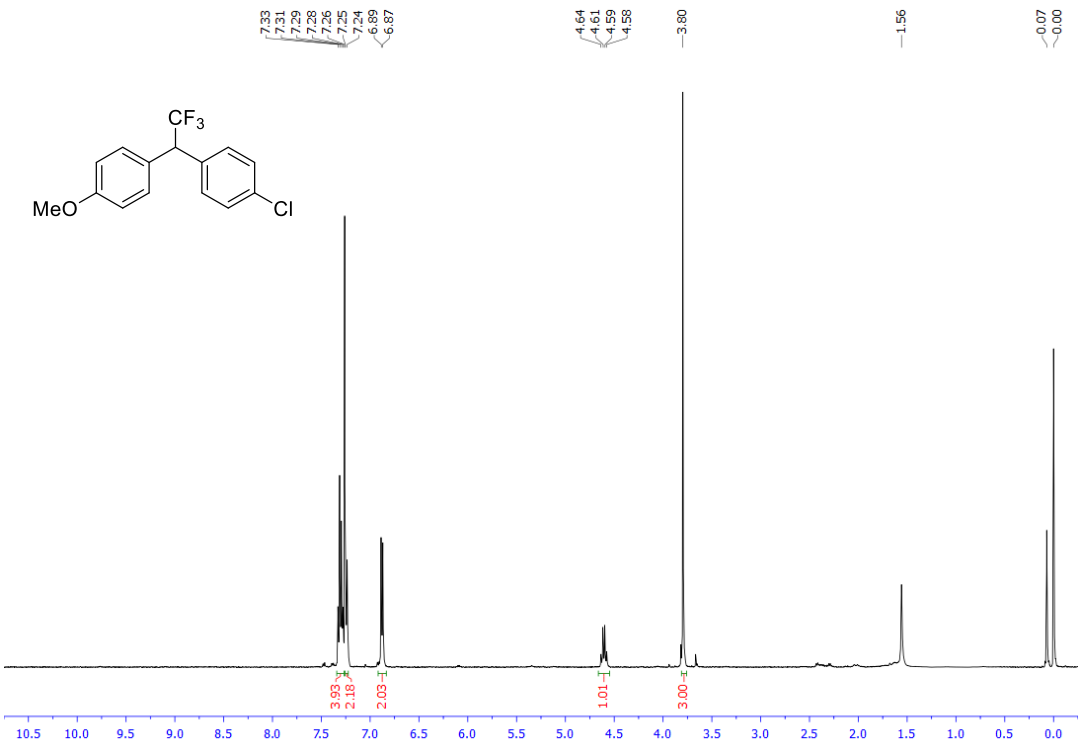


**Figure A6.1.** $^{1}$H NMR ($CDCl_3$, 500 MHz) spectrum of 1-chloro-4-(2,2,2-trifluoro-1-phenylethyl)benzene (**10a**)

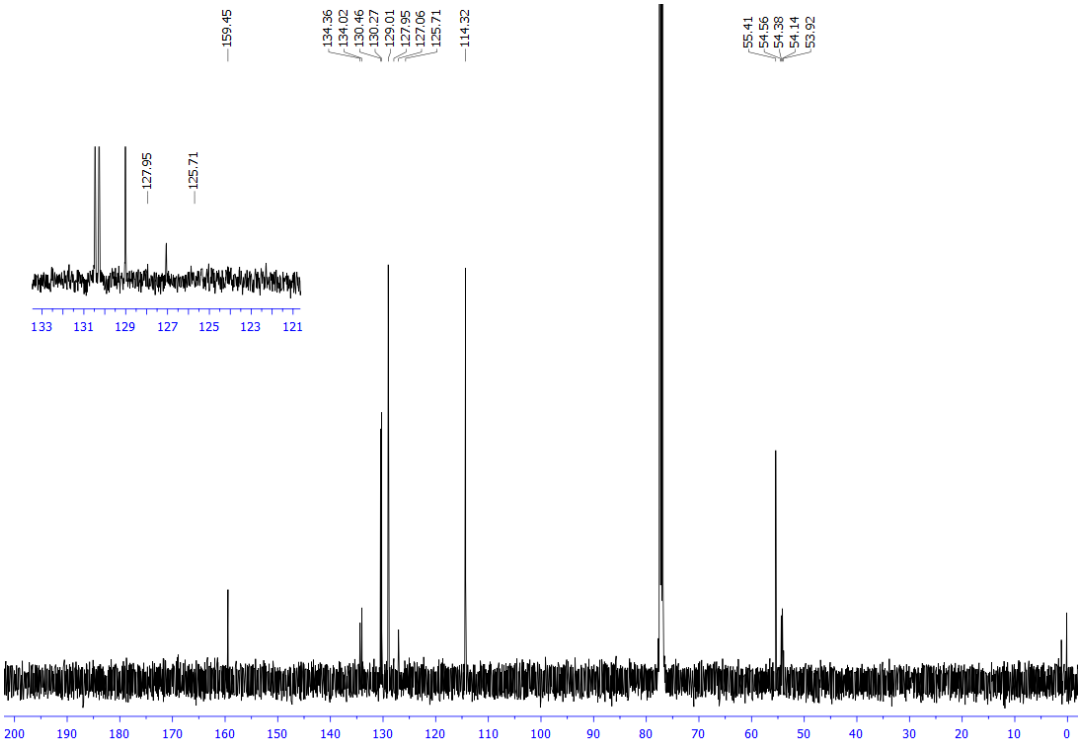


**Figure A6.2.** $^{13}$C NMR ($CDCl_3$, 126 MHz) spectrum of 1-chloro-4-(2,2,2-trifluoro-1-phenylethyl)benzene (**10a**)

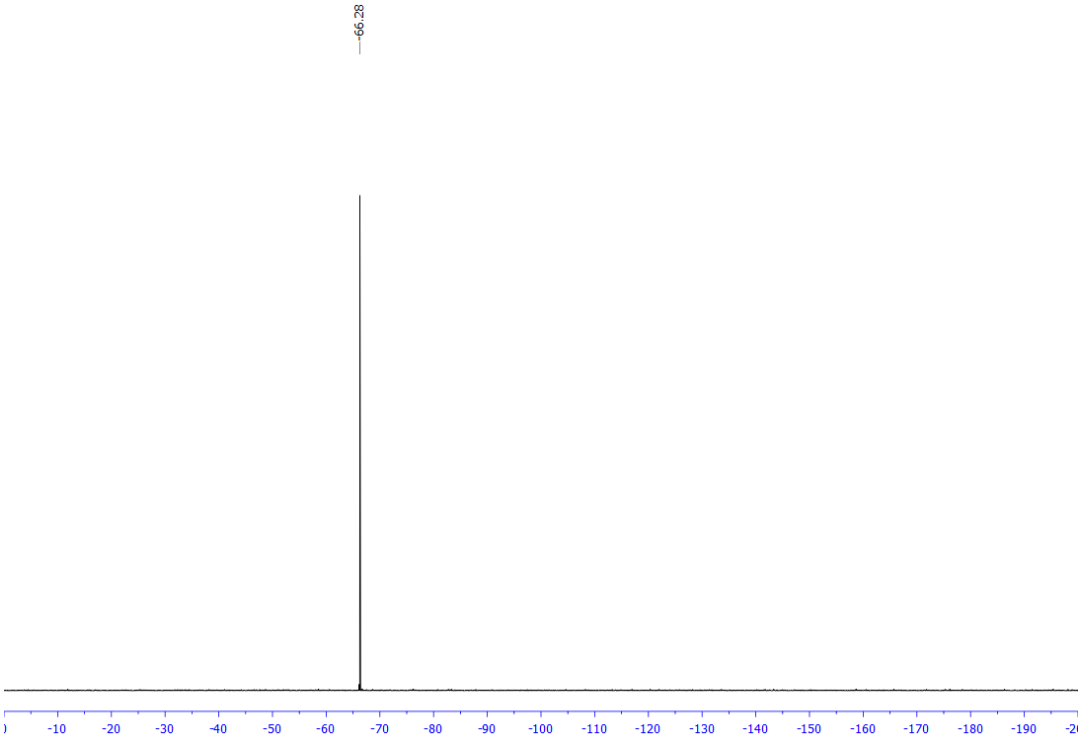


**Figure A6.3.** $^{19}F$ NMR ($CDCl_3$, 471 MHz) spectrum of 1-chloro-4-(2,2,2-trifluoro-1-phenylethyl)benzene (**10a**)

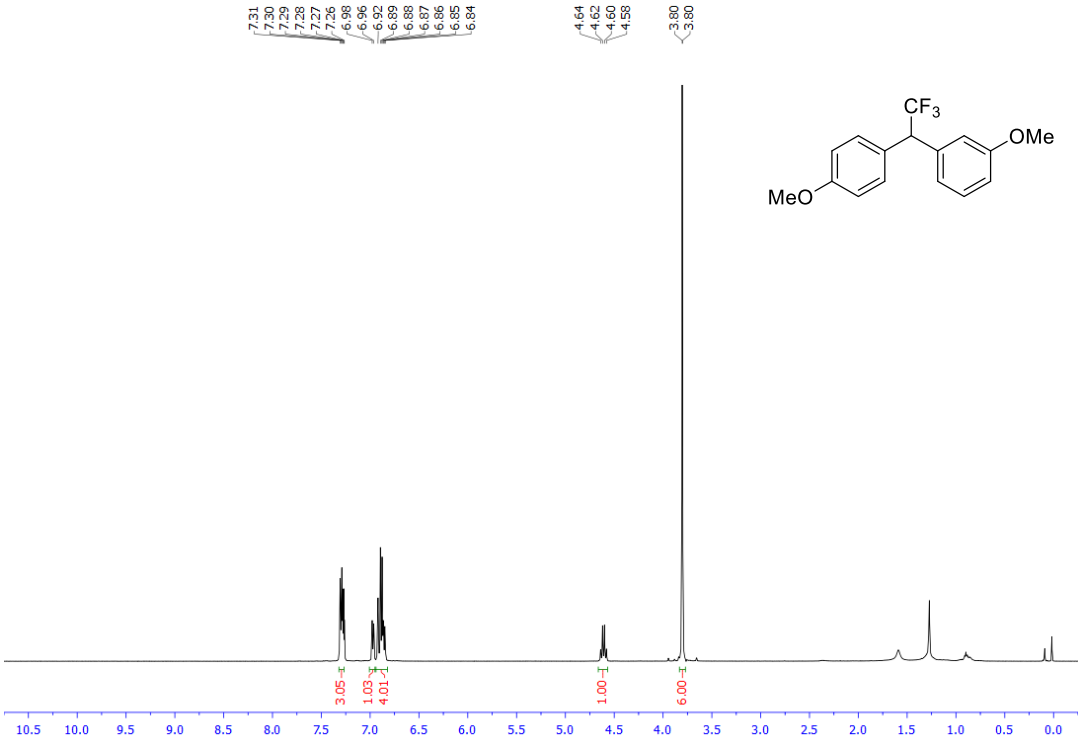


**Figure A6.4.** $^{1}H$ NMR ($CDCl_3$, 500 MHz) spectrum of 1-methoxy-3-(2,2,2-trifluoro-1-(4-methoxyphenyl)ethyl)benzene (**10b**)

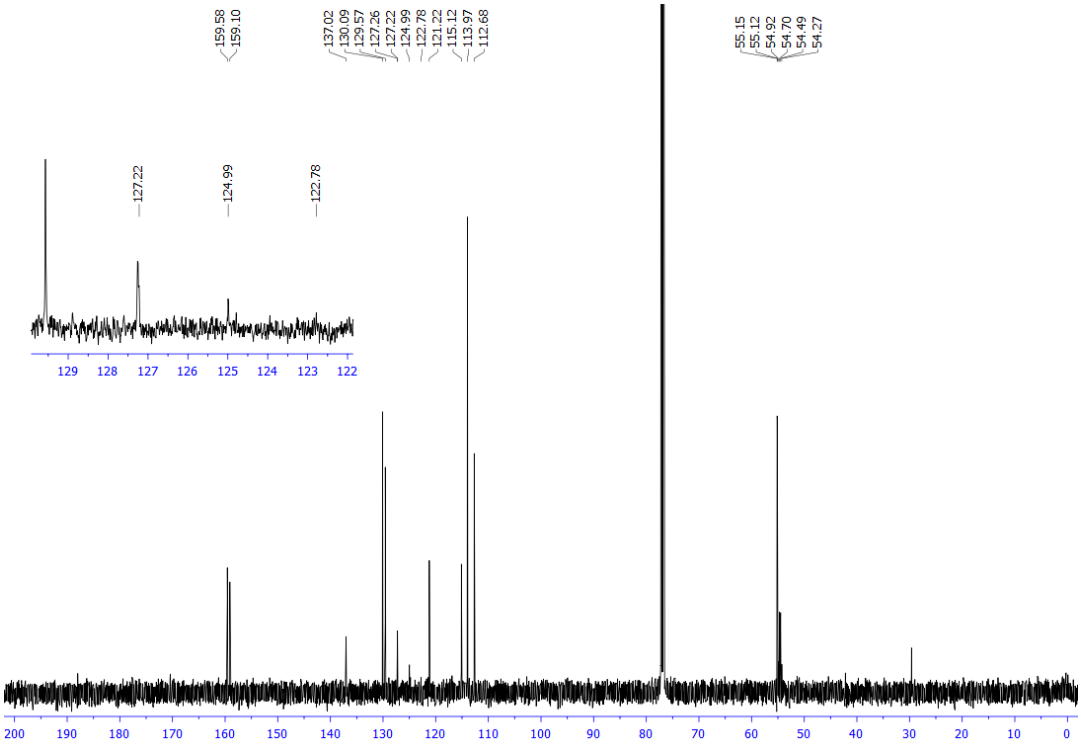


**Figure A6.5.** $^{13}C$ NMR ($CDCl_3$, 126 MHz) spectrum of 1-methoxy-3-(2,2,2-trifluoro-1-(4-methoxyphenyl)ethyl)benzene (**10b**)

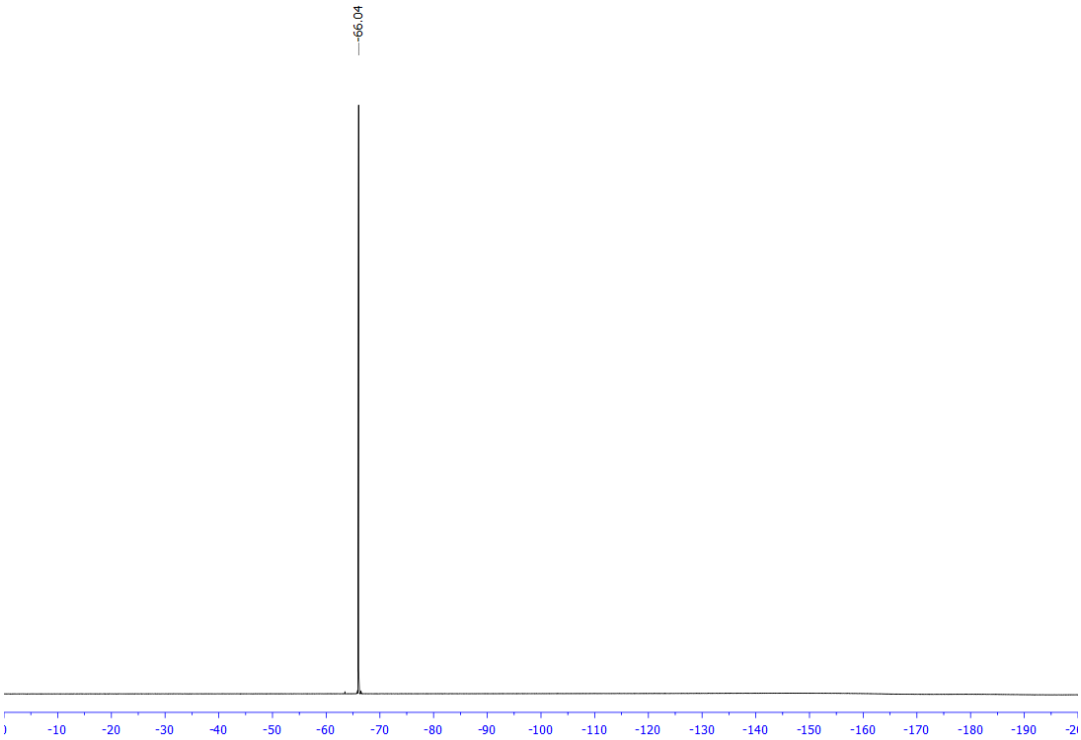


**Figure A6.6.** $^{19}F$ NMR ($CDCl_3$, 471 MHz) spectrum of 1-methoxy-3-(2,2,2-trifluoro-1-(4-methoxyphenyl)ethyl)benzene (**10b**)

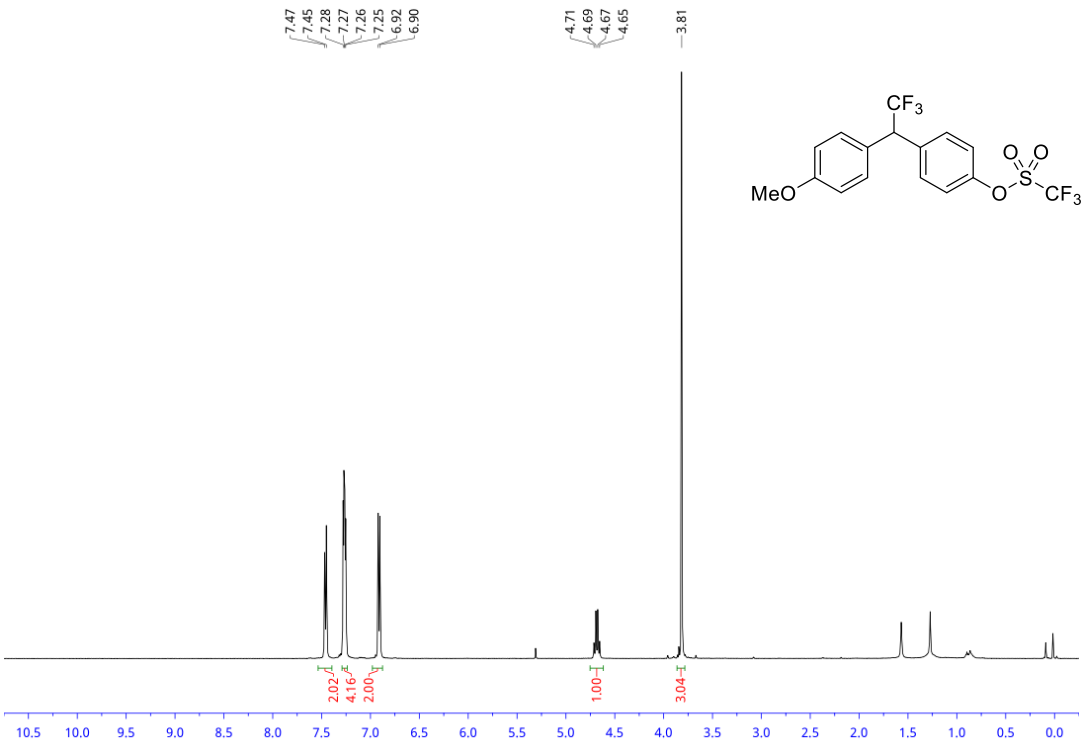


**Figure A6.7.** $^{1}$H NMR ($CDCl_3$, 500 MHz) spectrum of 4-(2,2,2-trifluoro-1-(4-methoxyphenyl)ethyl)phenyl trifluoromethanesulfonate (**10c**)

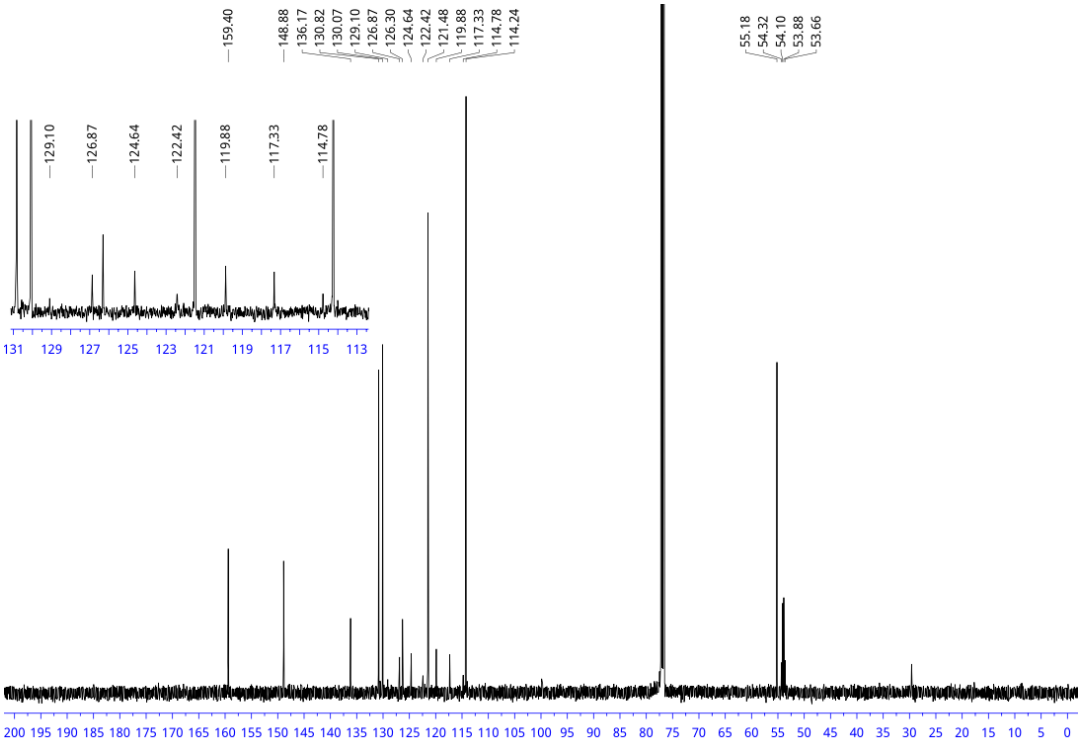


**Figure A6.8.** $^{13}$C NMR ($CDCl_3$, 126 MHz) spectrum of 4-(2,2,2-trifluoro-1-(4-methoxyphenyl)ethyl)phenyl trifluoromethanesulfonate (**10c**)

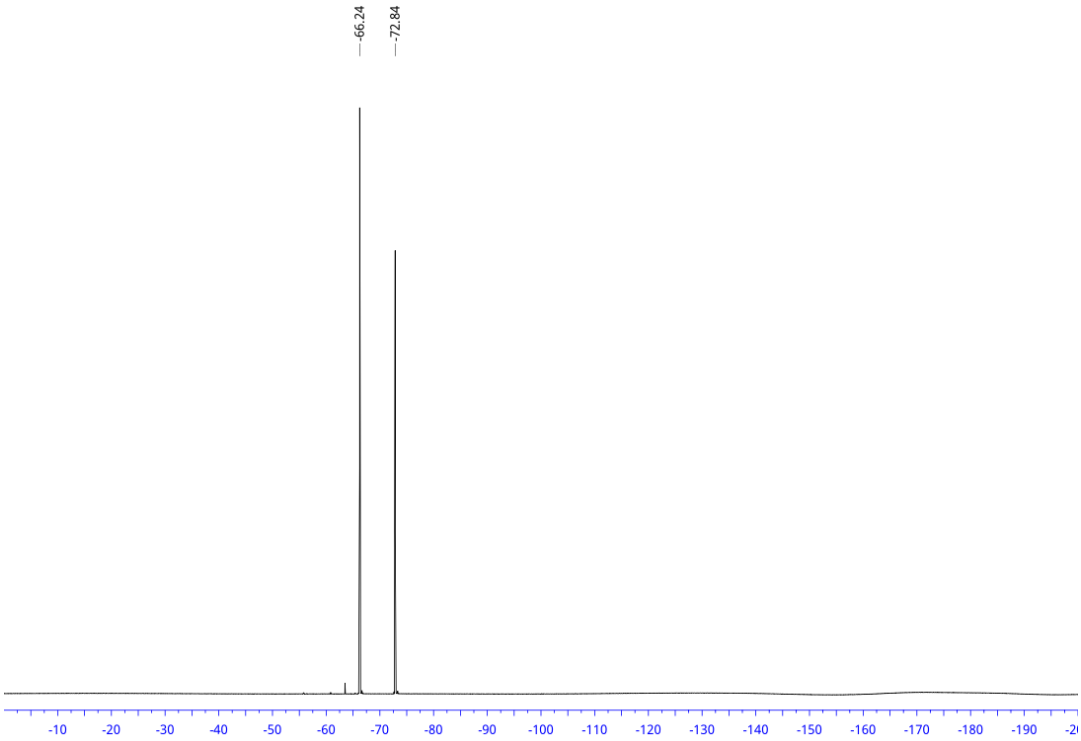


**Figure A6.9.** $^{19}$F NMR ($CDCl_3$, 471 MHz) spectrum of 4-(2,2,2-trifluoro-1-(4-methoxyphenyl)ethyl)phenyl trifluoromethanesulfonate (**10c**)

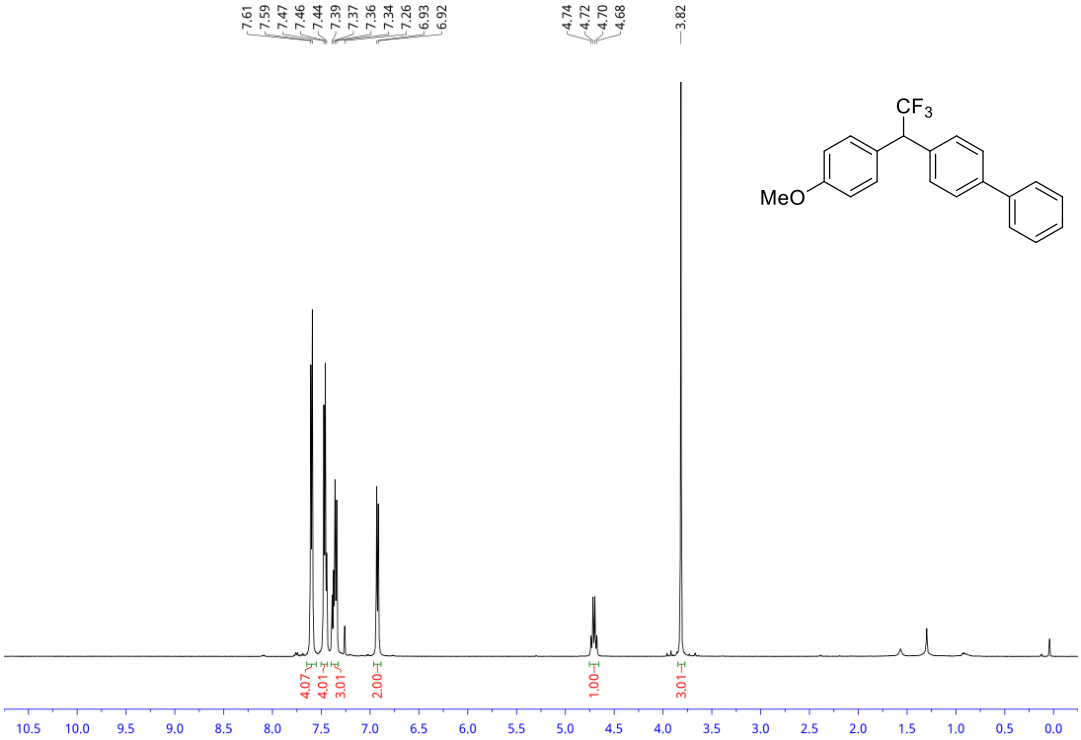


**Figure A6.10.** $^{1}$H NMR ($CDCl_3$, 500 MHz) spectrum of 4-(2,2,2-trifluoro-1-(4-methoxyphenyl)ethyl)-1,1'-biphenyl (**10d**)

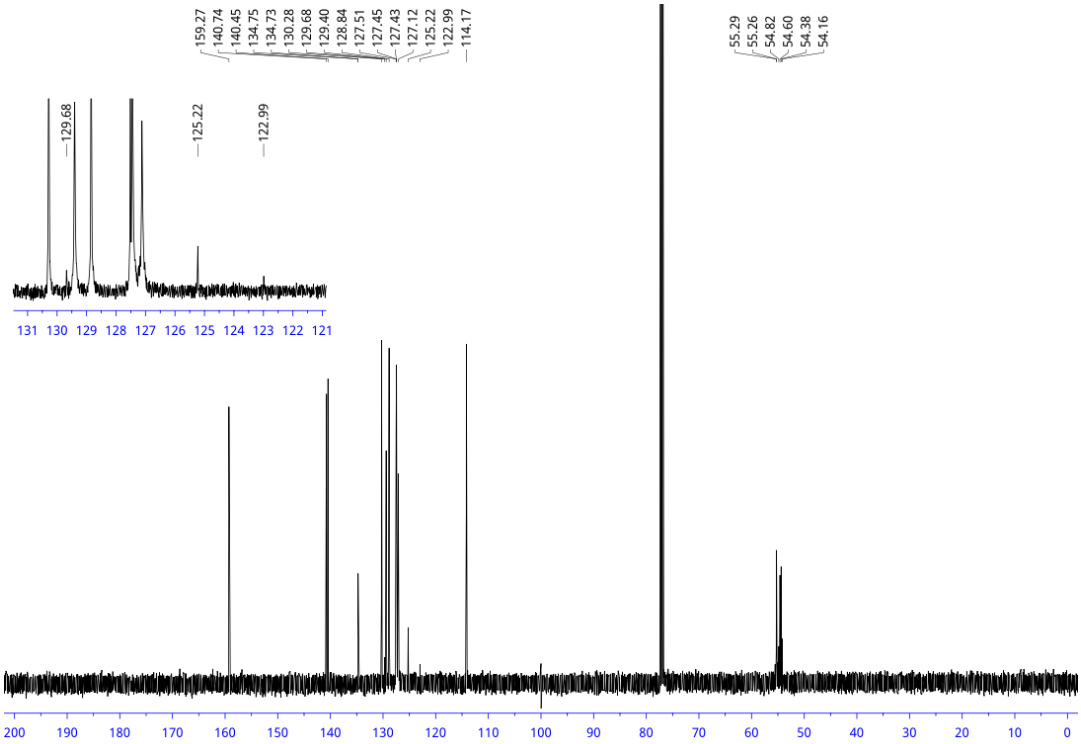


**Figure A6.11.** $^{13}C$ NMR ($CDCl_3$, 126 MHz) spectrum of 4-(2,2,2-trifluoro-1-(4-methoxyphenyl)ethyl)-1,1'-biphenyl (**10d**)

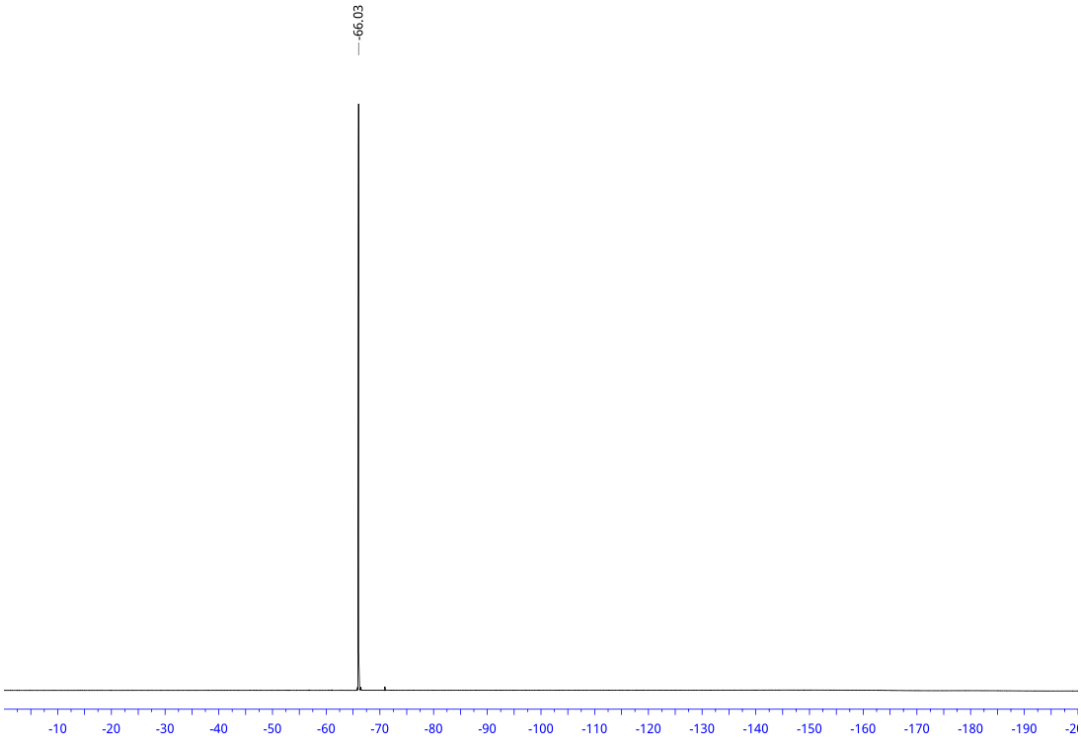


**Figure A6.12.** $^{19}F$ NMR ($CDCl_3$, 471 MHz) spectrum of 4-(2,2,2-trifluoro-1-(4-methoxyphenyl)ethyl)-1,1'-biphenyl (**10d**)

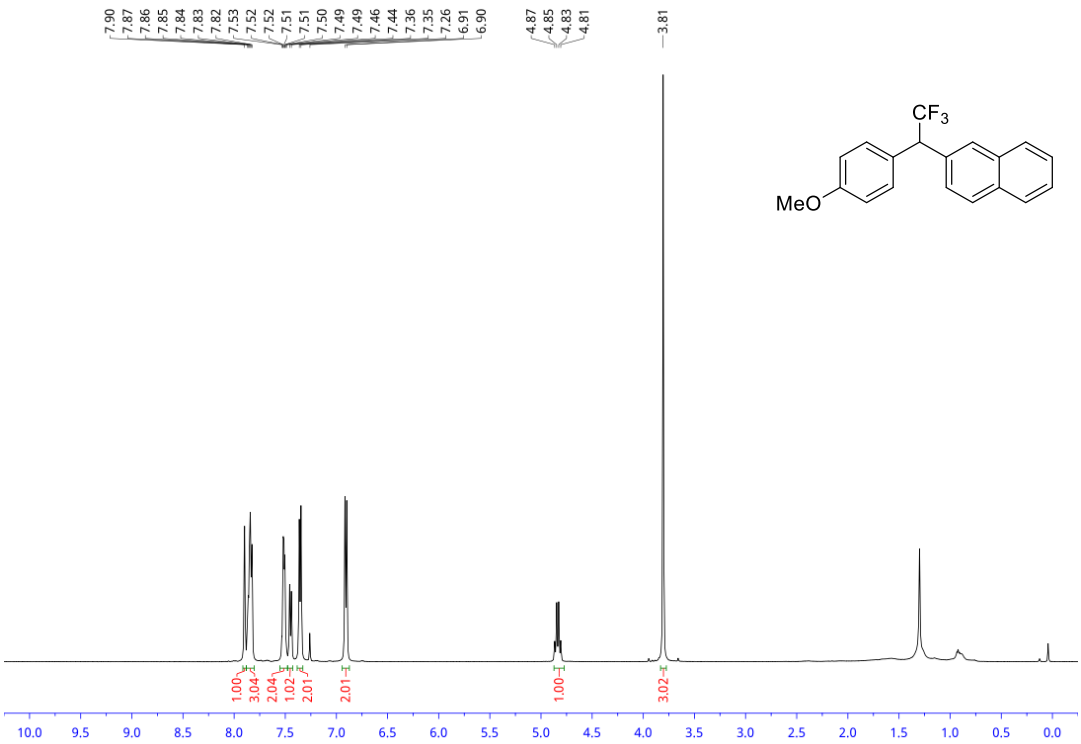


**Figure A6.13.** $^{1}$H NMR ($CDCl_3$, 500 MHz) spectrum of 2-(2,2,2-trifluoro-1-(4-methoxyphenyl)ethyl)naphthalene (**10e**)

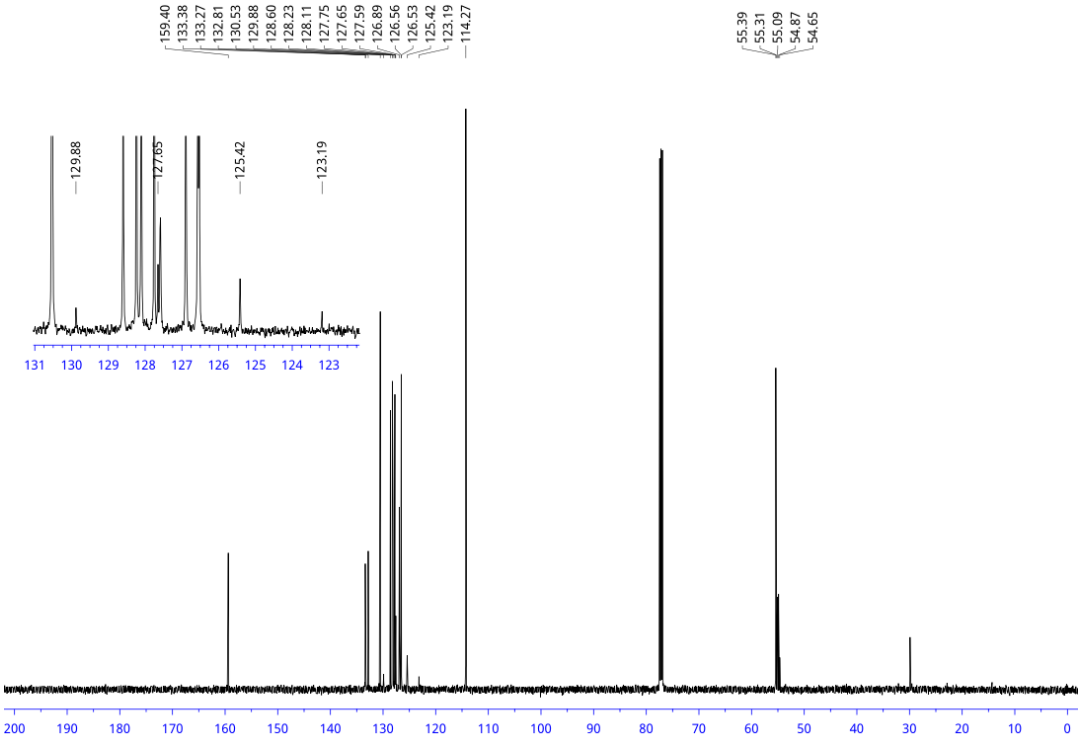


**Figure A6.14.** $^{13}$C NMR ($CDCl_3$, 126 MHz) spectrum of 2-(2,2,2-trifluoro-1-(4-methoxyphenyl)ethyl)naphthalene (**10e**)

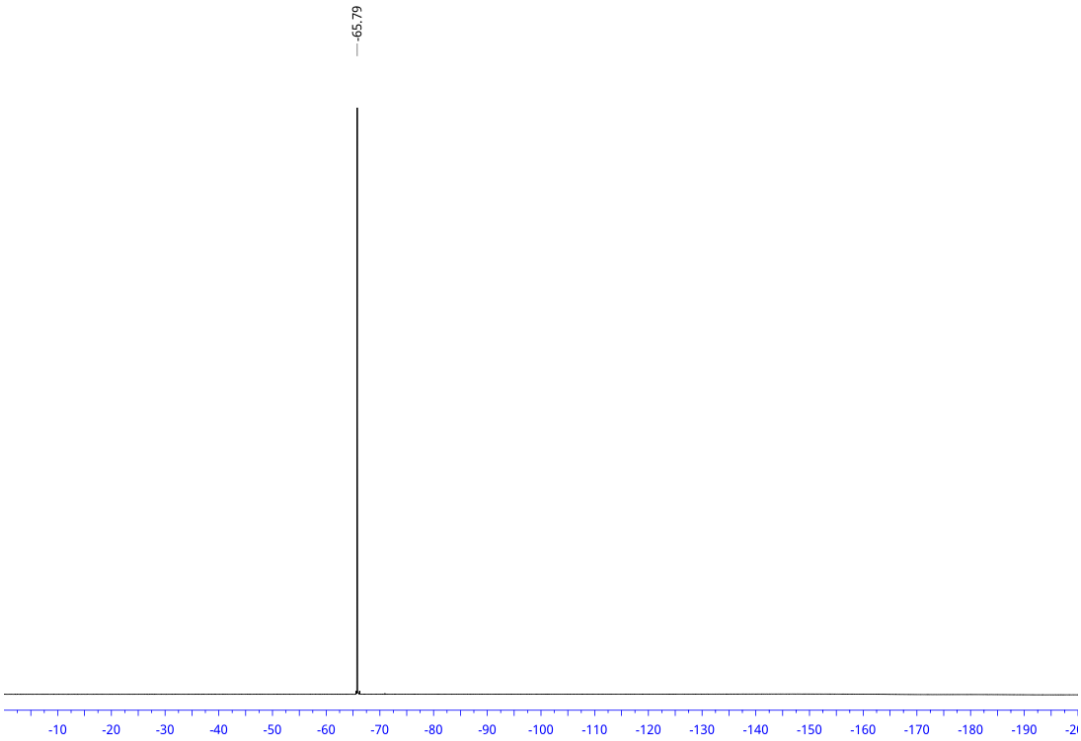


**Figure A6.15.** $^{19}F$ NMR ($CDCl_3$, 471 MHz) spectrum of 2-(2,2,2-trifluoro-1-(4-methoxyphenyl)ethyl)naphthalene (**10e**)

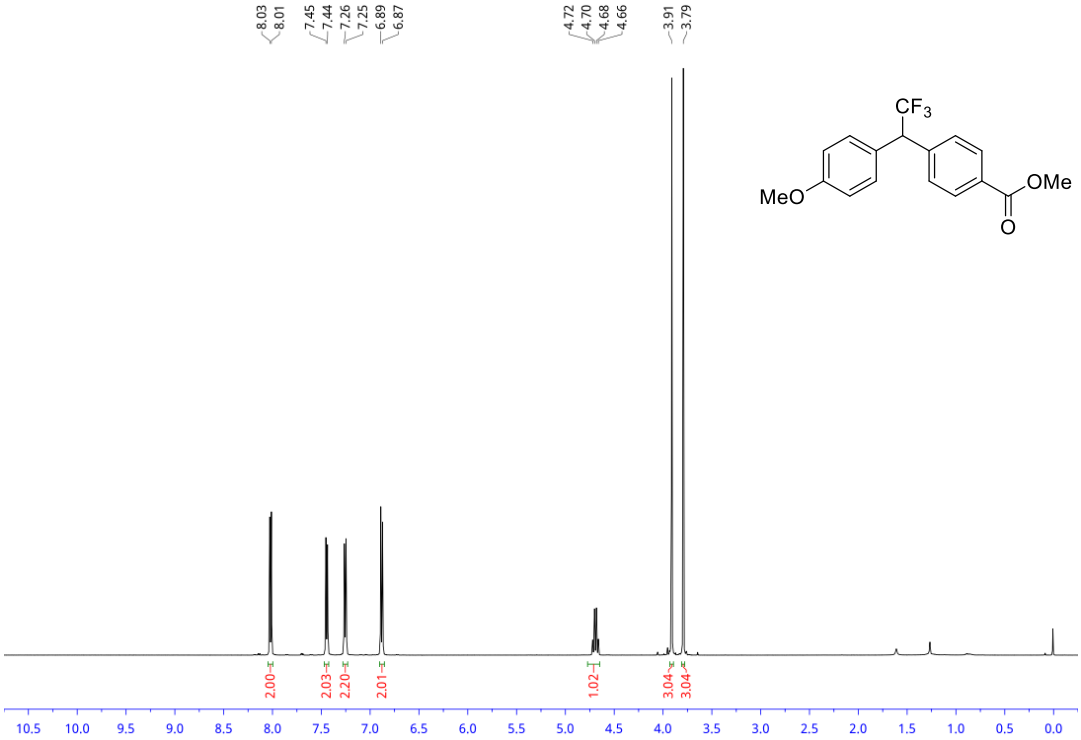


**Figure A6.16.** $^{1}H$ NMR ($CDCl_3$, 500 MHz) spectrum of methyl 4-(2,2,2-trifluoro-1-(4-methoxyphenyl)ethyl)benzoate (**10f**)

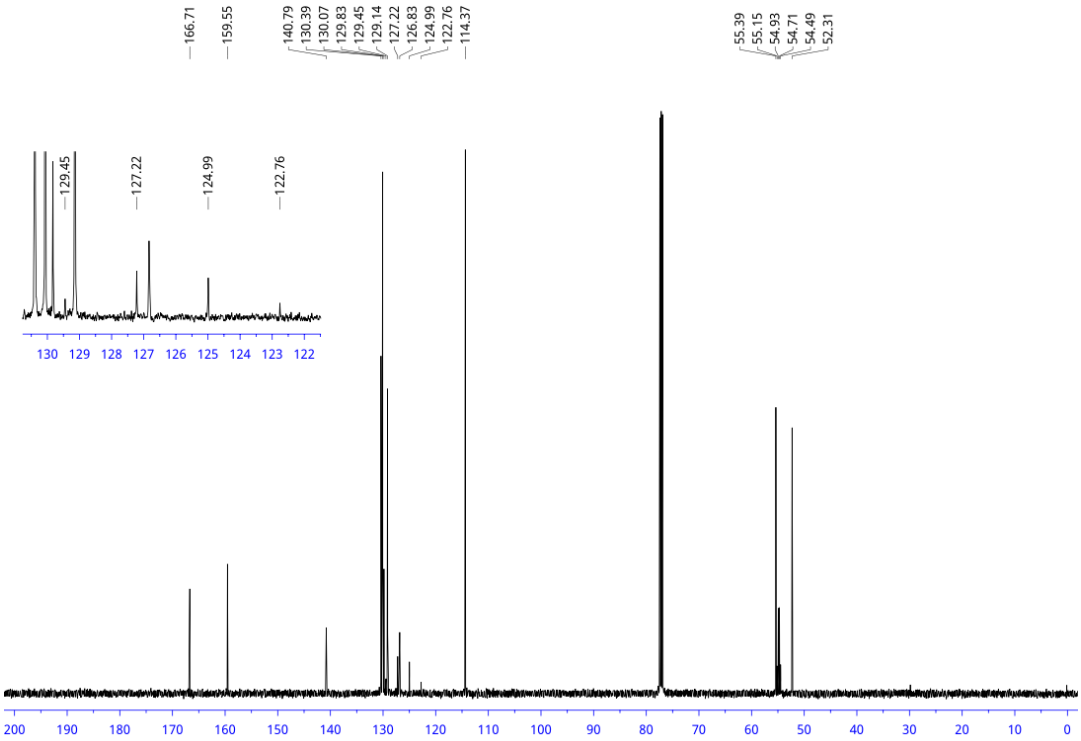


**Figure A6.17.** $^{13}C$ NMR ($CDCl_3$, 126 MHz) spectrum of methyl 4-(2,2,2-trifluoro-1-(4-methoxyphenyl)ethyl)benzoate (**10f**)

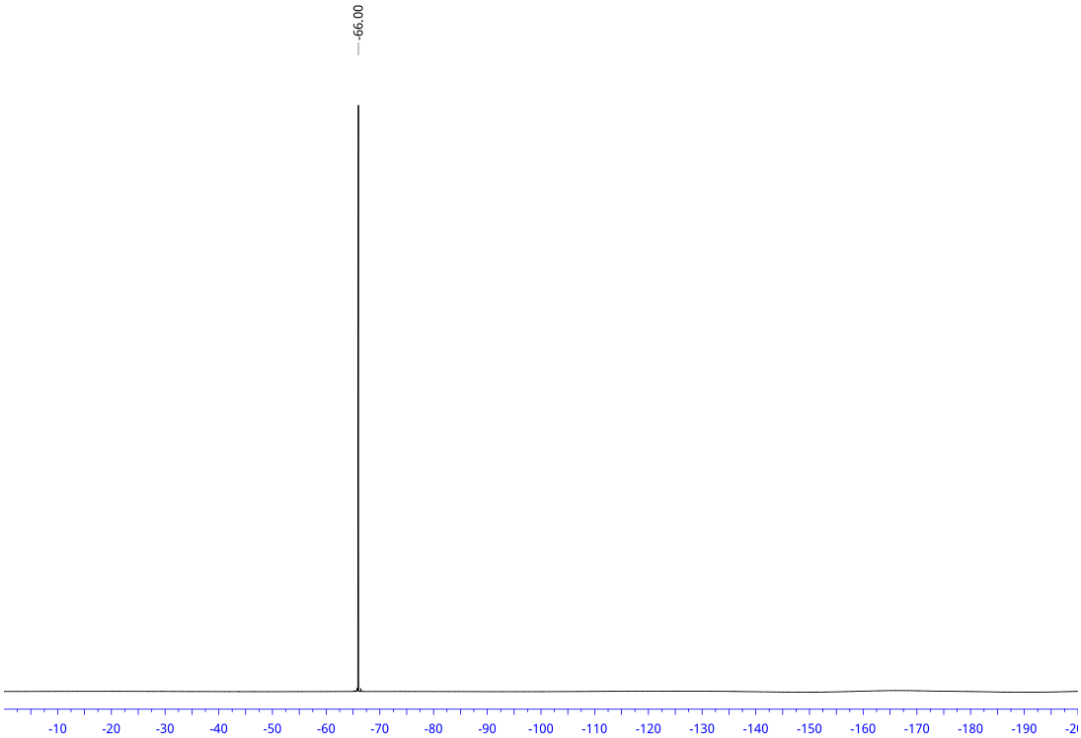


**Figure A6.18.** $^{19}F$ NMR ($CDCl_3$, 471 MHz) spectrum of methyl 4-(2,2,2-trifluoro-1-(4-methoxyphenyl)ethyl)benzoate (**10f**)

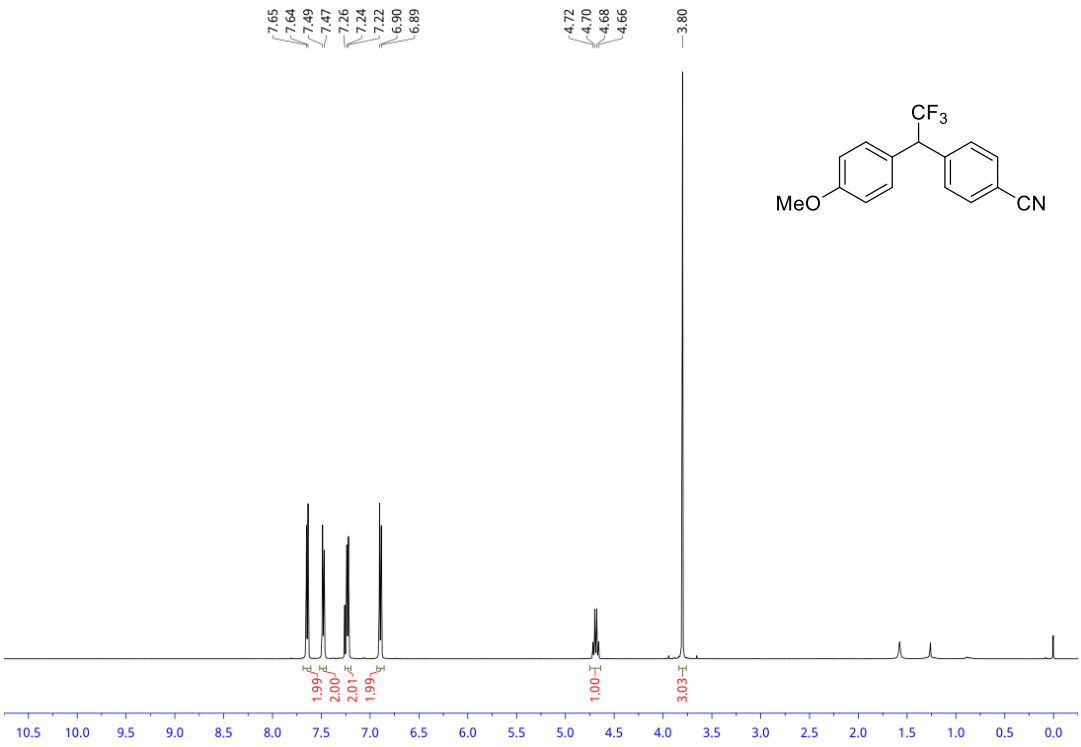


**Figure A6.19.** $^{1}$H NMR ($CDCl_3$, 500 MHz) spectrum of 4-(2,2,2-trifluoro-1-(4-methoxyphenyl)ethyl)benzonitrile (**10g**)

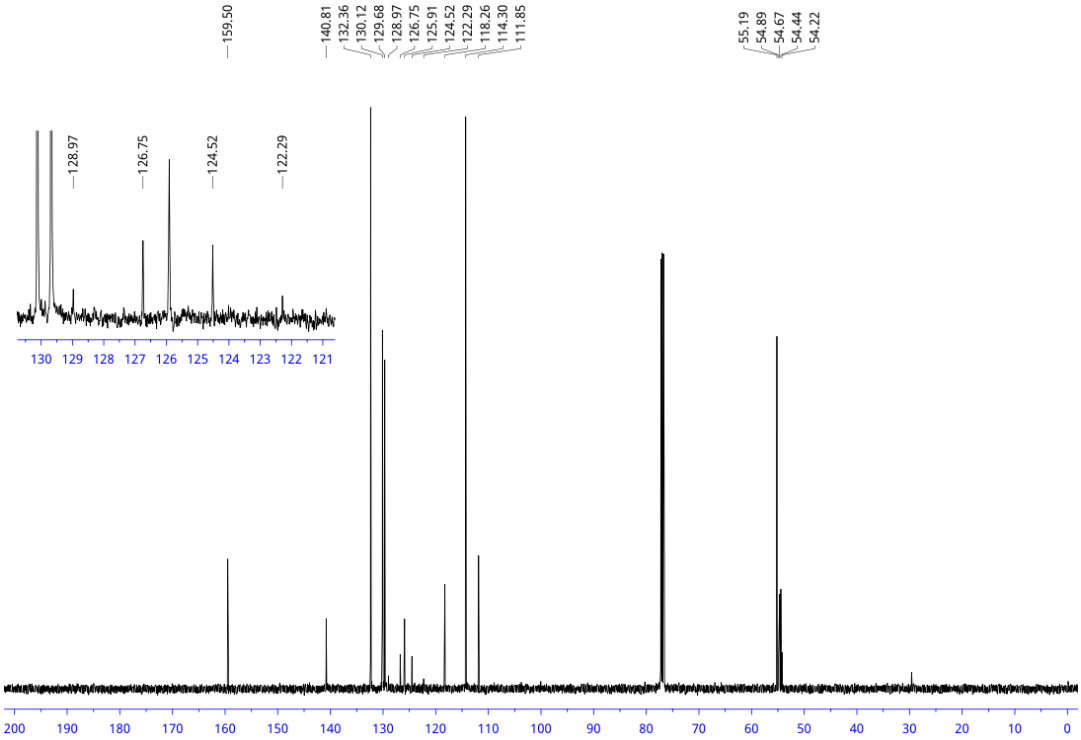


**Figure A6.20.** $^{13}$C NMR ($CDCl_3$, 126 MHz) spectrum of 4-(2,2,2-trifluoro-1-(4-methoxyphenyl)ethyl)benzonitrile (**10g**)

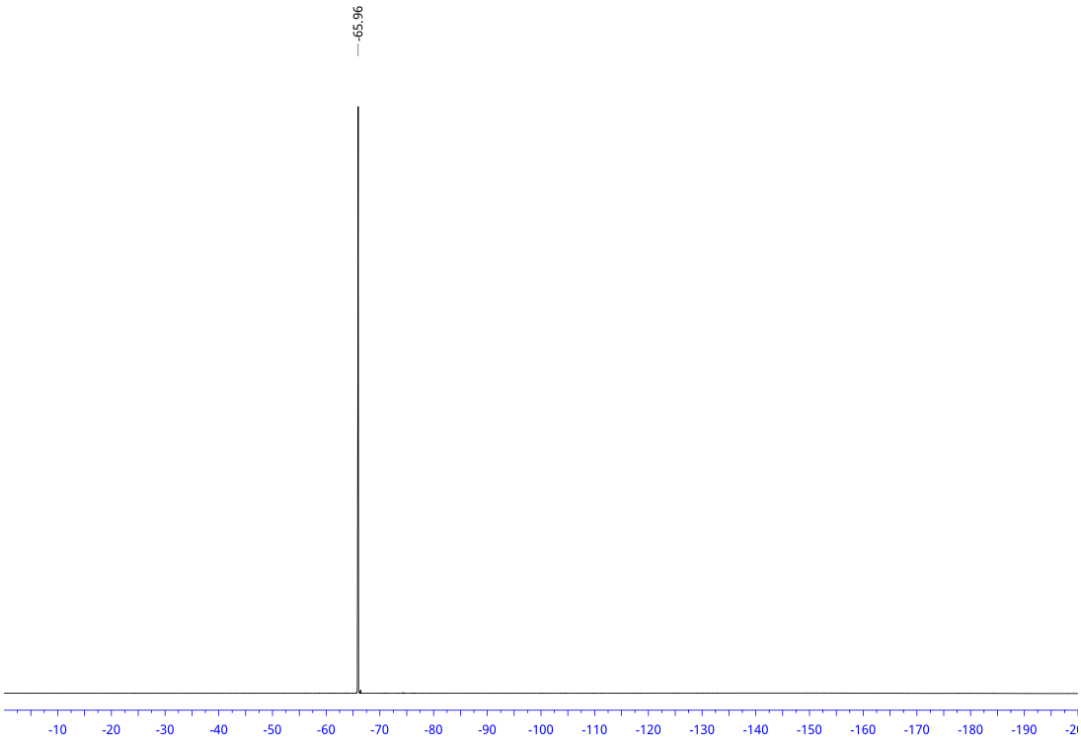


**Figure A6.21.** $^{19}F$ NMR ($CDCl_3$, 471 MHz) spectrum of 4-(2,2,2-trifluoro-1-(4-methoxyphenyl)ethyl)benzonitrile (**10g**)

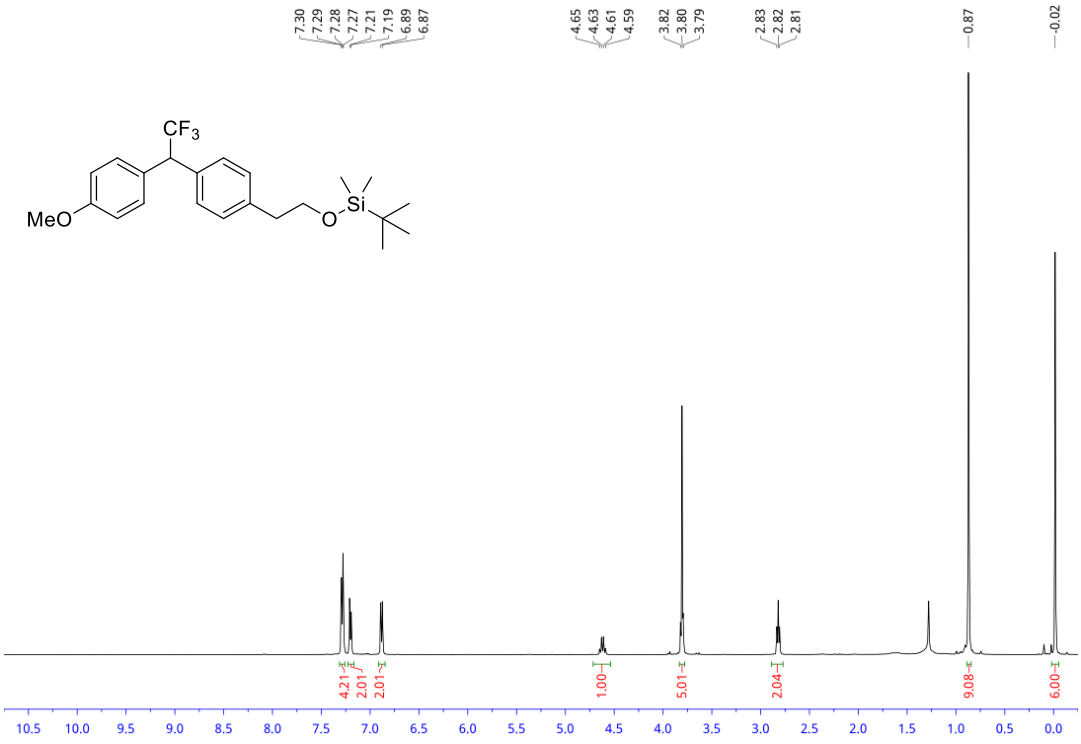


**Figure A6.22.** $^{1}H$ NMR ($CDCl_3$, 500 MHz) spectrum of *tert*-butyldimethyl(4-(2,2,2-trifluoro-1-(4-methoxyphenyl)ethyl)phenethoxy)silane (**10h**)

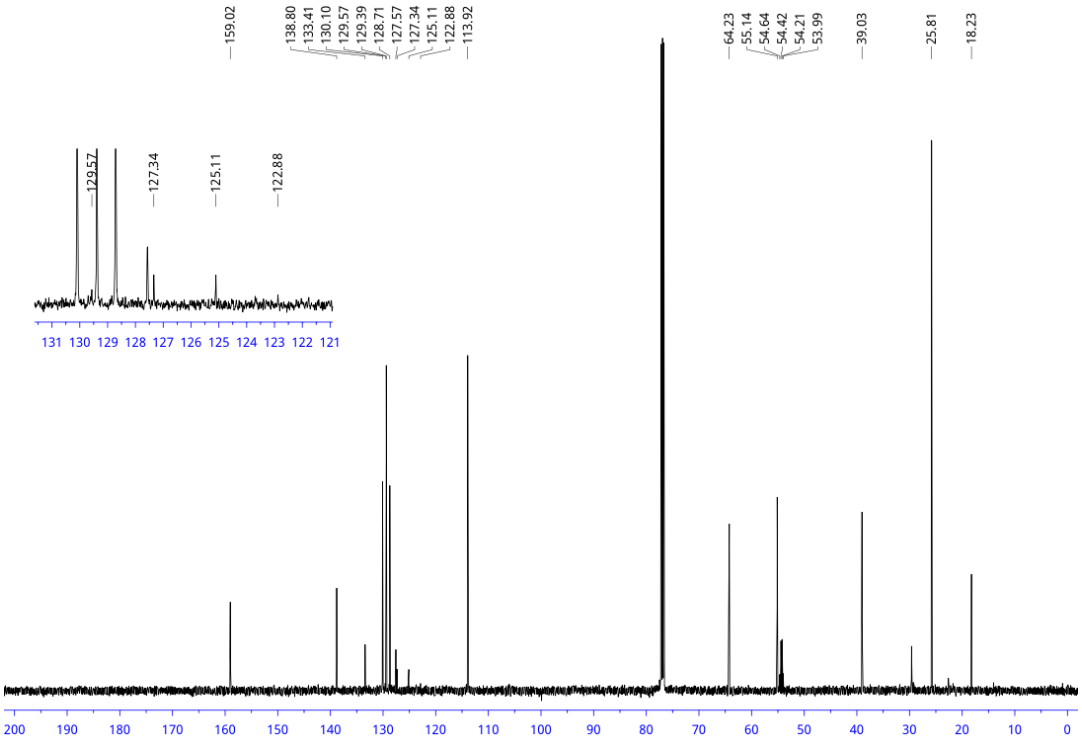


**Figure A6.23.** $^{13}C$ NMR ($CDCl_3$, 126 MHz) spectrum of *tert*-butyldimethyl(4-(2,2,2-trifluoro-1-(4-methoxyphenyl)ethyl)phenethoxy)silane (**10h**)

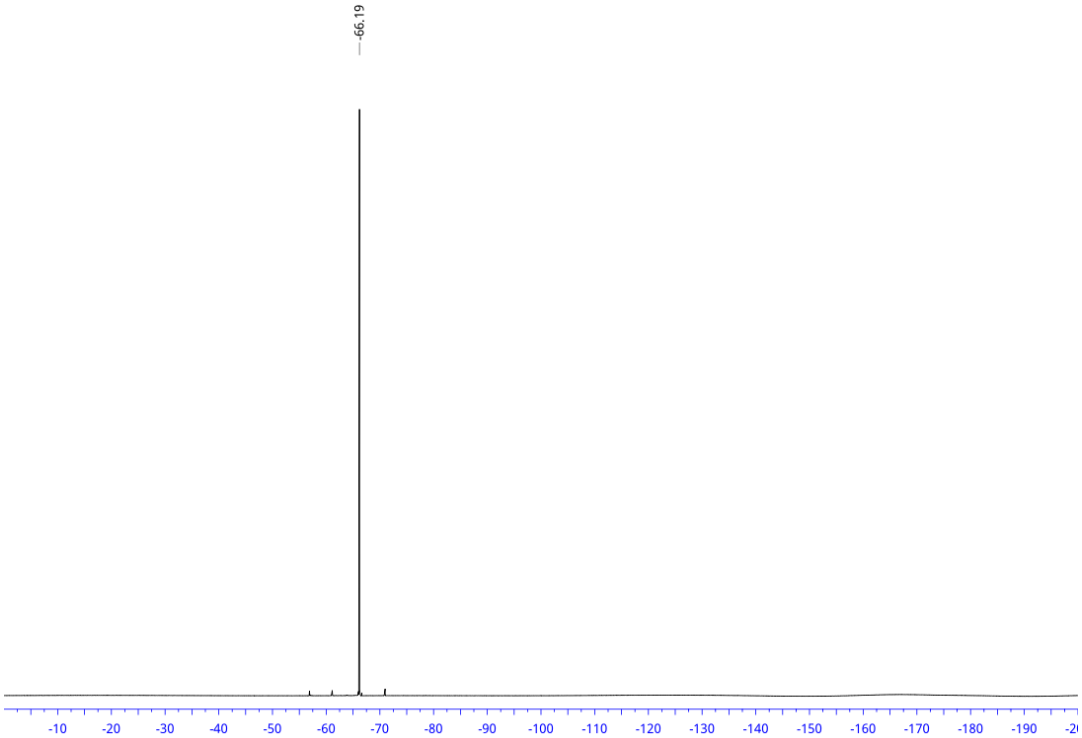


**Figure A6.24.** $^{19}F$ NMR ($CDCl_3$, 471 MHz) spectrum of *tert*-butyldimethyl(4-(2,2,2-trifluoro-1-(4-methoxyphenyl)ethyl)phenethoxy)silane (**10h**)

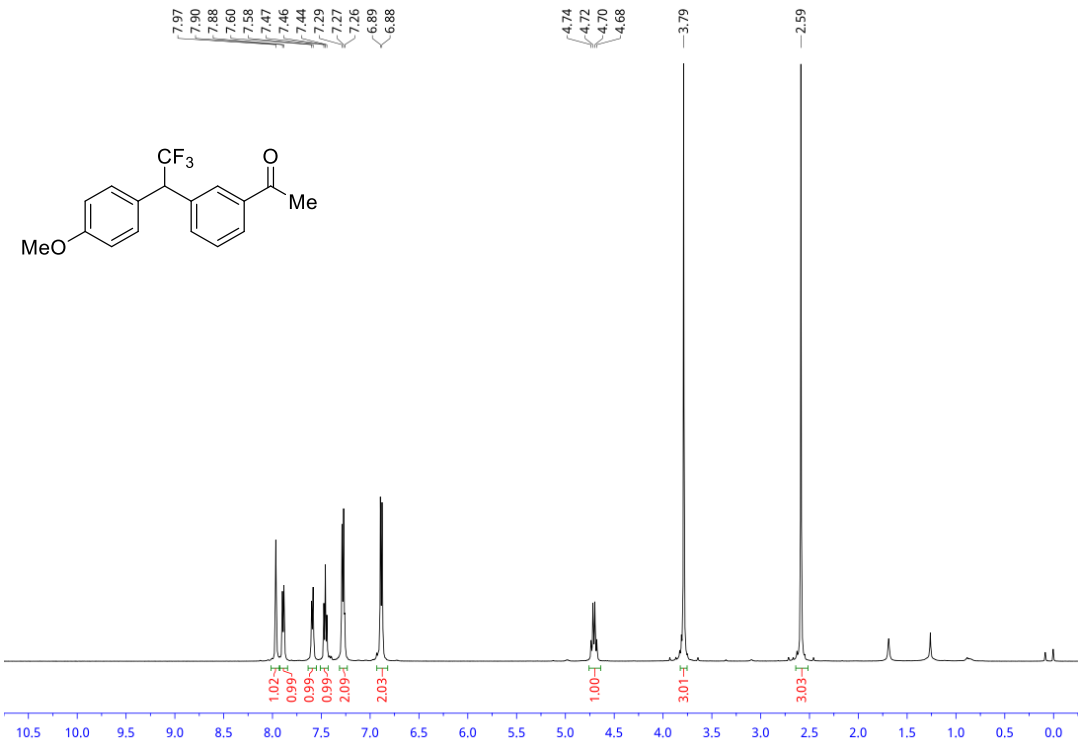


**Figure A6.25.** $^{1}$H NMR ($CDCl_3$, 500 MHz) spectrum of 1-(3-(2,2,2-trifluoro-1-(4-methoxyphenyl)ethyl)phenyl)ethan-1-one (**10i**)

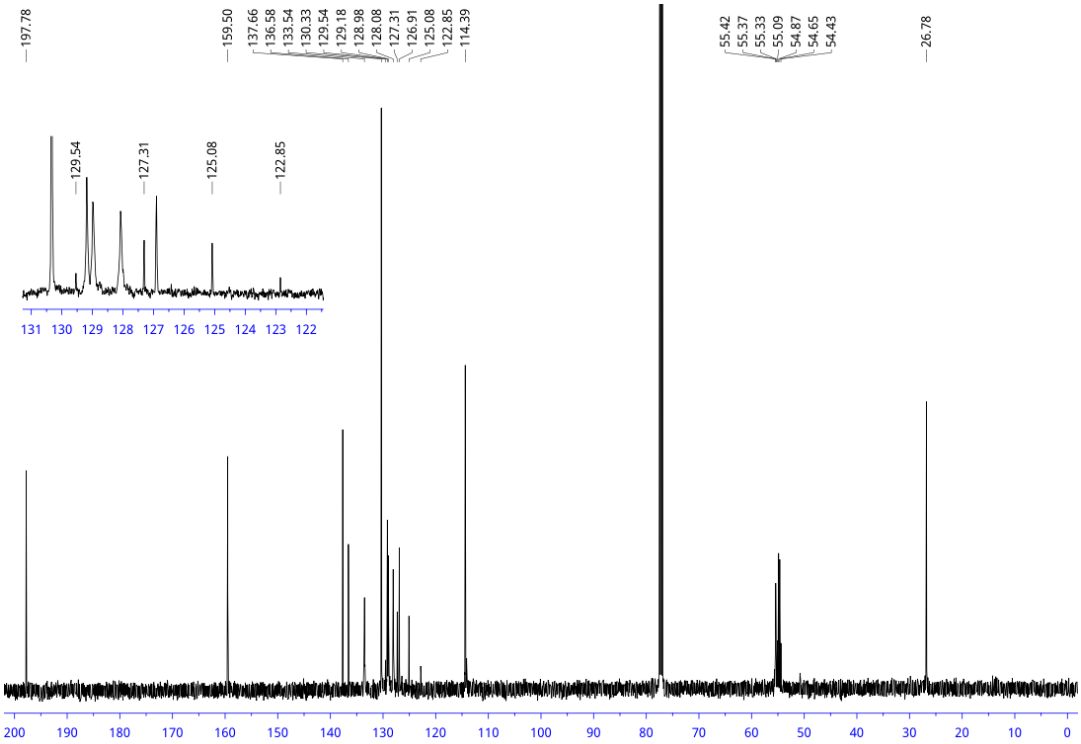


**Figure A6.26.** $^{13}$C NMR ($CDCl_3$, 126 MHz) spectrum of 1-(3-(2,2,2-trifluoro-1-(4-methoxyphenyl)ethyl)phenyl)ethan-1-one (**10i**)

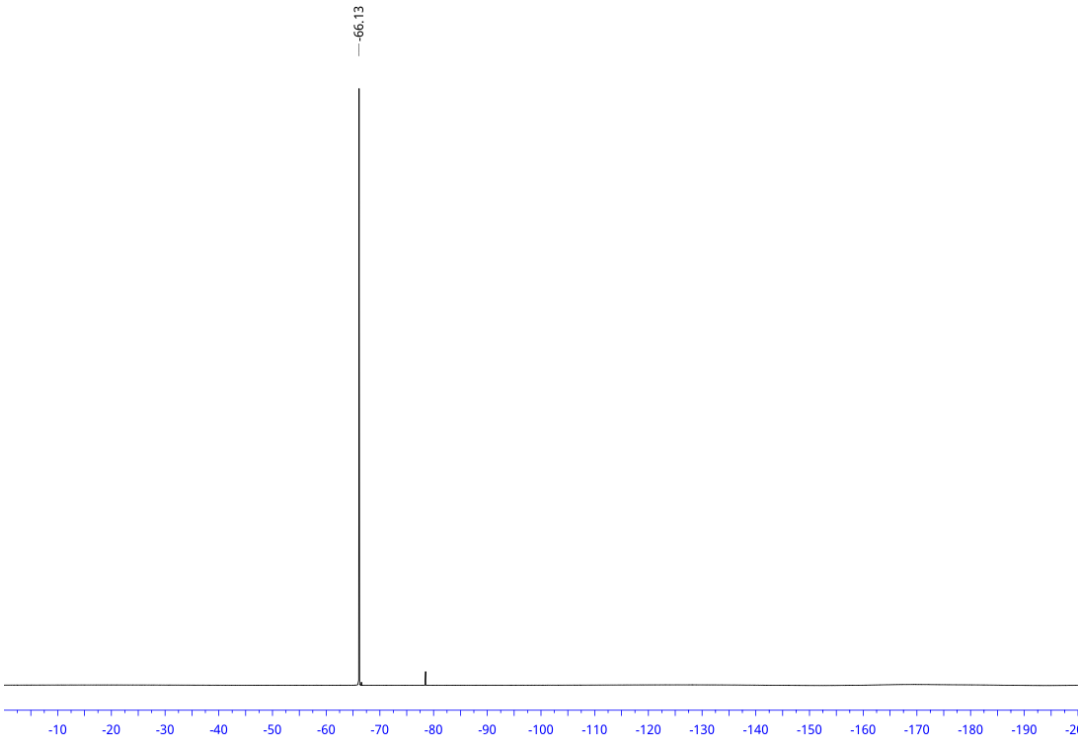


**Figure A6.27.** $^{19}F$ NMR ($CDCl_3$, 471 MHz) spectrum of 1-(3-(2,2,2-trifluoro-1-(4-methoxyphenyl)ethyl)phenyl)ethan-1-one (**10i**)

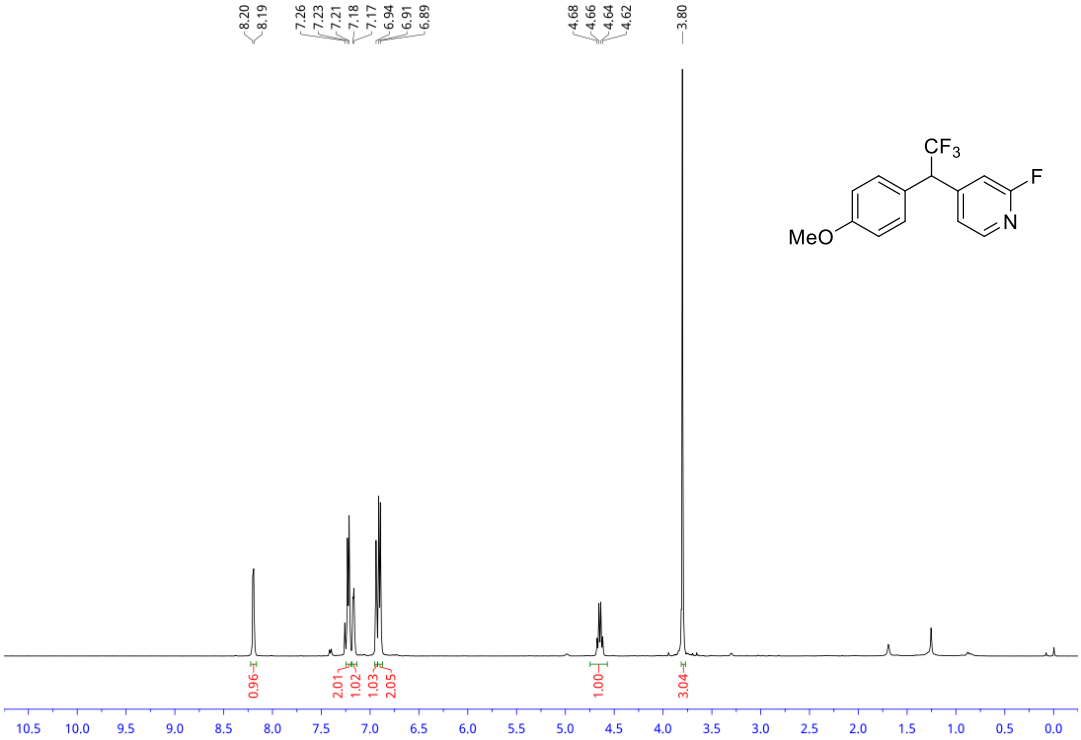


**Figure A6.28.** $^{1}H$ NMR ($CDCl_3$, 500 MHz) spectrum of 2-fluoro-4-(2,2,2-trifluoro-1-(4-methoxyphenyl)ethyl)pyridine (**10j**)

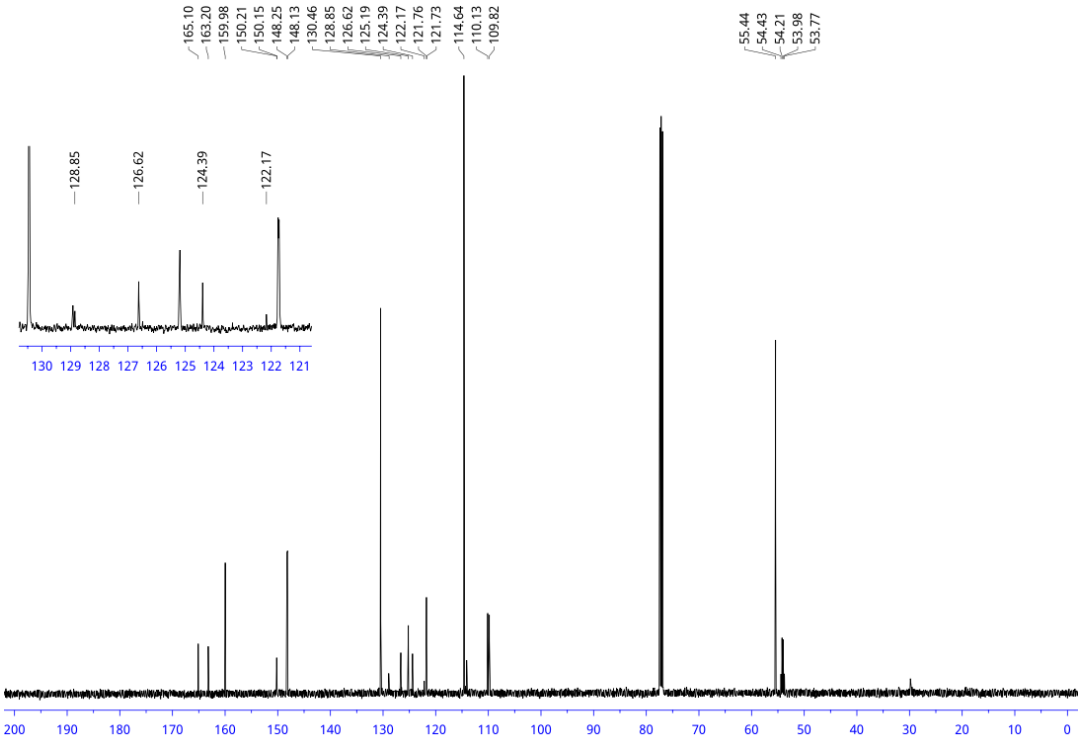


**Figure A6.29.** $^{13}C$ NMR ($CDCl_3$, 126 MHz) spectrum of 2-fluoro-4-(2,2,2-trifluoro-1-(4-methoxyphenyl)ethyl)pyridine (**10j**)

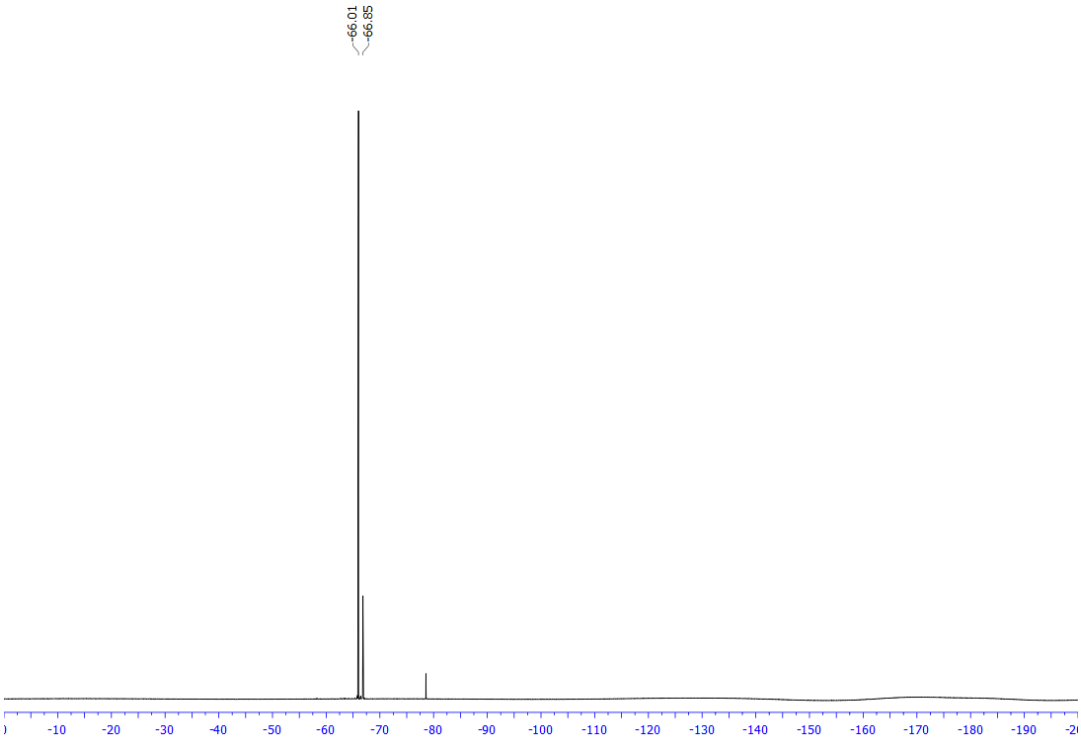


**Figure A6.30.** $^{19}F$ NMR ($CDCl_3$, 471 MHz) spectrum of 2-fluoro-4-(2,2,2-trifluoro-1-(4-methoxyphenyl)ethyl)pyridine (**10j**)

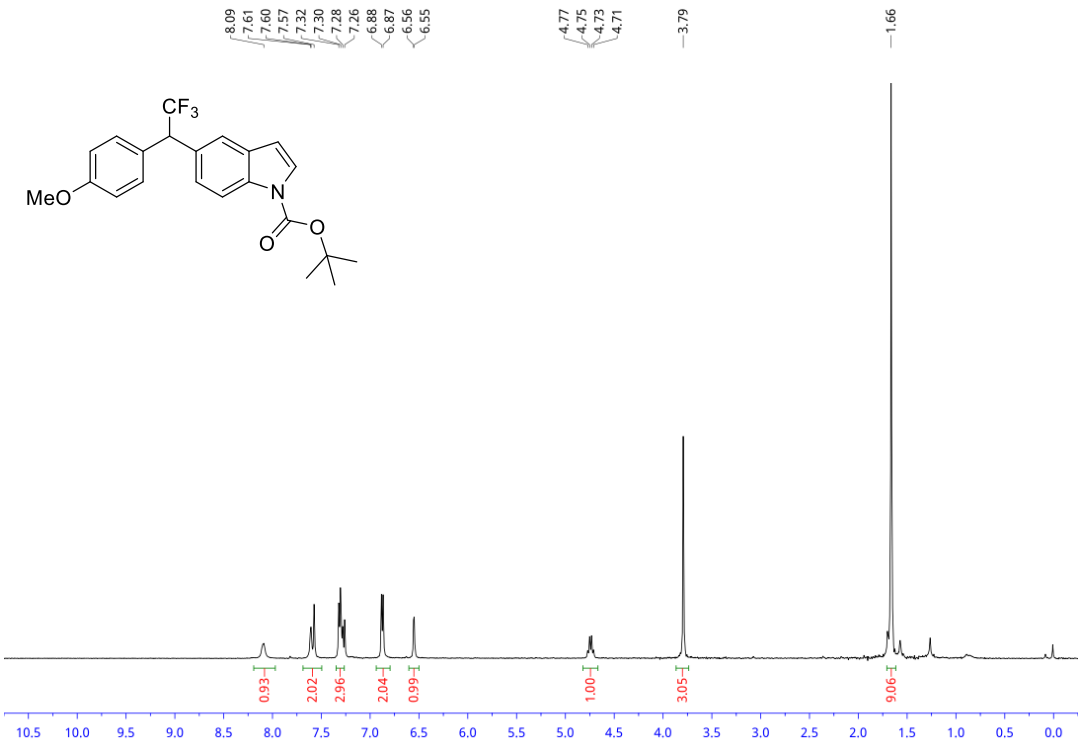


**Figure A6.31.** $^{1}$H NMR ($CDCl_3$, 500 MHz) spectrum of *tert*-butyl 5-(2,2,2-trifluoro-1-(4-methoxyphenyl)ethyl)-1*H*-indole-1-carboxylate (**10k**)

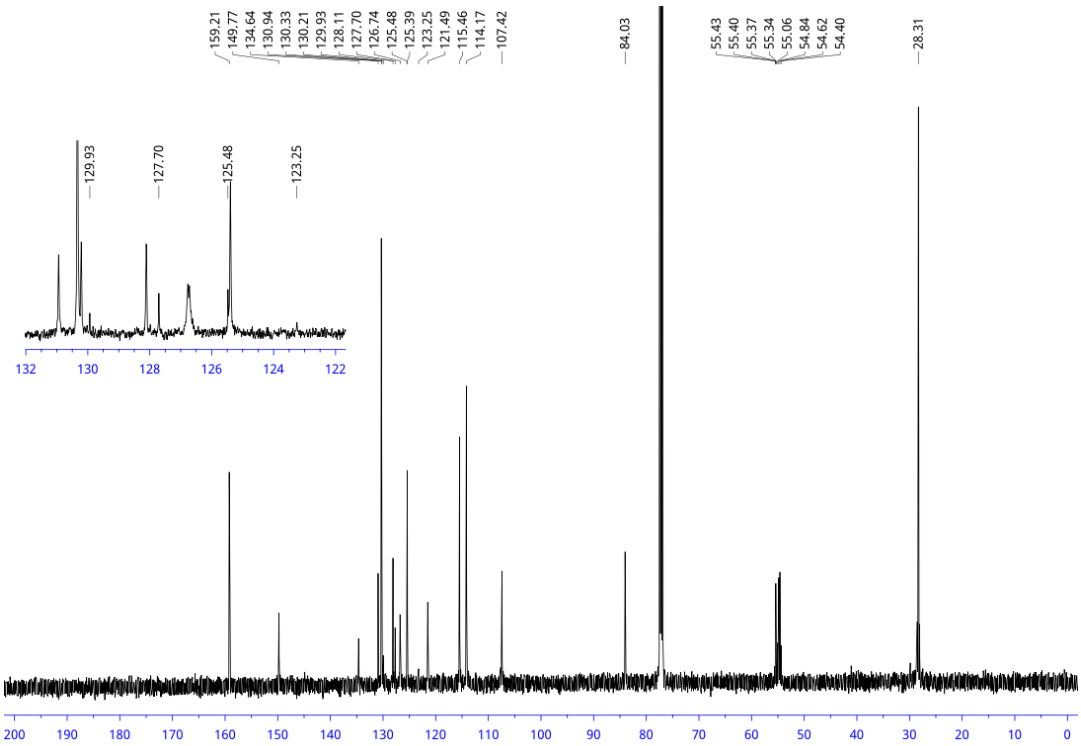


**Figure A6.32.** $^{13}$C NMR ($CDCl_3$, 126 MHz) spectrum of *tert*-butyl 5-(2,2,2-trifluoro-1-(4-methoxyphenyl)ethyl)-1*H*-indole-1-carboxylate (**10k**)

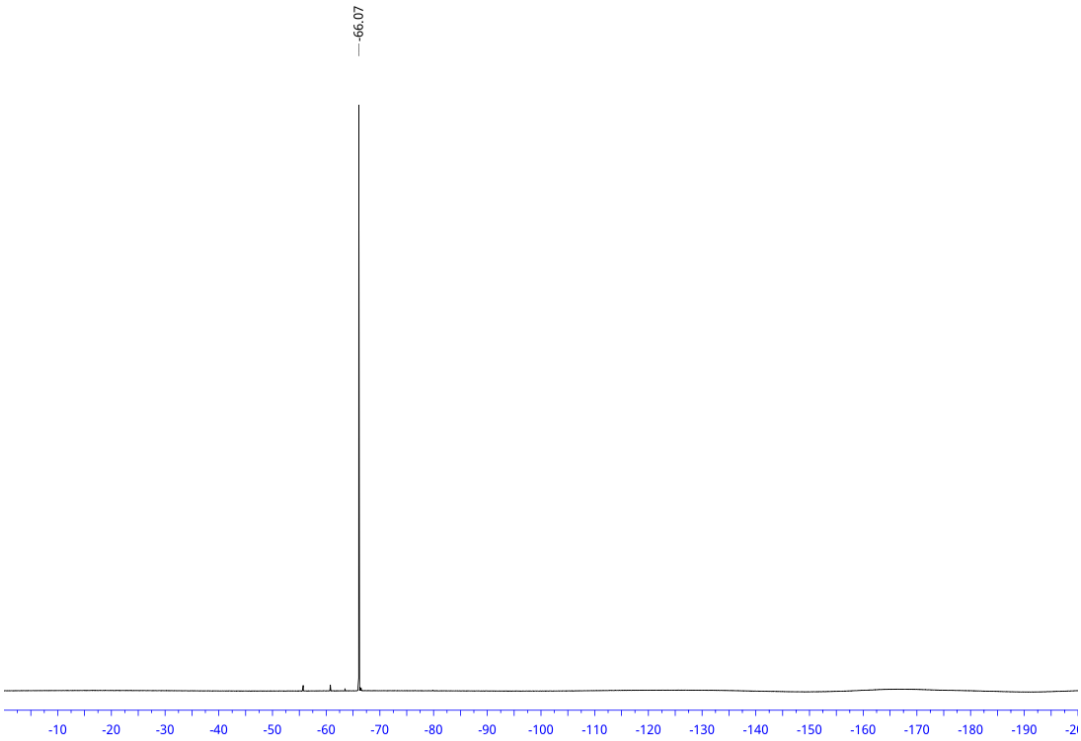


**Figure A6.33.** $^{19}$F NMR ($CDCl_3$, 471 MHz) spectrum of *tert*-butyl 5-(2,2,2-trifluoro-1-(4-methoxyphenyl)ethyl)-1*H*-indole-1-carboxylate (**10k**)

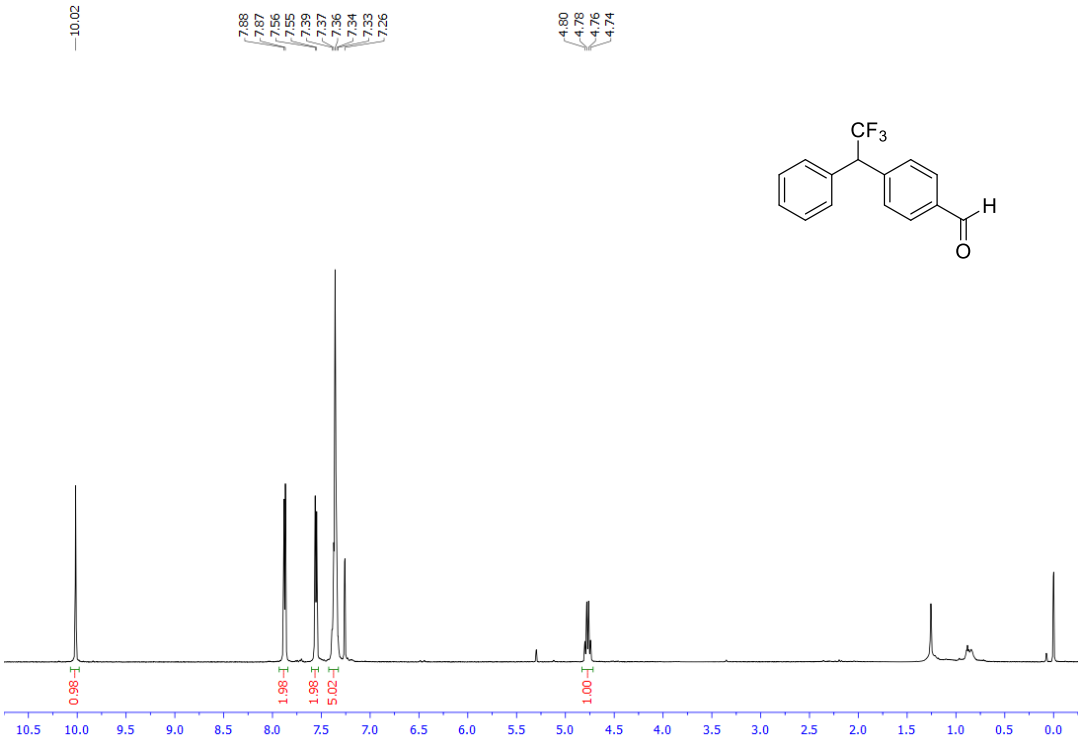


**Figure A6.34.** $^{1}$H NMR ($CDCl_3$, 500 MHz) spectrum of 4-(2,2,2-trifluoro-1-phenylethyl)benzaldehyde (**11a**)

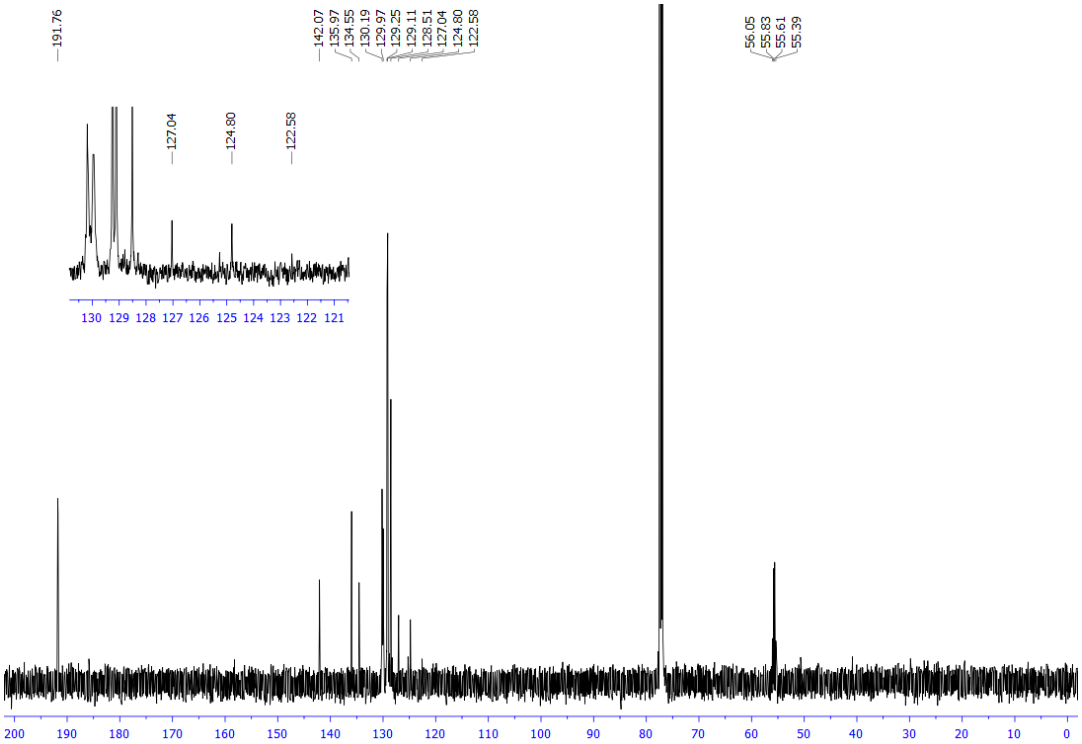


**Figure A6.35.** $^{13}C$ NMR ($CDCl_3$, 126 MHz) spectrum of 4-(2,2,2-trifluoro-1-phenylethyl)benzaldehyde (**11a**)

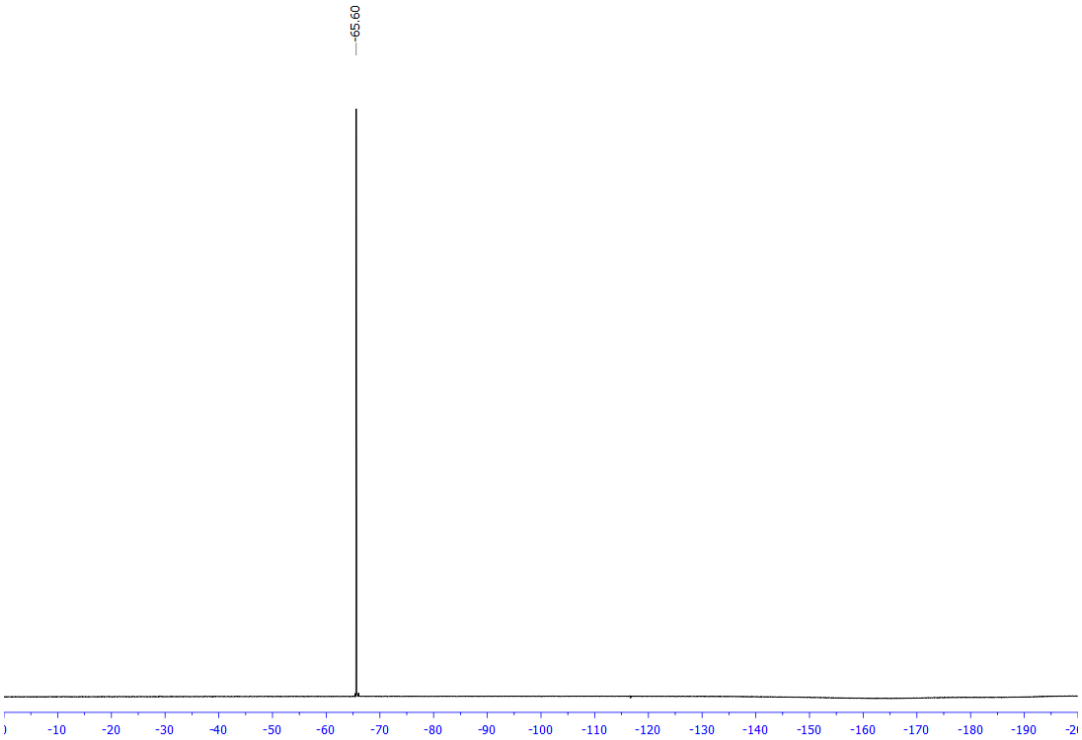


**Figure A6.36.** $^{19}F$ NMR ($CDCl_3$, 471 MHz) spectrum of 4-(2,2,2-trifluoro-1-phenylethyl)benzaldehyde (**11a**)

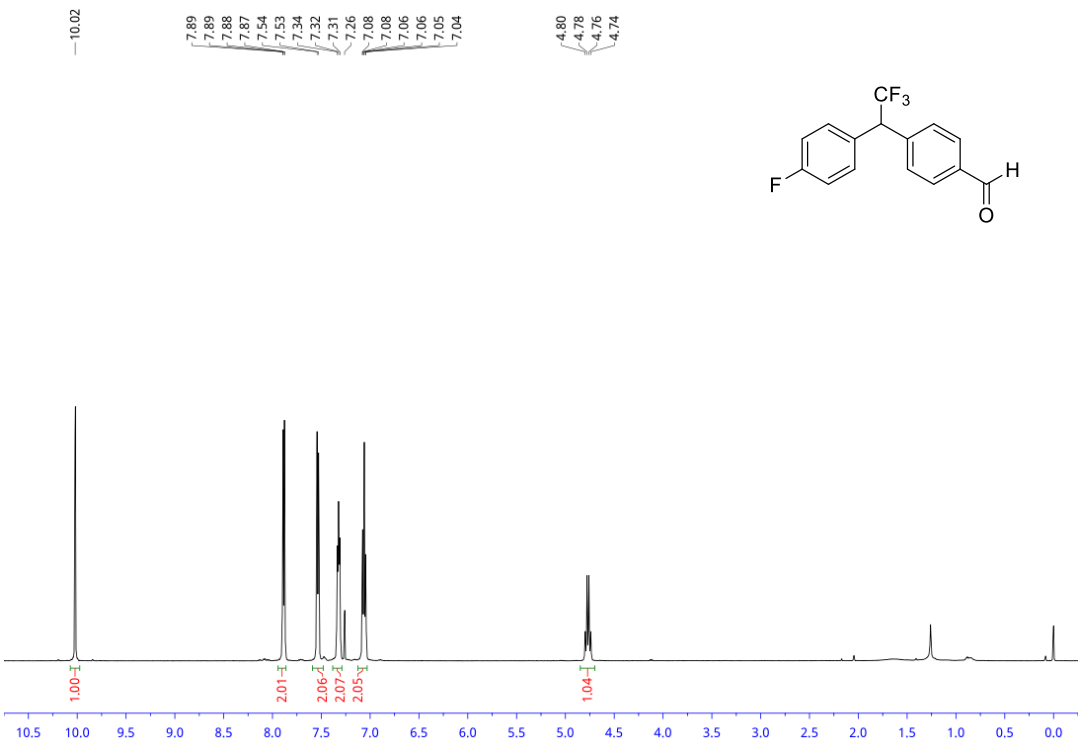


**Figure A6.37.** $^{1}$H NMR ($CDCl_3$, 500 MHz) spectrum of 4-(2,2,2-trifluoro-1-(4-fluorophenyl)ethyl)benzaldehyde (**11b**)

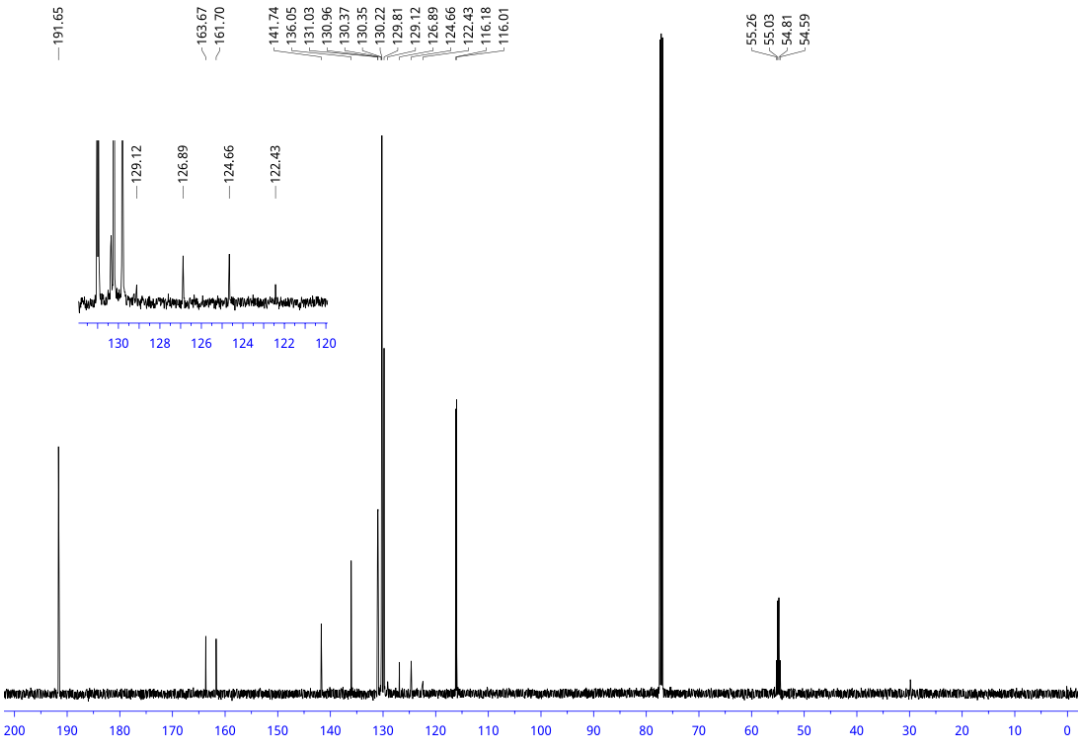


**Figure A6.38.** $^{13}$C NMR ($CDCl_3$, 126 MHz) spectrum of 4-(2,2,2-trifluoro-1-(4-fluorophenyl)ethyl)benzaldehyde (**11b**)

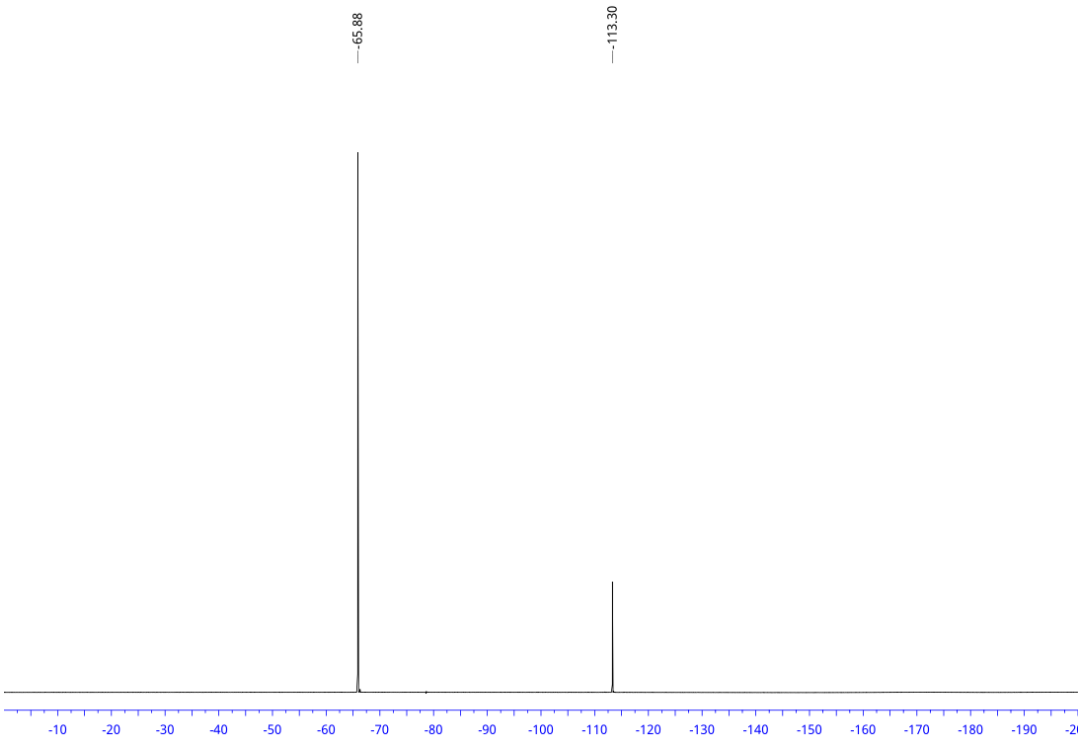


**Figure A6.39.** $^{19}$F NMR ($CDCl_3$, 471 MHz) spectrum of 4-(2,2,2-trifluoro-1-(4-fluorophenyl)ethyl)benzaldehyde (**11b**)

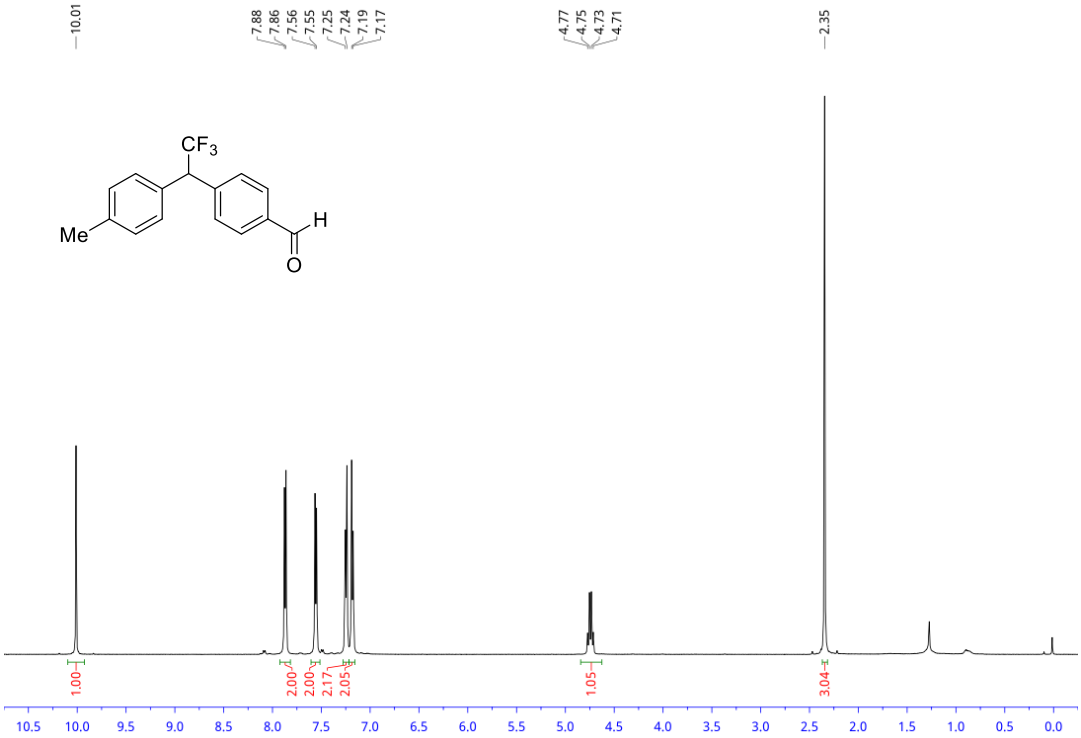


**Figure A6.40.** $^{1}$H NMR ($CDCl_3$, 500 MHz) spectrum of 4-(2,2,2-trifluoro-1-(p-tolyl)ethyl)benzaldehyde (**11c**)

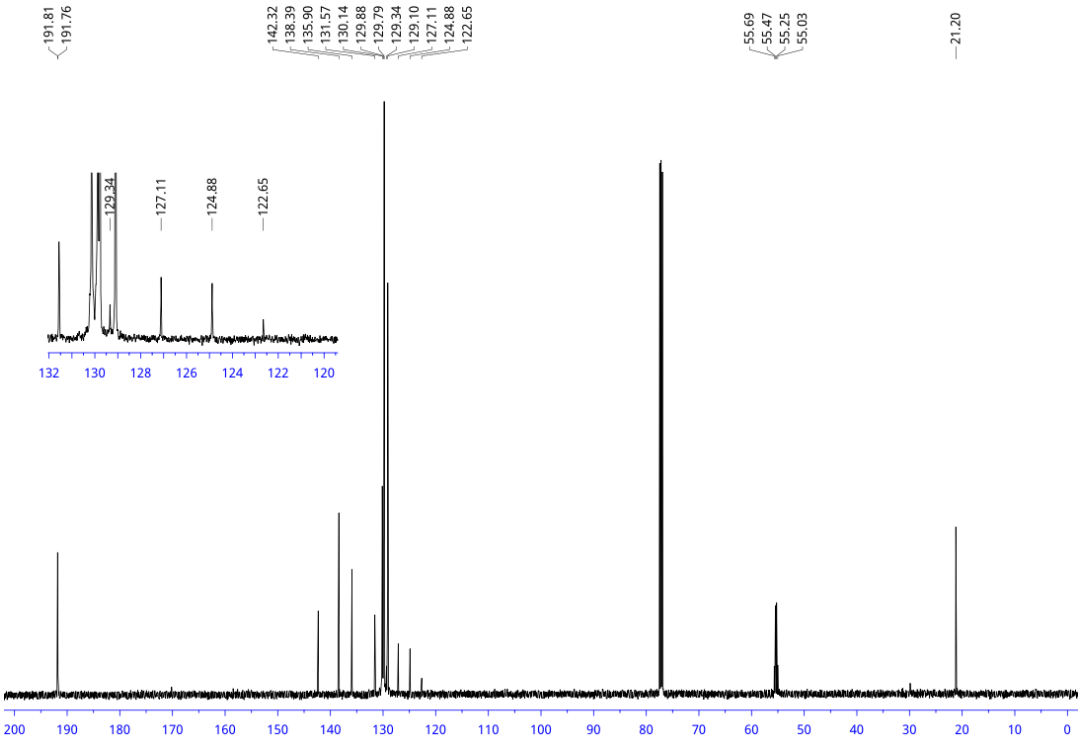


**Figure A6.41.** $^{13}C$ NMR ($CDCl_3$, 126 MHz) spectrum of 4-(2,2,2-trifluoro-1-(p-tolyl)ethyl)benzaldehyde (**11c**)

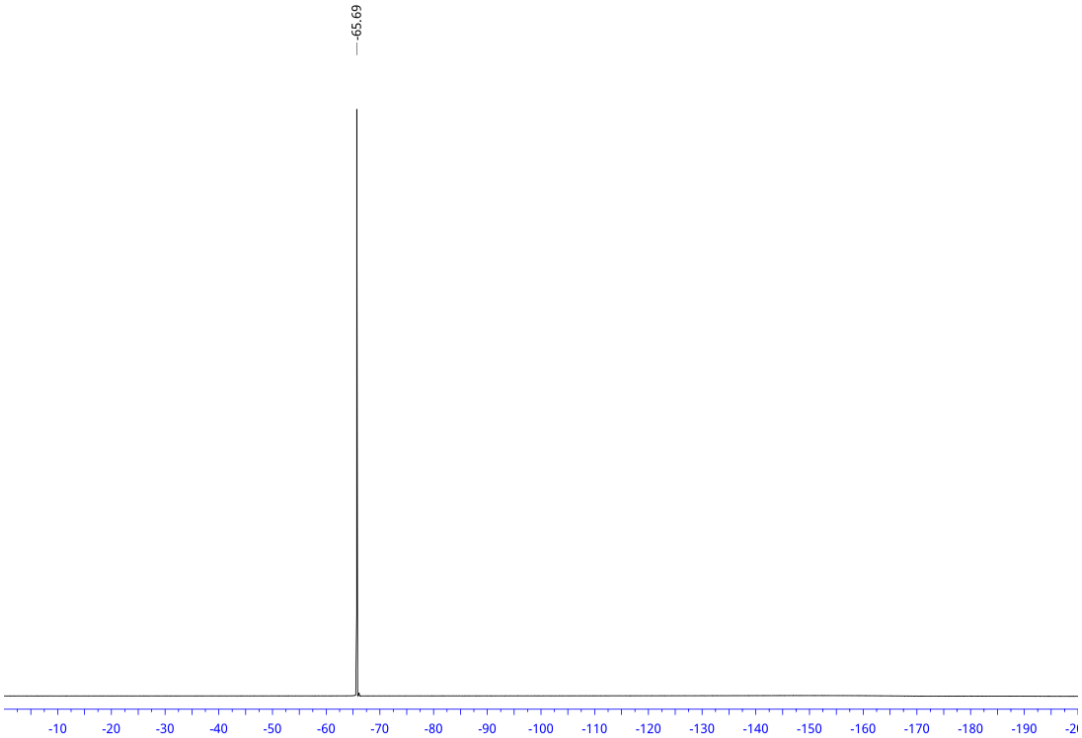


**Figure A6.42.** $^{19}F$ NMR ($CDCl_3$, 471 MHz) spectrum of 4-(2,2,2-trifluoro-1-(p-tolyl)ethyl)benzaldehyde (**11c**)


**Figure A6.43.** $^{1}$H NMR ($CDCl_3$, 500 MHz) spectrum of 4-(2,2,2-trifluoro-1-(4-methoxyphenyl)ethyl)benzaldehyde (**11d**)

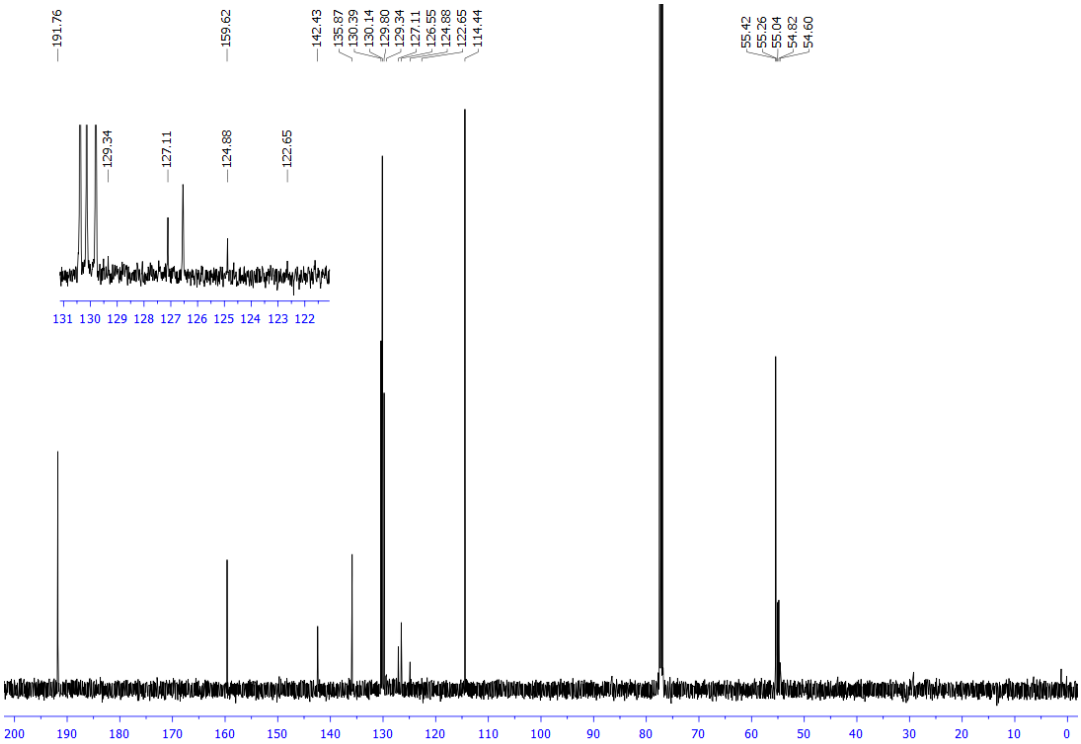


**Figure A6.44.** $^{13}$C NMR ($CDCl_3$, 126 MHz) spectrum of 4-(2,2,2-trifluoro-1-(4-methoxyphenyl)ethyl)benzaldehyde (**11d**)

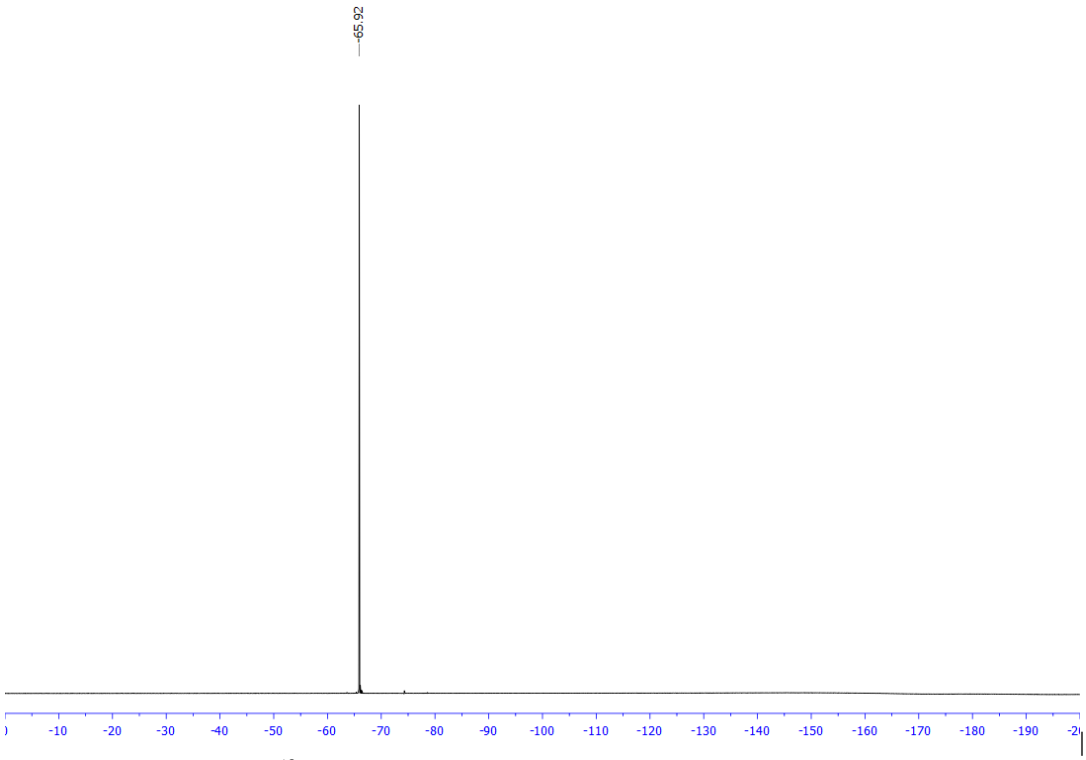


**Figure A6.45.** $^{19}F$ NMR ($CDCl_3$, 471 MHz) spectrum of 4-(2,2,2-trifluoro-1-(4-methoxyphenyl)ethyl)benzaldehyde (**11d**)

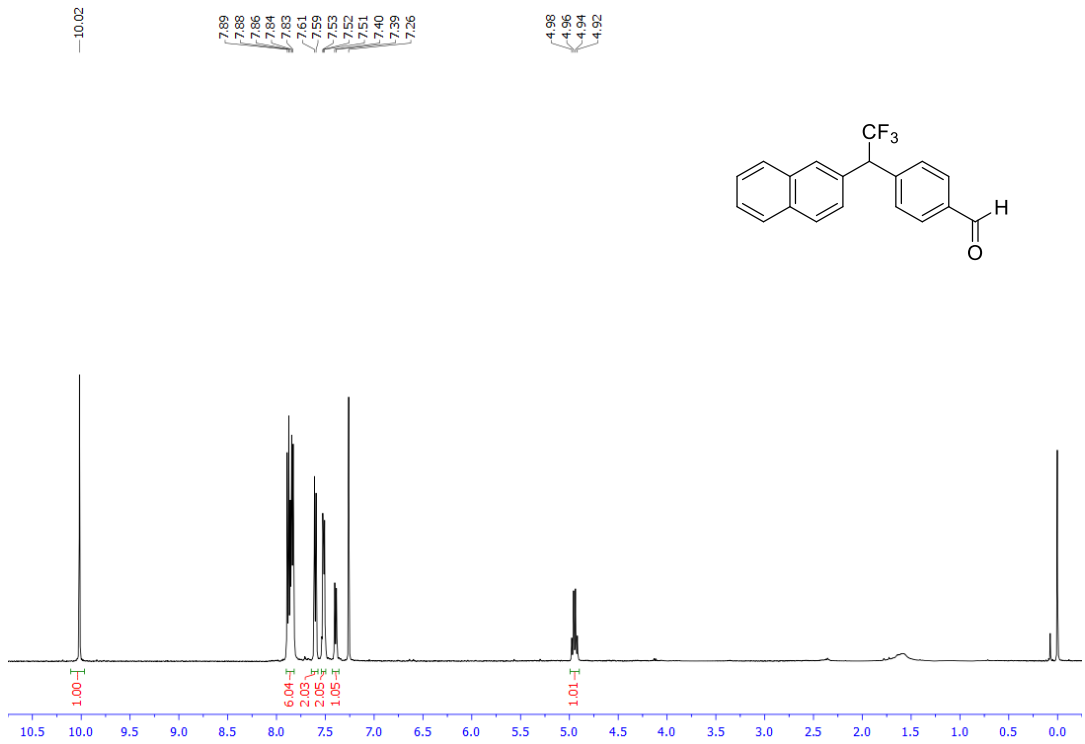


**Figure A6.46.** $^{1}H$ NMR ($CDCl_3$, 500 MHz) spectrum of 4-(2,2,2-trifluoro-1-(naphthalen-2-yl)ethyl)benzaldehyde (**11e**)

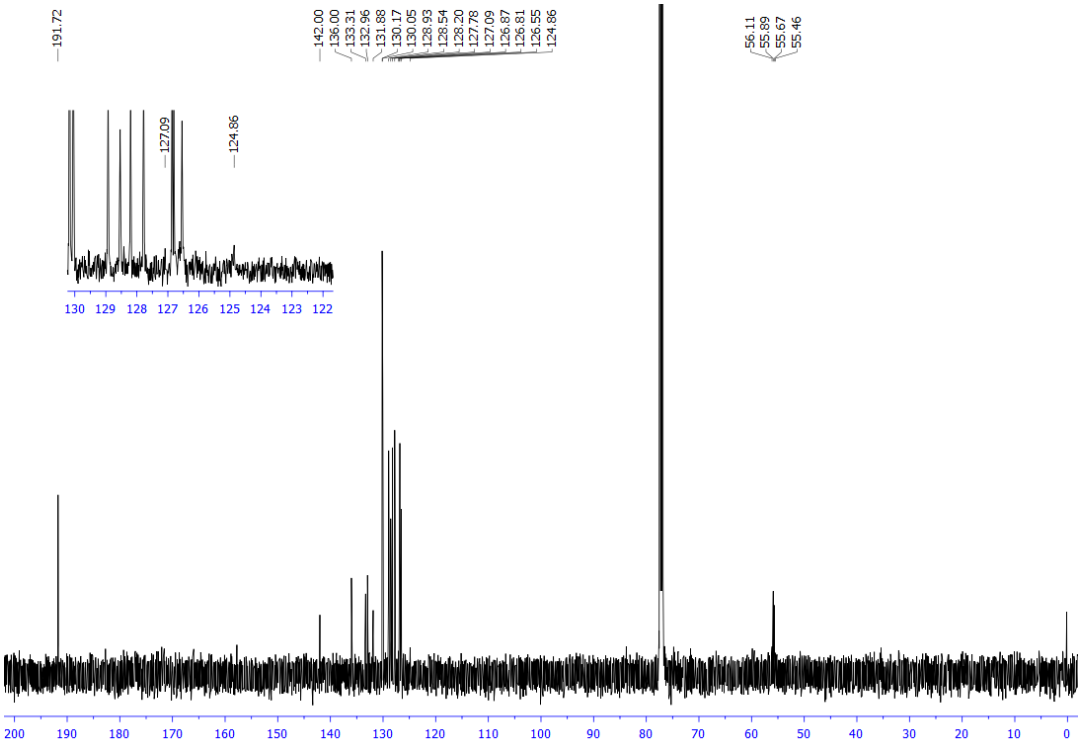


**Figure A6.47.** $^{13}C$ NMR ($CDCl_3$, 126 MHz) spectrum of 4-(2,2,2-trifluoro-1-(naphthalen-2-yl)ethyl)benzaldehyde (**11e**)

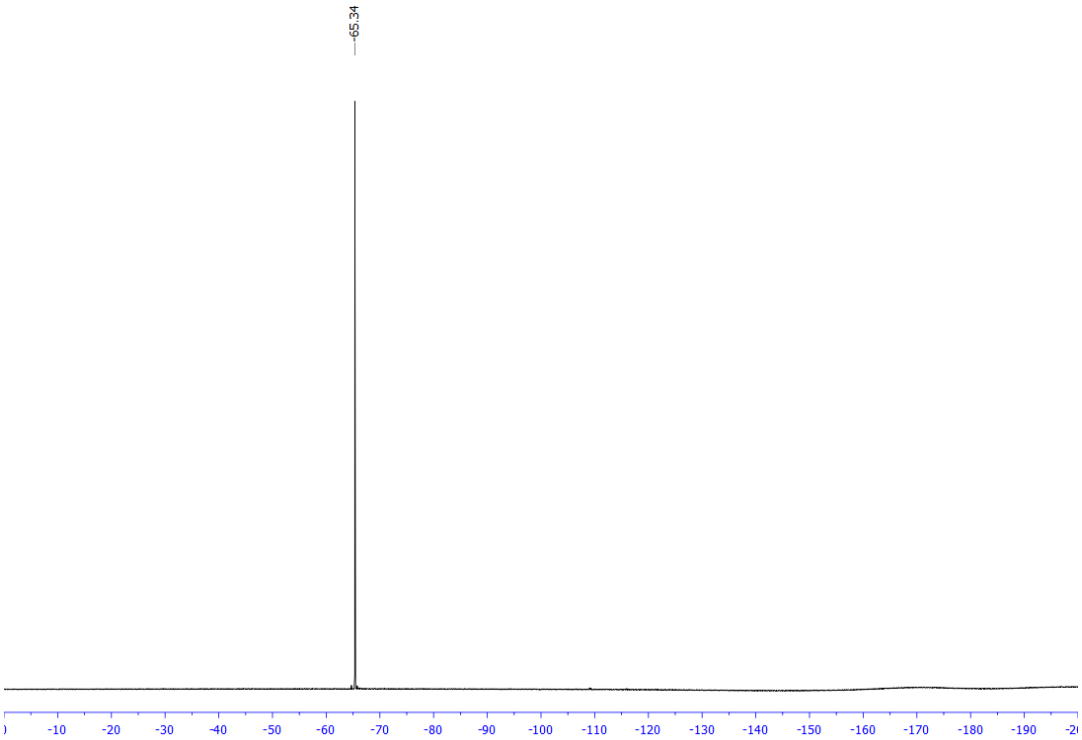


**Figure A6.48.** $^{19}F$ NMR ($CDCl_3$, 471 MHz) spectrum of 4-(2,2,2-trifluoro-1-(naphthalen-2-yl)ethyl)benzaldehyde (**11e**)

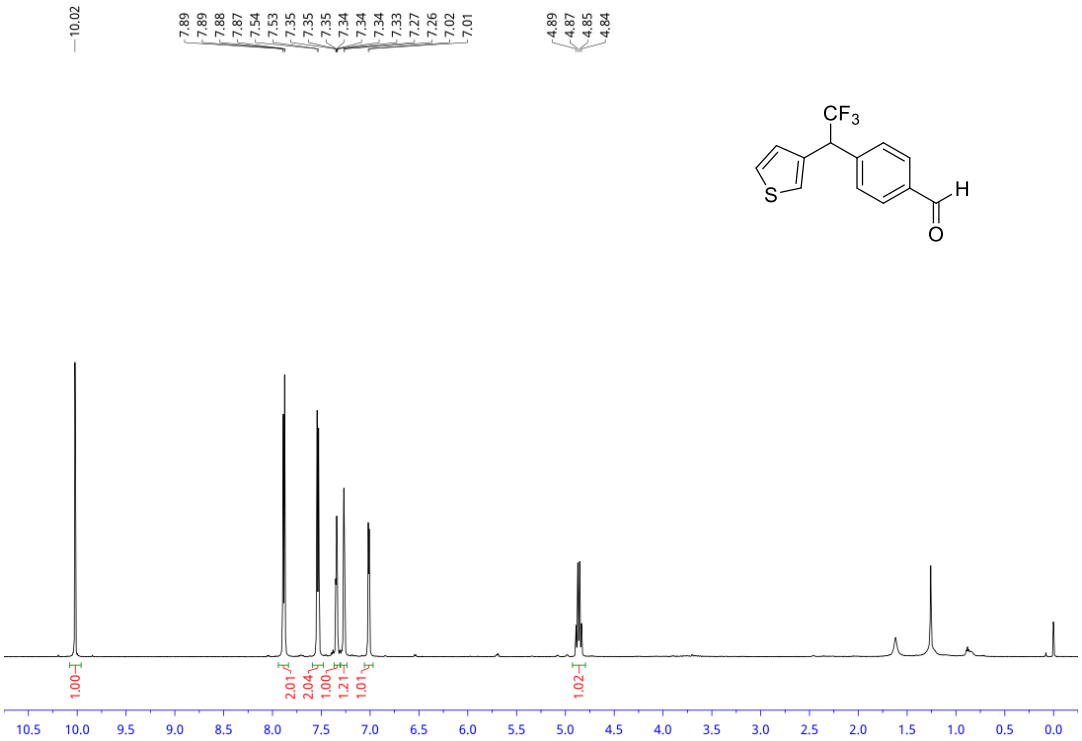


**Figure A6.49.** $^{1}$H NMR ($CDCl_3$, 500 MHz) spectrum of 4-(2,2,2-trifluoro-1-(thiophen-3-yl)ethyl)benzaldehyde (**11f**)

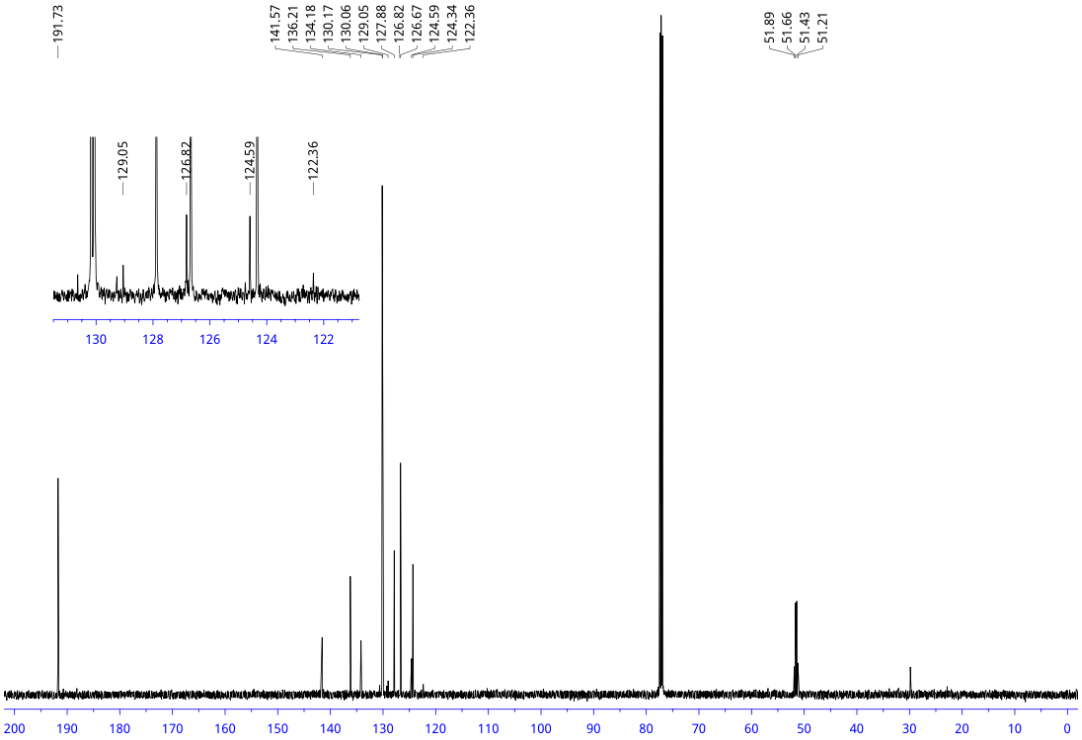


**Figure A6.50.** $^{13}$C NMR ($CDCl_3$, 126 MHz) spectrum of 4-(2,2,2-trifluoro-1-(thiophen-3-yl)ethyl)benzaldehyde (**11f**)

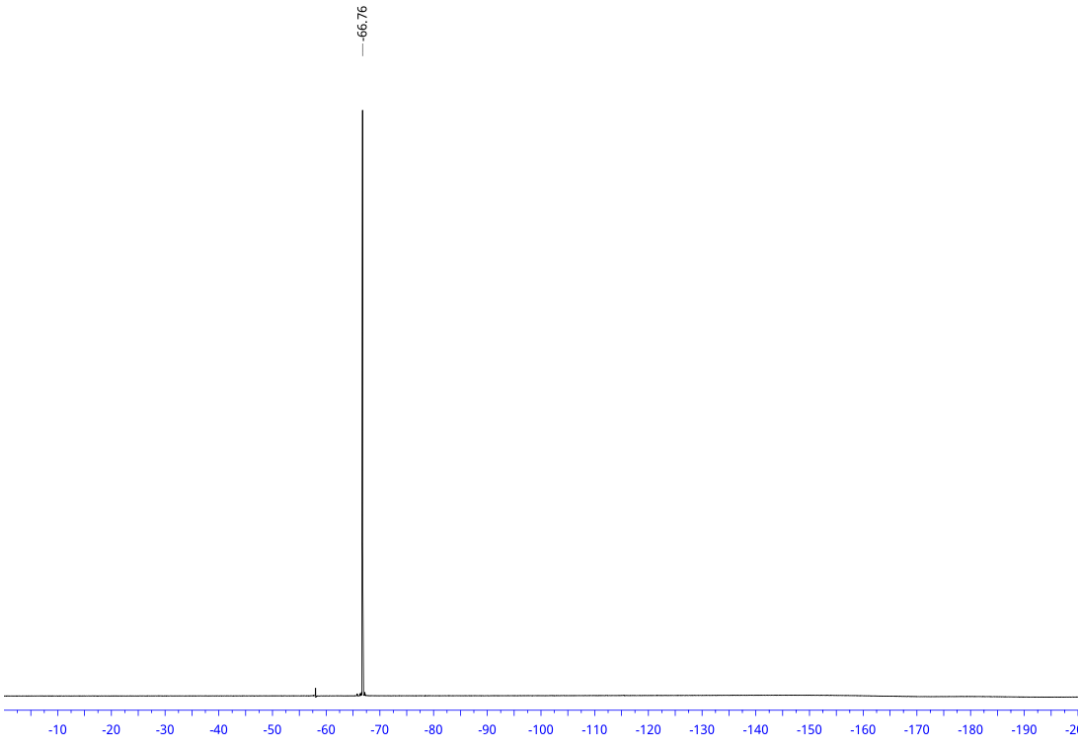


**Figure A6.51.** $^{19}$F NMR ($CDCl_3$, 471 MHz) spectrum of 4-(2,2,2-trifluoro-1-(thiophen-3-yl)ethyl)benzaldehyde (**11f**)

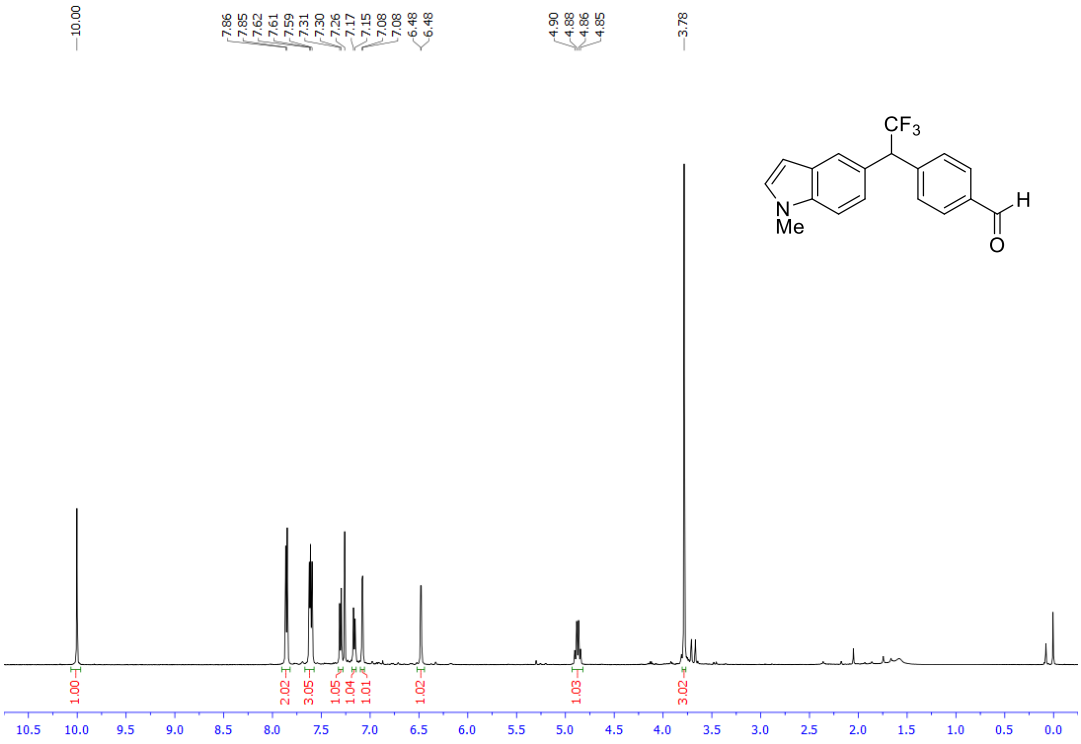


**Figure A6.52.** $^{1}$H NMR ($CDCl_3$, 500 MHz) spectrum of 4-(2,2,2-trifluoro-1-(1-methyl-1*H*-indol-5-yl)ethyl)benzaldehyde (**11g**)

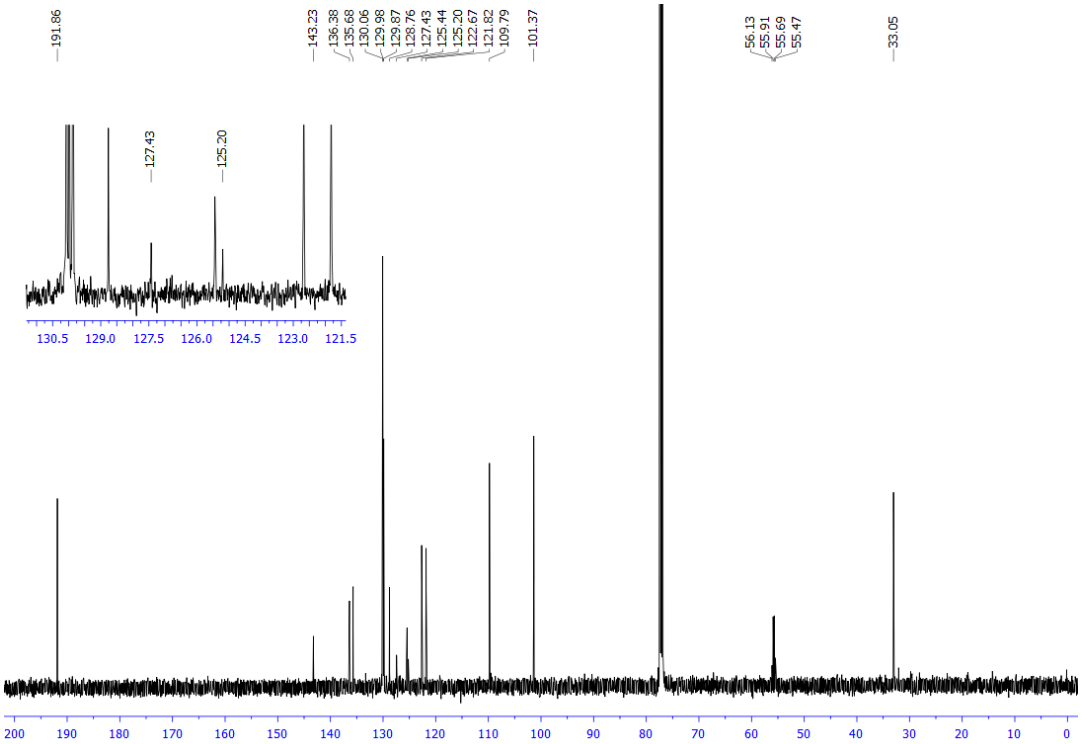


**Figure A6.53.** $^{13}C$ NMR ($CDCl_3$, 126 MHz) spectrum of 4-(2,2,2-trifluoro-1-(1-methyl-1*H*-indol-5-yl)ethyl)benzaldehyde (**11g**)

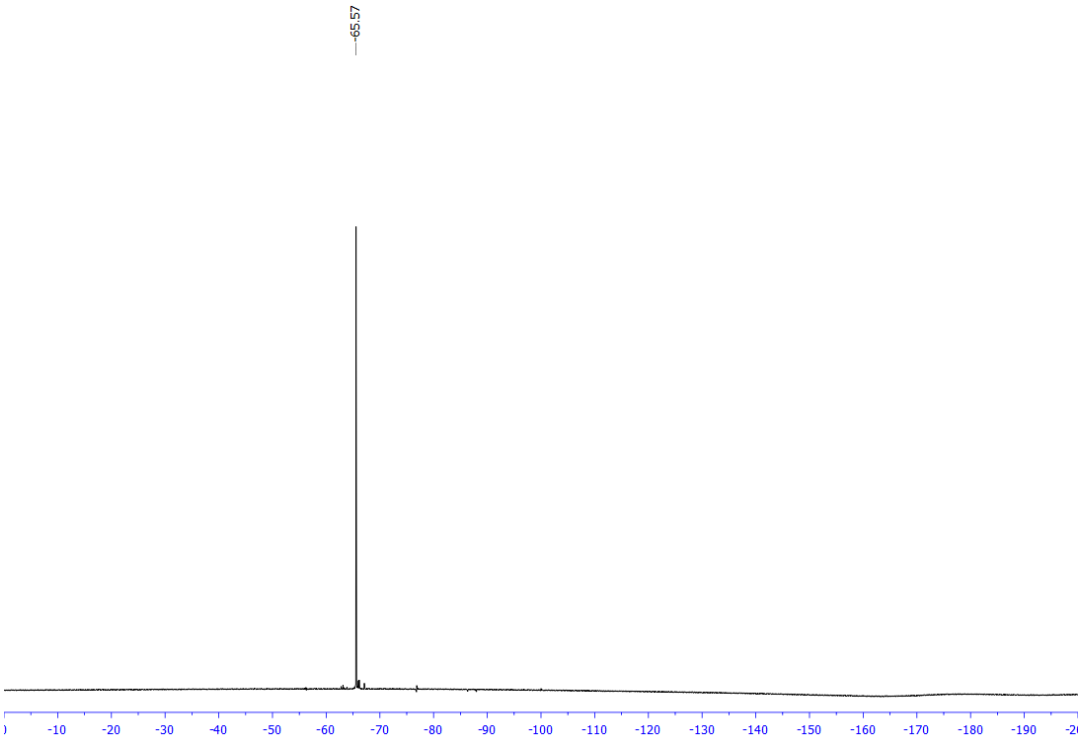


**Figure A6.54.** $^{19}F$ NMR ($CDCl_3$, 471 MHz) spectrum of 4-(2,2,2-trifluoro-1-(1-methyl-1*H*-indol-5-yl)ethyl)benzaldehyde (**11g**)

# Chapter 6. Construction of Quaternary Centers via Radical Mediated Alkyl Transfer

## 6.1 Introduction

The installation of quaternary centers has been a long-standing challenge going back to the earliest days in the art of steroid synthesis.[i] Woodward and coworkers succeeded in setting some of the first all-carbon stereocenters through cycloaddition chemistry over 60 years ago.[1] Although methods have evolved dramatically, there are still relatively few ways to install these centers reliably across a broad array of functionalized partners.[2–4] Among the most commonly employed methods, three predominate: 1) alkylation of 1,1-disubstituted allylic leaving groups,[5] 2) conjugate addition to α,β-unsaturated carbonyls,[6] and 3) alkylation of substituted enolate equivalents.[7] In many cases, each of these subclasses can cleanly access the requisite quaternary center, but are constrained by the requirement and natural reactivity pattern for a particular structural element (e.g., α,β-unsaturated carbonyls, allyl, or carbonyl systems). Most notably, none of these methods adequately address the synthesis of *arylated* quaternary centers.

In addition to these common approaches, a variety of niche metal-catalyzed reactions have also been developed for installing such centers between various nucleophile and electrophile combinations. Key contributions to highlight include Tsuji-Trost allylations,[8a] Heck couplings,[8b] Pauson-Khand cyclizations,[8c] redox relay arylations,[8d] and carbene C-H insertion reactions.[8e] These examples are by no means comprehensive, but represent landmark catalytic approaches to the installation of challenging quaternary centers.

---

[i] Reproduced in part from *Journal of the American Chemical Society*, manuscript accepted.

Although other metal-mediated catalytic reactions have enabled access to quaternary centers, there are, by contrast, vanishingly few examples of tertiary nucleophiles in classical cross-coupling chemistry. Seminal contributions from the Biscoe[9a] and Glorius[9b] groups have highlighted the success of Grignard reagents with *N*-heterocyclic carbene-ligated nickel complexes. Unfortunately, these strongly basic nucleophiles are poorly tolerant of electrophilic and protic functional groups and are often accompanied by isomerization, generating byproducts when the temperature of these reactions is not carefully controlled. Beyond these seminal reports, there are additional isolated examples using Kumada[10] or Negishi[11] reagents; however, these do not represent a unified strategy for tertiary cross-couplings. Particularly from a diversification perspective, approaches using these sensitive, pyrophoric reagents are wholly impractical when applied to a wide array of tertiary nucleophiles paired with an equally broad palette of aryl electrophiles. The clear absence of methods predicated on the use of bench-stable partners inspired the laboratory to explore tertiary organoboron nucleophiles more closely – especially given the recent surge in methods for their preparation.[13]

## 6.2 Results and Discussion

Studies were initiated using *tert*-butyltrifluoroborate **13** as the chosen nucleophile with 4'-bromoacetophenone as the aryl electrophile. Application of conditions[14] (**Figure 6.1A**) successful in previous studies proved completely ineffective for achieving the desired cross-coupling. For all bipyridyl ligands, only starting material or protodehalogenation products were observed. Furthermore, the alkyltrifluoroborate was often minimally consumed after 24 h. Given the lack of conversion under our initially developed conditions, we sought to understand in a more comprehensive manner the divergent reactivity of these tertiary radical precursors.

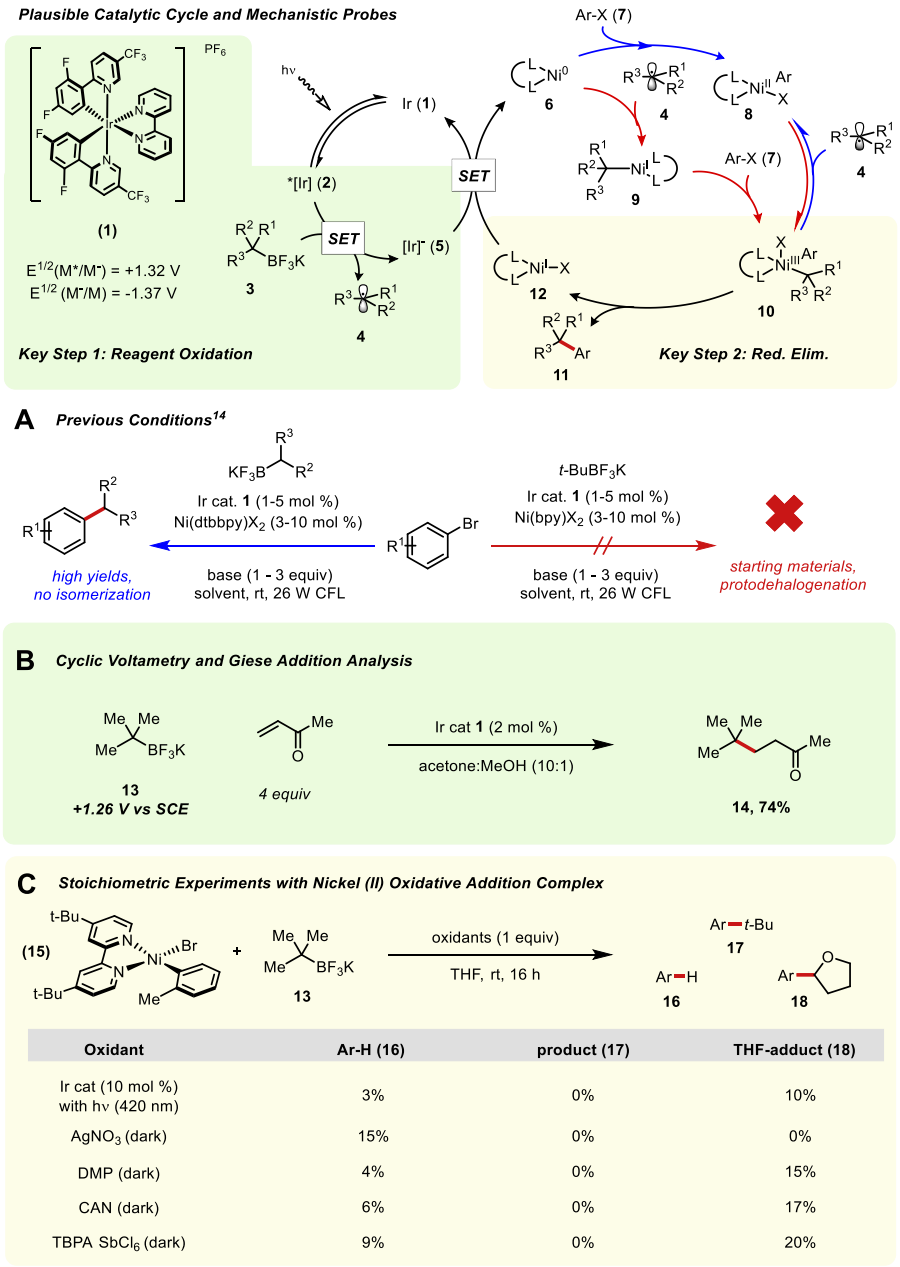


| Oxidant | Ar-H (16) | product (17) | THF-adduct (18) |
|---|---|---|---|
| Ir cat (10 mol %) with hν (420 nm) | 3% | 0% | 10% |
| $AgNO_3$ (dark) | 15% | 0% | 0% |
| DMP (dark) | 4% | 0% | 15% |
| CAN (dark) | 6% | 0% | 17% |
| TBPA $SbCl_6$ (dark) | 9% | 0% | 20% |

**Figure 6.1.** Plausible catalytic cycle and key mechanistic experiments

First, oxidation of the reagent was considered (**Figure 6.1B**). Notably, in previous work, static quenching of alkyltrifluoroborates in the presence of a cationic photocatalysts has been observed[15] – indicating the formation of a salt pre-complex that precedes a single-electron transfer (SET) event. Because of the enhanced steric bulk of these tertiary precursors, it seemed prudent to

confirm these reagents were indeed generating radical intermediates. Gratifyingly, both cyclic voltammetry analysis of the alkyltrifluoroborate ($E_{red}^{1/2}$ = +1.26 V vs SCE) and Giese-type trapping experiments[16] confirmed the viability of this oxidation, the latter affording the desired alkylated product **14** in 74% yield.

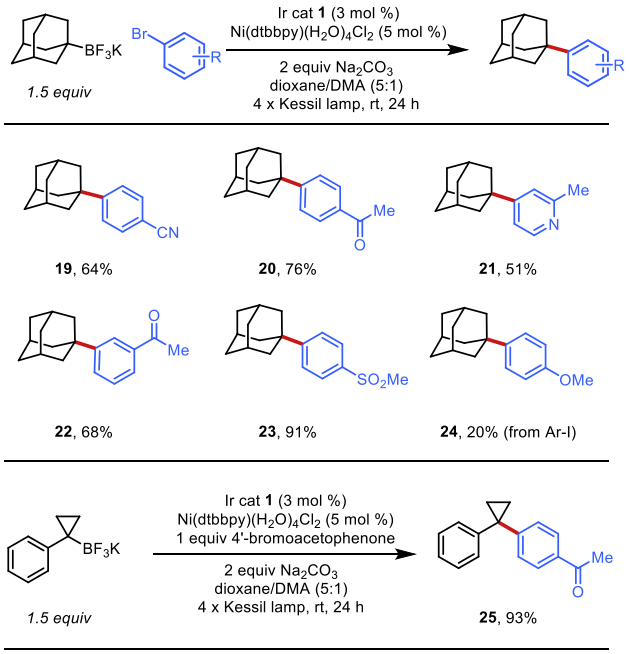


**Figure 6.2.** Constrained cyclic alkyltrifluoroborates in cross-coupling using slightly modified reaction conditions

Next, attention was turned to the key bond-forming reductive elimination step in these couplings (Figure 1C) Here, the desired $Ni^{III}$ intermediate was deemed to be accessible through the use of a preformed $Ni^{II}$(dtbbpy) oxidative addition complex **15** in the presence of alkyltrifluoroborate **13** and an appropriate oxidant. Surprisingly, stoichiometric experiments exposing this complex to a variety of oxidant combinations in the presence of alkyltrifluoroborate **13** failed to afford any of the desired coupling product even under prolonged reaction times. The only products observed were THF-adduct **18** (known to be generated under the reaction conditions through C-H abstraction[17] or halide abstraction pathways[18]) and protodehalogenation. Given these

results, it appeared unlikely that the established bipyridyl ligand systems for primary and secondary alkyl radicals would be broadly applicable to their tertiary counterparts.

Although daunted by the failures here, we did achieve targeted success with adamantyltrifluoroborate and other constrained ring systems because of their unique structural properties. As a tied back (tetrahedral) radical possessing no sites for possible β-hydride elimination, slight modification of the previously developed conditions allowed access to an array of compounds (Figure 2). Electron-poor (**19**–**23** , **25**), electron-rich (**24**) and heteroaryl halides (**20**) all proved viable. Unfortunately, this rather niche reactivity was not unprecedented[19,12a] and by no means represented a general solution to tertiary radical coupling.

To identify a set of more robust general conditions, a screening effort was initiated to evaluate a wide variety of ligand classes that might be amenable to tertiary radical progenitors. Representative ligands from the Ni cross-coupling literature ranging from phosphines,[20] pyridines,[21] terpyridines,[22] amino alcohols,[23] *N*-heterocyclic carbenes,[9] olefins,[24] to 1,3-diketones[25] were all introduced to both a Ni(0) and Ni(II) source in parallel. The reactions were then followed by UPLC to observe the desired coupling product (see Supporting Information for full details). Across all ligand classes, only diketonate-type species showed significant product formation. Interestingly, these ligands have seen use in mechanistically analogous reductive coupling chemistry reported by the Gong group in 2015.[25]

Further optimization of this ligand architecture identified a more bulky tetramethylheptanedione (TMHD) scaffold as being suitable for promoting the desired coupling. Additional evaluation of bases showed that the addition of inorganic bases served to reduce protodehalogenation byproducts and increase yield. A solvent screen showed that DMA was essential for coupling success. Use of other polar aprotic solvents such as DMF, DMSO, or NMP resulted in poorer conversions. Use of $ZnBr_2$ and other Lewis acids were tested as additives to facilitate the coupling. Although these additives were deemed non-essential, rate studies show that

these salts reduce the initial induction period observed for the coupling, particularly at larger reaction scales. A summary of the effect of deviations from the optimized conditions can be found in Table 1. It should be noted that although reactions run in front of the low wattage LEDs were sluggish (48–72 h), increasing the light intensity through the use of blue aquarium lamps as in Figure 1, entries **27** and **35**, substantially reduced the reaction times (24 h).

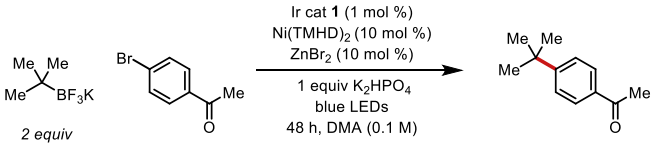


| entry | deviation | Ar-H / IS | SM / IS | P / IS | HPLC yield |
|---|---|---|---|---|---|
| 1 | no change | 0.29 | 0 | 3.61 | >95% |
| 2 | no light | 0.01 | 3.92 | 0 | <5% |
| 3 | no PC | 0.62 | 2.10 | 0.11 | <5% |
| 4 | no [Ni] | 0.63 | 3.65 | 0 | <5% |
| 5 | no $K_2HPO_4$ | 1.88 | 0.64 | 1.38 | 36% |
| 6 | no $ZnBr_2$ | 0.44 | 0 | 3.07 | 81% |
| 7 | $Ni(COD)_2$ (10%) $Zn(THMD)_2$ (20%) | 0.45 | 1.14 | 2.17 | 57% |
| 8 | $NiBr_2$ (10%) $Zn(THMD)_2$ (20%) | 0.11 | 3.26 | 0.31 | 8% |
| 9 | CzIPN[a] instead of Ir cat 1 | 2.07 | 0 | 1.35 | 35% |

**Table 6.1.** Optimized conditions for *tert*-butyltrifluoroborate cross-coupling and effects of deviation from standard conditions. [a]CzIPN = ;2,4,5,6-Tetra-9H-carbazol-9-yl-1,3-benzenedicarbonitrile

With suitable conditions in hand, an evaluation of this coupling across an array of aryl bromides was undertaken (Figure 3). The use of numerous electron-poor aryl bromides resulted in moderate to excellent yields. (**26–34**). Of note, a number of electrophilic functional groups that are intolerant of more reactive Kumada conditions could be employed to afford nitrile **27,** aldehyde **28**, sulfonyl fluoride **30**, amide **34**, and ketones **26** and **36**. A bromo sulfonamide could also be engaged in the coupling to give **31**, demonstrating tolerance of some protic functional groups. A heteroaryl thiophene and benzofuran were also acceptable partners to give products **35** and **36**. Unfortunately,

the more highly desirous *N*-heteroaryl bromides were ineffective under the coupling conditions (see **37**). At this time, we surmise that the pyridine serves to ligate the metal center competitively, inhibiting the active catalyst. This is supported by doping experiments where addition of 10 mol % of pyridine to the active catalyst mixture arrests conversion to desired product (see Supporting Information).

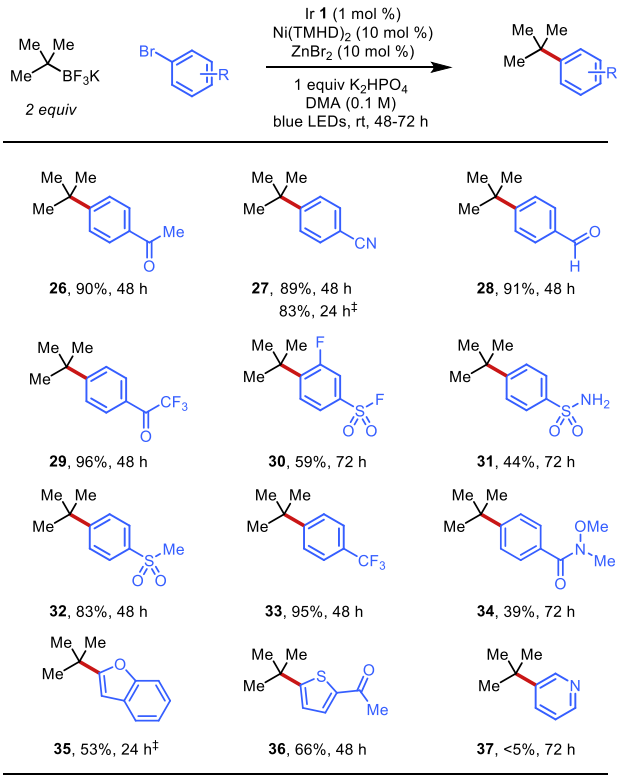


**Figure 6.3.** Aryl bromide scope in the cross-coupling of potassium *tert*-butyltrifluoroborate under the developed conditions. ‡Reactions irradiated with four H150 blue LED Kessil lamps.

To evaluate the scope further, an enone-derived alkyltrifluoroborate **38** was used to ease separation of reactions with incomplete conversion (Figure 4). Here, electron-poor systems worked well to give products **39**–**44**. Meta substitution was tolerated, giving compounds **43** and **46** in moderate yields. Overall, the use of electron-neutral bromides resulted in poorer yields (**45**–**46**) and

truly electron-rich systems such as 4-bromoanisole afforded trace product (**47**) under the developed conditions.

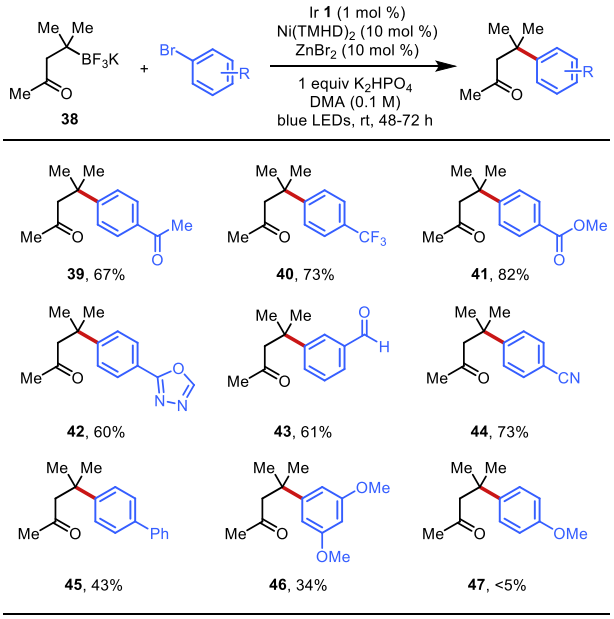


**Figure 6.4.** Further aryl bromide scope evaluation with enone derived alkyltrifluoroborate **38**

With this survey of electrophiles established, we next turned our attention to more complex tertiary alkyltrifluoroborate precursors using electron-poor bromides as model electrophiles (**Figure 6.5A**). Cyclohexanone- and cyclopentanone- based ring systems could be coupled with an array of substituted aryl bromides (aldehydes, sulfones, ketones) to afford products **48**–**51**. Notably, the products obtained from the coupling of these enone- and enoate-derived trifluoroborates are analogous to those accessed through 1,4 addition chemistry of aryl nucleophiles to α,β-unsaturated carbonyl systems.[26]As such, the coupling here represent an *umpolung* approach to these methods where the carbon β to the carbonyl has been rendered nucleophilic (**Figure 6.5B**). Considering the far greater number of commercially-available aryl electrophiles in comparison to the corresponding aryl nucleophiles, this alternative approach has clear advantages for diversity oriented synthesis. Other functionalized trifluoroborates could be employed to give quaternary centers in products **52**–

**56**. Here, ester-, ether-, and ketone-containing trifluoroborates all work well in the established protocol. The incorporation of an amide in a nearby position shut down the reaction, returning only β-hydride elimination and reduction products (see **57**), suggesting that changes in the ligation around the nickel have drastic effects on the reaction profile for this tertiary cross-coupling.

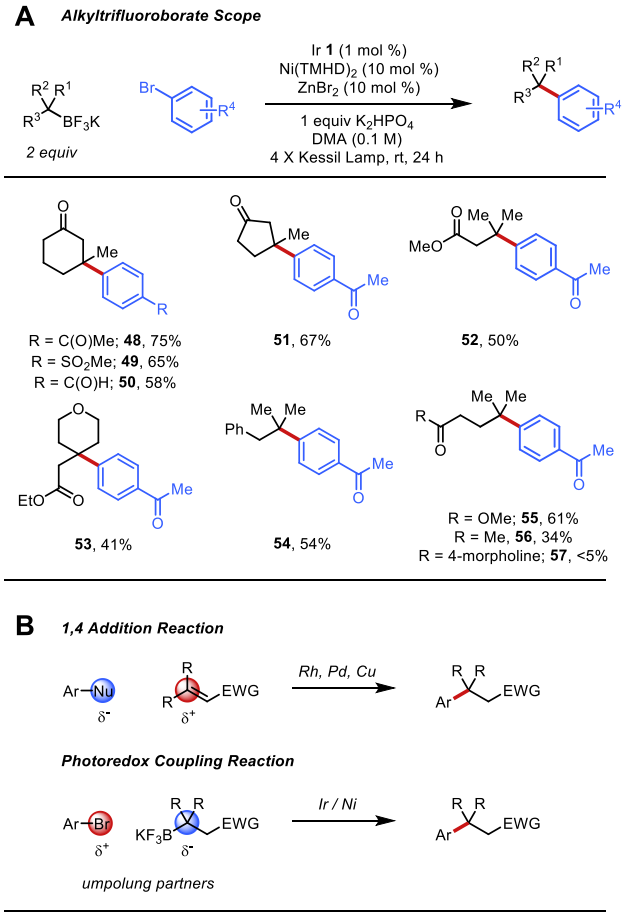


**Figure 6.5.** (A) Tertiary alkyltrifluoroborate scope with electron poor aryl bromides. (B) Comparison of enone and enoate derived trifluoroborate cross-coupling to metal catalyzed 1,4-addition chemistry.

## 6.3 Conclusion

In summary, the first general method for the cross-coupling of tertiary organotrifluoroborates has been described. The development of this protocol hinged on the use of photoredox high-throughput screening technology to identify a new ligand architecture amenable to more bulky tertiary radical nucleophiles. Using the conditions identified therein, an array of functionalized, unactivated tertiary organoboron reagents have been employed in transition metal-catalyzed cross-coupling for the first time.[27] These reactions generate notoriously challenging to access quaternary centers that are typically forged in cross-coupling through the use of highly reactive Kumada and Negishi partners. In contrast, these mild conditions are tolerant of a number of electrophilically-sensitive functional groups such as aldehydes, ketones, esters, and amides.

At present, a few key limitations of this protocol still remain, as the aryl bromide scope for this cross-coupling is currently limited to electron-poor and electron-neutral systems. From the standpoint of organoboron coupling, this limitation actually serves to complement existing metal-free tertiary coupling work by Aggarwal and others, wherein tertiary alkyl pinacol boronates can be best coupled with electron-rich arene systems.[28] The current method also exhibits a notable absence of *N*-containing heteroaryl partners. In some ways, this failure of heteroaryl systems is mitigated by the successful implementation of tertiary alkyltrifluoroborates in Minisci processes,[29] but extension to other electrophilic sites on heteroaryl compounds would still have significant value. Further refinement to the ligand scaffold and conditions will likely address these two limitations; efforts in the laboratory toward this end are an ongoing endeavor.

Given the growing suite of methods for the synthesis of tertiary organoboron compounds,[13] this photoredox cross-coupling serves as a timely addition, enabling tertiary organoboron reagents as partner in the installation of arylated quaternary centers. Although limitations remain, the ligand screening data and mechanistic interrogation will allow practitioners seeking to employ other

tertiary radical feedstocks (carboxylic acids, halides, aldehydes, silicates, etc.) to channel these lessons into developing new tertiary alkyl cross-couplings of broad interest. Taken together, these findings introduce tertiary alkyl radicals to the photoredox cross-coupling portfolio.

## 6.4 Experimental

### General considerations

All reactions were carried out under an inert atmosphere of nitrogen or argon unless otherwise noted. DMA was purchased as 99.9%, extra dry. $K_2HPO_4$ was stored and dispensed in a dry glovebox. $IrCl_3 \cdot xH_2O$, and $Ni(TMHD)_2$ were purchased from commercial sources. All other reagents were purchased commercially and used as received. Photoredox reactions were irradiated by 1.2 W/ft. blue LED (420 nm) light strips, coiled in a circular setup approximately 38 inches in length. To accelerate the reactions, irradiation with 2–4 Kessil H150 blue LED flood lamps can also be used to complete reactions in under 24 h. Melting points (°C) are uncorrected. NMR spectra were recorded on a 500 MHz spectrometer. $^{19}F$ NMR chemical shifts were referenced to external $CFCl_3$ (0.0 ppm). $^{11}B$ NMR spectra were obtained on a spectrometer equipped with the appropriate decoupling accessories. All $^{11}B$ NMR chemical shifts were referenced to an external $BF_3 \cdot OEt_2$ (0.0 ppm) with a negative sign indicating an upfield shift. Data are presented as follows: chemical shift (ppm), multiplicity (s = singlet, d = doublet, t = triplet, q = quartet, m = multiplet), coupling constant *J* (Hz) and integration. The $^{13}C$ signal of the carbon bonded to boron was not observed in all cases because of quadrupolar relaxation.

**General Procedure for Conversion of Boronic Acid Derivatives to Alkyltrifluoroborate:**

To a solution of boronic acid derivative in MeOH (0.1 M) at 0 °C was added saturated aq $KHF_2$ (4.5 M) dropwise over 30 min and then subsequently stirred for 3 h to rt. The resulting suspension was concentrated under reduced pressure. $H_2O$ was azeotropically removed by suspension in toluene (100–150 mL) followed by rotary evaporation. The remaining solid was dried under high vacuum overnight. The resultant solid was resuspended in hot acetone and filtered. The filtrate was then concentrated to minimal volume, and the trifluoroborates were precipitated by the addition of cold $Et_2O$, $CH_2Cl_2$, and/or pentanes.

**General Enone Borylation Procedure:**

Following a slightly modified literature procedure,[30] a flask was charged with CuBr (14.8 mg, 0.1 mmol), CyJohnPhos (35 mg, 0.1 mmol), bisboronic acid (537.9 mg, 6 mmol) and NaO*t*-Bu (144.2 mg, 1.5 mmol). The flask was evacuated and purged 3 times with argon. EtOH (50 mL) and enone (5.0 mmol) were added via syringe, and the mixture was stirred for 21 h. The reaction mixture was filtered through a plug of Celite and then rinsed with EtOAc (3 x 40 mL). The filtrate was concentrated, and the resultant oil was dissolved in MeOH (50 mL). This solution was cooled in an ice-bath, and then a solution of saturated $KHF_2$ (42.5 mmol, 4.5 M) was added dropwise. The mixture was warmed to rt and was stirred for 3.5 h. The suspension was then evaporated to dryness. The resultant solid was triturated and sonicated with hot acetone and filtered three times. The filtrate was then concentrated to a minimal volume, and the alkyltrifluoroborates were precipitated through dropwise addition of cold $Et_2O$ (10–50 mL). The mixture was filtered, washed with cold $Et_2O$ (5–20 mL), and dried on high vacuum overnight to yield the desired β-trifluoroboratoester or –ketone.

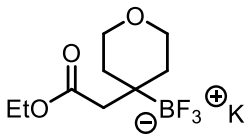

**S1**

**Potassium (4-(2-Ethoxy-2-oxoethyl)tetrahydro-2H-pyran-4-yl)trifluoroborate (S1)** prepared from ethyl 2-(tetrahydro-4H-pyran-4-ylidene)acetate (5 mmol) and obtained in 32% yield, 445 mg as a white crystalline solid, mp = 187 – 190 $^{0}$C. $^{1}$H NMR (500 MHz, acetone-$d_6$) δ 4.01 (q, $J$ = 7.1 Hz, 2H), 3.72 – 3.64 (m, 2H), 3.55 – 3.49 (m, 2H), 2.15 (s, 2H), 1.73 – 1.62 (m, 2H), 1.33 – 1.25 (m, 2H), 1.17 (t, $J$ = 7.1 Hz, 3H). $^{13}$C NMR (125.8 MHz, acetone-$d_6$) δ 175.3, 64.4, 58.9, 42.2, 33.5, 13.9. $^{19}$F NMR (XXX MHz, acetone-$d_6$) -146.8. $^{11}$B NMR (400 MHz, acetone-$d_6$) δ 5.42. IR (ATR): ν = 1720, 1688, 1308, 1228, 1088, 1016, 999, 964, 533 cm$^{-1}$. HRMS (ESI) m/z calc. for $C_9H_{15}BF_3O_3^-$ (M-) 238.1103, found 238.1095.

**Reductive Alkene Coupling Procedure:**

Based on a slightly modified literature procedure,[13b] to a solution of 4,4,5,5-tetramethyl-2-(prop-1-en-2-yl)-1,3,2-dioxaborolane (5.0 mmol) in 20 mL of EtOH was added anhydrous $Na_2HPO_4$ (2.12 g, 10.0 mmol), $Fe(acac)_3$ (177 mg, 10 mol %), acceptor olefin (15.0 mmol), and $PhSiH_3$ (1.62 g, 15.0 mmol). The resulting mixture was heated in an oil bath preheated to 60 °C with stirring (until GC analysis indicated the consumption of starting material boronate ester, usually 2–4 h). The reaction mixture was then cooled to rt and diluted with brine (20 mL) and EtOAc (20 mL). The organic layer was separated, and the aqueous layer was extracted with EtOAc (3 x 10 mL). The organic layers were combined, washed with brine (20 mL), dried ($Na_2SO_4$), filtered, and concentrated under reduced pressure. The resulting crude product was then purified by silica gel

flash column chromatography. The pinacol boronate obtained after column chromatography was dissolved in MeOH (10–20 mL) and converted to the alkyltrifluoroborate by addition of saturated aq $KHF_2$ (12 mL, 4.5 M, 54 mmol) at 0 °C. The mixture was then warmed to rt and stirred for 3.5 h. The suspension was then evaporated to dryness. The resultant solid was triturated and sonicated with warm acetone and filtered three times. The filtrate was then concentrated to a minimal volume, and the alkyltrifluoroborate was precipitated through dropwise addition of cold $Et_2O$ and/or pentanes (10–30 mL). The mixture was filtered, washed with cold $Et_2O$ (5–10 mL), and then dried on high vacuum overnight to yield the desired alkyltrifluoroborates.

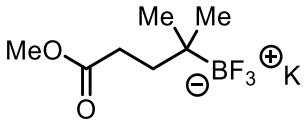


**S2**

**Potassium Trifluoro(5-methoxy-2-methyl-5-oxopentan-2-yl)borate (S2)** prepared using methyl methacrylate as the olefin acceptor and obtained in 44% yield, 522 mg as an off-white solid, mp = 129 – 131 $^0$C. $^1$H NMR (500 MHz, acetone-$d_6$) δ 3.55 (s, 3H), 2.47 – 2.17 (m, 2H), 1.55 – 1.30 (m, 2H), 0.68 (s, 6H). $^{13}$C NMR (126 MHz, acetone-$d_6$) δ 175.6, 137.0, 50.1, 36.0, 30.3, 24.1. $^{11}$B NMR (128.4 MHz, acetone-$d_6$) δ 6.19. $^{19}$F NMR (470.8 MHz, acetone-$d_6$) δ -150.5. IR (ATR): : ν = 1732, 1646, 1236, 1174, 1026, 981, 937, 750, 567 cm$^{-1}$. HRMS (ESI) m/z calc. for $C_7H_{13}BF_3O_2^-$ (M-) 196.0997, found 196.1975.

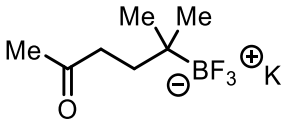


**S3**

**Potassium Trifluoro(2-methyl-5-oxohexan-2-yl)borate (S3)** prepared using methyl vinyl ketone as the olefin acceptor, 45% yield, 497 mg as a colorless, viscous oil. $^1$H NMR (500 MHz, acetone-

*d*$_6$) δ 2.47 – 2.28 (m, 2H), 2.03 (s, 3H), 1.37 – 1.30 (m, 2H), 0.67 (s, 6H) $^{13}$C NMR (125.8 MHz, acetone-*d*$_6$) δ 210.5, 40.1, 34.9, 28.6, 24.2. $^{11}$B NMR (128.4 MHz, acetone-*d*$_6$) δ 6.15 (with residual $BF_4$). $^{19}$F NMR (470.8 MHz, acetone-*d*$_6$) δ -149.0 (with residual $BF_4$). IR (ATR): : ν = 1696, 1471, 1296, 1254, 1016, 749, 480 cm$^{-1}$. HRMS (ESI) m/z calc. for $C_7H_{13}BF_3O^-$ (M-) 181.1012, found 181.1029.

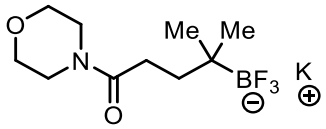


**S4**

**Potassium Trifluoro(2-methyl-5-morpholino-5-oxopentan-2-yl)borate (S4)** prepared using 1-morpholinoprop-2-en-1-one as the olefin acceptor, 53% yield, 764 mg as a white crystalline solid, mp = 164 – 166 $^0$C. $^1$H NMR (500 MHz, $CD_3CN$) δ 3.76–3.63 (m, 4H), 3.57 (s, 4H), 2.49–2.39 (m, 2H), 1.46–1.35 (m, 2H), 0.78 (s, 6H). $^{13}$C NMR (125.8 MHz, $CD_3CN$) δ 174.2, 66.5, 46.0, 41.4, 36.8, 29.8, 24.2. $^{11}$B NMR (128.4 MHz, $CD_3CN$) δ 6.00. $^{19}$F NMR (470.8 MHz, $CD_3CN$) δ -149.7. IR (ATR): ν = 1645, 1482, 1429, 1281, 1114, 1038, 1017, 963, 935, 524 cm$^{-1}$. HRMS (ESI) m/z calc. for $C_{10}H_{18}BF_3NO_2^-$ (M-) 252.1388, found 252.1383.

**Trifluoroborates below were synthesized according to known literature procedures:**

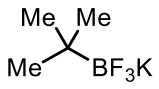


**13**

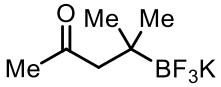


**38**

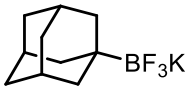


**S5**

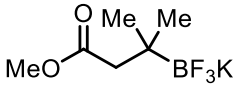


**S6**

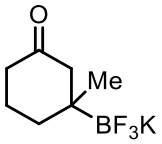


**S7**

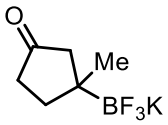


**S8**

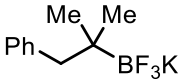


**S9**

Spectral data matched that reported in the literature literature[16,29-31]

**Selected reaction optimization studies:**

High Throughput Experimentation was performed at the Penn/Merck Center for High Throughput Experimentation at the University of Pennsylvania. The screens were analyzed by UPLC with addition of an internal standard. The areas for the internal standard (IS), aryl bromide (ArBr), and product (P) from each of the screens are shown in the tables below. The ratios calculated are pertinent only to that specific screen; the ratios from one screen should not be quantitatively compared to those from a different screen. The results of the screens are illustrated in a heat map. The information conveyed in these heat maps is two-fold. First, the size of the circle corresponds to the amount of product. The larger the circle, the more product formed during the reaction. Secondly, the shade of the circle corresponds to the amount of starting material, in this case aryl bromide, remaining. The lighter the circle, the less aryl bromide remaining after 24 h. Therefore, for a reaction resulting in high conversion and product formation, the circle will be both large and light.

*Procedure for screening at 10 μmol scale:*

To a 96 well plate reactor containing 1 mL reaction vials equipped with a Teflon-coated magnetic stir bar in a glovebox was added sequentially: 1) solution of Ni source (0.1 equiv) dissolved in THF for [$Ni(COD)_2$] or DMA [for all Ni(II) sources], and 2) ligand (0.1 equiv) in DMA. After addition, the plate was sealed and the vials were allowed to stir at 60 $^0$C for 1 h to ensure complexation of ligand to the catalyst. Then, 100 $\mu$L of a stock solution containing potassium *tert*-butyltrifluoroborate (1.5 equiv), aryl bromide (1.0 equiv – 10 $\mu$mol), photocatalyst (0.03 equiv), and internal standard (0.1 equiv) was added to each vial. The vials were sealed and stirred over blue LED lights at rt (~24 $^0$C). After 24 h the reactions were opened to air and diluted with 500 $\mu$L of MeCN. After stirring, the diluted block for fifteen minutes15 min, 25 $\mu$L aliquots were then

taken from the reaction vials and dosed into a 96-well UPLC block. These aliquots were further diluted by the addition of 700 $\mu$L of MeCN. The reaction mixtures were then analyzed by UPLC.

Note: If examining the effect of solid additives, these were added as slurries in THF or DCE (0.1 M) followed by solvent removal by Genovac evaporation before the following steps. If looking at the effect of liquid additives, these were added as stock solutions in DMA (1.0 M) after dosing all other ingredients

| Ni(COD)2 | | | | | | NiBr2dme | | | | | |
|---|---|---|---|---|---|---|---|---|---|---|---|
| L1 | L2 | L3 | L4 | L5 | L6 | L1 | L2 | L3 | L4 | L5 | L6 |
| L7 | L8 | L9 | L10 | L11 | L12 | L7 | L8 | L9 | L10 | L11 | L12 |
| L13 | L14 | L15 | L16 | L17 | L18 | L13 | L14 | L15 | L16 | L17 | L18 |
| L19 | L20 | L21 | L22 | L23 | L24 | L19 | L20 | L21 | L22 | L23 | L24 |
| L25 | L26 | L27 | L28 | L29 | L30 | L25 | L26 | L27 | L28 | L29 | L30 |
| L31 | L32 | L33 | L34 | L35 | L36 | L31 | L32 | L33 | L34 | L35 | L36 |
| L37 | L38 | L39 | L40 | L41 | L42 | L37 | L38 | L39 | L40 | L41 | L42 |
| L43 | L44 | L45 | L46 | L47 | L48 | L43 | L44 | L45 | L46 | L47 | L48 |

Conditions: 3 mol % Ir cat **1**, 10 mol % Ni, 10 mol % ligand, no base, 0.05 M DMA

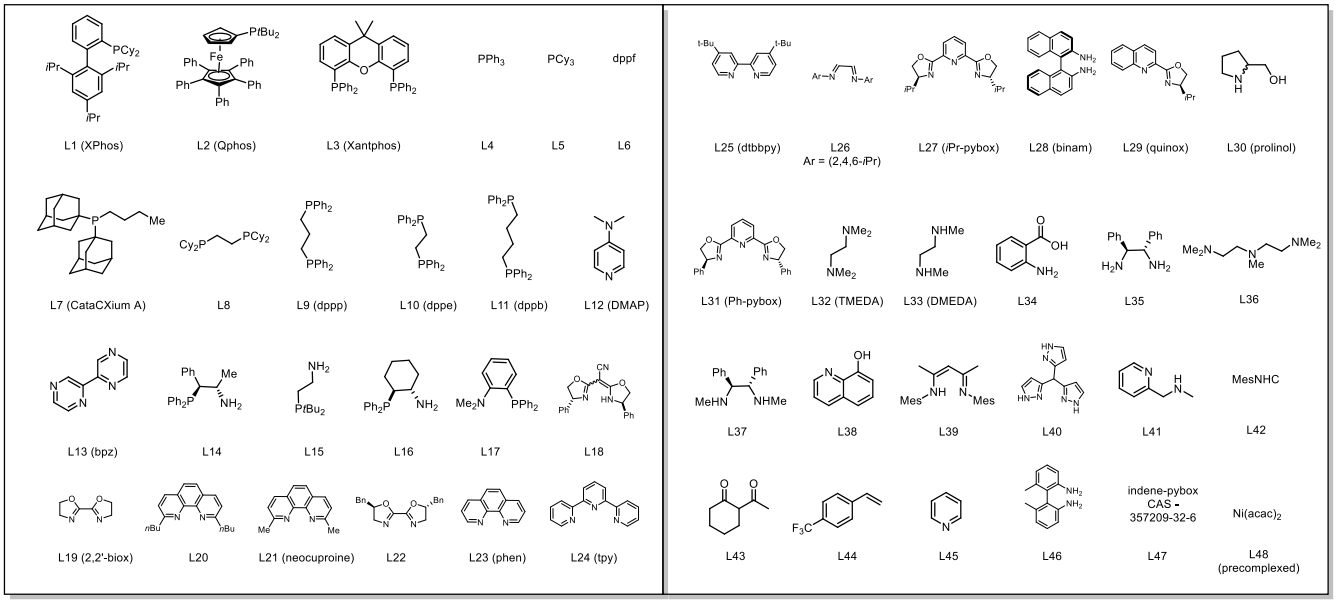


**Figure 6.6.** Broad Ligand Screening for Baseline Conversion

**Optimizing Precomplexed Diketonate Ligand Scaffold**

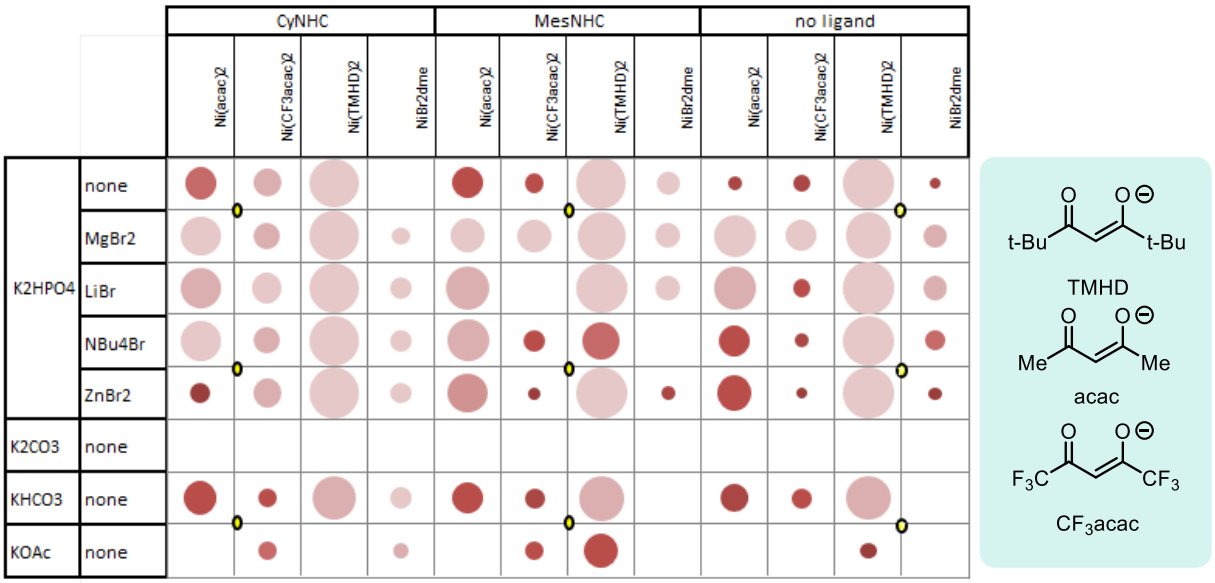


Conditions: 3 mol % Ir cat. **1**, 10 mol % Ni, 10 mol % ligand, 20 mol % additive, 1 equiv base, 0.05 M DMA

**Figure 6.7**. Effects of ligand structure, additives**, NHC additives, and bases on overall yield**

*Procedure for screening at 0.1 mmol scale:*

To a 1 dram vial containing a Teflon coated magnetic stir bar was added a stock solution of potassium *tert*-butyltrifluoroborate (2.0 equiv), aryl halide (1 equiv), photocatalyst **1** (3 mol %), and internal standard 4,4'-di-*tert*-butylbiphenyl (10 mol %) in THF. The solvent was then removed under high vacuum. To the reaction mixture was then added any additional base (1.0 equiv). The vial was then brought into a nitrogen filled glovebox and $Ni(TMHD)_2$ (10 mol %) was dosed in the reaction solvent of choice. The reactions were then monitored by GC analysis after stirring for 24 h with the product/IS ratios given below

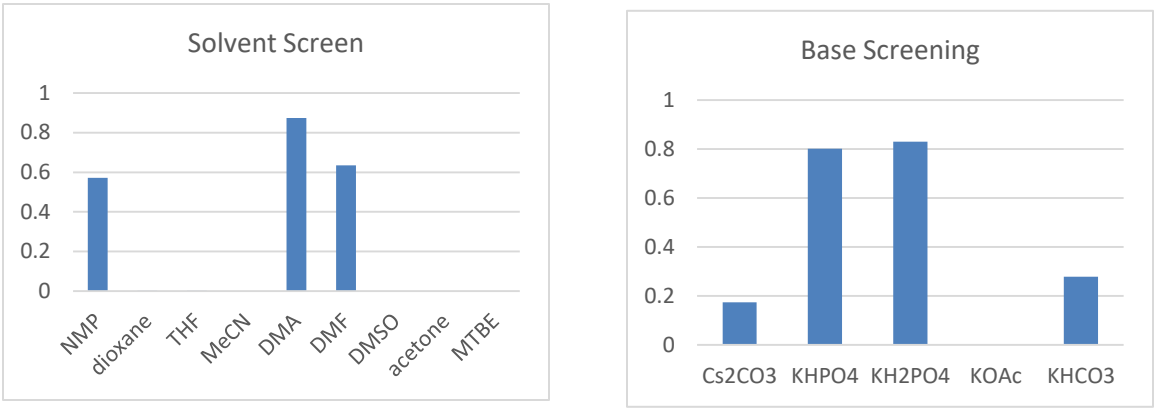


**Figure 6.8:** Benchtop Screening of Solvents and Bases

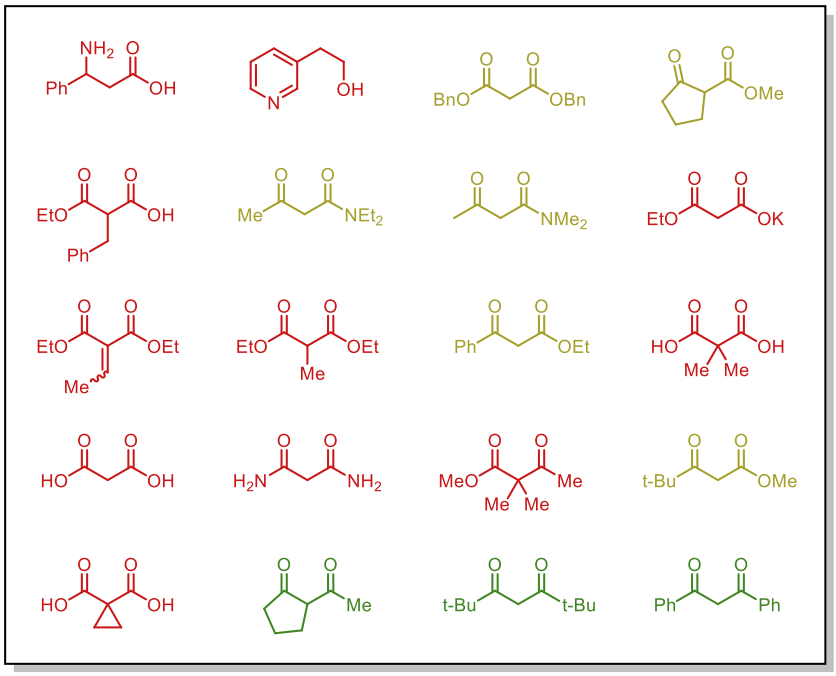

**Figure 6.9.** Similar Structures Examined as Ligands with Relative Conversion
(Red: <5%, Yellow: 5–50 %, Green: >50%)

**Procedure for nickel complexation with above ligands:**

Based on an adapted literature procedure,[6] 2.0 equiv of ligand (0.2 mmol) were dosed into a vial $Ni(OAc)_2$ x $4H_2O$ (1.8 mg, 0.1 mmol) . To the vial was added 0.5 mL of MeOH. The vial was then

capped and stirred at 50 ºC overnight to induce complexation of the ligand to the nickel center. The solvent was then removed under high vacuum to afford green to purple solids or semi-solids. The residual solid material was then dissolved in DMA and dosed as a 0.1 M stock solution.

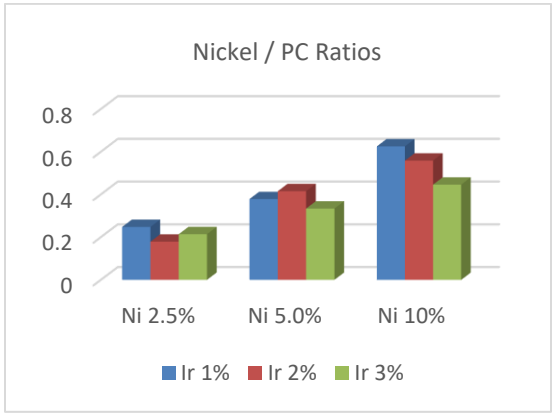


**Figure 6.10.** Nickel to Photocatalyst Ratio Array
(P/IS ratios under standard conditions after 24 h)

| | protodehalo / IS | SM / IS | prod / IS |
|---|---|---|---|
| CzIPN (3 mol %) | 2.073079791 | 0 | 1.354213274 |
| No PC | 0.623495552 | 2.10151753 | 0.107796965 |
| No base | 1.880733945 | 0.642201835 | 1.384301733 |
| No Ni | 0.623641304 | 3.65625 | 0 |
| No light | 0.011927181 | 3.925925926 | 0.026365348 |
| Ni(COD)2 / ligand | 0.450913242 | 1.146118721 | 2.171803653 |
| Std. cond | 0.298283262 | 0 | 3.617310443 |
| No Zn | 0.448275862 | 0 | 3.065922921 |
| NiI2 / ligand | 0.108389467 | 3.259644825 | 0.309246785 |
| pyridine (20 mol %) | 1.993569132 | 0.437299035 | 0.080385852 |

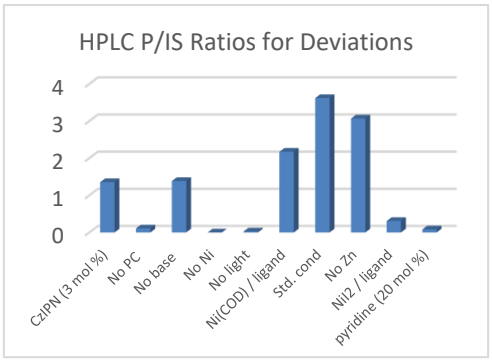


**Figure 6.11. Deviation from Standard Conditions (HPLC ratios after 48 h)**

**General procedure A for adamantyltrifluoroborates photoredox cross-coupling reactions:**

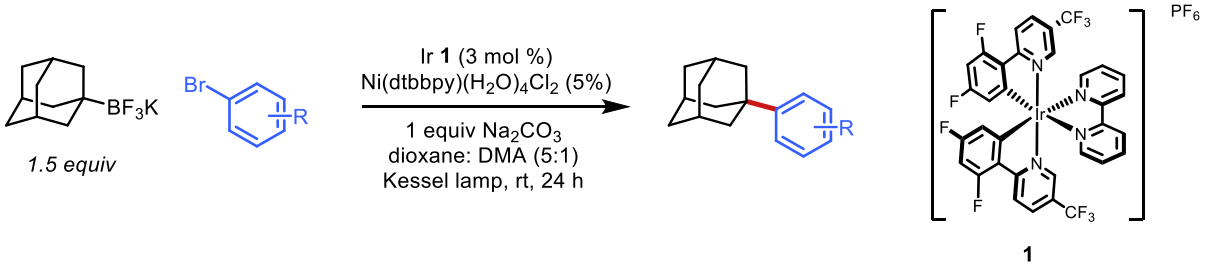


To a 4 dram borosilicate glass vial equipped with a Teflon-coated magnetic stir bar was added adamantyltrifluoroborate **S5** (181 mg, 0.75 mmol, 1.5 equiv), Ir[dFCF$_3$ppy]$_2$(bpy)PF$_6$ **1** (15.0 mg, 0.03 equiv), Ni(dtbbpy)(H$_2$O)$_4$Cl$_2$ (7.0 mg, 0.05 equiv), Na$_2$CO$_3$ (1.0 mmol, 2 equiv) and aryl bromide (0.5 mmol, 1 equiv) (liquid aryl bromides were added with solvent). The vial was then purged and evacuated 3x under argon atmosphere. To the vial was then added dioxane/DMA in a (6 mL in 5:1 mixture). The entire mixture was then sparged for 10 min with argon and then placed on a stir plate 4 cm away from 4 Kessil H150 blue flood lamps for 24 h. Two fans were placed above the reaction setup (shown below) to maintain an ambient temperature of 28–30 $^{o}$C. After completion, the reaction mixture was diluted with an equal volume of H$_2$O and extracted with EtOAc (3 x 5 mL). The organic layer was then dried (Na$_2$SO$_4$), filtered, concentrated onto silica, and then purified by silica gel chromatography, eluting with EtOAc and hexanes to obtain the products in pure form.

**General procedure B for tertiary photoredox cross-coupling reactions**

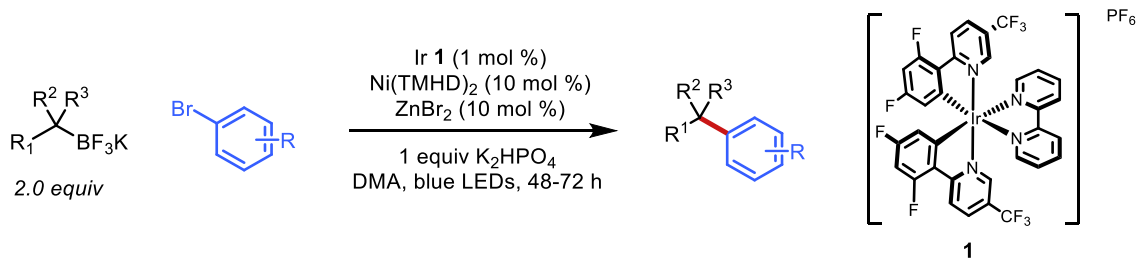

To a 4 dram borosilicate glass vial equipped with a Teflon-coated magnetic stir bar was added tertiary alkyltrifluoroborate (1.0 mmol, 2 equiv), $Ir[dFCF_3ppy]_2(bpy)PF_6$ **1** (5.0 mg, 0.01 equiv), and aryl bromide (0.5 mmol, 1 equiv) (liquid aryl bromides were added with solvent). The vial was then transferred into a glove box where $Ni(TMHD)_2$ (21.2 mg, 0.05 mmol), $ZnBr_2$ (11.3 mg, 0.05 mmol), and anhydrous $K_2HPO_4$ (87 mg, 0.5 mmol) were added. The vial was then capped and removed from the glovebox. Anhydrous DMA (5 mL) was added to the vial via syringe under inert atmosphere. The vial was then sparged with argon for 10 min. The vial containing all the reagents was further sealed with parafilm and Teflon tape and stirred for 48–72 h approximately 4 cm away from a ring of blue LED lights strips (see below). A fan was blown across the reaction setup to maintain an ambient temperature around 27 °C. After completion, the crude reaction mixture was diluted with $H_2O$ (10 mL) and extracted with $Et_2O$ (2 X 10 mL) EtOAc (5 mL). The organic layer was then washed with saturated aq NaCl (5 mL) and dried ($Na_2SO_4$). The resulting organics were then concentrated, and the residue was purified by column chromatography on silica gel, eluting with EtOAc and hexanes, to obtain products in pure form.

**General procedure C for tertiary photoredox cross-couplings**

Setup for these reactions remains the same as procedure B, however, the reactions are instead irradiated with 4 Kessil H150 blue flood lamps at 30 °C for 24 h. The greater light intensity in these systems significantly accelerates reaction progress and mirrors acceleration seen in other systems.[33]

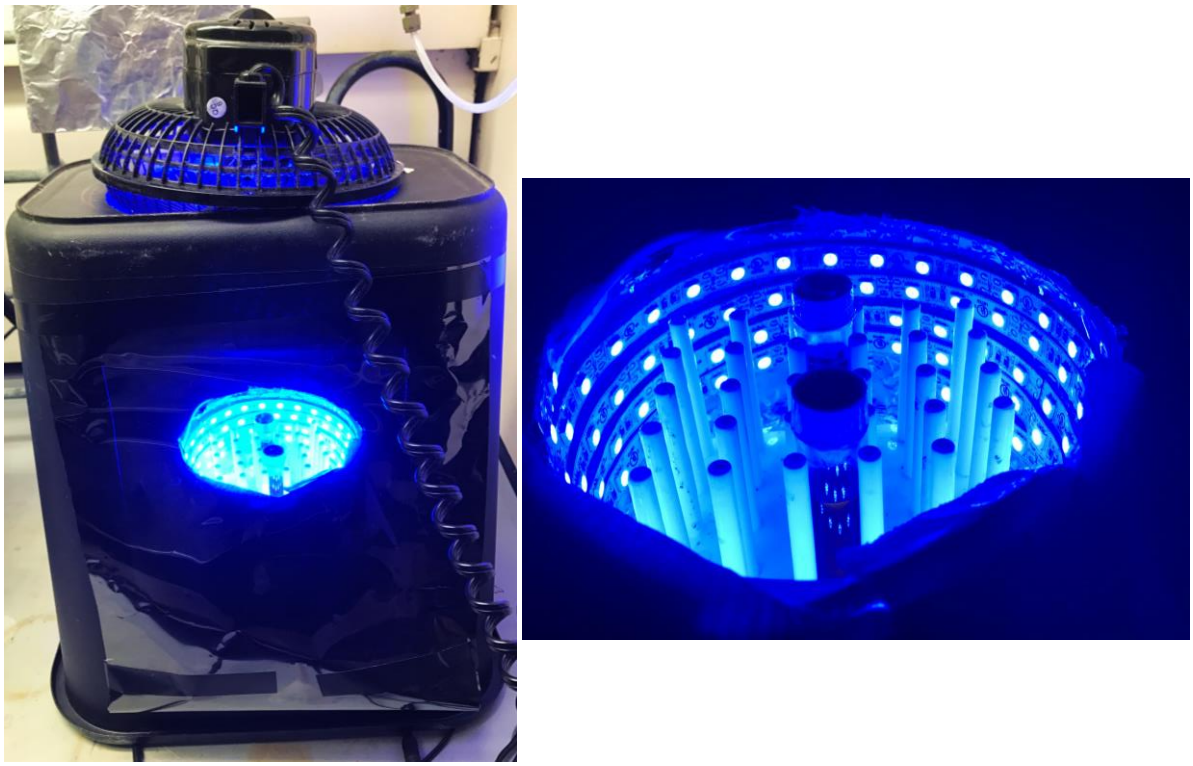

**Figure 6.12.** Procedure B photoredox cross-coupling reaction set-up (0.50 mmol scale)

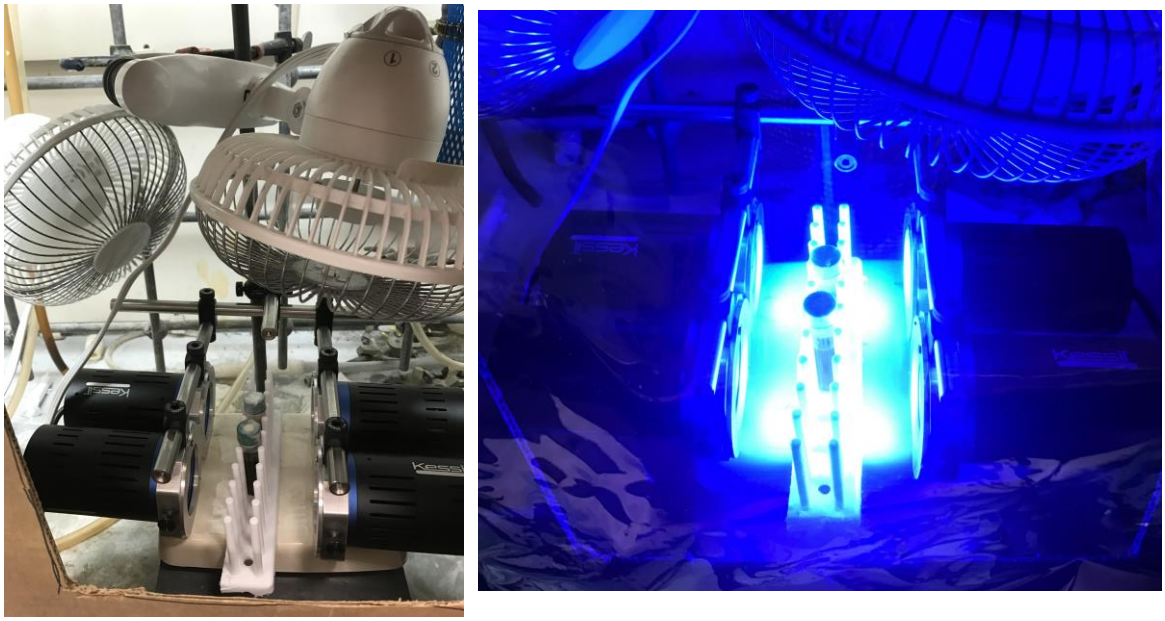

**Figure 6.13.** Procedure A and C Kessil lamp setup for shortened reaction times (0.25 – 0.50 mmol scale)

**Cyclic Voltammetry (CV) Data**

Electrochemical measurements were recorded on a CH Instruments: Model 600E Series Electrochemical Analyzer (observed in 0.002 M MeCN; $[N(Bu)_4](PF_6)$ = 0.1 M; Ag/AgCl = electrode; reported in SCE based on a ferrocene internal standard).

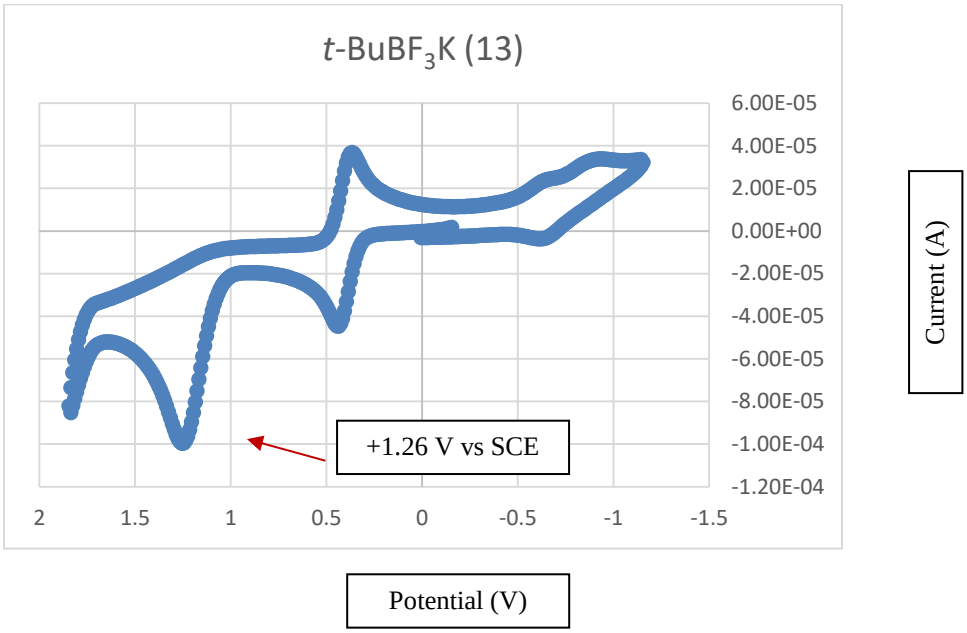


**Figure 6.14.** Oxidation Potential of Tertiary Alkyltrifluoroborate 13

**Alkyltrifluoroborate Oxidation Experiment**

Based on a literature procedure reported by Akita,[5] a one dram vial equipped with a Teflon coated magnetic stir bar was charged with alkyltrifluoroborate **13** (82 mg, 0.50 mmol) and $Ir[dFCF_3ppy]_2(bpy)PF_6$ **1** (10 mg, 0.01 mmol), then acetone (5.0 mL), MeOH (0.5 mL) and methyl vinyl ketone (140 mg, 2.0 mmol) were added under inert atmosphere. The vessel was degassed by Ar sparging for 10 min. The vial was then exposed to the blue LED setup in procedure B (vide supra) at rt for 24 h. The resulting mixture was extracted with $CH_2Cl_2$, and the combined organic

layers were dried ($Na_2SO_4$) and filtered. The filtrate was concentrated under vacuum, and the residue was purified by flash column chromatography on silica gel to afford **14** as a colorless oil (47 mg, 73%). $^1$H NMR (500 MHz, $CDCl_3$) δ 2.44-2.40 (m, 2H), 2.18 (s, 3H), 1.52-1.48 (m, 2H), 0.91 (s, 9H). $^{13}$C NMR (125.8 MHz, $CDCl_3$): δ 209.2, 39.1, 37.0, 29.5, 29.1, 28.8. Spectroscopic data matches that previously reported.[34]

**Compound Characterization Data**

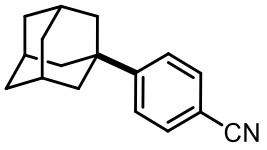


**19**

**4-(Adamantan-1-yl)benzonitrile (19):** obtained as a white amorphous solid using procedure A at 0.50 mmol scale (76 mg, 64%), mp = 125–128 $^0$C. $^1$H NMR (500 MHz, $CDCl_3$) δ 7.60 (d, *J* = 8.2 Hz, 2H), 7.45 (d, *J* = 8.3 Hz, 2H), 2.12 (s, 3H), 1.90 (s, 6H), 1.83 – 1.72 (m, 6H). $^{13}$C NMR (126 MHz, $CDCl_3$) δ 156.8, 132.2, 126.0, 119.4, 109.4, 42.9, 37.0, 36.7, 28.8. IR (ATR): ν = 2916, 2898, 2847, 2233, 1506, 1343, 1101, 849, 806, 563 cm$^{-1}$. HRMS (EI) m/z calc. for $C_{17}H_{19}N$ (M+) 237.1517, found 237.1501.

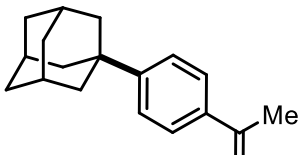


**20**

**1-(4-((3r,5r,7r)-Adamantan-1-yl)phenyl)ethan-1-one (20):** obtained as a white solid using procedure A at 0.50 mmol scale (97 mg, 76%), mp = 108–110 $^0$C. $^1$H NMR (500 MHz, $CDCl_3$) δ 7.92 (d, *J* = 8.4 Hz, 2H), 7.45 (d, *J* = 8.4 Hz, 2H), 2.59 (s, 3H), 2.12 (s, 3H), 1.92 (s, 6H), 1.83 – 1.72 (m, 6H). $^{13}$C NMR (126 MHz, $CDCl_3$) δ 198.1, 157.1, 134.8, 128.5, 125.3, 43.0, 36.8, 36.8,

28.9, 26.7. IR (ATR): ν = 2907, 2848, 1678, 1602, 1359, 1267, 1245, 832, 804, 596 $cm^{-1}$. HRMS (EI) m/z calc. for $C_{18}H_{22}O$ (M+) 254.1671, found 254.1675.

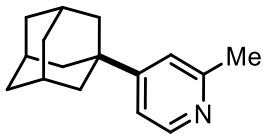


**21**

**4-((3r,5r,7r)-Adamantan-1-yl)-2-methylpyridine (21):** obtained as a pale yellow semi-solid using procedure A at 0.25 mmol scale (29 mg, 51%). $^{1}H$ NMR (500 MHz, $CDCl_3$) δ 8.40 (d, *J* = 5.4 Hz, 1H), 7.11 (s, 1H), 7.06 (d, *J* = 5.4 Hz, 1H), 2.55 (s, 3H), 2.11 (s, 3H), 1.89 (s, 6H), 1.83 – 1.75 (m, 6H). $^{13}C$ NMR (125.8 MHz, $CDCl_3$) δ 160.1, 158.0, 148.9, 119.7, 117.4, 42.3, 36.5, 36.0, 28.6, 24.5. IR (ATR): ν = 2901, 2848, 1602, 1550, 1449, 1397, 1296, 1038, 976, 837, 806 $cm^{-1}$. HRMS (EI) m/z calc. for $C_{16}H_{21}N$ (M+) 227.1674, found 227.1665.

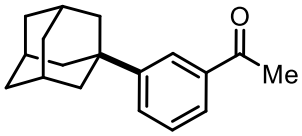


**22**

**1-(3-((3r,5r,7r)-Adamantan-1-yl)phenyl)ethan-1-one (22):** obtained as a colorless semi-solid with procedure A at 0.25 mmol scale (43 mg, 68%). $^{1}H$ NMR (500 MHz, $CDCl_3$) δ 7.98 (s, 1H), 7.77 (d, *J* = 7.6 Hz, 1H), 7.58 (d, *J* = 7.8 Hz, 1H), 7.41 (dd, *J* = 7.6, 7.8 Hz, 1H), 2.61 (s, 3H), 2.12 (s, 3H), 1.94 (s, 6H), 1.82 – 1.75 (m, 6H).$^{13}C$ NMR (125.8 MHz, $CDCl_3$) δ 193.8, 152.0, 137.2, 130.1, 128.5, 126.0, 124.8, 43.2, 36.8, 36.5, 29.0, 26.9. IR (ATR): ν = 2900, 1847, 1682, 1426, 1355, 1270, 963, 789, 695, 588 $cm^{-1}$. HRMS (EI) m/z calc. for $C_{18}H_{23}O$ (M+H) 255.1743, found 255.1748.

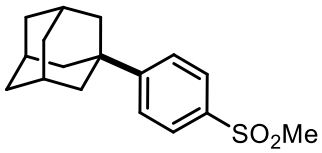


**23**

**1-(4-(Methylsulfonyl)phenyl)adamantane (23):** obtained as a white amorphous solid with procedure A at 0.25 mmol scale (66 mg, 91%), mp = 167–170 $^{0}$C. $^{1}$H NMR (500 MHz, $CDCl_3$) δ 7.87 (d, *J* = 8.6 Hz, 2H), 7.55 (d, *J* = 8.6 Hz, 2H), 3.04 (s, 3H), 2.13 (s, 3H), 1.92 (s, 6H), 1.83 – 1.72 (m, 6H). $^{13}$C NMR (126 MHz, $CDCl_3$) δ 157.8, 137.7, 127.4, 126.2, 44.7, 43.0, 37.0, 36.7, 28.8. IR (ATR): ν = 2902, 2848, 1596, 1449, 1308, 1291, 1148, 1090, 954, 777, 558, 473 cm$^{-1}$ HRMS (EI) m/z calc. for $C_{17}H_{22}O_2S$ (M+) 290.1341, found 290.1341.

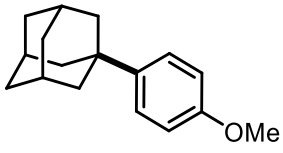


**24**

**(3r,5r,7r)-1-(4-Methoxyphenyl)adamantane (24)** obtained as a pale yellow oil using procedure A at 0.25 mmol scale (12 mg, 20%). $^{1}$H NMR (500 MHz, DMSO-*d*$_6$) δ 7.24 (d, *J* = 8.8 Hz, 2H), 6.83 (d, *J* = 8.8 Hz, 2H), 3.69 (s, 3H), 2.01 (s, 3H), 1.80 (s, 6H), 1.70 (s, 6H). $^{13}$C NMR (125.8 MHz, DMSO-*d*$_6$) δ 157.4, 143.4, 125.9, 113.8, 55.3, 43.2, 36.6, 35.4, 28.7. HRMS (EI) m/z calc. for $C_{17}H_{16}O$ (M+) 242.1671, found 242.1677. Spectroscopic data matches with previously reported data.[35]

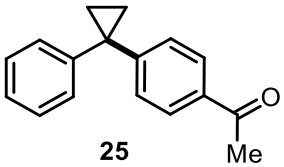


**25**

**1-(4-(1-Phenylcyclopropyl)phenyl)ethan-1-one (25):** obtained as a colorless oil with procedure A at 0.25 mmol scale (55 mg, 93% yield). $^{1}$H NMR (500 MHz, $CDCl_3$) δ 7.86 (d, *J* = 8.4 Hz, 2H), 7.34 – 7.19 (m, 7H), 2.57 (s, 3H), 1.43 – 1.32 (m, 4H). $^{13}$C NMR (125.8 MHz, $CDCl_3$) δ 197.9,

151.9, 144.6, 135.0, 129.1, 128.6, 128.6, 128.0, 126.6, 30.2, 26.7, 17.2. IR (ATR): ν = 3143, 2950, 1678, 1603, 1404, 1265, 957, 821, 760, 699, 598 $cm^{-1}$. HRMS (EI) m/z calc. for $C_{17}H_{16}O$ (M+) 236.1201, found 236.1206.

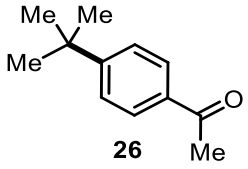


**26**

**1-(4-(*tert*-Butyl)phenyl)ethan-1-one** (**26)**: obtained as a colorless oil with procedure B (80 mg, 90%). $^1$H NMR ($CDCl_3$, 500 MHz): δ 7.90 (d, *J* = 8.0 Hz, 2H), 7.47 (d, *J* = 8.0 Hz, 2H), 2.58 (s, 3H), 1.36 (s, 9H). $^{13}$C NMR ($CDCl_3$, 125.8 MHz): δ 198.0, 157.0, 134.8, 128.4, 125.7, 35.2, 31.2. Spectroscopic data matches with previously reported data.[25]

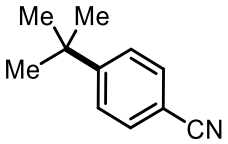


**27**

**4-(*tert*-Butyl)benzonitrile (27):** obtained as a colorless oil with procedure B (71 mg, 89%); with C (66 mg, 83%). $^1$H NMR (500 MHz, $CDCl_3$) δ 7.59 (d, *J* = 8.3 Hz, 2H), 7.49 (d, *J* = 8.3 Hz, 2H), 1.34 (s, 9H). $^{13}$C NMR (125.8 MHz, $CDCl_3$) δ 156.6, 131.9, 126.1, 119.0, 109.2, 35.2, 30.8. HRMS (ESI) m/z calc. for $C_{11}H_{14}N$ (M+H) 160.1126, found 160.1123. Spectroscopic data matches with previously reported data.[25]

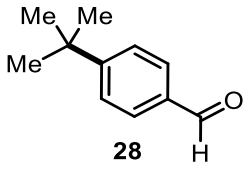


**28**

**4-(*tert*-Butyl)benzaldehyde (28):** obtained as a crystalline solid with procedure B (74 mg, 91%) (with <5% protodehalogenation). $^1$H NMR ($CDCl_3$, 500 MHz): δ 9.98 (s, 1H), 7.83 – 7.80 (m, 2H), 7.56 – 7.54 (m, 2H), 1.36 (s, 9H). $^{13}$C NMR ($CDCl_3$, 125.8 MHz): δ 192.2, 158.6, 134.2, 129.8, 126.1, 125.6, 35.5, 31.2.

HRMS (ESI) m/z calc. for $C_{11}H_{15}O$ (M+H) 163.1123, found 163.1129. Spectroscopic data matches with previously reported data.[25]

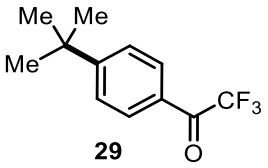


**29**

**1-(4-(*tert*-Butyl)phenyl)-2,2,2-trifluoroethan-1-one** (**29)**: obtained as a colorless oil with procedure B (109 mg, 96%). $^{1}$H NMR ($CDCl_3$, 500 MHz): δ 8.02 (d, *J* = 8.0 Hz, 2H), 7.57 – 7.55 (m, 2H), 1.37 (s, 9H). $^{13}$C NMR (125.8 MHz, $CDCl_3$) δ 180.2 (q, *J* = 34.7 Hz), 160.0, 130.3 (q, *J* = 2.5 Hz), 127.5, 126.3, 116.9 (q, *J* = 291.4 Hz), 35.58, 31.02. $^{19}$F NMR ($CDCl_3$, 282.4 MHz): δ -71.3. HRMS (ESI) m/z calc. for $C_{12}H_{16}O$ (M+) 230.0918, found 230.0904. Spectroscopic data matches with previously reported data.[36]

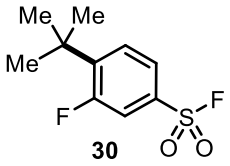


**30**

**4-(*tert*-Butyl)-3-fluorobenzenesulfonyl fluoride** (**30)**: obtained as a colorless oil with procedure B (69 mg, 59%). $^{1}$H NMR ($CDCl_3$, 500 MHz): δ 7.87 (m, 1H), 7.37 (d, *J* = 7.5 Hz, 1H), 7.33 (dd, *J* = 11.5, 1.5 Hz, 1H), 1.36 (s, 9H). $^{13}$C NMR ($CDCl_3$, 125.8 MHz): δ 182.0, 163.8 (d, *J* = 7.5 Hz), 160.7, 130.6, 122.1 (d, *J* = 3.3 Hz), 115.0 (d, *J* = 20.6 Hz), 36.0, 30.9. $^{19}$F NMR ($CDCl_3$, 470.8 MHz): δ 106.8(1), 106.8(3). IR (ATR): ν = 2970, 1607, 1571, 1420, 1215, 1203, 781, 644, 535 cm$^{-1}$.HRMS (EI) m/z calc. for $C_{10}H_{12}F_2O_2S$ (M+) 234.0526, found 234.0534.

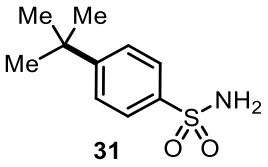


**31**

**1-(*tert*-Butyl)-4-(methylsulfonyl)benzene** (**32)**: obtained as a colorless oil with procedure B (88 mg, 83%),.

$^{1}$H NMR ($CDCl_3$, 500 MHz): δ 7.85 – 7.83 (m, 2H), 7.56 – 7.54 (m, 2H), 3.02 (s, 3H), 1.33 (s, 9H). $^{13}$C NMR ($CDCl_3$, 125.8 MHz): δ 157.7, 137.8, 127.3, 126.5, 44.7, 35.4, 31.2. HRMS (ESI) m/z calc. for $C_{11}H_{16}O_2S$ (M+) 212.0871, found 212.0863. Spectroscopic data matches with previously reported data.[25]

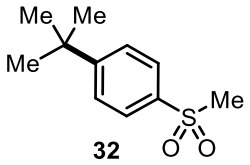

**32**

**1-(*tert*-Butyl)-4-(methylsulfonyl)benzene** (**32)**: obtained as a colorless oil with procedure B (88 mg, 83%), $^{1}$H NMR ($CDCl_3$, 500 MHz): δ 7.85 – 7.83 (m, 2H), 7.56 – 7.54 (m, 2H), 3.02 (s, 3H), 1.33 (s, 9H). $^{13}$C NMR ($CDCl_3$, 125.8 MHz): δ 157.7, 137.8, 127.3, 126.5, 44.7, 35.4, 31.2. HRMS (ESI) m/z calc. for $C_{11}H_{16}O_2S$ (M+) 212.0871, found 212.0863. Spectroscopic data matches with previously reported data.[10]

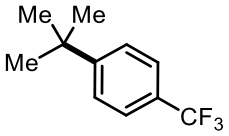

**33**

**1-(*tert*-Butyl)-4-(trifluoromethyl)benzene (33)** obtained as a pale yellow oil with procedure B (96 mg, 95%). $^{1}$H NMR (500 MHz, $CDCl_3$) δ 7.56 (d, *J* = 8.2 Hz, 2H), 7.50 (d, *J* = 8.2 Hz, 2H), 1.35 (s, 9H). $^{13}$C NMR ($CDCl_3$, 125.8 MHz): δ 155.3, 127.9 (q, *J* = 31.4 Hz), 125.8, 125.1 (q, *J* = 3.8 Hz), 124.5 (q, *J* = 271.8 Hz), 35.1, 31.3 (residual ligand peaks, less than 5% at 27.5, 90.9, 201.6). $^{19}$F NMR ($CDCl_3$, 282.4 MHz): δ 62.3. HRMS (ESI) m/z calc. for $C_{11}H_{13}F_3$ (M+) 202.0969, found 202.0958. Spectroscopic data matches with previously reported data.[38]

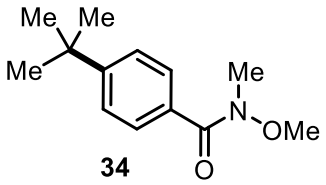

**34**

**4-(*tert*-Butyl)-N-methoxy-N-methylbenzamide** (**34**) obtained as yellow oil with procedure B (43 mg, 39%).

$^{1}$H NMR (500 MHz, $CDCl_3$) δ 7.64 (d, *J* = 8.5 Hz, 2H), 7.42 (d, *J* = 8.5 Hz, 2H), 3.59 (s, 3H), 3.36 (s, 3H), 1.34 (s, 9H). $^{13}$C NMR (126 MHz, $CDCl_3$) δ 169.9, 153.9, 131.0, 128.0, 124.9, 60.9 34.8, 33.9, 31.0. HRMS (ESI) m/z calc. for $C_{13}H_{20}NO_2$ (M+H) 222.1494, found 222.1492. Spectroscopic data matches with previously reported data.[38]

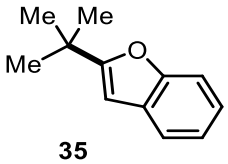


**35**

**2-(*tert*-Butyl)benzofuran (35):** obtained as a colorless oil with procedure C (46 mg, 53%).$^{1}$H NMR (500 MHz, $CDCl_3$) δ 7.50 (d, *J* = 7.4 Hz, 1H), 7.43 (d, *J* = 7.9 Hz, 1H), 7.25 – 7.14 (m, 2H), 6.37 (s, 1H), 1.40 (s, 9H). $^{13}$C NMR (126 MHz, $CDCl_3$) δ 167.1, 154.5, 128.8, 123.0, 122.2, 120.2, 110.7, 98.8, 32.9, 28.8. Spectroscopic data matches with previously reported data.[39]

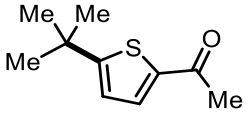


**36**

**1-(5-(*tert*-Butyl)thiophen-2-yl)ethan-1-one (36):** obtained as a yellow oil with procedure B (60 mg, 66%). $^{1}$H NMR (500 MHz, $CDCl_3$) δ 7.54 (d, *J* = 3.9 Hz, 1H), 6.88 (d, *J* = 3.9 Hz, 1H), 2.52 (s, 3H), 1.41 (s, 9H). $^{13}$C NMR (126 MHz, $CDCl_3$) δ 190.6, 167.2, 141.2, 132.5, 122.8, 35.1, 32.1, 26.4. HRMS (ESI) m/z calc. for $C_{10}H_{15}OS$ (M+H) 183.0844, found 183.0821. Spectroscopic data matches with previously reported data.[40]

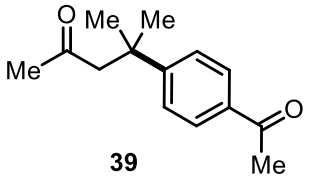


**39**

**4-(4-Acetylphenyl)-4-methylpentan-2-one** (**39)**: obtained as a colorless oil with procedure B (73 mg, 67%).$^{1}$H NMR ($CDCl_3$, 500 MHz): δ 7.93 – 7.91 (m, 2H), 7.47 – 7.44 (m, 2H), 2.82 (s, 2H), 2.59 (s, 3H), 1.89 (s, 3H), 1.45 (s, 6H). $^{13}$C NMR ($CDCl_3$, 125.8 MHz): δ 206.9, 197.6, 153.9, 134.9, 128.3, 125.7, 56.2, 37.4, 31.6, 28.8, 26.4. IR (ATR): ν = 2964, 1715, 1678, 1605, 1406,

1356, 1269, 1014, 958, 596 $cm^{-1}$. HRMS (ESI) m/z calc. for $C_{14}H_{18}O_2Na$ (M+Na) 241.1204, found 241.1210.

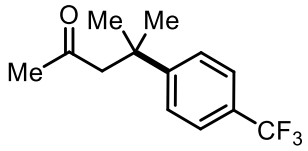


**40**

**4-Methyl-4-(4-(trifluoromethyl)phenyl)pentan-2-one** (**40)**: obtained as a clear oil, procedure B (89 mg, 73%). $^1H$ NMR ($CDCl_3$, 500 MHz): δ 7.57 (d, *J* = 7.5 Hz, 2H), 7.47 (d, *J* = 7.5 Hz, 2H), 2.81 (s, 2H), 1.91 (s, 3H), 1.45 (s, 6H). $^{13}C$ NMR ($CDCl_3$, 125.8 MHz): δ 206.8, 152.4 128.2, 125.8, 125.1 (q, *J* =3.8 Hz), 124.1 (q, *J* = 275.5 Hz) 56.1, 37.2, 31.6, 28.3. $^{19}F$ NMR ($CDCl_3$, 470.8 MHz): δ -62.4. IR (ATR): ν = 2967, 1718, 1618, 1409, 1325, 1112, 1104, 1068, 1014, 838, 530 $cm^{-1}$. HRMS (ESI) m/z calc. for $C_{13}H_{15}OF_3$ (M+) 244.1075, found 244.1072.

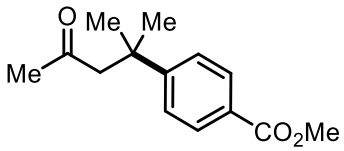


**41**

**Methyl 4-(2-Methyl-4-oxopentan-2-yl)benzoate** (**41)**: obtained as a colorless oil with procedure B (93 mg, 82%). $^1H$ NMR ($CDCl_3$, 500 MHz): δ 7.98 – 7.95 (m, 2H), 7.43 – 7.40 (m, 2H), 3.88 (s, 3H), 2.78 (s, 2H), 1.84 (s, 3H), 1.42 (s, 6H). $^{13}C$ NMR ($CDCl_3$, 125.8 MHz): δ 207.3, 167.1, 153.9, 129.7, 128.0, 125.7, 56.6, 52.1, 37.6, 31.8, 29.0. HRMS (ESI) m/z calc. for $C_{14}H_{19}O_3$ (M+H) 235.1334, found 235.1340. Spectroscopic data matches with previously reported data.[25]

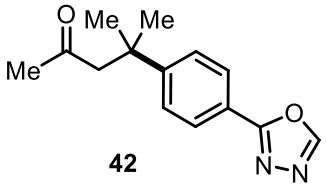


**42**

**4-(4-(1,3,4-Oxadiazol-2-yl)phenyl)-4-methylpentan-2-one** (**42)**: obtained as a yellow oil with procedure B (73 mg, 60%). $^1H$ NMR ($CDCl_3$, 500 MHz): δ 8.45 (s, 1H), 8.02 (d, *J* = 7.5 Hz, 2H),

7.51 (d, *J* = 7.5 Hz, 2H), 2.82 (s, 2H), 1.90 (s, 3H), 1.46 (s, 6H). $^{13}$C NMR ($CDCl_3$, 125.8 MHz): δ 207.1, 164.8, 153.0, 152.6, 127.2, 126.5, 121.3, 56.5, 37.6, 31.8, 29.0. IR (ATR): ν = 3250, 2965, 1714, 1616, 1494, 1380, 1097, 954, 713, 640 cm$^{-1}$. HRMS (ESI) m/z calc. for $C_{14}H_{17}N_2O_2$ (M+H) 245.1290, found 245.1282.

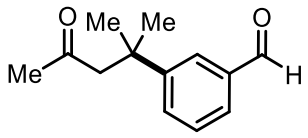


**43**

**3-(2-Methyl-4-oxopentan-2-yl)benzaldehyde** (**43)**: obtained as a colorless oil with procedure C (62 mg, 61%). $^1$H NMR ($CDCl_3$, 500 MHz): δ 10.02 (s, 1H), 7.88 (s, 1H), 7.72 – 7.70 (m, 1H), 7.66 – 7.63 (m, 1H), 7.51 – 7.48 (m, 1H), 2.82 (s, 2H), 1.90 (s, 3H), 1.46 (s, 6H). $^{13}$C NMR ($CDCl_3$, 125.8 MHz): δ 207.1, 192.7, 149.8, 136.6, 132.0, 129.1, 128.1, 126.5, 56.4, 37.4, 31.9, 29.1. IR (ATR): ν = 2964, 1694, 1603, 1361, 1261, 1177, 1083, 801, 697 cm$^{-1}$. HRMS (ESI) m/z calc. for $C_{13}H_{16}O_2$ (M+) 204.1150, found 204.1149.

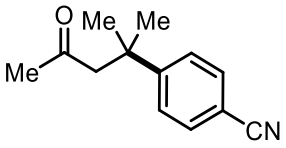


**44**

**4-(2-Methyl-4-oxopentan-2-yl)benzonitrile** (**44)**: obtained as a colorless oil with procedure C (73 mg, 73%). $^1$H NMR ($CDCl_3$, 500 MHz): δ 7.59 (d, *J* = 7.0 Hz, 2H), 7.45 (d, *J* = 7.0 Hz, 2H), 2.81 (s, 2H), 1.93 (s, 3H), 1.42 (s, 6H). $^{13}$C NMR ($CDCl_3$, 125.8 MHz): δ 206.6, 154.2, 132.2, 126.5, 119.1, 109.9, 56.1, 37.6, 31.7, 29.0. HRMS (ESI) m/z calc. for $C_{13}H_{16}NO$ (M+H) 202.1232, found 202.1240. Spectroscopic data matches with previously reported data.[41]

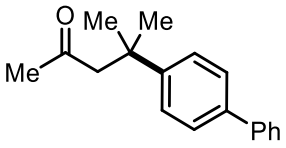


**45**

**4-([1,1'-Biphenyl]-4-yl)-4-methylpentan-2-one** (**45)**: obtained as a viscous oil with procedure C (54 mg, 43%). $^{1}$H NMR ($CDCl_3$, 500 MHz): δ 7.61 – 7.53 (m, 4H), 7.45 – 7.40 (m, 4H), 7.35 – 7.31 (m, 1H), 2.79 (s, 2H), 1.86 (s, 3H), 1.47 (s, 6H). $^{13}$C NMR ($CDCl_3$, 125.8 MHz): δ 208.1, 147.5, 140.9, 138.9, 128.9, 127.3, 127.1(1), 127.0(8), 126.1, 57.0, 37.3, 32.0, 29.1. IR (ATR): ν = 2962, 2927, 1715, 1702, 1487, 1356, 1161, 765, 697 $cm^{-1}$. HRMS (ESI) m/z calc. for $C_{18}H_{20}O$ (M+) 252.1514, found 252.1521.

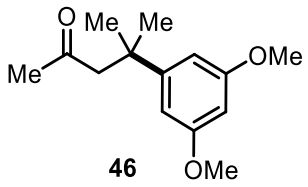

**46**

**4-(3,5-Dimethoxyphenyl)-4-methylpentan-2-one** (**46)**: obtained as a colorless oil with procedure B (40 mg, 34%). $^{1}$H NMR ($CDCl_3$, 500 MHz): δ 6.52 (d, *J* = 2.0 Hz, 2H), 6.33 (d, *J* = 2.0 Hz, 1H), 3.81 (s, 6H), 2.71 (s, 2H), 1.86 (s, 3H), 1.40 (s, 6H). $^{13}$C NMR ($CDCl_3$, 125.8 MHz): δ 207.9, 160.6, 150.9, 104.4, 97.1, 56.7, 55.1, 37.5, 31.7, 28.8. IR (ATR): ν = 2961, 1838, 1703, 1594, 1423, 1315, 1203, 1154, 1052, 700 $cm^{-1}$. HRMS (ESI) m/z calc. for $C_{14}H_{20}O_3Na$ (M+Na) 259.1310, found 259.1313.

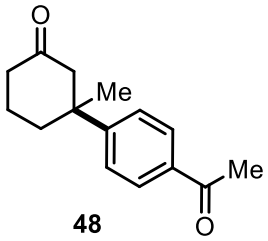

**48**

**3-(4-Acetylphenyl)-3-methylcyclohexan-1-one** (**48)**: obtained as a colorless oil with procedure C (97 mg, 75%). $^{1}$H NMR (500 MHz, $CDCl_3$) δ 7.91 (d, *J* = 7.9 Hz, 2H), 7.41 (d, *J* = 7.9 Hz, 2H), 2.89 (d, *J* = 14.2 Hz, 1H), 2.57 (s, 3H), 2.46 (d, *J* = 14.2 Hz, 1H), 2.37 – 2.13 (m, 3H), 2.00 – 1.83 (m, 2H), 1.63 (bs, 1H), 1.33 (s, 3H).$^{13}$C NMR (125.8 MHz, $CDCl_3$) δ 210.9, 197.8, 153.0, 135.4, 128.8, 126.1, 53.0, 43.4, 40.8, 37.9, 29.9, 26.7, 22.1. HRMS (ESI) m/z calc. for $C_{15}H_{19}O_2$ (M+H) 231.1385, found 231.1372. Spectroscopic data matches with previously reported data.[42]

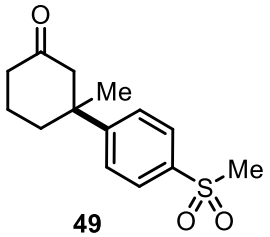


**49**

**3-Methyl-3-(4-(methylsulfonyl)phenyl)cyclohexan-1-one** (**49)**: obtained as a colorless oil with procedure C (87 mg, 65%). $^{1}$H NMR (500 MHz, $CDCl_3$) δ 7.89 (d, *J* = 8.6 Hz, 2H), 7.53 (d, *J* = 8.6 Hz, 2H), 3.05 (s, 3H), 2.89 (d, *J* = 14.2 Hz, 1H), 2.50 (d, *J* = 14.2 Hz, 1H), 2.38 – 2.19 (m, 3H), 1.97 (d, *J* = 12.6 Hz, 2H), 1.68 – 1.62 (m, 1H), 1.35 (s, 3H). $^{13}$C NMR (125.8 MHz, $CDCl_3$) δ 210.2, 153.7, 138.4, 127.6, 126.7, 52.6, 44.4, 43.3, 40.6, 37.6, 29.7, 21.9. IR (ATR): ν = 2929, 1705, 1596, 1305, 1146, 1094, 954, 727, 538 $cm^{-1}$. HRMS (ESI) m/z calc. for $C_{14}H_{18}O_3S$ (M+) 266.0977, found 266.0987.

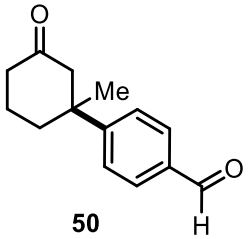


**50**

**4-(1-Methyl-3-oxocyclohexyl)benzaldehyde** (**50**): obtained as a colorless oil with procedure C (63 mg, 58%). $^{1}$H NMR (500 MHz, $CDCl_3$) δ 9.99 (s, 1H), 7.84 (d, *J* = 8.4 Hz, 2H), 7.50 (d, *J* = 8.4 Hz, 2H), 2.90 (d, *J* = 14.1 Hz, 1H), 2.49 (d, *J* = 14.1 Hz, 1H), 2.38 – 2.18 (m, 3H), 2.02 – 1.85 (m, 2H), 1.70 – 1.62 (m, 1H), 1.35 (s, 3H). $^{13}$C NMR (125.8 MHz, $CDCl_3$) δ 210.5, 191.7, 154.4, 134.6, 129.9, 126.3, 52.7, 43.4, 40.6, 37.7, 29.6, 21.9. IR (ATR): ν = 2936, 1701, 1608, 1226, 825 $cm^{-1}$. HRMS (ESI) m/z calc. for $C_{14}H_{16}O_2$ (M+) 216.1150, found 216.1146.

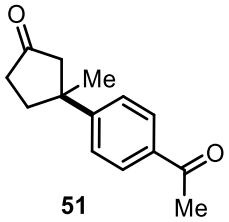


**51**

**3-(4-Acetylphenyl)-3-methylcyclopentan-1-one** (**51**): obtained as a white semi-solid with procedure C (72 mg, 67%).$^{1}$H NMR (500 MHz, $CDCl_3$) δ 7.94 (d, *J* = 8.6 Hz, 2H), 7.38 (d, *J* = 8.6 Hz, 2H), 2.64 (d, *J* = 17.5 Hz, 1H), 2.59 (s, 3H), 2.54 – 2.28 (m, 5H), 1.40 (s, 3H). $^{13}$C NMR (125.8 MHz, $CDCl_3$) δ 217.8, 197.8, 154.1, 135.5, 128.9, 125.9, 52.0, 44.2, 36.7, 35.7, 29.3, 26.7. IR (ATR): ν = 2960, 1739, 1679, 1605, 1406, 1271, 1156, 958, 836, 601 cm$^{-1}$. HRMS (ESI) m/z calc. for $C_{14}H_{16}O_2$ (M+) 216.1150, found 216.1165.

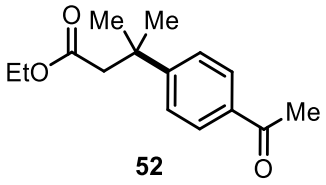


**52**

**Ethyl 3-(4-Acetylphenyl)-3-methylbutanoate (52)** obtained as a colorless oil with procedure C (62 mg, 50 %). $^{1}$H NMR (500 MHz, $CDCl_3$) δ 7.91 (dd, *J* = 6.7, 1.8 Hz, 2H), 7.46 (dd, *J* = 6.7, 1.8 Hz, 2H), 3.97 (q, *J* = 7.1 Hz, 2H), 2.64 (s, 2H), 2.58 (s, 3H), 1.47 (s, 6H), 1.08 (t, *J* = 7.1 Hz, 3H). $^{13}$C NMR (125.8 MHz, $CDCl_3$) δ 198.0, 171.3, 154.0, 135.1, 128.4, 126.0, 60.2, 48.2, 37.6, 29.0, 26.7, 14.2. IR (ATR): ν = 2971, 1730, 1682, 1606, 1406, 1366, 1270, 1034, 837 cm$^{-1}$. HRMS (EI) m/z calc. for $C_{15}H_{20}O_3$ (M+) 248.1412, found 248.1416.

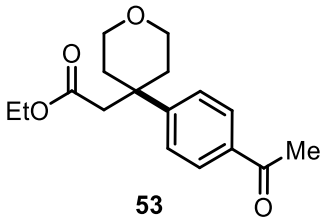


**53**

**Ethyl 2-(4-(4-Acetylphenyl)tetrahydro-2H-pyran-4-yl)acetate (53)** obtained as a colorless oil with procedure C (60 mg, 41%). $^{1}$H NMR (500 MHz, $CDCl_3$) δ 7.94 (d, *J* = 8.5 Hz, 2H), 7.42 (d, *J* = 8.5 Hz, 2H), 3.89 – 3.76 (m, 4H), 3.66 – 3.48 (m, 2H), 2.65 (s, 2H), 2.59 (s, 3H), 2.34 – 2.22 (m, 2H), 2.12 – 1.98 (m, 2H), 0.98 (t, *J* = 7.1 Hz, 3H). $^{13}$C NMR (125.8 MHz, $CDCl_3$) δ 197.9, 170.6, 150.0, 135.5, 128.6, 127.1, 64.2, 60.3, 46.9, 39.0, 36.2, 26.8, 14.1. IR (ATR): ν = 2956, 1727, 1682, 1605, 1407, 1358, 1114, 1030, 831 cm$^{-1}$. HRMS (EI) m/z calc. for $C_{17}H_{22}O_4$ (M+) 290.1518, found 290.1537.

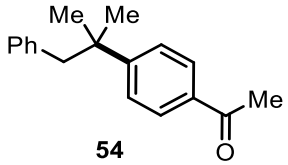

**54**

**1-(4-(2-Methyl-1-phenylpropan-2-yl)phenyl)ethan-1-one (54)** obtained as a colorless oil using procedure C (68 mg 54%). $^{1}$H NMR (500 MHz, $CDCl_3$) δ 7.88 (d, *J* = 8.4 Hz, 2H), 7.38 (d, *J* = 8.4 Hz, 2H), 7.15 – 7.10 (m, 3H), 6.84 – 6.72 (m, 2H), 2.89 (s, 2H), 2.60 (s, 3H), 1.35 (s, 6H). $^{13}$C NMR (125.8 MHz, $CDCl_3$) δ 197.9, 154.6, 138.1, 134.7, 130.2, 128.0, 127.5, 126.4, 126.0, 50.7, 39.2, 28.0, 26.5. IR (ATR): ν = 3028, 2966, 2926, 1682, 1605, 1357, 1269, 1015, 838, 702 cm$^{-1}$. HRMS (EI) m/z calc. for $C_{18}H_{20}O$ (M+) 252.1514, found 252.1529.

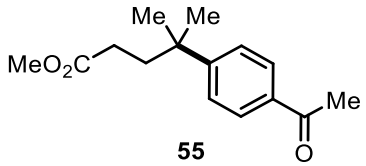

**55**

**Methyl 4-(4-Acetylphenyl)-4-methylpentanoate (55)** obtained as a colorless oil with procedure C (76 mg, 61 %). $^{1}$H NMR (500 MHz, $CDCl_3$) δ 7.92 (d, *J* = 8.3 Hz, 2H), 7.43 (d, *J* = 8.3 Hz, 2H), 3.60 (s, 3H), 2.60 (s, 3H), 2.18 – 1.92 (m, 4H), 1.35 (s, 6H). $^{13}$C NMR (126 MHz, $CDCl_3$) δ 198.0, 174.3, 154.0, 135.1, 128.6, 126.2, 51.7, 38.8, 37.9, 30.0, 28.7, 26.7. IR (ATR): ν = 2963, 1736,

1682, 1606, 1566, 1435, 1357, 1269, 1118, 958, 601 $cm^{-1}$. HRMS (EI) m/z calc. for $C_{15}H_{20}O_3$ (M+) 248.1412, found 248.1413.

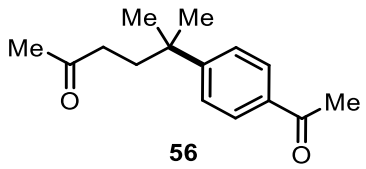

**56**

**5-(4-Acetylphenyl)-5-methylhexan-2-one (56)** obtained as a colorless oil with procedure C (40 mg, 34%). $^1$H NMR (500 MHz, $CDCl_3$) δ 7.91 (d, *J* = 8.4 Hz, 2H), 7.42 (d, *J* = 8.4 Hz, 2H), 2.60 (s, 3H), 2.16 (t, *J* = 8.0 Hz, 2H), 2.04 (s, 3H), 1.95 (t, *J* = 8.0 Hz, 2H), 1.34 (s, 6H). $^{13}$C NMR (125.8 MHz, $CDCl_3$) δ 208.5, 197.7, 154.0, 134.8, 128.3, 126.0, 39.3, 37.5, 37.2, 29.8, 28.6, 26.4. IR (ATR): ν = 2964, 1713, 1682, 1606, 1271, 838, 640, 556 $cm^{-1}$. HRMS (EI) m/z calc. for $C_{15}H_{20}O_2$ (M+) 232.1463, found 232.1460.

## 6.5 References

(1) Woodward, R. B.; Sondheimer, F.; Taub, D.; Heusler, K.; McLamore, W. M. *J. Am. Chem. Soc.* **1952**, *74*, 4223.

(2) Quasdorf, K. W.; Overman, L. E. *Nature* **2014**, *516*, 181.

(3) Das, J. P.; Marek, I.; Lam, J. K.; Wang, D.-H.; Yu, J.-Q.; Monde, K.; Harada, N.; Harada, N. *Chem. Commun.* **2011**, *47*, 4593.

(4) Christoffers, J.; Baro, A. *Adv. Synth. Catal.* **2005**, *347*, 1473.

(5) Wu, C.; Yue, G.; Nielsen, C. D.-T.; Xu, K.; Hirao, H.; Zhou, J. *J. Am. Chem. Soc.* **2016**, *138*, 742.

(6) d'Augustin, M.; Palais, L.; Alexakis, A. *Angew. Chem. Int. Ed.* **2005**, *44*, 1376.

(7) Minko, Y.; Marek, I. *Chem. Commun.* **2014**, *50*, 12597.

(8) (a) Mohr, J. T.; Behenna, D. C.; Harned, A. M.; Stoltz, B. M. *Angew. Chem. Int. Ed.* **2005**, *44*, 6924. (b) Atsuyuki, A.; Bachand, B.; Overman, L. E.; Poon, D. J. *J. Am. Chem. Soc.* **1998**, *120*, 6477. (c) Jiang, B.; Xu, M. *Angew. Chem. Int. Ed.* **2004**, *43*, 2543. (d) Mei, T.-S.; Patel, H. H.; Sigman, M. S. *Nature* **2014**, *508*, 340. (e) Kubiak, R. W.; Mighion, J. D.; Wilkerson-Hill, S. M.; Alford, J. S.; Yoshidomi, T.; Davies, H. M. L. *Org. Lett.* **2016**, *18*, 3118.

(9) (a) Joshi-Pangu, A.; Wang, C.-Y.; Biscoe, M. R. *J. Am. Chem. Soc.* **2011**, *133*, 8478. (b) Lohre, C.; Dröge, T.; Wang, C.; Glorius, F. *Chem. - A Eur. J.* **2011**, *17*, 6052.

(11) (a) Nugent, W. A. *Org. Lett.* **2002**, *4*, 2133. (b) Hayashi, T.; Konishi, M.; Yokota, K.-I.; Kumada, M. *Chem. Lett.* **1980**, 767. (c) Hintermann, L.; Xiao, L.; Labonne, A. *Angew. Chem. Int. Ed.* **2008**, *47*, 8246.

(12) (a) Sämann, C.; Dhayalan, V.; Schreiner, P. R.; Knochel, P. *Org. Lett.* **2014**, *16*, 2418. (b) Gurung, S. K.; Thapa, S.; Kafle, A.; Dickie, D. A.; Giri, R. *Org. Lett.* **2014**, *16*, 1264.

(13) (a) Silvi, M.; Sandford, C.; Aggarwal, V. K. *J. Am. Chem. Soc.* **2017**, *139*, 5736. (b) Li, C.; Wang, J.; Barton, L. M.; Yu, S.; Tian, M.; Peters, D. S.; Kumar, M.; Yu, A. W.; Johnson, K. A.; Chatterjee, A. K.; Yan, M.; Baran, P. S. *Science* **2017**. (c) Lo, J. C.; Gui, J.; Yabe, Y.; Pan, C.-M.; Baran, P. S. *Nature* **2014**, *516*, 343. (d) Kerchner, H. A.; Montgomery, J. *Org. Lett.* **2016**, *18*, 5760. (e) Atack, T. C.; Cook, S. P. *J. Am. Chem. Soc.* **2016**, *138*, 6139. (f) Kischkewitz, M.; Okamoto, K.; Mück-Lichtenfeld, C.; Studer, A. *Science* **2017**, *355*.

(14) (a) Tellis, J. C.; Primer, D. N.; Molander, G. A. *Science* **2014**, *345*, 433. (b) Primer, D. N.; Karakaya, I.; Tellis, J. C.; Molander, G. A. *J. Am. Chem. Soc.* **2015**, *137*, 2195.

(15) Matsui, J. K.; Molander, G. A. *Org. Lett.* **2017**, *19*, 950.

(16) Yasu, Y.; Koike, T.; Akita, M. *Adv. Synth. Catal.* **2012**, *354*, 3414.

(17) (a) Blanksby, S. J.; Ellison, G. B. *Acc. Chem. Res.* **2003**, *36*, 255. (b) Laarhoven, L. J. J.; Mulder, P. *J. Phys. Chem. B* **1997**, *101*, 73.

(18) (a) Heitz, D. R.; Tellis, J. C.; Molander, G. A. *J. Am. Chem. Soc.* **2016**, *138*, 12715. (b) Shields, B. J.; Doyle, A. G. *J. Am. Chem. Soc.* **2016**, *138*, 12719.

(19) Zhang, P.; Le, C.; MacMillan, D. W. C. *J. Am. Chem. Soc.* **2016**, *138*, 8084.

(20) Yu, D.-G.; Wang, X.; Zhu, R.-Y.; Luo, S.; Zhang, X.-B.; Wang, B.-Q.; Wang, L.; Shi, Z.-J. *J. Am. Chem. Soc.* **2012**, *134*, 14638.

(21) Liao, L.-Y.; Kong, X.-R.; Duan, X.-F. *J. Org. Chem.* **2014**, *79*, 777.

(22) Joshi-Pangu, A.; Ganesh, M.; Biscoe, M. R. *Org. Lett.* **2011**, *13*, 1218.

(23) González-Bobes, F.; Fu, G. C. *J. Am. Chem. Soc.* **2006**, *128*, 5360.

(24) Huang, C.-Y.; Doyle, A. G. *J. Am. Chem. Soc.* **2012**, *134*, 9541.

(25) Wang, X.; Wang, S.; Xue, W.; Gong, H. *J. Am. Chem. Soc.* **2015**, *137*, 11562.

(26) Shockley, S. E.; Holder, J. C.; Stoltz, B. M. *Org. Process Res. Dev.* **2015**, *19*, 974.

(27) The use of tertiary cyclopropyltrifluoroborates has been achieved previously: Harris, M. R.; Li, Q.; Lian, Y.; Xiao, J.; Londregan, A. T. *Org. Lett.* **2017**, *19*, 2450.

(28) Sandford, C.; Aggarwal, V. K. *Chem. Commun.* **2017**, *53*, 5481.

(29) Matsui, J. K.; Primer, D. N.; Molander, G. A. *Chem. Sci.* **2017**, *8*, 3512..

(30) Molander, G. A.; McKee, S. A. *Org. Lett.* **2011**, *13*, 4684.

(31) Verbelen, B.; Cunha Dias Rezende, L.; Boodts, S.; Jacobs, J.; Van Meervelt, L.; Hofkens, J.; Dehaen, W. *Chem. – A Eur. J.* **2015**, *21*, 12667.

(32) Woods, J.; Omoregie, H. O. *Int. J. Chem.* **2011**, *3*, 24.

(33) Le, C.; Wismer, M. K.; Shi, Z.-C.; Zhang, R.; Conway, D. V.; Li, G.; Vachal, P.; Davies, I. W.; MacMillan, D. W. C. *ACS Cent. Sci.* **2017**, DOI: acscentsci.7b00159.

(34) Kerr, W. J.; Mudd, R. J.; Brown, J. A. *Chem. - A Eur. J.* **2016**, *22*, 4738.

(35) Udding, A. C.; Strating, J.; Wynberg, H. *Tetrahedron Lett.* **1968**, *9*, 1345.

(36) Rudzinski, D. M.; Kelly, C. B.; Leadbeater, N. E. *Chem. Commun.* **2012**, *48*, 9610.

(37) Roizen, J. L.; Zalatan, D. N.; Du Bois, J. *Angew. Chem. Int. Ed.* **2013**, *52*, 11343.

(38) Lin, X.; Hou, C.; Li, H.; Weng, Z. *Chem. - A Eur. J.* **2016**, *22*, 2075.

(39) Ortega, N.; Urban, S.; Beiring, B.; Glorius, F. *Angew. Chem. Int. Ed.* **2012**, *51*, 1710.

(40) Kim, B. H.; Jeon, I.; Han, T. H.; Park, H. J.; Jun, Y. M. *J. Chem. Soc. Perkin Trans. 1* **2001**, *0*, 2035.

(41) Carlson, G. L. B.; Quina, F. H.; Zarnegar, B. M.; Whitten, D. G. *J. Am. Chem. Soc.* **1975**, *97*, 347.

(42) Kikushima, K.; Holder, J. C.; Gatti, M.; Stoltz, B. M. *J. Am. Chem. Soc.* **2011**, *133*, 6902.

**Author Contributions:**

D.N.P. designed the experiments, optimized the reaction, prepared all the compounds, and wrote and edited the manuscript.

## Appendix A7. $^{1}H$, $^{13}C$, $^{11}B$, and $^{19}F$ NMR Spectra Relevant to Chapter 6

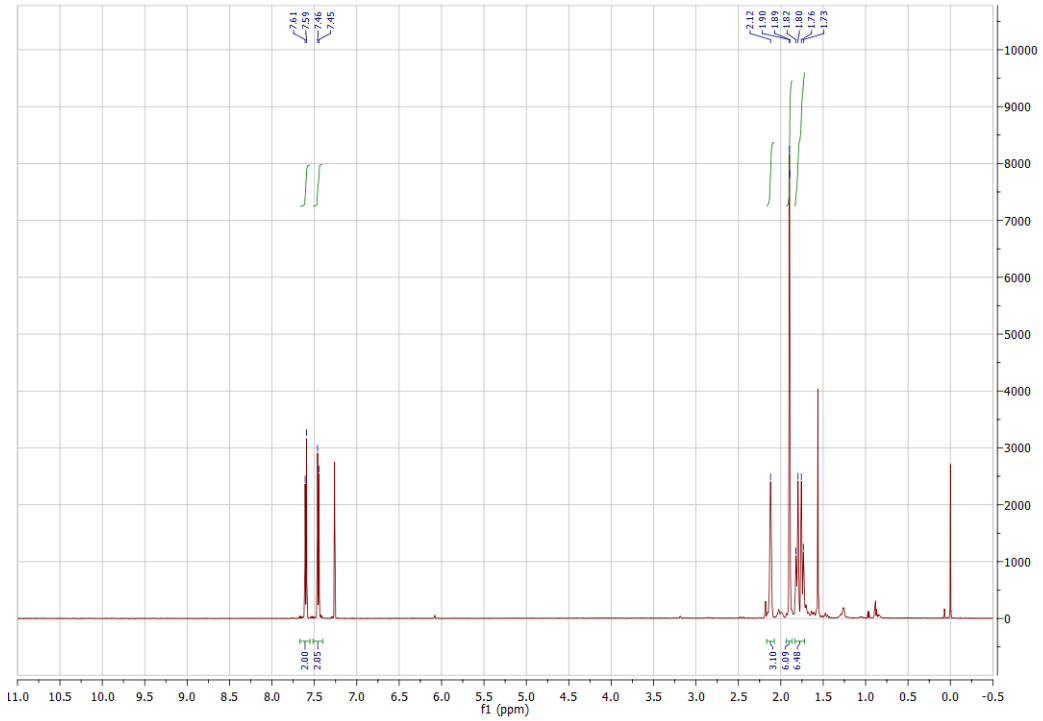


**Figure A7.1.** $^{1}$H NMR ($CDCl_3$, 500 MHz) of 4-(adamantan-1-yl)benzonitrile (**19**)

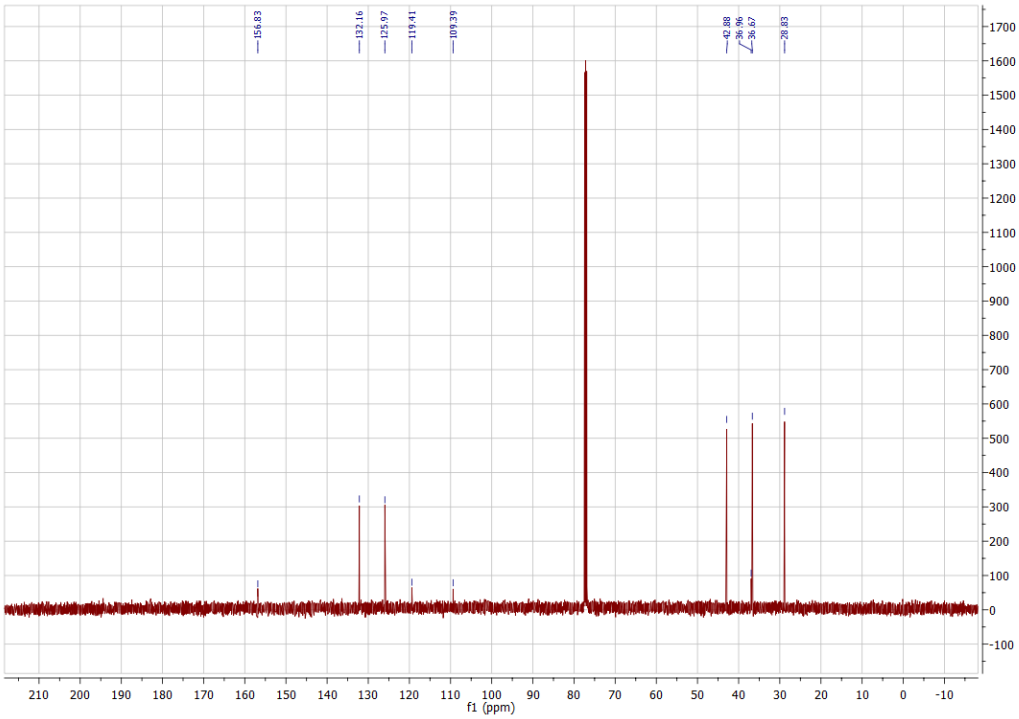


**Figure A7.2.** $^{13}$C NMR ($CDCl_3$, 125.8 MHz) of 4-(adamantan-1-yl)benzonitrile (**19**)

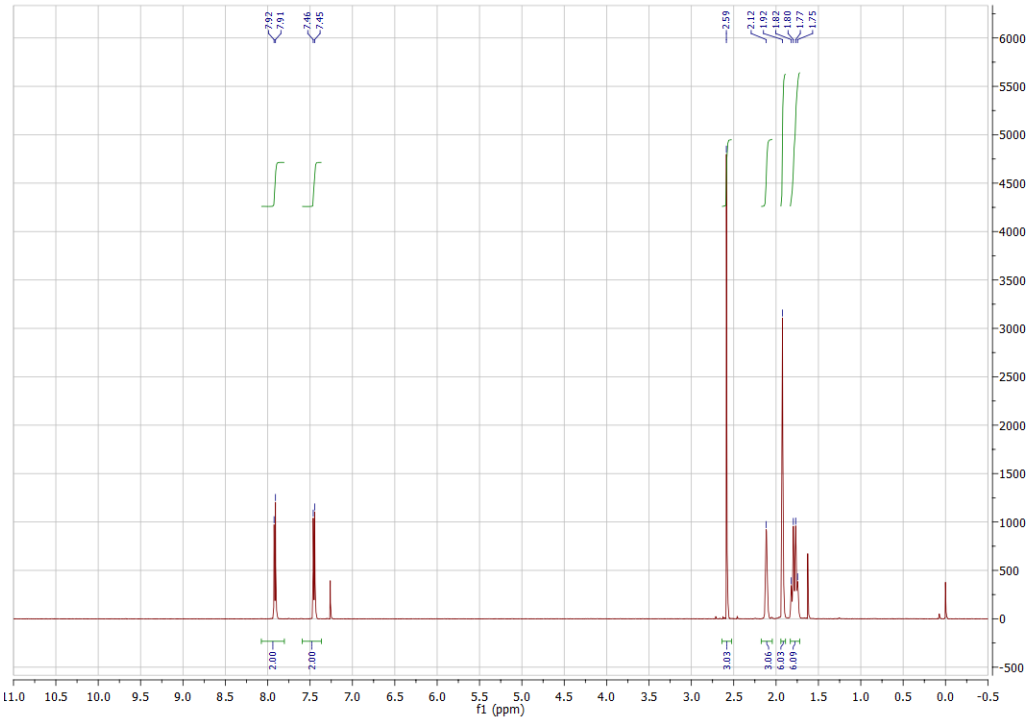


**Figure A7.3.** $^{1}H$ NMR ($CDCl_3$, 500 MHz) of 1-(4-((3r,5r,7r)-Adamantan-1-yl)phenyl)ethan-1-one (**20**)

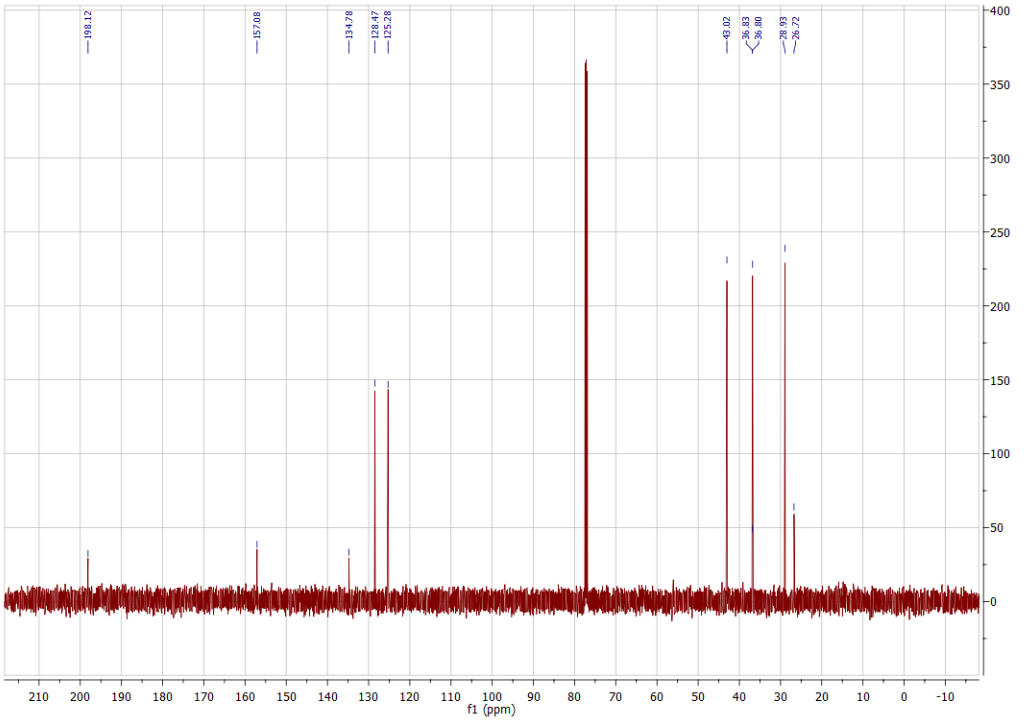


**Figure A7.4.** $^{13}C$ NMR ($CDCl_3$, 125.8 MHz) of 1-(4-((3r,5r,7r)-Adamantan-1-yl)phenyl)ethan-1-one (**20**)

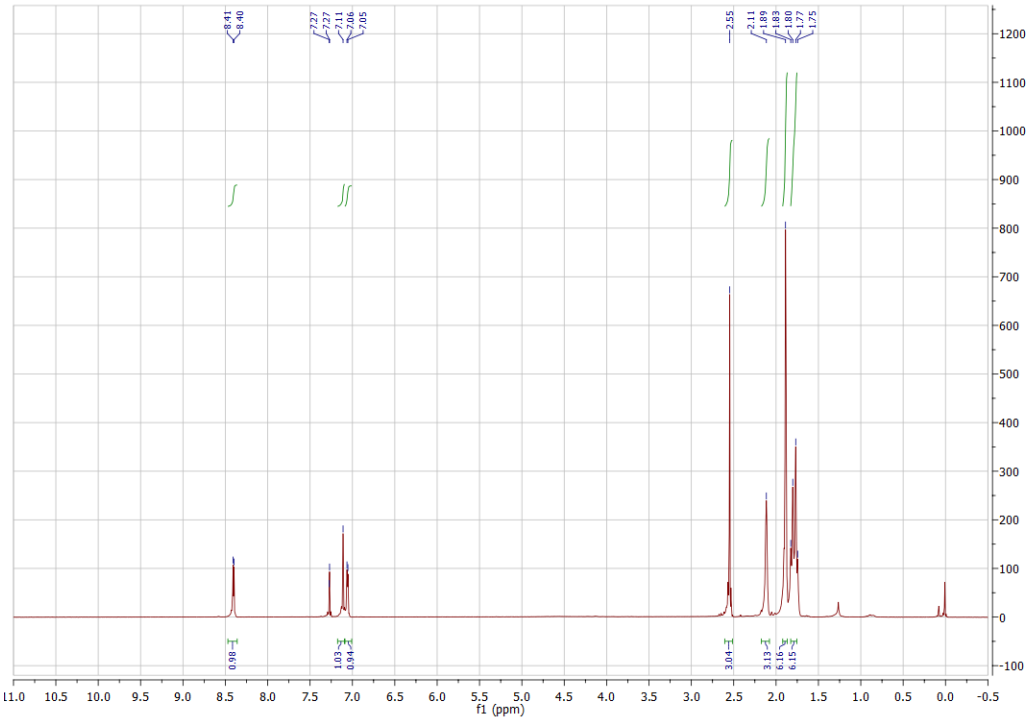


**Figure A7.5.** $^{1}H$ NMR ($CDCl_3$, 500 MHz) spectrum of 4-((3r,5r,7r)-adamantan-1-yl)-2-methylpyridine (**21**)

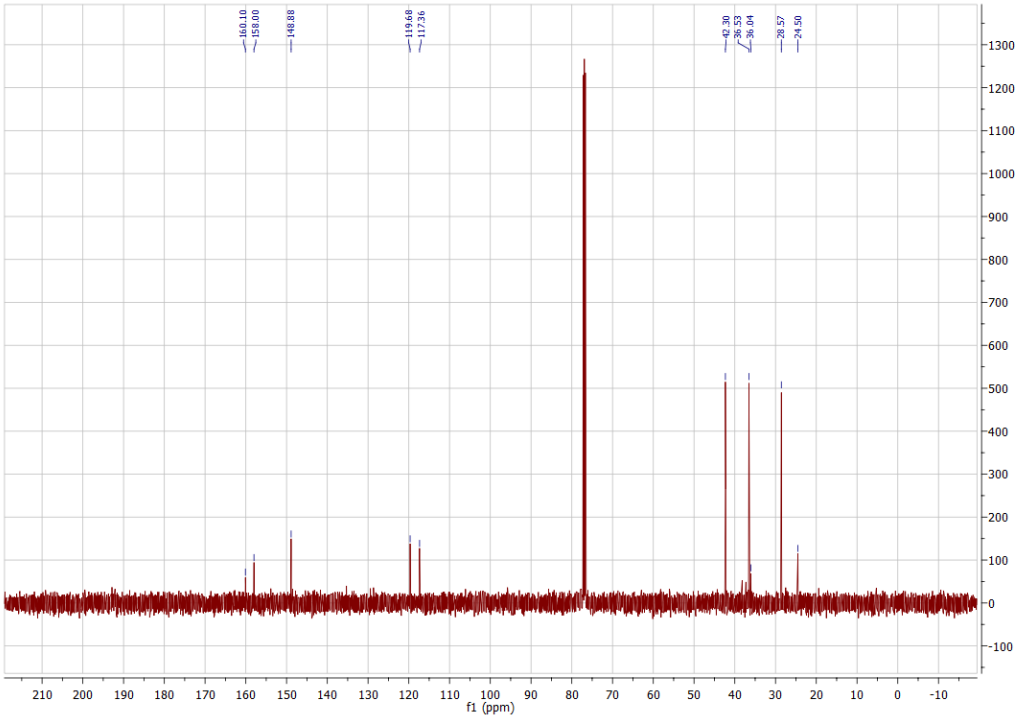


**Figure A7.6.** $^{13}C$ NMR ($CDCl_3$, 125.8 MHz) spectrum of 4-((3r,5r,7r)-adamantan-1-yl)-2-methylpyridine (**21**)

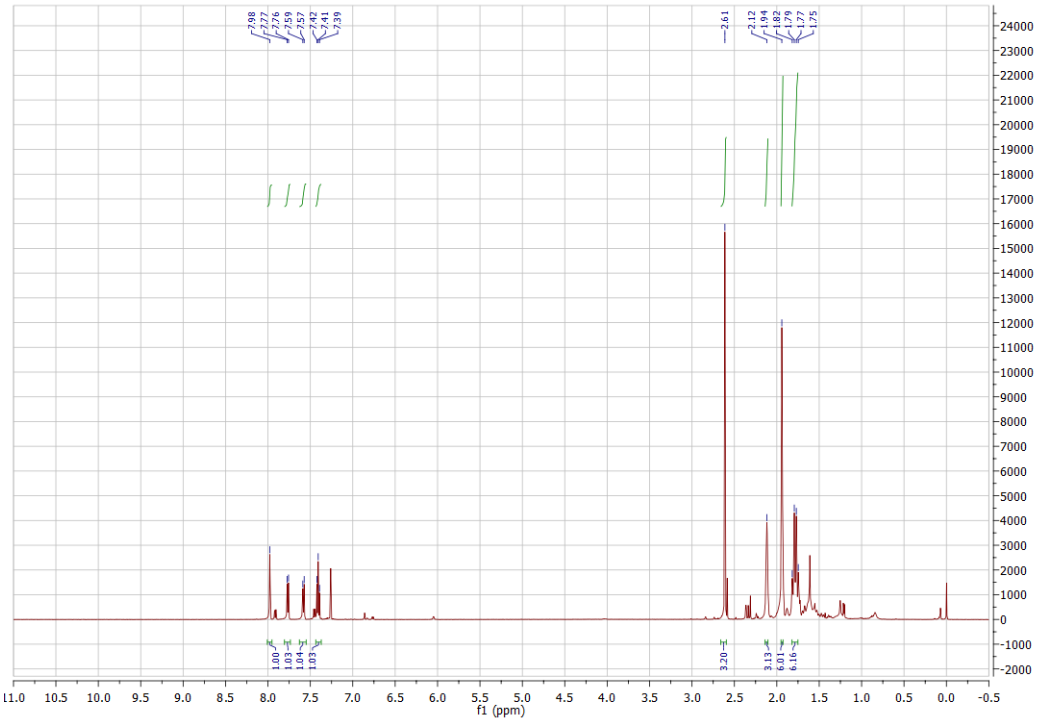


**Figure A7.7.** $^{1}$H NMR ($CDCl_3$, 500 MHz) spectrum of 1-(3-((3r,5r,7r)-Adamantan-1-yl)phenyl)ethan-1-one (**22**)

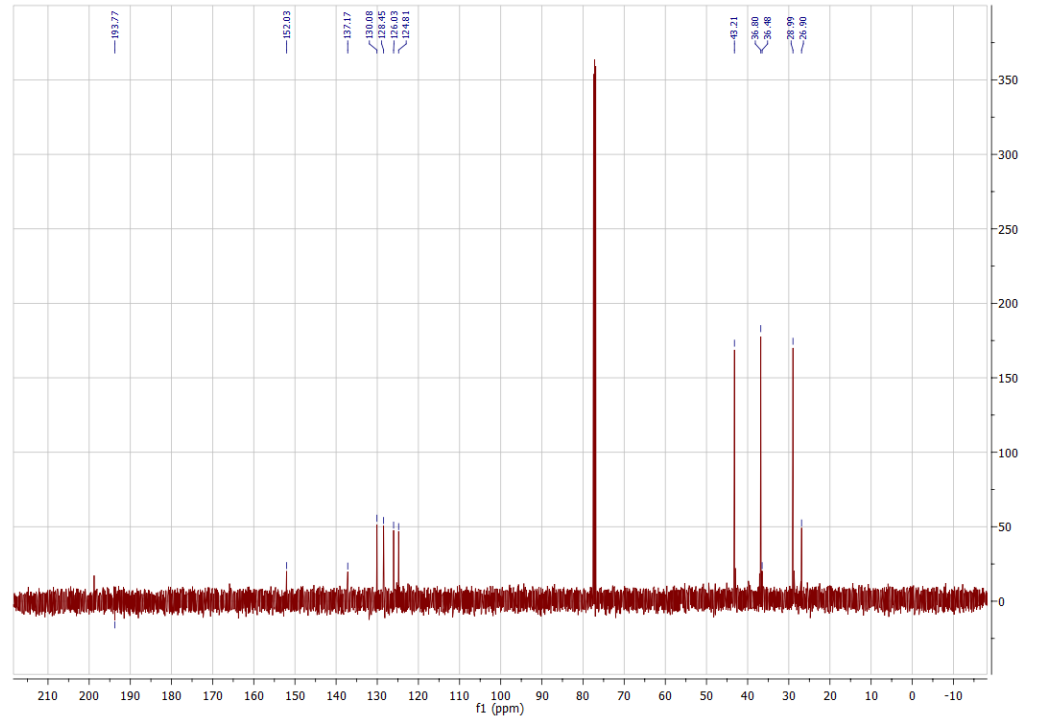


**Figure A7.8.** $^{13}$C NMR ($CDCl_3$, 125.8 MHz) spectrum of 1-(3-((3r,5r,7r)-Adamantan-1-yl)phenyl)ethan-1-one (**22**)

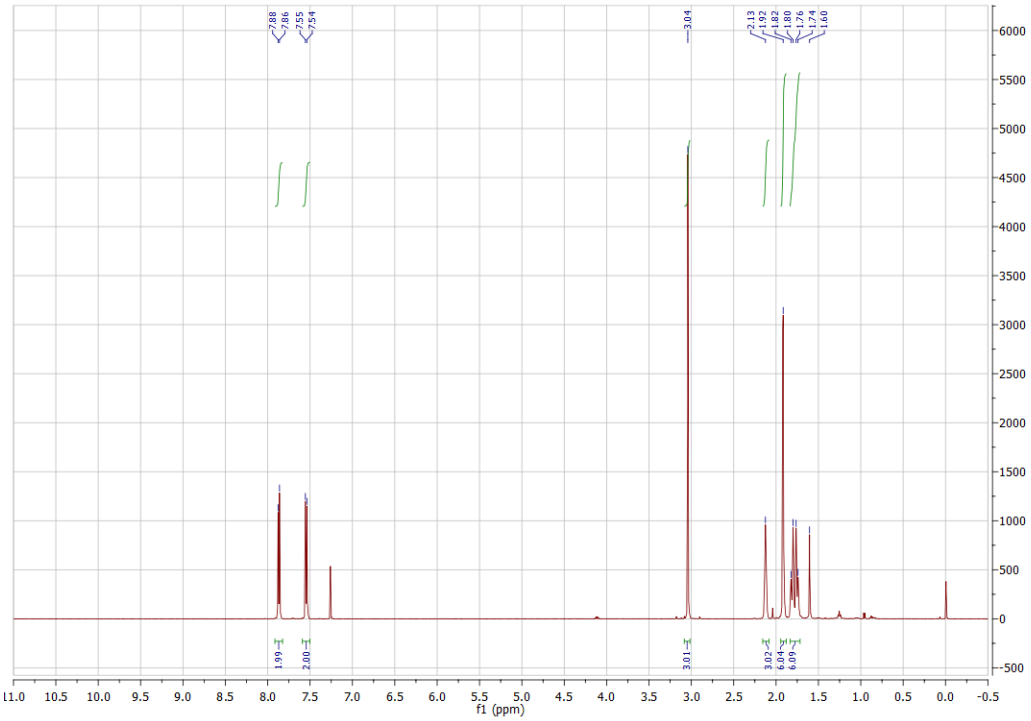


**Figure A7.9.** $^{1}$H NMR ($CDCl_3$, 500 MHz) spectrum of 1-(4-(methylsulfonyl)phenyl)adamantane (**23**)

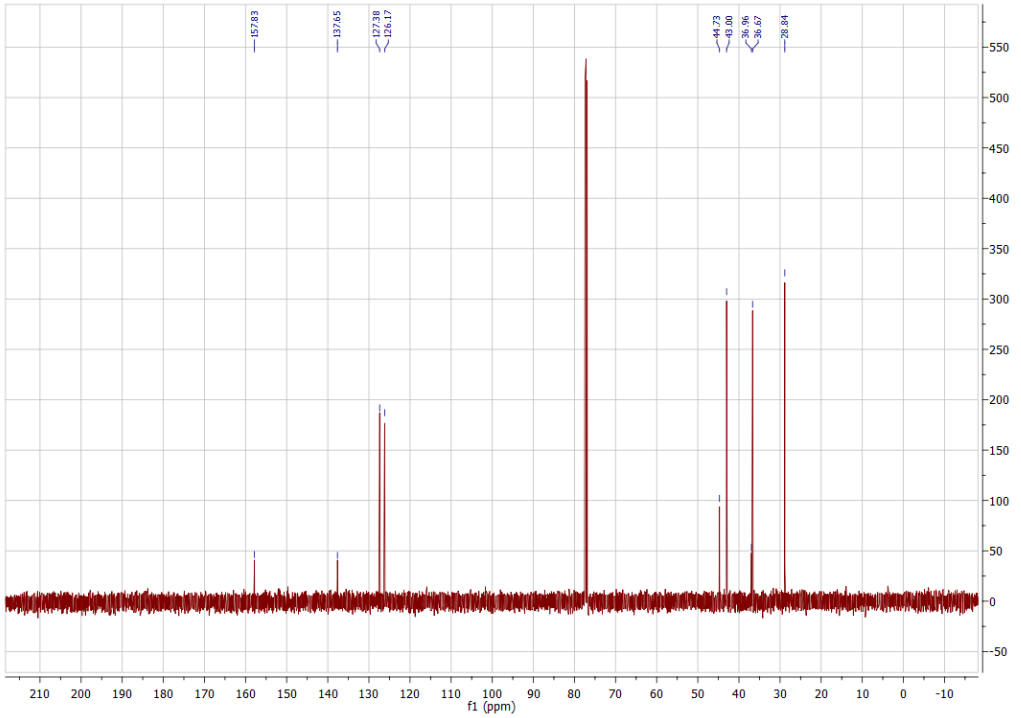


**Figure A7.10.** $^{13}$C NMR ($CDCl_3$, 125.8 MHz) spectrum of 1-(4-(methylsulfonyl)phenyl)adamantane (**23**)

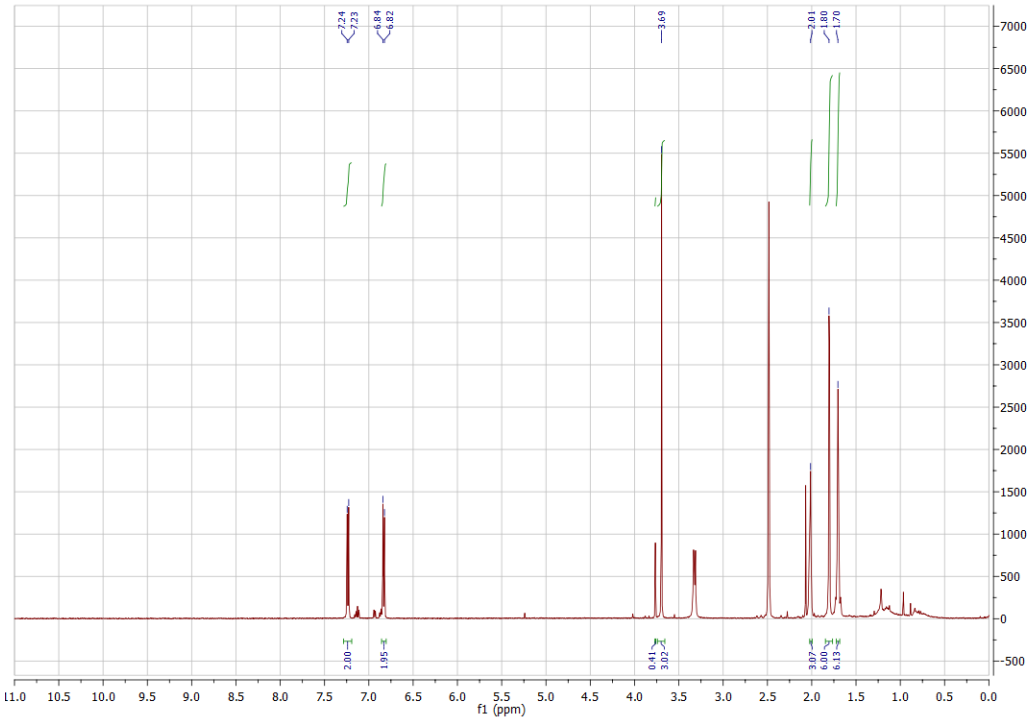


**Figure A7.11.** $^{1}$H NMR ($CDCl_3$, 500 MHz) spectrum of(3r,5r,7r)-1-(4-methoxyphenyl)adamantane (**24**)

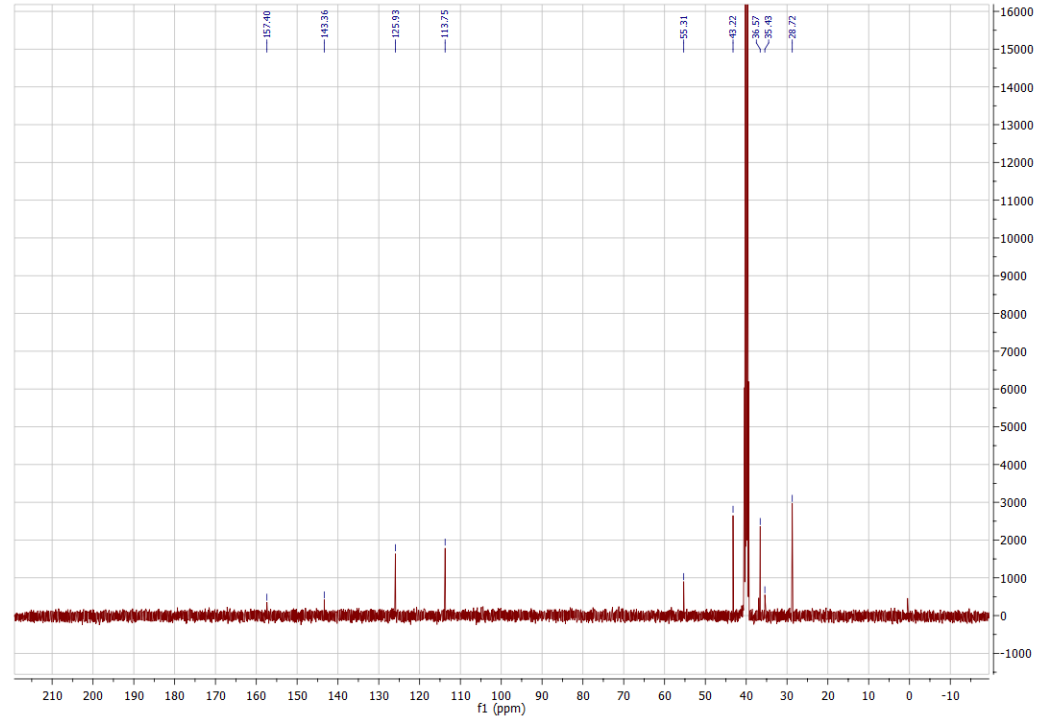


**Figure A7.12.** $^{13}$C NMR ($CDCl_3$, 125.8 MHz) spectrum of (3r,5r,7r)-1-(4-methoxyphenyl)adamantane (**24**)

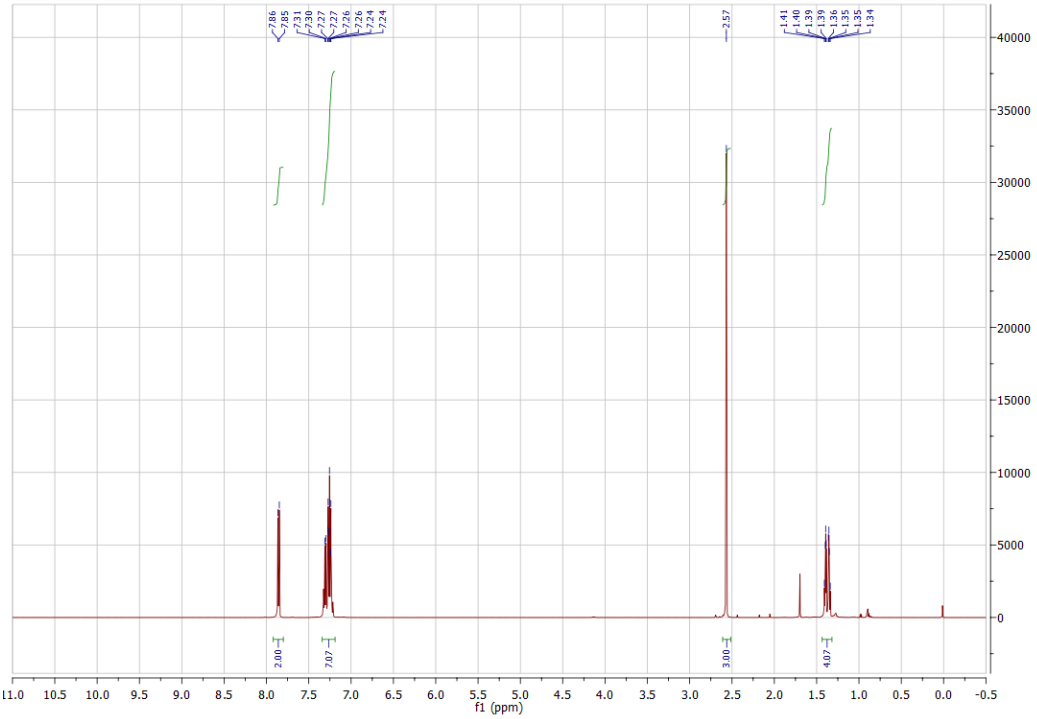


**Figure A7.13.** $^{1}$H NMR ($CDCl_3$, 500 MHz) spectrum of 1-(4-(1-phenylcyclopropyl)phenyl)ethan-1-one (**25**)

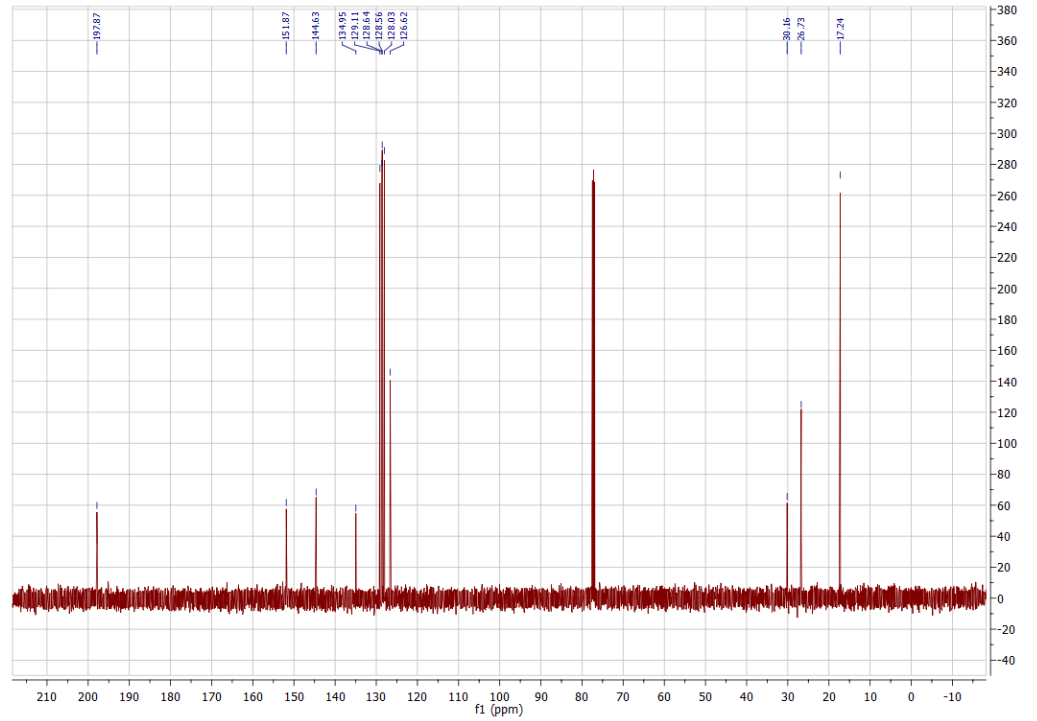


**Figure A7.14.** $^{13}$C NMR ($CDCl_3$, 125.8 MHz) spectrum of 1-(4-(1-phenylcyclopropyl)phenyl)ethan-1-one (**25**)

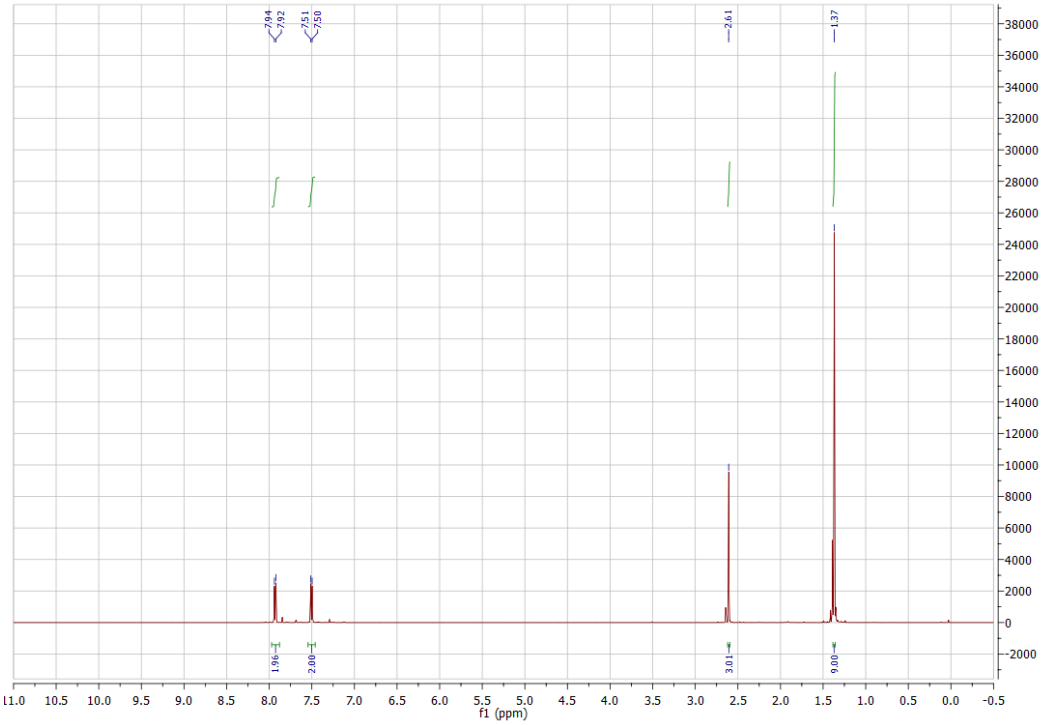


**Figure A7.15.** $^{1}$H NMR ($CDCl_3$, 500 MHz) spectrum of 1-(4-(*tert*-Butyl)phenyl)ethan-1-one (**26**)

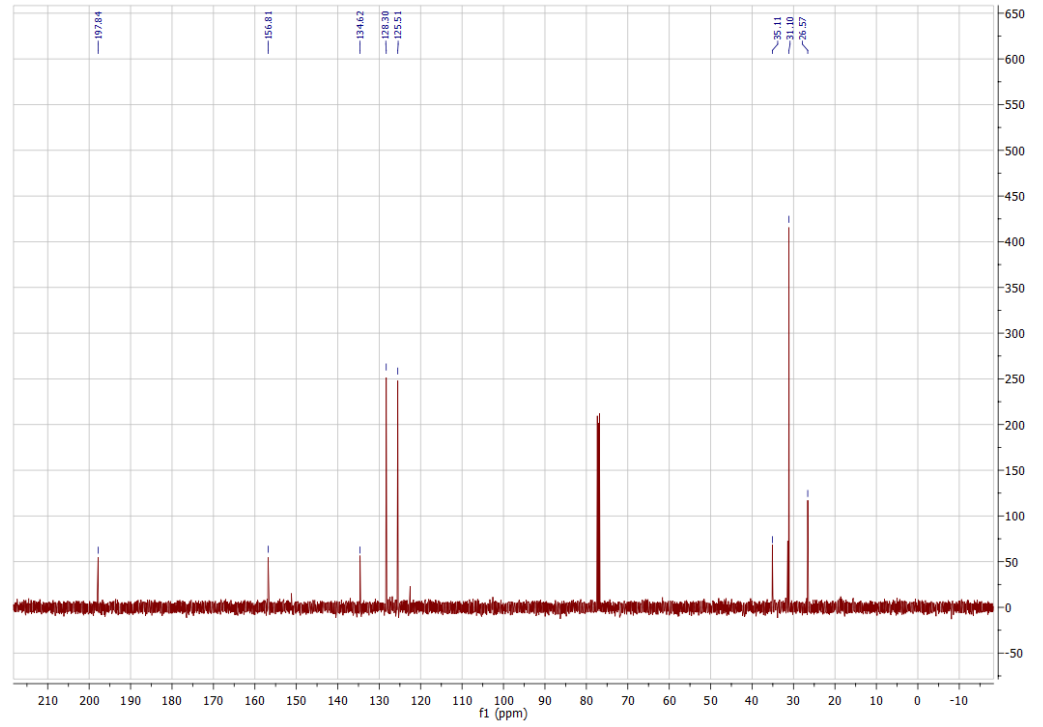


**Figure A7.16.** $^{13}$C NMR ($CDCl_3$, 125.8 MHz) spectrum of 1-(4-(*tert*-Butyl)phenyl)ethan-1-one (**26**)

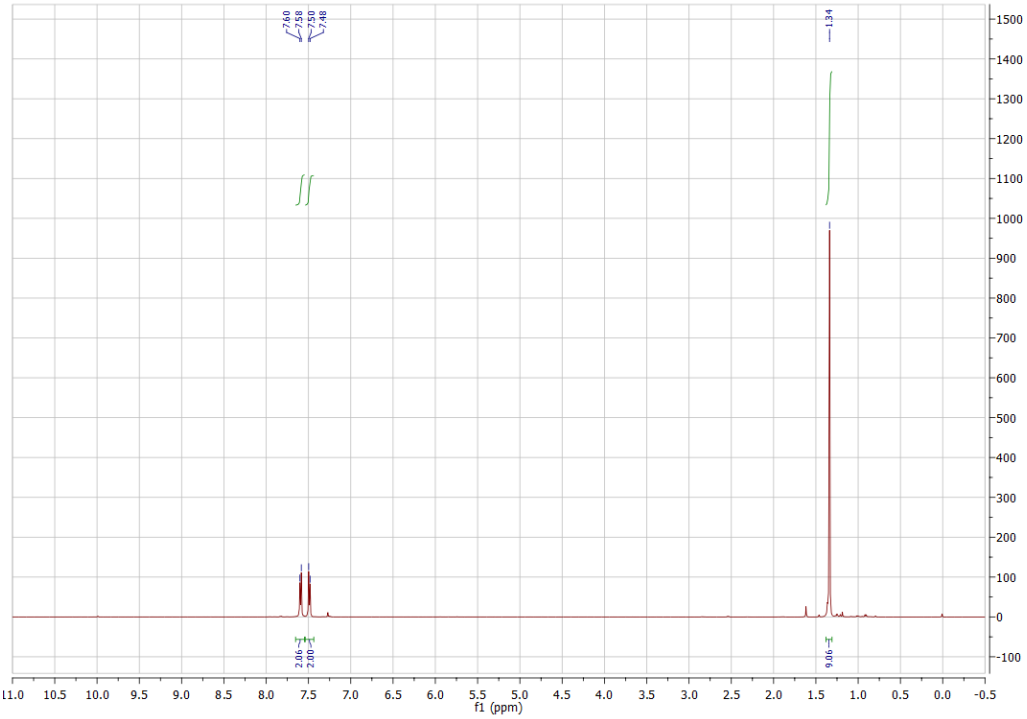


**Figure A7.17.** $^{1}$H NMR ($CDCl_3$, 500 MHz) spectrum of 4-(*tert*-Butyl)benzonitrile (**27**)

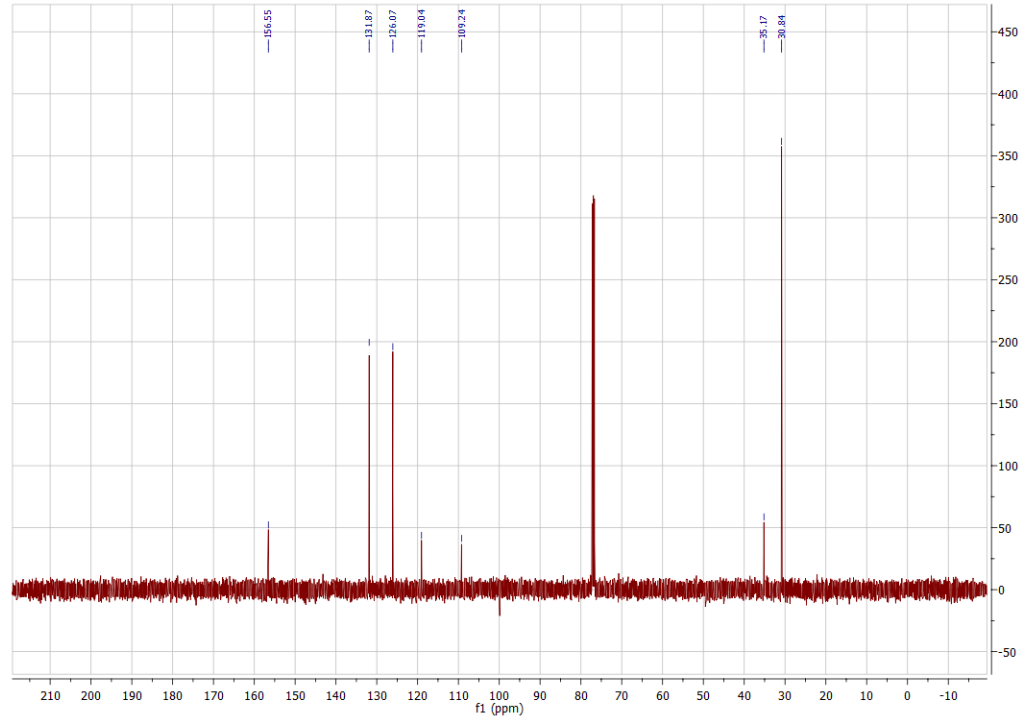


**Figure A7.18.** $^{13}$C NMR ($CDCl_3$, 125.8 MHz) spectrum of 4-(*tert*-Butyl)benzonitrile (**27**)

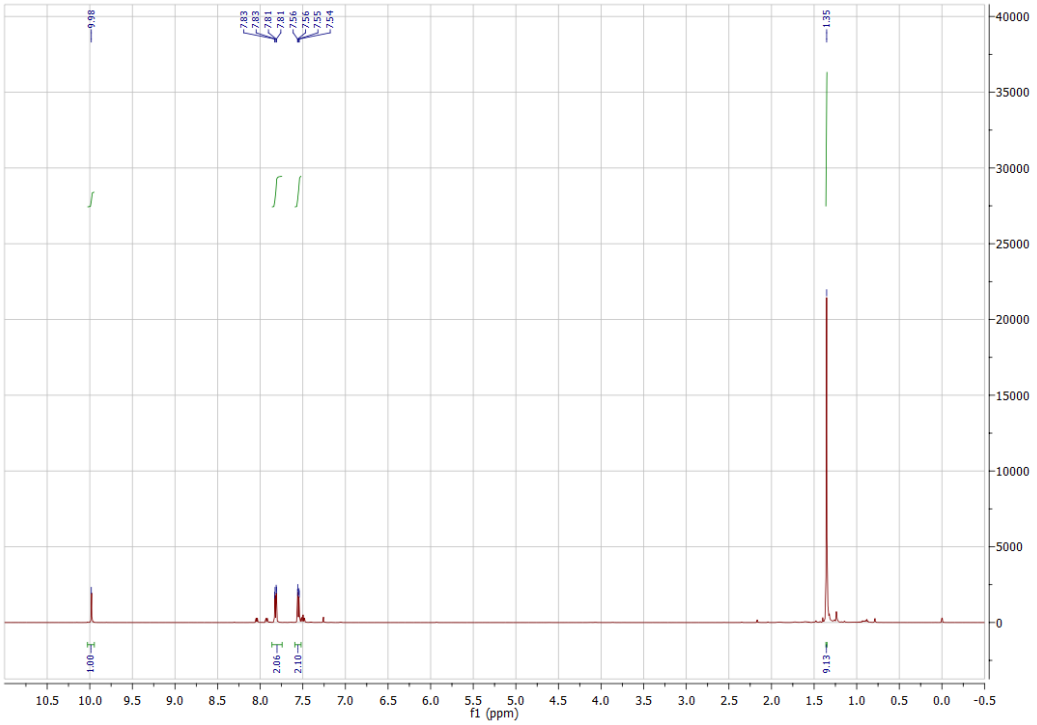


**Figure A7.19.** $^{1}$H NMR ($CDCl_3$, 500 MHz) spectrum of 4-(*tert*-Butyl)benzaldehyde (**28**)

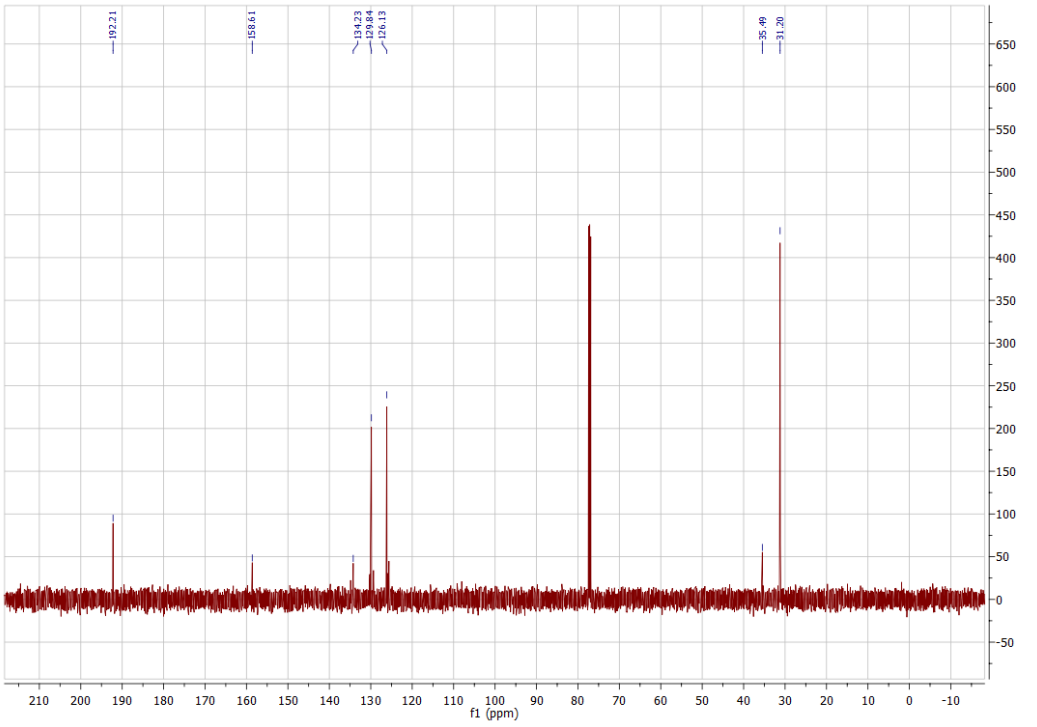


**Figure A7.20.** $^{13}$C NMR ($CDCl_3$, 125.8 MHz) spectrum of 4-(*tert*-Butyl)benzaldehyde (**28**)

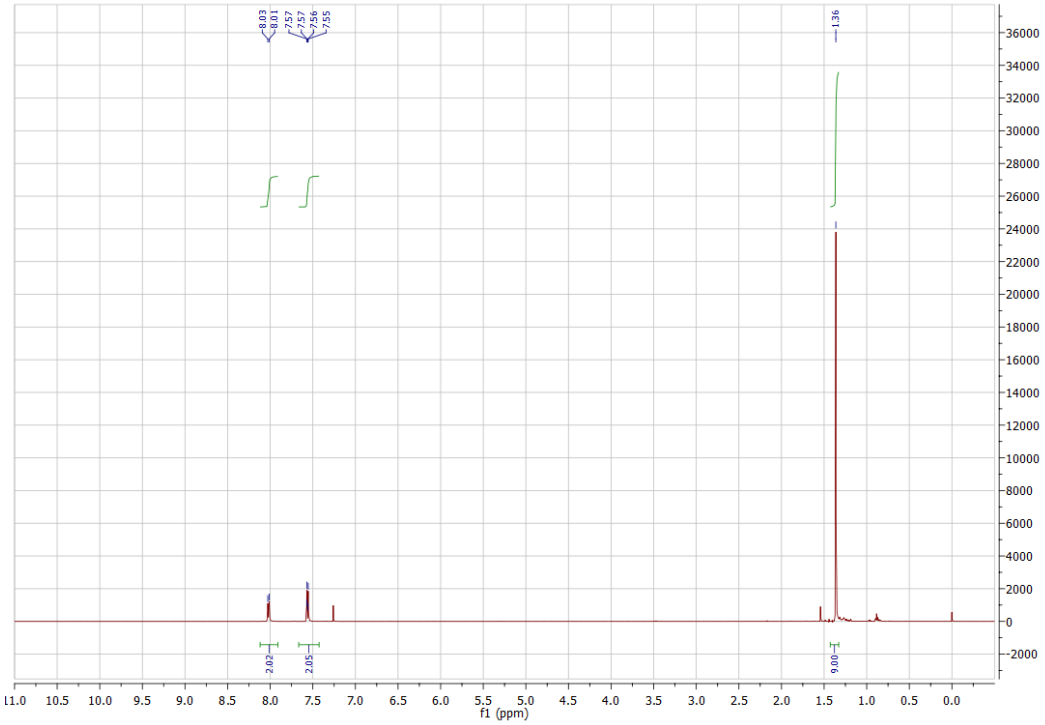


**Figure A7.21.** $^{1}H$ NMR ($CDCl_3$, 500 MHz) spectrum of 1-(4-(tert-butyl)phenyl)-2,2,2-trifluoroethan-1-one (**29**)

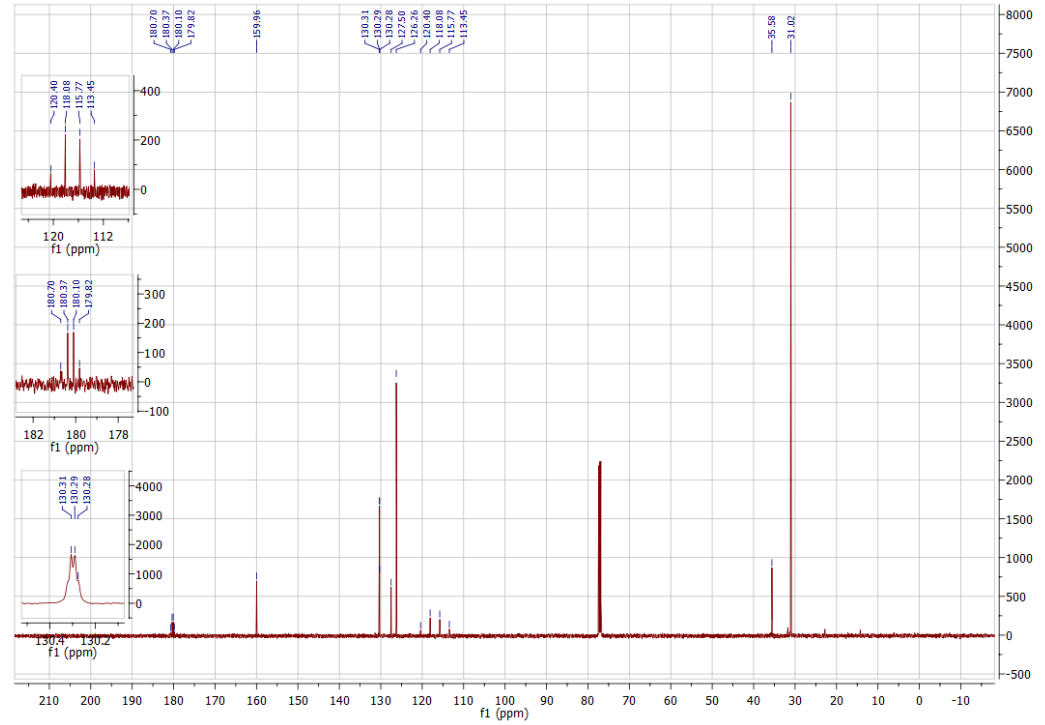


**Figure A7.22.** $^{13}C$ NMR ($CDCl_3$, 125.8 MHz) spectrum of 1-(4-(tert-butyl)phenyl)-2,2,2-trifluoroethan-1-one (**29**)

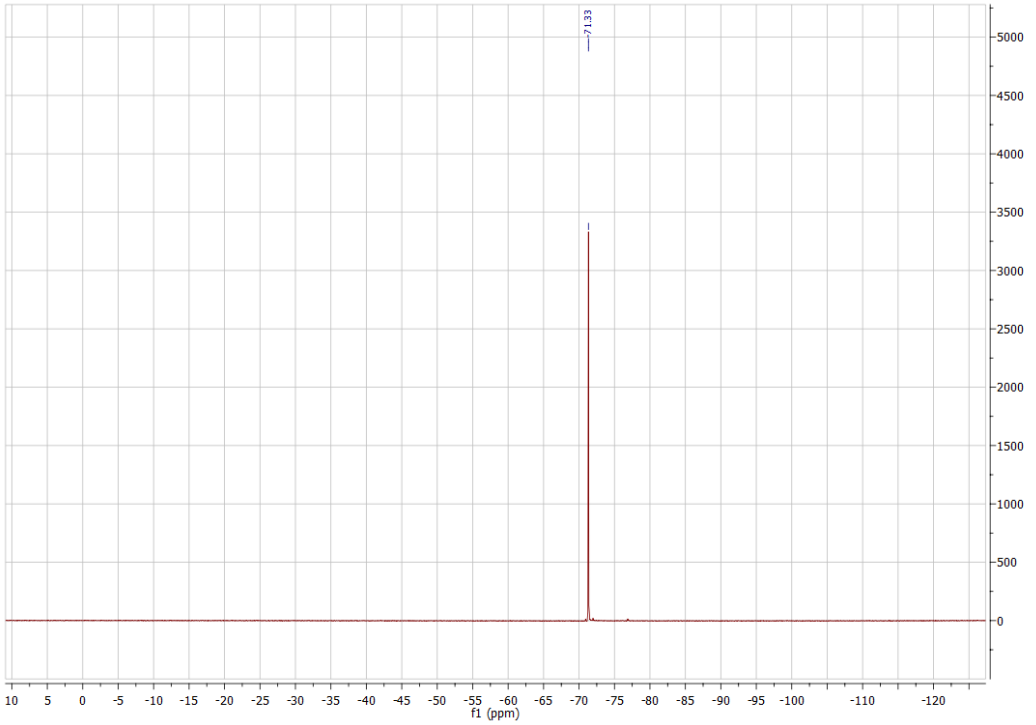


**Figure A7.23.** $^{19}F$ NMR ($CDCl_3$, 470.8 MHz) spectrum of 1-(4-(tert-butyl)phenyl)-2,2,2-trifluoroethan-1-one (**29**)

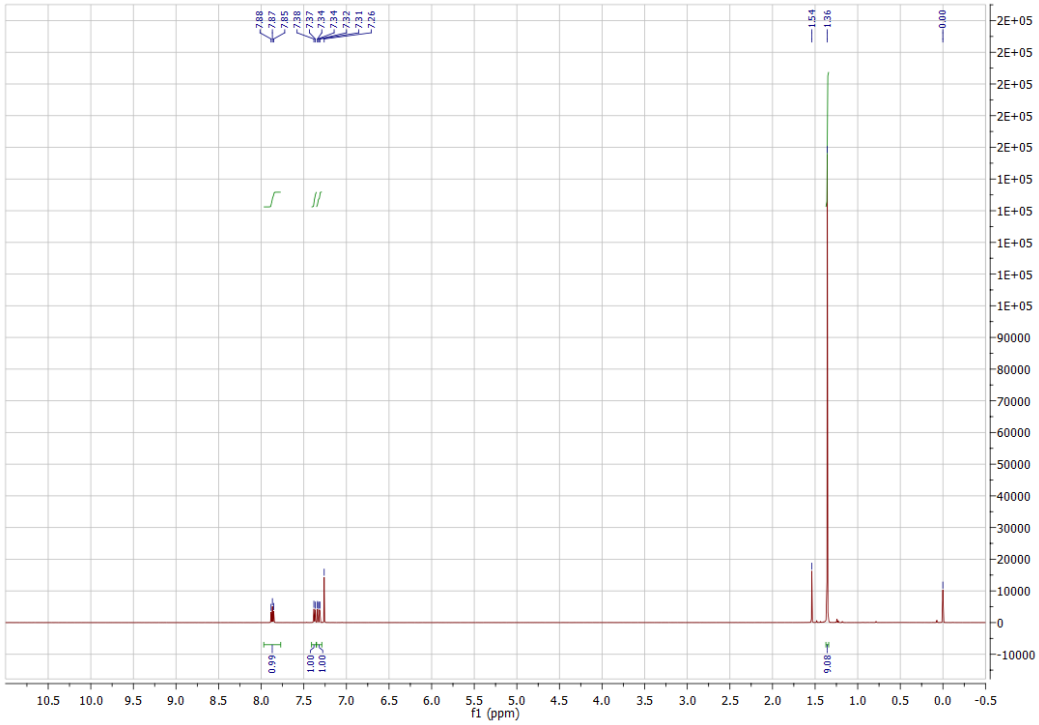


**Figure A7.24.** $^{1}H$ NMR ($CDCl_3$, 500 MHz) spectrum of 4-(tert-butyl)-3-fluorobenzenesulfonyl fluoride (**30**)

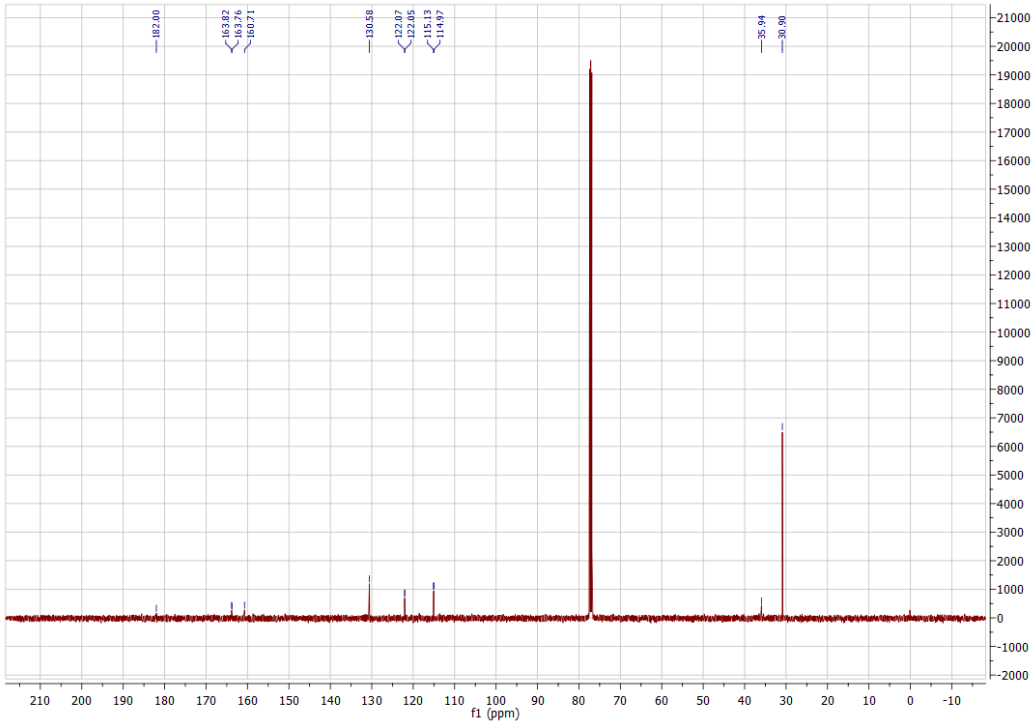


**Figure A7.25.** $^{13}C$ NMR ($CDCl_3$, 125.8 MHz) spectrum of 4-(tert-butyl)-3-fluorobenzenesulfonyl fluoride (**30**)

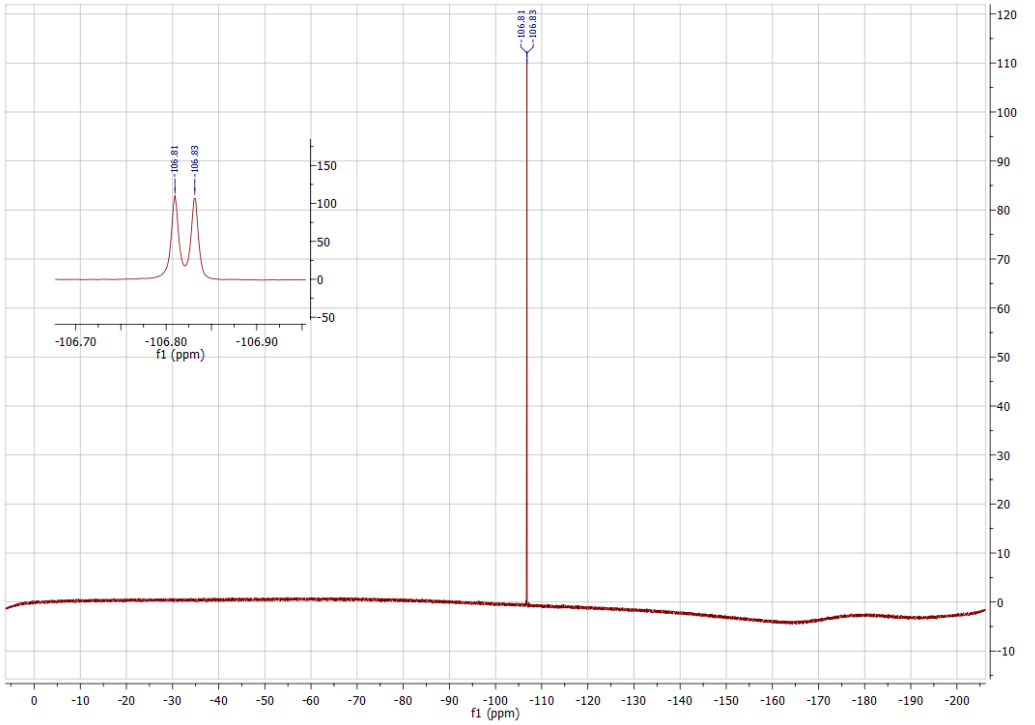


**Figure A7.26.** $^{19}F$ NMR ($CDCl_3$, 470.8 MHz) spectrum of of 4-(tert-butyl)-3-fluorobenzenesulfonyl fluoride (**30**)

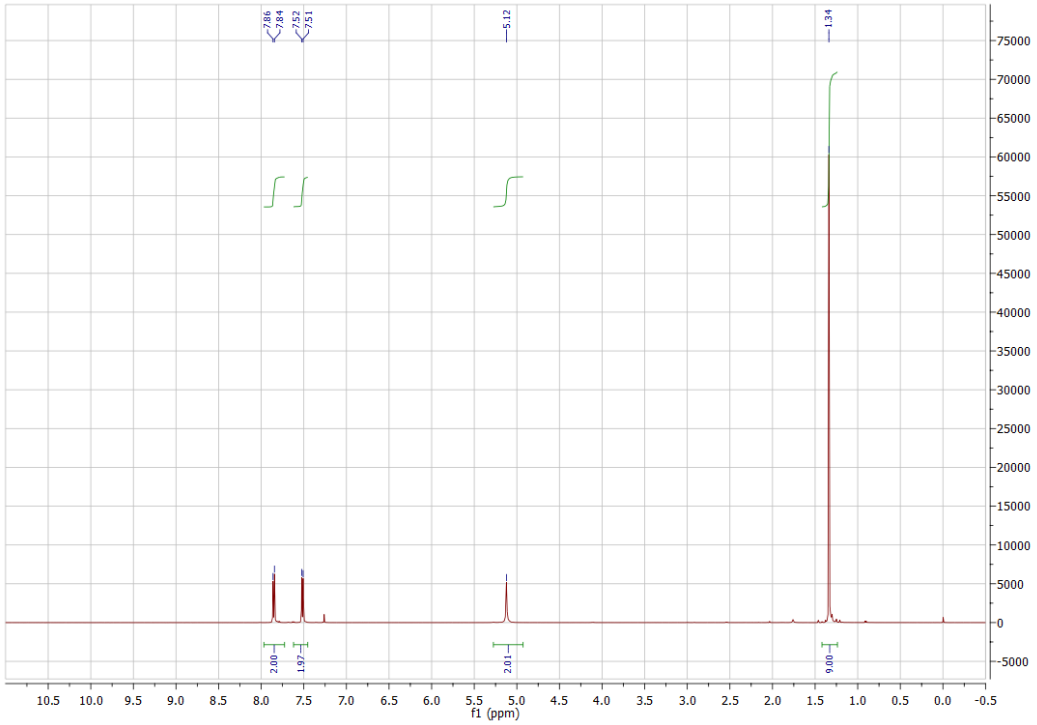


**Figure A7.27.** $^{1}$H NMR ($CDCl_3$, 500 MHz) spectrum of 4-(*tert*-Butyl)benzenesulfonamide (**31**)

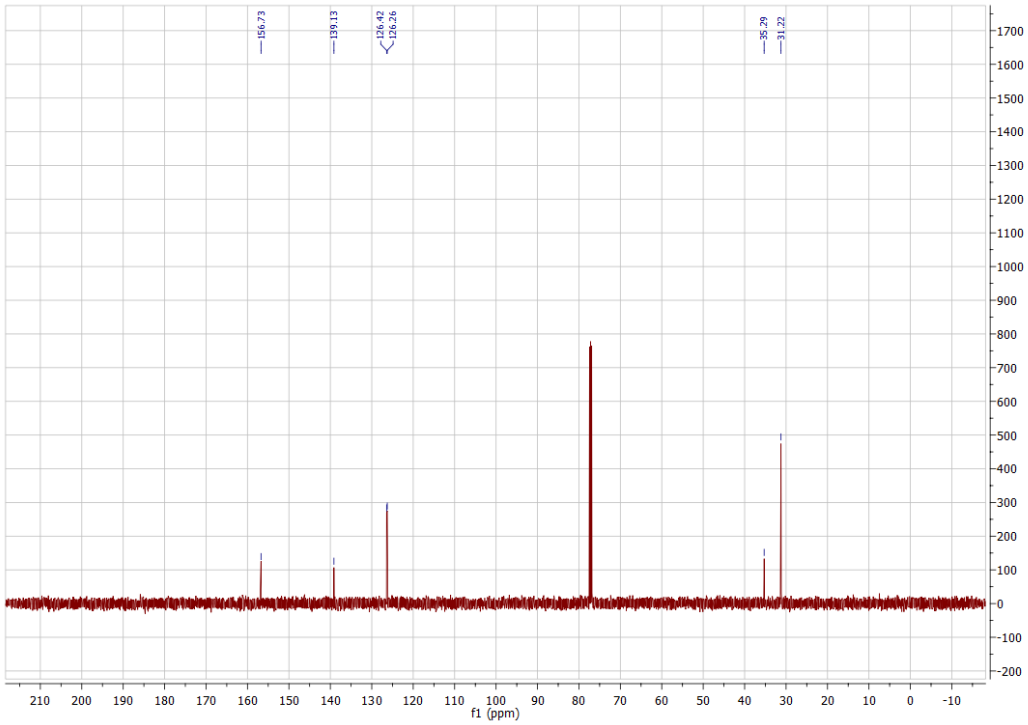


**Figure A7.28.** $^{13}$C NMR ($CDCl_3$, 125.8 MHz) spectrum of 4-(*tert*-Butyl)benzenesulfonamide (**31**)

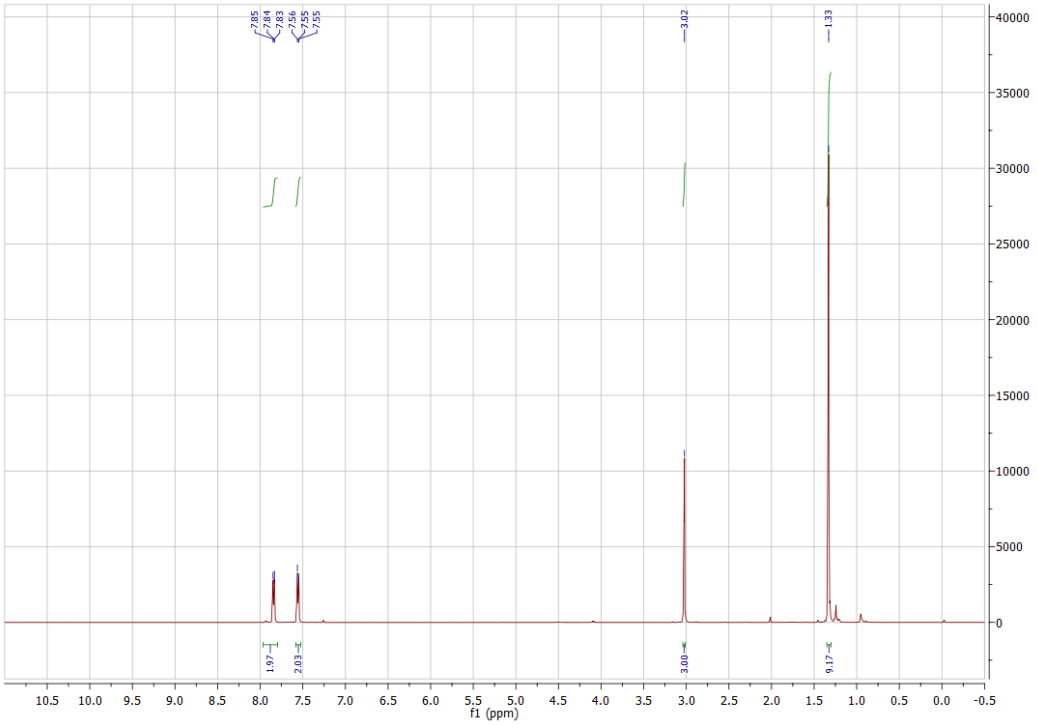


**Figure A7.29.** $^{1}$H NMR ($CDCl_3$, 500 MHz) spectrum of 1-(*tert*-Butyl)-4-(methylsulfonyl)benzene (**32**)

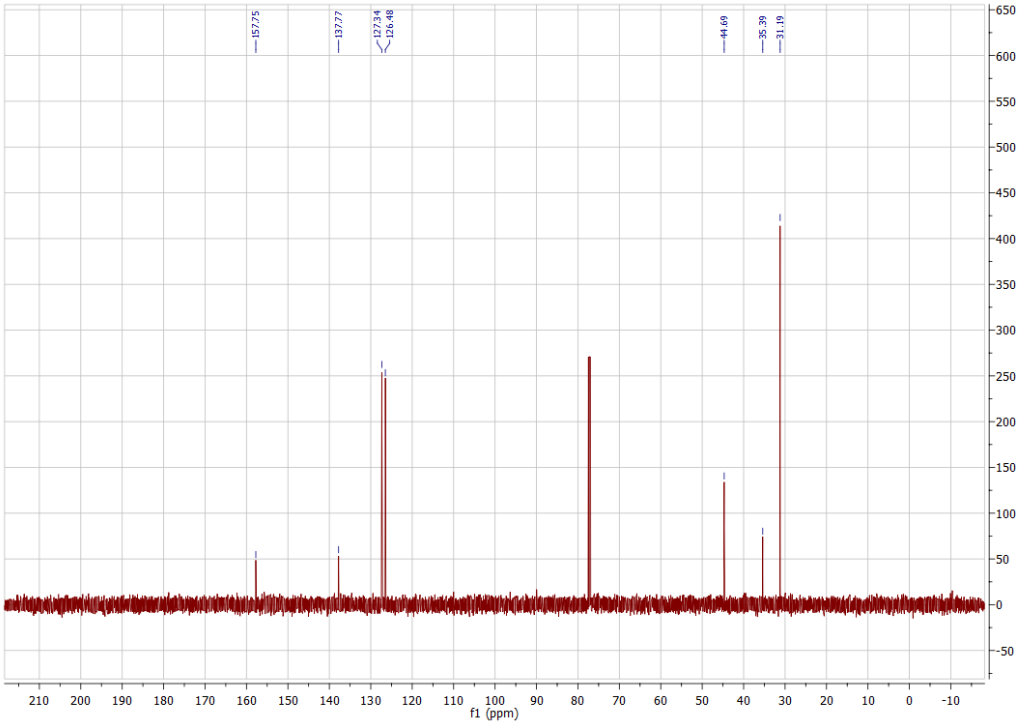


**Figure A7.30.** $^{13}$C NMR ($CDCl_3$, 125.8 MHz) spectrum of 1-(*tert*-Butyl)-4-(methylsulfonyl)benzene (**32**)

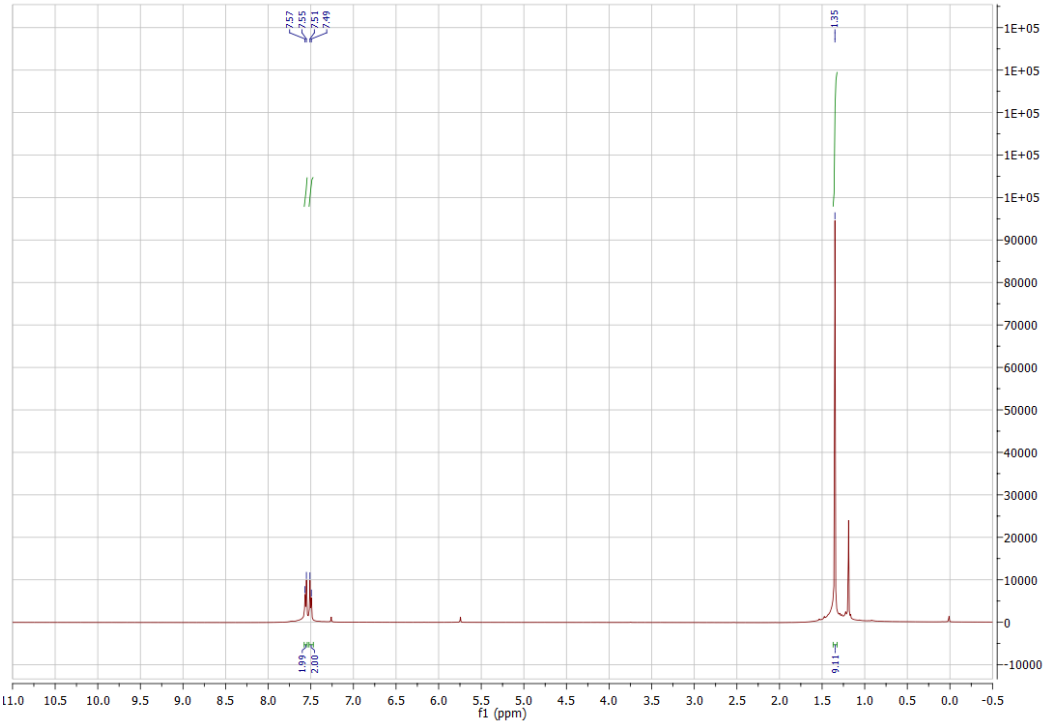


**Figure A7.31.** $^{1}H$ NMR ($CDCl_3$, 500 MHz) spectrum of 1-(tert-butyl)-4-(trifluoromethyl)benzene (**33**)

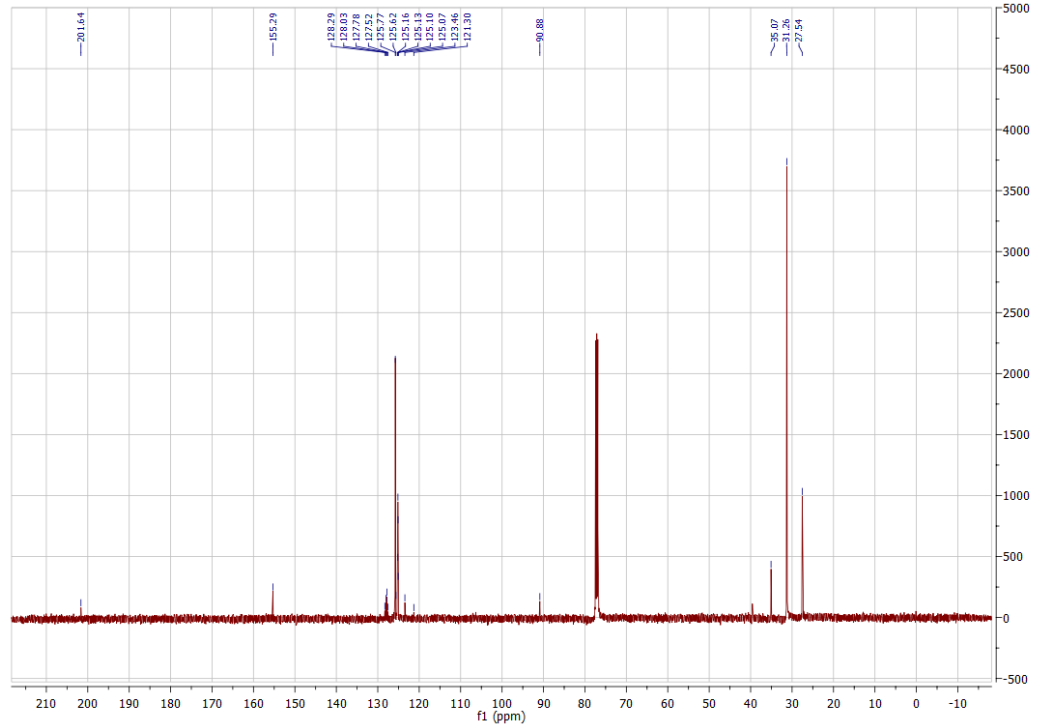


**Figure A7.32.** $^{13}C$ NMR ($CDCl_3$, 125.8 MHz) spectrum of 1-(tert-butyl)-4-(trifluoromethyl)benzene (**33**)

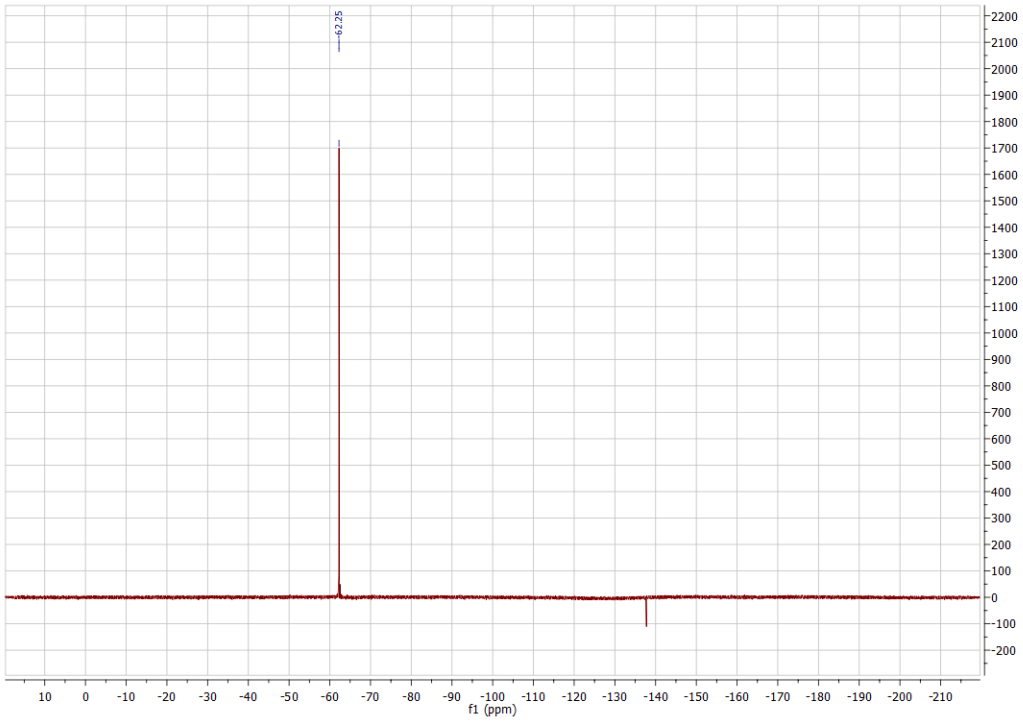


**Figure A7.33.** $^{19}F$ NMR ($CDCl_3$, 125.8 MHz) spectrum of 1-(tert-butyl)-4-(trifluoromethyl)benzene (**33**)

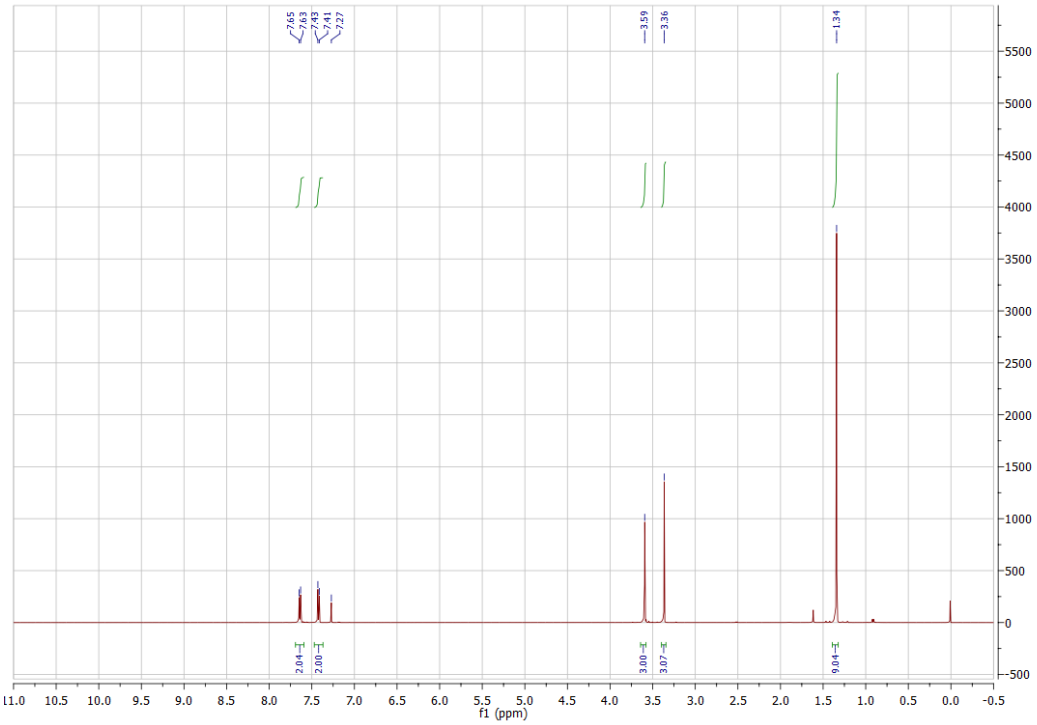


**Figure A7.34.** $^{1}H$ NMR ($CDCl_3$, 500 MHz) spectrum of 4-(tert-butyl)-N-methoxy-N-methylbenzamide (**34**)

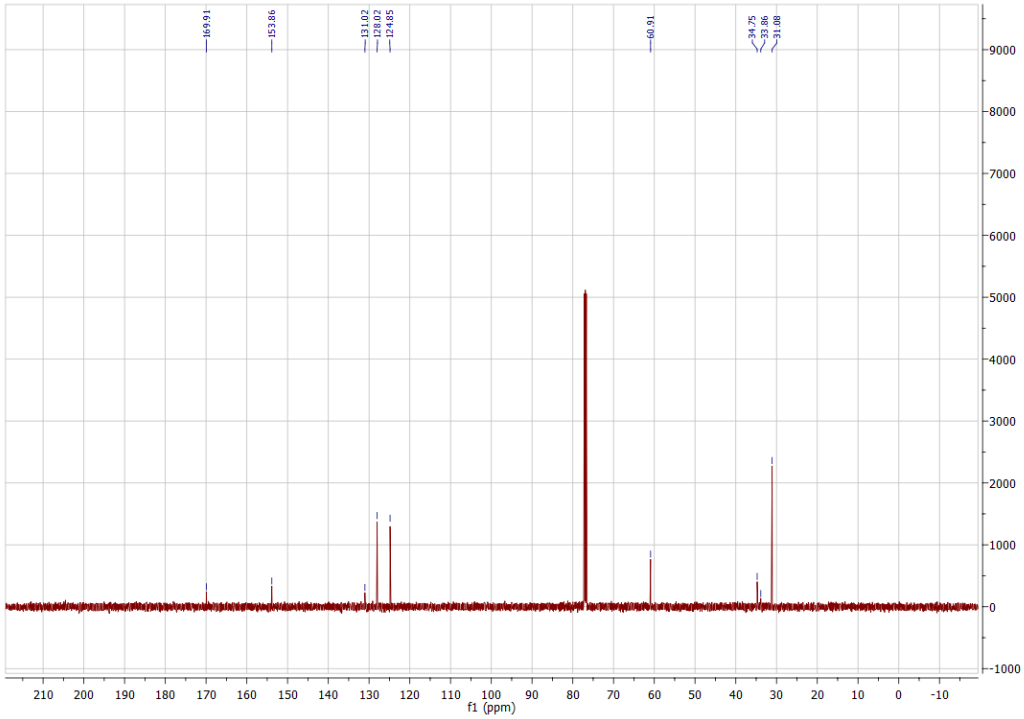


**Figure A7.35.** $^{13}C$ NMR ($CDCl_3$, 125.8 MHz) spectrum of 4-(tert-butyl)-N-methoxy-N-methylbenzamide (**34**)

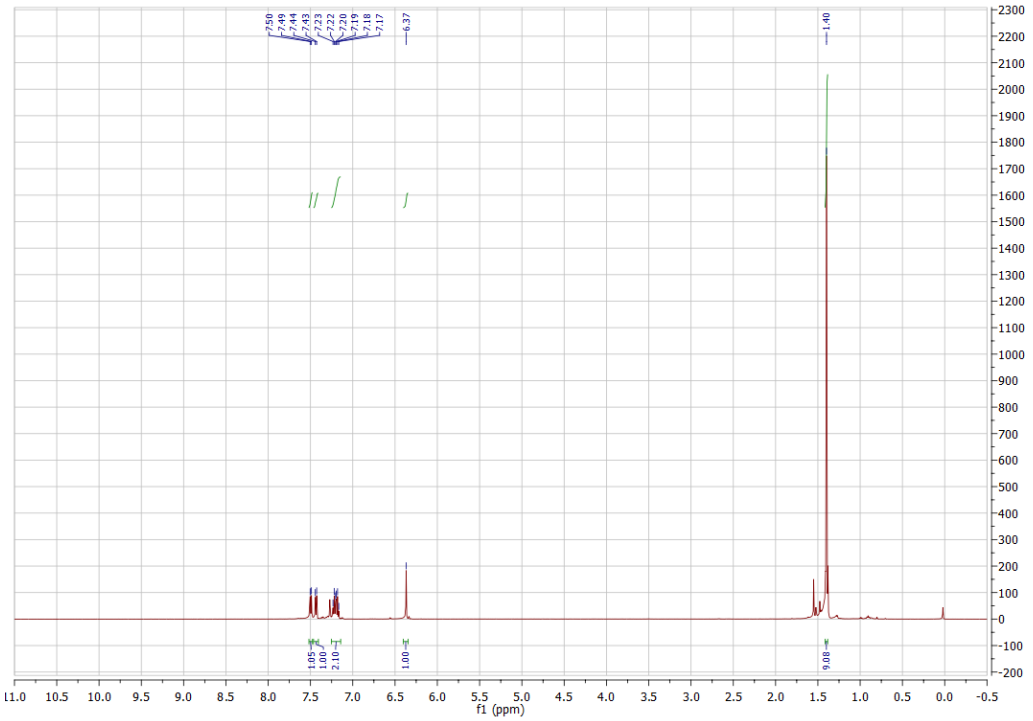


**Figure A7.36.** $^{1}H$ NMR ($CDCl_3$, 500 MHz) spectrum of 2-(*tert*-Butyl)benzofuran (**35**)

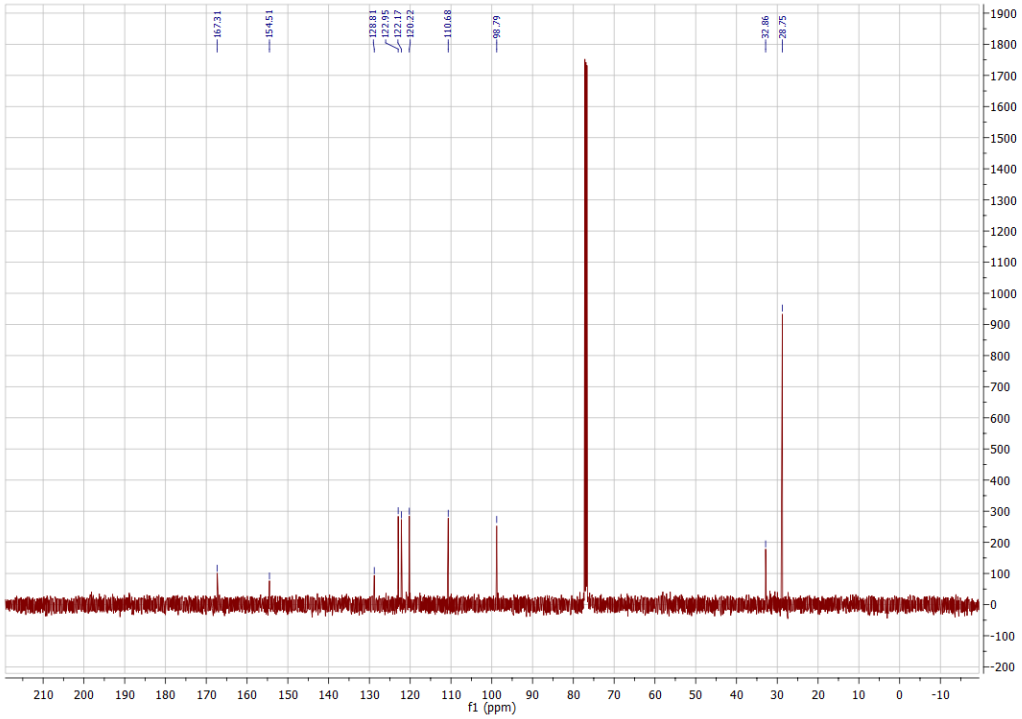


**Figure A7.37.** $^{13}C$ NMR ($CDCl_3$, 125.8 MHz) spectrum of 2-(*tert*-Butyl)benzofuran (**35**)

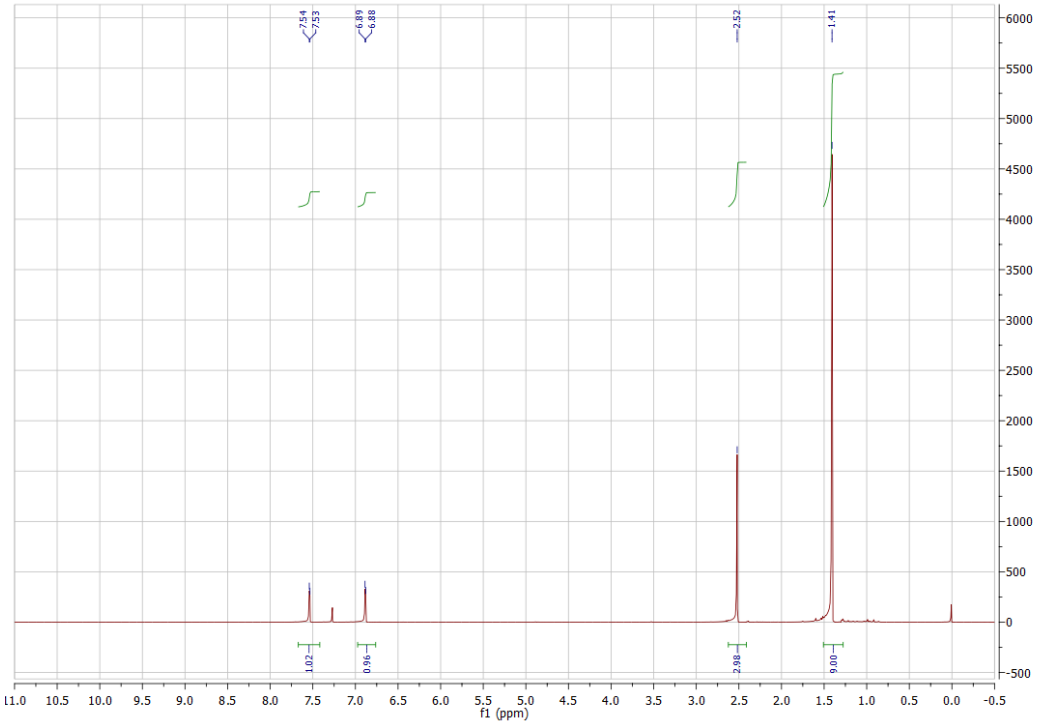


**Figure A7.38.** $^{1}H$ NMR ($CDCl_3$, 500 MHz) spectrum of 1-(5-(tert-butyl)thiophen-2-yl)ethan-1-one (**36**)

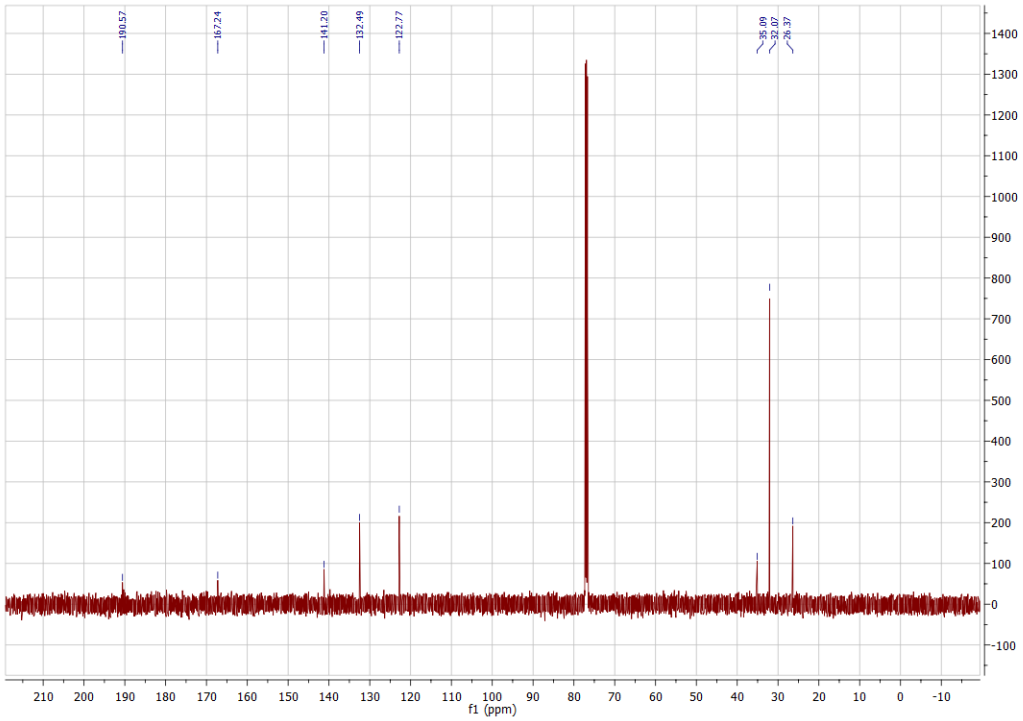


**Figure A7.39.** $^{13}C$ NMR ($CDCl_3$, 125.8 MHz) spectrum of 1-(5-(tert-butyl)thiophen-2-yl)ethan-1-one (**36**)

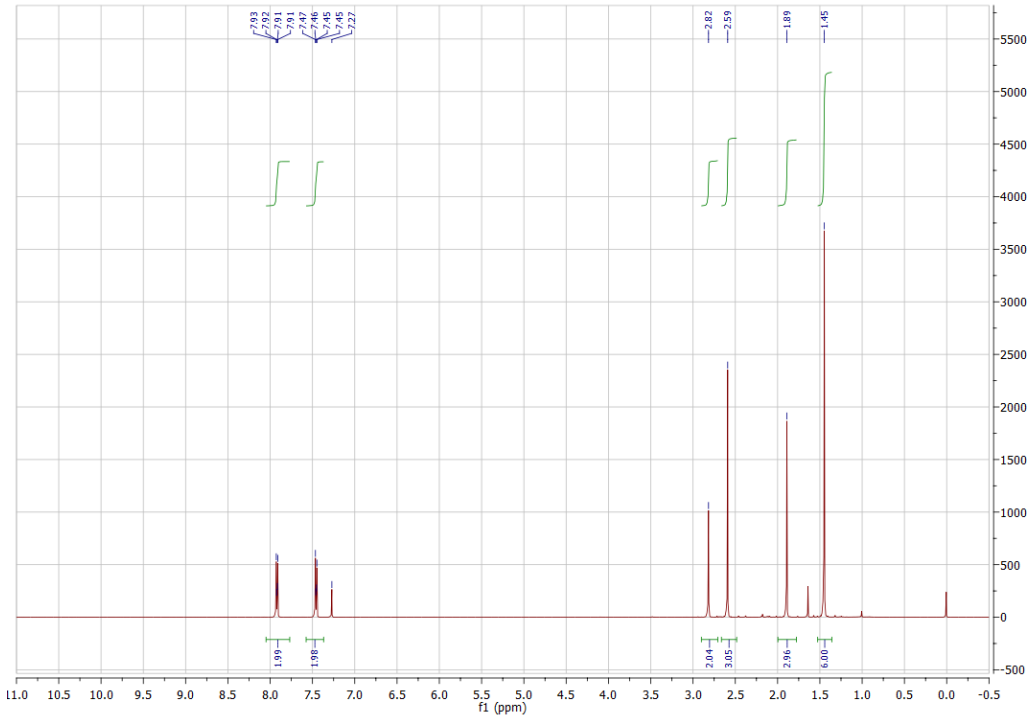


**Figure A7.40.** $^{1}H$ NMR ($CDCl_3$, 500 MHz) spectrum of 4-(4-Acetylphenyl)-4-methylpentan-2-one (**39**)

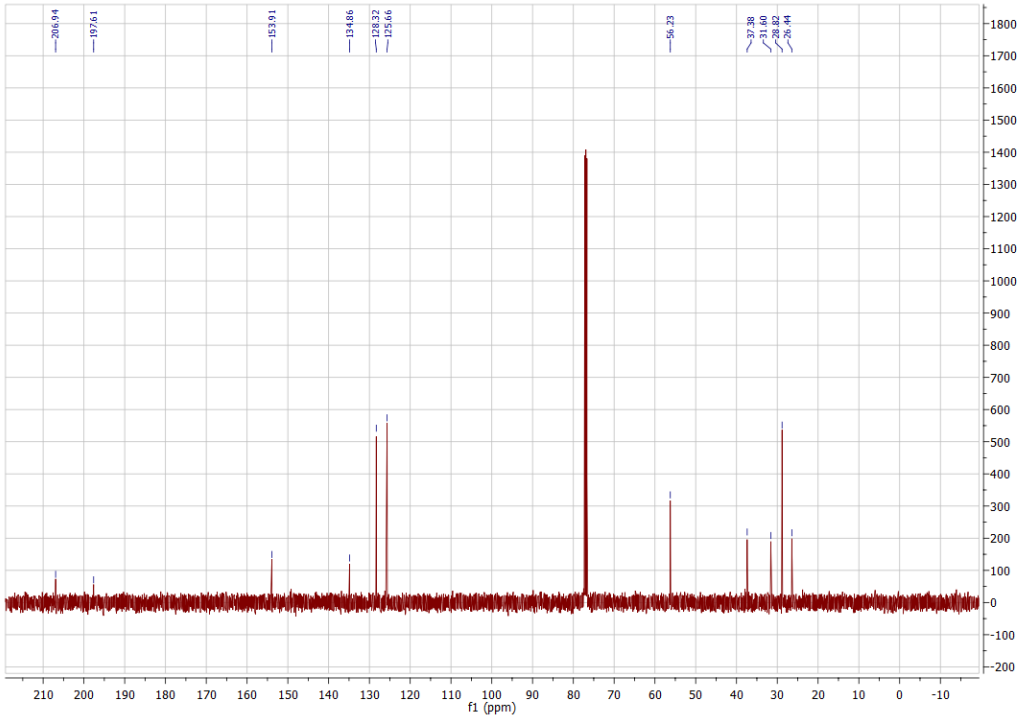


**Figure A7.41.** $^{13}C$ NMR ($CDCl_3$, 125.8 MHz) spectrum of 4-(4-Acetylphenyl)-4-methylpentan-2-one (**39**)

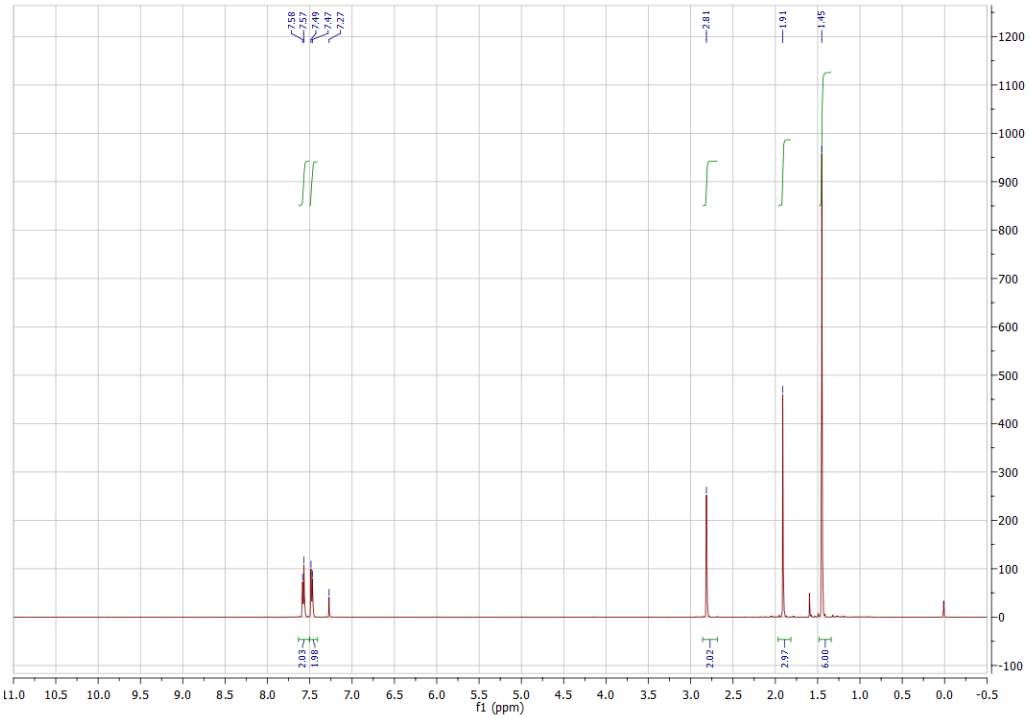


**Figure A7.42.** $^{1}H$ NMR ($CDCl_3$, 500 MHz) spectrum of 4-Methyl-4-(4-(trifluoromethyl)phenyl)pentan-2-one (**40**)

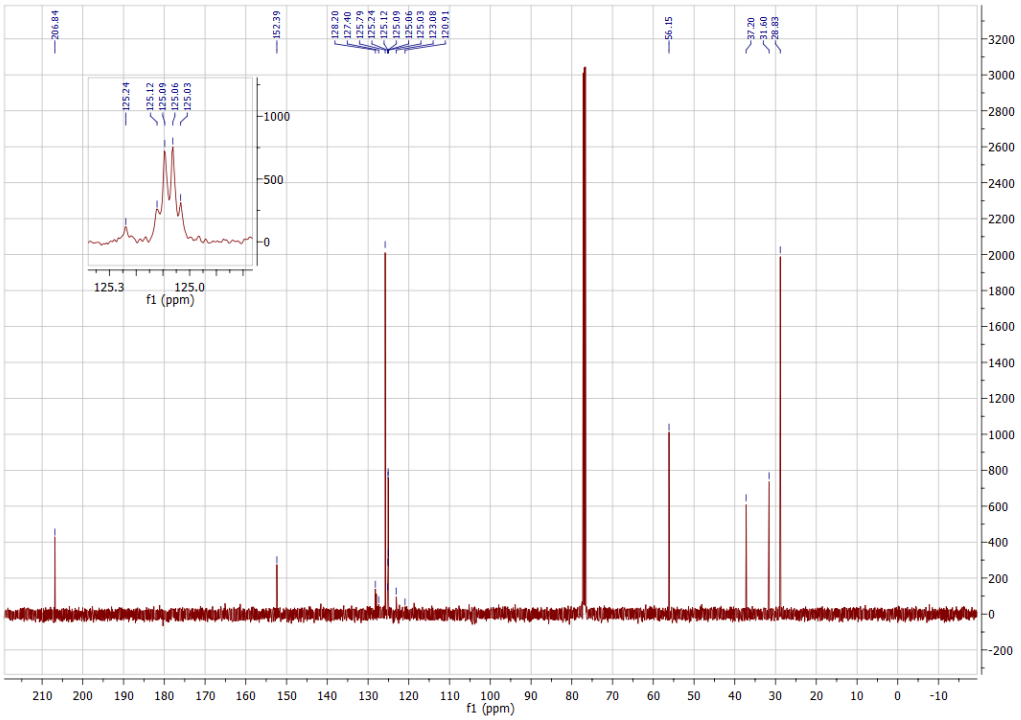


**Figure A7.43.** $^{13}C$ NMR ($CDCl_3$, 125.8 MHz) spectrum of 4-Methyl-4-(4-(trifluoromethyl)phenyl)pentan-2-one (**40**)

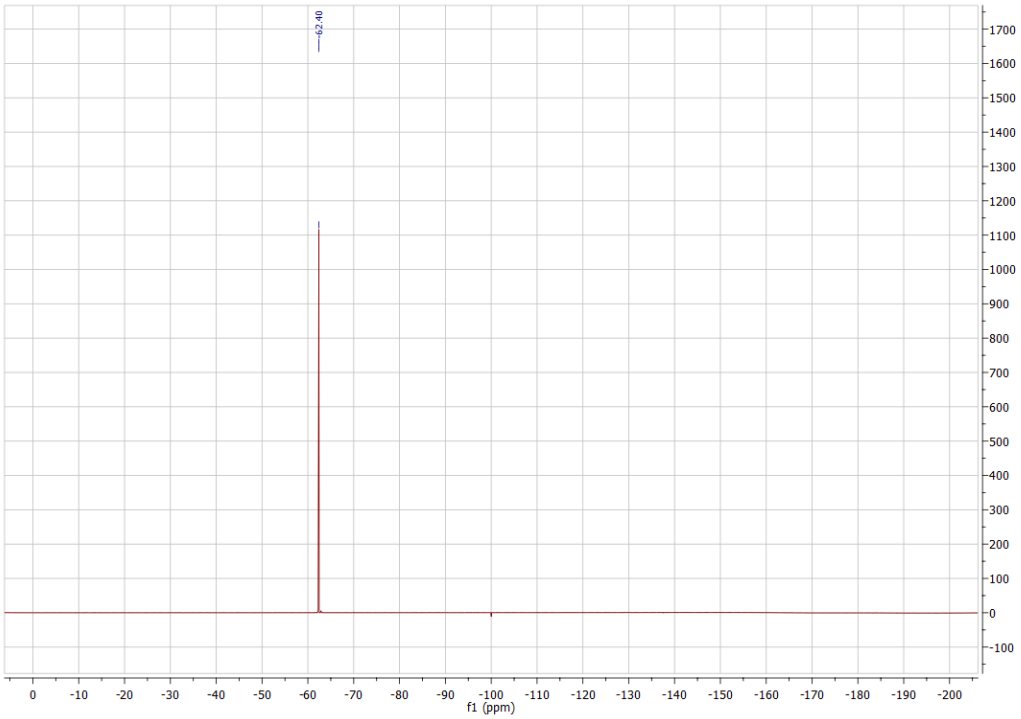


**Figure A7.44.** $^{19}F$ NMR ($CDCl_3$, 470.8 MHz) spectrum of 4-Methyl-4-(4-(trifluoromethyl)phenyl)pentan-2-one (**40)**

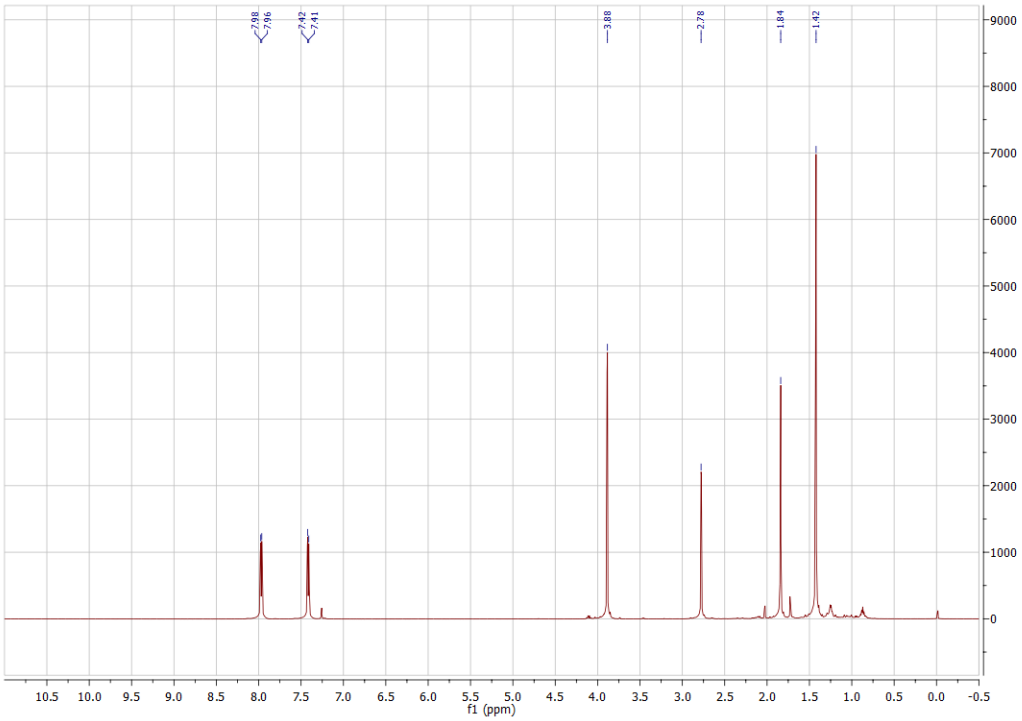


**Figure A7.45.** $^{1}$H NMR ($CDCl_3$, 500 MHz) spectrum of Methyl 4-(2-methyl-4-oxopentan-2-yl)benzoate (**41**)

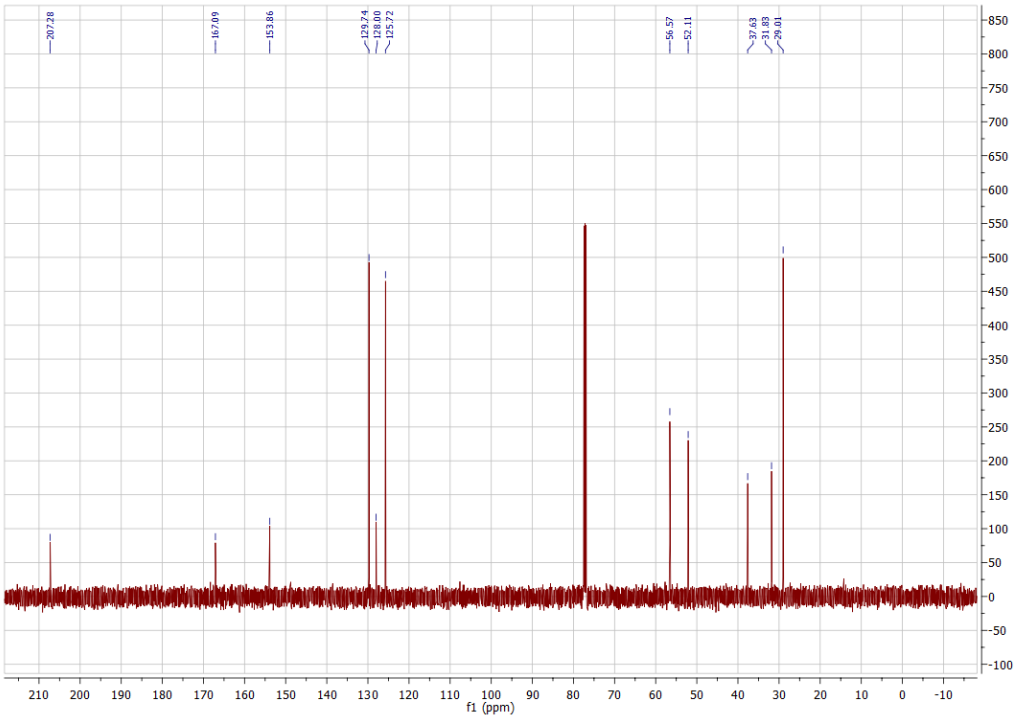


**Figure A7.46.** $^{13}$C NMR ($CDCl_3$, 125.8 MHz) spectrum of Methyl 4-(2-methyl-4-oxopentan-2-yl)benzoate (**41**)

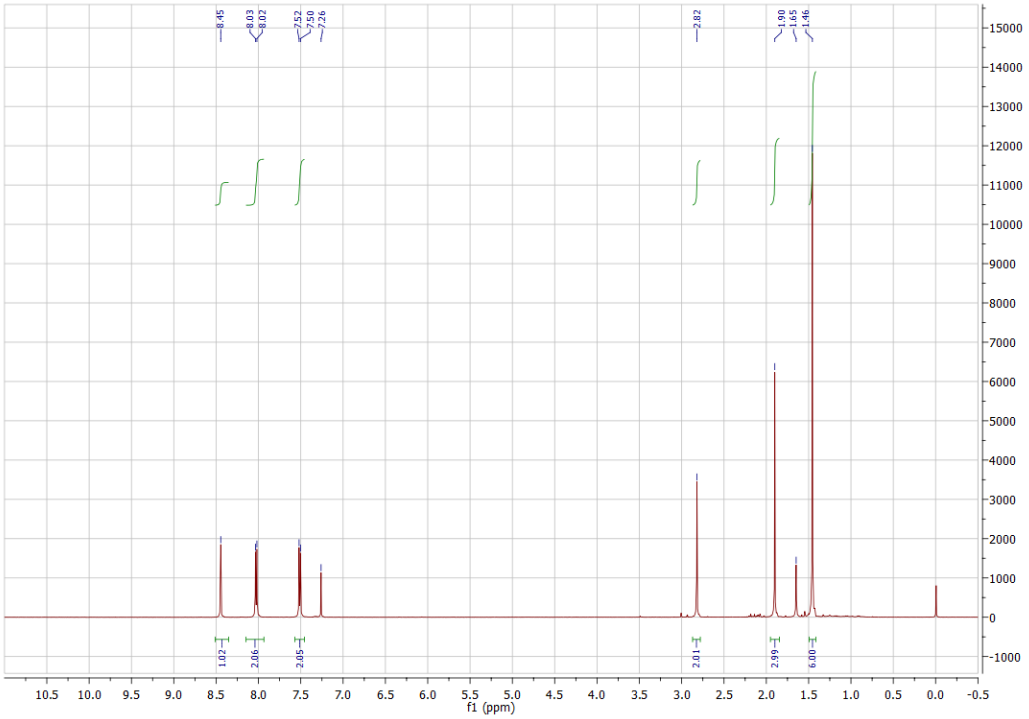


**Figure A7.47.** $^{1}$H NMR ($CDCl_3$, 500 MHz) spectrum of 4-(4-(1,3,4-Oxadiazol-2-yl)phenyl)-4-methylpentan-2-one (**42)**

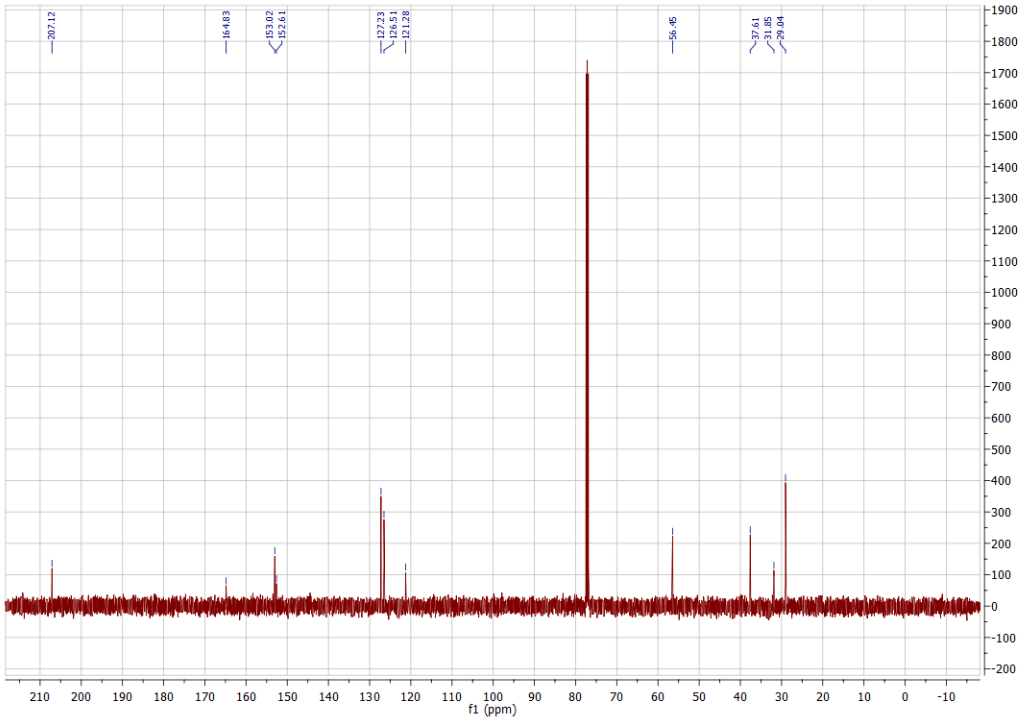


**Figure A7.48.** $^{13}$C NMR ($CDCl_3$, 125.8 MHz) spectrum of 4-(4-(1,3,4-Oxadiazol-2-yl)phenyl)-4-methylpentan-2-one (**42**)

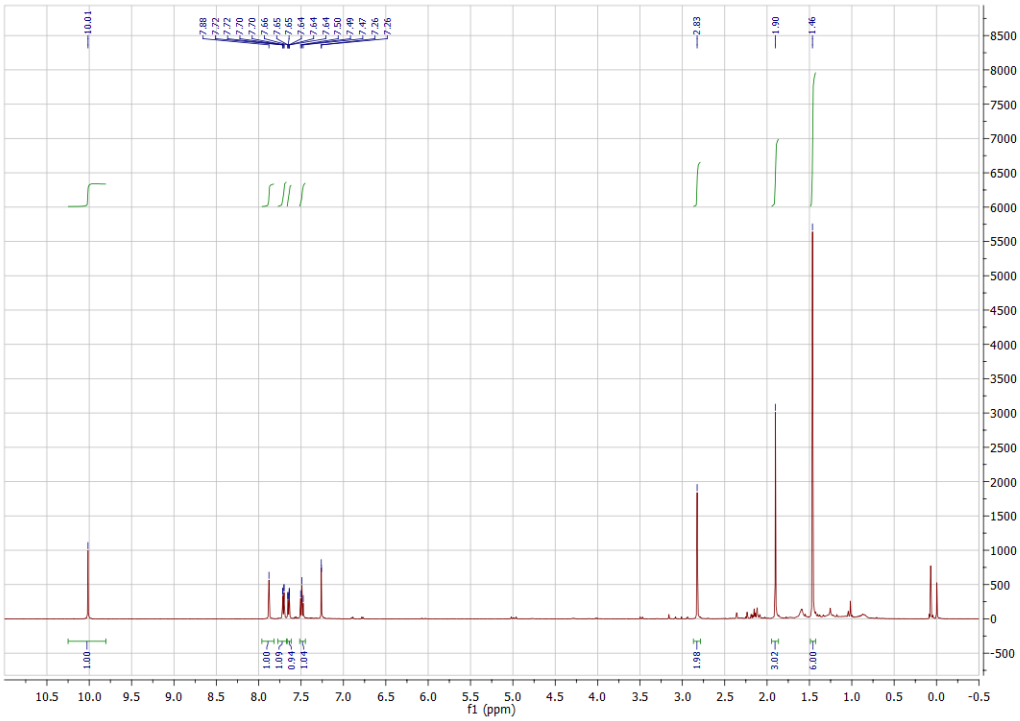


**Figure A7.49.** $^{1}$H NMR ($CDCl_3$, 500 MHz) spectrum of 3-(2-Methyl-4-oxopentan-2-yl)benzaldehyde (**43**)

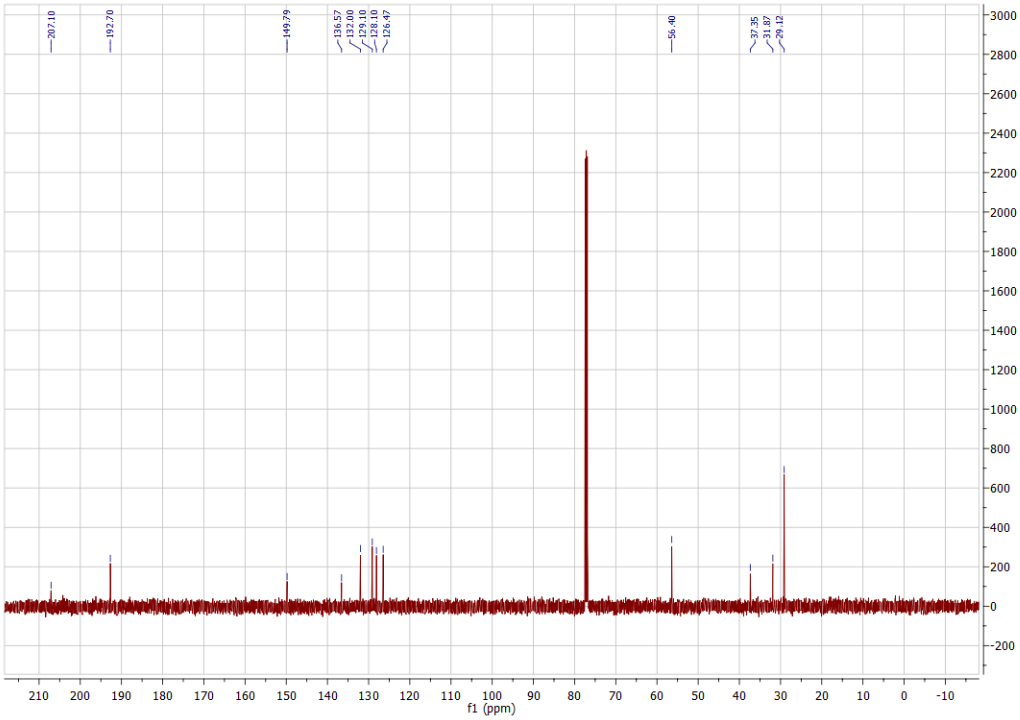


**Figure A7.50.** $^{13}$C NMR ($CDCl_3$, 125.8 MHz) spectrum of 3-(2-Methyl-4-oxopentan-2-yl)benzaldehyde (**43**)

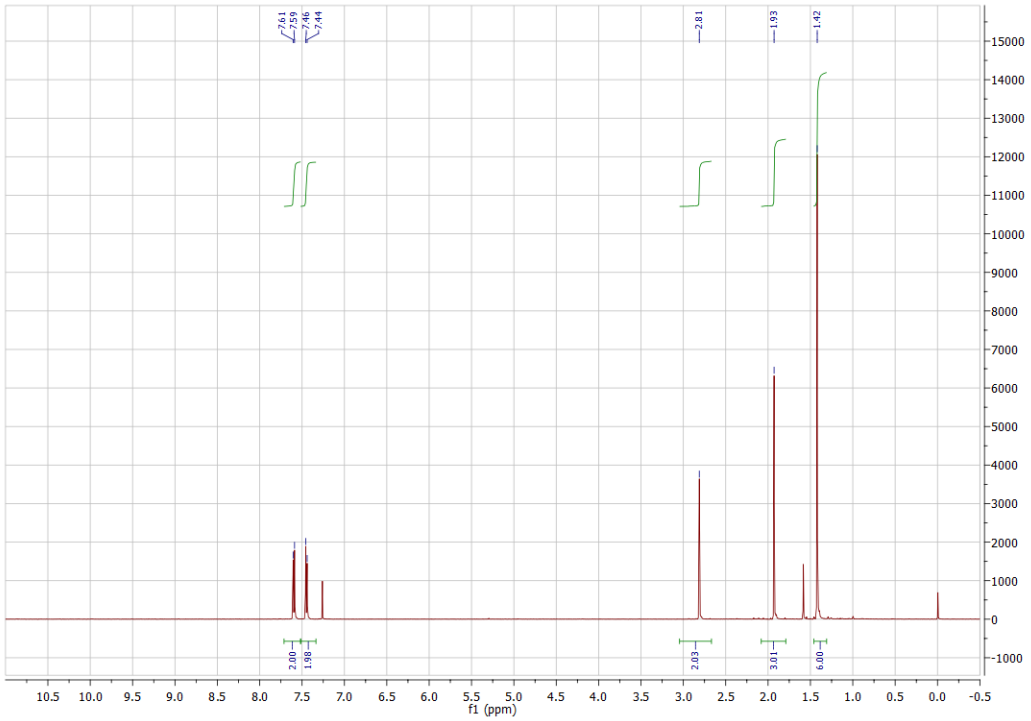


**Figure A7.51.** $^{1}$H NMR ($CDCl_3$, 500 MHz) spectrum of 4-(2-Methyl-4-oxopentan-2-yl)benzonitrile (**44**)

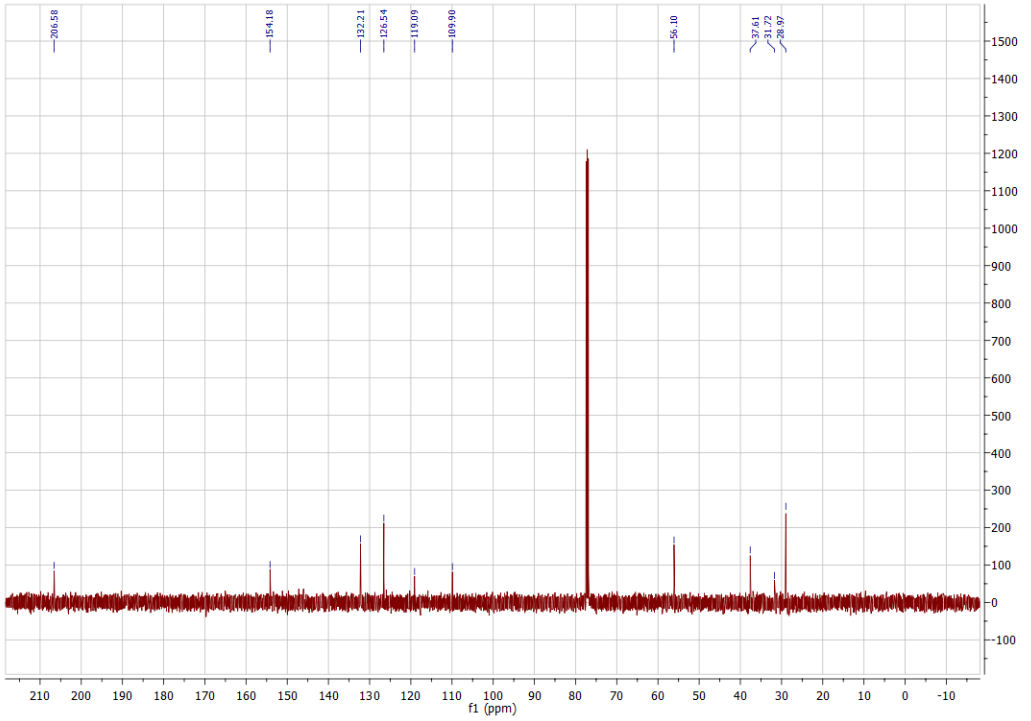


**Figure A7.52.** $^{13}$C NMR ($CDCl_3$, 125.8 MHz) spectrum of 4-(2-Methyl-4-oxopentan-2-yl)benzonitrile (**44**)

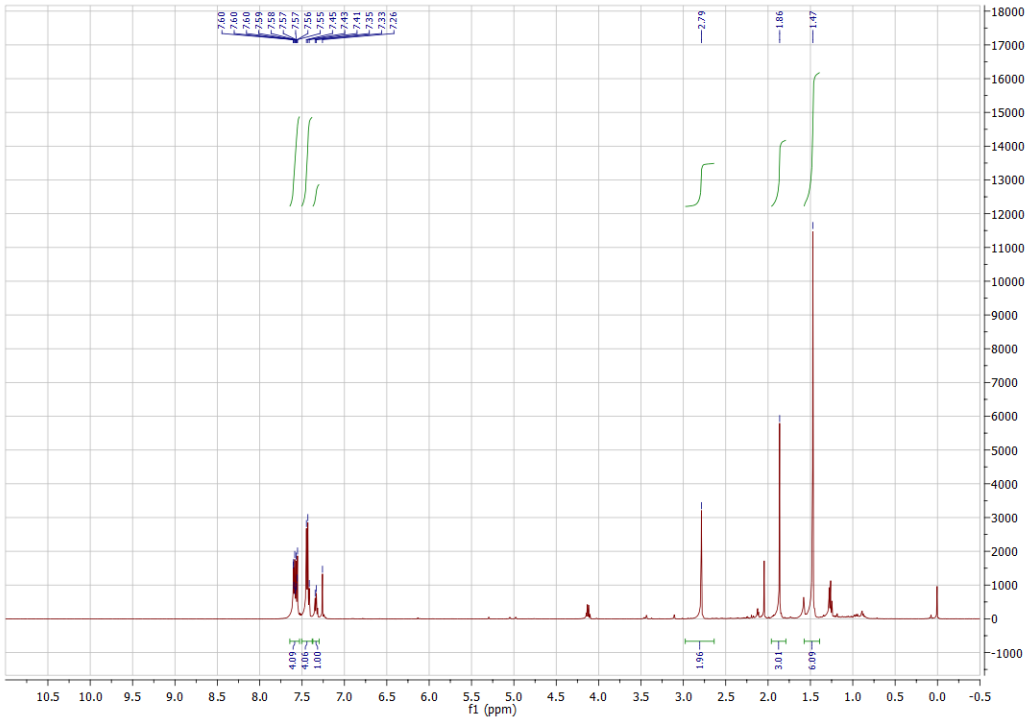


**Figure A7.53.** $^{1}$H NMR ($CDCl_3$, 500 MHz) spectrum of 4-([1,1'-Biphenyl]-4-yl)-4-methylpentan-2-one (**45**)

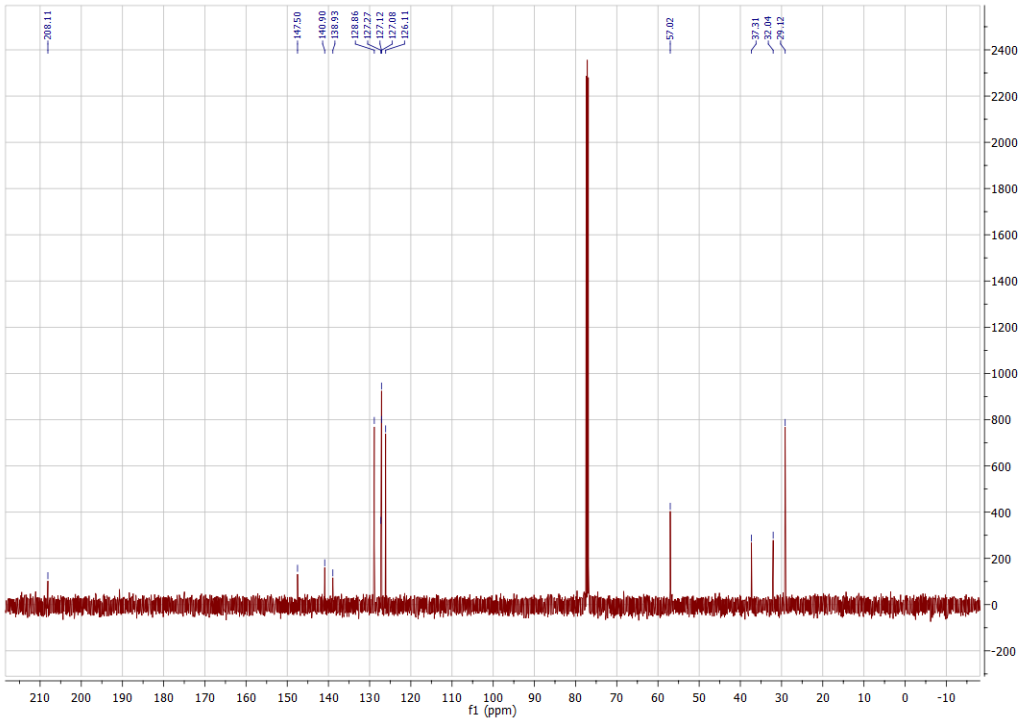


**Figure A7.54.** $^{13}$C NMR ($CDCl_3$, 125.8 MHz) spectrum of 4-([1,1'-Biphenyl]-4-yl)-4-methylpentan-2-one (**45**)

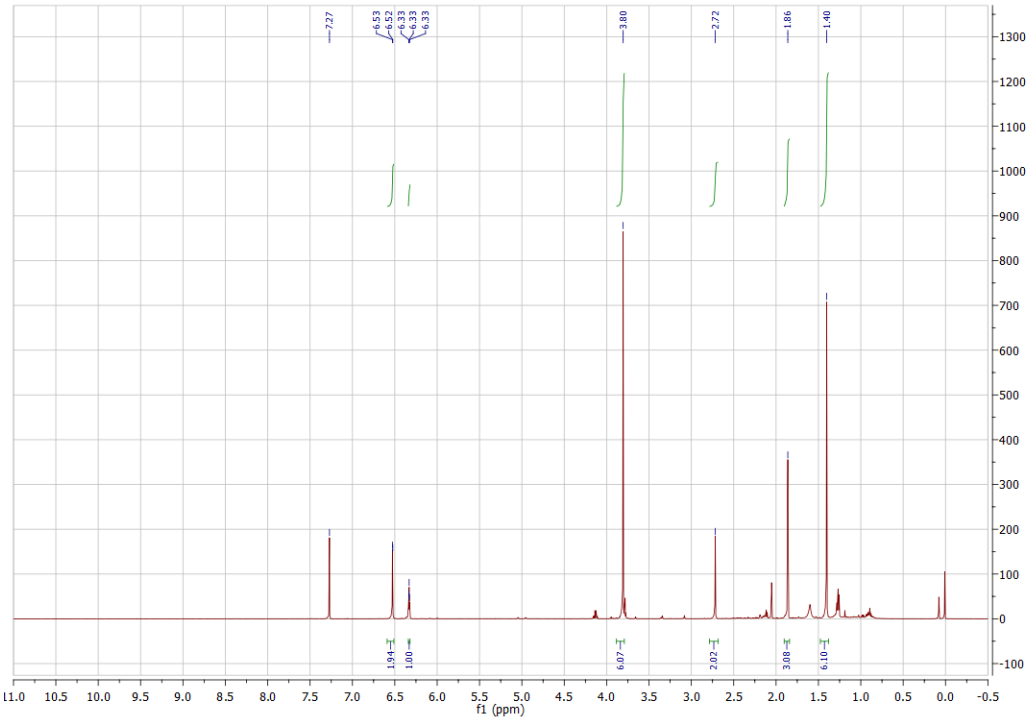


**Figure A7.55.** $^{1}$H NMR ($CDCl_3$, 500 MHz) spectrum of 4-(3,5-Dimethoxyphenyl)-4-methylpentan-2-one (**46**)

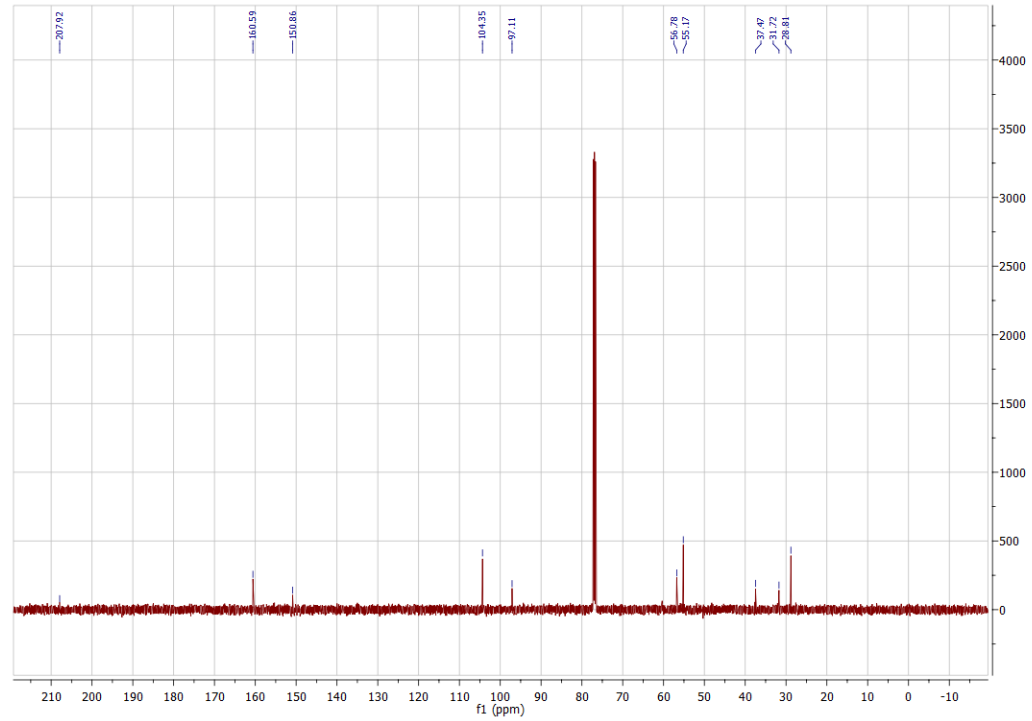


**Figure A7.56.** $^{13}$C NMR ($CDCl_3$, 125.8 MHz) spectrum of 4-(3,5-Dimethoxyphenyl)-4-methylpentan-2-one (**46**)

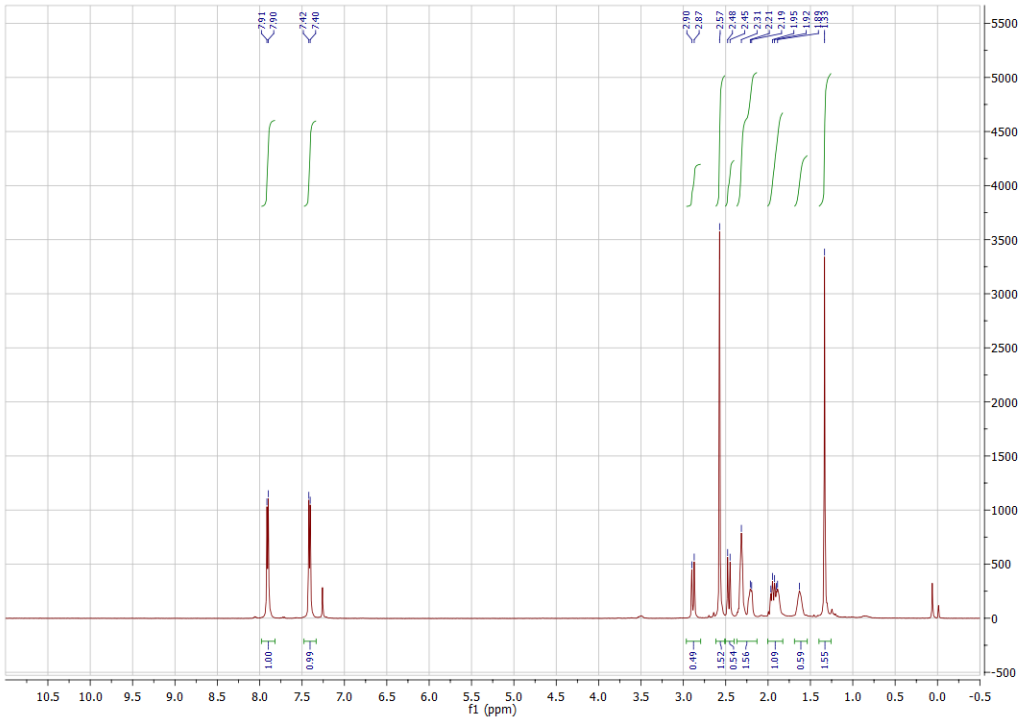


**Figure A7.57.** $^{1}$H NMR ($CDCl_3$, 500 MHz) spectrum of 3-(4-acetylphenyl)-3-methylcyclohexan-1-one (**48**)

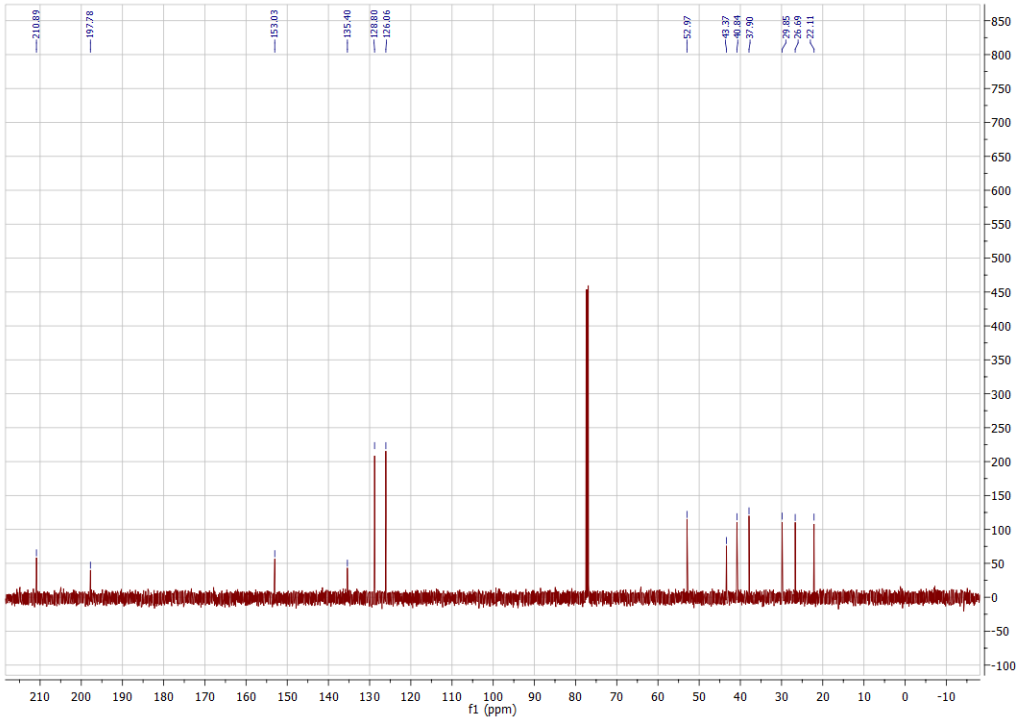


**Figure A7.58.** $^{13}$C NMR ($CDCl_3$, 125.8 MHz) spectrum of 3-(4-acetylphenyl)-3-methylcyclohexan-1-one (**48**)

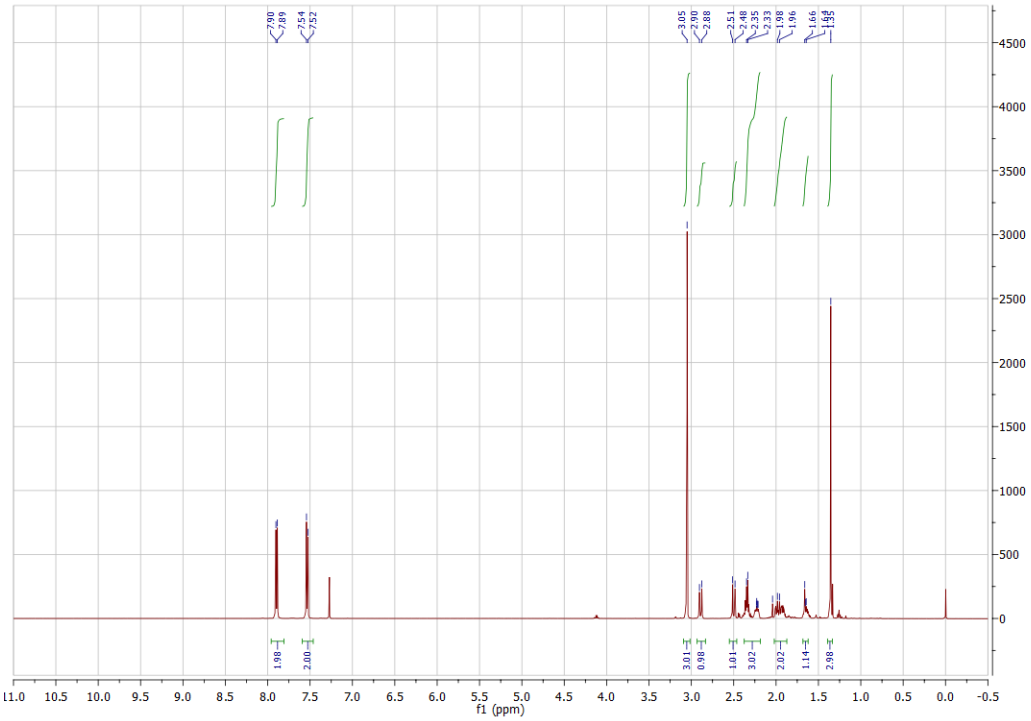


**Figure A7.59.** $^{1}$H NMR ($CDCl_3$, 500 MHz) spectrum of 3-methyl-3-(4-(methylsulfonyl)phenyl)cyclohexan-1-one (**49**)

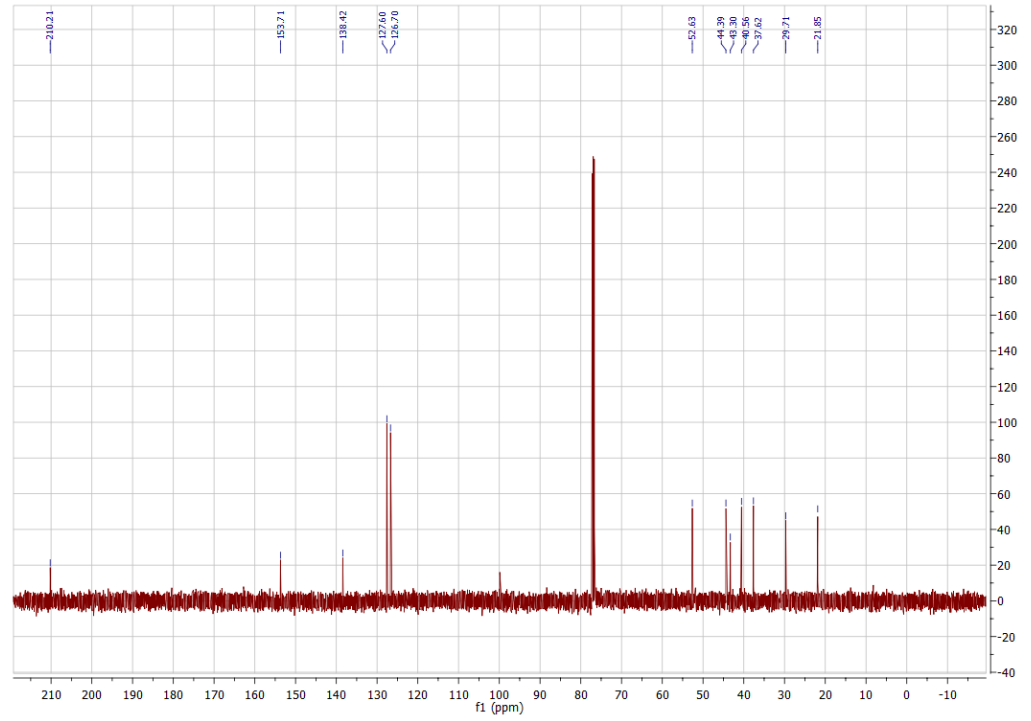


**Figure A7.60.** $^{13}$C NMR ($CDCl_3$, 125.8 MHz) spectrum of 3-methyl-3-(4-(methylsulfonyl)phenyl)cyclohexan-1-one (**49**)

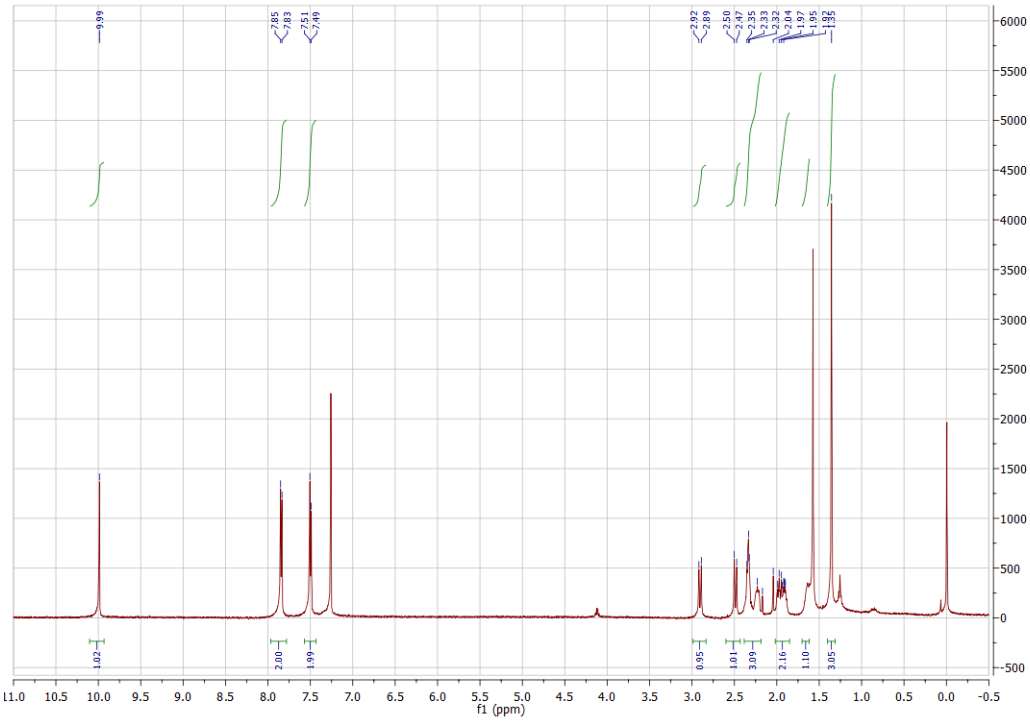

**Figure A7.61.** $^{1}$H NMR ($CDCl_3$, 500 MHz) spectrum of 4-(1-Methyl-3-oxocyclohexyl)benzaldehyde (**50**)

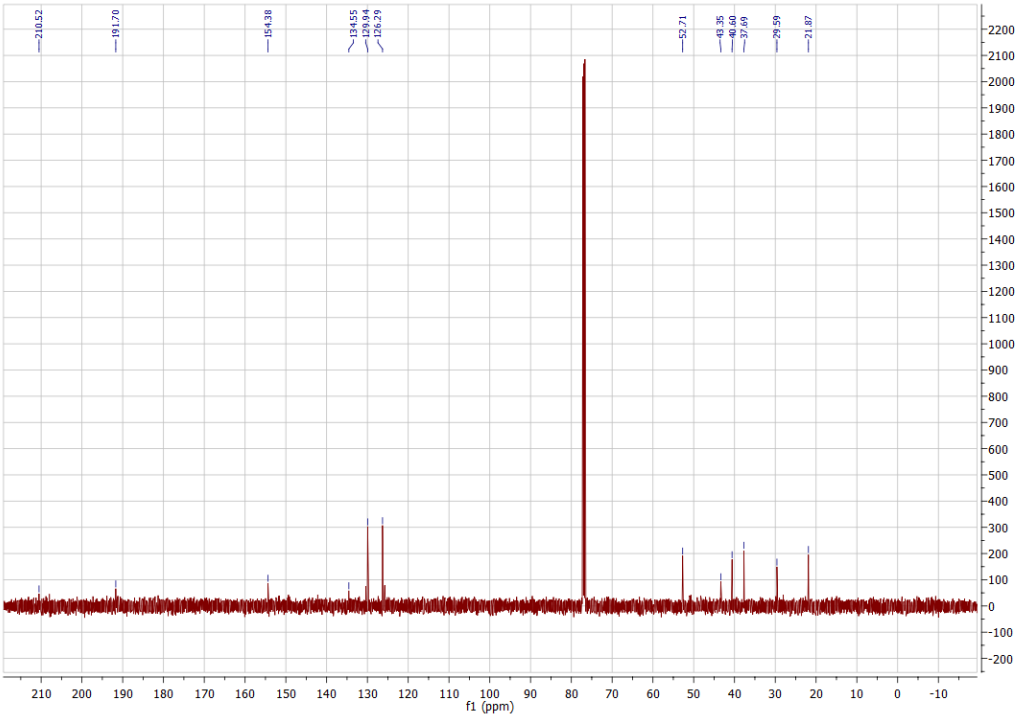

**Figure A7.62.** $^{13}$C NMR ($CDCl_3$, 125.8 MHz) spectrum of 4-(1-Methyl-3-oxocyclohexyl)benzaldehyde (**50**)

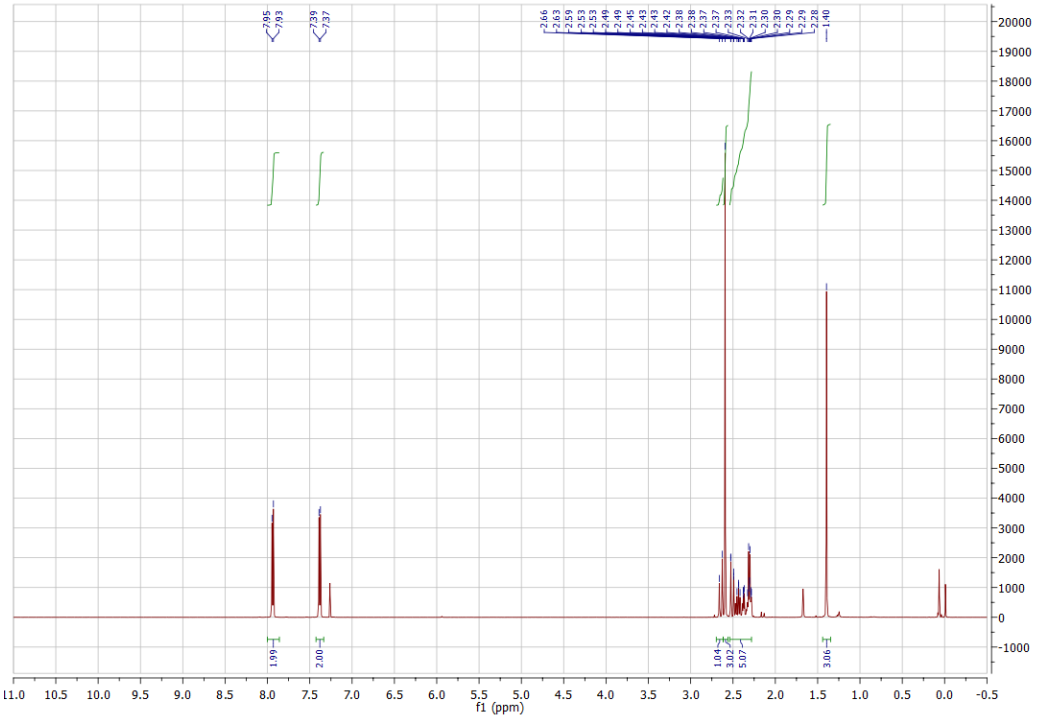


**Figure A7.63.** $^{1}$H NMR ($CDCl_3$, 500 MHz) spectrum of 3-(4-Acetylphenyl)-3-methylcyclopentan-1-one (**51**)

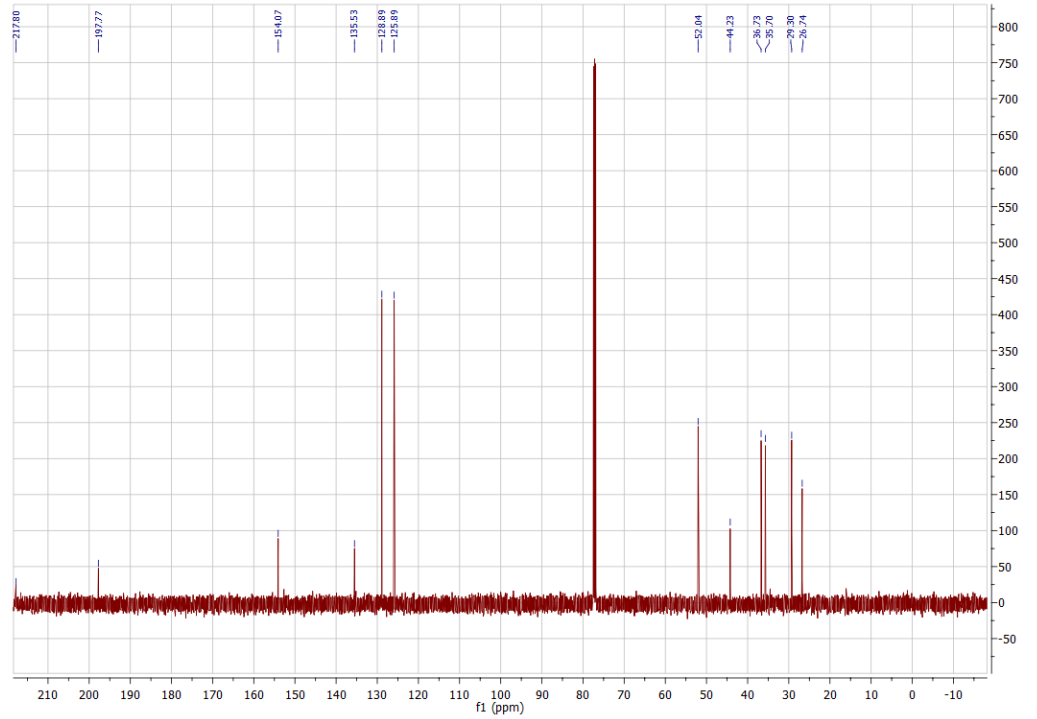


**Figure A7.64.** $^{13}$C NMR ($CDCl_3$, 125.8 MHz) spectrum of 3-(4-Acetylphenyl)-3-methylcyclopentan-1-one (**51**)

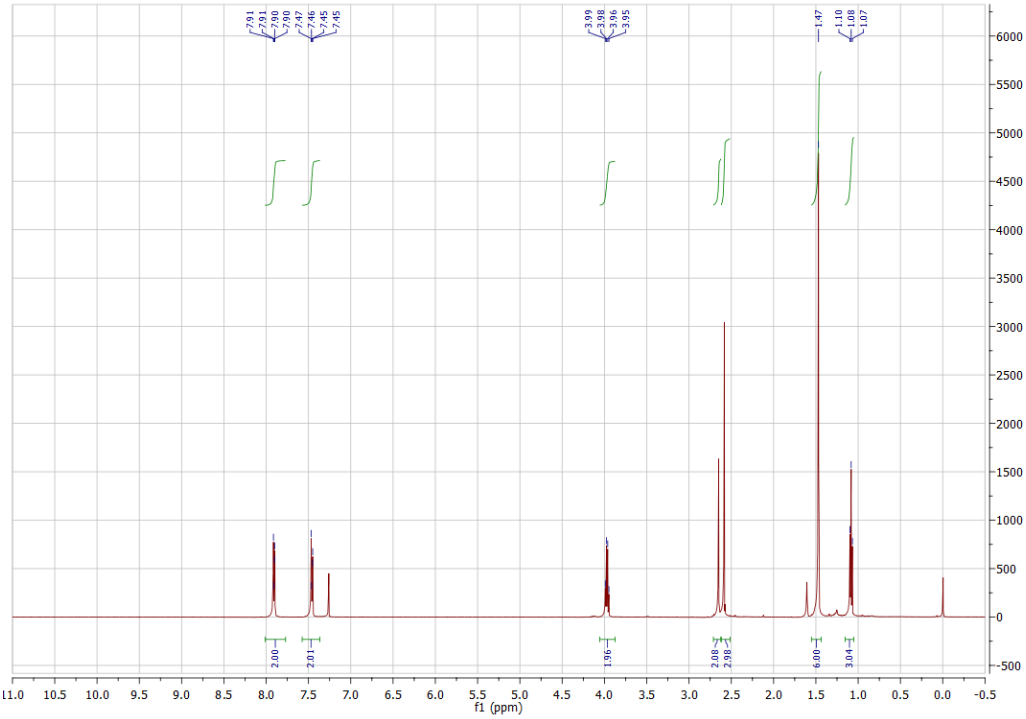


**Figure A7.65.** $^{1}$H NMR ($CDCl_3$, 500 MHz) spectrum of ethyl 3-(4-acetylphenyl)-3-methylbutanoate (**52**)

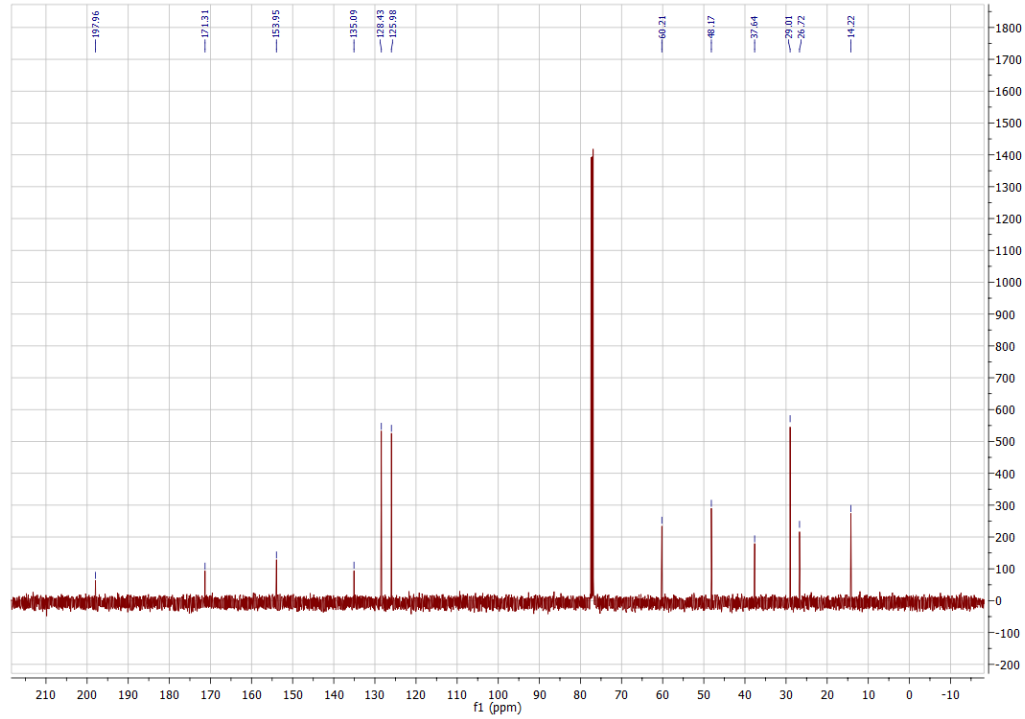


**Figure A7.66.** $^{13}$C NMR ($CDCl_3$, 125.8 MHz) spectrum of ethyl 3-(4-acetylphenyl)-3-methylbutanoate (**52**)

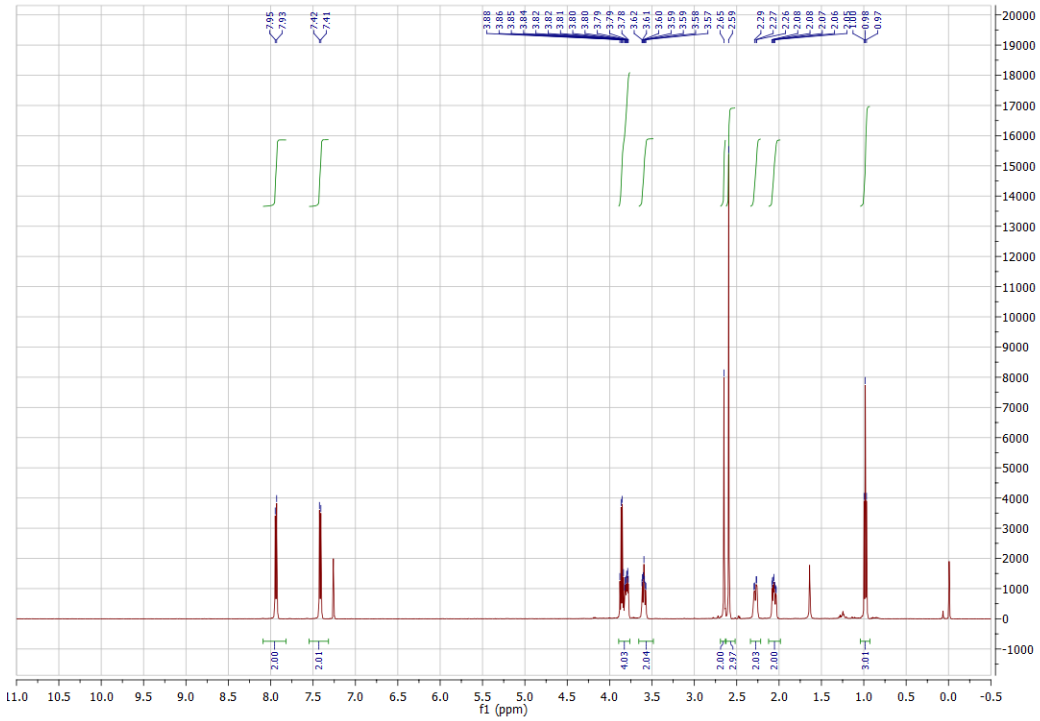

**Figure A7.67.** $^{1}$H NMR ($CDCl_3$, 500 MHz) spectrum of ethyl 2-(4-(4-acetylphenyl)tetrahydro-2H-pyran-4-yl)acetate (**53**)

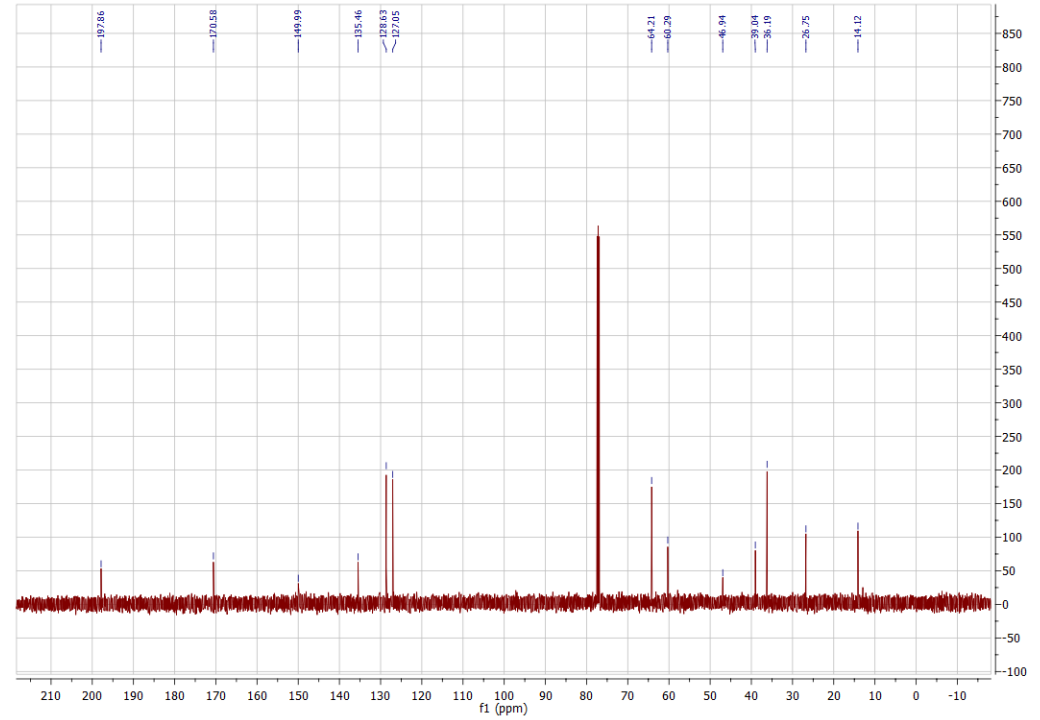

**Figure A7.68.** $^{13}$C NMR ($CDCl_3$, 125.8 MHz) spectrum of ethyl 2-(4-(4-acetylphenyl)tetrahydro-2H-pyran-4-yl)acetate (**53**)

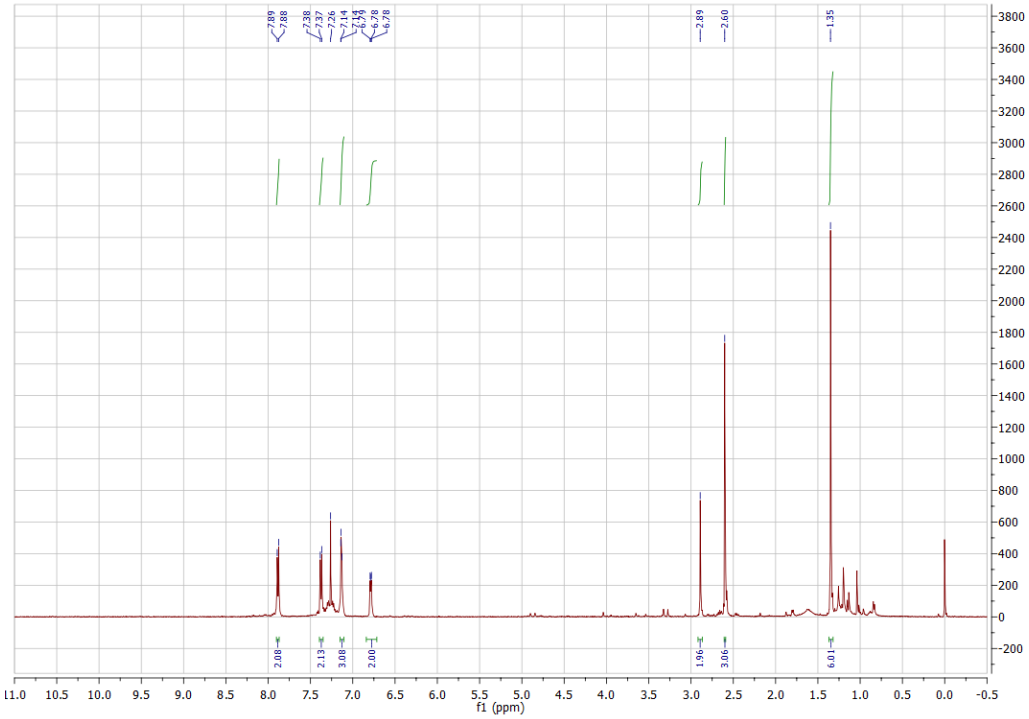


**Figure A7.69.** $^{1}$H NMR ($CDCl_3$, 500 MHz) spectrum of XX (**54**)

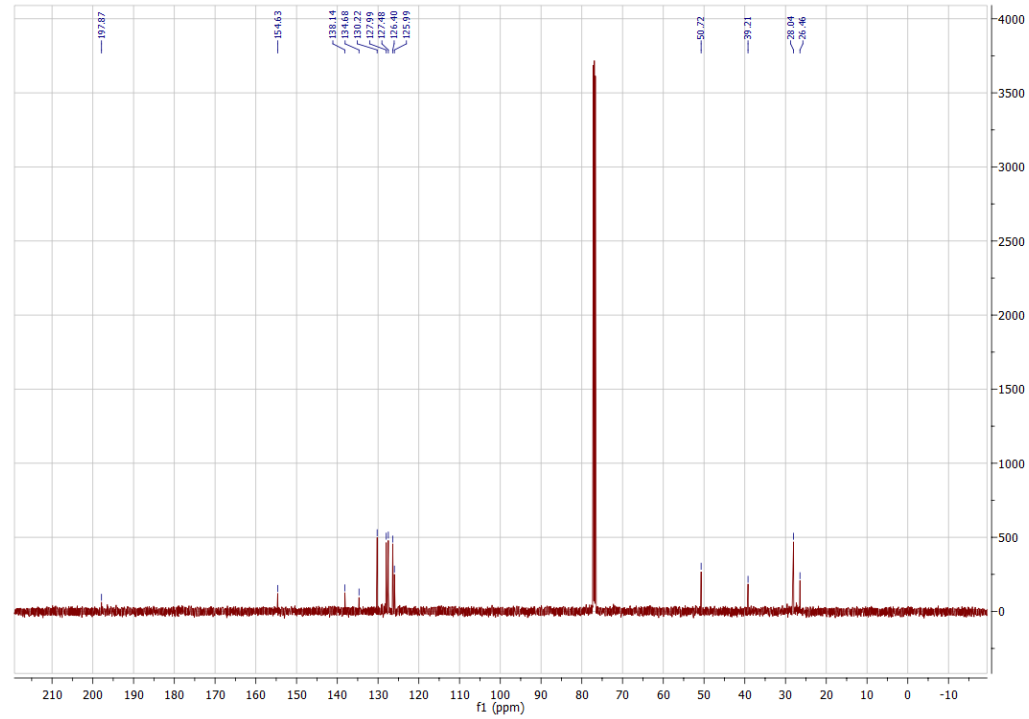


**Figure A7.70.** $^{13}$C NMR ($CDCl_3$, 125.8 MHz) spectrum of XX (**54**)

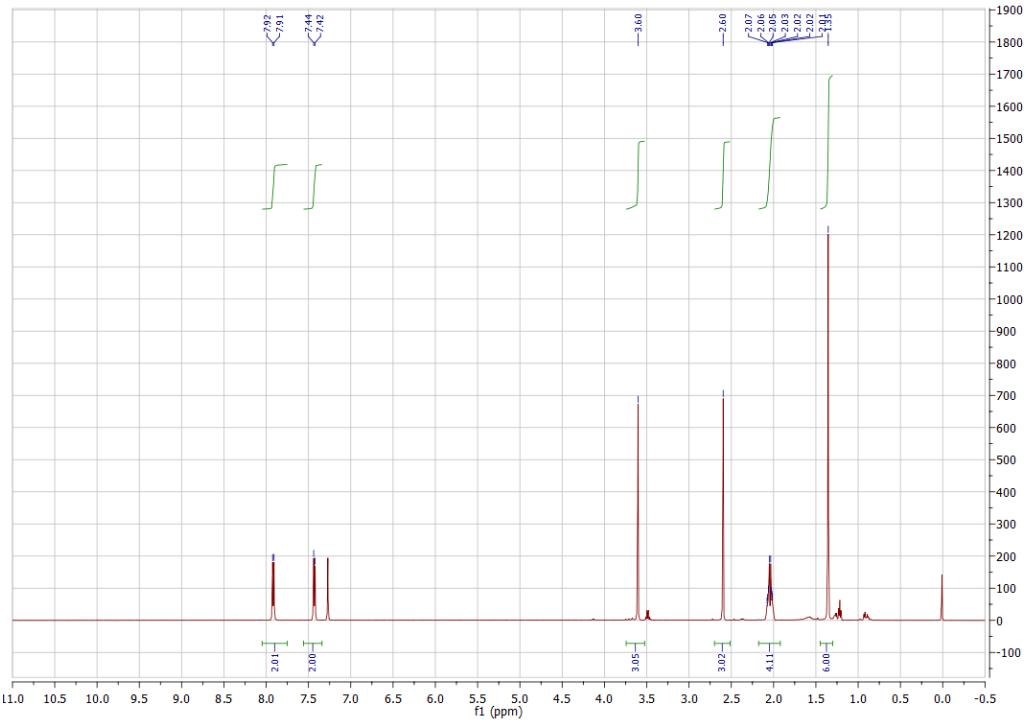


**Figure A7.71.** $^{1}$H NMR ($CDCl_3$, 500 MHz) spectrum of methyl 4-(4-acetylphenyl)-4-methylpentanoate (**55**)

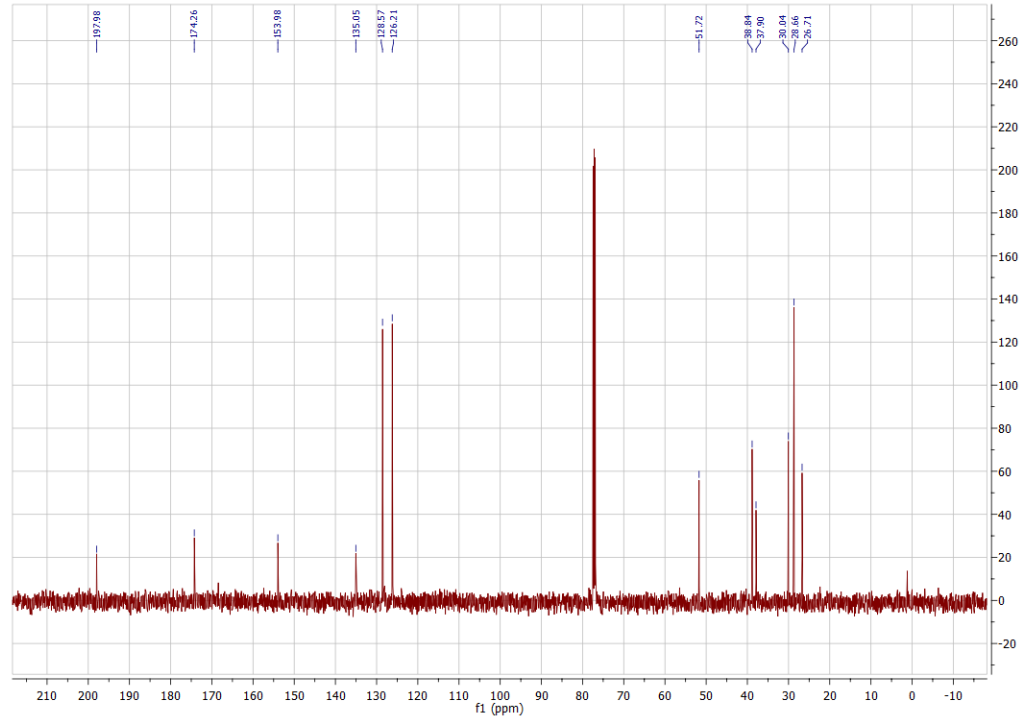


**Figure A7.72.** $^{13}$C NMR ($CDCl_3$, 125.8 MHz) spectrum of methyl 4-(4-acetylphenyl)-4-methylpentanoate (**55**)

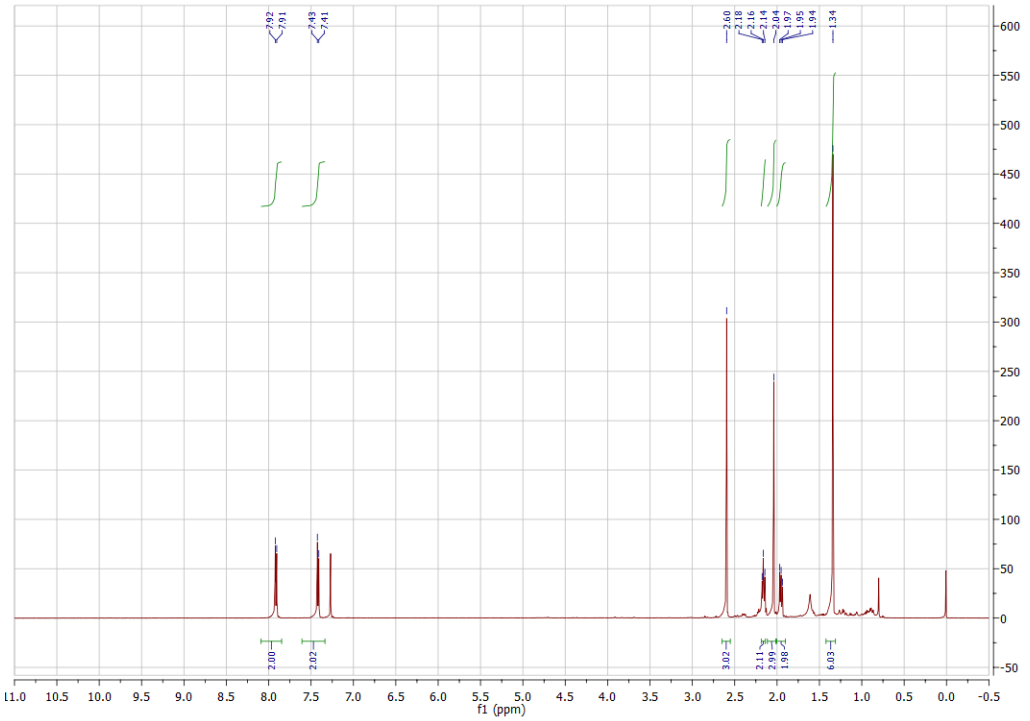


**Figure A7.73.** $^{1}$H NMR ($CDCl_3$, 500 MHz) spectrum of XX (**56**)

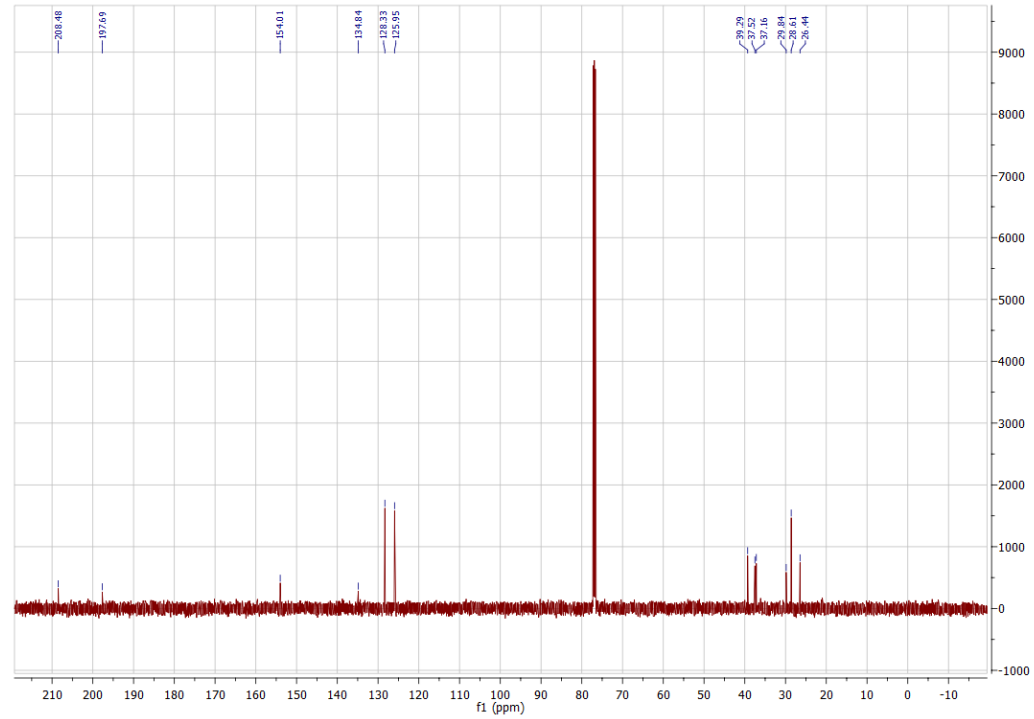


**Figure A7.74.** $^{13}$C NMR ($CDCl_3$, 125.8 MHz) spectrum of XX (**56**)

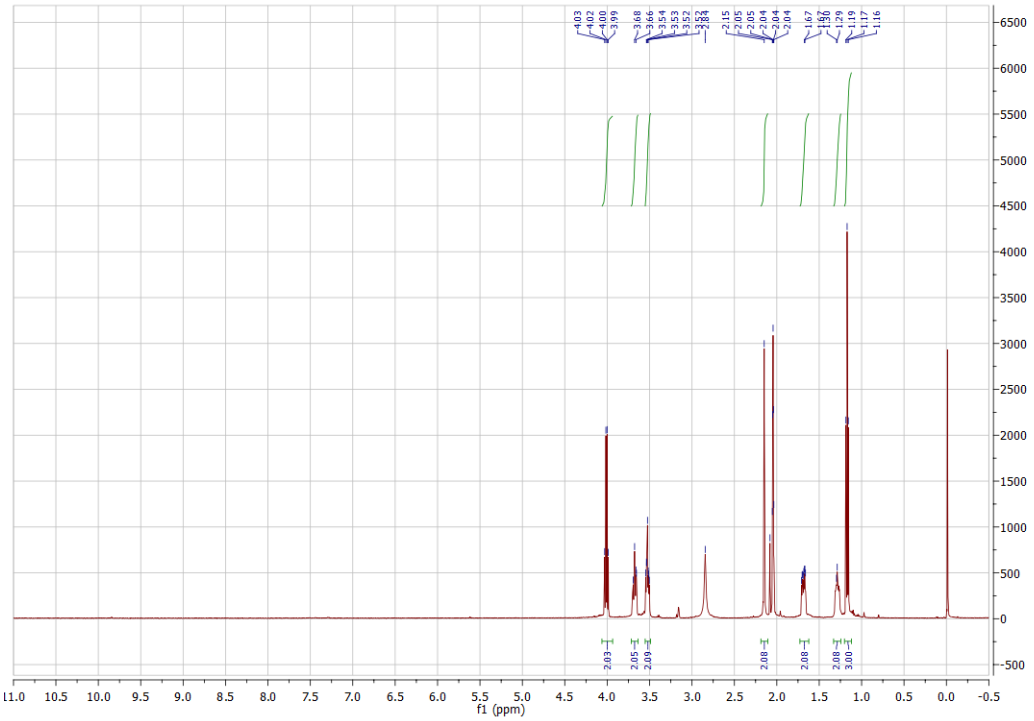


**Figure A7.75.** $^{1}$H NMR (acetone-$d_6$, 500 MHz) of potassium (4-(2-ethoxy-2-oxoethyl)tetrahydro-2H-pyran-4-yl)trifluoroborates (**S1**)

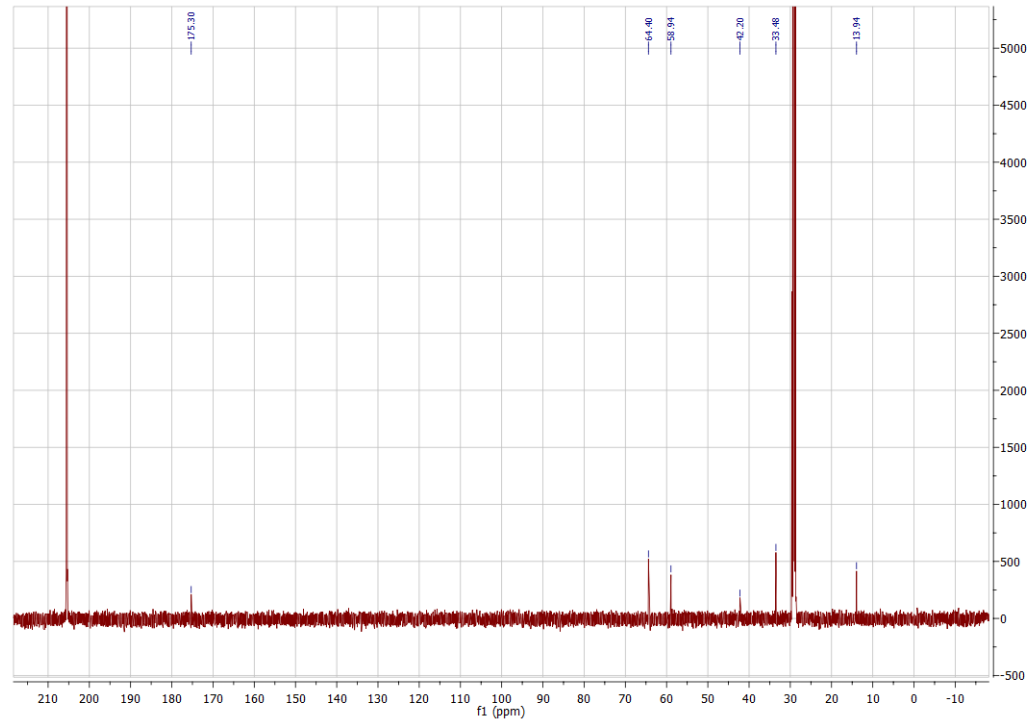


**Figure A7.76.** $^{13}$C NMR (acetone-$d_6$, 500 MHz) of potassium (4-(2-ethoxy-2-oxoethyl)tetrahydro-2H-pyran-4-yl)trifluoroborates (**S1**)

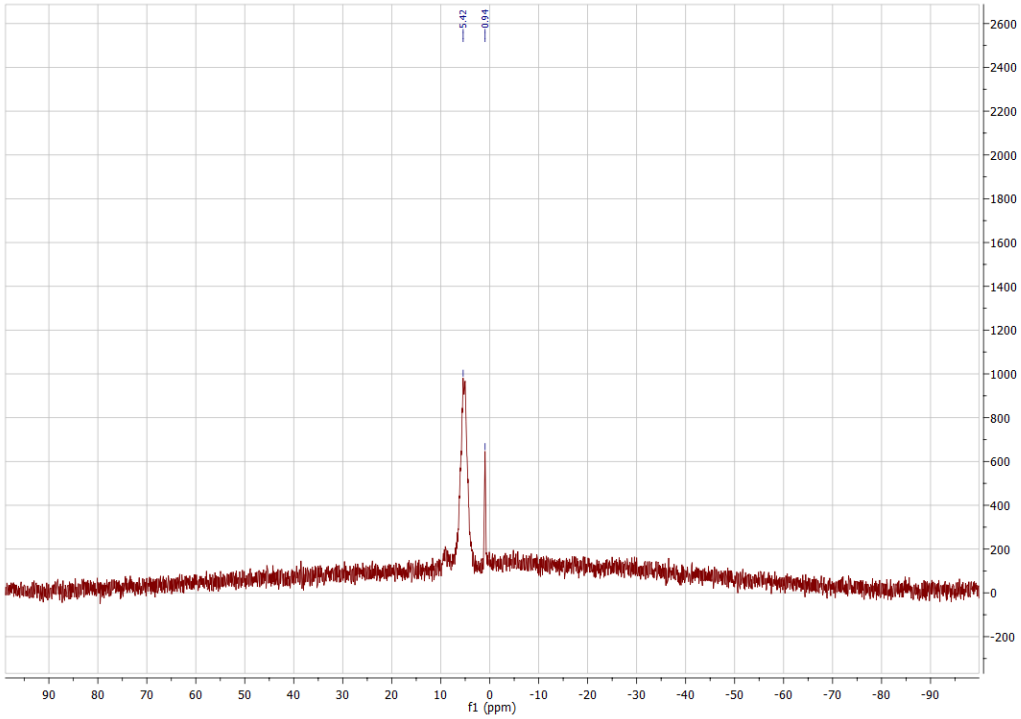


**Figure A7.77.** $^{11}$B NMR (acetone-$d_6$, 500 MHz) of potassium (4-(2-ethoxy-2-oxoethyl)tetrahydro-2H-pyran-4-yl)trifluoroborates (**S1**)

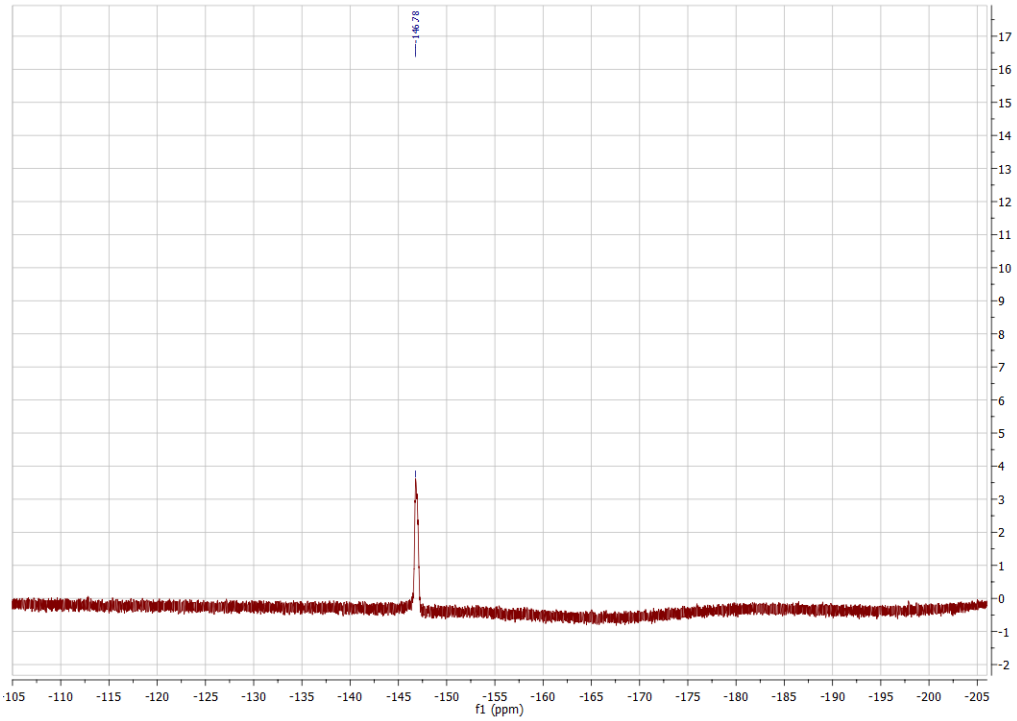


**Figure A7.78.** $^{19}$F NMR (acetone-$d_6$, 500 MHz) of potassium (4-(2-ethoxy-2-oxoethyl)tetrahydro-2H-pyran-4-yl)trifluoroborates (**S1**)

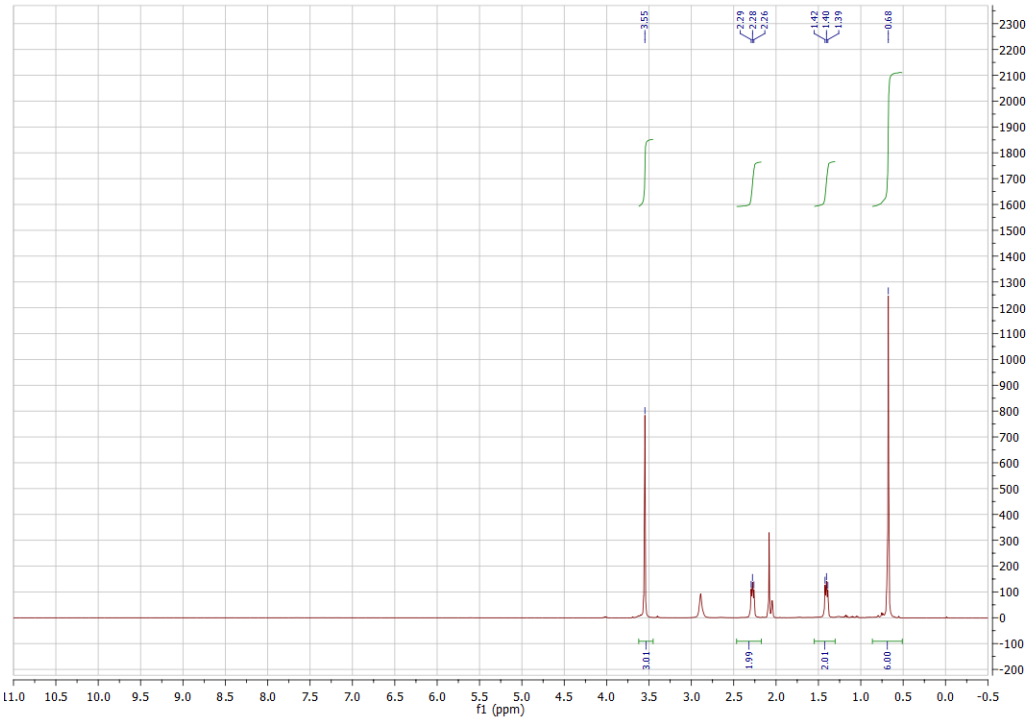


**Figure A7.79.** $^{1}$H NMR (acetone-$d_6$, 500 MHz) of potassium trifluoro(5-methoxy-2-methyl-5-oxopentan-2-yl)borate **(S2)**

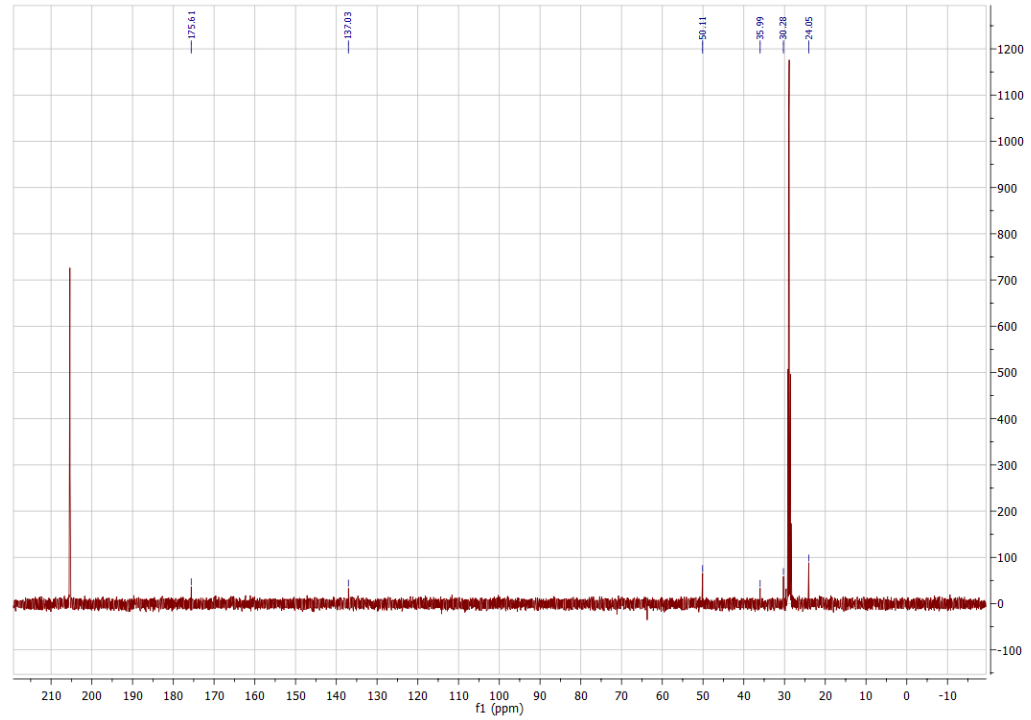


**Figure A7.80.** $^{13}$C NMR (acetone-$d_6$, 500 MHz) of potassium trifluoro(5-methoxy-2-methyl-5-oxopentan-2-yl)borate **(S2)**

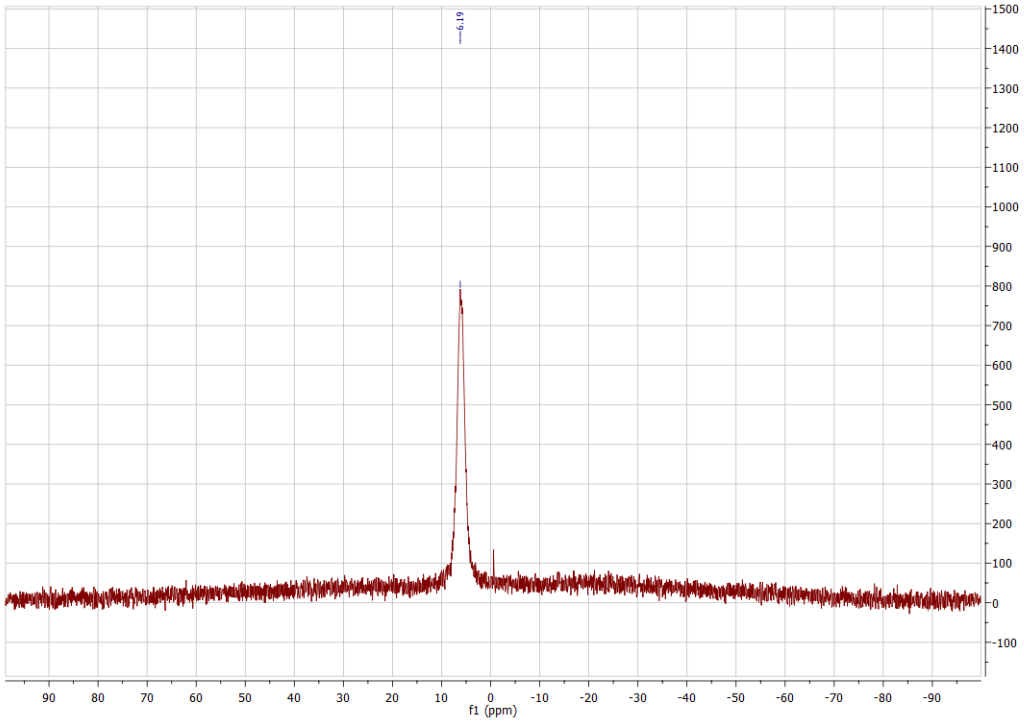


**Figure A7.81.** $^{11}$B NMR (acetone-$d_6$, 500 MHz) of potassium trifluoro(5-methoxy-2-methyl-5-oxopentan-2-yl)borate **(S2)**

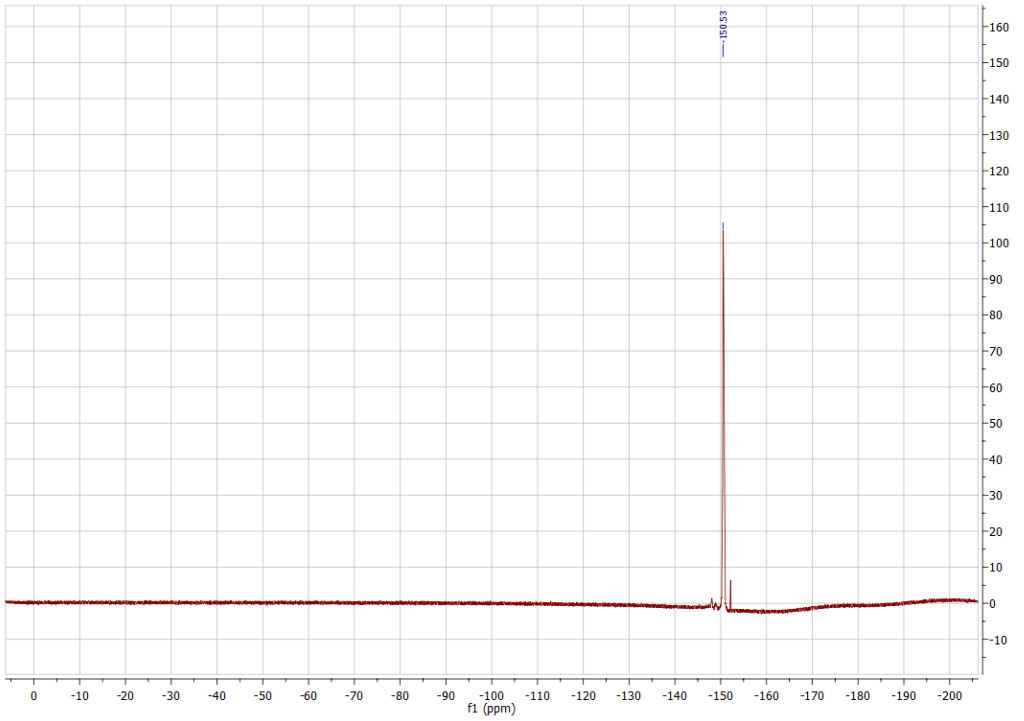


**Figure A7.82.** $^{19}$F NMR (acetone-$d_6$, 500 MHz) of potassium trifluoro(5-methoxy-2-methyl-5-oxopentan-2-yl)borate **(S2)**

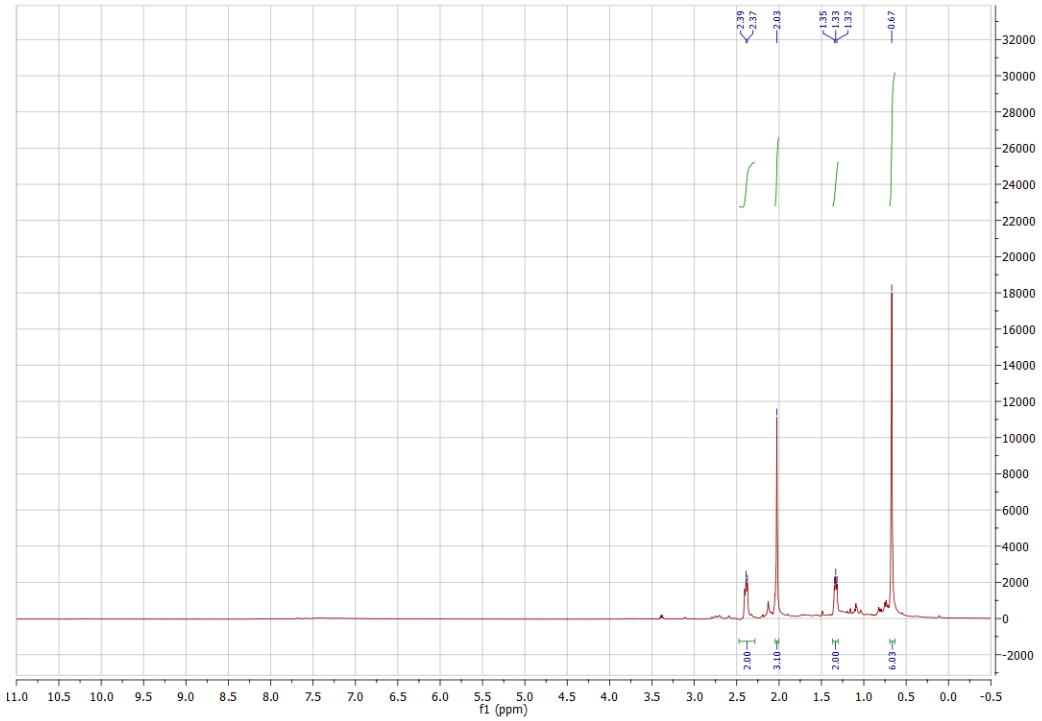


**Figure A7.83.** $^{1}$H NMR (acetone-$d_6$, 500 MHz) of potassium trifluoro(2-methyl-5-oxohexan-2-yl)borate (**S3**)

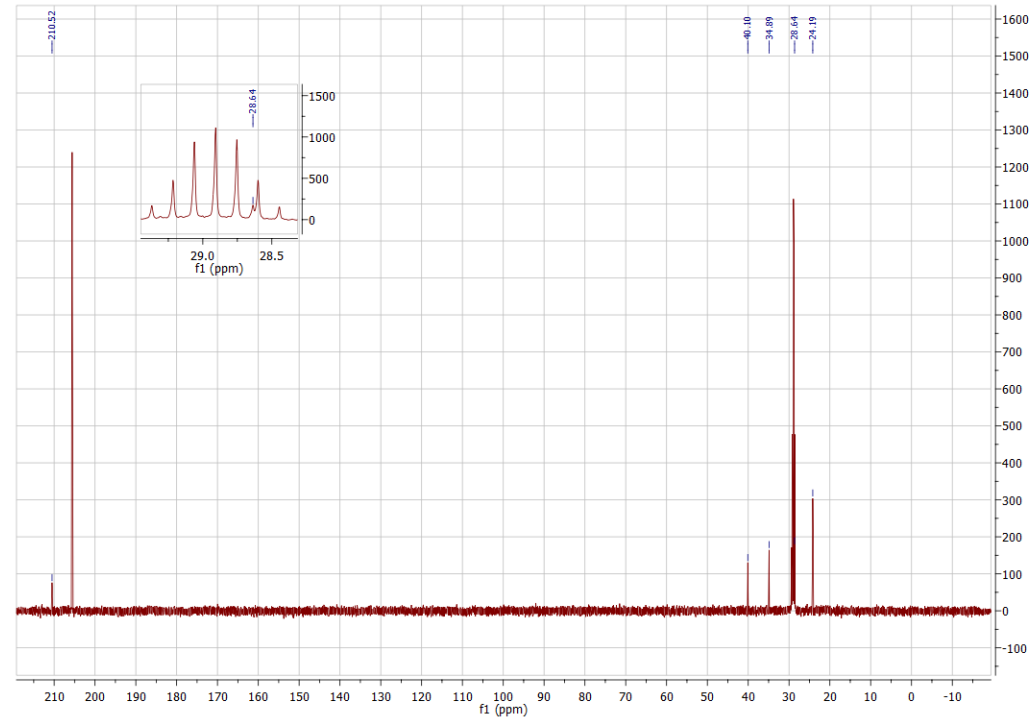


**Figure A7.84.** $^{13}$C NMR (acetone-$d_6$, 500 MHz) of potassium trifluoro(2-methyl-5-oxohexan-2-yl)borate (**S3**)

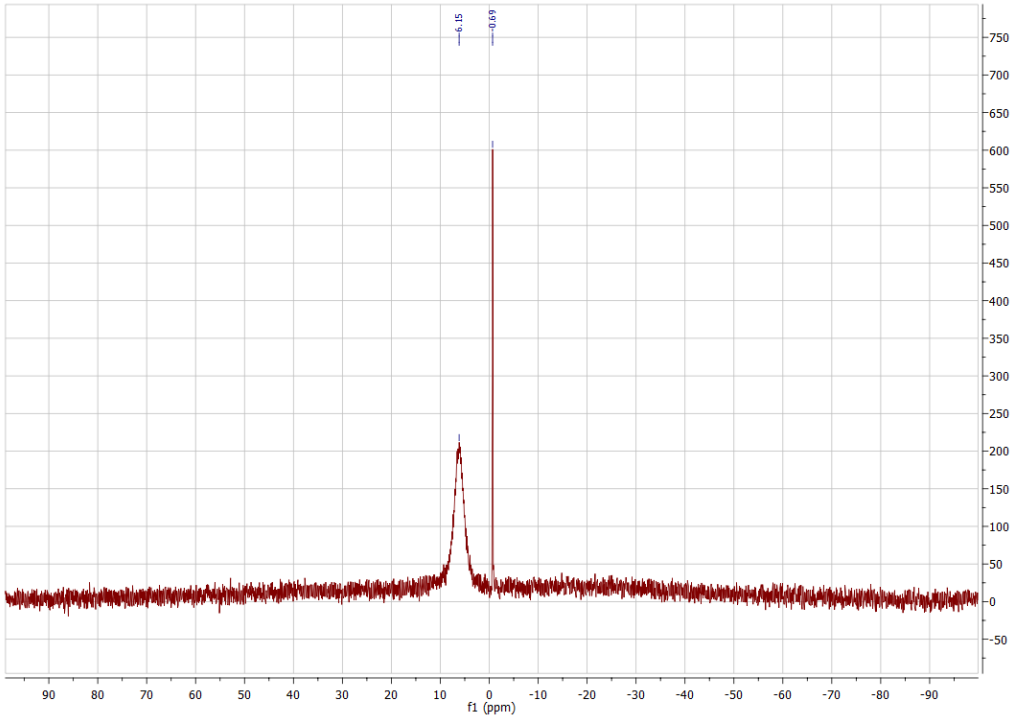


**Figure A7.85.** $^{11}$B NMR (acetone-$d_6$, 500 MHz) of potassium trifluoro(2-methyl-5-oxohexan-2-yl)borate (**S3**)

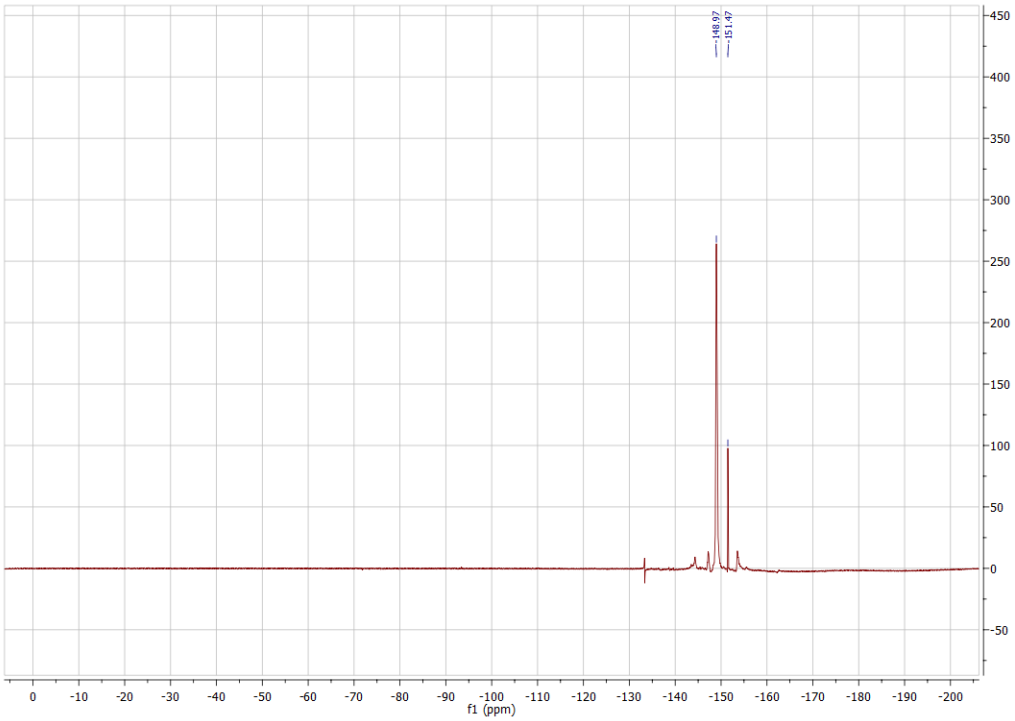


**Figure A7.86.** $^{19}$F NMR (acetone-$d_6$, 500 MHz) of potassium trifluoro(2-methyl-5-oxohexan-2-yl)borate (**S3**)

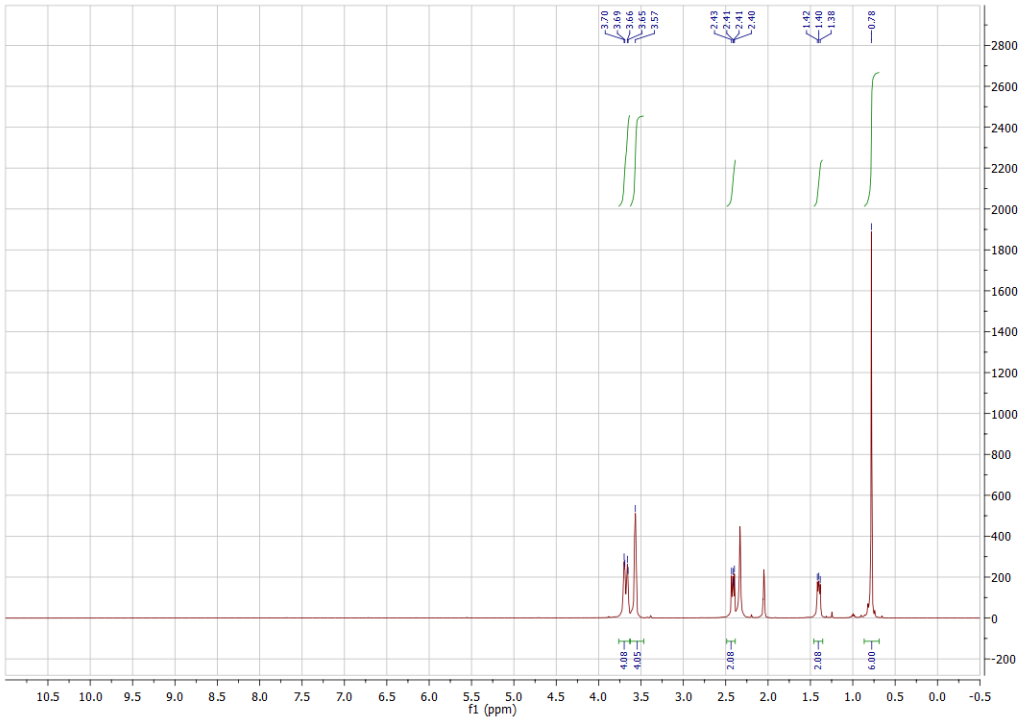


**Figure A7.87.** $^{1}$H NMR ($CD_3CN$, 500 MHz) of potassium trifluoro(2-methyl-5-morpholino-5-oxopentan-2-yl)borate (**S4**)

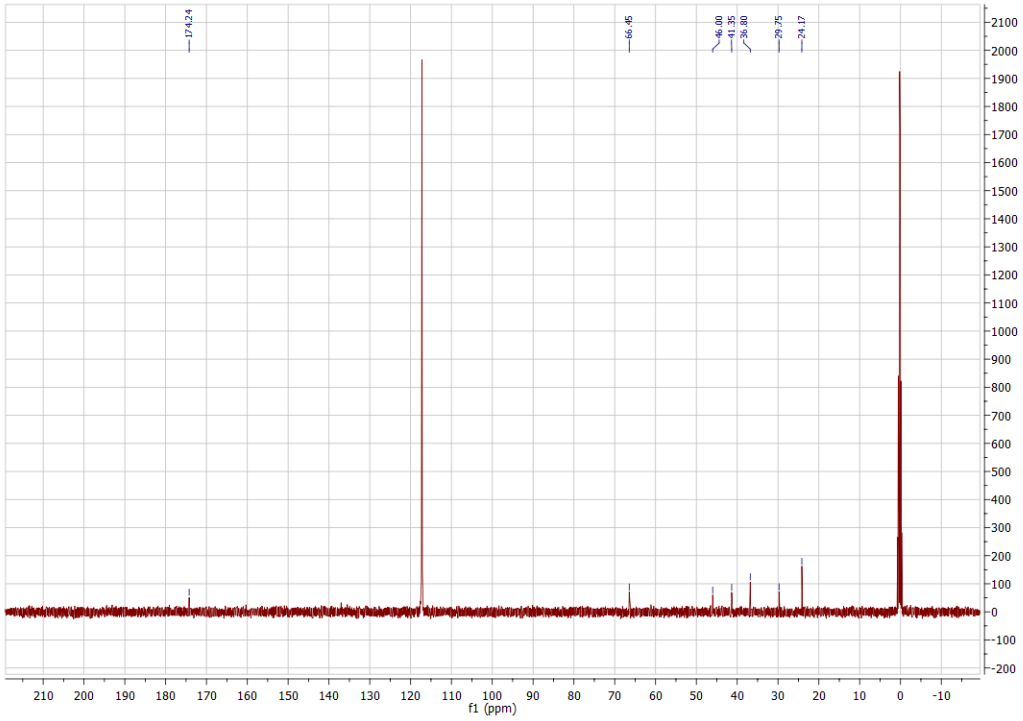


**Figure A7.88.** $^{13}$C NMR ($CD_3CN$, 500 MHz) of potassium trifluoro(2-methyl-5-morpholino-5-oxopentan-2-yl)borate (**S4**)

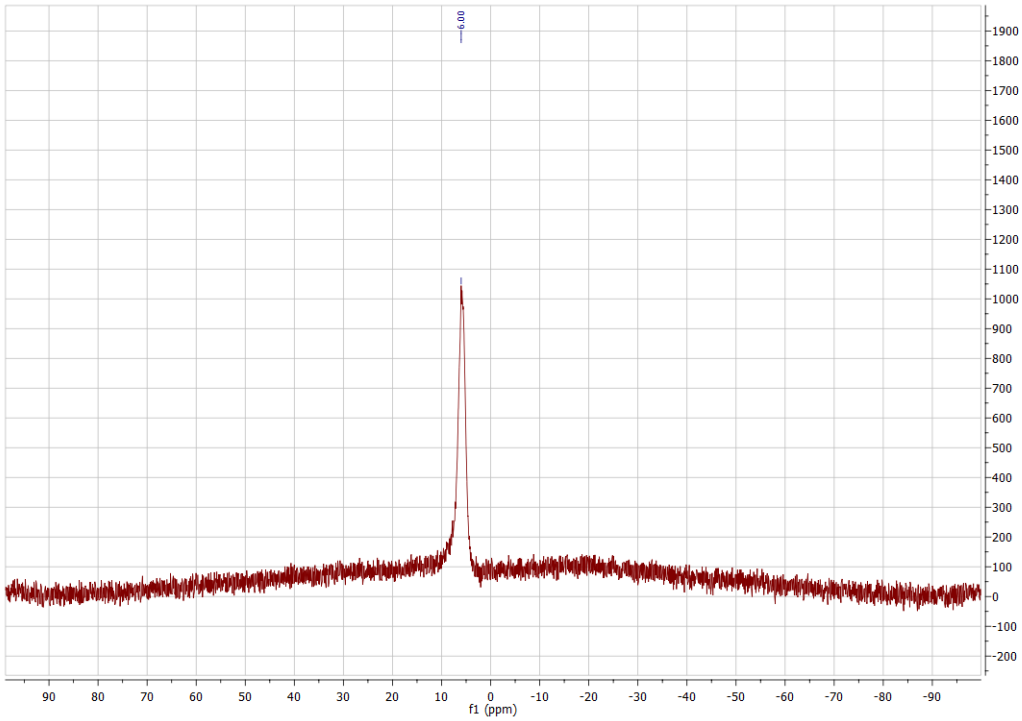


**Figure A7.89.** $^{11}$B NMR ($CD_3CN$, 500 MHz) of potassium trifluoro(2-methyl-5-morpholino-5-oxopentan-2-yl)borate (**S4**)

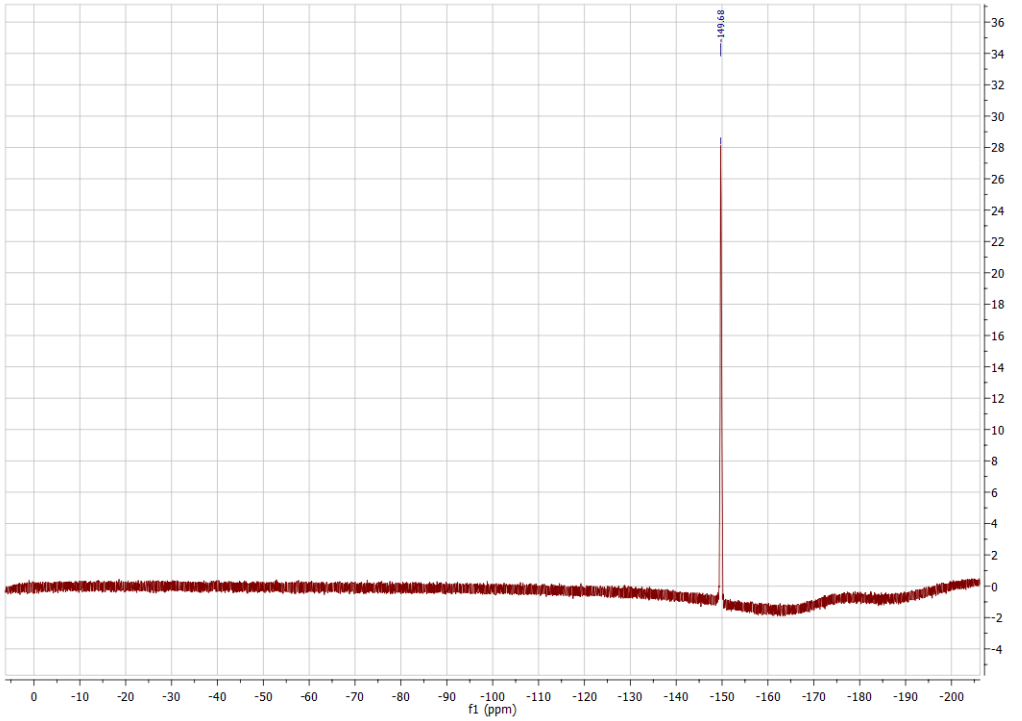


**Figure A7.90.** $^{19}$F NMR ($CD_3CN$, 500 MHz) of potassium trifluoro(2-methyl-5-morpholino-5-oxopentan-2-yl)borate (**S4**)

# Chapter 7. Hypervalent Silicates as Alternative Radical Precursors

## 7.1 Introduction

Having demonstrated the use of alkyltrifluoroborates extending from benzylic systems all the way to the highly congested tertiary variants, we became interested in developing a palette of potential radical feedstocks to complement the existing protocols. In much the same way as cross-coupling benefits from a diverse collection of organometallic nucleophiles (Negishi, Kumada, Suzuki, etc), in the single electron transmetalation paradigm, no one particular radical source is best in all cases. In certain situations, an organoboron reagent may be easier to access, more reactive/selective, or inexpensive. In others, a competing reagent may be more suitable.

For alkyltrifluoroborates, a number of notable shortcomings currently exist. First, in the SET cross-coupling reaction, an expensive Ir-based photocatalyst is required because of the high oxidation potentials of the boron reagents, and consequently primary alkyl radicals are inaccessible because the trifluoroborate precursor ($E^0$ ~ +1.90 V *vs* SCE)[1] is not readily oxidized by photoexcited Ir catalysts ($E^0$ = +1.32 V *vs* SCE).[2] Second, the initial oxidation of the alkyltrifluoroborates releases $BF_3$, which is corrosive on scale and has been demonstrated to be an inhibitor of reactivity, thereby requiring addition of excess base. Finally, alkyltrifluoroborates are often minimally soluble in many organic solvents, thus obstructing the transmission of light in photoredox reactions.[i]

---

[i] Reproduced in part from *J. Am. Chem. Soc.*, **2016**, *138*, 475.

In our quest to find new coupling partners able to address these issues, we considered that the alkylborate anion present in trifluoroborates has striking similarities to hypercoordinate silicate complexes that are often invoked as intermediates in Hiyama type cross-couplings.[3] Therefore, we wondered if this hypercoordinate complex (**Figure 7.1**) or some stable isolable complex thereof could be generated and oxidized in the presence of an appropriate photocatalyst.

v

**Figure 7.1.** Similarities between organoborates and silicate intermediates

Examination of the literature identified a number of stable, isolable hypercoordinate silicon complexes that had been reported going back as early as the 1960s.[4,5] Follow-up investigations into these complexes were largely focused on their structural features, particularly the well-defined square pyramidal structure adopted by the bis-catecholatosilicate structures. It was not until the mid 1990s that these structures were used in productive synthetic chemistry. DeShong was the first to employ the aryl structures in aryl-aryl cross-couplings.[6]

Most excitingly, in our quest to identify new silicate coupling partners, we noted the seminal studies of Nishigaishi *et al.* on the allylation of nitrile-containing arenes using photoexcited, hypercoordinate tetramethylammonium allylbis(catecholato)silicate. These investigations were suggestive that these complexes were a ready and easily oxidized source of alkyl radicals.[7] Most notably, these bis(catecholato)silicates appeared amenable to photoredox/Ni dual catalysis and were intriguing because the benign byproducts generated from their fragmentation (biscatecholsilane and tetramethylammonium bromide) would obviate the need for basic additives required in all heretofore reported SET mediated cross-couplings.

During the course of our investigations into these hypercoordinate reagents, the groups of Fensterbank and Goddard described the use of related potassium organobis(catecholato)silicates as alkyl radical precursors.[8] This contribution demonstrated that, as expected, both primary and secondary alkyl radicals could be generated from the corresponding pentacoordinate silicon species and employed in a number of transformations. In addition, six such silicates were used in dual photoredox/nickel-catalyzed cross-coupling with a single aryl halide. Unfortunately, this brief study did not fully outline the advantages or potential of such synthons. For example, in these protocols, an expensive Ir catalyst was utilized, whereas the oxidation potentials of the silicates ($E^0$ = +0.75 V *vs* SCE for 1º alkylsilicate **5**, **Figure 7.2**)[9] lie in the range of the less expensive, photoexcited $[Ru(bpy)_3](PF_6)_2$ catalyst ($E^0$ = +0.77 V *vs* SCE) (bpy: 2,2'-bipyridine).[10] Secondly, the use of potassium as a counterion forced the authors to employ the cost-prohibitive 18–crown–6 as both stabilizer and solubilizer,[11,12] making the corresponding silicates unusable for practical large scale/industrial purposes. Given these restrictions, we hoped to improve the synthesis and application of these silicates in photoredox cross-coupling protocols.

## 7.2 Results and Discussion

Prior to the publication of the Fensterbank/Goddard study, we had begun our own investigation with the synthesis of alkylbis(catecholato)silicate derivatives having a triethylammonium cation, using modified literature reaction conditions.[5] Reaction of a substoichiometric amount of catechol with benzyltrimethoxysilane in refluxing THF using triethylamine as base afforded the corresponding silicate **1** in 92% yield (cation = $Et_3NH$, **Figure 7.2**). This economical ($90/Kg of catechol, $80/Kg of triethylamine) and straightforward, multigram scale reaction could be extended to secondary (**2**, **3**) and other primary (**4-6**, **11**, **13**) alkyltrimethoxysilanes without modification of the reaction conditions. In some cases, an

improvement of the yield was observed by using the higher boiling dioxane instead of THF (**7**-**10**). Interestingly, we noticed a significant decrease in the solubility of the corresponding silicates (**3**, **8**-**10**, **12**) in ethereal solvents when replacing triethylamine with diisopropylamine as base, allowing the isolation of the latter salts as fine, fluffy powders ($R^1$ = H, $R^2$ = *i*–Pr). In the case of the primary alkylamine **14**, the amine group serves as both base and counterion. All these silicate derivatives are non-hygroscopic, colorless, bench stable powders that can be stored at room temperature under air without noticeable decomposition even after 5 months (see Experimental).

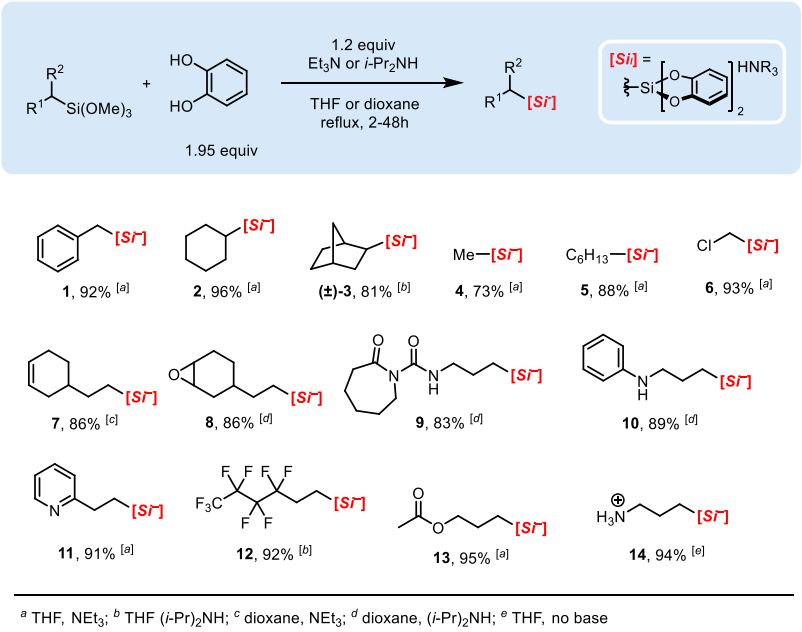


**Figure 7.2**. Preparation of Primary and Secondary Ammonium Alkylbis(catecholato)silicates.

With a suitable library of substrates in hand, attention was turned to the development of a practical photoredox/Ni dual catalyzed cross-coupling using aryl bromide electrophiles. Screening of the reaction conditions using 4-bromobenzonitrile and triethylammonium cyclohexylbis(catecholato)silicate **2** indicated that the catalyst system previously established for the cross-coupling of secondary alkyltrifluoroborate[13] {5.0 mol % of [$NiCl_2$(dme)], 5.0 mol % of

4,4'-di-*tert*-butyl-2,2'-bipyridine (dtbbpy), and 2.0 mol % of $[Ir(dFCF_3ppy)_2(bpy)]PF_6$, using a 26 W compact fluorescent lightbulb (CFL)} could be applied almost directly to alkylbis(catecholato)silicates [$dFCF_3ppy$: 2-(2,4-difluorophenyl)-5-(trifluoromethyl)pyridine]. However, the use of DMF as solvent at higher concentration (0.1 M instead of 0.05 M) led to significantly improved conversions (see Experimental). Whereas additives have proven to be crucial in previously reported photoredox/Ni and conventional cross-couplings with organotrifluoroborates, their use here proved detrimental. Various photocatalysts were assessed to replace the expensive Ir photocatalysts, and, as anticipated from the low oxidation potential of organobis(catecholato)silicate,[9] the $[Ru(bpy)_3](PF_6)_2$ could be substituted without any loss in yield (see Supporting Information).

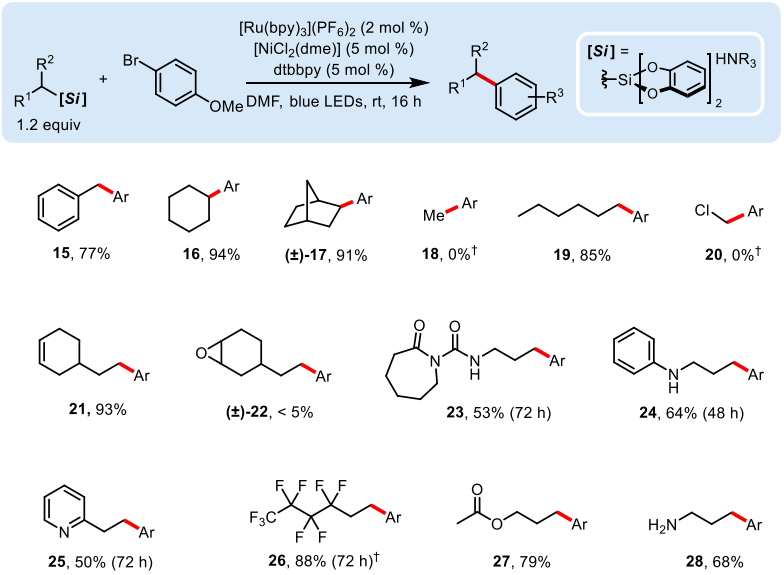


**Figure 7.3.** Photoredox Cross-coupling of Ammonium Alkylbis(catecholato)silicates with Bromoanisole.

Using these reaction conditions with the electron rich 4-bromoanisole and **1**, coupled product **15** was obtained in 77% isolated yield (**Figure 7.3**). The study was extended to all other silicates synthesized, affording coupled products in good to excellent yield with both 2º and 1º

alkylsilicates. These reactions, which involve highly reactive 1º and 2º alkyl radicals, proved to be applicable in sterically demanding systems (**17**) and tolerant of reactive functional groups such as esters (**27**) and lactams/ureas (**23**). Remarkably, substrates containing coordinating groups such as pyridine (**25**) and primary alkylamines (**28**) coupled in good yields. Furthermore, to the best of our knowledge, substrate **14** represents the first successful example of an alkylmetallic cross-coupling partner bearing a free primary alkylamine functional group. As the introduction of primary alkylamines is a common method for increasing solubility and/or biocompatibility of lead candidates in medicinal chemistry, this tolerance is highly relevant for diversification efforts in drug discovery.[14] Also noteworthy, very few examples of the cross-coupling of free secondary alkylamine-containing nucleophiles have been reported in the literature.[15] Of further importance, the use of the less highly oxidizing Ru photocatalyst allows the incorporation of oxidizable amines such as that found in aniline **24** ($E^0$ = +0.76 V *vs* SCE).[16] Unfortunately, silicates **4**, **6**, and **8** failed to give any cross-coupling product. We suspect this is likely because of the high oxidation potentials and greater reactivity of the generated radicals, favoring C-H abstraction and aryl addition pathways.

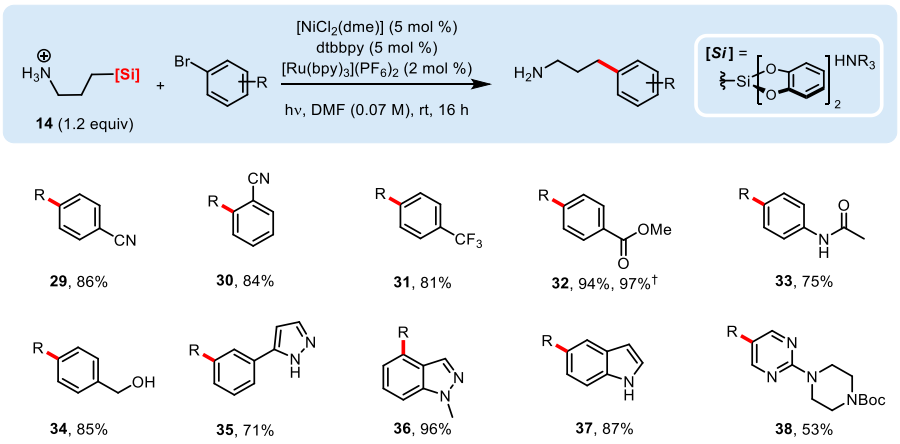


**Figure 7.4.** Aryl- and Heteroaryl Bromide Scope with Primary Amine-Containing Silicate **14.**

To assess the limitations of the primary amine coupling reaction, silicate **14** was reacted with various aryl- and heteroaryl electrophiles using unmodified reaction conditions (**Figure 7.4**). Electron-rich (**33**, **34**), electron-poor (**29**–**32**), and ortho-substituted (**30**) cross-coupled products were accessed in good to excellent yield. In particular, the presence of further protic functional groups such as those found in acetanilide **33**, benzyl alcohol **34**, and *unprotected* pyrazole **35** and indole **37** did not affect the reaction, which is surprising because these substrates have proven recalcitrant coupling partners under previous cross-coupling protocols.[13,17] Nitrogen-containing heterocycles (**35**–**38**), which represent important substructures in pharmaceutical libraries,[18] were well tolerated and afforded the corresponding coupling products in reasonable (**38**) to excellent (**36**) yields. Although poorer reactivity was observed in accessing **38**, the remaining mass balance could be accounted for as unreacted aryl halide after 16 h. To confirm the scalability of this primary alkylamine cross-coupling, a gram-scale reaction was performed and afforded coupled product **32** in 97% isolated yield after only 4 h. This increase in reaction rate when compared to that of organotrifluoroborates was achieved through the use of high-intensity, broadband white LEDs, accompanied with a slight increase in reaction temperature (36 ºC, see Experimental).

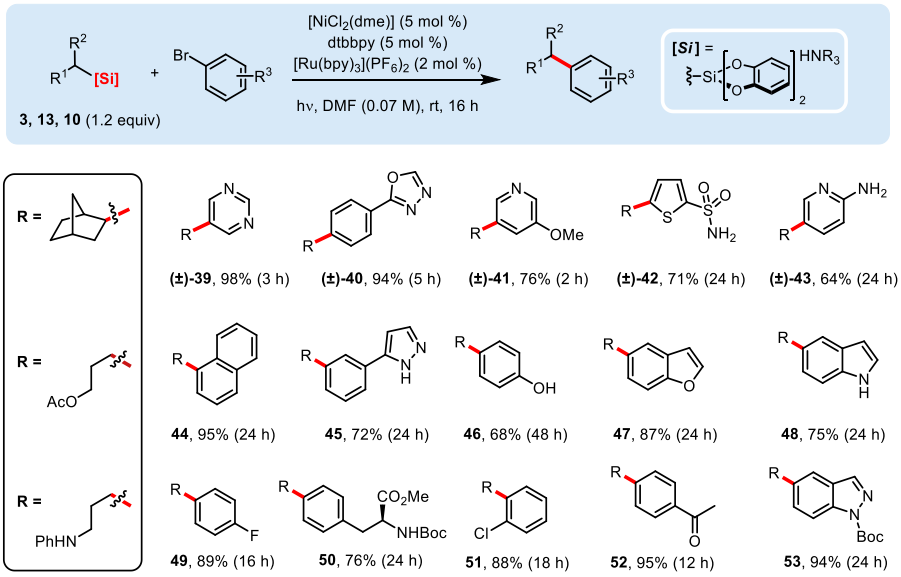


**Figure 7.5.** Aryl- and Heteroaryl Bromide Scope with both Primary and Secondary Ammonium Alkylbis(catecholato)silicate.

The scope of the reaction was next extended to sterically encumbered 2º alkyl- (**3**) as well as 1º alkylsilicates bearing acetoxy (**13**) or secondary alkylamine (**10**) functional groups (**Figure 7.5**). The use of 2º alkylsilicon reagents in cross-coupling is perhaps unremarkable in light of our previous success with 2º alkylboron reagents, but it still represents the first time that unactivated secondary Hiyama-type reagents[19–21] have been widely employed in cross-coupling.[22] Furthermore, the far lower oxidation potentials and/or higher solubility of these reagents in organic media leads in many cases to reactions that are complete in dramatically shorter time-frames (as short as 2 h for pyridyl derivative **41**) than their trifluoroborate or carboxylic acid counterparts,[23,24] and even those previously developed by Fensterbank/Goddard (24 h).[8]

A wide variety of aryl- and heteroaryl bromides were assessed to highlight the broad compatibility of these extremely mild cross-coupling conditions. Coupled products bearing electron-withdrawing (**49**, **51**, **52**) or electron-donating groups (**44**, **46**) were easily accessed, as well as more sterically encumbered systems (**44**) or those bearing a potential competitive site for oxidative addition (**51**). Nitrogen heterocycles (**39**, **41**, **43**, **48**, **53**) could be acquired in the process

in good to excellent yield (even for the challenging aminopyridine **43**). Oxygen- (**47**) and sulfur- (**42**) containing heteroaryls could be procured as well. Furthermore, target structures bearing protic groups (**43, 45**, **46**, **48**, **50**) were readily synthesized. Overall, the success of ammonium organobis(catechol)silicates makes them partners of choice for metal-catalyzed carbon-carbon bond-forming reactions, as both their functional group tolerance and reactivity outperform previously reported photoredox/Ni dual catalysis methods and conventional Hiyama/Suzuki cross-couplings.[3]

As a final showcase of these hypercoordinate silicates, two successive, photoredox/Ni dual cross-couplings were carried out with dibrominated arenes **54** and **56** (**Figure 7.6**). In both cases, an initial cross-coupling with a 2º alkyltrifluoroborate was first performed under conditions previously optimized in our laboratory using the iridium photoredox catalyst. After filtration of the resulting salts in air, concentration, solvent switch, and addition of a primary silicate **13** (**1** for aryl **56**), a second cross-coupling was then completed to provide functionalized arenes **55** and **57**. Most notably, these transformations require no intermediate isolation and can be performed without the further addition of *either* the photoredox or cross-coupling catalyst, underlining the robustness of both dual catalysis systems. This chemistry has the potential to be applied to successive one-pot cross-coupling operations in either batch or photo-flow systems. Furthermore, given the reports by Burke and co-workers on successive MIDA boronate cross-couplings[25] and our own on mechanistically orthogonal boron couplings,[26] innumerable opportunities exist for rapid complexity-building operations without isolation of intermediates.

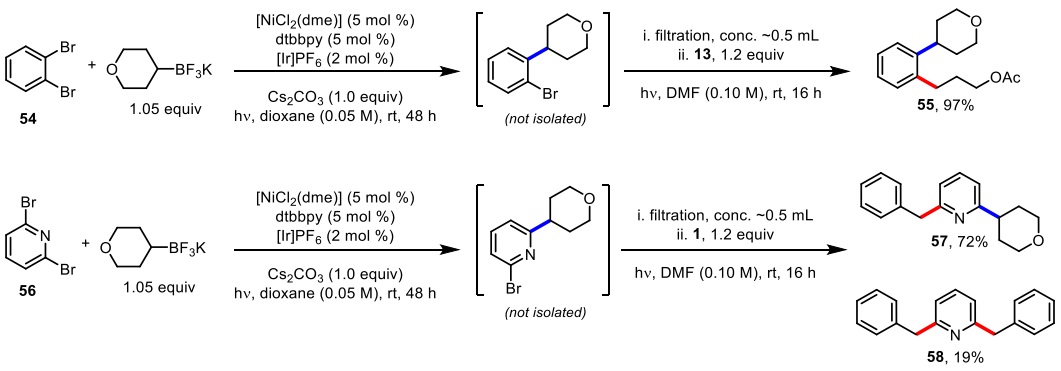


**Figure 7.6** Successive Photoredox/Ni Dual Cross Couplings Using Organotrifluoroborate then Organobis(catecholato)silicate Nucleophiles.

## 7.3 Conclusion

In summary, we have developed a synthetic procedure for the photoredox cross-coupling of ammonium organobis(catecholato)silicates that is operationally simple and does not require the use of expensive crown ether additives. These silicates represent ideal radical precursors because of their low oxidation potentials, excellent physical properties, and the innocuous byproducts formed upon oxidation. Further, these silicates have been demonstrated for the first time as 1º and 2º alkyl radical precursors in the dual catalytic Ru/Ni cross-coupling. The conditions developed herein are general, functional group tolerant and, when dealing with protic functional groups, unmatched by competing alkyltrifluoroborate[13] and carboxylic acid protocols.[24,23]

Most remarkably, the use of these reagents allows the selective coupling of an alkylmetallic reagent in the presence of primary amines for the first time – representing an expansion into new reactivity space. Whereas traditional two-electron cross-couplings of alkylmetallics feature strongly basic reagents and/or additives that favor amine deprotonation and coordination,[32] the use of a base-free, odd-electron transmetalation manifold inhibits competitive metal-catalyzed amination. Considering the absence of a single-step method for the introduction of primary alkylamines onto (hetero)aryl halide cores, aminoalkylsilicates have the potential to improve the

late stage introduction of primary amines into bioactive compounds. Taken together, these findings introduce alkylsilicates as key players in the photoredox/Ni dual catalytic cross-coupling regime.

## 7.4 Experimental

### General considerations

All reactions were carried out under an inert atmosphere of nitrogen or argon unless otherwise noted. DMF (99.9%, extra dry) was used as received. Triethylamine and diisopropylamine were distilled prior to use and stored over activated molecular sieves. Catechol (99%) was sublimed prior to use. [$NiCl_2$(dme)] was purchased from commercial sources and all other reagents were purchased commercially and used as received, unless otherwise noted. Column chromatography was performed by Combiflash$^{(R)}$ using RediSep Rf Gold Normal-Phase Silica$^{(R)}$ columns. Photoredox reactions were irradiated with a standard 26 W compact fluorescent light bulb and the temperature was controlled using an external fan. Melting points (°C) are uncorrected. Mass spectra (ESI-TOF) were recorded using $CH_2Cl_2$, MeCN or MeOH as the solvent. NMR spectra were recorded with Bruker FT spectrometers. $^{1}H$ (500.4 MHz) and $^{13}C$ $\{^{1}H\}$ (125.8 MHz) NMR chemical shifts are reported relative to internal TMS ($\delta = 0.00$ ppm) or to residual protiated solvent, and $^{19}F$ $\{^{1}H\}$ NMR (470.8 MHz) chemical shifts were referenced to external $CFCl_3$ (0.0 ppm). Data are presented as follows: chemical shift (ppm), multiplicity (s = singlet, d = doublet, t = triplet, q = quartet, sept = septet, m = multiplet, br = broad), coupling constant *J* (Hz) and integration.

**Procedure for the synthesis of alkyltrimethoxysilanes from alkyltrichlorosilanes**

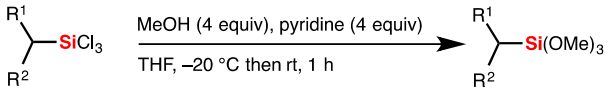


To an oven-dried double neck round bottom flask equipped with an inert gas inlet, an addition funnel and a stir bar were successively introduced organotrichlorosilane (1 equiv) and THF (0.3 M). The resulting solution was cooled to –20 °C, then MeOH (4 equiv) and pyridine (4 equiv) were placed into the addition funnel and added dropwise to the trichlorosilane solution under vigorous stirring, resulting in an immediate precipitation of pyridinium chloride salt. After addition, the reaction mixture was allowed to reach rt for 1 h before being diluted with chilled $H_2O$ (same volume as THF) and extracted with $Et_2O$ (3 × THF volume). The combined organic extracts were dried ($MgSO_4$) and concentrated under vacuum, affording a colorless oil. The latter was finally distilled under reduced pressure to obtain the product in pure form.

**Procedure for the synthesis of alkylbis(catechol)silicates**

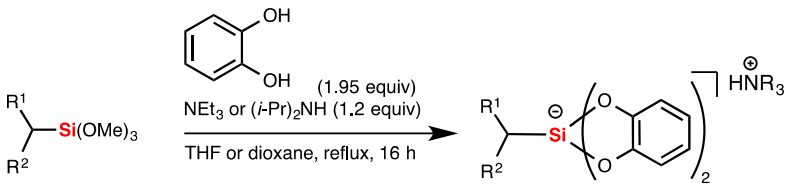


Catechol (1.95 equiv) was introduced into a microwave vial with a stirring bar. The vial was sealed with a Teflon-coated septum cap then purged with $N_2$ and evacuated four times. THF or 1,4–dioxane (0.5 M) and the corresponding amine (1.2 equiv) were introduced, and the resulting light pink solution was stirred at rt for 15 min before addition of alkyltrimethoxysilane derivative (1 equiv) (*note: no amine base was needed for the synthesis of* ***14***). The reaction mixture was refluxed for 16 h, then an aliquot was taken and analyzed by $^1$H NMR. In the case of an incomplete reaction,

the vial was cooled to rt and the reaction mixture concentrated to a glue (to remove MeOH formed during the reaction) before the amine (0.5 equiv) and solvent (1.0 M) were introduced, and the vial was heated at reflux for another 16 h. The vial was finally cooled to rt and the reaction mixture concentrated to a glue before the $Et_2O$ (0.1 M) was introduced. The mixture was then sonicated 15 min to allow the corresponding product to precipitate as a white powder. Note that for some silicates, evaporation in vacuo for a prolonged period of time (16 h) was required before sonication. The vial was finally unsealed and the precipitate was collected by vacuum filtration. The filter cake was washed with $Et_2O$ to afford the desired silicate. In some cases, a trace amount (less than 5%) of tris(catechol)silicate could be detected in the final product, but the latter did not affect the efficiency of the dual photoredox/nickel catalyzed cross coupling. If desired, the product could be purified by dissolving in $CH_2Cl_2$ followed by precipitation with pentane and filtration.

**Synthesis of photocatalyst $[Ru(bpy)_3](PF_6)_2$**

The synthesis of photocatalyst $[Ru(bpy)_3](PF_6)_2$ has been realized using a modified method of the literature.[27]

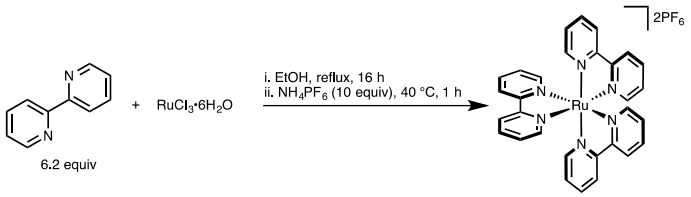


2,2'-Bipyridyl (968 mg, 6.20 mmol) and $RuCl_3•6H_2O$ (316 mg, 1.00 mmol) were introduced in a microwave vial with a stirring bar. The vial was sealed with a Teflon-coated septum cap then purged with $N_2$ and evacuated four times. The content was solved in degassed EtOH (40 mL) then stirred at reflux for 16 h. After cooling to rt, the vial was unsealed and $NH_4PF_6$ (1.63 g, 10 mmol) was added, resulting in an immediate precipitation of an orange suspension. The mixture was heated 15 min at 40 °C then cooled to 0 °C in an ice bath. After 2 h, the precipitate was collected

by vacuum filtration and the cake washed thoroughly with $H_2O$ (~200 mL) then EtOH (~100 mL) and finally $Et_2O$ (~100 mL) to afford the title compound as a brick red solid (710 mg, 83%). mp >250 °C. Characterization data for this compound matched that reported in the literature.[1]

**High Throughput Experimentation Information**

High Throughput Experimentation was performed at the Penn/Merck Center for High Throughput Experimentation at the University of Pennsylvania. The screens were run on a 0.01 mmol scale (relative to ArBr) and analyzed by HPLC with addition of 4,4′-di-*tert*-butylbiphenyl (0.1 equiv) as internal standard (IS). The graphs depicted hereafter represent product or starting material to internal standard ratios (P/IS or SM/IS, respectively). The ratios calculated are pertinent only to that specific screen; the ratios from one screen should not be quantitatively compared to those from a different screen.

**General Procedure for Screens**

Reactions were run in glass vials in 24 or 96 well plate reactor blocks having hollowed bottoms, and the vials were equipped with Teflon coated magnetic stir bar (Figure 1). The plate was placed in a glovebox, then the various compounds (silicates, ArBr, ligands, metallic precursors, photoredox catalyst) were added as solutions using micropipettes. If needed, carrying solvents were removed using a centrifugal evaporator. The plate was sealed with a screwed top lid equipped with a PTFE gasket then removed from the glovebox and placed on an LED (white or blue) plate on the top a magnetic stirrer (500 rpm). After 16 h, the plate was unsealed and reaction mixtures were diluted with MeCN (0.50 mL). Aliquots (25 μL) were taken and introduced into a 96 well HPLC plate, diluted with MeCN (0.70 mL) and finally analyzed by HPLC.

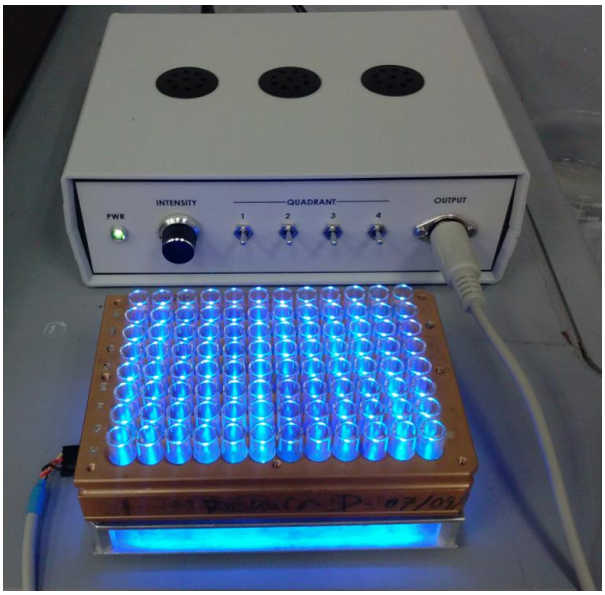


**Figure 7.6**. Hollow bottom 96 well plate reactor block equipped with glass vials and blue LED plate.

**Screens using HTE Screening Center**

**Screen 1.** Optimization of metal catalyzed photoredox cross-coupling using cyclohexylbis(catecholato)silicate•$HNEt_3$ (**2**) – Variation of solvents, metal sources and ligands.

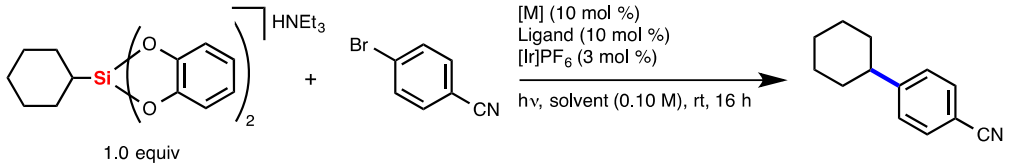


| Solvent | Metal source | Ligand [Ni] | Ligand [Pd] |
|---|---|---|---|
| THF<br>DMF | $[Ni(COD)_2]$<br>$[NiCl_2(dme)]$<br>$[Pd_2(dba)_3]$<br>$[Pd(OAc)_2]$ | dppe<br>$PPh_3$<br>$P(Cy)_3$<br>dppf<br>$P(t\text{-}Bu)_3$<br>PhOx | |
| | | dppp<br>dppbz<br>$P(o\text{-}Tol)_3$<br>blank<br>bphen<br>dtbBpy | IMes<br>DuPhos<br>CyJohnPhos<br>XPhos<br>RuPhos<br>Cataxcium A |

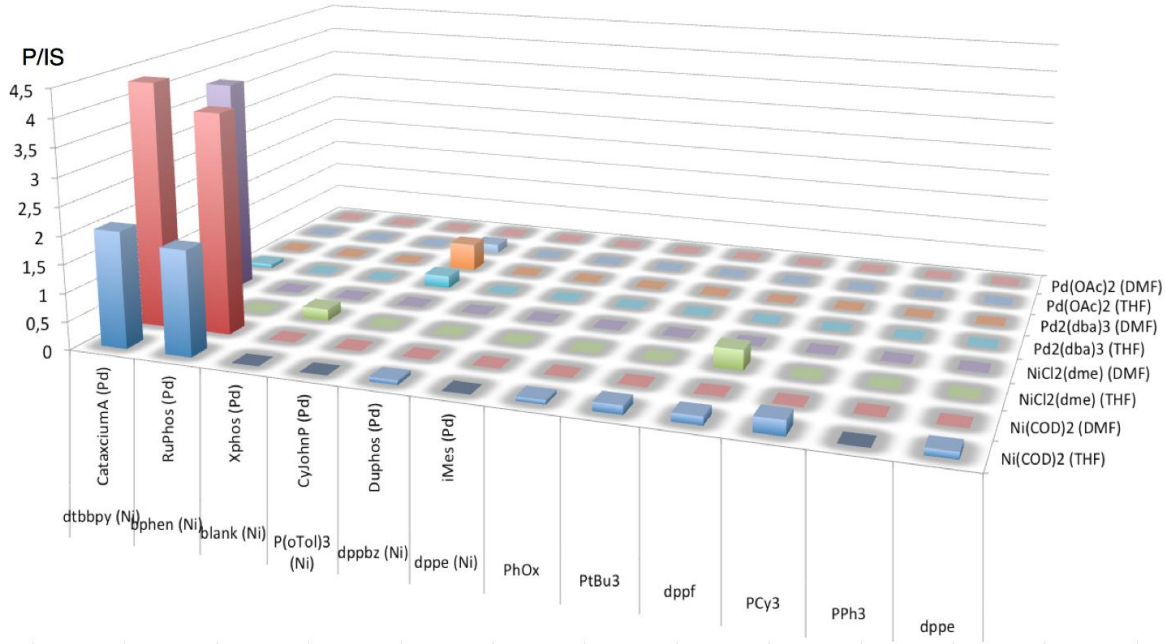


**Figure 7.7**. Optimization of metal catalyzed photoredox cross-coupling using cyclohexylbis(catecholato)silicate•$HNEt_3$ and various metal sources, ligands and solvents. *Note*: $[Ir]PF_6$ stands for $[Ir(dFCF_3ppy)_2(bpy)]PF_6$ ($dFCF_3ppy$ = 2-(2,4- difluorophenyl)-5-(trifluoromethyl)pyridine; bpy = bipyridine)

**Screen 2**. Optimization of metal catalyzed photoredox cross-coupling using cyclohexylbis(catecholato)silicate•$HNEt_3$ (**2**) – Variation of Ni(II) sources and solvents.

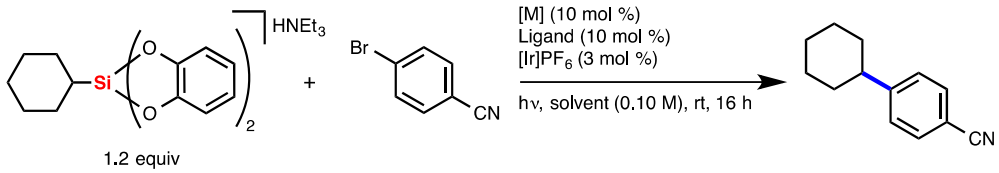


| Nickel (II) source | Solvent |
|---|---|
| $[NiCl_2(dme)]$ | THF |
| $[Ni(NO_3)_2]6H_2O$ | MeCN |
| | 2-methylbutan-2-ol |
| | DMA |
| | DMF |
| | DMSO |
| | DCE |
| | AcOEt |
| | CPME |
| | MeTHF |
| | DME |
| | dimethylcarbonate |

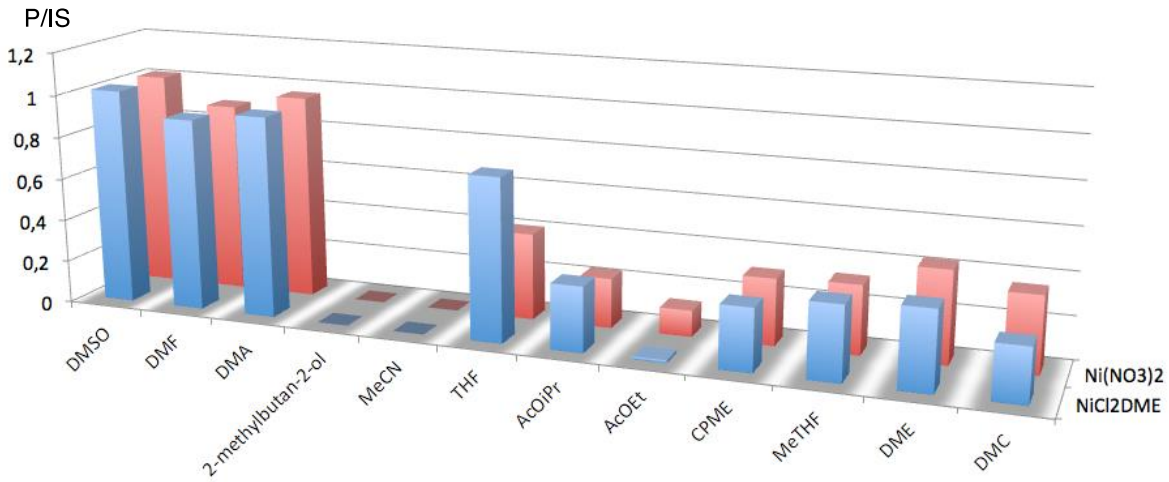


**Figure 7.8.** Optimization of metal catalyzed photoredox cross-coupling using cyclohexylbis(catecholato)silicate•$HNEt_3$. and various Nickel (II) sources and solvents.

**Screen 3.** Optimization of metal catalyzed photoredox cross-coupling using organobis(catecholato)silicate•$HNEt_3$ – Variation of photoredox catalysts.

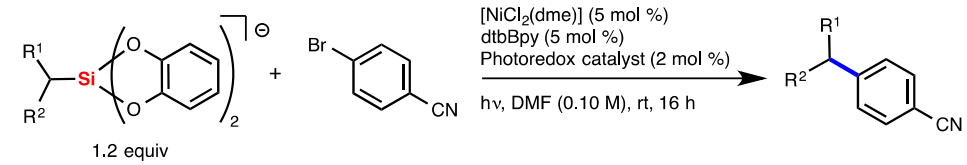


| Silicate | Photoredox catalyst |
|---|---|
| **1** | $[Ir(dFCF_3ppy)_2(bpy)]PF_6$ |
| **2** | $[Ru(bpy)_3]2PF_6$ |
| **14** | $[Ru(phen)_3]2PF_6$ |
| **5** | $[Ru(bpz)_3]2PF_6$ |
| | $[Ru(bpm)_3]2PF_6$ |
| | EosinY |

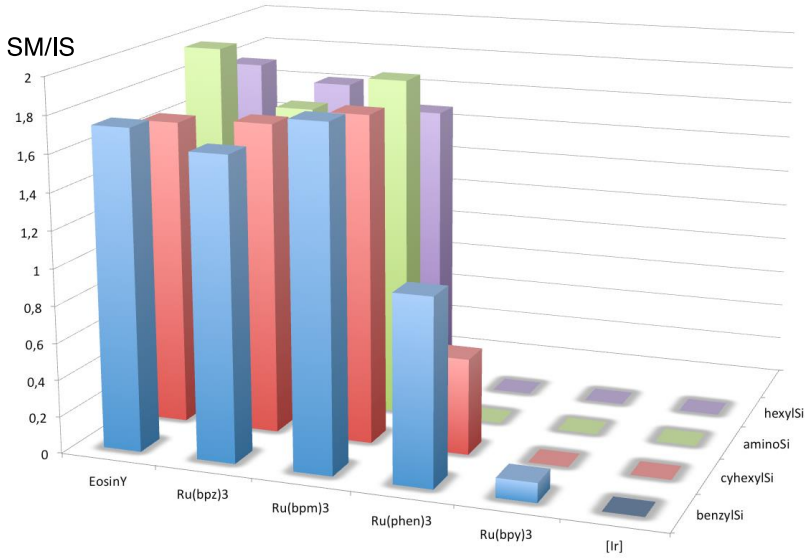


**Figure 7.9.** Screening of photoredox catalyst for the cross-coupling of various organobis(catecholato)silicates with bromobenzonitrile. *SM/IS graph.*

**General procedure for photoredox cross-coupling reactions**

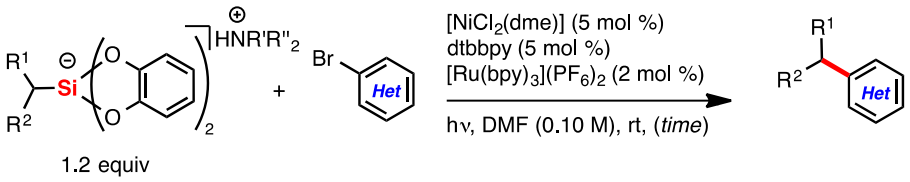


**0.5 mmol scale reaction:** To a 2-dram clear glass vial equipped with a Teflon-coated magnetic stir bar was added 4,4'-di-*tert*-butyl-2,2'-bipyridine (6.7 mg, 0.025 mmol), and [$NiCl_2$(dme)] (5.5 mg, 0.025 mmol). The vial was capped and purged with nitrogen, then 1.5 mL THF was introduced. The resulting suspension was heated briefly with a heat gun until the nickel and ligand were fully solubilized, yielding a pale green solution. The solution was cooled in an ice bath, resulting in the immediate precipitation of an evergreen solid. Solvents were then evaporated in vacuo to give a fine coating of the ligated nickel complex. Once dry, aryl bromide (0.5 mmol, 1.0 equiv) (liquid aryl bromides were added with solvent), aalkylsilicates (0.6 mmol, 1.2 equiv), and [$Ru(bpy)_3$]$2PF_6$ (8.6 mg, 0.01 mmol) were added in succession. The vial was then capped and purged four times. Under inert atmosphere, DMF (5 mL) was introduced. The vial containing all the reagents was further sealed with Parafilm and stirred approximately 4 cm away from a 26 W fluorescent light bulb. A fan was blown across the reaction setup to suppress the heat generated by the latter (the reaction temperatures were estimated to be ~30 °C). After 16-24 h, an aliquot was taken and analyzed by HPLC to monitor reaction completion.

*General work up:* The crude reaction mixture was poured in a separatory funnel and diluted with $H_2O$ (20 mL). The resulting suspension was extracted with $Et_2O$ (3 × 30 mL), and the combined organic extracts were washed with a saturated solution of $Na_2CO_3$ (2 × 20 mL) then $H_2O$ (20 mL), dried ($MgSO_4$) and concentrated. The residue was purified by column chromatography on silica

gel, eluting with EtOAc and hexanes (or with $CH_2Cl_2$ and *i*–PrOH, when needed), to obtain products in pure form.

*Special work up for amine-containing compounds:* After completion, the crude reaction mixture was diluted with EtOAc (10 mL), filtered through an approximately 6 cm x 4 cm cylindrical plug of Celite, washing with EtOAc (50 mL). The resulting solution was concentrated, retaken in EtOAc (20 mL), poured in a separatory funnel and washed with a saturated solution of $Na_2CO_3$ (2 × 10 mL) then $H_2O$ (10 mL), dried ($MgSO_4$) and concentrated. The residue was purified by column chromatography on silica gel, eluting with MeOH and $CH_2Cl_2$ containing $NH_4OH$ (1 %, *v*/*v*), to obtain the product in pure form.

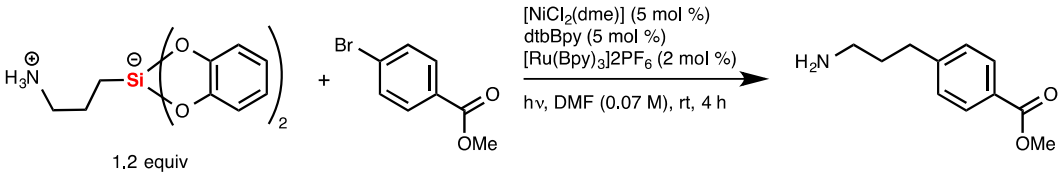


**Gram scale reaction:** To a 100 mL Schlenk flask equipped with a Teflon-coated magnetic stir bar was added [$NiCl_2$(dme)] (55 mg, 0.25 mmol) and 4,4'-di-*tert*-butyl-2,2'-bipyridine (67 mg, 0.25). The flask was capped and purged with nitrogen, then 5.0 mL THF was introduced. The resulting suspension was heated briefly with a heat gun until the nickel and ligand were fully solubilized, yielding a pale green solution. The solution was cooled in an ice bath, resulting in the immediate precipitation of an evergreen solid. Solvents were then evaporated in vacuo to give a fine coating of the ligated nickel complex. Once dry, methyl 4-bromobenzoate (1.075 g, 5.00 mmol), silicate **14** (1.325 g, 6.00 mmol) and [Ru(bpy)$_3$]2$PF_6$ (86 mg, 0.10 mmol) were added in succession. The vial was then capped and purged four times. Under inert atmosphere, DMF (80 mL) was introduced. The vial containing all the reagents was further sealed with Parafilm and stirred in the "light

chamber" depicted below. Two fans were blown across the reaction setup to suppress the heat generated by the LEDs, reaching 36 °C after 1 h. Reaction completion was monitored by taking aliquots of the reaction mixture and analyzing them by HPLC. After completion (4 h), the crude reaction mixture was diluted with EtOAc (50 mL), filtered through an approximately 6 cm x 4 cm cylindrical plug of Celite, washing with EtOAc (150 mL). The resulting solution was concentrated, retaken in EtOAc (100 mL), poured into a separatory funnel and washed with a saturated solution of $Na_2CO_3$ (2 × 50 mL) then $H_2O$ (50 mL), dried ($MgSO_4$) and concentrated. The residue was purified by column chromatography on silica gel, eluting with MeOH and $CH_2Cl_2$ containing $NH_4OH$ (1 %, *v*/*v*), to obtain methyl 4-(3-aminopropyl)benzoate in pure form (891 mg, 92%).

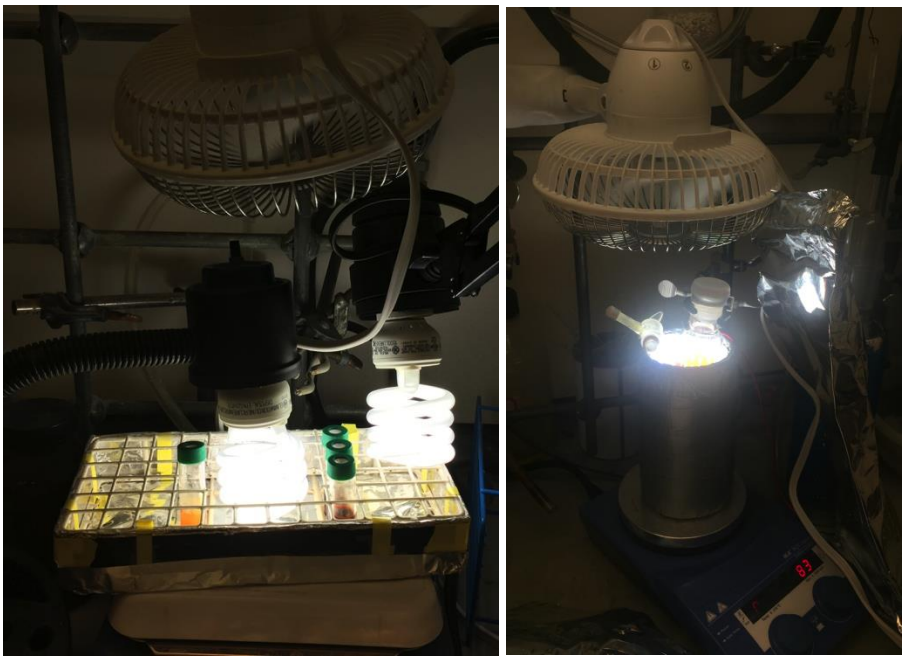

**Figure 7.10.** 0.5 mmol (left) and gram (right) scale photoredox cross-coupling reaction set-up.

**General procedure for successive photoredox cross-coupling reactions**

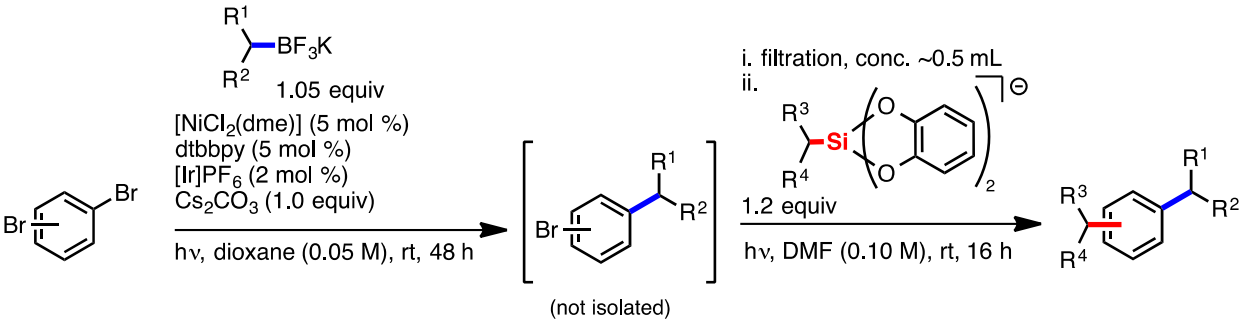


To a 4-dram clear glass vial equipped with a Teflon-coated magnetic stir bar was added 4,4'-di-*tert*-butyl-2,2'-bipyridine (6.7 mg, 0.025 mmol), and [$NiCl_2$(dme)] (5.5 mg, 0.025 mmol). The vial was capped and purged with nitrogen, then 1.5 mL THF was introduced. The resulting suspension was heated briefly with a heat gun until the nickel and ligand were fully solubilized, yielding a pale green solution. The solution was cooled in an ice bath, resulting in the immediate precipitation of an evergreen solid. Solvents were then evaporated in vacuo to give a fine coating of the ligated nickel complex. Once dry, aryl bromide (0.5 mmol, 1.0 equiv) (liquid aryl bromides were added with solvent), alkyltrifluoroborate (0.51 mmol, 1.05 equiv), and [$Ir(dFCF_3ppy)_2(bpy)]PF_6$ (10.1 mg, 0.01 mmol) were added in succession. The vial was then capped and purged four times. Under inert atmosphere, dioxane (10 mL) was introduced. The vial containing all the reagents was further sealed with Parafilm and stirred approximately 4 cm away from a 26 W fluorescent light bulb. A fan was blown across the reaction setup to suppress the heat generated by the latter (the reaction temperatures were estimated to be ~30 °C). After 48 h, the crude reaction mixture was filtered through an approximately 2 cm x 2 cm cylindrical plug of Celite in air, washing with dioxane (10 mL). The resulting solution was concentrated to approximately 0.5 mL in vacuo, then alkylsilicate (0.6 mmol, 1.2 equiv) and DMF (5 mL) were added successfully. The resulting solution was then capped and flushed with inert gas. The vial was further sealed with Parafilm and stirred approximately 4 cm away from a 26 W fluorescent light bulb for 16 h. Finally, the crude reaction

mixture was poured in a separatory funnel and diluted with $H_2O$ (20 mL). The resulting suspension was extracted with $Et_2O$ (3 × 30 mL), and the combined organic extracts were washed with a saturated solution of $Na_2CO_3$ (2 × 20 mL) then $H_2O$ (20 mL), dried ($MgSO_4$) and concentrated. The residue was purified by column chromatography on silica gel, eluting with EtOAc and hexanes, to obtain products in pure form.

**Compound Characterization Data**

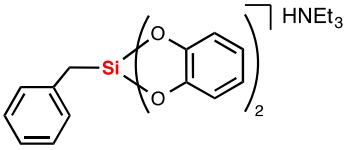


**Triethylammonium benzylbis(catecholato)silicate** (**1**): obtained as a white powder using THF as solvent (1.89 g, 92%), mp = 118 °C; $^1$H NMR ($CDCl_3$, 500.4 MHz): δ 7.00 (t, *J* = 7.7 Hz, 2 H), 6.90 (t, *J* = 7.7 Hz, 1 H), 6.85 (d, *J* = 7.7 Hz, 2 H), 6.72–6.66 (m, 8 H), 3.07 (q, *J* = 7.2 Hz, 6 H), 2.25 (s, 2 H), 1.14 (t, *J* = 7.6 Hz, 9 H) ppm; $^{13}$C {$^1$H} NMR ($CDCl_3$, 125.8 MHz): δ 149.3, 142.0, 129.0, 127.2, 122.9, 118.7, 110.7, 46.1, 26.0, 8.4 ppm; IR: ν = 3031, 2928, 1528, 1482, 1235, 816, 739, 695 cm$^{-1}$; HRMS (ESI) m/z calc. for $C_{19}H_{15}O_4Si$ [M – $HNEt_3$]$^-$ 335.0740, found 335.0744; $E_{pa}$ = + 0.70 V *vs* SCE.

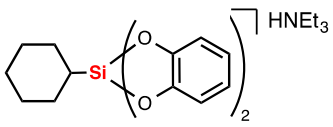


**Triethylammonium cyclohexylbis(catecholato)silicate** (**2**): obtained as a white powder using THF as solvent (1.14 g, 96%), mp 158 °C; $^1$H NMR ($CDCl_3$, 500.4 MHz): δ 6.74–6.68 (m, 4 H), 6.67–6.62 (m, 4 H), 3.24 (q, *J* = 7.2 Hz, 6 H), 1.63 (d, *J* = 14.0 Hz, 2 H), 1.54–1.51 (m, 3 H), 1.30 (t, *J* = 7.6 Hz, 9 H), 1.22–1.12 (m, 2 H), 1.12–1.01 (m, 3 H), 0.92–0.82 (tt, *J* = 12.2, 3.3 Hz, 1 H)

ppm; $^{13}$C NMR {$^{1}$H} ($CDCl_3$, 125.8 MHz): δ 150.0, 118.4, 110.3, 46.1, 29.4, 28.4, 28.1, 30.0, 8.53 ppm; IR: ν = 3030, 2944, 1486, 1458, 1357, 1262, 1231, 1205, 1101, 1015, 816, 742, 731, 685 cm$^{-1}$; HRMS (ESI) m/z calc. for $C_{18}H_{19}O_4Si$ [M – $HNEt_3$]$^-$ 327.1053, found 327.1055; $E_{pa}$ = + 0.74 V *vs* SCE.

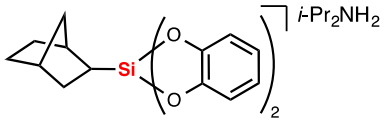


**Diisopropylammonium *exo*-2-bicyclo[2.2.1]heptylbis(catecholato)silicate** (**3**): obtained as a white powder using THF as solvent (1.14 g, 81%), mp 188 °C; $^{1}$H NMR ($CDCl_3$, 500.4 MHz): δ 6.74–6.68 (m, 4 H), 6.67–6.62 (m, 4 H), 3.24 (q, *J* = 7.2 Hz, 6 H), 2.22 (br s, 1 H), 2.02 (br s, 1 H), 1.65–1.58 (m, 1 H), 1.37–1.31 (m, 2 H), 1.28 (t, *J* = 7.5 Hz, 9 H), 1.22–1.16 (m, 1 H), 1.09–1.01 (m, 3 H), 0.91 (dt, *J* = 8.7, 2.6 Hz, 1 H), 0.79–0.74 (m, 1 H) ppm; $^{13}$C {$^{1}$H} NMR ($CDCl_3$, 125.8 MHz): δ 149.9, 149.7, 118.5, 118.4, 110.5, 110.4, 46.1, 38.4, 38.3, 36.6, 33.3, 32.9, 31.1, 29.1, 8.6 ppm; IR: ν = 3025, 2941, 1485, 1262, 1241, 1207, 1191, 1101, 1017, 816, 732, 704 cm$^{-1}$; HRMS (ESI) m/z calc. for $C_{19}H_{19}O_4Si$ [M – *i*-$Pr_2NH_2$]$^-$ 339.1058, found 339.1062.

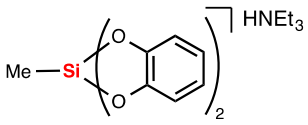


**Triethylammonium methylbis(catecholato)silicate** (**4**): obtained as a gray powder using THF as solvent (1.63 g, 73%), mp 168 °C; $^{1}$H NMR ($CDCl_3$, 500.4 MHz): δ 6.74–6.71 (m, 4 H), 6.69–6.64 (m, 4 H), 3.23 (q, *J* = 7.5 Hz, 6 H), 1.29 (t, *J* = 7.5 Hz, 9 H), 0.14 (s, 3 H) ppm; $^{13}$C {$^{1}$H} NMR ($CDCl_3$, 125.8 MHz): δ 149.2, 118.6, 110.7, 46.1, 8.5, –1.1 ppm; IR: ν = 3045, 1598, 1483, 1354, 1277, 1240, 1225, 1153, 1098, 1013, 826, 740 cm$^{-1}$; HRMS (ESI) m/z calc. for $C_{13}H_{11}O_4Si$ [M – $HNEt_3$]$^-$ 259.0432, found 259.0435.

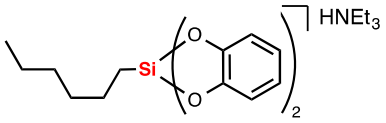


**Triethylammonium hexylbis(catecholato)silicate** (**5**): obtained as a white powder using THF as solvent (1.21 g, 88%), mp 116 °C; $^{1}$H NMR ($CDCl_3$, 500.4 MHz): δ 6.74–6.68 (m, 4 H), 6.67–6.62 (m, 4 H), 3.24 (q, *J* = 7.2 Hz, 6 H), 1.34–1.25 (m, 11 H), 1.18–1.10 (m, 6 H), 0.78 (t, *J* = 7.0 Hz, 3 H), 0.69–0.64 (m, 2 H) ppm; $^{13}$C {$^{1}$H} NMR ($CDCl_3$, 125.8 MHz): δ 149.9, 118.7, 110.8, 46.3, 33.2, 31.8, 24.5, 22.8, 17.1, 14.3, 8.9 ppm; IR: ν = 3035, 2924, 1484, 1355, 1239, 1100, 1014, 818, 734 cm$^{-1}$; HRMS (ESI) m/z calc. for $C_{18}H_{21}O_4Si$ [M – $HNEt_3$]$^-$ 329.1215, found 329.1212; $E_{pa}$ = + 0.75 V *vs* SCE.

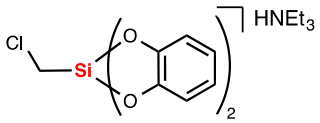


**Triethylammonium chloromethylbis(catecholato)silicate** (**6**): obtained as a light brown powder using THF as solvent (2.16 g, 93%), mp 108 °C; $^{1}$H NMR ($CDCl_3$, 500.4 MHz): δ 6.76–6.73 (m, 4 H), 6.72–6.68 (m, 4 H), 3.32 (q, *J* = 7.1 Hz, 6 H), 2.90 (s, 2 H), 1.37 (t, *J* = 7.1 Hz, 9 H) ppm; $^{13}$C {$^{1}$H} NMR ($CDCl_3$, 125.8 MHz): δ 149.0, 119.0, 110.8, 46.4, 30.4, 8.5 ppm; IR: ν = 2995, 1483, 1390, 1351, 1239, 1221, 1172, 1153, 1101, 1060, 1012, 829, 783, 771, 739 cm$^{-1}$; HRMS (ESI) m/z calc. for $C_{13}H_{10}ClO_4Si$ [M – $HNEt_3$]$^-$ 293.0037, found 293.0032.

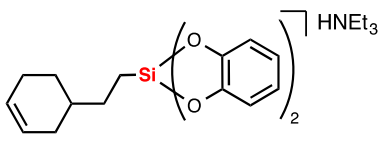

**Triethylammonium 2-(3-cyclohexenyl)ethylbis(catecholato)silicate** (**7**): obtained as a white powder using 1,4–dioxane as solvent (1.70 g, 86%), mp 102 °C; $^{1}$H NMR ($CDCl_3$, 500.4 MHz): δ 6.75–6.70 (m, 4 H), 6.68–6.64 (m, 4 H), 5.59–5.55 (m, 2 H), 3.27 (q, *J* = 7.3 Hz, 6 H), 2.01–1.85 (m, 3 H), 1.64–1.58 (m, 1 H), 1.51–1.43 (m, 1 H), 1.31 (t, *J* = 7.3 Hz, 9 H), 1.29–1.24 (m, 3 H), 1.07–0.97 (m, 1 H), 0.73–0.68 (m, 2 H) ppm; $^{13}$C {$^{1}$H} NMR ($CDCl_3$, 125.8 MHz): δ 149.6, 149.5, 127.0, 126.8, 118.5, 118.4, 110.6, 46.1, 36.2, 31.6, 31.0, 28.5, 25.4, 13.7, 8.4 ppm; IR: ν = 2913, 1484, 1390, 1356, 1261, 1241, 1227, 1205, 1014, 817, 759, 733, 679 cm$^{-1}$; HRMS (ESI) m/z calc. for $C_{20}H_{21}O_4Si$ [M – $HNEt_3$]$^-$ 353.1215, found 353.1217.

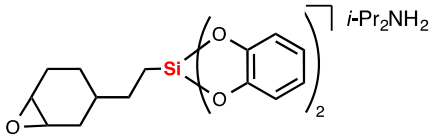


**Diisopropylammonium 2-(3,4-epoxycyclohexyl)ethylbis(catecholato)silicate** (**8**): obtained as a white powder using 1,4–dioxane as solvent (3.29 g, 86%), mp 140 °C; $^{1}$H NMR (DMSO–$d_6$, 500.4 MHz): δ 6.52–6.47 (m, 4 H), 6.44–6.40 (m, 4 H), 3.33 (sept, *J* = 6.4 Hz, 2 H), 3.19–3.15 (d, *J* = 10 Hz, 0.5 H), 3.00–2.93 (m, 1.5 H), 1.91–1.79 (m, 1.5 H), 1.58–1.48 (m, 1 H), 1.37–1.24 (m, 1 H), 1.18 (d, *J* = 6.4 Hz, 12 H), 1.14–0.99 (m, 4 H), 0.99–0.88 (m, 0.5 H), 0.82–0.63 (m, 1 H), 0.46–0.40 (m, 2 H) ppm; $^{13}$C {$^{1}$H} NMR (DMSO–$d_6$, 125.8 MHz): δ 151.1, 151.0, 117.4, 117.3, 109.8, 52.4, 52.0, 51.3, 51.2, 46.7, 35.1, 32.3, 31.8, 31.5, 30.9, 30.7, 26.7, 25.4, 24.4, 23.4, 19.4, 15.6, 15.4 ppm; IR: ν = 2986, 2919, 1485, 1238, 891, 813, 736 cm$^{-1}$; HRMS (ESI) m/z calc. for $C_{20}H_{21}O_5Si$ [M – *i*-$Pr_2NH_2$]$^-$ 369.1164, found 369. 1169.

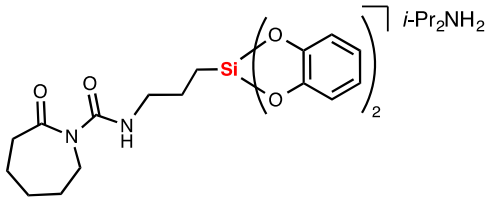

**Diisopropylammonium *N*-[5-(bis(catecholato)silicate)-2-aza-1-oxopentyl]caprolactam (9):** obtained as a white powder using 1,4–dioxane as solvent (2.74 g, 83%), mp 146 °C; $^{1}$H NMR ($CD_3CN$, 500.4 MHz): δ 9.10 (br s, 1 H), 6.67–6.62 (m, 4 H), 6.58–6.53 (m, 4 H), 3.89 (t, *J* = 4.5 Hz, 2 H), 3.53 (tt, *J* = 6.7, 6.7 Hz, 2 H), 3.03 (sept, *J* = 6.4 Hz, 2 H), 2.67–2.61 (m, 2 H), 1.73–1.65 (m, 4 H), 1.63–1.54 (m, 2 H), 1.46–1.37 (m, 2 H), 1.31 (d, *J* = 6.4 Hz, 12 H), 0.58–0.50 (m, 2 H) ppm; $^{13}$C {$^{1}$H} NMR (DMSO-$d_6$, 125.8 MHz): δ 179.3, 154.3, 150.9, 117.5, 109.9, 46.7, 43.4, 43.0, 39.3, 28.6, 28.3, 25.0, 23.3, 19.4, 15.9 ppm; IR: ν = 2928, 1698, 1485, 1239, 813, 738 cm$^{-1}$; HRMS (ESI) m/z calc. for $C_{22}H_{25}N_2O_6Si$ [M – *i*-$Pr_2NH_2$]$^-$ 441.1446, found 441.1441.

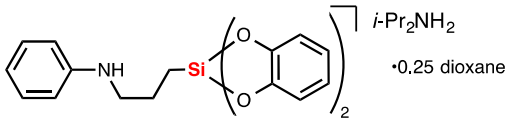


**Diisopropylammonium 3-(phenylamino)propylbis(catecholato)silicate (10):** obtained as a white powder using 1,4–dioxane as solvent (3.50 g, 89%), crystallized with 0.25 equiv 1,4–dioxane and a trace amount of $Et_2O$, mp 154 °C; $^{1}$H NMR (DMSO-$d_6$, 500.4 MHz): δ 8.01 (br s, 2 H), 6.99 (t, *J* = 7.3 Hz, 2 H), 6.54–6.51 (m, 4 H), 6.45–6.41 (m, 7 H), 5.32 (t, *J* = 5.1 Hz, 1 H), 3.34 (sept, *J* = 6.4 Hz, 2 H), 2.79 (td, *J* = 7.9, 5.1 Hz, 2 H), 1.46 (tt, *J* = 7.9, 7.9 Hz, 2 H), 1.19 (d, *J* = 6.4 Hz, 12 H), 0.54 (t, *J* = 7.9 Hz, 2 H) ppm; $^{13}$C {$^{1}$H} NMR (DMSO-$d_6$, 125.8 MHz): δ 151.0, 145.5, 129.1, 117.5, 115.2, 112.1, 109.9, 66.7, 16.8, 46.6, 24.7, 19.2, 16.2 ppm; IR: ν = 2859, 1601, 1484, 1239, 1149, 813, 739 cm$^{-1}$; HRMS (ESI) m/z calc. for $C_{21}H_{20}NO_4Si$ [M – *i*-$Pr_2NH_2$]$^-$ 378.1167, found 378.1167.

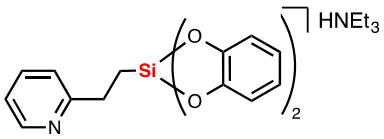


**Triethylammonium 2-(pyridin-2-yl)ethylbis(catecholato)silicate (11):** obtained as a white powder using THF as solvent (3.54 g, 91%), together with 8% of SM, mp = 168 °C; $^{1}$H NMR ($CDCl_3$, 500.4 MHz): δ 9.53 (br s, 1 H), 8.34 (d, *J* = 5.4 Hz, 1 H), 7.48 (dd, *J* = 7.9, *J* = 6.3 Hz, 1 H), 7.10 (d, *J* = 7.9 Hz, 1 H), 6.98 (dd, *J* = 6.3, *J* = 5.3 Hz, 1 H), 6.71–6.67 (m, 4 H), 6.65–6.60 (m, 4 H), 3.12 (q, *J* = 6.5 Hz, 6 H), 2.84 (m, 2 H), 1.22 (t, *J* = 6.5 Hz, 9 H), 1.12–1.07 (m, 2 H) ppm; $^{13}$C {$^{1}$H} NMR ($CDCl_3$, 125.8 MHz): δ 149.6, 147.6, 136.7, 125.5, 120.6, 118.4, 114.8, 110.7, 46.0, 32.6, 16.7, 9.2 ppm; IR: ν = 2859, 1601, 1484, 1239, 813, 739, 692 cm$^{-1}$; HRMS (ESI) m/z calc. for $C_{19}H_{16}NO_4Si$ $[M - HNEt_3]^-$ 350.0854, found 350.0851.

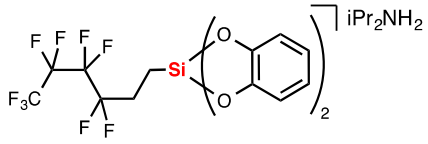


**Diisopropylammonium 3,3,4,4,5,5,6,6,6-nonafluorohexylbis(catecholato)silicate (12):** obtained as a white powder using THF as solvent (1.48 g, 92%), mp 65 °C; $^{1}$H NMR ($CDCl_3$, 500.4 MHz): δ 6.76–6.73 (m, 4 H), 6.69–6.66 (m, 4 H), 3.34 (sept, *J* = 6.6 Hz, 2 H), 2.16–2.02 (m, 2 H), 1.41 (d, *J* = 6.6 Hz, 12 H), 0.95–0.88 (m, 2 H) ppm; $^{13}$C {$^{1}$H} NMR ($CDCl_3$, 125.8 MHz): δ 149.3, 119.2, 111.0, 46.4, 26.4 (t, *J* = 22 Hz), 8.6, 5.9 ppm; $^{19}$F {$^{1}$H} NMR ($CDCl_3$, 470.8 MHz): –81.1, –116.4, –124.4, –126.1 ppm; IR: ν = 3049, 1599, 1484, 1352, 1238, 121, 1129, 1101, 1059, 1013, 877, 822, 792, 737, 690 cm$^{-1}$; HRMS (ESI) m/z calc. for $C_{18}H_{12}F_9O_4Si$ $[M - i\text{-}Pr_2NH_2]^-$ 491.0361, found 491.0361.

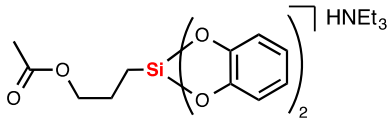

**Triethylammonium 3-acetoxypropylbis(catecholato)silicate (13):** obtained as a white powder using THF as solvent (1.92 g, 95%), mp 88 °C; $^{1}$H NMR ($CDCl_3$, 500.4 MHz): δ 6.75–6.73 (m, 4 H), 6.68–6.65 (m, 4 H), 3.89 (t, *J* = 7.2 Hz, 2 H), 3.28 (q, *J* = 6.6 Hz, 6 H), 1.94 (s, 3 H), 1.69–1.66 (m, 2 H), 1.32 (t, *J* = 6.6 Hz, 9 H), 0.71–0.66 (m, 2 H) ppm; $^{13}$C {$^{1}$H} NMR ($CDCl_3$, 125.8 MHz): δ 171.2, 149.4, 118.6, 110.7, 67.3, 46.1, 23.6, 21.0, 12.4, 8.4 ppm; IR: ν = 3038, 1725, 1483, 1238, 1197, 1030, 1016, 815, 735, 701, 664 cm$^{-1}$; HRMS (ESI) m/z calc. for $C_{17}H_{17}O_6Si$ [M – $HNEt_3$]$^-$ 345.0794, found 345.0796.

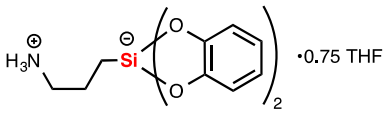


**3-Ammoniumpropylbis(catecholato)silicate (14):** obtained as a white powder using THF as solvent (1.97 g, 94%), crystallized with 0.75 equiv THF, mp >250 °C; $^{1}$H NMR (DMSO-$d_6$, 500.4 MHz): δ 7.43 (br s, 3 H), 6.55–6.51 (m, 4 H), 6.47–6.42 (m, 4 H), 2.59 (t, *J* = 7.6 Hz, 2 H), 1.48 (td, *J* = 7.6, 7.6 Hz, 2 H), 0.53–0.48 (m, 2 H) ppm; $^{13}$C {$^{1}$H} NMR (DMSO-$d_6$, 125.8 MHz): δ 150.8, 117.6, 110.0, 42.3, 23.3, 15.3 ppm; IR: ν = 3048, 2930, 1601, 1483, 1355, 1242, 1101, 1048, 1013, 889, 826, 733, 705 cm$^{-1}$; HRMS (ESI) m/z calc. for $C_{15}H_{16}NO_4Si$ [M – H]$^-$ 302.0854, found 302.0859.

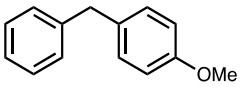


**1-Benzyl-4-methoxybenzene (15):** obtained as a colorless oil (76 mg, 77%); $^{1}$H NMR ($CDCl_3$, 500.4 MHz): δ 7.28 (t, *J* = 7.5 Hz, 2 H), 7.20–7.16 (m, 3 H), 7.10 (d, *J* = 9.0 Hz, 2 H), 6.83 (d, *J* = 9.0 Hz, 2 H), 3.92 (s, 2 H), 3.78 (s, 3 H) ppm; $^{13}$C {$^{1}$H} NMR ($CDCl_3$, 125.8 MHz): 158.1, 141.7, 133.4, 130.0, 129.0, 128.6, 126.1, 114.0, 55.4, 41.2 ppm; HRMS (ESI) m/z calc. for $C_{14}H_{14}O$ [M]$^+$ 198.1045, found 198.1048.[28]

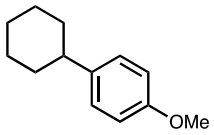


**1-Cyclohexyl-4-methoxybenzene (16):** obtained as a colorless oil (89 mg, 94%); $^{1}$H NMR ($CDCl_3$, 500.4 MHz): δ 7.13 (d, *J* = 7.6 Hz, 2 H), 6.84 (d, *J* = 7.6 Hz, 2 H), 3.78 (s, 3 H), 2.47–2.41 (m, 1 H), 1.86–1.71 (m, 4 H), 1.73 (dd, *J* = 13.0, 4.7 Hz, 1 H), 1.44–1.32 (m, 4 H), 1.29–1.19 (m, 1 H) ppm; $^{13}$C NMR ($CDCl_3$, 125.8 MHz): 157.8, 140.5, 127.8, 113.8, 55.4, 43.9, 34.9, 27.1, 26.3 ppm; HRMS (ESI) m/z calc. for $C_{13}H_{18}O$ $[M]^+$ 190.1358, found 190.1359.[29]

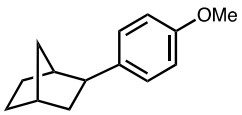


***exo*-2-(4-Methoxyphenyl)bicyclo[2.2.1]heptane (17):** obtained as a colorless oil (92 mg, 91%); $^{1}$H NMR ($CDCl_3$, 500.4 MHz): δ 7.16 (d, *J* = 8.6 Hz, 2 H), 6.86 (d, *J* = 8.6 Hz, 2 H), 3.81 (s, 3 H), 2.71 (dd, *J* = 6.3, 8.8 Hz, 1 H), 2.37 (d, *J* = 5.8 Hz, 2 H), 1.77 (ddd, *J* = 2.4, 9.9, 9.9 Hz, 1 H), 1.69–1.52 (m, 4 H), 1.41–1.34 (m, 1 H), 1.31–1.26 (m, 1 H), 1.19 (d, *J* = 4.5 Hz, 1 H) ppm; $^{13}$C {$^{1}$H} NMR ($CDCl_3$, 125.8 MHz): 157.6, 139.9, 128.1, 113.7, 55.4, 46.7, 43.3, 39.3, 37.0, 36.1, 30.7, 29.1 ppm; IR: ν = 2948, 2848, 2833, 1611, 1510, 1463, 1454, 1441, 1294, 1277, 1245, 1208, 1178, 1139, 1107, 1035, 822, 763, 600, 532 $cm^{-1}$; HRMS (ESI) m/z calc. for $C_{14}H_{18}O$ $[M]^+$ 202.1358, found 202.1356.

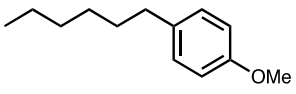

**1-Hexyl-4-methoxybenzene (19):** obtained as a colorless oil (82 mg, 85%); $^{1}$H NMR ($CDCl_3$, 500.4 MHz): δ 7.09 (d, *J* = 8.7 Hz, 2 H), 6.82 (d, *J* = 8.7 Hz, 2 H), 3.78 (s, 3 H), 2.54 (t, *J* = 7.4 Hz, 2 H), 1.57 (q, *J* = 7.2 Hz, 2 H), 1.35–1.26 (m, 6 H), 0.88 (t, *J* = 6.9 Hz, 3 H) ppm; $^{13}$C {$^{1}$H} NMR ($CDCl_3$, 125.8 MHz): 157.7, 146.1, 129.4, 113.8, 55.4, 35.2, 31.9, 29.1, 22.8, 14.7 ppm; HRMS (ESI) m/z calc. for $C_{13}H_{19}O$ $[M - H]^+$ 191.1436, found 191.1426.[30]

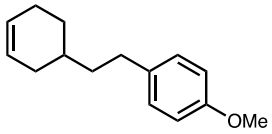


**1-(2-(Cyclohex-3-en-1-yl)ethyl)-4-methoxybenzene (21):** obtained as a colorless oil (100 mg, 93%); $^{1}$H NMR ($CDCl_3$, 500.4 MHz): δ 7.12 (d, *J* = 8.0 Hz, 2 H), 6.84 (d, *J* = 8.0 Hz, 2 H), 5.67 (br s, 2 H), 3.80 (s, 3 H), 2.61 (t, *J* = 7.3 Hz, 2 H), 2.16 (dd, *J* = 17.3, 4.0 Hz, 1 H), 2.09–2.02 (m, 2 H), 1.83–1.77 (m, 1 H), 1.76–1.68 (m, 1 H), 1.63–1.55 (m, 3 H), 1.33–1.22 (m, 1 H) ppm; $^{13}$C {$^{1}$H} NMR ($CDCl_3$, 125.8 MHz): 157.5, 134.9, 129.1, 126.9, 126.4, 113.6, 55.2, 38.7, 32.9, 32.2, 31.7, 28.8, 25.1 ppm; IR: ν = 3021, 2910, 2834, 1612, 1511, 1489, 1454, 1440, 1300, 1242, 1176, 1141, 1109, 1037, 820, 727, 653, 562, 521 $cm^{-1}$; HRMS (ESI) m/z calc. for $C_{15}H_{20}O$ $[M]^+$ 216.1514, found 216.1511.

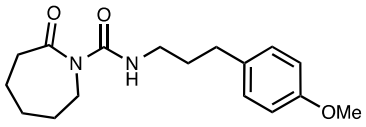


***N*-[(3-(4-Methoxyphenyl)propyl)-2-aza-1-oxopentyl]caprolactam (23):** obtained as a colorless oil (81 mg, 53%); $^{1}$H NMR ($CDCl_3$, 500.4 MHz): δ 9.30 (br s, 1 H), 7.10 (d, *J* = 8.3 Hz, 2 H), 6.82 (d, *J* = 8.3 Hz, 2 H), 3.98 (d, *J* = 2.1 Hz, 2 H), 3.77 (s, 3 H), 3.29 (q, *J* = 6.4 Hz, 2 H), 2.71–2.68 (m, 2 H), 2.61 (t, *J* = 8.3 Hz, 2 H), 1.85 (q, *J* = 7.7 Hz, 2 H), 1.80–1.68 (m, 6 H) ppm; $^{13}$C {$^{1}$H}

NMR ($CDCl_3$, 125.8 MHz): 179.6, 157.9, 155.0, 133.7, 129.4, 113.9, 55.4, 43.9, 40.1, 39.9, 32.4, 31.4, 29.3, 28.5, 23.7 ppm; IR: ν = 2930, 1695, 1610, 1529, 1510, 1462, 1454, 1437, 1317, 1350, 1332, 1300, 1242, 1213, 1175, 1164, 969, 809 $cm^{-1}$; HRMS (ESI) m/z calc. for $C_{17}H_{25}N_2O_3$ $[M + H]^+$ 305.1865, found 305.1861.

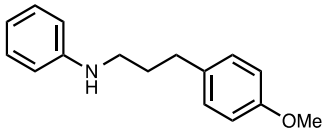


***N*-(3-(4-Methoxyphenyl)propyl)aniline (24):** obtained as a yellow crystalline solid (77 mg, 64%); mp, 66-67 °C, $^1H$ NMR ($CDCl_3$, 500.4 MHz): δ 7.18 (td, *J* = 7.4, 1.1 Hz, 2 Hz), 7.13 (d, *J* = 8.2 Hz, 2 H), 6.86 (d, *J* = 8.9 Hz, 2 H), 6.71 (tt, *J* = 7.3, 1.1 Hz, 1 H), 6.60 (dd, *J* = 8.6, 1.1 Hz, 2 H), 3.81 (s, 3 H), 3.38–3.92 (br s, 1 H), 3.16 (t, *J* = 7.5 Hz, 2 H), 2.70 (t, *J* = 7.5 Hz, 2 H), 1.94 (tt, *J* = 7.5, 7.5 Hz, 2 H) ppm; $^{13}C$ {$^1H$} NMR ($CDCl_3$, 125.8 MHz): 157.8, 148.3, 133.6, 129.8, 129.1, 117.2, 113.8, 112.7, 55.2, 43.4, 32.4, 31.2 ppm; IR: ν = 3388, 2911, 2851, 1603, 1507, 1472, 1320, 1255, 1237, 1176, 1095, 1057, 991, 811, 768, 748, 557, 511 $cm^{-1}$; HRMS (ESI) m/z calc. for $C_{16}H_{20}NO$ $[M + H]^+$ 242.1545, found 242.1550.

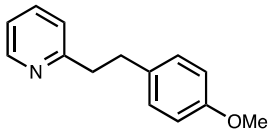


**2-(4-Methoxyphenethyl)pyridine (25):** obtained as a colorless oil (53 mg, 50%); $^1H$ NMR ($CDCl_3$, 500.4 MHz): δ 8.55 (dd, *J* = 4.5, 2.3 Hz, 1 H), 7.55 (ddd, *J* = 7.5, 7.5, 2.1 Hz, 1 H), 7.12–7.08 (m, 3 H), 7.06 (d, *J* = 7.7 Hz, 1 H), 6.81 (d, *J* = 8.6 Hz, 2 H), 3.77 (s, 3 H), 3.09–3.03 (m, 2 H), 3.02–2.96 (m, 2 H) ppm; $^{13}C$ {$^1H$} NMR ($CDCl_3$, 125.8 MHz): 161.3, 157.8, 149.2, 136.2,

133.6, 129.3, 122.9, 121.0, 113.7, 55.15, 40.42, 35.1 ppm; IR: ν = 3006, 2932, 1610, 1588, 1568, 1510, 1473, 1454, 1434, 1300, 1242, 1177, 1149, 1034, 822, 749 $cm^{-1}$; HRMS (ESI) m/z calc. for $C_{14}H_{16}NO$ $[M + H]^+$ 214.1232, found 214.1236.

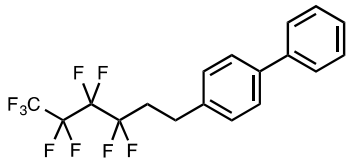

**4-(3,3,4,4,5,5,6,6,6-Nonafluorohexyl)-1,1'-biphenyl (26):** obtained as a colorless solid (177 mg, 88%), mp 55 °C; $^1H$ NMR ($CDCl_3$, 500.4 MHz): δ 7.57 (d, *J* = 7.8 Hz, 2 H), 7.54 (d, *J* = 7.8 Hz, 2 H), 7.43 (dd, *J* = 7.7, 7.4 Hz, 2 H), 7.33 (t, *J* = 7.4 Hz, 1 H), 7.27 (d, *J* = 7.7 Hz, 2 H), 2.98–2.84 (m, 2 H), 2.47–2.34 (m, 2 H) ppm; $^{13}C$ {$^1H$} NMR ($CDCl_3$, 125.8 MHz): 140.7, 139.7, 138.1, 128.7, 128.6, 127.4, 127.2, 126.9, 32.8 (t, *J* = 22.3 Hz), 26.0 ppm; $^{19}F$ {$^1H$} NMR ($CDCl_3$, 470.8 MHz): –81.1, –114.2, –124.4, –125.9 ppm; IR: ν = 1488, 1357, 1301, 1215, 1167, 1130, 1089, 1049, 1007, 983, 881, 838, 760, 750, 734, 693 $cm^{-1}$; HRMS (ESI) m/z calc. for $C_{18}H_{13}F_9$ $[M]^+$ 400.0874, found 400.0875.

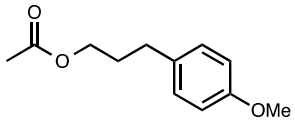

**3-(4-Methoxyphenyl)propyl acetate (27):** obtained as a colorless oil (82 mg, 79%); $^1H$ NMR ($CDCl_3$, 500.4 MHz): δ 7.10 (d, *J* = 8.4 Hz, 2 H), 6.83 (d, *J* = 8.4 Hz, 2 H), 4.07 (t, *J* = 6.5 Hz, 2 H), 3.79 (s, 3 H), 2.63 (t, *J* = 7.9 Hz, 2 H), 2.06 (s, 3 H), 1.92 (tt, *J* = 6.5, 7.9 Hz, 2 H) ppm; $^{13}C$ {$^1H$} NMR ($CDCl_3$, 125.8 MHz): 171.3, 158.0, 133.4, 129.4, 114.0, 64.0, 55.4, 31.4, 30.6, 21.2

ppm; IR: ν = 2953, 1735, 1612, 1511, 1464, 1386, 1365, 1300, 1235, 1177, 1113, 1033, 951, 810, 700, 532 $cm^{-1}$; HRMS (ESI) m/z calc. for $C_{12}H_{16}O_3$ $[M]^+$ 208.1299, found 208.1297.

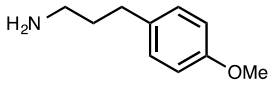


**3-(4-Methoxyphenyl)propan-1-amine (28):** obtained as a yellow oil (56 mg, 68%); $^1H$ NMR ($CDCl_3$, 500.4 MHz): δ 7.09 (d, *J* = 7.0 Hz, 2 H), 6.82 (d, *J* = 7.0 Hz, 2 H), 3.78 (s, 3 H), 2.71 (t, *J* = 6.8 Hz, 2 H), 2.59 (t, *J* = 7.8 Hz, 2 H), 1.78 (tt, *J* = 6.8, 7.8 Hz 2 H) 1.39 (br s, 2 H) ppm; $^{13}C$ {$^1H$} NMR ($CDCl_3$, 125.8 MHz): 157.7, 134.1, 129.2, 113.7, 55.1, 41.6, 35.5, 32.2 ppm; IR: ν = 3320, 2925, 2854, 1663, 1611, 1584, 1512, 1464, 1300, 1245, 1177, 1093, 1035, 907, 648, 530 $cm^{-1}$; HRMS (ESI) m/z calc. for $C_{10}H_{16}NO$ $[M + H]^+$ 166.1231, found 166.1232.

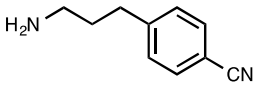


**4-(3-Aminopropyl)benzonitrile (29):** obtained as a light brown oil (69 mg, 86%); $^1H$ NMR ($CDCl_3$, 500.4 MHz): δ 7.57 (d, *J* = 8.0 Hz, 2 H), 7.29 (d, *J* = 8.0 Hz, 2 H), 2.88–2.80 (br s, 2 H), 2.80–2.70 (m, 4 H), 1.81 (tt, *J* = 7.7, 7.5 Hz, 2 H) ppm; $^{13}C$ {$^1H$} NMR ($CDCl_3$, 125.8 MHz): 147.5, 132.1, 129.1, 119.0, 109.7, 41.0, 33.8, 33.2 ppm; IR: ν = 3124, 3110, 2869, 2270, 1678, 1607, 1554, 1452, 1403, 1179, 850, 698 $cm^{-1}$; HRMS (ESI) m/z calc. for $C_{10}H_{13}N_2$ $[M + H]^+$ 161.1079, found 161.1082.

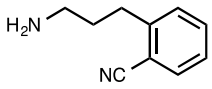

**2-(3-Aminopropyl)benzonitrile (30):** obtained as a dark yellow oil (67 mg, 84%); $^{1}$H NMR ($CDCl_3$, 500.4 MHz): δ 7.58 (d, *J* = 8.0 Hz, 1 H), 7.49 (t, *J* = 7.5 Hz, 1 H), 7.31 (d, *J* = 7.5 Hz, 1 H), 7.29–7.24 (m, 1 H), 2.87 (t, *J* = 6.6 Hz, 2 H), 2.76 (t, *J* = 5.7 Hz, 2 H), 2.24 (br s, 2 H), 1.87–1.77 (m, 2 H) ppm; $^{13}$C {$^{1}$H} NMR ($CDCl_3$, 125.8 MHz): 146.2, 133.0, 132.9, 129.7, 126.7, 118.2, 112.4, 41.5, 34.4, 32.0 ppm; IR: ν = 3364, 2933, 2867, 2223, 1710, 1661, 1599, 1573, 1448, 1364, 1314, 1164, 1035, 844, 759, 665, 539, 508 cm$^{-1}$; HRMS (ESI) m/z calc. for $C_{10}H_{12}N_2Na$ $[M + Na]^+$ 183.0898, found 183.0901.

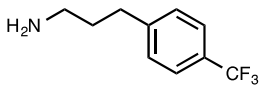


**3-(4-(Trifluoromethyl)phenyl)propan-1-amine (31):** obtained as a brown oil (82 mg, 81%); $^{1}$H NMR ($CDCl_3$, 500.4 MHz): 7.54 (d, *J* = 7.5 Hz, 2 H), 7.31 (d, *J* = 7.5 Hz, 2 H), 2.78–2.71 (m, 4 H), 1.80 (tt, *J* = 7.3, 7.2 Hz, 2 H), 1.36 (br s, 2 H) ppm; $^{13}$C {$^{1}$H} NMR ($CDCl_3$, 125.8 MHz): 146.9, 128.6, 128.1, 125.2 (q, *J* = 3.4 Hz), 123.2, 41.5, 34.9, 33.02 ppm; $^{19}$F {$^{1}$H} NMR ($CDCl_3$, 470.8 MHz): –62.3 ppm; IR: ν = 2934, 2862, 1617, 1585, 1454, 1418, 1322, 1160, 1112, 1065, 1018, 953, 840, 815, 730, 630 cm$^{-1}$; HRMS (ESI) m/z calc. for $C_{10}H_{13}NF_3$ $[M + H]^+$ 204.1002, found 204.1000.

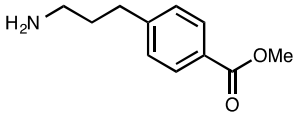


**Methyl 4-(3-aminopropyl)benzoate (32):** obtained as a colorless solid (91 mg, 94%), mp 104 °C; $^{1}$H NMR ($CDCl_3$, 500.4 MHz): 7.94 (d, *J* = 7.7 Hz, 2 H), 7.24 (d, *J* = 7.7 Hz, 2 H), 3.89 (s, 3 H), 2.75–2.66 (m, 4 H), 2.43–2.00 (m, 2 H), 1.78 (tt, *J* = 7.2, 7.4 Hz, 2 H) ppm; $^{13}$C {$^{1}$H} NMR ($CDCl_3$, 125.8 MHz): 166.9, 147.5, 129.6, 128.3, 127.7, 51.8, 41.5, 34.7, 33.2 ppm; IR: ν = 2922, 2857,

1717, 1608, 1574, 1435, 1416, 1392, 1310, 1271, 1210, 1177, 110, 1020, 763, 701 $cm^{-1}$; HRMS (ESI) m/z calc. for $C_{11}H_{16}NO_2$ $[M + H]^+$ 194.1181, found 194.1183.

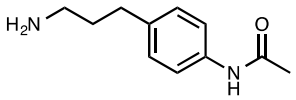

***N*-(4-(3-Aminopropyl)phenyl)acetamide (33):** obtained as an off white powder (72 mg, 75%), mp 94 °C; $^1H$ NMR (DMSO-$d_6$, 500.4 MHz): δ 9.91 (s, 1 H), 7.49 (d, *J* = 8.9 Hz, 2 H), 7.10 (d, *J* = 8.9 Hz, 2 H), 4.21 (br s, 2 H), 2.61 (br s, 1 H), 2.55 (t, *J* = 6.6 Hz, 2 H), 2.52–2.49 (m, 1 H), 2.02 (s, 3 H), 1.77–1.66 (m, 2 H) ppm; $^{13}C$ {$^1H$} NMR (DMSO-$d_6$, 125.8 MHz): 168.4, 137.6, 136.6, 128.7, 119.4, 33.1, 32.8, 32.1, 24.3 ppm; IR: ν = 3244, 3180, 3112, 3030, 2930, 2858, 1662, 1601, 1536, 1813, 1410, 1370, 1316, 1264, 828, 790, 745 $cm^{-1}$; HRMS (ESI) m/z calc. for $C_{11}H_{16}N_2ONa$ $[M + Na]^+$ 215.1166, found 215.1160.

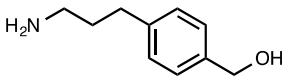

**(4-(3-Aminopropyl)phenyl)methanol (34):** obtained as a brown oil (69 mg, 85%); $^1H$ NMR ($CDCl_3$, 500.4 MHz): δ 7.30 (d, *J* = 8.2 Hz, 2 H), 7.19 (d, *J* = 8.9 Hz, 2 H), 4.67 (s, 2 H), 2.74 (t, *J* = 7.1 Hz, 2 H), 2.67 (t, *J* = 7.9 Hz, 2 H), 1.78 (tt, *J* = 7.1, 7.9 Hz, 2 H), 1.51 (br s, 3 H) ppm; $^{13}C$ {$^1H$} NMR ($CDCl_3$, 125.8 MHz): 141.4, 138.5, 128.5, 127.1, 65.0, 41.6, 35.2, 32.9 ppm; IR: ν = 3338, 2970, 2933, 2883, 1466, 1407, 1378, 1341, 1306, 1160, 1128, 1108, 951, 817, 644, 487 $cm^{-1}$; HRMS (ESI) m/z calc. for $C_{10}H_{16}NO$ $[M + H]^+$ 166.1236, found 166.1232.

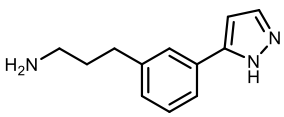

**3-(3-(1H-Pyrazol-5-yl)phenyl)propan-1-amine (35):** obtained as a dark yellow oil (71 mg, 71%); $^{1}$H NMR ($CDCl_3$, 500.4 MHz): δ 7.58-7.52 (m, 3 H), 7.26 (dd, *J* = 7.5, 7.5 Hz, 1 H), 7.08 (d, *J* = 7.5 Hz, 1 H), 6.55 (s, 1 H), 5.15–4.81 (br s, 3 H), 2.70 (tt, *J* = 7.0, 7.0 Hz, 2 H), 2.61 (t, *J* = 7.0 Hz, 2 H), 1.76 (t, *J* = 7.0 Hz, 2 H) ppm; $^{13}$C {$^{1}$H} NMR ($CDCl_3$, 125.8 MHz): 148.7, 142.6, 133.7, 132.3, 128.9, 128.2, 125.8, 123.5, 102.6, 41.5, 34.8, 30.7 ppm; IR: ν = 3158, 3049, 2924, 2855, 1661, 1607, 1587, 1471, 1434, 1352, 1248, 1097, 1041, 923, 907, 794, 759, 699, 609 cm$^{-1}$; HRMS (ESI) m/z calc. for $C_{12}H_{16}N_3$ $[M + H]^+$ 202.1343, found 202.1344.

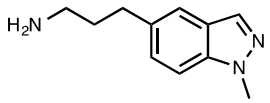


**3-(1-Methyl-1*H*-indazol-5-yl)propan-1-amine (36):** obtained as a light brown oil (91 mg, 96%); $^{1}$H NMR ($CDCl_3$, 500.4 MHz): δ 7.98 (s, 1 H), 7.27 (dd, *J* = 6.8, 7.4 Hz, 1 H), 7.20 (d, *J* = 7.4 Hz, 1 H), 6.89 (d, *J* = 6.8 Hz, 1 H), 4.03 (s, 3 H), 2.91 (t, *J* = 6.9 H, 2 H), 2.85–2.59 (m, 2 H), 1.92 (t, *J* = 8.2 H, 2 H), 1.27 (br s, 1 H), 0.97 (br s, 1 H) ppm; $^{13}$C {$^{1}$H} NMR ($CDCl_3$, 125.8 MHz): 140.1, 135.2, 131.4, 126.6, 123.9, 119.7, 107.0, 41.4, 35.7, 32.6, 30.7 ppm; IR: ν = 2928, 2848, 2727, 1611, 1463, 1449, 1440, 1432, 1392, 1230, 1152, 987, 970, 954, 817, 783, 744, 730 cm$^{-1}$; HRMS (ESI) m/z calc. for $C_{11}H_{16}N_3$ $[M + H]^+$ 190.1344, found 190.1346.

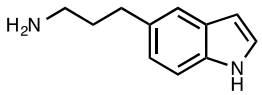


**3-(1*H*-Indol-5-yl)propan-1-amine (37):** obtained as a light yellow oil (76 mg, 87%); $^{1}$H NMR ($CDCl_3$, 500.4 MHz): δ 8.54 (br s, 1 H), 7.45 (s, 1 H), 7.29 (d, *J* = 5.1 Hz, 1 H), 7.15 (s, 1 H), 7.02 (d, *J* = 5.1 Hz, 1 H), 6.49 (s, 1 H), 2.92–2.71 (m, 4 H), 1.87 (br s, 2 H), 1.34–1.21 (m, 2 H) ppm;

$^{13}C$ {$^{1}H$} NMR ($CDCl_3$, 125.8 MHz): δ 134.39, 133.0, 126.0, 124.4, 122.7, 119.0, 110.8, 101.9, 33.4, 33.2, 29.6 ppm; IR: ν = 3229, 2922, 1615, 1512, 1476, 1422, 1343, 1046, 1022, 999, 820, 767 $cm^{-1}$; HRMS (ESI) m/z calc. for $C_{11}H_{15}N_2$ $[M + H]^+$ 175.1235, found 175.1239.

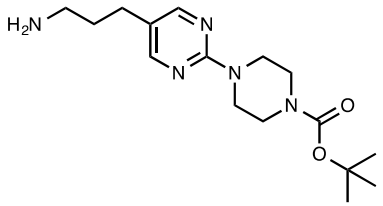

***tert*-Butyl 4-(5-(3-aminopropyl)pyrimidin-2-yl)piperazine-1-carboxylate (38):** obtained as an off white powder (86 mg, 53%), mp 126 °C; $^{1}H$ NMR ($CDCl_3$, 500.4 MHz): δ 8.16 (s, 2 H), 4.60–4.07 (m, 2 H), 3.74 (br s, 4 H), 3.47 (br s, 4 H), 2.90–2.70 (m, 2 H), 2.48 (br s, 2 H), 1.86–1.69 (m, 2 H), 1.47 (s, 9 H) ppm; $^{13}C$ {$^{1}H$} NMR ($CDCl_3$, 125.8 MHz): 180.7, 157.4, 154.7, 122.3, 79.8, 43.7, 44.4–42.8 (m, 2 C) 43.1, 28.35, 26.6 ppm; IR: ν = 2922, 2858, 1683, 1603, 1537, 1487, 1450, 1417, 1365, 1243, 1166, 1126, 1085, 997, 949 $cm^{-1}$; HRMS (ESI) m/z calc. for $C_{16}H_{28}N_5O_2$ $[M + H]^+$ 322.2243, found 322.2238.

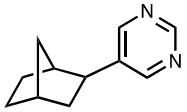

**5-(*exo*-Bicyclo[2.2.1]heptan-2-yl)pyrimidine (39):** reaction carried out starting from 0.368 mmol of ArBr, obtained as a colorless oil (63 mg, 98%); $^{1}H$ NMR ($CDCl_3$, 500.4 MHz): δ 9.02 (s, 1 H), 8.58 (s, 2 H), 2.72 (dd, *J* = 5.6, 9.3 Hz, 1 H), 2.42 (t, *J* = 4.6 Hz, 1 H), 2.38 (d, *J* = 3.3 Hz, 1 H), 1.83 (ddd, *J* = 2.4, 9.4, 11.2 Hz, 1 H), 1.71–1.57 (m, 3 H), 1.48 (dt, *J* = 2.0, 2.0, 10.0 Hz, 1 H), 1.42–1.36 (m, 1 H), 1.32–1.23 (m, 2 H) ppm; $^{13}C$ {$^{1}H$} NMR ($CDCl_3$, 125.8 MHz): 156.1, 155.6, 139.8, 42.9, 42.3, 38.4, 36.8, 36.0, 30.2, 28.5 ppm; IR: ν = 3041, 2950, 2870, 1557, 1454, 1411, 1330, 1312, 1298, 1273, 1236, 1208, 1190, 1166, 1138, 1036, 728 $cm^{-1}$; HRMS (ESI) m/z calc. for $C_{11}H_{15}N_2$ $[M + H]^+$ 175.1235, found 175.1238.

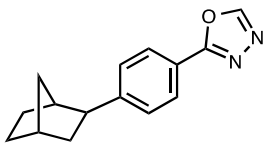


**2-(4-(*exo*-Bicyclo[2.2.1]heptan-2-yl)phenyl)-1,3,4-oxadiazole (40):** obtained as a colorless solid (113 mg, 94%), mp 101 °C; $^{1}$H NMR ($CDCl_3$, 500.4 MHz): δ 8.44 (s, 1 H), 7.99 (d, *J* = 7.7 Hz, 2 H), 7.37 (d, *J* = 7.7 Hz, 2 H), 2.82 (dd, *J* = 5.7, 8.9 Hz, 1 H), 2.38–2.34 (m, 2 H), 1.78 (ddd, *J* = 2.2, 9.5, 11.9 Hz, 1 H), 1.71–1.57 (m, 3 H), 1.53 (dd, *J* = 2.8, 9.4 Hz, 1 H), 1.39 (t, *J* = 9.2 Hz, 1 H), 1.34–1.27 (m, 1 H), 1.24 (dd, *J* = 2.8, 9.3 Hz, 1 H) ppm; $^{13}$C {$^{1}$H} NMR ($CDCl_3$, 125.8 MHz): 164.8, 152.3, 152.1, 127.7, 126.9, 120.5, 47.4, 42.6, 39.0, 36.8, 36.1, 30.5, 28.7 ppm; IR: ν = 3110, 2955, 2867, 1611, 1578, 1504, 1493, 1453, 1413, 1097, 1066, 1015, 954, 895, 847, 831, 713 $cm^{-1}$; HRMS (ESI) m/z calc. for $C_{15}H_{16}N_2ONa$ $[M + Na]^+$ 263.1160, found 263.1163.

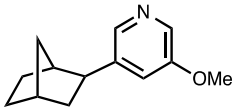


**3-(*exo*-Bicyclo[2.2.1]heptan-2-yl)-5-methoxypyridine (41):** obtained as a light brown oil (77 mg, 76%); $^{1}$H NMR ($CDCl_3$, 500.4 MHz): δ 8.09 (br s, 2 H), 7.02 (s, 1 H), 3.83 (s, 3 H), 2.72 (dd, *J* = 5.6, 9.0 Hz, 1 H), 2.38–2.34 (m, 2 H), 1.78 (ddd, *J* = 2.0, 10.0, 11.0 Hz, 1 H), 1.65–1.52 (m, 3 H), 1.49 (dd, *J* = 2.5, 9.7 Hz, 1 H), 1.36 (t, *J* = 9.0 Hz, 1 H), 1.30–1.24 (m, 1 H), 1.21 (dd, *J* = 2.8, 9.3 Hz, 1 H) ppm; $^{13}$C {$^{1}$H} NMR ($CDCl_3$, 125.8 MHz): 155.5, 143.4, 141.6, 133.7, 119.5, 55.40, 44.7, 42.6, 38.7, 36.7, 36.1, 30.4, 28.6 ppm; IR: ν = 2949, 2869, 1585, 1456, 1242, 1283, 1264, 1178, 1158, 1039, 866, 716 $cm^{-1}$; HRMS (ESI) m/z calc. for $C_{13}H_{18}NO$ $[M + H]^+$ 204.1388, found 204.1392.

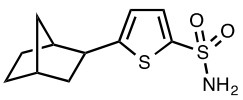

**5-(*exo*-Bicyclo[2.2.1]heptan-2-yl)thiophene-2-sulfonamide (42):** obtained as a colorless oil (91 mg, 71%); $^{1}$H NMR ($CDCl_3$, 500.4 MHz): δ 7.48 (d, *J* = 4.1 Hz, 1 H), 6.74 (d, *J* = 4.1 Hz, 1 H), 5.13 (br s, 2 H), 2.95 (dd, *J* = 5.5, 8.8 Hz, 1 H), 2.40–2.35 (m, 2 H), 1.87 (ddd, *J* = 3.4, 9.8, 10.9 Hz, 1 H), 1.71–1.57 (m, 3 H), 1.53 (dt, *J* = 2.0, 2.0, 10.0 Hz, 1 H), 1.40–1.34 (m, 1 H), 1.29–1.24 (m, 2 H) ppm; $^{13}$C {$^{1}$H} NMR ($CDCl_3$, 125.8 MHz): 160.4, 138.9, 131.8, 122.7, 44.8, 43.5, 40.5, 36.5, 36.2, 29.7, 28.4 ppm; IR: ν = 3264, 2950, 2870, 1593, 1545, 1440, 1330, 1154, 1083, 1013, 892, 810, 804, 729, 671 cm$^{-1}$; HRMS (ESI) m/z calc. for $C_{11}H_{14}NO_2S_2$ $[M - H]^-$ 256.0466, found 256.0464.

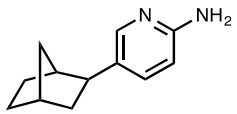


**5-(*exo*-Bicyclo[2.2.1]heptan-2-yl)pyridin-2-amine (43):** obtained as a light brown solid (60 mg, 64%), mp 104 °C; $^{1}$H NMR ($CDCl_3$, 500.4 MHz): δ 7.93 (d, *J* = 1.9 Hz, 1 H), 7.29 (dd, *J* = 1.9, 8.3 Hz, 1 H), 6.44 (d, *J* = 8.3 Hz, 1 H), 4.31 (br s, 2 H), 2.60 (dd, *J* = 5.9, 8.9 Hz, 1 H), 2.34 (br s, 1 H), 2.26 (br s, 1 H), 1.72 (ddd, *J* = 3.3, 9.1, 10.0 Hz, 1 H), 1.60–1.55 (m, 3 H), 1.47 (dt, *J* = 1.9, 1.9, 10.1 Hz, 1 H), 1.36–1.20 (m, 2 H), 1.17 (d, *J* = 8.3 Hz, 1 H) ppm; $^{13}$C {$^{1}$H} NMR ($CDCl_3$, 125.8 MHz): 156.2, 146.4, 136.7, 132.8, 108.2, 44.2, 42.9, 38.8, 36.7, 35.9, 30.4, 28.7 ppm; IR: ν = 3352, 3186, 2948, 2868, 1621, 1499, 1454, 1392, 1257, 1204, 1147, 823, 766, 742 cm$^{-1}$; HRMS (ESI) m/z calc. for $C_{12}H_{17}N_2$ $[M + H]^+$ 189.1392, found 189.1394.

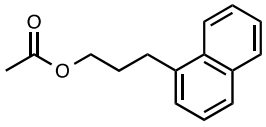

**3-(Naphthalen-1-yl)propyl acetate (44):** obtained as a colorless oil (108 mg, 95%); $^{1}$H NMR ($CDCl_3$, 500.4 MHz): δ 8.06 (d, *J* = 8.4 Hz, 1 H), 7.89 (d, *J* = 7.9 Hz, 1 H), 7.76 (d, *J* = 7.9 Hz, 1 H), 7.57–7.49 (m, 2 H), 7.43 (t, *J* = 7.8 Hz, 1 H), 7.36 (d, *J* = 6.7 Hz, 1 H), 4.20 (t, *J* = 6.7 Hz, 2 H), 3.19 (t, *J* = 8.0 Hz, 2 H), 1.92 (tt, *J* = 6.7, 8.0 Hz, 2 H), 2.11 (s, 3 H) ppm; $^{13}$C NMR ($CDCl_3$, 125.8 MHz): 171.1, 137.2, 133.9, 131.7, 128.8, 126.8, 126.0, 125.8, 125.4, 125.3, 123.5, 64.0, 29.4, 29.2, 20.9 ppm; IR: ν = 2954, 1733, 1596, 1510, 1464, 1434, 1386, 1232, 1166, 1038, 976, 950, 876, 791, 776, 734 cm$^{-1}$; HRMS (ESI) m/z calc. for $C_{15}H_{16}O_2Na$ $[M + Na]^+$ 251.1048, found 251.1049.

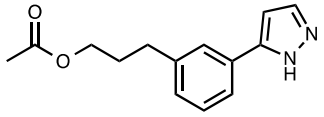


**3-(3-(1H-Pyrazol-5-yl)phenyl)propyl acetate (45):** obtained as a pale yellow oil (88 mg, 72%); $^{1}$H NMR ($CDCl_3$, 500.4 MHz): δ 12.8–10.2 (br s, 1 H), 7.61-7.59 (m, 3 H), 7.32 (dd, *J* = 8.0, 7.5 Hz, 1 H), 7.15 (d, *J* = 7.5 Hz, 1 H), 6.61 (s, 1 H), 4.10 (t, *J* = 6.5 Hz, 2 H), 2.71 (t, *J* = 7.5 Hz, 2 H), 2.05 (s, 3 H), 1.92 (tt, *J* = 6.5, 7.5 Hz, 2 H) ppm $^{13}$C NMR ($CDCl_3$, 125.8 MHz): 171.5, 149.1, 141.9, 133.5, 132.3, 129.1, 128.3, 125.9, 123.7, 102.8, 64.0, 32.3, 30.3, 21.2 ppm; IR: ν = 3173, 3055, 2954, 1733, 1610, 1470, 1450, 1366, 1095, 1037, 972, 933, 898, 764, 699, 605 cm$^{-1}$; HRMS (ESI) m/z calc. for $C_{14}H_{16}N_2O_2Na$ $[M + Na]^+$ 267.1109, found 267.1121.

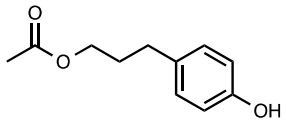


**3-(4-Hydroxyphenyl)propyl acetate (46):** obtained as a light brown oil (66 mg, 68%); $^{1}$H NMR ($CDCl_3$, 500.4 MHz): δ 7.04 (dd, *J* = 8.0, 2.0 Hz, 2 H), 6.79 (dd, *J* = 8.0, 2.0 Hz, 2 H), 5.29 (s br,

1 H), 4.08 (m, 2 H), 2.61 (t, *J* = 7.5 Hz, 2 H), 2.06 (s, 3 H), 1.93 (m, 2 H) ppm; $^{13}$C NMR ($CDCl_3$, 125.8 MHz): 171.8, 154.1, 133.3, 129.6, 115.4, 64.1, 31.3, 30.5, 21.2 ppm; IR: ν = 3385, 3090, 2905, 1734, 1707, 1614, 1596, 1390, 1229, 1172, 1035, 846, 822, 746, 555 $cm^{-1}$; HRMS (ESI) m/z calc. for $C_{11}H_{13}O_3$ $[M - H]^-$ 193.0865, found 193.0864.

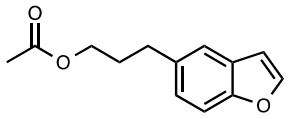

**3-(Benzofuran-5-yl)propyl acetate (47):** obtained as a colorless oil (95 mg, 87%); $^1$H NMR ($CDCl_3$, 500.4 MHz): δ 7.60 (d, *J* = 2.0 Hz, 1 H), 7.43-7.40 (m, 2 H), 7.12 (d, *J* = 8.5, 1.5 Hz, 1 H), 6.71 (dd, *J* = 1.5, 2.0 Hz, 1 H), 4.10 (t, *J* = 7.0 Hz, 2 H), 2.78 (t, *J* = 7.5 Hz, 2 H), 2.06 (s, 3 H), 1.99 (tt, *J* = 7.0, 7.5 Hz, 2 H) ppm; $^{13}$C NMR ($CDCl_3$, 125.8 MHz): 171.3, 153.8, 145.3, 135.8, 127.7, 125.0, 120.6, 111.3, 106.5, 64.0, 32.3, 30.9, 21.1 ppm; IR: ν = 2953, 1734, 1468, 1445, 1387, 1365, 1197, 1126, 1110, 1031, 978, 884, 813, 792, 767, 631, 606 $cm^{-1}$; HRMS (ESI) m/z calc. for $C_{13}H_{14}O_3Na$ $[M + Na]^+$ 241.0841, found 251.0844.

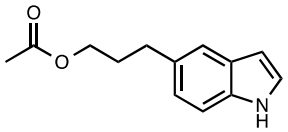

**3-(1H-Indol-5-yl)propyl acetate (48):** obtained as a white crystalline solid (81 mg, 75%); mp 121 °C, $^1$H NMR ($CDCl_3$, 500.4 MHz): δ 8.10 (s br, 1 H), 7.46 (s, 1 H), 7.31 (d, *J* = 8.0 Hz, 1 H), 7.18 (s, 1 H), 7.04 (d, *J* = 8.0 Hz, 1 H), 6.51 (s, 1 H), 4.13 (t, *J* = 6.5 Hz, 2 H), 2.80 (t, *J* = 7.5 Hz, 2 H), 2.09 (s, 3 H), 1.93 (tt, *J* = 6.5, 7.5 Hz, 2 H) ppm; $^{13}$C NMR ($CDCl_3$, 125.8 MHz): 171.6, 134.6, 132.6, 128.3, 124.6, 123.0, 120.1, 111.1, 102.3, 64.3, 32.4, 31.1, 21.2 ppm ; IR: ν = 3281, 2852, 1702, 1368, 1238, 1142, 1070, 896, 868, 809, 760, 731, 631, 607, 573 $cm^{-1}$; HRMS (ESI) m/z calc. for $C_{13}H_{16}NO_2$ $[M + H]^+$ 218.1181, found 218.1186.

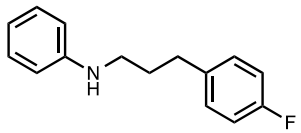

***N*-(3-(4-Fluorophenyl)propyl)aniline (49):** obtained as a pale yellow oil (102 mg, 89%); $^{1}$H NMR ($CDCl_3$, 500.4 MHz): δ 7.18–7.09 (m, 4 H), 6.79 (t, *J* = 8.5 Hz, 2 H), 6.68 (t, *J* = 7.3 Hz, 1 H), 6.56 (t, *J* = 7.8 Hz, 2 H), 3.57 (br s, 1 H), 3.11 (t, *J* = 7.3 Hz, 2 H), 2.68 (t, *J* = 7.3 Hz, 2 H), 1.90 (q, *J* = 7.3 Hz, 2 H) ppm; $^{13}$C {$^{1}$H} NMR ($CDCl_3$, 125.8 MHz): 161.5 (d, *J* = 240.9 Hz), 148.5, 137.5 (d, *J* = 3.9 Hz), 129.9 (d, *J* = 9.0 Hz), 129.4, 117.4, 115.2 (d, *J* = 21.1 Hz), 112.9, 43.4, 32.7, 31.4 ppm; $^{19}$F {$^{1}$H} NMR ($CDCl_3$, 470.8 MHz): –117.5 ppm; IR: ν = 2932, 2860, 1601, 1505, 1476, 1454, 1430, 1318, 1256, 1218, 1179, 1156, 1095, 869, 848, 820, 747, 691, 542, 500 cm$^{-1}$; HRMS (ESI) m/z calc. for $C_{15}H_{16}NF$ $[M]^+$ 229.1267, found 229.1260.

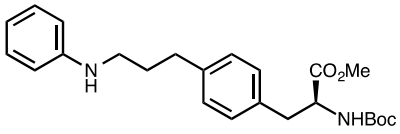

**Methyl (*S*)-2-((*tert*-butoxycarbonyl)amino)-3-(4-(3-(phenylamino)propyl)phenyl)propanoate (50):** obtained as a colorless oil (158 mg, 76%); $[\alpha]^{20}_{D}$ = –89.5 ($CHCl_3$, *c* = 1.0); $^{1}$H NMR ($CDCl_3$, 500.4 MHz): δ 7.18 (t, *J* = 7.4 Hz, 2 H), 7.14 (d, *J* = 8.2 Hz, 2 H), 7.07 (d, *J* = 7.4 Hz, 2 H), 6.71 (t, *J* = 7.5 Hz, 1 H), 6.60 (d, *J* = 8.5 Hz, 2 H), 5.04 (d, *J* = 9.4 Hz, 1 H),4.60 (dd, *J* = 9.4, 4.7 Hz, 1 H), 3.88–3.45 (br s, 1 H), 3.71 (s, 3 H), 3.15 (t, *J* = 6.9 Hz, 2 H), 3.13–3.01 (m, 2 H), 2.72 (t, *J* = 7.8 Hz, 2 H), 1.92 (tt, *J* = 6.9, 7.8 Hz, 2 H), 1.44 (s, 9 H) ppm; $^{13}$C {$^{1}$H} NMR ($CDCl_3$, 125.8 MHz): 172.3, 155.1, 148.3, 140.3, 133.5, 129.3, 129.2, 128.5, 117.2, 112.7, 79.8, 54.4, 52.1, 43.4, 37.9, 32.9, 30.9, 28.3 ppm; IR: ν = 3352, 2976, 1742, 1704, 1602, 15034, 1435, 1365, 1320, 1252, 1214, 1161, 1115, 1058, 1020, 991, 910, 748, 732, 692 cm$^{-1}$; HRMS (ESI) m/z calc. for $C_{24}H_{32}N_2O_4Na$ $[M + Na]^+$ 435.2260, found 435.2263.

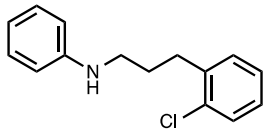

***N*-(3-(2-Chlorophenyl)propyl)aniline (51):** obtained as a yellow oil (108 mg, 88%); $^{1}$H NMR ($CDCl_3$, 500.4 MHz): δ 7.33 (d, *J* = 7.4 Hz, 1 H), 7.22–7.09 (m, 5 H), 6.68 (t, *J* = 7.4 Hz, 1 H), 6.58 (d, *J* = 8.1 Hz, 2 H), 3.62 (br s, 1 H), 3.15 (t, *J* = 6.8 Hz, 2 H), 2.83 (t, *J* = 7.6 Hz, 2 H), 1.92 (tt, *J* = 6.8, 7.6 Hz, 2 H) ppm; $^{13}$C {$^{1}$H} NMR ($CDCl_3$, 125.8 MHz): 148.5, 139.4, 134.1, 130.6, 129.7, 129.4, 127.7, 127.1, 117.4, 112.9, 43.6, 31.3, 29.7 ppm; IR: ν = 3310, 2930, 2862, 1601, 1504, 1473, 1256, 1153, 1131, 1051, 992, 744, 691, 680, 508 cm$^{-1}$; HRMS (ESI) m/z calc. for $C_{15}H_{17}NCl$ $[M + H]^+$ 246.1050, found 246.1048.

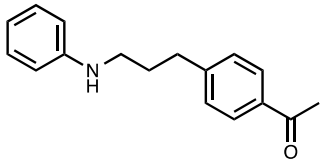

**1-(4-(3-(Phenylamino)propyl)phenyl)ethan-1-one (52):** obtained as a colorless crystalline solid (120 mg, 95%); mp 104-105 °C, $^{1}$H NMR ($CDCl_3$, 500.4 MHz): δ 7.90 (d, *J* = 7.6 Hz, 2 H), 7.30 (d, *J* = 7.6 Hz, 2 H), 7.18 (t, *J* = 7.6 Hz, 2 H), 6.71 (t, *J* = 7.6 Hz, 1 H), 6.58 (d, *J* = 7.6 Hz, 2 H), 3.64 (br s, 1 H), 3.11 (t, *J* = 7.5 Hz, 2 H), 2.68 (t, *J* = 7.5 Hz, 2 H), 2.59 (s, 3 H), 1.98 (q, *J* = 7.5 Hz, 2 H) ppm; $^{13}$C {$^{1}$H} NMR ($CDCl_3$, 125.8 MHz): 197.9, 148.3, 147.7, 135.4, 129.4, 128.8 [× 2], 117.5, 112.9, 43.4, 33.6, 30.9, 26.8 ppm; IR: ν = 3358, 2118, 1642, 1604, 1503, 1413, 1361, 1258, 1236, 1118, 1082, 891, 870, 748, 693, 614, 539 cm$^{-1}$; HRMS (ESI) m/z calc. for $C_{17}H_{20}NO$ $[M + H]^+$ 254.1545, found 254.1549.

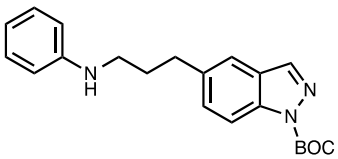


***tert*-Butyl 5-(3-(phenylamino)propyl)-1*H*-indazole-1-carboxylate (53):** obtained as a yellow oil (165 mg, 94%); $^{1}$H NMR ($CDCl_3$, 500.4 MHz): δ 8.12 (s, 1 H), 8.08 (s, 1 H), 7.64 (d, *J* = 8.3 Hz, 1 H), 7.20–7.14 (m, 3 H), 6.70 (t, *J* = 7.5 Hz, 1 H), 6.59 (d, *J* = 8.1 Hz, 2 H), 3.65 (br s, 1 H), 3.18 (t, *J* = 6.8 Hz, 2 H), 2.91 (t, *J* = 8.0 Hz, 2 H), 2.03 (m, 2 H), 1.72 (s, 9 H) ppm; $^{13}$C {$^{1}$H} NMR ($CDCl_3$, 125.8 MHz): 149.6, 148.4, 143.6, 140.5, 139.6, 129.4, 125.0, 124.5, 121.1, 117.4, 114.1, 112.9, 85.0, 43.5, 34.2, 31.4, 28.4 ppm; IR: ν = 3342, 2980, 2854, 1735, 1712, 1602, 1480, 1345, 1291, 1251, 1150, 1028, 938, 764, 748, 730, 692 cm$^{-1}$; HRMS (ESI) m/z calc. for $C_{21}H_{26}N_3O_2$ [M + H]$^{+}$ 352.2025, found 352.2023.

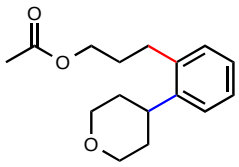


**3-(2-(Tetrahydro-2*H*-pyran-4-yl)phenyl)propyl acetate (55):** obtained as a crystalline powder (127 mg, 97%), mp 46 °C; $^{1}$H NMR ($CDCl_3$, 500.4 MHz): δ 7.28–7.25 (m, 1 H), 7.24–7.20 (m, 1 H), 7.18–7.14 (m, 2 H), 4.16–4.09 (m, 4 H), 3.56 (t, *J* = 11.2 Hz, 2 H), 2.99 (tt, *J* = 11.9, 3.0 Hz, 1 H), 2.75 (t, *J* = 8.1 Hz, 2 H), 2.09 (s, 3 H), 1.96–1.94 (m, 4 H), 1.69–1.64 (m, 2 H) ppm; $^{13}$C {$^{1}$H} NMR ($CDCl_3$, 125.8 MHz): 171.0, 143.3, 138.8, 129.5, 126.6, 126.2, 126.1, 68.6, 63.9, 36.8, 34.0, 30.5, 29.0, 20.9 ppm; IR: ν = 2923, 2848, 1734, 1493, 1465, 1385, 1365, 1236, 1126, 1087, 1034, 1019, 980, 901, 838, 764 cm$^{-1}$; HRMS (ESI) m/z calc. for $C_{16}H_{23}O_3$ [M + H]$^{+}$ 263.1647, found 263.1653.

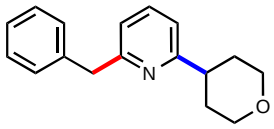


**2-Benzyl-6-(tetrahydro-2*H*-pyran-4-yl)pyridine (57):** obtained as a light yellow oil (91 mg, 72%); $^{1}$H NMR ($CDCl_3$, 500.4 MHz): δ 7.52 (d, *J* = 7.9 Hz, 1 H), 7.4–7.27 (m, 4 H), 7.25-7.20 (m, 1 H), 7.00 (d, *J* = 7.7 Hz, 1 H), 6.92 (d, *J* = 7.7 Hz, 1 H), 4.15 (s, 2 H), 4.11 (dt, *J* = 10.9, 2.7 Hz, 2 H), 3.61–3.53 (m, 2 H), 2.98 (q, *J* = 7.8 Hz, 1 H), 1.95–1.87 (m, 4 H) ppm; $^{13}$C {$^{1}$H} NMR ($CDCl_3$, 125.8 MHz): 163.8, 160.3, 139.6, 136.9, 129.0, 128.4, 126.2, 120.6, 117.8, 68.1, 44.7, 43.4, 32.5 ppm; IR: ν = 2949, 2917, 2841, 1588, 1575, 1494, 1451, 1386, 1237, 1128, 1086, 1029, 980, 866, 823, 774 cm$^{-1}$; HRMS (ESI) m/z calc. for $C_{17}H_{20}NO$ $[M + H]^+$ 254.1545, found 254.1548.

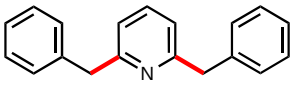


**2,6-Dibenzylpyridine (58):** obtained as a light yellow oil (24 mg, 19%); $^{1}$H NMR ($CDCl_3$, 500.4 MHz): δ 7.46 (t, *J* = 7.9 Hz, 1 H), 7.34–7.26 (m, 8 H), 7.26–7.21 (m, 2 H), 6.90 (d, *J* = 7.2 Hz, 2 H), 4.18 (s, 4 H) ppm; $^{13}$C {$^{1}$H} NMR ($CDCl_3$, 125.8 MHz): 160.4, 139.5, 136.9, 129.1, 128.4, 126.2, 120.5, 44.5 ppm; IR: ν = 3026, 2919, 1588, 1573, 1494, 1450, 1427, 1260, 1217, 1091, 1074, 1029, 769, 737, 696 cm$^{-1}$; HRMS (ESI) m/z calc. for $C_{19}H_{18}N$ $[M + H]^+$ 260.1439, found 260.1445.

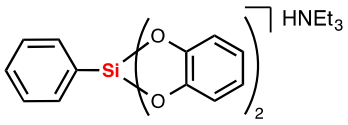


**Triethylammonium phenylbis(catecholato)silicate** (**59**): obtained as a white powder using THF as solvent (3.28 g, 93%), mp = 203 °C; $^{1}$H NMR (DMSO-$d_6$, 500.4 MHz): δ 8.79 (br. s, 1 H), 7.51

(d, *J* = 7.0 Hz, 2 H), 7.16–7.10 (m, 3 H), 6.63–6.58 (m, 4 H), 6.51–6.48 (m, 4 H), 3.06 (q, *J* = 7.5 Hz, 6 H), 1.14 (t, *J* = 7.5 Hz, 9 H) ppm; $^{13}C$ {$^{1}H$} NMR (DMSO-$d_6$, 125.8 MHz): δ 150.8, 142.3, 135.1, 128.2, 127.1, 117.9, 110.2, 46.2, 9.0 ppm; IR: ν = 1483, 1439, 1388, 1351, 1240, 1227, 1157, 1113, 1101, 1012, 889, 819, 761, 737, 723, 700 $cm^{-1}$; HRMS (ESI) m/z calc. for $C_{18}H_{13}O_4Si$ $[M – HNEt_3]^-$ 321.0582, found 321.0588; $E_{pa}$ = + 0.76 V *vs* SCE.

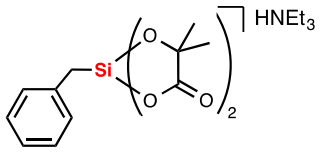


**Triethylammonium benzylbis(methyl-2-hydroxyisobuyro)silicate (60)**: Alpha-hydroxyisobutyric acid (477 mg, 4.89 mmol, 1.95 equiv) was introduced into a microwave vial with a stirring bar. The vial was sealed with a Teflon-coated septum cap then purged with $N_2$ and evacuated four times. 1,4–Dioxane (5 mL) and triethylamine (0.39 mL, 287 mg, 2.88 mmol, 1.2 equiv) were introduced, and the resulting slurry was stirred at rt for 15 min before addition of benzyltrimethoxysilane (500 mg, 2.35 mmol, 1 equiv). The reaction mixture was refluxed for 16 h, then the vial was cooled to rt and the reaction mixture concentrated to a glue before the $Et_2O$ (25 mL) was introduced. The mixture was then sonicated 15 min to allow the corresponding product to precipitate as a white powder. The filter cake was finally washed with $Et_2O$ to afford **60** as a white powder (810 mg, 81%), mp = 96 °C; $^{1}H$ NMR (DMSO-$d_6$, 500.4 MHz): δ 8.89 (br. s, 1 H), 7.09 (t, *J* = 7.1 Hz, 2 H), 6.99 (t, *J* = 7.1 Hz, 2 H), 6.93 (d, *J* = 7.1 Hz, 1 H), 3.85 (q, *J* = 7.3 Hz, 6 H), 2.04–1.93 (m, 2 H), 1.16 (t, *J* = 7.3 Hz, 9 H), 1.10 (s, 6 H), 0.84 (s, 6 H) ppm; $^{13}C$ {$^{1}H$} NMR (DMSO-$d_6$, 125.8 MHz): δ 179.2, 141.8, 129.1, 127.8, 123.5, 73.5, 46.2, 28.9, 28.3, 26.7, 9.1 ppm; IR: ν = 1707, 1668, 1470, 1378, 1357, 1325, 1204, 1187, 1164, 1012, 861, 810, 796, 778, 694 $cm^{-1}$; HRMS (ESI) m/z calc. for $C_{15}H_{19}O_6Si$ $[M – HNEt_3]^-$ 323.0950, found 323.0945; $E_{pa}$ > + 2.00 V *vs* SCE.

## 7.5 References


(1) Yasu, Y.; Koike, T.; Akita, M. *Adv. Synth. Catal.* **2012**, *354*, 3414.

(2) Koike, T.; Akita, M. *Inorg. Chem. Front.* **2014**, *1*, 562.

(3) Chang, W.-T. T.; Smith, R. C.; Regens, C. S.; Bailey, A. D.; Werner, N. S.; Denmark, S. E. In *Organic Reactions*; John Wiley & Sons, Inc.: Hoboken, NJ, USA, 2011; pp 213–746.

(4) Frye, C. L. *J. Am. Chem. Soc.* **1970**, *92*, 1205.

(5) Frye, C. L. *J. Am. Chem. Soc.* **1964**, *86*, 3170.

(6) Seganish, M. W.; DeShong, P. *Org. Lett.*, **2004**, *6*, 4379

(7) Matsuoka, D.; Nishigaichi, Y. *Chem. Lett.* **2015**, *44*, 163.

(8) Corcé, V.; Chamoreau, L.-M.; Derat, E.; Goddard, J.-P.; Ollivier, C.; Fensterbank, L. *Angew. Chem. Int. Ed.* **2015**, *54*, 11414.

(9) Nishigaichi, Y.; Suzuki, A.; Takuwa, A. *Tetrahedron Lett.* **2007**, *48*, 211.

(10) Prier, C. K.; Rankic, D. A.; MacMillan, D. W. C. *Chem. Rev.* **2013**, *113*, 5322.

(11) Brefort, J. L.; Corriu, R. J. P.; Guerin, C.; Henner, B. J. L.; Wong Chi Man, W. W. C. *Organometallics* **1990**, *9*, 2080.

(12) Yamaguchi, S.; Akiyama, S.; Tamao, K. **1999**.

(13) Primer, D. N.; Karakaya, I.; Tellis, J. C.; Molander, G. A. *J. Am. Chem. Soc.* **2015**, *137*, 2195.

(14) Foye, W. O.; Lemke, T. L.; Williams, D. A. *Foye's principles of medicinal chemistry*, 7th ed.; Wolters Kluwer Health/Lippincott Williams & Wilkins: Philadelphia, 2013.

(15) Fleury-Brégeot, N.; Raushel, J.; Sandrock, D. L.; Dreher, S. D.; Molander, G. A. *Chemistry* **2012**, *18*, 9564.

(16) Leedy, D. W.; Adams, R. N. *J. Am. Chem. Soc.* **1970**, *92*, 1646.

(17) Karakaya, I.; Primer, D. N.; Molander, G. A. *Org. Lett.* **2015**, *17*, 3294.

(18) Welsch, M. E.; Snyder, S. A.; Stockwell, B. R. *Curr. Opin. Chem. Biol.* **2010**, *14*, 347.

(19) Beaulieu, L.-P. B.; Delvos, L. B.; Charette, A. B. *Org. Lett.* **2010**, *12*, 1348.

(20) Nakao, Y.; Takeda, M.; Matsumoto, T.; Hiyama, T. *Angew. Chem. Int. Ed.* **2010**, *49*, 4447.

(21) Wu, L.; Hartwig, J. F. *J. Am. Chem. Soc.* **2005**, *127*, 15824.

(22) Matsuhashi, H.; Kuroboshi, M.; Hatanaka, Y.; Hiyama, T. *Tetrahedron Lett.* **1994**, *35*, 6507.

(23) Chu, L.; Lipshultz, J. M.; MacMillan, D. W. C. *Angew. Chem. Int. Ed.* **2015**, *54*, 7929.

(24) Zuo, Z.; Ahneman, D.; Chu, L.; Terrett, J.; Doyle, A. G.; MacMillan, D. W. C. *Science* **2014**, *345*, 437.

(25) Li, J.; Ballmer, S. G.; Gillis, E. P.; Fujii, S.; Schmidt, M. J.; Palazzolo, A. M. E.; Lehmann, J. W.; Morehouse, G. F.; Burke, M. D. *Science* **2015**, *347*, 6227.

(26) Yamashita, Y.; Tellis, J. C.; Molander, G. A. *Proc. Natl. Acad. Sci.* **2015**, *112*, 12026.

(27) Mabrouk, P. A.; Wrighton, M. S. *Inorg. Chem.* **1986**, *25*, 526.

(28) Schmink, J. R.; Leadbeater, N. E. *Org. Lett.* **2009**, *11*, 2575.

(29) Kretchmer, R. A.; McCloskey, S. M. B. *J. Org. Chem.* **1972**, *37*, 1989.

(30) Ackermann, L.; Kapdi, A. R.; Schulzke, C. *Org. Lett.* **2010**, *12*, 2298.

**Author Contributions**:

D.N.P. conceived and designed the project, co-wrote and edited the manuscript, and prepared some of the compounds made in this study. Matthieu Jouffroy co-wrote and edited the manuscript, optimized the reaction conditions, synthesized the alkylsilicates, and prepared a number of the compounds made in this study.

## Appendix A8. $^{1}H$, $^{13}C$, and $^{19}F$ NMR Spectra Relevant to Chapter 7

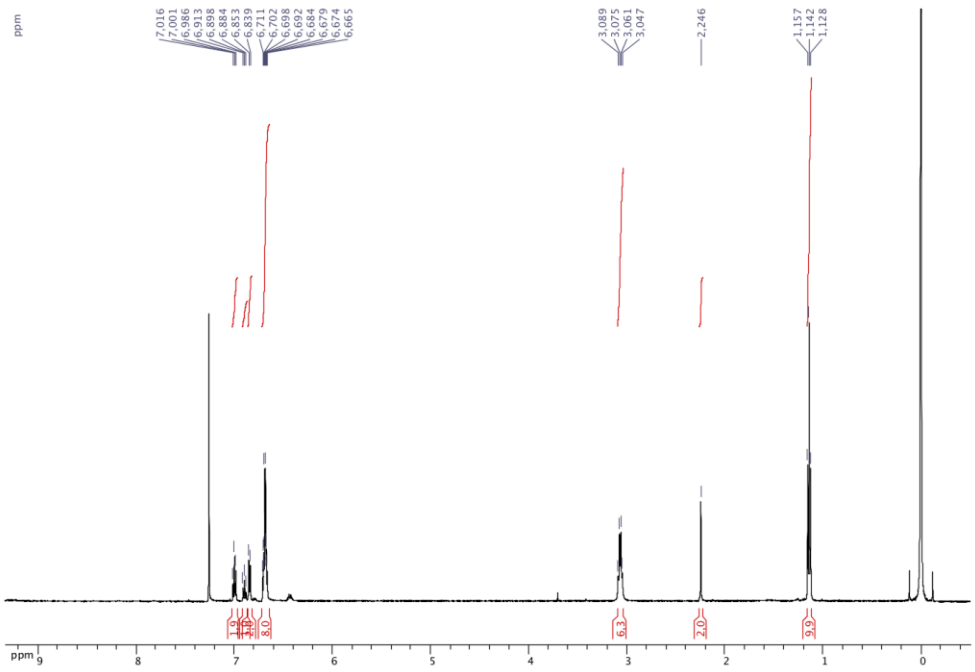


$^{1}$H NMR ($CDCl_3$, 500.4 MHz) of triethylammonium benzylbis(catecholato)silicate (**1**)

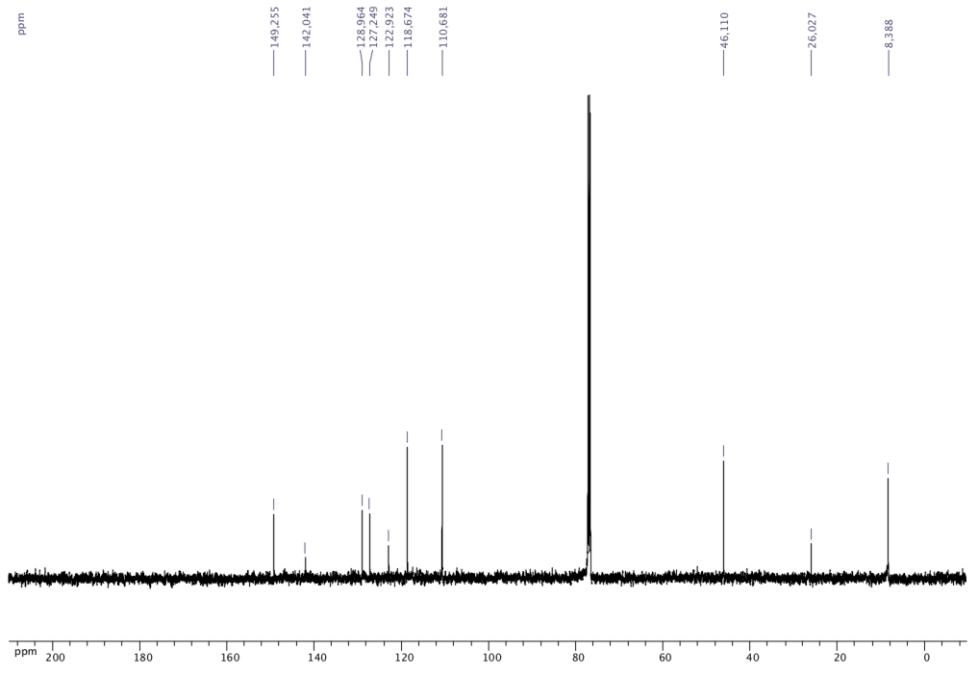


$^{13}$C {$^{1}$H} NMR ($CDCl_3$, 125.8 MHz) of triethylammonium benzylbis(catecholato)silicate (**1**)

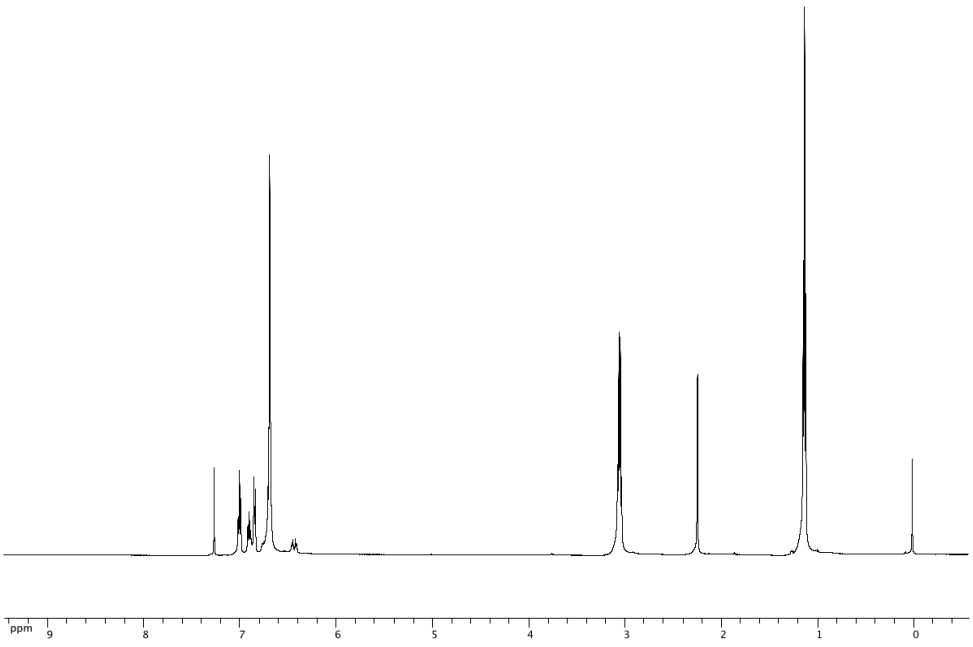


$^{1}$H NMR ($CDCl_3$, 500.4 MHz) of triethylammonium benzylbis(catecholato)silicate (**1**) after 3 months on benchtop.

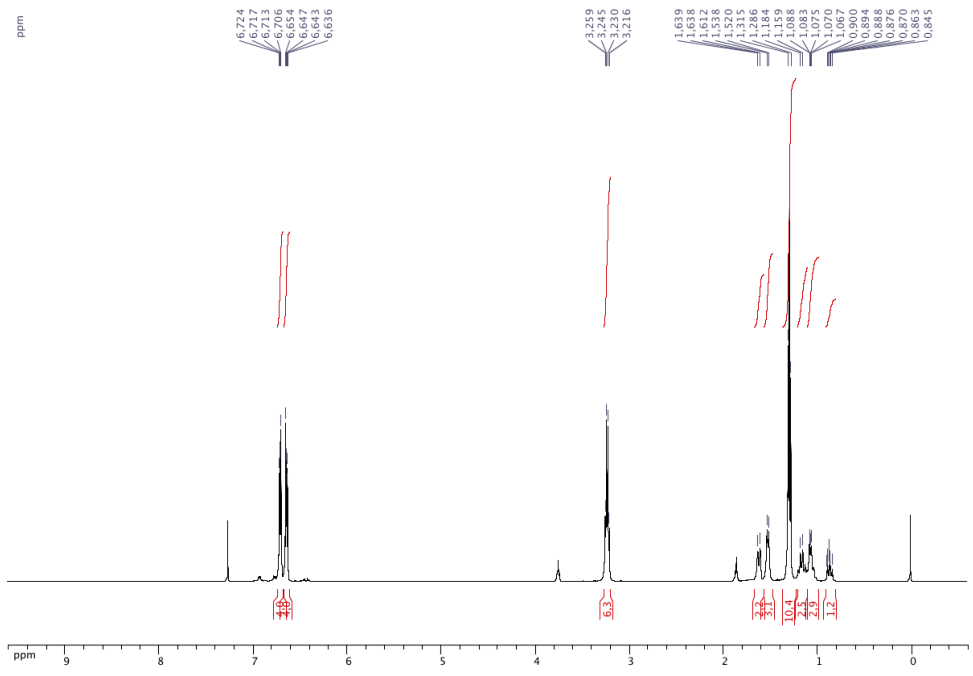


$^{1}$H NMR ($CDCl_3$, 500.4 MHz) of triethylammonium cyclohexylbis(catecholato)silicate (**2**)

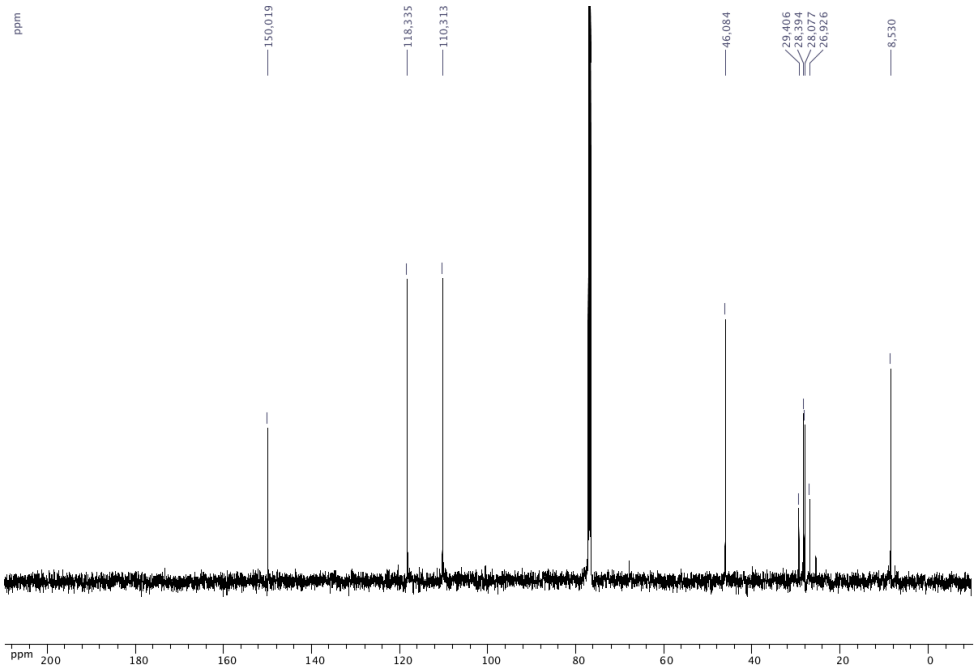


$^{13}C$ {$^{1}H$} NMR ($CDCl_3$, 125.8 MHz) of triethylammonium cyclohexylbis(catecholato)silicate (**2**)

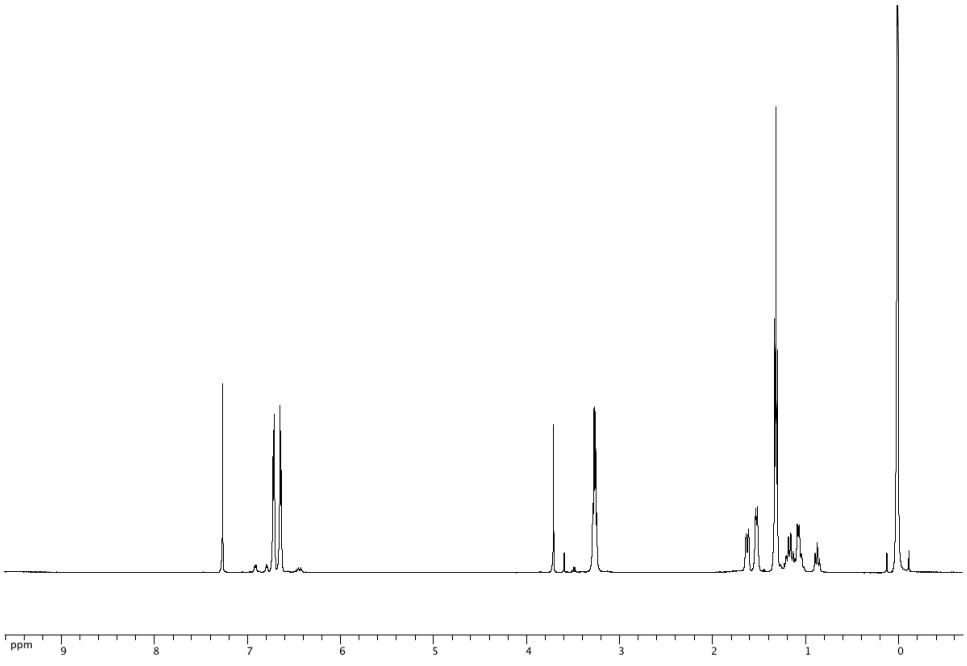


$^{1}H$ NMR ($CDCl_3$, 500.4 MHz) of triethylammonium cyclohexylbis(catecholato)silicate (**2**) after 3 months on benchtop.

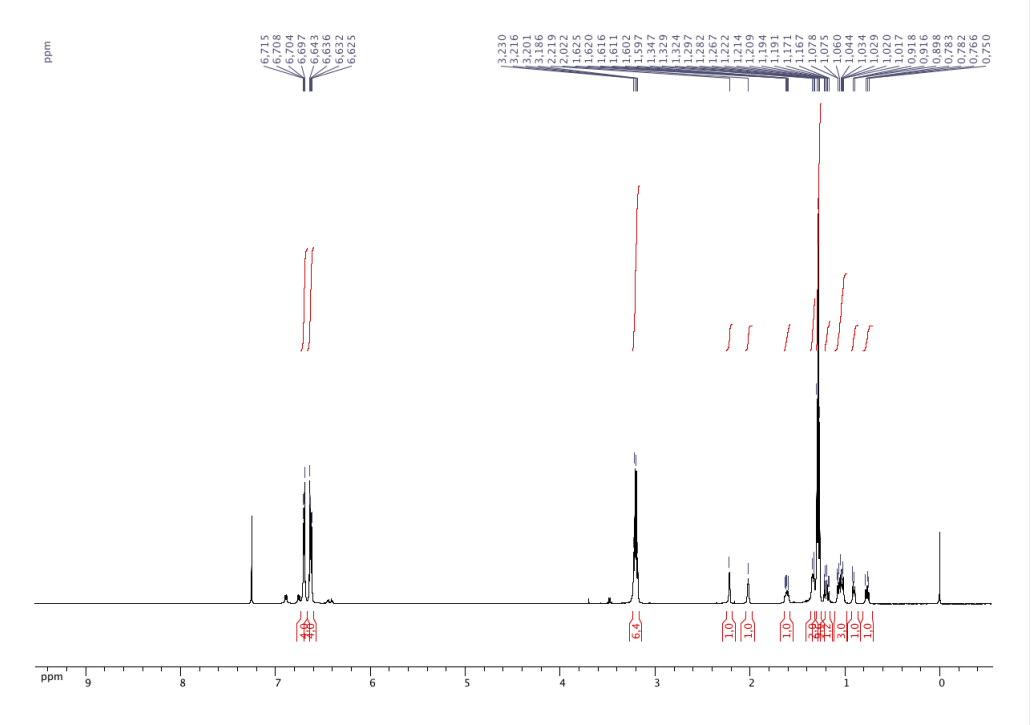

$^{1}$H NMR ($CDCl_3$, 500.4 MHz) of triethylammonium *exo*-2-bicyclo[2.2.1]heptylbis(catecholato)silicate (**3**)

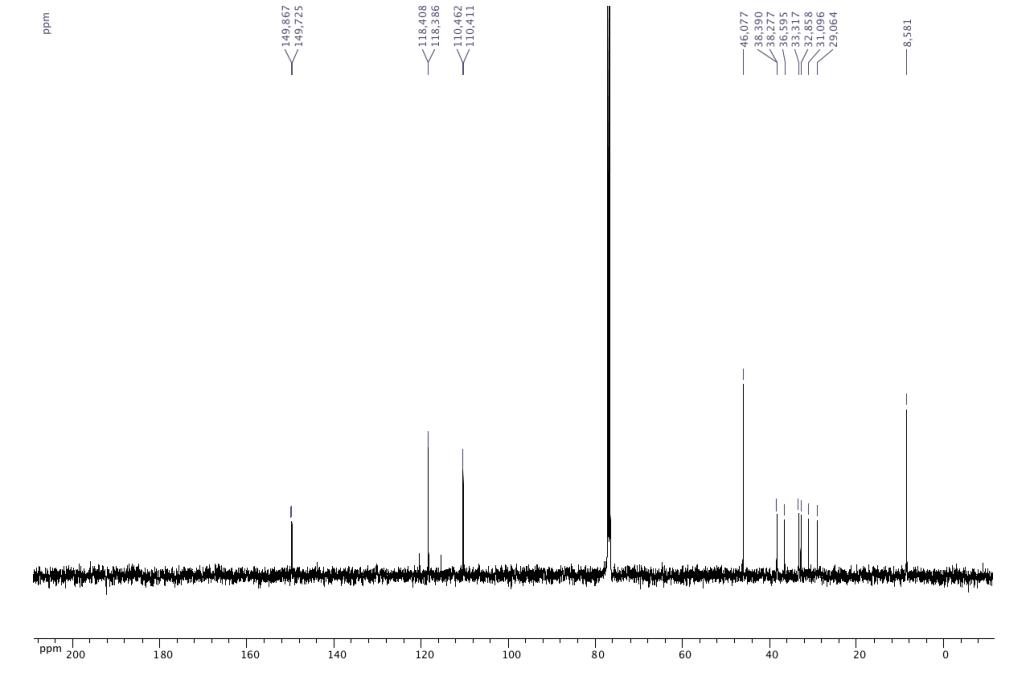

$^{13}$C NMR {$^{1}$H} ($CDCl_3$, 125.8 MHz) of triethylammonium *exo*-2-bicyclo[2.2.1]heptylbis(catecholato)silicate (**3**)

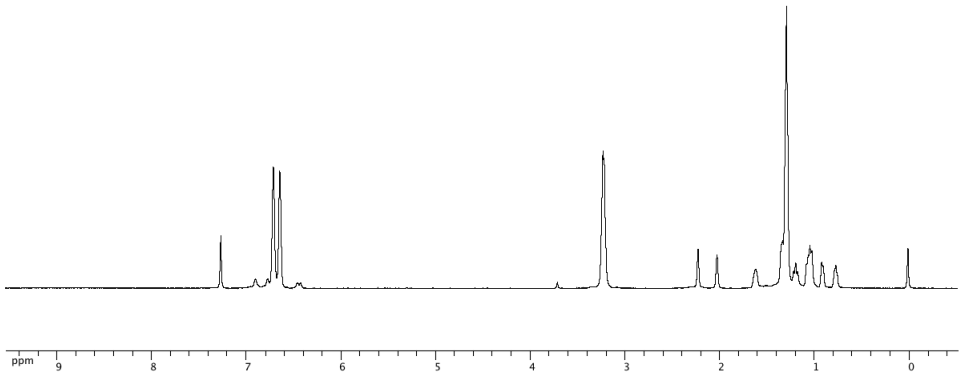


$^{1}$H NMR ($CDCl_3$, 500.4 MHz) of triethylammonium *exo*-2-bicyclo[2.2.1]heptylbis(catecholato)silicate (**3**) after 3 months on benchtop.

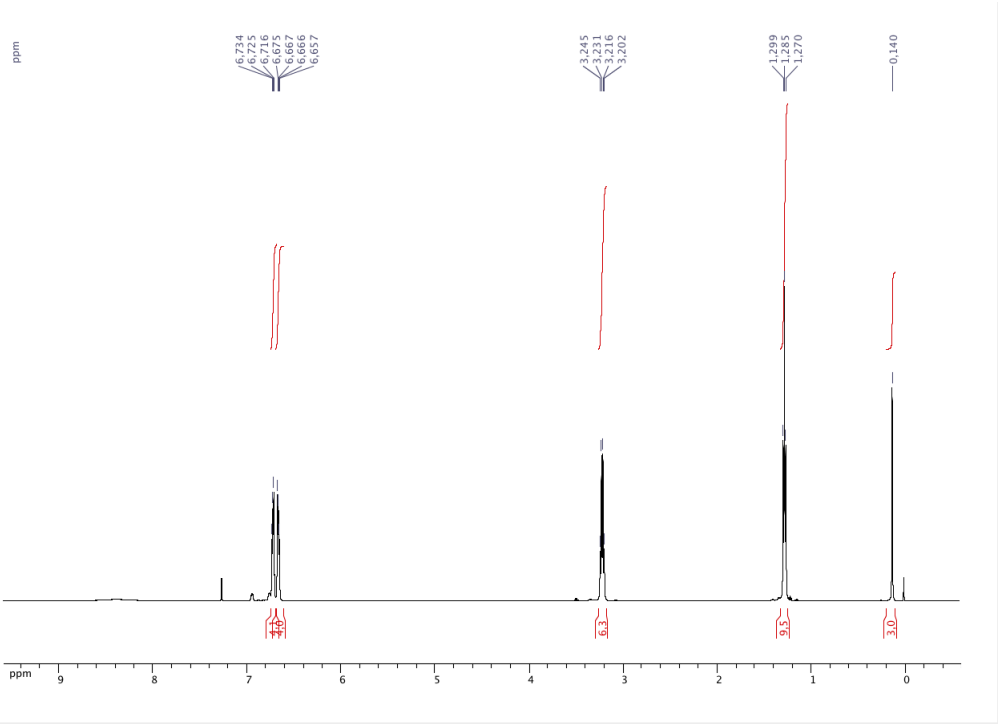


$^{1}$H NMR ($CDCl_3$, 500.4 MHz) of triethylammonium methylbis(catecholato)silicate (**4**)

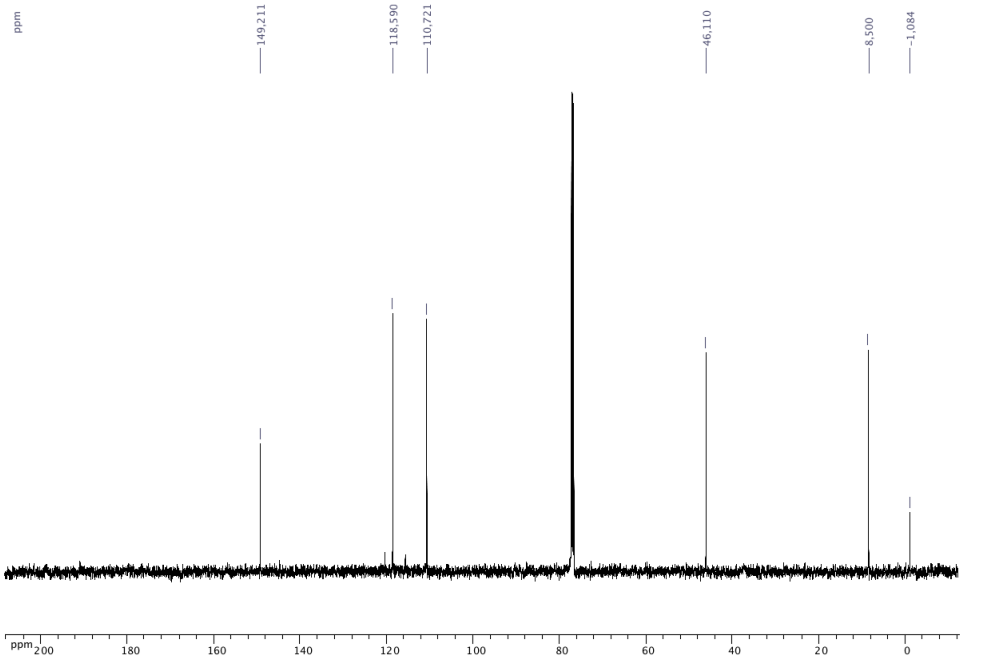


$^{13}$C NMR {$^{1}$H} ($CDCl_3$, 125.8 MHz) of triethylammonium methylbis(catecholato)silicate (**4**)

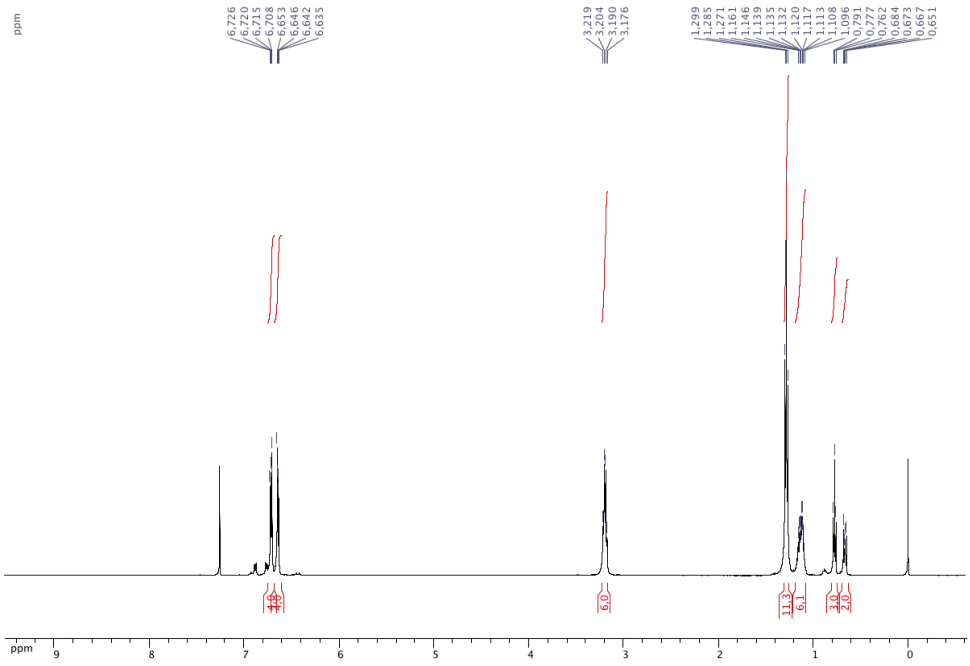


$^{1}$H NMR ($CDCl_3$, 500.4 MHz) of triethylammonium hexylbis(catecholato)silicate (**5**)

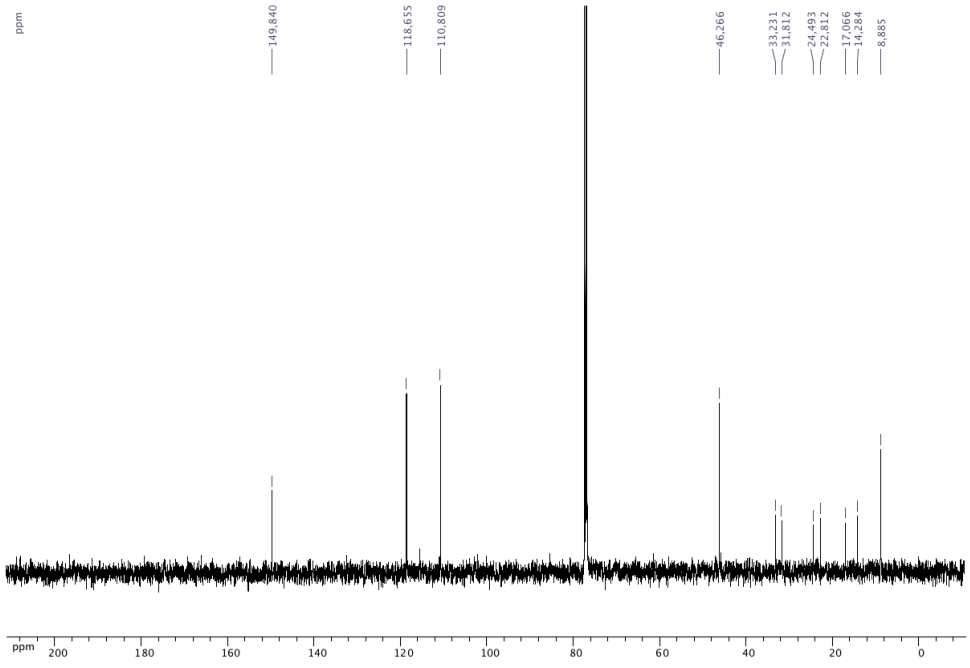


$^{13}$C NMR {$^{1}$H} ($CDCl_3$, 125.8 MHz) of triethylammonium hexylbis(catecholato)silicate (**5**)

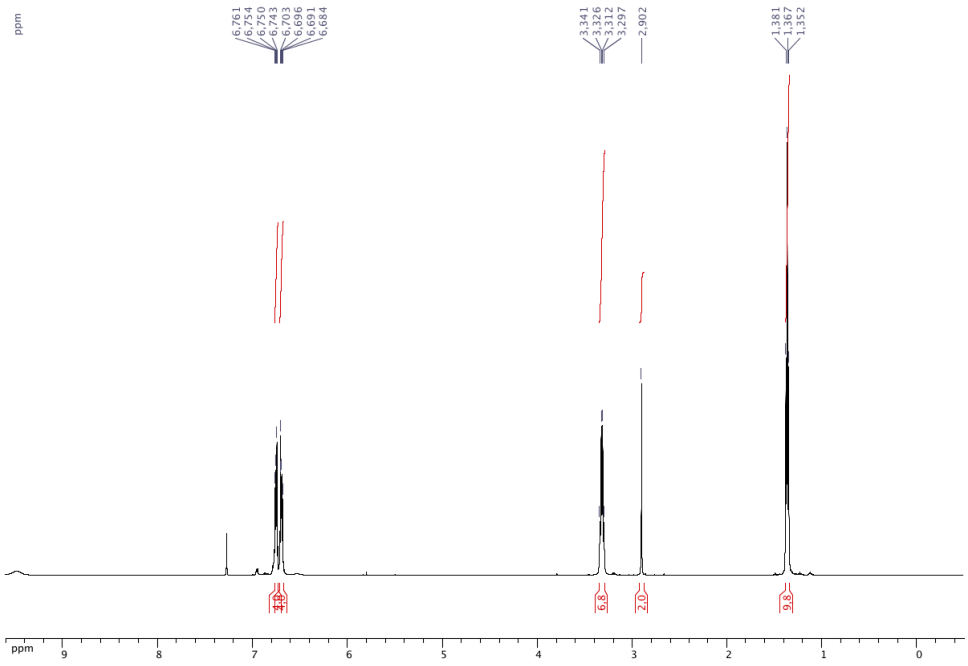


$^{1}$H NMR ($CDCl_3$, 500.4 MHz) of triethylammonium chloromethylbis(catecholato)silicate (**6**)

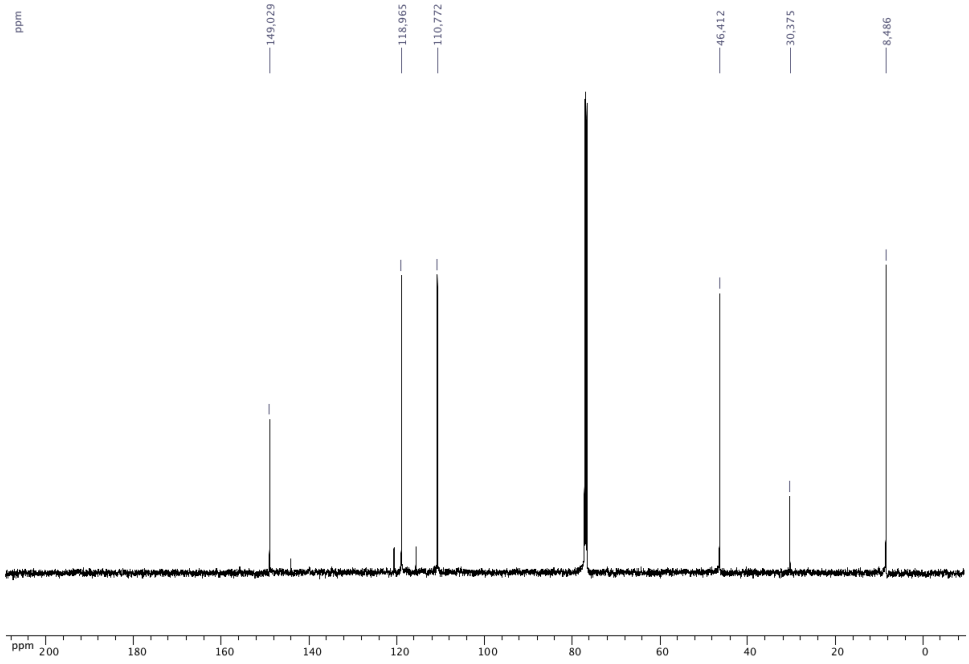


$^{13}$C NMR {$^{1}$H} ($CDCl_3$, 125.8 MHz) of triethylammonium chloromethylbis(catecholato)silicate (**6**)

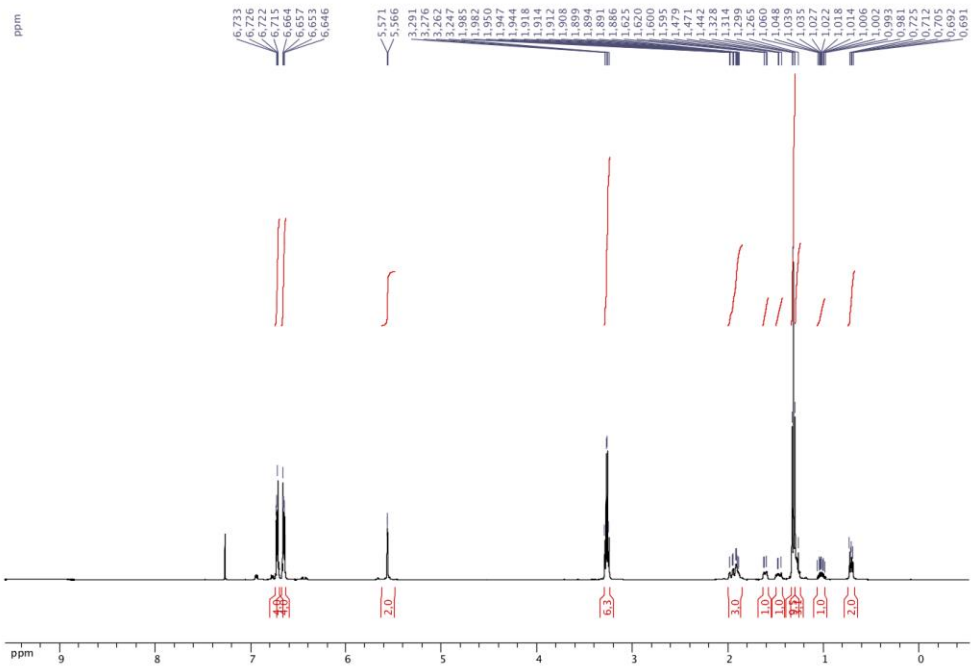

$^{1}$H NMR ($CDCl_3$, 500.4 MHz) of triethylammonium 2-(3-cyclohexenyl)ethylbis(catecholato)silicate (**7**)

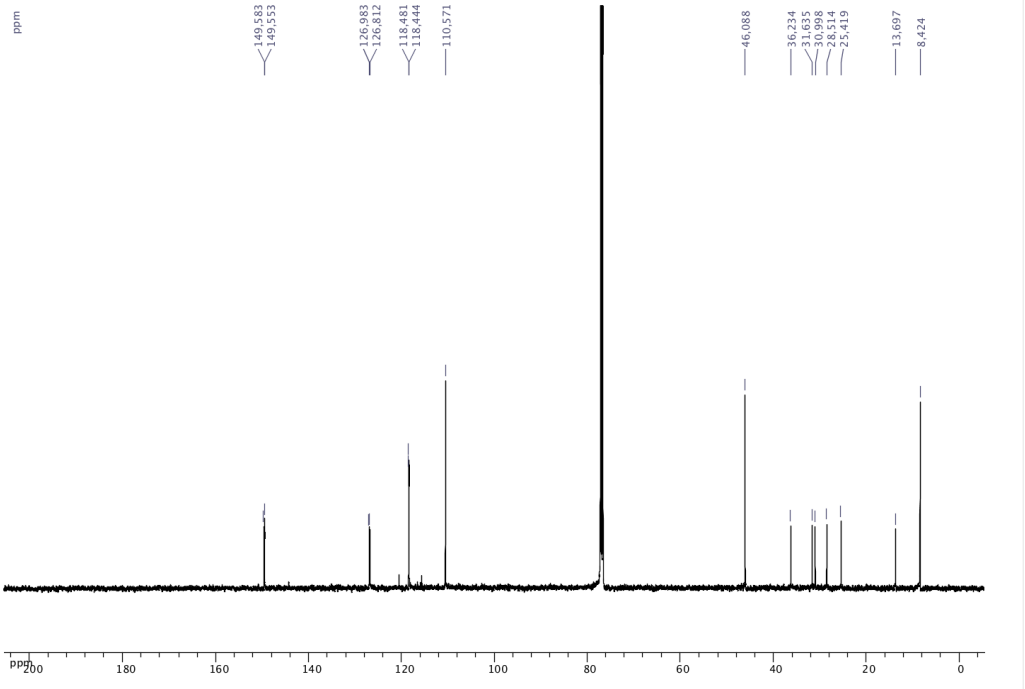

$^{13}$C NMR {$^{1}$H} ($CDCl_3$, 125.8 MHz) of triethylammonium 2-(3-cyclohexenyl)ethylbis(catecholato)silicate (**7**)

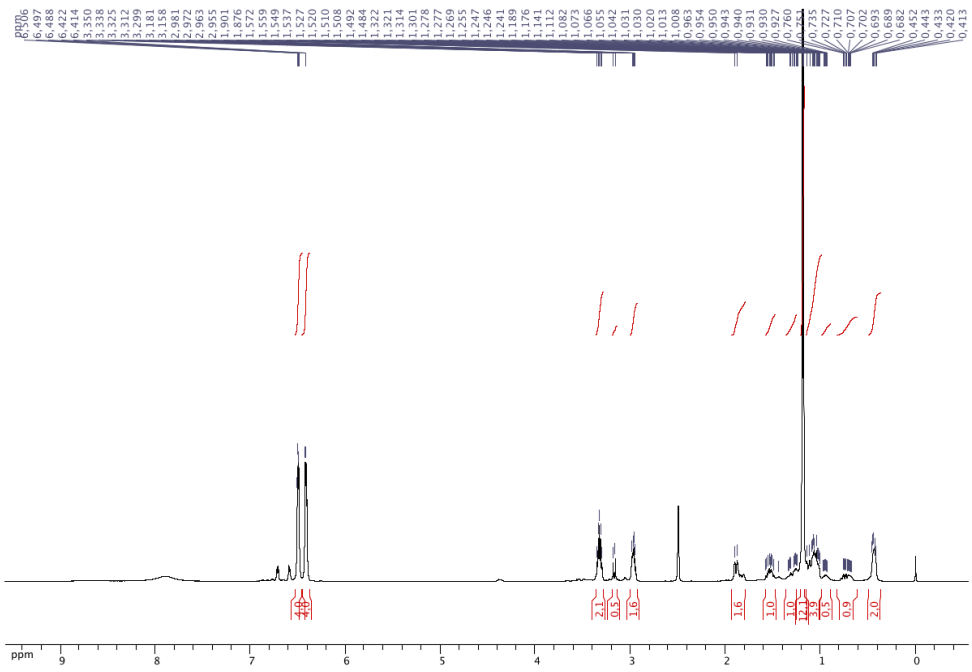

$^{1}$H NMR (DMSO–$d_6$, 500.4 MHz) of diisopropylammonium 2-(3,4-epoxycyclohexyl)ethylbis(catecholato)silicate (**8**)

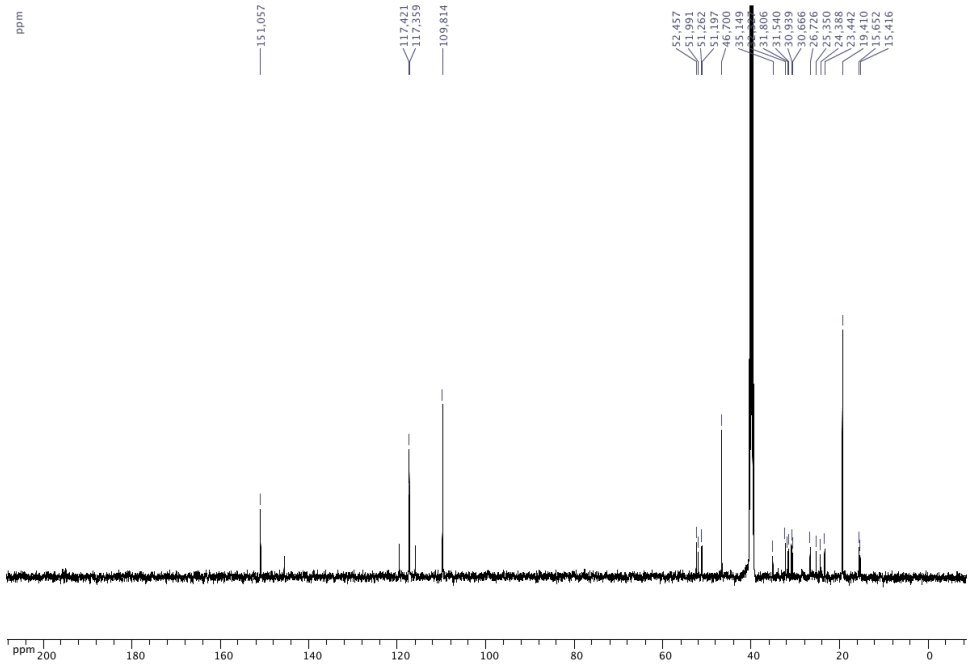

$^{13}$C NMR {$^{1}$H} (DMSO–$d_6$, 125.8 MHz) of diisopropylammonium 2-(3,4-epoxycyclohexyl)ethylbis(catecholato)silicate (**8**)

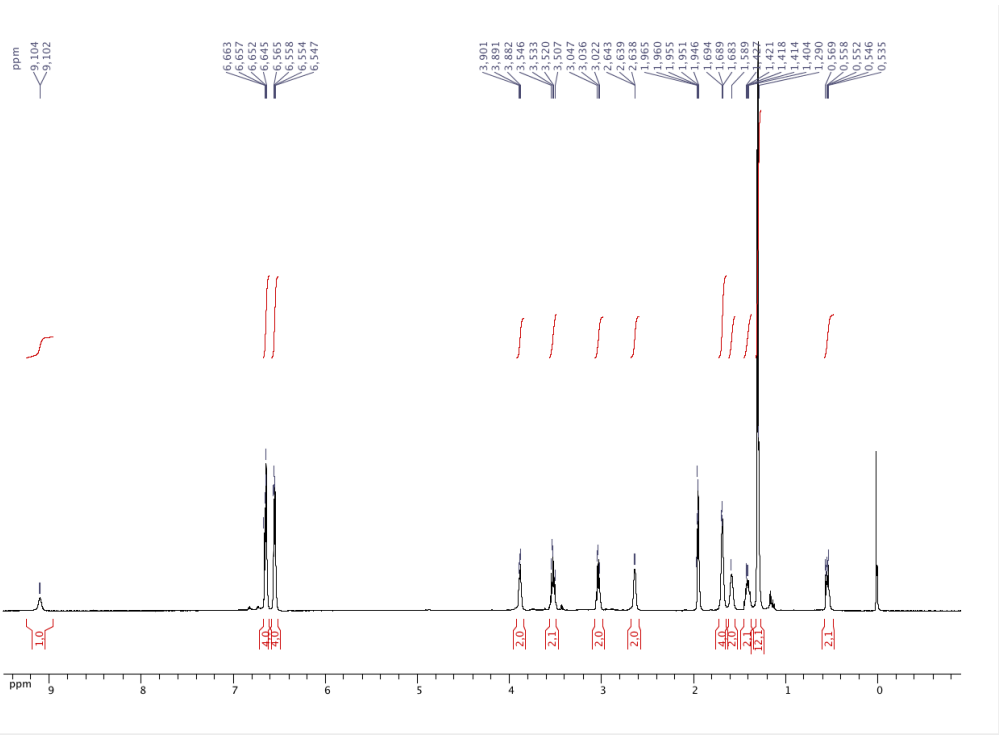

$^{1}$H NMR ($CD_3CN$, 500.4 MHz) of diisopropylammonium *N*-[5-(bis(catecholato)silicate)-2-aza-1-oxopentyl]caprolactam (**9**)

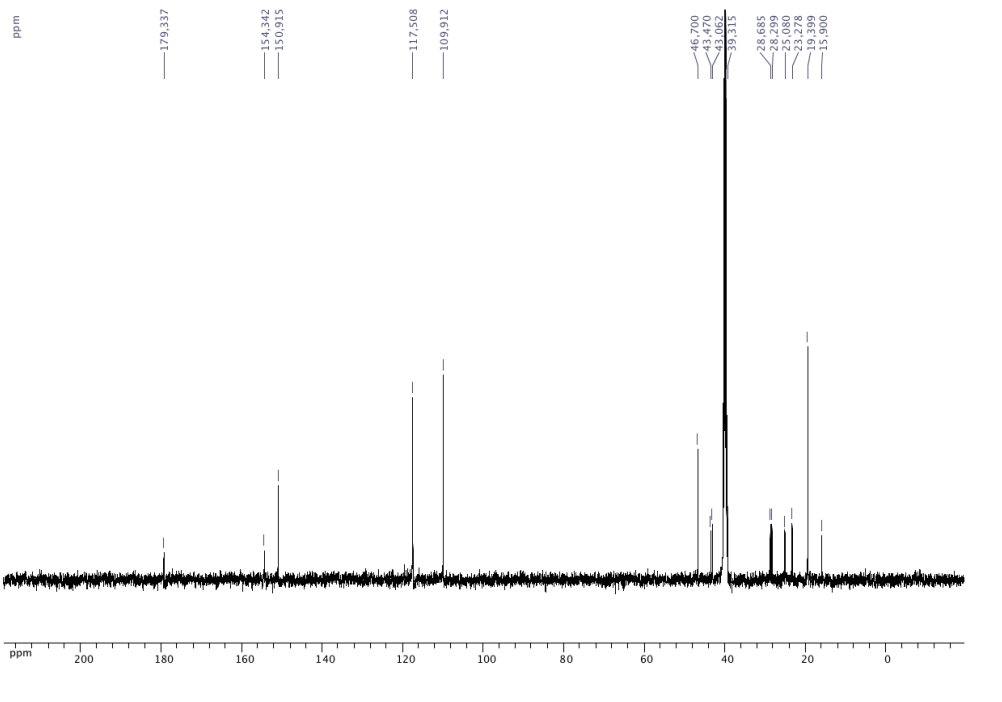

$^{13}$C NMR {$^{1}$H} (DMSO-$d_6$, 125.8 MHz) of diisopropylammonium *N*-[5-(bis(catecholato)silicate)-2-aza-1-oxopentyl]caprolactam (**9**)

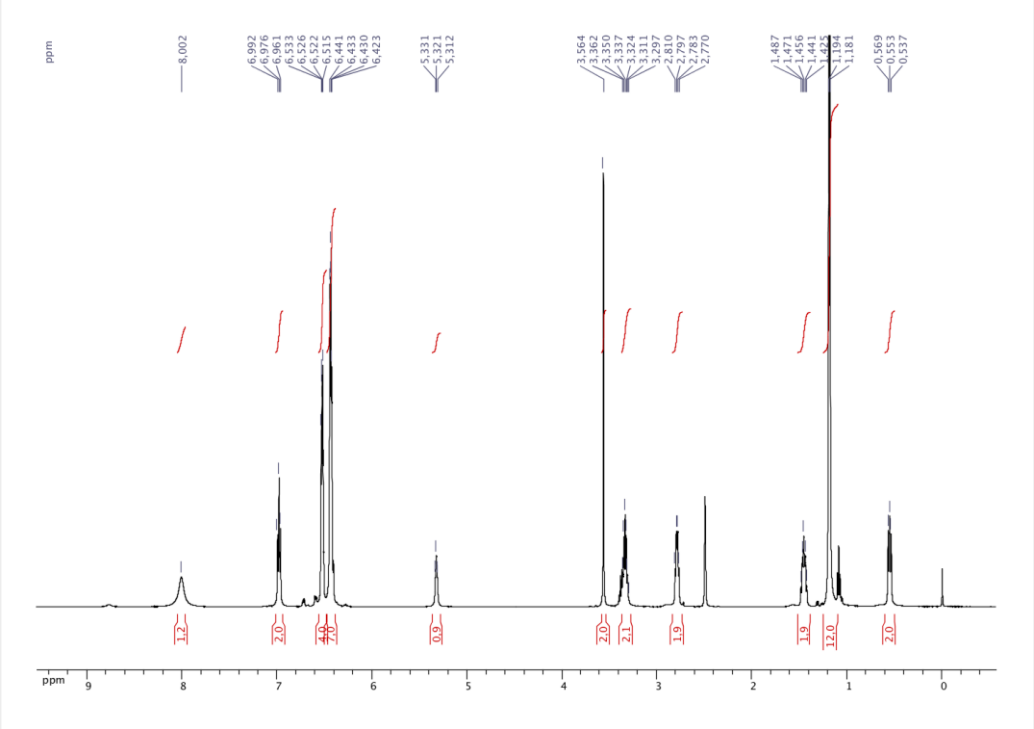

$^{1}$H NMR (DMSO-$d_6$, 500.4 MHz) of diisopropylammonium 3-(phenylamino)propylbis(catecholato)silicate (**10**)

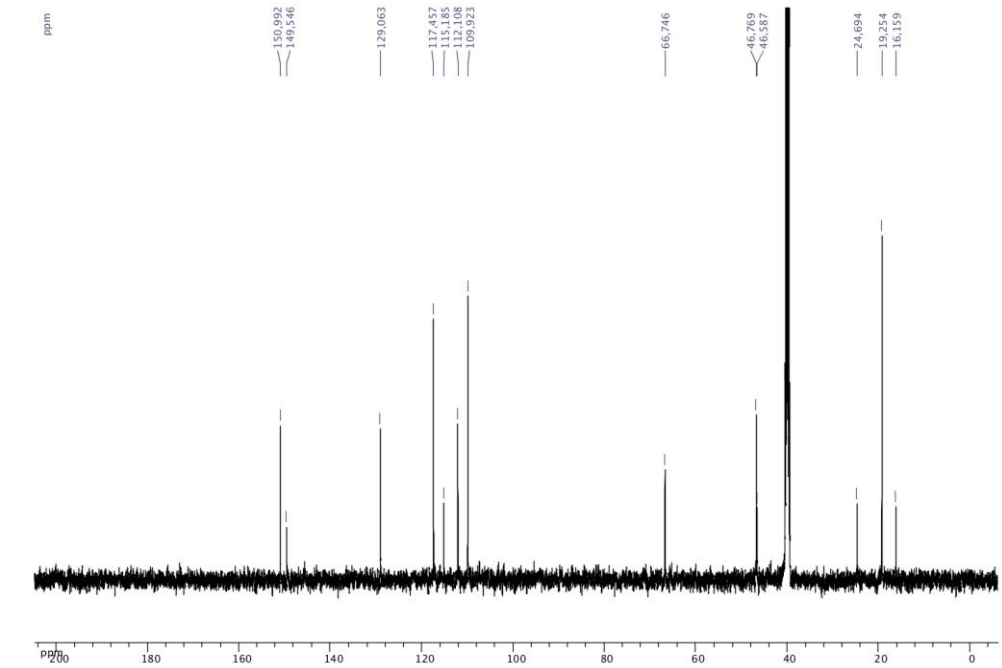

$^{13}$C NMR {$^{1}$H} (DMSO-$d_6$, 125.8 MHz) of diisopropylammonium 3-(phenylamino)propylbis(catecholato)
silicate (**10**)

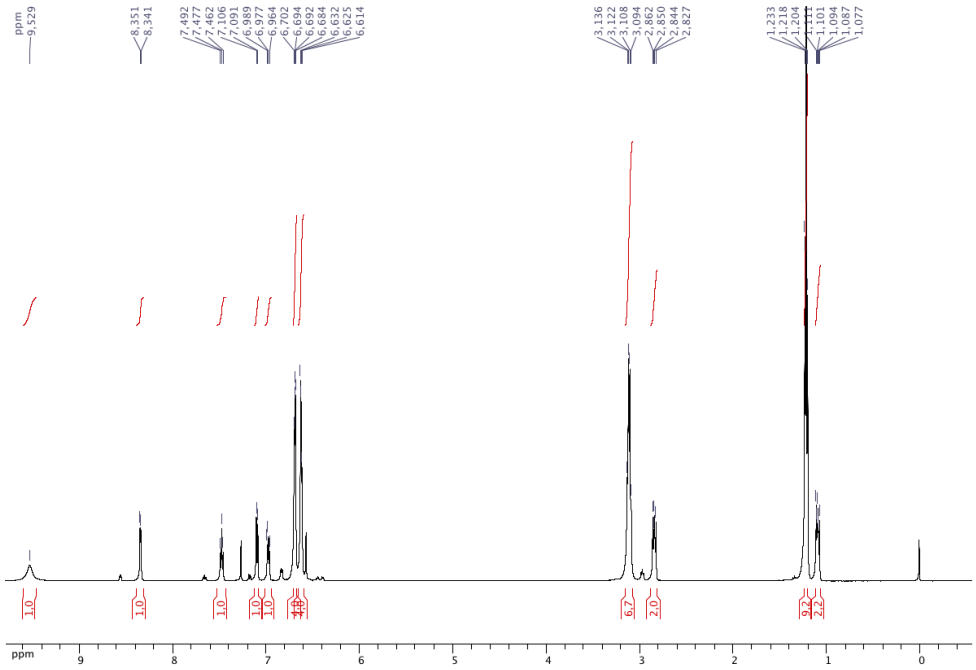


$^{1}$H NMR ($CDCl_3$, 500.4 MHz) of triethylammonium 2-(pyridin-2-yl)ethylbis(catecholato)silicate (**11**)

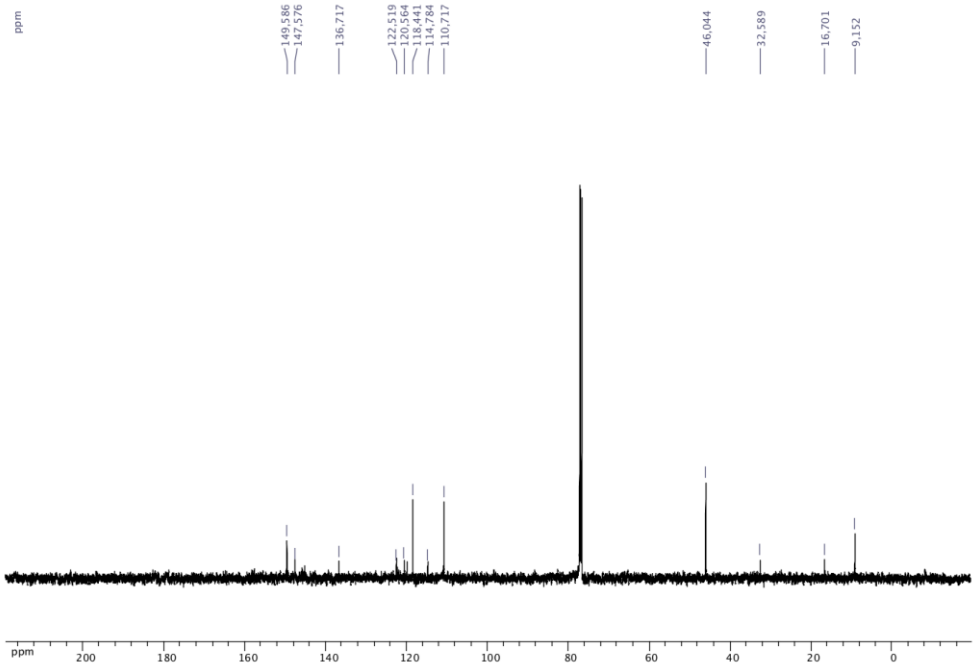


$^{13}$C NMR {$^{1}$H} ($CDCl_3$, 125.8 MHz) of of triethylammonium 2-(pyridin-2-yl)ethylbis(catecholato)silicate (**11**)

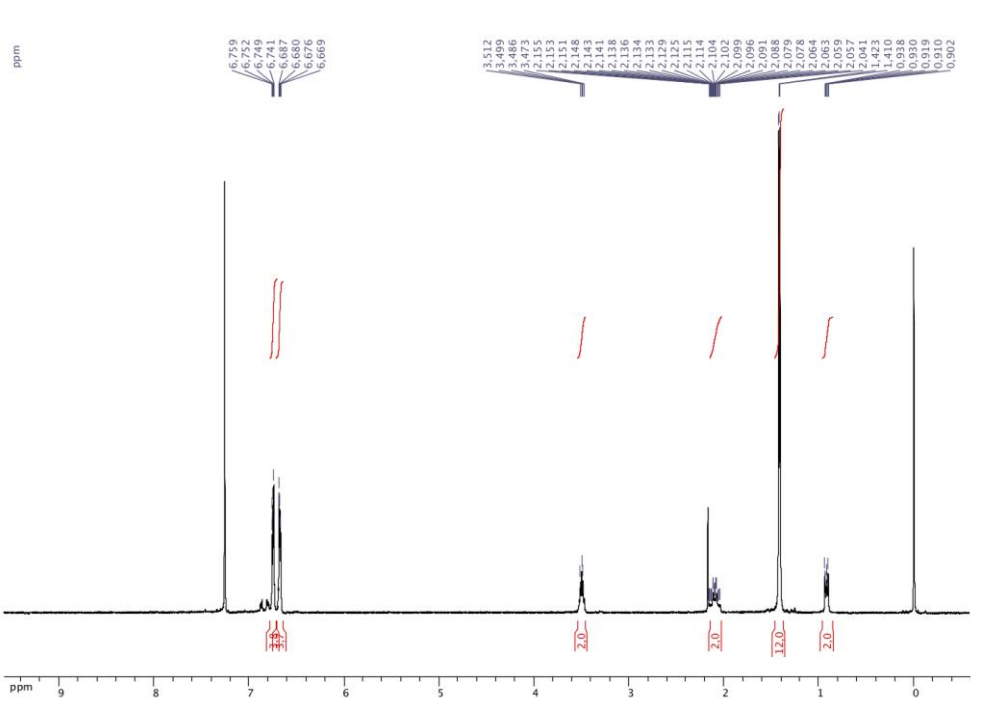

$^{1}$H NMR ($CDCl_3$, 500.4 MHz) of diisopropylammonium 3,3,4,4,5,5,6,6,6-nonafluorohexylbis(catecholato)silicate (**12**)

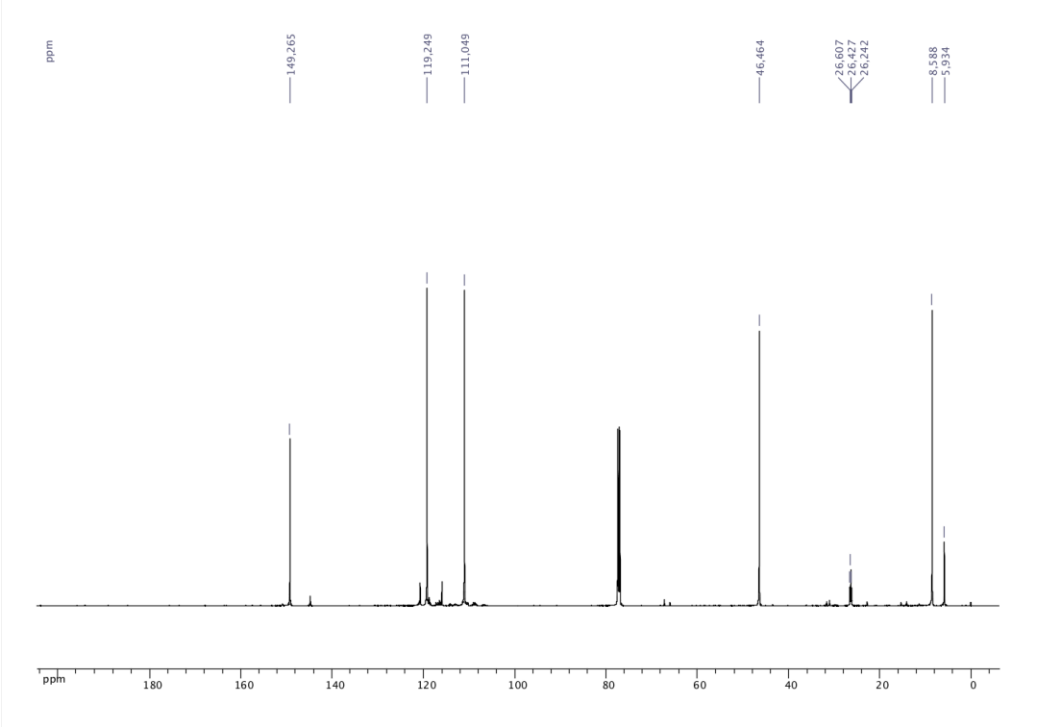

$^{13}$C NMR {$^{1}$H} ($CDCl_3$, 125.8 MHz) of diisopropylammonium 3,3,4,4,5,5,6,6,6-nonafluorohexylbis(catecholato)silicate (**12**)

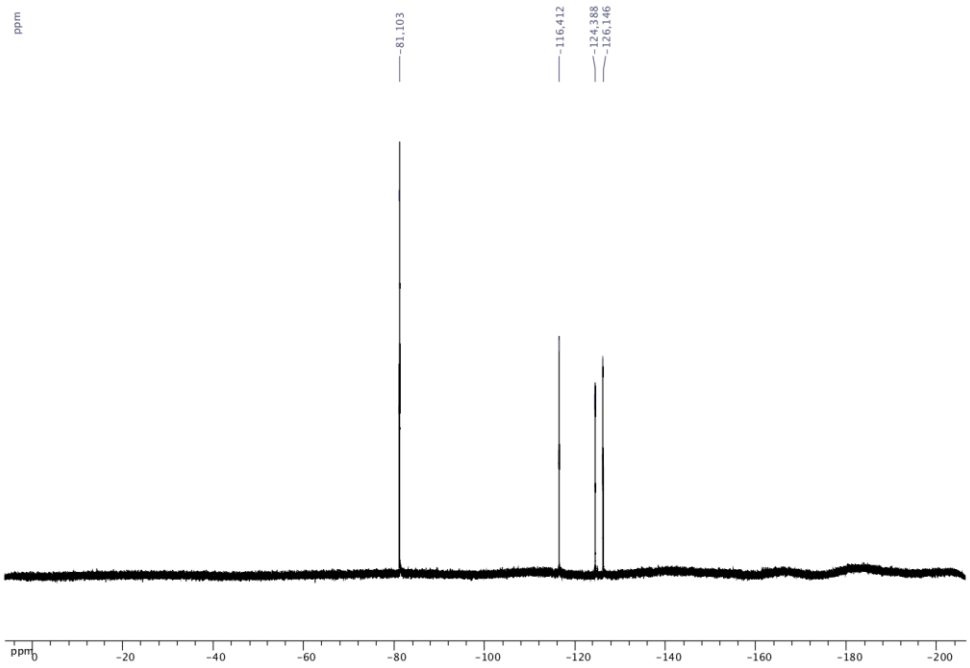


$^{19}F$ NMR {$^{1}H$} ($CDCl_3$, 470.8 MHz) of diisopropylammonium 3,3,4,4,5,5,6,6,6-nonafluorohexylbis(catecholato)silicate (**12**)

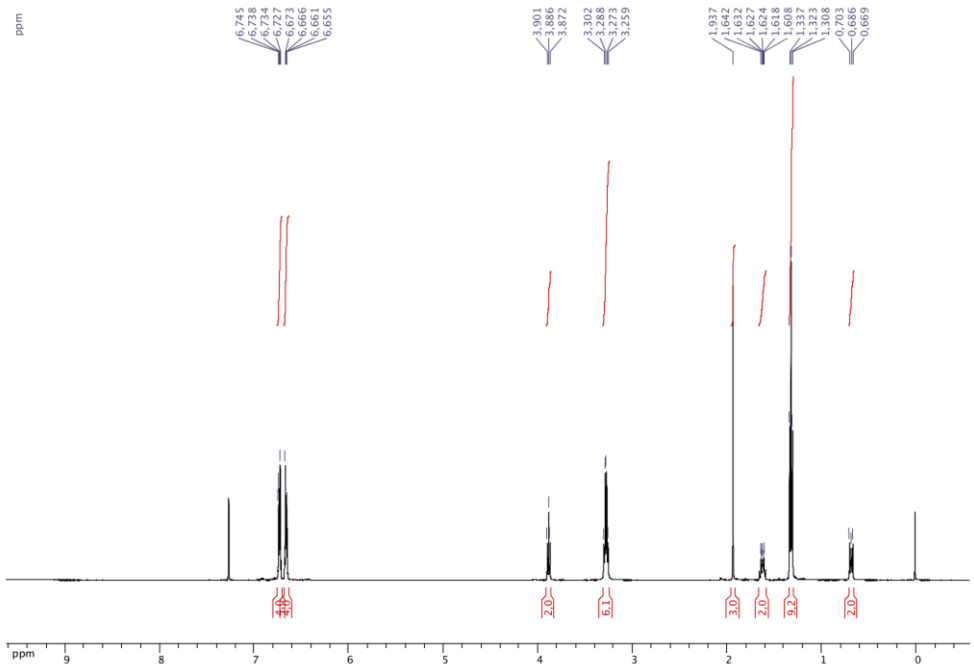


$^{1}$H NMR ($CDCl_3$, 500.4 MHz) of triethylammonium 3-acetoxypropylbis(catecholato)silicate (**13**)

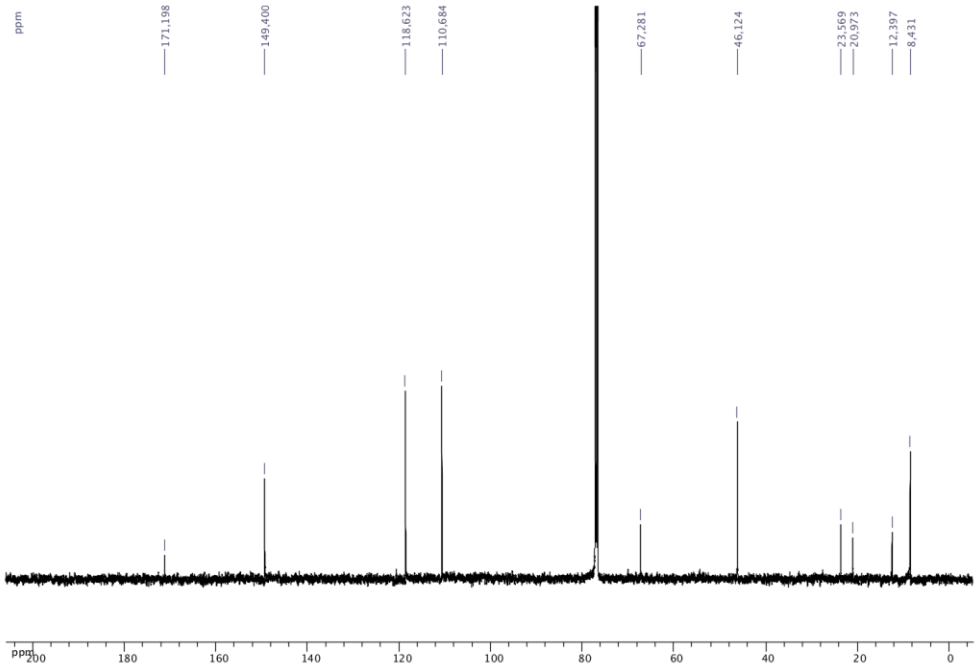


$^{13}$C NMR {$^{1}$H} ($CDCl_3$, 125.8 MHz) of triethylammonium 3-acetoxypropylbis(catecholato)silicate (**13**)

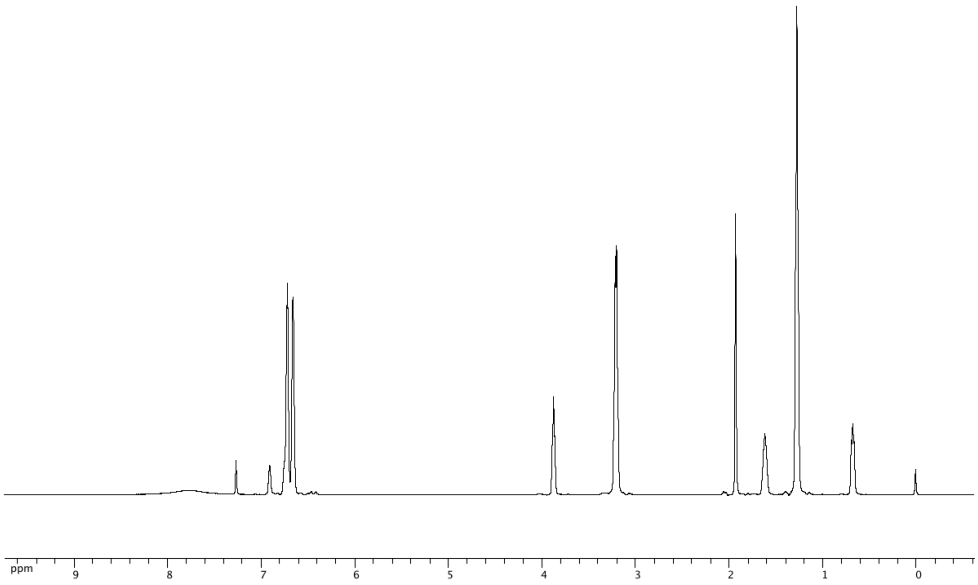


$^{1}$H NMR ($CDCl_3$, 500.4 MHz) of triethylammonium 3-acetoxypropylbis(catecholato)silicate (**13**) after 3 months on benchtop.

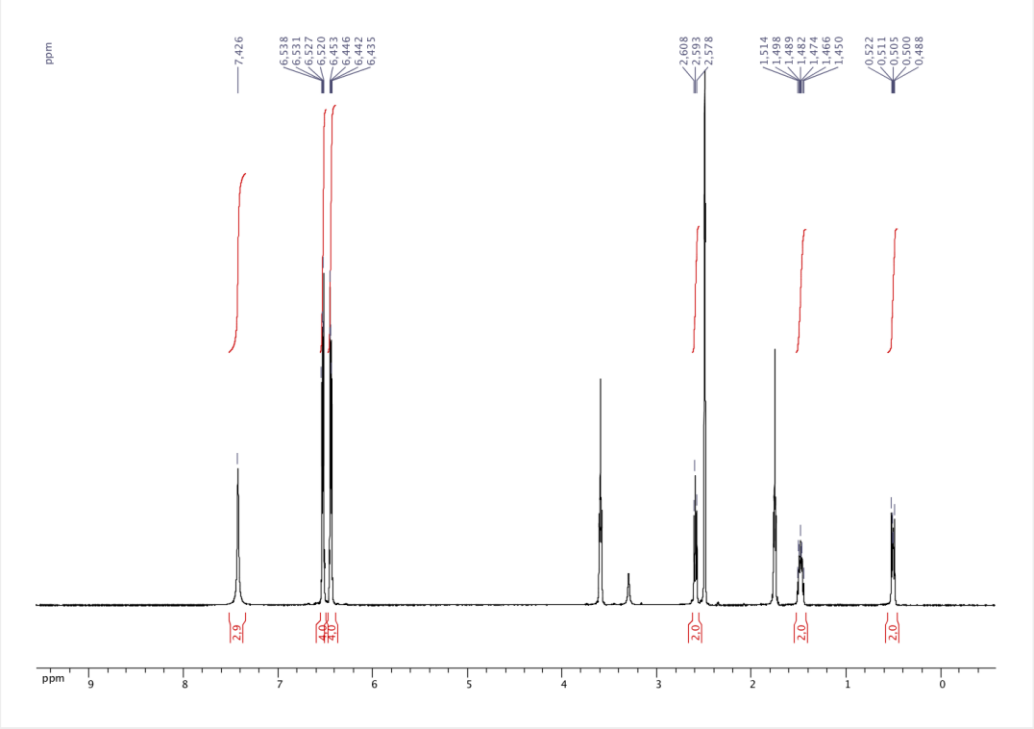


$^{1}$H NMR (DMSO-$d_6$, 500.4 MHz) of 3-ammoniumpropylbis(catecholato)silicate (**14**)

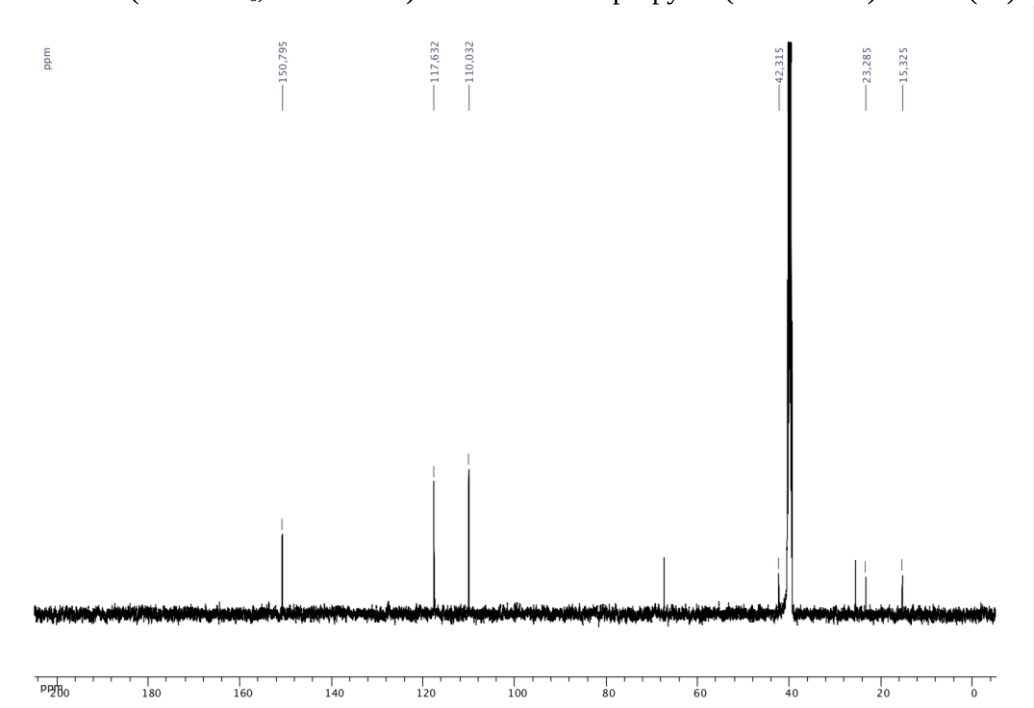


$^{13}$C NMR {$^{1}$H} (DMSO-$d_6$, 125.8 MHz) of 3-ammoniumpropylbis(catecholato)silicate (**14**)

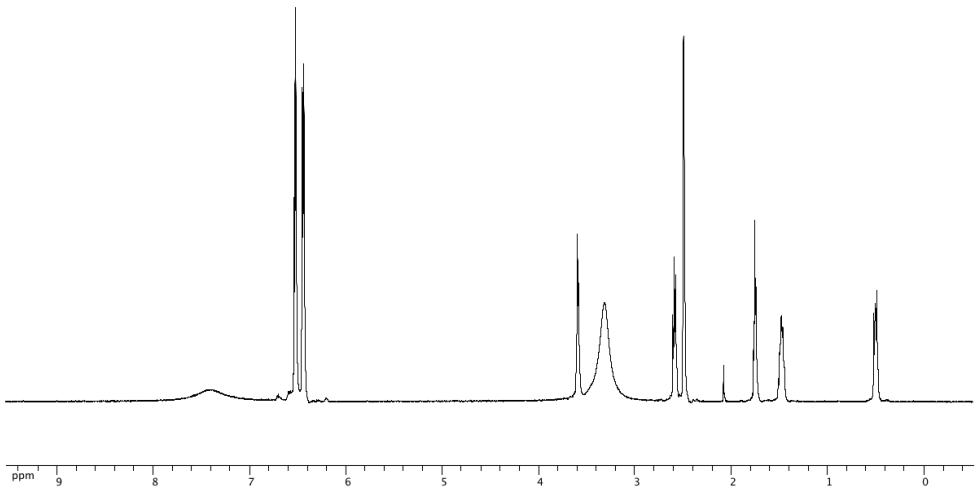


$^{1}$H NMR (DMSO-$d_6$, 500.4 MHz) of 3-ammoniumpropylbis(catecholato)silicate (**14**) after 3 months on benchtop.

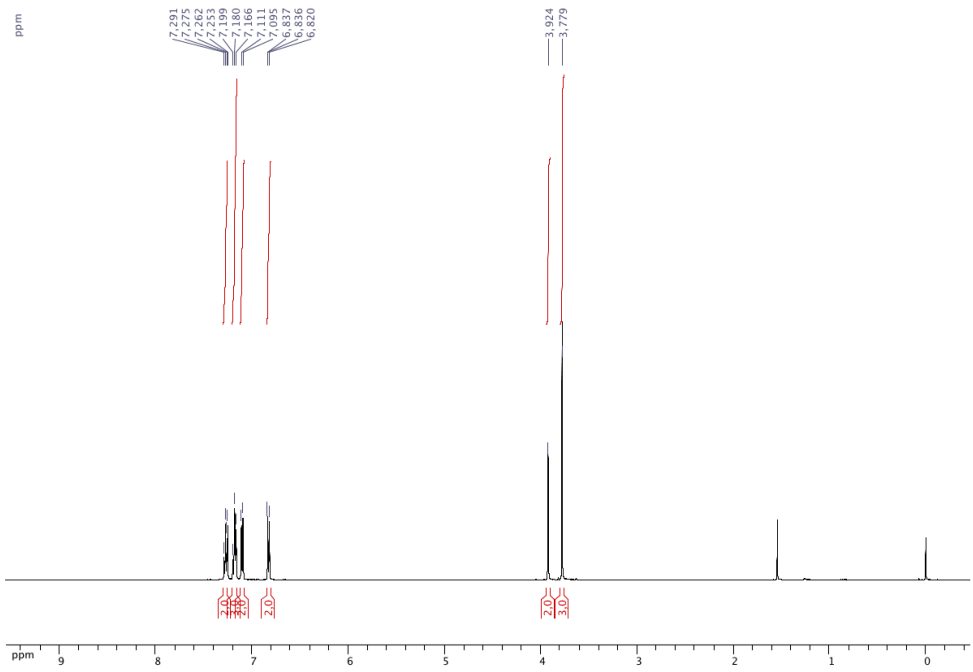


$^{1}$H NMR ($CDCl_3$, 500.4 MHz) of 1-benzyl-4-methoxybenzene (**15**)

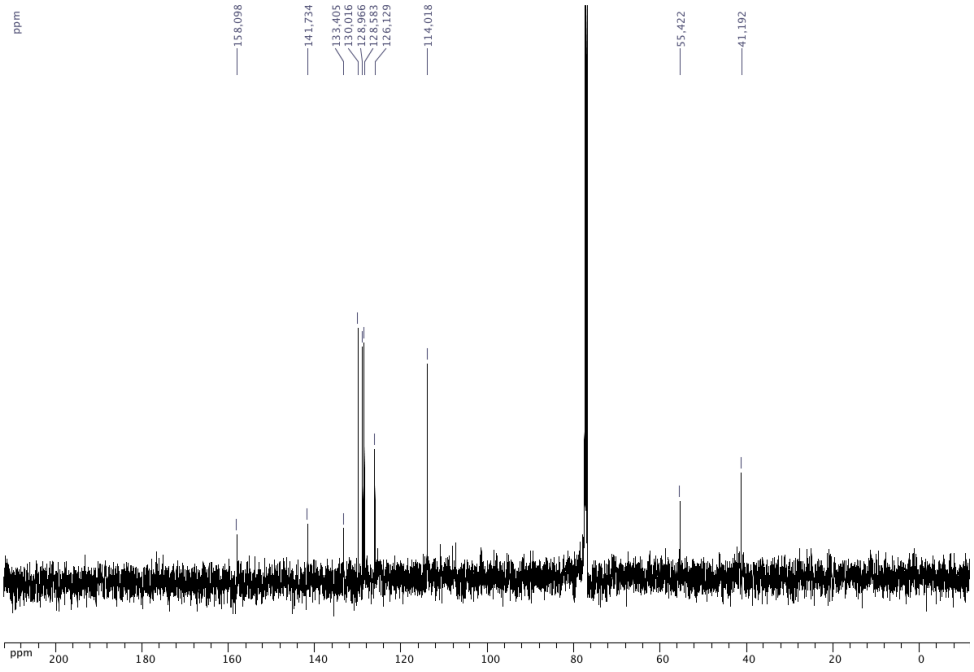


$^{13}$C NMR {$^{1}$H} ($CDCl_3$, 125.8 MHz) of 1-benzyl-4-methoxybenzene (**15**)

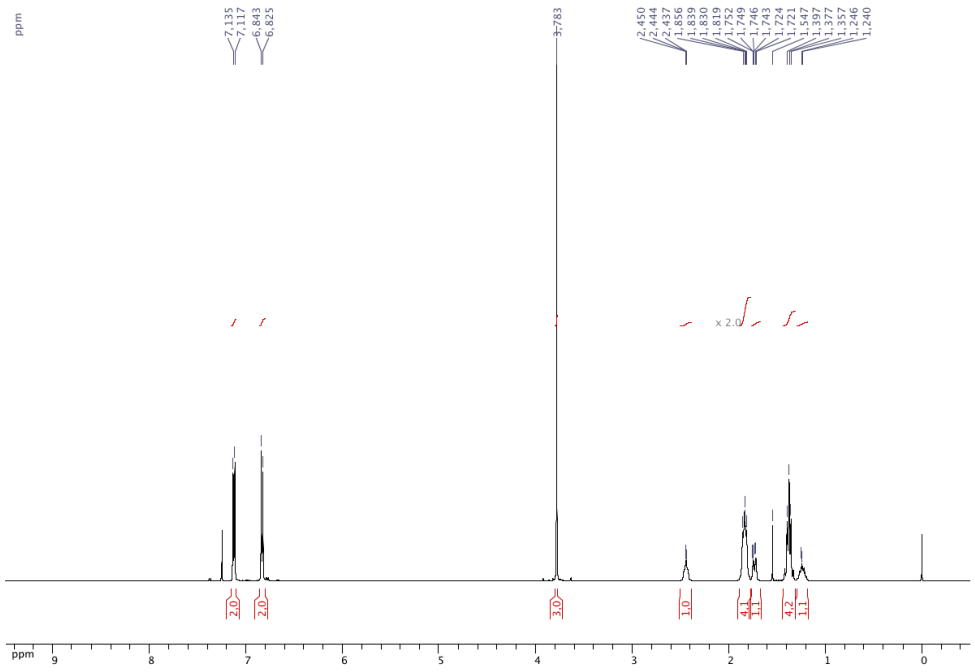


$^{1}$H NMR ($CDCl_3$, 500.4 MHz) of 1-cyclohexyl-4-methoxybenzene (**16**)

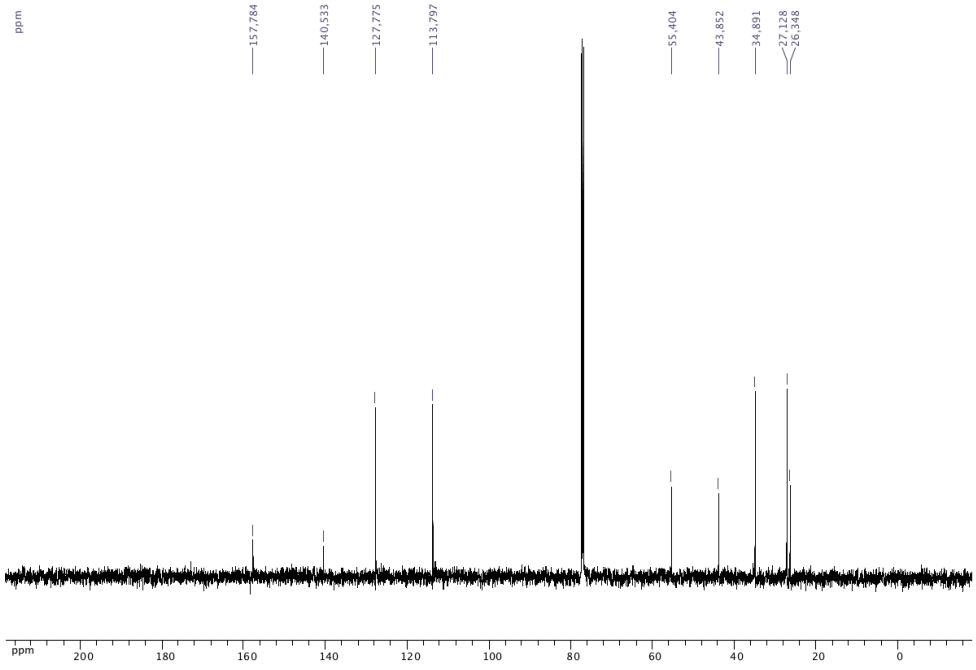


$^{13}$C NMR {$^{1}$H} ($CDCl_3$, 125.8 MHz) of 1-cyclohexyl-4-methoxybenzene (**16**)

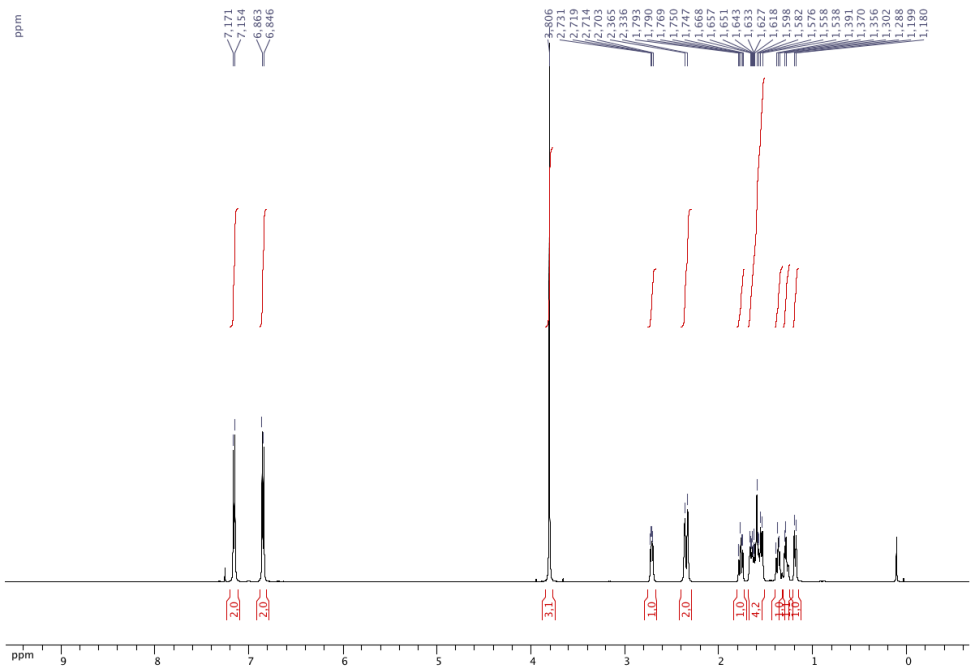

$^{1}$H NMR ($CDCl_3$, 500.4 MHz) of *exo*-2-(4-methoxyphenyl)bicyclo[2.2.1]heptane (**17**)

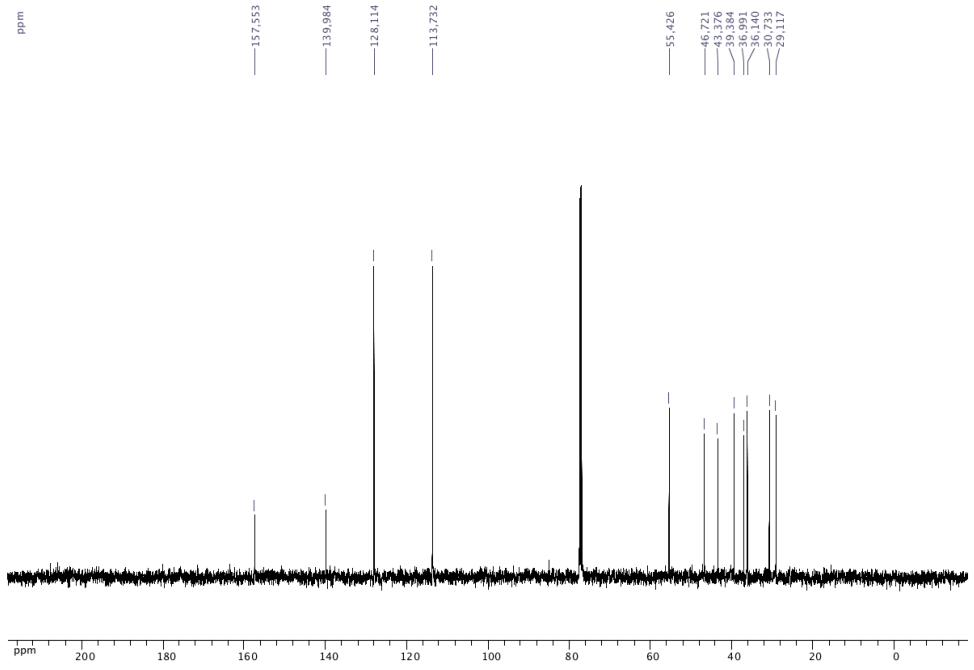

$^{13}$C NMR {$^{1}$H} ($CDCl_3$, 125.8 MHz) of *exo*-2-(4-methoxyphenyl)bicyclo[2.2.1]heptane (**17**)

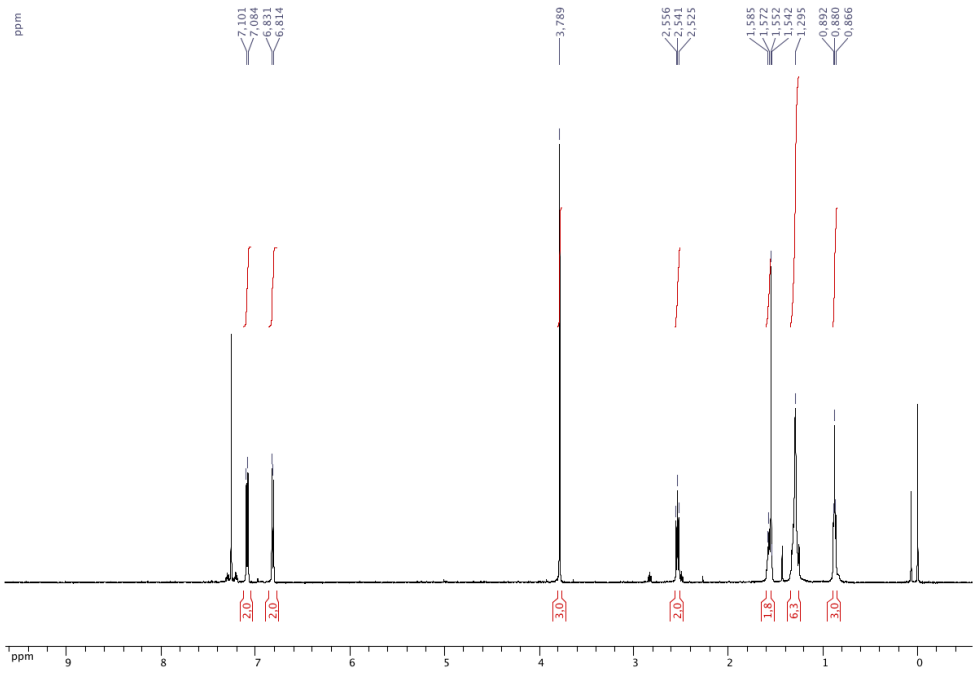


$^{1}$H NMR ($CDCl_3$, 500.4 MHz) of 1-hexyl-4-methoxybenzene (**19**)

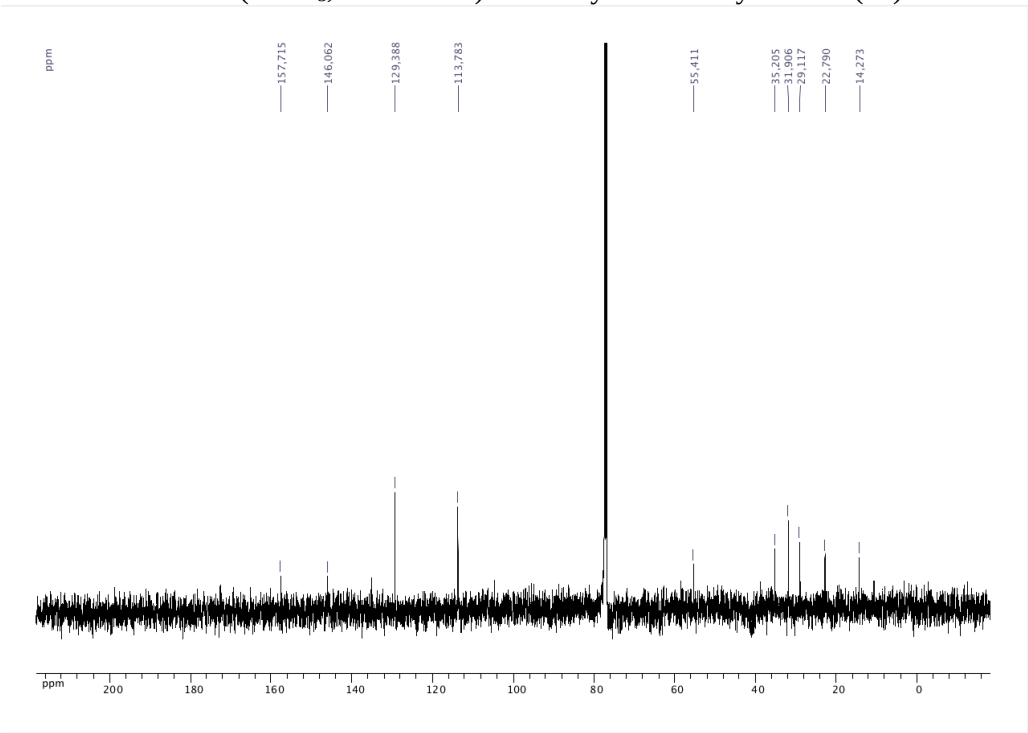


$^{13}$C NMR {$^{1}$H} ($CDCl_3$, 125.8 MHz) of 1-hexyl-4-methoxybenzene (**19**)

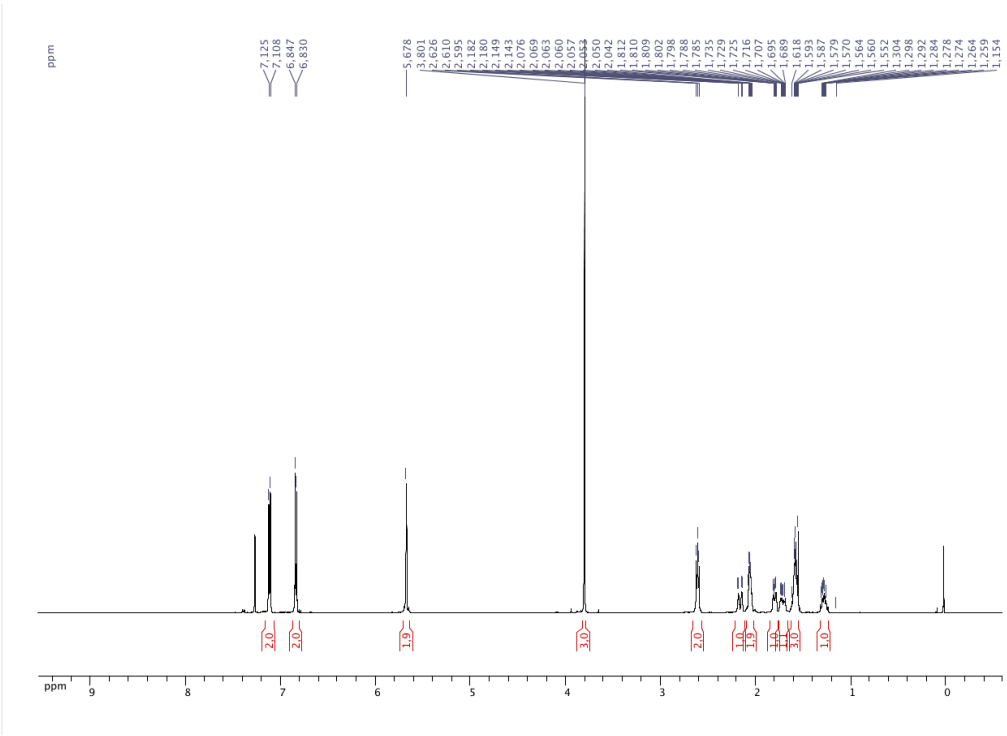

$^{1}$H NMR ($CDCl_3$, 500.4 MHz) of 1-(2-(cyclohex-3-en-1-yl)ethyl)-4-methoxybenzene (**21**)

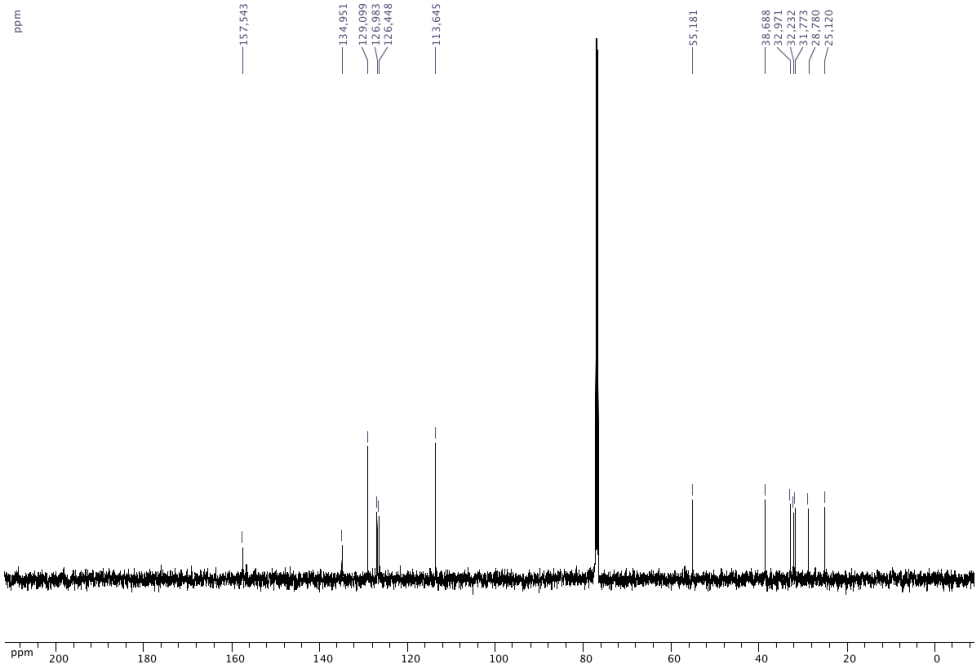

$^{13}$C NMR {$^{1}$H} ($CDCl_3$, 125.8 MHz) of 1-(2-(cyclohex-3-en-1-yl)ethyl)-4-methoxybenzene (**21**)

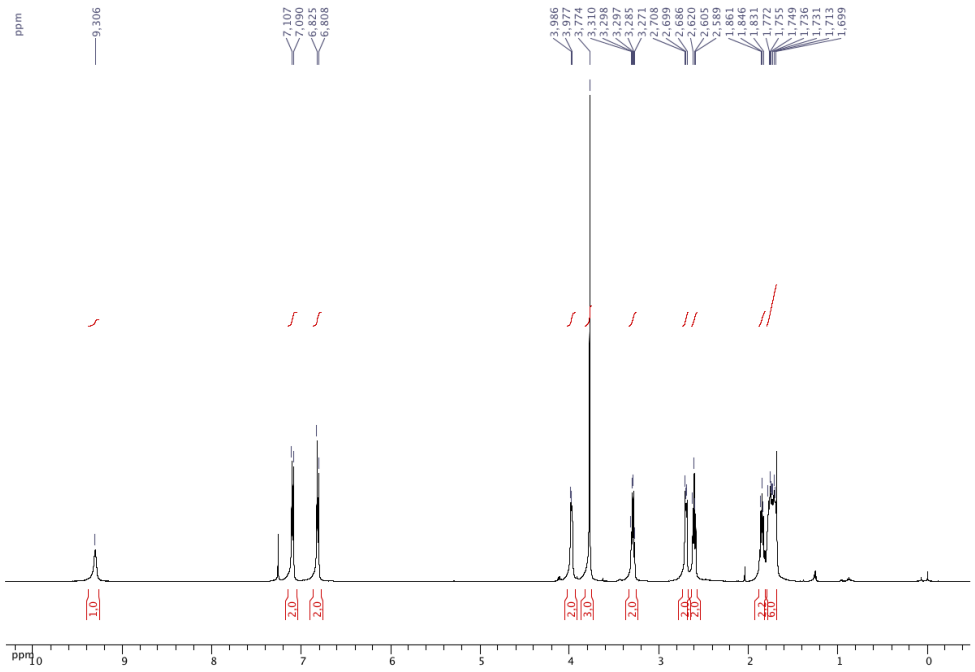


$^{1}$H NMR ($CDCl_3$, 500.4 MHz) of *N*-[(3-(4-methoxyphenyl)propyl)-2-aza-1-oxopentyl]caprolactam (**23**)

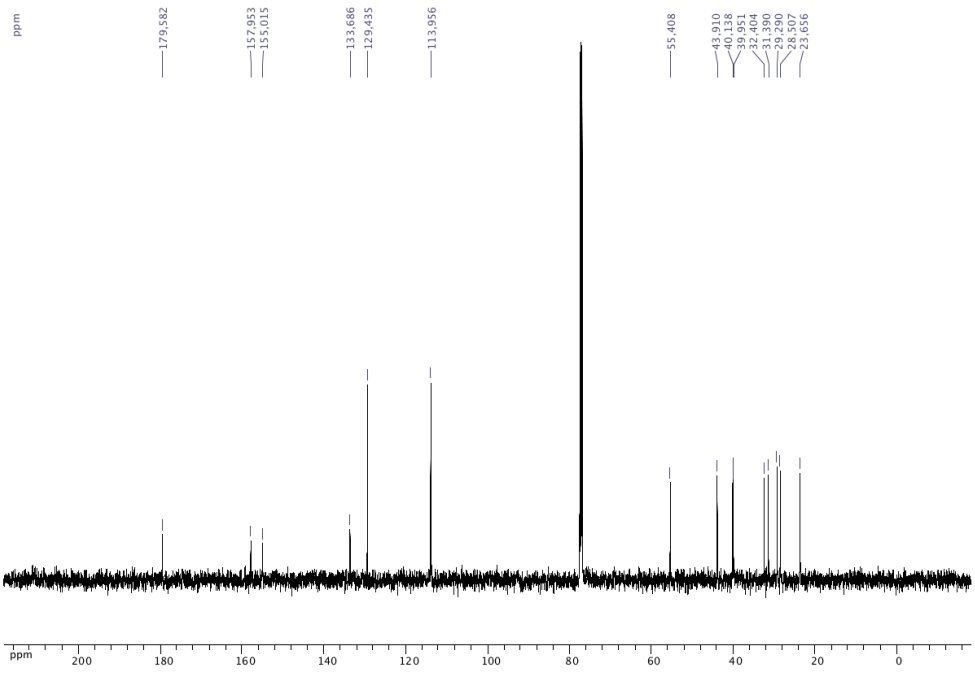


$^{13}$C NMR {$^{1}$H} ($CDCl_3$, 125.8 MHz) of *N*-[(3-(4-methoxyphenyl)propyl)-2-aza-1-oxopentyl]caprolactam (**23**)

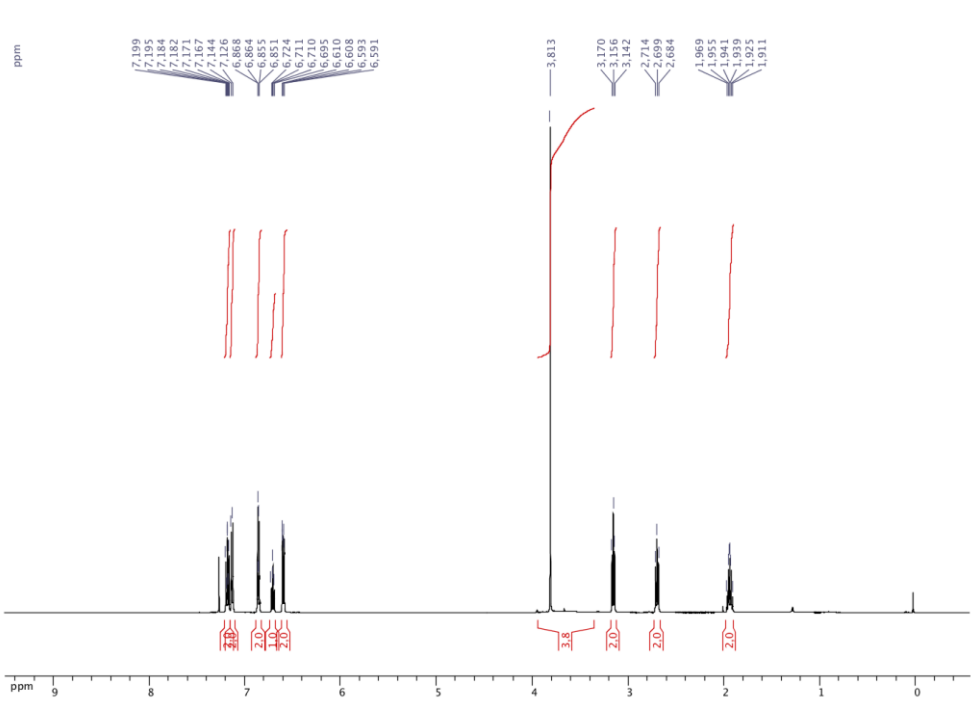


$^{1}$H NMR ($CDCl_3$, 500.4 MHz) of *N*-(3-(4-methoxyphenyl)propyl)aniline (**24**)

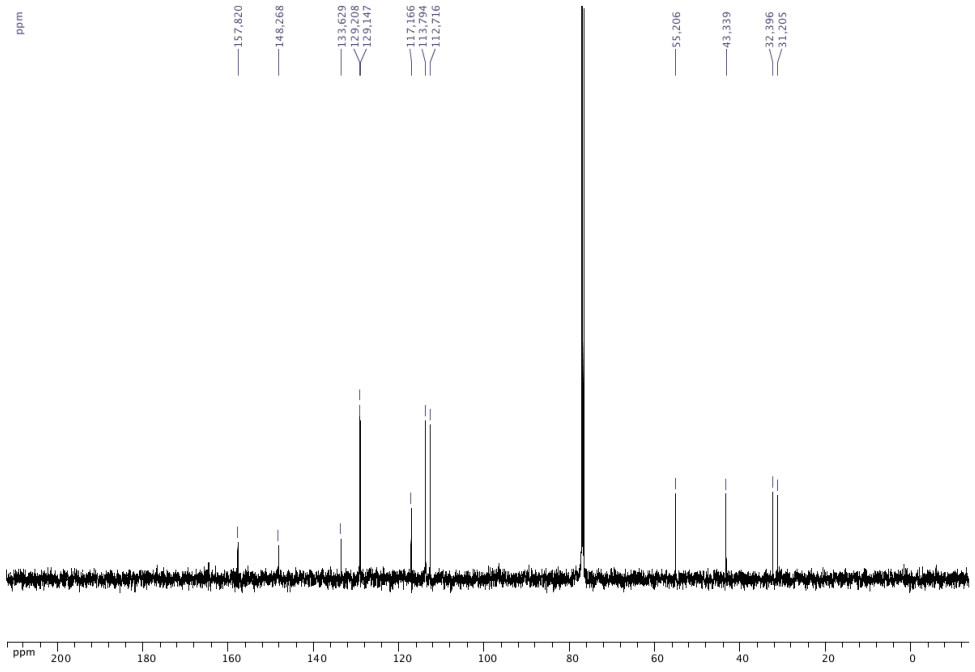


$^{13}$C NMR {$^{1}$H} ($CDCl_3$, 125.8 MHz) of *N*-(3-(4-methoxyphenyl)propyl)aniline (**24**)

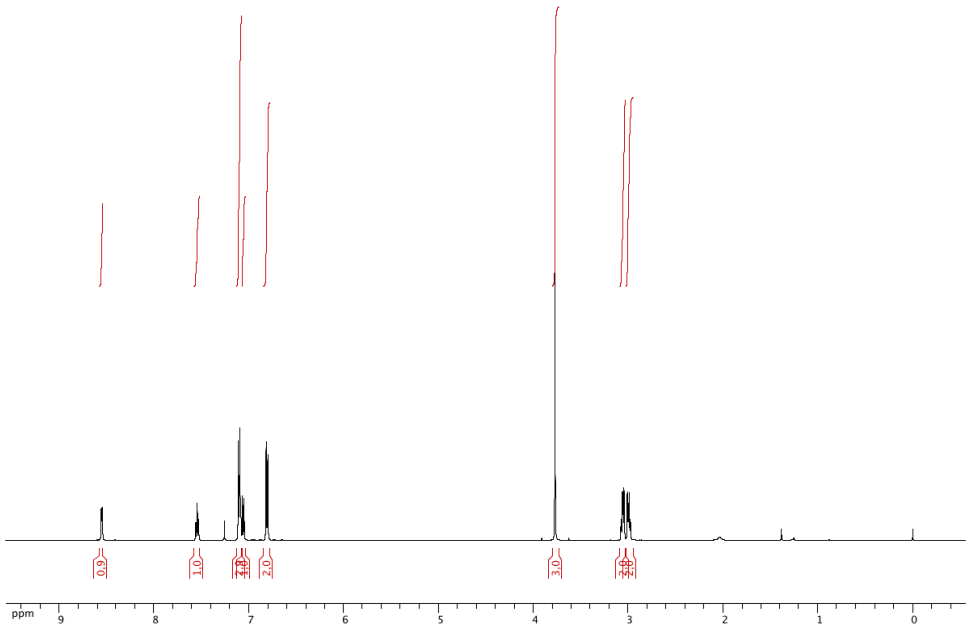


$^{1}$H NMR ($CDCl_3$, 500.4 MHz) of 2-(4-methoxyphenethyl)pyridine (**25**)

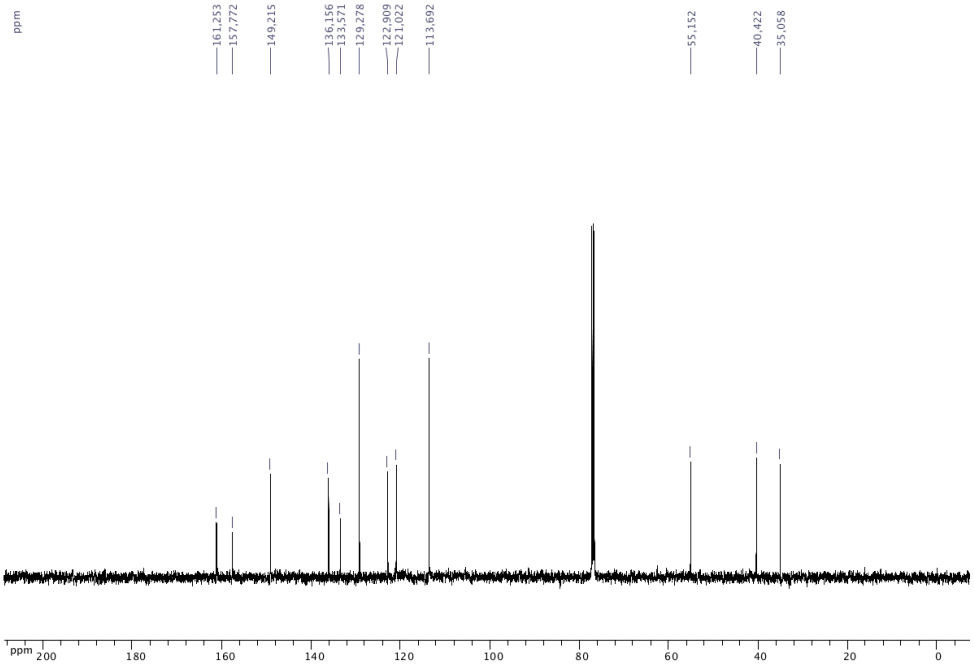


$^{13}$C NMR {$^{1}$H} ($CDCl_3$, 125.8 MHz) of 2-(4-methoxyphenethyl)pyridine (**25**)

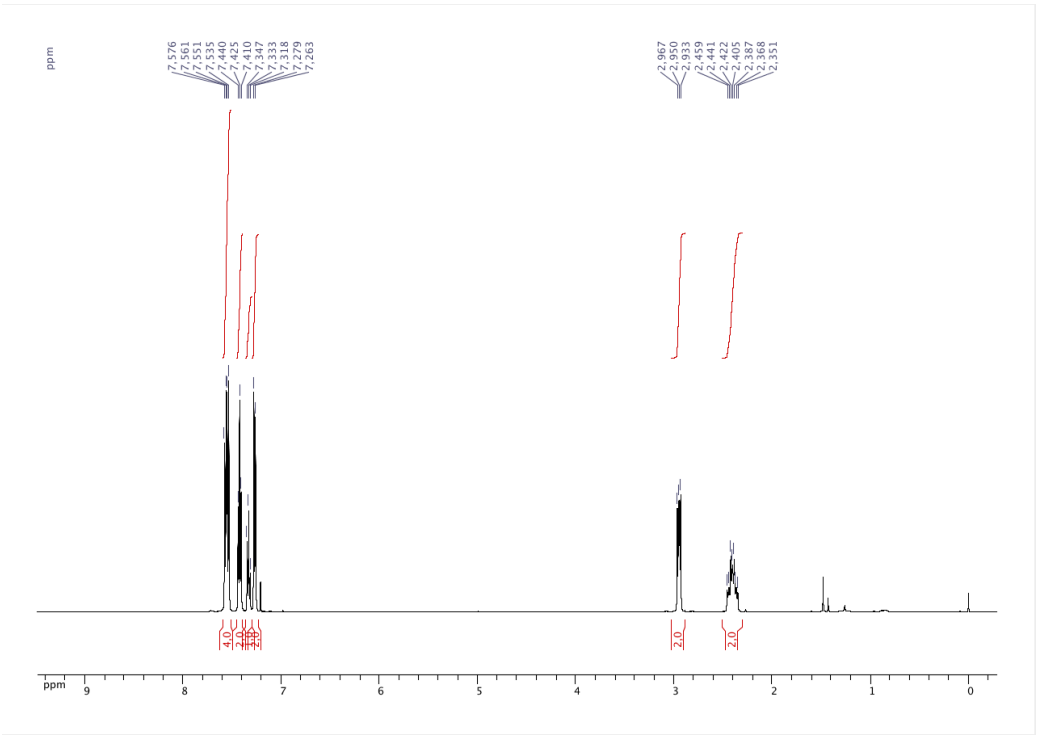


$^{1}$H NMR ($CDCl_3$, 500.4 MHz) of 4-(3,3,4,4,5,5,6,6,6-nonafluorohexyl)-1,1'-biphenyl (**26**)

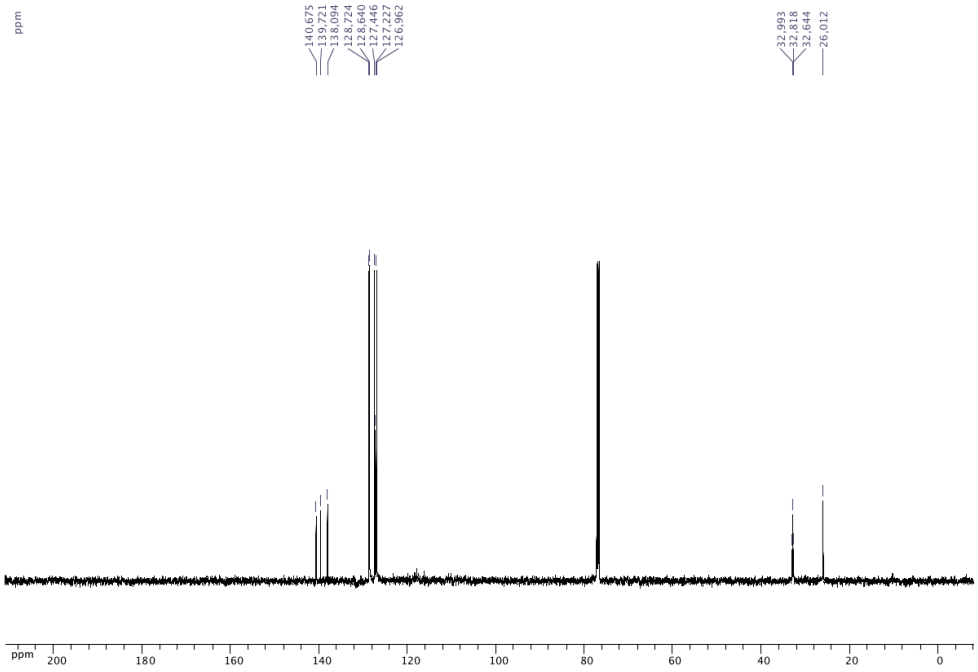


$^{13}$C NMR {$^{1}$H} ($CDCl_3$, 125.8 MHz) of 4-(3,3,4,4,5,5,6,6,6-nonafluorohexyl)-1,1'-biphenyl (**26**)

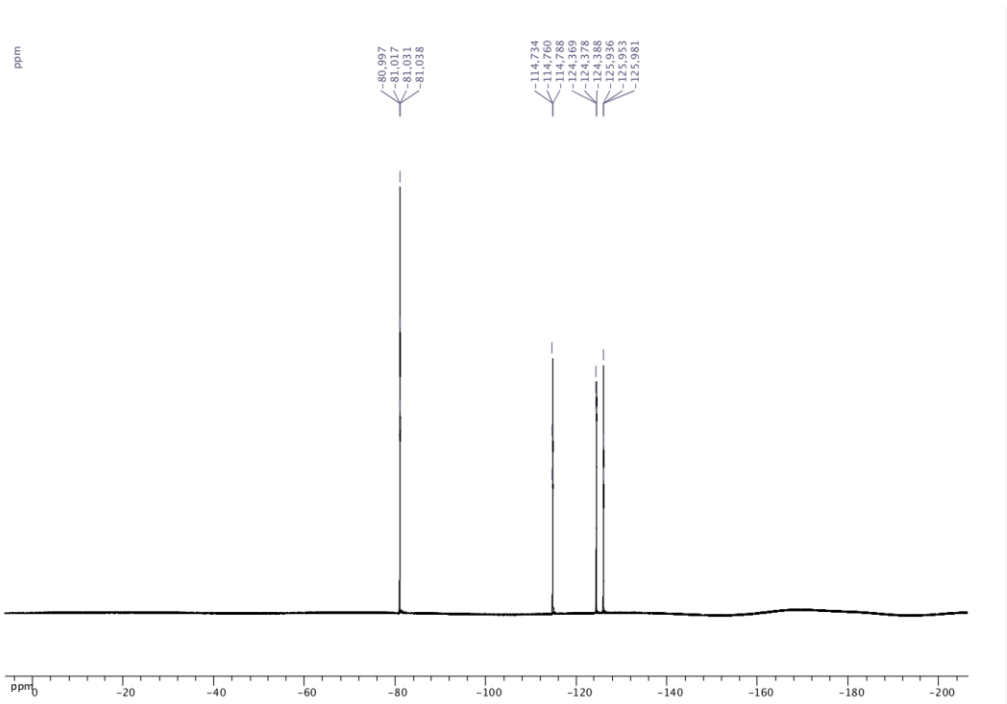


$^{19}F$ NMR {$^{1}H$} ($CDCl_3$, 470.8 MHz) of 4-(3,3,4,4,5,5,6,6,6-nonafluorohexyl)-1,1'-biphenyl (**26**)

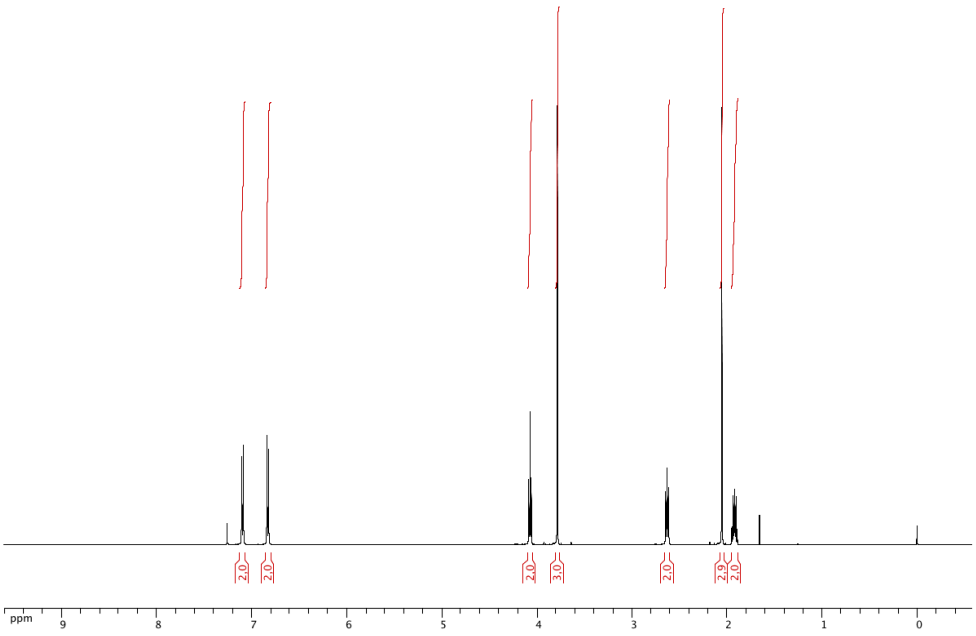


$^{1}$H NMR ($CDCl_3$, 500.4 MHz) of 3-(4-methoxyphenyl)propyl acetate (**27**)

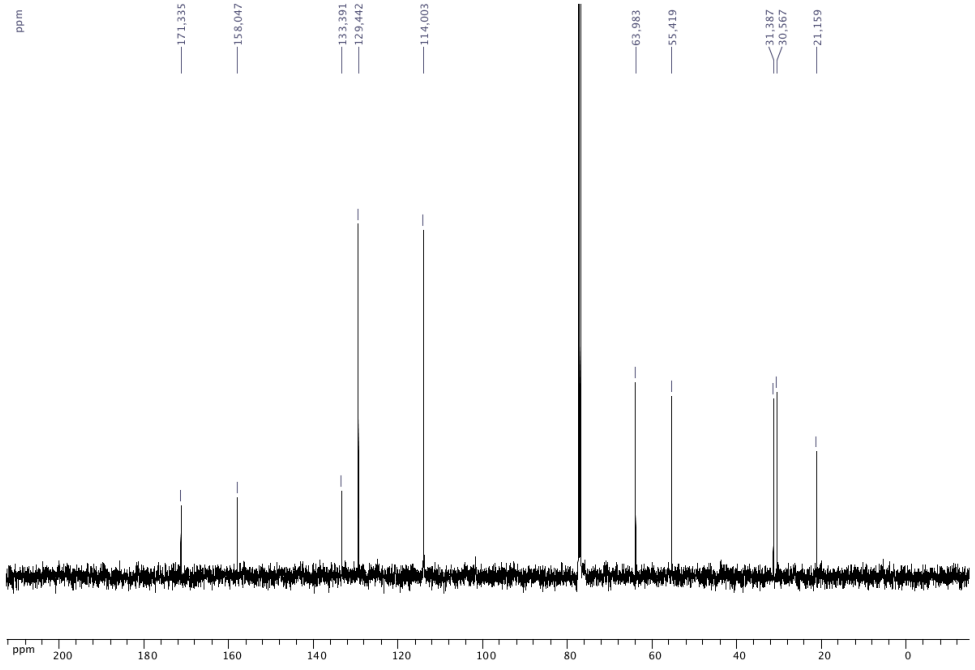


$^{13}$C NMR {$^{1}$H} ($CDCl_3$, 125.8 MHz) of 3-(4-methoxyphenyl)propyl acetate (**27**)

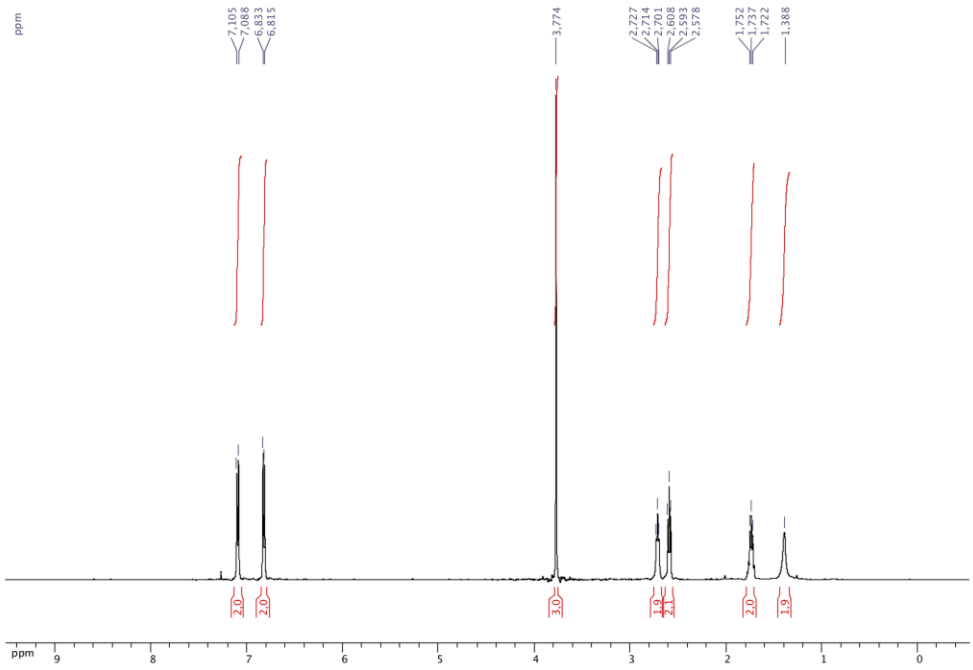


$^{1}$H NMR ($CDCl_3$, 500.4 MHz) of 3-(4-methoxyphenyl)propan-1-amine (**28**)

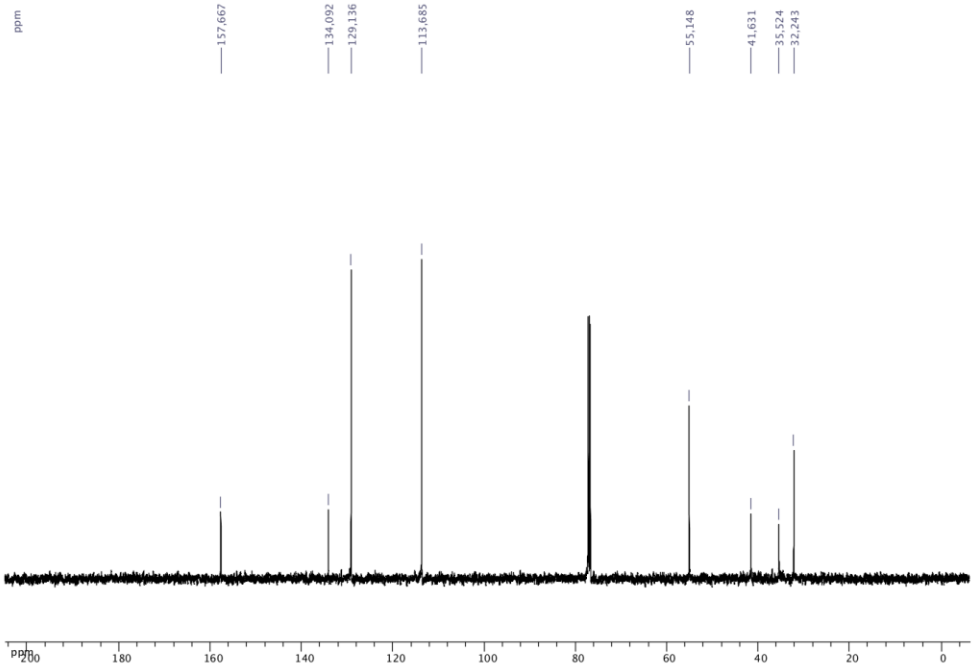


$^{13}$C NMR {$^{1}$H} ($CDCl_3$, 125.8 MHz) of 3-(4-methoxyphenyl)propan-1-amine (**28**)

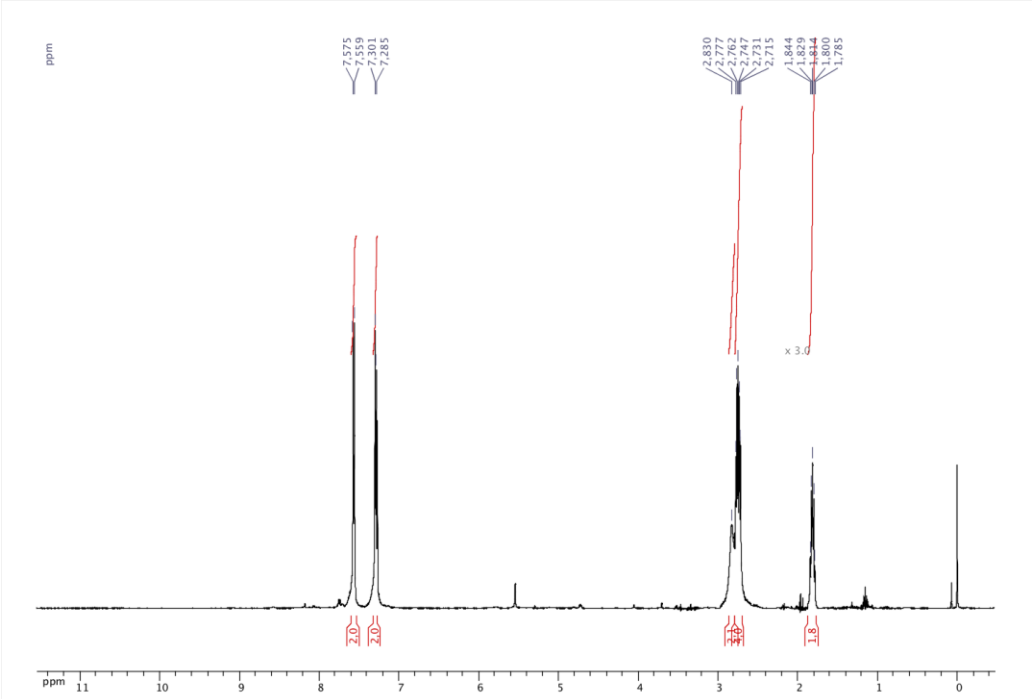


$^{1}$H NMR ($CDCl_3$, 500.4 MHz) of 4-(3-aminopropyl)benzonitrile (**29**)

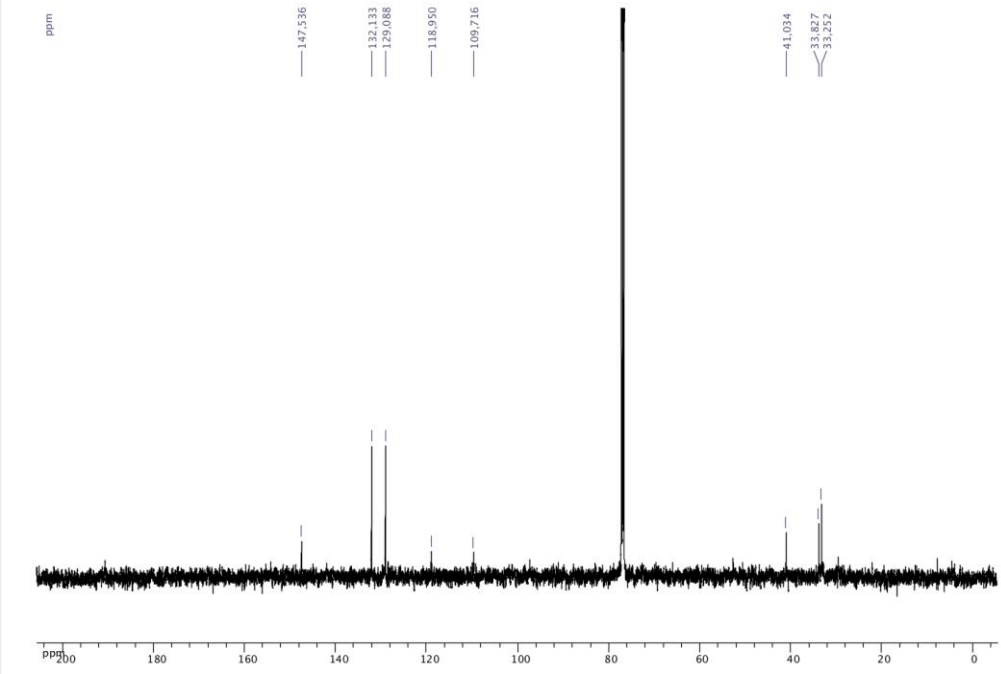


$^{13}$C NMR {$^{1}$H} ($CDCl_3$, 125.8 MHz) of 4-(3-aminopropyl)benzonitrile (**29**)

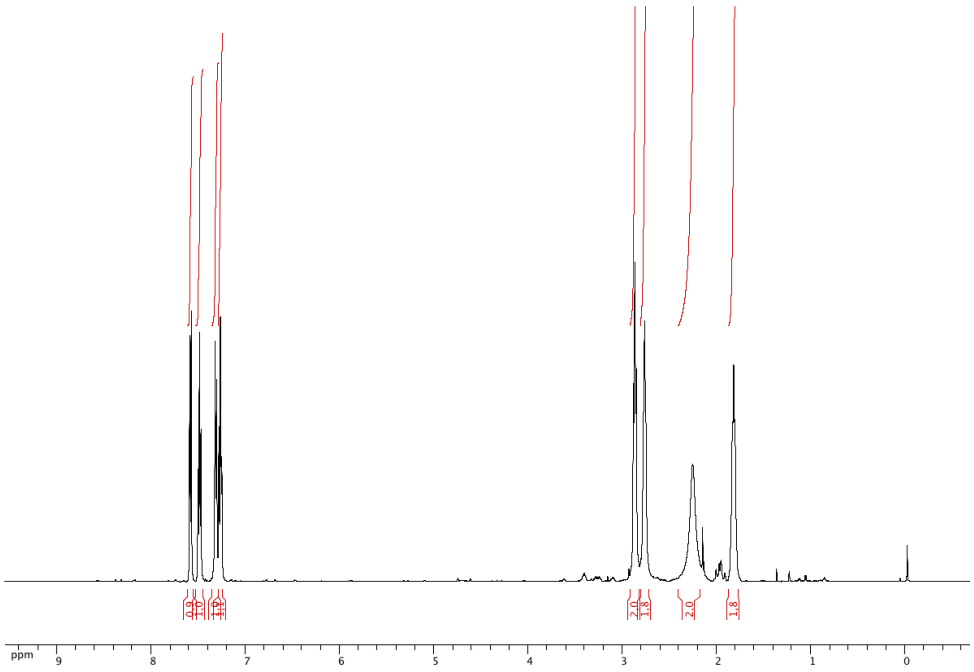


$^{1}$H NMR ($CDCl_3$, 500.4 MHz) of 2-(3-aminopropyl)benzonitrile (**30**)

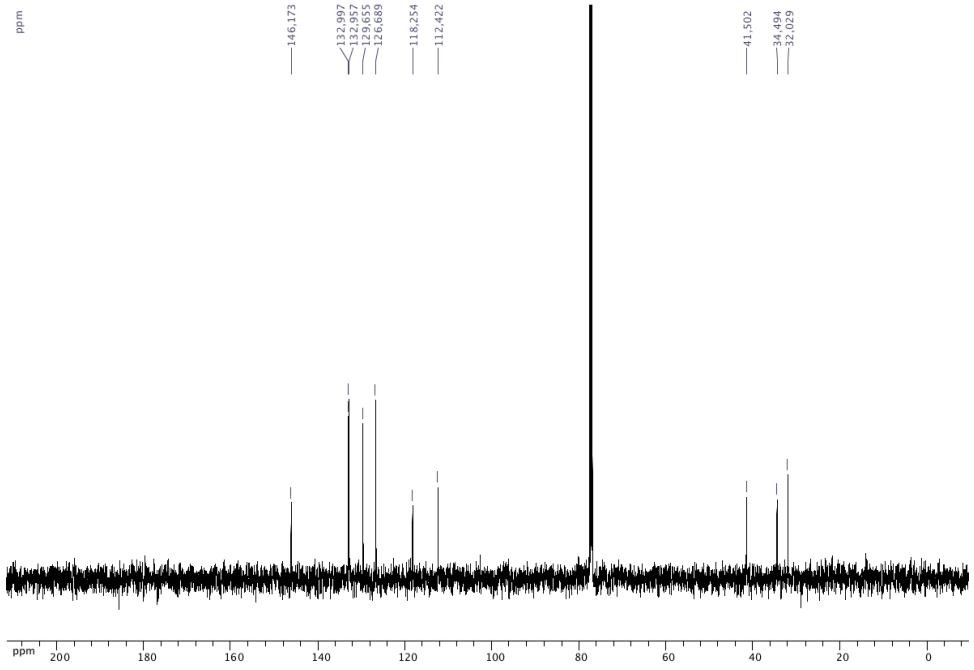


$^{13}$C NMR {$^{1}$H} ($CDCl_3$, 125.8 MHz) of 2-(3-aminopropyl)benzonitrile (**30**)

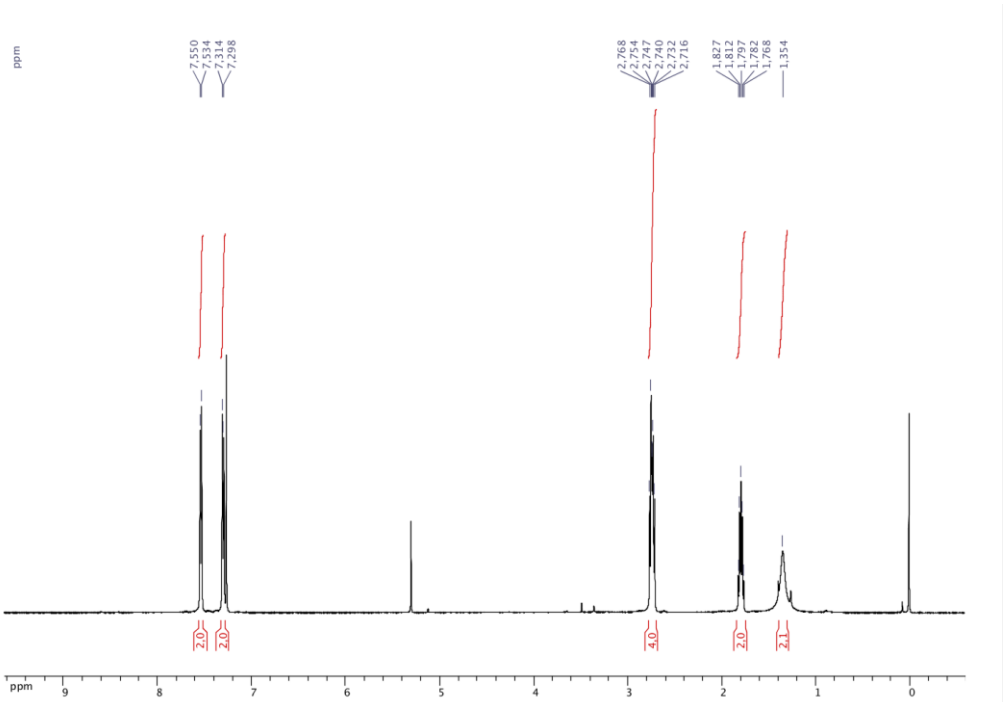


$^{1}$H NMR ($CDCl_3$, 500.4 MHz) of 3-(4-(trifluoromethyl)phenyl)propan-1-amine (**31**)

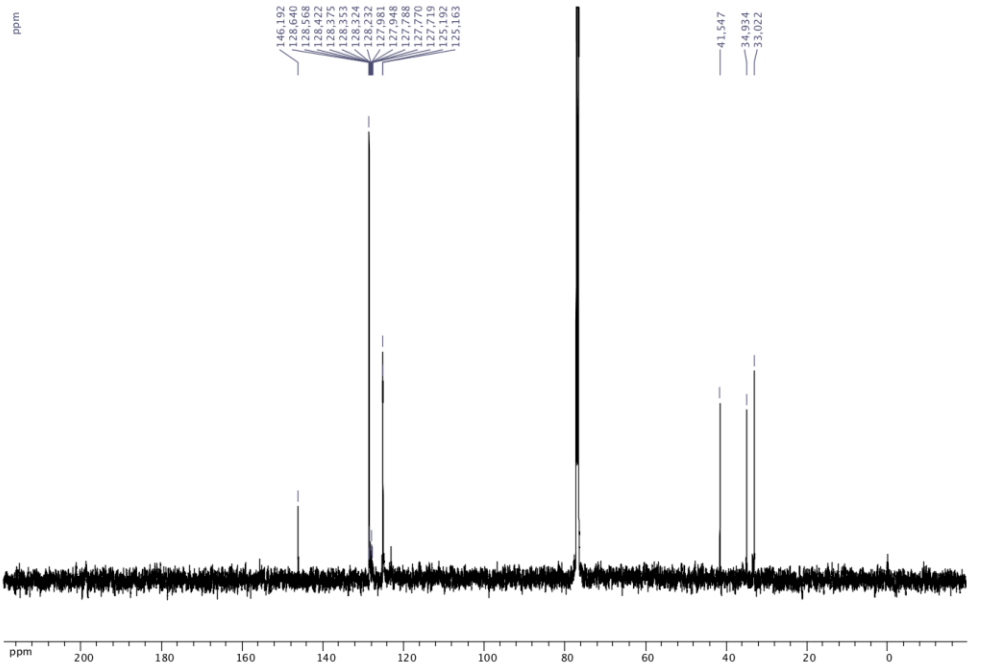


$^{13}$C NMR {$^{1}$H} ($CDCl_3$, 125.8 MHz) of 3-(4-(trifluoromethyl)phenyl)propan-1-amine (**31**)

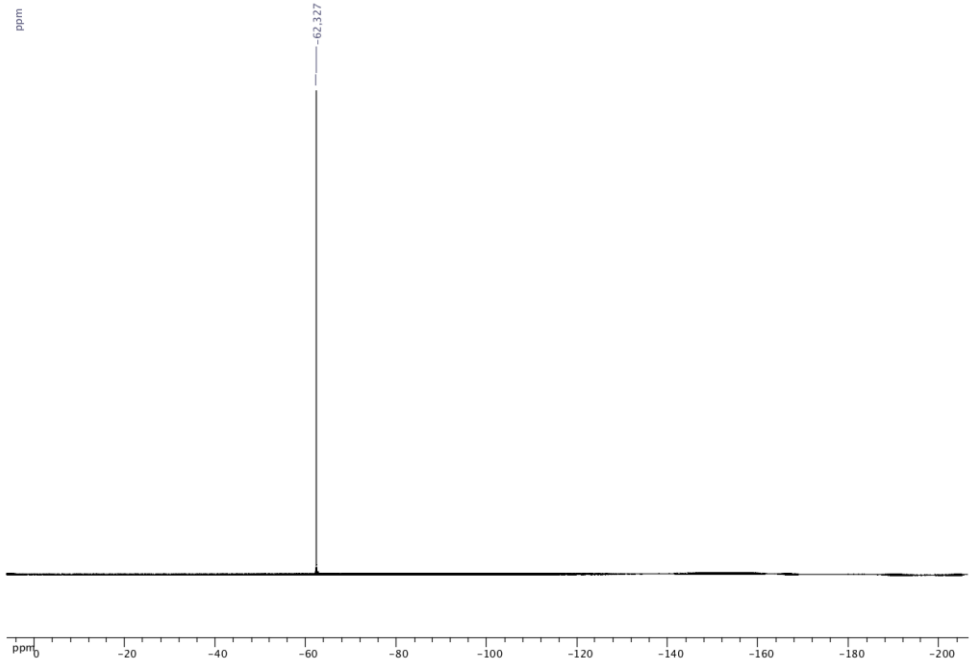


$^{19}F$ NMR {$^{1}H$} ($CDCl_3$, 470.8 MHz) of 3-(4-(trifluoromethyl)phenyl)propan-1-amine (**31**)

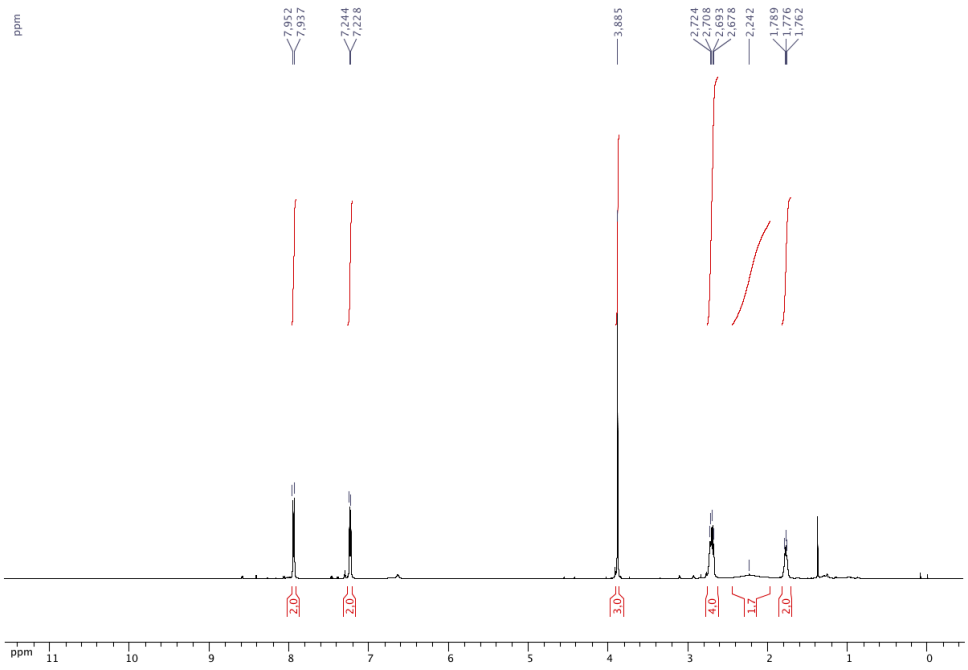


$^{1}$H NMR ($CDCl_3$, 500.4 MHz) of methyl 4-(3-aminopropyl)benzoate (**32**)

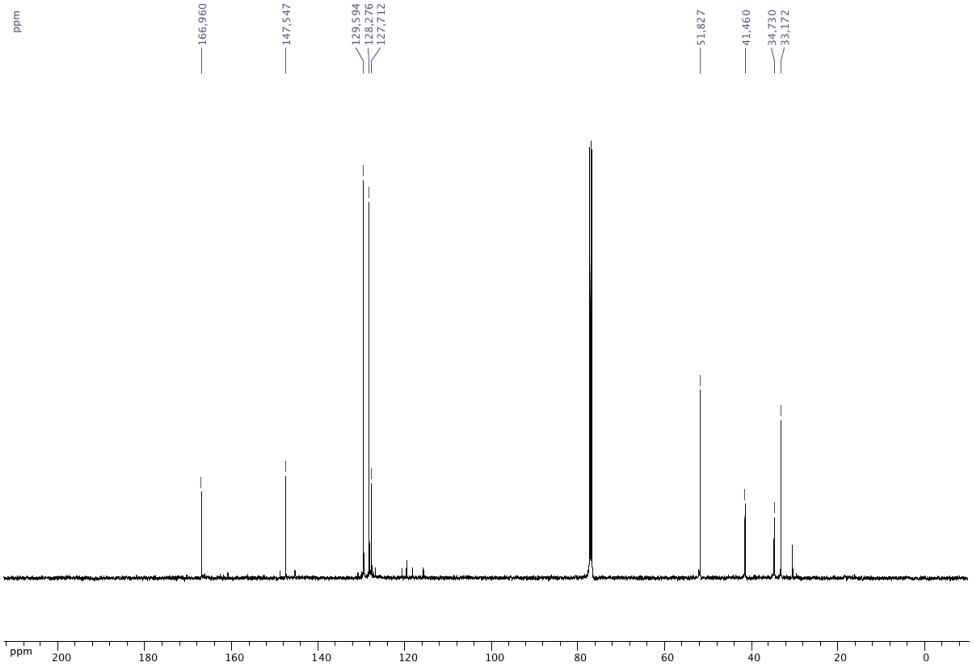


$^{13}$C NMR {$^{1}$H} ($CDCl_3$, 125.8 MHz) of methyl 4-(3-aminopropyl)benzoate (**32**)

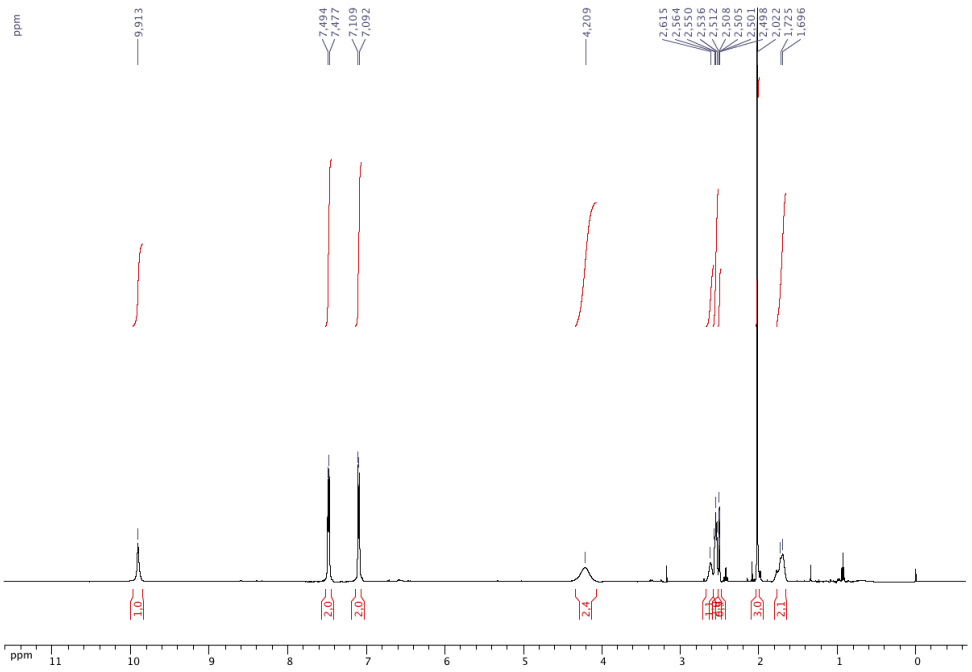


$^{1}$H NMR (DMSO-$d_6$, 500.4 MHz) of *N*-(4-(3-aminopropyl)phenyl)acetamide (**33**)

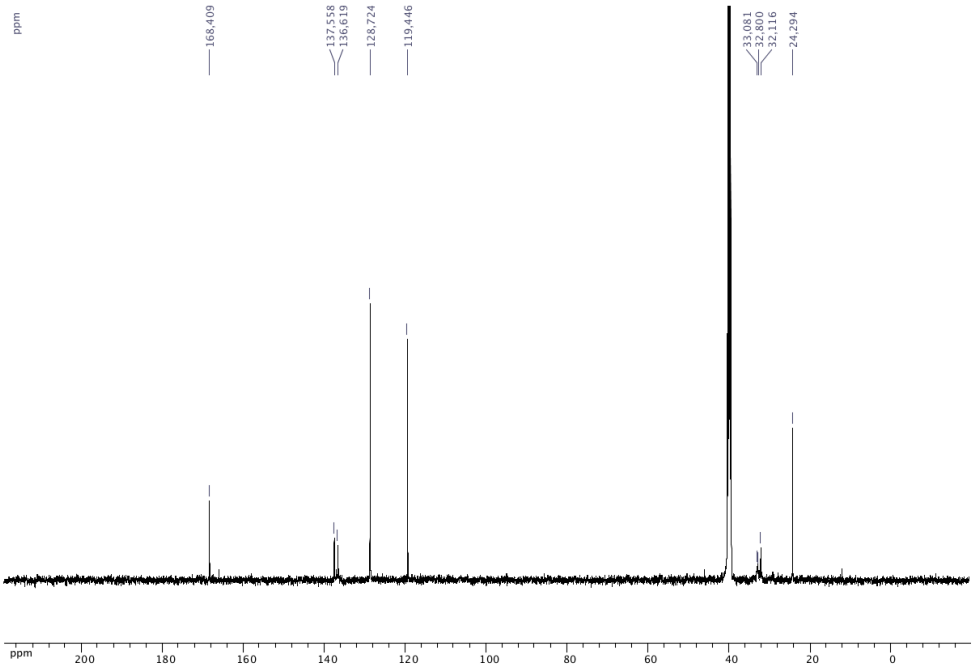


$^{13}$C NMR {$^{1}$H} (DMSO-$d_6$, 125.8 MHz) of *N*-(4-(3-aminopropyl)phenyl)acetamide (**33**)

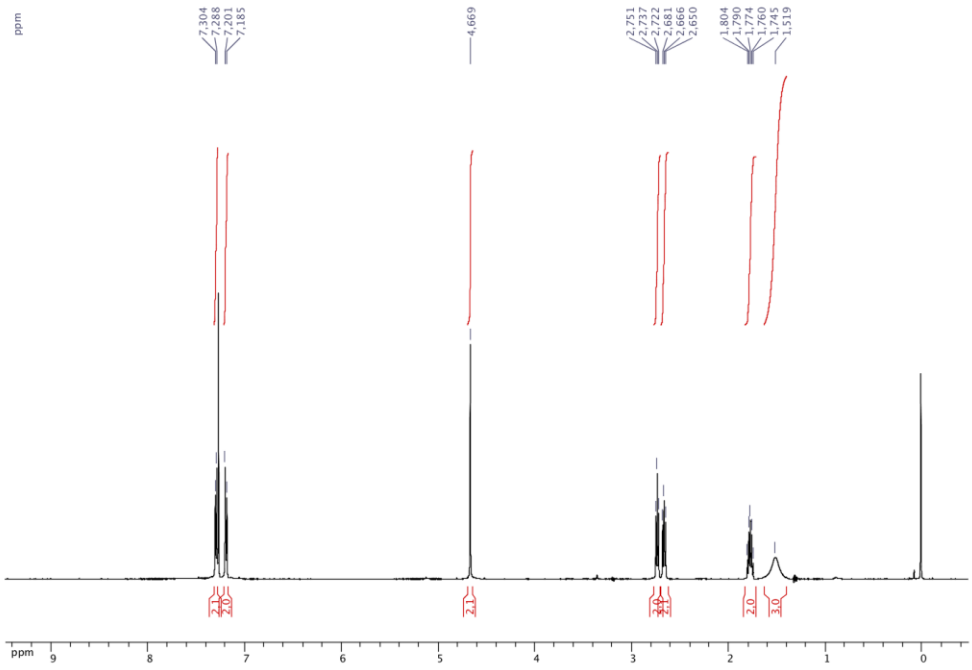


$^{1}$H NMR ($CDCl_3$, 500.4 MHz) of (4-(3-aminopropyl)phenyl)methanol (**34**)

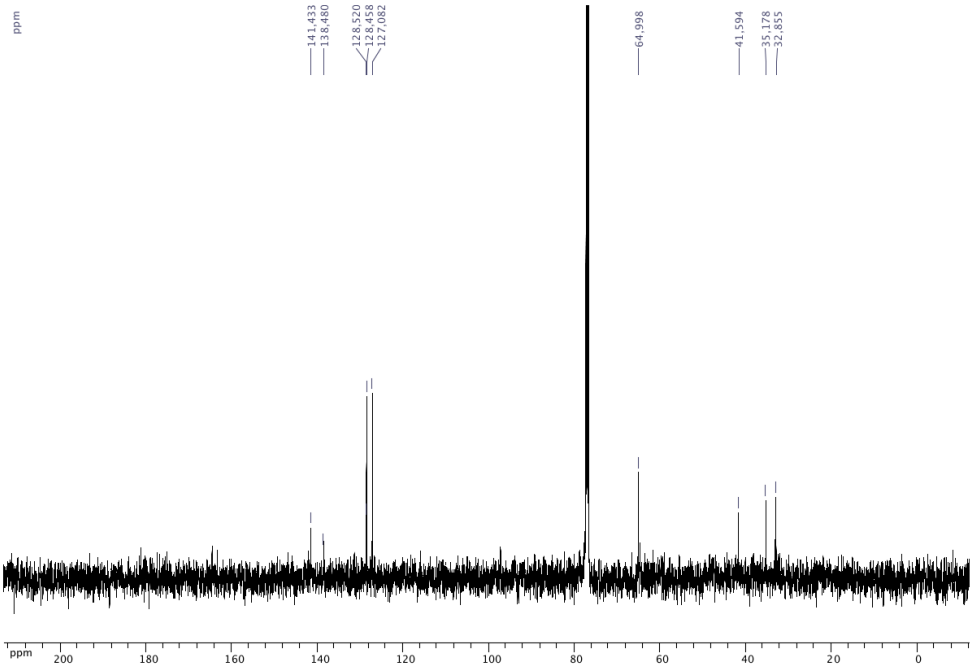


$^{13}$C NMR {$^{1}$H} ($CDCl_3$, 125.8 MHz) of (4-(3-aminopropyl)phenyl)methanol (**34**)

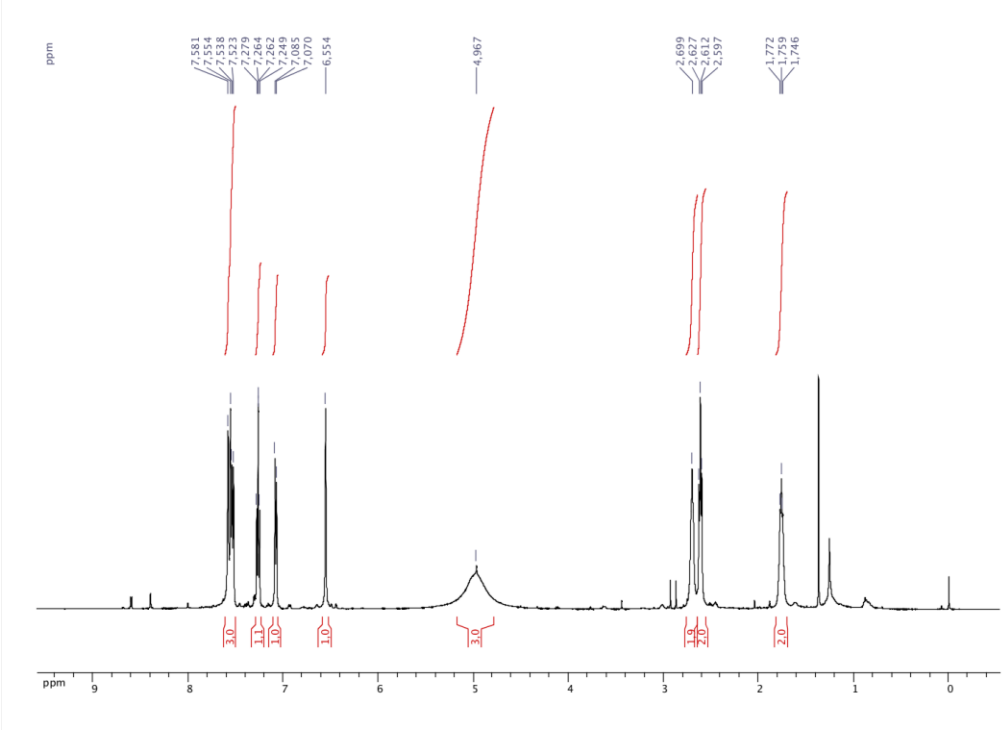


$^{1}$H NMR ($CDCl_3$, 500.4 MHz) of 3-(3-(1*H*-pyrazol-5-yl)phenyl)propan-1-amine (**35**)

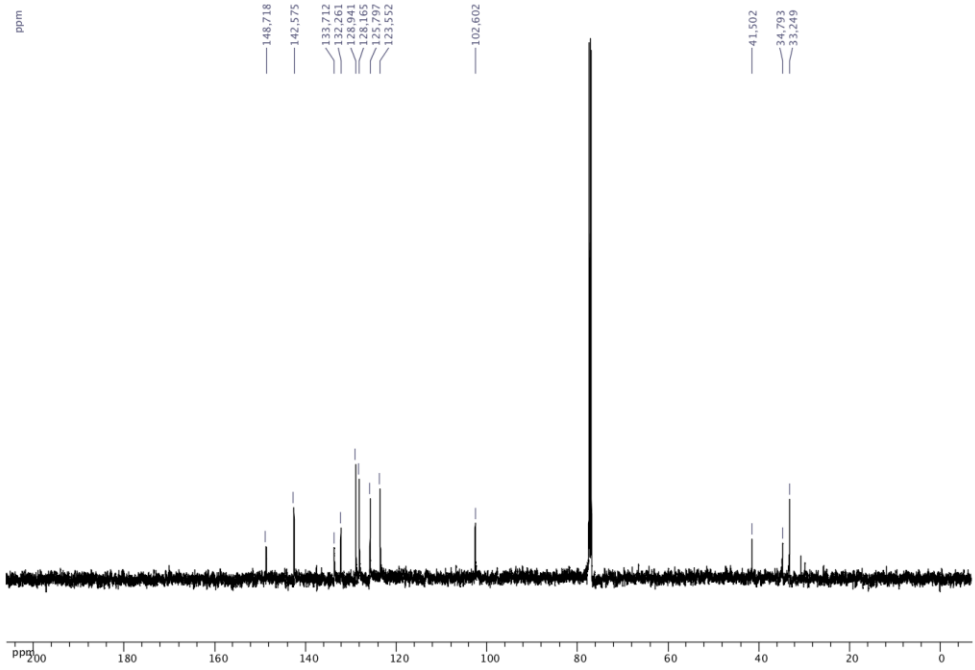


$^{13}$C NMR {$^{1}$H} ($CDCl_3$, 125.8 MHz) of 3-(3-(1*H*-pyrazol-5-yl)phenyl)propan-1-amine (**35**)

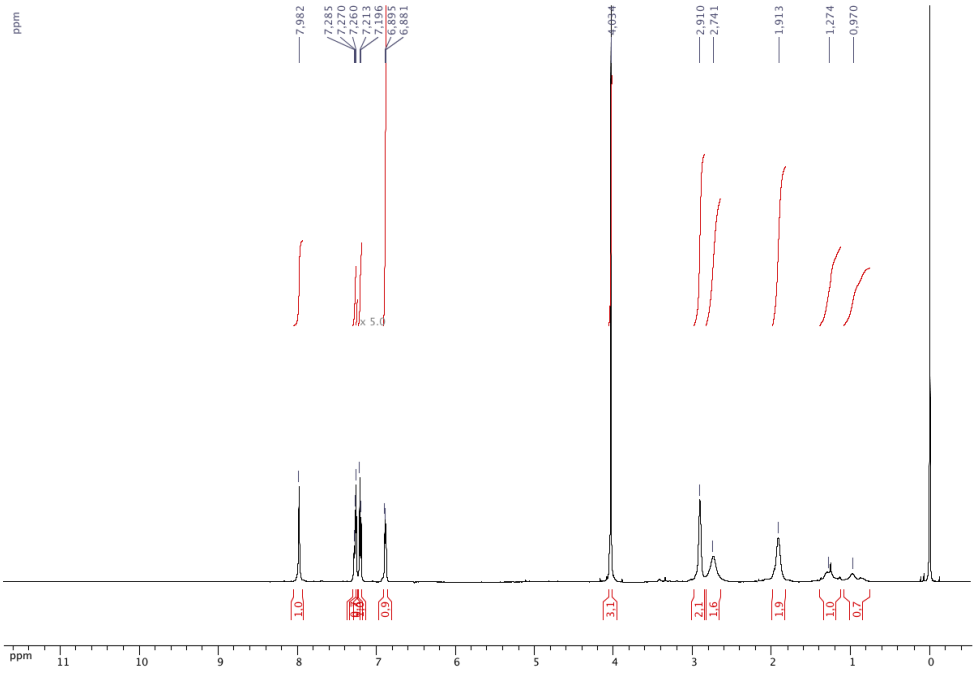


$^{1}$H NMR ($CDCl_3$, 500.4 MHz) of 3-(1-methyl-1*H*-indazol-5-yl)propan-1-amine (**36**)

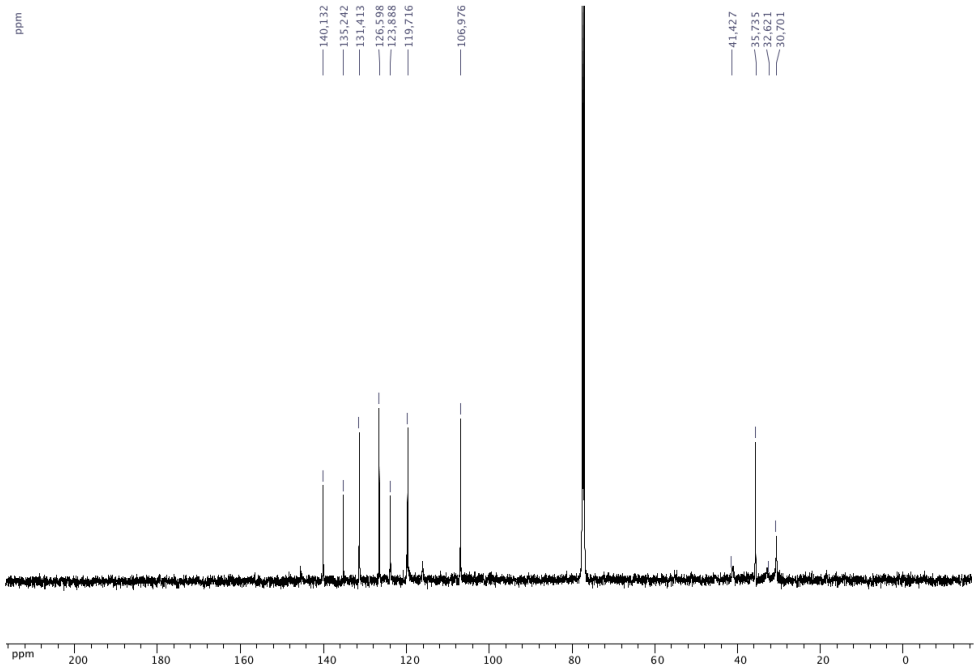


$^{13}$C NMR {$^{1}$H} ($CDCl_3$, 125.8 MHz) of 3-(1-methyl-1*H*-indazol-5-yl)propan-1-amine (**36**)

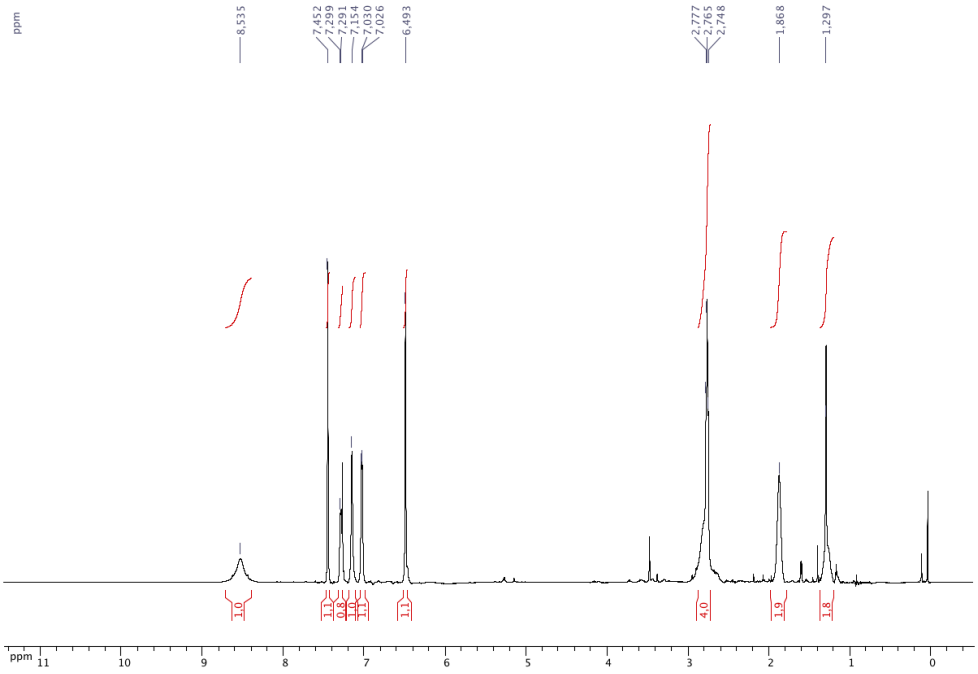


$^{1}$H NMR ($CDCl_3$, 500.4 MHz) of 3-(1*H*-indol-5-yl)propan-1-amine (**37**)

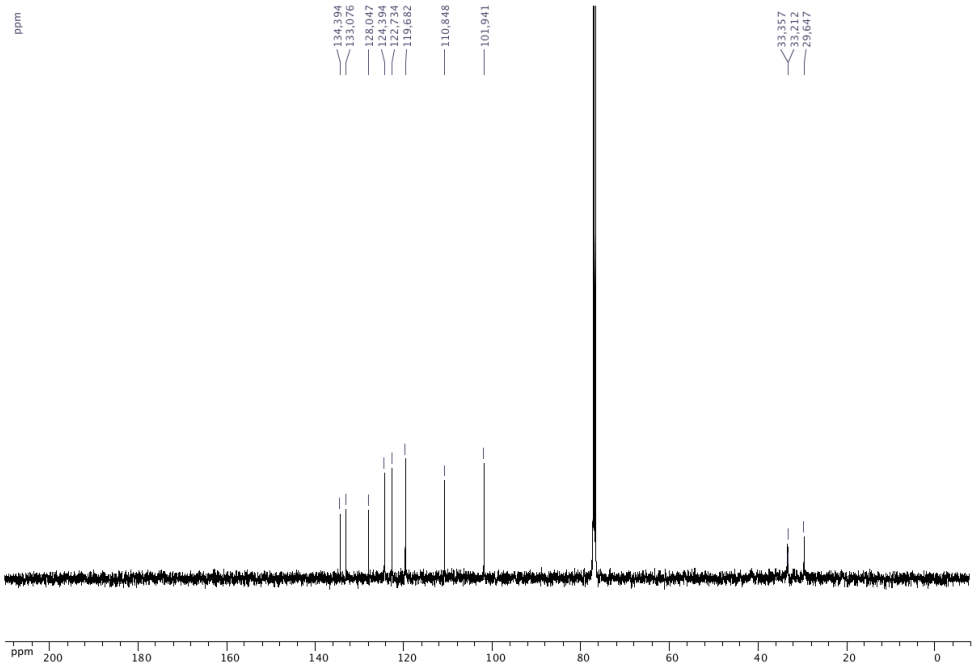


$^{13}$C NMR {$^{1}$H} ($CDCl_3$, 125.8 MHz) of 3-(1*H*-indol-5-yl)propan-1-amine (**37**)

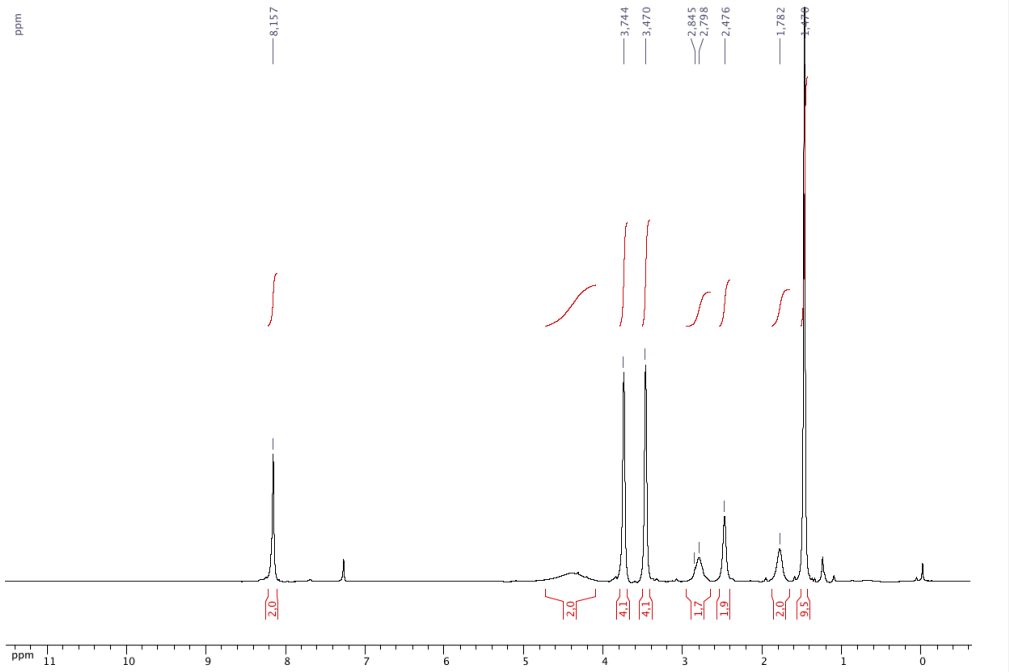


$^{1}$H NMR ($CDCl_3$, 500.4 MHz) of *tert*-butyl 4-(5-(3-aminopropyl)pyrimidin-2-yl)piperazine-1-carboxylate (**38**)

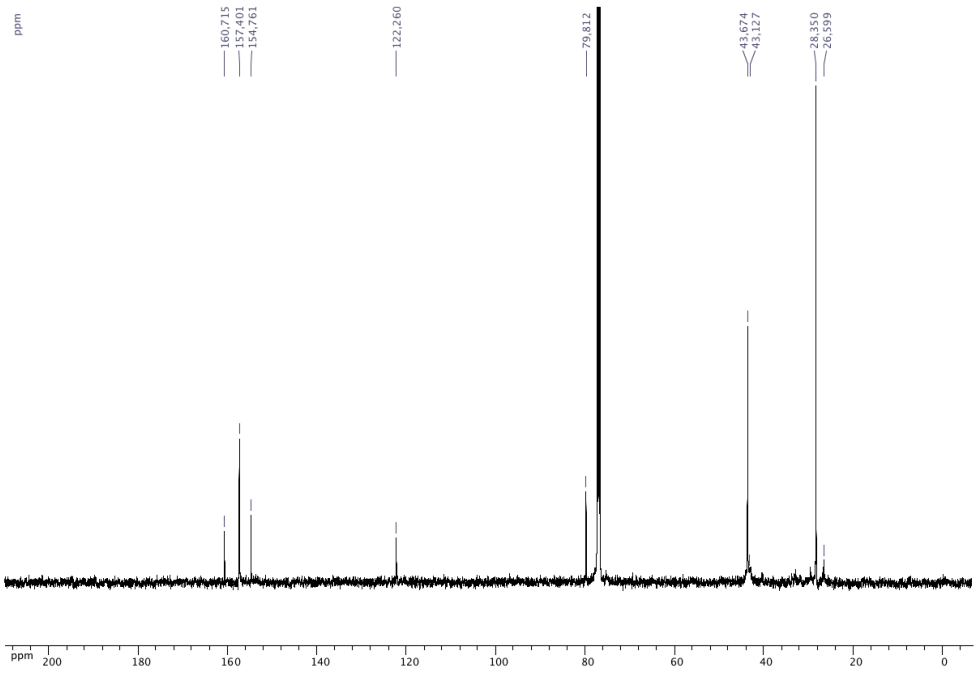


$^{13}$C NMR {$^{1}$H} ($CDCl_3$, 125.8 MHz) of *tert*-butyl 4-(5-(3-aminopropyl)pyrimidin-2-yl)piperazine-1-carboxylate (**38**)

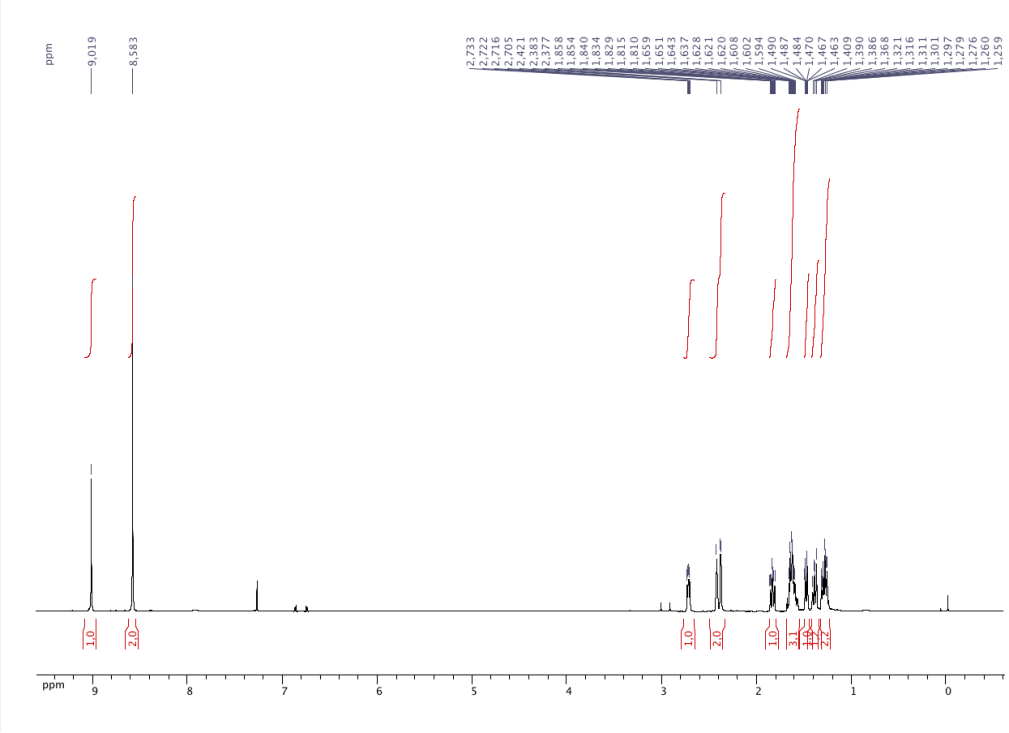


$^{1}$H NMR ($CDCl_3$, 500.4 MHz) of 5-(*exo*-bicyclo[2.2.1]heptan-2-yl)pyrimidine (**39**)

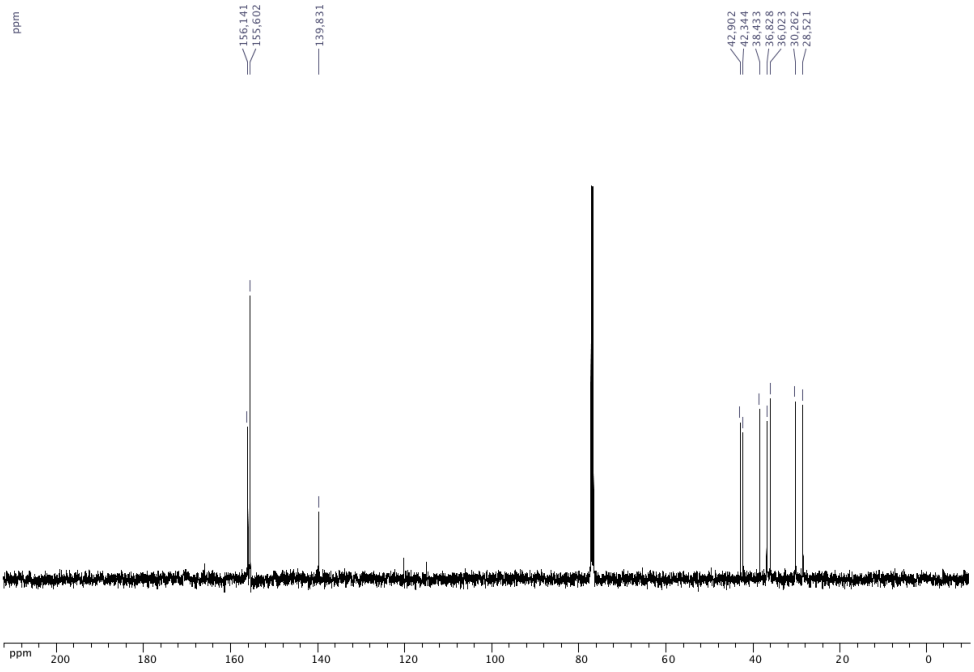


$^{13}$C NMR {$^{1}$H} ($CDCl_3$, 125.8 MHz) of 5-(*exo*-bicyclo[2.2.1]heptan-2-yl)pyrimidine (**39**)

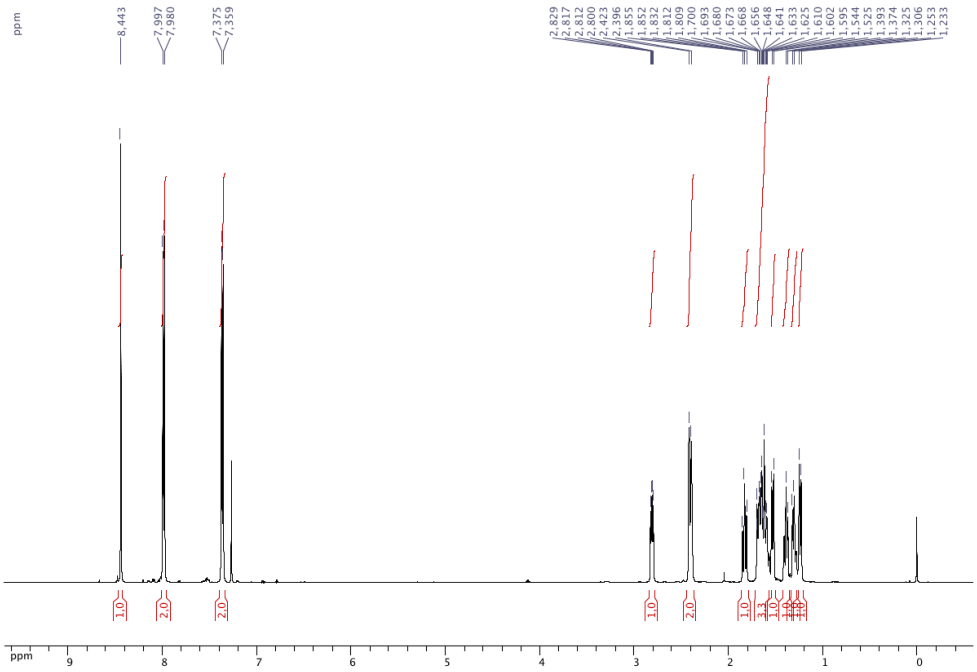


$^{1}$H NMR ($CDCl_3$, 500.4 MHz) of 2-(4-(*exo*-bicyclo[2.2.1]heptan-2-yl)phenyl)-1,3,4-oxadiazole (**40**)

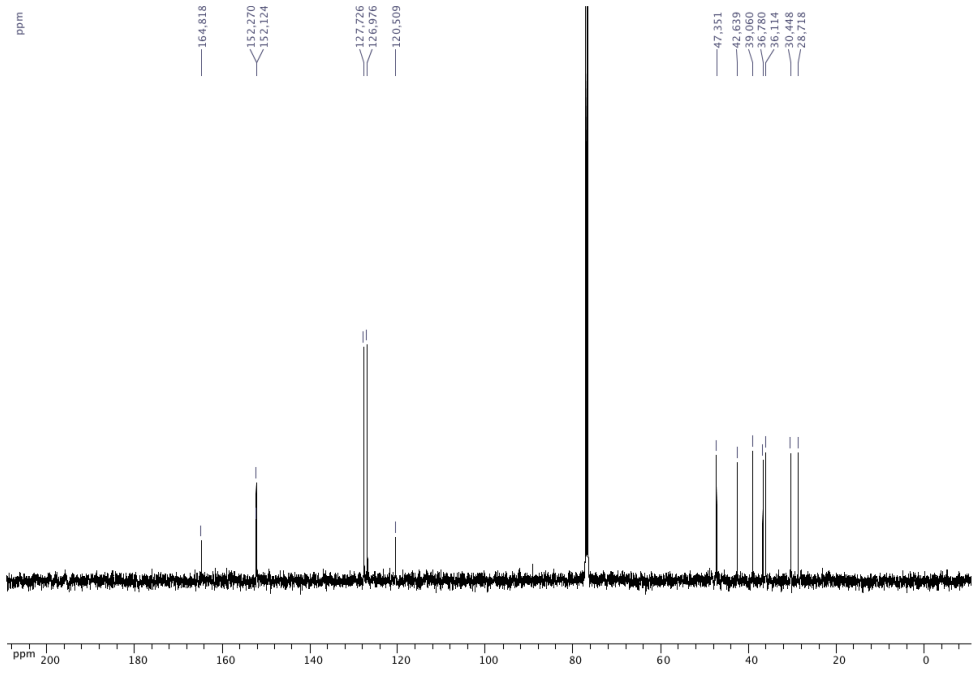


$^{13}$C NMR {$^{1}$H} ($CDCl_3$, 125.8 MHz) of 2-(4-(*exo*-bicyclo[2.2.1]heptan-2-yl)phenyl)-1,3,4-oxadiazole (**40**)

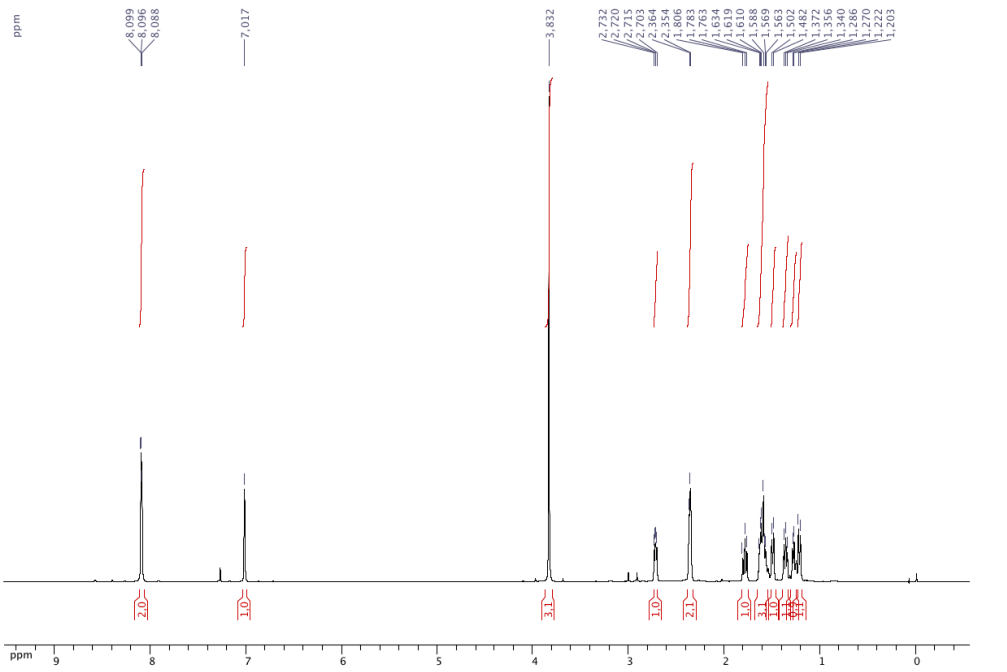


$^{1}$H NMR ($CDCl_3$, 500.4 MHz) of 3-(*exo*-bicyclo[2.2.1]heptan-2-yl)-5-methoxypyridine (**41**)

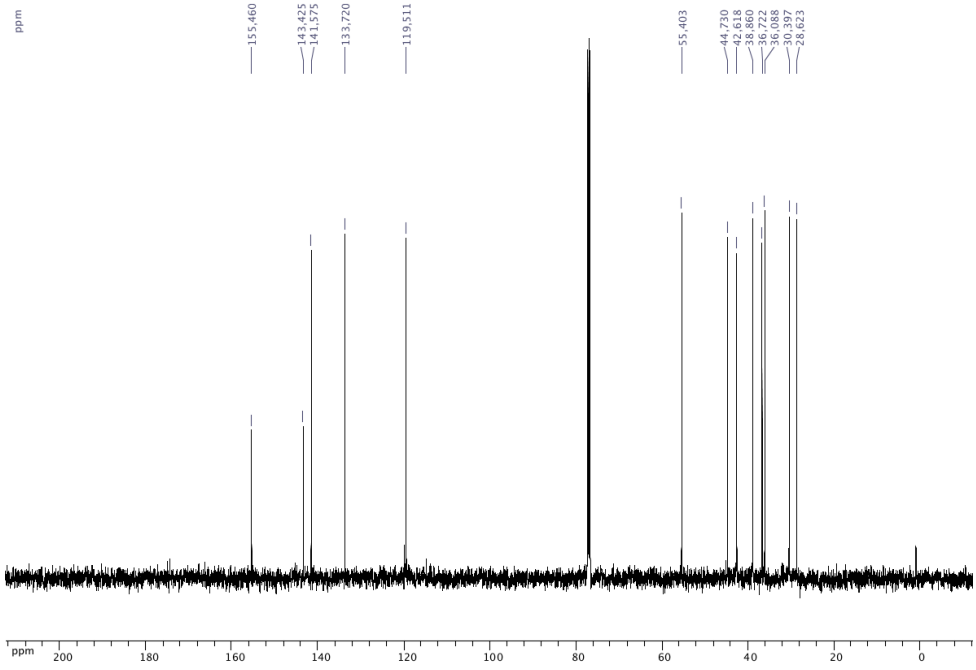


$^{13}$C NMR {$^{1}$H} ($CDCl_3$, 125.8 MHz) of 3-(*exo*-bicyclo[2.2.1]heptan-2-yl)-5-methoxypyridine (**41**)

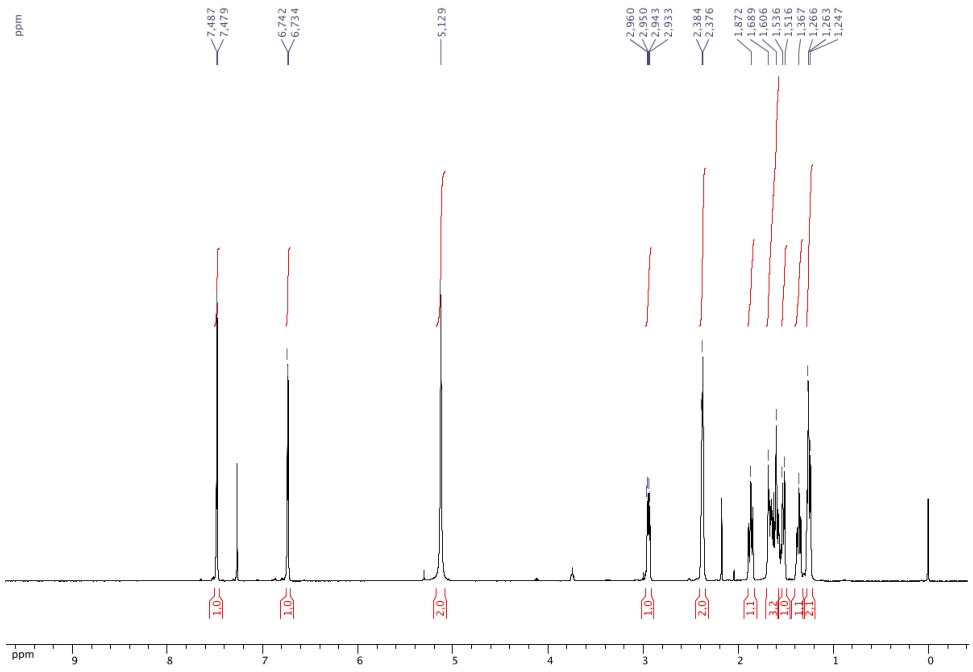


$^{1}$H NMR ($CDCl_3$, 500.4 MHz) of 5-(*exo*-bicyclo[2.2.1]heptan-2-yl)thiophene-2-sulfonamide (**42**)

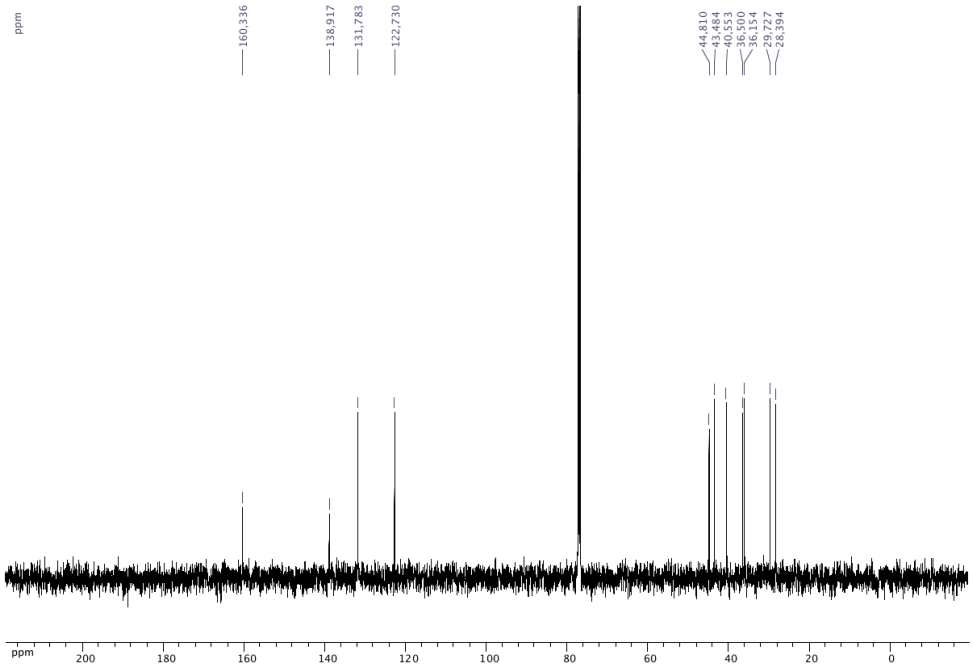


$^{13}$C NMR {$^{1}$H} ($CDCl_3$, 125.8 MHz) of 5-(*exo*-bicyclo[2.2.1]heptan-2-yl)thiophene-2-sulfonamide (**42**)

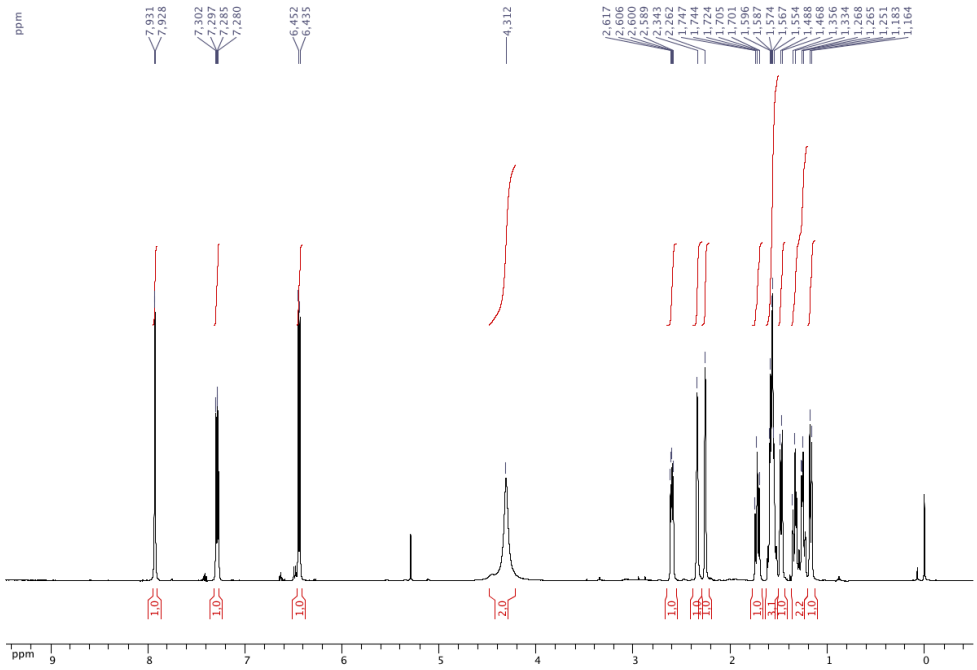

$^{1}$H NMR ($CDCl_3$, 500.4 MHz) of 5-(*exo*-bicyclo[2.2.1]heptan-2-yl)pyridin-2-amine (**43**)

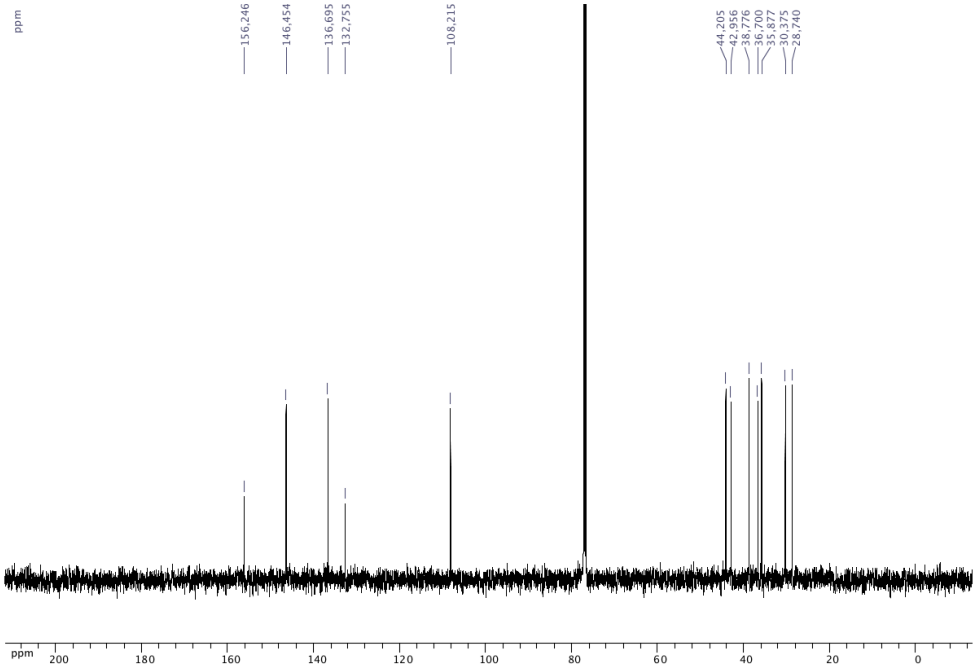

$^{13}$C NMR {$^{1}$H} ($CDCl_3$, 125.8 MHz) of 5-(*exo*-bicyclo[2.2.1]heptan-2-yl)pyridin-2-amine (**43**)

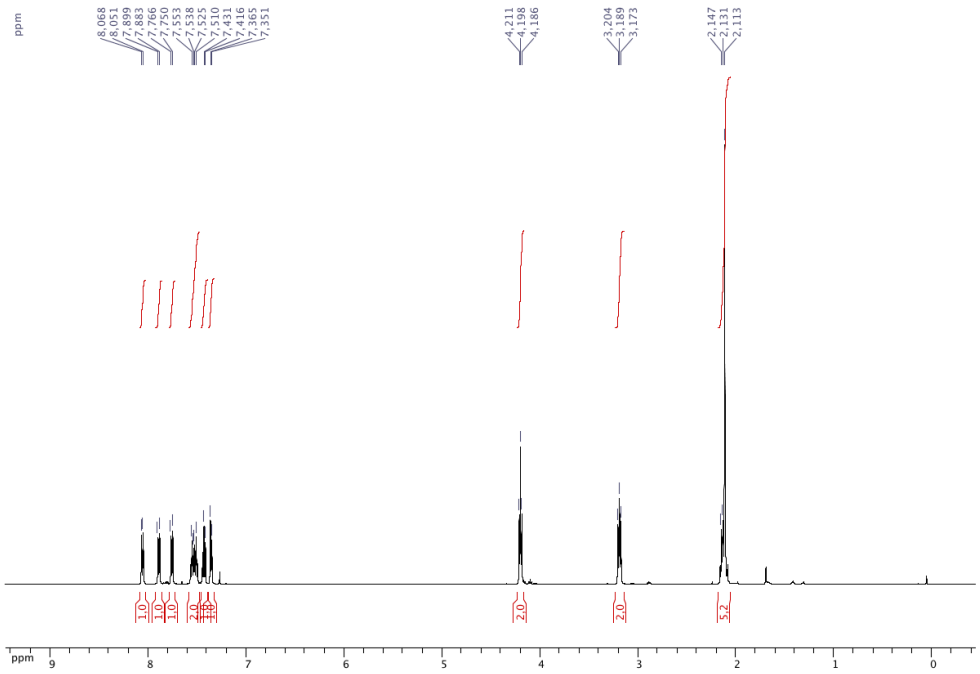


$^{1}$H NMR ($CDCl_3$, 500.4 MHz) of 3-(naphthalen-1-yl)propyl acetate (**44**)

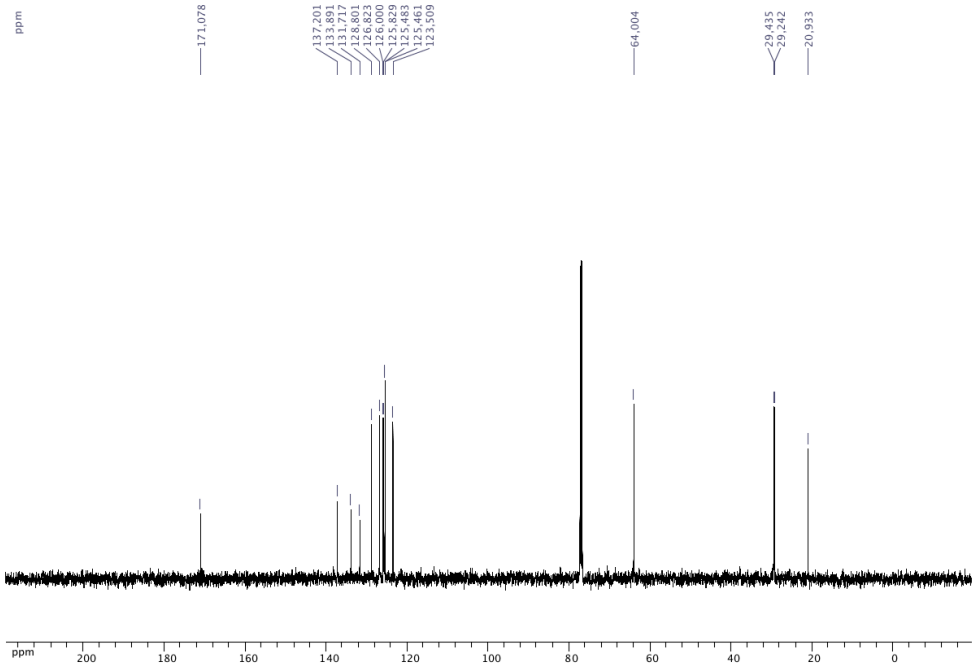


$^{13}$C NMR {$^{1}$H} ($CDCl_3$, 125.8 MHz) of 3-(naphthalen-1-yl)propyl acetate (**44**)

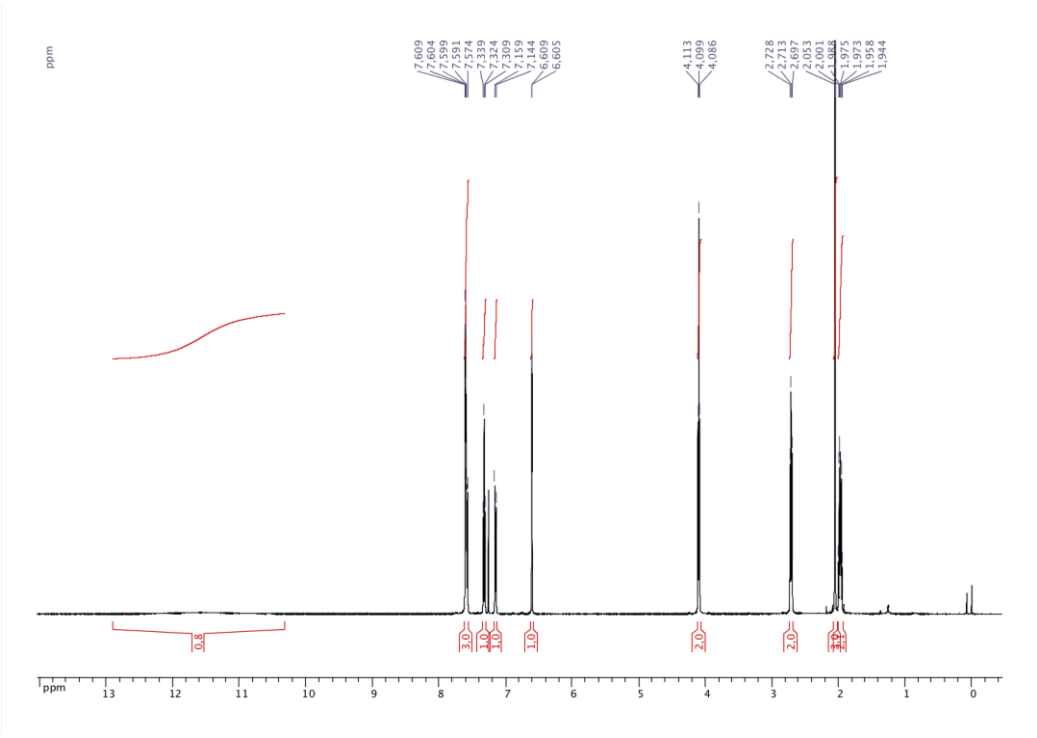


$^{1}$H NMR ($CDCl_3$, 500.4 MHz) of 3-(3-(1H-pyrazol-5-yl)phenyl)propyl acetate (**45**)

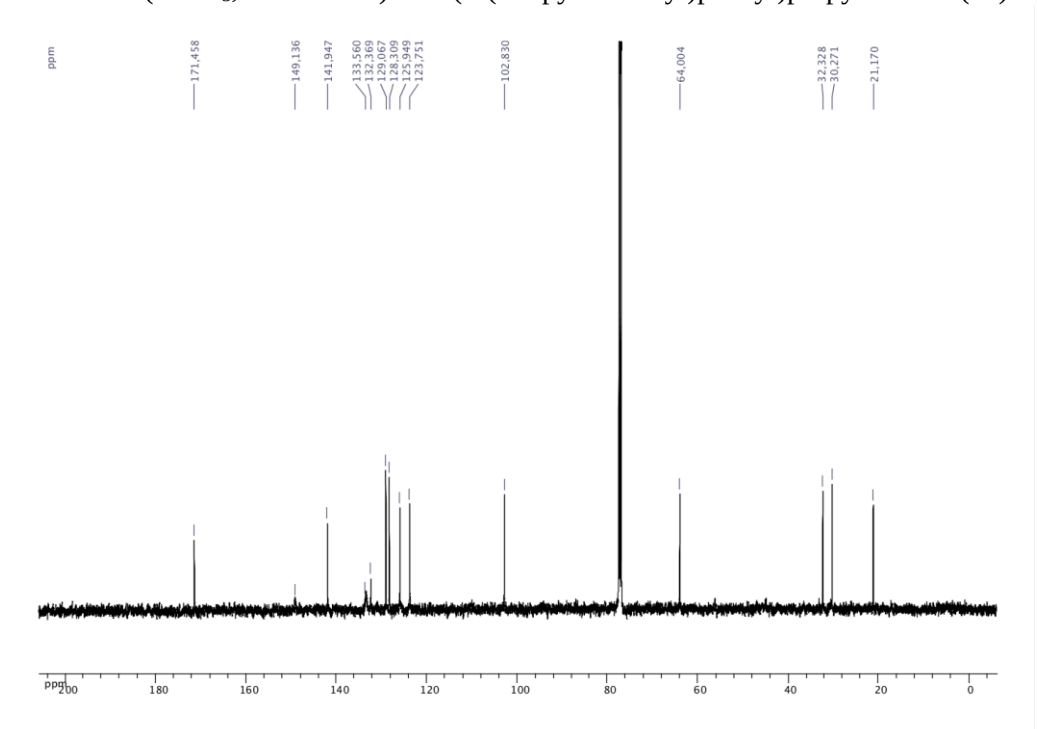


$^{13}$C NMR {$^{1}$H} ($CDCl_3$, 125.8 MHz) of 3-(3-(1H-pyrazol-5-yl)phenyl)propyl acetate (**45**)

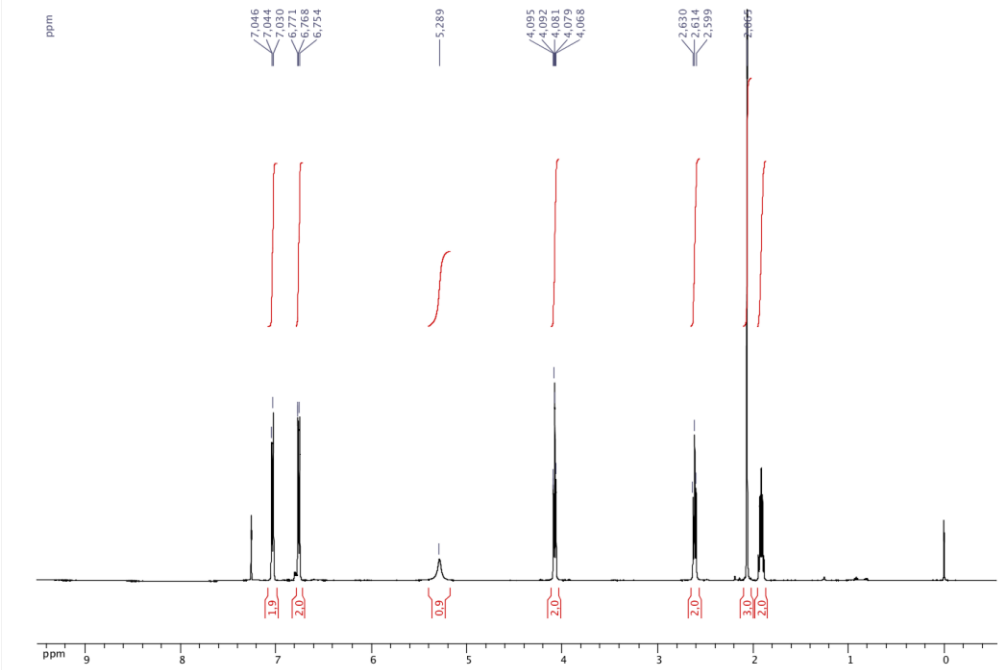


$^{1}$H NMR ($CDCl_3$, 500.4 MHz) of 3-(4-hydroxyphenyl)propyl acetate (**46**)

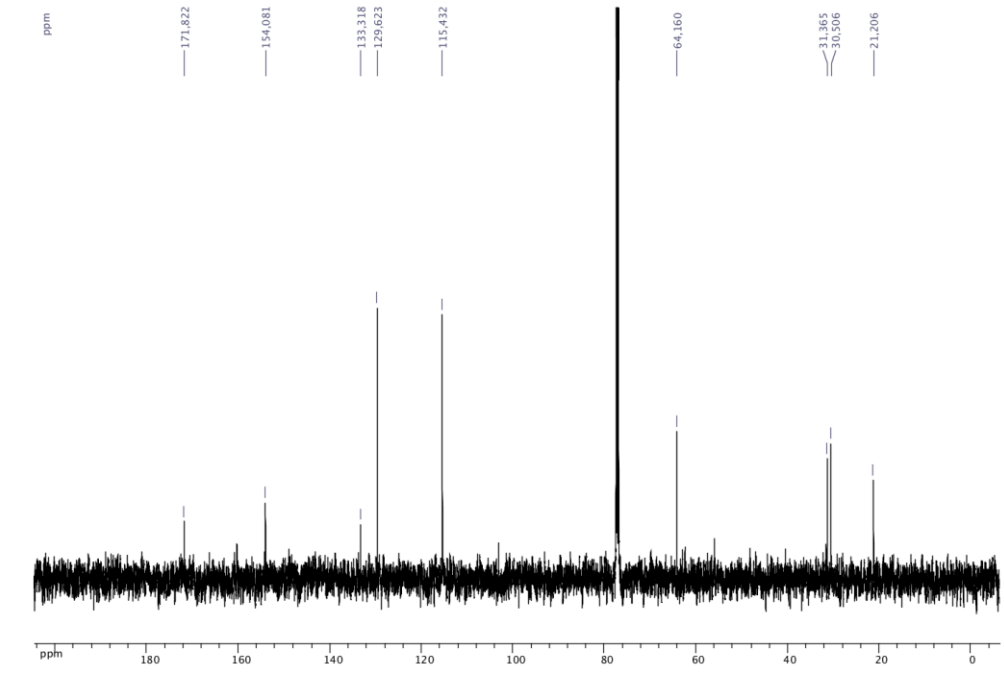


$^{13}$C NMR {$^{1}$H} ($CDCl_3$, 125.8 MHz) of 3-(4-hydroxyphenyl)propyl acetate (**46**)

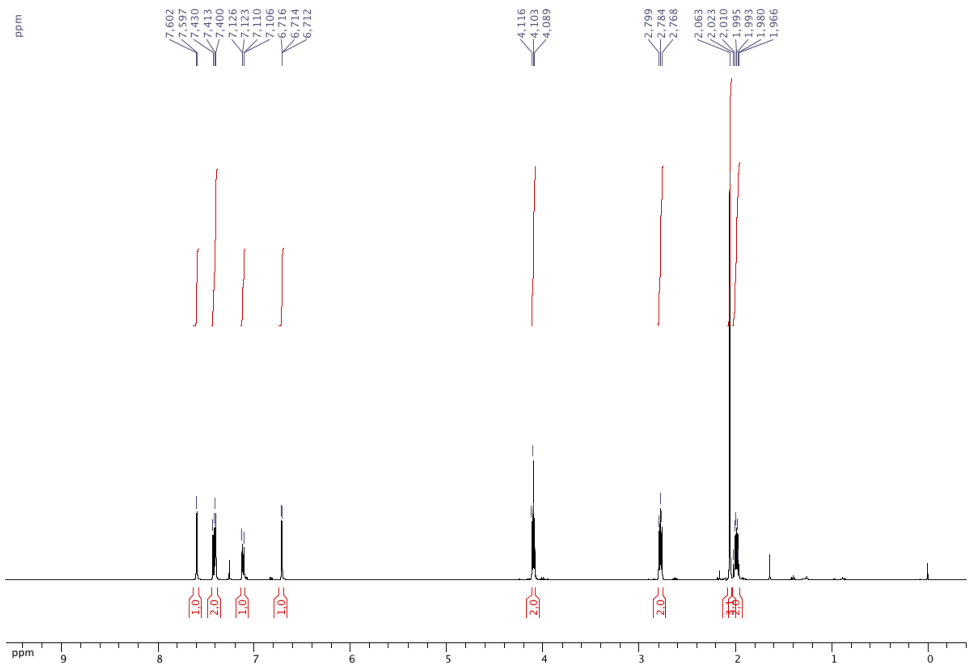


$^{1}$H NMR ($CDCl_3$, 500.4 MHz) of 3-(benzofuran-5-yl)propyl acetate (**47**)

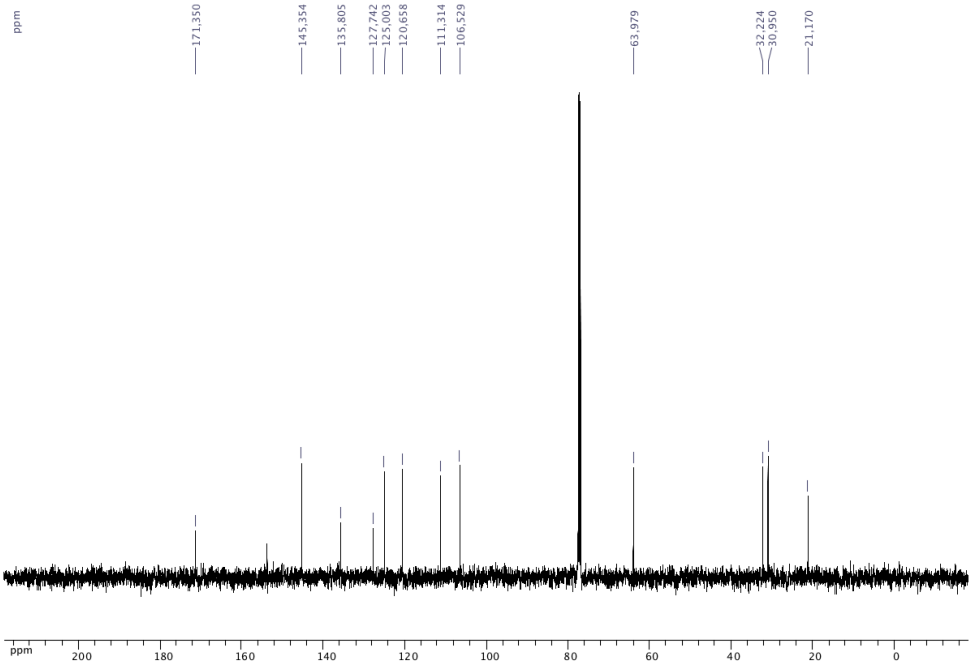


$^{13}$C NMR {$^{1}$H} ($CDCl_3$, 125.8 MHz) of 3-(benzofuran-5-yl)propyl acetate (**47**)

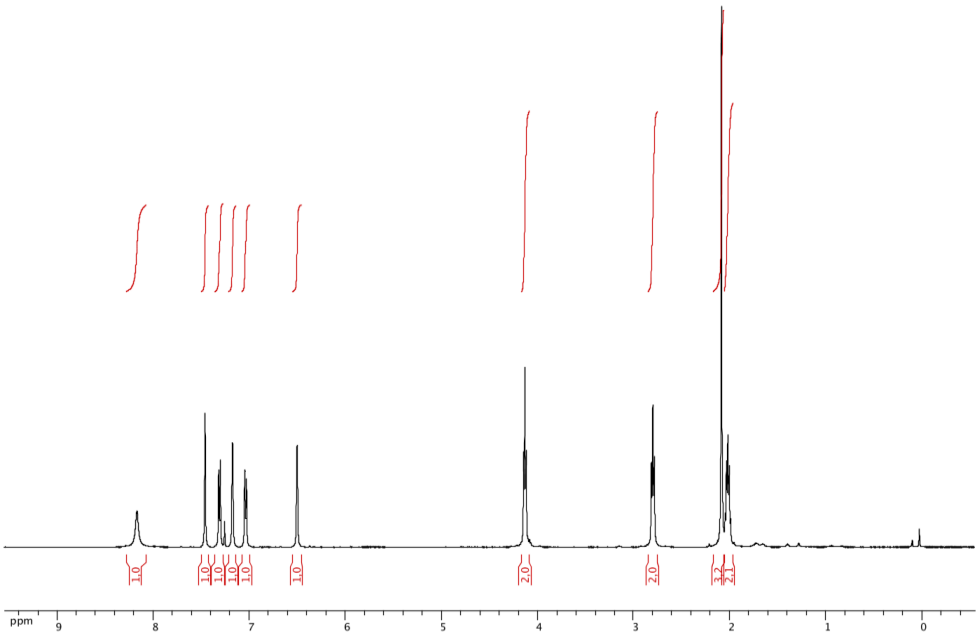


$^{1}$H NMR ($CDCl_3$, 500.4 MHz) of 3-(1H-indol-5-yl)propyl acetate (**48**)

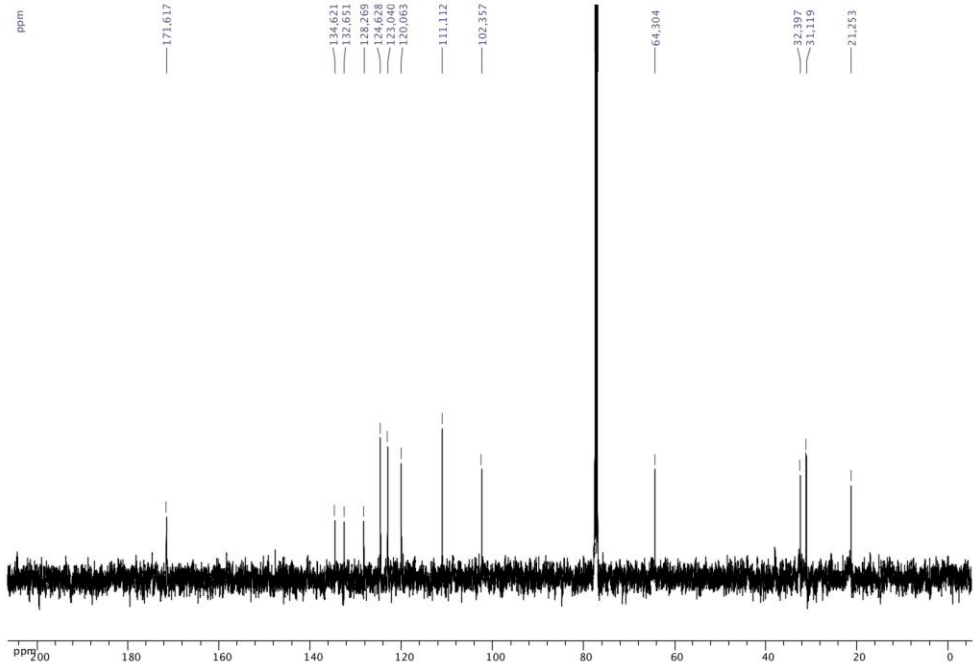


$^{13}$C NMR {$^{1}$H} ($CDCl_3$, 125.8 MHz) of 3-(1H-indol-5-yl)propyl acetate (**48**)

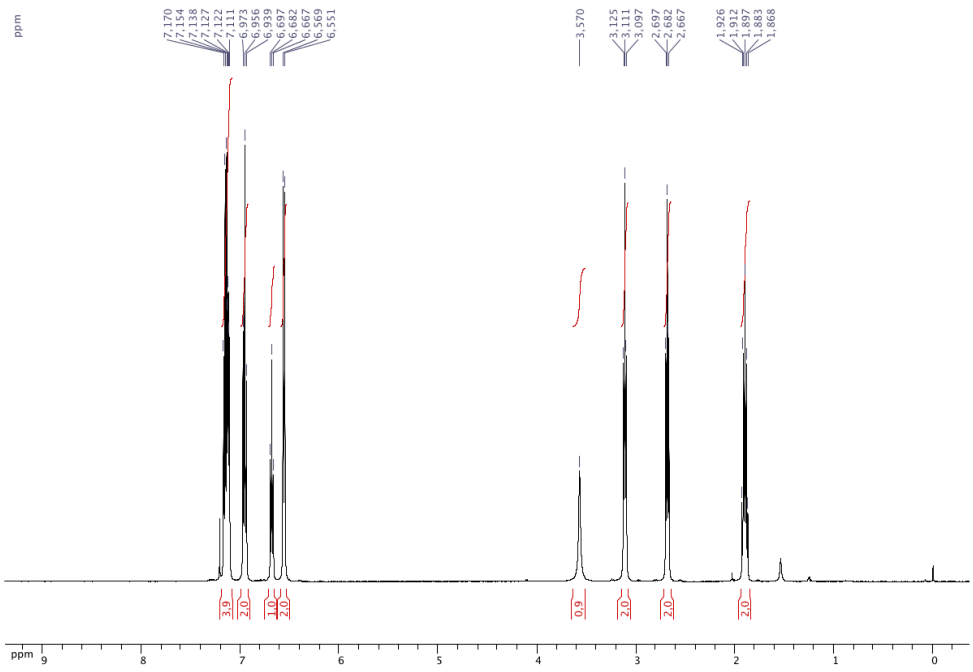


$^{1}$H NMR ($CDCl_3$, 500.4 MHz) of *N*-(3-(4-fluorophenyl)propyl)aniline (**49**)

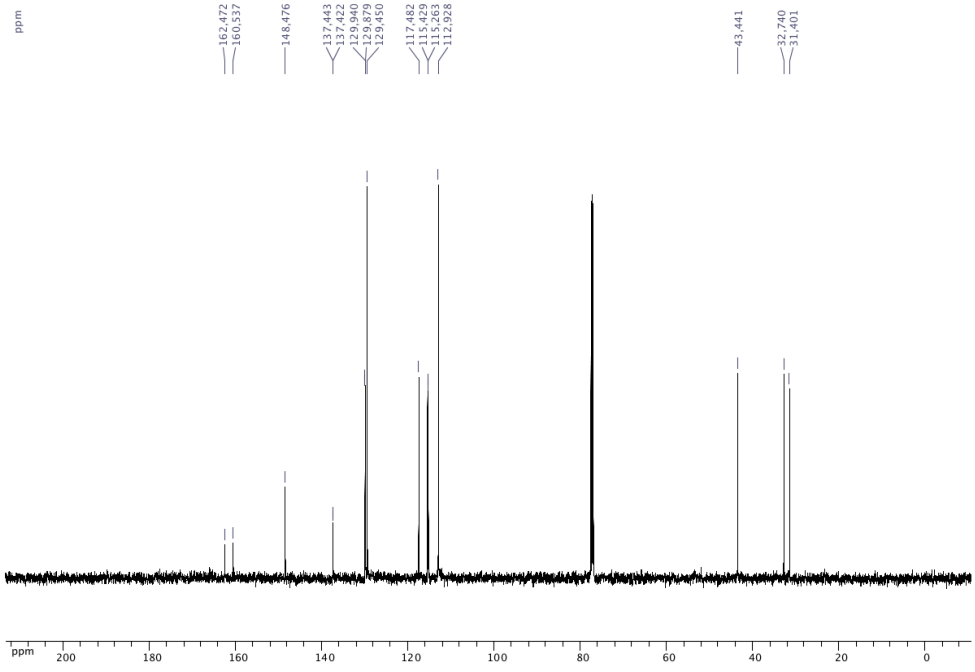


$^{13}$C NMR {$^{1}$H} ($CDCl_3$, 125.8 MHz) of *N*-(3-(4-fluorophenyl)propyl)aniline (**49**)

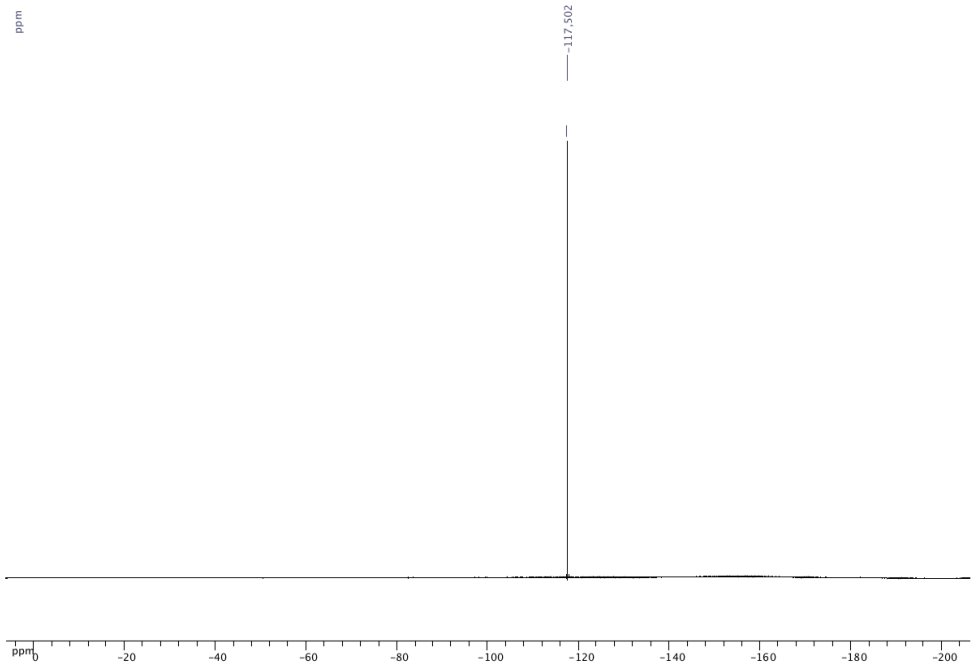


$^{19}F$ NMR {$^{1}H$} ($CDCl_3$, 470.8 MHz) of *N*-(3-(4-fluorophenyl)propyl)aniline (**49**)

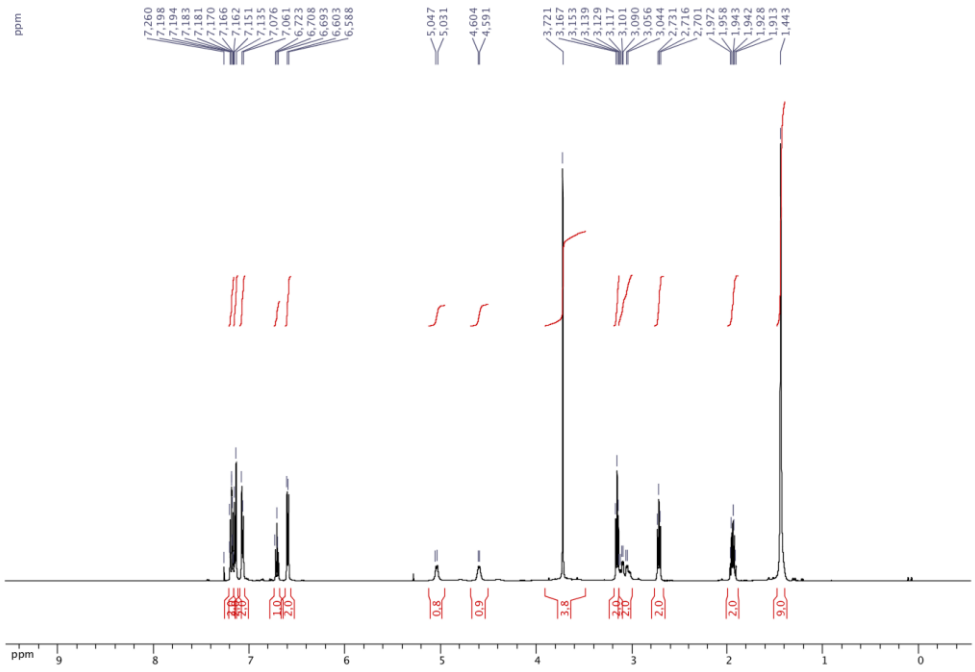

$^{1}$H NMR ($CDCl_3$, 500.4 MHz) of methyl (*S*)-2-((*tert*-butoxycarbonyl)amino)-3-(4-(3-(phenylamino)propyl)phenyl)propanoate (**50**).

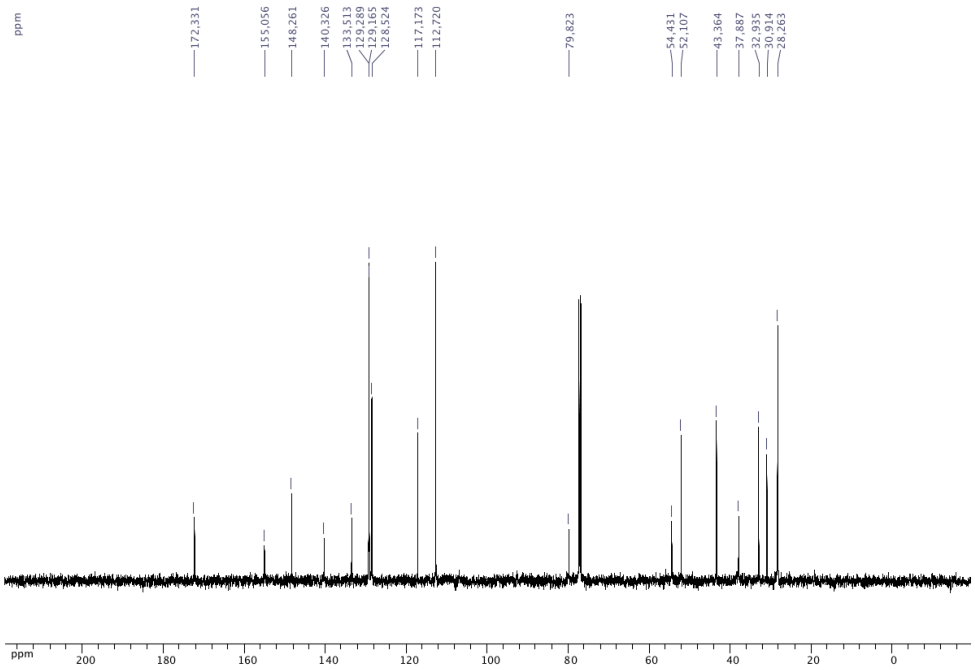

$^{13}$C NMR {$^{1}$H} ($CDCl_3$, 125.8 MHz) of methyl (*S*)-2-((*tert*-butoxycarbonyl)amino)-3-(4-(3-(phenylamino)propyl)phenyl)propanoate (**50**).

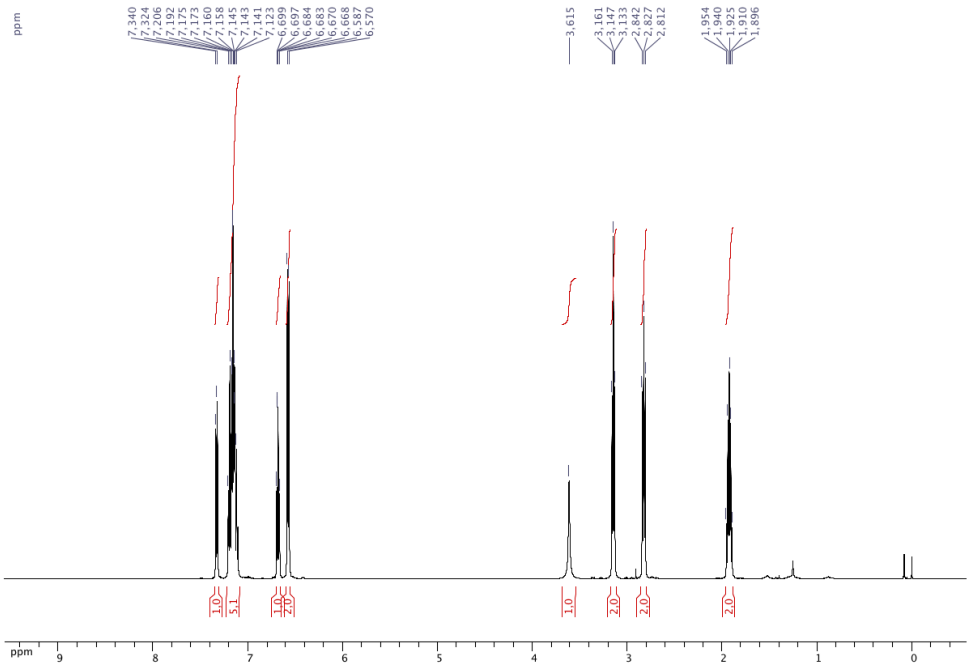


$^{1}$H NMR ($CDCl_3$, 500.4 MHz) of *N*-(3-(2-chlorophenyl)propyl)aniline (**51**)

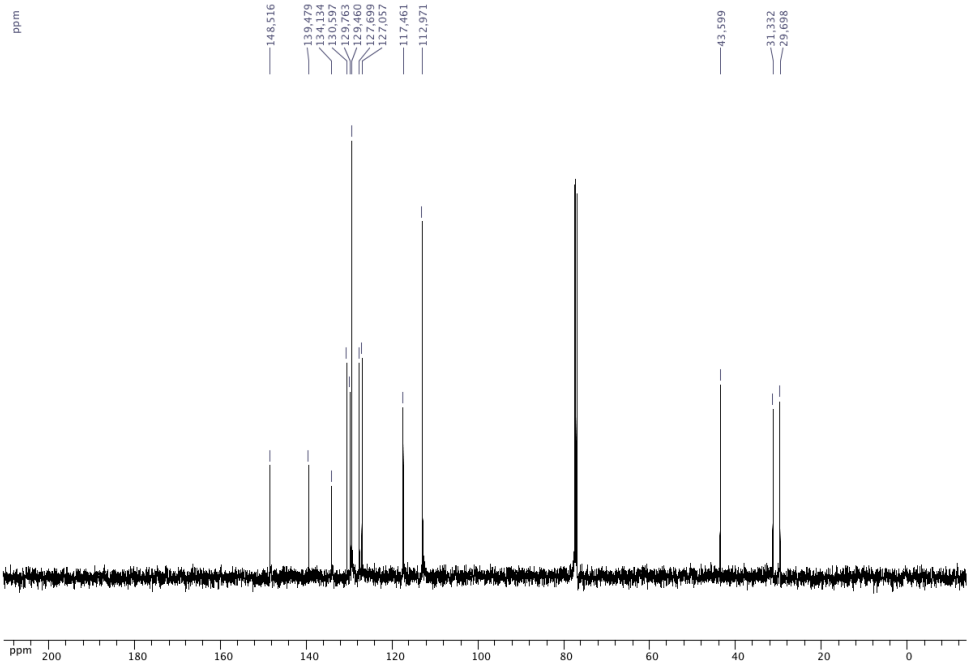


$^{13}$C NMR {$^{1}$H} ($CDCl_3$, 125.8 MHz) of *N*-(3-(2-chlorophenyl)propyl)aniline (**51**)

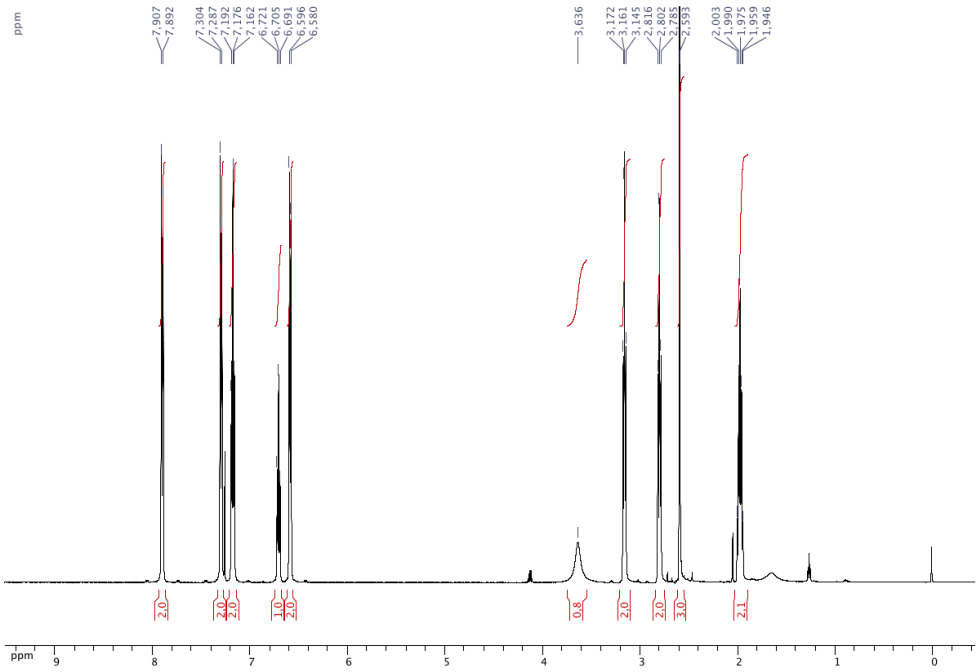


$^{1}$H NMR ($CDCl_3$, 500.4 MHz) of 1-(4-(3-(phenylamino)propyl)phenyl)ethan-1-one (**52**)

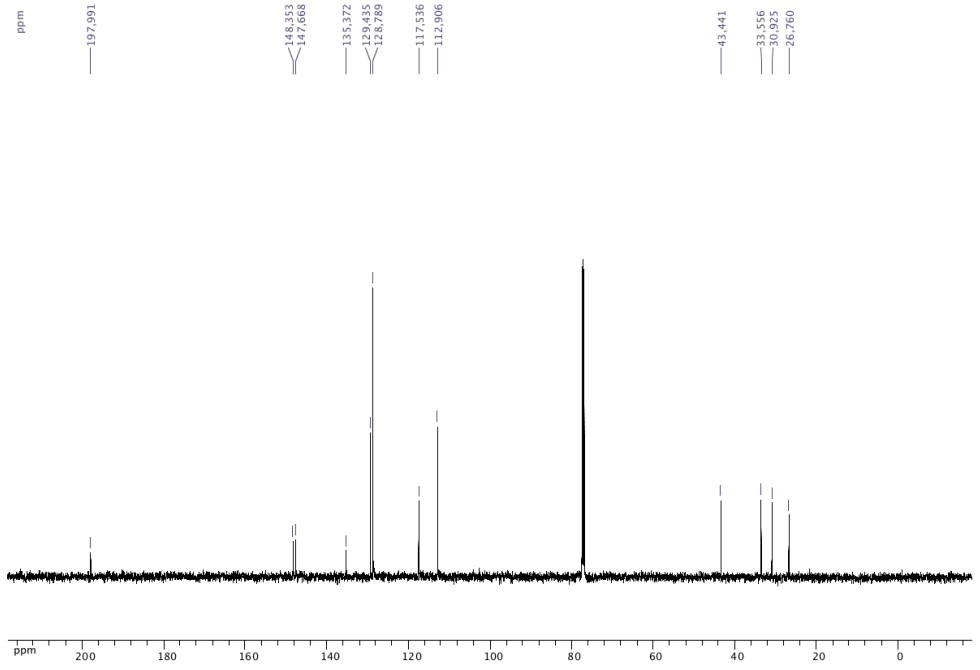


$^{13}$C NMR {$^{1}$H} ($CDCl_3$, 125.8 MHz) of 1-(4-(3-(phenylamino)propyl)phenyl)ethan-1-one (**52**)

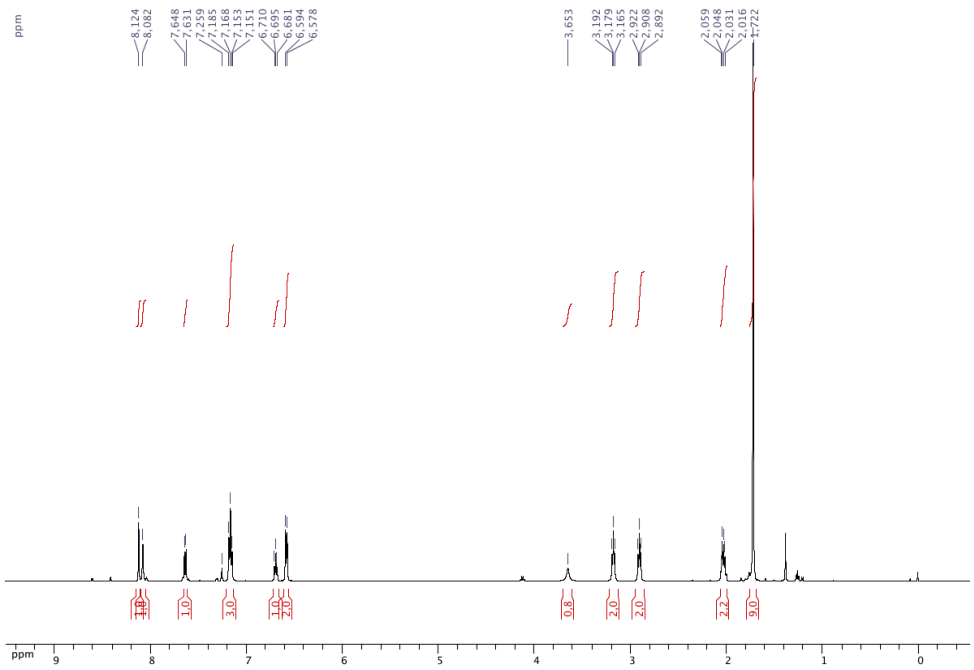


$^{1}$H NMR ($CDCl_3$, 500.4 MHz) of *tert*-butyl 5-(3-(phenylamino)propyl)-1*H*-indazole-1-carboxylate (**53**)

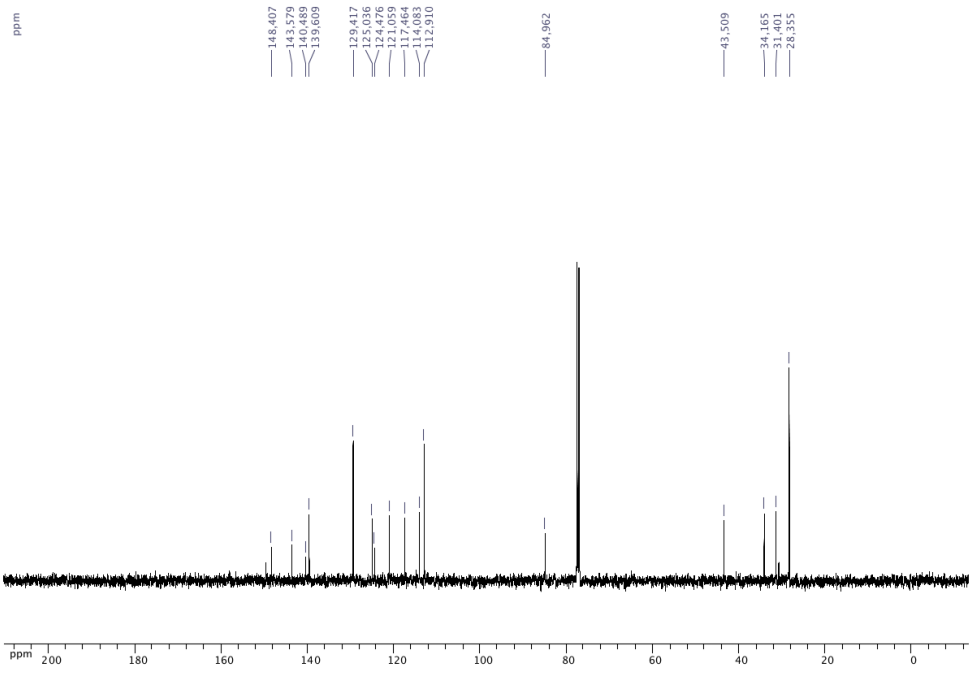


$^{13}$C NMR {$^{1}$H} ($CDCl_3$, 125.8 MHz) of *tert*-butyl 5-(3-(phenylamino)propyl)-1*H*-indazole-1-carboxylate (**53**)

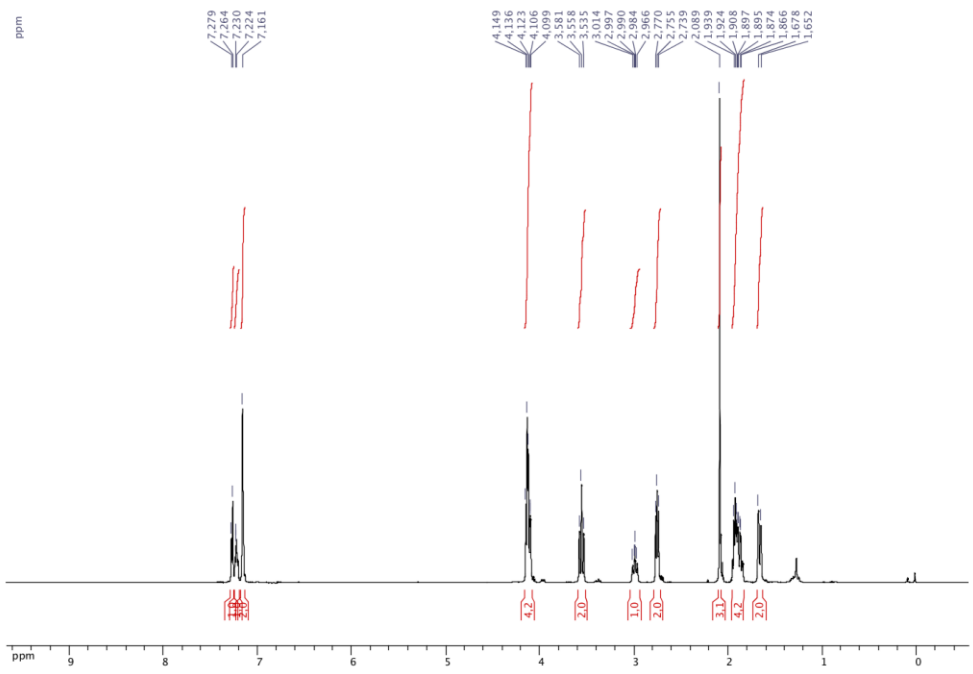

$^{1}$H NMR ($CDCl_3$, 500.4 MHz) of 3-(2-(tetrahydro-2*H*-pyran-4-yl)phenyl)propyl acetate (**55**)

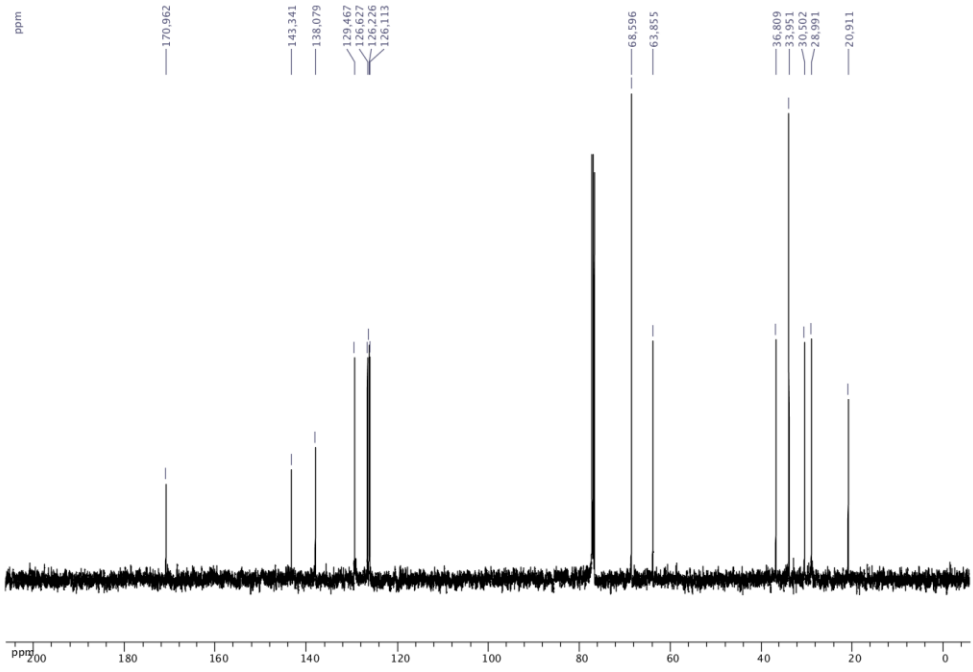

$^{13}$C NMR {$^{1}$H} ($CDCl_3$, 125.8 MHz) of 3-(2-(tetrahydro-2*H*-pyran-4-yl)phenyl)propyl acetate (**55**)

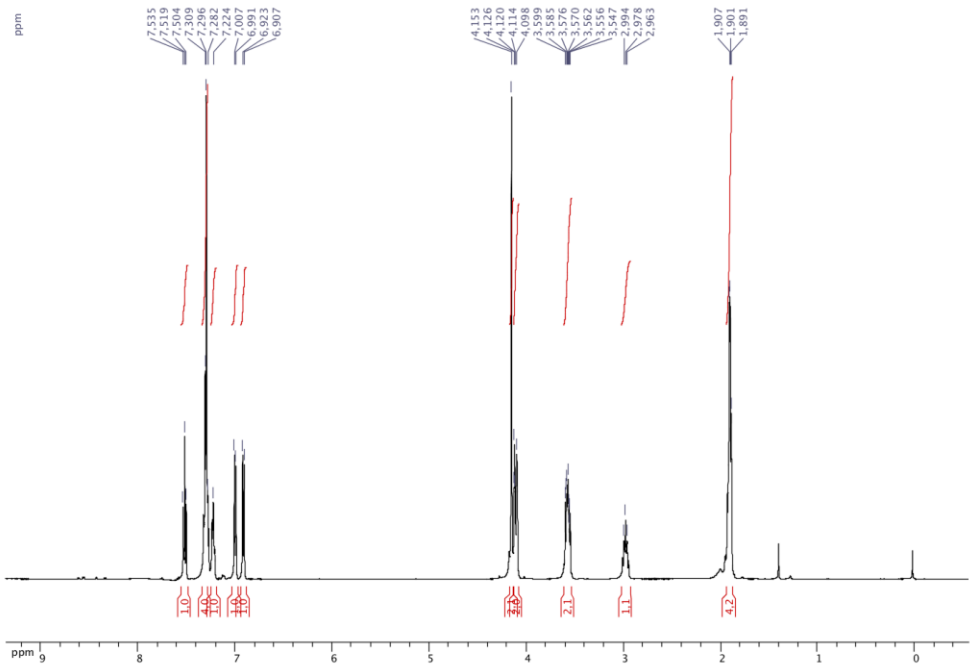


$^{1}$H NMR ($CDCl_3$, 500.4 MHz) of 2-benzyl-6-(tetrahydro-2*H*-pyran-4-yl)pyridine (**57**)

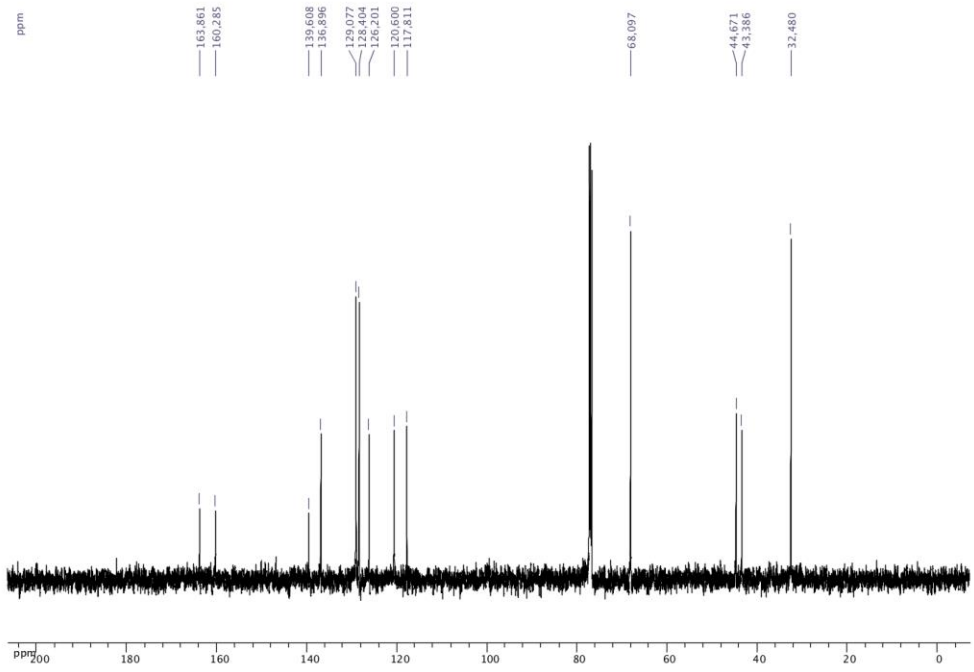


$^{13}$C NMR {$^{1}$H} ($CDCl_3$, 125.8 MHz) of 2-benzyl-6-(tetrahydro-2*H*-pyran-4-yl)pyridine (**57**)

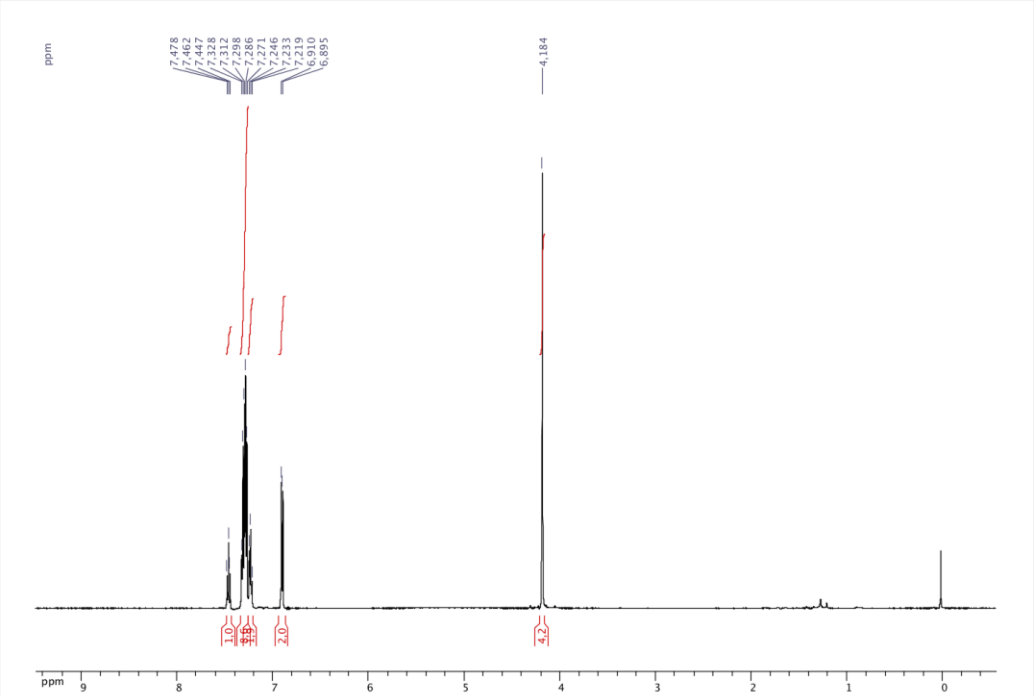


$^{1}$H NMR ($CDCl_3$, 500.4 MHz) of 2,6-dibenzylpyridine (**58**)

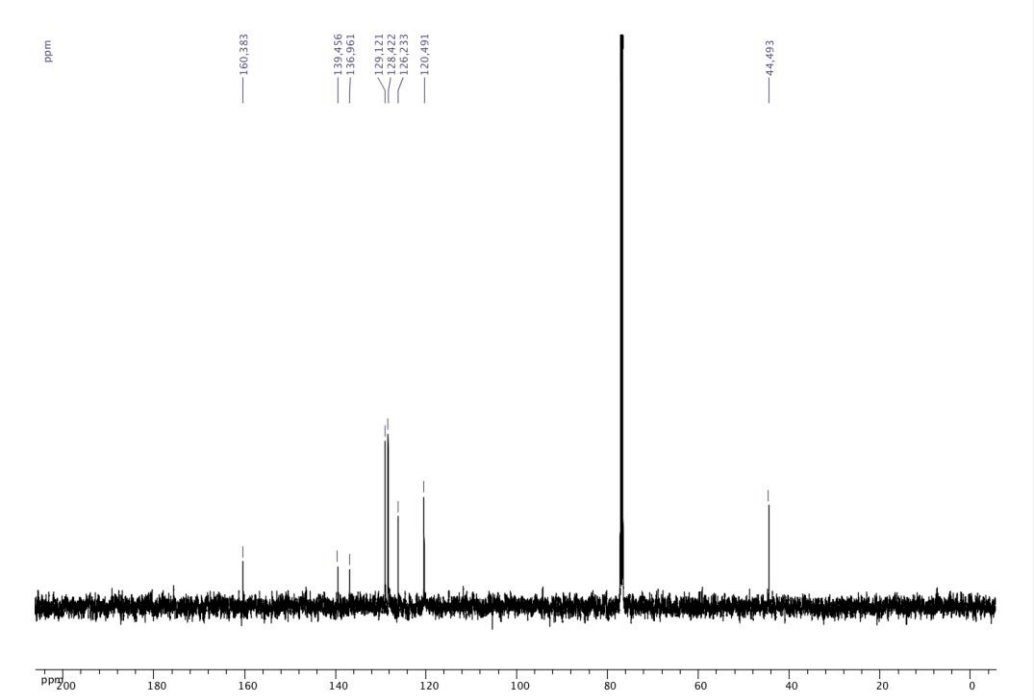


$^{13}$C NMR {$^{1}$H} ($CDCl_3$, 125.8 MHz) of 2,6-dibenzylpyridine (**58**)

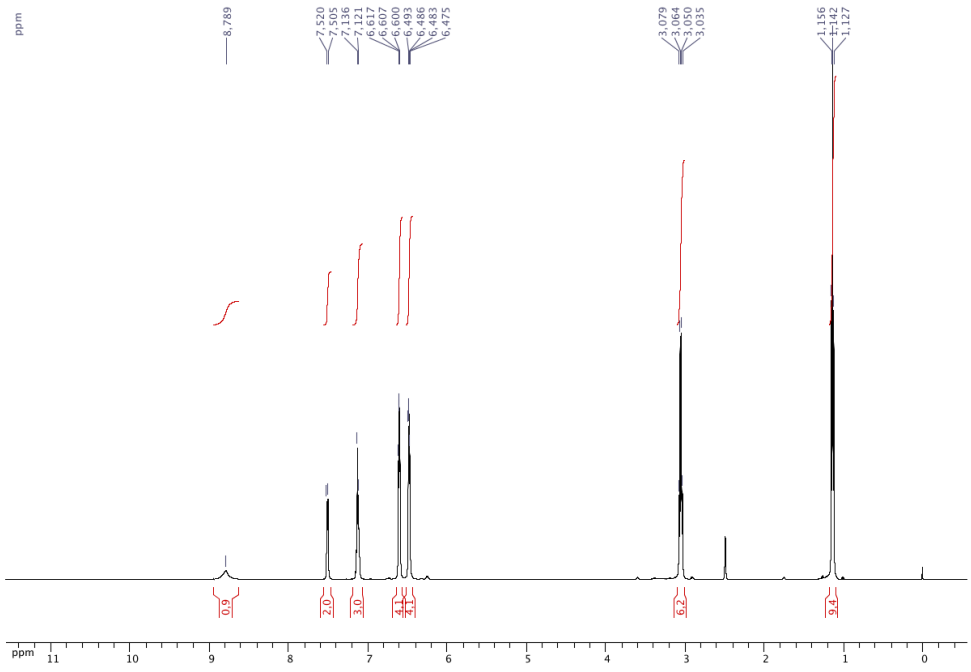


$^{1}$H NMR (DMSO-$d_6$, 500.4 MHz) of triethylammonium phenylbis(catecholato)silicate (**59**)

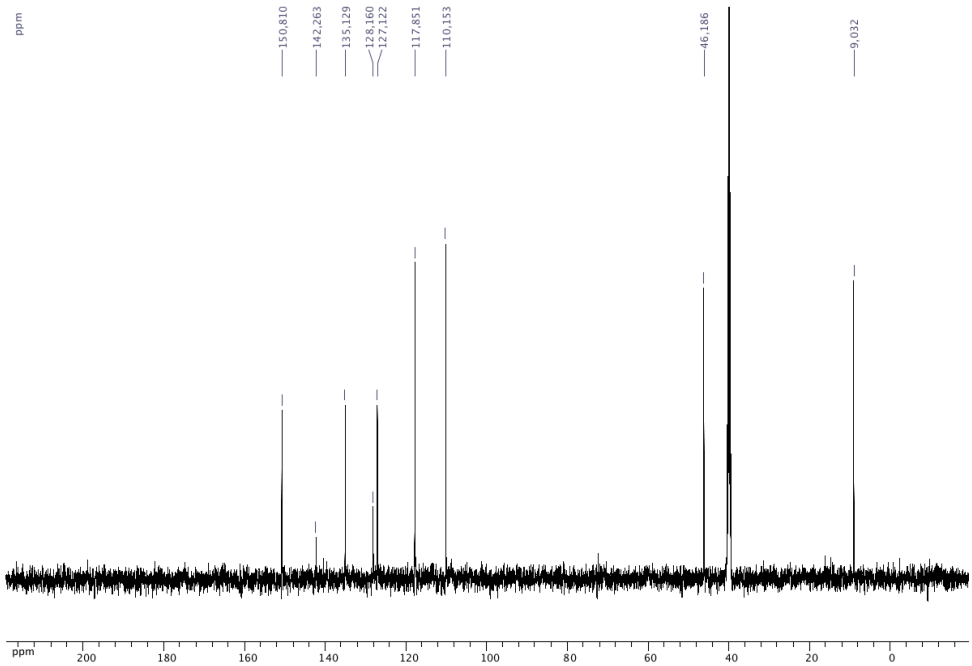


$^{13}$C NMR {$^{1}$H} (DMSO-$d_6$, 125.8 MHz) of triethylammonium phenylbis(catecholato)silicate (**59**)

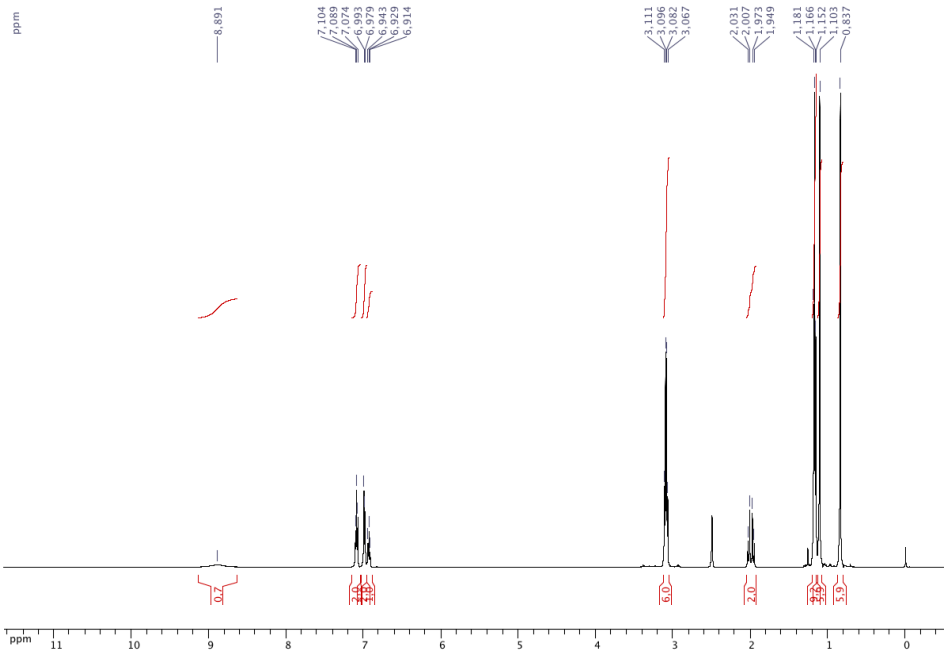


$^{1}$H NMR (DMSO-$d_6$, 500.4 MHz) of triethylammonium benzylbis(methyl-2-hydroxyisobuyro)silicate (**60**)

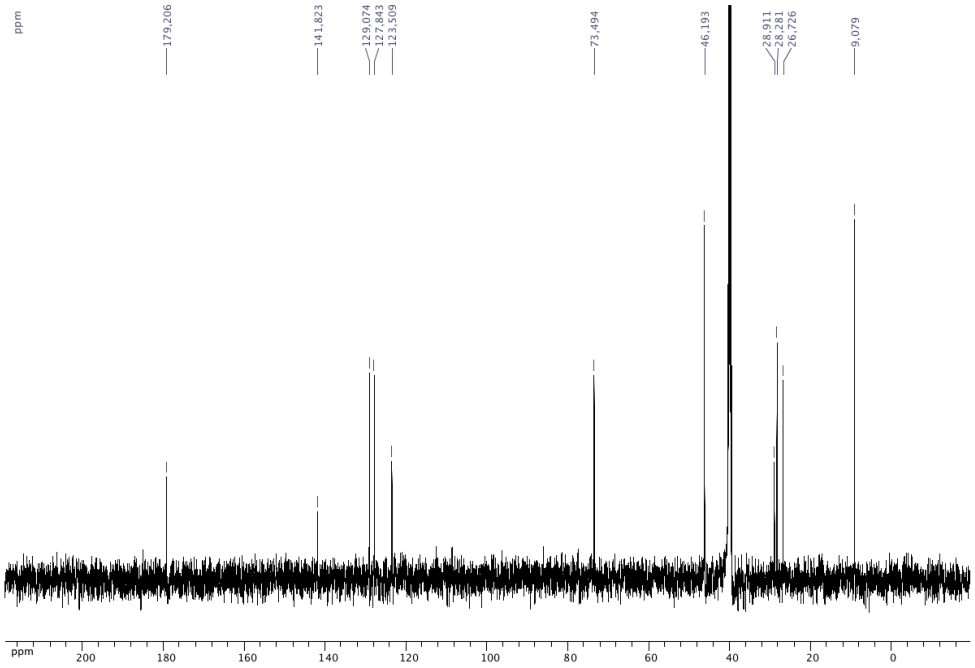


$^{13}$C NMR {$^{1}$H} (DMSO-$d_6$, 125.8 MHz) of triethylammonium benzylbis(methyl-2-hydroxyisobuyro)silicate (**60**)

**Appendix A9. Cyclic Voltammetry Data Relevant to Chapter 7**

Voltammetric measurements were recorded on a CH Instruments: Model 600E Series Electrochemical Analyzer using a standard three electrodes setup in dry and degassed MeCN (10 mL), with ferrocene as internal reference ($E^0_{1/2}$ = + 0.40 V *vs* SCE) and tetrabutylammonium hexafluorophosphate as electrolyte (0.10 mmol). Cyclic voltammograms were recorded with a step potential of 0.002 V at a scan rate of 0.1 V/s.

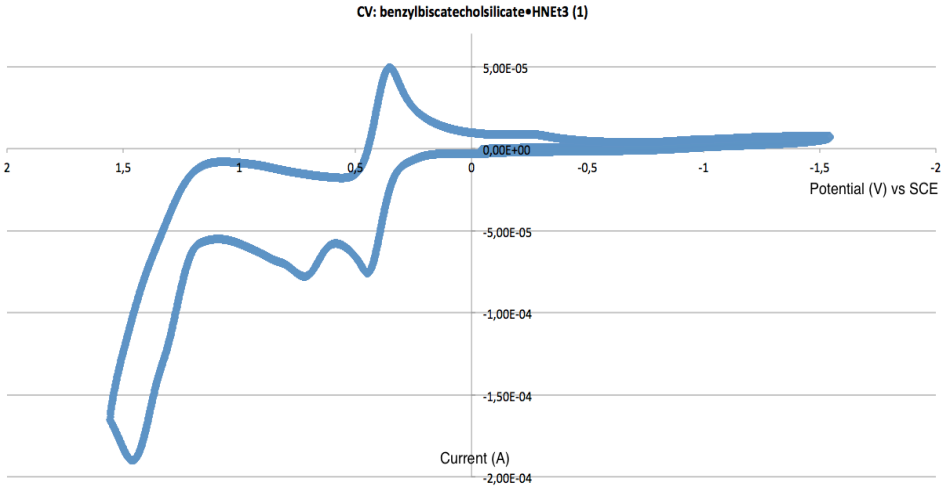


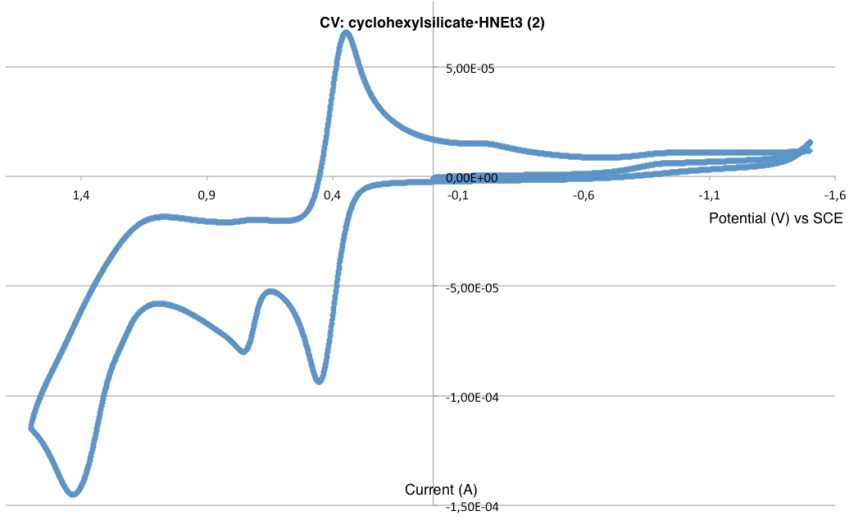

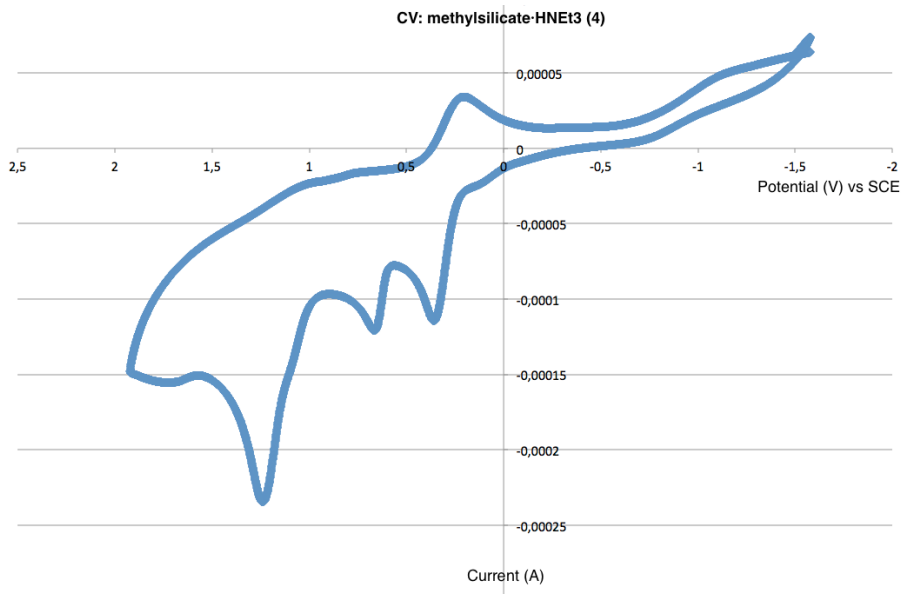
CV: methylsilicate·HNEt3 (4)
0,00005
0
2,5
2
1,5
1
0,5
0
-0,5
-1
-1,5
-2
Potential (V) vs SCE
-0,00005
-0,0001
-0,00015
-0,0002
-0,00025
Current (A)

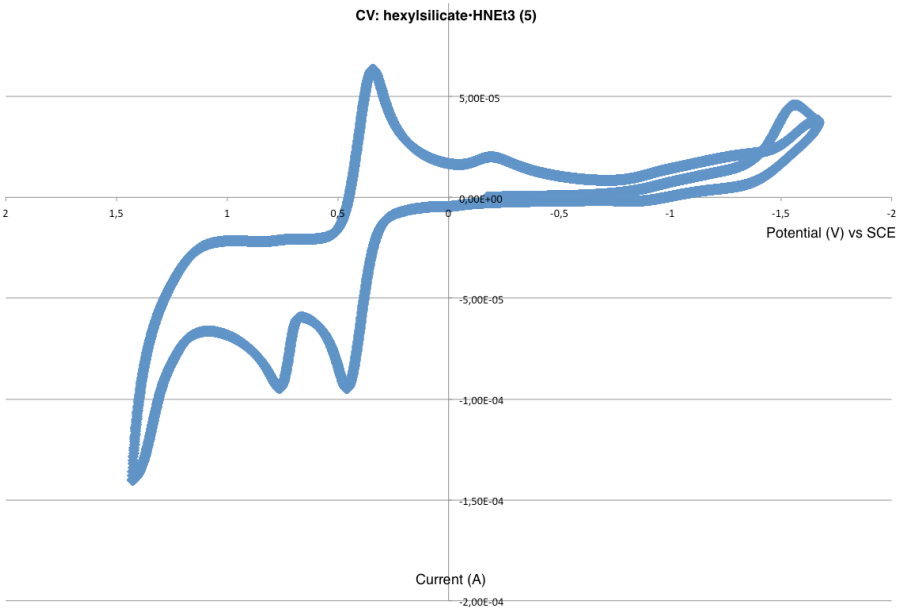
CV: hexylsilicate·HNEt3 (5)
5,00E-05
0,00E+00
2
1,5
1
0,5
0
-0,5
-1
-1,5
-2
Potential (V) vs SCE
-5,00E-05
-1,00E-04
-1,50E-04
Current (A)
-2,00E-04

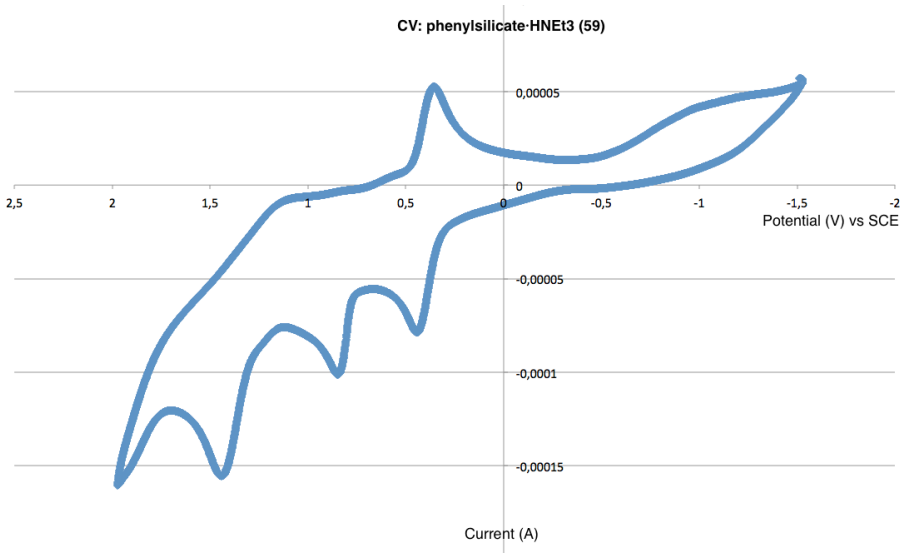
CV: phenylsilicate·HNEt3 (59)
0,00005
0
-0,00005
-0,0001
-0,00015
2,5
2
1,5
1
0,5
0
-0,5
-1
-1,5
-2
Potential (V) vs SCE
Current (A)

# Chapter 8. Computational and Experimental Investigations into Reaction Mechanism

## 8.1 Introduction

In the originally proposed reaction mechanism for these photoredox mediated cross-couplings,[1] we hypothesized that the Ni(0) catalyst **1** first engages the aryl bromide in oxidative addition to afford arylnickel(II) complex **3** (**Figure 8.1**, red). In parallel, oxidative fragmentation of an alkyltrifluoroborate **6** by the excited state of Ir photoredox catalyst **4** yields a carbon-centered radical that is rapidly captured by this Ni(II) complex. Reductive elimination from the resultant Ni(III) species **10** yields the cross-coupled product and Ni(I) complex **12**. Finally, single-electron reduction of Ni(I) by anionic Ir complex **8** simultaneously regenerates the Ni(0) catalyst and the ground state photocatalyst. MacMillan, Doyle, and coworkers hypothesized a similar mechanistic scenario for the related cross-coupling of α-amino acids and N,N-dialkyl-N-arylamines with aryl halides.[2]

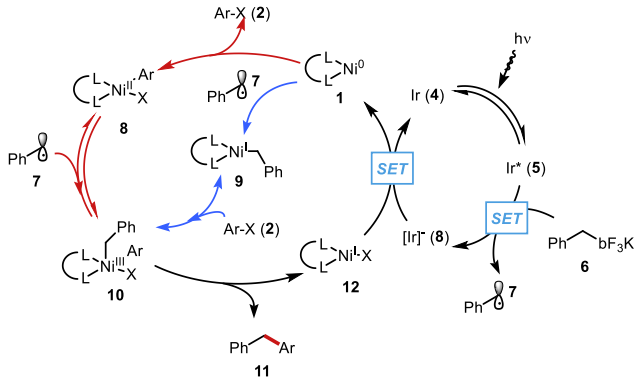


**Figure 8.1**: Possible catalytic cycles (red: oxidative addition first; blue: radical addition first)

Although there are no clear faults with the original mechanism,[i] we also recognized the possibility of an alternative pathway in which radical addition precedes oxidative addition (**Figure 8.1**, blue). Considering the success of this chemistry in achieving stereoconvergent transformations as highlighted in the cross-coupling of a secondary alkyltrifluoroborate in the presence of a chiral Ni complex (**Figure 8.2**), we deemed it necessary to parse out the differences between these two competing mechanisms. Greater understanding of this reaction coordinate would improve our development of these stereoconvergent cross-couplings by giving us clues about how to alter ligand structure and reaction conditions to achieve enhanced stereocontrol. As these reactions are difficult to monitor experimentally (variable induction period, visible light irradiation, and multiple catalysts), we hoped that a computational collaboration between the Molander group and the Kozlowski group.

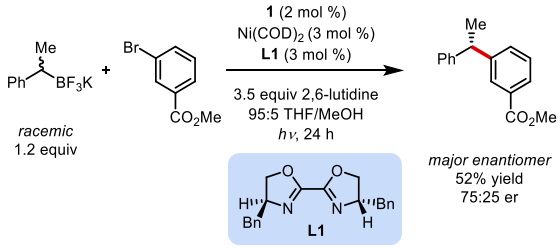


**Figure 8.2**. Stereoconvergent cross-coupling of a secondary benzylic trifluoroborate

Here, to paint the differences between these two mechanistic scenarios, we undertook a computational analysis of the Ni catalytic cycle with the goal of addressing two key questions, (1) to which oxidation state of Ni does the radical add? and (2) which step in the catalytic cycle is enantio-determining? Importantly, although there have been numerous computational and experimental studies of traditional transition-metal catalyzed CCRs,[3] there are limited

[i] Reproduced in part from *J. Am. Chem. Soc.*, **2015**, *137*, 4896,

computational analyses of nickel-catalyzed CCRs in which carbon-centered radicals and paramagnetic Ni species are invoked.[4–6]

To address this, we began a detailed DFT study of the catalytic cross-coupling of alkyltrifluoroborates and aryl bromides via single electron transmetalation. Results reveal that the final reductive elimination accounts for the origin of stereoinduction for this important transformation. A stereochemical model is proposed and supported by experiments with a series of substituted aryl bromides. These mechanistic findings are proposed to have far-reaching implications related to other stereoconvergent CCRs.

## 8.2 Results and Discussion

We initiated our studies by calculating the Gibbs free energy profile with 2,2'-bipyridine as a model ligand for the 4,4'-dtbbpy ligand used experimentally (Figure 2). Because of the presence of radicals and low-spin nickel intermediates, all optimizations were performed using a spin-unrestricted broken-symmetry UB3LYP functional with both the LANL2DZ and 6-31G(d) basis sets (with the Guess=mix keyword as implemented in Gaussian09).[7] Multiple spin states were considered for all intermediates and transition states. This method has been used before to rationalize selectivities accurately,[8] model radical nickel systems,[6] and account for changes associated with ligands.[9] Single point energy calculations of optimized structures were carried out in water (SMD solvation model) at the (U)M06/6-311+G(d,p) level of theory. For comparison, we computed the energetic profile by varying the basis set [6-311+G(d,p) for C, N, O, Br, H and SDD for Ni] and solvent (SMD in acetone), which showed similar energetics (see Experimental). Exhaustive conformational searches were performed for all intermediates to map out the lowest energy profile, and intrinsic reaction coordinate (IRC) calculations were undertaken to ensure transitions states connected the illustrated ground states.

Beginning from square planar Ni(bpy)(COD) **A**, dissociation of 1,5,-cyclooctadiene (COD) and complexation to bromobenzene is energetically disfavored by 6-8 kcal/mol (**Figure 8.3**). However, oxidative addition is energetically feasible (15-18 kcal/mol) leading to square planar Ni(II) intermediate **A2**, which is ~26 kcal/mol downhill in energy. The Ni(II) to Ni(III) process, occurring via addition of a benzyl radical (presumably generated in the concomitant photocatalytic cycle[1,2,10] from Figure 1), is found to proceed via a low barrier (~4 kcal/mol) transition state **A2-TS** and is reversible. Significantly, the reductive elimination transition state (**C-TS**) leading to the CCR product and Ni(bpy)Br intermediate is ~6 kcal/mol higher in energy than the radical addition/dissociation.

In an alternative mechanistic pathway, the nickel catalytic cycle can proceed via an alkylnickel(I) intermediate preceding oxidative addition (**Figure 8.1** red). Ligand dissociation and radical $\eta^2$-complexation to nickel(0) leads to intermediate **B1**, which proceeds via a ~5 kcal/mol energy barrier to form benzyl nickel(I) intermediate **B2**, a process that is favorable by ~10-15 kcal/mol. This Ni(I) intermediate can undergo facile and irreversible oxidative addition (via **B2-TS**) to merge the two energetically feasible pathways via the pentacoordinated Ni(III) intermediate C. This implies that, irrespective of the specific pathway, e.g., radical capture of Ni(0) or Ni(II), the dual photoredox/cross-coupling cycle *converges onto a Ni(III) intermediate that can dissociate the stabilized radical to form Ni(II) more rapidly than undergoing reductive elimination!* Subsequent reduction by the photoredox cycle will generate the Ni(0) intermediate to restart the catalytic cycle.

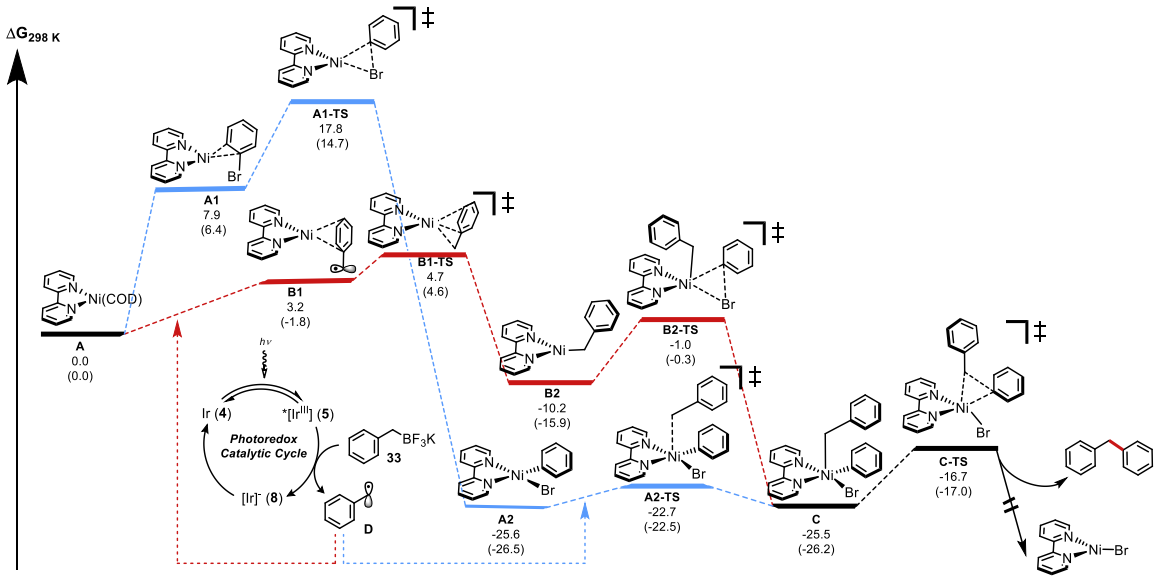


**Figure 8.3.** Reaction coordinate for the competing pathways using 2,2'-bipyridine. Relative Gibbs free energy values calculated with SMD-water-(U)M06/6-311+G(d,p)//UB3LYP/6-31G(d,p) and SMD-water-(U)M06/6-311+G(d,p) //UB3LYP/LANL2DZ (in parentheses).

In our recent report, we observed modest enantioselectivity (75:25 er) with the use of chiral 4,4'-dibenzyl-2,2'-bis(2-oxazoline) ligand, **L1** (**Figure 8.2**). We had previously suggested that the origin of enantioselectivity in the single-electron transmetalation of secondary alkyltrifluoroborates arises from facial selectivity in the addition of the prochiral radical to the ligated nickel(II) center, followed by stereoretentive reductive elimination. However, if homolytic equilibration of the Ni(III)/Ni(II) pair is faster than reductive elimination, as these calculations indicate, then the origin of stereoselectivity should be found in the reductive elimination step. Thus, we propose that enantioselectivity arises from a process best described as a dynamic kinetic resolution (DKR)[11] of Ni(III) complex **C'**. In other words, addition of the secondary radical to the Ni center operates under Curtin-Hammett conditions[12] furnishing two equilibrating diastereomeric Ni(III) complexes, one of which reductively eliminates at a faster rate, leading to the major enantiomer. Stereoconvergence then results via stereochemical scrambling of the secondary alkyl subunit

through dissociation and recombination. Indeed, computations of the diastereomeric transition states C' correlate well with experiment; specifically, a Boltzmann distribution from calculated free energies of the eight lowest energy diastereomeric transition states predicts a 68% ee vs the experimental 50% ee. Examination of the structures reveals that the α-methylbenzyl group rotates to avoid gauche-like interactions along the forming C-C bond (**Figure 8.4**). In the lower energy diastereomeric transition state these interactions are minimized.

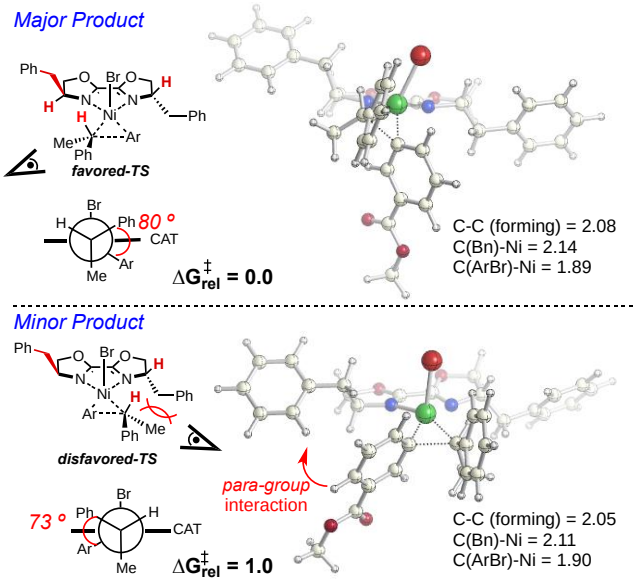


**Figure 8.4**. Competing diastereomeric transition states in the reductive elimination. Relative free energies, (kcal/mol) are computed using SMD-water-(U)M06/6-311+G(d,p)//UB3LYP/6-31G(d,p).

Having established reductive elimination as the enantio-determining step in these systems, other potential substrates were probed with the aim of establishing a correlation between the calculated and experimental selectivities. Calculations of the diastereomeric transition states for several substrates suggested that substituents at the para-position of the aryl bromide could enhance the enantioselectivity. In particular, larger para-substituents encounter steric interactions with the ligand benzyl group in the transition state leading to the minor enantiomeric product (see bottom structure in **Figure 8.4**). Notably, the stereochemical influence of these substituents distal from the bond-forming site would not be evident in the absence of this computational model. Gratifyingly,

these predictions correlated well with experiment and afforded improved enantioselectivity in generating 1,1-diarylethane **13-15** (**Figure 8.5**).

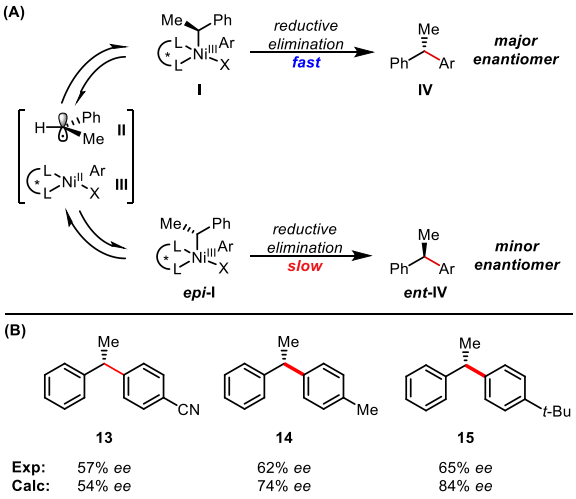


**Figure 8.5**. Predicted and experimental reaction enantioselectivities.

Moving forward, we became curious whether this DKR-controlled enantioselectivity operates in other asymmetric nickel-catalyzed cross-coupling processes. Of particular interest are reports documenting nickel-catalyzed asymmetric cross-couplings (Suzuki, Negishi, Hiyama, and Kumada)[13,14] and reductive cross-couplings.[15,16] Importantly, it can be argued that the "black box" nature of these transformations have limited their widespread development and adaptation, as no general model for stereoinduction has yet been proposed despite the large number of processes reported to date. Although a number of these asymmetric cross-couplings employ alkyl groups that would be precursors to stabilized radicals (i.e., benzylic, allylic, α-carbonyl, etc.), several examples of asymmetric cross-couplings of electronically unactivated alkyl subunits have been reported.[17,18] Although the analogy of the former examples to that reported here is readily apparent, it was less clear whether the proposed Ni(III) DKR manifold would be viable for systems in which less stable (e.g., unstabilized secondary alkyl) radicals were generated via homolysis of the Ni(III) intermediate. In an effort to address this question, the stereoconvergent cross-coupling of

unactivated secondary alkyl bromides and primary alkylboranes reported by Fu and coworkers (**Figure 8.6**)[19] was examined computationally.

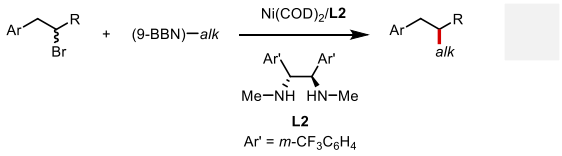


**Figure 8.6.** Stereoconvergent unactivated alkyl cross-coupling

Beginning from the putative Ni(III) complex, the transition states for homolysis of the secondary alkyl substituent and C-C bond-forming reductive elimination were computed. As shown in **Figure 8.7**, these calculations convincingly support a scenario analogous to that described above; that is, Ni(III) complex **10a** exists in homolytic equilibrium with Ni(II) complex **3a** and the free alkyl radical in a process that is much faster than the subsequent reductive elimination leading to Ni(I) complex **12a** and cross-coupled alkane product. As such, we propose that stereoconvergence in these processes occurs by the same Ni(III) DKR process that we have elucidated for photoredox/nickel dual catalytic organoboron cross-coupling. This newfound knowledge regarding the fundamental origin of enantioinduction in Ni-catalyzed stereoconvergent processes can be used to augment stereoselectivity in known transformations through rational design and may be helpful in identifying new substrate classes that can participate via this reactivity manifold. These results are in agreement with the lack of products with long-lived radical intermediates. Specifically, radicals that quickly and favorably complex to the nickel center as proposed in **Figure 8.3** avoid radical pathways such as cyclization by a pendant alkene. We are currently investigating the full scope of this proposal for various Ni-catalyzed C-C bond-forming processes involving alkyl radical intermediates, including the factors that might change the enantiodetermining step.

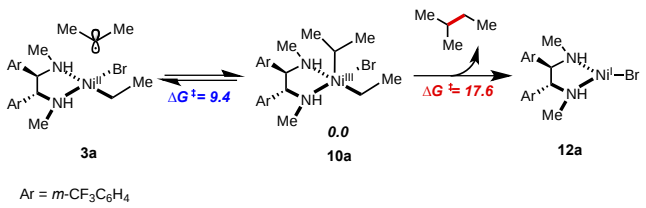


**Figure 8.7.** Energy barriers for the competing stabilized alkyl radical dissociation and reductive elimination transition states with chiral diamine ligand **L2**. Relative free energies (kcal/mol) are computed at the UM06/6-311+g(d,p) in SMD (water) level of theory.

## 8.3 Conclusion

In summary, we have employed DFT calculations to investigate the reaction pathway of the nickel/photoredox dual catalytic cross-coupling of aryl bromides with carbon-centered radicals derived from alkyltrifluoroborates. These computations suggest a mechanistic scenario wherein the radical can enter the cross-coupling cycle by addition to either Ni(0) or Ni(II).[20] The two pathways converge upon a common Ni(III) intermediate that is able to release the stabilized alkyl radical via Ni-C bond homolysis, thus establishing an unexpected equilibrium between this high valent Ni(III) and the Ni(II)/radical pair. The cross-coupled product is then generated via irreversible reductive elimination. The reductive elimination barrier was computed to be significantly higher in energy than the barrier associated with the reversible homolysis process. Calculations show that the stereoinduction occurs through DKR of the Ni(III) intermediate according to the Curtin-Hammett principle. Experimental results have offered support for the proposed stereochemical model. Most importantly, the Curtin-Hammett DKR stereoinduction model appears to be broadly operative in various related stereoconvergent Ni-catalyzed processes, offering a rationalization for the mechanism of stereoselectivity in these transformations for the first time.

## 8.4 Experimental

### General Considerations

All reactions were carried out under an inert atmosphere of nitrogen or argon unless otherwise noted. 2,6-Lutidine (>99%, purified by redistillation) was used without further purification. Ni(COD)2 and 2,2′-Bis[(4*S*)-4-benzyl-2-oxazoline] were purchased from commercial sources. Potassium trifluoro(1-phenylethyl)borate was prepared according to a published procedure.[21] THF (99.9% for HPLC, unstabilized) was dried by passing through activated alumina under an argon atmosphere using a J. C. Meyer solvent system. All other reagents were purchased commercially and used as received. Photocatalyst **4** was prepared according to the previously reported procedure.[1] Photoredox reactions were irradiated with a standard 26 W compact fluorescent light bulb (CFL) or blue LED light strips (~425 nm). NMR spectra were recorded on a 500 MHz spectrometer. Data are presented as follows: chemical shift (ppm), multiplicity (s = singlet, d = doublet, t = triplet, dd = doublet of doublets, q = quartet, m = multiplet, br = broad), coupling constant J (Hz) and integration. Optical rotation data was collected on a Jasco P-2000 polarimeter.

### General Procedure for Preparation of Enantioenriched 1,1-Diarylethanes

To a two dram (8 mL) borosilicate glass vial equipped with a Teflon-coated magnetic stir bar was added aryl bromide (0.5 mmol, 1 equiv), potassium trifluoro(1-phenylethyl)borate (127 mg, 0.6 mmol, 1.2 equiv), $Ir[dFCF_3ppy]_2(bpy)PF_6$ **2.1** (15 mg, 0.015 mmol), and **L1** (8.0 mg, 0.025 mmol). The vial was taken into a glovebox and $Ni(COD)_2$ (6.8 mg, 0.025 mmol) was added. The vial was sealed with a plastic screw cap containing a Teflon-lined silicone septum, removed from the glovebox, and evacuated and purged with inert gas three times. Under an inert atmosphere THF (5

mL) and 2,6-lutidine (202 μL, 1.75 mmol, 3.5 equiv) were introduced successively. The vial was sealed with parafilm and stirred for the specified time with irradiation from a 26 W CFL or blue LED light strips. The crude reaction mixture was filtered through a plug of Celite, washing with EtOAc (3 x 4 mL). The residue was purified using the method specified below to obtain the products in pure form.

**Computational Details**

Full Reference of Gaussian09:

Gaussian 09, Revision B.01, M. J. Frisch, G. W. Trucks, H. B. Schlegel, G. E. Scuseria, M. A. Robb, J. R. Cheeseman, G. Scalmani, V. Barone, B. Mennucci, G. A. Petersson, H. Nakatsuji, M. Caricato, X. Li, H. P. Hratchian, A. F. Izmaylov, J. Bloino, G. Zheng, J. L. Sonnenberg, M. Hada, M. Ehara, K. Toyota, R. Fukuda, J. Hasegawa, M. Ishida, T. Nakajima, Y. Honda, O. Kitao, H. Nakai, T. Vreven, J. A. Montgomery, Jr., J. E. Peralta, F. Ogliaro, M. Bearpark, J. J. Heyd, E. Brothers, K. N. Kudin, V. N. Staroverov, T.Keith, R. Kobayashi, J. Normand, K. Raghavachari, A. Rendell, J. C. Burant, S. S. Iyengar, J. Tomasi, M. Cossi, N. Rega, J. M. Millam, M. Klene, J. E. Knox, J. B. Cross, V. Bakken, C. Adamo, J. Jaramillo, R. Gomperts, R. E. Stratmann, O. Yazyev, A. J. Austin, R. Cammi, C. Pomelli, J. W. Ochterski, R. L. Martin, K. Morokuma, V. G. Zakrzewski, G. A. Voth, P. Salvador, J. J. Dannenberg, S. Dapprich, A. D. Daniels, O. Farkas, J. B. Foresman, J. V. Ortiz, J. Cioslowski, and D. J. Fox, Gaussian, Inc., Wallingford CT, 2010.

All optimizations were performed using spin-unrestricted broken-symmetry DFT using UB3LYP[22–24] with both the LANL2DZ[25] and 6-31G(d) basis sets (with the guess=mix keyword as implemented in Gaussian09) in the gas phase. Vibrational frequencies were computed at the same

level to obtain thermal corrections (at 298 K; enthalpic and free energy) and to characterize the stationary points as transition states (one and only one imaginary frequency) or minima (zero imaginary frequencies). For comparison, free energies were corrected (+1.89 kcal/mol) on going from standard state to 1 M in solution. Single point energy calculations in solvent [both water (ε =78.3553) and acetone (ε=20.493)] were performed using the SMD[26]-solvation model using the UM06[27] functional with the 6-311+G(d,p) basis set on both UB3LYP/LANL2DZ and UB3LYP/6-31G(d) optimized geometries. For comparison, we also computed single point energy calculations using UM06 functional and split basis [6-311+G(d,p) basis for C, H, N, Br, O atoms and SDD basis set with effective core potential[28] for Ni]. The choice of method had a minor effect on the relative energetics and did not change the overall conclusions. Exhaustive conformational searches were performed for all intermediates to map out the lowest energy profile, and intrinsic reaction coordinate (IRCs) calculations were undertaken to ensure transitions states connected the illustrated ground states.

**Compound Characterization Data**

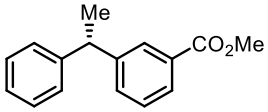


**Methyl (*S*)-3-(1-phenylethyl)benzoate (S1):** Prepared as part of a prior publication.[1] Absolute stereochemistry was assigned as (*S*) based on data reported in the literature.[29]

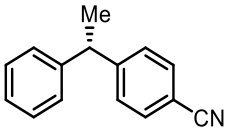

**(*S*)-4-(1-Phenylethyl)benzonitrile (13):** Reaction time was 24 h; purified by flash column chromatography on silica gel; obtained as a colorless oil; $^{1}$H NMR ($CDCl_3$, 500 MHz): δ 7.56 (d, *J* = 8.2 Hz, 2 H), 7.30 (dd, *J* = 8.1, 8.1 Hz, 4 H), 7.22 (t, *J* = 7.4 Hz, 1 H), 7.20-7.15 (m, 2 H), 4.20 (q, *J* = 7.2 Hz, 1 H), 1.65 (d, *J* = 7.2 Hz, 3 H) ppm; $^{13}$C NMR ($CDC_3$, 125.8 MHz): δ 152.1, 144.8, 132.4, 128.8, 128.6, 127.1, 126.8, 119.1, 110.1, 45.0, 21.6 ppm; Chiral SFC analysis indicated that the product was formed in 57% ee [ChiralPak OJ-H column: 5% *i*-PrOH in $CO_2$, 2.0 mL/min, $t_r$ = 8.48 (major peak) $t_r$ = 9.88 (minor peak)]; $[\alpha]_D^{22}$ = 3.1 (*c* = 0.10, $CHCl_3$); Absolute stereochemistry was assigned as (*S*) based on analogy to **S1**; Characterization data matched that previously reported in the literature.[30]

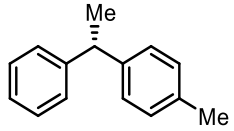


**(*S*)-1-Methyl-4-(1-phenylethyl)benzene (14):** Reaction time was 48 h; purified by preparatory high performance liquid chromatography (Waters AutoPure system, Sunfire C18 column, 49 x 100 mm, 5 μm particle size, 50% → 96% MeCN/$H_2O$, 0.1% TFA); obtained as a colorless oil; $^{1}$H NMR ($CDCl_3$, 500 MHz): δ 7.28 (m, 2 H), 7.22 (d, *J* = 7.0 Hz, 2 H), 7.17 (t, *J* = 7.2 Hz, 1 H), 7.14-7.06 (m, 4 H), 4.12 (q, *J* = 7.2 Hz, 1 H), 2.31 (s, 3 H), 1.63 (d, *J* = 7.2 Hz, 3 H); $^{13}$C NMR ($CDC_3$, 125.8 MHz): δ 146.7, 143.5, 135.6, 129.2, 128.5, 127.7, 127.6, 126.1, 44.5, 22.1, 21.1; Chiral SFC analysis indicated that the product was formed in 62% ee [ChiralPak OJ-H column: 3% *i*-PrOH in $CO_2$, 2.0 mL/min, $t_r$ = 10.63 (major peak) $t_r$ = 14.47 (minor peak)]; $[\alpha]_D^{22}$ = 0.5 (*c* = 0.10, $CHCl_3$); Absolute stereochemistry was assigned as (*S*) based on analogy to **S1**; Characterization data matched that previously reported in the literature.[31]

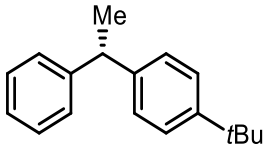


**(*S*)-1-(*tert*-Butyl)-4-(1-phenylethyl)benzene (15):** Reaction time was 24 h; purified by preparatory high performance liquid chromatography (Waters AutoPure system, Sunfire C18 column, 49 x 100 mm, 5 μm particle size, 50% → 96% MeCN/$H_2O$, 0.1% TFA); obtained as a colorless oil; $^1$H NMR ($CDCl_3$, 500 MHz): δ 7.31-7.23 (m, 6 H), 7.19-7.15 (m, 3 H), 4.12 (q, *J* = 7.2 Hz, 1 H), 1.64 (d, *J* = 7.2 Hz, 3 H), 1.30 (s, 9 H); $^{13}$C NMR ($CDC_3$, 125.8 MHz): δ 148.8, 146.8, 143.4, 128.5, 127.8, 127.3, 126.1, 125.4, 44.5, 34.5, 31.5, 22.0; Chiral SFC analysis indicated that the product was formed in 65% ee [ChiralPak OJ-H column: 3% *i*-PrOH in $CO_2$, 2.0 mL/min, $t_r$ = 5.67 (major peak) $t_r$ = 6.80 (minor peak)]; $[\alpha]_D^{22}$ = 2.5 (*c* = 0.10, $CHCl_3$); Absolute stereochemistry was assigned as (*S*) based on analogy to **S1**; Characterization data matched that previously reported in the literature.[32]

**Experiments with Enantioenriched Starting Materials**

To rule out the possibility of stereoselectivity arising from classical kinetic resolution of potassium (±)-1-phenylethyltrifluoroborate, potassium (*R*)-1-phenylethyltrifluoroborate was prepared according to literature procedures. All characterization data were consistent with those previously reported.[33,34] This compound, prepared as an 85:15 mixture of *R* and *S* enantiomers as judged by oxidation to the corresponding alcohols and chromatographic analysis thereof, was subjected to asymmetric photoredox cross-coupling with 4-bromobenzonitrile according to the general procedure described for **13** above using **L1** as a ligand. The enantioselectivity and absolute configuration of the major cross-coupled enantiomer of **13** observed in this reaction were the same as those observed using racemic potassium 1-phenylethyltrifluoroborate. Furthermore, reaction of

the enantioenriched trifluoroborate with 4-bromobenzonitrile under dual catalytic photoredox conditions using achiral 2,2'-bioxazoline as a ligand generated racemic product. These data are consistent with the proposed stereoconvergent pathway and provide strong evidence against a classical kinetic resolution as the source of stereoselectivity.

## 8.5 References


(1) Tellis, J. C.; Primer, D. N.; Molander, G. A. *Science* **2014**, *345*, 433.

(2) Zuo, Z.; Ahneman, D.; Chu, L.; Terrett, J.; Doyle, A. G.; MacMillan, D. W. C. *Science* **2014**, *345*, 437.

(3) Ananikov, V. P. *Understanding organometallic reaction mechanisms and catalysis*; WILEY-VCH: Weinheim, Germany, 2015.

(4) Ren, Q.; Jiang, F.; Gong, H. *J. Organomet. Chem.* **2014**, *770*, 130.

(5) Li, Z.; Jiang, Y.-Y.; Fu, Y. *Chem. - A Eur. J.* **2012**, *18*, 4345.

(6) Lin, X.; Phillips, D. L. *J. Org. Chem.* **2008**, *73*, 3680.

(7) *Frisch, M. J.; et al. Gaussian 09, rev C.01; Gaussian, Inc.: Wallington CT, 2009*.

(8) Um, J. M.; Gutierrez, O.; Schoenebeck, F.; Houk, K. N.; MacMillan, D. W. C. *J. Am. Chem. Soc.* **2010**, *132*, 6001.

(9) Jones, G. D.; Martin, J. L.; McFarland, C.; Allen, O. R.; Hall, R. E.; Haley, A. D.; Brandon, R. J.; Konovalova, T.; Desrochers, P. J.; Pulay, P.; Vicic, D. A. *J. Am. Chem. Soc.* **2006**, *128*, 13175.

(10) Primer, D. N.; Karakaya, I.; Tellis, J. C.; Molander, G. A. *J. Am. Chem. Soc.* **2015**, *137*, 2195.

(11) Beak, P.; Basu, A.; Gallagher, D. J.; Park, Y. S.; Thayumanavan, S. *Acc. Chem. Res.* **1996**, *29*, 552.

(12) Seeman, J. I. *J. Chem. Educ.* **1986**, *63*, 42.

(13) Rudolph, A.; Lautens, M. *Angew. Chem. Int. Ed.* **2009**, *48*, 2656.

(14) Tasker, S. Z.; Standley, E. A.; Jamison, T. F. *Nature* **2014**, *509*, 299.

(15) Cherney, A. H.; Kadunce, N. T.; Reisman, S. E. *J. Am. Chem. Soc.* **2013**, *135*, 7442.

(16) Cherney, A. H.; Reisman, S. E. *J. Am. Chem. Soc.* **2014**, *136*, 14365.

(17) Zultanski, S. L.; Fu, G. C. *J. Am. Chem. Soc.* **2013**, *135*, 624.

(18) Wilsily, A.; Tramutola, F.; Owston, N. A.; Fu, G. C. *J. Am. Chem. Soc.* **2012**, *134*, 5794.

(19) Saito, B.; Fu, G. C. *J. Am. Chem. Soc.* **2008**, *130*, 6694.

(20) Schley, N. D.; Fu, G. C. *J. Am. Chem. Soc.* **2014**, *136*, 16588.

(21) Cazorla, C.; Métay, E.; Lemaire, M. *Tetrahedron* **2011**, *67*, 8615.

(22) Becke, A. D. *J. Chem. Phys.* **1993**, *98*, 1372.

(23) Lee, C.; Yang, W.; Parr, R. G. *Phys. Chem. Rev. B.* **1988**, *37*, 785.

(24) Stephens, P. J.; Devlin, F. J.; Chabalowski, C. F.; Frisch, M. J. *J. Phys. Chem.* **1994**, *98*, 11623.

(25) Hay, P. J.; Wadt, W. R. *J. Chem. Phys.* **1985**, *82*, 270.

(26) Marenich, A. V; J, C. C.; Thrular, D. G. I. *Phys. Chem. B* **2009**, *113*, 6378.

(27) Zhao, Y.; Truhlar, D. G. *Theor. Chem. Acc.* **2008**, *120*, 215.

(28) Fuentealba, P.; Preuss, H.; Stoll, H.; Von Szentpaly, L. *Chem. Phys. Lett.* **1982**, *89*, 418.

(29) Fessard, C.; Andrews, S. P.; Motoyoshi, H.; Carreira, E. M. *Angew. Chem. Int. Ed.* **2007**, *46*, 9331.

(30) Liu, Z.; Dong, N.; Zu, M.; Sun, Z.; Tu, T. *J. Org. Chem.* **2013**, 78, 7436.

(31) Schafer, G.; Bode, J. W. *Angew. Chem. Int. Ed.* **2011**, *50*, 10913.

(32) Najamura, R.; Obora, Y.; Ishii, Y. *Chem. Commun.* **2008**, 3417.

(33) Crudden, C. M.; Hleba, Y. B.; Chen, A. C. *J. Am. Chem. Soc.* **2004**, *126*, 9200.

(34) Bagutski, V.; Ros, A.; Aggarwal, V. K. *Tetrahedron* **2009**, *65*, 9956.

**Author Contributions**

D.N.P. contributed to the design of the experiments and optimized conditions for enantioselective cross-coupling. John C. Tellis contributed to the conception of the project, prepared the compounds, and was involved in interpretation of the data. Osvaldo Gutierrez performed the computational studies. All wrote and edited the manuscript.

## Appendix A10. $^{1}H$, $^{13}C$ Spectra and Chiral SFC Chromatograms Relevant to Chapter 8

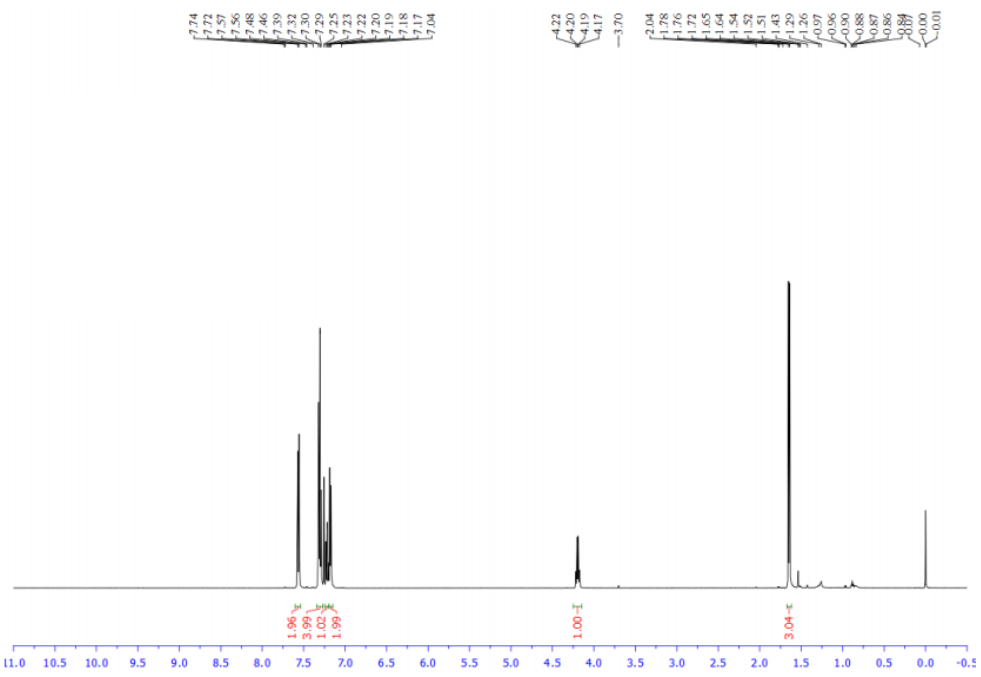

**Figure A10.1.** $^{1}$H NMR ($CDCl_3$, 500 MHz) spectrum of (S)-4-(1-phenylethyl)benzonitrile (**13**)

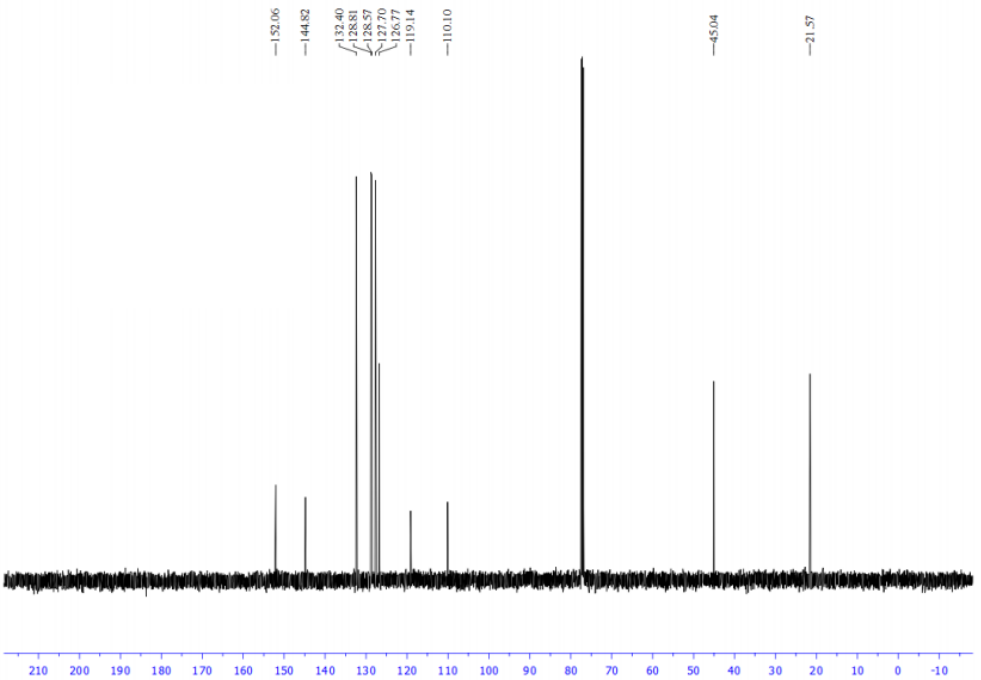

**Figure A10.2.** $^{13}$C NMR ($CDCl_3$, 125.8 MHz) spectrum of (S)-4-(1-phenylethyl)benzonitrile (**13**)

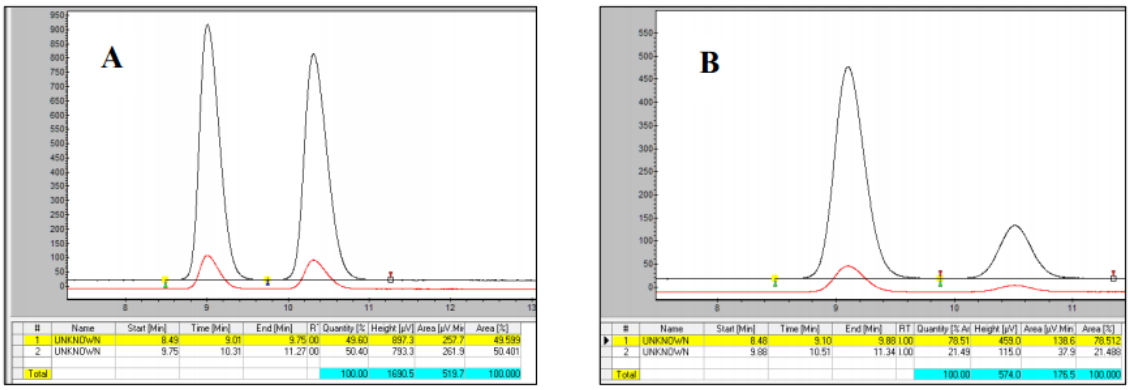


**Figure A10.3.** Chiral SFC chromatogram (OJ-H column: 5% *i*-PrOH in $CO_2$, 2.0 mL/min) of racemic (A) and enantioenriched (B) 4-(1-phenylethyl)benzonitrile (**13**)

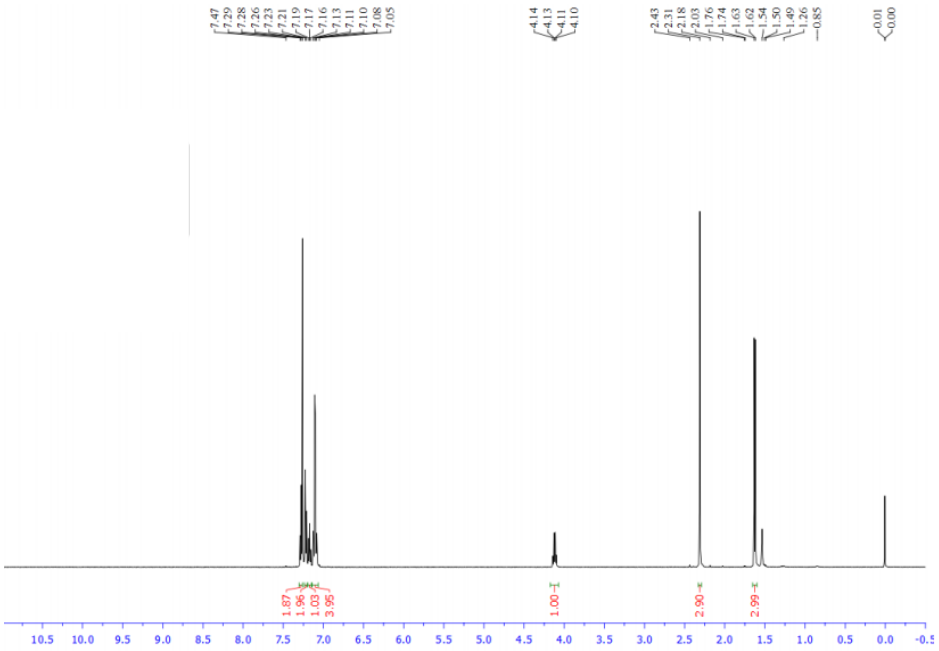

**Figure A10.4.** $^{1}H$ NMR ($CDCl_3$, 500 MHz) spectrum of (S)-1-methyl-4-(1-phenylethyl)benzene (**14**)

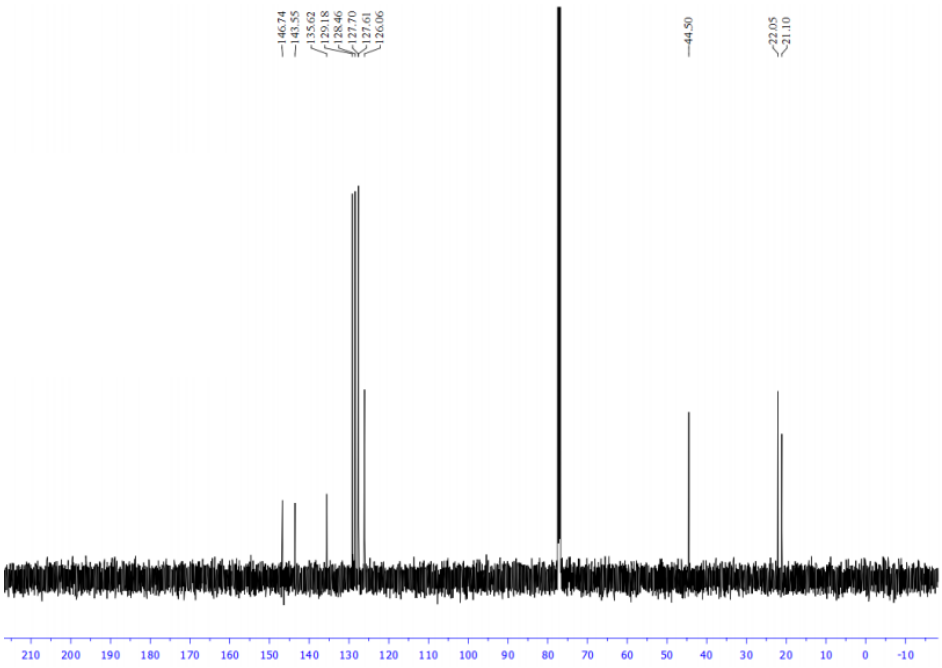

**Figure A10.5.** $^{13}C$ NMR ($CDCl_3$, 500 MHz) spectrum of (S)-1-methyl-4-(1-phenylethyl)benzene (**14**)

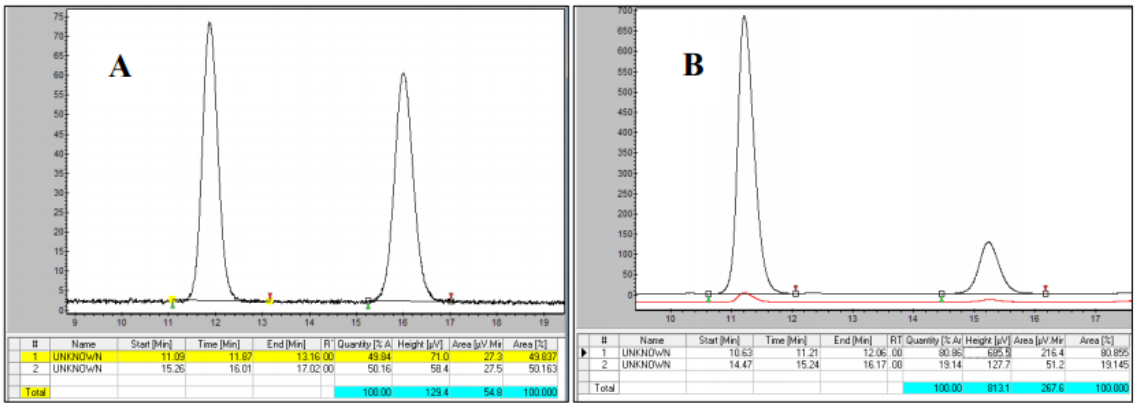


**Figure A10.6.** Chiral SFC chromatogram (OJ-H column: 3% *i*-PrOH in $CO_2$, 2.0 mL/min) of racemic (A) and enantioenriched (B) 1-methyl-4-(1-phenylethyl)benzene (**14**)

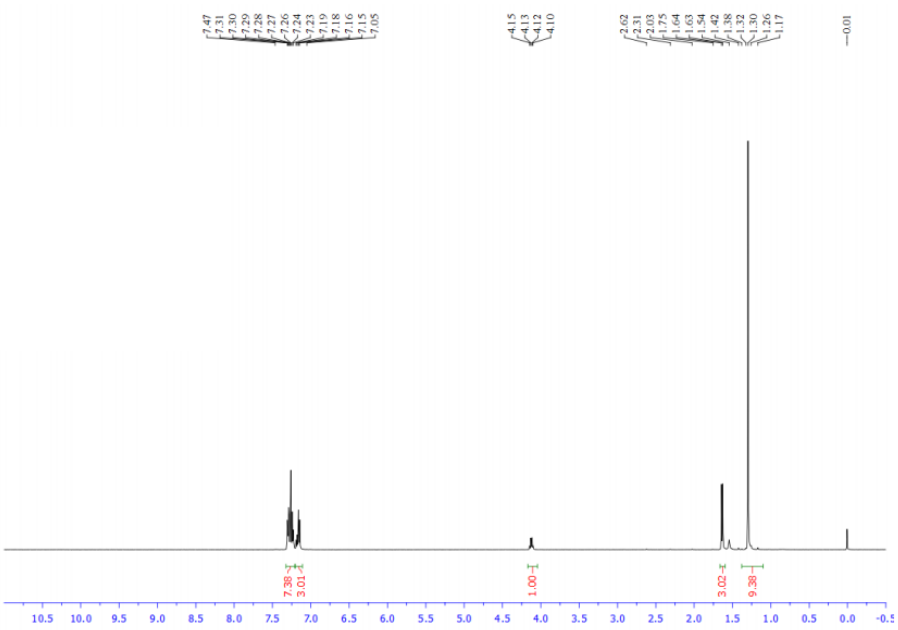

**Figure A10.7.** $^{1}$H NMR ($CDCl_3$, 500 MHz) spectrum of (S)-1-(*tert*-butyl)-4-(1-phenylethyl)benzene (**15**)

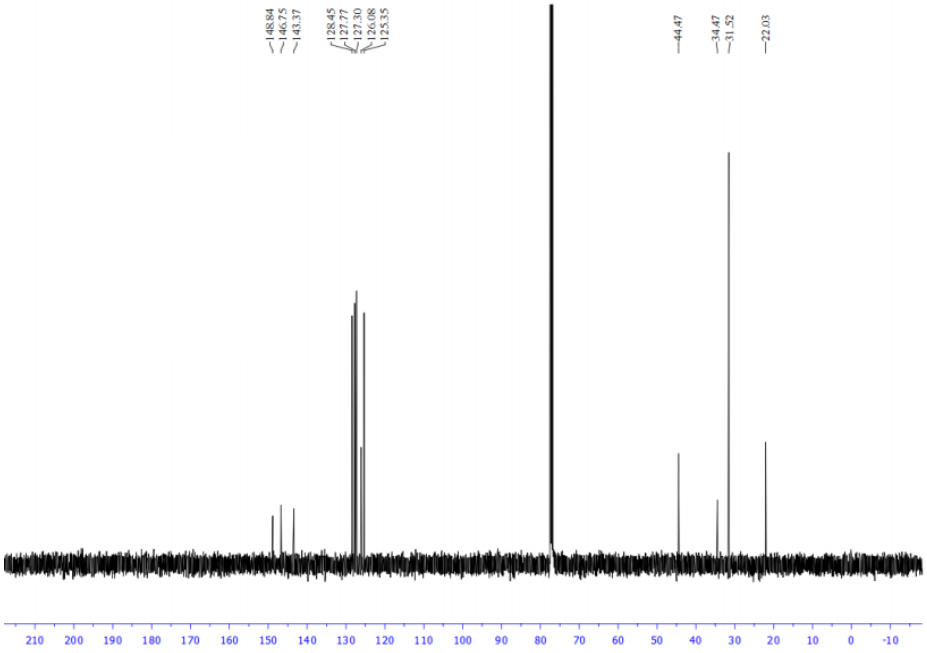

**Figure A10.8.** $^{13}$C NMR ($CDCl_3$, 125.8 MHz) spectrum of (S)-1-(*tert*-butyl)-4-(1-phenylethyl)benzene (**15**)

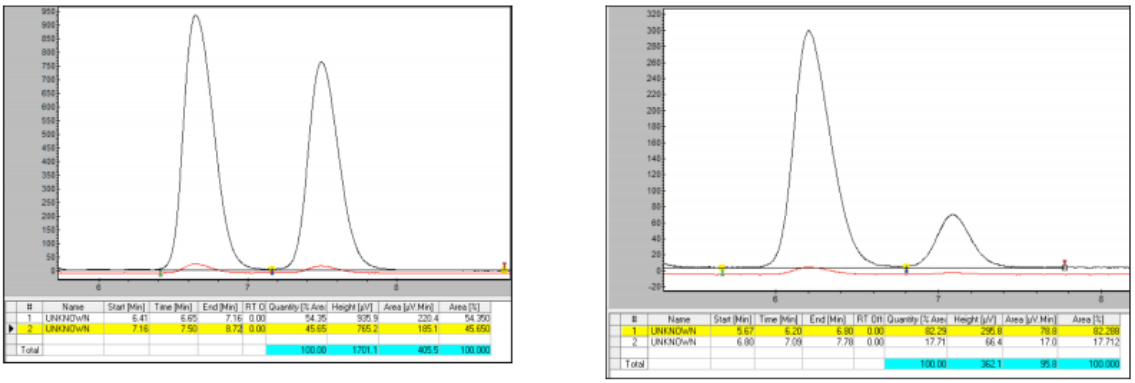

| # | Name | Start [Min] | Time [Min] | End [Min] | RT Diff | Quantity [% Area] | Height [µV] | Area [µV Min] | Area [%] |
|---|---|---|---|---|---|---|---|---|---|
| 1 | UNKNOWN | 6.41 | 6.65 | 7.16 | 0.00 | 54.35 | 935.9 | 220.4 | 54.350 |
| 2 | UNKNOWN | 7.16 | 7.50 | 8.72 | 0.00 | 45.65 | 765.2 | 185.1 | 45.650 |
| Total | | | | | | 100.00 | 1701.1 | 405.5 | 100.000 |

| # | Name | Start [Min] | Time [Min] | End [Min] | RT Diff | Quantity [% Area] | Height [µV] | Area [µV Min] | Area [%] |
|---|---|---|---|---|---|---|---|---|---|
| 1 | UNKNOWN | 5.67 | 6.20 | 6.80 | 0.00 | 82.29 | 295.8 | 78.8 | 82.288 |
| 2 | UNKNOWN | 6.80 | 7.09 | 7.78 | 0.00 | 17.71 | 66.4 | 17.0 | 17.712 |
| Total | | | | | | 100.00 | 362.1 | 95.8 | 100.000 |

**Figure A10.9.** Chiral SFC chromatogram (OJ-H column: 3% *i*-PrOH in $CO_2$, 2.0 mL/min)of racemic (A) and enantioenriched (B) 1-(*tert*-butyl)-4-(1- phenylethyl)benzene (**15**)

# Chapter 9. Photoredox Generated Radicals in Minisci Chemistry

## 9.1 Introduction

Heteroaryl subunits are among the most commonly employed,[i] privileged structures in medicinal chemistry.[1] Unfortunately, the synthesis of many of these structures is often predicated on cyclization reactions[2] from simple starting materials (e.g., aldehydes, hydrazines, alkynes, etc.). Although these methods often prove advantageous when the precursors needed for a particular molecular target are inexpensive and commercially available, these sequences are untenable when attempting to access a diverse library of structurally rich heteroarenes with a common core (**Figure 9.1**).

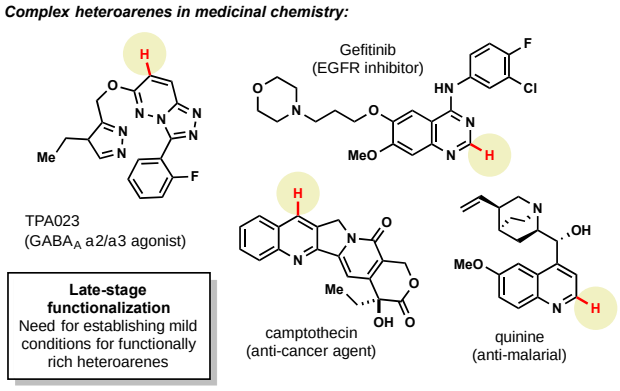


**Figure 9.1.** Complex heteroarenes poised for diversification.

To overcome this challenge, two predominant anionic strategies have emerged for diversifying common heteroaryl motifs: fluorination to enable facile $S_NAr$-based chemistry[3] and halogenation (bromination,[4] chlorination[5]) to provide a site for cross-coupling.[6] These methods are

[i] Reproduced in part from *Chem. Sci.*, **2017**, *8*, 3512.

highly effective for many systems, but in numerous cases installation of the halide at the desired site is unselective or impossible, requiring re-evaluation of the synthetic strategy. Furthermore, when successful incorporation of halides has occurred, heteroarenes are often obstinate partners in cross-coupling chemistry,[7] requiring careful screening to achieve fruitful union. Most importantly, from an efficiency standpoint, these strategies are sub-optimal as they first require a functional handle to be installed, only to be immediately replaced in a subsequent displacement reaction.

Radical alkylations of heteroarenes (Minisci reactions)[8] represent a more direct functionalization of specific C-H bonds. For this reason, radical alkylation strategies have recently risen to prominence for the late-stage functionalization of heteroaryl systems. Although Minisci and coworkers initially used silver oxidants at elevated temperatures to generate alkyl radicals from the corresponding carboxylic acids,[9] advances in alkyl radical generation have enabled much milder methods to be developed (**Figure 9.2**). These have included methods using boronic acids,[10] peresters,[11] and other precursors[12] under much less forcing conditions. Most notably, the Baran laboratory has pioneered the use of sulfinate salts[13] that have enabled the extremely facile introduction of functionalized alkyl radicals into an impressive array of heteroarenes. These methods allow the formal C-H alkylation of heterocycles in a mild, *metal-free* manner – drawing rapid adoption by medicinal chemists for the late stage diversification of pharmaceutically relevant compounds.[14]

Unfortunately, even with these advances, current methods are not without their limitations, particularly with regard to the continued requirement for high loadings of both the radical partner

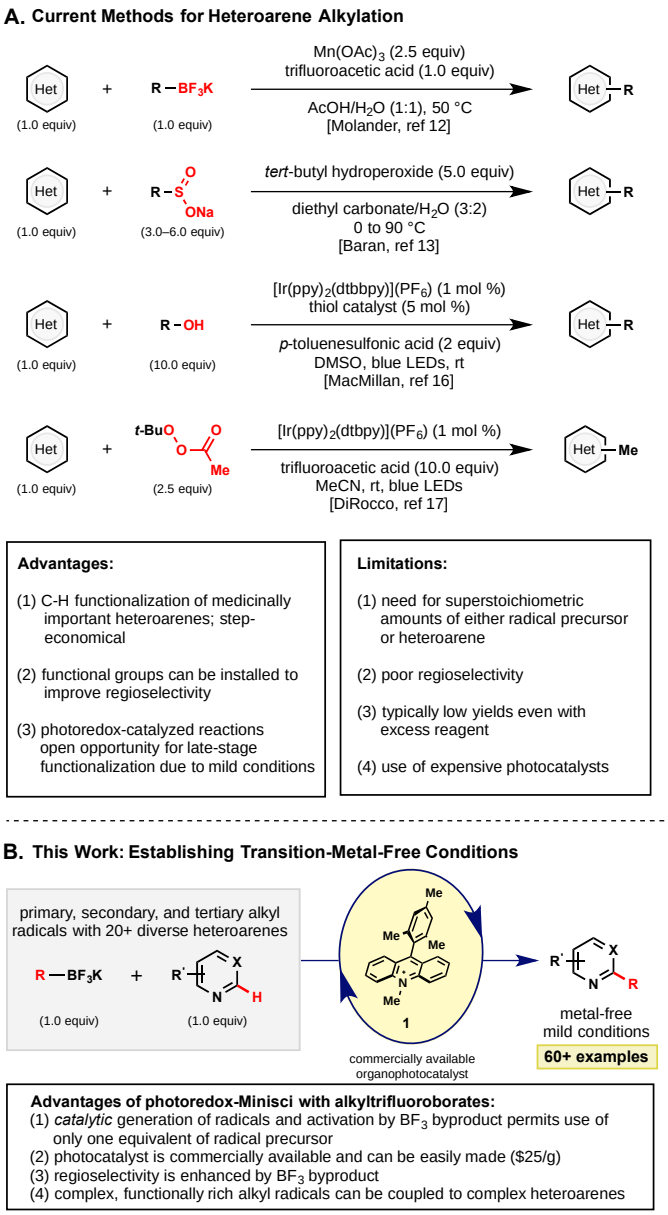


**Figure 9.2.** Approaches to Heteroarene Functionalization

and oxidant. Even the milder methods employing sulfinate salts often require a significant excess of an expensive and synthetically demanding precursor (3–6 equiv) and oxidant (5–10 equiv) to achieve good yields.[13] To date, methods grounded on *stoichiometric* radical generation have been continually limited by parasitic reactivity (e.g., homocoupling, H-atom abstraction, and chain

processes) that appear to outcompete the desired Minisci alkylation. As such, often the only solution has been to push reactions to completion with increased reagent loadings or successive dosing (**Figure 9.2A**).

To combat the disproportionate stoichiometry and typically harsh conditions, other groups have turned to photoredox catalysis for the efficient generation of radicals.[15] Contributions by the MacMillan,[16] DiRocco,[17] Chen,[18] and Barriault[19] groups have all highlighted the advantages afforded under this paradigm. Although a variety of alkyl radicals precursors were presented in these photoredox contributions, each method exhibits some inherent limitations. For example, the MacMillan group targets weak C-H bonds and were largely limited to α-heteroatom bonds. Barriault and coworkers demonstrated that alkyl bromides could be reduced to generate the corresponding alkyl radicals, but 3 equivalents of these precursors and a UVA LED light source were required. Additionally, MacMillan and Barriault used expensive iridium or gold photocatalysts, respectively. The recent report by Chen addressed many of these issues with the use of sustainable boronic acid partners and inexpensive $Ru(bpy)_3$, but their method employs the use of a stoichiometric iodine oxidant that seems uniquely required for activation.

In light of these advances, we recognized the potential to marry photoredox Minisci chemistry with our laboratory's interest in alkyltrifluoroborate reagents, especially given reports by our laboratory and others[20] on the favorable single electron oxidation potentials of these salts to form alkyl radicals ($E_{red}$ = +1.10 V *vs* SCE for 1° benzylic[20a] and +1.50 V *vs* SCE for 2° alkyltrifluoroborates[20b]). Here, with appropriate organic photocatalyst selection (for **1**: $*E_{red}$ = +2.06 V *vs* SCE[21]), all representative radical classes could be activated under identical reaction conditions (**Figure 9.2B**). In this scenario, one can envision photocatalyst excitation serving as a chaperone for steady, synchronized, *catalytic* radical generation. Such a protocol insures that an excess of radicals are not generated, minimizing at least some of the byproducts formed through stoichiometric processes. The photoredox catalyst-coordinated generation of radicals in this

manner leads to improvement in reagent and oxidant loading, thus enhancing the efficiency and sustainability of these methods. Serendipitiously, these aforementioned concepts, in conjuction with the generation of Lewis acidic $BF_3$ byproduct, also led to enhanced reactivity and selectivity in these transformations.

## 9.2 Results and Discussion

Mechanistically, we anticipated that visible light irradiation of organic photocatalyst **1** would generate the excited complex **1***, which is highly oxidizing and capable of oxidizing an alkyltrifluoroborate to release the desired alkyl radical **3** and $BF_3$ (**Figure 9.3**). The generated radical **3** can then intercept the protonated heteroarene to form the radical cation **5**. Reduction of persulfate ($E_{red}$ = > +0.35 V *vs* SCE[22]) by the reduced form of the photocatalyst **4** ($E_{red}$ = +0.49 V *vs* SCE[21]) generates the sulfate dianion and sulfate radical anion, regenerating photocatalyst **1**.[21] Finally, H-atom abstraction of **5** by the sulfate radical anion leads to rearomatization, affording the desired alkylated heteroarene **6**.[16] Quantum yield studies indicate this is not a radical chain process as evidenced by a $\phi$ of 0.31 (see experimental). Furthermore, addition of excess allyl acetate (a known sulfate radical anion trap[23]) did not interfere with reaction efficiency or conversion.

To begin this optimization, we keyed in on tertiary radical partners for our initial studies – in particular, *tert*-butyltrifluoroborate as the appropriate radical precursor and isoquinoline carboxylate as the heteroaryl partner. Before screening various photocatalysts, controls probing the need for oxidant (**Table 9.1**, entry 2), light (entry 3), and photocatalyst (entry 4) were completed. Additionally, the absence of acid (entry 5) afforded 30% conversion to product, although as alkyl radical **3** is generated, $BF_3$ (an electron-deficient Lewis acid) is concomitantly being formed.

Performing the reaction in air provided a comparable yield (entry 6) to a reaction carried out under inert conditions (entry 1).

The mesityl acridinium photocatalyst was then compared to other photocatalysts (entries 7–10). Noting the need for a relatively high oxidizing potential of the photocatalyst, it was expected that ruthenium photocatalysts (with significantly lower oxidation potentials than the acridinium dyes) would experience diminished yields, which proved to be the case (entries 7, 8). During the period that photoredox catalysis has gained traction in the organic chemistry community, one major criticism has been the high cost of the key metal-based photocatalysts (i.e., those based on iridium and ruthenium). Nicewicz[24] and Zhang[25] have explored alternative organophotocatalysts that have been shown to exhibit similar reactivity to their metal-based counterparts. Surprisingly, 4CzIPN (entry 10) significantly outperformed MesAcr over a 12 h period. Neither excess alkyltrifluoroborate (entry 11) nor excess oxidant (entry 12) provided any perceived advantages. Of note, acridine afforded only trace amounts of alkylation product at the C9 position during our heteroarene scope investigation. For mesityl acridinium, the C9 position is occupied by the mesityl substituent and is therefore unable to participate in Minisci alkylation, thus making it a suitable photocatalyst for the reactions described herein.

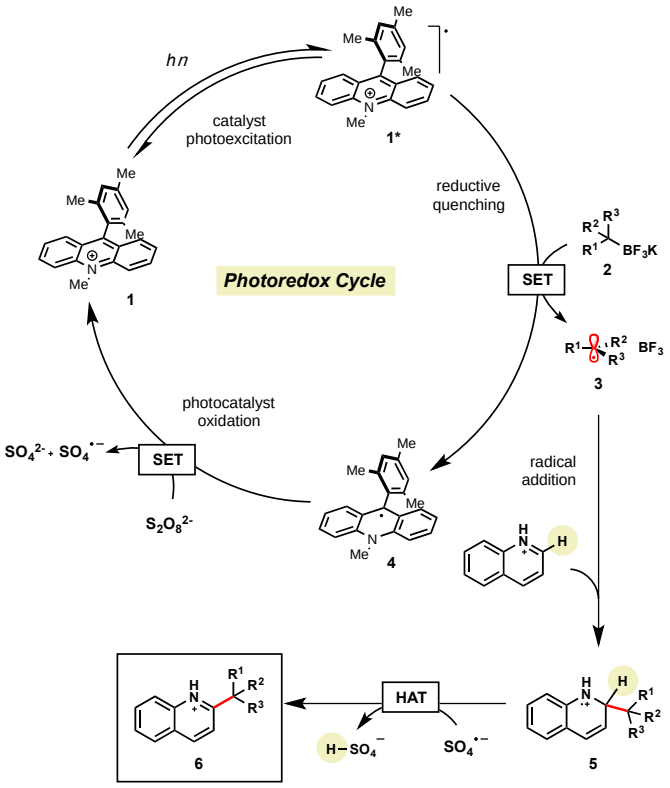


**Figure 9.3**. Proposed Mechanism

In view of their low cost and ease of access, going forward we focused on the two organophotocatalysts, MesAcr and 4CzIPN. To determine the most suitable organic photocatalyst for our purposes, we scaled up the reactions described in entries 1 and 10, and discovered that running the reaction for 16 h afforded similar yields, consistent with the small scale reactions. It was important for this protocol to be general for primary, secondary, and tertiary alkyltrifluoroborates. Because primary alkyltrifluoroborates have a markedly higher oxidation potential ($E_{red}$ = +1.80 V vs SCE[20k]) than secondary or tertiary alkyltrifluoroborates, MesAcr and 4CzIPN were compared with a primary alkyltrifluoroborate (**Figure 9.4**). In this assay, MesAcr outperformed CzIPN with 76% versus <10% isolated yields, respectively.

**Table 9.1.** Optimization for Tertiary Alkyl Coupling[a]

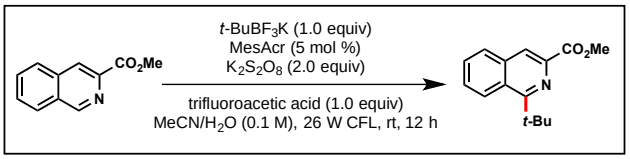


| Entry | Deviation from Standard Conditions | % Yield [b] |
|---|---|---|
| 1 | none | 57 |
| 2 | no persulfate | <5 |
| 3 | no light | <**5** |
| 4 | no photocatalyst | 0 |
| 5 | no acid | 30 |
| 6 | open to air (needle puncture) | 53 |
| 7 | $Ru(bpy)_3Cl_2$ (photocatalyst) | 8 |
| 8 | $Ru(bpz)_3$ (photocatalyst) | 16 |
| 9 | $Ir[dFCF_3ppy]_2(bpy)PF_6$ (photocatalyst) | 86 |
| 10 | 4CzIPN (photocatalyst) | 96 |
| 11 | 2.0 equiv trifluoroborate | 45 |
| 12 | 4.0 equiv persulfate | 84 |

**Photocatalysts**

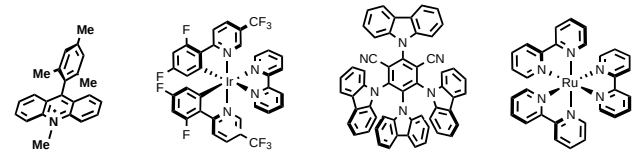

**MesAcr** $E_{red}$ = +2.06 V | **$Ir[dFCF_3ppy]_2(bpy)$** $E_{red}$ = +1.32 V | **4CzIPN** $E_{red}$ = +1.35 V | **$Ru(bpy)_3$** $E_{red}$ = +0.77 V

[a]Optimization reactions were run with heteroarene (1.0 equiv), *tert*-butyltrifluoroborate (1.0 equiv), photocatalyst (5 mol %), $K_2S_2O_8$ (2.0 equiv), trifluoroacetic acid (1.0 equiv) in $MeCN/H_2O$ (1:1) on 0.1 mmol scale. [b]Yields were obtained by HPLC using a calibration curve.

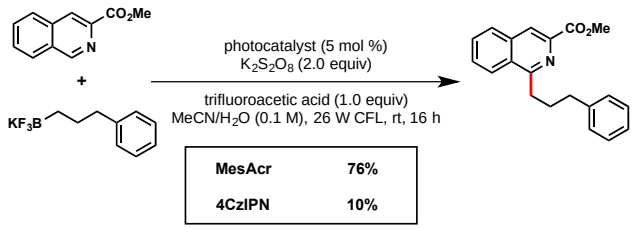


**Figure 9.4.** Comparing Organophotocatalysts

Tricoordinate organoboron compounds are isoelectronic with carbocations, and thus would not be expected to be easily oxidized by single electron transfer (SET) processes. To confirm that this chemistry was unique to alkyltrifluoroborates, a variety of organoboron reagents were synthesized and analyzed by cyclic voltammetry to determine their relative oxidation potentials

(**Table 9.2**). As expected, the trivalent organoboron variants exhibit very high oxidation potentials as compared to their tetravalent, "ate" complex analogues. Consequently, under the reaction conditions, no radical formation from the boronic acids and/or esters was observed. For the tetravalent species, triolborates exhibit comparatively low reduction potentials. Unfortunately, the swift hydrolysis of triolborates under the acidic, aqueous reaction conditions forms the redox inactive boronic acid.[26] By contrast, alkyltrifluoroborates are both stable to the reaction conditions and redox amenable, resulting in an excellent 72% yield with methyl isoquinoline carboxylate after 16 h.

**Table 9.2.** Exploring Various Alkylboron Compounds[a]

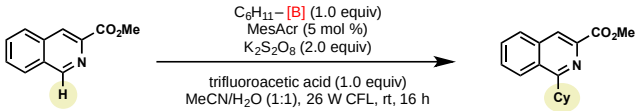


| Alkylboron | Reduction Potential | Result | Drawbacks |
|---|---|---|---|
| 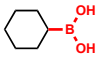 | >2.5 V vs SCE | no conversion | · air sensitive<br>· poor redox properties |
| 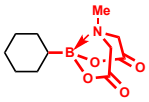 | >2.5 V vs SCE | no conversion | · limited commerical availability<br>· poor atom economy<br>· poor redox properties |
| 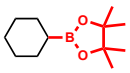 | >2.5 V vs SCE | <5% conversion | · air sensitive<br>· poor atom economy<br>· poor redox properties |
| 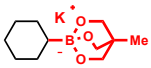 | +1.1 V vs SCE | no conversion | · limited commercial availability<br>· hydrolytically unstable<br>· poor atom economy |
| 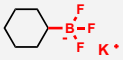 | $E_{red}$ = +1.5 V vs SCE<br>72% isolated yield | | · **commerically available**<br>· **bench-stable**<br>· **excellent redox properties** |

[a]Reactions were run with heteroarene (1.0 equiv), alkylboron reagent (1.0 equiv), MesAcr (5 mol %), $K_2S_2O_8$ (2.0 equiv), trifluoroacetic acid (1.0 equiv) in MeCN/$H_2O$ (1:1) on 0.2 mmol scale.

*tert*-Butyltrifluoroborate was selected to examine the amenability of various heteroarene partners (**Figure 9.5**). Regioselectivity was probed using quinoline itself, leaving both the C2 and C4 positions available for alkylation. Currently there are two methods for installing tertiary radicals

regioselectively into the quinoline core structure. Namgoong and coworkers reported the use of excess TMP-zincate to deprotonate selectively at the C2 position, followed by incorporation of the *tert*-butyl substituent.[27] This was a singular transformation, with no demonstrated scope. Additionally, Minisci and coworkers have reported selective C2 C-H substitution on quinolines using a 3-fold excess of alkyl iodide radical precursors.[8b] Although efficient, drawbacks of this approach included using peroxide as the oxidant, thereby limiting functional group tolerance, and the limited number of commercially available, complex alkyl iodides. Therefore, we were pleased to observe *regioselective* addition to the C2 position of the heteroarene in 72% yield (**1a**). With substitution at the C4 position of quinoline, the reaction reached full conversion to product within 16 h as determined by GC-MS analysis (**1b**). When isolated, a 95% yield of the desired product was achieved. Beyond alkyl substituents, halides and trifluoromethyl groups incorporated within the heteroaromatics allowed excellent conversion to product (**1c**, **1d**).

In addition to quinoline cores, indazole (**1e**), isoquinoline (**1g**), and quinoxaline (**1h**, **1i**) moieties were successful partners under standard conditions. Indazole **1e** is particularly notable because of the prevalence in medicinal chemistry[1] and, to the best of our knowledge, the absence of Minisci examples in the literature. As expected, the use of the benzimidazole core resulted in no conversion **(1f**) because of the electron-rich nature of the C2 site. Additionally, *N*-methyl benzimidazole was similarly unreactive. Pyridines also exhibited selective mono-addition (**1j**–**1l, 1n**). Only one reported of nicotinamide alkylation *via* Minisci chemistry has been previously, wherein three equiv of the corresponding carboxylic acid were necessary under silver catalyzed conditions.[28] A medicinally relevant core, quinazolinone **1p**, afforded product in 90% yield. Purine **1q** contains two sites of potential radical addition, but substitution was observed only on the pyrimidine subunit. Overall, this method is broadly tolerant of a wide range of functional groups as demonstrated with quinine **1r** (possessing alkene, alcohol, tertiary amine groups). Notably, the

tertiary amine embedded within quinine did not interfere with the photocatalytic cycle despite its propensity for competitive oxidation.

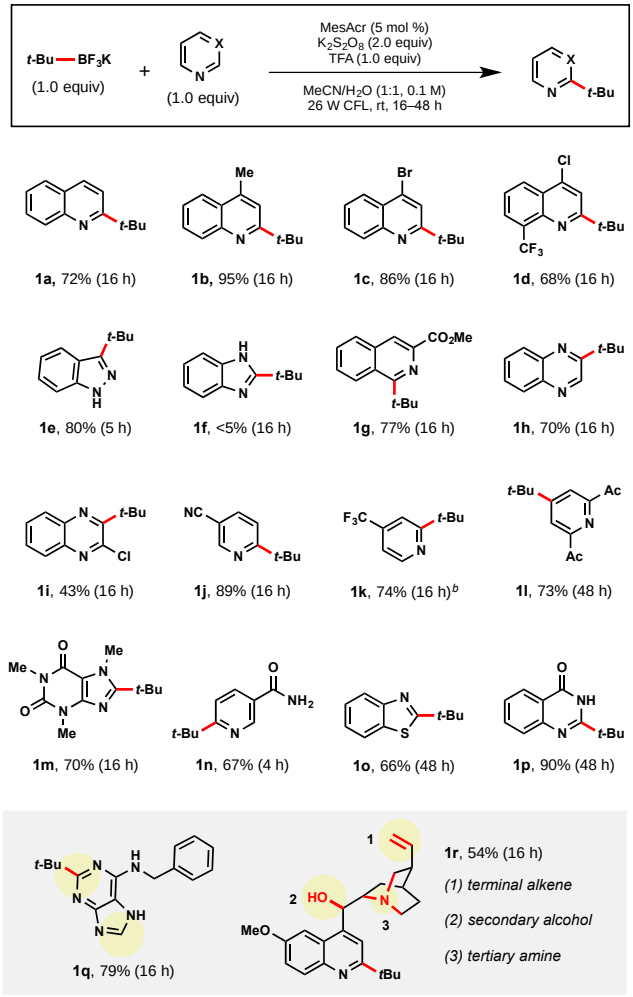


**Figure 9.5.** Heteroarene Scope[a]

[a]Reactions were run with heteroarene (1.0 equiv), *tert*-butyltrifluoroborate (1.0 equiv), MesAcr (5 mol %), $K_2S_2O_8$ (2.0 equiv), trifluoroacetic acid (1.0 equiv) in MeCN/$H_2O$ (1:1) on 0.3 mmol scale.
[b]Yield determined by fluorine NMR using fluorobenzene as internal standard.

Currently, there are a limited number of tertiary alkylboranes commercially available and no alkyltrifluoroborates. Presumably, this is a result of narrow synthetic utility compared to their primary and secondary counterparts. Although we demonstrated that *tert*-butyltrifluoroborate was viable, more highly elaborated systems could also be incorporated. Cook and coworkers recently

reported a manganese-catalyzed borylation of alkyl bromides. Using Cook's procedure,[29] >1 g of pinacolborane intermediate **1t** was synthesized from the corresponding alkyl bromide **1s**. This borylation was followed by treatment with saturated $KHF_2$ to afford the corresponding alkyltrifluoroborate **1u** (**Figure 9.6**).

With tertiary alkyltrifluoroborate **1u** in hand, radical addition to caffeine **1v** and benzothiophene **1w** was carried out. The development of the Cook approach to 3° alkyltrifluoroborates thus allows access to an even greater array of coupling partners.

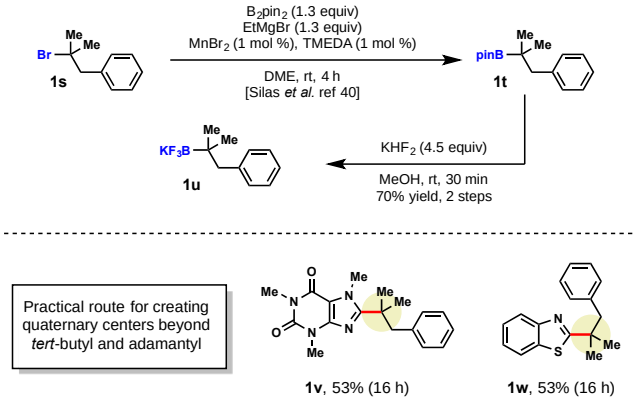


**Figure 9.6.** Synthesis of Tertiary Alkyltrifluoroborate[a]

[a]Reactions were run with heteroarene (1.0 equiv), tertiary alkyltrifluoroborate (1.0 equiv), MesAcr (5 mol %), $K_2S_2O_8$ (2.0 equiv), trifluoroacetic acid (1.0 equiv) in MeCN/$H_2O$ (1:1) on 0.3 mmol scale.

In further studies, a wide range of alkyltrifluoroborates were found to be suitable partners in the developed photoredox Minisci conditions (**Figure 9.7**). First, a benzyl protected □-alkoxyalkyltrifluoroborate afforded **2a** in 58% yield. Additional examples of unactivated, secondary alkyl radical precursors could be appended as in **2b**–**2j**. For **2b**, the successful addition of fluorinated isosteres is encouraging, given the well-documented propensity these subunits have for modulating solubility and binding affinity in medicinal chemistry.[30] For **2c**–**2e,** the tetrahydropyranyl and piperidinyl moieties are commonly introduced ring structures that serve as useful probes for H-bond donors/acceptors in SAR efforts.[31]

To the best of our knowledge, primary alcohols appended to the radical coupling partner have not been reported in Minisci-type reactions, perhaps owing to their propensity to undergo H-atom abstraction alpha to the hydroxyl group. Therefore, we were pleased to obtain **2f**, albeit in low yield. Of note, this selecitivity is complementary to the MacMillan group's work on alcohols as radical precursors in photoredox-Minisci couplings.[16a] A further exploration of 5- and 4-membered heterocycles (**2g**–**2i**) was conducted with promising results, where tetrahydrofuran **2g** was afforded in 34% yield, but access to pyrrolidine **2h** was not successful. For azetidine **2i**, standard solvent conditions provided only trace amounts of product, but switching to DCE/$H_2O$ (1:1) proved to be beneficial. Cyclopropyltrifluoroborate, although unproductive in previously reported photoredox/Ni dual cross-coupling methods,[20b] afforded **2j**, albeit in 20% yield. 1-Adamantyltrifluoroborate has never been used in Minisci-type alkylations. Using the standard conditions, **2k** was isolated in 45% yield. Lastly, chemoselective radical addition to the isoquinoline was observed for **2l** despite containing an alternate site for alkylation within the alkyltrifluoroborate partner.

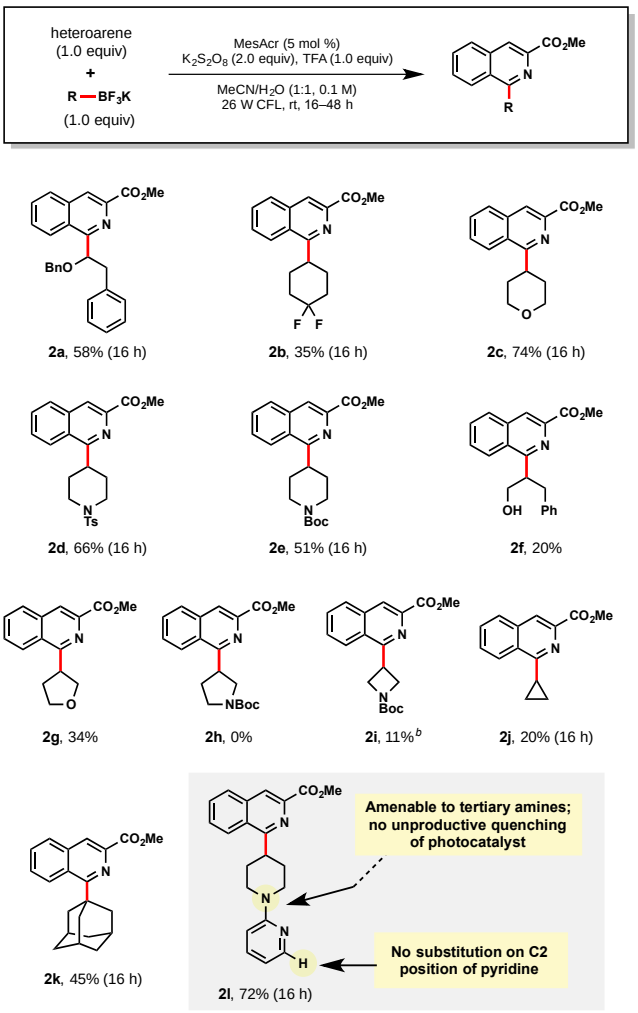


**Table 9.7.** Secondary and Tertiary Alkyltrifluoroborate Scope[a]

[a]Reactions were run with methyl isoquinoline-3-carboxylate (1.0 equiv), alkyltrifluoroborate (1.0 equiv), MesAcr (5 mol %), $K_2S_2O_8$ (2.0 equiv), trifluoroacetic acid (1.0 equiv) in $MeCN/H_2O$ (1:1) on 0.3 mmol scale. [b]Reaction run in $DCE/H_2O$ (1:1).

Moving forward, this Minisci process was anticipated to be broadly applicable even to primary alkyltrifluoroborates, which possess relatively high oxidation potentials (**Table 9.8**). As an initial foray, we first investigated whether stabilized primary α-alkoxymethyltrifluoroborates could be competent partners in this process (**3a**–**3d**). Non-stabilized alkyl radicals were also demonstrated in examples **3e**–**3l**. Notably, **3j** contains an *ortho* bromide functional handle for further elaboration. Unfortunantely, electron deficient 3,3,3-trifluoropropyltrifluoroborate afforded **3l** in diminished

yield, likely because of its high oxidation potential and resultant destabilization of the generated radical. These trends track with other recent reports specifically targeting more electrophilic radicals.[13e, 16b]

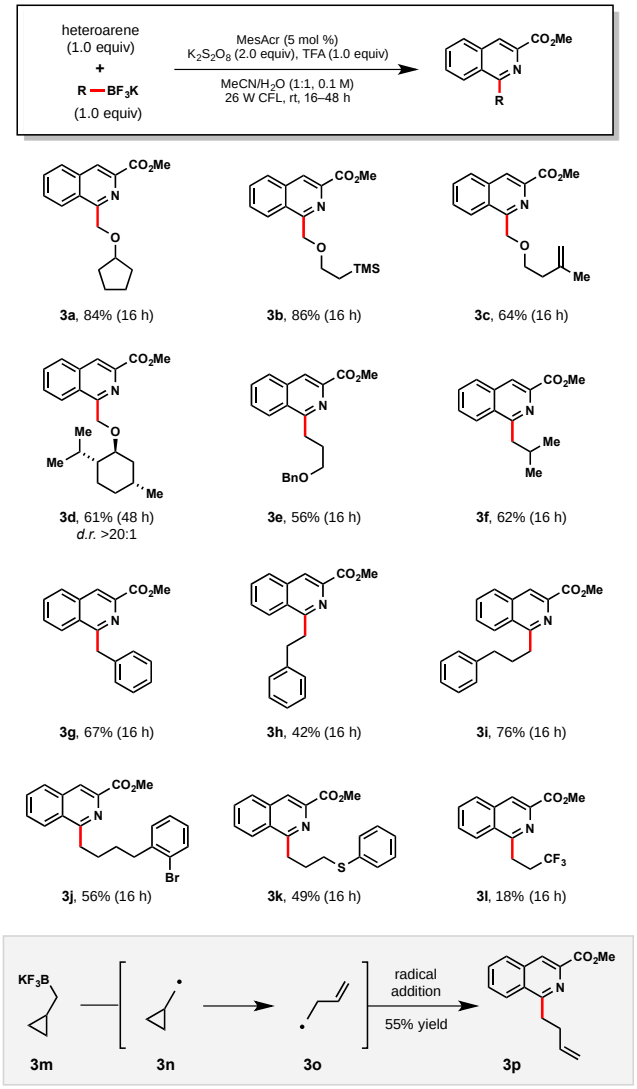


**Figure 9.8.** Primary Alkyltrifluoroborate Scope[a]

[a]Reactions were run with 1-methyl isoquinolinecarboxylate (1.0 equiv), primary alkyltrifluoroborate (1.0 equiv), MesAcr (5 mol %), $K_2S_2O_8$ (2.0 equiv), trifluoroacetic acid (1.0 equiv) in MeCN/$H_2O$ (1:1) on 0.3 mmol scale.

As would be anticipated for the radical-based mechanism of the transformation, cyclopropylcarbinyltrifluoroborate **3m** formed the corresponding radical **3o** after SET oxidation

and subequent rearrangement. Following radical addition to the activated heteroaromatic, **3p** was isolated in 55% yield.

The diversity of the process was expanded to underline the potential for widespread utility (**Figure 9.9**). Lepidine was coupled with a variety of stabilized α-alkoxy (**4a**–**4c**) and unstabilized (**4d**–**4f**) radicals. With quinoline, C2 regiospecificity was again observed (**4d**, **4e**), albeit in diminished yields. This is particularly noteworthy given the challenges associated with avoiding complex mixtures of isomers in prior Minisci-type reaction reports.[32] With heteroarene cores such as pyridine (**4f**), benzothiazole (**4g**), indazole (**4h**), and quinazolinone (**4i**, **4j**), exceptional yields were observed. When exploring reactivity with caffeine, methylcyclopentyltrifluoroborate afforded **4k** in 37% yield. Additionally, a secondary alkyl radical was successfully appended to functionally rich quinine as demonstrated in **4l**.

Given the success of this method, the use of this technology for selective ligand modifications was envisioned (**Figure 9.10**). As a case study, difunctionalization of a bipyridine-based ligand was selected for further investigation. Commonly these ligands are synthesized through the $S_NAr$ reaction of strong nucleophiles (e.g., *tert*-butyllithium) to a fluorinated bipyridine precursor, which is unfortunate given the popularity of these ligands in Cu and Ni catalysis.[33] In contrast to the use of such pyrophoric alkylating agents, bench-stable alkyltrifluoroborates represent an attractive alternative. Gratifyingly, unfunctionalized substructures **5a** and **5c** were converted to the desired products in 84% and 68% yields, respectively. Pyridine ligands are also valuable for the synthesis of iridium photocatalysts. Under the same reaction conditions, heteroarene **5e** afforded mono-alkylated product **5f** in 82% yield. When tridentate ligand terpyridine **5g** was subjected to the standard conditions with two equivalents of *tert*-butyltrifluoroborate, mono-alkylated **5h** was formed exclusively.[34]

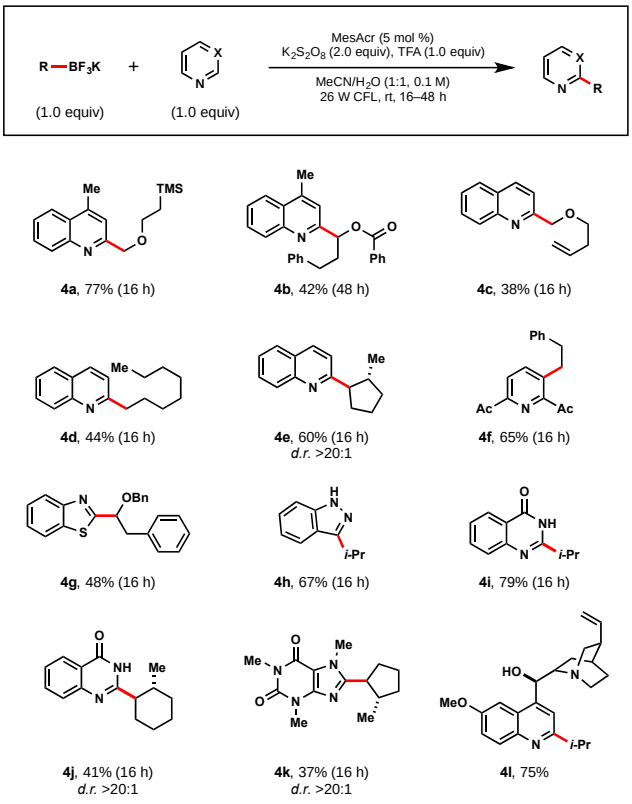


**Figure 9.9.** Demonstration of Diversity[a]

[a]Reactions were run with heteroarene (1.0 equiv), primary alkyltrifluoroborate (1.0 equiv), MesAcr (5 mol %), $K_2S_2O_8$ (2.0 equiv), trifluoroacetic acid (1.0 equiv) in $MeCN/H_2O$ (1:1) on 0.3 mmol scale.

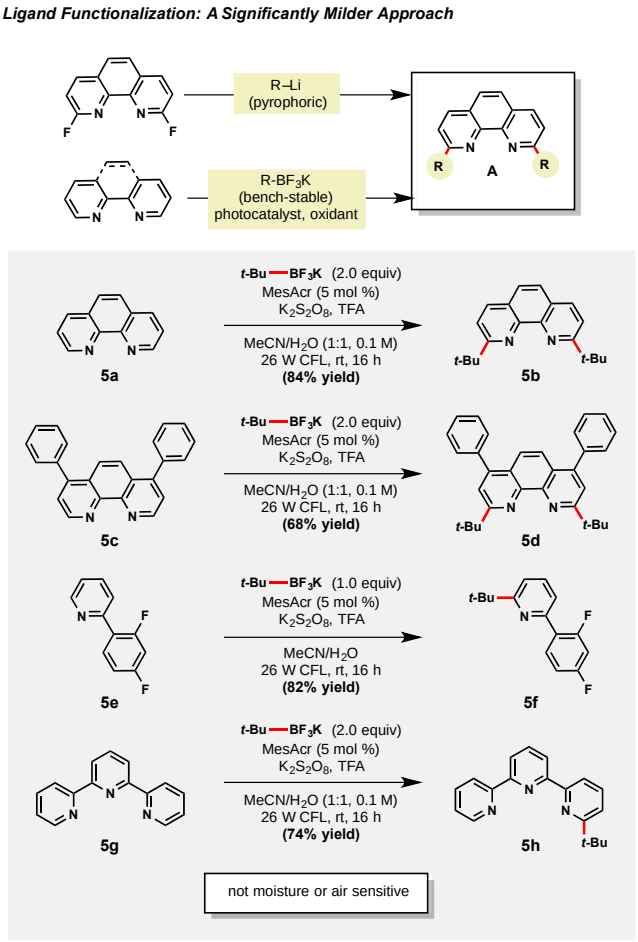


**Figure 9.10.** Mild Alternative for Ligand Synthesis[a]

[a]Reactions were run with heteroarene (1.0 equiv), alkyltrifluoroborate (1.0 or 2.0 equiv), MesAcr (5 mol %), $K_2S_2O_8$ (2.0 equiv), trifluoroacetic acid (1.0 equiv) in MeCN/$H_2O$ (1:1) on 0.3 mmol scale.

Although medicinal chemists have principally capitalized on late-stage Minisci heteroarene alkylation,[9] it can be advantageous to introduce alkyl substitution earlier in a synthetic sequence.[35] Using the present protocol, the installation of alkyl subunits on brominated heteroarenes provides an excellent opportunity to highlight divergency in molecular synthesis. Furthermore, the halides installed within a variety of heteroarenes can serve a dual purpose: they may serve as an electronic bias for regioselective alkylations *ortho* to the halide,[13d] and they provide a functional handle for cross-coupling reactions, etc.[5c] To initiate studies to explore these concepts, a number of brominated heteroarenes were selected (Table 7). First, pyrimidine **6a** was paired with an □-

alkoxyalkyltrifluoroborate to yield exclusively the C4-substituted product. When moving to pyridines, a mixture of C2 and C6 alkylation occurred with tosyl-protected piperidinyltrifluoroborate (**6b**). Conversely, with primary alkyltrifluoroborates, only the C2-substituted products were observed in examples **6c** and **6d**. Chloride substitution was also well tolerated as demonstrated in **6d**. When 4-bromoisoquinoline was utilized as a substrate, a mixture of regioisomers **6e** and **6f** was generated. Based on these studies, **6a** and **6c** contrast favorably with previous findings in the Baran laboratory wherein regiomeric isomers were observed for heteroaryl bromides and chlorides.[13d]

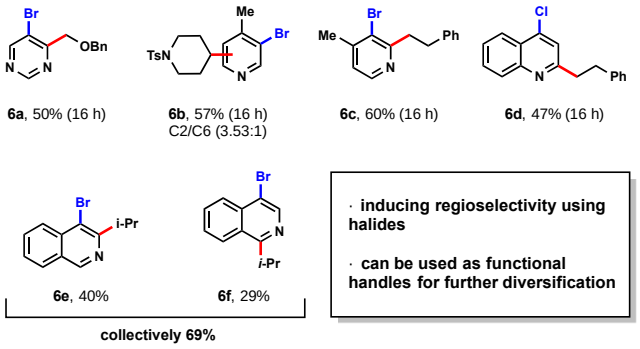


**Figure 9.11.** Utilizing Heteroarenes with Functional Handles

As a final highlight of the potential for late-stage functionalization, camptothecin (CPT) was selected as an appropriate, complex heteroarene. In medicinal chemistry, CPT was identified as an anti-cancer drug candidate because of its cytotoxic activity in a number of cancer cell lines. Unfortunately, poor solubility was a systemic issue and prevented moving it forward as a drug candidate.[36] To tackle this challenge, various alkyl substitutions on the C7 position of the natural alkaloid were introduced, resulting in a more highly-active clinical candidate.[37] Although SAR studies were conducted to confirm the promising properties of alkyl decoration, the alkyl substituents were primarily limited to simple alkyl groups (e.g., methyl, ethyl) using the corresponding alkyl bromides, peroxide, and acid under thermal conditions.[38] To demonstrate the

advantages of using the currently developed, mild photoredox conditions, secondary and primary alkyltrifluoroborates were selected as reagents for generation of analogues. As displayed in **Figure 9.12**, primary α-alkoxyalkyl subunits could be incorporated, along with secondary alkyl moieties (**7a**, **7b**).

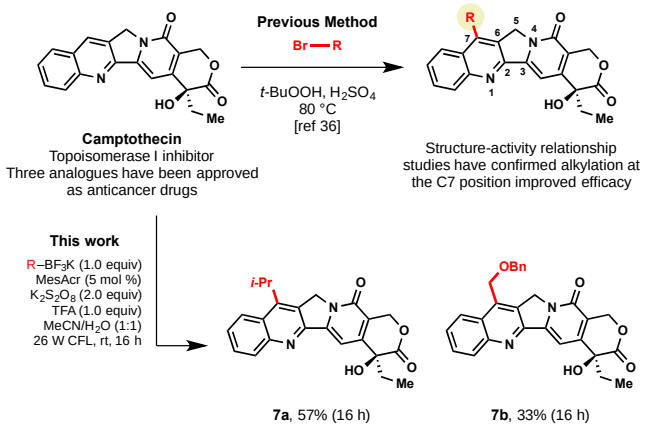


**Figure 9.12.** Camptothecin Analogues: Examples of Late-Stage Functionalization

Based on our previous reports on Minisci chemistry[12] and the results provided herein, it became clear that the use of alkyltrifluoroborates provided clear advantages in terms of both reactivity (permitting a single equivalent of radical precursor to be employed) and regioselectivity in heteroarene alkylation. Given these observations, it seemed that there might be some inherent advantage to the generation of $BF_3$ byproduct during the course of the reaction. Two distinct possibilities were considered: (1) the $BF_3$ produced was intimately involved with the generated radical, providing a shepherding effect in delivering the radical with enhanced selectivity, or (2) the $BF_3$ was coordinating to the heteroarene prior to the radical addition, activating the heteroaryl substrate and enhancing preference for one site beyond the activation provided by the added protic acid.

To assess the first hypothesis, DFT calculations were performed to determine the effective "bond order" for radical association with $BF_3$ in solution. This potential interaction was of particular interest as this escorting effect has little precedent in the chemical literature; currently, there are only examples of nitrogen- and oxygen-centered radicals interacting with $BF_3$ in solution.[39] Indeed, preliminary calculations suggest that a strong preference exists for the free radical over a $BF_3$-bound complex in solution (see experimental). Noting this lack of association, we were quick to investigate an alternative hypothesis.

To probe each of the possible heteroarene complexes, we prepared stoichiometric solutions of one of our successful, selective substrates, quinoline, with no additive, trifluoroacetic acid (TFA) alone, $BF_3$ alone, and finally TFA with added $BF_3$, hoping to probe the effect of coordination on the proton and carbon shifts of heteroarene and provide some rationale for the differences between our chemistry and previously established protocols.

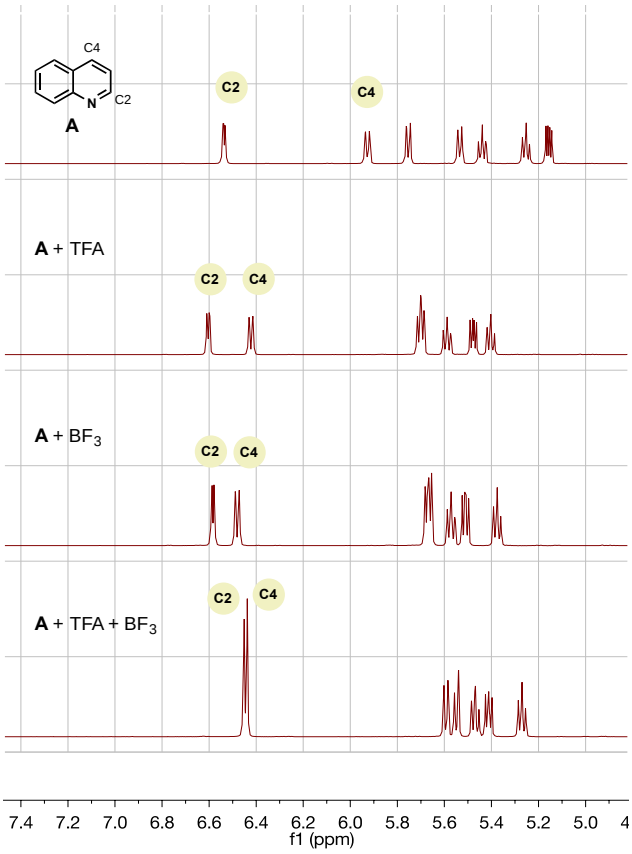


**Figure 9.13.** $^{1}$H NMR of **A** with trifluoroacetic acid and/or $BF_3$ additive in $CD_3CN/H_2O$ (1:1). TMS was used as a reference.

For trifluoroacetic acid, a clear downfield shift was observed in the H2 and H4 protons of quinoline (**Figure 9.13**). Likewise, for the addition of $BF_3$, a slightly less pronounced, but clear, downfield shift was also observed for the same protons. However, the combination of both additives together produced a wholly different shift in resonances to a unique heteroarene species.

Most importantly, the carbon shifts of C2 relative to C4 (the best indicator of relative radicophilicity) possess enhanced differentiation in relative downfield shift (~3 ppm) in comparison to the $BF_3$ and trifluoroacetic acid complexes alone (~1 ppm) (**Figure 9.14**). Based on these chemical shifts, it is reasonable to suggest the C2 position is preferentially activated over the C4

position[40] under the reaction conditions, resulting in the enhanced regioselective mono-alkylation observed for the quinoline system and, by analogy, many of the other systems in which alkyltrifluoroborates appear uniquely reactive and selective (*vida infra*).

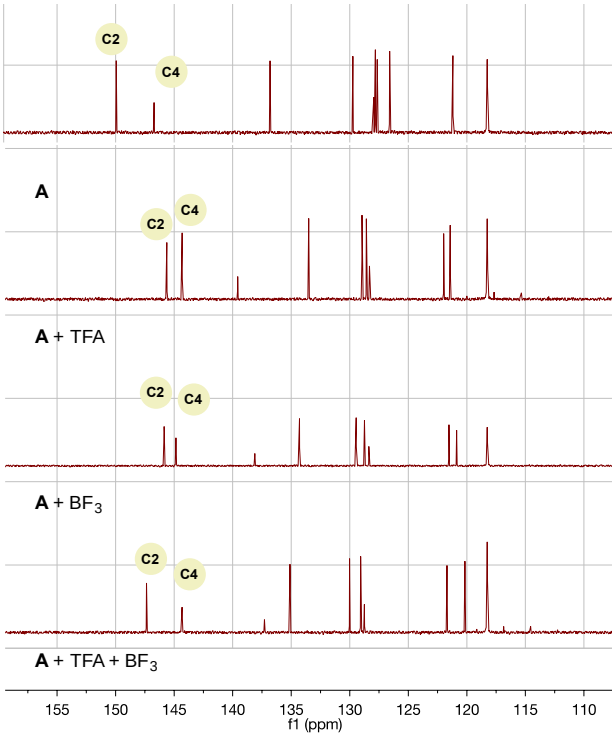


**Figure 9.14**. $^{13}C$ NMR of **A** with trifluoroacetic acid and/or $BF_3$ additive in $CD_3CN/H_2O$ (1:1). $CD_3CN$ solvent peak was used as a reference.

To probe these findings further, we hoped that the use of alternative radical precursors (e.g., sulfinate salts or carboxylic acids) could be used in the presence and/or absence of $BF_3$ to achieve the same desired regioselectivity. Unfortunately, under our standard conditions, sulfinate salts were universally ineffective, and carboxylic acids gave the same regiomixture, even with added $BF_3$. Given this current ambiguity, this enhanced reactivity and regioselectivity appears to remain unique to the trifluoroborate precursors (see experimental).

At this time, although it is impossible to propose a structure for this *distinct,* activated species, we speculate that $BF_3$ activation of either the heteroarene π-cloud[41] or polarization of the trifluoroacetic acid[42] to increase its effective pKa may be responsible. Intriguingly, this type of dual activation could perhaps be more broadly operative in the selective alkylation of other heteroaryl cores.

## 9.3 Conclusion

In summary, a mild, room temperature method for the introduction of a diverse palette of alkyl groups has been developed. Under a set of unified reaction conditions, primary, secondary, and tertiary alkyltrifluoroborates can be employed in photoredox Minisci chemistry for the first time. This chemistry makes use of an inexpensive, mild oxidant, organic photocatalyst, and requires *only one equivalent of alkyl radical partner*, providing one of the most cost efficient and sustainable approaches to date. Additionally, enhanced regioselectivity was observed compared to current "state of the art" Minisci-type alkylations. Both of these phenomena may be related to the *synchronized, catalytic* generation of radicals in conjunction with the in situ generation of $BF_3$ during the course of the reaction. The resultant method has been demonstrated broadly with respect to the heteroarene and alkyltrifluoroborate partners. Furthermore, access to bipyridine-type ligands as well as the late stage diversification of medicinally relevant substructures has been showcased. Finally, NMR studies provided support for a unique, highly activated species caused by the formation of $BF_3$ upon the single-electron oxidation of alkyltrifluoroborates. Currently, further mechanistic studies are underway to elucidate the nature of this complex.

Given the wide array of commercially available alkyltrifluoroborates, in addition to those synthesized by our laboratory and emerging from other groups, this approach provides a valuable

contribution to the Minisci-type alkylation literature that is both highly competitive with, and complementary to, existing protocols. As alkyltrifluoroborates are well behaved, bench stable salts, these reagents will continue to serve as useful "radicals in a bottle" for synthetic chemists.

## 9.4 Experimental

NMR Spectra ($^{1}H$, $^{13}C$, $^{19}F$) were performed at 298 K. $^{1}H$ NMR spectra were referenced to residual non-deuterated chloroform (δ 7.26) in $CDCl_3$, residual DMSO-$d_5$ (δ 2.50) in DMSO-$d_6$, acetone-$d_5$ (δ 2.09) in acetone-$d_6$, and residual MeCN-$d_2$ (δ 1.94) in MeCN-$d_3$. $^{13}C$ NMR spectra were referenced to $CDCl_3$ (δ 77.2) and DMSO-$d_6$ (δ 39.5). Reactions were monitored by HPLC, GC/MS, $^{1}H$ NMR, and/or by TLC on silica gel plates (60 Å porosity, 250 μm thickness). TLC analysis was performed using hexanes/EtOAc as the eluant and visualized using UV light. Silica plugs utilized flash silica gel (60 Å porosity, 32–63 μm). Flash chromatography was accomplished using an automated system (visualizing at 254 nm, monitoring at 280 nm) with silica cartridges (60 Å porosity, 20–40 μm). Solvents were purified by use of drying cartridges through a solvent delivery system. Melting points (°C) are uncorrected.

Deuterated NMR solvents were either used as purchased (DMSO-$d_6$) or were stored over 4Å molecular sieves and/or $K_2CO_3$ ($CDCl_3$). $Na_2SO_4$, $MgSO_4$, MeOH, $CH_2Cl_2$, MeCN, pentane, $Et_2O$, trifluoroacetic acid, and $K_2S_2O_8$ were used as purchased. Heteroarenes were purchased from commercial suppliers and used without further purification. MeCN/$H_2O$ was degassed thoroughly with $N_2$ and stored under $N_2$. The photocatalyst *N*-Me-9-mesityl acridinium tetrafluoroborate was donated by Pfizer and used without further purification.

### General Procedure

To a 4.0 mL vial, alkyltrifluoroborate (0.30 mmol, 1.0 equiv), heteroarene (0.30 mmol, 1.0 equiv), photocatalyst (6.2 mg, 0.015 mmol, 0.05 equiv), and $K_2S_2O_8$ (162.2 mg, 0.60 mmol, 2.0 equiv) were added. Open to air, a mixture of 3.0 mL MeCN/$H_2O$ (1:1) was added, followed by trifluoroacetic acid (34.2 mg, 0.30 mmol, 1.0 equiv). The mixture was stirred under white LEDs for 5–48 h under a fan. The reaction mixture was quenched with saturated $NaHCO_3$ and extracted with $CH_2Cl_2$ (3 x 20 mL). The organic extracts were combined and concentrated on Celite. The crude mixture was purified by silica gel column chromatography.

## HETEROARENE SCOPE WITH *TERT*-BUTYLTRIFLUOROBORATE


2-(*tert*-Butyl)quinoline (**1a**). **Physical state:** 40 mg, 72% yield, clear oil. **$^1$H NMR** (500 MHz, $CDCl_3$) δ 8.07 (d, *J* = 8.6 Hz, 2H), 7.77 – 7.75 (m, 1H), 7.68 – 7.64 (m, 1H), 7.54 – 7.52 (m, 1H), 7.49 – 7.46 (m, 1H), 1.48 (s, 9H). **$^{13}$C NMR** (126 MHz, $CDCl_3$) δ 169.4, 147.6, 136.0, 129.6, 129.1, 127.4, 126.6, 125.7, 118.3, 38.3, 30.3. **HRMS (ES+)** m/z calc. for $C_{13}H_{16}N$ [M+H] 186.1283, found 186.1280. **FT-IR** ($cm^{-1}$, neat, ATR) 2961, 1619, 1601, 1565, 1504, 1364, 1138, 1103, 829, 756, 478.

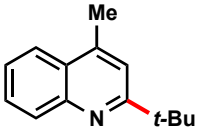


2-(*tert*-Butyl)-4-methylquinoline (**1b**) Reference: Gabriele, B.; Mancuso, R; Salerno, G.; Ruffolo, G.; Plastina, P. *J. Org. Chem.* **2007**, *72*, 6873. **Physical state:** 57 mg, 95% yield, clear oil. **$^1$H NMR** (500 MHz, $CDCl_3$) δ 8.05 (d, *J* = 8.4 Hz, 1H), 7.93-7.90 (m, 1H), 7.66-7.64 (m, 1H), 7.49-7.27 (m,

1H), 7.34 (s, 1H), 2.67 (s, 3H), 1.47 (s, 9H). **$^{13}$C NMR** (126 MHz, $CDCl_3$) δ 169.1, 147.5, 143.7, 130.1, 128.8, 126.7, 125.5 123.5, 119.0, 38.1, 30.3, 19.1.

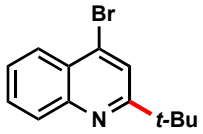


4-Bromo-2-(*tert*-butyl)quinoline (**1c**) **Physical state:** 68 mg, 86% yield, clear oil. **$^{1}$H NMR** (500 MHz, $CDCl_3$) δ 8.10 (d, *J* = 8.4 Hz, 1H), 8.06-8.02 (m, 1H), 7.79 (s, 1H), 7.69 (dd *J* = 7.7, 7.6 Hz, 1H), 7.54 (dd, *J* = 7.7, 7.6 Hz, 1H), 1.45 (s, 9H). **$^{13}$C NMR** (126 MHz, $CDCl_3$) δ 169.5, 148.3, 134.0, 130.1, 130.0, 127.0, 126.5, 126.2, 122.5, 38.3, 30.2. **HRMS (ES+)** m/z calc. for $C_{13}H_{15}BrN$ [M+H] 264.0388, found 264.0397. **FT-IR** ($cm^{-1}$, neat, ATR) 2957, 1585, 1488, 820, 756.

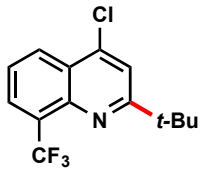


2-(*tert*-Butyl)-4-chloro-8-(trifluoromethyl)quinoline (**1d**). **Physical state:** 78 mg, 70% yield, clear oil. **$^{1}$H NMR** (500 MHz, $CDCl_3$) δ 8.38 (d, *J* = 8.4 Hz, 1H), 8.08 (d, *J* = 7.2 Hz, 1H), 7.68 (s, 1H), 7.61-7.59 (m, 1H), 1.47 (s, 9H). **$^{13}$C NMR** (126 MHz, $CDCl_3$) δ 170.5, 144.9, 142.6, 128.5 (q, *J* = 5.5 Hz), 128.3 (q, *J* = 29.1 Hz), 128.2, 125.3, 125.2, 123.1, 119.3, 38.9, 29.9. **HRMS (ES+)** m/z calc. for $C_{14}H_{14}ClF_3N$ [M+H] 288.0767, found 288.0762. **FT-IR** ($cm^{-1}$, neat, ATR) 2965, 1592, 1489, 1463, 1293, 1145, 1118, 766.

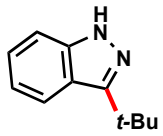

3-(*tert*-Butyl)-1*H*-indazole (**1e**). Reference: Li, P.; Wu, C.; Zhao, J.; Rogness, D. C.; Shi, F. *J. Org. Chem.* **2012**, *77*, 3149. **Physical state:** 41 mg, 80% yield, clear oil. **$^{1}$H NMR** (500 MHz, $CDCl_3$) δ 10.07 (bs, 1H), 7.91 (d, *J* = 8.2 Hz, 1H), 7.44 (d, *J* = 8.2 Hz, 1H), 7.36-7.33 (m, 1H), 7.14-7.11 (m, 1H), 1.55 (s, 9H). **$^{13}$C NMR** (126 MHz, $CDCl_3$) δ 154.8, 142.1, 126.3, 122.3, 120.7, 120.0, 110.1, 34.0, 30.2. **HRMS (ES+)** m/z calc. for $C_{11}H_{15}N_2$ [M+H] 175.1235, found 175.1229. **FT-IR** ($cm^{-1}$, neat, ATR) 3146, 3112, 3073, 2963, 2928, 2900, 1342, 739.

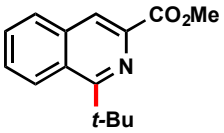


Methyl 1-(*tert*-Butyl)isoquinoline-3-carboxylate (**1g**). **Physical state:** 55 mg isolated, 77% yield, white solid (mp = 55 °C). **$^{1}$H NMR** (500 MHz, $CDCl_3$) δ 11.64 (s, 1H), 8.50 – 8.45 (m, 2H), 7.72 – 7.70 (m, 2H), 4.06 (s, 3H), 1.64 (s, 9H). **$^{13}$C NMR** (126 MHz, $CDCl_3$) δ 171.8, 158.0, 155.4, 129.6, 129.3, 129.0, 128.8, 127.3, 124.3, 118.4, 52.9, 39.7, 31.2. **FT-IR** ($cm^{-1}$, neat, ATR) 2953, 1661, 1450, 1337, 1242, 1164.

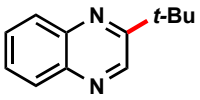


2-(*tert*-Butyl)quinoxaline (**1h**). **Physical state:** 39 mg, 70% yield, clear oil. **$^{1}$H NMR** (500 MHz, $CDCl_3$) δ 8.99 (s, 1H), 8.06 (dd, *J* = 8.0, 3.8 Hz, 2H), 7.71 (m, 2H), 1.52 (s, 9H). **$^{13}$C NMR** (126 MHz, $CDCl_3$) δ 163.8, 143.6, 141.8, 141.0, 129.8, 129.5, 129.1, 129.0, 37.4, 29.9. **HRMS (ES+)** m/z calc. for $C_{12}H_{15}N_2$ [M+H] 186.1157, found 186.1158. **FT-IR** ($cm^{-1}$, neat, ATR) 2963, 1558, 1492, 1464, 1365, 1237, 1155, 1128, 1097, 1014, 968, 761, 607.

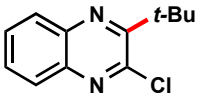

2-(*tert*-Butyl)-3-chloroquinoxaline (**1i**). **Physical state:** 28 mg isolated, 43% yield, clear oil. **$^{1}$H NMR** (500 MHz, $CDCl_3$) δ 8.99 (s, 1H), 8.07 – 8.05 (m, 2H), 7.74 – 7.68 (m, 2H), 1.52 (s, 9H). **$^{13}$C NMR** (126 MHz, $CDCl_3$) δ 163.8, 143.6, 141.8, 141.0, 129.8, 129.5, 129.1, 129.0, 37.4, 29.9. **HRMS (ES+)** m/z calc. for $C_{12}H_{15}ClN_2$ [M+H] 221.0846, found 221.0844. **FT-IR** ($cm^{-1}$, neat, ATR) 2977, 1167, 1104, 1008, 761.

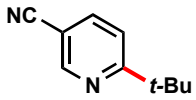


6-(*tert*-Butyl)nicotinonitrile (**1j**). **Physical state:** 42 mg, 89% yield, yellow oil. **$^{1}$H NMR** (500 MHz, $CDCl_3$) δ 8.82 (s, 1H), 7.87 (d, *J* = 8.2 Hz, 1H), 7.46 (d, *J* = 8.2 Hz, 1H), 1.38 (s, 9H). **$^{13}$C NMR** (126 MHz, $CDCl_3$) δ 174.1, 151.7, 139.5, 119.3, 117.3, 106.9, 38.4, 30.0. **HRMS (ES+)** m/z calc. for $C_{10}H_{13}N_2$ [M+H] 161.1079, found 161.1078. **FT-IR** ($cm^{-1}$, neat, ATR) 2960, 2050, 1721, 1596.

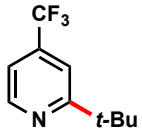


2-(*tert*-Butyl)-4-(trifluoromethyl)pyridine (**1k**). Reference: Stowers, K. J.; Fortner, K. C.; Sanford, M. S. *J. Am. Chem. Soc.* **2011**, *133*, 6541. **Physical state:** 58 mg, 95% yield, light yellow oil. **$^{1}$H NMR** (500 MHz, $CDCl_3$) δ 8.74 (d, *J* = 4.9 Hz, 1H), 7.53 (s, 1H), 7.31 (d, *J* = 5.0 Hz, 1H), 1.40 (d, *J* = 1.9 Hz, 9H). **$^{13}$C NMR** (126 MHz, $CDCl_3$) δ 171.2, 149.7, 138.7 (q, *J* = 34.0 Hz), 123.4 (q, *J* = 271.0), 116.4 (q, *J* = 4.0 Hz), 114.8, 114.81, 38.0, 30.2. **$^{19}$F NMR** (500 MHz) δ -64.70.

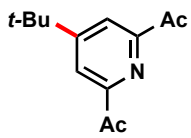

1,1'-(4-(*tert*-Butyl)pyridine-2,6-diyl)bis(ethan-1-one) (**1l**). **Physical state:** 48 mg, 73% yield, clear oil. **$^{1}$H NMR** (500 MHz, $CDCl_3$) δ 8.22 (s, 2H), 2.78 (s, 6H), 1.36 (s, 9H). **$^{13}$C NMR** (126 MHz, $CDCl_3$) δ 200.1, 162.9, 153.0, 122.0, 35.6, 30.6, 25.9. **HRMS (ES+)** m/z calc. for $C_{13}H_{18}NO_2$ [M+H] 220.1338, found 220.1334. **FT-IR** ($cm^{-1}$, neat, ATR) 2968, 2975, 1700, 1362, 1244, 1131, 610.

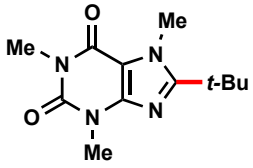


8-(*tert*-Butyl)-1,3,7-trimethyl-3,7-dihydro-1*H*-purine-2,6-dione (**1m**) **Physical state:** 52 mg, 70% yield, white solid (173 °C). **$^{1}$H NMR** (500 MHz, $CDCl_3$) δ 4.11 (s, 3H), 3.56 (s, 3H), 3.39 (s, 3H), 1.47 (s, 9H). **$^{13}$C NMR** (126 MHz, $CDCl_3$) δ 160.1, 155.8, 151.9, 147.1, 108.4, 34.3, 34.2, 29.7, 29.1, 28.0. **HRMS (ES+)** m/z calc. for $C_{12}H_{19}N_4O_2$ [M+H] 251.1508, found 251.1505. **FT-IR** ($cm^{-1}$, neat, ATR) 2974, 1699, 1656, 1543, 1492, 1428, 1364, 1240, 740.

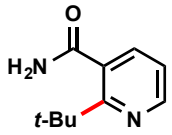


2-(*tert*-Butyl)nicotinamide **(1n**) Reference: Tada, M.; Yokoi, Y. *J. Heterocyclic Chem.* **1989**, *26*, 45. **Physical state:** 36 mg, 67% yield, light yellow solid (mp = 94 °C). **$^{1}$H NMR** (500 MHz, DMSO-$d_6$) δ 8.95 (d, *J* = 2.3 Hz, 1H), 8.17 – 7.99 (m, 2H), 7.51 (d, *J* = 8.2 Hz, 2H), 1.31 (s, 9H). **$^{13}$C NMR** (126 MHz, DMSO) δ 171.2, 166.5, 147.6, 135.6, 127.0, 118.5, 20.8, 14.1. **HRMS (ES+)** m/z calc. for $C_{10}H_{15}N_2O$ [M+H] 179.1184, found 179.1190. **FT-IR** ($cm^{-1}$, neat, ATR) 3433, 2253, 2127, 1667, 1394, 1051, 1023, 820, 760.

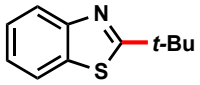


2-(*tert*-Butyl)benzo[*d*]thiazole (**1o**). **Physical state:** 38 mg, 66% yield, yellow oil. **$^{1}$H NMR** (500 MHz, $CDCl_3$) δ 8.00 (d, *J* = 8.2 Hz, 1H), 7.85 (d, *J* = 7.9 Hz, 1H), 7.46 – 7.43 (m, 1H), 7.35 – 7.32 (m, 1H), 1.53 (s, 9H). **$^{13}$C NMR** (126 MHz, $CDCl_3$) δ 182.0, 153.4, 135.1, 125.9, 124.6, 122.8, 121.6, 38.5, 30.9. **HRMS (ES+)** m/z calc. for $C_{11}H_{14}NS$ [M+H] 192.0847, found 192.0847. **FT-IR** ($cm^{-1}$, neat, ATR) 2965, 1513, 1438, 1044, 1008, 758.

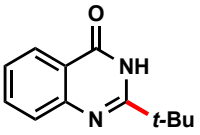


2-(*tert*-Butyl)quinazolin-4(3*H*)-one (**1p**). Reference: Li, Z.; Dong, J.; Chen, X.; Li, Q.; Zhou, Y.; Yin, S. -F. *J. Org*, *Chem.* **2015**, *80*, 9392. **Physical state:** 54 mg, 90% yield, white solid (mp = 110–113 °C). **$^{1}$H NMR** (500 MHz, $CDCl_3$) δ 11.40 (s, 1H), 8.29 (d, *J* = 7.6 Hz, 1H), 7.74 (d, *J* = 9.8 Hz, 2H), 7.45 (t, *J* = 7.6 Hz, 1H), 1.50 (s, 9H). **$^{13}$C NMR** (126 MHz, $CDCl_3$) δ 164.1, 162.3, 149.4, 134.6, 127.8, 126.4, 126.3, 120.7, 100.1, 37.6, 28.4. **HRMS (ES+)** m/z calc. for $C_{12}H_{15}N_2O$ [M+H] 203.1184, found 203.1183. **FT-IR** ($cm^{-1}$, neat, ATR) 3189, 3079, 2968, 1667, 1611, 772.

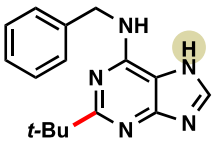


*N*-Benzyl-2-(*tert*-butyl)-7*H*-purin-6-amine (**1q**). **Physical state:** 67 mg, 79% yield, yellow solid (mp = 125–127 °C). **$^{1}$H NMR** (500 MHz, $CDCl_3$) δ 8.45 (s, 1H), 7.44 – 7.41 (m, 2H), (dd, *J* = 7.5, 7.5 Hz, 2H), 7.29 (d, *J* = 7.5 Hz, 1H), 6.12 (bs, 1H), 4.89 (s, 2H), 1.53 (s, 9H) (highlighted proton not observed). **$^{13}$C NMR** (126 MHz, $CDCl_3$) δ 160.7, 154.2, 151.6, 138.7, 128.8, 128.7, 128.2,

127.6, 100.1, 33.9, 29.6, 27.8. **HRMS (ES+)** m/z calc. for $C_{16}H_{20}N_5$ [M+H] 282.1719, found 282.1718. **FT-IR** ($cm^{-1}$, neat, ATR) 2972, 1619, 1598, 1351, 1299.

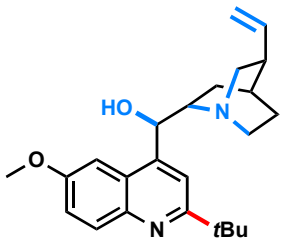


(1*R*)-(2-(*tert*-Butyl)-6-methoxyquinolin-4-yl)(5-vinylquinuclidin-2-yl)methanol (**1r**). Reference: Yardley, J. P.; Bright, R. E.; Rane, L.; Rees, R. W.; Russell, P. B.; Smith, H. *J. Med. Chem.* **1971**, *14*, 62. **Physical state:** 62 mg, 54% yield, light yellow oil. **$^1$H NMR** (500 MHz, $CDCl_3$) δ 7.98 (d, *J* = 9.2 Hz, 1H), 7.67 (s, 1H), 7.30 (d, *J* = 9.2 Hz, 1H), 7.20 (s, 1H), 5.73 (dt, *J* = 17.6, 9.0 Hz, 1H), 5.58 (s, 1H), 4.97 – 4.90 (m, 2H), 3.89 (s, 3H), 3.50 – 3.45 (m, 1H), 3.20 – 3.08 (m, 2H), 2.71 – 2.65 (m, 2H), 2.29 – 2.25 (m, 1H), 1.81 (s, 1H), 1.79 – 1.65 (m, 2H), 1.52 – 1.43 (m, 11H). **$^{13}$C NMR** (126 MHz, $CDCl_3$) δ 166.6, 157.4, 146.9, 143.8, 142.0, 131.9, 124.7, 120.9, 115.5, 114.6, 101.3, 72.6, 60.1, 57.3, 55.8, 43.5, 40.1, 38.1, 30.3, 28.1, 27.8, 21.6. **HRMS (ES+)** m/z calc. for $C_{24}H_{32}N_2O_2$ [M+H] 381.2536, found 381.2543. **FT-IR** ($cm^{-1}$, neat, ATR)2954, 1621, 1601, 1561, 1505, 1471, 1363, 1343, 1263, 1231, 1106, 1034, 911, 832, 734, 645.

**TERTIARY EXAMPLES**

---

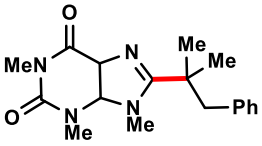


1,3,9-Trimethyl-8-(2-methyl-1-phenylpropan-2-yl)-3,9-dihydro-1H-purine-2,6-dione (**1v**).**Physical state:** 52 mg, 53% yield, pale yellow solid (mp = 101–103 °C). **$^1$H NMR** (500 MHz, $CDCl_3$) δ 7.23-7.21 (m, 3H), 6.88-6.85 (m, 2H), 3.80 (s, 3H), 3.56 (s, 3H), 3.41 (s, 3H), 3.03 (s,

2H), 1.51 (s, 6H). **$^{13}$C NMR** (126 MHz, $CDCl_3$) δ 158.7, 155.5, 146.9(4), 146.9(1), 137.4, 129.8, 128.1, 126.7, 107.7, 48.2, 39.4, 33.8, 29.5, 27.8, 27.2. **HRMS (ES+)** m/z calc. for $C_{17}H_{23}N_4O_2$ [M+H] 327.1821, found 327.1820. **FT-IR** ($cm^{-1}$, neat, ATR) 3055, 2987, 1758, 1699, 1656, 1422, 1040, 896, 733, 703.

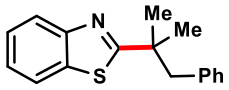


2-(2-Methyl-1-phenylpropan-2-yl)benzo[d]thiazole (**1w**). **Physical state:** 52 mg, 53% yield, pale yellow oil. **$^{1}$H NMR** (500 MHz, $CDCl_3$) δ 8.05 (d, *J* = 8.2 Hz, 1H), 7.86 (dd, *J* = 8.0, 0.5 Hz, 1H), 7.53 – 7.44 (m, 1H), 7.41 – 7.32 (m, 1H), 7.27 – 7.12 (m, 3H), 7.09 – 6.98 (m, 2H), 3.18 (s, 2H), 1.52 (s, 6H). **$^{13}$C NMR** (126 MHz, $CDCl_3$) δ 180.7, 153.2, 137.6, 134.8, 130.4, 127.8, 126.3, 125.7, 124.5, 122.7, 121.4, 49.5, 42.2, 28.0. **HRMS (ES+)** m/z calc. for $C_{17}H_{18}NS$ [M+H] 268.1160, found 268.1168. **FT-IR** ($cm^{-1}$, neat, ATR) 3028, 2927, 1505, 1495, 1385, 1280, 1005, 743, 687.

## SECONDARY AND TERTIARY ALKYLTRIFLUOROBORATE SCOPE

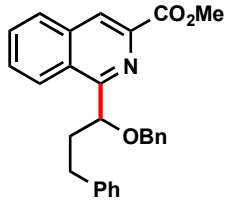


Methyl 1-(1-(Benzyloxy)-3-phenylpropyl)isoquinoline-3-carboxylate (**2a**). **Physical state:** 71 mg, 58% yield, clear oil. **$^{1}$H NMR** (500 MHz, $CDCl_3$) δ 8.88 (d, *J* = 8.5 Hz, 1H), 8.52 (s, 1H), 7.98 (d, *J* = 8.0 Hz, 1H), 7.78 – 7.76 (m, 1H), 7.70 – 7.66 (m, 1H), 7.41 – 7.35 (m, 1H), 7.31 – 7.22 (m, 7H), 7.19 – 7.12 (m, 2H), 5.26 – 5.22 (m, 1H), 4.52 – 4.43 (m, 2H), 4.08 (s, 3H), 3.12 – 2.96 (m, 1H), 2.78 – 2.72 (m, 1H), 2.61 – 2.53 (m, 1H), 2.33 – 2.25 (m, 1H). **$^{13}$C NMR** (126 MHz, $CDCl_3$) δ 166.4, 161.5, 141.7, 140.2, 138.1, 136.5, 130.6, 129.1, 128.8, 128.4, 128.2, 128.1(9), 127.8, 127.7,

127.5, 126.2, 125.7, 124.2, 85.1, 71.5, 52.8, 37.8, 32.5. **HRMS (ES+)** m/z calc. for $C_{27}H_{25}NO_3Na$ [M+Na] 434.1732, found 434.1734. **FT-IR** ($cm^{-1}$, neat, ATR) 3052, 2950, 1736, 1717, 1373, 1147, 1027, 908, 782, 490.

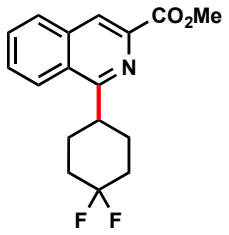


Methyl 1-(4,4-Difluorocyclohexyl)isoquinoline-3-carboxylate (**2b**). **Physical state:** 32 mg, 35% yield, yellow oil. **$^1$H NMR** (500 MHz, $CDCl_3$) δ 8.43 (s, 1H), 8.22 (d, *J* = 7.8 Hz, 1H), 7.98 – 7.95 (m, 1H), 7.77 – 7.72 (m, 2H), 4.02 (s, 3H), 3.72 – 3.58 (m, 1H), 2.40 – 2.27 (m, 4H), 2.16 – 1.90 (m, 4H). **$^{13}$C NMR** (126 MHz, $CDCl_3$) δ 166.7, 163.5, 163.5, 140.6, 136.1, 130.4, 129.4, 129.4, 129.3, 127.6, 125.2, 124.5, 123.3, 122.9, 121.4, 52.7, 39.7, 28.3, 28.2. **$^{19}$F NMR** (471 MHz, $C_6D6$) δ 2.26 (d, *J* = 235.5 Hz), 6.03 (d, *J* = 235.5 Hz). **HRMS (ES+)** m/z calc. for $C_{17}H_{17}F_2NO_3$ [M+Na] 328.1125, found 328.1124. **FT-IR** ($cm^{-1}$, neat, ATR) 2951, 1736, 1450, 1374, 1236, 1205, 1101, 956, 784.

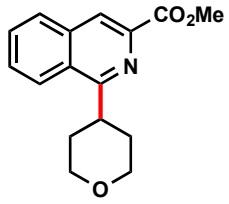


Methyl 1-(Tetrahydro-2H-pyran-4-yl)isoquinoline-3-carboxylate (**2c**). **Physical state:** 60 mg, 74% yield, white semi-solid. **$^1$H NMR** (300 MHz, $CDCl_3$) δ 8.45 (s, 1H), 8.35 – 8.22 (m, 1H), 8.07 – 7.90 (m, 1H), 7.76 (dt, *J* = 5.4, 3.2 Hz, 2H), 4.20 (dd, *J* = 11.4, 2.6 Hz, 2H), 4.05 (s, 3H), 3.93 – 3.56 (m, 3H), 2.51 – 2.23 (m, 2H), 1.91 (dd, *J* = 13.4, 1.5 Hz, 2H). **$^{13}$C NMR** (126 MHz, $CDCl_3$) δ 166.9, 163.9, 141.0, 140.9, 136.3, 130.4, 129.4, 127.7, 124.6, 122.9, 68.3, 52.8, 39.4, 32.0. **HRMS**

**(ES+)** m/z calc. for $C_{16}H_{17}NO_3Na$ [M+Na] 294.1106, found 294.1111. **FT-IR** ($cm^{-1}$, neat, ATR) 2962, 1589, 1489, 1387, 850.

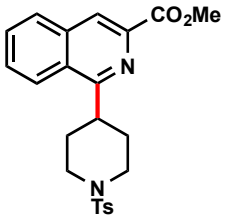


Methyl 1-(1-Tosylpiperidin-4-yl)isoquinoline-3-carboxylate (**2d**). **Physical state:** 84 mg, 66% yield, pale yellow solid (mp = dec ~195 $^0$C). **$^1$H NMR** (500 MHz, $CDCl_3$) δ 8.42 (s, 1H), 8.11 (d, *J* = 8.5 Hz, 1H), 7.97 (d, *J* = 8.0 Hz, 1H), 7.74-7.66 (m, 4H), 7.37 (d, *J* = 8.0 Hz, 2H), 4.03 (s, 3H), 3.98 (d, *J* = 11.5 Hz, 2H), 3.53-3.48 (m, 1H), 2.62-2.52 (m, 2H), 2.48 (s, 3H), 2.45-2.32 (m, 2H), 2.05-2.03 (m, 2H). **$^{13}$C NMR** (126 MHz, $CDCl_3$) δ 166.5, 162.9, 143.3, 140.6, 133.3, 130.2, 129.5, 129.2, 129.1(9), 128.8, 127.8, 127.4, 124.1, 122.8, 52.6, 46.3, 39.1, 30.4, 21.5. **HRMS (ES+)** m/z calc. for $C_{23}H_{25}N_2O_4S$ [M+H] 425.1535, found 425.1531. **FT-IR** ($cm^{-1}$, neat, ATR) 2962, 1589, 1489, 1387, 850.

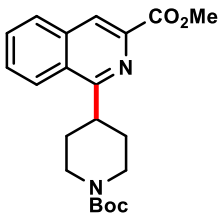


Methyl 1-(1-(*tert*-Butoxycarbonyl)piperidin-4-yl)isoquinoline-3-carboxylate (**2e**). **Physical state:** 41 mg, 51% yield, white semi-solid. **$^1$H NMR** (500 MHz, $CDCl_3$) δ 8.42 (s, 1H), 8.25 (d, *J* = 7.3 Hz, 1H), 8.06 – 7.89 (m, 1H), 7.84 – 7.64 (m, 2H), 4.32 (m, 2H), 4.02 (s, 3H), 3.72 (t, *J* = 11.4 Hz, 1H), 2.99 (m, 2H), 2.03 (m, 4H), 1.49 (s, 9H). **$^{13}$C NMR** (126 MHz, $CDCl_3$) δ 166.8, 164.1, 154.9, 140.8, 136.3, 130.5, 129.4, 127.8, 124.6, 122.9, 79.6, 58.5, 52.8, 40.2, 31.2, 28.7. **HRMS (ES+)** m/z calc. for $C_{21}H_{27}N_2O_4$ [M+H] 371.1971, found 371.1984. **FT-IR** ($cm^{-1}$, neat, ATR) 2962, 1589, 1489, 1387, 850.

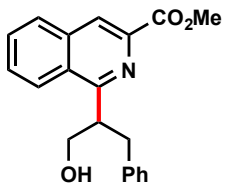


Methyl 1-(1-Hydroxy-3-phenylpropan-2-yl)isoquinoline-3-carboxylate (**2f**). **Physical state:** 20 mg, 20% yield, clear oil. **$^1$H NMR** (500 MHz, $CDCl_3$) δ 8.48 (s, 1H), 8.13 (d, *J* = 8.4 Hz, 1H), 7.98 (d, *J* = 8.1 Hz, 1H), 7.78 – 7.75 (m, 1H), 7.72 – 7.68 (m, 1H), 7.34 – 7.18 (m, 5H), 5.65 (d, *J* = 10.1 Hz, 1H), 4.19 (d, *J* = 11.3 Hz, 1H), 4.05 (s, 3H), 3.98 – 3.93 (m, 1H), 3.88 – 3.84 (m, 1H), 3.39 – 3.34 (m, 1H), 3.12 – 3.07 (m, 1H). **$^{13}$C NMR** (126 MHz, $CDCl_3$) δ 166.2, 165.4, 140.1, 139.6, 136.3, 131.1, 129.9, 129.5, 129.4, 128.7, 128.0, 126.5, 125.0, 123.2, 63.1, 53.0, 44.4, 38.1. **HRMS (ES+)** m/z calc. for $C_{20}H_{20}NO_2$ [M+H] 322.1443, found 322.1452. **FT-IR** ($cm^{-1}$, neat, ATR) 1734, 1451, 1244, 1207, 749, 702.

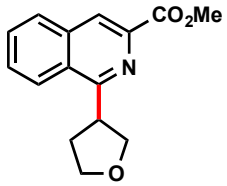


Methyl 1-(Tetrahydrofuran-3-yl)isoquinoline-3-carboxylate (**2g**). Physical state: 43.7 mg, 34% yield, colorless oil. **$^1$H NMR** (500 MHz, $CDCl_3$) δ 8.45 (s, 1H), 8.27 (d, *J* = 7.2 Hz, 1H), 8.00 – 7.93 (m, 1H), 7.80 – 7.70 (m, 2H), 4.42 – 4.32 (m, 2H), 4.25 – 4.15 (m, 2H), 4.08 – 3.96 (m, 4H), 2.79 – 2.57 (m, 1H), 2.53 – 2.31 (m, 1H). **$^{13}$C NMR** (126 MHz, $CDCl_3$) δ 166.5, 161.2, 136.0, 134.0, 130.4, 129.4, 129.0, 128.4, 124.8, 123.0, 112.7, 77.2, 68.8, 52.6, 43.4, 32.1. **HRMS (ES+)** m/z calc. for $C_{15}H_{16}NO_3$ [M+H] 258.1130, found 258.1140. **FT-IR** ($cm^{-1}$, neat, ATR) 2987, 2870, 1208, 1063, 861, 837.

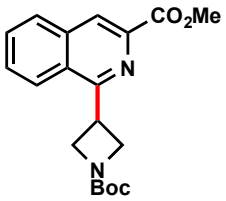


Methyl 1-(1-(*tert*-Butoxycarbonyl)azetidin-3-yl)isoquinoline-3-carboxylate (**2i**). **$^{1}$H NMR** (500 MHz, $CDCl_3$) δ 8.50 (s, 1H), 8.01 (d, *J* = 8.1 Hz, 1H), 7.89 (d, *J* = 8.2 Hz, 1H), 7.82 – 7.71 (m, 2H), 4.64 – 4.45 (m, 5H), 4.05 (s, 3H), 1.47 (s, 9H). **$^{13}$C NMR** (126 MHz, $CDCl_3$) δ 166.3, 159.7, 156.3, 140.3, 135.9, 130.7, 129.7, 129.2, 127.7, 124.3, 123.4, 79.4, 52.6, 33.0, 28.3. **HRMS (ES+)** m/z calc. for $C_{19}H_{23}N_2O_4$ [M+H] 343.1658, found 343.1666. **FT-IR** ($cm^{-1}$, neat, ATR) 2987, 2870, 1208, 1063, 861, 837.

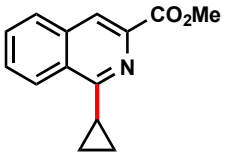


Methyl 1-Cyclopropylisoquinoline-3-carboxylate (**2j**). **Physical state:** 21 mg, 31% yield, clear oil. **$^{1}$H NMR** (500 MHz, $CDCl_3$) δ 8.54 – 8.44 (m, 1H), 8.36 (s, 1H), 8.01 – 7.89 (m, 1H), 7.76 – 7.73 (m, 2H), 4.01 (s, 3H), 2.75 (tt, *J* = 8.5, 4.9 Hz, 1H), 1.37 – 1.34 (m, 2H), 1.17 – 1.13 (m, 2H). **$^{13}$C NMR** (126 MHz, $CDCl_3$) δ 166.9, 162.5, 140.7, 135.8, 130.6, 129.5, 129.4, 129.0, 125.6, 122.3, 52.9, 14.4, 9.3. **HRMS (ES+)** m/z calc. for $C_{14}H_{13}NO_2$ [M+H] 228.1025, found 228.1019. **FT-IR** ($cm^{-1}$, neat, ATR) 2951, 1737, 1321, 1269, 1244, 988.

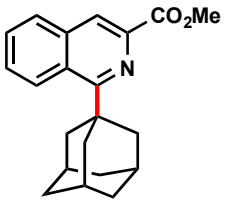


Methyl 1-((3*r*,5*r*,7*r*)-Adamantan-1-yl)isoquinoline-3-carboxylate (**2k**). **Physical state:** 43.4 mg, 45% yield, off-white solid (mp = 210–212 °C). **$^{1}$H NMR** (500 MHz, $CDCl_3$) δ 11.63 (s, 1H), 8.73

– 8.71 (m, 1H), 8.58 – 8.38 (m, 1H), 7.71 – 7.70 (m, 2H), 4.08 (s, 3H), 2.38 (s, 6H), 2.21 (s, 3H), 1.89 (m, 6H). **$^{13}$C NMR** (126 MHz, $CDCl_3$) δ 171.6, 157.4, 155.1, 129.5, 129.1, 128.6, 128.4, 126.8, 124.2, 118.5, 52.7, 42.2, 41.9, 37.0, 29.1. **HRMS (ES+)** m/z calc. for $C_{21}H_{24}NO_2$ [M+H] 322.1807, found 322.1797. **FT-IR** ($cm^{-1}$, neat, ATR) 2951, 1737, 1321, 1269, 1244, 988.

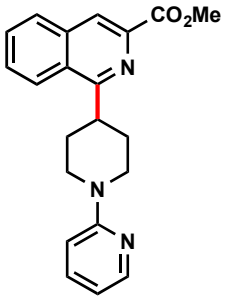


Methyl 1-(1-(Pyridin-2-yl)piperidin-4-yl)isoquinoline-3-carboxylate (**2l**). **Physical state:** 75 mg, 72% yield, yellow solid (mp = 154–157 °C). **$^{1}$H NMR** (500 MHz, $CDCl_3$) δ 8.42 (s, 1H), 8.31 (s, 1H), 8.20 (s, 1H) 7.98 (d, *J* = 3.5 Hz, 1H), 7.76 – 7.74 (m, 2H), 7.49 – 7.45 (m, 1H), 6.74 (d, *J* = 8.5 Hz, 1H), 6.60-6.59 (m, 1H), 4.52 (d, *J* = 12.5 Hz, 2H), 4.00 (s, 3H), 3.82-3.80 (m, 1H), 3.12 (t, *J* = 12.5 Hz, 2H), 2.34-2.26 (m, 2H), 2.10-2.04 (m, 2H). **$^{13}$C NMR** (126 MHz, $CDCl_3$) δ 166.9, 164.3, 159.6, 148.1, 140.9, 137.5, 136.3, 130.4, 129.4, 129.4, 127.8, 124.8, 122.9, 112.8, 107.4, 52.8, 45.8, 40.7, 31.2. **HRMS (ES+)** m/z calc. for $C_{21}H_{22}N_3O_2$ [M+H] 348.1712, found 348.1714. **FT-IR** ($cm^{-1}$, neat, ATR) 2962, 1589, 1489, 1387, 850, 1236.

**PRIMARY ALKYLTRIFLUOROBORATE COUPLING**

---

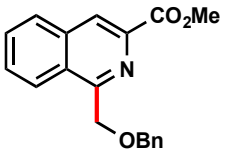

Methyl 1-((Benzyloxy)methyl)isoquinoline-3-carboxylate (**3a**). **Physical state:** 52 mg, 56% yield, clear oil. **$^{1}$H NMR** (500 MHz, $CDCl_3$) δ 8.45 (s, 1H), 8.21 (d, *J* = 8.3 Hz, 1H), 8.03 (d, *J* = 7.4 Hz, 2H), 7.96 (d, *J* = 8.1 Hz, 1H), 7.74 (t, *J* = 7.5 Hz, 1H), 7.68 (t, *J* = 7.6 Hz, 1H), 7.54 (t, *J* = 7.0 Hz, 1H), 7.42 (t, *J* = 7.6 Hz, 2H), 4.41 (t, *J* = 6.4 Hz, 2H), 4.04 (s, 3H), 3.46 (t, *J* = 7.9 Hz, 2H). **$^{13}$C NMR** (126 MHz, $CDCl_3$) δ 166.8, 166.8, 162.5, 140.8, 136.1, 133.0, 133.0, 130.7, 130.6, 129.7, 129.7, 129.52, 129.1, 128.5, 125.6, 123.1, 100.1, 77.4, 77.2, 76.9, 64.9, 64.8, 62.6, 53.0, 35.3, 29.4, 29.0, 26.4, 25.4. **HRMS (ES+)** m/z calc. for $C_{19}H_{17}NO_3$ [M+Na] 308.1287, found 308.1283. **FT-IR** ($cm^{-1}$, neat, ATR) 2951, 1716, 1315, 1275, 1246, 712.

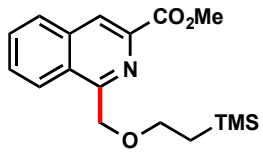


Methyl 1-((2-(Trimethylsilyl)ethoxy)methyl)isoquinoline-3-carboxylate (**3b**). **Physical state:** 61 mg, 86% yield, clear oil. **$^{1}$H NMR** (500 MHz, $CDCl_3$) δ 8.53 (s, 1H), 8.47 (d, *J* = 7.9 Hz, 1H), 7.96 (d, *J* = 7.9 Hz, 1H), 7.78 – 7.71 (m, 2H), 5.13 (s, 2H), 4.04 (s, 3H), 3.76 – 3.55 (m, 2H), 1.11 – 0.90 (m, 2H), -0.03 (s, 9H). **$^{13}$C NMR** (126 MHz, $CDCl_3$) δ 166.5, 158.4, 140.4, 136.3, 130.9, 129.6, 129.0, 128.6, 126.6, 124.7, 73.5, 68.5, 52.9, 18.5, -1.3. **HRMS (ES+)** m/z calc. for $C_{17}H_{23}NO_3Si$ [M+Na] 340.1345, found 340.1347. **FT-IR** ($cm^{-1}$, neat, ATR) 2951, 1740, 1719, 1247, 1208, 860.

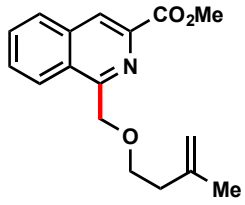


Methyl 1-(((3-Methylbut-3-en-1-yl)oxy)methyl)isoquinoline-3-carboxylate (**3c**). **Physical state:** 55 mg, 64% yield, clear oil. **$^{1}$H NMR** (500 MHz, $CDCl_3$) δ 8.54 (s, 1H), 8.49 (d, *J* = 8.2 Hz, 1H), 7.96 (d, *J* = 7.9 Hz, 1H), 7.78 – 7.70 (m, 2H), 5.16 (s, 2H), 4.74 (s, 1H), 4.70 (s, 1H), 4.04 (s, 3H),

3.68 (t, *J* = 6.9 Hz, 2H), 2.32 (t, *J* = 6.9 Hz, 2H), 1.68 (s, 3H). **$^{13}$C NMR** (126 MHz, $CDCl_3$) δ 166.4, 158.2, 142.8, 140.3, 136.3, 131.0, 129.6, 129.0, 128.6, 126.6, 124.8, 111.7, 74.2, 69.4, 53.0, 37.9, 22.7. **HRMS (ES+)** m/z calc. for $C_{17}H_{19}NO_3Na$ [M+Na] 308.1263, found 308.1263. **FT-IR** ($cm^{-1}$, neat, ATR) 2950, 1738, 1450, 1295, 1209, 1109.

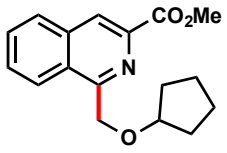


Methyl 1-((Cyclopentyloxy)methyl)isoquinoline-3-carboxylate (**3d**). **Physical state:** 72 mg, 84% yield, clear viscous oil. **$^{1}$H NMR** (500 MHz, $CDCl_3$) δ 8.52 (s, 1H), 8.45 (d, *J* = 7.7 Hz, 1H), 7.94 (d, *J* = 7.4 Hz, 1H), 7.74 (s, 2H), 5.10 (s, 2H), 4.13 (s, 1H), 4.04 (s, 3H), 1.52 (m, 8H). **$^{13}$C NMR** (126 MHz, $CDCl_3$) δ 166.5, 158.6, 140.3, 136.3, 130.9, 129.6, 129.1, 128.6, 126.7, 124.7, 82.3, 77.4, 77.2, 76.9, 72.5, 53.0, 32.4, 23.6. **HRMS (ES+)** m/z calc. for $C_{17}H_{20}NO_3$ [M+H] 286.1443, found 286.1454. **FT-IR** ($cm^{-1}$, neat, ATR) 2952, 1737, 1334, 1246, 1110, 1096, 791.

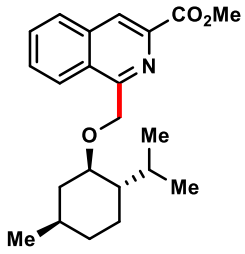


Methyl 1-((((1*R*,2*S*,5*R*)-2-Isopropyl-5-methylcyclohexyl)oxy)methyl)isoquinoline-3-carboxylate (**3e**). **Physical state:** 65 mg, 61% yield, clear oil. **$^{1}$H NMR** (500 MHz, $CDCl_3$) δ 8.53 (s, 1H), 8.46 (d, *J* = 7.7 Hz, 1H), 7.95 (d, *J* = 8.2 Hz, 1H), 7.79 – 7.70 (m, 2H), 5.30 (d, *J* = 11.3 Hz, 1H), 5.04 (d, *J* = 11.3 Hz, 1H), 4.04 (s, 3H), 3.28 (td, *J* = 10.5, 4.1 Hz, 1H), 2.07 – 2.03 (m, 1H), 1.67 – 1.54 (m, 2H), 1.43 – 1.17 (m, 3H), 0.97 – 0.75 (m, 9H), 0.43 (d, *J* = 6.9 Hz, 3H). **$^{13}$C NMR** (126 MHz, $CDCl_3$) δ 166.6, 158.9, 140.3, 136.3, 130.9, 129.4, 129.2, 128.6, 127.0, 124.8, 79.3, 71.3, 52.9,

48.5, 40.4, 34.6, 31.6, 25.3, 23.1, 22.5, 21.1, 15.7. **HRMS (ES+)** m/z calc. for $C_{22}H_{29}NO_3Na$ [M+Na] 378.2047, found 378.2045. **FT-IR** ($cm^{-1}$, neat, ATR) 2954, 2869, 1722, 1244, 1108, 984, 907, 688, 646.

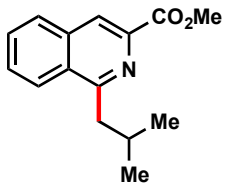


Methyl 1-Isobutylisoquinoline-3-carboxylate (**3f**). **Physical state:** 45 mg, 62% yield, clear oil. **$^1$H NMR** (500 MHz, $CDCl_3$) δ 8.43 (s, 1H), 8.21 (d, *J* = 8.0 Hz, 1H), 7.94 (d, *J* = 7.8 Hz, 1H), 7.71 (m, 2H), 4.03 (s, 3H), 3.25 (d, *J* = 7.3 Hz, 2H), 2.32 (m, 1H), 0.98 (d, *J* = 6.7 Hz, 6H). **$^{13}$C NMR** (126 MHz, $CDCl_3$) δ 166.9, 162.5, 140.8, 136.1, 130.5, 129.2, 129.0, 129.0, 125.9, 122.8, 52.9, 44.1, 29.8, 22.9. **HRMS (ES+)** m/z calc. for $C_{15}H_{17}NO_2Na$ [M+Na] 266.1157, found 266.1161. **FT-IR** ($cm^{-1}$, neat, ATR) 2955, 1737, 1718, 1294, 1242, 1205.

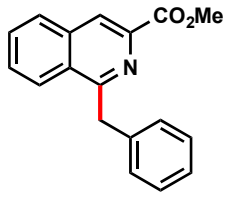


Methyl 1-Benzylisoquinoline-3-carboxylate (**3g**). **Physical state:** 56 mg, 67% yield, clear oil. **$^1$H NMR** (500 MHz, $CDCl_3$) δ 8.51 (s, 1H), 8.16 (d, *J* = 8.4 Hz, 1H), 7.95 (d, *J* = 8.1 Hz, 1H), 7.73 – 7.68 (m, 1H), 7.64 – 7.60 (m, 1H), 7.27 – 7.20 (m, 4H), 7.19 – 7.13 (t, *J* = 7.0 Hz, 1H), 4.78 (s, 2H), 4.07 (s, 3H). **$^{13}$C NMR** (126 MHz, $CDCl_3$) δ 166.7, 160.9, 140.8, 139.2, 136.4, 130.7, 129.6, 129.0, 128.8, 128.7 128.7, 126.5, 126.4, 123.7, 53.0, 42.6. **HRMS (ES+)** m/z calc. for $C_{18}H_{16}NO_2$ [M+H] 278.1181, found 278.1171. **FT-IR** ($cm^{-1}$, neat, ATR) 2949, 1736, 1568, 1438, 1242, 1208, 1150, 1106, 742, 692.

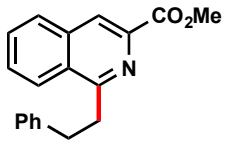


Methyl 1-Phenethylisoquinoline-3-carboxylate (3**h**). **Physical state:** 28 mg, 32% yield, clear oil. **$^{1}$H NMR** (500 MHz, $CDCl_3$) δ 8.47 (s, 1H), 8.19 (d, *J* = 8.2 Hz, 1H), 7.96 (d, *J* = 7.9 Hz, 1H), 7.78 – 7.66 (m, 2H), 7.32 – 7.15 (m, 5H), 4.06 (s, 3H), 3.76 – 3.62 (m, 2H), 3.28 – 3.15 (m, 2H). **$^{13}$C NMR** (126 MHz, $CDCl_3$) δ 166.8, 166.8, 162.0, 141.8, 140.8, 136.1, 130.7, 129.5, 129.1, 128.6, 128.6, 126.2, 125.5, 123.2, 53.0, 37.4, 35.6 (one aryl carbon peak overlaps). **HRMS (ES+)** m/z calc. for $C_{19}H_{18}NO_2$ [M+H] 314.1157, found 314.1157. **FT-IR** ($cm^{-1}$, neat, ATR) 2949, 1737, 1716, 1240, 1208, 749.

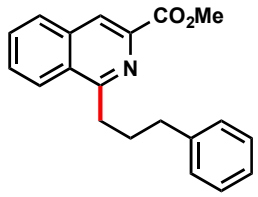


Methyl 1-(3-Phenylpropyl)isoquinoline-3-carboxylate (**3i**). **Physical state:** 76% yield, clear oil. **$^{1}$H NMR** (500 MHz, $CDCl_3$) δ 8.44 (s, 1H), 8.06 (d, *J* = 8.3 Hz, 1H), 7.94 (d, *J* = 8.0 Hz, 1H), 7.76 – 7.68 (m, 2H), 7.35 – 7.26 (m, 2H), 7.25 – 7.16 (m, 3H), 4.05 (s, 3H), 3.48 – 3.27 (m, 2H), 2.81 (t, *J* = 7.7 Hz, 2H), 2.26 – 2.19 (m, 2H). **$^{13}$C NMR** (126 MHz, $CDCl_3$) δ 166.8, 162.8, 142.1, 140.8, 136.1, 130.6 129.4, 129.0, 128.7, 128.5, 128.5, 126.0, 125.6, 123.1, 53.0, 36.1, 35.2, 31.6. **HRMS (ES+)** m/z calc. for $C_{20}H_{20}NO_2$ [M+H] 306.1494, found 306.1492. **FT-IR** ($cm^{-1}$, neat, ATR) 2949, 1736, 1716, 1242, 1209, 747.

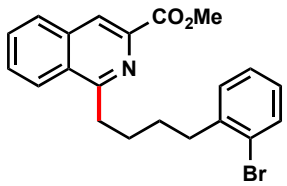

Methyl 1-(4-(2-Bromophenyl)butyl)isoquinoline-3-carboxylate (**3j**). **Physical state:** 67 mg, 56% yield, clear oil. **$^1$H NMR** (500 MHz, $CDCl_3$) δ 8.44 (s, 1H), 8.20 (d, *J* = 8.0 Hz, 1H), 7.95 (d, *J* = 7.8 Hz, 1H), 7.75 – 7.70 (m, 2H), 7.51 (d, *J* = 8.0 Hz, 1H), 7.24 – 7.19 (m, 2H), 7.03 (s, 1H), 4.04 (s, 3H), 3.42 (t, *J* = 8.1 Hz, 2H), 2.85 – 2.76 (m, 2H), 2.01 – 1.90 (m, 2H), 1.85 – 1.76 (m, 2H). **$^{13}$C NMR** (126 MHz, $CDCl_3$) δ 166.8, 162.9, 141.7, 140.8, 136.1, 132.9, 130.6, 130.5, 129.4, 129.0, 128.5, 127.6, 125.7, 124.6, 123.0, 53.0, 36.2, 35.7, 30.2, 29.8. **HRMS (ES+)** m/z calc. for $C_{21}H_{20}BrNO_2$ [M+Na] 420.0575, found 420.0576. **FT-IR** ($cm^{-1}$, neat, ATR) 2946, 1735, 1438, 1239, 1207, 1020, 748.

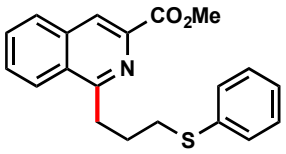


Methyl 1-(3-(Phenylthio)propyl)isoquinoline-3-carboxylate (3**k**) **Physical state:** 50 mg, 49% yield, clear oil. **$^1$H NMR** (500 MHz, $CDCl_3$) δ 8.44 (s, 1H), 8.15 (d, *J* = 8.4 Hz, 1H), 7.95 (d, *J* = 8.1 Hz, 1H), 7.76 – 7.70 (m, 1H), 7.70 – 7.64 (m, 1H), 7.36 (d, *J* = 7.7 Hz, 2H), 7.31 – 7.21 (m, 2H), 7.19 – 7.14 (m, 1H), 4.04 (s, 3H), 3.58 – 3.46 (m, 2H), 3.11 (t, *J* = 7.0 Hz, 2H), 2.30 – 2.21 (m, 2H). **$^{13}$C NMR** (126 MHz, $CDCl_3$) δ 166.7, 161.9, 140.7, 136.5, 136.1, 130.7, 129.6, 129.4, 129.0, 128.5, 126.1 125.6, 123.2, 53.0, 34.4, 33.6, 29.0 (one aryl peak overlaps). **HRMS (ES+)** m/z calc. for $C_{20}H_{20}NO_2S$ [M+H] 338.1215, found 338.1198. **FT-IR** ($cm^{-1}$, neat, ATR) 2950, 1737, 1716, 1449, 1325, 1294, 1243, 1210.

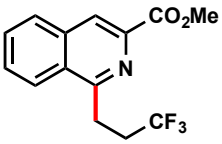


Methyl 1-(3,3,3-Trifluoropropyl)isoquinoline-3-carboxylate (**3l**). **Physical state:** 15 mg, 18% yield, viscous oil. **$^1$H NMR** (500 MHz, $CDCl_3$) δ 8.48 (s, 1H), 8.20 (d, *J* = 8.6 Hz, 1H), 8.06 – 7.93 (m, 1H), 7.86 – 7.74 (m, 2H), 4.05 (s, 3H), 3.68 – 3.57 (m, 2H), 2.96 – 2.77 (m, 2H). **$^{13}$C NMR** (126 MHz, $CDCl_3$) δ 166.5, 158.7, 140.6, 136.0, 131.1, 130.1, 129.3, 128.4, 124.8, 123.7, 53.1,

32.5 (q, *J* = 29.0 Hz), 29.0, 27.4. **$^{19}$F NMR** (471 MHz, $CDCl_3$) δ -66.42. **HRMS (ES+)** m/z calc. for $C_{14}H_{12}F_3NO_2Na$ [M+Na] 306.0718, found 306.0721. **FT-IR** ($cm^{-1}$, neat, ATR) 3071, 1715, 1240, 1126.

**TANDEM RING OPENING EXAMPLE**

---

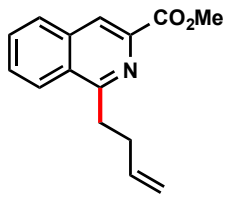


Methyl 1-(But-3-en-1-yl)isoquinoline-3-carboxylate (**3p**). **Physical state:** 40 mg, 55% yield, crystalline powder (mp = 54–57 °C). **$^1$H NMR** (500 MHz, $CDCl_3$) δ 8.44 (s, 1H), 8.21 (d, *J* = 7.9 Hz, 1H), 7.95 (d, *J* = 7.9 Hz, 1H), 7.76 – 7.68 (m, 2H), 6.05 – 5.90 (m, 1H), 5.12 (d, *J* = 17.0 Hz, 1H), 5.01 (d, *J* = 10.2 Hz, 1H), 4.04 (s, 3H), 3.47 (t, *J* = 8.2 Hz, 2H), 2.70 – 2.60 (m, 2H). **$^{13}$C NMR** (126 MHz, $CDCl_3$) δ 166.7, 162.3, 140.8, 137.8, 136.1, 130.6, 129.5, 129.1, 128.5, 125.6, 123.1, 115.3, 53.0, 35.0, 33.8. **HRMS (ES+)** m/z calc. for $C_{15}H_{15}NO_2$ [M+Na] 264.1000, found 264.0998. **FT-IR** ($cm^{-1}$, neat, ATR) 1748, 1656, 1596, 1157.

**MIXED TABLE**

---

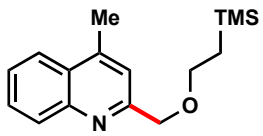

4-Methyl-2-((2-(Trimethylsilyl)ethoxy)methyl)quinoline (**4a**). Reference: Molander, G. A.; Colombel, V.; Braz, V. *Org. Lett.* **2011**, *13*, 1852. **Physical state:** 62 mg, 77% yield, clear oil. **$^1$H NMR** (500 MHz, $CDCl_3$) δ 8.05 (d, *J* = 8.4 Hz, 1H), 7.98 (d, *J* = 8.3 Hz, 1H), 7.71 – 7.66 (m, 1H), 7.55 – 7.51 (m, 1H), 7.46 (s, 1H), 4.74 (s, 2H), 3.72 – 3.63 (m, 2H), 2.71 (s, 3H), 1.11 – 1.03 (m, 2H), -0.03 (s, 9H). **$^{13}$C NMR** (126 MHz, $CDCl_3$) δ 159.3, 147.5, 145.0, 129.7, 129.3, 127.7, 126.1, 123.8, 120.2, 74.1, 68.6, 19.0, 18.5, -1.2. **FT-IR** ($cm^{-1}$, neat, ATR) 2953, 1603, 1249, 1101, 850, 836, 757.

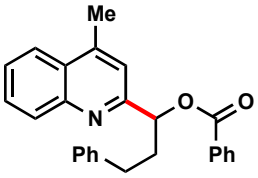


1-(4-Methylquinolin-2-yl)-3-phenylpropyl benzoate (**4b**). **Physical state:** 48 mg, 42% yield, clear oil. **$^1$H NMR** (500 MHz, $CDCl_3$) δ 8.15 (d, *J* = 7.7 Hz, 2H), 8.10 (d, *J* = 8.4 Hz, 1H), 7.97 (d, *J* = 8.3 Hz, 1H), 7.72 – 7.69 (m, 1H), 7.62 – 7.59 (m, 1H), 7.56 – 7.52 (m, 1H), 7.51 – 7.47 (m, 2H), 7.34 (s, 1H), 7.30 – 7.12 (m, 5H), 6.20 (dd, *J* = 8.3, 5.1 Hz, 1H), 2.90 – 2.78 (m, 2H), 2.69 (s, 3H), 2.60 – 2.45 (m, 2H). **$^{13}$C NMR** (126 MHz, $CDCl_3$) δ 166.1, 159.7, 147.6, 145.3, 141.5 133.3, 130.3, 130.0, 129.4, 128.8, 128.6, 128.4, 127.8, 126.5, 126.4, 126.1, 123.8, 119.1, 36.9, 32.1, 19.1. **HRMS (ES+)** m/z calc. for $C_{26}H_{23}NO_2$ [M+Na] 404.1626, found 404.1630. **FT-IR** ($cm^{-1}$, neat, ATR) 1719, 1602, 1451, 1270, 1111, 1070, 1027, 713.

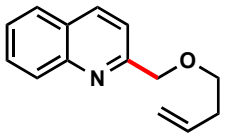


2-((But-3-en-1-yloxy)methyl)quinoline (4**c**). **Physical state:** 24 mg, 38% yield, clear oil. **$^1$H NMR** (500 MHz, $CDCl_3$) δ 8.18 (d, *J* = 8.4 Hz, 1H), 8.05 (d, *J* = 8.7 Hz, 1H), 7.82 (d, *J* = 8.4 Hz, 1H),

7.72 – 7.68 (m, 1H), 7.64 – 7.61 (m, 1H), 7.54 – 7.51 (m, 1H), 5.92 – 5.84 (m, 1H), 5.15 – 5.06 (m, 2H), 4.82 (s, 2H), 3.65 (t, *J* = 6.6 Hz, 2H), 2.45 (m, 2H). **$^{13}$C NMR** (126 MHz, $CDCl_3$) δ 159.6, 147.7, 136.9, 135.3, 129.7, 129.1, 127.8, 127.7, 126.4, 119.5, 116.7, 74.6, 70.5, 34.4. **HRMS (ES+)** m/z calc. for $C_{14}H_{16}NO$ [M+H] 214.1232, found 214.1234. **FT-IR** ($cm^{-1}$, neat, ATR) 2858, 1601, 1506, 1428, 1359, 1106, 996, 916, 829, 784, 755, 618.

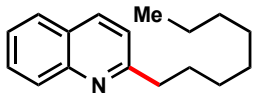


2-Octylquinoline (**4d**). **Physical state:** 32 mg, 44% yield, yellow oil. **$^{1}$H NMR** (500 MHz, $CDCl_3$) δ 8.80 (d, *J* = 4.4 Hz, 1H), 8.11 (d, *J* = 8.4 Hz, 1H), 8.04 (d, *J* = 8.4 Hz, 1H), 7.71 – 7.68 (m, 1H), 7.57 – 7.54 (m, 1H), 7.23 (d, *J* = 4.3 Hz, 1H), 3.09 – 3.04 (m, 2H), 1.80 – 1.73 (m, 2H), 1.47 – 1.41 (m, 2H), 1.40 – 1.17 (m, 8H), 0.88 (t, *J* = 6.6 Hz, 3H). **$^{13}$C NMR** (126 MHz, $CDCl_3$) δ 150.4, 148.9, 148.5, 130.4, 129.1, 127.8, 126.3, 123.8, 120.9, 32.3, 32.0, 30.3, 29.9, 29.6, 29.4, 22.8, 14.2. **HRMS (ES+)** m/z calc. for $C_{17}H_{24}N$ [M+H] 242.1909, found 242.1904. **FT-IR** ($cm^{-1}$, neat, ATR) 2924, 2855, 1592, 1508, 1463, 760.

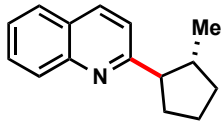


2-((2*R*)-2-Methylcyclopentyl)quinoline (**4e**). **Physical state:** 38 mg, 60% yield, clear oil. **$^{1}$H NMR** (500 MHz, $CDCl_3$) δ 8.08 – 8.04 (m, 2H), 7.77 (d, *J* = 8.1 Hz, 1H), 7.69 – 7.65 (m, 1H), 7.49 – 7.45 (m, 1H), 7.31 (d, *J* = 8.6 Hz, 1H), 2.90 – 2.84 (m, 1H), 2.33 – 2.17 (m, 2H), 2.09 – 1.93 (m, 2H), 1.92 – 1.77 (m, 2H), 1.45 – 1.37 (m, 1H), 1.01 (d, *J* = 6.5 Hz, 3H). **$^{13}$C NMR** (126 MHz, $CDCl_3$) δ 165.6, 148.1, 136.2, 129.3, 129.2, 127.6, 127.1, 125.7, 120.4, 57.3, 42.5, 35.2, 34.3, 24.5, 19.0. **HRMS (ES+)** m/z calc. for $C_{15}H_{18}N$ [M+H] 212.1439, found 212.1444. **FT-IR** ($cm^{-1}$, neat, ATR) 3050, 2946, 1601, 1255.

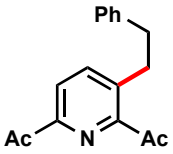


1,1'-(3-Phenethylpyridine-2,6-diyl)bis(ethan-1-one) (**4f**). **Physical state:** 52 mg, 65% yield, clear oil. **$^{1}$H NMR** (500 MHz, $CDCl_3$) δ 8.04 (d, *J* = 8.0 Hz, 1H), 7.62 (d, *J* = 8.0 Hz, 1H), 7.30 – 7.25 (m, 2H), 7.22 – 7.18 (m, 3H), 3.33 – 3.30 (m, 2H), 2.93 – 2.90 (m, 2H), 2.75 (s, 3H), 2.73 (s, 3H). **$^{13}$C NMR** (126 MHz, $CDCl_3$) δ 201.8, 199.4, 151.1, 150.6, 142.0, 141.0, 140.9, 128.8, 128.6, 126.4, 123.7, 37.4, 35.4, 28.4, 25.7. **HRMS (ES+)** m/z calc. for $C_{17}H_{18}NO_2$ [M+H] 268.1338, found 268.1339. **FT-IR** ($cm^{-1}$, neat, ATR) 1699, 1358, 1296, 700.

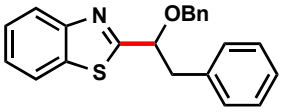


2-(1-(Benzyloxy)-2-phenylethyl)benzo[*d*]thiazole (**4g**). **Physical state:** 52 mg, 53% yield, colorless oil. **$^{1}$H NMR** (500 MHz, $CDCl_3$) δ 8.07 – 8.00 (m, 1H), 7.92 (d, *J* = 8.0 Hz, 1H), 7.52 – 7.47 (m, 1H), 7.43 – 7.36 (m, 5H), 7.35 – 7.31 (m, 1H), 7.28 – 7.24 (m, 2H), 7.17 (d, *J* = 7.8 Hz, 3H), 4.85 (dd, *J* = 8.3, 4.8 Hz, 1H), 4.70 (d, *J* = 11.4 Hz, 1H), 4.52 (d, *J* = 11.4 Hz, 1H), 2.93 – 2.82 (m, 1H), 2.82 – 2.71 (m, 1H), 2.41 – 2.29 (m, 1H), 2.29 – 2.19 (m, 2H). **$^{13}$C NMR** (126 MHz, $CDCl_3$) δ 175.4, 153.3, 141.3, 137.6, 135.1, 128.7, 128.6(5), 128.5(7), 128.3, 128.1, 126.1(5), 126.1(3), 125.3, 123.2, 122.1, 79.0, 72.3, 38.9, 31.7. **HRMS (ES+)** m/z calc. for $C_{23}H_{23}NOS$ [M+H] 360.1422, found 360.1420. **FT-IR** ($cm^{-1}$, neat, ATR) 3027, 2922, 2861, 1516, 1495, 1093, 1027, 1014, 758, 697.

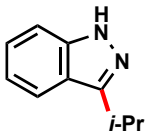

3-Isopropyl-1*H*-indazole (**4h**). **Physical state:** 33 mg, 69% yield, clear oil. **$^{1}$H NMR** (500 MHz, $CDCl_3$) δ 9.84 (bs, 1H), 7.78 (d, *J* = 8.1 Hz, 1H), 7.45 – 7.42 (m, 1H), 7.38 – 7.35 (m, 1H), 7.15 – 7.12 (m, 1H), 3.44 (sept, *J* = 7.0 Hz, 1H), 1.48 (d, *J* = 7.0 Hz, 6H). **$^{13}$C NMR** (126 MHz, $CDCl_3$) δ 152.8, 141.6, 126.7, 121.4, 120.8, 120.2, 109.9, 27.9, 22.3. **HRMS (ES+)** m/z calc. for $C_{10}H_{12}N_2$ [M+] 160.1000, found 160.1001. **FT-IR** ($cm^{-1}$, neat, ATR) 3189, 2968, 1623, 1501, 1349, 742.

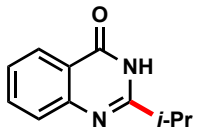


2-Isopropylquinazolin-4(3*H*)-one (**4i**). Reference: Shen, G.; Zhou, H.; Sui, Y.; Liu, Q.; Zou, K. *Tetrahedron Lett.* **2016**, *57*, 587. **Physical state:** 45 mg, 79% yield, white solid (mp = 123 °C). **$^{1}$H NMR** (500 MHz, $CDCl_3$) δ 11.64 (s, 1H), 8.30 (d, *J* = 7.9 Hz, 1H), 7.79 – 7.72 (m, 2H), 7.47 – 7.45 (m, 1H), 3.06 (sept, *J* = 7.0 Hz, 1H), 1.45 (d, *J* = 7.0 Hz, 6H). **$^{13}$C NMR** (126 MHz, $CDCl_3$) δ 164.4, 161.0, 149.6, 134.8, 127.5, 126.4, 126.4, 120.9, 35.1, 20.6. **HRMS (ES+)** m/z calc. for $C_{11}H_{12}N_2ONa$ [M+Na] 211.0847, found 211.0851. **FT-IR** ($cm^{-1}$, neat, ATR) 2970, 2932, 1622, 1609, 1472, 1384, 1252, 772.

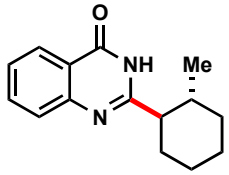


2-((1*R*,2*R*)-2-Methylcyclohexyl)quinazolin-4(3*H*)-one (**4j**). **Physical state:** 30 mg, 41% yield, white powder (mp = 89–93 °C). **$^{1}$H NMR** (500 MHz, $CDCl_3$) δ 11.48 (s, 1H), 8.29 (d, *J* = 7.9 Hz, 1H), 7.80 – 7.71 (m, 2H), 7.48 – 7.46 (m, 1H), 2.39 – 2.33 (m, 1H), 2.05 – 1.96 (m, 2H), 1.92 – 1.73 (m, 4H), 1.57 – 1.49 (m, 1H), 1.43 – 1.35 (m, 1H), 1.26 – 1.12 (m, 1H), 0.88 (d, *J* = 6.5 Hz, 3H). **$^{13}$C NMR** (126 MHz, $CDCl_3$) δ 164.1, 159.9, 149.6, 134.8, 127.5, 126.4, 120.9, 100.1, 52.9,

35.2, 35.2, 31.5, 26.2, 26.1, 20.6. **HRMS (ES+)** m/z calc. for $C_{15}H_{19}N_2O$ [M+H] 243.1497, found 243.1500. **FT-IR** ($cm^{-1}$, neat, ATR) 2926, 1668, 1471, 773.

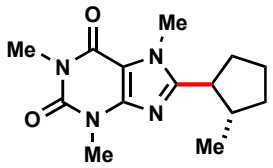


1,3,7-Trimethyl-8-((2*S*)-2-methylcyclopentyl)-3,7-dihydro-1*H*-purine-2,6-dione (**4k**). **Physical state:** 31 mg, 37%, light yellow oil. **$^1$H NMR** (500 MHz, $CDCl_3$) δ 3.93 (s, 3H), 3.56 (s, 3H), 3.40 (s, 3H), 2.67 – 2.63 (m, 1H), 2.50 -2.40 (m, 1H), 2.14 – 2.01 (m, 2H), 1.96 – 1.76 (m, 4H), 1.02 (d, *J* = 6.5 Hz, 3H). **$^{13}$C NMR** (126 MHz, $CDCl_3$) δ 157.6, 155.5, 152.0, 148.4, 107.4, 44.8, 41.3, 34.6, 32.4, 31.7, 29.9, 28.0, 24.2, 19.2. **HRMS (ES+)** m/z calc. for $C_{14}H_{21}N_4O_2$ [M+H] 277.1658, found 277.1661. **FT-IR** ($cm^{-1}$, neat, ATR) 2954, 1703, 1661, 1543, 1436, 1221, 1041, 981, 747.

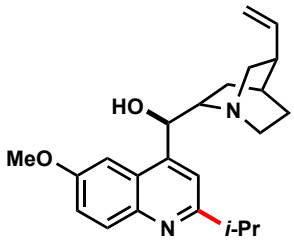


(1*R*)-(2-Isopropyl-6-methoxyquinolin-4-yl)(5-vinylquinuclidin-2-yl)methanol (**4l**). **Physical state:** 82 mg, 75% yield, light yellow solid (mp = 145 °C). **$^1$H NMR** (500 MHz, $CDCl_3$) δ 7.89 (d, *J* = 9.1 Hz, 1H), 7.52 (s, 1H), 7.22 (d, *J* = 9.1 Hz, 1H), 7.07 (s, 1H), 5.80 (s, 1H), 5.73 – 5.60 (m, 1H), 5.00 – 4.92 (m, 2H), 3.81 – 3.73 (m, 4H), 3.26 – 3.08 (m, 3H), 2.85 – 2.75 (m, 3H), 2.42 – 2.35 (m, 1H), 1.90 – 1.80 (m, 2H), 1.65 – 1.60 (m, 1H), 1.49 – 1.39 (m, 1H), 1.34 (d, *J* = 6.9 Hz, 6H). **$^{13}$C NMR** (126 MHz, $CDCl_3$) δ 164.7, 157.6, 146.3, 143.8, 140.1, 131.3, 124.7, 121.5, 116.5, 115.8, 100.6, 60.2, 60.1, 56.2, 55.9, 43.7, 39.0, 37.2, 27.7, 26.4, 22.7, 20.2. **HRMS (ES+)** m/z calc. for $C_{23}H_{30}N_2O_2$ [M+H] 367.2361, found 367.2394. **FT-IR** ($cm^{-1}$, neat, ATR) 2962, 1674, 1620,

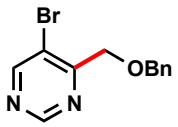


4-((Benzyloxy)methyl)-5-bromopyrimidine (**5a**). **Physical state:** 42 mg, 50% yield, clear oil. **$^{1}$H NMR** (500 MHz, $CDCl_3$) δ 9.13 (s, 1H), 8.77 (s, 1H), 7.43 – 7.30 (m, 5H), 4.73 (s, 2H), 4.71 (s, 2H). **$^{13}$C NMR** (126 MHz, $CDCl_3$) δ 164.1, 158.9, 157.1, 137.4, 128.7, 128.2, 128.2, 120.3, 73.7, 71.1. **HRMS (ES+)** m/z calc. for $C_{12}H_{12}BrN_3O$ [M+H] 279.0133, found 279.0135. **FT-IR** ($cm^{-1}$, neat, ATR) 2860, 1560, 1454, 1388, 1360, 1216, 1097, 1036, 738, 698.

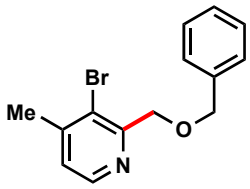


2-((Benzyloxy)methyl)-3-bromo-4-methylpyridine (**5b**). **Physical state:** 55 mg, 63% yield, clear oil. **$^{1}$H NMR** (500 MHz, $CDCl_3$) δ 8.33 (d, *J* = 4.8 Hz, 1H), 7.30 (m, 4H), 7.22 (m, 1H), 7.03 (d, *J* = 4.8 Hz, 1H), 3.40 – 3.21 (m, 2H), 3.05 (dd, *J* = 10.2, 6.7 Hz, 2H), 2.43 (s, 3H). **$^{13}$C NMR** (126 MHz, $CDCl_3$) δ 159.9, 148.0, 147.2, 141.9, 128.7, 128.6, 126.2, 124.4, 124.0, 40.4, 34.8, 23.6. **HRMS (ES+)** m/z calc. for $C_{14}H_{15}BrNO$ [M+H] 292.0701, found 292.0701. **FT-IR** ($cm^{-1}$, neat, ATR) 1735, 1716, 1452, 1296, 1243, 1211, 794.

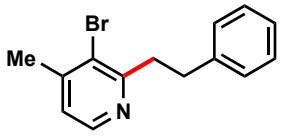


3-Bromo-4-methyl-2-phenethylpyridine (**5c**). **Physical state:** 50 mg, 60% yield, clear oil. **$^{1}$H NMR** (500 MHz, $CDCl_3$) δ 8.33 (d, *J* = 4.8 Hz, 1H), 7.30 (d, *J* = 4.4 Hz, 4H), 7.21 (p, *J* = 4.1 Hz, 1H),

7.03 (d, *J* = 4.8 Hz, 1H), 3.37 – 3.22 (m, 2H), 3.05 (dd, *J* = 10.2, 6.7 Hz, 2H), 2.43 (s, 3H). **$^{13}$C NMR** (126 MHz, $CDCl_3$) δ 159.9, 147.9, 147.2, 141.9, 128.6, 128.5, 126.1, 124.3, 123.9, 40.4, 34.8, 23.6. **HRMS (ES+)** m/z calc. for $C_{14}H_{14}BrN$ [M+H] 276.0388, found 276.0388. **FT-IR** ($cm^{-1}$, neat, ATR) 1727, 1591, 1435, 1281, 1258, 1084, 738, 698.

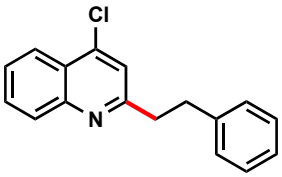


4-Chloro-2-phenethylquinoline (**5d**). **Physical state:** 38 mg, 47% yield, clear oil. **$^{1}$H NMR** (500 MHz, $CDCl_3$) δ 8.20 (d, *J* = 8.3 Hz, 1H), 8.08 (d, *J* = 8.4 Hz, 1H), 7.76 (t, *J* = 7.7 Hz, 1H), 7.60 (t, *J* = 7.6 Hz, 1H), 7.35 (s, 1H), 7.30 (t, *J* = 7.5 Hz, 2H), 7.22 (dd, *J* = 15.9, 8.7 Hz, 2H), 3.29 – 3.23 (m, 2H), 3.16 (dd, *J* = 9.7, 6.3 Hz, 2H). **$^{13}$C NMR** (126 MHz, $CDCl_3$) δ 161.9, 149.0, 142.7, 141.3, 130.5, 129.4, 128.6, 126.9, 126.3, 125.2, 124.1, 121.7, 40.9, 35.8. **HRMS (ES+)** m/z calc. for $C_{17}H_{15}ClN$ [M+H] 268.0893, found 268.0896. **FT-IR** ($cm^{-1}$, neat, ATR) 3062, 3027, 1589, 1493, 1149, 866, 759, 698.

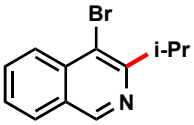


4-Bromo-3-isopropylisoquinoline (**5e**). **Physical state:** 30 mg, 40% yield, clear oil. **$^{1}$H NMR** (500 MHz, $CDCl_3$) δ 8.67 (s, 1H), 8.24 – 8.18 (m, 2H), 7.79 – 7.76 (m, 1H), 7.67 – 7.64 (m, 1H), 3.91 (sept, *J* = 6.8 Hz, 1H), 1.43 (d, *J* = 6.8 Hz, 6H). **$^{13}$C NMR** (126 MHz, $CDCl_3$) δ 166.1, 143.8, 135.0, 130.9, 127.9, 127.7, 127.0, 125.2, 117.7, 31.2, 22.3. **HRMS (ES+)** m/z calc. for $C_{12}H_{13}BrN$ [M+H] 250.0231, found 250.0224. **FT-IR** ($cm^{-1}$, neat, ATR) 2965, 2929, 1565, 1387, 1240, 1009, 928.

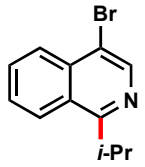


4-Bromo-1-isopropylisoquinoline (**5f**). **Physical state:** 22 mg, 29% yield, clear oil. **$^{1}$H NMR** (500 MHz, $CDCl_3$) δ 8.51 (s, 1H), 8.35 (d, *J* = 8.5 Hz, 1H), 7.62 – 7.59 (m, 1H), 7.52 – 7.49 (m, 1H), 7.43 (d, *J* = 8.5 Hz, 1H), 4.08 (sept, *J* = 6.8 Hz, 1H), 1.55 (d, *J* = 6.8 Hz, 6H). **$^{13}$C NMR** (126 MHz, $CDCl_3$) δ 166.8, 143.2, 136.3, 129.9, 127.1, 126.9, 126.3, 125.9, 125.1, 31.3, 22.4. **HRMS (ES+)** m/z calc. for $C_{12}H_{14}BrN$ [M+H] 250.0231, found 250.0224. **FT-IR** ($cm^{-1}$, neat, ATR) 2965, 1556, 1502, 1388, 1246, 765.

**LIGAND FUCNTIONALIZATION**

---

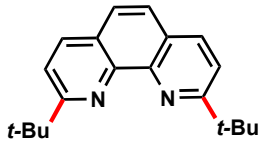


2,9-Di-*tert*-butyl-1,10-phenanthroline (**9**). Reference: Xu, C.; Zhang, L.; Dong, C.; Xu, J.; Pan, Y.; Li, Y.; Zhang, H.; Li, H.; Yu, Z.; Xu, L. *Adv. Synth. Catal.* **2016**, *358*, 567. **Physical state:** 38 mg, 42% yield, white semi-solid. **$^{1}$H NMR** (500 MHz, $CDCl_3$) δ 8.13 (d, *J* = 8.4 Hz, 2H), 7.84 – 7.48 (m, 4H), 1.60 (s, 18H). **$^{13}$C NMR** (126 MHz, $CDCl_3$) δ 169.4, 145.0, 136.0, 127.0, 125.5, 119.7, 38.8, 30.4. **HRMS (ES+)** m/z calc. for $C_{20}H_{25}N$ [M+H] 293.2018, found 293.2020. **FT-IR** ($cm^{-1}$, neat, ATR) 2962, 1589, 1489, 1387, 850.

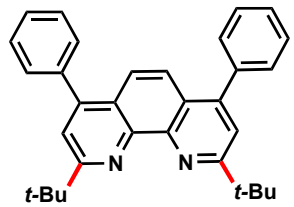

2,9-Di-*tert*-butyl-4,7-diphenyl-1,10-phenanthroline (**11**). Reference: Sugihara, S.; Okada, T.; Hiratani, K. *Anal. Sci.* **1993**, *9*, 593. **Physical state:** 152 mg, 68% yield, yellow oil. **$^1$H NMR** (500 MHz, $CDCl_3$) δ 7.72 (s, 2H), 7.63 (s, 2H), 7.56 – 7.43 (m, 10H), 1.64 (s, 18H). **$^{13}$C NMR** (126 MHz, $CDCl_3$) δ 168.8, 148.4, 145.7, 139.2, 129.9, 128.6, 128.2, 124.9, 123.1, 120.1, 38.9, 30.5.

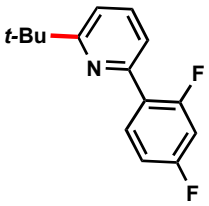


2-(*tert*-Butyl)-6-(2,4-difluorophenyl)pyridine (**13**). **Physical state:** 61 mg, 82% yield, light yellow oil. **$^1$H NMR** (500 MHz, $CDCl_3$) δ 8.61 (d, *J* = 5.1 Hz, 1H), 7.96 (m, 1H), 7.72 (s, 1H), 7.28 – 7.22 (m, 1H), 6.99 (t, *J* = 8.4 Hz, 1H), 6.91 (m, 1H), 1.36 (s, 9H). **$^{13}$C NMR** (126 MHz, $CDCl_3$) δ 163.2 (dd, *J* = 250.5, 12.1 Hz), 160.6 (dd, *J* = 252.0, 11.9 Hz), 160.6, 149.8, 132.4 (dd, *J* = 9.7, 4.6 Hz), 124.5 (dd, *J* = 12.0, 3.9 Hz), 122.6, 121.5 (d, *J* = 8.9 Hz), 119.7, 111.9 (dd, *J* = 21.0, 3.8 Hz), 104.4 (m), 35.0, 30.7. **HRMS (ES+)** m/z calc. for $C_{15}H_{16}F_2N$ [M+H] 248.1251, found 248.1241. **FT-IR** ($cm^{-1}$, neat, ATR) 2949, 1736, 1716, 1242, 1209, 747, 700.

## CAMPTOTHECIN ANALOGUES

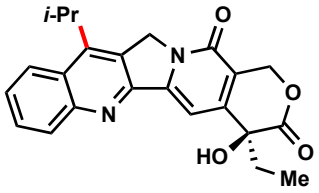


(*S*)-4-Ethyl-4-hydroxy-11-isopropyl-1,12-dihydro-14*H*-pyrano[3',4':6,7]indolizino[1,2-*b*]quinoline-3,14(4*H*)-dione (**5a**). Reference: Miao, Z. *et al. J. Med. Chem.* **2013**, *56*, 7902 **Physical state:** 67 mg, 57% yield, light yellow solid (mp = 192 °C). **$^1$H NMR** (500 MHz, $CDCl_3$) δ 8.25 – 8.20 (m, 2H), 7.79 – 7.76 (m, 1H), 7.70 – 7.61 (m, 2H), 5.74 (d, *J* = 16.1 Hz, 1H), 5.38 (s, 2H),

5.30 (d, *J* = 16.1 Hz, 1H), 4.05 – 3.92 (m, 1H), 3.90 (bs, 1H), 1.94 – 1.84 (m, 2H), 1.56 (d, *J* = 8.3 Hz, 6H), 1.03 (t, *J* = 7.4 Hz, 3H). **$^{13}$C NMR** (126 MHz, $CDCl_3$) δ 174.1, 157.7, 152.5, 150.4, 149.9, 149.5, 146.6, 130.9, 130.1, 127.8, 126.9, 125.5, 123.9, 118.5, 98.0, 72.9, 66.5, 50.4, 31.8, 21.7, 21.6, 8.0. **HRMS (ES+)** m/z calc. for $C_{23}H_{22}N_2O_4$ [M+Na] 413.1477, found 413.1460. **FT-IR** ($cm^{-1}$, neat, ATR) 3320, 2971, 1748, 1657, 1157, 727.

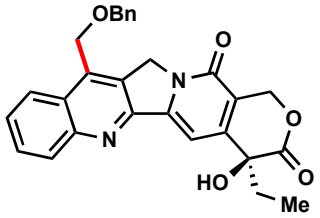


(*S*)-11-((Benzyloxy)methyl)-4-ethyl-4-hydroxy-1,12-dihydro-14*H*-pyrano[3',4':6,7]indolizino[1,2-*b*]quinoline-3,14(4*H*)-dione (**5b**). **Physical state:** 23 mg, 33% yield, yellow oil. **$^{1}$H NMR** (500 MHz, $CDCl_3$) δ 8.22 (d, *J* = 8.5 Hz, 1H), 7.96 (d, *J* = 8.5 Hz, 1H), 7.80 -7.76 (m, 1H), 7.69 – 7.59 (m, 2H), 7.42 – 7.34 (m, 5H), 5.75 (d, *J* = 16.2 Hz, 1H), 5.42 (s, 2H), 5.31 (d, *J* = 16.2 Hz, 1H), 5.18 (s, 2H), 4.78 (s, 2H), 3.78 (s, 1H), 1.95 – 1.86 (m, 2H), 1.04 (t, *J* = 7.4 Hz, 3H). **$^{13}$C NMR** (126 MHz, $CDCl_3$) δ 174.1, 157.8, 152.8, 150.1, 149.1, 146.5, 139.4, 137.1, 130.7, 130.3, 128.9, 128.5, 128.1, 128.1, 127.2, 126.0, 123.5, 118.8, 97.9, 73.9, 72.9, 67.2, 66.6, 51.0, 31.8, 8.0. **HRMS (ES+)** m/z calc. for $C_{28}H_{25}N_2O_5$ [M+H] 469.1763, found 469.1774. **FT-IR** ($cm^{-1}$, neat, ATR) 2987, 2870, 1208, 1063, 861, 837.

**Cyclic Voltammetry of Organoboron Reagents:**

Electrochemical measurements were recorded on a CH Instruments: Model 600E Series Electrochemical Analyzer (observed in 0.002 M MeCN; $[N(Bu)_4](PF_6)$ = 0.1 M; Ag/AgCl = electrode; reported in SCE based on a ferrocene internal standard).

Of the organoboron reagents examined, only the potassium cyclohexyltriolborate (~1.1 V *vs SCE*) and potassium cyclohexyltrifluoroborate (~1.5 V *vs SCE*) exhibited oxidations within the solvent window of MeCN. These potentials have been reported previously by Akita and coworkers. No features were observed for oxidation of the cyclohexyl boronic acid, MIDA, and pincaol boronates.

## 9.5 References


(1) M. E. Welsch, S. A. Snyder, and B. R. Stockwell, *Curr. Opin. Chem. Biol.*, 2010, **14**, 347.

(2) (a) D. Yang, S. Burugupalli, D. Daniel, and Y. Chen, *J. Org. Chem.*, 2012, **77**, 4466. (b) L. Zheng, J. Ju, Y. Bin, and R. Hua, *J. Org. Chem.*, 2012, **77**, 5794. (c) G. Zhang, H. Ni, W. Chen, J. Shao, H. Liu, B. Chen, and Y. Yu, *Org. Lett.*, 2013, **15**, 5967. (d) J. -A. Jiang, W. -B. Huang, J. -J. Zhai, H. -W. Liu, Q. Cai, L. -X. Xu, W. Wang, and Y. -F. Ji, *Tetrahedron*, 2013, **69**, 627. (e) M. R. Kumar, A. Park, N. Park, and S. Lee, *Org. Lett.*, 2011, **13**, 3542.

(3) (a) J. F. Bunnett and R. E. Zahler, *Chem. Rev.*, 1951, **49**, 273. (b) O. F. Terrier, *Modern Nucleophilic Aromatic Substitution*; Wiley-VCH: Weinheim, Germany, 2013. (c) P. S. Fier, J. F. Hartwig, *J. Am. Chem. Soc.*, 2014, **136**, 10139.

(4) G. Joshi and S. Adimurthy, *Ind. Eng. Chem. Res.*, 2011, **50**, 12271.

(5) R. A. Rodriguez, C. -M. Pan, Y. Yabe, Y. Kawamata, M. D. Eastgate, and P. S. Baran, *J. Am. Chem. Soc.*, 2014, **136**, 6908.

(6) (a) K. L. Billingsley, K. W. Anderson, and S. L. Buchwald, *Angew. Chem. Int. Ed.*, 2006, **45**, 3484. (b) K. Billingsley and S. L. Buchwald, *J. Am. Chem. Soc.*, 2007, **129**, 3358.

(7) S. Ge and J. F. Hartwig, *Angew. Chem. Int. Ed.*, 2012, **51**, 12837.

(8) (a) F. Minisci, *Acc. Chem. Res.*, 1975, **8**, 165. (b) F. Minisci, E. Vismara, and F. J. Fontana, *J. Org. Chem.*, 1989, **54**, 5224. (b) W. -M. Zhao, X. -L. Chen, J. -W. Yuan, L. -B. Qu, L. -K. Duan and Y. -F. Zhao, *Chem. Commun.* 2014, **50**, 2018. (c) R. Xia, M. -S. Xie, H. -Y. Niu, G. -R. Qu, H. -M. Guo, *Org. Lett.* 2014, **16**, 444.

(9) F. Minisci, R. Bernardi, F. Bertini, R. Galli, and M. Perchinummo, *Tetrahedron*, 1971, **27**, 3575.

(10) I. B. Seiple, S. Su, R. A. Rodriguez, R. Gianatassio, Y. Fujiwara, A. L. Sobel, and P. S. Baran, *J. Am. Chem. Soc.*, 2010, **132**, 13194.

(11) K. Foo, E. Sella, I. Thome, M. D. Eastgate, and P. S. Baran, *J. Am. Chem. Soc.*, 2014, **136**, 5279.

(12) (a) G. A. Molander, V. Colombel, and V. A. Braz, *Org. Lett.*, 2011, **13**, 1852. (b) M. Presset, N. Fleury-Brégeot, D. Oehlrich, F. Rombouts, and G. A. Molander, *J. Org. Chem.*, 2013, **78**, 4615.

(13) (a) R. Gianatassio, S. Kawamura, C. L. Eprile, K. Foo, J. Ge, A. C. Burns, M. R. Collins, and P. S. Baran, *Angew. Chem. Int. Ed.*, 2014, **53**, 9851. (b) Q. Zhou, A. Ruffoni, R. Gianatassio, Y. Fujiwara, E. Sella, D. Shabat, and P. S. Baran, *Angew. Chem. Int. Ed.*, 2013, **52**, 3949. (c) Y. Ji, T. Brueckl, R. D. Baxter, Y. Fujiwara, I. B. Seiple, S. Su, D. G. Blackmond, and P. S. Baran, *Proc. Natl. Acad. Sci.*, 2011, **108**, 14411. (d) F. O'Hara, D. G. Blackmond, and P. S. Baran, *J. Am. Chem. Soc.*, 2013, **135**, 12122. (e) Y. Fujiwara, J. A. Dixon, F. O'Hara, E. D. Funder, D. D. Dixon, R. A. Rodriguez, R. D. Baxter, B. Herle, N. Sach, M. R. Collins, Y. Ishihara, and P. S. Baran, *Nature*, 2012, **492**, 95.

(14) M. A. Duncton, *J. Med. Chem. Commun.*, 2011, **2**, 1135.

(15) J. -P. Goddard, C. Ollivier, and L. Fensterbank, *Acc. Chem. Res.*, 2016, **49**, 1924.

(16) (a) J. Jin and D. W. C. MacMillan, *Nature*, 2015, **525**, 87. (b) D. A. Nagib and D. W. C. MacMillan, *Nature*, 2011, **480**, 224. (c) J. Jin and D. W. C. MacMillan, *Angew. Chem. Int.*

*Ed.*, 2015, **54**, 1565.

(17) D. A. DiRocco, K. Dykstra, S. Krska, P. Vachal, D. V. Conway, and M. Tudge, *Angew. Chem. Int. Ed.*, 2014, **53**, 4802.

(18) G. -X. Li, C. A. Morales-Rivera, Y. Wang, F. Gao, G. He, P. Liu, and G. Chen, *Chem. Sci.*, 2016, **7**, 6407.

(19) T. McCallum and L. Barriault, *Chem. Sci.*, 2016, **7**, 4754.

(20) (a) J. C. Tellis, D. N. Primer, and G. A. Molander, *Science*, 2014, **345**, 433. (b) D. N. Primer, I. Karakaya, J. C. Tellis, and G. A. Molander, *J. Am. Chem. Soc.*, 2015, **137**, 2195. (c) I. Karakaya, D. N. Primer, and G. A. Molander, *Org. Lett.*, 2015, **17**, 3294. (d) Y. Yamashita, J. C. Tellis, and G. A. Molander, *Proc. Natl. Acad. Sci. U.S.A.*, 2015, **112**, 12026. (e) M. El Khatib, R. A. Serafim, and G. A. Molander, *Angew. Chem. Int. Ed.*, 2016, **55**, 254. (f) D. Ryu, D. N. Primer, J. C. Tellis, and. G. A. Molander, *Chem. Eur. J.*, 2016, **22**, 120. (g) J. Amani, E. Sodagar, and G. A. Molander, *Org. Lett.*, 2016, **18**, 732. (h) R. Karimi-Nami, J. C. Tellis, and G. A. Molander, *Org. Lett.*, 2016, **18**, 2572. (i) J. C. Tellis, J. Amani, and G. A.Molander, *Org. Lett.*, 2016, **18**, 2572. (j) Y. Yasu, T. Koike, and M. Akita, *Adv. Synth. Catal.*, 2012, **354**, 3414. (k) T. Chinzei, K. Miyazawa, Y. Yasu, T. Koike, and M. Akita, *RSC Adv.*, 2015, **5**, 21297. (l) G. Sorin, R. M. Mallorquin, Y. Contie, A. Baralle, M. Malacria, J. -P. Goddard, and L. Fensterbank, *Angew. Chem. Int. Ed.*, 2010, **49**, 8721.

(21) S. Fukuzumi, H. Kotani, K. Ohkubo, S. Ogo, N. V. Tkachenko, and H. Lemmetyinen, *J. Am. Chem. Soc.*, 2004, **126**, 1600.

(22) R. J. Memming, *J. Electrochem. Soc.*, 1969, **116**, 785.

(23) (a) A. J. Kalb and T. L. Allen, *J. Am. Chem. Soc.*, 1964, **86**, 5107. (b) N. R. Patel and R. A. Flowers, II, *J. Am. Chem. Soc.*, 2013, **135**, 4672.

(24) (a) D. S. Hamilton and D. A. Nicewicz, *J. Am. Chem. Soc.*, 2012, **134**, 18577. (b) P. D. Morse and D. A. Nicewicz, *Chem. Sci.*, 2015, **6**, 270. (c) D. A. Nicewicz and T. M. Nguyen, *ACS*

*Catal.*, 2014, **4**, 355. (d) J. Grandjean and D. A. Nicewicz, *Angew. Chem. Int. Ed.*, 2013, **52**, 3967. (e) M. Riener and D. A. Nicewicz, *Chem. Sci.*, 2013, **4**, 2625. (f) D. J. Wilger, N. J. Gesmundo, and D. A. Nicewicz, *Chem. Sci.*, 2013, **4**, 3160. (g) T. M. Nguyen and D. A. Nicewicz, *J. Am. Chem. Soc.*, 2013, **135**, 9588. (h) A. J. Perkowski and D. A. Nicewicz, *J. Am. Chem. Soc.*, 2013, **135**, 10334. (i) D. A. Nicewicz and D. S. Hamilton, *Synthesis*, 2014, **25**, 1191. (j) T. M. Nguyen, N. Manohar, and D. A. Nicewicz, *Angew. Chem. Int. Ed.*, 2014, **53**, 6198. (k) N. Romero and D. A. Nicewicz, *J. Am. Chem. Soc.*, 2014, **136**, 17024. (k) M. A. Zeller, M. Riener, and D. A. Nicewicz, *Org. Lett.*, 2014, **16**, 4810. (l) N. J. Gesmundo, J. -M. M. Grandjean, and D. A. Nicewicz, *Org. Lett.*, 2015, **17**, 1316.

(25) J. Luo and J. Zhang, *ACS Catal.*, 2016, **6**, 873.

(26) M. Butters, J. N. Harvey, J. Jover, A. J. J. Lennox, G. C. Lloyd-Jones, and P. M. Murray, *Angew. Chem. Int. Ed.*, 2010, **49**, 5156.

(27) H. J. Seo, S. J. Yoon, S. H. Jang, and S. K. Namgoong, *Tetrahedron Lett.*, 2011, **52**, 3747.

(28) M. Tada and Y. Yokoi, *J. Heterocyclic Chem.*, 1989, **26**, 45.

(29) T. C. Atack and S. P. Cook, *J. Am. Chem. Soc.*, 2016, **138**, 6139.

(30) (a) E. P. Gillis, K. J. Eastman, M. D. Hill, D. J. Donnelly, and N. A. Meanwell, *J. Med. Chem.*, 2015, **58**, 8315. (b) S. Purser, P. R. Moore, S. Swallow, and V. Gouverneur, *Chem. Soc. Rev.*, 2008, **37**, 320.

(31) K. E. Murphy-Benenato, N. Olivier, A. Choy, P. L. Ross, M. D. Miller, J. Thresher, N. Gao, and M. R. Hale, *ACS Med. Chem. Lett.*, 2014, **5**, 1213.

(32) (a) G. -X. Li, C. A. Morales-Rivera, Y. Wang, F. Gao, G. He, P. Liu, and, G. Chen, G. *Chem. Sci.*, 2016, **7**, 6407. (b) Y. Siddaraju, M. Lamani, and K. R. Prabhu, *J. Org. Chem.*, 2014, **79**, 3856.

(33) (a) P. G. Sammes and G. Yahioglu, *Chem. Soc. Rev*,. 1994, **23**, 327.

(34) We suspect that for the bipyridine system, initial alkylation enhances the rate of alkylation to

the adjacent pyridine. For the larger, more diffuse terpyridine ligand, this rate acceleration is not seen due to both stereo- and electronic effects.

(35) R. Gianatassio, S. Kawamura, C. L. Eprile, K. Foo, J. Ge, A. C. Burns, M. R. Collins, and P. S. Baran, *Angew. Chem. Int. Ed.*, 2014, **53**, 9851.

(36) V. J. Venditto and E. E. Simanek, *Mol. Pharm.*, 2010, **7**, 307.

(37) C. D. Britten, S. G. Hilsenbeck, S. G. Eckhardt, J. Marty, G. Mangold, J. R. MacDonald, E. K. Rowinsky, D. D. Von Hoff, and S. Weitman, *Cancer Res.*, 1999, **59**, 1049.

(38) M. Li, W. Jin, C. Jiang, C. Zheng, W. Tang, T. You, and L. Lou, *Bioorg. Med. Chem. Lett.*, 2009, **19**, 4107.

(39) (a) S. Sekiguchi, K. Akiyama, and S. Tero-Kubota, *J. Chem. Soc., Perkin Trans. 2.*, 1997, 1619. (b) Y. Y. Lim and R. S. Drago, *Inorg. Chem.*, 1972, **11**, 1334.

(40) Note that although enhanced C2/C4 differentiation is also observed for the heteroaryl in the absence of Bronsted/Lewis acid, the radical addition and/or oxidation steps are substantially slowed by their absence.

(41) (a) H. B. Mansaray, A. D. L. Rowe, N. Phillips, J. Niemeyer, M. Kelly, D. A. Addy, J. I. Bates, and S. Aldridge, S. *Chem. Commun.*, 2011, **47**, 12295. (b) P. Tarakeshwar, S. J. Lee, J. Y. Lee, and K. S. Kim, *J. Phys. Chem. B.* 1999, **103**, 184.

(42) (a) J. Ren, C. J. Cramer, and R. R. Squires, *J. Am. Chem. Soc.*, 1999, **121**, 2633. (b) H. Yamamoto and K. Futatsugi, *Angew. Chem. Int. Ed.*, 2005, **44**, 1924.

**Author Contributions**:

D.N.P. designed the mechanistic experiments and prepared some of the alkyltrifluoroborates used in this study. D.N.P. also synthesized a number of the compounds prepared in this study. Jennifer Matsui optimized the reaction conditions and prepared most of the compounds synthesized in this study. Both D.N.P. and Jennifer Matsui wrote and edited the manuscript.

## Appendix A11. $^{1}H$, $^{13}C$, $^{11}B$, $^{19}F$ Spectra Relevant to Chapter 9

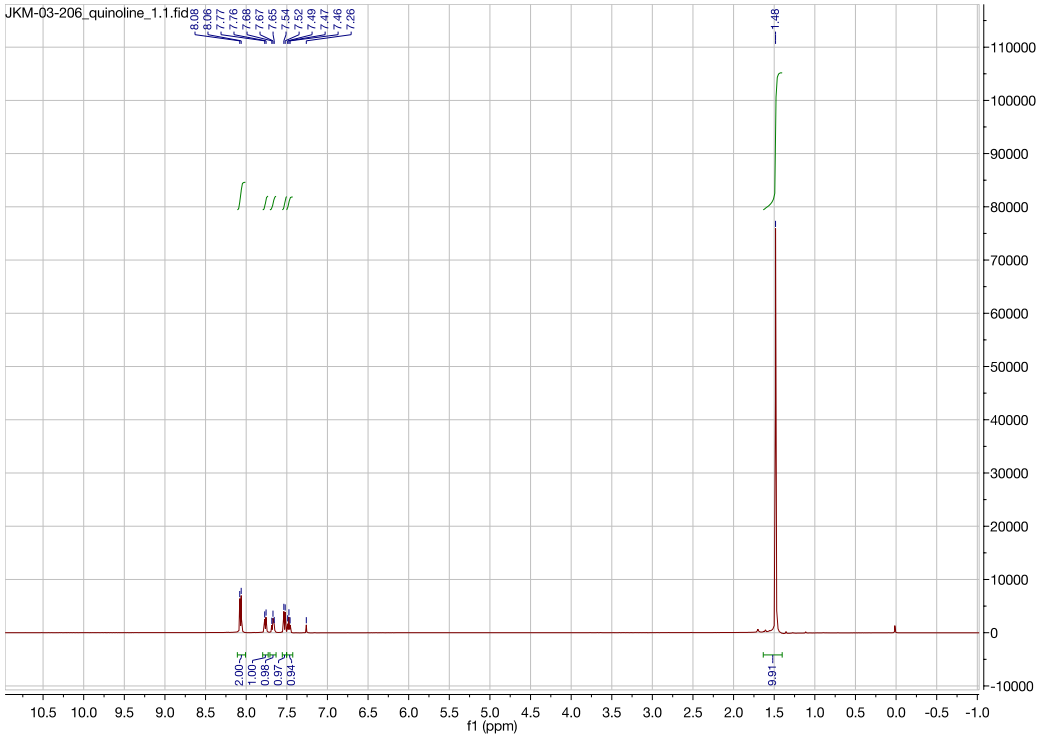


**Figure A11.1.** $^{1}$H NMR ($CDCl_3$, 500 MHz) spectrum of 2-(*tert*-butyl)quinoline (**1a**)

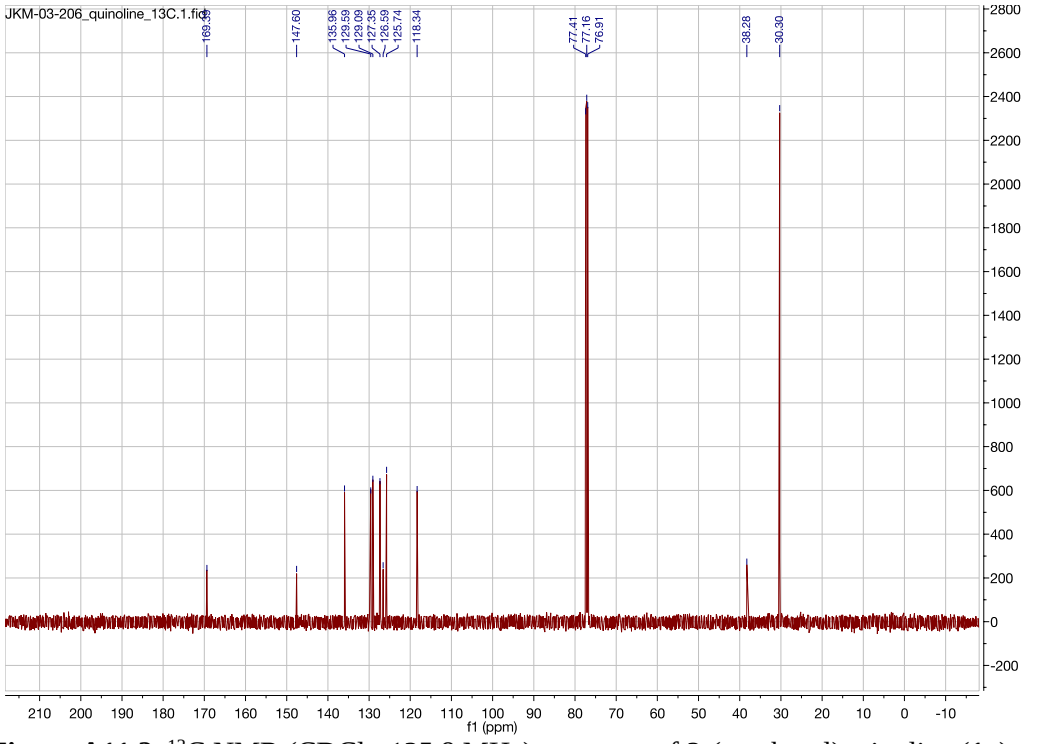


**Figure A11.2.** $^{13}$C NMR ($CDCl_3$, 125.8 MHz) spectrum of 2-(*tert*-butyl)quinoline (**1a**)

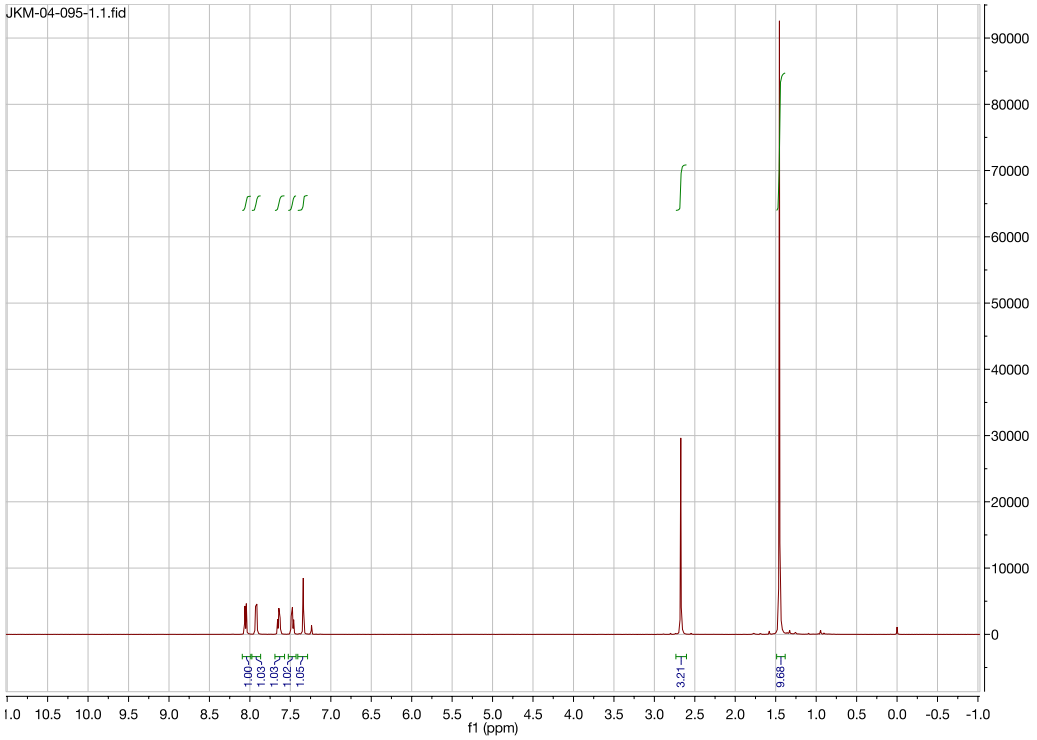


**Figure A11.3.** $^{1}$H NMR ($CDCl_3$, 500 MHz) spectrum of 2-(*tert*-butyl)-4-methylquinoline (**1b**)

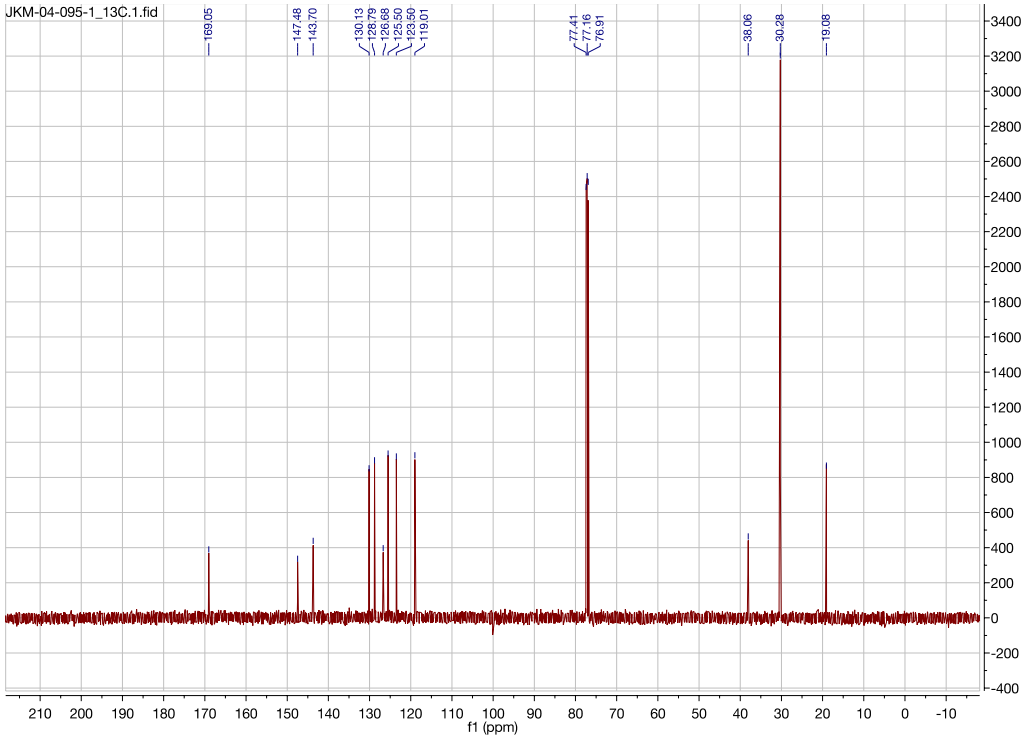


**Figure A11.4.** $^{13}$C NMR ($CDCl_3$, 125.8 MHz) spectrum of 2-(*tert*-butyl)-4-methylquinoline (**1b**)

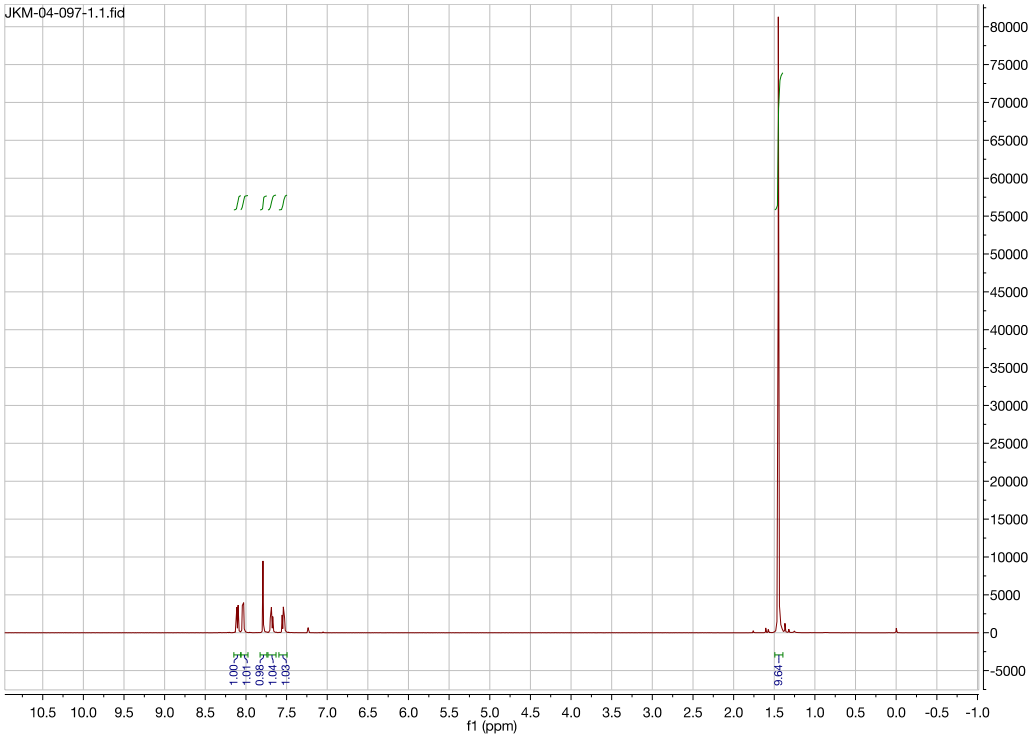


**Figure A11.5.** $^{1}$H NMR ($CDCl_3$, 500 MHz) spectrum of 4-bromo-2-(*tert*-butyl)quinoline (**1c**)

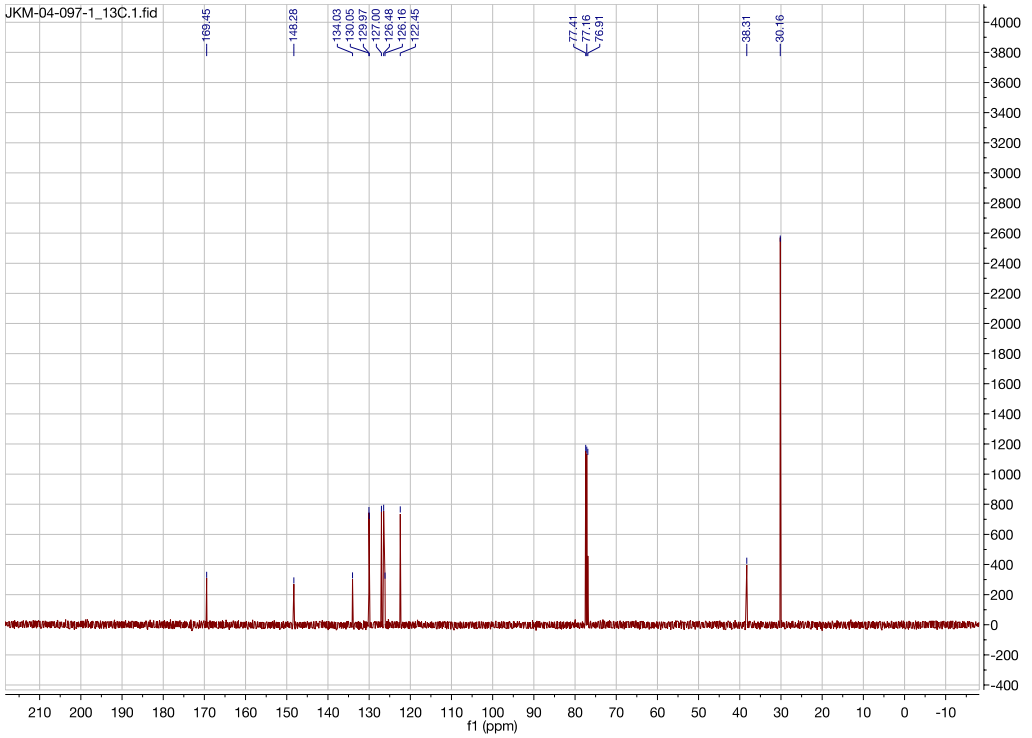


**Figure A11.6.** $^{13}$C NMR ($CDCl_3$, 125.8 MHz) spectrum of 4-bromo-2-(*tert*-butyl)quinoline (**1c**)

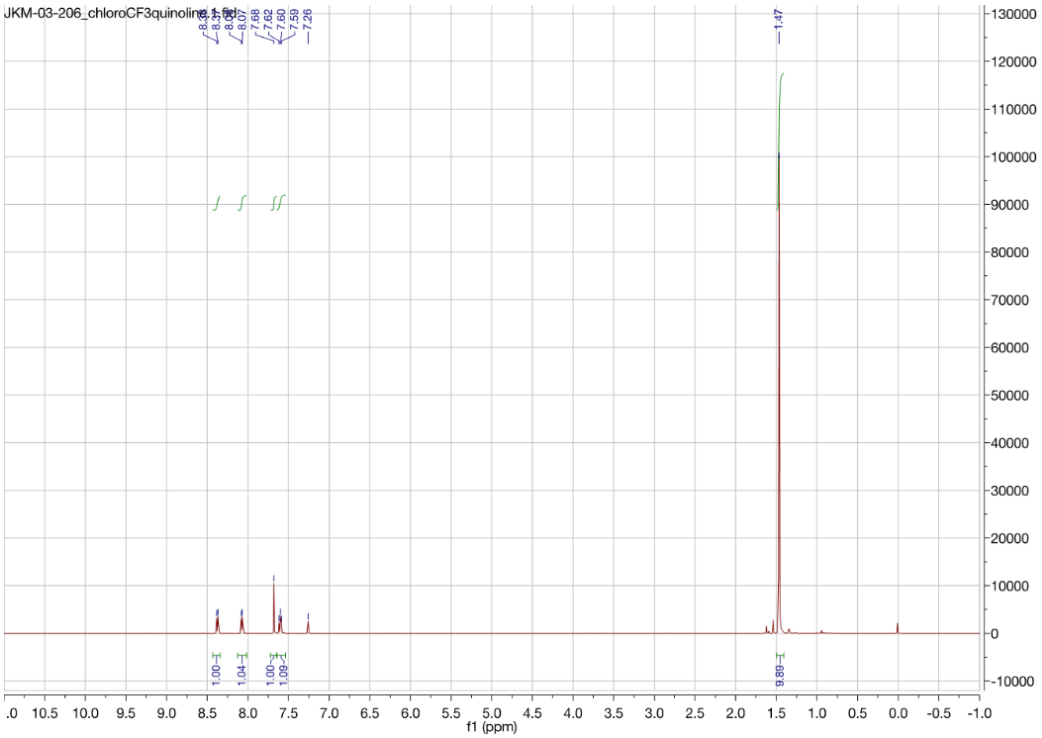


**Figure A11.7.** $^{1}$H NMR ($CDCl_3$, 500 MHz) spectrum of 2-(*tert*-butyl)-4-chloro-8-(trifluoromethyl)quinoline (**1d**)

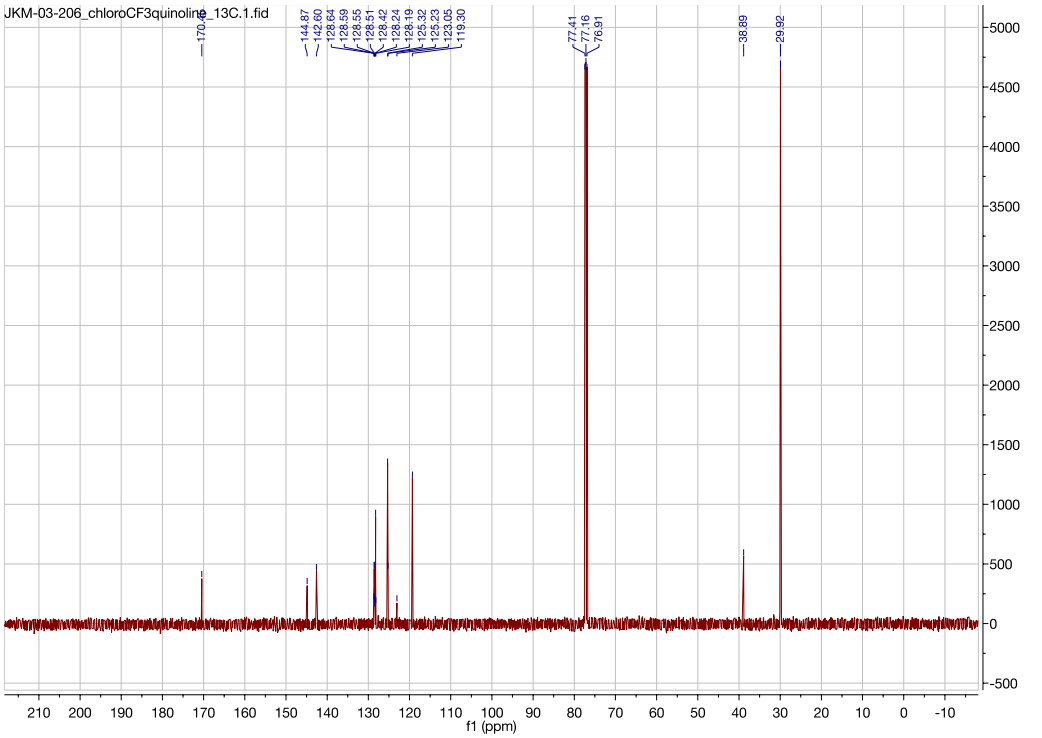


**Figure A11.8.** $^{13}$C NMR ($CDCl_3$, 125.8 MHz) spectrum of 2-(*tert*-butyl)-4-chloro-8-(trifluoromethyl)quinoline (**1d**)

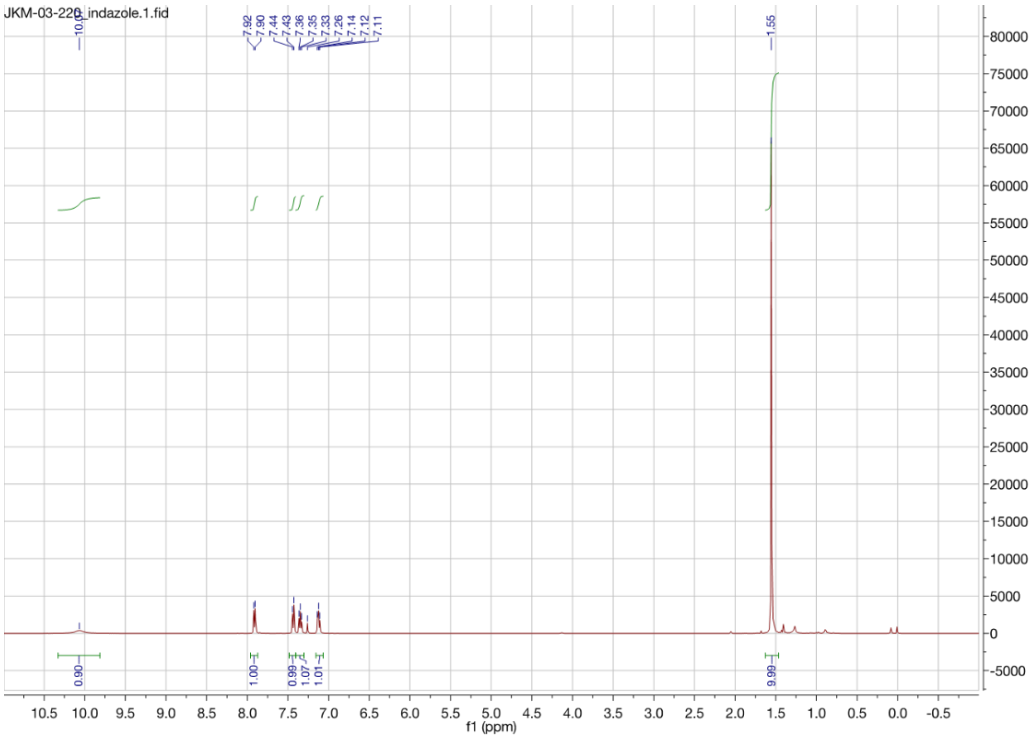


**Figure A11.9.** $^{1}$H NMR ($CDCl_3$, 500 MHz) spectrum of 3-(*tert*-butyl)-1*H*-indazole (**1e**)

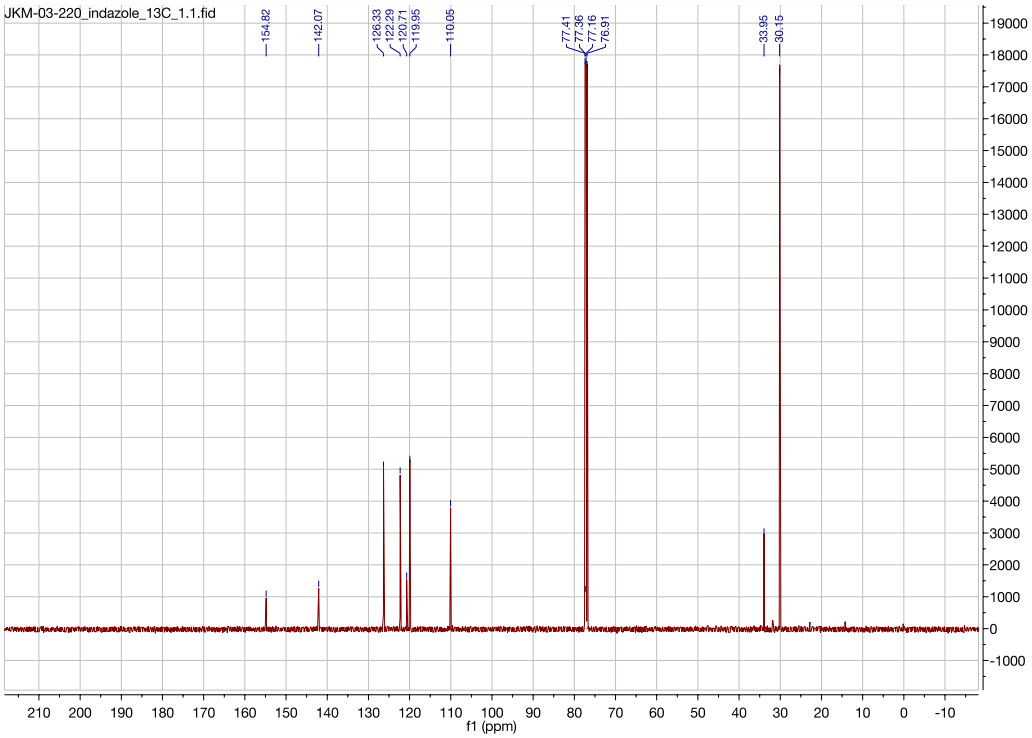


**Figure A11.10.** $^{13}$C NMR ($CDCl_3$, 125.8 MHz) spectrum of 3-(*tert*-butyl)-1*H*-indazole (**1e**)

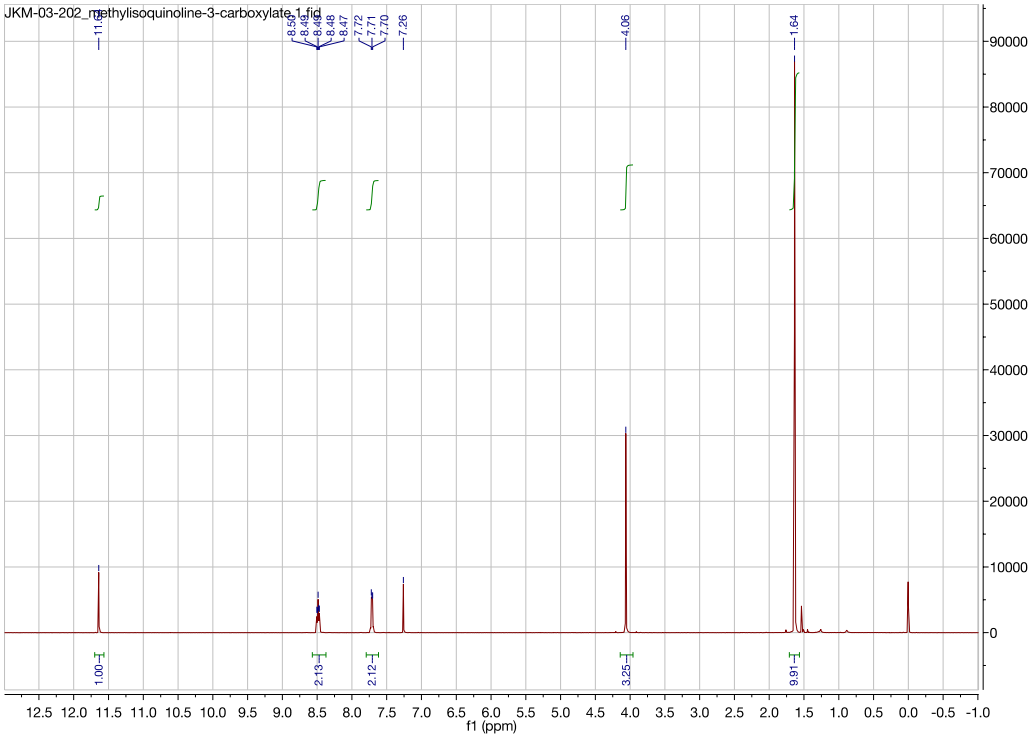


**Figure A11.9.** $^{1}$H NMR ($CDCl_3$, 500 MHz) spectrum of methyl 1-(*tert*-butyl)isoquinoline-3-carboxylate (**1g**)

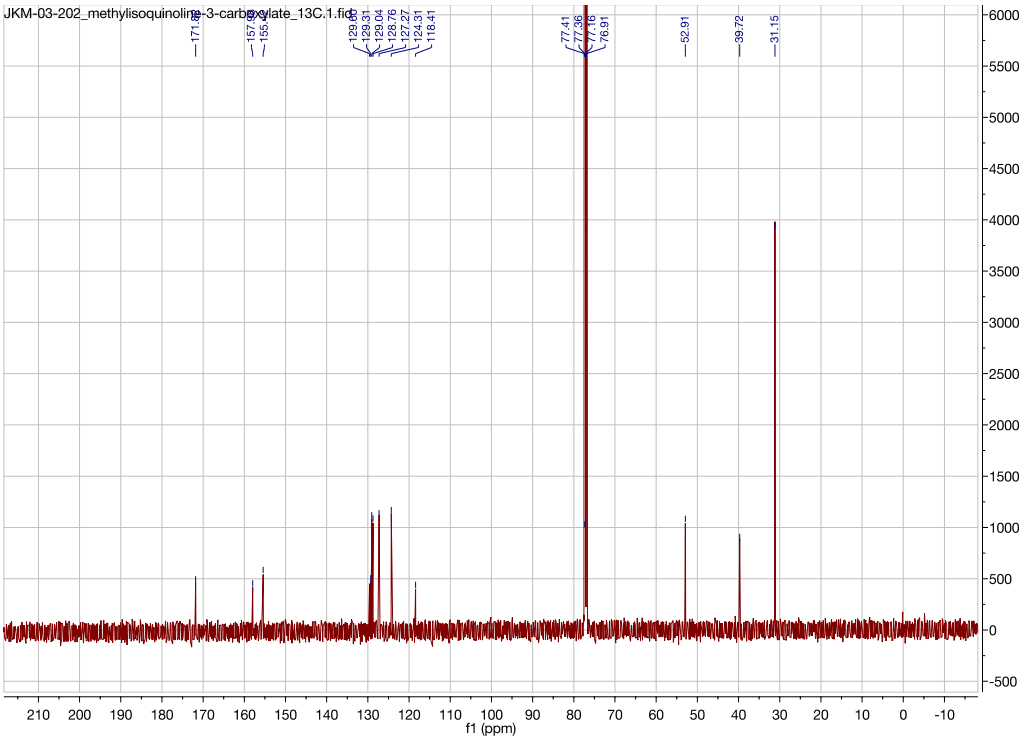


**Figure A11.10.** $^{13}$C NMR ($CDCl_3$, 125.8 MHz) spectrum of methyl 1-(*tert*-butyl)isoquinoline-3-carboxylate (**1g**)

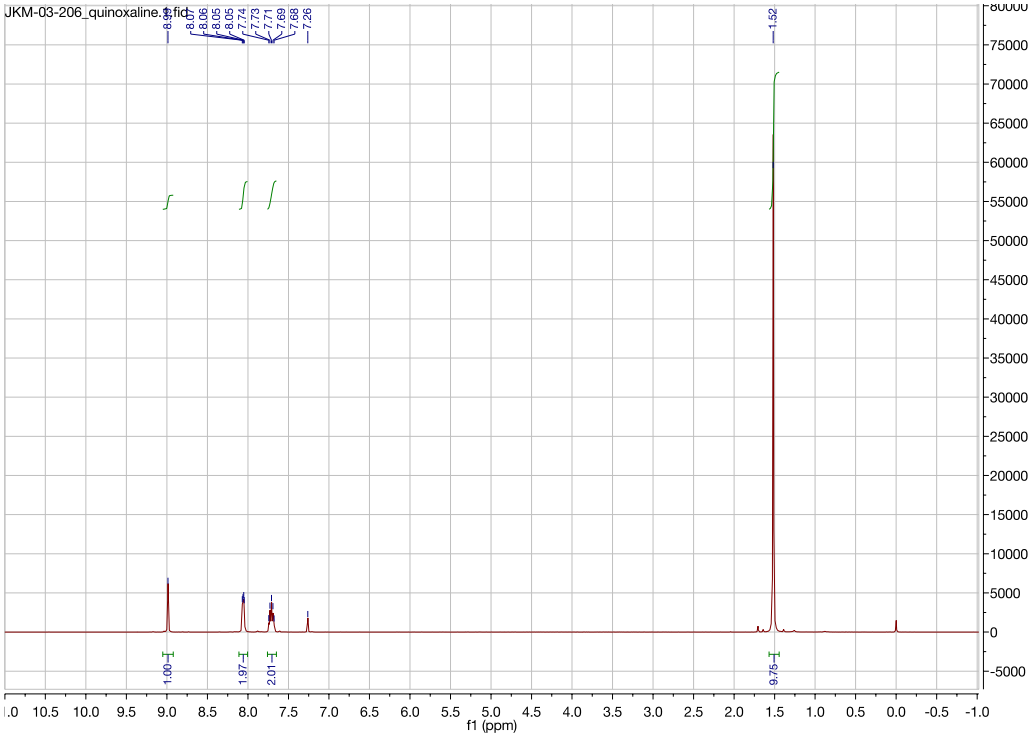


**Figure A11.11.** $^{1}$H NMR ($CDCl_3$, 500 MHz) spectrum of 2-(*tert*-butyl)quinoxaline (**1h**)

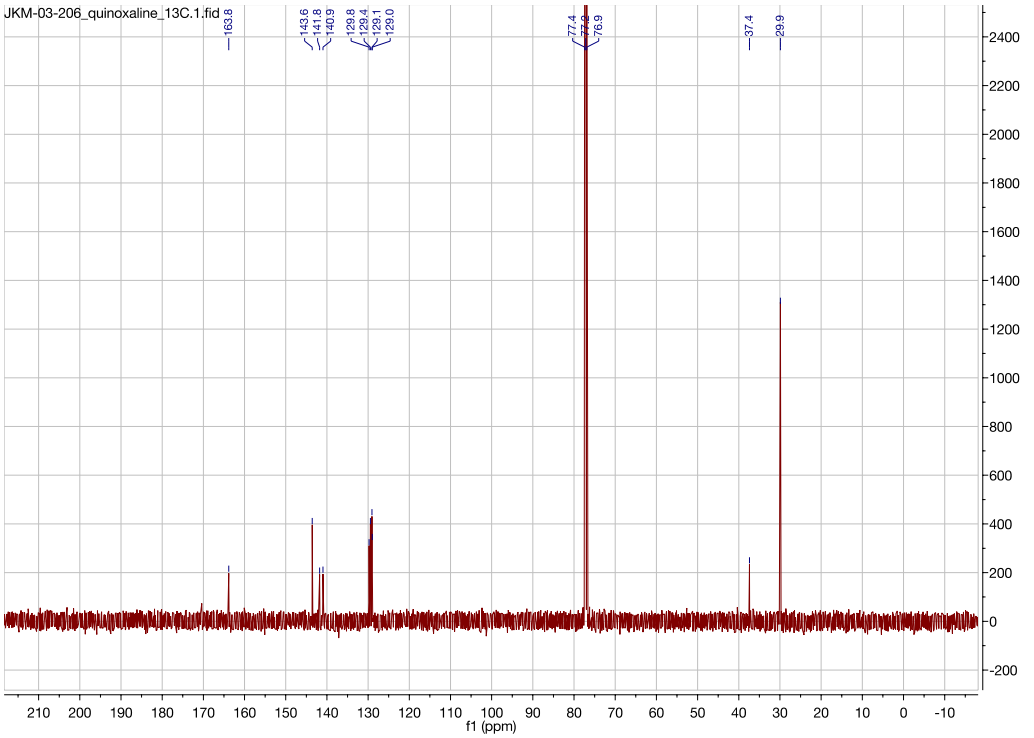


**Figure A11.12.** $^{13}$C NMR ($CDCl_3$, 125.8 MHz) spectrum of 2-(*tert*-butyl)quinoxaline (**1h**)

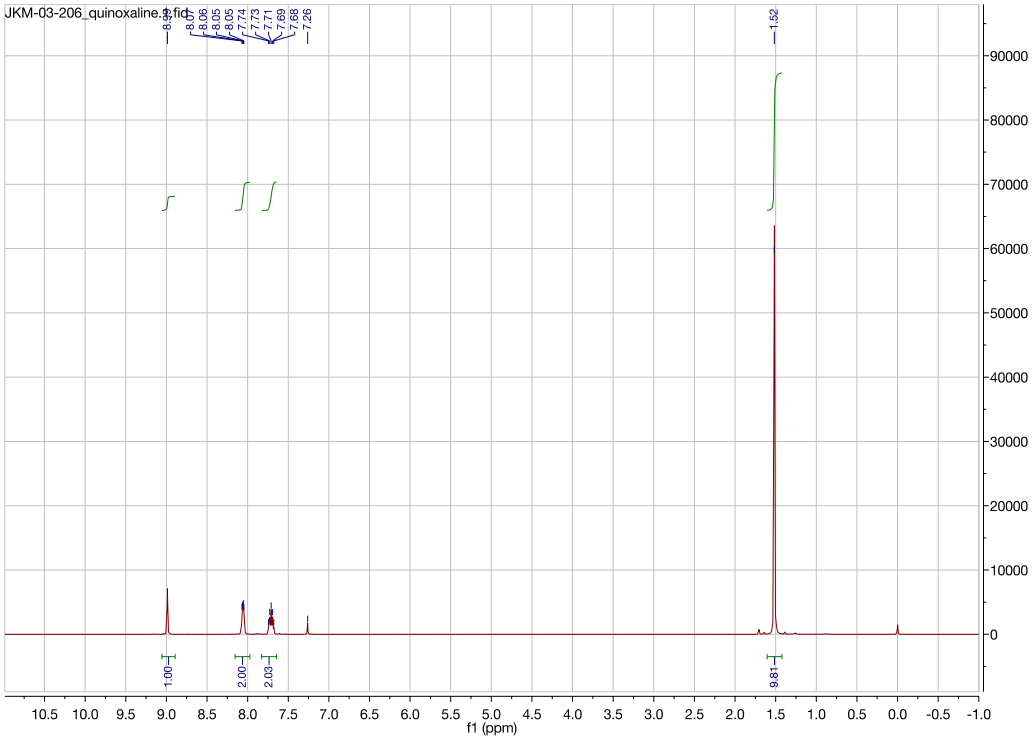


**Figure A11.13.** $^{1}$H NMR ($CDCl_3$, 500 MHz) spectrum of 2-(*tert*-butyl)-3-chloroquinoxaline (**1i**)

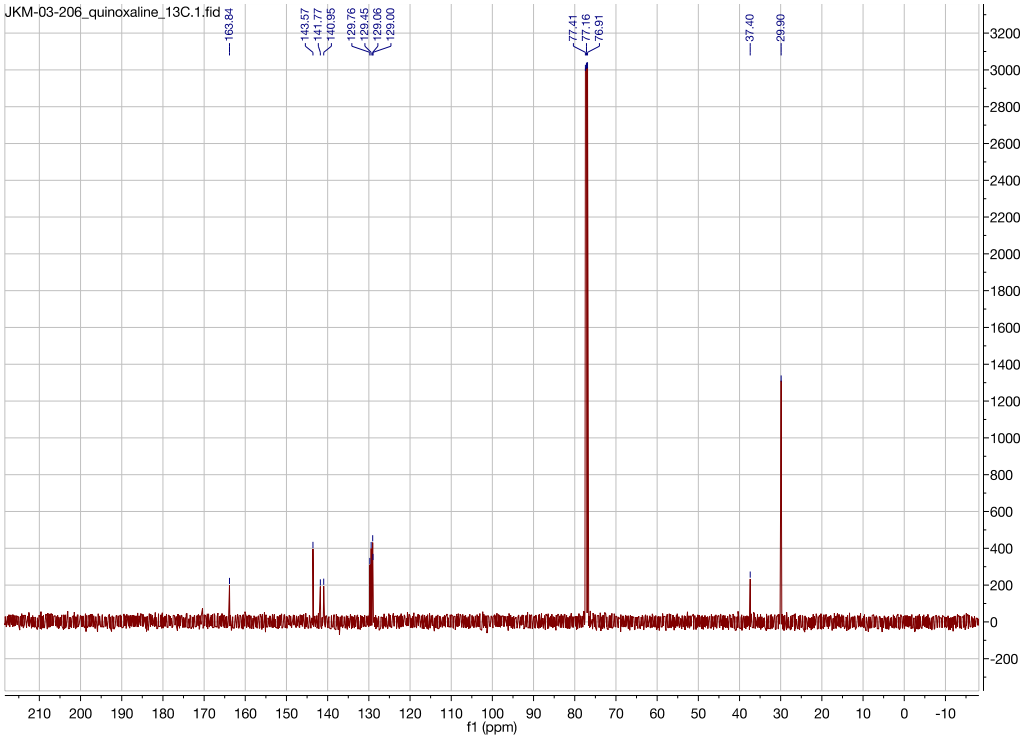


**Figure A11.14.** $^{13}$C NMR ($CDCl_3$, 125.8 MHz) spectrum of 2-(*tert*-butyl)-3-chloroquinoxaline (**1i**)

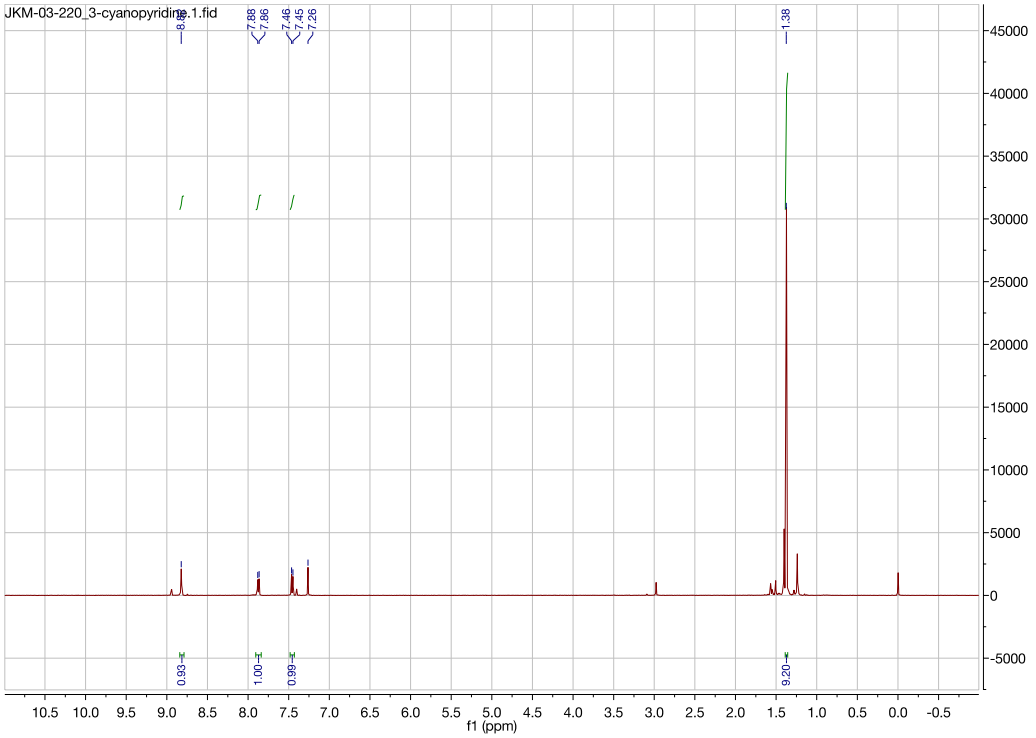


**Figure A11.15.** $^{1}$H NMR ($CDCl_3$, 500 MHz) spectrum of 6-(*tert*-butyl)nicotinonitrile (**1j**)

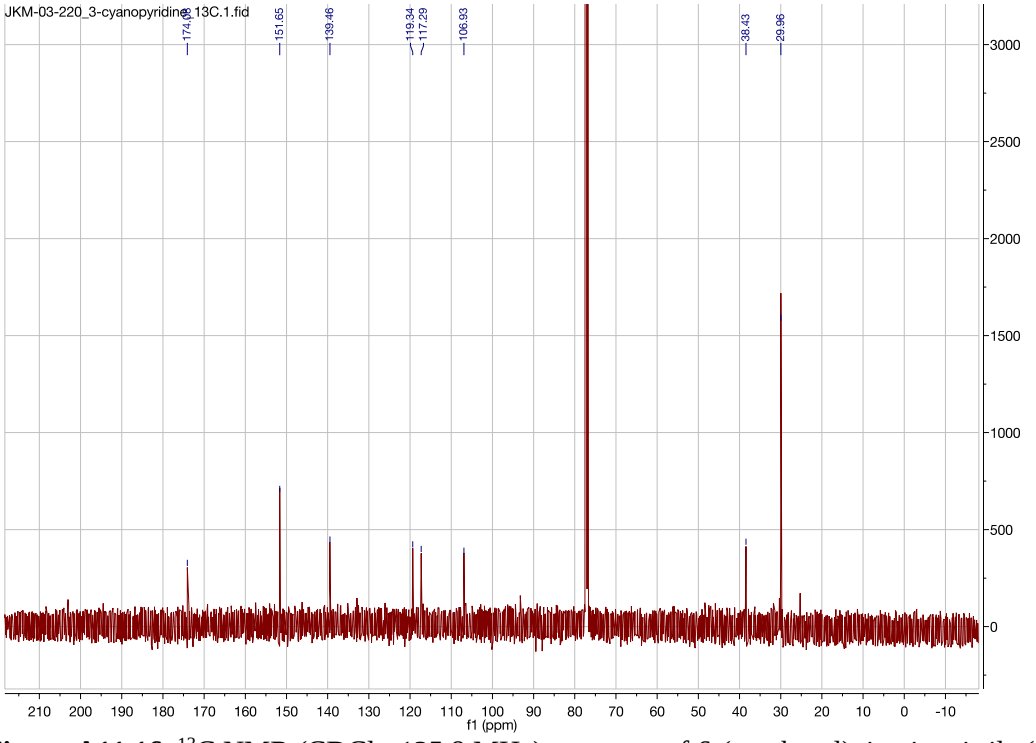


**Figure A11.16.** $^{13}$C NMR ($CDCl_3$, 125.8 MHz) spectrum of 6-(*tert*-butyl)nicotinonitrile (**1j**)

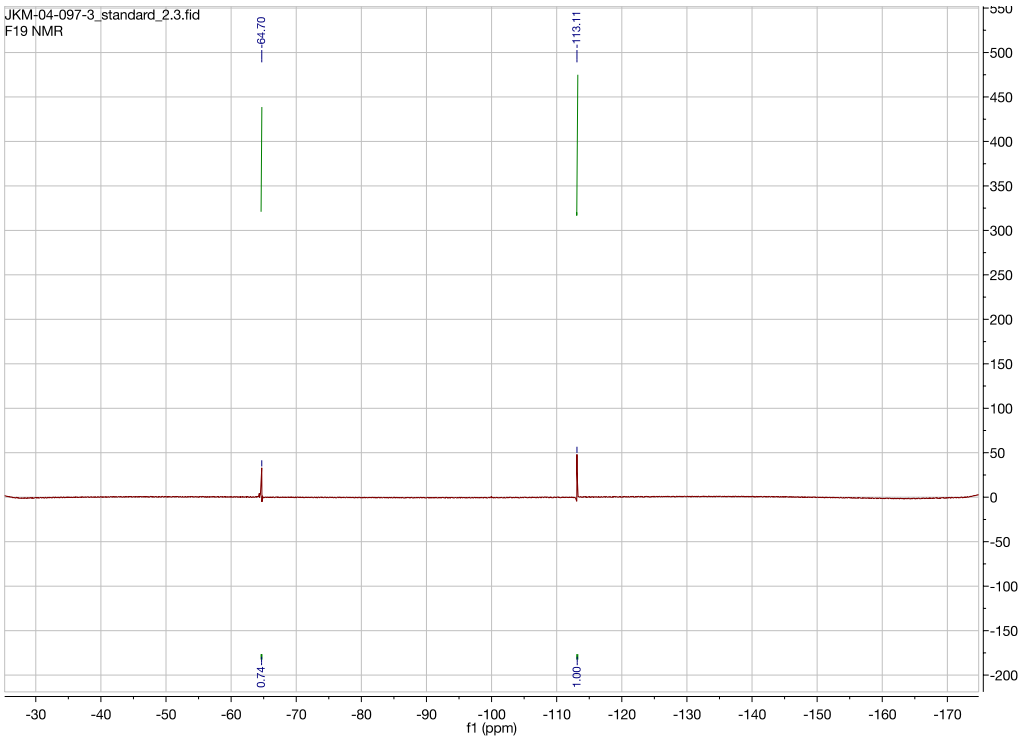


**Figure A11.17.** $^{19}F$ NMR ($CDCl_3$, 470.8 MHz) spectra of 2-(*tert*-Butyl)-4-(trifluoromethyl)pyridine (**1k**) with fluorobenzene

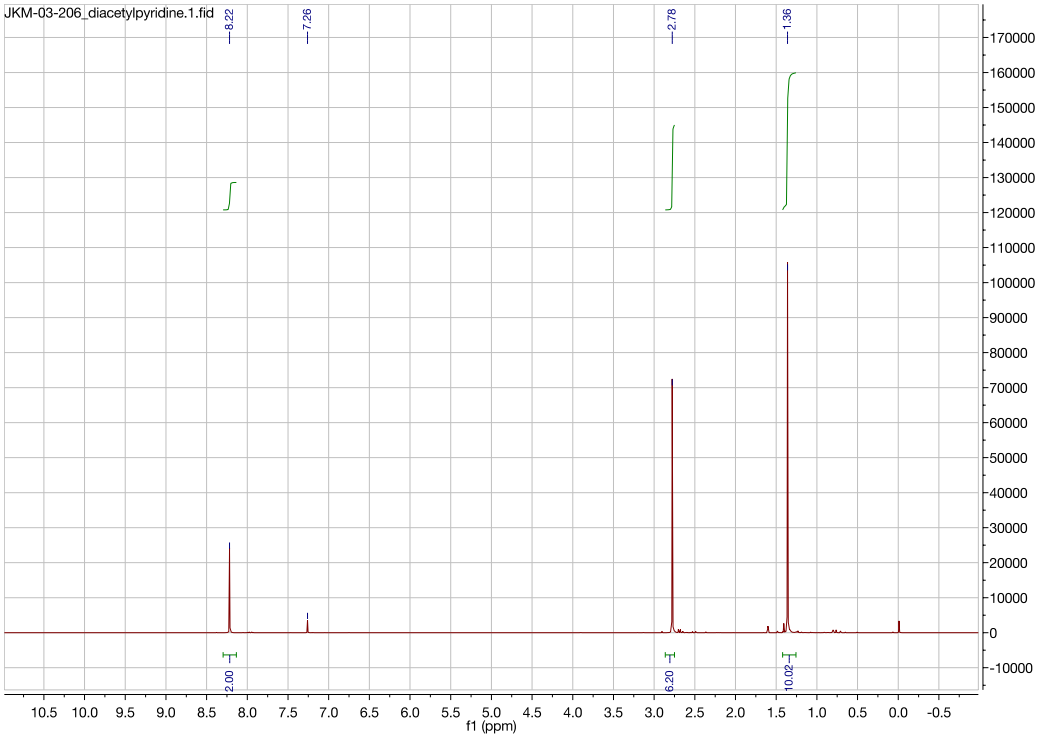


**Figure A11.18.** $^{1}$H NMR ($CDCl_3$, 500 MHz) spectrum of 1,1'-(4-(*tert*-butyl)pyridine-2,6-diyl)bis(ethan-1-one) (**1l**)

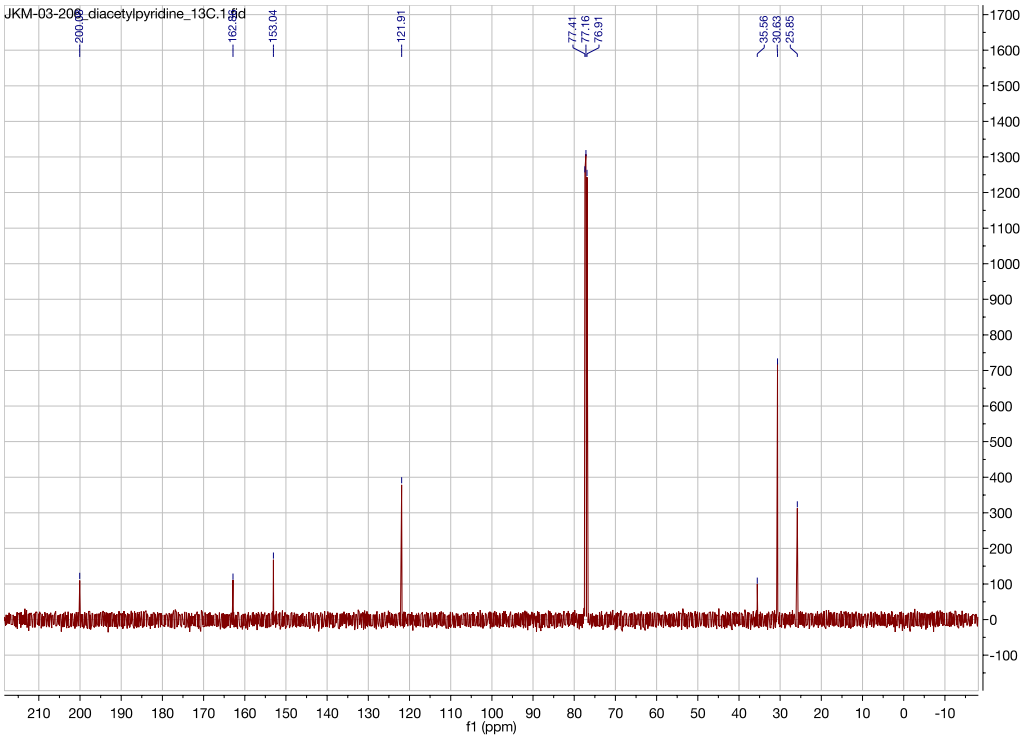


**Figure A11.19.** $^{13}$C NMR ($CDCl_3$, 125.8 MHz) spectrum of 1,1'-(4-(*tert*-butyl)pyridine-2,6-diyl)bis(ethan-1-one) (**1l**)

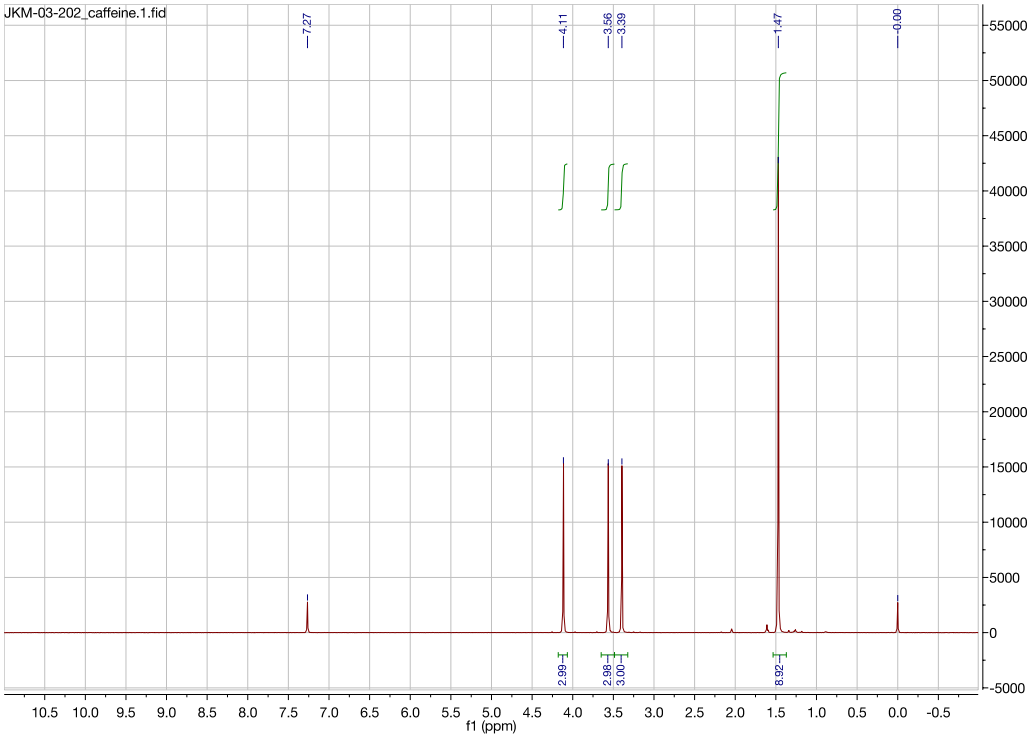


**Figure A11.20.** $^{1}$H NMR ($CDCl_3$, 500 MHz) spectrum of 8-(*tert*-butyl)-1,3,7-trimethyl-3,7-dihydro-1*H*-purine-2,6-dione (**1m**)

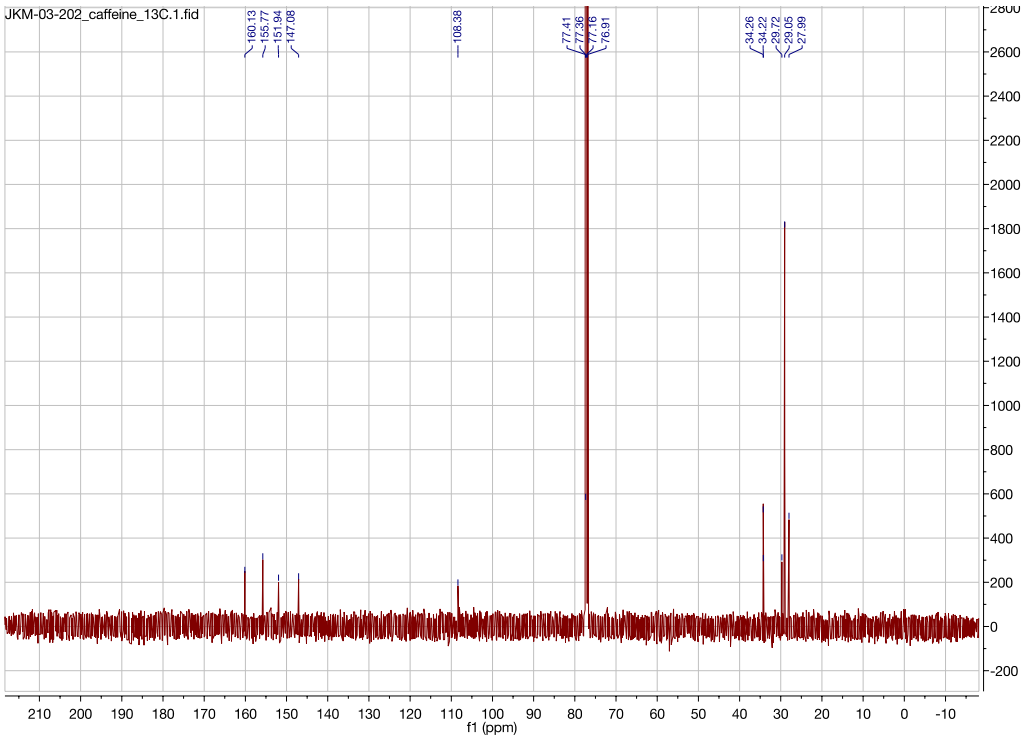


**Figure A11.21.** $^{13}$C NMR ($CDCl_3$, 125.8 MHz) spectrum of 8-(*tert*-butyl)-1,3,7-trimethyl-3,7-dihydro-1*H*-purine-2,6-dione (**1m**)

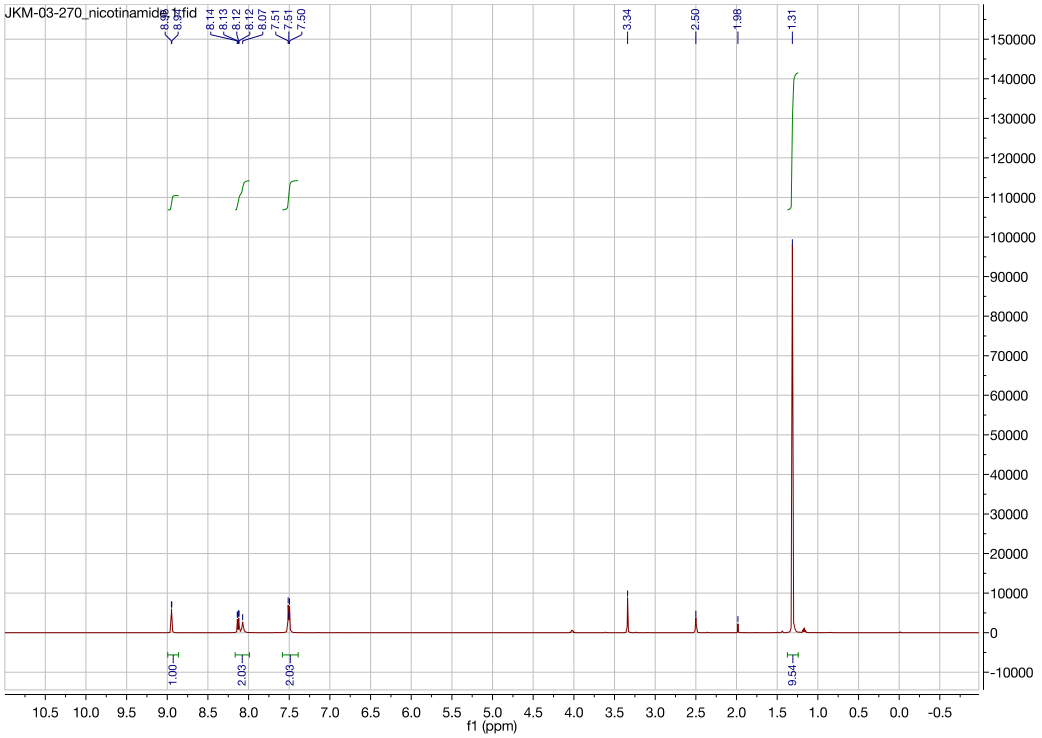


**Figure A11.22.** $^{1}$H NMR ($CDCl_3$, 500 MHz) spectrum of 6-(*tert*-butyl)nicotinamide (**1n**)

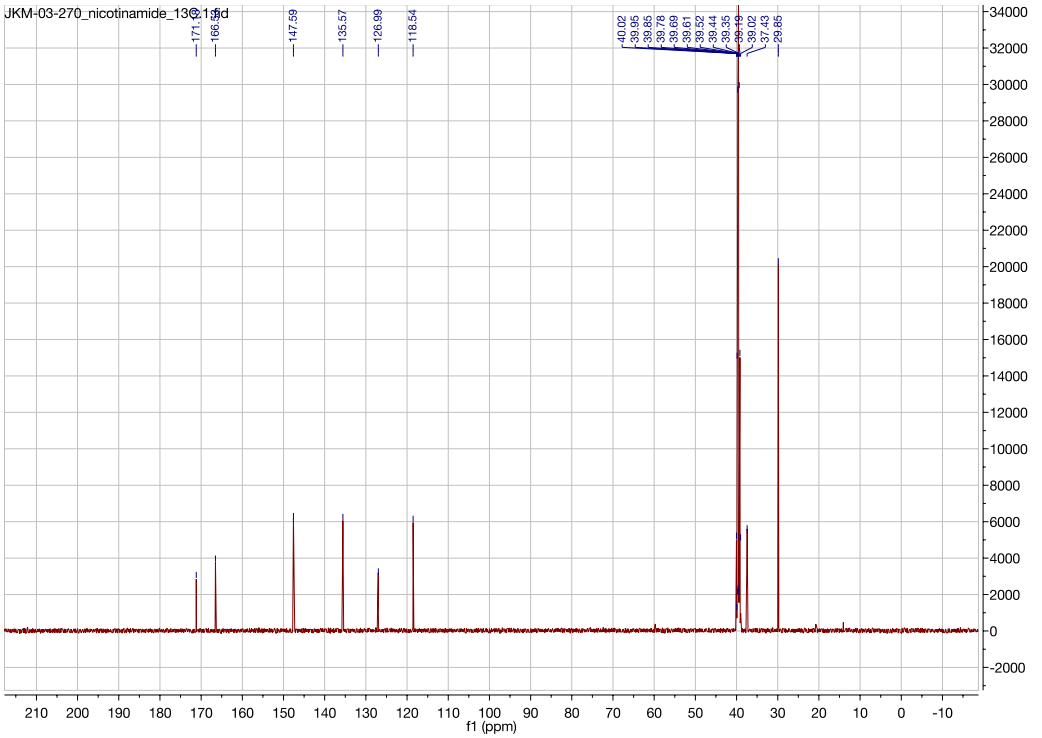


**Figure A11.23.** $^{13}$C NMR ($CDCl_3$, 125.8 MHz) spectrum of 6-(*tert*-butyl)nicotinamide (**1n**)

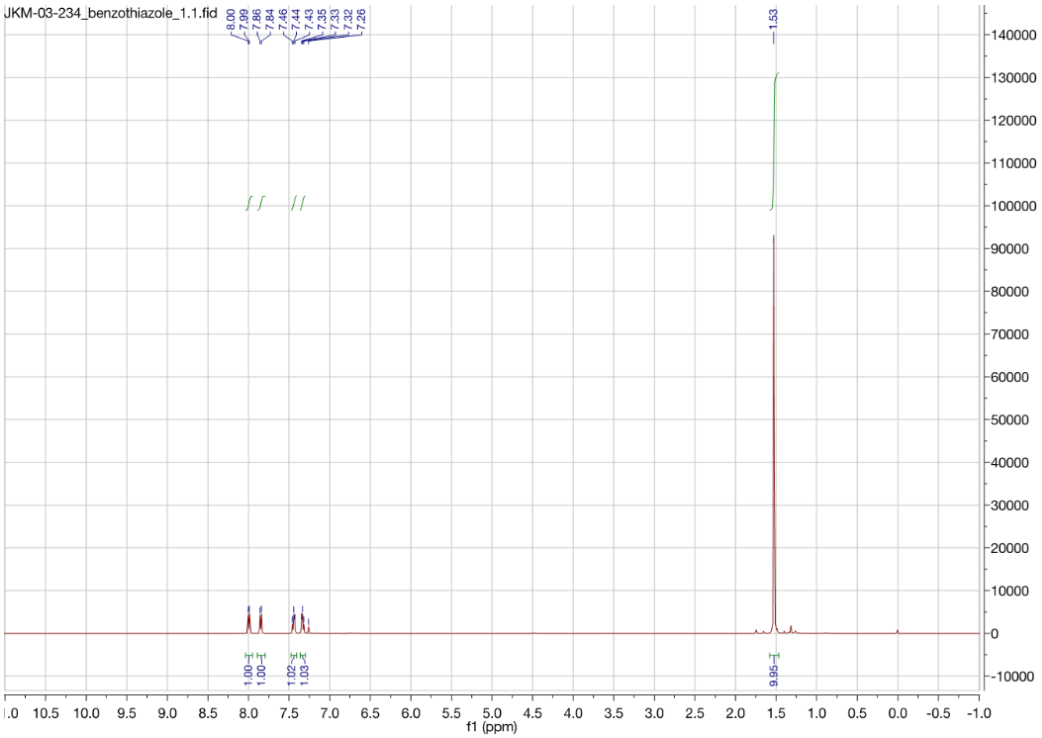


**Figure A11.24.** $^{1}$H NMR ($CDCl_3$, 500 MHz) spectrum of 2-(*tert*-butyl)benzo[*d*]thiazole (**1o**)

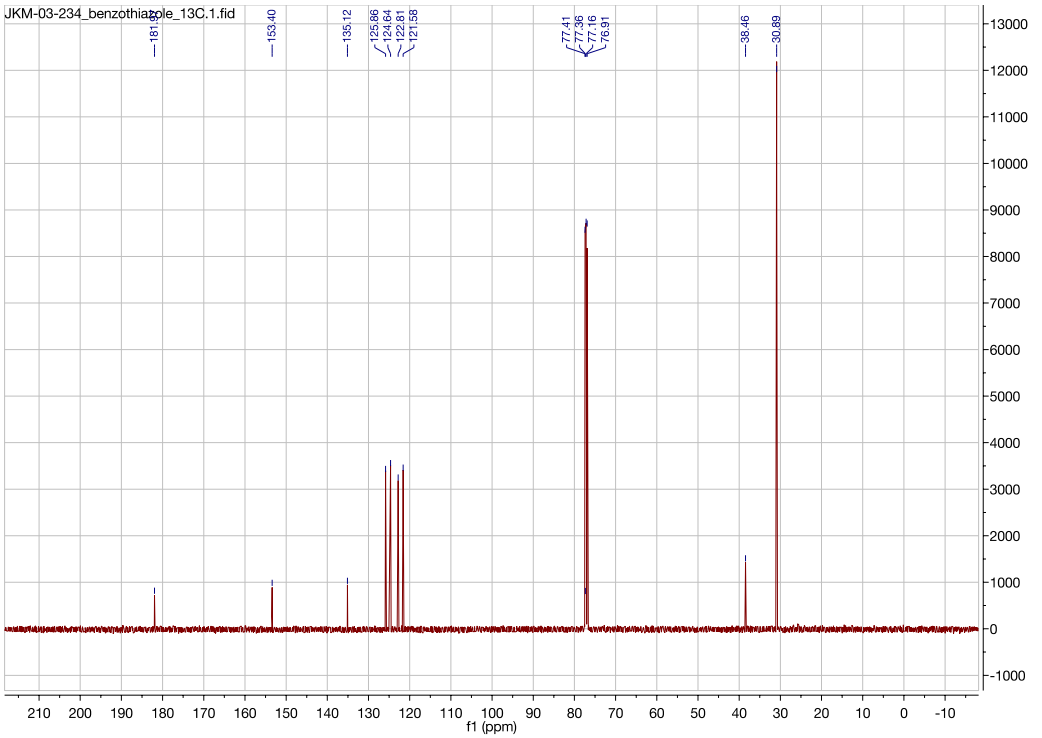


**Figure A11.25.** $^{13}$C NMR ($CDCl_3$, 125.8 MHz) spectrum of 2-(*tert*-butyl)benzo[*d*]thiazole (**1o**)

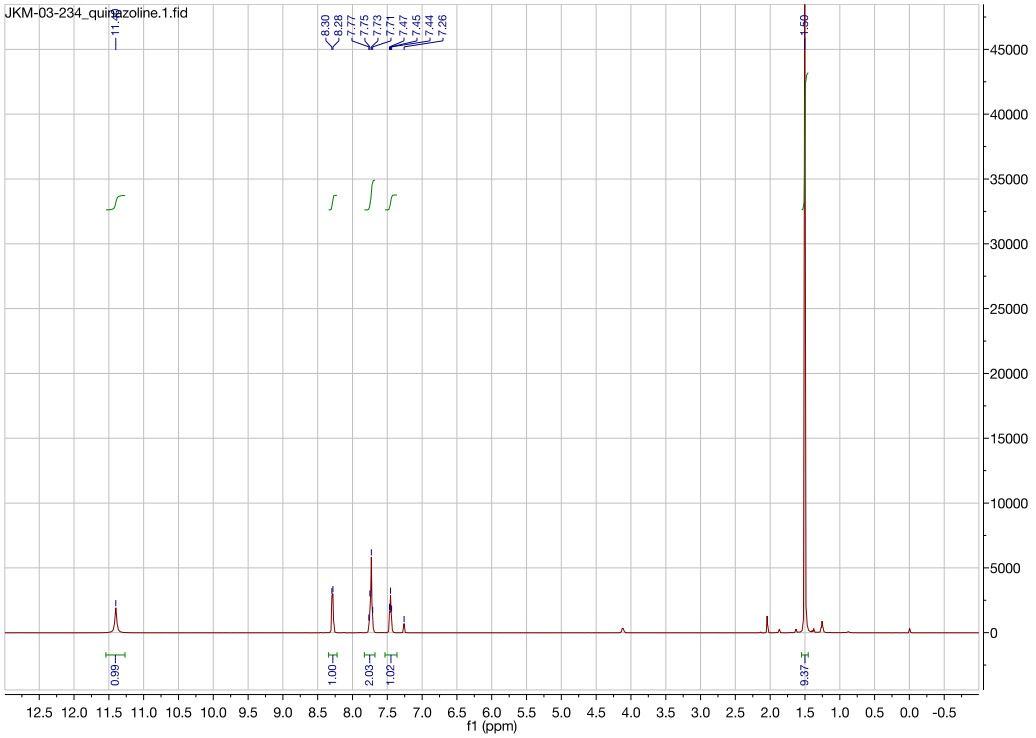


**Figure A11.26.** $^{1}$H NMR ($CDCl_3$, 500 MHz) spectrum of 2-(*tert*-butyl)quinazolin-4(3*H*)-one (**1p**)

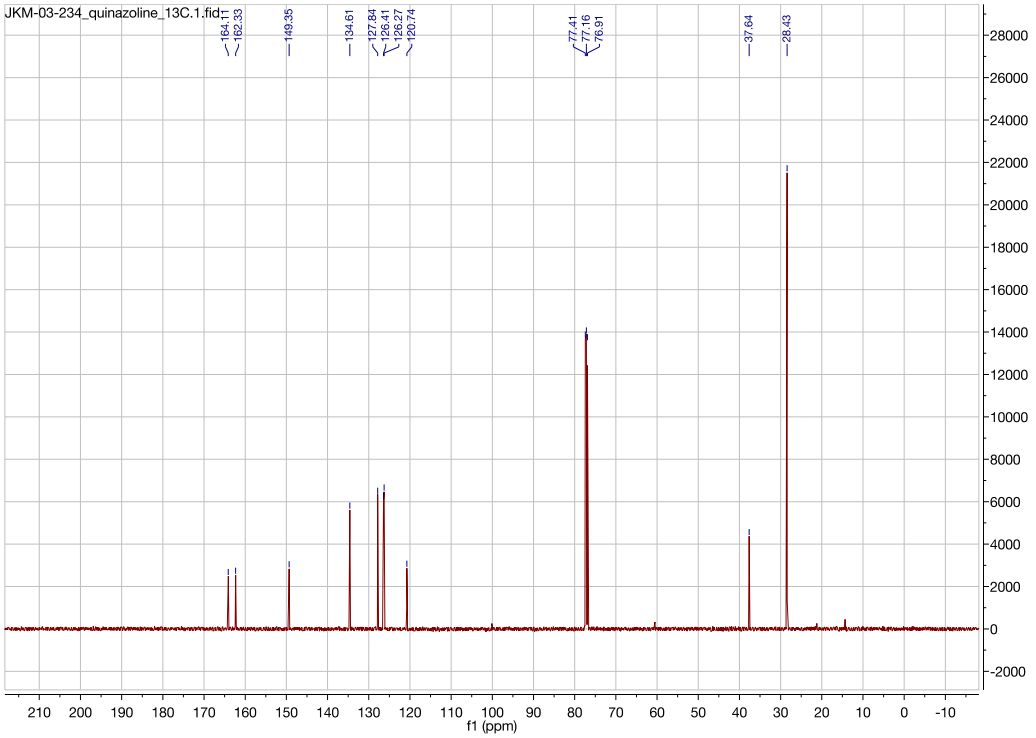


**Figure A11.27.** $^{13}$C NMR ($CDCl_3$, 125.8 MHz) spectrum of 2-(*tert*-butyl)quinazolin-4(3*H*)-one (**1p**)

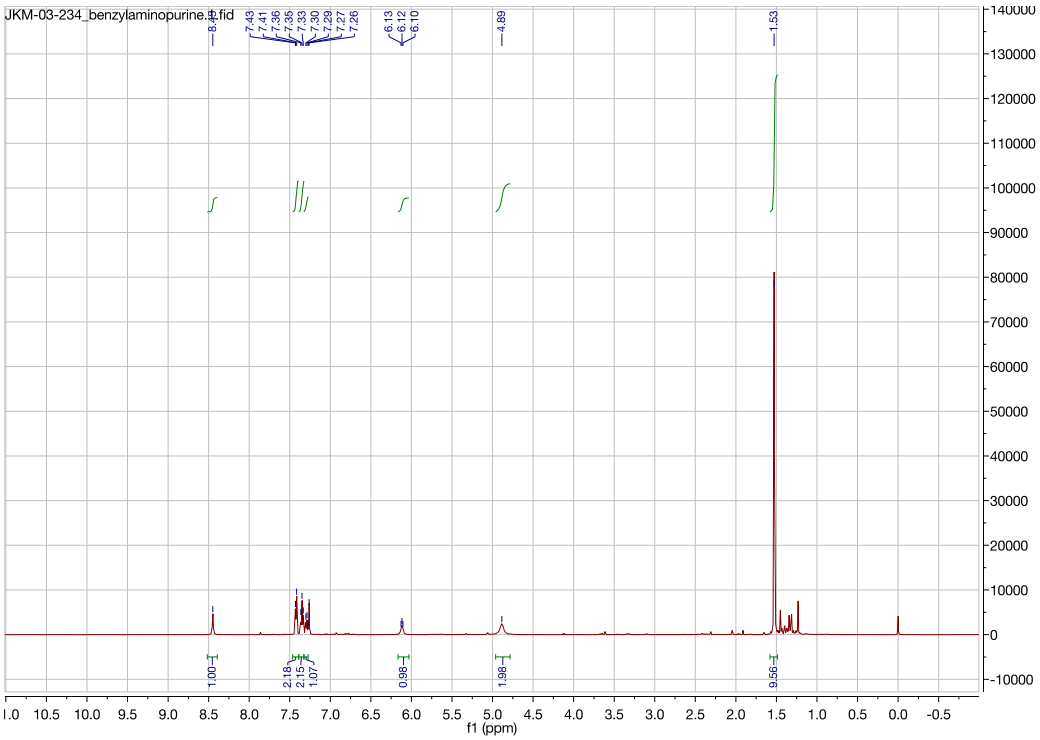


**Figure A11.28.** $^{1}$H NMR ($CDCl_3$, 500 MHz) spectrum of *N*-benzyl-2-(*tert*-butyl)-7*H*-purin-6-amine (**1q**)

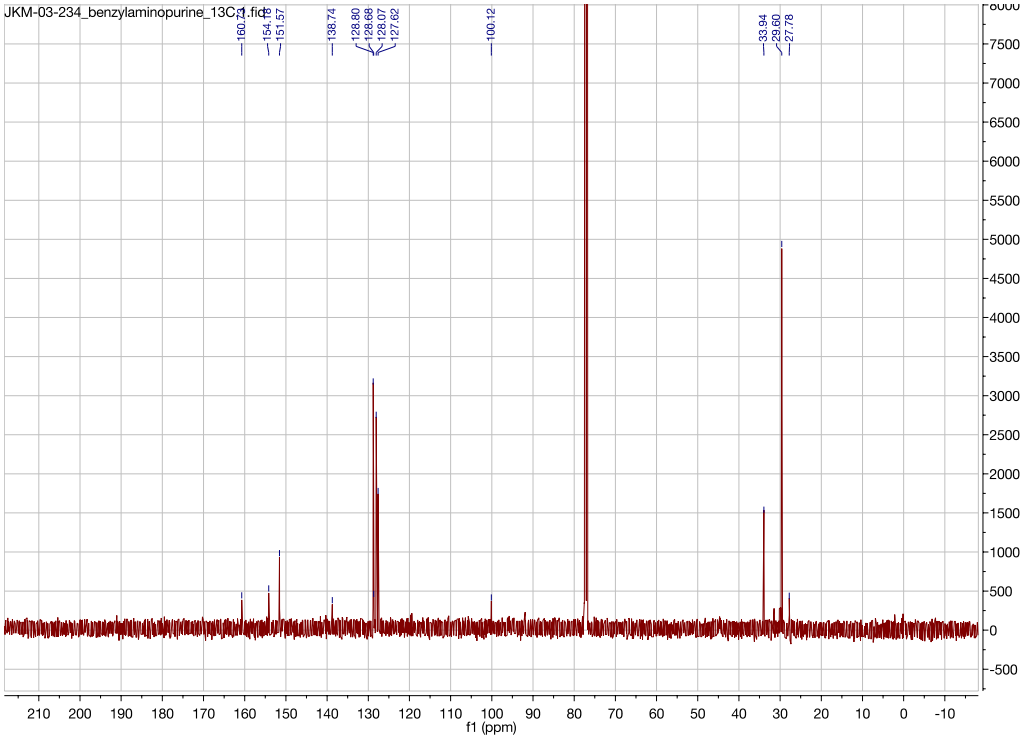


**Figure A11.29.** $^{13}$C NMR ($CDCl_3$, 125.8 MHz) spectrum of *N*-benzyl-2-(*tert*-butyl)-7*H*-purin-6-amine (**1q**)

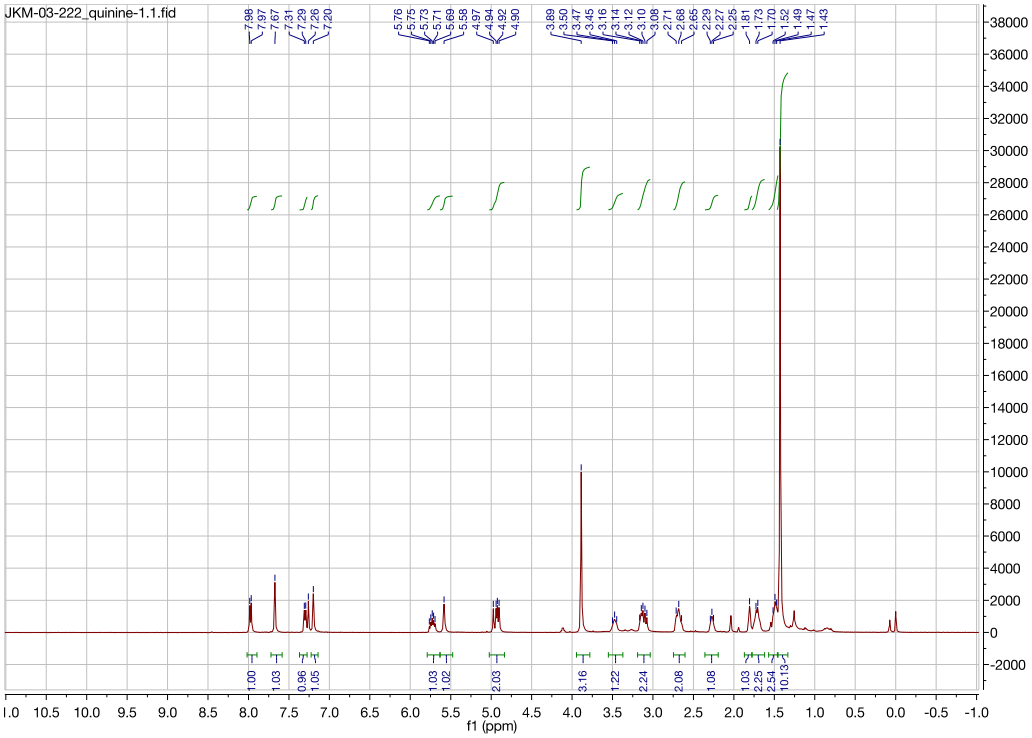


**Figure A11.30.** $^{1}$H NMR ($CDCl_3$, 500 MHz) spectrum of (1*R*)-(2-(*tert*-butyl)-6-methoxyquinolin-4-yl)(5-vinylquinuclidin-2-yl)methanol (**1r**)

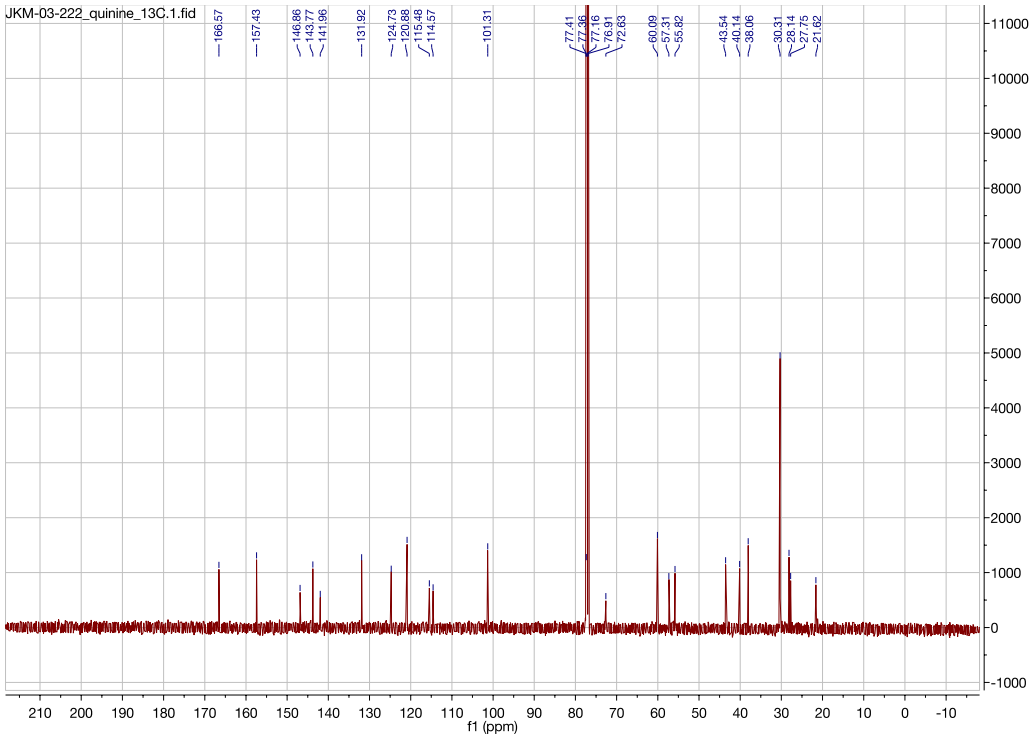


**Figure A11.31.** $^{13}$C NMR ($CDCl_3$, 125.8 MHz) spectrum of (1*R*)-(2-(*tert*-butyl)-6-methoxyquinolin-4-yl)(5-vinylquinuclidin-2-yl)methanol (**1r**)

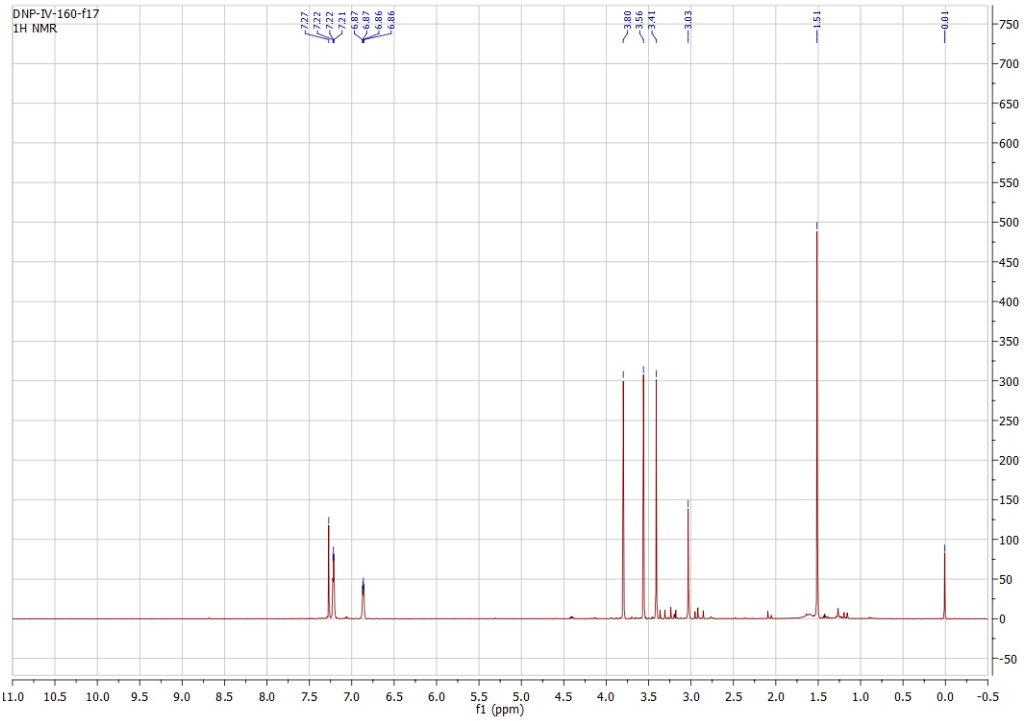


**Figure A11.32.** $^{1}H$ NMR ($CDCl_3$, 500 MHz) spectrum of 1,3,9-trimethyl-8-(2-methyl-1-phenylpropan-2-yl)-3,9-dihydro-1H-purine-2,6-dione (**1v**)

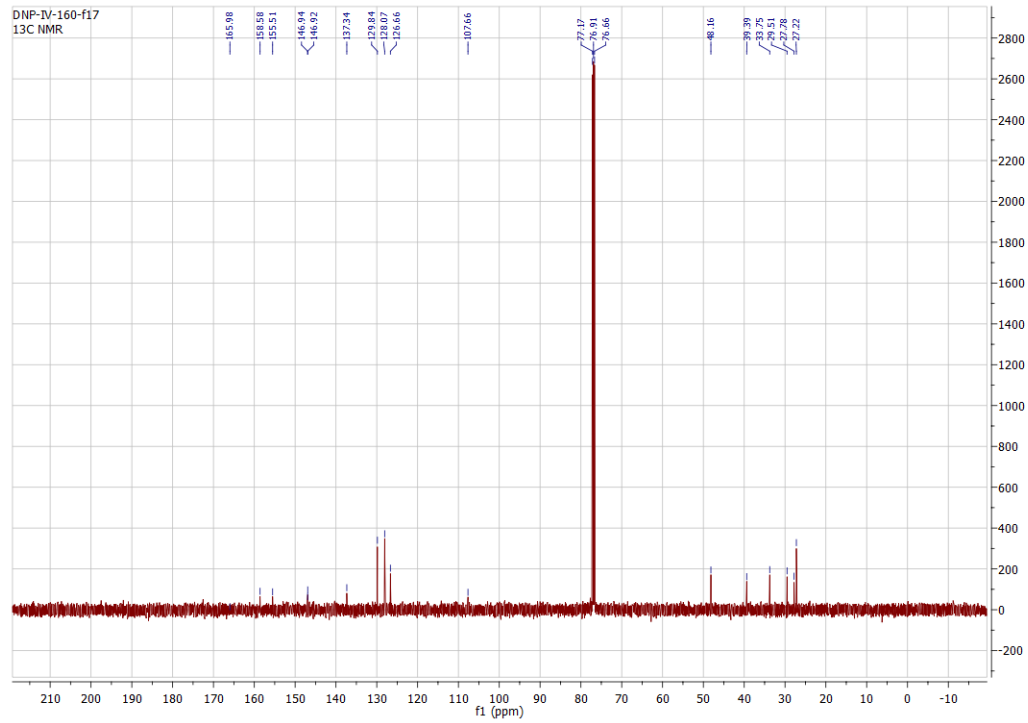


**Figure A11.33.** $^{13}C$ NMR ($CDCl_3$, 125.8 MHz) spectrum of 1,3,9-trimethyl-8-(2-methyl-1-phenylpropan-2-yl)-3,9-dihydro-1H-purine-2,6-dione (**1v**)

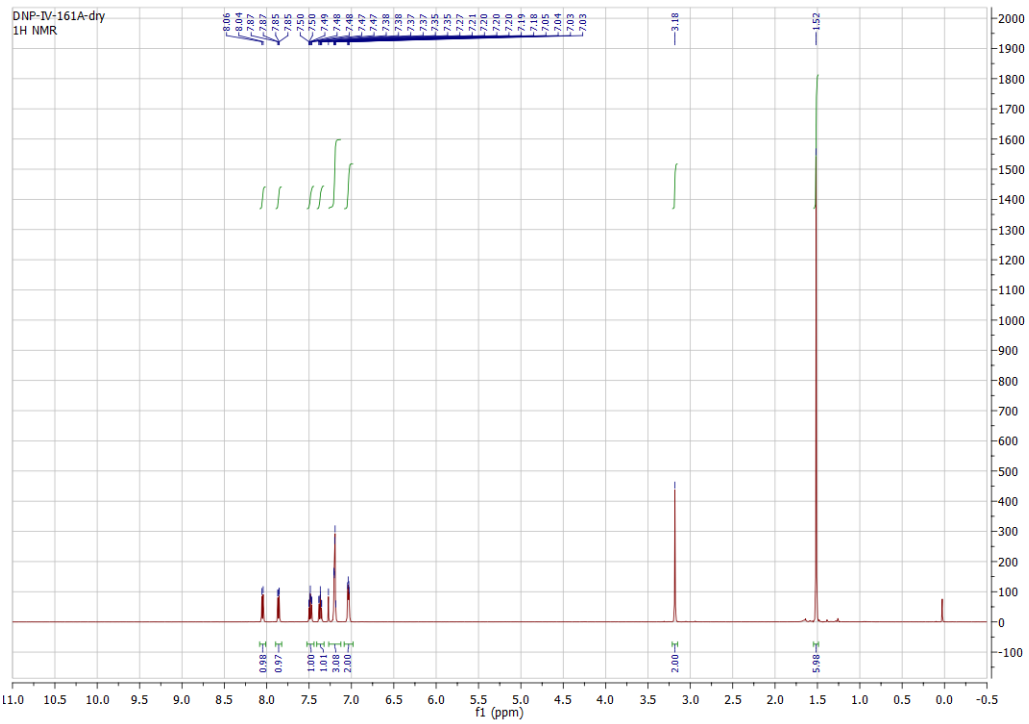


**Figure A11.34.** $^{1}$H NMR ($CDCl_3$, 500 MHz) spectrum of 2-(2-methyl-1-phenylpropan-2-yl)benzo[d]thiazole (**1w**)

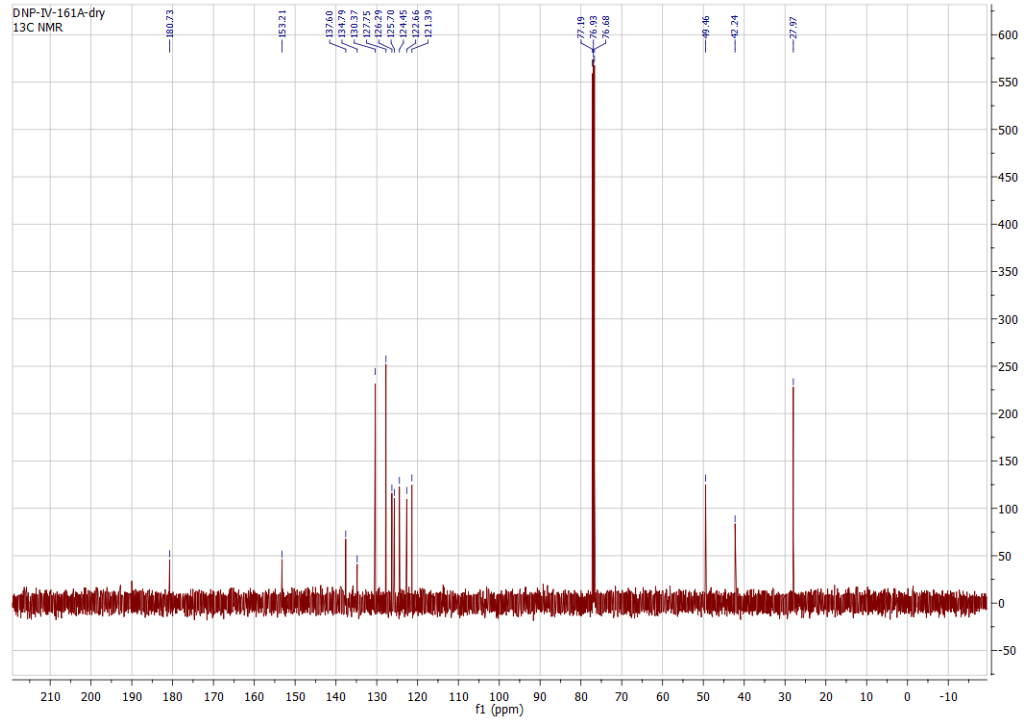


**Figure A11.35.** $^{13}$C NMR ($CDCl_3$, 125.8 MHz) spectrum of 2-(2-methyl-1-phenylpropan-2-yl)benzo[d]thiazole (**1w**)

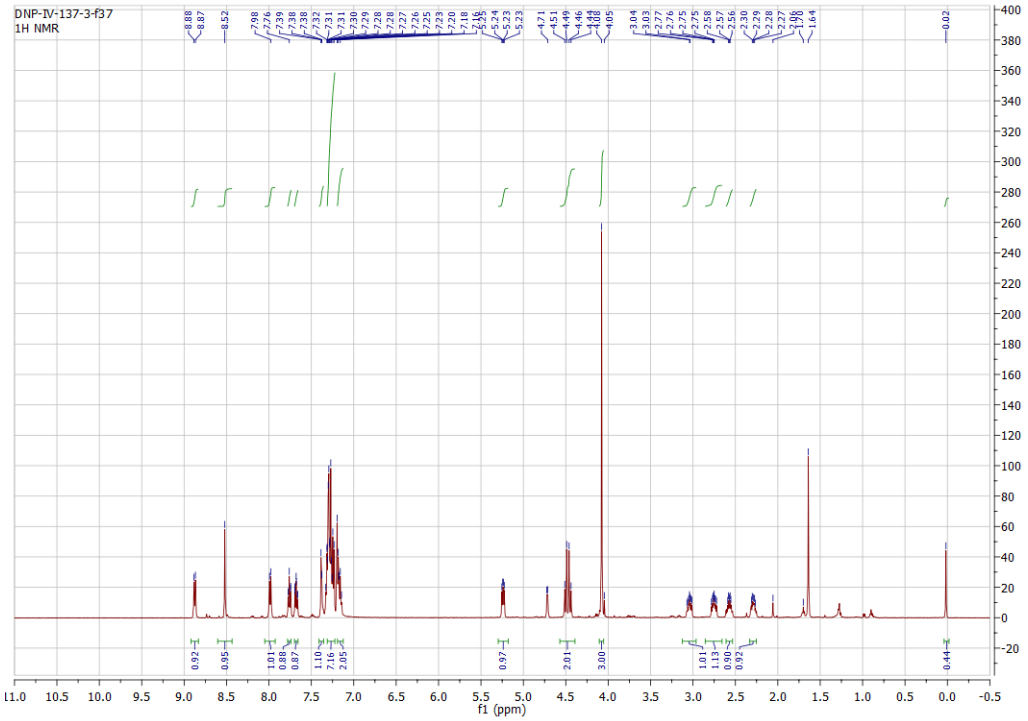


**Figure A11.36.** $^{1}$H NMR ($CDCl_3$, 500 MHz) spectrum of methyl 1-(1-(benzyloxy)-3-phenylpropyl)isoquinoline-3-carboxylate (**2a**)

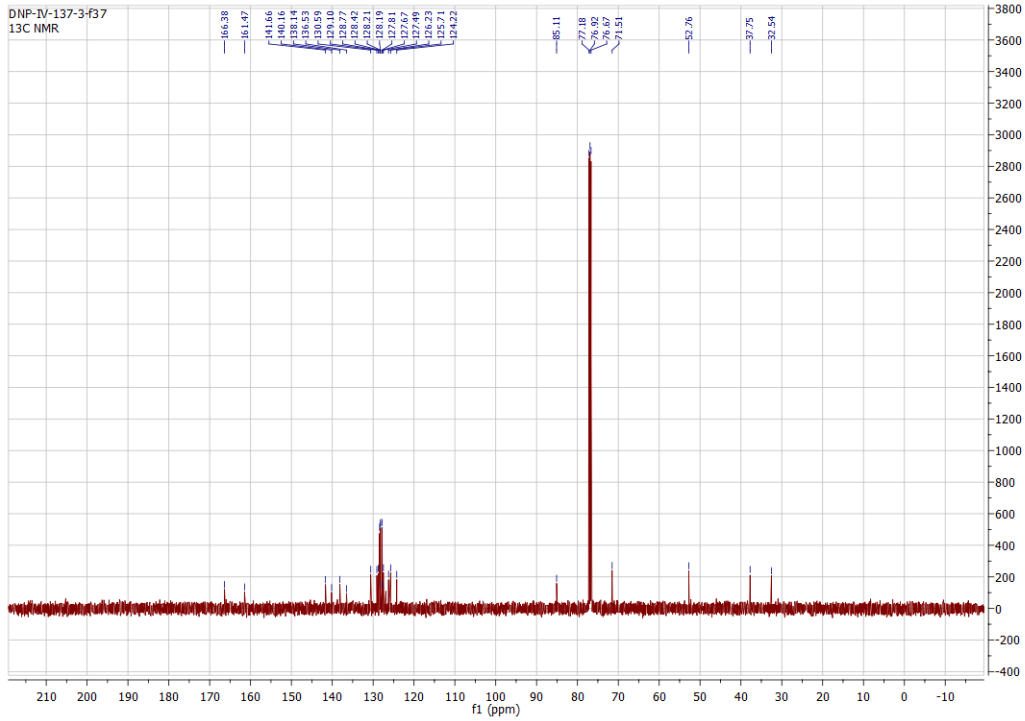


**Figure A11.37.** $^{13}$C NMR ($CDCl_3$, 125.8 MHz) spectrum of methyl 1-(1-(benzyloxy)-3-phenylpropyl)isoquinoline-3-carboxylate (**2a**)

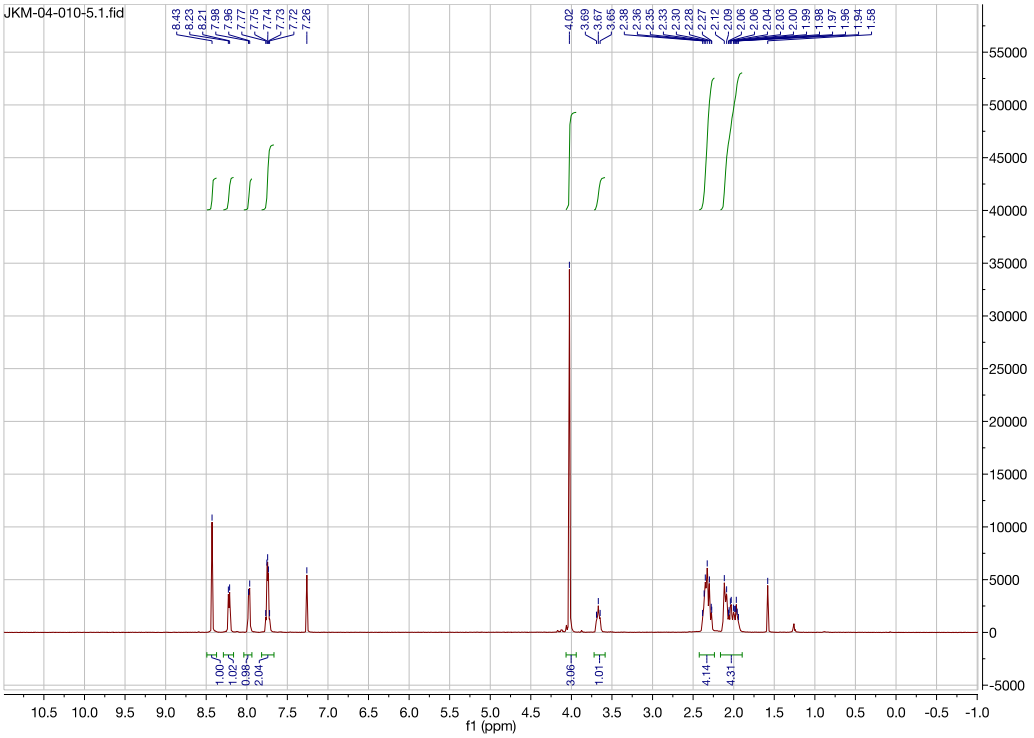


**Figure A11.38.** $^{1}$H NMR ($CDCl_3$, 500 MHz) spectrum of methyl 1-(4,4-difluorocyclohexyl)isoquinoline-3-carboxylate (**2b**)

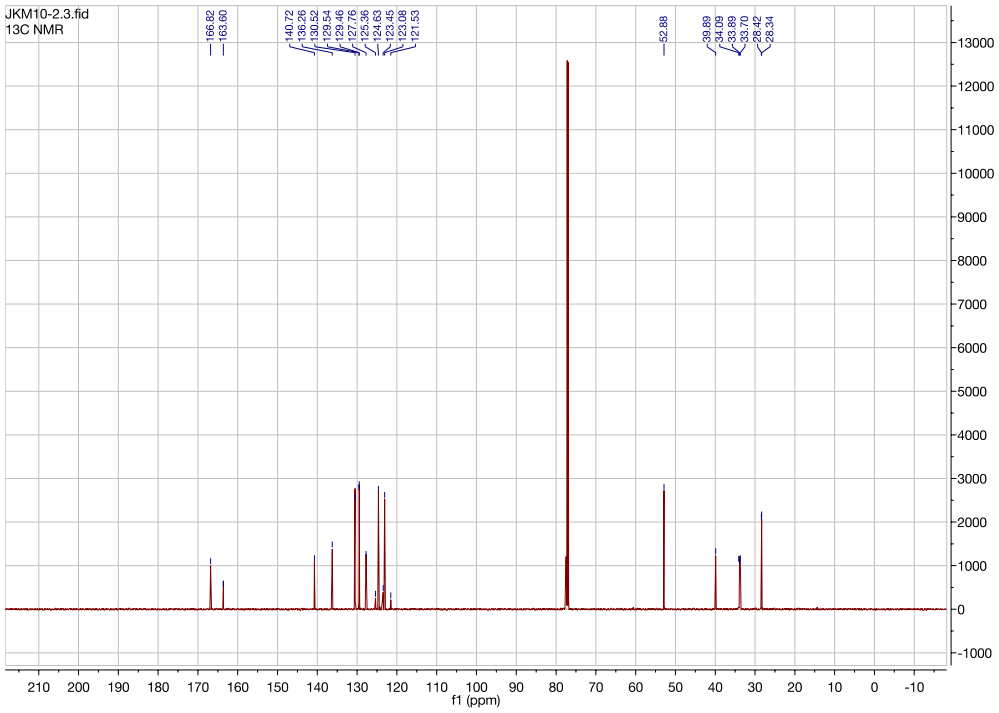


**Figure A11.39.** $^{13}$C NMR ($CDCl_3$, 125.8 MHz) spectrum of methyl 1-(4,4-difluorocyclohexyl)isoquinoline-3-carboxylate (**2b**)

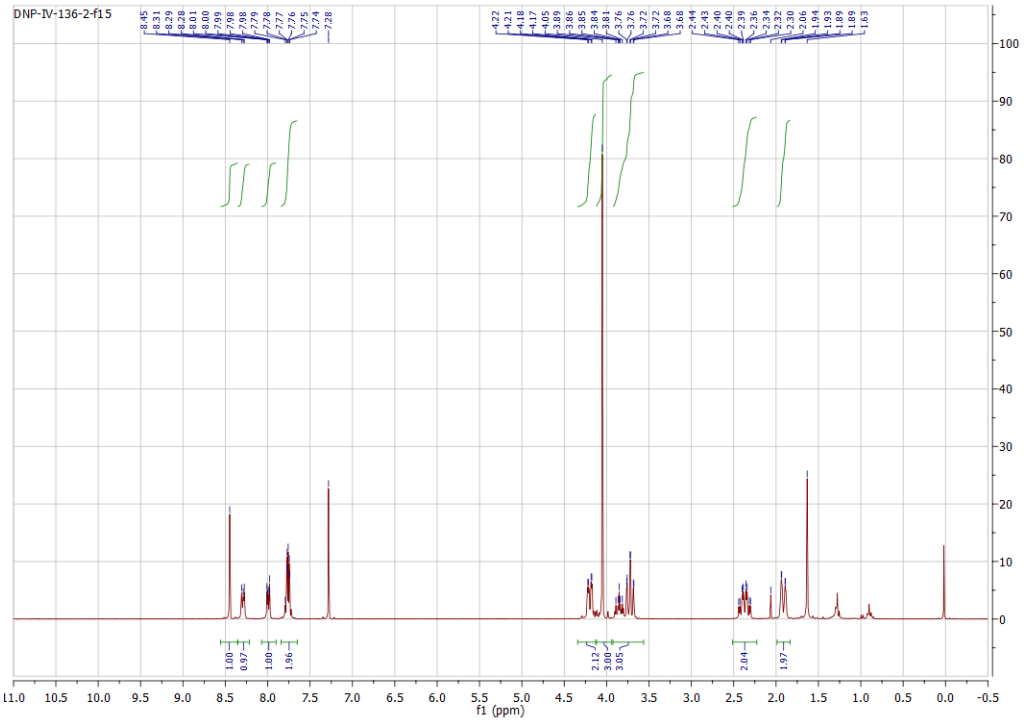


**Figure A11.40.** $^{1}$H NMR ($CDCl_3$, 500 MHz) spectrum of methyl 1-(tetrahydro-2H-pyran-4-yl)isoquinoline-3-carboxylate (**2c**)

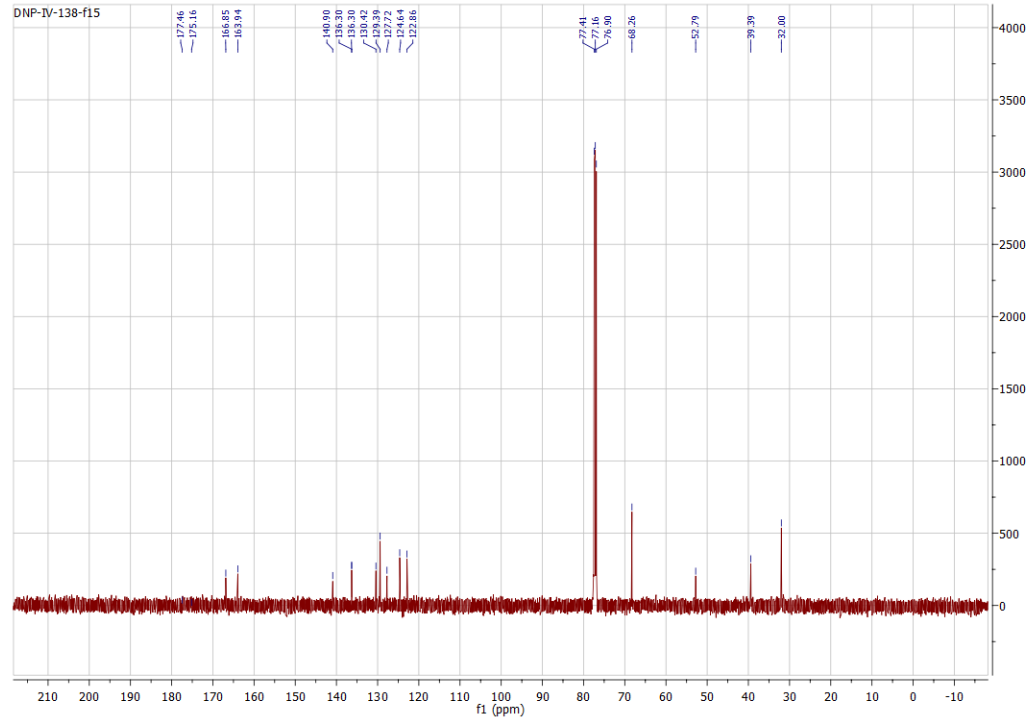


**Figure A11.41.** $^{13}$C NMR ($CDCl_3$, 125.8 MHz) spectrum of methyl 1-(tetrahydro-2H-pyran-4-yl)isoquinoline-3-carboxylate (**2c**)

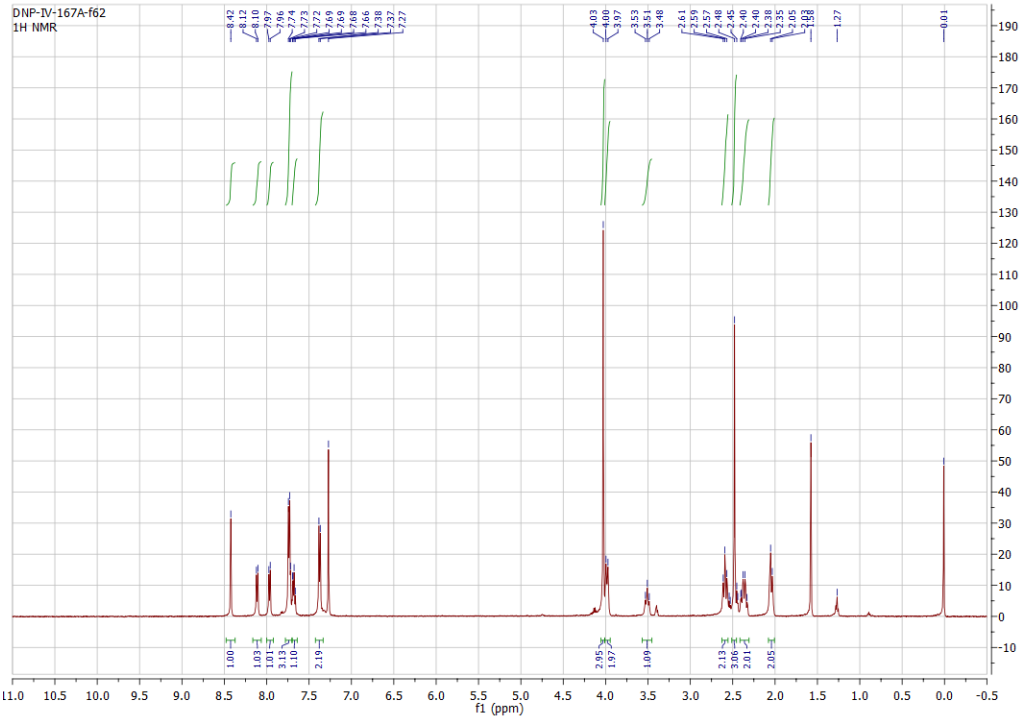


**Figure A11.42.** $^{1}$H NMR ($CDCl_3$, 500 MHz) spectrum of methyl 1-(1-tosylpiperidin-4-yl)isoquinoline-3-carboxylate (**2d**)

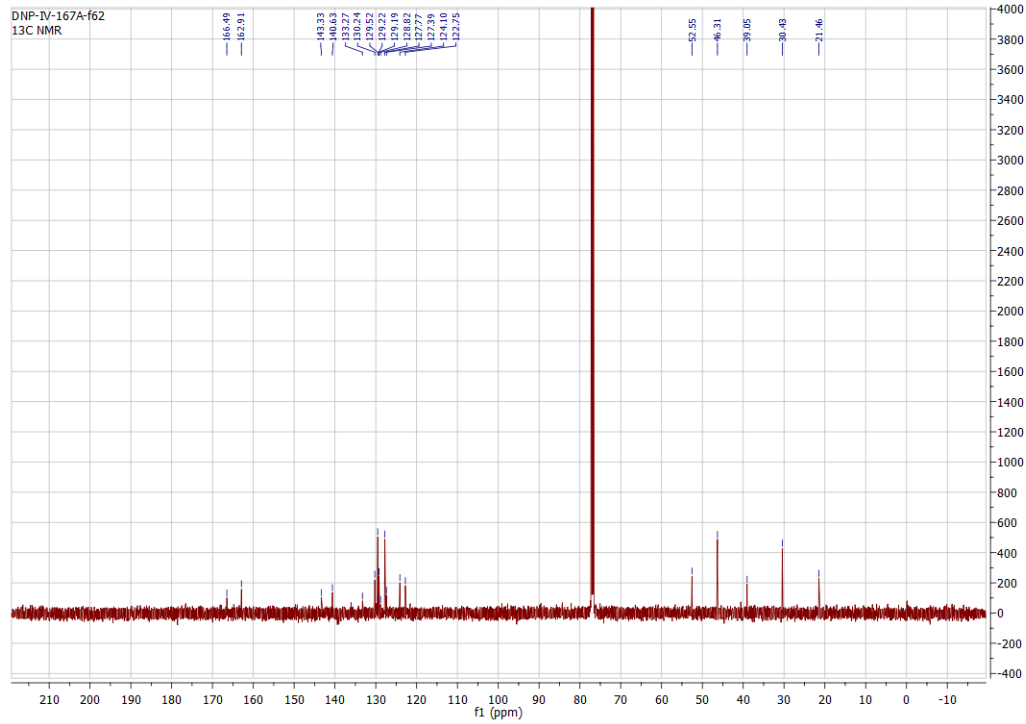


**Figure A11.43.** $^{13}$C NMR ($CDCl_3$, 125.8 MHz) spectrum of methyl 1-(1-tosylpiperidin-4-yl)isoquinoline-3-carboxylate (**2d**)

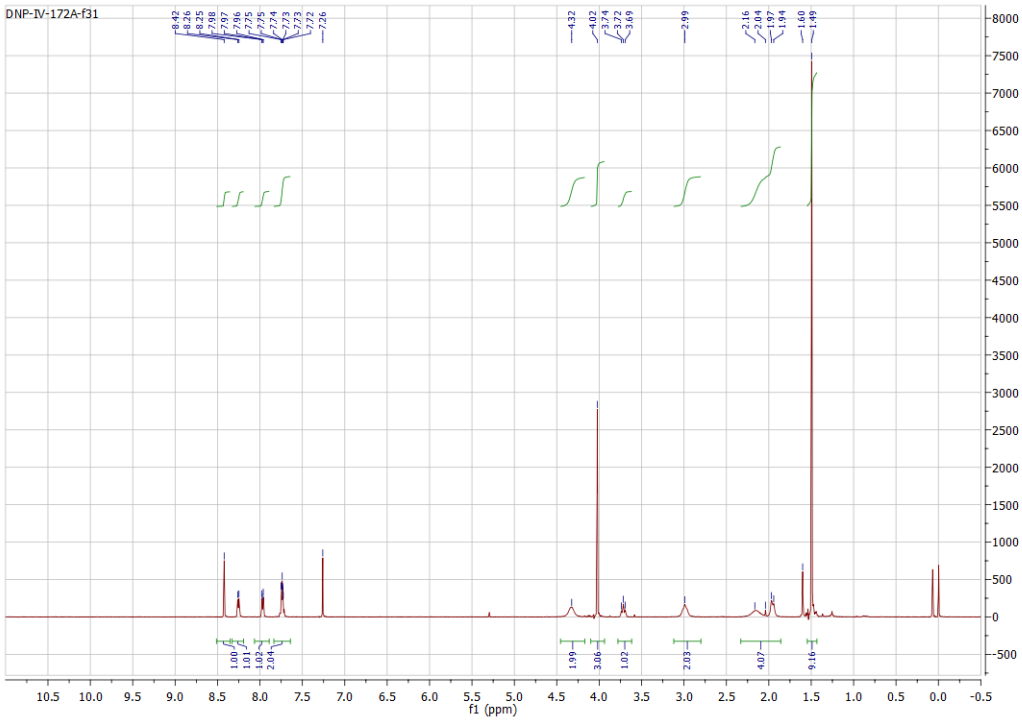


**Figure A11.44.** $^{1}$H NMR ($CDCl_3$, 500 MHz) spectrum of methyl 1-(1-(*tert*-butoxycarbonyl)piperidin-4-yl)isoquinoline-3-carboxylate (**2e**)

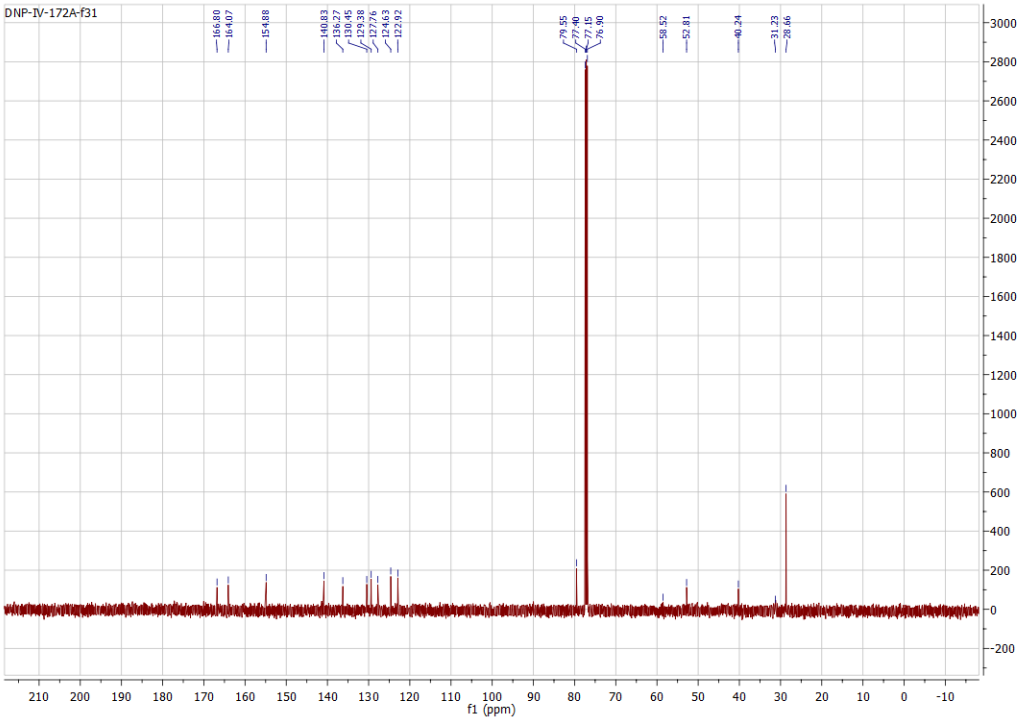


**Figure A11.45.** $^{13}$C NMR ($CDCl_3$, 125.8 MHz) spectrum of methyl 1-(1-(*tert*-butoxycarbonyl)piperidin-4-yl)isoquinoline-3-carboxylate (**2e**)

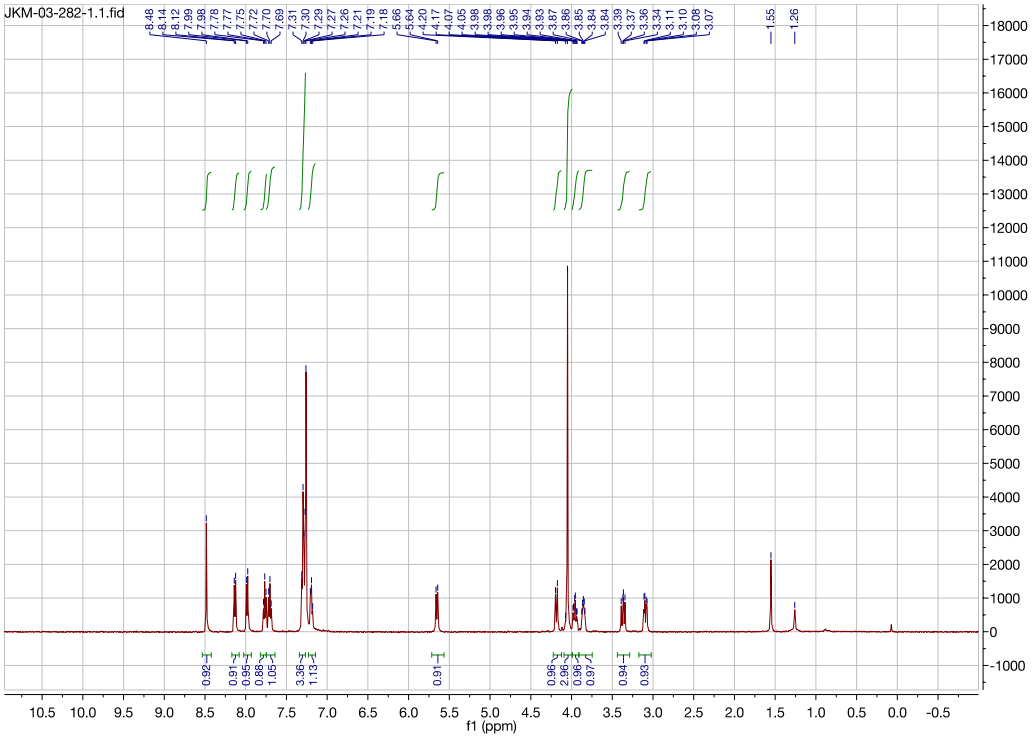


**Figure A11.46.** $^{1}$H NMR ($CDCl_3$, 500 MHz) spectrum of methyl 1-(1-hydroxy-3-phenylpropan-2-yl)isoquinoline-3-carboxylate (**2f**)

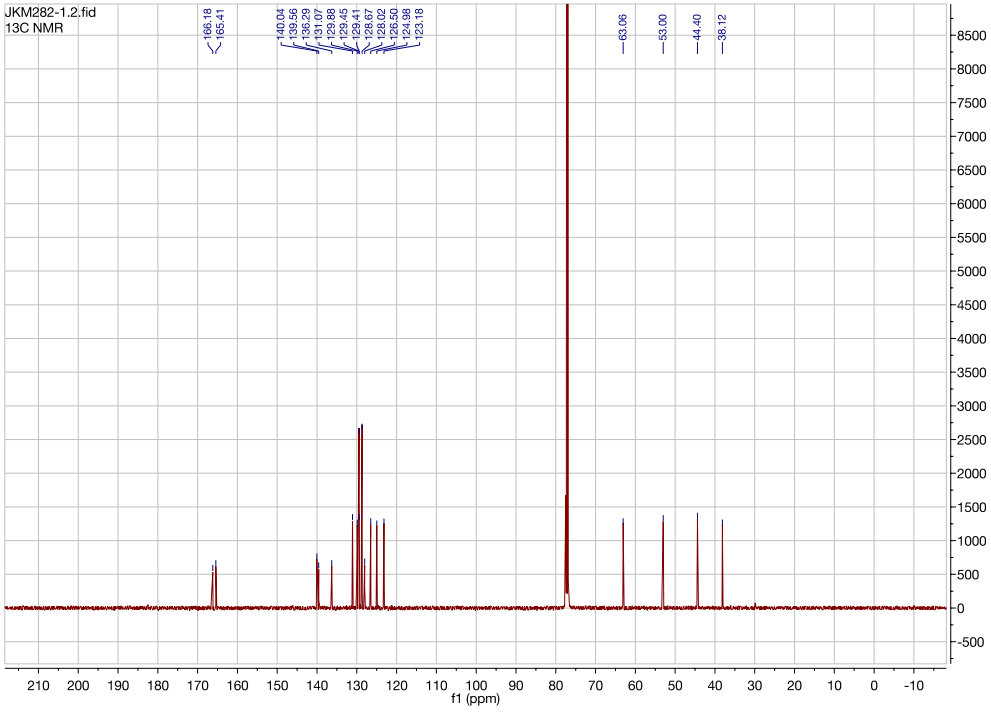


**Figure A11.47.** $^{13}$C NMR ($CDCl_3$, 125.8 MHz) spectrum of methyl 1-(1-hydroxy-3-phenylpropan-2-yl)isoquinoline-3-carboxylate (**2f**)

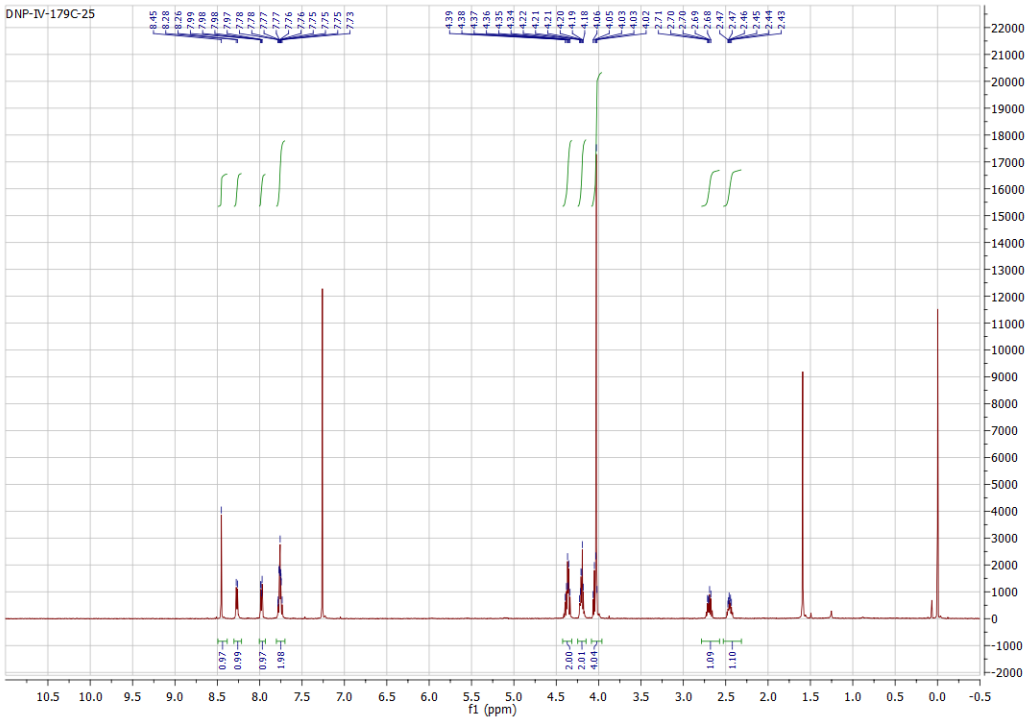


**Figure A11.48.** $^{1}$H NMR ($CDCl_3$, 500 MHz) spectrum of methyl 1-(tetrahydrofuran-3-yl)isoquinoline-3-carboxylate (**2g**)

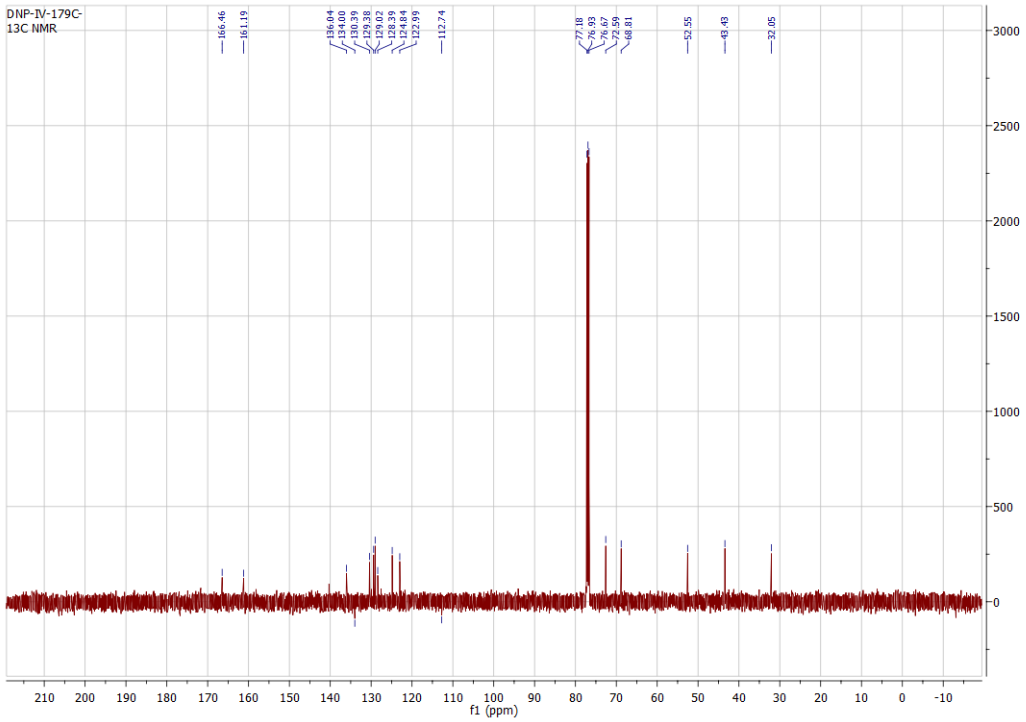


**Figure A11.49.** $^{13}$C NMR ($CDCl_3$, 125.8 MHz) spectrum of methyl 1-(tetrahydrofuran-3-yl)isoquinoline-3-carboxylate (**2g**)

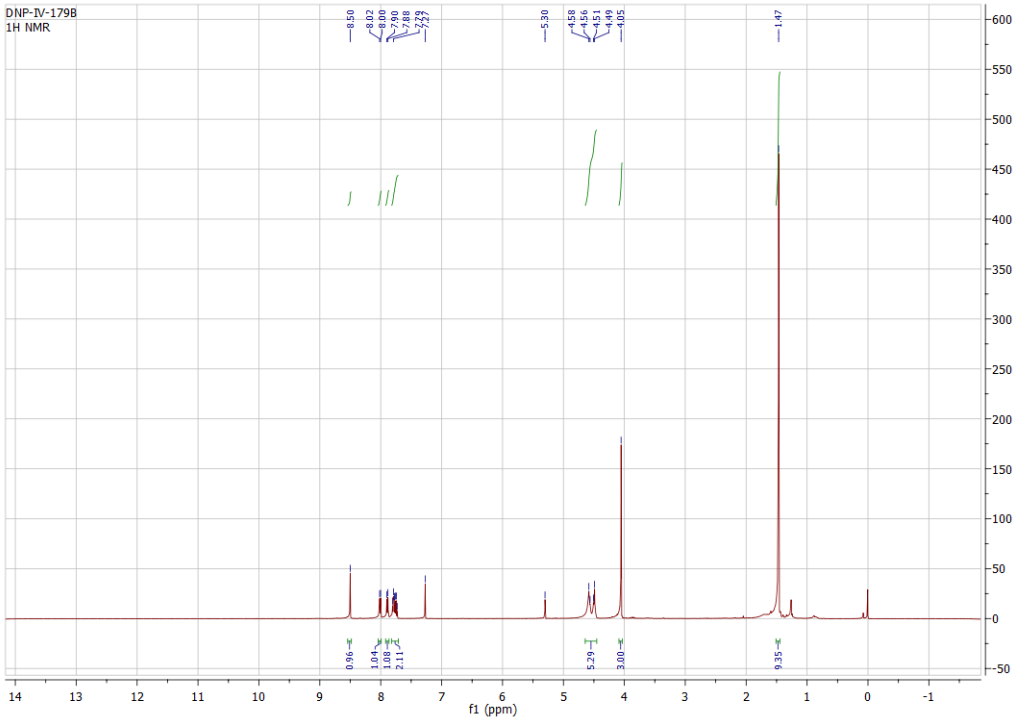


**Figure A11.50.** $^{1}$H NMR ($CDCl_3$, 500 MHz) spectrum of methyl 1-(1-(*tert*-butoxycarbonyl)azetidin-3-yl)isoquinoline-3-carboxylate (**2i**)

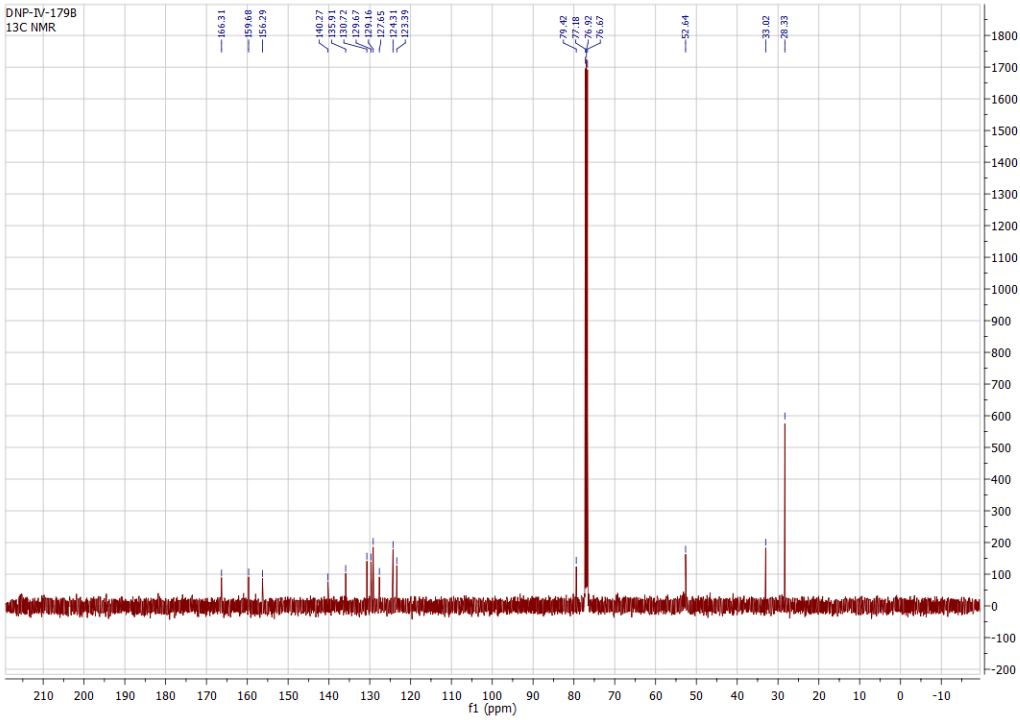


**Figure A11.51.** $^{13}$C NMR ($CDCl_3$, 125.8 MHz) spectrum of methyl 1-(1-(*tert*-butoxycarbonyl)azetidin-3-yl)isoquinoline-3-carboxylate (**2i**)

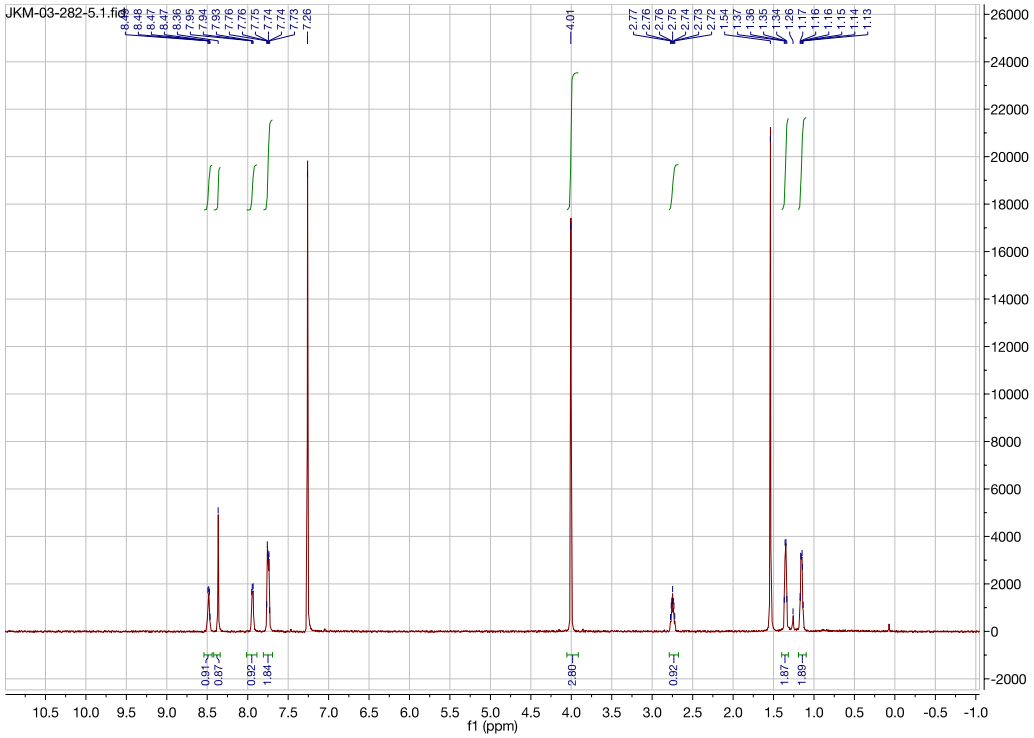


**Figure A11.52.** $^{1}$H NMR ($CDCl_3$, 500 MHz) spectrum of methyl 1-cyclopropylisoquinoline-3-carboxylate (**2j**)

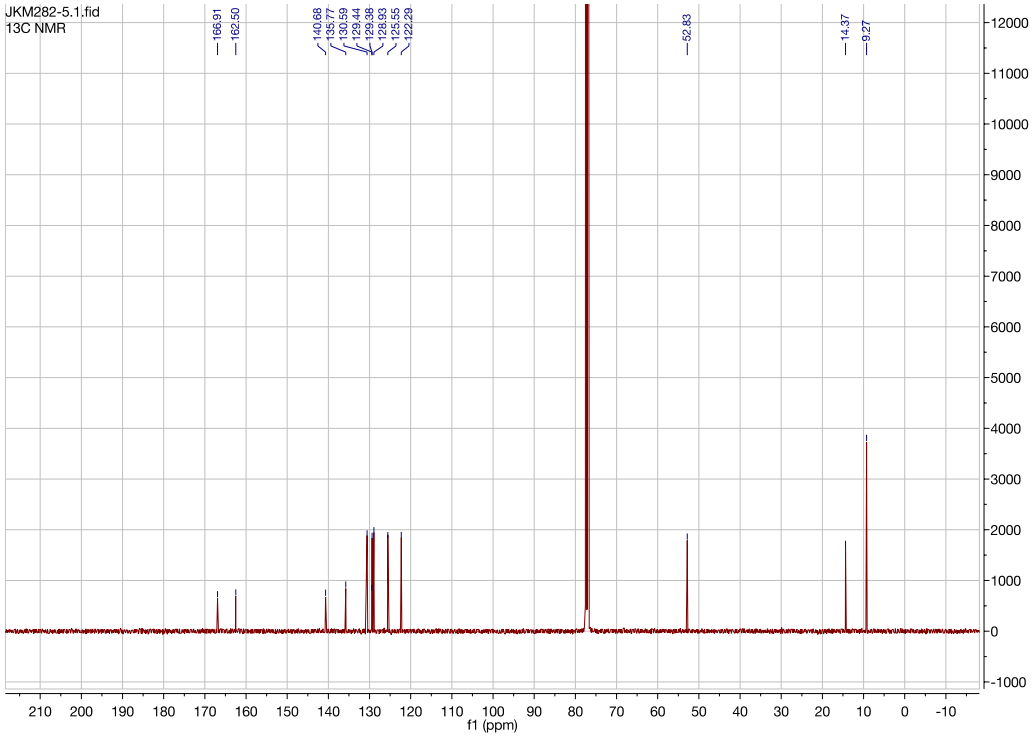


**Figure A11.53.** $^{13}$C NMR ($CDCl_3$, 125.8 MHz) spectrum of methyl 1-cyclopropylisoquinoline-3-carboxylate (**2j**)

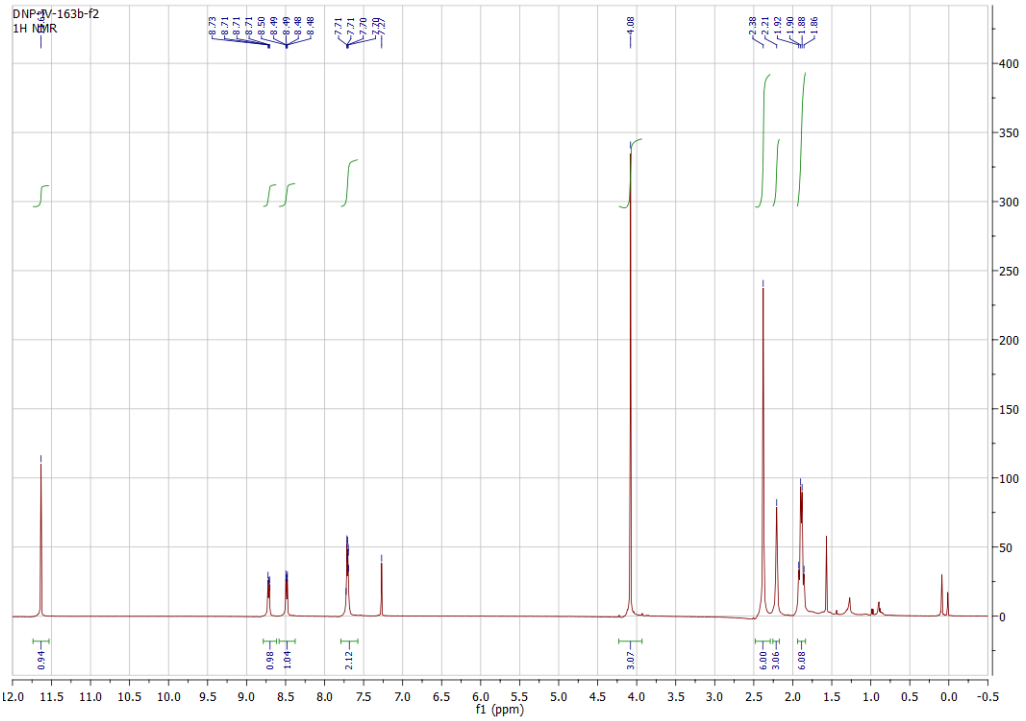


**Figure A11.54.** $^{1}$H NMR ($CDCl_3$, 500 MHz) spectrum of methyl 1-((3*r*,5*r*,7*r*)-adamantan-1-yl)isoquinoline-3-carboxylate (**2k**)

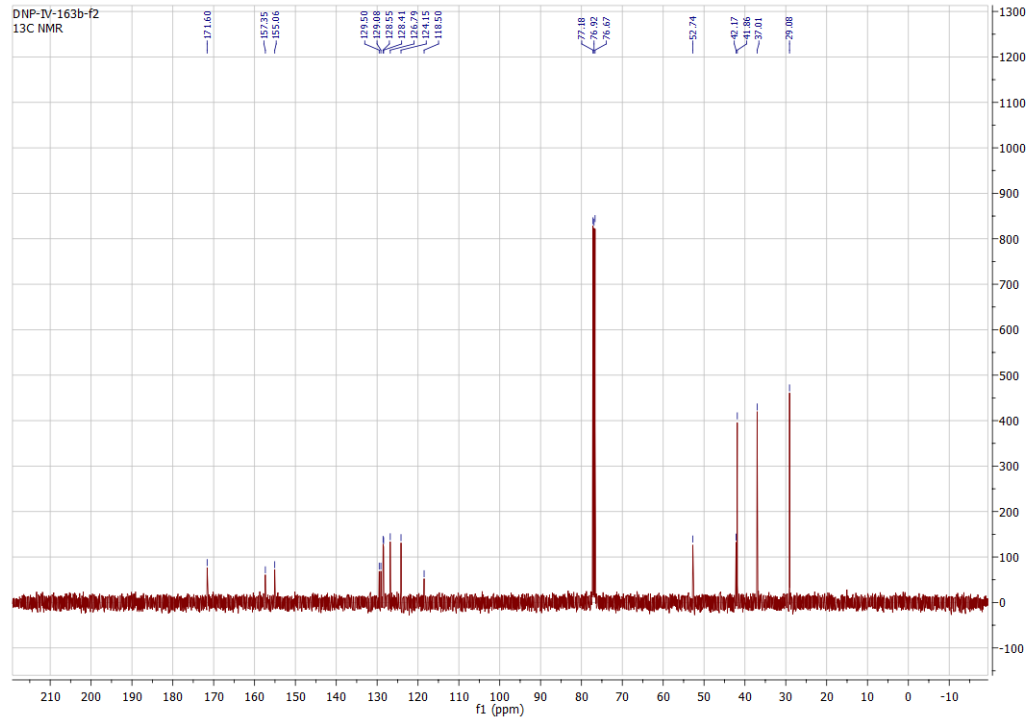


**Figure A11.55.** $^{13}$C NMR ($CDCl_3$, 125.8 MHz) spectrum of XX methyl 1-((3*r*,5*r*,7*r*)-adamantan-1-yl)isoquinoline-3-carboxylate (**2k**)

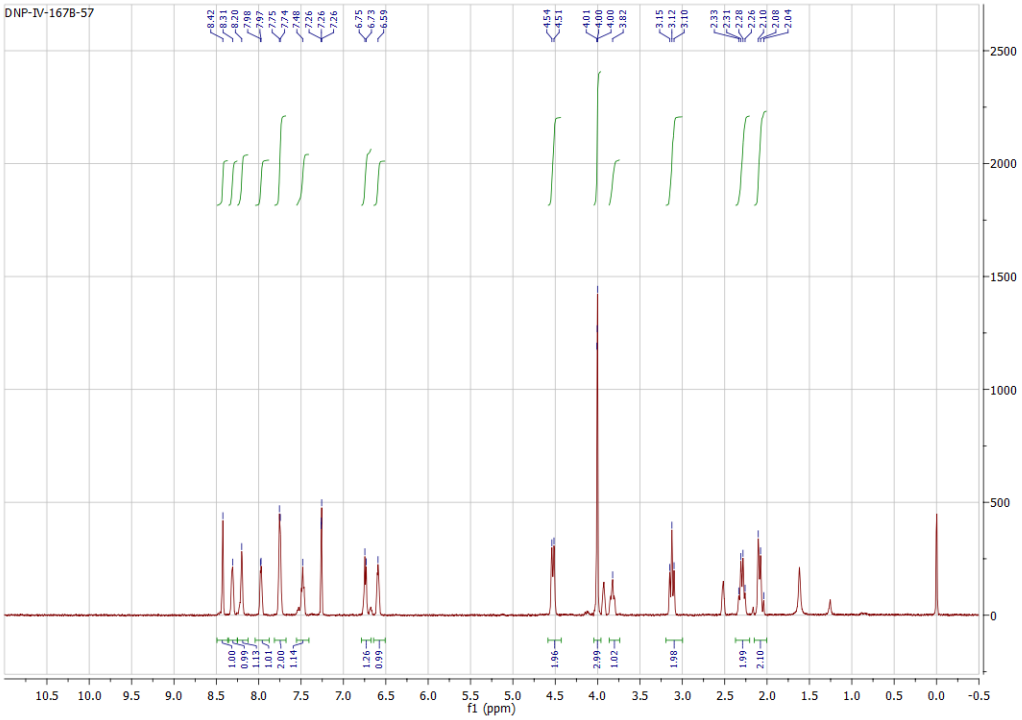


**Figure A11.56.** $^{1}$H NMR ($CDCl_3$, 500 MHz) spectrum of methyl 1-(1-(pyridin-2-yl)piperidin-4-yl)isoquinoline-3-carboxylate (**2l**)

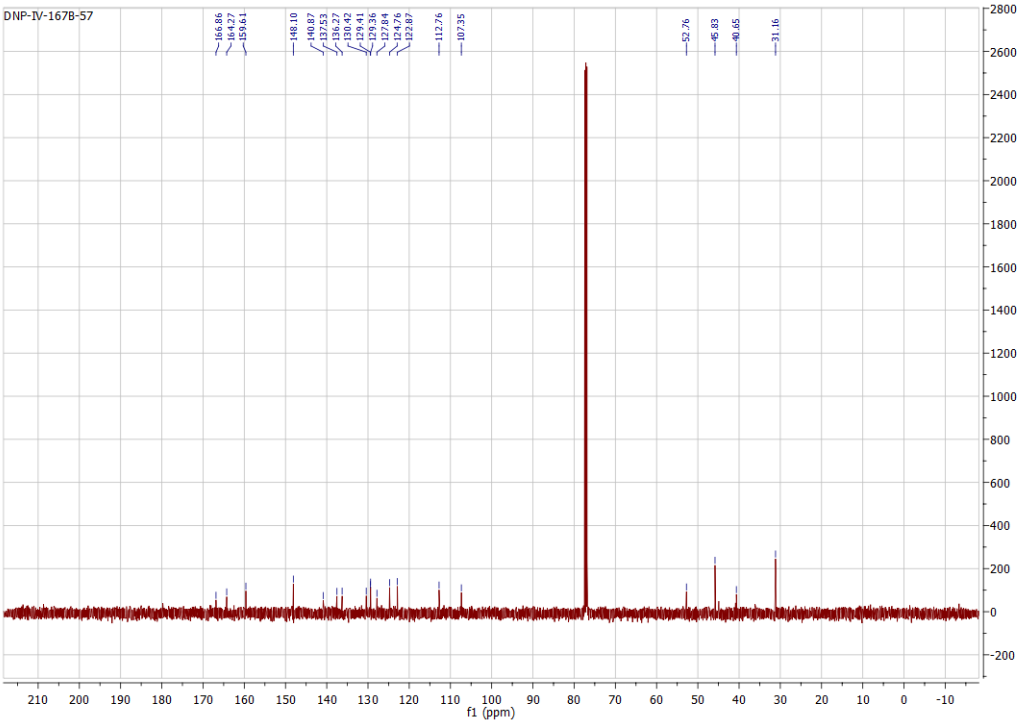


**Figure A11.57.** $^{13}$C NMR ($CDCl_3$, 125.8 MHz) spectrum of methyl 1-(1-(pyridin-2-yl)piperidin-4-yl)isoquinoline-3-carboxylate (**2l**)

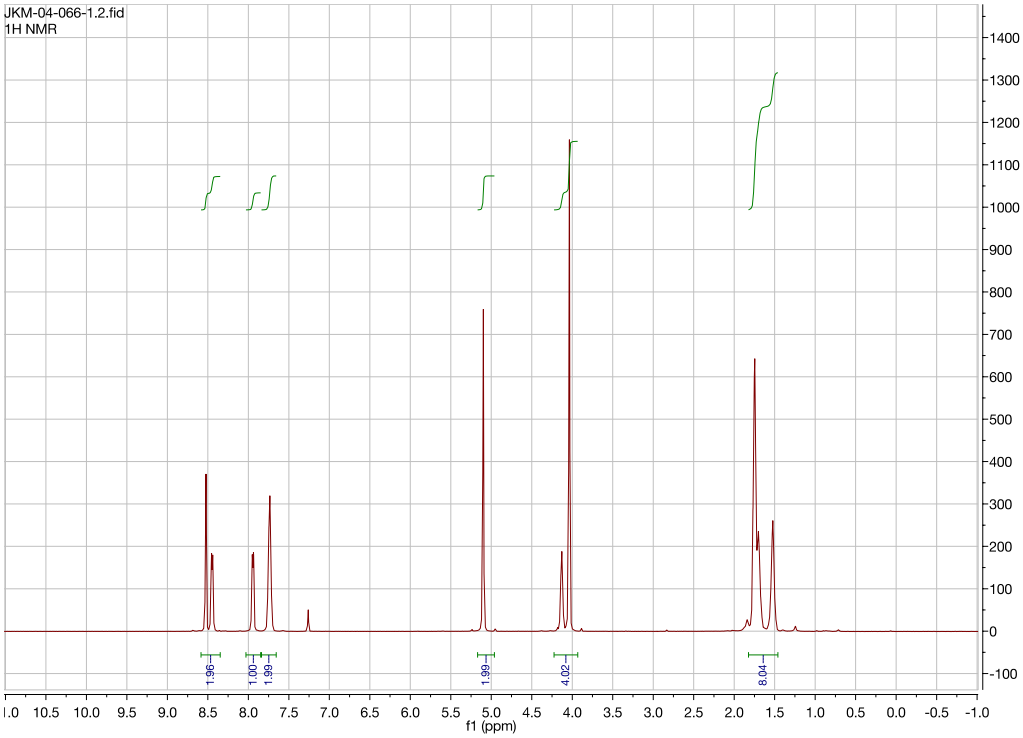


**Figure A11.58.** $^{1}H$ NMR ($CDCl_3$, 500 MHz) spectrum of methyl 1-((cyclopentyloxy)methyl)isoquinoline-3-carboxylate (**3a**)

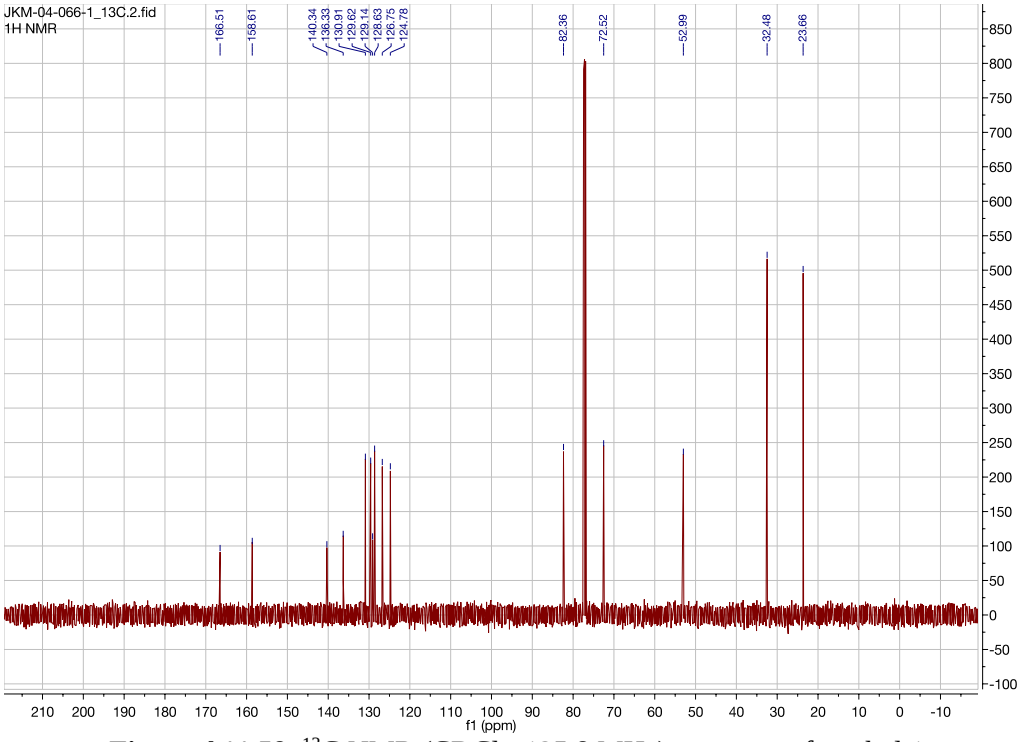


**Figure A11.59.** $^{13}C$ NMR ($CDCl_3$, 125.8 MHz) spectrum of methyl 1-((cyclopentyloxy)methyl)isoquinoline-3-carboxylate (**3a**)

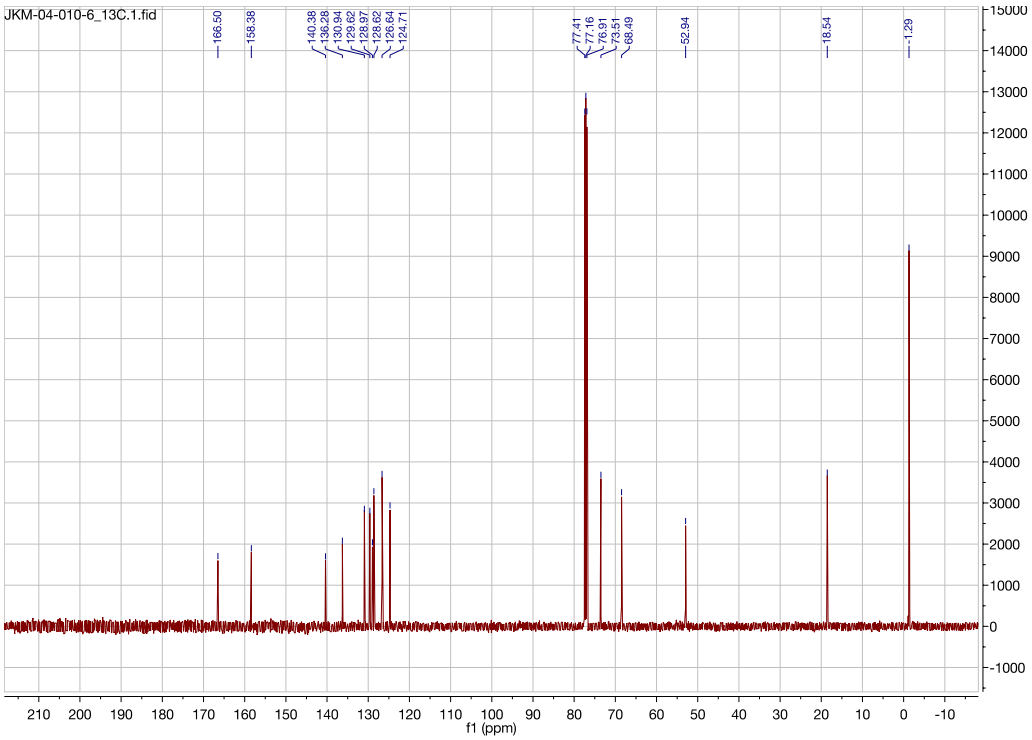


**Figure A11.60.** $^{1}H$ NMR ($CDCl_3$, 500 MHz) spectrum of methyl 1-((2-(trimethylsilyl)ethoxy)methyl)isoquinoline-3-carboxylate (**3b**)

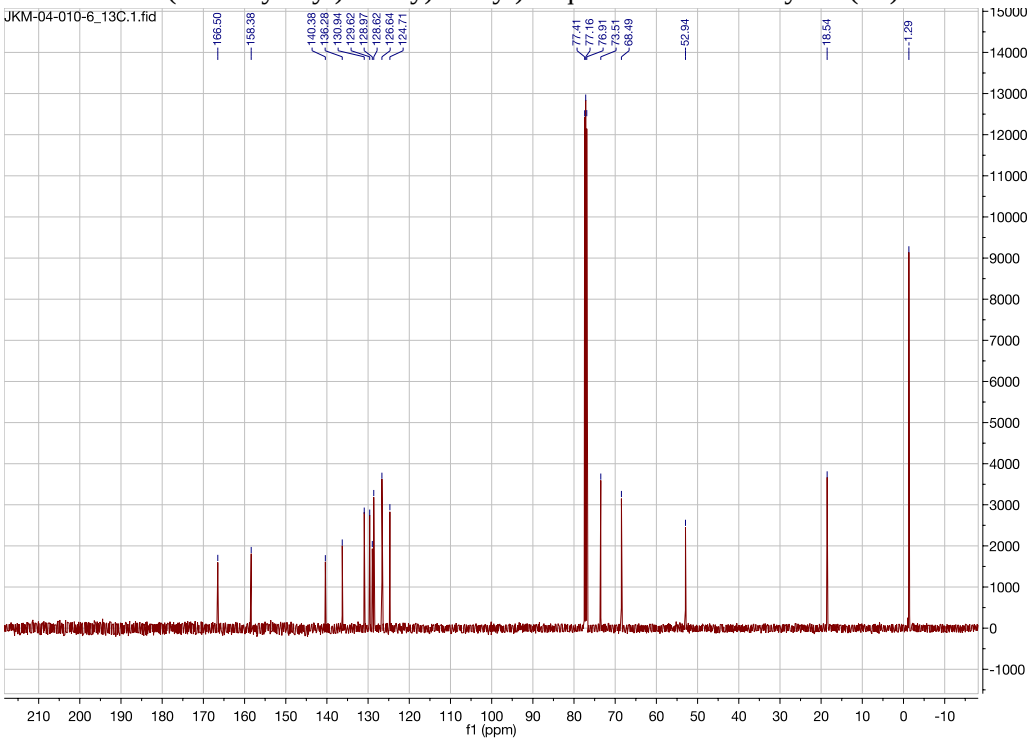


**Figure A11.61.** $^{13}C$ NMR ($CDCl_3$, 125.8 MHz) spectrum of methyl 1-((2-(trimethylsilyl)ethoxy)methyl)isoquinoline-3-carboxylate (**3b**)

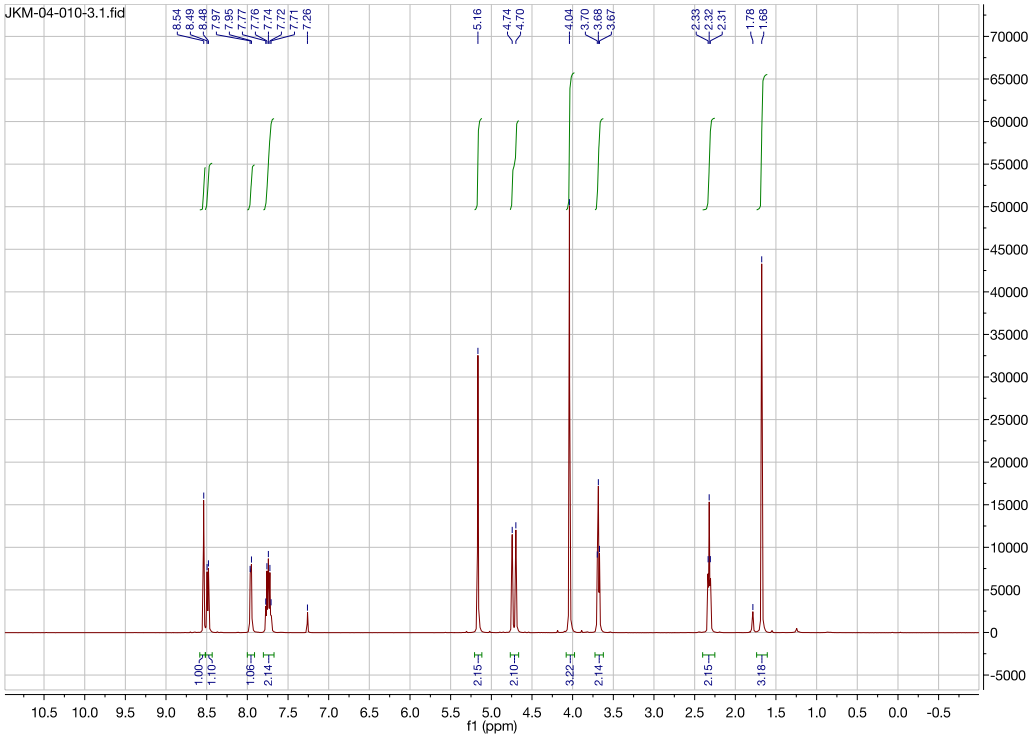


**Figure A11.62.** $^{1}$H NMR ($CDCl_3$, 500 MHz) spectrum of methyl 1-(((3-methylbut-3-en-1-yl)oxy)methyl)isoquinoline-3-carboxylate (**3c**)

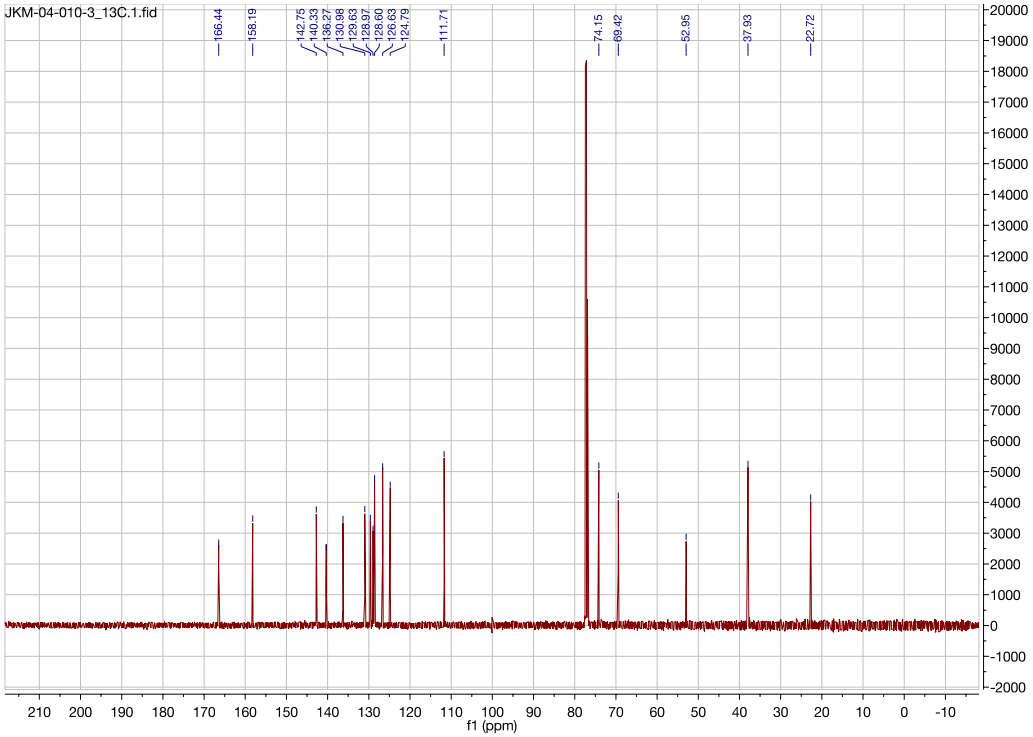


**Figure A11.63.** $^{13}$C NMR ($CDCl_3$, 125.8 MHz) spectrum of methyl 1-(((3-methylbut-3-en-1-yl)oxy)methyl)isoquinoline-3-carboxylate (**3c**)

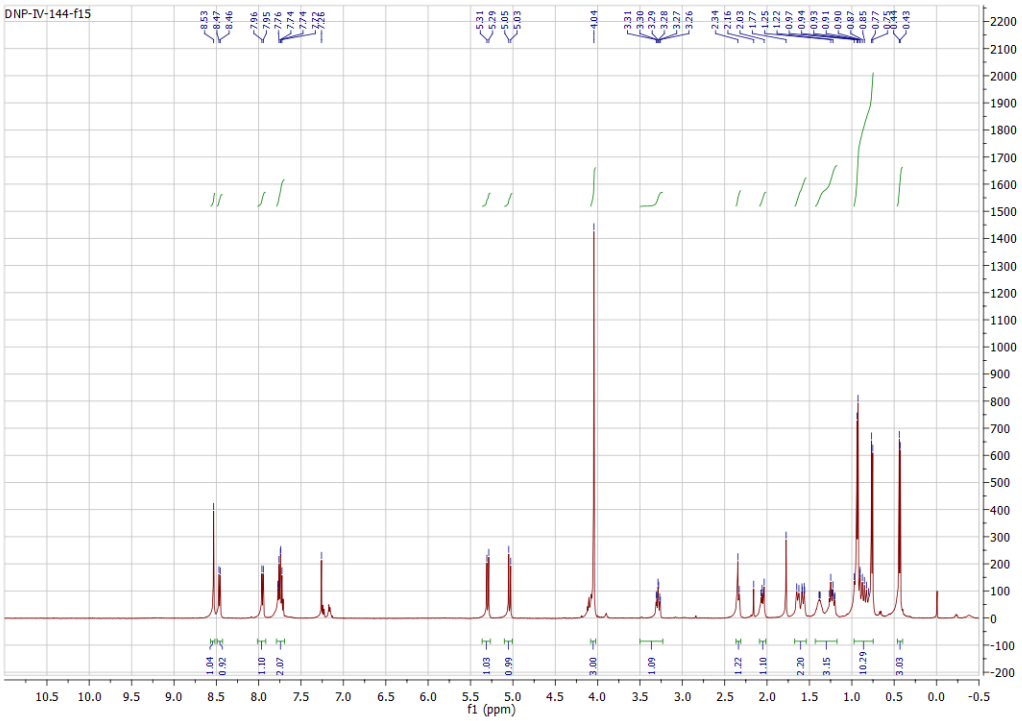


**Figure A11.64.** $^{1}$H NMR ($CDCl_3$, 500 MHz) spectrum of methyl 1-((((1*R*,2*S*,5*R*)-2-isopropyl-5-methylcyclohexyl)oxy)methyl)isoquinoline-3-carboxylate (**3d**)

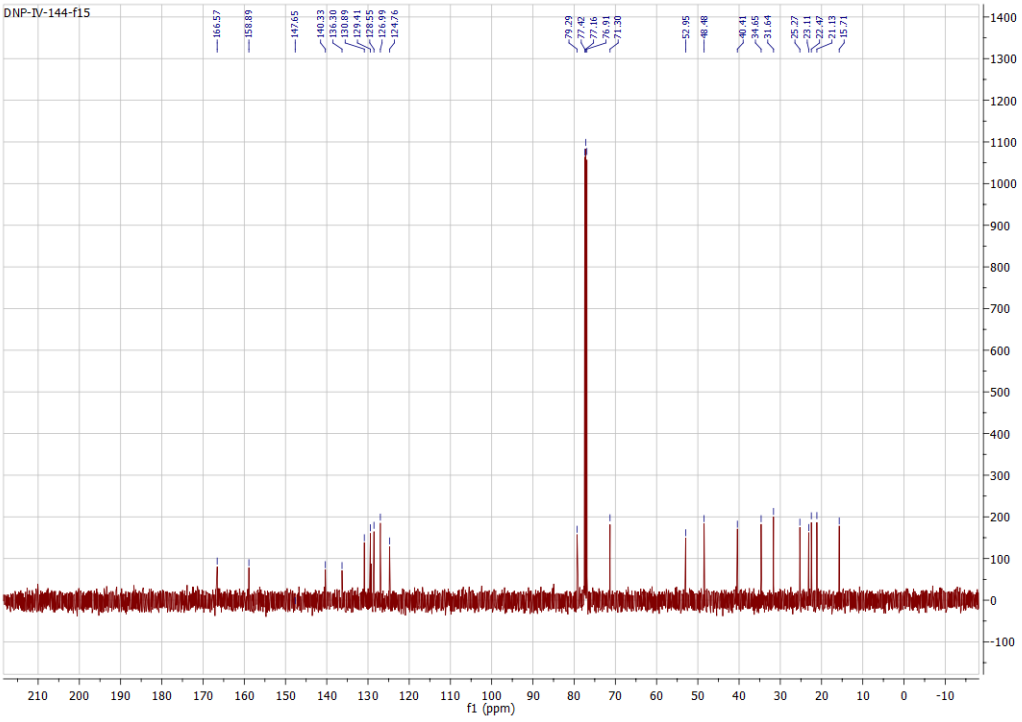


**Figure A11.65.** $^{13}$C NMR ($CDCl_3$, 125.8 MHz) spectrum of methyl 1-((((1*R*,2*S*,5*R*)-2-isopropyl-5-methylcyclohexyl)oxy)methyl)isoquinoline-3-carboxylate (**3d**)

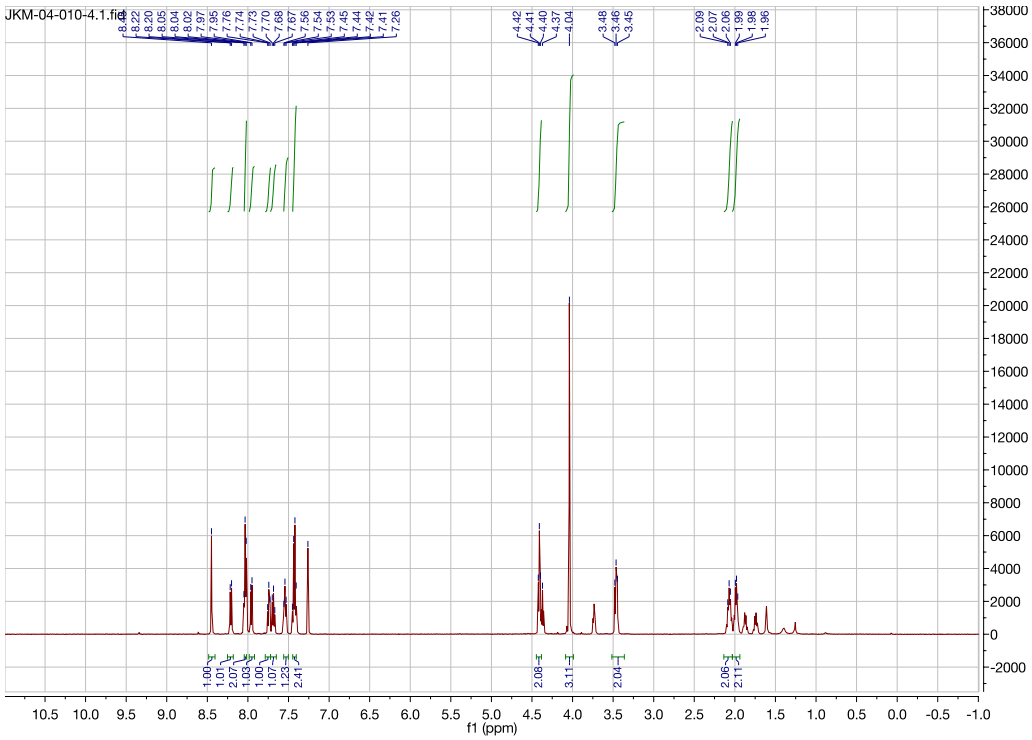


**Figure A11.66.** $^{1}$H NMR ($CDCl_3$, 500 MHz) spectrum of methyl 1-(3-(benzyloxy)propyl)isoquinoline-3-carboxylate (**3e**)

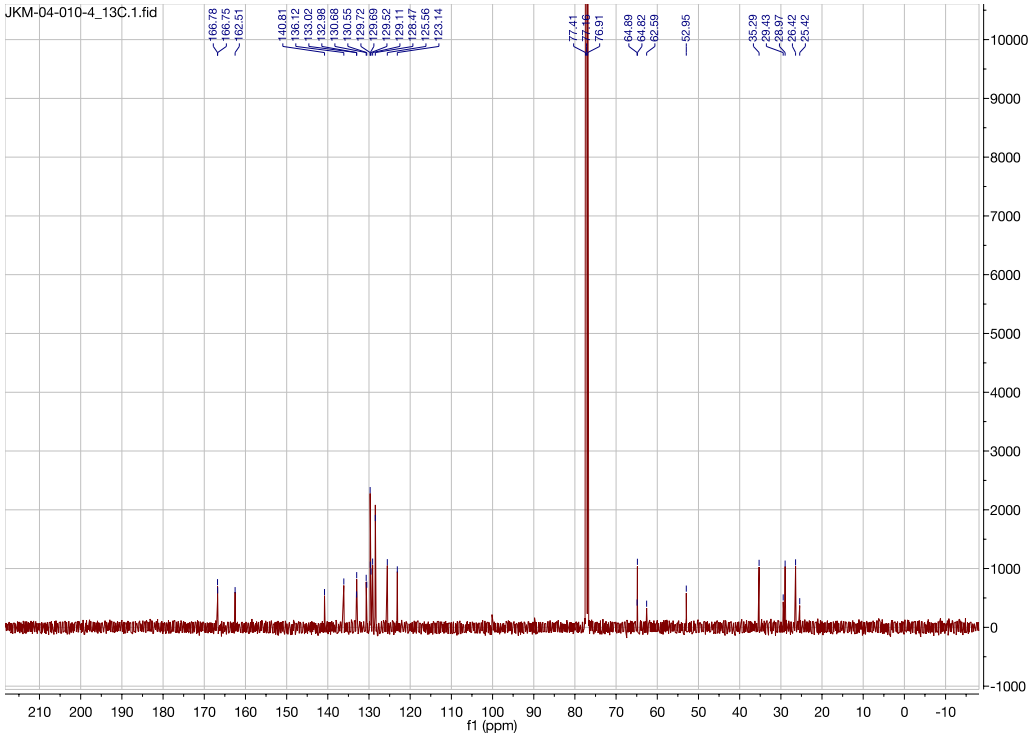


**Figure A11.67.** $^{13}$C NMR ($CDCl_3$, 125.8 MHz) spectrum of methyl 1-(3-(benzyloxy)propyl)isoquinoline-3-carboxylate (**3e**)

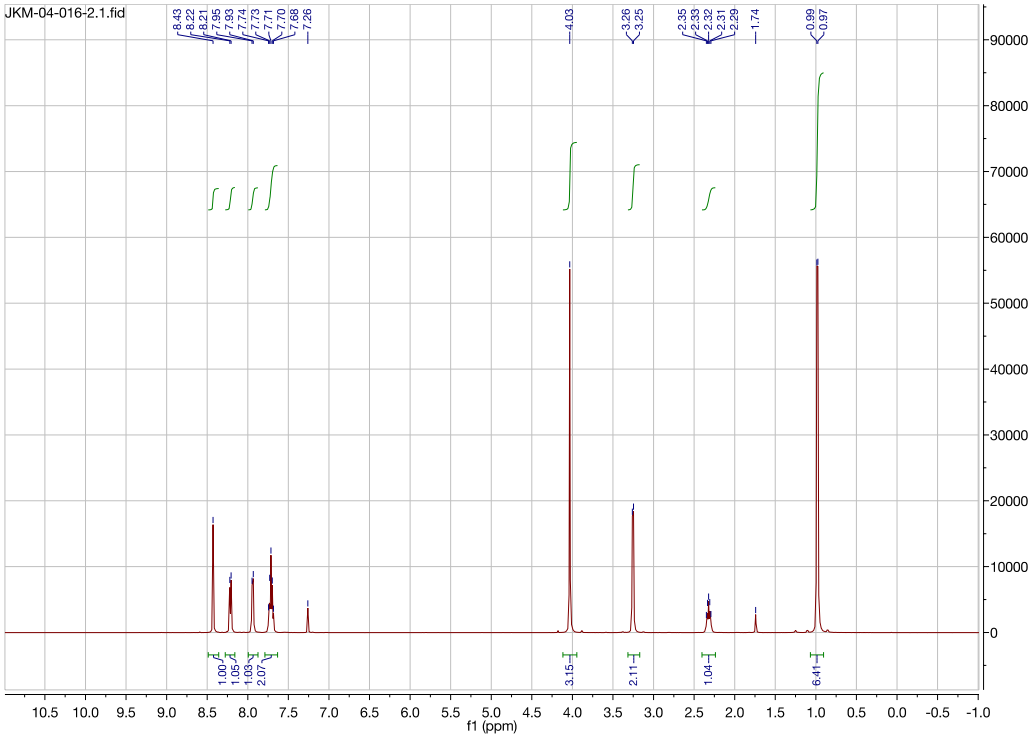


**Figure A11.68.** $^{1}$H NMR ($CDCl_3$, 500 MHz) spectrum of methyl 1-isobutylisoquinoline-3-carboxylate (**3f**)

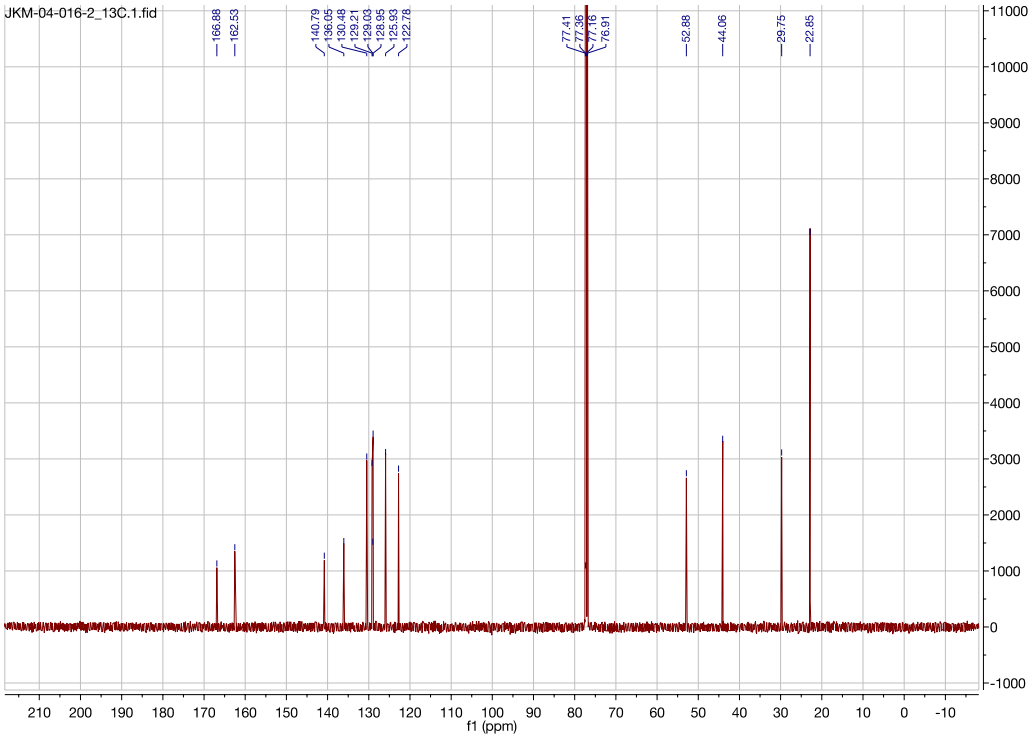


**Figure A11.69.** $^{13}$C NMR ($CDCl_3$, 125.8 MHz) spectrum of methyl 1-isobutylisoquinoline-3-carboxylate (**3f**)

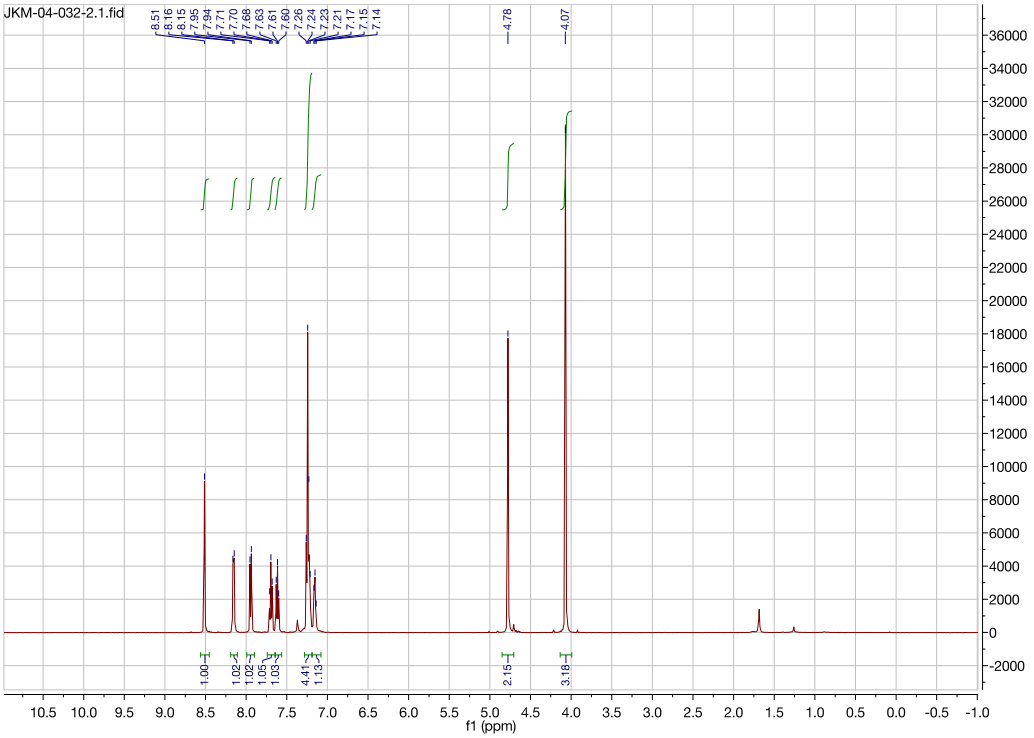


**Figure A11.70.** $^{1}$H NMR ($CDCl_3$, 500 MHz) spectrum of methyl 1-benzylisoquinoline-3-carboxylate (**3g**)

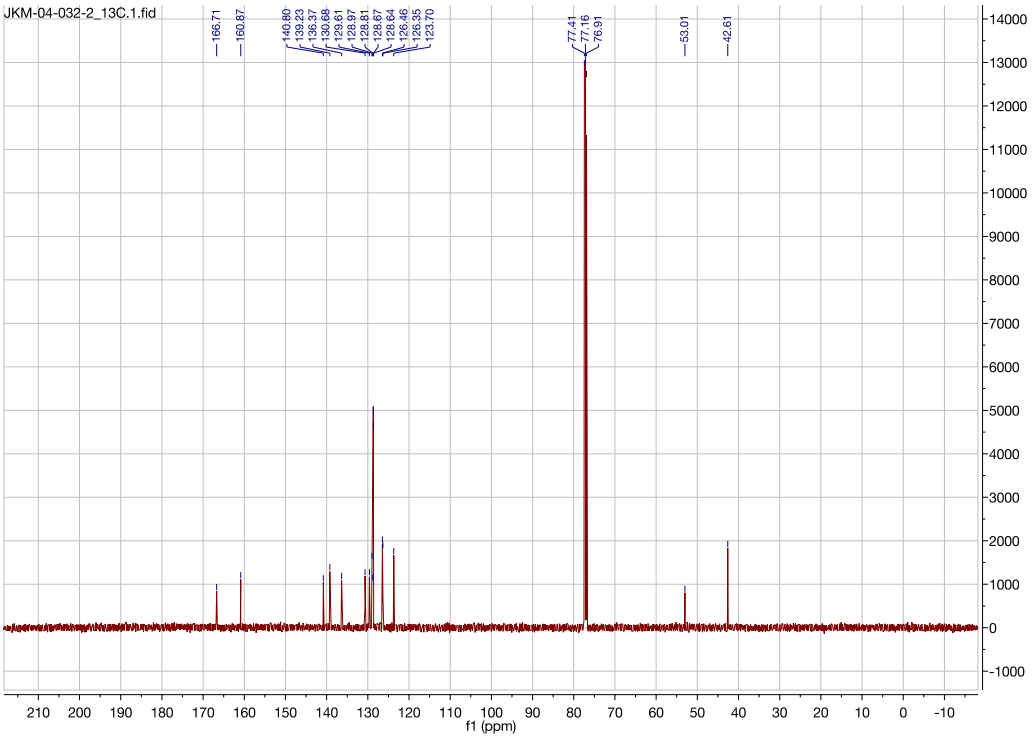


**Figure A11.71.** $^{13}$C NMR ($CDCl_3$, 125.8 MHz) spectrum of methyl 1-benzylisoquinoline-3-carboxylate (**3g**)

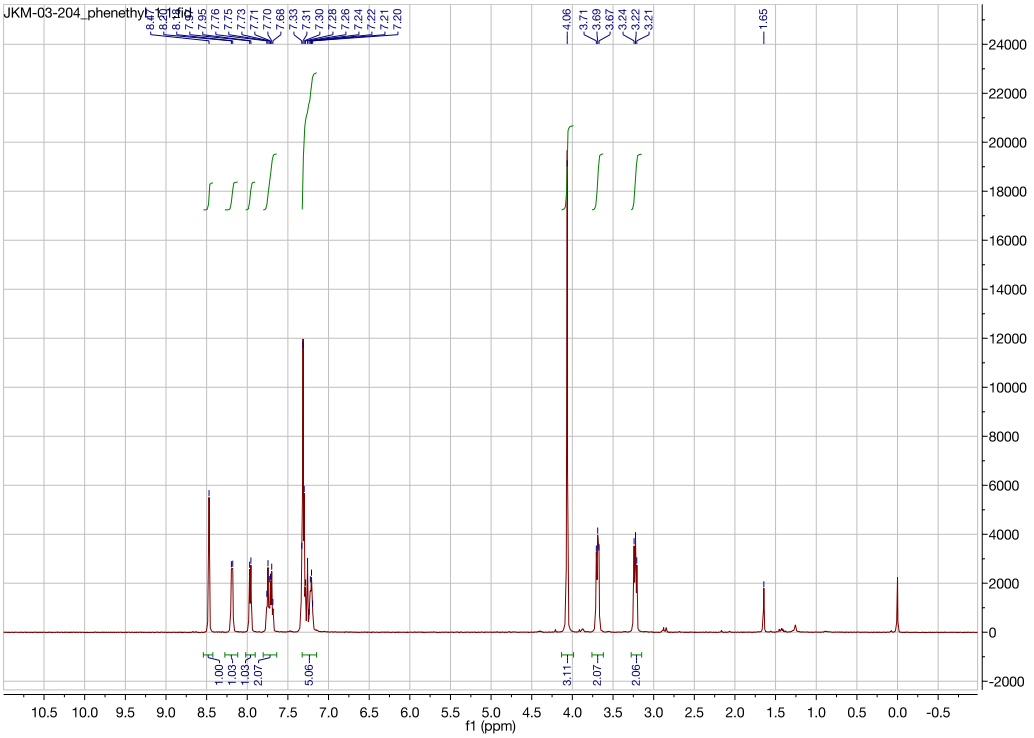


**Figure A11.72.** $^{1}$H NMR ($CDCl_3$, 500 MHz) spectrum of ethyl 1-phenethylisoquinoline-3-carboxylate (**3h**)

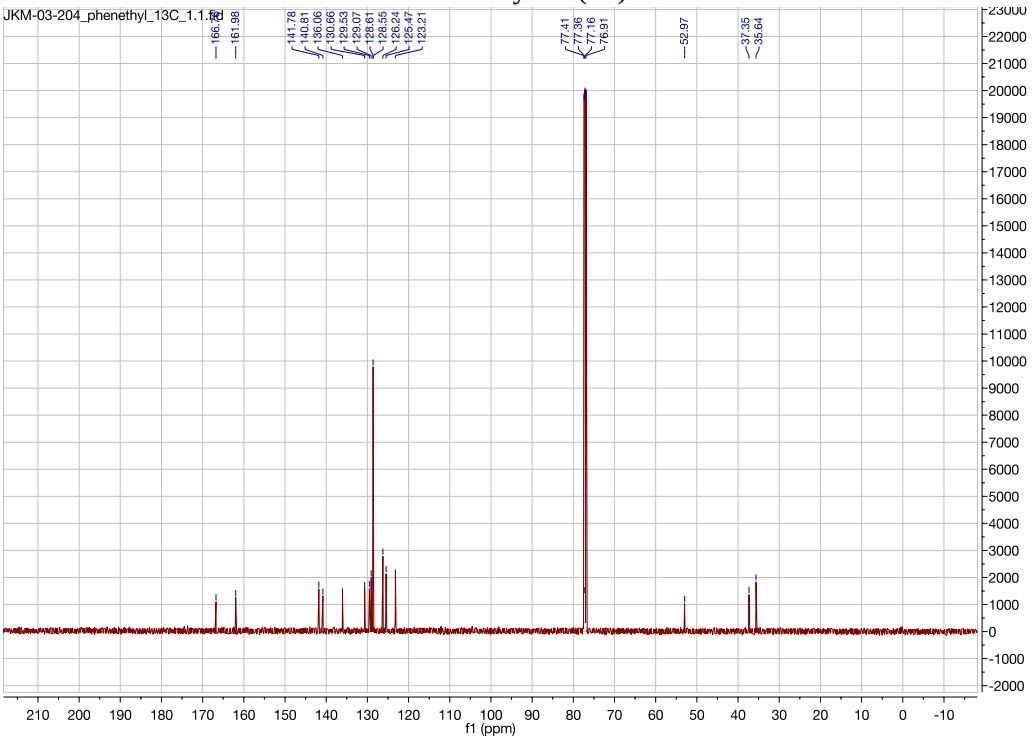


**Figure A11.73.** $^{13}$C NMR ($CDCl_3$, 125.8 MHz) spectrum of ethyl 1-phenethylisoquinoline-3-carboxylate (**3h**)

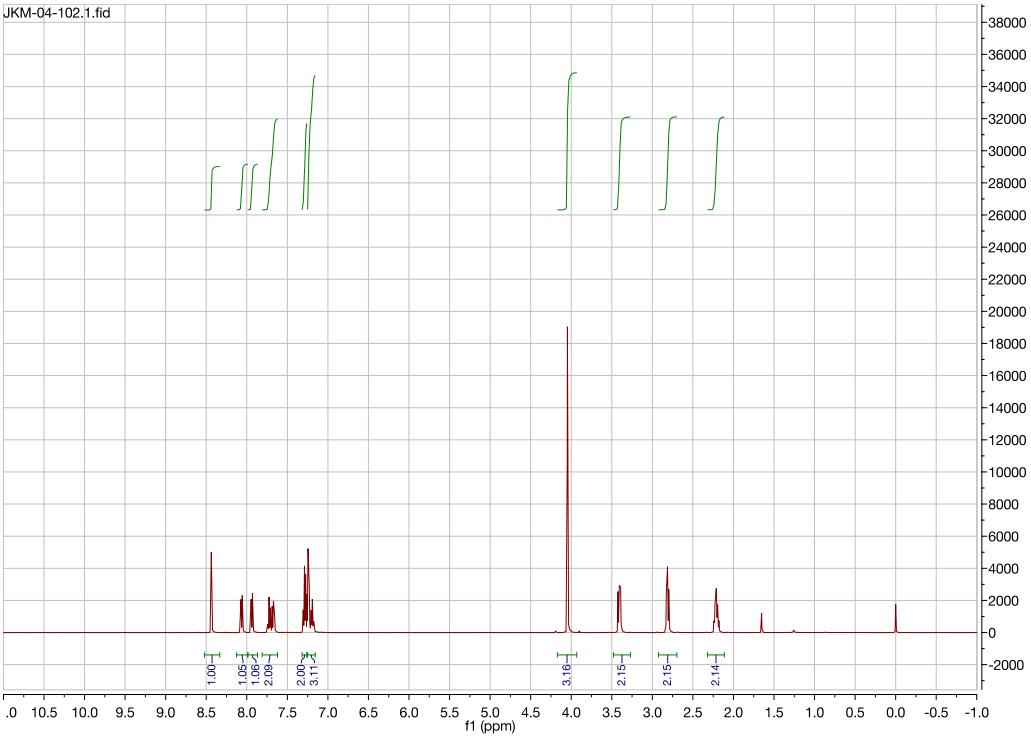


**Figure A11.74.** $^{1}$H NMR ($CDCl_3$, 500 MHz) spectrum of methyl 1-(3-phenylpropyl)isoquinoline-3-carboxylate (**3i**)

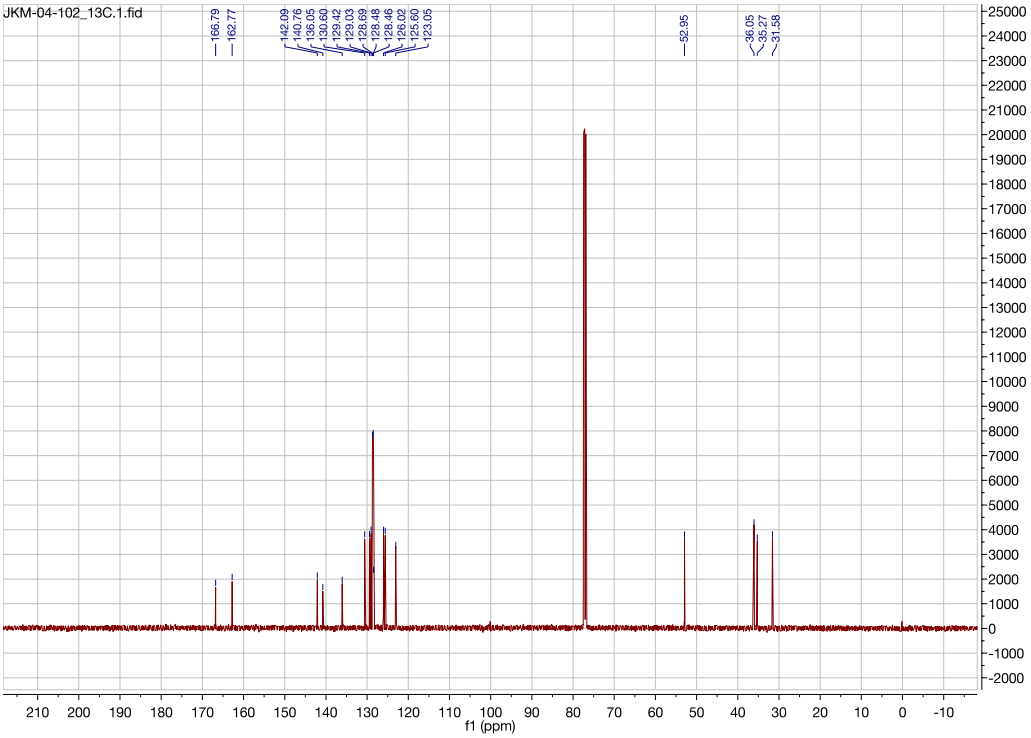


**Figure A11.75.** $^{13}$C NMR ($CDCl_3$, 125.8 MHz) spectrum of methyl 1-(3-phenylpropyl)isoquinoline-3-carboxylate (**3i**)

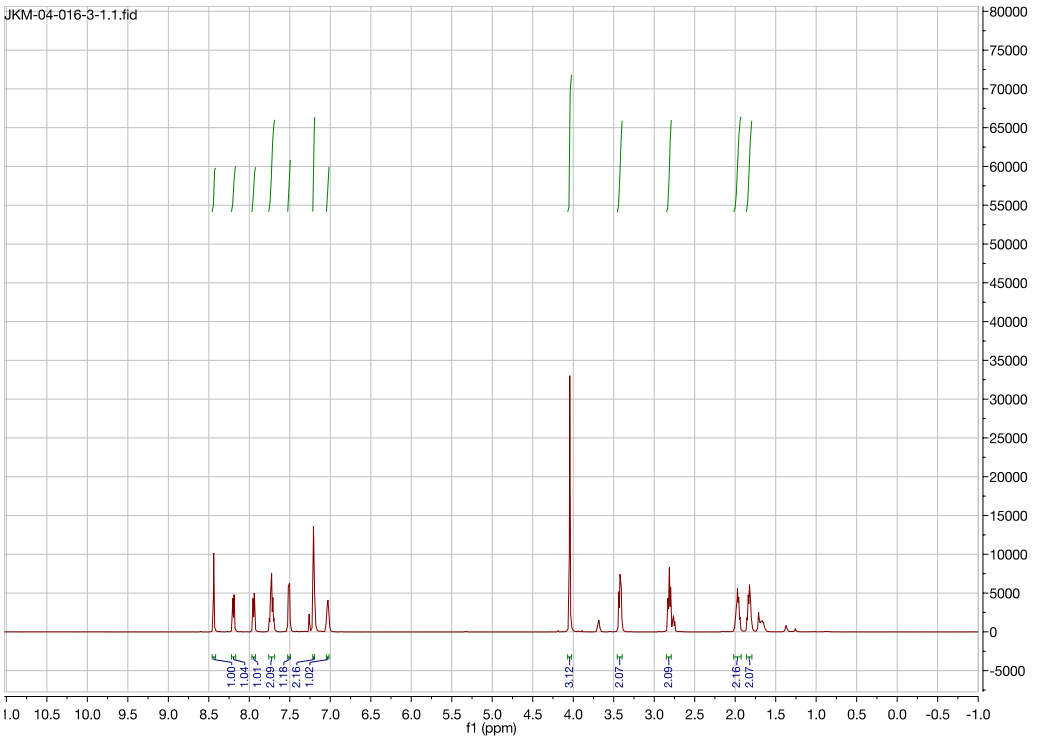


**Figure A11.76.** $^{1}$H NMR ($CDCl_3$, 500 MHz) spectrum of methyl 1-(4-(2-bromophenyl)butyl)isoquinoline-3-carboxylate (**3j**)

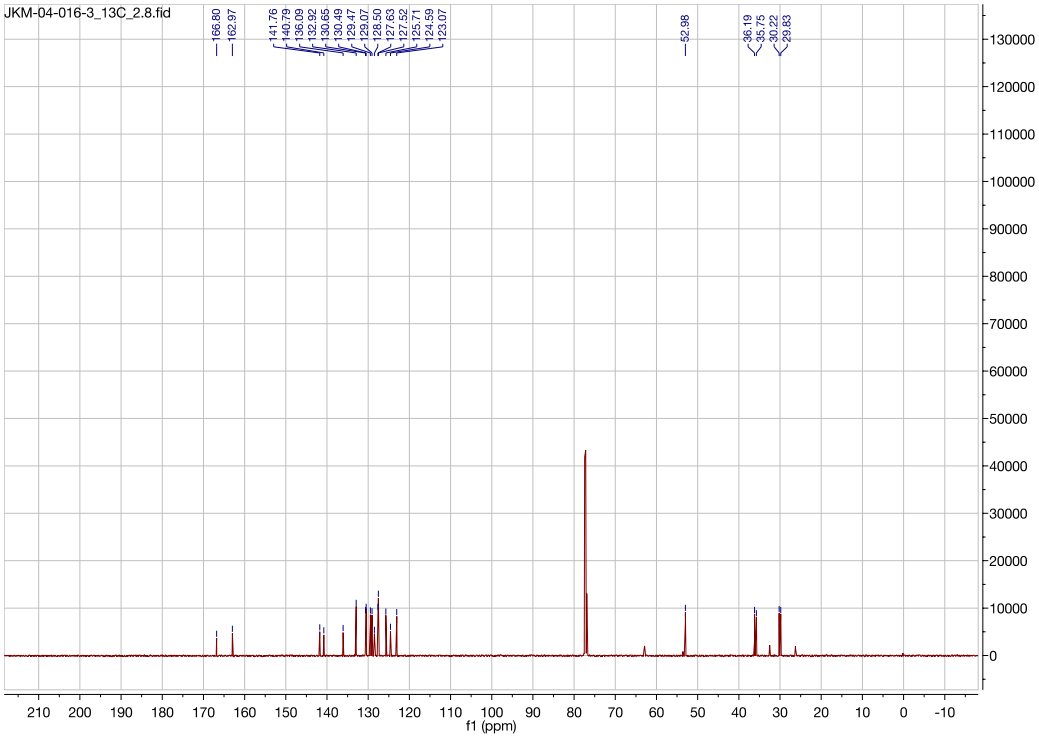


**Figure A11.77.** $^{13}$C NMR ($CDCl_3$, 125.8 MHz) spectrum of methyl 1-(4-(2-bromophenyl)butyl)isoquinoline-3-carboxylate (**3j**)

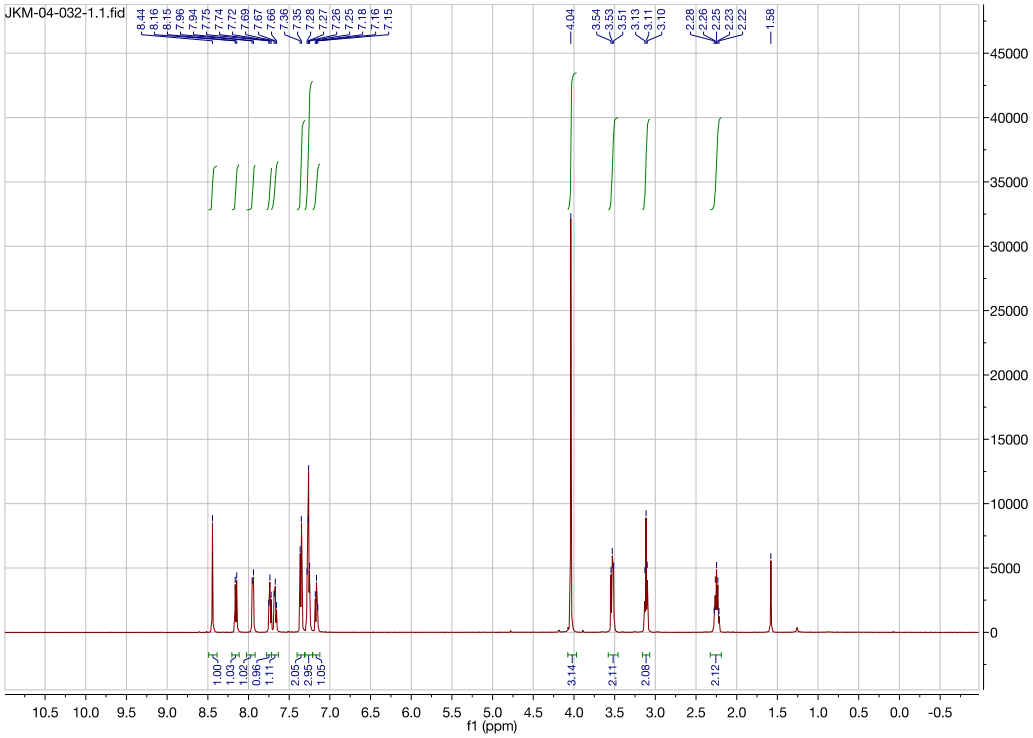


**Figure A11.78.** $^{1}$H NMR ($CDCl_3$, 500 MHz) spectrum of methyl 1-(3-(phenylthio)propyl)isoquinoline-3-carboxylate (**3k**)

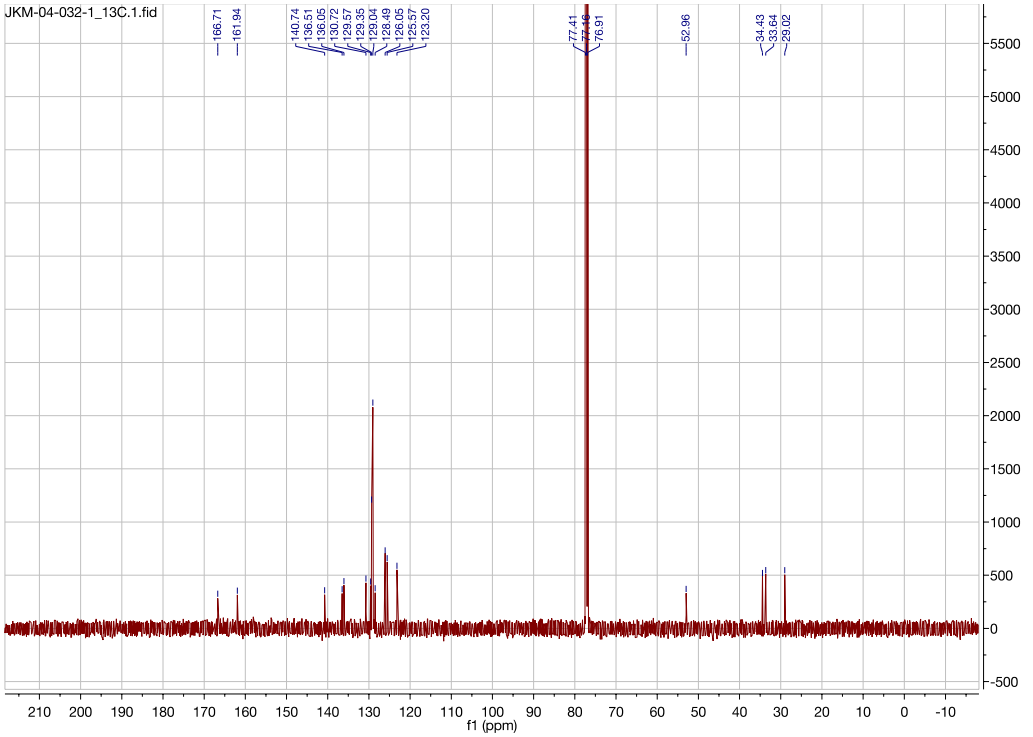


**Figure A11.79.** $^{13}$C NMR ($CDCl_3$, 125.8 MHz) spectrum of methyl 1-(3-(phenylthio)propyl)isoquinoline-3-carboxylate (**3k**)

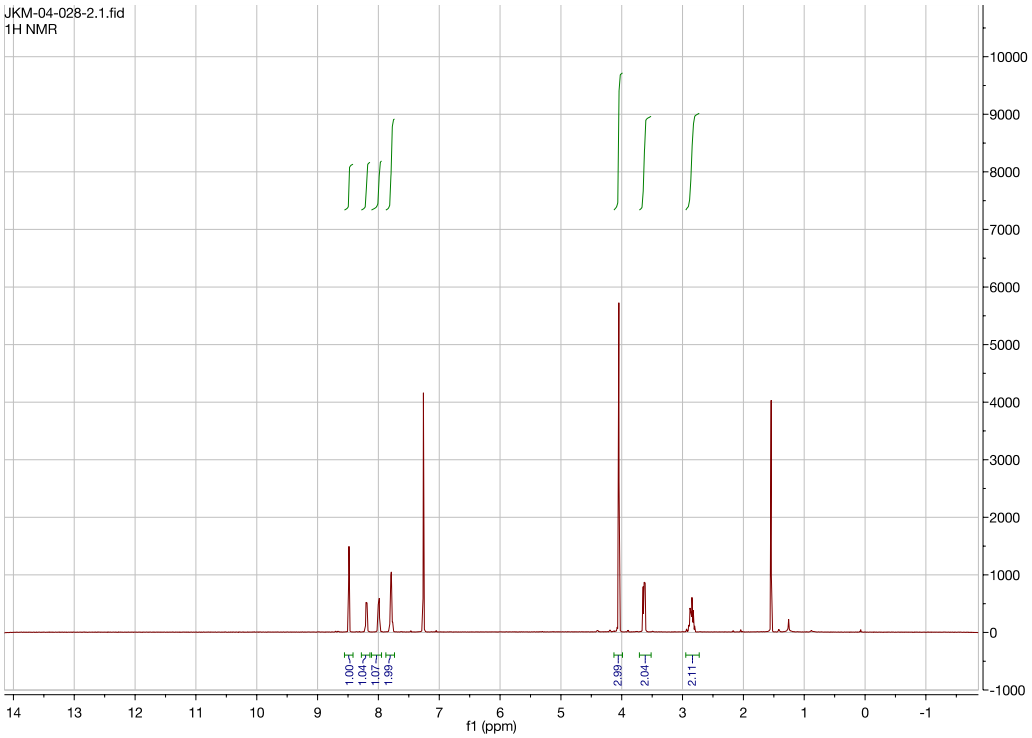


**Figure A11.80.** $^{1}H$ NMR ($CDCl_3$, 500 MHz) spectrum of methyl 1-(3,3,3-trifluoropropyl)isoquinoline-3-carboxylate (**3l**)

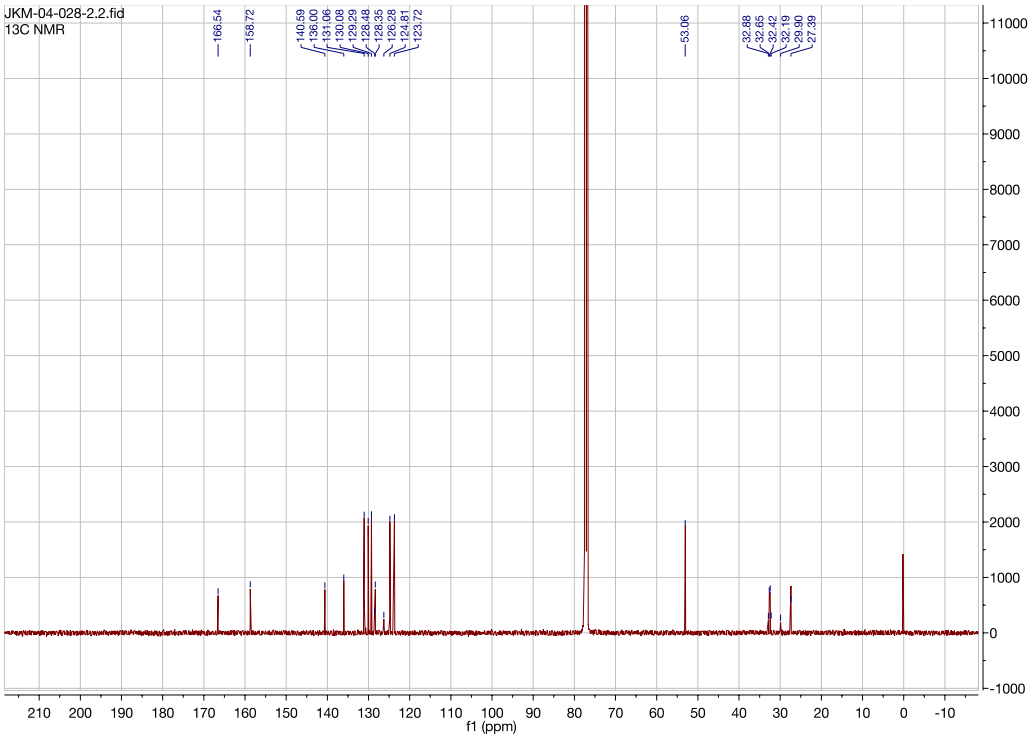


**Figure A11.81.** $^{13}C$ NMR ($CDCl_3$, 125.8 MHz) spectrum of methyl 1-(3,3,3-trifluoropropyl)isoquinoline-3-carboxylate (**3l**)

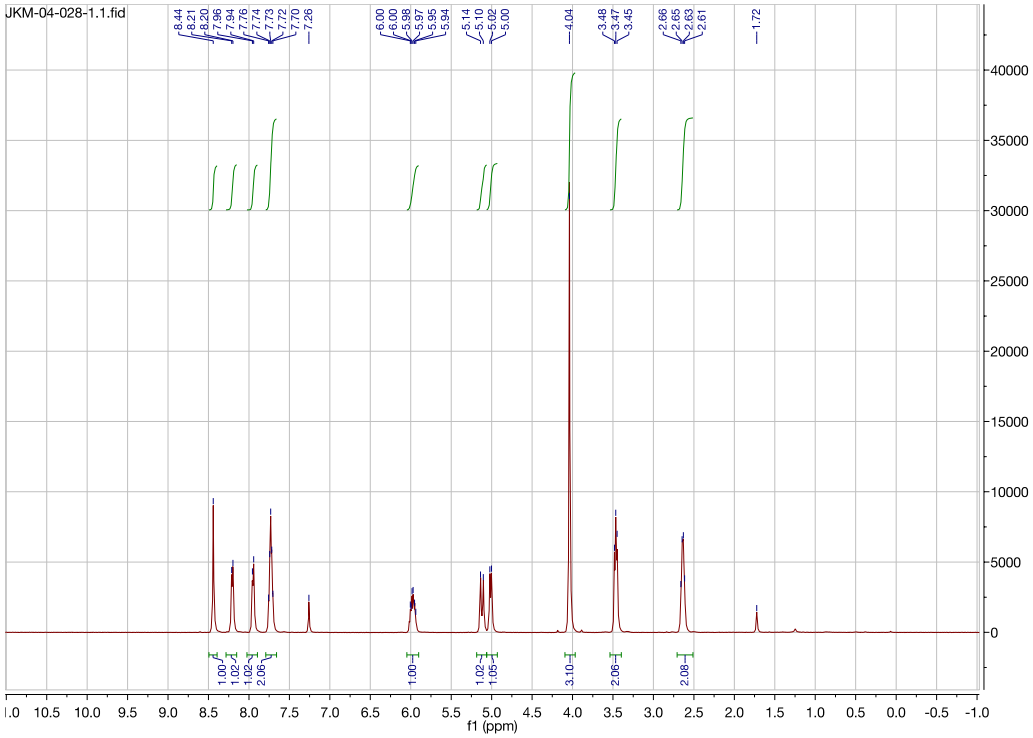


**Figure A11.82.** $^{1}$H NMR ($CDCl_3$, 500 MHz) spectrum of methyl 1-(but-3-en-1-yl)isoquinoline-3-carboxylate (**3p**)

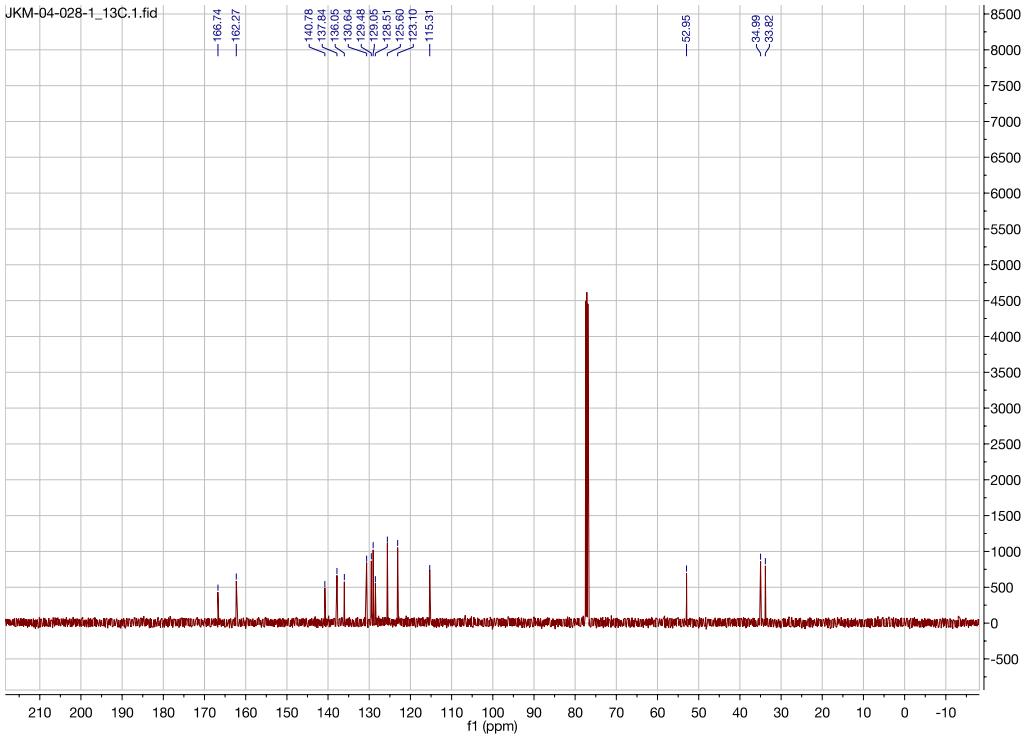


**Figure A11.83.** $^{13}$C NMR ($CDCl_3$, 125.8 MHz) spectrum of methyl 1-(but-3-en-1-yl)isoquinoline-3-carboxylate (**3p**)

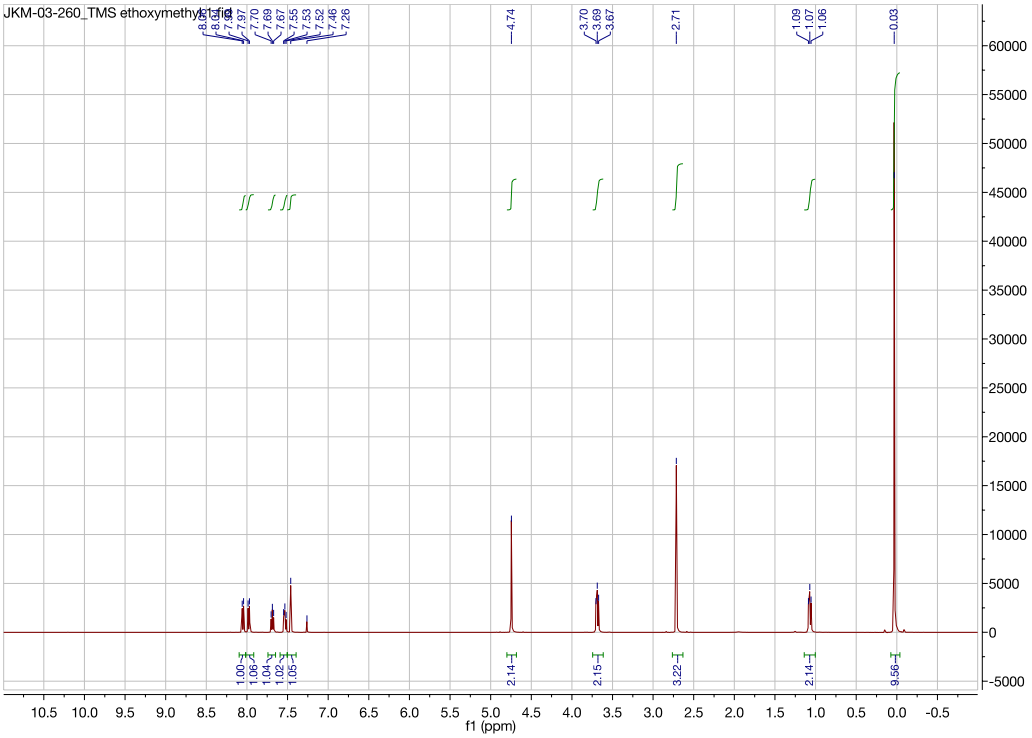


**Figure A11.84.** $^{1}$H NMR ($CDCl_3$, 500 MHz) spectrum of 4-methyl-2-((2-(trimethylsilyl)ethoxy)methyl)quinoline (**4a**)

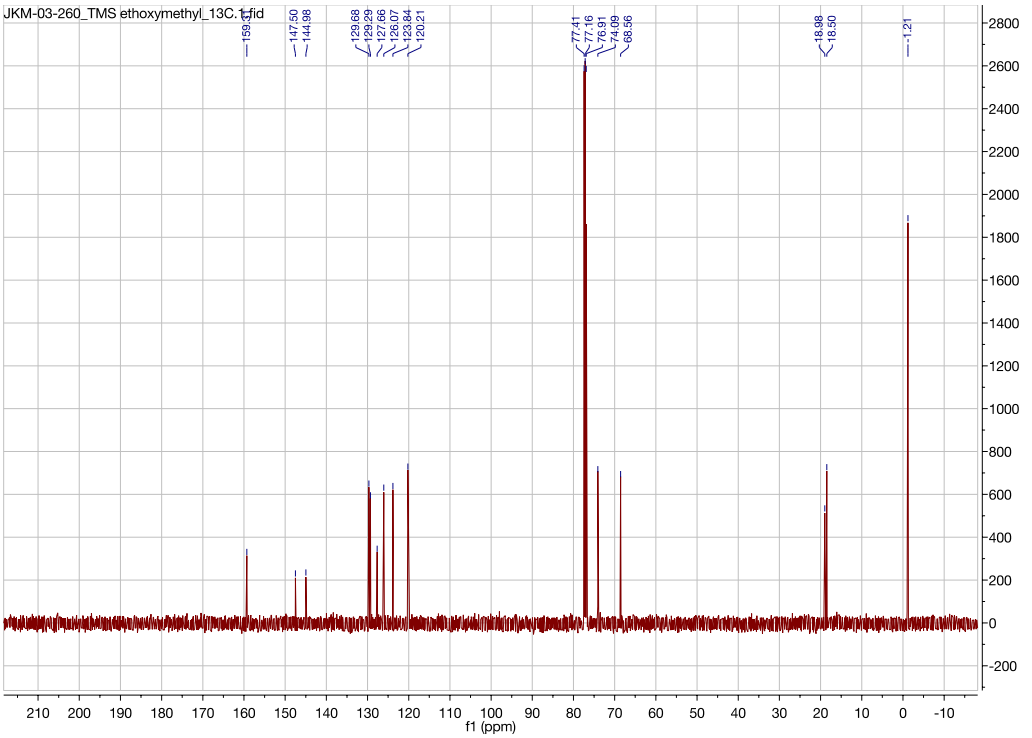


**Figure A11.85.** $^{13}$C NMR ($CDCl_3$, 125.8 MHz) spectrum of 4-methyl-2-((2-(trimethylsilyl)ethoxy)methyl)quinoline (**4a**)

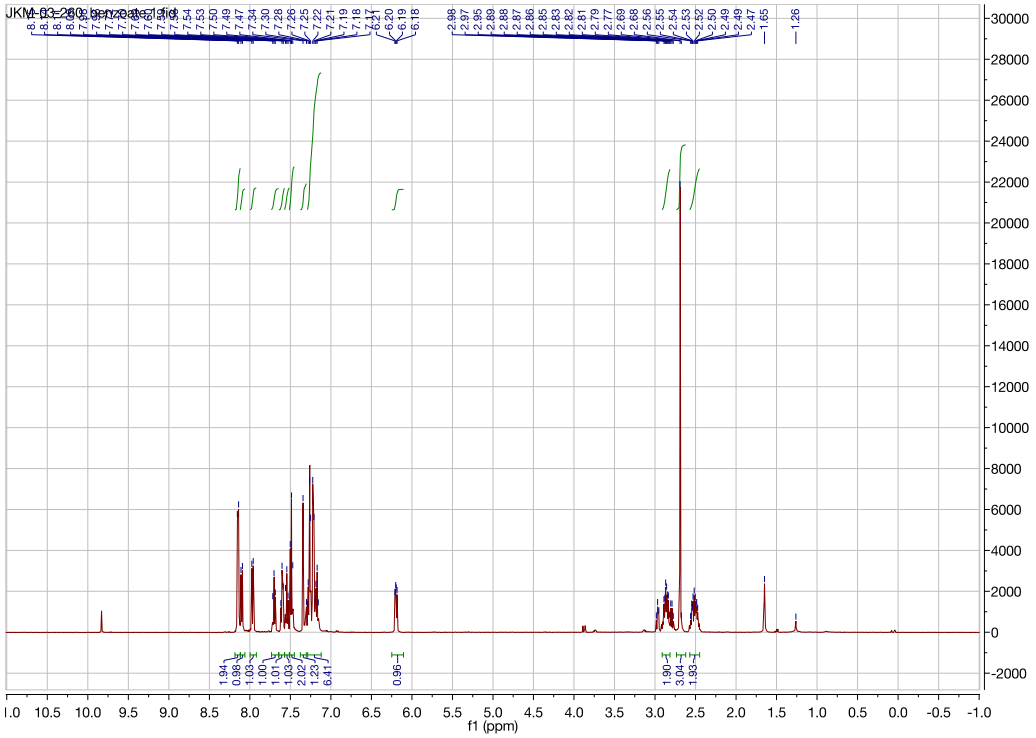


**Figure A11.86.** $^{1}H$ NMR ($CDCl_3$, 500 MHz) spectrum of 1-(4-methylquinolin-2-yl)-3-phenylpropyl benzoate (**4b**)

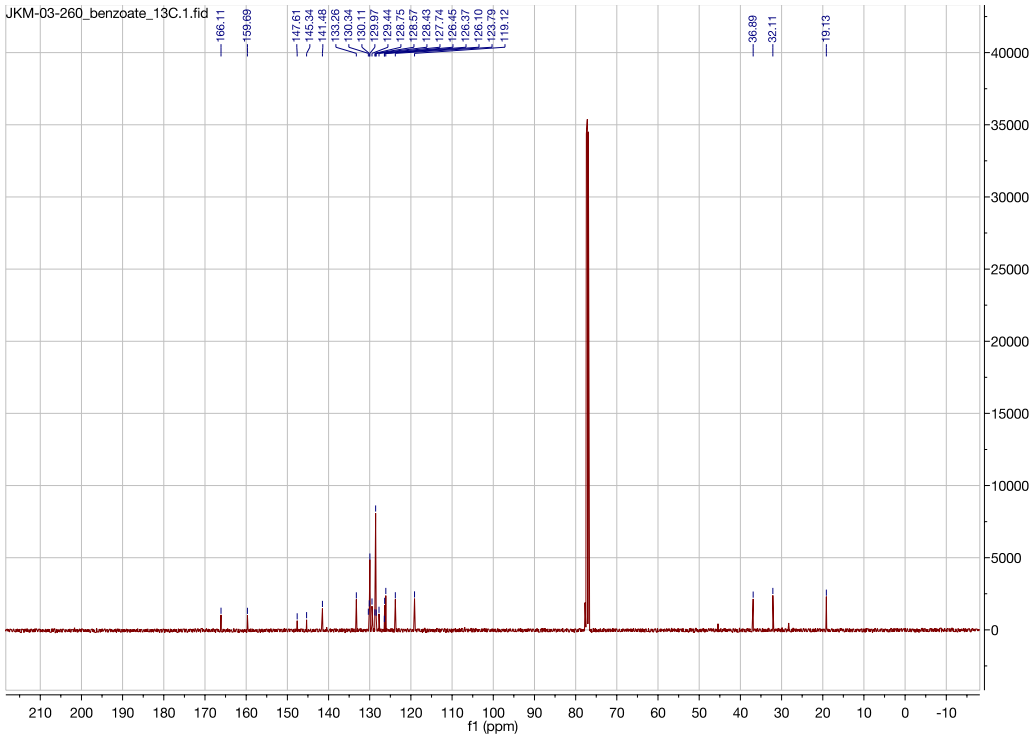


**Figure A11.87.** $^{13}C$ NMR ($CDCl_3$, 125.8 MHz) spectrum of 1-(4-methylquinolin-2-yl)-3-phenylpropyl benzoate (**4b**)

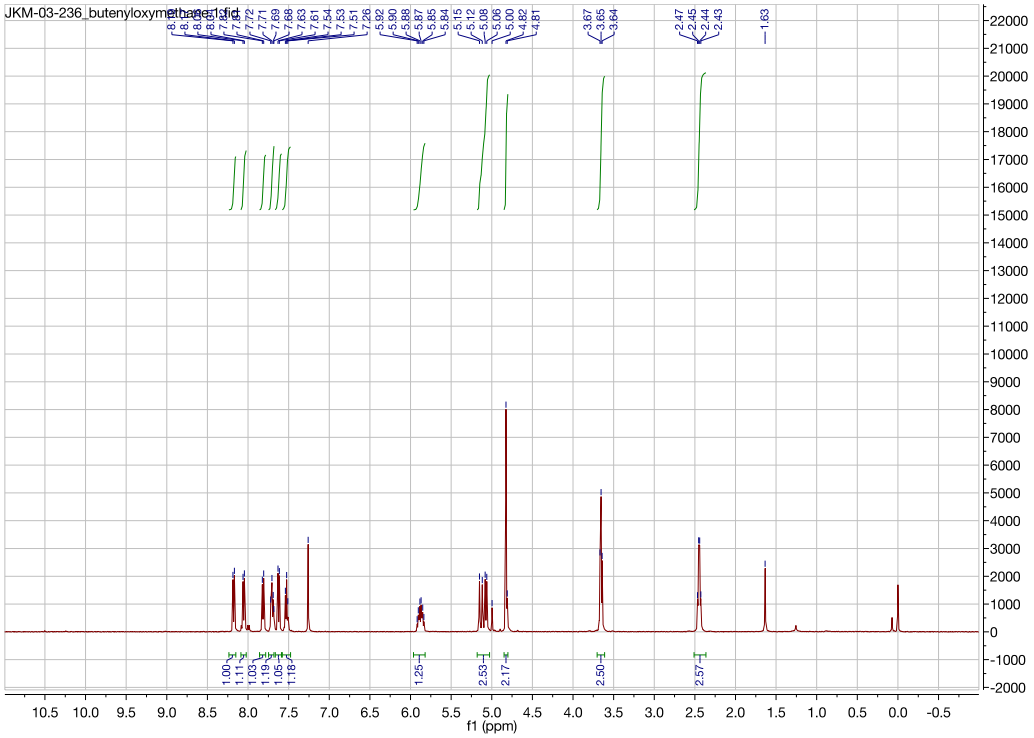


**Figure A11.88.** $^{1}$H NMR ($CDCl_3$, 500 MHz) spectrum of 2-((but-3-en-1-yloxy)methyl)quinoline (**4c**)

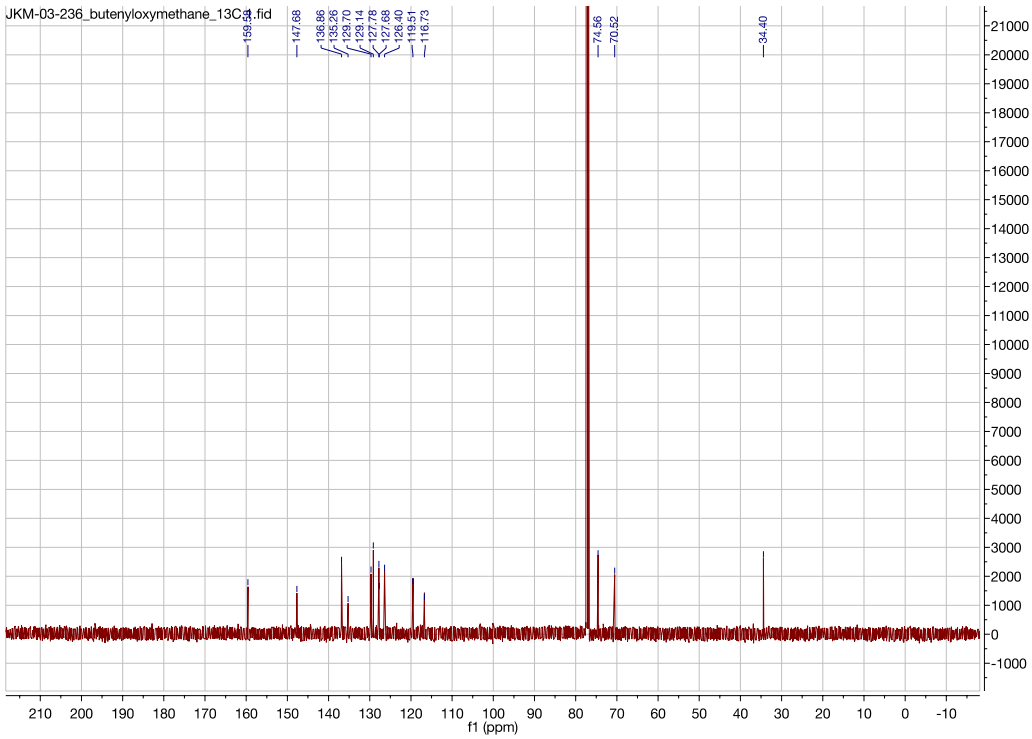


**Figure A11.89.** $^{13}$C NMR ($CDCl_3$, 125.8 MHz) spectrum of 2-((but-3-en-1-yloxy)methyl)quinoline (**4c**)

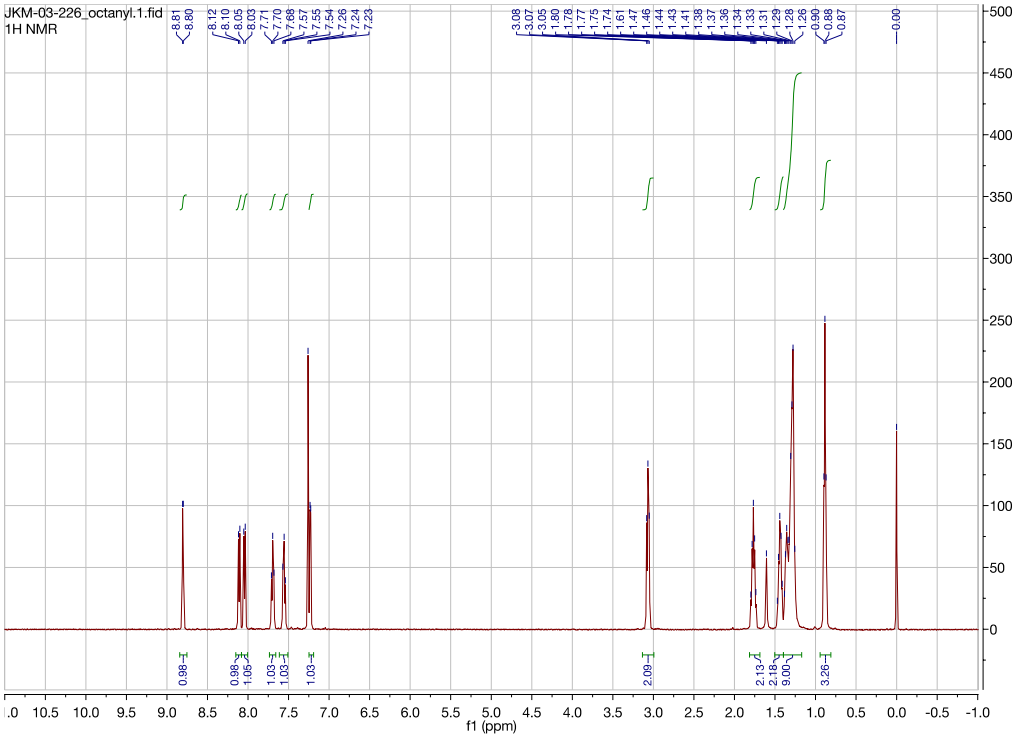


**Figure A11.90.** $^{1}$H NMR ($CDCl_3$, 500 MHz) spectrum of 2-octylquinoline (**4d**)

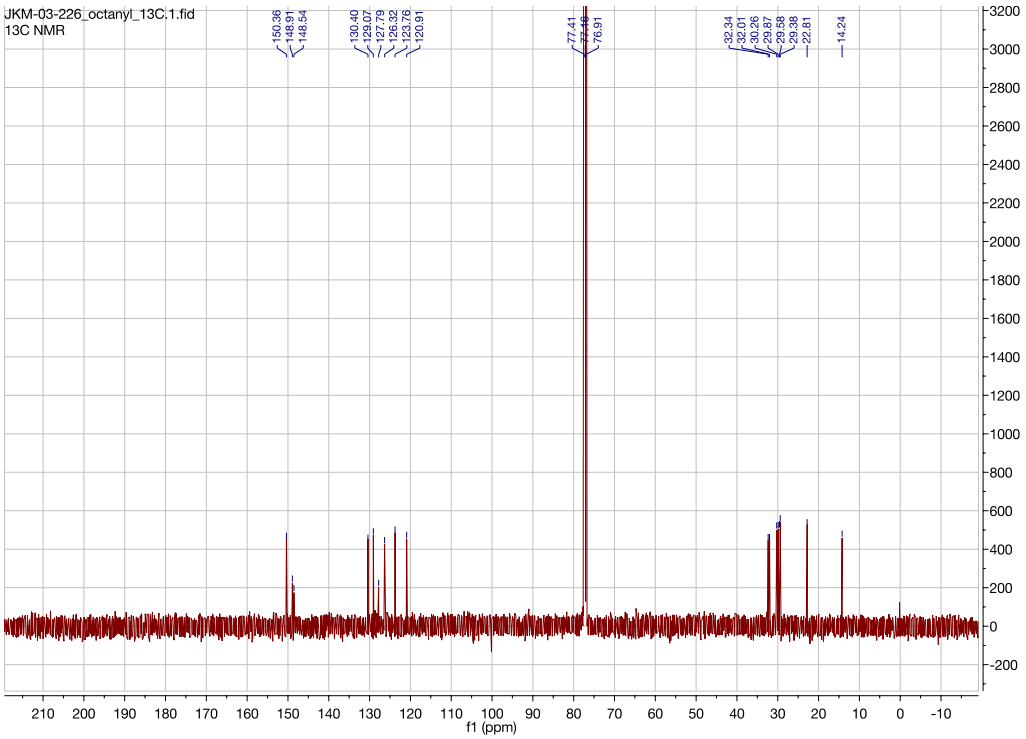


**Figure A11.91.** $^{13}$C NMR ($CDCl_3$, 125.8 MHz) spectrum of 2-octylquinoline (**4d**)

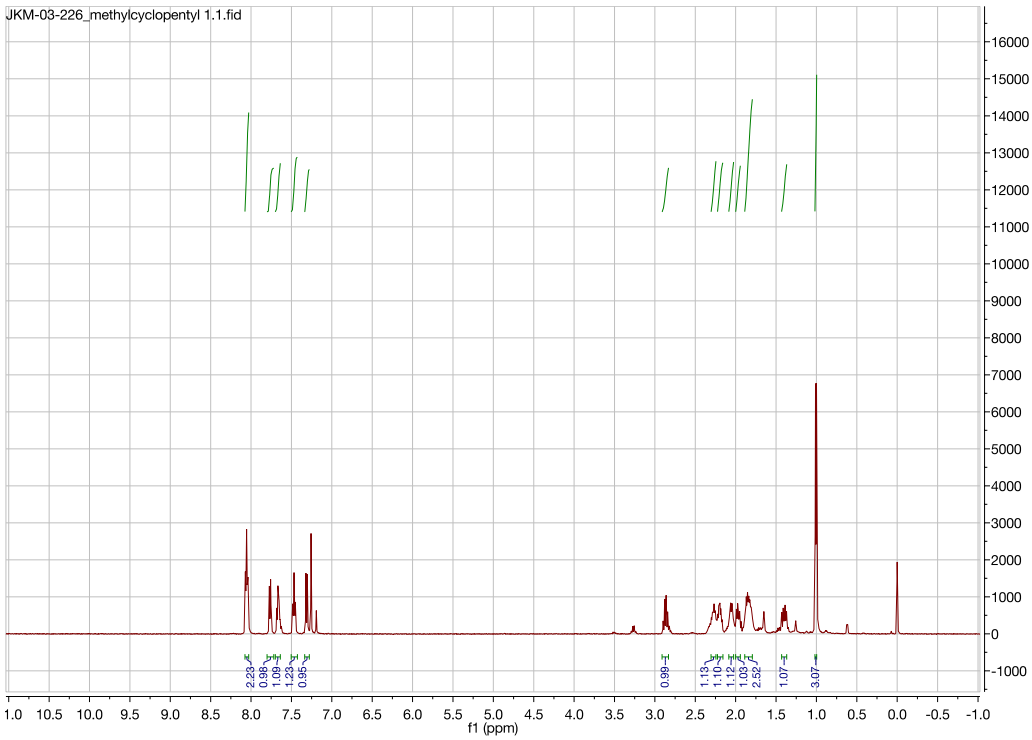


**Figure A11.92.** $^{1}$H NMR ($CDCl_3$, 500 MHz) spectrum of 2-((*trans*)-2-methylcyclopentyl)quinoline (4**e**)

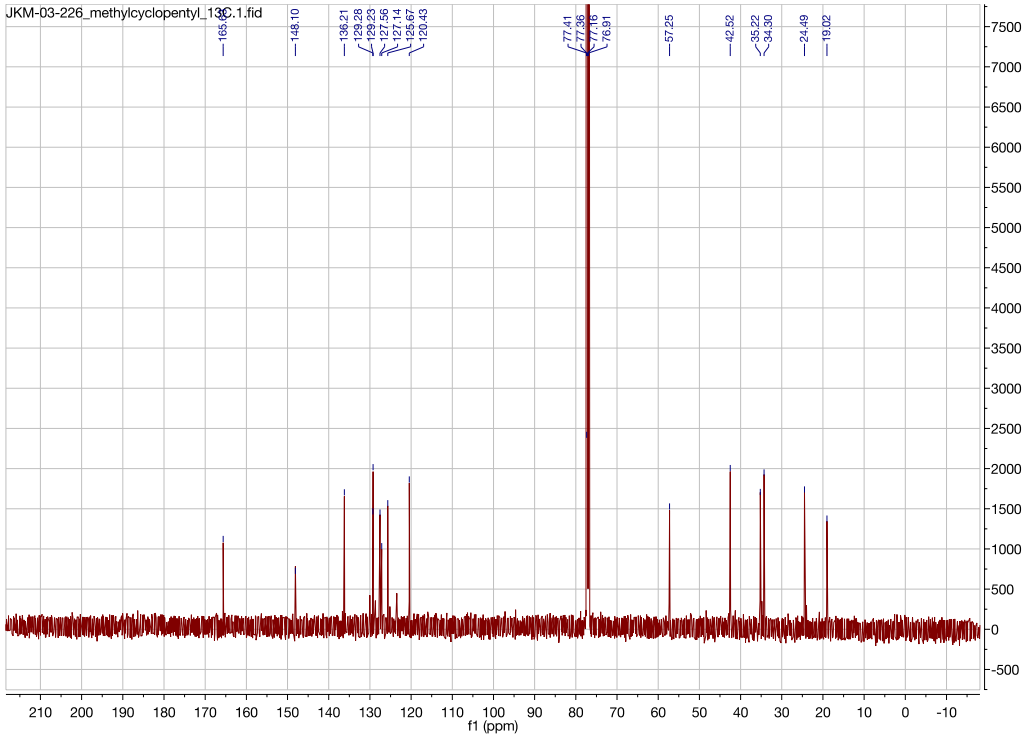


**Figure A11.93.** $^{13}$C NMR ($CDCl_3$, 125.8 MHz) spectrum of 2-((*trans*)-2-methylcyclopentyl)quinoline (4**e**)

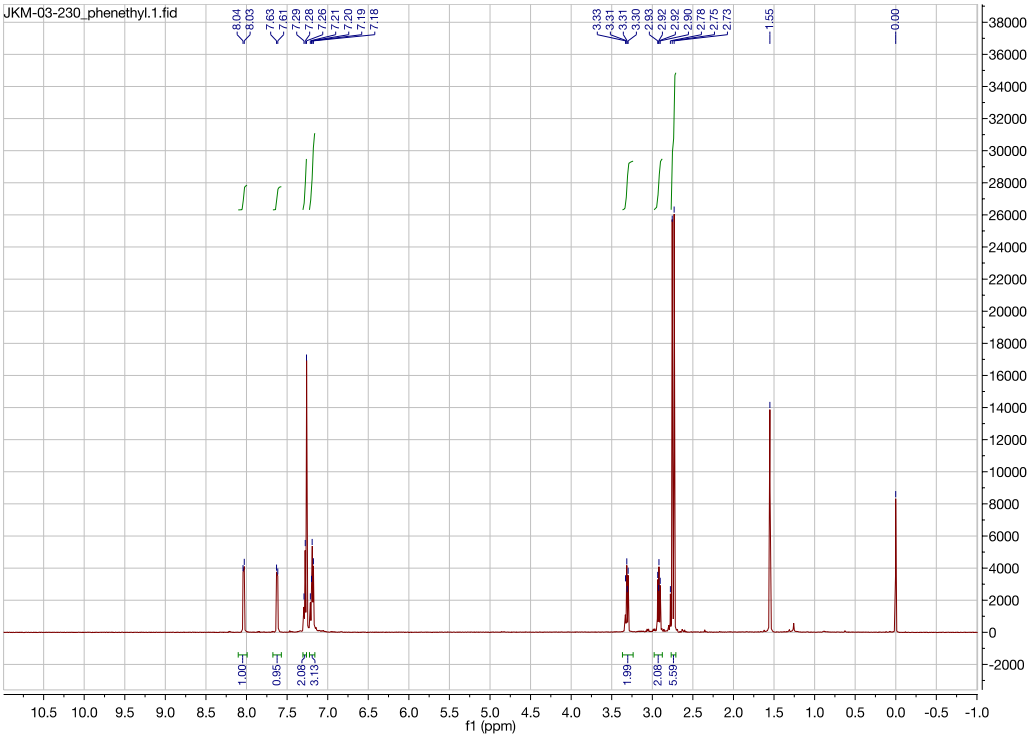


**Figure A11.94.** $^{1}$H NMR ($CDCl_3$, 500 MHz) spectrum of 1,1'-(3-phenethylpyridine-2,6-diyl)bis(ethan-1-one) (**4f**)

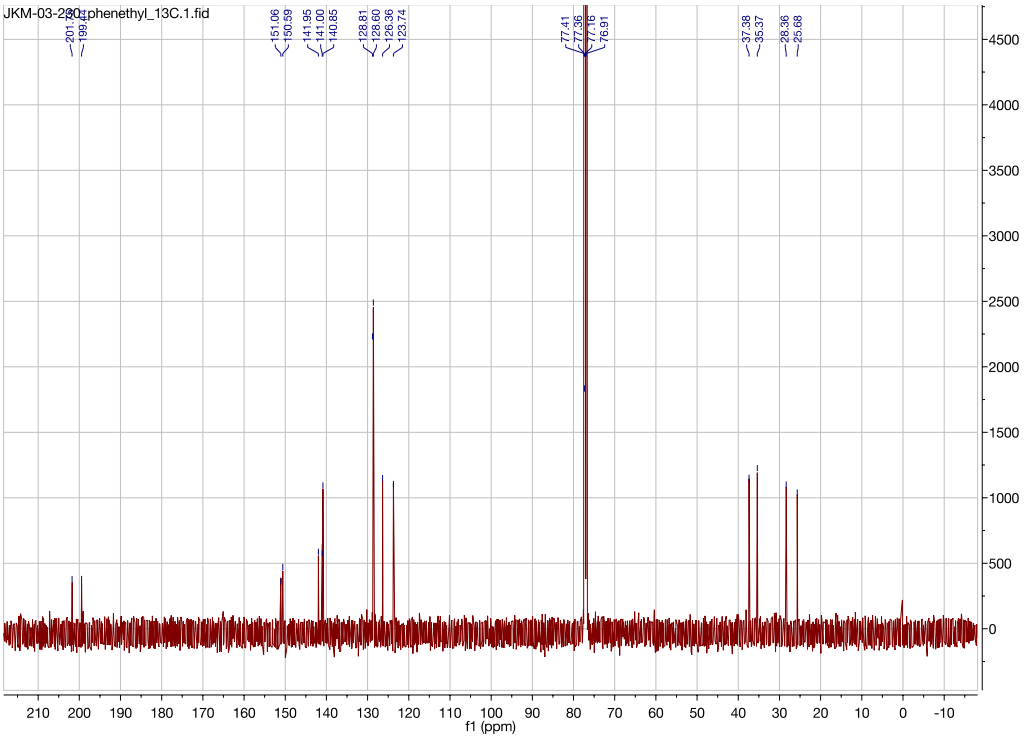


**Figure A11.95.** $^{13}$C NMR ($CDCl_3$, 125.8 MHz) spectrum of 1,1'-(3-phenethylpyridine-2,6-diyl)bis(ethan-1-one) (**4f**)

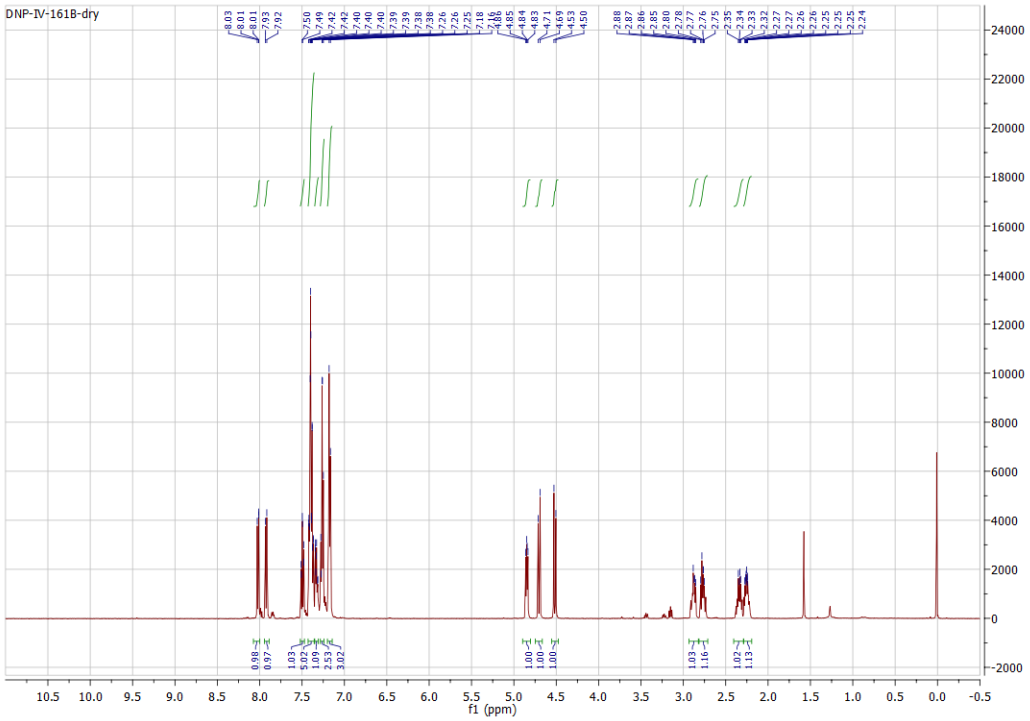


**Figure A11.96.** $^{1}$H NMR ($CDCl_3$, 500 MHz) spectrum of 2-(1-(benzyloxy)-2-phenylethyl)benzo[*d*]thiazole (**4g**)

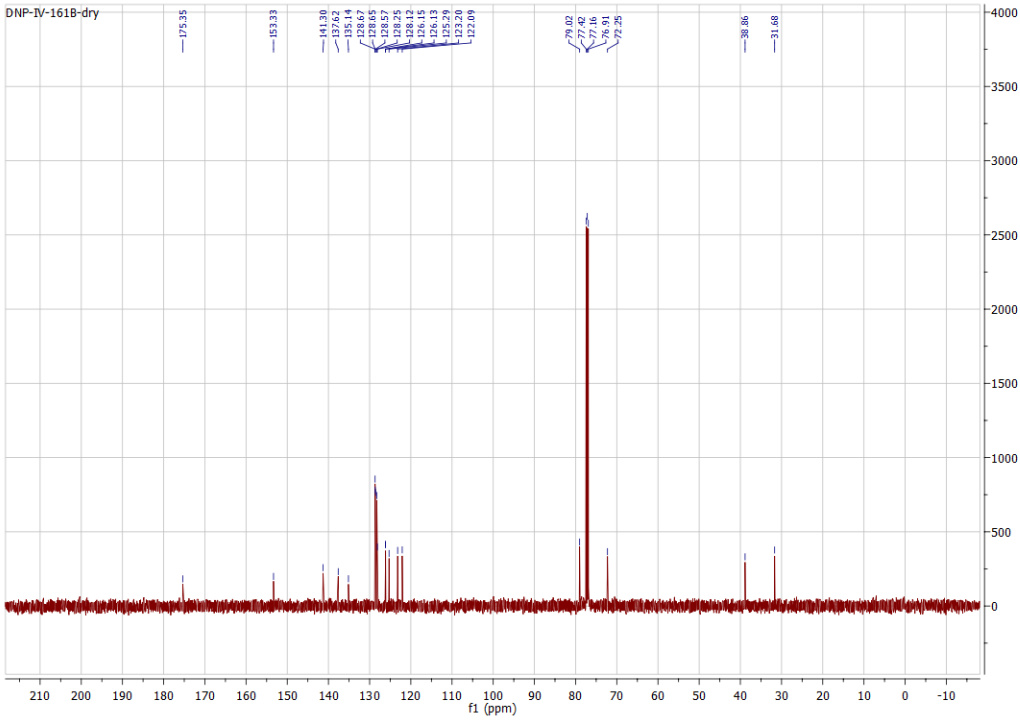


**Figure A11.97.** $^{13}$C NMR ($CDCl_3$, 125.8 MHz) spectrum of 2-(1-(benzyloxy)-2-phenylethyl)benzo[*d*]thiazole (**4g**)

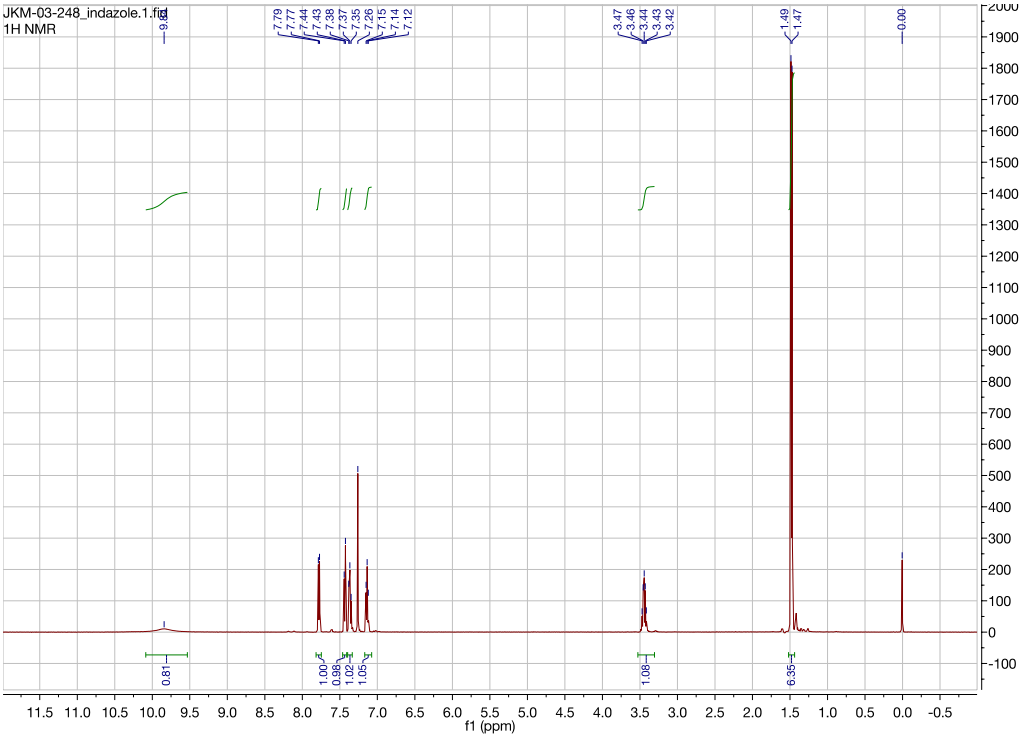


**Figure A11.98.** $^{1}$H NMR ($CDCl_3$, 500 MHz) spectrum of 3-Isopropyl-1*H*-indazole (**4h**)

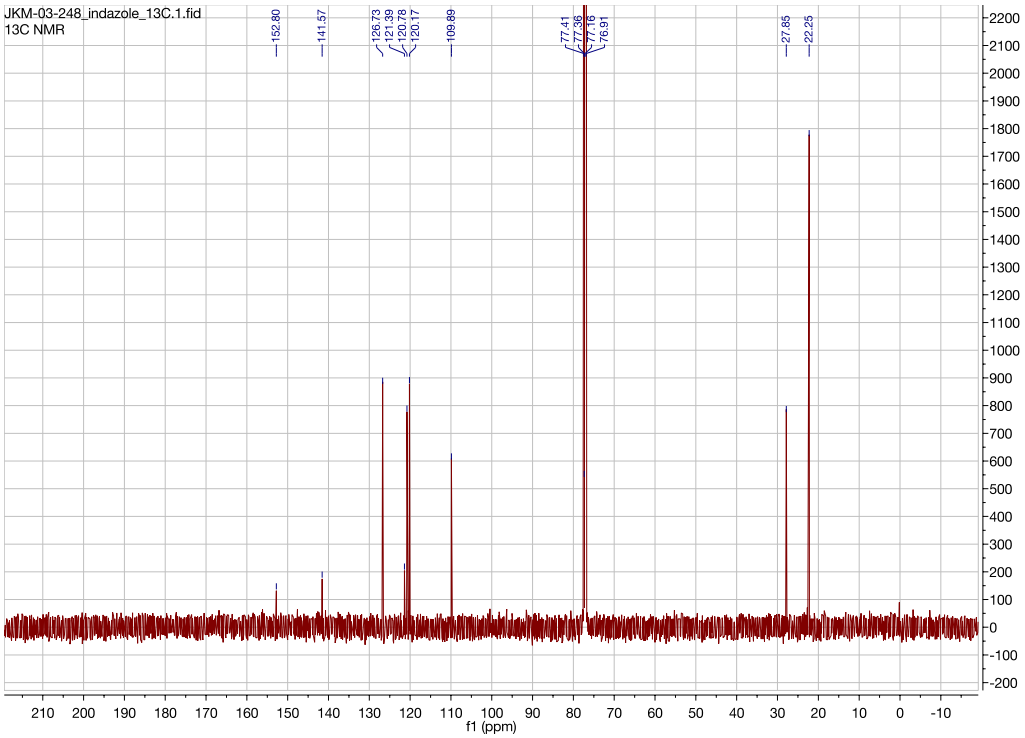


**Figure A11.99.** $^{13}$C NMR ($CDCl_3$, 125.8 MHz) spectrum of 3-Isopropyl-1*H*-indazole (**4h**)

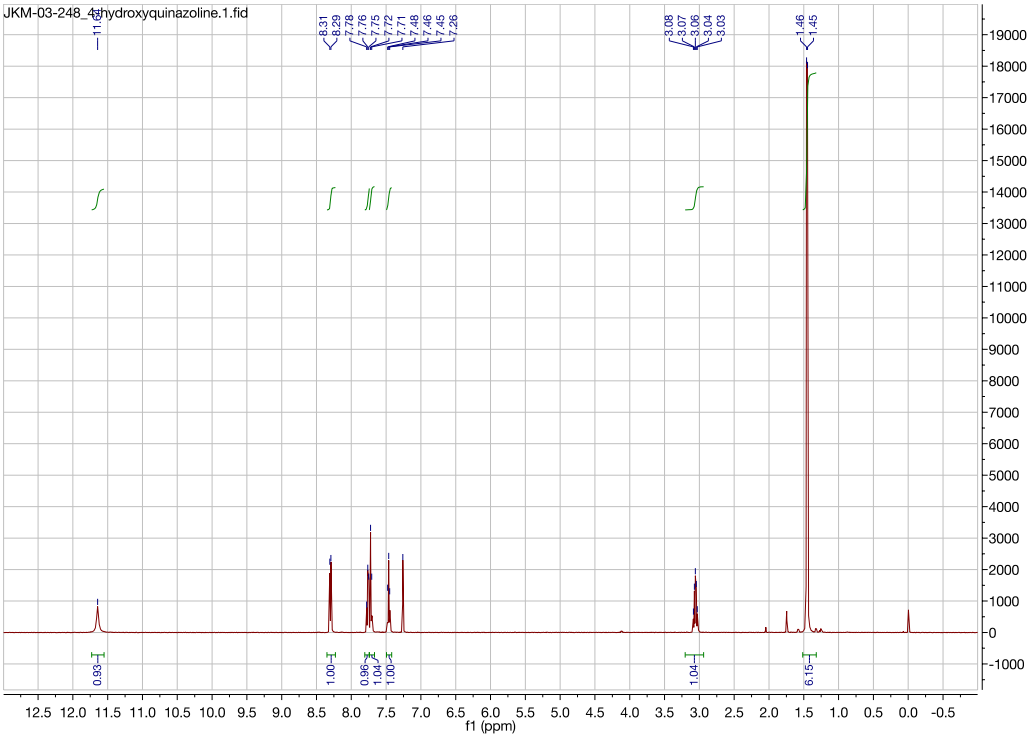


**Figure A11.100.** $^{1}$H NMR ($CDCl_3$, 500 MHz) spectrum of 2-isopropylquinazolin-4(3*H*)-one (4**i**)

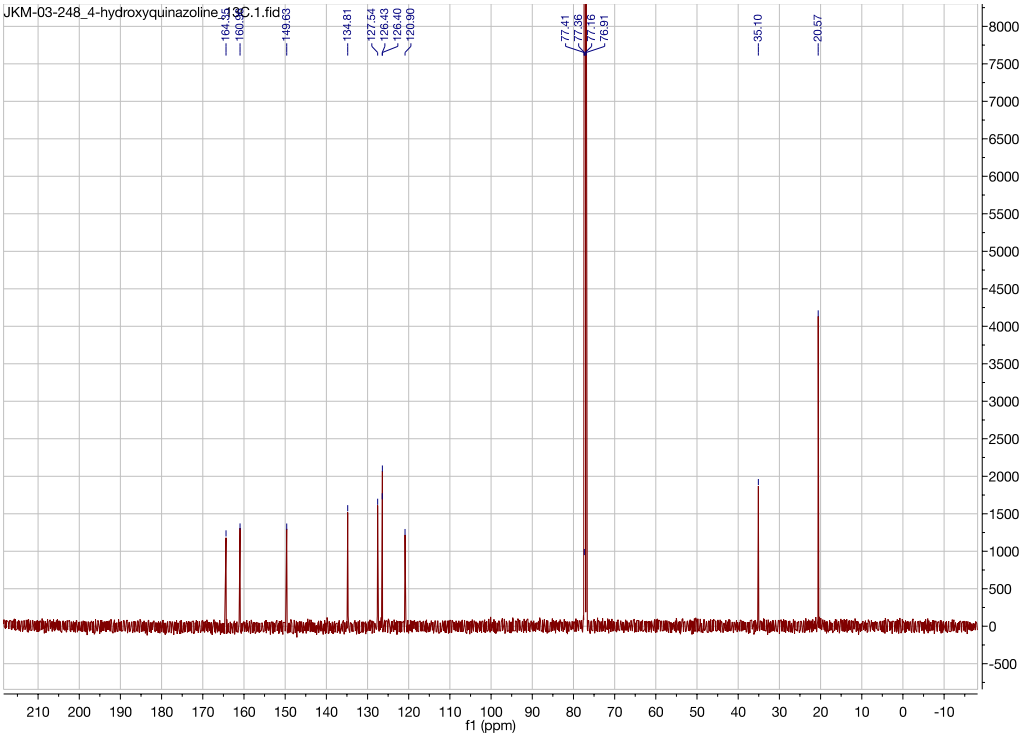


**Figure A11.101.** $^{13}$C NMR ($CDCl_3$, 125.8 MHz) spectrum of 2-isopropylquinazolin-4(3*H*)-one (4**i**)

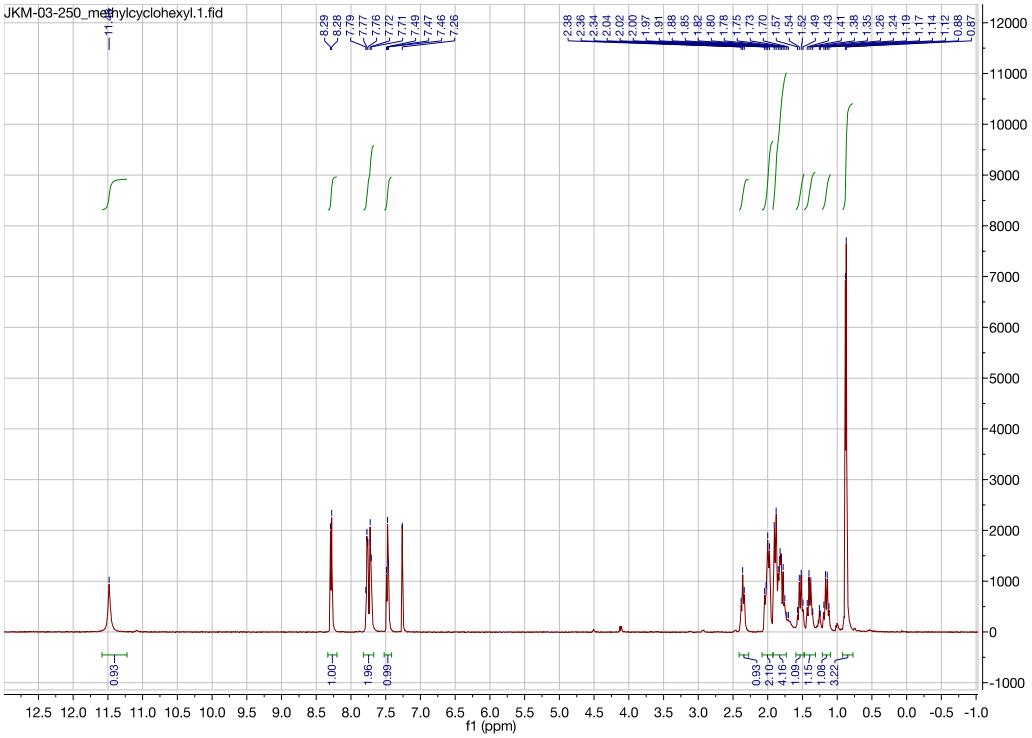


**Figure A11.102.** $^{1}$H NMR ($CDCl_3$, 500 MHz) spectrum of 2-((*trans*)-2-methylcyclohexyl)quinazolin-4(3*H*)-one (**4j**)

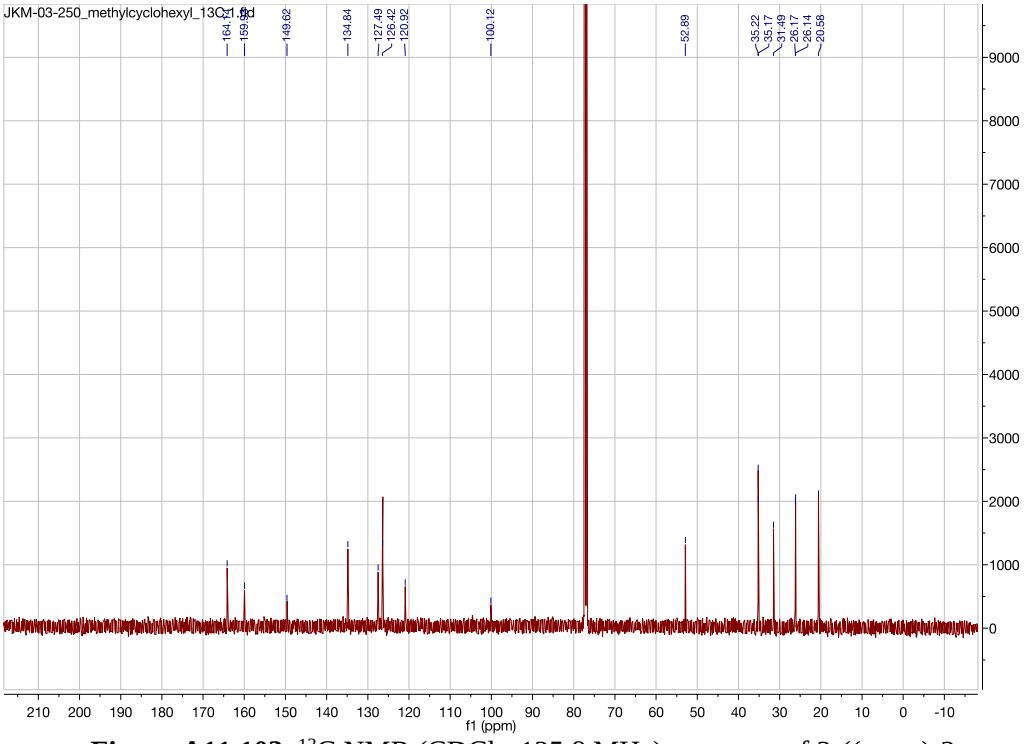


**Figure A11.103.** $^{13}$C NMR ($CDCl_3$, 125.8 MHz) spectrum of 2-((*trans*)-2-methylcyclohexyl)quinazolin-4(3*H*)-one (**4j**)

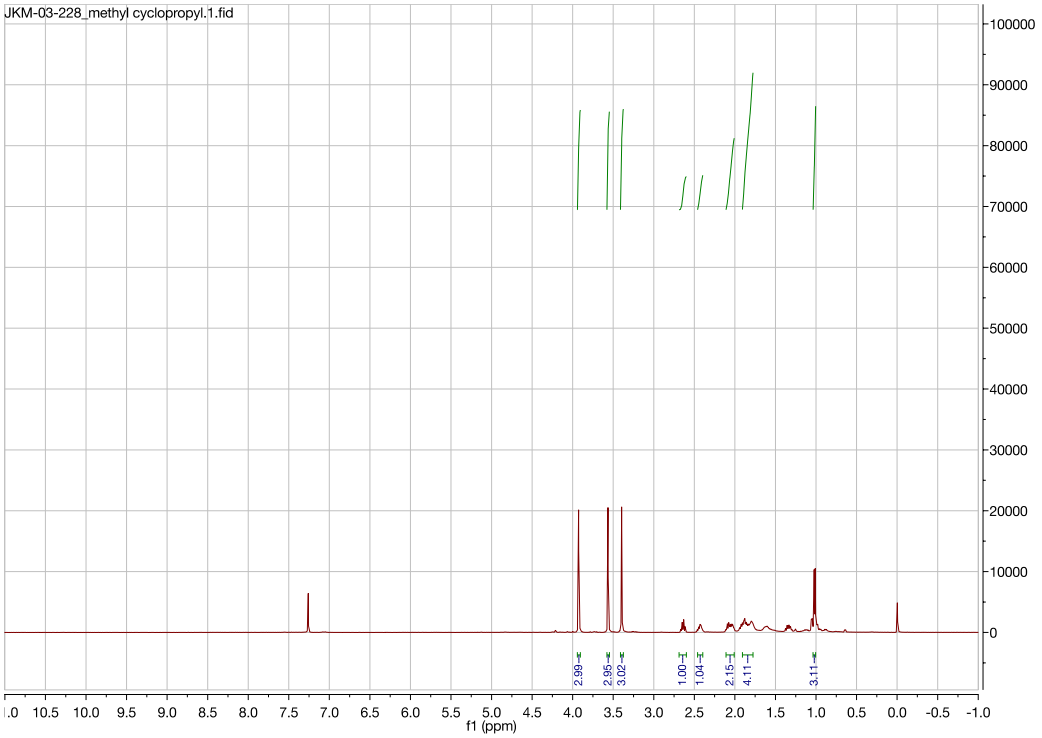


**Figure A11.104.** $^{1}$H NMR ($CDCl_3$, 500 MHz) spectrum of 1,3,7-trimethyl-8-((2*S*)-2-methylcyclopentyl)-3,7-dihydro-1*H*-purine-2,6-dione (**4k**)

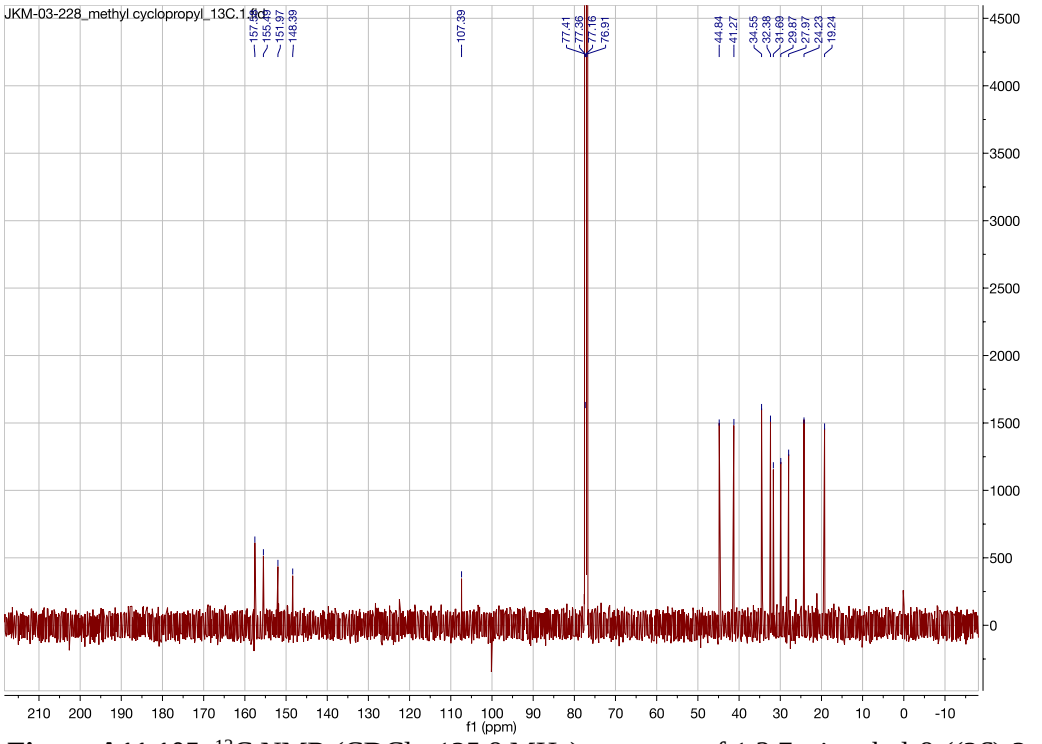


**Figure A11.105.** $^{13}$C NMR ($CDCl_3$, 125.8 MHz) spectrum of 1,3,7-trimethyl-8-((2*S*)-2-methylcyclopentyl)-3,7-dihydro-1*H*-purine-2,6-dione (**4k**)

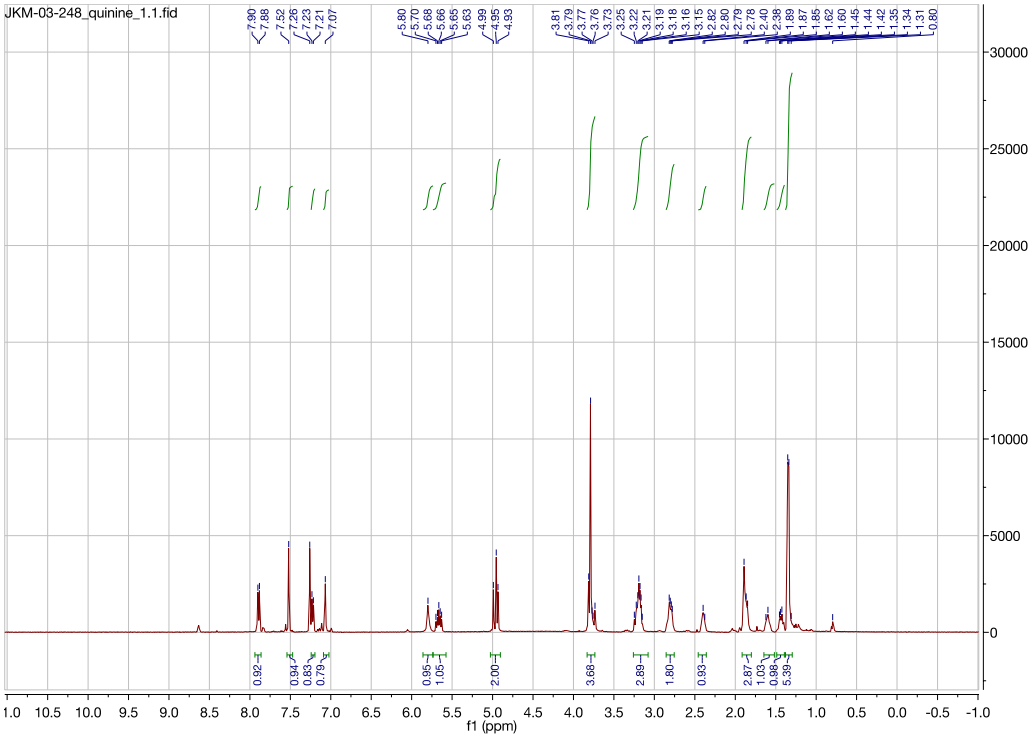


**Figure A11.106.** $^{1}$H NMR ($CDCl_3$, 500 MHz) spectrum of (1*R*)-(2-isopropyl-6-methoxyquinolin-4-yl)(5-vinylquinuclidin-2-yl)methanol (**4l**)

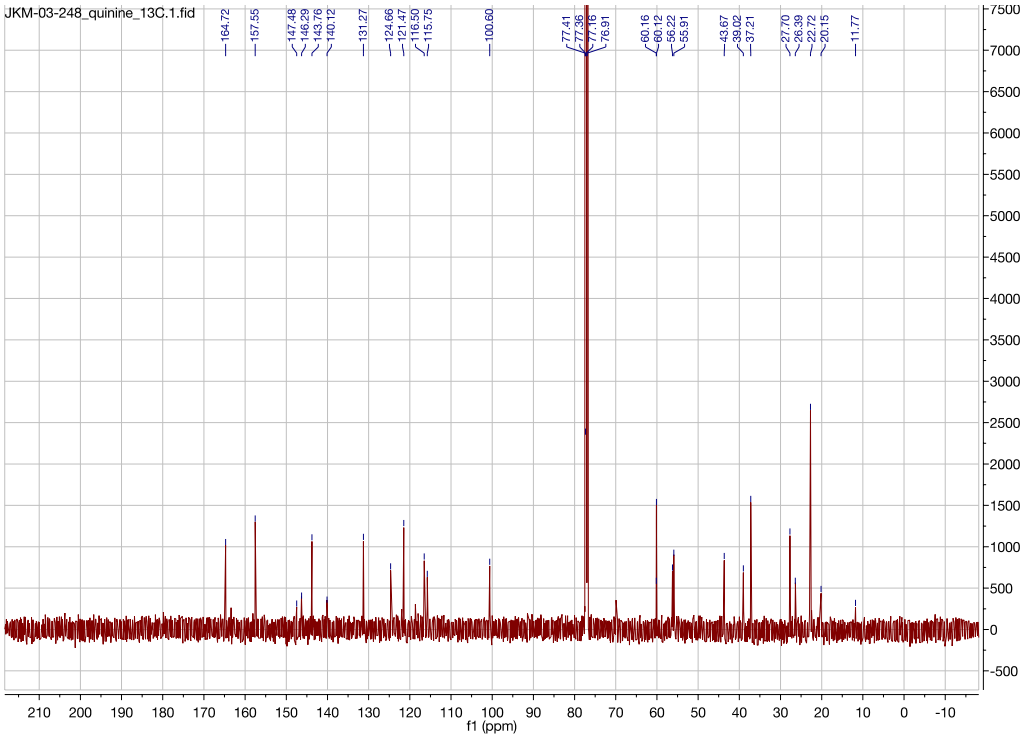


**Figure A11.107.** $^{13}$C NMR ($CDCl_3$, 125.8 MHz) spectrum of (1*R*)-(2-isopropyl-6-methoxyquinolin-4-yl)(5-vinylquinuclidin-2-yl)methanol (**4l**)

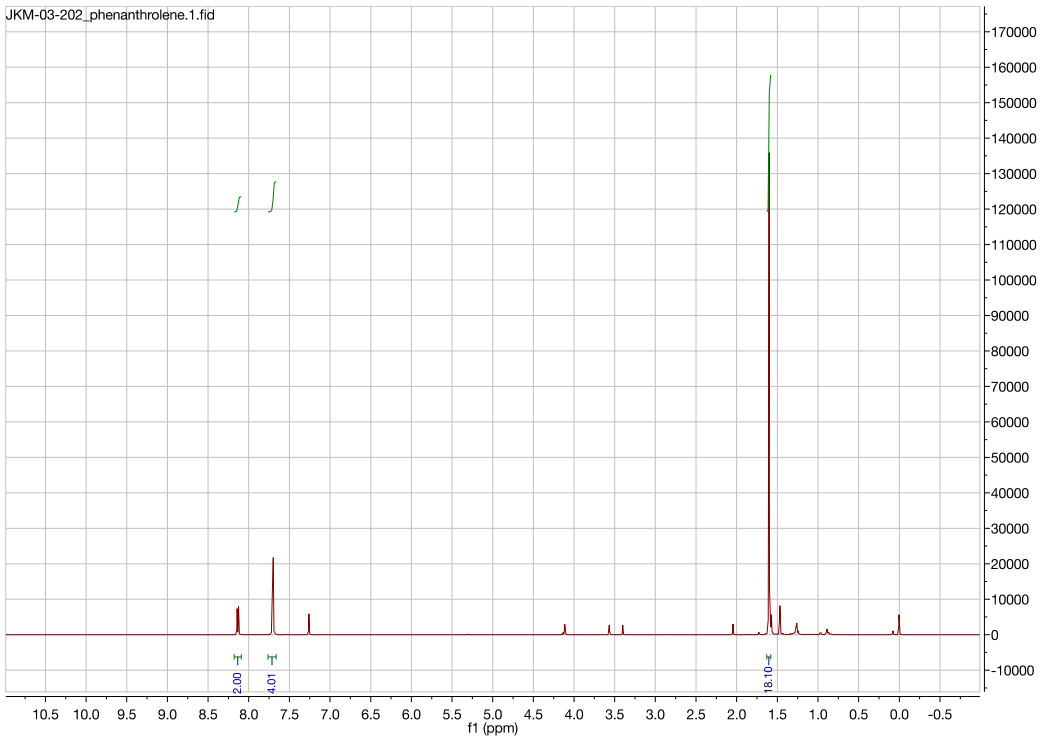


**Figure A11.108.** $^{1}H$ NMR ($CDCl_3$, 500 MHz) spectrum of 2,9-di-*tert*-butyl-1,10-phenanthroline (**5b**)

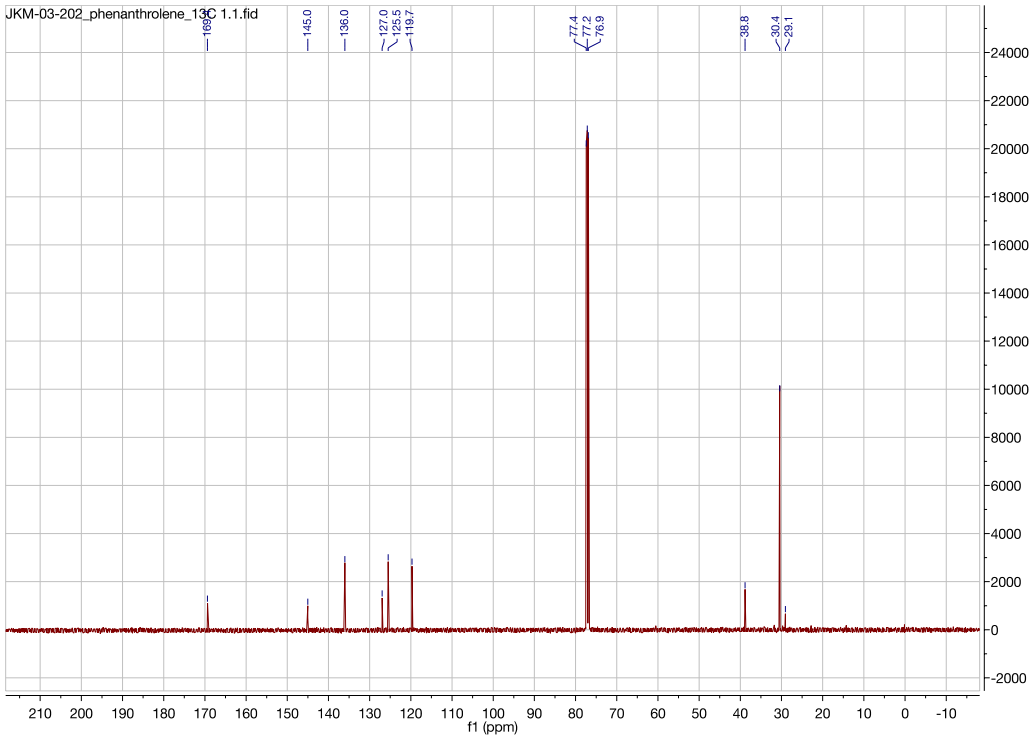


**Figure A11.109.** $^{13}C$ NMR ($CDCl_3$, 125.8 MHz) spectrum of 2,9-di-*tert*-butyl-1,10-phenanthroline (**5b**)

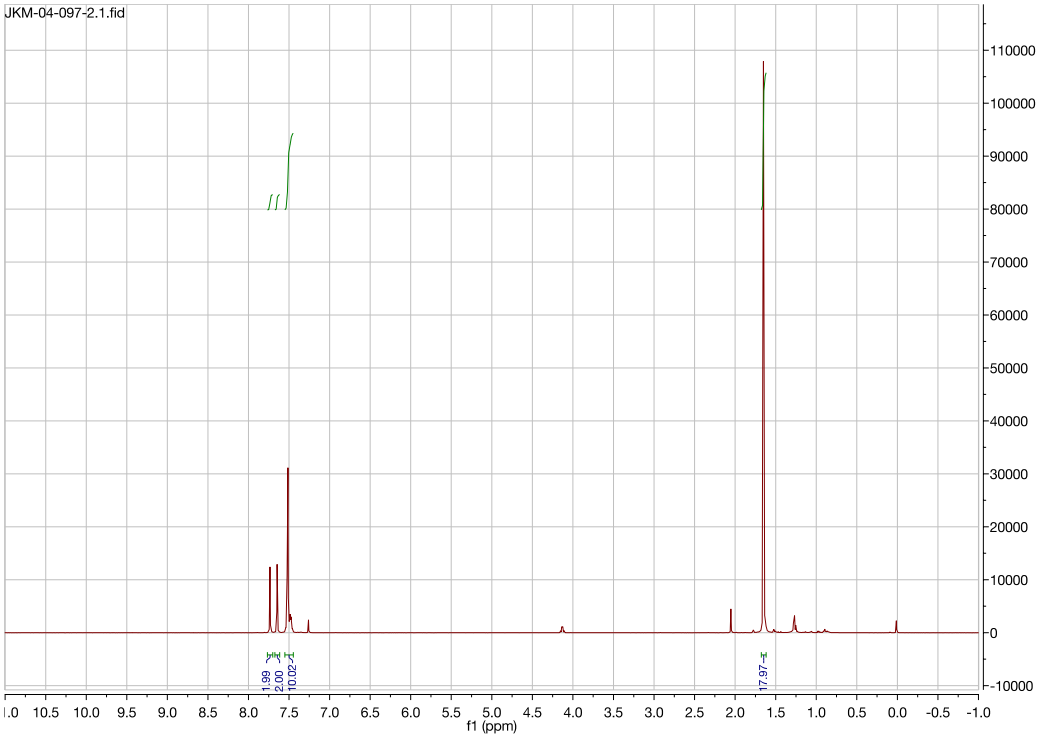


**Figure A11.110.** $^{1}$H NMR ($CDCl_3$, 500 MHz) spectrum of 2,9-di-*tert*-butyl-4,7-diphenyl-1,10-phenanthroline (**5d**)

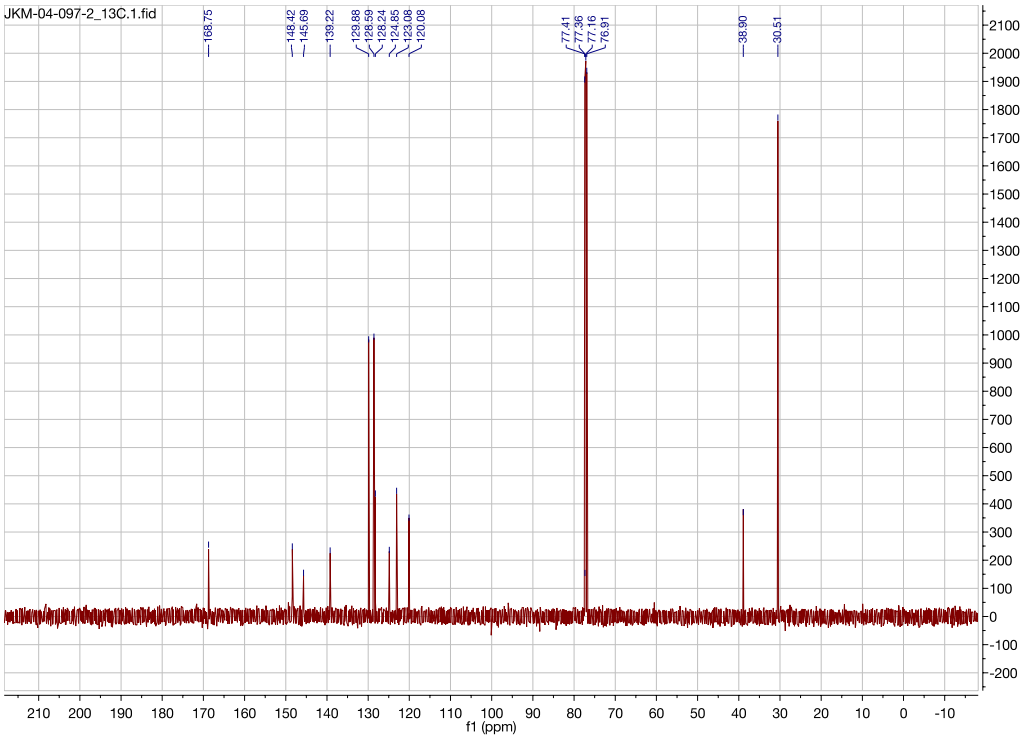


**Figure A11.111.** $^{13}$C NMR ($CDCl_3$, 125.8 MHz) spectrum of 2,9-di-*tert*-butyl-4,7-diphenyl-1,10-phenanthroline (**5d**)

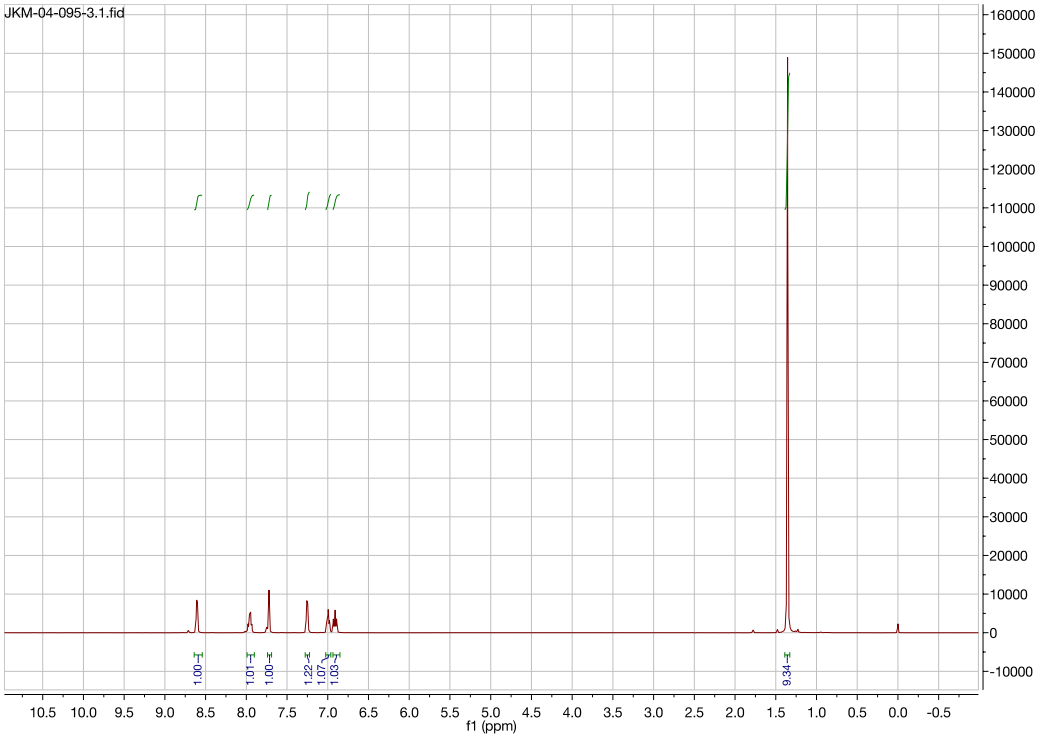


**Figure A11.112.** $^{1}$H NMR ($CDCl_3$, 500 MHz) spectrum of 2-(*tert*-butyl)-6-(2,4-difluorophenyl)pyridine (**5f**)

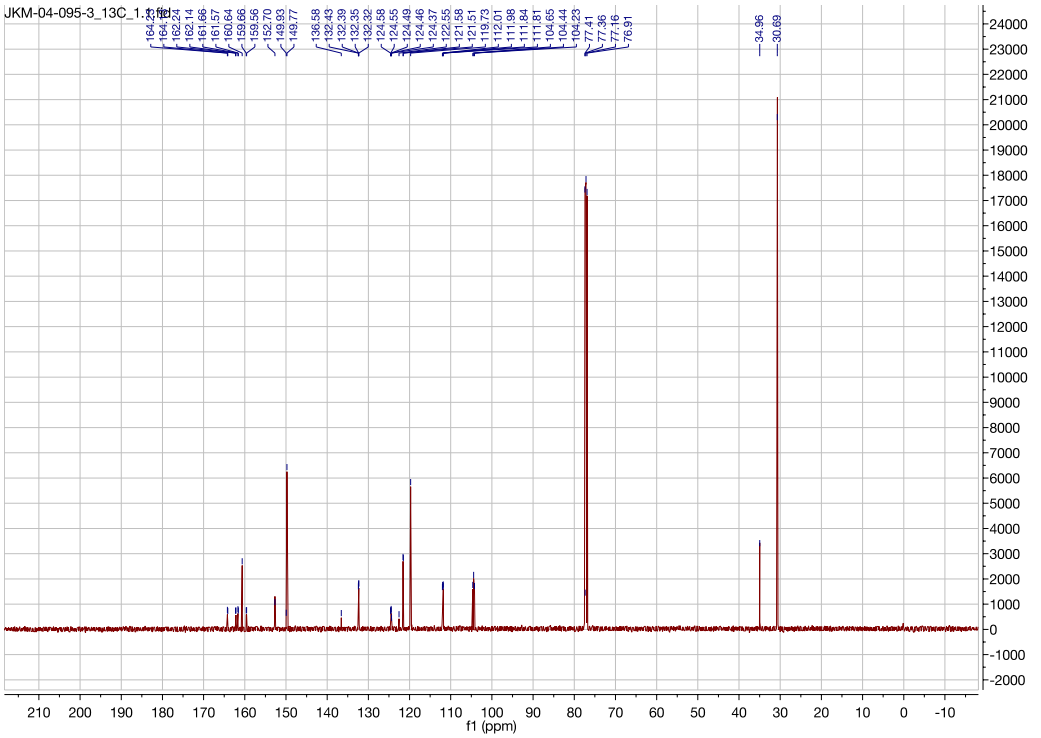


**Figure A11.113.** $^{13}$C NMR ($CDCl_3$, 125.8 MHz) spectrum of 2-(*tert*-butyl)-6-(2,4-difluorophenyl)pyridine (**5f**)

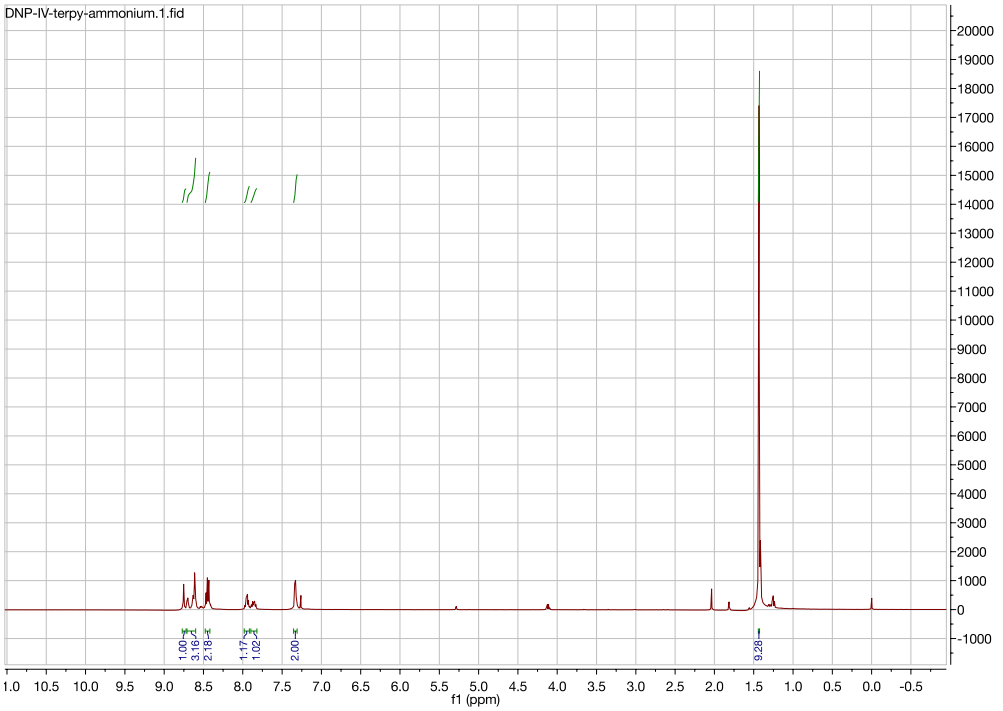


**Figure A11.114.** $^{1}$H NMR ($CDCl_3$, 500 MHz) spectrum of 6-(*tert*-butyl)-2,2':6',2"-terpyridine (**5h**)

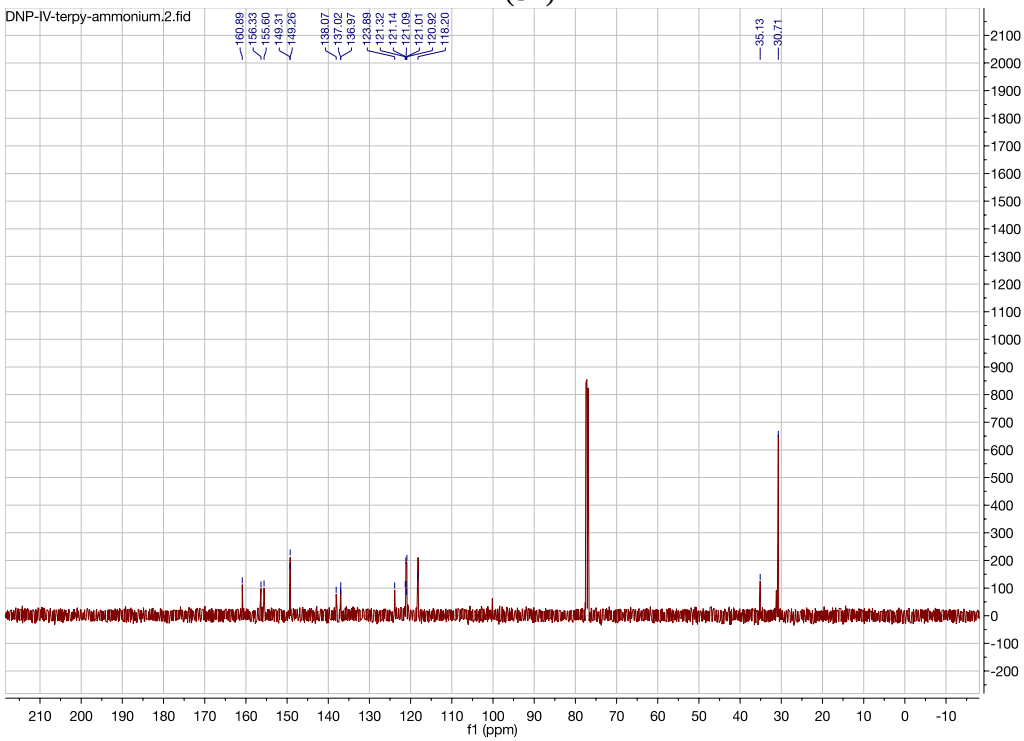


**Figure A11.115.** $^{13}$C NMR ($CDCl_3$, 125.8 MHz) spectrum of 6-(*tert*-butyl)-2,2':6',2"-terpyridine (**5h**)

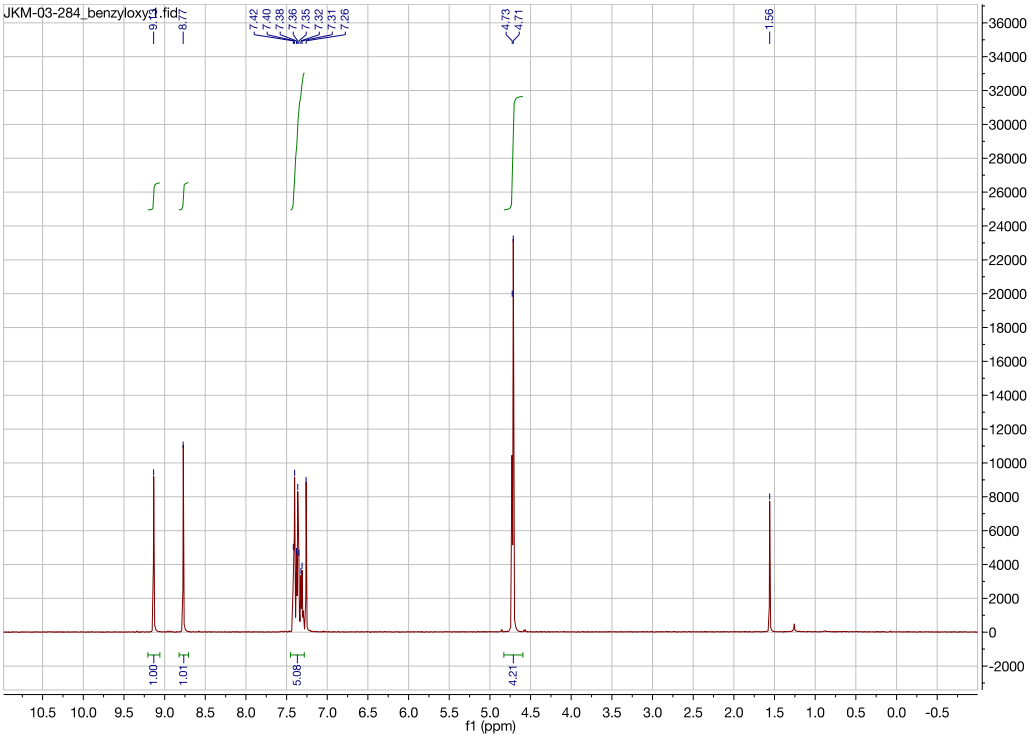


**Figure A11.116.** $^{1}$H NMR ($CDCl_3$, 500 MHz) spectrum of 4-((benzyloxy)methyl)-5-bromopyrimidine (**6a**)

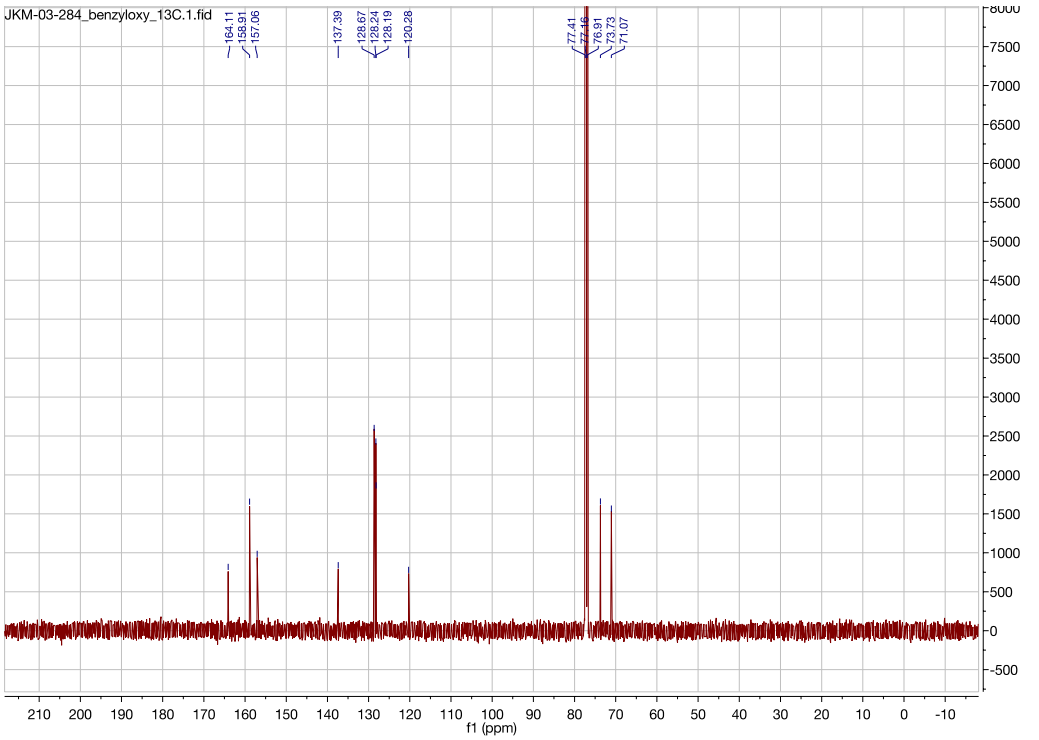


**Figure A11.117.** $^{13}$C NMR ($CDCl_3$, 125.8 MHz) spectrum of 4-((benzyloxy)methyl)-5-bromopyrimidine (**6a**)

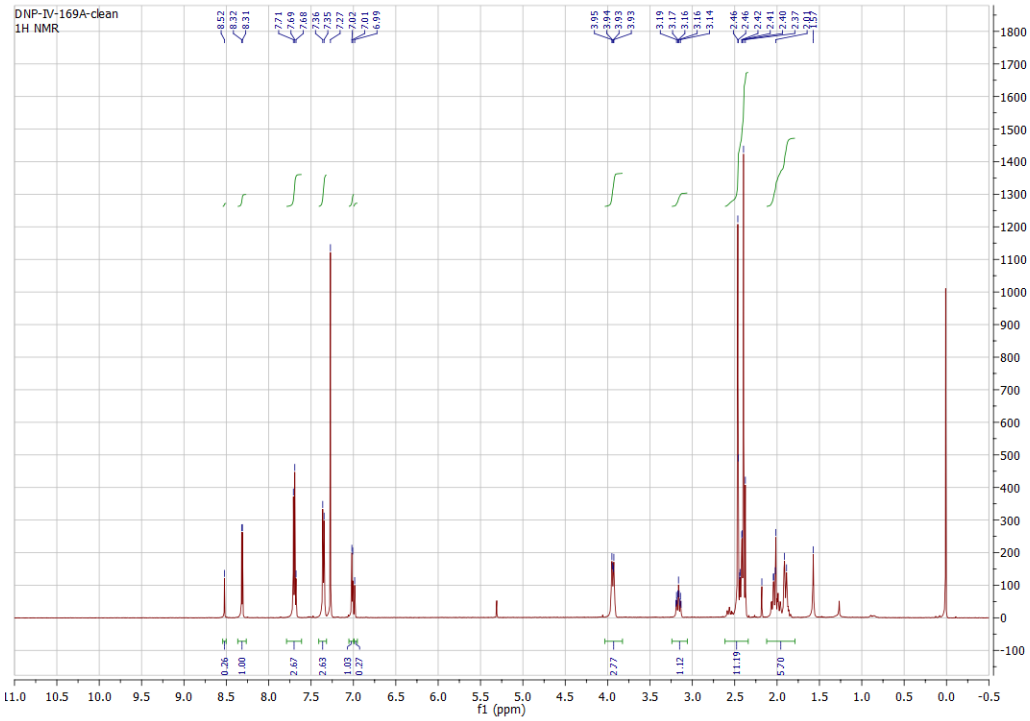


**Figure A11.118.** $^{1}H$ NMR ($CDCl_3$, 500 MHz) spectrum of 3-bromo-4-methyl-2-(1-tosylpiperidin-4-yl)pyridine and 5-bromo-4-methyl-2-(1-tosylpiperidin-4-yl)pyridine (**6b**)

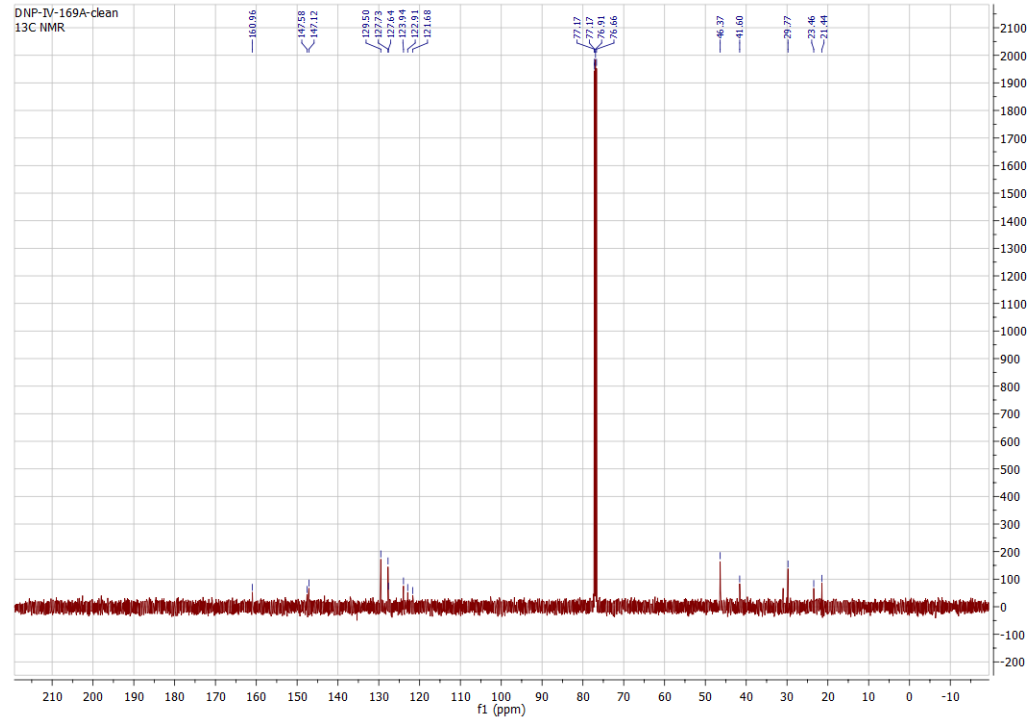


**Figure A11.119.** $^{13}C$ NMR ($CDCl_3$, 125.8 MHz) spectrum of 3-bromo-4-methyl-2-(1-tosylpiperidin-4-yl)pyridine and 5-bromo-4-methyl-2-(1-tosylpiperidin-4-yl)pyridine (**6b**)

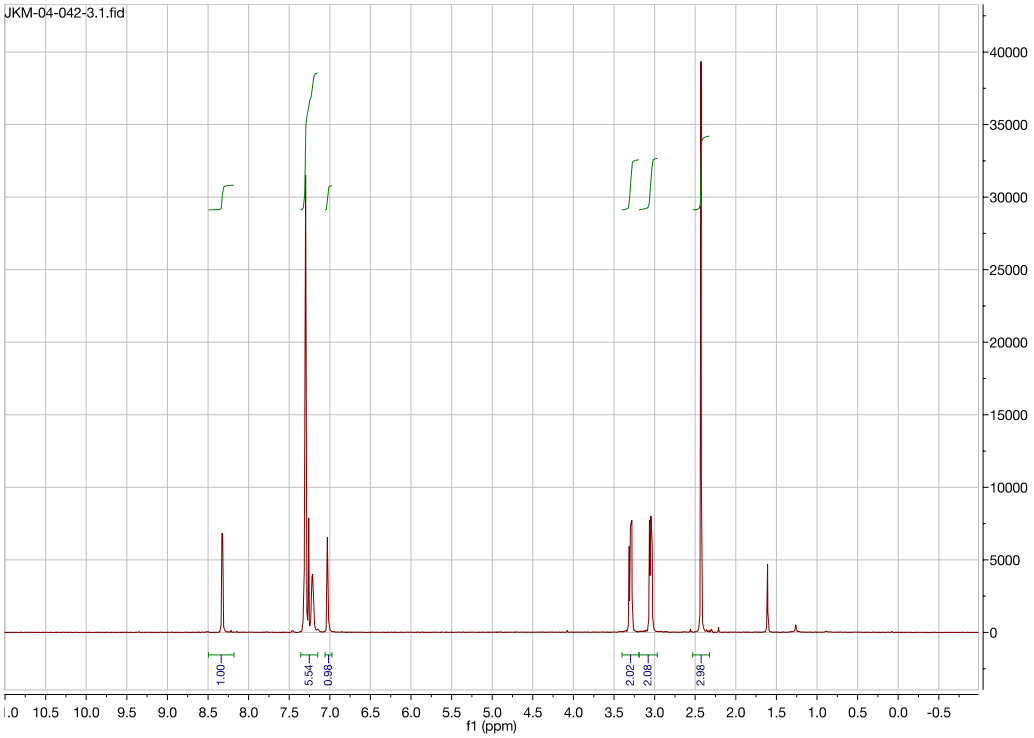


**Figure A11.120.** $^{1}$H NMR ($CDCl_3$, 500 MHz) spectrum of 3-bromo-4-methyl-2-phenethylpyridine (**6c**)

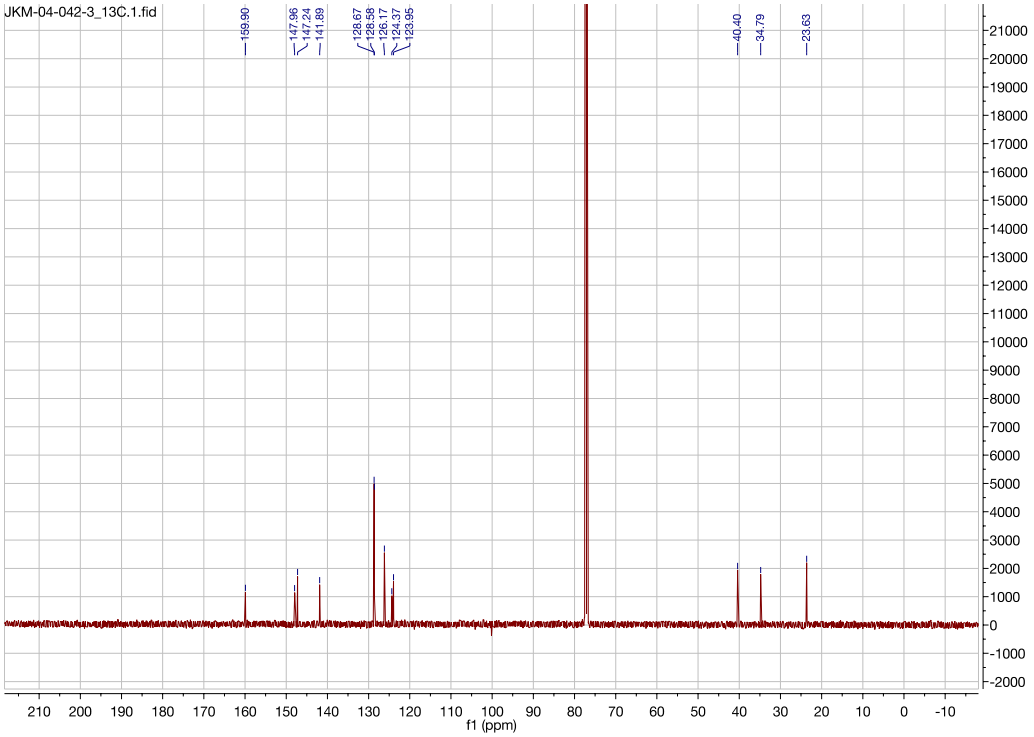


**Figure A11.121.** $^{13}$C NMR ($CDCl_3$, 125.8 MHz) spectrum of 3-bromo-4-methyl-2-phenethylpyridine (**6c**)

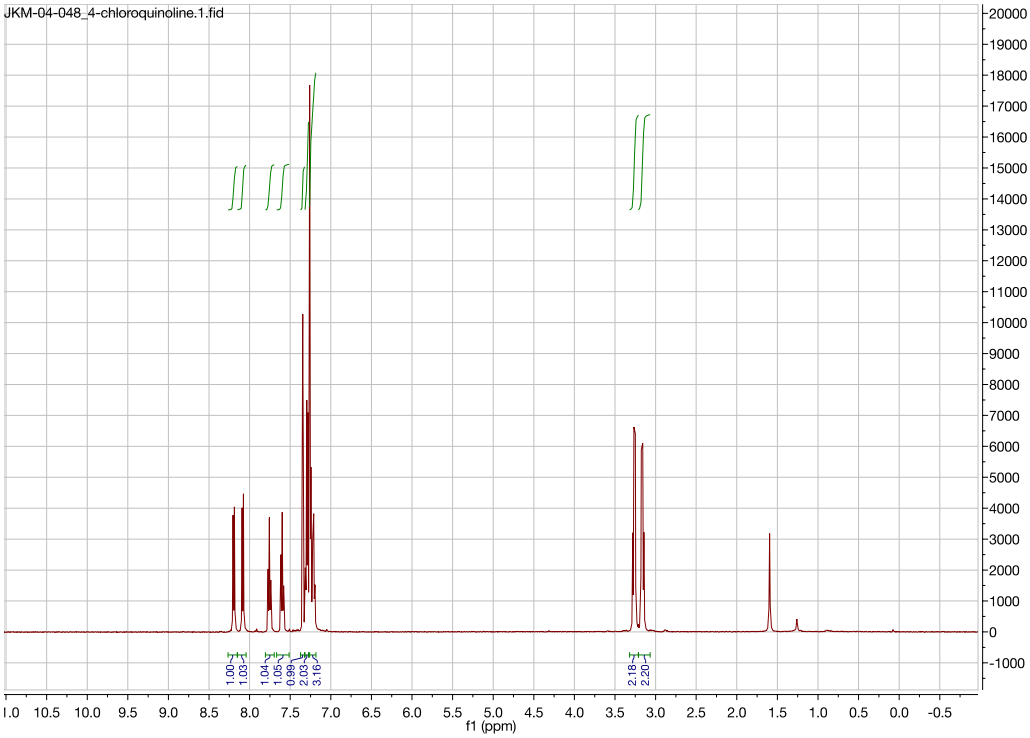


**Figure A11.122.** $^{1}$H NMR ($CDCl_3$, 500 MHz) spectrum of 4-chloro-2-phenethylquinoline (**6d**)

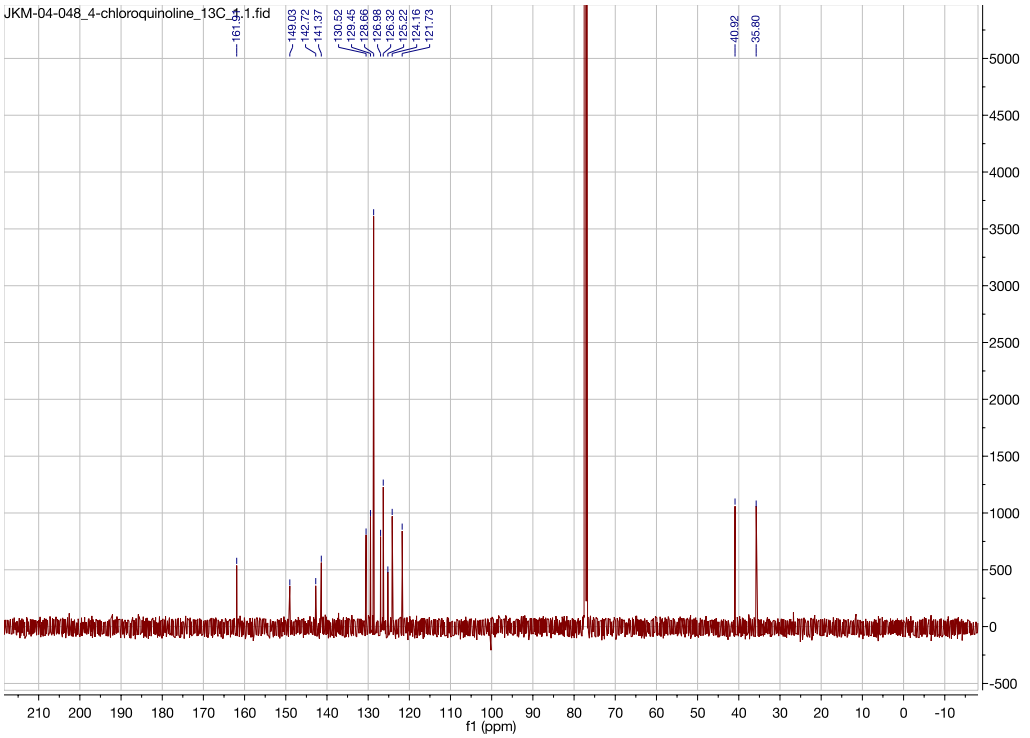


**Figure A11.123.** $^{13}$C NMR ($CDCl_3$, 125.8 MHz) spectrum of 4-chloro-2-phenethylquinoline (**6d**)

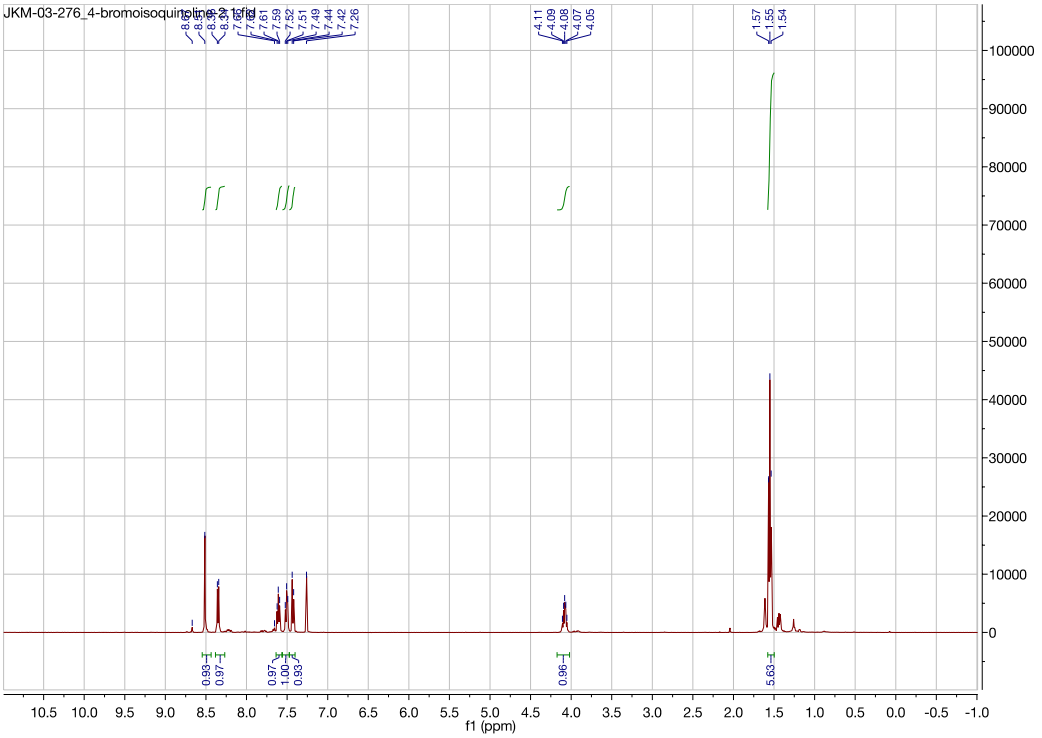


**Figure A11.124.** $^{1}$H NMR ($CDCl_3$, 500 MHz) spectrum of 4-bromo-3-isopropylisoquinoline (**6e**)

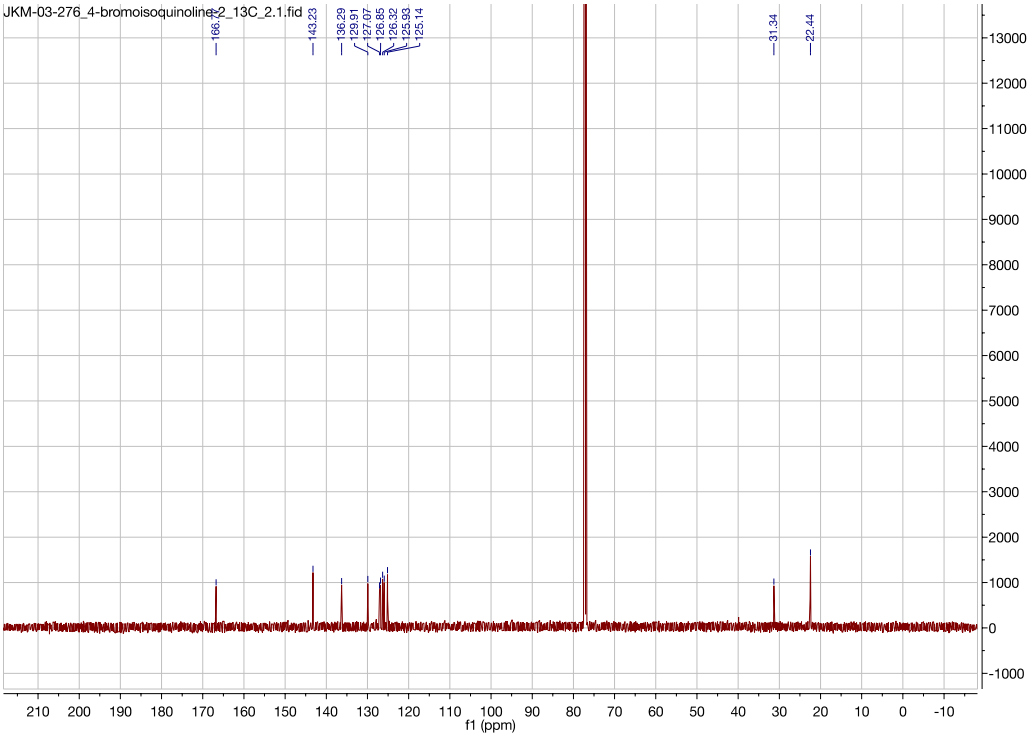


**Figure A11.125.** $^{13}$C NMR ($CDCl_3$, 125.8 MHz) spectrum of 4-bromo-3-isopropylisoquinoline (**6e**)

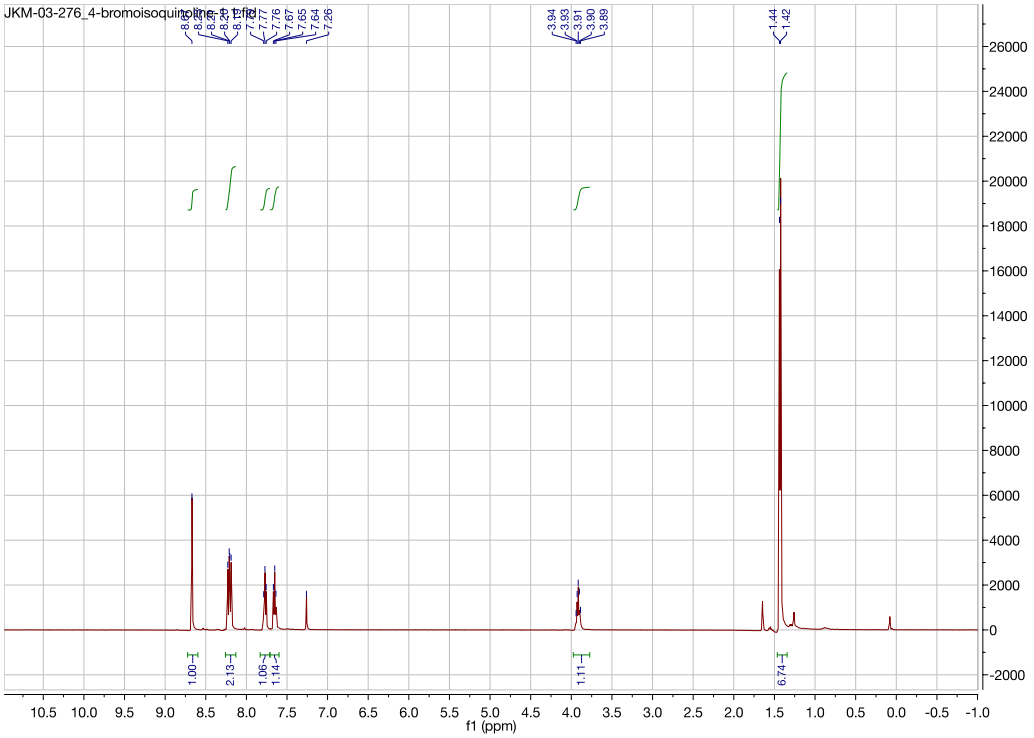


**Figure A11.126.** $^{1}$H NMR ($CDCl_3$, 500 MHz) spectrum of 4-bromo-1-isopropylisoquinoline (**6f**)

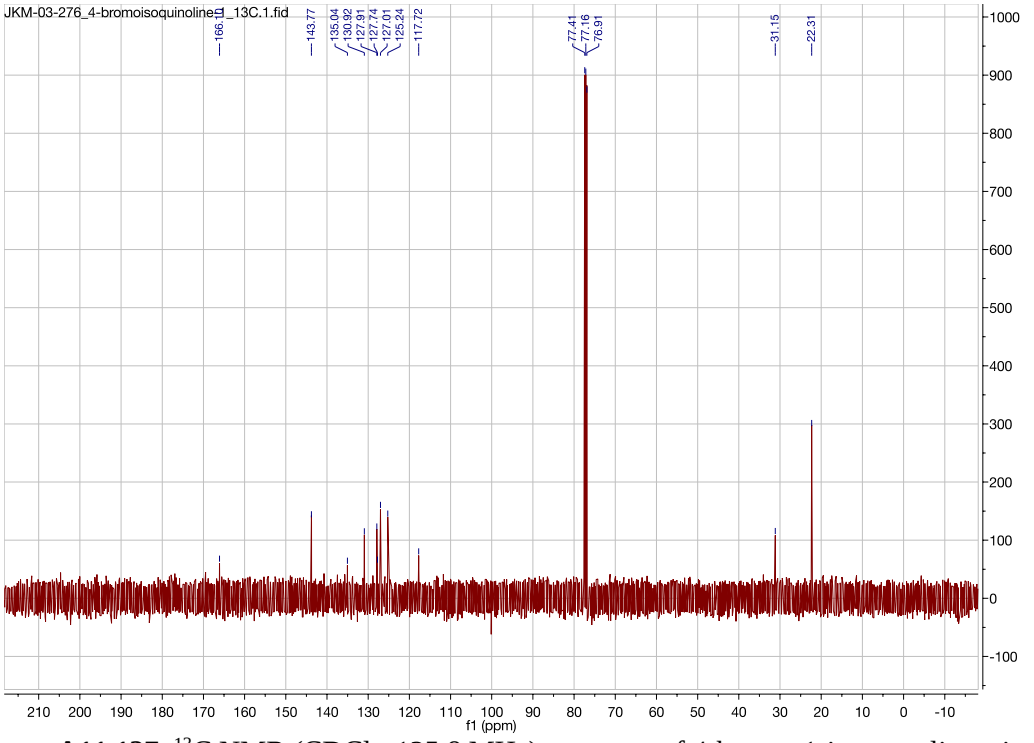


**Figure A11.127.** $^{13}$C NMR ($CDCl_3$, 125.8 MHz) spectrum of 4-bromo-1-isopropylisoquinoline (**6f**)

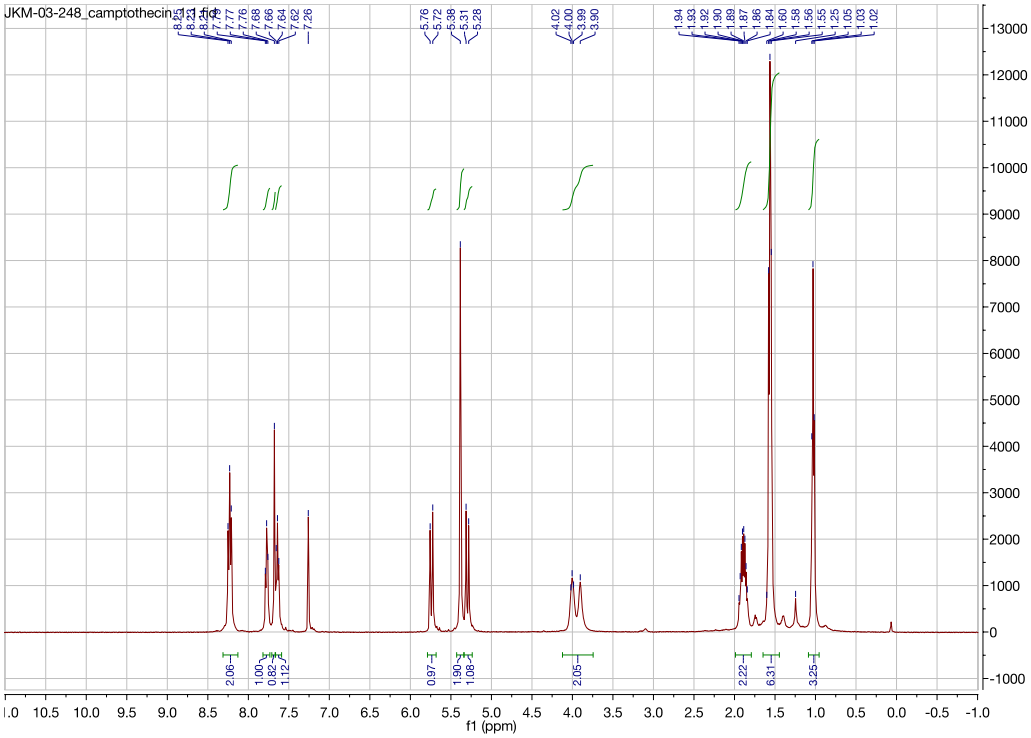


**Figure A11.128.** $^{1}$H NMR ($CDCl_3$, 500 MHz) spectrum of (*S*)-4-ethyl-4-hydroxy-11-isopropyl-1,12-dihydro-14*H*-pyrano[3',4':6,7]indolizino[1,2-*b*]quinoline-3,14(4*H*)-dione (**7a**)

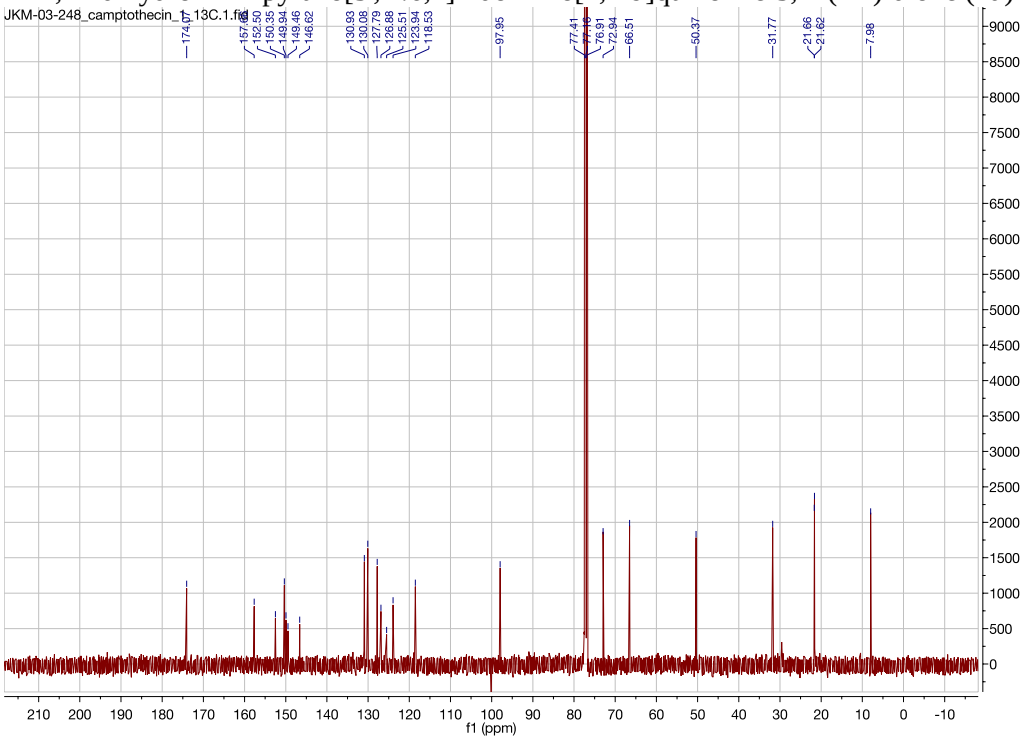


**Figure A11.129.** $^{13}$C NMR ($CDCl_3$, 125.8 MHz) spectrum of (*S*)-4-ethyl-4-hydroxy-11-isopropyl-1,12-dihydro-14*H*-pyrano[3',4':6,7]indolizino[1,2-*b*]quinoline-3,14(4*H*)-dione (**7a**)

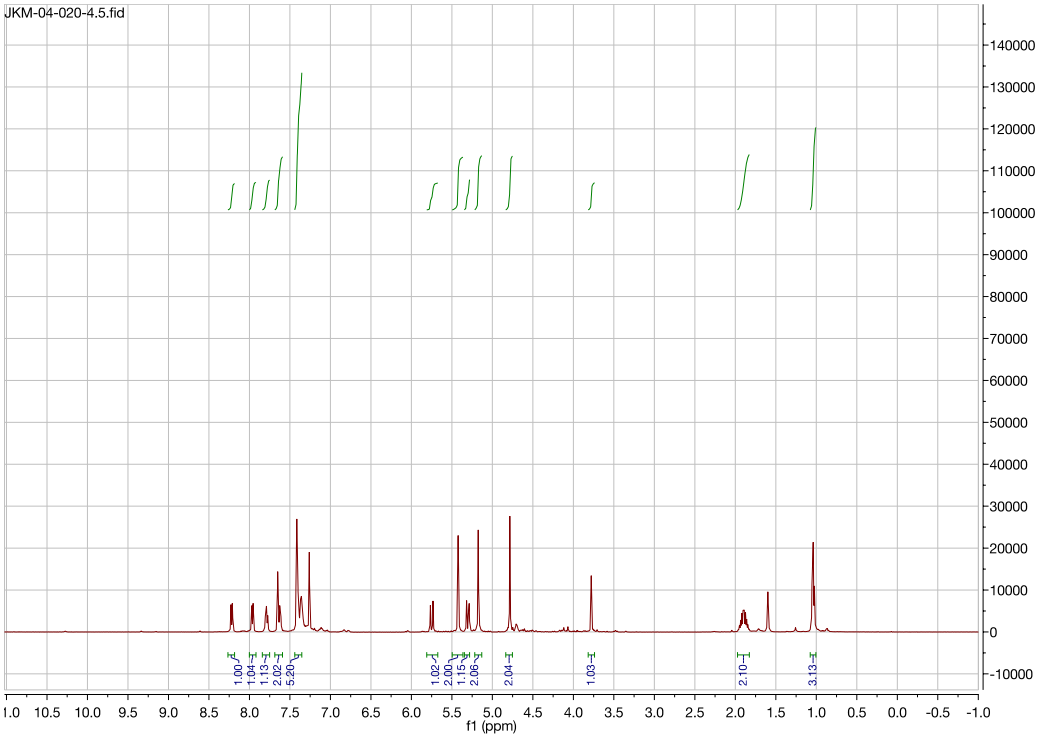


**Figure A11.130.** $^{1}$H NMR ($CDCl_3$, 500 MHz) spectrum of (*S*)-11-((benzyloxy)methyl)-4-ethyl-4-hydroxy-1,12-dihydro-14*H*-pyrano[3',4':6,7]indolizino[1,2-*b*]quinoline-3,14(4*H*)-dione (**7b**)

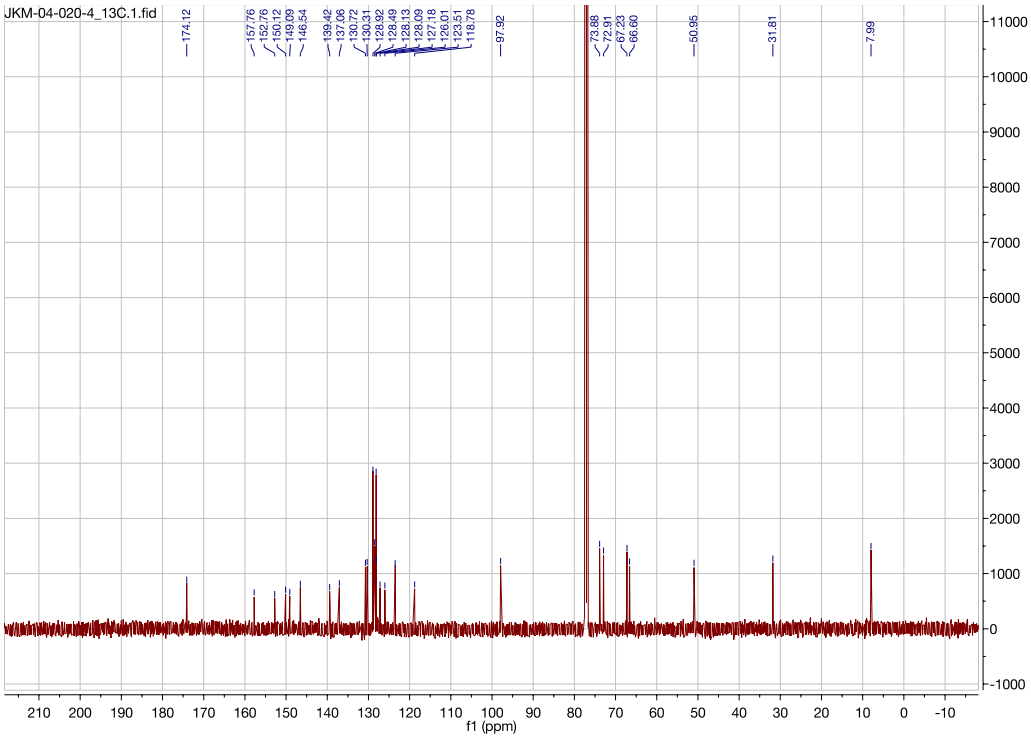


**Figure A11.131.** $^{13}$C NMR ($CDCl_3$, 125.8 MHz) spectrum of (*S*)-11-((benzyloxy)methyl)-4-ethyl-4-hydroxy-1,12-dihydro-14*H*-pyrano[3',4':6,7]indolizino[1,2-*b*]quinoline-3,14(4*H*)-dione (**7b**)


**Figure A11.132.** $^{1}$H NMR (acetone-$d_6$, 125.8 MHz) spectrum of potassium trifluoro(2-methyl-1-phenylpropan-2-yl)borate (**1u**)

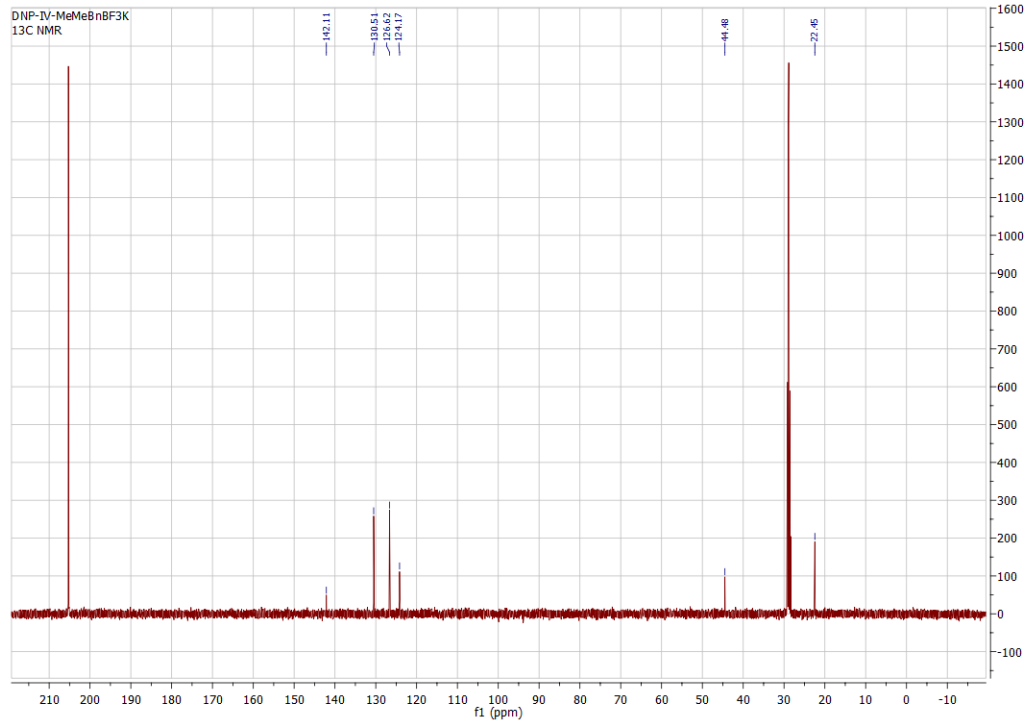


**Figure A11.133.** $^{13}$C NMR (acetone-$d_6$, 125.8 MHz) spectrum of potassium trifluoro(2-methyl-1-phenylpropan-2-yl)borate (**1u**)

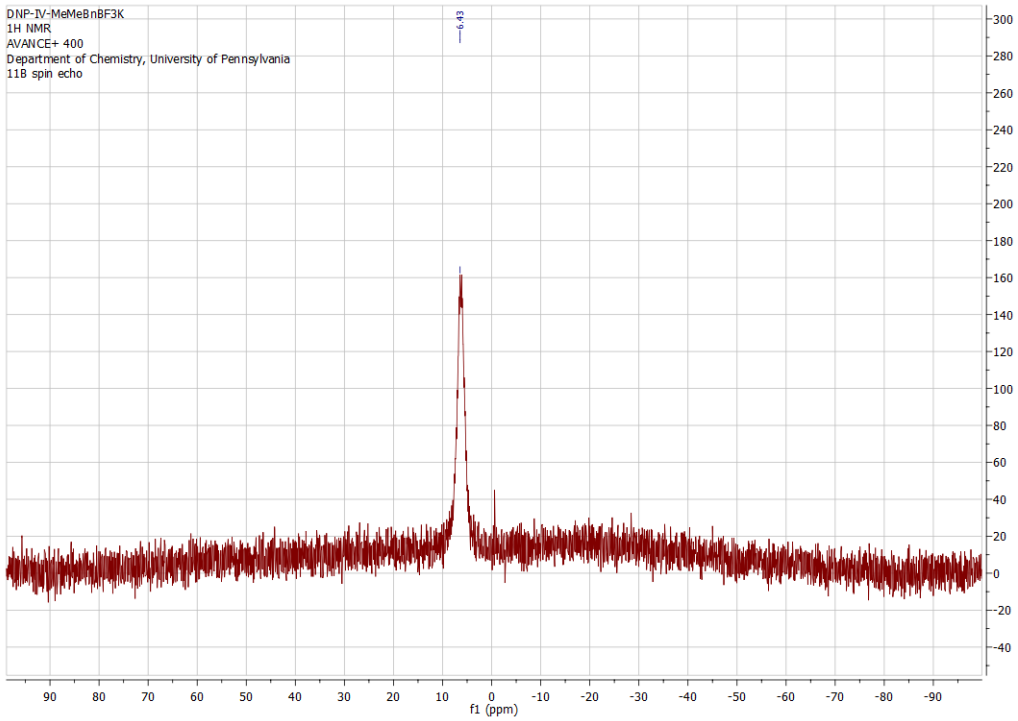


**Figure A11.134.** $^{11}$B NMR (acetone-$d_6$, 128.4 MHz) spectrum of potassium trifluoro(2-methyl-1-phenylpropan-2-yl)borate (**1u**)

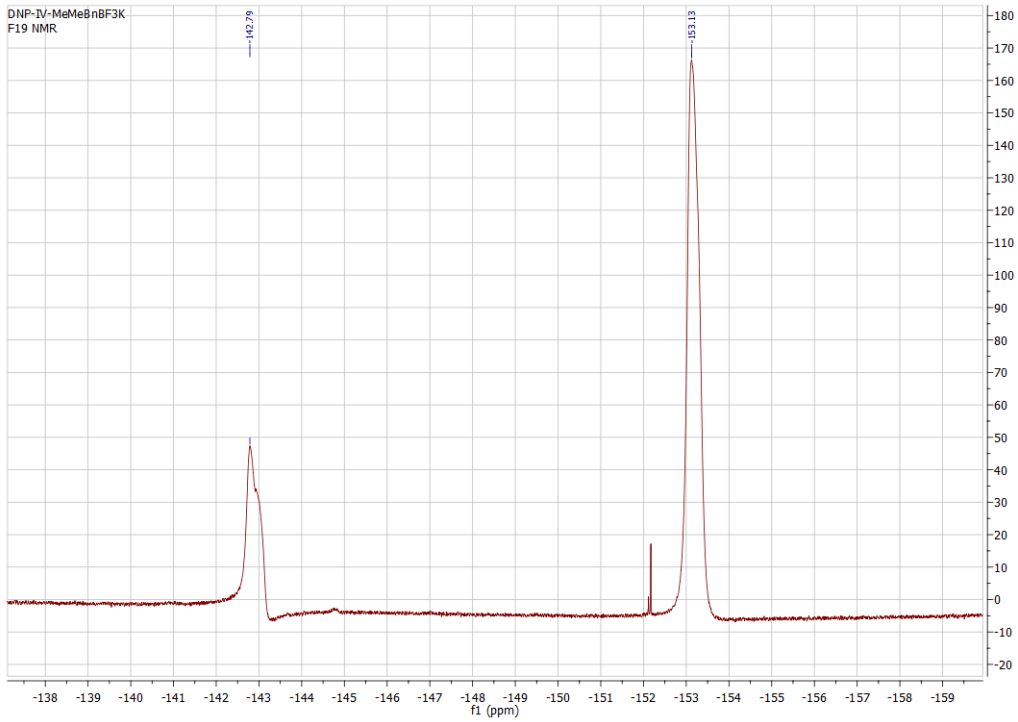


**Figure A11.135.** $^{19}$F NMR ($CDCl_3$, 470.8 MHz) spectrum of potassium trifluoro(2-methyl-1-phenylpropan-2-yl)borate (**1u**)

## About the Author

David Neal Primer was born on December 20, 1989 in Baltimore, Maryland to Benjamin and Terry-Thomas Primer. He spent his early years with his older brother, Chris, in New Jersey where he attended Hopewell Valley Central High School. Here, his early interest in science and math developed. In particular, his science teachers pushed him to pursue a possible career in academic research and drug discovery and, after a summer interning at Jacobus Pharmaceutical Company, Dave was certain of what career and impact he hoped to have.

In 2008, he began his undergraduate studies at Emory University in Atlanta, GA. After taking an outstanding introductory course in organic chemistry taught by Professor Jose Soria, Dave developed a deep interest in the art and creativity of organic synthesis. Inspired to begin research, Dave cut his teeth in the laboroatory of Professor Huw M. L Davies. Here, he learned to problem solve while investigating some chiral Au-catalyzed carbenoid chemistry; in particular, the mentorship of Fred Briones and Brendan Parr helped shape him into a solid, thoughtful scientist. In 2012, David graduated with a B.S. in chemistry and opted to continue to his studies before testing the job market.

Encouraged by his Uncle John Caldwell, David applied to and was accepted to the University of Pennsylvania, where he began his graduate studies in the laboratory of Professor Gary A. Molander. Over his past four years, David has worked closely with a number of his colleagues (in particular, John Tellis and Jennifer Matsui) to collectively publish eight papers and two reviews on the use of photoredox catalysis to enable radical mediated C-C bond-forming reactions with alkylorganometallics. He plans to complete his thesis in July 2017 before joining the process team at Celgene Corporation in New Jersey. While in the New Jersey area, David will have a chance to be close to his family, friends and his amazing girlfriend of the last seven years, Nicole.